Monday, May 20, 2019
11:00AM - 12:00PM
AI/Faster Scans, Less Contrast, Better Diagnoses?

3420

11:00AM - 11:06AM

10x Reduction of Gadolinium Dosage in Clinical Contrast-Enhanced Brain MRI Using Deep Learning

E Gong[1], T Zhang[2]
[1]Subtle Medical Inc., Menlo Park, CA, [2]Subtle Medical, Menlo Park, CA

Purpose
Gadolinium Deposition is one of the most pressing MR safety issues facing clinical imaging community. In this work, we further validated a Deep Learning based contrast-boost method, on 200 patients with mixed indications, and demonstrated the generalization and robustness of the deep learning based solution to reducing gadolinium dosage while maintaining diagnostic quality.
Materials and Methods
Dataset A cohort of 200 patients were included in this study, with mixed indications and receiving clinically routine contrast-enhanced MRI (CE-MRI) exams. Sequences: Pre-contrast (zero-dose), post-contrast after 10% dosage administration (low-dose) and post-contrast after 100% dosage administration (full-dose) was collected with 3D T1 IR-FSPGR sequences for each patient. The dataset include scans from multiple sites and multiple scanner models to demonstrate the generalization of the proposed method. Method Different series from the same patient were co-registered and normalized using histogram matching technique to ensure consistency of image intensity. A deep convolutional neural network (3D U-Net) was trained to learn the approximation of the full-dose CE-MRI using low-dose and zero-dose images. 5-fold cross-validation was used to generate results for evaluation. Evaluation Quantitative metrics (PSNR, RMSE, SSIM) were used to evaluate the improvement of the enhanced contrast using deep learning. Qualitative metrics (image quality, contrast enhancement quality) were used to evaluate the result of the DL based enhancement. A non-inferiority test was conducted to demonstrate the performance of the method and validate the capability of reducing dosage without image quality loss.
Results
Quantitative metrics demonstrated consistent (~4dB in PSNR and 10% in SSIM) and significant ($p<0.001$) quality improvement of the deep learning based solution, compared with low-dose CE-MRI. Qualitative ratings showed non-significant differences between the proposed method and acquired full-dose CE-MRI images, which was also verified with the non-inferiority testing.
Conclusions
With a large dataset, we demonstrated the DL solution can generalize well, achieving robust and significant quality improvement over the low-dose CE-MRI, using 10% or even less gadolinium dosage. It enables significantly (at least 10x) gadolinium dosage reduction without sacrificing diagnostic quality. This Deep Learning solution is valuable in clinical radiology for providing alternative solutions against gadolinium deposition.

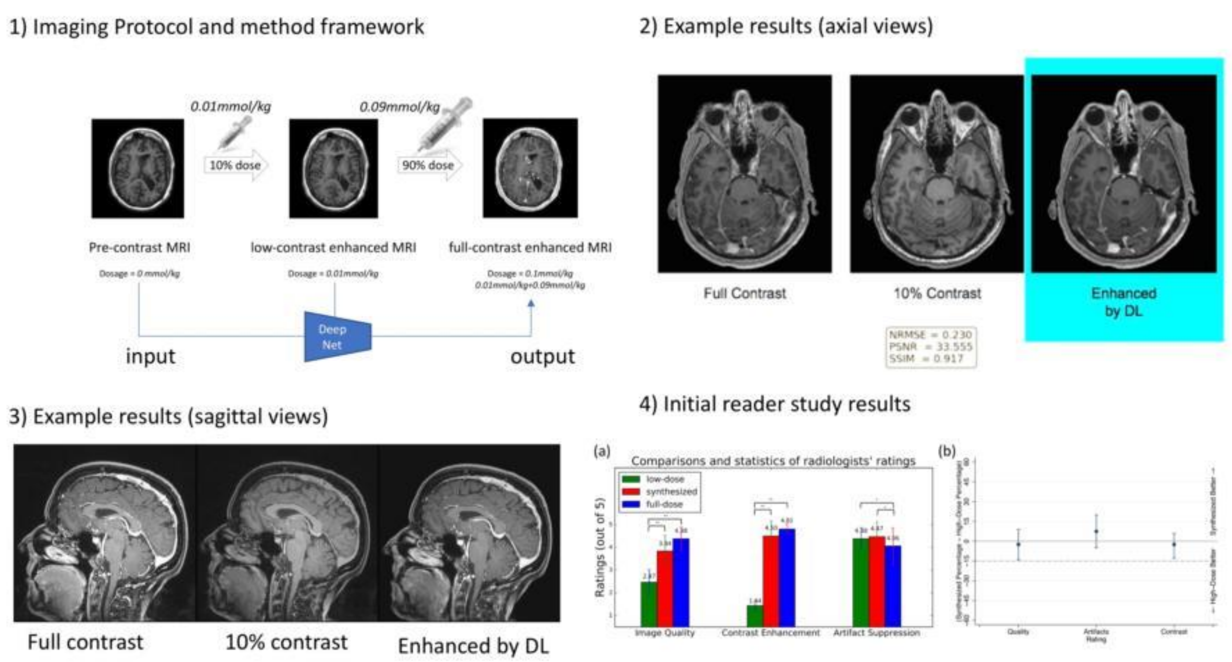

(Filename: TCT_3420_ASNR_Gad.jpg)

3395

11:06AM - 11:12AM

3x Acceleration of Clinical Brain and Spine MRI Using Deep Learning and Generative Adversarial Network

E Gong[1], T Zhang[1], A Shankaranarayanan[2]
[1]Subtle Medical Inc., Menlo Park, CA, [2]N/A, N/A

Purpose
Magnetic Resonance Imaging (MRI) is widely used in clinical neuroimaging exams and provides superior tissue contrasts for diagnosis. However for numbers of clinical applications, such as acute stroke and trauma imaging, MRI exams are sometimes time-consuming and may delay clinical decision making. In this work we present the technology using Deep Learning and Generative Adversarial Network to achieve 3-times speed up of routine clinical brain MRI and spine MRI.
Materials and Methods
Dataset Routine brain and spine protocols are collected with two settings: standard exam and 3x~4x faster exams by adjusting acquisition parameters (repetition NEX time, acceleration rate and matrix size). With IRB approval, 40 patients from 3 sites with clinical indication for routine brain and spine imaging are blindly included in the analysis to use this protocol to collect paired datasets consisting of slower (standard, high-quality) scans and faster (accelerated, low-quality) scans. For brain scans, the analysis focus on the 3D T1w and T2w series in the routine brain MRI protocol, while Sagittal T1w and PDw series are processed for spine MRI. Method A deep learning model was trained to post-reconstruct the faster (low-quality) MR images, with high-quality MR images from slower acquisition as reference. 3D Patch based method is used to augment the samples available for training. A mixed loss function, combining voxel-wise L1 loss, perceptual loss and Adversarial loss [Ref 1.] from Generative Adversarial Network, was used. The network structure is similar as in [Ref 1.] which is a recurrent type of Convolutional Neural Network structure based on ResNet modules. 50 epochs were used with Adam optimizer to ensure convergence. Evaluation To Evaluate the performance, both quantitative evaluation

and qualitative visual check is involved. Quantitative metrics (PSNR, SSIM) was used to demonstrate the enhanced MR images using the proposed method achieve significantly better quality than faster low-quality scans. Visual examples show similar quality comparing with the standard high-quality MRI from 3x slower scans.

Results

Evaluating using Peak-Signal-to-Noise-Ratio (PSNR) and structure-similarity-metric (SSIM), the reconstructed images using the proposed Deep Learning have significantly higher quality than the input images, with over 2dB PSNR and 5% SSIM increase in average. The results are also similar qualitatively compared with standard high-quality image.

Conclusions

The proposed method provide potentials to 3x accelerate routine clinical brain and spine MR exams without significant degradation of image quality, which benefit clinical applications with effiecient neuroradiology exams.

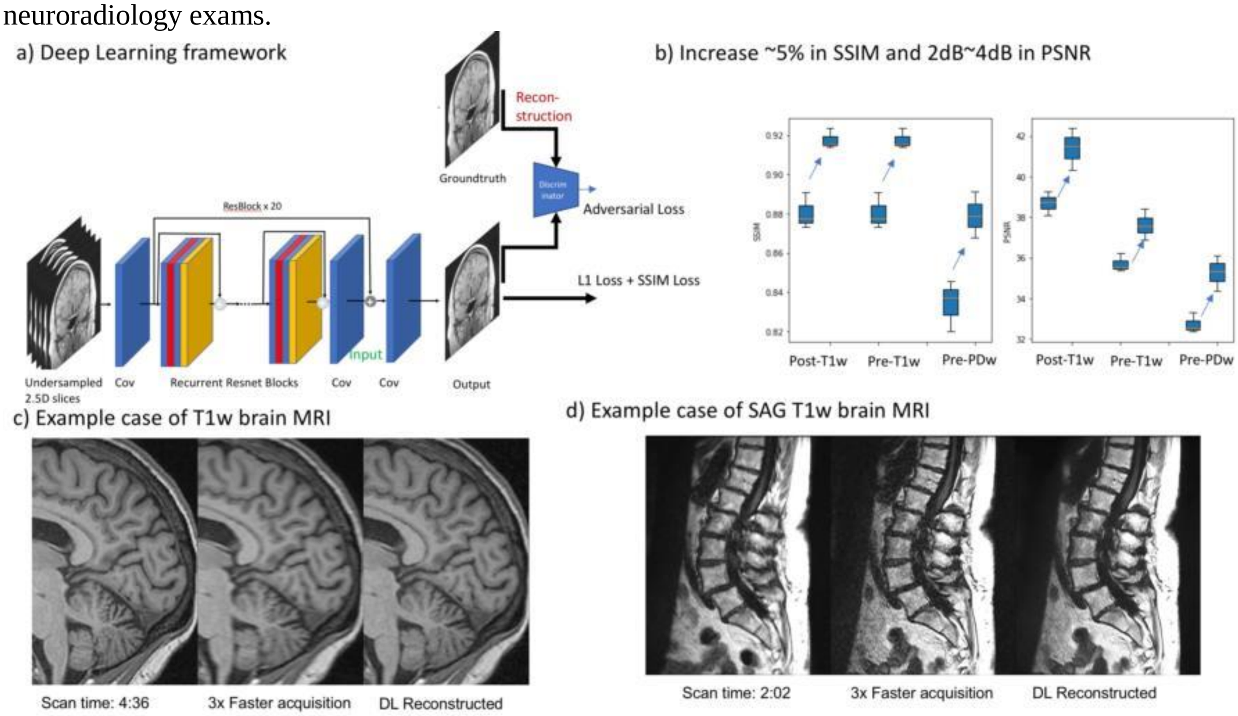

(Filename: TCT_3395_ASNR_MRI.jpg)

2415

11:12AM - 11:18AM

A Generalizable Deep Learning Network for Imaging Neuropathology with Ultra-low-dose PET/MRI

K Chen[1], M Schürer[2], E Gong[3], M Khalighi[1], O Sabri[2], G Zaharchuk[4], H Barthel[2]
[1]Stanford University, Stanford, CA, [2]University of Leipzig, Leipzig, Saxony, [3]Stanford, stanford, CA, [4]STANFORD UNIVERSITY, STANFORD, CA

Purpose

We have previously used deep learning networks to generate diagnostic amyloid PET images from PET/MRI scan protocols with markedly reduced injected radiotracer dose and/or reduced imaging time [1]. We aim to apply this trained network to data acquired at various sites with different scanners, scan protocols, and reconstruction pipelines. This will form the basis to allow larger multi-center trials to acquire simultaneous PET/MR imaging at radiation dose levels equivalent to those accrued during cross-country air travel.

Materials and Methods

PET/MRI data acquisition: 40 PET/MRI scans (39 participants, 19 female, 67±8 yrs) were obtained from Scanner 1 (Signa, GE Healthcare) while 40 other participants (23 female, 64±11 yrs) were scanned on another PET/MRI scanner (mMR, Siemens Healthineers; "Scanner 2"). The T1-weighted and T2-weighted MR images were acquired on both scanners while T2 FLAIR was acquired on Scanner 1 only. The amyloid radiotracer 18F-florbetaben was injected into the subject and PET data were acquired simultaneously 90-110 minutes after injection. The raw list-mode PET data was reconstructed for the full-dose ground truth image and was also either randomly undersampled to simulate 1% dose (Scanner 1) or framed for 1 minute from the start of PET acquisition (Scanner 2) for reconstruction to produce a low-dose equivalent (5% dose) PET image. U-net implementation: We trained a convolutional neural network ("U-net") with the proposed structure (Figure 1a) [2,3], using data from Scanner 1. 5-fold cross-validation was used for testing the data. The inputs of the network are the multi-contrast MR images (T1-weighted, T2-weighted, T2 FLAIR) and the low-dose PET image. For incomplete data, the T1-weighted images were used as inputs for the missing T2 FLAIR channel in the network. No fine-tuning was performed when applying the trained network to Scanner 2 data. Data analysis: Using the software FreeSurfer, a T1-based brain mask of each subject was used for voxel-based analyses. For each axial slice of the volumes, the image quality of the synthesized PET image and the low-dose PET images within the brain mask were compared to the original full-dose image using the metrics peak signal-to-noise ratio (PSNR), structural similarity (SSIM), and root mean square error (RMSE). Paired t-tests were used to assess the difference of metrics across datasets.

Results

Diagnostic-quality amyloid PET images were generated from the U-net using simultaneously-acquired MR images and ultra-low-dose PET data. The U-net reduced the noise from the low-dose reconstructions; the MR information added diagnostic value to the images while increasing image quality (Figure 1b, top) [1]. Similarly, applying the network on low-dose images reconstructed from Scanner 2 data, even with a different PET/MRI acquisition and reconstruction protocol, also produced images with greatly reduced noise (Figure 1b, bottom) and increased PSNR, SSIM, and reduced RMSE ($p<0.001$ for all comparisons; Figure 1c). The metrics obtained from Scanner 2 data are slightly lower than those obtained from Scanner 1 data due to the image quality difference and the bias in training data for the network but can be improved with further fine-tuning of the network using Scanner 2 data.

Conclusions

We have developed a U-net trained to generate diagnostic-quality amyloid PET images of the head from 100-fold undersampled PET images combined with MR inputs. Furthermore, we have applied the trained network to data acquired with a different scanner vendor and data acquisition protocol showing improved image quality. This can form the basis for actual low-dose PET/MRI acquisitions as well as the generalization of a trained amyloid PET/MRI imaging neural network model for use in multi-center studies.

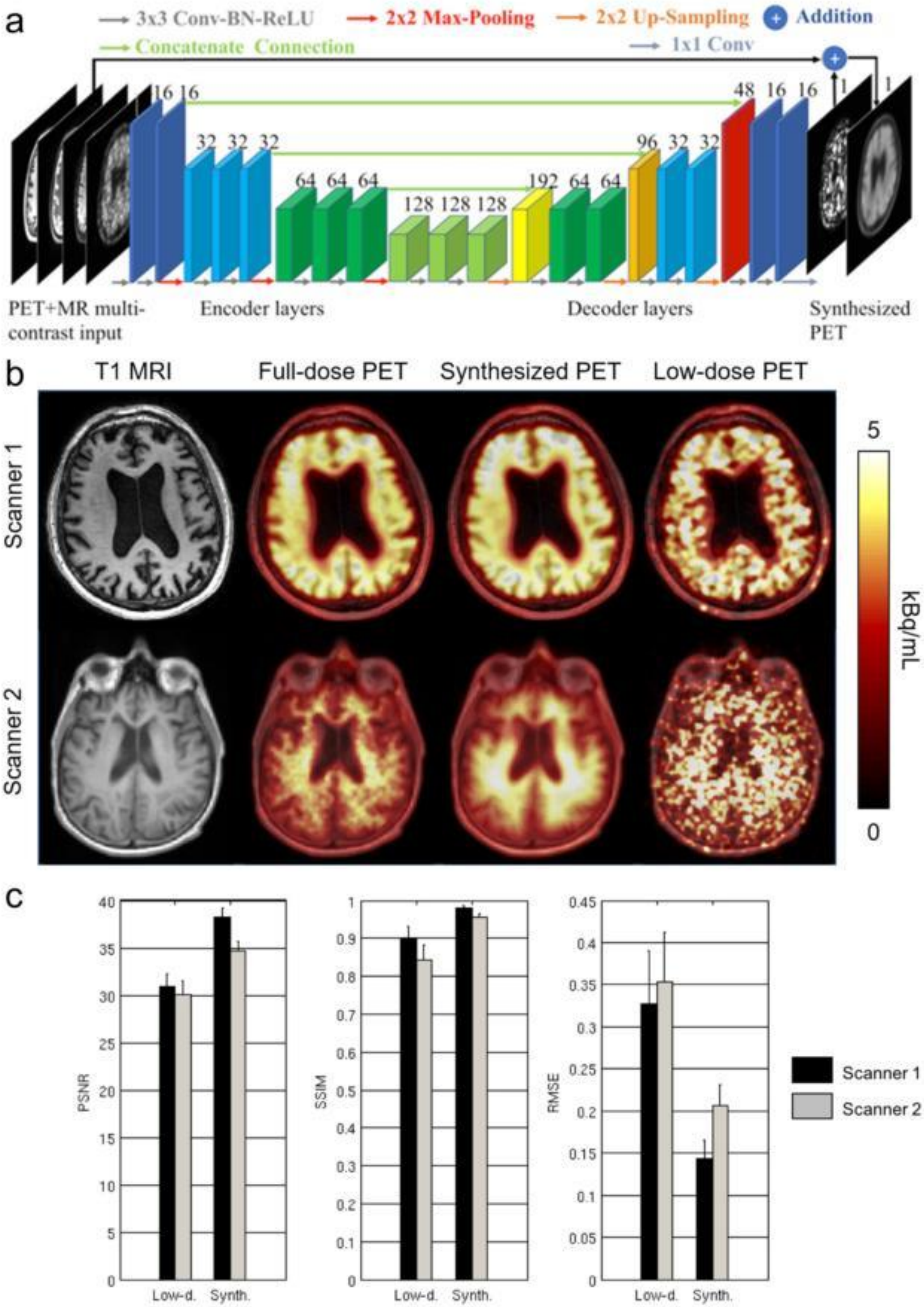
a
3x3 Conv-BN-ReLU
2x2 Max-Pooling
2x2 Up-Sampling
Addition
Concatenate Connection
1x1 Conv
16 16
32 32 32
64 64 64
128 128 128
192 64 64
96 32 32
48 16 16
1
1
PET+MR multi-contrast input
Encoder layers
Decoder layers
Synthesized PET
b
T1 MRI
Full-dose PET
Synthesized PET
Low-dose PET
Scanner 1
Scanner 2
5
kBq/mL
0
c
PSNR
SSIM
RMSE
Low-d.
Synth.
Scanner 1
Scanner 2

(Filename: TCT_2415_ASNR_image_compiled.jpg)

3299

11:18AM - 11:24AM

Artificial Intelligence Based Clinical Diagnostic Decision Support System in Neuroradiology

S Mohan[1], J Rudie[2], A Rauschecker[3], E Botzolakis[1], I Nasrallah[1], E Herskovits[4], L Desiderio[1], H Kundel[1], R Bryan[5]
[1]University of Pennsylvania, Philadelphia, PA, [2]Perelman School of Medicine at University of Pennsylvania, Philadelphia, PA, [3]UCSF, San Francisco, CA, [4]UNVERSITY OF MARYLAND, BALTIMORE, MD, [5]Univ. Pennsylvania, Philadlephia, PA

Purpose
Despite an exponential growth of artificial intelligence (AI) methods, applications assisting in formulating radiological differential-diagnosis (D/Dx) are limited. We have developed a 'personal belief' Bayesian Expert System (BES), which takes as input key features (KFs) extracted by radiologists from brain MRI, and outputs a rank-ordered D/Dx. We hypothesize that the diagnostic accuracy of the BES-D/Dx , using KFs extracted by attending radiologists, would perform at the level of a neuroradiology fellow.
Materials and Methods
13 neuroradiology attendings and 11 neuroradiology fellows set out to randomly select 8 examples of all adult neuroradiology diseases from our radiology archives, representing the spectrum of adult neuroradiology diagnoses (n=124) including 'normal'. The consensus diagnoses for these cases, based upon the clinical, radiologic and pathologic records, , were taken as the ground truth (GT). 33 diagnosis-blind readers, in 3 level-of-training groups, 13 neuroradiology attendings, 11 neuroradiology fellows and 9 radiology residents, were randomized in 2 groups and asked to report predefined signal and spatial KFs, and their 3 highest probability diagnoses for each case.. Six reads were obtained for each case, two each from each group. Each reader's KFs were entered into the BES, which generated a probability rank-ordered D/Dx (BES-D/Dx). We compared Radiologist Group-D/Dx and BES/Radiologist Group-D/Dx to the GT diagnoses using receiver operating characteristic (ROC) analysis.
Results
Of the 124 adult neuroradiology diseases we found examples of 92 diseases, with a total of 481 cases. 2400 cases (out of 2886 assigned cases), thus far, have been reviewed. Greater diagnostic accuracy was associated with higher levels of training, with Attendings, Fellows, and Residents ranking the correct diagnosis first 53, 47, and 33% of the time, respectively, and reporting the correct diagnosis as one of their 3 top choices 67, 60 and 47% of the time. BES performance was below that of the same-level-of-training radiologists, ranking the correct diagnosis first 28, 27, 21% of the time, respectively, and reporting the correct diagnosis as one of its 3 top choices 47, 43 and 38% of the time. However, the BES using Attending KFs performed at approximately the level of the resident group.
Conclusions
A neuroradiological diagnostic decision-support application was developed and evaluated using a set of 481 diagnosis-proven clinical neuroradiology MRI examinations. BES performance was below that of the radiologists, but using KFs extracted by Attendings , the BES performed at a resident level. Future optimization of the BES is expected to improve its performance, with potential to reduce the variability of radiology reports, improve report quality, reduce missed diagnoses and increase the efficiency of practicing radiologists.

3574

11:24AM - 11:30AM

Contrast-free MRI Contrast Enhancement with Deep Learning

J Liu[1], E Gong[2], G Zaharchuk[3], K Chen[4]

[1]*Tsinghua University, Beijing, China,* [2]*Stanford University, Sunnyvale, CA,* [3]*STANFORD UNIVERSITY, STANFORD, CA,* [4]*Stanford University, Stanford, CA*

Purpose
Given the issues surrounding gadolinium contrast agent, we tested whether a deep learning framework could be used to predict diagnostic post-contrast MRI images based on pre-contrast MRI images.
Materials and Methods
404 adult clinical patients were scanned with a protocol that included 6 sequences (3D IR-prepped FSPGR T1w, T2w, FLAIR T2w, 3D ASL, diffusion-weighted imaging [DWI] with 2 b values (0-1000), and T2*w) acquired before contrast agent injection and one sequence (3D IR-prepped FSPGR T1w) acquired after injection. A deep attention generative adversarial network was trained to predict post-contrast T1w images with five neighboring slices from the six pre-contrast sequences as inputs.
Results
We evaluated the performance of the proposed method on the test set with peak signal-to-noise ration (PSNR) and structural similarity (SSIM) index. The generated images have PSNR of 27.5 ± 5.6 and SSIM of 0.939 ± 0.031 compared to acquired post-contrast T1w images. The image similarity metrics show that the model is able to synthesize post-contrast T1w images with superior image quality and great resemblance to the ground truth image. Restoration of the contrast uptake is clearly noted on the synthesized post-contrast images even in small vessels and lesions, though there are also failing cases.
Conclusions
The recent identifications of gadolinium deposition within human brain and body suggest that the dosage of GBCA should be as low as possible to reduce the degree of gadolinium accumulation and toxicity. Our study shows that CNNs are capable of synthesizing post-contrast T1w images from a combination of pre-contrast MR images. With more training cases and further validation, this approach could have great clinical value especially for patients who cannot receive contrast agent injection.

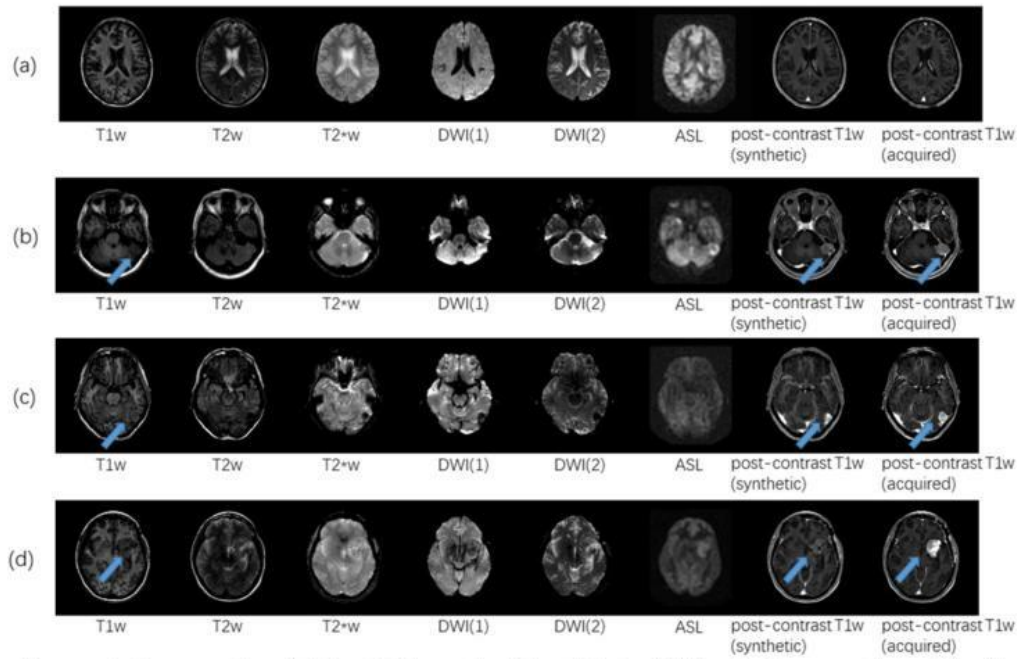

Figure. Representative examples. (a) Result from a healthy subject; (b) Result from a patient with glioma; (c) Result from a patient with meningioma after resection and radiation. (d) Result from a patient with residual meningioma. In (b)(c), the synthesized and acquired T1w images show similar contrast uptakes in the lesions, which are completely unseen in the pre-contrast T1w images. In (d), the lesion is missing in the synthetic image.

(Filename: TCT_3574_2.jpg)

2868

11:30AM - 11:36AM

Creating Realistic T1-Weighted Magnetic Resonance Images from Diffusion-Weighted Acquisitions Using a Generative Adversarial Network

V Patel[1]
[1]*Keck School of Medicine of USC, Los Angeles, CA*

Purpose
Advanced MR imaging techniques have enabled many unique and powerful investigations in recent decades. Functional MRI (fMRI), for example, relies on blood oxygen level dependent changes in the local magnetic field to draw inferences about the underlying brain activity. Diffusion tensor imaging (DTI) and its advanced variants (HARDI, DSI, etc.) utilize the directional dependence of the diffusion-weighted signal to produce maps of white matter fiber orientation. Both fMRI and DTI typically rely on fast echo planar imaging techniques, with associated compromises in terms of image resolution and artifacts. Accordingly, for most research studies in which spatial normalization of the data is ultimately desired, a separate "anatomical" T1-weighted image is acquired for each subject to provide a reference for image registration algorithms. The need for these additional sequences increases the total time and cost of image acquisition, which may be significant when aggregated over a large research study. Recently, new developments in the field of artificial intelligence -- in particular, various applications of multilayered convolutional neural networks, or deep learning -- have yielded impressive results for the classification and segmentation of radiological images in specific problem domains [1]. A new and less commonly used

machine learning technique, that of generative adversarial networks (GANs), relies on similar principles while essentially placing two neural networks in direct competition to yield convincing synthetic images of a particular type [2]. Conditional GANs are a subtype of GAN capable of translating an image of one type or style into another. In this work, we sought to determine: 1) whether it is possible to train a conditional GAN to produce synthetic T1-weighted images based solely on directional diffusion-weighted EPI input, and 2) whether any deficiencies in the generated images significantly impact the accuracy of MR image registration

Materials and Methods

At the time of our study, the MGH-USC Human Connectome Project (HCP) had made diffusion-weighted and T1-weighted data for 35 subjects available for public download [3]; these served as the source data for our investigation. The HCP diffusion-weighted data was collected using a dedicated protocol at 5 different b-values and up to 128 distinct gradient directions. However, for the purposes of the current study, we discarded all but the 64 samples obtained at the b-value of 1000 s/mm2, a typical q-shell accessible to most researchers and clinicians. As is necessary in deep learning experiments to guard against overfitting and ensure generalizability, we randomly divided the HCP data into training (29 subjects) and testing (6 subjects) groups. We developed our network by extending the well-known conditional GAN pix2pix construction of Isola [4] to accept 3-D data using custom code written in the Python programming language and version 2.2.2 of the open source Keras machine learning library with a TensorFlow backend. We used a batch size of 1 and trained the network for 200 epochs using data from the training group, which was augmented through the conventional means of scaling, flipping, and rotation. The trained model was then applied to the unseen data from the test group to generate T1-weighted images directly from the diffusion-weighted samples of those 6 subjects. To determine the suitability of the generated T1-weighted images for the purpose of image registration, we used the FLIRT and FNIRT utilities from version 6.0 of the FSL suite [5] to perform nonlinear registration of the MNI-152 brain template to the native space of each test subject, using both the generated and acquired T1-weighted volumes as the fixed images. The displacement maps for both registrations were compared voxelwise for each subject and both the mean and the maximum displacement discrepancy (in mm) was quantified for all voxels within the brain.

Results

Training the GAN for 200 epochs on the diffusion-weighted data from the 29 subjects in the training set required 14 hours and 32 minutes of computation time on a GeForce 1080 Ti GPU. Generating the synthetic T1-weighted volumes for all 6 test subjects required only 48 seconds. A representative example of the GAN output is provided in the attached figure, shown alongside the acquired T1-weighted data for purposes of qualitative comparison. We note that the GAN output appears quite realistic on cursory examination, and that a careful inspection is required to appreciate the differences between the two T1-weighted images (which are most evident in the basal ganglia and along the right frontal lobe gyri in this sample). The quantitative analysis of the differences between nonlinear registration displacement fields produced by targeting the generated and acquired T1-weighted volumes revealed that these minor differences between the images had negligible impact on the ultimate spatial normalization. Across the 6 test subjects, the mean difference in the displacement map was 0.053 mm, and the largest single-point difference in the displacement maps was 0.45 mm. As a reference for evaluating the significance of these differences, we note that the resolution of the acquired diffusion-weighted data set was 1.5 mm isotropic.

Conclusions

We have demonstrated a method for using a conditional GAN to generate realistic T1-weighted images directly from diffusion-weighted echo planar volumes. We have shown that these generated volumes can be used as target images for spatial normalization with negligible differences in the displacement fields compared to using conventionally acquired T1-weighted images. These results have the potential to reduce scanning times and costs for many research studies by eliminating the acquisition of dedicated sequences that are currently obtained for the sole purpose of image registration. These time and cost savings may then be converted to acquire greater numbers of or higher quality versions of the actual sequences of interest (e.g., DTI or DSI). Further work will establish whether similar results can be achieved with the T2*-weighted images used in fMRI. Ultimately, a well-trained generative model may be developed using data contributed by multiple sites and provided as a resource to the research community.

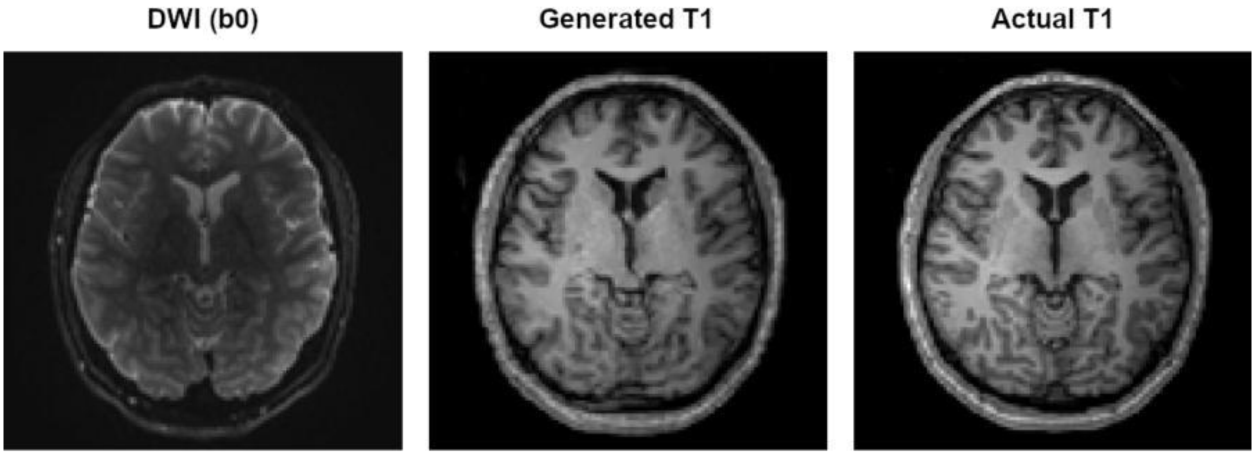

Representative GAN performance on the test dataset. The multi-direction diffusion-weighted data set (b0 volume shown on left) served as input to the GAN, which produced the corresponding T1-weighted image (center). The true acquired T1-weighted image is shown (right) for comparison.

(Filename: TCT_2868_gan.jpg)

3593

11:36AM - 11:42AM

Deep Learning Enables High Quality One-minute EPIMix Brain MRI Scans

J Liu[1], E Gong[2], G Zaharchuk[3], S Skare[4]
[1]Tsinghua University, Beijing, China, [2]Stanford University, Sunnyvale, CA, [3]STANFORD UNIVERSITY, STANFORD, CA, [4]Karolinska Institutet, Stockholm, SE-171 76 Stockholm

Purpose
EPIMix is a newly proposed one-minute multi-contrast echo-planar imaging based sequence for brain magnetic resonance imaging (MRI). Despite the ultra-fast acquisition speed, EPIMix images suffer from lower signal-to-noise ratio (SNR) and resolution than standard scans. In this study, we tested whether a deep learning framework could improve the image quality of EPIMix.
Materials and Methods
The MR protocol included 6 EPI Mix sequences (T2, T2-FLAIR, T1-FLAIR, ADC, GRE, DWI) and 2 standard sequences (T2, T2 FLAIR). 50 patients were scanned. 40 cases from the cohort were random chosen for training and the rest were used for testing. A deep cycle-consistent generative adversarial network was trained to enhance EPIMix images including denoising and super-resolution.
Results
The proposed method was applied to T2 and T2-FLAIR images. The results show that the enhanced images look sharper and have higher similarity with standard images than the original EPIMix images. In addition, the pathologies in the original images are well-preserved. Several examples are shown in the Figure (enhanced and reference images are of 512 × 512 pixels, while EPIMix images are of 256 × 256 pixels and enlarged via bicubic interpolation for uniform display).
Conclusions
Our study shows that the proposed method is capable of enhancing the ultra-fast EPIMix scans and generating visually pleasing results. The results suggest that deep learning can enable ultra-fast MRI scans without losing image quality. With further validation, this approach could improve patients' MRI

scan experience, potentially reduce the cost of MRI scans, and most importantly help patients with acute diseases such as acute cerebral infarction who can get better diagnosis and treatment with MRI images while they cannot afford to spend the time needed for standard MRI.

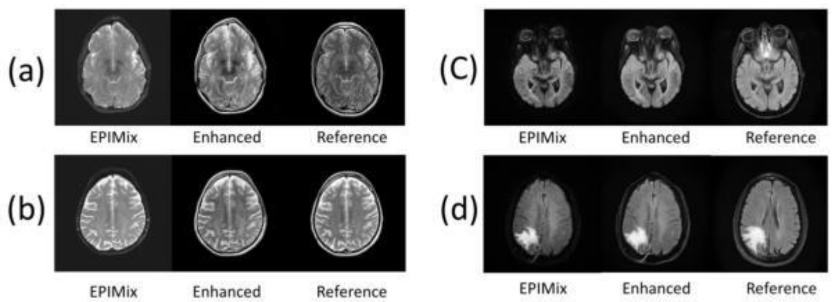

Figure. Examples of enhanced images from the test set. (a) (b): T2; (c) (d): T2 FLAIR. Reference images are taken from nearby positions in standard image volumes for visual comparisons. Enhanced and reference images are of 512 × 512 pixels, while EPIMix images are of 256 × 256 pixels and enlarged via bicubic interpolation for uniform display.

(Filename: TCT_3593_EPIMix_poster.jpg)

2736

11:42AM - 11:48AM

DIR and FLAIR Correlate of Gadolinium Enhancing Lesions in Multiple Sclerosis: Is Contrast Needed for Follow-up MRI?

R Hu[1], G Sadigh[1], A Waldman[1], A Saindane[1]
[1]*Emory University School of Medicine, Atlanta, GA*

Purpose

Gadolinium enhanced MRI is routinely used for follow-up of patients with multiple sclerosis (MS). Motivated by concerns about gadolinium deposition, recent studies have questioned the necessity of contrast on routine follow-up by showing that lesion enhancement is highly associated with FLAIR progression. We sought to evaluate the performance of DIR, a sequence more sensitive to cortical and infratentorial lesions than FLAIR, as a surrogate marker for lesion enhancement.

Materials and Methods

In this IRB approved study, we retrospectively reviewed 252 consecutive MRIs in 172 unique patients performed using a dedicated MS protocol including 3D DIR, 2D FLAIR and 3D post-contrast T1 weighted imaging on a single 3T scanner. Patients were included based on clinically confirmed MS and were excluded for other intracranial pathologies. Three neuroradiologists independent reviewed all images, blinded to clinical and demographic information, grading the co-presence or absence of DIR, FLAIR and contrast enhancing lesions. In a subset of patients with prior comparisons, we counted the number of progressive lesions on each of the 3 sequences. Consensus interpretation was used for further analysis.

Results

34 of 252 MRIs (13%) demonstrated a total of 55 enhancing lesions, of which 52 (95%) had corresponding hyperintensity on DIR and FLAIR. All lesions were concordant on DIR and FLAIR, and the 3 enhancing lesions not visible on either sequence were small (< 2 mm) and cortical/subcortical (2) or periventricular (1) in location. 18 (24%) of the 76 MRIs with a prior comparison had imaging evidence of progression: 11 (61%) of these showed new lesions on DIR or FLAIR only, 6 (33%) showed progression on all sequences, and 1 (6%) had an enhancing lesion occurring in an area of unchanged confluent DIR and FLAIR abnormality (Figure).

Conclusions

There is a high but imperfect concordance between enhancing lesions and hyperintensity on either DIR or FLAIR. Very small cortical/subcortical and periventricular enhancing lesions can be difficult to appreciate on DIR or FLAIR. Serial follow-up using DIR or FLAIR alone may capture the majority of imaging progression, but isolated enhancing lesions in confluent areas of white matter abnormality could present a pitfall for this approach.

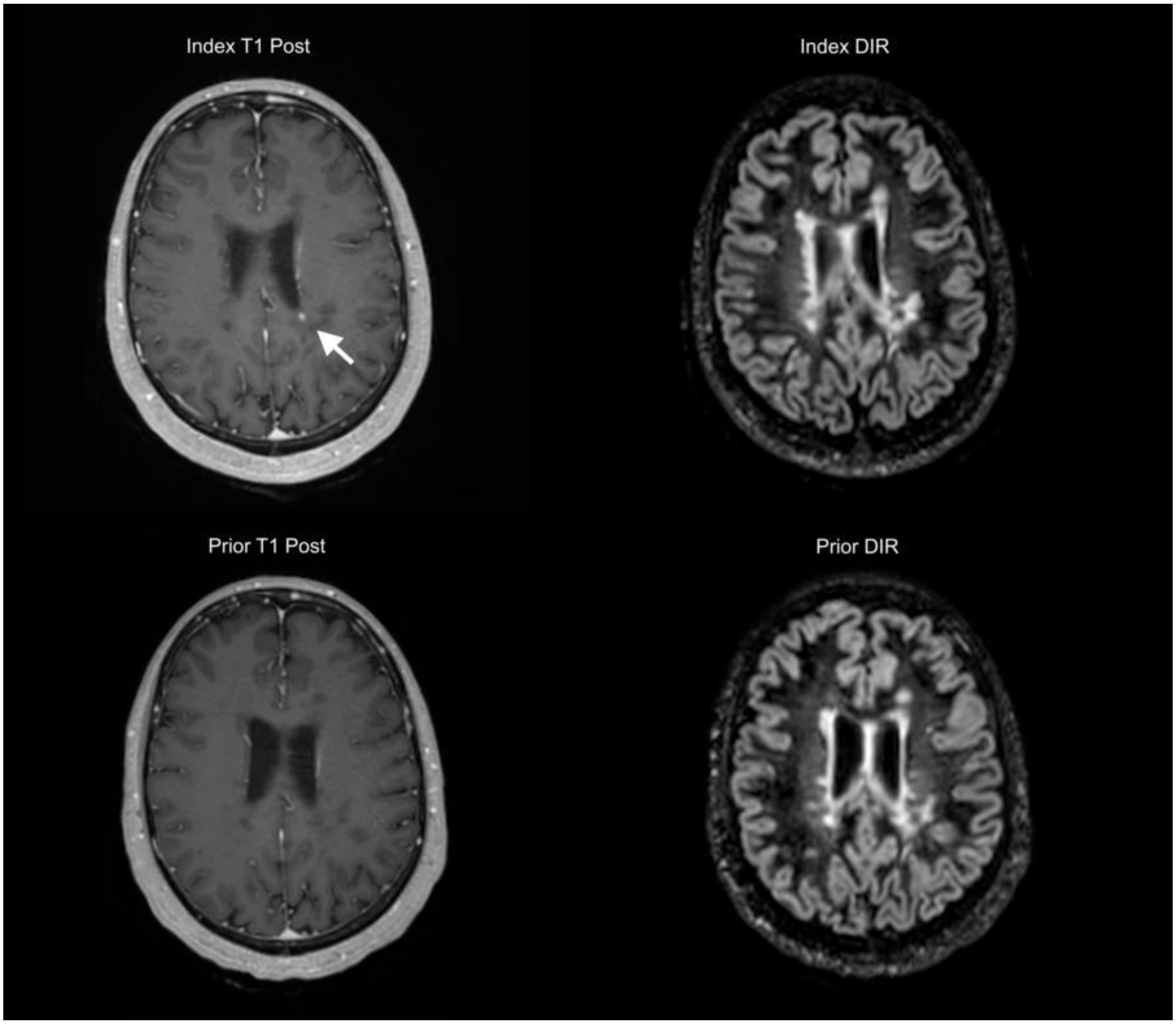

(Filename: TCT_2736_Figure1.jpg)

2384

11:48AM - 11:54AM

Fully Automated Diagnosis in Neuroradiology: Combining Deep Learning and Bayesian Networks

J Rudie[1], L Xie[1], J Wang[1], E Botzolakis[2], R Bryan[3], I Nasrallah[1], S Mohan[1], J Gee[1], A Rauschecker[4]
[1]University of Pennsylvania School of Medicine, Philadelphia, PA, [2]Mecklenburg Radiology Associates, Charlotte, NC, [3]Dell Medical School, University of Texas, Austin, Austin, TX, [4]Univeristy of California San Francisco, Philadelphia, PA

Purpose
As both the complexity and volume of medical imaging increases, there is a pressing need for automated quantitative and probabilistic image analyses that can improve the efficiency and accuracy of the radiology workflow. We leveraged customized image processing, convolutional neural networks and subspecialty expertise encapsulated within Bayesian networks to create a transparent automated system to quantitatively characterize multimodal brain MRIs and automatically a generate probabilistic differential diagnosis for 35 disease entities.

Materials and Methods
390 clinically-validated cases were split into training (n = 288) and validation (n = 102) samples. Seven clinical MR modalities (T1W, T2W, FLAIR, T1post, GRE, DWI/ADC) were incorporated into a customized image-processing pipeline (A) using ANTs tissue segmentation [1] and 3D U-Net convolutional neural networks [2]. Features derived from the image processing pipeline were combined with clinical information (age, gender, chronicity, immune status) in an expert-trained naïve Bayes network focused on 35 diseases known to involve deep gray matter (B). Within the validation sample the performance of the fully automated system was compared to radiology residents, neuroradiology fellows, community radiologists and academic neuroradiology attendings.
Results
The accuracy of the image processing and feature extraction pipelines were overall ~89% accurate compared to attending extracted ground truth features. The fully automated pipeline, integrating imaging and clinical features, determined an accurate differential diagnosis in 77% of the cases (top 3) and the exact diagnosis in 60% of the cases, which was significantly better than residents (55%/36%) and community radiology attendings (52%/33%), not significantly different than neuroradiology fellows (72%/59%), and below academic neuroradiology attendings (84%/67%).
Conclusions
Using a hybrid approach, which computationally mirrors the two fundamental steps to image interpretation by combining customized image processing, convolutional neural networks and Bayesian networks, we developed an AI based system that can diagnose a wide array of neurologic diseases, performing at the level of a neuroradiology fellow. This general approach, when working in conjunction with a radiologist, has the potential to improve radiologists' accuracy and efficiency.

(Filename: TCT_2384_ASNR_Figure.jpg)

Monday, May 20, 2019
11:00AM - 12:00PM
Neuroinflammatory Diseases Adult Brain

2638

11:00AM - 11:06AM

Abnormal Brain FDG PET Findings in Post-Treatment Lyme Disease Syndrome

M Larvie[1], A COUTINHO[2], N Zubcevik[3]
[1]Cleveland Clinic, Cambridge, MA, [2]University of São Paulo, São Paulo, SP, [3]Spaulding Rehabilitation Hospital, Charlestown, MA

Purpose
Lyme disease is a tick-borne infection of the spirochete, Borrelia burgdorferi. In many cases, prompt diagnosis and appropriate antibiotic therapy leads to an effective and durable cure. In a minority of cases, despite standard-of-care treatment, patients report persistent symptoms involving multiple organ systems, particularly the central nervous system (CNS) and the musculoskeletal system, and this condition has been termed post-treatment Lyme disease syndrome (PTLDS), in contrast to a more controversial condition putatively described as chronic Lyme disease1. Among the many challenges that these patients present, accurate diagnosis is one of the largest. These patients no longer harbor the Borrelia organism, and so their condition is not defined by infection status. The CNS-related complaints have been referred to as "brain fog" and include poorly defined symptoms such as fatigue, diminished memory, impaired cognitive function and behavior changes2. Routine diagnostic imaging with CT and MRI in these patients

typically show no abnormality. An earlier report has identified FDG brain PET abnormalities in patients with Lyme disease3. To test the hypothesis that there is a functional brain abnormality in PTLDS, we have used brain FDG PET examinations to look for an objective biomarker of brain abnormality.

Materials and Methods

Research subjects were recruited from patients presenting to a specialized clinic for the evaluation and management of the chronic sequelae following exposure to tick borne illness. A total of 68 subjects are included in this study. In addition to clinical examination and laboratory testing that is routine for the specialized clinic from which the patients were recruited, brain FDG PET examinations were obtained on all subjects. Brain PET imaging was obtained approximately 45 minutes following intravenous injection of 5.0 mCi of 18F-fluorodeoxyglucose (FDG) using an ECAT HR+ scanner (Siemens/CTI, Knoxville, TN). Sixty-three planes were acquired simultaneously over a 15.5 cm field of view. Images were acquired in 3D mode. Attenuation correction was performed using a transmission scan obtained with a 68Ge source. A maximum likelihood reconstruction method was used, yielding images with in-plane resolution of approximately 4.6 mm (full width at half maximum). All patients were screened with fingerstick blood glucose measurement, and PET imaging was not performed in those patients with blood glucose greater than 150 mg/dl. Brain FDG PET examinations were reviewed using syngo.via and NeuroMIM software. Visual qualitative inspection as well as parametric Z-score comparisons using age-stratified normal patient populations were used in each case. The brain FDG PET scans were classified as normal, possibly abnormal, definitely abnormal, and definitely abnormal with a pattern suggestive of a high confidence diagnosis.

Results

Demographic characteristics of the 68 subjects are shown in Table 1. Of note, 69% of subjects were female and the average age was 48 years old. Table 1. Subject characteristics Total subjects 68 Gender Female 47 (69% Male 21 (31%) Age range 19-76 Average age 48.4 Classification of brain FDG PET scan results according to the categories described in the Methods section is shown in Table 2. Brain FDG PET findings were predominantly regions of hypometabolism, indicated by decreased FDG uptake. A single exception was possible mild relative hypermetabolism in the frontal lobes in a single subject. Areas of possible or definitive hypometabolism were identified in the temporal, frontal, parietal and occipital lobes, the thalami, and the cerebellum. Among the scans classified as possibly abnormal, temporal hypometabolism was the most common possible abnormality (14/32 subjects, 43.8%). Of the scans classified as definitively abnormal, temporal lobe hypometabolism was also the most common finding (9/10, 90%). The one scan classified as abnormal with a pattern consistent with a high confidence diagnosis was a 74 year old male with brain FDG PET findings typical of Alzheimer pathology. One subject with definite abnormality on an initial PET scan was treated with a course of antibiotic therapy4 and on subsequent brain FDG PET examination the abnormality had resolved, with concordant improvement in neuropsychiatric symptoms. Table 2. Brain FDG PET classification Classification Number Percent Normal 27 38.6 Possibly abnormal 32 45.7 Definitely abnormal 10 14.3 High confidence diagnosis 1 1.4 Figure 1 shows images from a brain FDG PET scan of a 50 year old man with neuropsychiatric features suggestive of PTLDS. There is hypometabolism in the temporal lobes and cerebellum bilaterally.

Conclusions

Abnormal brain FDG PET scans were seen in 14.3% of subjects with PTLDS. The dominant abnormality in this population was temporal lobe hypometabolism, a feature that has been identified in other encephalitides, including Lyme disease and auto-antibody encephalitis syndromes. Although a causal relationship cannot be established from this data, these findings raise the possibility that brain FDG PET may be a useful biomarker in the evaluation of this difficult patient population5 and may be useful for stratifying patients who may benefit from additional treatment. Further studies should be directed at exploring long term outcomes in PTLDS patients with abnormal brain FDG PET findings, as well as possible etiologies of brain abnormality in PTLDS.

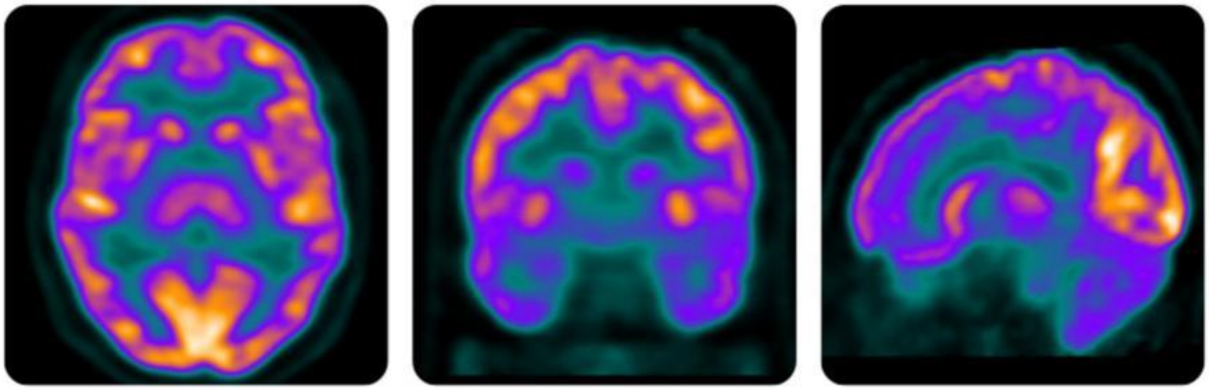

(Filename: TCT_2638_ASNR_Fig-1.jpg)

3643

11:06AM - 11:12AM

Automated Segmentation in Multiple Sclerosis: Clinical Imaging Completion by 3D Volumetry

t nguyen[1]
[1]*C.H.N.O. des Quinze Vingts, Paris, France*

Purpose
Evaluation of delineation accuracy and reproducible volumetry of hypersignals in MS follow-up.
Materials and Methods
Twenty patients underwent M.R. Imaging at 3T for multiple sclerosis, 3D sequences including T1-weighted SE, FLAIR and Double Inversion Recovery, before Gadolinium injection. Temporal imaging was performed at T0 and approximately 1 year later for all patients. Data were afterwards submitted to digital segmentation and volumetric summation using volBrain 1.0 software for individual comparison.
Results
Segmentation demonstrated a precise delineation of abnormal hypersignals in periventricular areas and in the corona radiata. Contiguous hypersignals were segmented throughout the subcortical white matter, whereas isolated subcortical hypersignals were excluded from segmentation in most cases concerning lesions under 5 mm of diameter, and in nearly 50% of lesions with diameter superior to 5 mm. Segmentation appeared more pertinent to delineate subcortical hypersignals in 3D FLAIR sequences when compared to 3D DIR sequences . Anatomical registration onto MNI templates allowed a temporal follow up of 3D FLAIR or 3D DIR sequences in individuals, when superimposed on 3D T1. Anatomical references in 3D T1, such as anterior or posterior commissures, were efficiently coregistrated en 17 patients, using rigid spatial transformation. Three patients were discarded, due to spatial mismatch in 3D T1 volumes superior to 1.5 voxel.
Conclusions
Anatomical registration and hypersignal segmentation can be routinely achieved for multiple sclerosis, with a reliable temporal evaluation based on adequate volume superimposition. These preliminary results suggest a short-term application to machine-learning in AI, with accurate signal detection in improved MR sequence quality.

3419

11:12AM - 11:18AM

Common and Uncommon Imaging Findings in Neuromyelitis Optica: A Retrospective Review

D Ray[1], S Salama[2], M Khan[1], M Levy[3], I Izbudak[1]

[1]*Johns Hopkins Medical Institute, Department of Radiology, Baltimore, MD,* [2]*Johns Hopkins Medical Institute, Department of Neurology; University of Alexandria, Egypt, Baltimore, MD,* [3]*Johns Hopkins Medical Institute, Department of Neurology, Baltimore, MD*

Purpose
To evaluate the frequency of initial imaging findings in patients with neuromyelitis optica with a documented relapse at a single tertiary care institution.
Materials and Methods
Following institutional review board approval, 95 patients with confirmed neuromyelitis optica were retrospectively reviewed to evaluate the initial imaging findings. Imaging criteria used were in concordance with the International Consensus Diagnostic Criteria for Neuromyelitis Optica Spectrum Disorders to appropriately collect data. Patient charts were reviewed to determine the clinical relapse.
Results
A total of 95 patients were reviewed with a diagnosis of neuromyelitis optica. The average age of our patients was 40 years made up of 20 males and 75 females. Common imaging findings included subcortical lesions (48%), optic neuritis (46%), longitudinally extensive transverse myelitis (63%), central spinal cord involvement (67%), and involvement of both the cervical and thoracic spine (49%), and enhancement of the cord lesions (43%) with many patients having multifocal lesions. Uncommon imaging findings included lesions in the dorsal medulla (7%) and fourth ventricle periependymal lesions (12%). Average time in months between initial presentation and first relapse was 13 months.
Conclusions
This study demonstrates the frequency of imaging findings in patients with clinically proven neuromyelitis optica at initial presentation. The most common findings were classic including lesions of the spinal cord and optic neuritis with less common findings involving the dorsal medulla and periependymal fourth ventricle. This study highlights the importance of imaging to assist in the diagnosis of neuromyelitis optica. Radiologists should be aware of the common and uncommon imaging findings in neuromyelitis optica to ensure the appropriate and timely management for patients.

2957

11:18AM - 11:24AM

Fluorescence Molecular Imaging of Myeloperoxidase in Bacterial Cerebritis

B Pulli[1], C Wang[1], N Jalali Motlagh[1], G Wojtkiewicz[1], A Li[1], J Chen[1]
[1]*Massachusetts General Hospital, Boston, MA*

Purpose
Myeloperoxidase (MPO) is a highly oxidative enzyme crucial for defense against pathogens (1). We sought to develop a molecular imaging probe sensitive and specific for MPO that is suitable for fluorescence imaging applications.
Materials and Methods
We incubated the MPO activatable biotinylated sensor (MABS) with human MPO and two other human peroxidases (LPO and EPO) to determine specificity. To induce bacterial cerebritis, three female C57BL/6J (wildtype) mice and three MPO-knockout (KO) mice were injected stereotactically with salmonella or saline in the right or left cerebral hemispheres, respectively. 23 hours after induction, mice were injected with MABS. Brains were harvested and imaged with a fluorescence reflectance imaging system followed by immunohistochemistry for MPO protein.
Results
MABS contains 5-hydroxytyptamide moieties that can be activated by MPO, and a biotin moiety for detection with fluorochrome-tagged streptavidin (figure, A). Upon oxidation by MPO, but not other peroxidases (EPO and LPO), MABS binds to proteins and forms probe-protein oligomers ($p<0.01$, one-way ANOVA, figure, B). In wildtype mice but not MPO-KO mice with bacterial cerebritis, increased

fluorescent signal was seen in the right but not in the left hemisphere ($p<0.001$, student t-test, figure, C). Immunofluorescence demonstrated MPO activity and protein within the region of cerebritis but not in the left hemisphere. Interestingly, in regions close to the cerebritis, MPO protein without MPO activity was detected. Neither MPO activity nor MPO protein were detected in the brains of MPO-KO mice (figure, D).

Conclusions

MABS specifically detects MPO activity and reports active inflammation in bacterial cerebritis. MPO activity does not always co-localize with MPO protein, revealing that not all MPO protein is enzymatically active in vivo and underscoring the importance of monitoring enzymatic activity. Upon translation, this technology can be used in neurosurgical and catheter-based applications to detect oxidative stress and inflammation in patients.

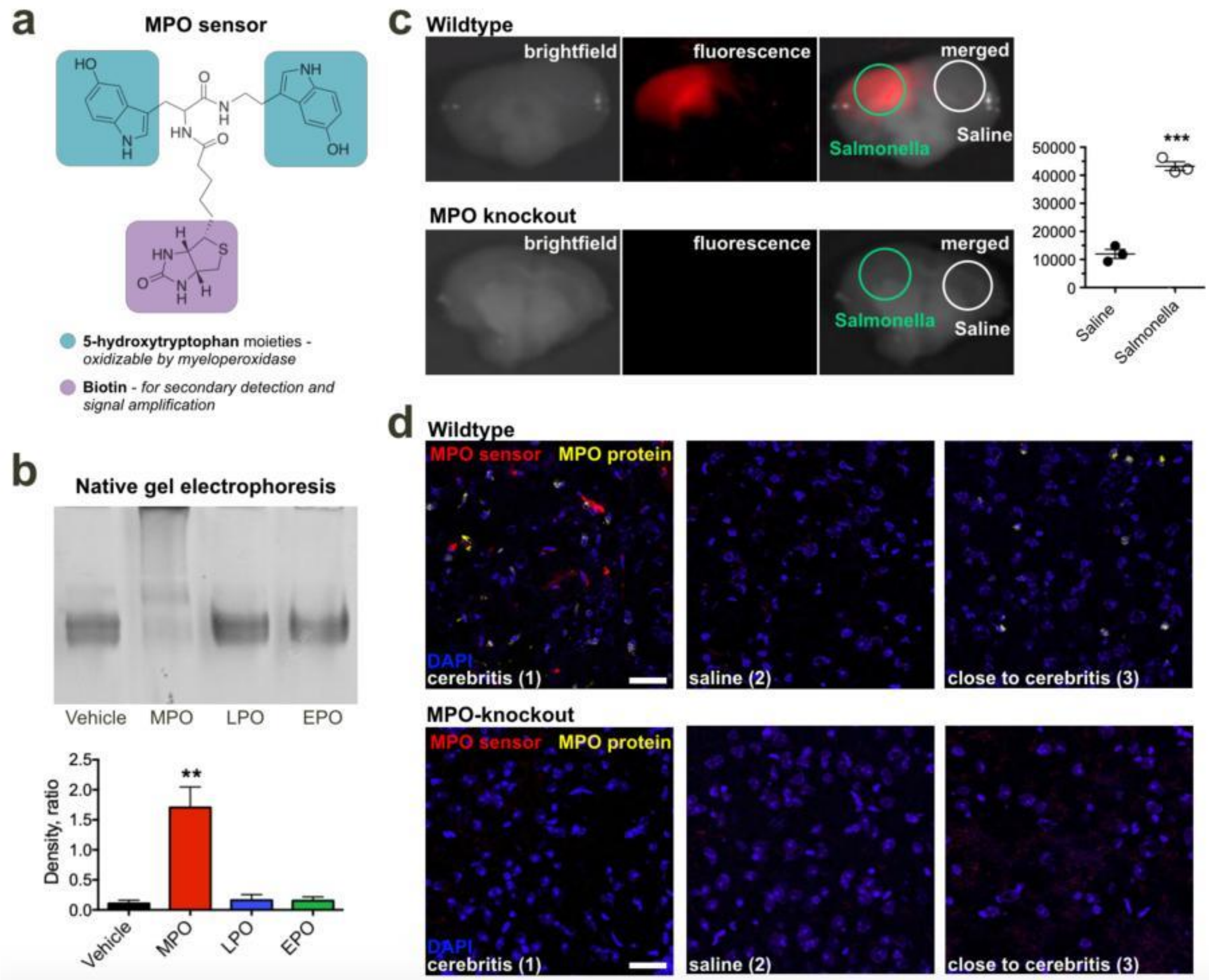

(Filename: TCT_2957_ASNR_figure.jpg)

2440

11:24AM - 11:30AM

Measurement of ADC Values to Differentiate Tumefactive Active Demyelinating Lesions from Primary CNS Lymphoma and Glioblastoma.

R Guillory[1], F Kebbel[2], P Rabiei[3], R Riascos[3], J Zhu[3], Y Esquenazi[3], R Patel[3], A Kamali[4]

[1]*University of Texas at Houston, Houston, TX,* [2]*McGovern Medical School, University of Texas Health Sciences Center at Houston, Houston, TX,* [3]*The University of Texas Health Science Center at Houston, Houston, TX,* [4]*UT HEALTH, HOUSTON, TX*

Purpose
Clinical management of patients with active demyelinating disease is much different from patients with primary CNS lymphoma or Glioblastoma. Our purpose was to evaluate whether tumefactive active demyelinating lesions could be distinguished from primary CNS lymphoma and from Glioblastoma using ADC values measured from the PACS workstation.
Materials and Methods
We retrospectively identified 30 patients from our institution with tumefactive active demyelinating lesions demonstrating restricted diffusion on MRI. Within the areas of active demyelination, the minimum ADC and average ADC values were measured from the PACS workstation. Comparative statistical analysis was performed comparing these values to the ADC values obtained from 30 cases of primary CNS lymphoma and 42 cases of Glioblastoma.
Results
Our results show that there was a statistically significant difference between the ADC values of tumefactive active demyelinating lesions and Glioblastoma (The ADC values of the demyelinating lesions are significantly lower than Glioblastoma; $p<0.001$) and between lymphoma and Glioblastoma (The ADC values of the lymphoma are significantly lower than Glioblastoma; $p<0.001$). There was no statistically significant difference between the ADC values of tumefactive active demyelinating lesions and lymphoma (minimum ADC $p=0.21$; average ADC $p=0.099$).
Conclusions
Our findings suggest that it is possible to use ADC values measured from the PACS workstation to differentiate tumefactive active demyelinating lesions from Glioblastoma and to differentiate lymphoma from Glioblastoma in the brain. However, we were not able to distinguish active demyelinating lesions from lymphoma with statistical significance using ADC values.

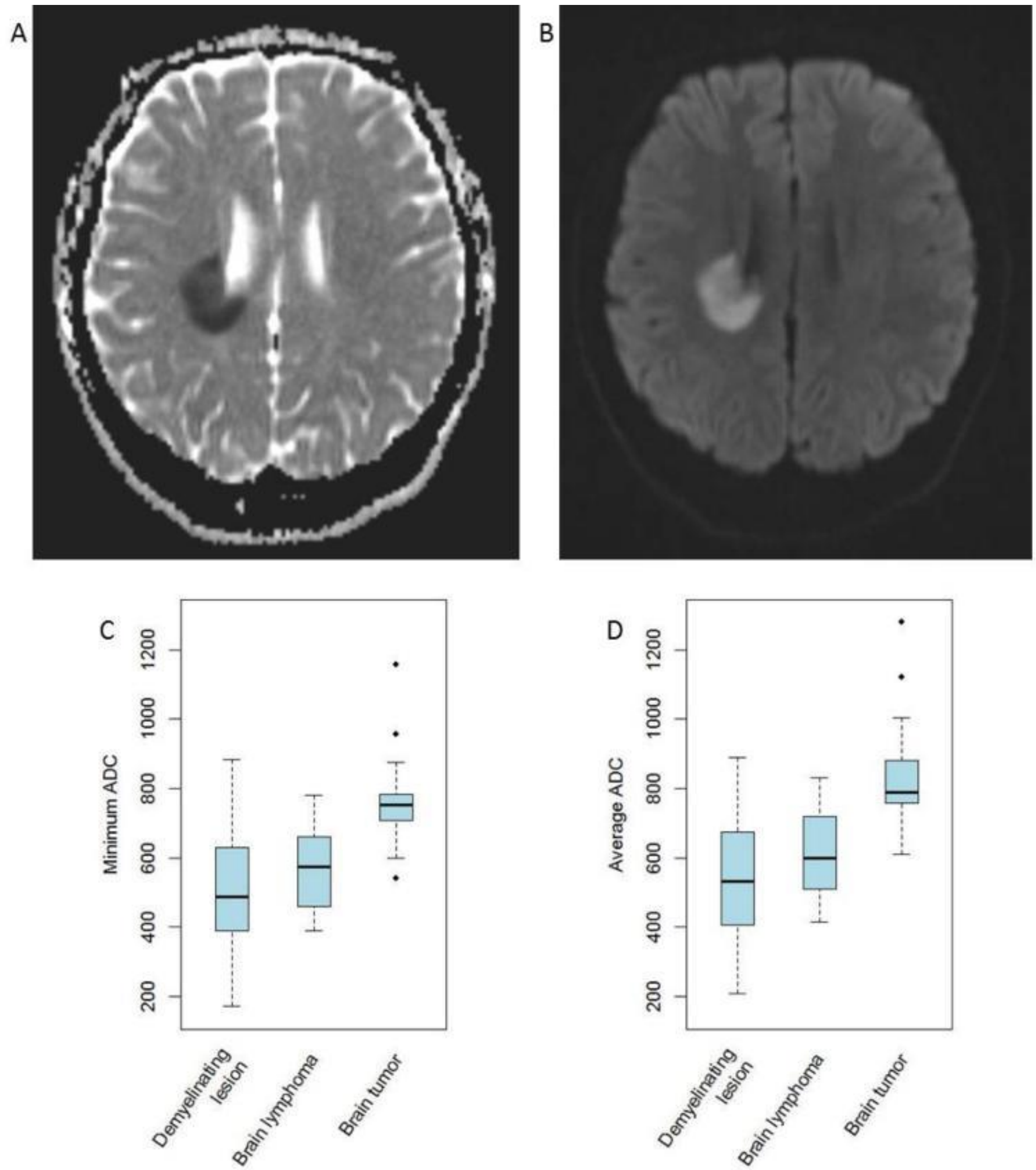

ADC map (A) and DWI (B) demonstrating restricted diffusion in an active demyelinating lesion. Minimum ADC values (C) and average ADC values (D) found in demyelinating lesions, CNS lymphoma and Glioblastomas.

(Filename: TCT_2440_ADCgraphicfile.jpg)

2364

11:30AM - 11:36AM

Temporal Evolution of DWI and Gadolinium Enhancement in Balo's Variant of Multiple Sclerosis suggests a Cytotoxic Oligodendrocytopathy preceding Blood Brain Barrier Breakdown in Acute Demyelination

P Morris[1], W Tobin[1], C Lucchinetti[1], Y Guo[1], N Zalewski[1], E Jolliffe[2], A Raghunathan[1]

[1]*Mayo Clinic, Rochester, MN,* [2]*Wellington Regional Hospital, Wellington, MN*

Purpose
Balo's Sclerosis is an uncommon variant of multiple sclerosis (MS) characterized by concentric ring formation on various MRI sequences. The clinical course is variable, but the atypical clinical and imaging features at presentation mean that this group of patients is more likely than typical MS patients to undergo repeated MRI examinations and even biopsy during the initial acute period. This paper takes advantage of the repeated imaging performed during the acute phase of illness in a group of patients with Balo or Balo-like imaging findings to analyze the temporal evolution of the MR imaging features of evolving demyelination.
Materials and Methods
A retrospective review was performed of clinical and imaging data in 41 patients with changes of Balo's concentric sclerosis (2+ bands on T2 imaging) or Balo-like changes (2+ bands on other sequences). Date of recorded onset of symptoms was tabulated. Sequential MRIs following that date were evaluated and analyzed for evolution of imaging characteristics. CT images in the acute phase, when available, were also reviewed. Axial cross-sectional area measurements were performed on DWI, ADC, FLAIR, T2 and Axial post-gadolinium T1 images for the dominant or index lesion in each patient and followed over time. Post-biopsy images were omitted from the analysis. The relative size and its change over time of the area of diffusion-restriction, T2 signal, and T1 enhancement were evaluated using a linear fit model.
Results
Sequential MRI examinations in the acute phase of illness were available in 27 adult patients (F/M 16/11, mean age 44y). Long term clinical status was documented in 20, with 7 lost to follow-up. Among the documented patients 13 ultimately met the McDonald Criteria for diagnosis of relapsing remitting multiple sclerosis. One further patient died during initial presentation. The MRI examinations demonstrated a consistent pattern of changes whereby lesion prominence varied over time depending on the MR sequence. Most prominently, DWI, T2 dark bands, and gadolinium T1 images fluctuated out of phase with one another. A pattern of circumferential, centrifugal, band-like propagation of lesion size was seen characterized by initial restriction of diffusion, followed by later development of gadolinium enhancement as the DWI images faded, or as the DWI restricting zone migrated peripherally. T2 changes also evolved from initial subtle elevation of signal, intermediate formation of T2 dark bands, later central uniformly bright signal and ultimately prominent regression of lesion size. Statistical correlation of relative size of the lesion on DWI and T1Gd+ demonstrated a correlation with time (F Ratio 0.94, $p < 0.02$) Non-contrast CT images were available in 15 patients during acute presentation. With 2 exceptions, these lesions were exclusively hypodense throughout.
Conclusions
Compromise of the blood-brain barrier in MS is generally thought to be a prerequisite for the "outside in" model of disease. It is likely that evidence of Gadolinium enhancement on T1 weighted imaging correlates with blood-brain barrier breakdown. In this study, imaging findings on DWI are prominent in areas of active demyelination, often occurring before the appearance of T2 hypointensity and gadolinium enhancement suggesting that the inciting event occurs prior to the breakdown of the blood-brain barrier. The temporal evolution of DWI restriction following later by T1 gadolinium enhancement seen in this study is also seen in other types acute CNS injuries including hypoxic and metabolic injuries. These findings point, therefore, to a pivotal cytotoxic event preceding blood-brain barrier breakdown, as the initial trigger of demyelination

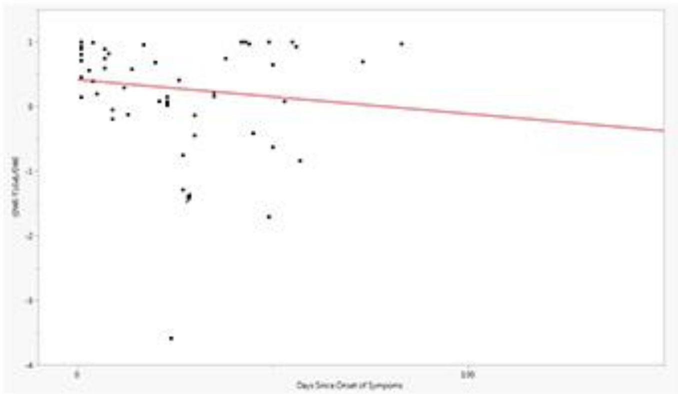

Correlation of lesion size on DWI and T1Gad+
over time in days

(Filename: TCT_2364_ASNR2019ppmFigure1.jpg)

2550

11:42AM - 11:48AM

Tumefactive Primary Central Nervous System Vasculitis: MRI Findings of a Rare and Underrecognized Neuroinflammatory Disease

S SUTHIPHOSUWAN[1], A Bharatha[1], C Hsu[2], A Lin[1], D Munoz[1], A Osborn[3]
[1]St. Michael's hospital, University of Toronto, Toronto, ON, Canada, [2]Gold Coast University Hospital, Queensland, Australia, [3]University of Utah, Salt Lake City, UT, USA

Purpose
Primary central nervous system vasculitis(PCNSV) can rarely be "tumefactive" mimicking a brain neoplasm.(1-3) This is an underrecognized entity(2, 3) especially in the radiology literature. In this study, we present a case series of biopsy proven tumefactive PCNSV with analysis of the neuroimaging findings.
Materials and Methods
A collaborative retrospective case series was conducted between two tertiary institutions. Eight patients(5 males, 3 females; mean age 49 years) with biopsy proven PCNSV. Conventional MRI, CT angiogram(CTA) or MR angiogram(MRA), and when available MR perfusion were reviewed. Clinical findings and histopathology findings were also documented.
Results
Tumefactive PCNSV typically present as single intra-axial mass(5/8;63%) and less commonly as multifocal lesions(3/8;37%). Variable parenchymal enhancement patterns were observed: small nodular or ring enhancement(4/8;50%), mixed linear/perivascular enhancement(2/8;25%), and large irregular heterogeneous enhancement(2/8;25%). Leptomeningeal enhancement was found in 2 cases(2/8;25%),

while ependymal enhancement were seen in 3 cases(3/8;37%). In the majority of cases, the lesions involved cortex and subcortical white matter(6/8;75%). 3 cases(3/8;37%) had deep and periventricular white matter involvement. Involvement of basal ganglia were found in 3 cases(3/8;37%). Only one case(1/8;13%) had brain stem involvement. Petechial hemorrhages were present in 5 of 8 cases (63%). Only one case showed diffusion restriction(1/8;13%). MR perfusion was performed in three cases, which showed a low relative cerebral blood volume(rCBV). No abnormality of the large or medium-sized intracranial arteries were detected on either the CTA or MRA(6/6;100%).

Conclusions

Tumefactive PCNSV can have myriad radiologic appearance with all cases showing variable enhancement patterns. Specifically, when MRI shows unusual tumor-like, cortical-subcortical lesions with petechial hemorrhages, but no diffusion restriction or high rCBV, tumefactive PCNSV should be included in the differential diagnosis. Normal morphology of the large or medium size vessel on imaging should not be used as exclusion for tumefactive PCNSV.

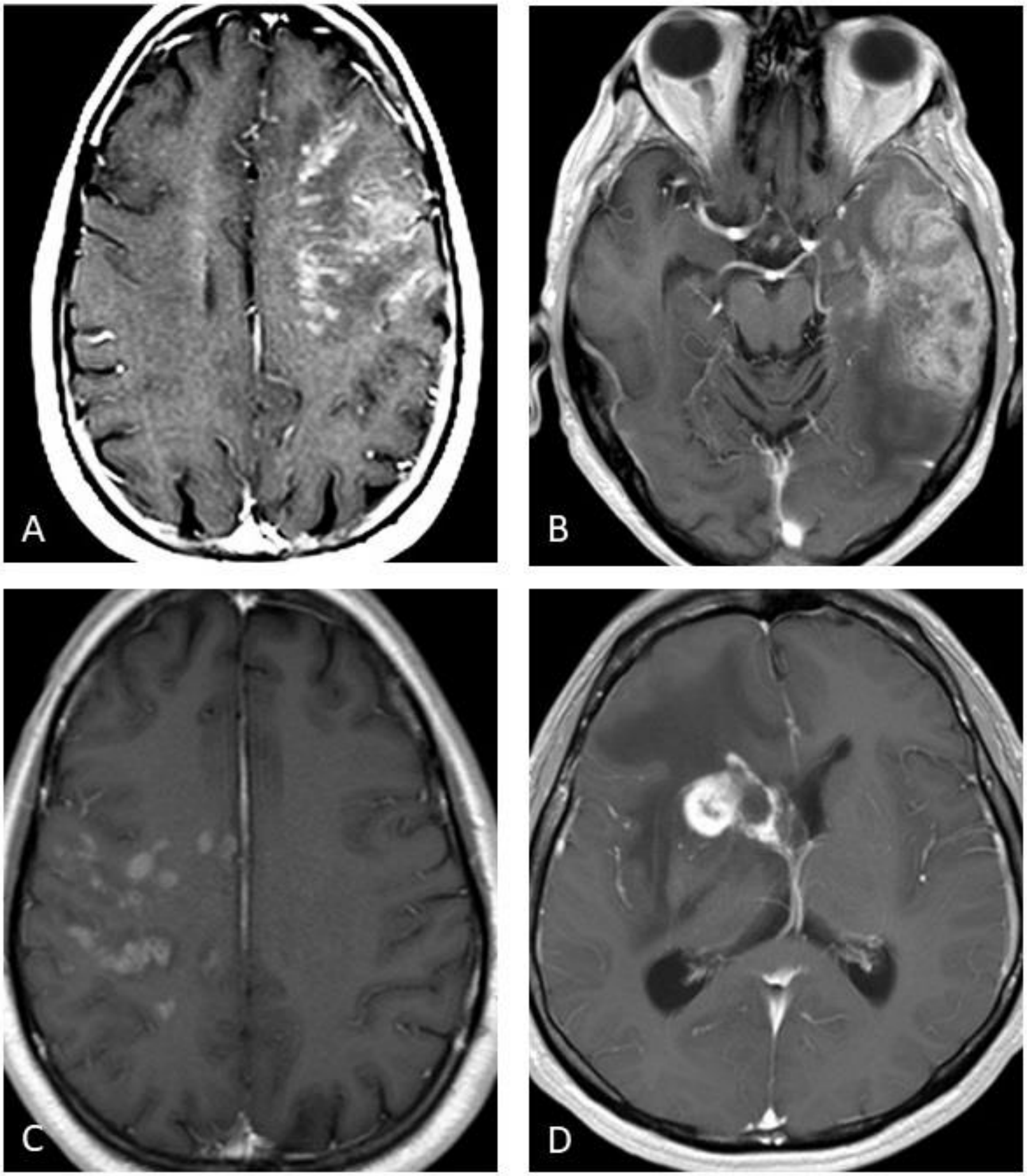

(Filename: TCT_2550_imageforasnrabstract.jpg)

Monday, May 20, 2019
11:00AM - 12:00PM
Practice & Training Issues

2368

11:07AM - 11:14AM

Accuracy of On-call Residents Interpretation of Spinal Cord and Cauda Equina Compression

C Huang[1], A Ali[1], Y Chang[1], A Bezuidenhout[1], R Rojas[1], R Bhadelia[1]
[1]Beth Israel Deaconess Medical Center, Boston, MA

Purpose
Acute neurological deficits due to suspected spinal cord compression (SCC) and cauda equine compression (CEC) may require immediate clinical management (1). Therefore, accurate on-call interpretation of imaging studies is essential. Our purpose was to assess the accuracy of on-call radiology residents' interpretation of emergent total spine MRI scans performed for SCC/CEC.
Materials and Methods
We reviewed consecutive after hour total spine MRI cases performed over one-year period by the emergency room at our institution for SCC/CEC. Results of preliminary readings by residents and final readings by faculty were compared to determine agreements/disagreements for SCC/CEC and presence of other significant findings-OSF (intramedullary spinal cord lesion, trauma-related findings, hematoma, and infection/tumor) that may impact clinical management. The results were classified as true positive (TP), true negative (TN), false positive (FP), false negative (FN) to determine the sensitivity, specificity and accuracy of preliminary reads by on-call residents for SCC/CEC and OSF.
Results
There were 189 studies which had preliminary reads done by 2nd- 4th year residents. 48/189 had SCC/CEC according to the final reads with TP=45, TN=138, FP=3 and FN=3. The sensitivity, specificity and accuracy of resident preliminary reads for SCC/CEC were 93.8 %, 97.9% and 96.8% respectively. All 3 FN cases belonged to 2nd year residents. Sensitivity of preliminary reads increased with years of training and was 100% for 3-4 year residents. 41/189 had OSF with TP=38, TN=148, FP=0 and FN=3. The sensitivity, specificity and accuracy of resident preliminary reads for OSF were 92.7 %, 100% and 98.4% respectively. No effect of level of training was seen in detecting OSF.
Conclusions
Overall accuracy of on-call residents' interpretation of total spine MRI was high and sensitivity of SCC/CEC detection improved with level of training. However, the sensitivity of 2nd year residents for diagnosing SCC/CEC was relatively low. Focused training of 2nd year residents for SCC/CEC may help reduce inaccuracies.

2906

11:14AM - 11:21AM

An Economic Implication: Variation in Brain MRI Interpretation Time Based on Practice Setting

R Mattay[1], M Salehi Sadaghiani[2], D Leake[3], R Bryan[3], S Mohan[1]
[1]Perelman School of Medicine at the University of Pennsylvania, Philadelphia, PA, [2]UHS Hospitals, Johnson City, NY, [3]University of Texas at Austin Dell Medical School, Austin, TX

Purpose
With the ever-increasing availability of imaging modalities and the number of MRI scans being performed (1), along with the steadily declining reimbursements for imaging procedures (2), there is an increasing pressure on radiologists to read more with major economic implications. It is therefore imperative to determine all the tasks radiologists perform and understand the variation in timing based on practice setting.
Materials and Methods
This observational study tracked attending radiologists interpreting brain MRIs in three settings: a private practice, a tertiary care academic institution where scans were read independently, and the same academic institution where drafts were created by trainees. Data was gathered from a total of 14 radiologists

interpreting 352 brain MRIs. We measured the total time taken from opening each scan to report signing, and for each of the 5 activities performed during this period: image viewing, obtaining clinical data, report transcription, education of trainees and/or clinicians, and 'other'.
Results
The average time taken to interpret a Brain MRI was 8.66 minutes +/- 6.88 minutes. There was no statistical difference between academic attendings reading independently or over-reading drafts by a trainee (10.03 +/- 5.49 min vs. 10.85 +/- 8.82 min; p=0.3). However, there was a statistically significant difference between attendings reading in either academic setting when compared to attendings in private practice (4.29 +/- 2.18 min, P<.0001).
Conclusions
The variation in total time taken to interpret a brain MRI based on the practice setting is likely due to a variety of factors including case complexity mix, where academic cases likely included a higher preponderance of complex and uncommon/rare diagnoses. Additionally, there was a significant difference between the amount of education that was provided between the settings. These findings have implications on the economics of neuroradiology, and suggest that factors such as case-complexity and the time spent on trainee education could be factored into fee schedules, possibly mirroring similar reimbursement models of many clinical specialties.

Assignment	Observation	Transcription	Education	Clinical correlation	Total-Other
Academic-Independent (N=124)	4.76 +/- 2.82 min	3.68 +/- 2.33 min	0.18 +/- 0.84 min	1.93 +/- 2.10 min	10.03 +/- 5.49 min
Academic-Review of Trainee (N=124)	5.15 +/- 3.60 min	2.68 +/- 3.13 min	1.13 +/- 2.37 min	2.55 +/- 3.74 min	10.95 +/- 8.82 min
Private Practice (N=104)	2.15 +/- 0.83 min	1.39 +/- 1.27 min	0.00 +/- 0.00 min	0.56 +/- 0.67 min	4.29 +/- 2.18 min

(Filename: TCT_2906_Abstract_Timing_Figure300.jpg)

3044

11:21AM - 11:28AM

Critical Care Radiology Shift Simulation: A Neuroradiology Educational Assessment Tool

J Rees[1], R Slater[1], C Sistrom[1], R DeJesus[1], T Massini[1], A Mancuso[1]
[1]*UNIVERSITY OF FLORIDA COLLEGE OF MEDICINE, Gainesville, FL*

Purpose
Purpose: As radiology resident physicians advance in their training, they move from full supervision through graded levels of independent decision making situations. The ACGME has asked training programs for objective documentation of the adequacy of their training and preparation to begin independent imaging interpretation. In response to this mandate, the University of Florida Radiology Department has developed and implemented an objective assessment methodology, the Critical Care Radiology Shift Simulation (CCRS - aka SIMS) to assess each residents readiness to interpret, advise and provide action priorities of critical imaging studies. In this paper we will focus on the Neuroradiology component of this training and assessment program.
Materials and Methods
Materials and Methods: The Critical Care Radiology Shift (CCRS) Simulation experience takes approximately 8 hours and requires viewing of a full resolution set of DICOM images in the selected studies. Sixty-five cases across all radiology sub-specialties, with a range of difficulty including normal studies, constitute this 8 hour simulation experience. The participants are asked, in their own words, to determine whether the study is normal or abnormal and deliver their consultation in a short written response format. The CCRS Simulation embodies the required components of the consultative process

and the professional behavior objectives of understanding clinical context and properly communicating the acuity of the given clinical scenario. The cases provided were selected by sub-specialists in each discipline and were graded by sub-specialists following agreed upon standards and point systems designed to accurately reflect the depth of knowledge and accuracy displayed by the trainee.

Results

Results: The CCRS Simulation has now been delivered 7 times over the last 7 years at the UF Residency and also for residents at 46 other Radiology training programs. The results of four recent iterations (yrs. 2014-2017) of the CCRS Simulation, after it had undergone a testing and maturation period of 3 years, are the subject of this report. The program (and our analytic sample) grew steadily over the four years of study (2014-2017). Table 1 shows numbers of unique graders (N=15), programs (N=34), residents (N=538), cases (N=256), sessions (N=670), and scores (N=43,170) stratified by cycle year. Table 1. Counts of unique graders, programs, residents, cases, sessions, and analyzed scores by simulation session (year). (See Table 1) Neuroradiology cases were the most difficult to interpret correctly (P<0.0001) with effect size of 2.41 (95% CI 1.64-3.19) points lower than body and musculoskeletal cases. Multiple analyses by other investigators of resident-attending discrepancy reflect this trend with Neuroradiology overnight readings having significantly higher miss rates compared with other sub-specialties . Over these 4 testing cycles 57 of the 256 cases were in the Neuroradiology domain. The general distribution of these cases were approximately 50% brain, 25% spine and 25% ENT. 5 normal studies were included in the total. Out of 10 possible points awarded for each case scores of under 4 were considered failing and potentially significantly harmful to patients according to this grading scheme. 28 out of the 57 Neuroradiology domain questions had minimum average scores of under 4. In some specific clinical scenarios, the rate of potentially harmful was 95% of the participants, and, in aggregate these 28/57 cases were missed by about 90% of participants in each unique instance. The primary cause of error was observational, in 80% or more cases.

Conclusions

Conclusions: The CCRS (nicknamed SIMS) has become an integral part of the UF Neuroradiology resident training and preparation, in conjunction with the more traditional case based attending resident teaching activities which occur every day, and it has become a valued component of Radiology Resident assessment at 46 other Radiology Residency programs as of 2018. The SIMS testing provides us direct objective feedback on the fitness of each resident to proceed in their training, and also identifies specific shortcomings which must be addressed. Through its use, we have discovered educational gaps in Neuroradiology training which can be alleviated by focused educational methodology especially with regard to observational discipline, and also to a lesser extent arising from incorrect interpretation of correctly observed findings.

simulation cycle	unique graders	unique programs	unique residents	unique cases	unique sessions	resident scores
2014	2	9	103	65	103	6,674
2015	4	16	127	65	127	8,202
2016	10	25	197	65	197	12,671
2017	11	29	243	65	243	15,623
Total*	**15**	**34**	**538**	**256**	**670**	**43,170**

*Note: Totals are for unique (distinct) counts and will less than the column sums except for unique sessions and scores.

(Filename: TCT_3044_Table1-SIMSSessions.JPG)

2983

11:28AM - 11:35AM

Effectiveness of Prophylactic Strategies in Preventing Acute Allergic-Like Reactions to Gadolinium-Based Contrast Agents in Patients with a History of Reaction

J Mcdonald[1], A Kolbe[2], R Hartman[2], D Kallmes[2], R Mcdonald[1]
[1]*MAYO CLINIC - ROCHESTER, MN, ROCHESTER, MN*, [2]*Mayo Clinic, Rochester, MN*

Purpose
To examine and compare prophylactic strategies for avoiding repeat acute allergic-like reactions to gadolinium-based contrast agents (GBCAs) in patients with a history of reaction.
Materials and Methods
All patients with a prior allergic-like reaction to a GBCA that received intravenous GBCA for a subsequent magnetic resonance (MR) exam at our institution from June, 2009 to May, 2017 were identified. Prior reaction details, including the specific GBCA that caused the reaction, symptoms of the reaction, and severity of the reaction (American College of Radiology criteria of mild, moderate, and severe) were retrieved from the medical record. Prophylactic premedication administered prior to the subsequent MR exam and any allergic-like acute reactions that occurred at the time of the subsequent MR exam were retrieved. The effectiveness of various prophylactic strategies was compared.
Results
: A total of 191 patients were identified who received a total of 448 subsequent MR exams. Patients were premedicated for approximately half of the exams (n=206, 46%), most commonly premedicated with methylprednisolone at 12 and 2 hours prior to exam (n=105, 51%), with smaller subsets of patients also premedicated with diphenhydramine within 2 hours prior to exam (n=53, 26%) or diphenhydramine alone within 2 hours prior to exam (n=47, 23%). A total of 38 subsequent allergic-like reactions (8.4% of exams) in 36 patients (18% of patients) occurred. Reaction rates from lowest to highest were observed with exams where: a different GBCA was used and the patient was not premedicated (2/149, 1.3%), a different GBCA was used and the patient was premedicated (6/95, 6.3%), the same GBCA was used and the patient was not premedicated (11/77, 14%), and the same GBCA was used and the patient was premedicated (16/67, 24%). Exams where the patient was premedicated had significantly higher repeat reaction rates than exams where premedication was not administered (25/204, 12% vs. 13/244, 5.3%, p=.0088). Switching to a different GBCA was associated with a significantly lower rate of repeat reactions than using the same GBCA (also premedicated: p=.0003; not also premedicated: p<.0001).
Conclusions
Only a small percentage of patients with a history of acute allergic-like reaction to GBCAs had a repeat reaction. Switching GBCAs is significantly more effective at preventing repeat reactions than premedication.

2921

11:35AM - 11:42AM

Out with the Old and in with the New: Streamlining, Modernizing and Automating Radiology Scheduling in a Large Academic Medical Center

M Keiper[1], S Osborn[2], J Pelz[1]
[1]*UNIVERSITY OF NEBRASKA MEDICAL CENTER, OMAHA, NE*, [2]*University of Nebraska Medical Center, Omaha, NE*

Purpose
To determine the feasibility of workforce manipulation and streamlining radiology scheduling workflow in order to improve call center metrics and customer service in a large academic medical center.
Materials and Methods
Baseline call center metrics with emphasis on abandoned call rate (AR) and percent of calls answered in 30 seconds or less (TSF) were established over a 6-month period. After baseline call center metrics were obtained, two specific interventions were instituted. The first and more urgent initiative entailed replacing highly paid call center nurses with less expensive call center staff in a 2.5:1 ratio while maintaining

budget neutrality. The second and subsequent initiative entailed rewriting and streamlining scheduling workflow, scheduling guidelines and scheduling requirements. The streamlining process was performed with the goal of reducing the steps to schedule a radiology exam in order to completely automate the scheduling process. After streamlining the live scheduling process, the scheduling platform was automated. Call center parameters were measured actively both during and after the interventions were completed.

Results

Baseline call center metrics demonstrated a mean AR of 6.2% (4.2-8.1%) and mean TSF service indicator of 58% (42-73%). A portion of the call center nursing staff was successfully replaced by lower paid employees consisting primarily of medical assistants and former radiology technologists. The overall call center workforce increased in absolute size by 32%. The scheduling process was also successfully streamlined by significantly decreasing scheduling guidelines from 457 initial guidelines to less than 50. Patient preparation guidelines and questionnaires were also similarly reduced and consolidated. After instituting these changes and reducing the absolute requirements for live scheduling by employees, the entire process was successfully automated in the electronic health record by IT personnel. The call center metrics improved to a mean AR of 4.7% (2.7-5.1) and mean TSF of 69% (57-78%) after partially replacing the call center nursing staff personnel. After completely automating the process, the metrics improved to a mean AR of 2.7% (1.9-3.7) and mean TSF of 82% (74-91%).

Conclusions

Workforce manipulation as well as streamlining and automating the radiology scheduling process in a large academic medical center is possible and may lead to marked improvement in call center metrics, customer service and, potentially, radiology imaging volumes and revenues. The automation of the process may also lead to additional downstream benefits such as automated on line scheduling, improved patient satisfaction, and decreasing scheduling costs.

2257

11:42AM - 11:49AM

Productivity Data of First-Year Neuroradiology Fellows at a Large Academic Institution

J Masur[1], S Mohan[2], J Schmitt[2], L Bagley[2], A Nayate[3]
[1]Hospital of the University of Pennsylvania, Philadelphia, PA, [2]University of Pennsylvania, Philadelphia, PA, [3]University Hospitals Cleveland Medical Center, Cleveland, OH

Purpose

ACGME has established guidelines for trainees to gain minimum proficiency during Neuroradiology fellowship. However, there is no published data on the trends or expectations for the number of studies Neuroradiology fellows should interpret during fellowship. The purpose of this study was to evaluate the productivity of first-year Neuroradiology fellows at our academic institution during recent years and propose baseline trends in Neuroradiology subspecialty training.

Materials and Methods

We retrospectively determined the number of Neuroradiology studies (CT/CTA and MRI/MRA) dictated by each first-year fellow from 2012-13 through 2016-2017. We determined if the study was dictated during a regular weekday or while the fellow was on independent evening call. The total number of studies read by each fellow year both on clinical service and on call were compared with ANOVA. The number of studies read monthly by each fellow were evaluated with linear regression to evaluate for trends in productivity throughout the year.

Results

Data were analyzed for a total of 33 fellows. There was a statistically significant upward trend in the number of studies interpreted during subsequent academic years ($F(6,42) = 68.2$, $p<0.0001$) (Figure 1). The number of cases read on call by each fellow was statistically significantly higher than studies read during normal clinical service ($F(4,27)=89.1$, p-value < 0.0001). We found a small but statistically

significant increase in average monthly read volume over the fellowship year (beta 8.3, F=35.52 (1,10 df) p = 0.0001).
Conclusions
Our results demonstrate a positive correlation between the number of studies dictated by fellows while on independent evening call, with a significant upward trend in more recent years. We found a small but statistically significant upward trend throughout the year in productivity for each fellow. Our findings can be utilized by Neuroradiology fellowship programs to evaluate the progress of Neuroradiology fellows during an academic year.

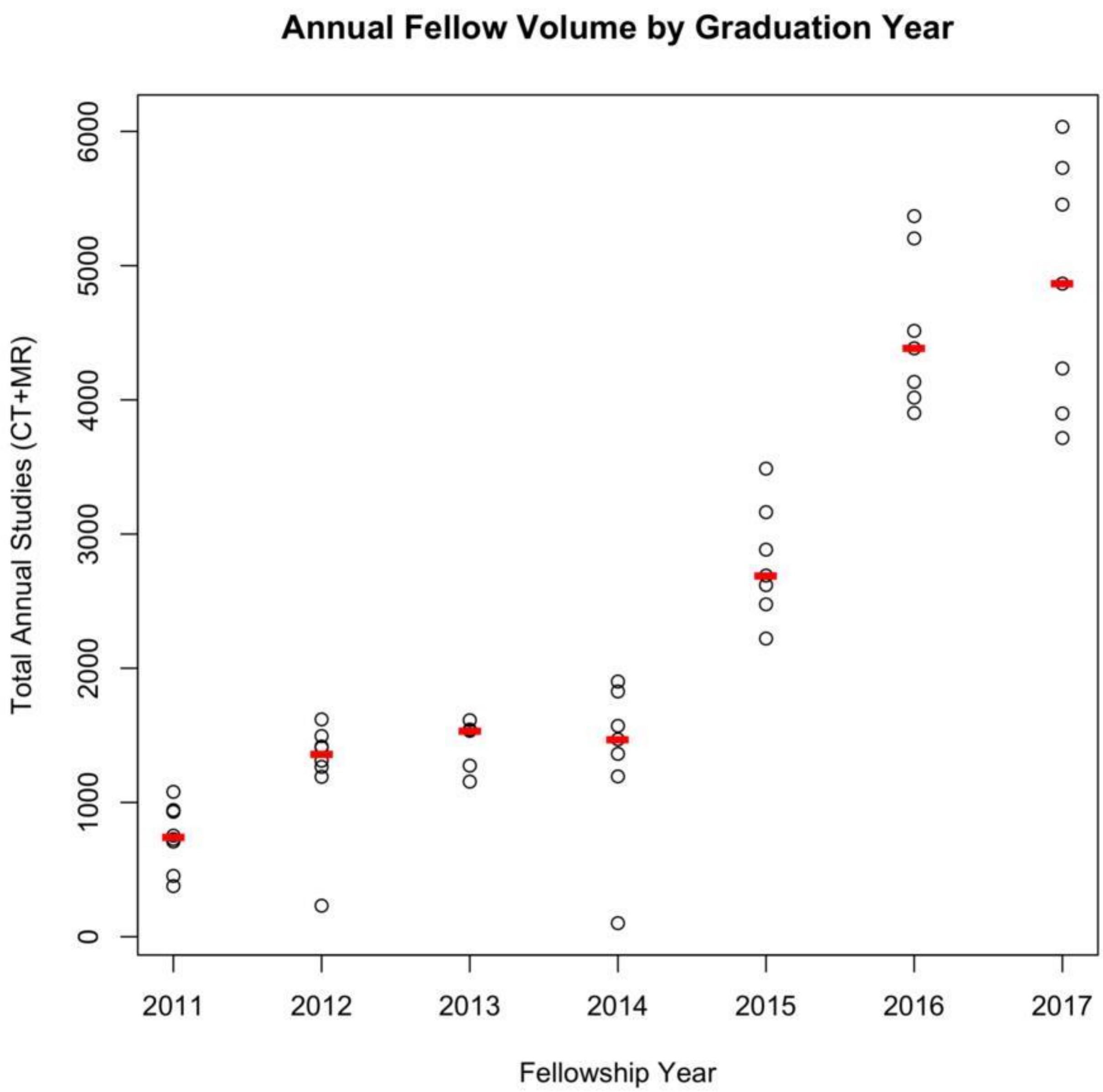

(Filename: TCT_2257_FellowsAnnual.jpg)

3004

11:49AM - 11:56AM

What are Neuroradiology Ordering Practices from the Emergency Department at an Academic Tertiary Referral Center

R Griesbach[1], R Bruce[1], J YU[1]
[1]*University of Wisconsin School of Medicine and Public Health, Madison, WI*

Purpose
The ordering practices of neuroradiology imaging is important for appropriate resource allotment by the radiology department, and to assess the variability in applying best practice imaging recommendations. Our purpose was to assess whether there is variability in the usage of resource intensive neuroradiology imaging studies between ordering providers in the emergency care setting.
Materials and Methods
This HIPPA compliant study was granted an Institutional Review Board exemption as a quality improvement initiative. All CT and MR examinations ordered from the emergency department between 7/1/2015 and 9/30/2018 were collected. For these exams, the neuroradiology and non-neuroradiology studies for each provider were cataloged. Providers who had ordered at least 200 total exams were selected. For these providers, the ordered neuroradiology studies were reviewed and the resource intensive exams; CT angiography head and neck with perfusion, MR "Stroke Deluxe" (MRI head with and without contrast, MRA neck with and without contrast, MRA head without contrast), and MRI Total Spine were tabulated by provider.
Results
A total of 48 ordering providers were included in the study. The average provider ordered a total of 1966 (SD = 1255) CT and MR scans during the selected period (Figure A). Neuroradiology exams accounted for an average of 55.78% (SD = 2.56%) of these scans (Figures B and C). Resource intensive neuroradiology imaging studies accounted for an average of 6.71% (SD = 2.37%) of the average provider's ordered neuroradiology scans (Figure D). 6 of the 48 ordering providers (12.5%) were statistical outliers (1.5 standard deviations above or below the 3rd or 1st quartile, respectively) based how many resource intensive neuroradiology imaging studies they ordered.
Conclusions
The providers in the emergency department at an academic tertiary care center have large variability in the ordering of resource intensive neuroradiology imaging studies. High variability in ordering practices can create resource allocation challenges for the radiology department and highlights pragmatic and policy challenges in applying best practice imaging recommendations in a high utilization setting.

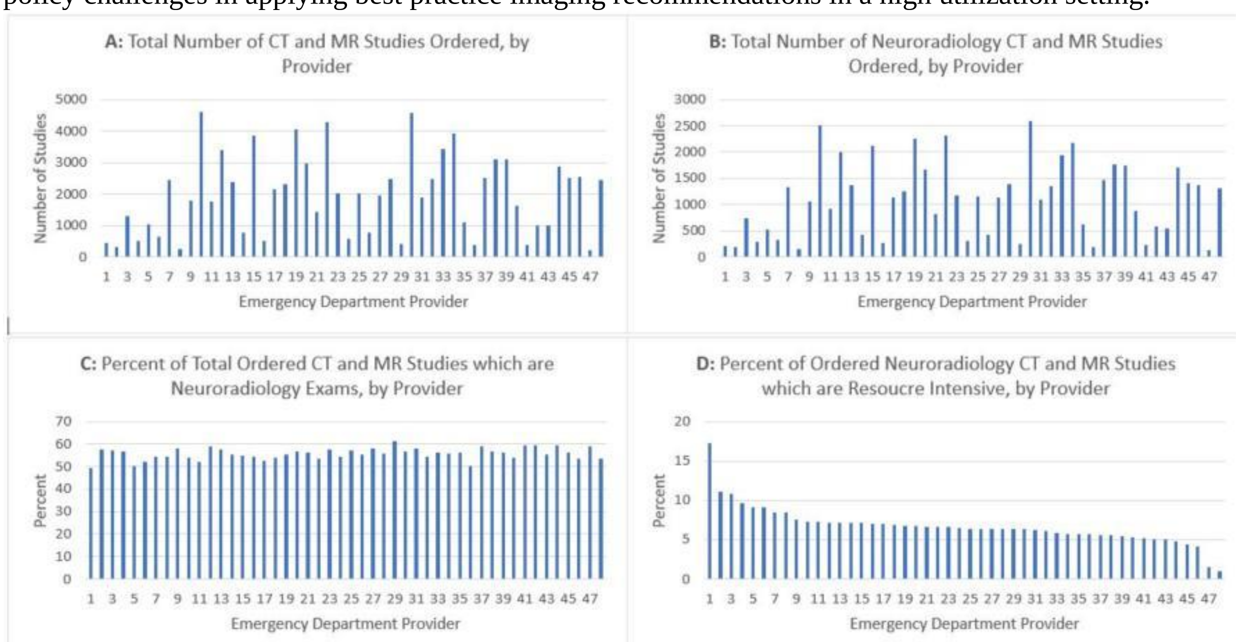

(Filename: TCT_3004_EDNeuroradiologyGraphs.JPG)

Monday, May 20, 2019
1:00PM - 2:30PM
Adult Brain Potpourri Topics 1

2321

1:00PM - 1:07PM

A Case Report on Intracranial Metastasizing Pleomorphic Adenoma from Parotid Gland

Y Ota[1], J Tazoe[1], K Yamada[1], m Yasuike[1], K Aita[1], K Akazawa[1]
[1]*Kyoto Prefectural University of Medicine, Kyoto, Japan*

Purpose
To present the imaging characteristics of intracranial metastasizing pleomorphic adenoma from parotid gland and to perform literature review of cases reported in English journals
Materials and Methods
A 70-year-old woman presented with right sided weakness and gradual development of hemiplegia. Her cognitive function declined along the time course. At this admission, all blood tests were within normal limit. On physical examination, she showed right facial palsy and right hemiplegia. She received left parotidectomy for a pleomorphic adenoma 37 years ago. In this admission, multiple imaging examinations of brain (non-contrast CT, non-contrast MRI, contrast MRI, FDG PET/CT, Angiogram) were performed. All imaging showed an extra-axial tumor at her left parietal-occipital region. Under the imaging diagnosis of meningioma, the tumor was removed surgically. Pathologically, it turned out to be a pleomorphic adenoma and the diagnosis of metastasizing pleomorphic adenoma was made accordingly. There is no consensus in previous reports about imaging findings of metastasizing pleomorphic adenoma. Moreover, the metastases are found more frequently in bone, lymph nodes, lung and liver.
Results
CT showed a heterogenous tumor with multiple small high-density nodules suggesting calcification or hemorrhage at left parieto-occipital region. The tumor presented with perifocal edema and mass effects, which caused midline shift towards the right. On MR, the tumor showed multinodular shape, heterogenous hyper-intensity on T2WI and hypo-intensity on T1WI, and homogenous enhancement on Gd-T1WI. The tumor showed no diffusion restriction. On SWI, low-intensity inside the tumor suggesting hemorrhage was depicted. FDG-PET showed low uptakes. Angiography showed increased vascularity with blood supply from left falx cerebral artery.
Conclusions
We experienced a rare case of metastasizing pleomorphic adenoma from parotid gland and it should be remembered that pleomorphic adenoma can metastasize to intracranial resion.

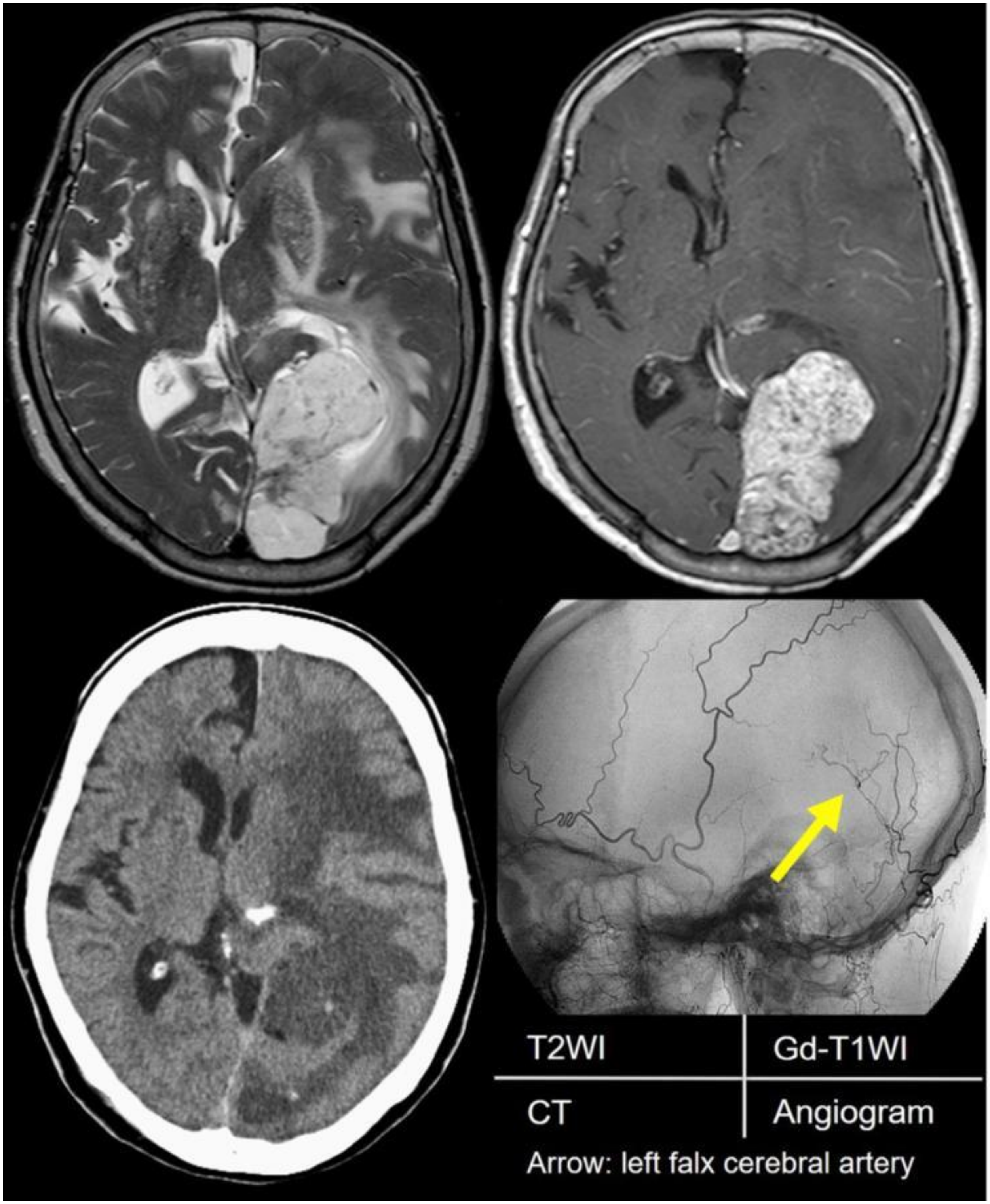

(Filename: TCT_2321_drota014.jpg)

3132

1:07PM - 1:14PM

Brain Tumor Reporting and Data Systems (BT-RADS): Novel Structured Template for More Reliable Reporting of Brain Tumors

J Zhang[1], B Weinberg[2], R Hu[1], A Saindane[1], M Mullins[3], J Allen[1], M Hoch[2]
[1]Emory University, Atlanta, GA, [2]Emory University Hospital, Atlanta, GA, [3]EMORY UNIVERSITY, ATLANTA, GA

Purpose

Structured reporting systems, such as those used for breast imaging and head and neck cancers, have provided a framework for more reliable and accurate image interpretation. We have developed and implemented an institution-wide reporting system, BT-RADS, in order to monitor the post-treatment progression of gliomas. The purpose of this study was to determine whether implementation of BT-RADS resulted in improvements in reporting parameters, including completeness, usage of "hedge" words, and consistent reiteration of relevant clinical history.

Materials and Methods

Complete past reports of gliomas of 6 experienced neuroradiologists from a large academic center were obtained from 2 months prior to implementation of BT-RADS (July-August 2017, n = 211) and 2 months after implementation of BT-RADS (July-August 2018, n = 172). Of the total cases, a similar proportion of cases were read by the 6 different neuroradiologists for both pre- and post-BT-RADS. Two sets of key words were identified: hedge words and history words, which were surrogates of consistent reporting. Hedge words convey ambiguity, such as: "somewhat," "possibly," and "likely". History words included 1) those related to medications, such as "Temozolomide" (including variants "Temodar" and "TMZ"), "Avastin," and "steroid" (including the variant "dexamethasone"), 2) those related to tumor mutations, such as "MGMT" and "IDH," and 3) those related to "radiation" treatment.

Results

Pre-BT-RADS reports demonstrated poor reporting of history words, including "Avastin" (7.1% of cases, n = 211), "Temozolomide" (18%), "IDH" (4.3%), and "MGMT" (10.9%). There was also inconsistent reporting of "radiation" history (40.3%). There was high usage of hedge words (60.7%), with the most commonly used being "likely" (49.8%). Implementation of BT-RADS resulted in significant increases in the proportion of cases for which there was reporting of history words, including "Avastin" (18.0%), "Temozolomide" (58.7%), "IDH" (19.2%), "MGMT" (31.4%), and "radiation" (95.9%). Furthermore, BT-RADS demonstrated significant reductions of hedge word usage (44.2%, n = 172), for instance "likely" (28.5%).

Conclusions

The implementation of BT-RADS has demonstrated tremendous promise in this initial period within a single large academic center. Specifically, BT-RADS has resulted in significant improvements in reporter consistency and reliability, including greater reproducibility in reporting key clinical history elements, especially medication and radiation history, as well as lesser reliance on hedge words that can introduce ambiguity and skepticism into the report. These initial compelling results support further deployment of BT-RADS across other medical centers and further expansion into other tumor types.

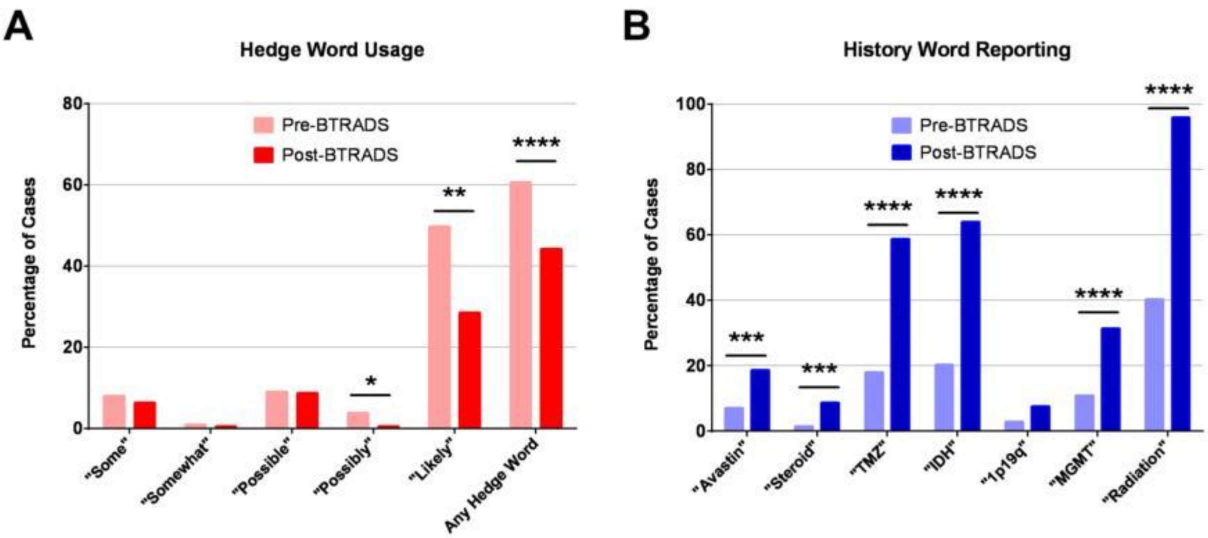

Figure 1. Language analysis of reports both before and after implementation of BT-RADS. A. Exported reports were evaluated for instances of hedge words, and cases containing individual or any hedge words were analyzed as a percentage of total cases. BT-RADS implementation resulted in significant decreases in overall hedge word usage, as well as specifically usage of "Possibly" and "Likely". **B.** Exported reports were evaluated for consistency of history reporting. BT-RADS implementation resulted in significantly greater reporting of 1) medication history markers "Avastin," "Steroid," and "TMZ;" 2) tumor mutation marker "IDH;" and 3) "Radiation."
*: p<0.05, **: p<0.01, ***: p<0.001, ****: p<0.0001, Fisher's exact test.

(Filename: TCT_3132_BTRADS-words_analysis-181105-abstractfinal_JWA.jpg)

2780

1:14PM - 1:21PM

Computed Tomography Perfusion Can Predict In-Hospital Mortality in Patients with Severe Traumatic Brain Injury at Hospital Presentation: A Pilot Study

J Shankar[1], K Virani[2], H Wong[3], K Eddy[3]
[1]University of Manitoba, Winnipeg, MB, Manitoba, [2]Dalhousie University, Halifax, Nova Scotia, [3]Dalhousie University, Halifax, Halifax, Nova Scotia

Purpose
The severity of TBI is commonly classified into mild, moderate, and severe categories using the Glasgow Coma Scale (GCS), with "severe TBI" defined as a GCS score ≤ 8. The maximum in-hospital mortality has been shown in the first 48 hrs of their admission and this time frame is also the most resource-intensive period for medical and surgical activity. Recognizing the limitations of traditional diagnostic imaging techniques in prognostication of patients with severe TBI, our research focuses on correlating computed tomography perfusion (CTP) parameters with in hospital mortality. The purpose of the proposed pilot study was first to assess feasibility and safety of CTP in the initial imaging protocol in severe TBI patients and to examine whether CTP features can help in prognostication. Hypothesis- CTP can determine brainstem death, when present, in patients with severe TBI at the time of their presentation.
Materials and Methods
The study was approved by institutional research ethics board (REB) with deferral of consent from the

next to kin within a week of CTP. A prospective cohort study was conducted from September 2017 to December 2018 and included patients with severe TBI (defined as a GCS score ≤ 8 before intubation). CTP was performed at the time of initial imaging work-up immediately after hospital arrival. CTP images were acquired but not processed and all patients received the standard of care clinical care as dictated by their injuries. CTP images were processed at the end of the study and assessed for presence of features of brainstem death. The CTP features were then compared with clinical outcome.

Results

A total 21 patients (Male-15, 71%; mean age-36, median age 27.5 yrs) were enrolled. Consent could be obtained from all except 1 for whom we got waiver of consent from REB. No complications were seen from CTP. Average hospital stay was 2 weeks. In the first 48 hours of admission, 4 patients (19%) died. CTP in severe TBI patients, done at the time of their first diagnostic imaging, is 75% sensitive, 100% specific with 100% PPV and 93.75% NPV for predicting in-hospital mortality.

Conclusions

Our pilot study confirmed the feasibility and safety of performing CTP in patients with severe TBI at their hospital presentation. CTP findings showed 75% sensitivity and very high specificity, PPV and NPV to predict in-hospital mortality.

3405

1:21PM - 1:28PM

Contrast Staining on Post-Thrombectomy Dual Energy CT in MTICI 2B and 3 Reperfusion Predicts Post-procedural Intracerebral Hemorrhage

D Byrne[1], J Walsh[2], F Settecase[3], M Heran[1], A Salmeen[1], B Rohr[2], T Field[1], A Rohr[4]
[1]Vancouver General Hospital, Vancouver, BC, [2]University of British Columbia, Vancouver, BC, [3]University of British Columbia, Vancouver, British Columbia, [4]Vancouver General Hospital and University of British Columbia Hospital, Vancouver, BC

Purpose

A good reperfusion result alone does not predict a patient's course immediately after thrombectomy. A better understanding of risk for post-procedural hemorrhage can inform antithrombotic strategy, monitoring needs and prognosis. We evaluated the frequency of immediate post-procedural contrast staining on DECT in patients who achieved good reperfusion and its relationship with intracerebral hemorrhage (ICH).

Materials and Methods

We reviewed immediate post-thrombectomy DECT studies of 60 consecutive patients who underwent endovascular treatment for an anterior circulation LVO with pre-procedural ASPECTS ≥7 and mTICI 2B/3 The presence of parenchymal contrast staining was recorded using DECT post-processing SyngoVia software. Four cases with ICH on this immediate post-thrombectomy DECT were excluded. Follow-up non-contrast single energy CT studies were evaluated for the presence of ICH.

Results

DECT parenchymal contrast staining was present in 41/56 (73%) of cases. Of cases with contrast staining, 10/41 (24%) developed ICH on follow-up CT. In patients with no contrast staining on DECT immediately post-procedure, none had ICH on follow-up CT.

Conclusions

Contrast staining is a frequent finding on immediate post-thrombectomy DECT. Despite successful reperfusion, the presence of contrast staining is an imaging biomarker of patients who are more likely to develop post-procedural ICH.

3083

1:28PM - 1:35PM

Does Variant Anatomy Affect Normal RAPID Posterior Circulation CT-Perfusion?

A Goldman-Yassen[1], M Uhouse[2], S Dehkharghani[3]
[1]NYU Langone Medical Center, Bronx, NY, [2]New York Medical College, Valhalla, NY, [3]NEW YORK UNIVERSITY-NYU MEDICAL CENTER, NEW YORK, NY

Purpose
Perfusion-based patient selection is supported through expert consensus and facilitates late-time window therapy in patients with acute ischemic stroke (AIS). Endovascular trials have emphasized anterior circulation (predominately ICA and MCA) large vessel occlusion (LVO), and generalizability to posterior circulation LVO may not be straightforward due to relative delays in anatomic territories of the posterior circulation, the propensity for anatomical variation and asymmetries in the posterior circulation, and the delay sensitivity inherent to deconvolved time-to-maximum (Tmax) parametric maps approximating features of canonical tissue residue functions. A description of thresholded Tmax and CBF volumetric lesions in normal tissues without LVO is thus critical before CTP criteria can be extended to patients with posterior circulation AIS. We sought to establish the extent and magnitude of putative perfusion deficits in the posterior circulation, amongst subjects without steno-occlussive disease, hypothesizing a greater tendency for benign oligemic delay and interactions with normal variations in vertebrobasilar anatomy and arterial input function (AIF) selection in a fully user-independent, auto-thresholded and auto-segmented perfusion analysis tool.
Materials and Methods
AIS patients undergoing CTP and CTA were retrospectively identified from a radiologic and clinical informatics query. CTP were analyzed using RAPID (iSchemnaView, Menlo Park, CA) to generate automated maps of critically hypoperfused tissue (Tmax>6s) volumes, thresholded voxel-wise at delays of 4s, 6s, 8s, and 10s, as well as estimates of the infarction core (relative CBF<30%). CTA of the cerebrovascular circulation were reviewed to exclude significant cervical or intracranial steno-occlusive disease, as well as for characterization of the posterior circulation with respect to anatomical dominance or visible asymmetries in the principal branches of the vertebrobasilar system or posterior communicating arteries. Automated AIF detection was employed using an operator-independent algorithm weighted for arterial tracer kinetic features. Studies with high grade stenosis or occlusion of any vessel, acute stroke at follow up, or other acute intracranial pathology were excluded.
Results
Twenty-nine cases were included in the analysis (median age 64 years, 52% Female). Nine subjects (22%) had either bilateral (n=3) or unilateral (n=6) diminutive or absent P1 posterior cerebral artery (PCA) segments and prominent posterior communicating (PCOM) arteries (fetal or near-fetal origin). Eight subjects were right vertebral artery dominant and 11 left dominant. Nineteen arterial AIF over the MCA, 7 over the basilar, and 6 over the ACA. Median volume of Tmax for the cohort was 14ml over 4 seconds (range 0-208ml) and 0ml over 6 seconds (range 0-12ml). CBF values were normal in call cases. There is no statistically significant difference in Tmax values between subjects with fetal / near-fetal PCA origins, those with vertebral artery dominance, or the location of the AIF.
Conclusions
In subjects without significant cerebrovascular steno-occlusive disease, physiologic elevations in posterior circulation Tmax values do not appear to engender false positive imputation of critically hypoperfused tissue volumes, irrespective of anatomic (co)dominance or other asymmetries and anatomic variation or AIF placement. Benign oligemic delays may be encountered in this setting but are not likely to impact perfusion-based patient selection criteria in endovascular trials.

2179

1:35PM - 1:42PM

Evaluation of 3D-FatNav based Motion Correction in the Clinical Setting of Patients with Brain Tumors

C Glessgen[1], D Gallichan[2], N Hainc[3], M Moor[4], C Federau[5]
[1]Universitätsspital Basel, Basel, Switzerland, [2]Cardiff University, Cardiff, Wales, [3]Universitätsspital Zürich, Zürich, Zürich, [4]Universitätsspital Basel, Basel, Basel, [5]University Hospital Basel, Basel, CA

Purpose
The purpose of this study was to evaluate 3D fat-navigator based motion correction in patients with brain tumors.
Materials and Methods
An MRI-based fat-excitation motion navigator was incorporated into a standard MPRAGE sequence and acquired in 40 consecutive brain tumor patients, pre and post-Gadolinium injection, and reconstructed with and without motion correction. Following key anatomical landmarks were evaluated: the temporal lobes, the pons and cerebellum, the basal ganglia and, after contrast administration, the bifurcations of the middle cerebral artery and the A2 segment of the anterior cerebral artery. The severity of motion score was assessed quantitatively and subjectively by two radiologists using a 5-point score from 0 (no artifacts) to 4 (non-diagnostic) for each pair and landmark. An image quality improvement following motion correction (IQIMC) score was assessed from 0 (identical) to 3 (important correction). Student t-tests were used to test for statistical significance.
Results
The mean IQIMC score throughout the datasets was 0.54, significantly differing from 0 ($p<0.001$). The IQIMC score increased with the severity of the motion artefacts. In the cases with and light artefacts, the mean IQIMC score was 0.50 and 0.13 respectively. In the cases with moderate artifacts and severe artifacts, the mean IQIMC score was 1.17 and 2.25 respectively. In the cases with non-diagnostic image quality, the mean IQIMC score 1.38.
Conclusions
Fat-navigator based motion correction significantly improved MPRAGE image quality in restless patients during MRI acquisition. There was no loss of image quality in patients with little or no motion.

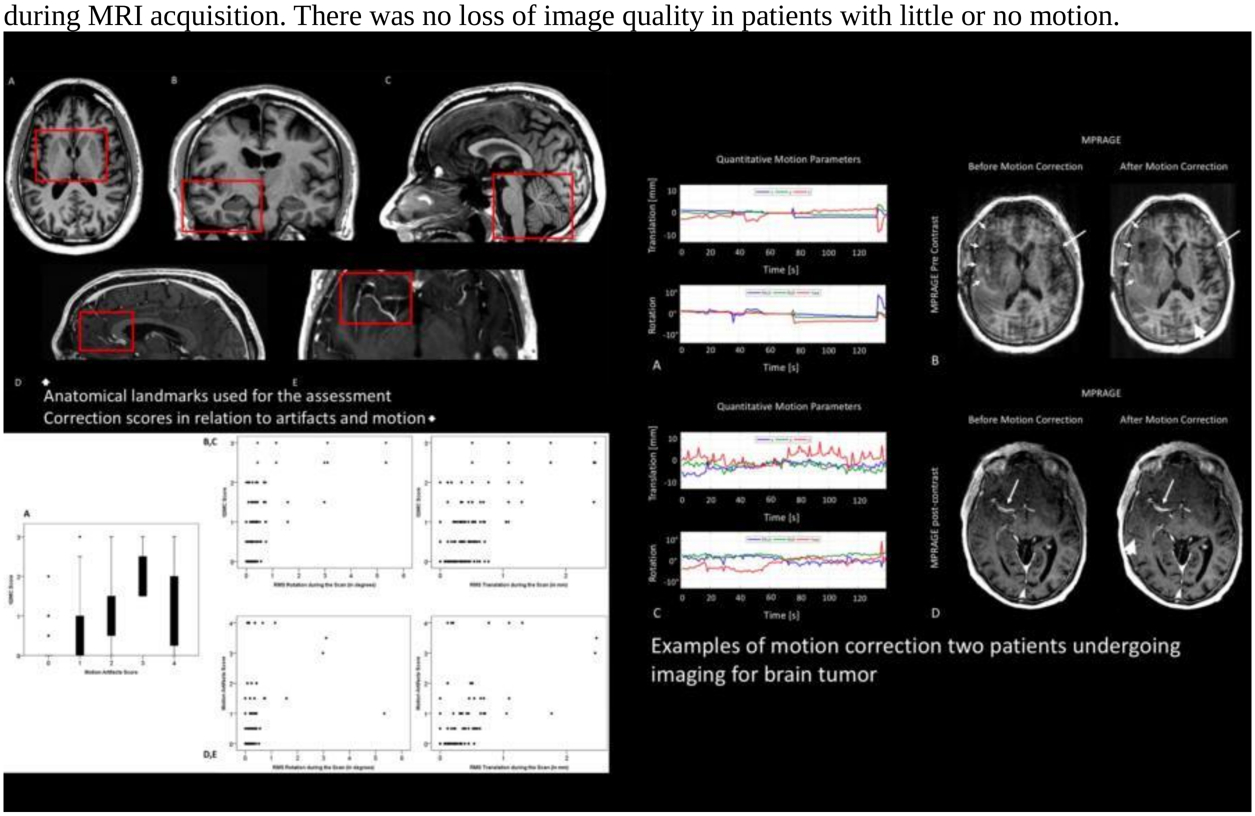

(Filename: TCT_2179_Infografic.jpg)

3246

1:42PM - 1:49PM

Highly Accelerated 3D T1-Weighted SPACE for Rapid Intracranial Vessel Wall Imaging using Wave-CAIPI: Implementation and SNR Considerations

J Conklin[1], M Longo[1], S Cauley[2], K Setsompop[2], J Kirsch[1], E Obusez[1], J Romero[1], R Gonzalez[1], P Schaefer[1], S Huang[3], O Rapalino[1]
[1]Massachusetts General Hospital, Boston, MA, [2]Harvard Medical School, Boston, MA, [3]Massachusetts General Hospital / Athinoula A. Martinos Center for Biomedical Imaging, Boston, MA

Purpose
Intracranial vessel wall imaging is a promising technique for a variety of clinical applications [1], however current approaches suffer from lengthy acquisition times. At our institution for example, high-resolution pre- and post-contrast 3D T1-SPACE is performed requiring > 15 minutes of scanning. The Wave-CAIPI parallel imaging approach enables high acceleration factors with negligible g-factor penalty [2], and may facilitate vessel wall imaging in more clinically feasible scan times. We evaluated highly accelerated 3D T1-SPACE using Wave-CAIPI (Wave-T1-SPACE) in a healthy volunteer, and compared this sequence to our current clinical protocol (standard T1-SPACE) in terms of image quality and SNR.
Materials and Methods
The study was IRB approved and HIPAA compliant. A prototype Wave-T1-SPACE sequence was implemented on a 3T MRI system (MAGNETOM Prisma; Siemens Healthcare GmbH, Erlangen) and a healthy volunteer was scanned using a 32-channel head coil. Wave-T1-SPACE (R=9, acquisition time 2:38 min) and standard T1-SPACE (R=4, acquisition time 7:39 min) were matched in terms of voxel size (0.9 mm isotropic) and other scan parameters. Each sequence was acquired twice, and quantitative SNR maps were calculated using the difference method [3]. The average SNR for the deep brain (basal ganglia and thalami) was compared between the two sequences. Images were then co-registered and compared side-by-side in multiple planes for visualization of the intracranial arteries.
Results
SNR maps showed mildly reduced SNR for Wave-T1-SPACE compared to standard T1-SPACE (Figure A). Deep brain SNR (the most SNR limited portion of the brain) was 88.1 for standard T1-SPACE compared to 53.6 for Wave-T1-SPACE, scaling approximately with $1/\sqrt{R}$ and suggesting the Wave-CAIPI approach was successful in mitigating g-factor related SNR losses. Both sequences provided excellent black blood contrast and visualization of the major branches of the circle of Willis (Figure B), noting a mild but perceptible increase in image noise on the Wave-T1-SPACE sequence.
Conclusions
Evaluation of the intracranial arteries using Wave-T1-SPACE is feasible with sub-millimeter isotropic resolution and sub-3 minute acquisition time, with preservation of reasonable SNR (>50) in the central and most SNR limited portions of the brain. This technique could facilitate broader adoption of vessel wall imaging for a variety of clinical indications, and further study with post-contrast images in a clinical setting is recommended.

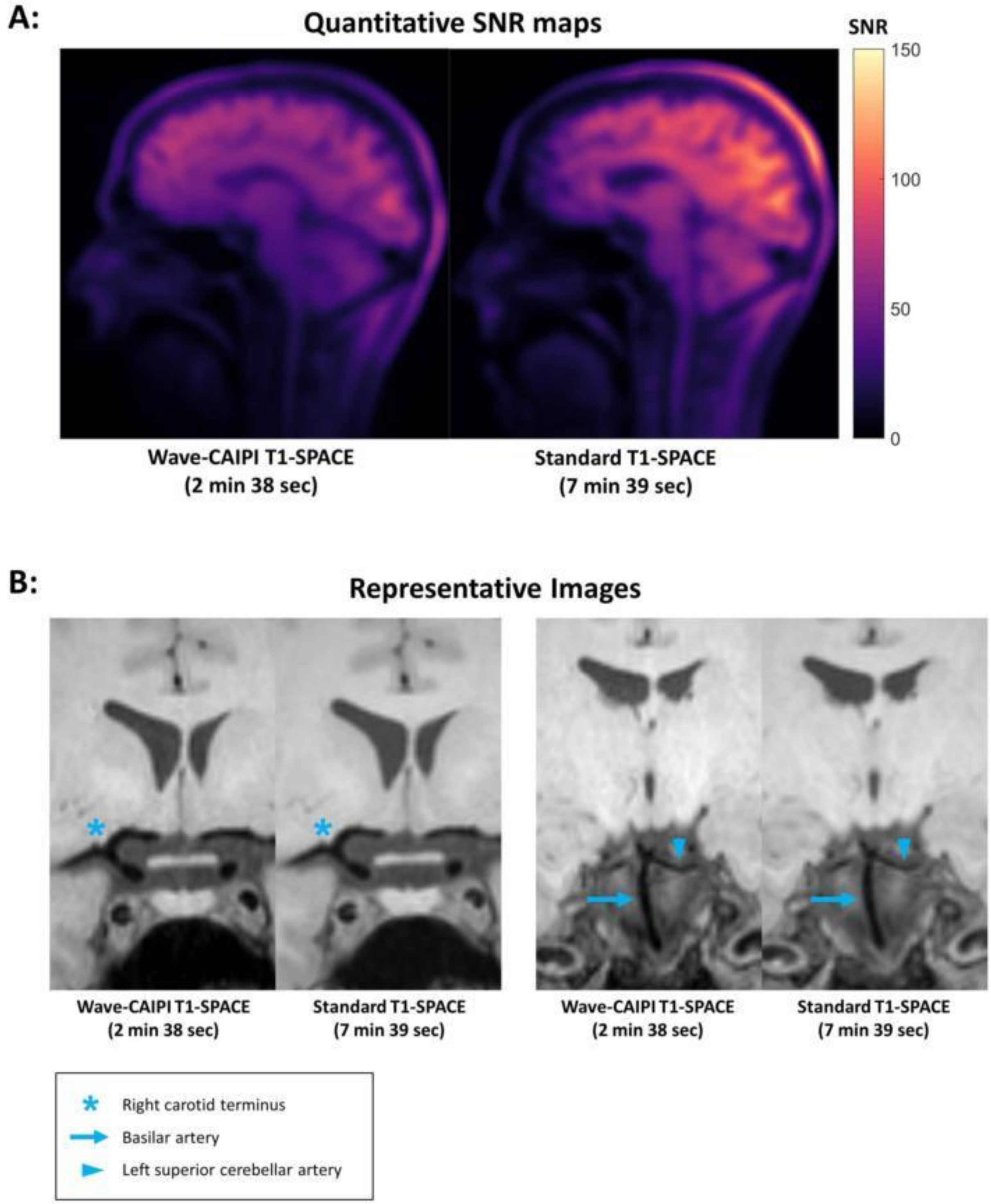

(Filename: TCT_3246_Figure1.jpg)

2800

1:49PM - 1:56PM

Olfactory Neuroblastoma (Esthesioneuroblastoma): Variable Imaging Features

E Kipervasser[1], S Kamalian[1], C Soneru[2], P Sasson[1], S Teoh[1], E Kipervasser[1]
[1]Mount Auburn Hospital, Cambridge, MA, [2]Mt. Auburn Hospital, Cambridge, MA

Purpose
To review imaging characteristics of olfactory neuroblastoma and potential pitfalls.
Materials and Methods
A 64-year-old male with history of hypertension presented to the emergency department with recurrent right-sided epistaxis. His daily medications included aspirin. His physical exam revealed a bleeding source in the anterior portion of the right nasal cavity which was cauterized. At follow-up consultation with an Otolaryngologist, the patient endorsed chronic hyposmia, but no other sinonasal symptoms. On physical exam, anterior rhinoscopy showed a lesion between the nasal septum and right inferior turbinate. Nasal endoscopy revealed a vascular sinonasal mass which was filling the right nasal cavity and extended through a septal defect to the superior portion of the left nasal cavity. The remainder of the head and neck exam found no palpable cervical lymphadenopathy and intact cranial nerves. He was sent for a sinus CT. Biopsy of the mass revealed olfactory neuroblastoma.
Results
Sinus CT shows a large soft tissue mass involving the right nasal cavity with destruction of the nasal septum involving the middle turbinate, extending into the right ethmoid and frontal sinuses, and intracranially along the inferior aspect of right olfactory recess. On MRI, there is a T1-isointense, T2-hypointense expansile mass with homogeneous enhancement and restricted diffusion filling the right nasal cavity and extending to the upper left nasal cavity. The mass is extending to the right anterior cranial fossa/olfactory recess with associated dural enhancement. Extension into the right medial peri-orbital fat is seen with mass effect on the medial rectus (Figure 1).
Conclusions
While the invasive characteristics and enhancement pattern were typical for olfactory neuroblastoma, the T2-hypointensity was unusual and given the associated restricted diffusion we initially favored primary tumors such as T-cell lymphoma or amelanotic melanoma. Given the variable imaging features, we need to remain open-minded about differential diagnosis of sinonasal masses, as highlighted in this case.

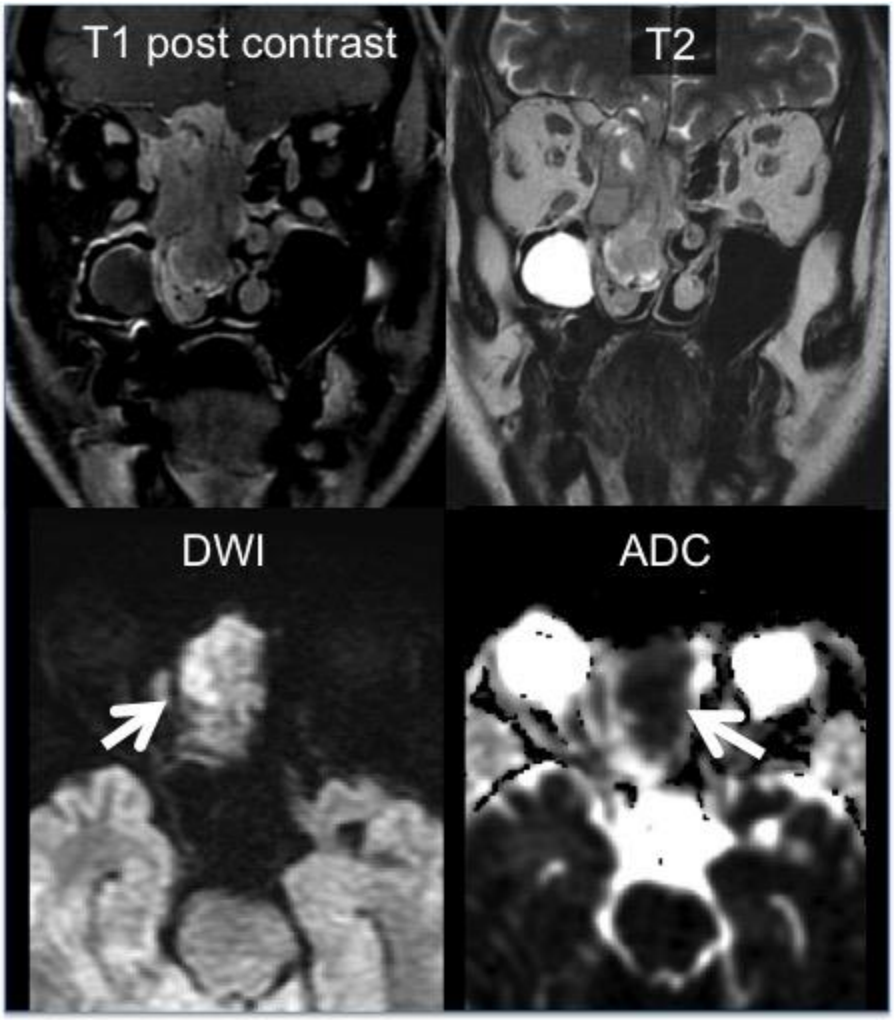

(Filename: TCT_2800_Imagingolfactoryneuroblastoma.jpg)

2271

1:56PM - 2:03PM

Pointwise encoding time reduction with radial acquisition (PETRA) in the Follow-up after Stent-assisted Coil Embolization for Anterior Circulation Aneurysms

Y Heo[1], H Jeong[2], J Beak[3]
[1]INJE UNIVERSITY, BUSAN PAIK HOSPITAL, BUSAN, Busan, [2]INJE UNIVERSITY, BUSAN PAIK HOSPITAL, Busan, Busan, [3]Inje university Busan Paik hospital, Busan, Busan

Purpose
TOF MR angiography is widely used, but has limitations in the follow-up after stent-assisted coil embolization due to magnetic susceptibility and radiofrequency shielding. We applied PETRA sequence using an ultrashort-echo time in the follow-up after stent-assisted coil embolization for anterior circulation aneurysms. The purpose of this study was to compare blood flow within intracranial stent using TOF MR angiography and PETRA MR angiography.
Materials and Methods
Twenty-six patients treated with stent-assisted coil embolization for anterior circulation aneurysms underwent TOF MR angiography and PETRA MR angiography in the same session. Two

neuroradiologists independently reviewed the both MR angiography and subjectively graded (1, not visible; 2, poor; 3, good; 4, excellent) using latest DSA as a reference of standard. We also compared according to the types of intracranial stents.

Results

PETRA MR angiography (3.27 ± 0.962 in reader 1, 3.62 ± 0.752 in reader 2) showed significantly higher grades than TOF MR angiography (2.23 ± 0.863 in reader 1, 2.42 ± 0.758 in reader 2). Inter-observer agreement showed almost perfect between two readers (0.810 for PETRA MRA, 0.861 for TOF MRA). Neuroform stents showed higher grade than Enterprise stent in both PETRA and TOF MR angiography, but there were no significant differences between two types of intracranial stents in both readers.

Conclusions

PETRA MR angiography may be useful in the follow-up after stent-assisted coil embolization for anterior circulation aneurysms.

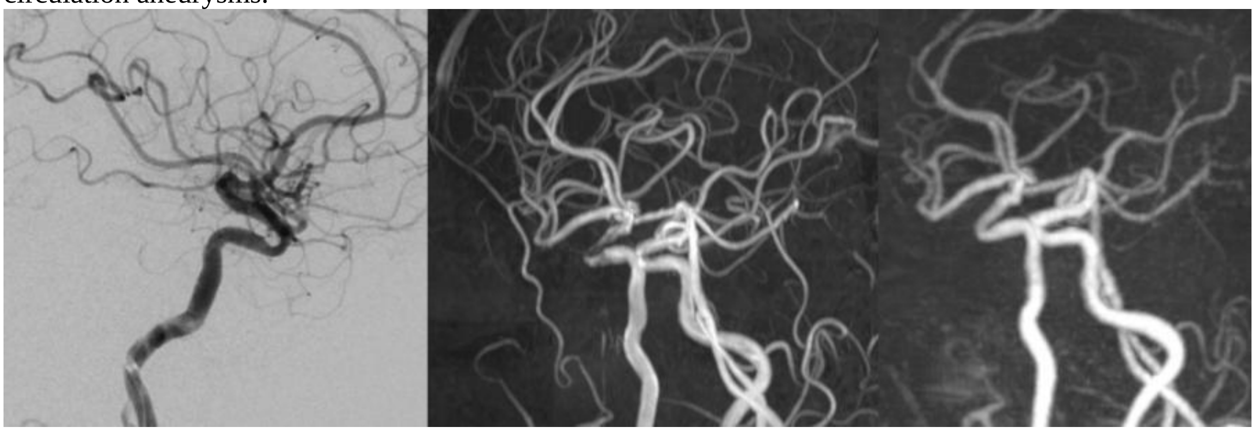

(Filename: TCT_2271_ASNRFigure.jpg)

3384

2:03PM - 2:10PM

Spindle Cell Oncocytoma of the Pituitary Gland: an Oddball with a Twist

B Laguna[1], E Sloan[1], A Bollen[2], S Cha[2]
[1]UCSF, San Francisco, CA, [2]University of California San Francisco, San Francisco, CA

Purpose

While the vast majority of primary pituitary lesions represent pituitary adenomas, craniopharyngiomas, meningiomas, oncocytomas, pituitocytomas also present as masses of the adenohypophysis. Here we aim to describe specific imaging features of spindle cell oncocytoma.

Materials and Methods

A 48 year old man presented with intermittent headaches, hypogonadism and fatigue, prompting endocrinologic work up, including brain imaging. Patient denied symptoms of polydipsia, polyuria, and had normal visual fields on confrontation testing. Based on imaging findings, patient underwent open biopsy via lamina terminalis, which identified a highly vascular tumor. Initial frozen section suggested underlying meningioma. Given degree of vascularity, only a biopsy was performed, opting for subsequent safer trans-frontal transcortical transventricular tinea forniceal approach. Gross total resection was accomplished two days later, and intraoperative pathology again suggested meningioma. On formal histopathology review, the mass was identified as a vascular, spindled and epithelioid neoplasm, negative for STAT6 and SSTR2A, eliminating hemangiopericytoma and meningioma from the differential. Immunohistochemical stains were strongly positive anti-mitochondrial antigen and TTF1, and in combination with the number of spindle cells and vascularity, a diagnosis was made of spindle cell oncocytoma.

Results
Initial imaging demonstrated a large, solid, avidly enhancing suprasellar mass, displacing the optic chiasm superiorly, and exerting mass effect on the anterior third ventricle. The mass had no definitive involvement of the sella or the infundibulum, both of which were normal in size and appearance.
Conclusions
Spindle cell oncocytomas are WHO grade I neoplasms which arise from the adenohypophysis, with patients typically presenting with visual symptoms or sequelae of panhypopituitarism. Lesions are rarely confined to the sella, often suprasellar, and highly vascular. On imaging, they can demonstrate internal flow voids, susceptibility artifact, and unlike adenomas, will demonstrate early avid enhancement. Purely suprasellar, solid mass with definite imaging connection the pituitary gland could still represent a pituitary oddball, the spindle cell oncocytoma.

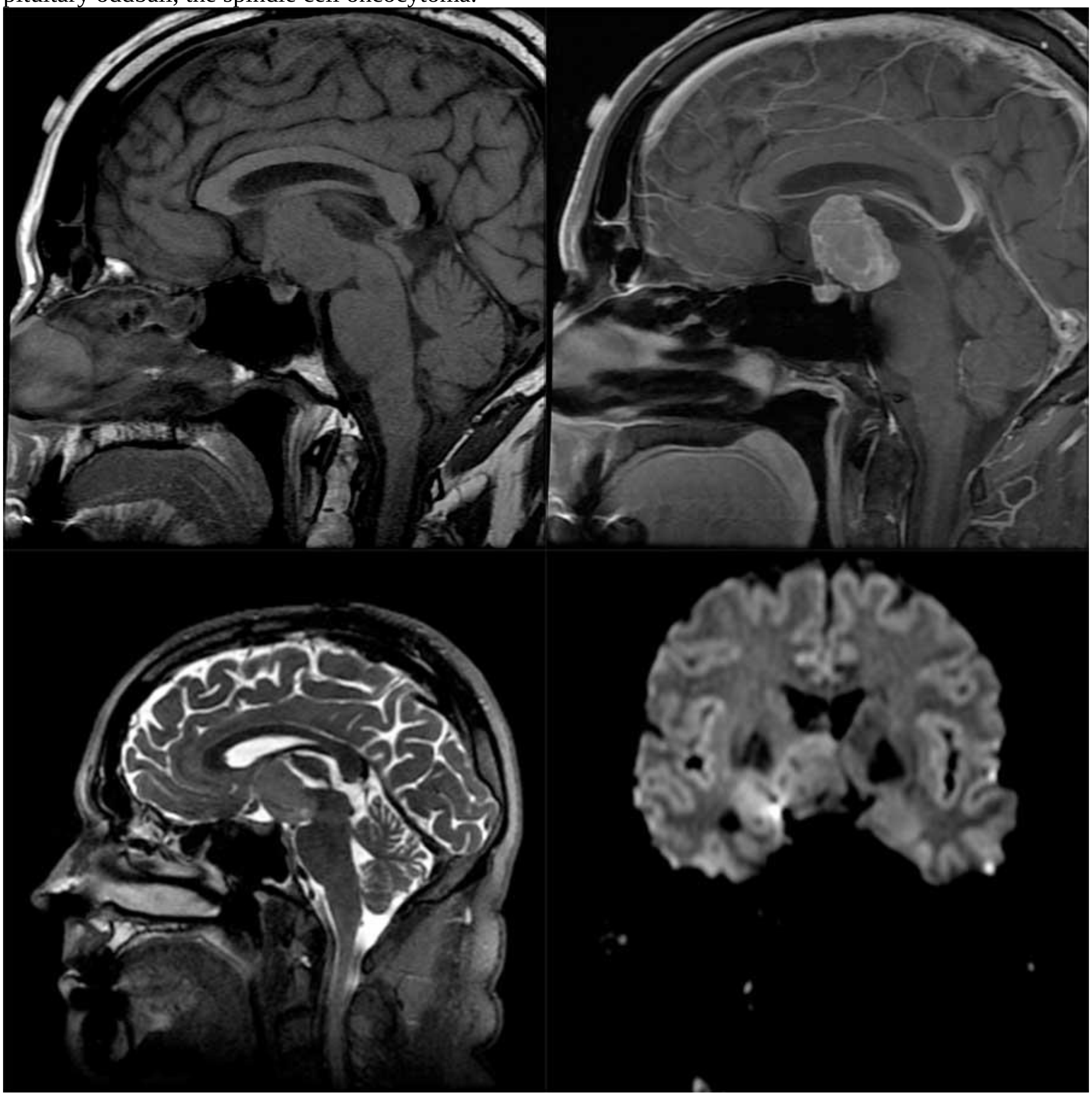

(Filename: TCT_3384_Untitled-2.jpg)

2109

2:10PM - 2:17PM

The Atypical 'Diving' Lesion: Congenitally Dilated Imperforate Submandibular Duct

V Yedavalli[1], K Yeom[2]
[1]Stanford University, San Francisco, CA, [2]Stanford University, Palo alto, CA

Purpose
Congenital dilated imperforate submandibular duct (CDISD) is an extremely rare condition found in neonates, often resulting in poor feeding. We present a case of this entity in a one-week old male who warranted workup after tachypnea with breastfeeding.
Materials and Methods
A one-week old male patient was found to have difficulty breastfeeding. The patient had difficulty latching and varying degrees of tachypnea during feedings. Physical exam uncovered a palpable lesion along the floor of the tongue on the left. Sonographic evaluation showed an avascular tubular structure in the area of interest. Subsequent MR demonstrated a serpentine faintly rim enhancing tubular structure along the floor of the mouth arising from the left submandibular gland extending into the sublingual space. The patient then underwent a frenulotomy which resulted in immediate decompression and resolution.
Results
One-week old male neonate with difficulty breastfeeding. A) Axial T2W demonstrates a dilated hyperintense tubular structure within the left sublingual and submandibular spaces. B-C) Axial T1W postcontrast shows corresponding faint rim enhancement with an abrupt cutoff anteriorly and extension into the submandibular space. D) Coronal T1W postcontrast demonstrates contiguity with an asymmetrically enlarged left submandibular gland.
Conclusions
Although diving ranula is often invoked when encountering a tubular floor of the mouth cystic lesion, in a symptomatic neonate, CDISD is an easily treatable entity that should also be considered in a differential diagnosis.

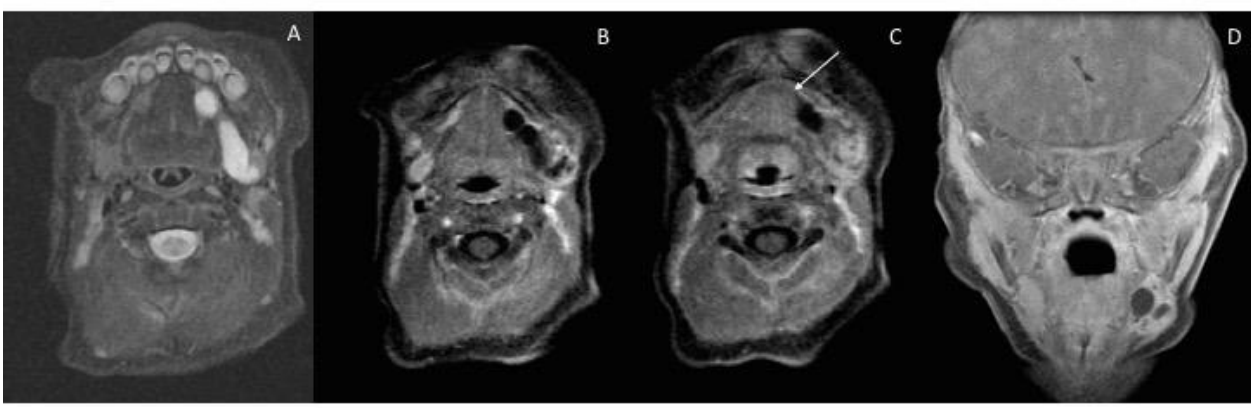

One week old male neonate with difficulty breastfeeding. A) Axial T2W demonstrates a dilated hyperintense tubular structure within the left sublingual and submandibular spaces. B-C) Axial T1W postcontrast shows corresponding faint rim enhancement with an abrupt cutoff anteriorly (arrow) and extension into the submandibular space. D) Coronal T1W postcontrast demonstrates contiguity with an asymmetrically enlarged left submandibular gland.

(Filename: TCT_2109_CongenitalSubmandibularDuct.jpg)

3661

2:17PM - 2:24PM

Utility of CT Angiography (CTA) for Evaluation of Acute Vision Loss from Emergency Department

A Malhotra[1], K Al-Dasuqi[2], S Onderi[3], X Wu[4], K Seifert[5]
[1]YALE UNIVERSITY SCHOOL OF MEDICINE, NEW CANAAN, CT, [2]Yale New-Haven Hospital, New Haven, CT, [3]Boston Medical Center, Boston University School of Medicine, Boston, MA, [4]Yale University School of Medicine, New Haven, CT, [5]YALE NEW HAVEN HOSPITAL, NEW HAVEN, CT

Purpose
Imaging is frequently performed for evaluation of acute vision changes/vision loss. Guidelines recommend the combination of urgent brain magnetic resonance imaging with diffusion-weighted imaging, vascular imaging, and clinical assessment to identify monocular vision loss, branch or central retinal artery occlusion in patients at highest risk for recurrent stroke. The purpose of the study was to assess the utility of CT Angiography (CTA) in patients presenting to the ED with acute vision loss or blurry vision as an isolated symptom.
Materials and Methods
After IRB approval, the institutional medical records were searched for patients who received CT Angiography from the Emergency Department for acute presentation with vision loss or blurry vision over a 3 year period at a tertiary, academic center. Demographic data was collected, as well as risk factors and prior imaging where available. The CTA studies were assessed for positive findings - both vascular and brain parenchymal changes. Follow- up imaging performed within one year was subsequently recorded where available.
Results
A search of the medical records revealed 465 patients who received a CT Angiography from the Emergency Department during the study period. Decreased or non-visualization of the Ophthalmic artery was reported in 4 cases, complete occlusion of the ipsilateral ICA was reported in 3 cases and incidental alternate diagnosis like Posterior cerebral artery infarct, prior MR evidence of Optic nerve lesions or demyelinating plaques were noted in 24 patients.
Conclusions
CT angiography is uncommonly positive in patients with acute vision loss and vision changes in the absence of other focal neurologic signs. Its utility and cost-effectiveness when performed from the Emergency Department need further study.

Monday, May 20, 2019
1:00PM - 2:30PM
AI/Advanced Imaging in Vascular Disease and Tumors

2111

1:00PM - 1:07PM

Artificial Intelligence in Radiology Literature: Trends in Publication from 2008-2017 with a Focus on the American Journal of Neuroradiology

J Perchik[1], A Murray[2], A Gunn[2]
[1]University of Alabama, Birmingham, BIRMINGHAM, AL, [2]University of Alabama, Birmingham, Birmingham, AL

Purpose

From aiding in detection of stroke to workflow optimization, artificial intelligence (AI) is becoming increasingly important for radiologists. We seek to assess if an increase in applications of AI in radiology practice resulted in an increased representation in radiology journals and how the American Journal of Neuroradiology (AJNR) compares to these trends.

Materials and Methods

The top 10 radiology journals were selected based on their impact factor (IF), scimagojr.com ranking, and SCOPUS 2017 Cite-Score; AJNR was included among these journals. All articles published by the respective journals from 2008-2017 were selected. Article information and citation statistics were collected from SCOPUS. Articles with titles, MeSH terms, or keywords that included the phrases "Artificial Intelligence", "Deep Learning", "Machine Learning", or "Neural Network" were included for analysis.

Results

Of the 34,529 articles published in the selected journals from 2008-2017, 172 articles met the criteria for inclusion (0.5%). AI articles were, on average, cited more frequently (mean 19.3; range 0-239) than articles published by the selected journals (mean16.6; range 0-1191); however, this difference was not statistically significant ($p=0.29$). AJNR tied with Radiology for the most AI articles published with 28 articles, had the third highest proportion of articles devoted to AI, 0.63%, and the third highest average citation of AI articles, 27.4 (range 0-239). An increase in AI articles per year was not observed overall nor in AJNR ($R^2 = 0.0052$, $R^2 = 0.0013$ respectively).

Conclusions

AI publication makes up a small proportion of radiology literature, but is highly cited and has widespread interest. AJNR is a top journal in the field of AI in radiology, but AI publication remains low and has not increased with time. AJNR should continue to be a leader in the field and encourage research in AI.

Figure 1. AI articles published per journal by year

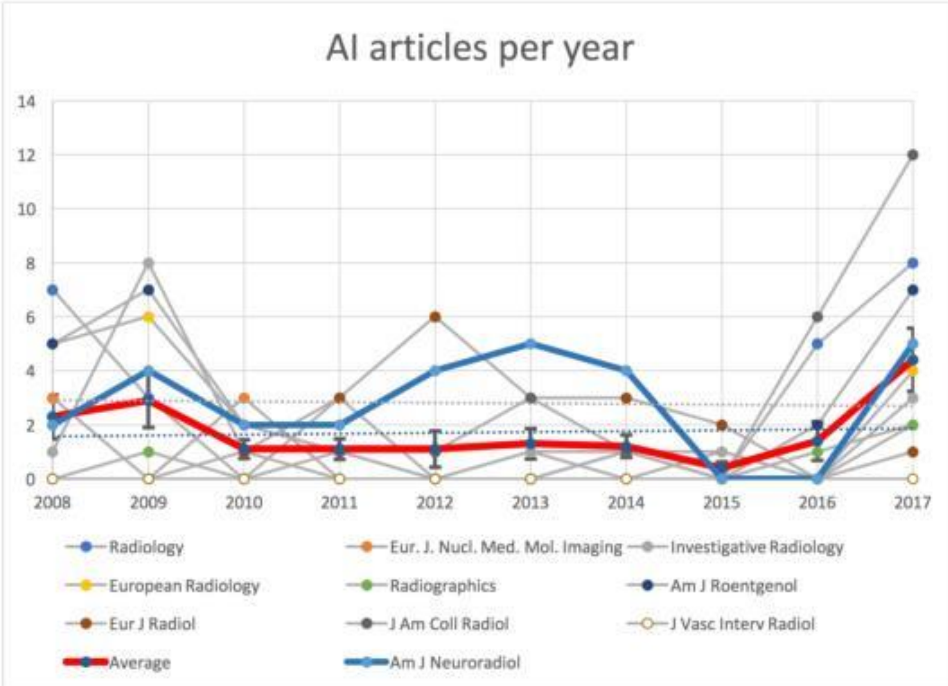

Table 1.

	Total AI articles	AI as percent of publications	Average citation-AI articles[1]	Overall average article citation[1]
Am J of Neuroradiol	28	0.63%	27.39	18.45
Radiology	28	0.52%	39.29	30.12
Am J Roentgenol	25	0.38%	17.68	17.1
J Am Coll Radiol	24	0.75%	3.125	5.18
Eur J Radiol	19	0.49%	10.42	12.65
Eur Radiol	19	0.48%	25	19.1
Invest Radiol	15	1.4%	22.67	22.24
Eur J Nucl Med Mol Imaging	10	0.33%	19.67	25.85
Radiographics	4	0.23%	28	19.57
J Vasc Interv Radiol	0	0%	0	5.32
Average	17.2	0.52%	19.3	17.6

1: Citations of articles published 2008-2017 as of August 10, 2018

(Filename: TCT_2111_AIprojectforASNRfiguresfinalJPEG.jpg)

3446

1:07PM - 1:14PM

Assessment of Global and Regional Difference of Resting State Cerebral Vascular Reactivity index in Patient with Brain Tumor

M Jenabi[1], K Peck[1], M Gene[1], A Holodny[2]
[1]Memorial Sloan Kettering Cancer Center, New York, NY, [2]MSKCC, DEMAREST, NJ

Purpose
We utilized resting state fMRI (rfMRI)[1] to estimate the BOLD signal change in response to natural breathing to measure the impairment of cerebral vascular Reactivity (CVR)[23] due to the presence of tumor and to determine whether this tumor-induced CVR can be corrected using specific frequency band.
Materials and Methods
10 controls (49.25±8.15) and 60 patients (49.73 s±15.36: glioma grade IV(GBM) (N=24), grade III (N=7), grade II and I (N=19) and metastases(MET) (N= 10)) were included in this study. Four CVR associated values (standard deviation of residual error (SD map), regression coefficient (R map), amplitude of low-frequency fluctuation (ALFF)[4] and regional homogeneity based on the Kendall's coefficient of concordance (KCC map)[5]) were obtained from the low frequency fluctuation (LFF) of rfMRI in three frequency band (0.01-0.02, 0.02-0.04, 0.04-0.08) and averaged over whole brain (WB) and tumor region of interests (ROIs) to measure the global and regional frequency related CVR properties respectively.
Results
ALFF was highly correlated with SD (r>0.95) and R (r>0.6) maps in WB and tumor ROIs in all 3-frequency band. The SD value in controls and patients, across ROIs increases with frequency (p< 〖1×10〗^(-5),q<0.01). The R value in controls and patients across ROIs are independent on frequency (whole brain:0.99±0.008, tumor: 0.57±0.063). The R value for GBM was higher globally (GBM: 1>control) and lower in tumor ROI (GBM: 0.5). The KCC value in controls and patients is significantly increased with frequency (p< 〖1×10〗^(-13), q< 〖1×10〗^(-11)) across WB ROI, but not in tumor ROI (p<0.02).
Conclusions
CVR mapping can determine the area of potential neuro-vascular uncoupling (NVU) in the brain to provide more accurate information in pre-surgical planning. The low SD value with less intrasubject variability in lower band suggest that LFF in lower frequency is more reliable to estimate NVU-related false-negative effects. Furthermore, rfMRI is a feasible alternative to estimate CVR map.

3253

1:14PM - 1:21PM

Automated Detection and Segmentation of Brain Metastases Using Deep-Learning Neural-Networks Utilizing Multi-Modal MRI

E Tong[1], M Iv[1], D Yi[1], E Groevik[1], D Rubin[2], G Zaharchuk[1]
[1]Stanford University, Stanford, CA, [2]Stanford University, San Francisco, CA

Purpose
Accurate detection and precise segmentation of brain metastases is crucial for staging, treatment-decision, and radiation-planning. While this important task is time-consuming and tedious for radiologists, it poses as a challenge well suited for Deep-learning Neural-Networks. Our work aims to train a fully Convolutional-Neural-Network (CNN) on multi-modal MRI for automatic detection and segmentation of brain metastases.
Materials and Methods
Brain metastases of 156 patients (mean age 63±12yrs, 64(41%) with 1-3 metastases, 47(30%) with 4-10 metastases, and 45(29%) with >10 metastases) were manually segmented by 2 neuroradiologists on post-

gadolinium T1-BRAVO sequences, which serve as ground-truth. Pre- and post-gadolinium T1-weighted 3D-fast-spin-echo(CUBE) and post-gadolinium T1 3D-BRAVO and 3D-CUBE-FLAIR sequences performed on 1.5T and 3T MR scanners were used to train a 2.5D fully convolutional network based on GoogLeNet architecture (Figure 1). Input to CNN was a slab of slices (from each sequence) depicting each metastasis. The neural-network was optimized for segmentation and trained using the TensorFlow framework, which outputs a probability-map (0-100%) of metastasis detection. Performance was evaluated by estimating precision, recall, Dice-coefficient, Intersection-over-Union-score(IoU), and ROC-curve statistics. Dataset was split into 100/5/51 patients for training/validation/testing.

Results

Area under the ROC-curve, averaged across all patients, was 0.96(Graph 1). Based on ROC statistics, the average optimal probability-threshold for metastasis was 0.91. Using this threshold, the average precision, recall, and segmentation IoU-and Dice-score were 0.69, 0.55, 0.44, and 0.58, respectively. No apparent impact on performance in datasets degraded by motion artifact was detected in our preliminary results. Subgroup analyses, according to number of metastases and size of metastases, are shown in Table 2. . Figure 2 shows predictions (probability-maps) generated by CNN, overlaid on a post-contrast BRAVO image in a patient with three lung metastases. Visual inspection shows good agreement between the CNN predictions and the 'ground-truth' as delineated by neuroradiologists (highlighted in yellow circle).

Conclusions

Our study demonstrates that Deep-Learning Neural-Network, trained on multi-modal MRI, has the potential to automate detection and segmentation of brain metastases. As we continue to increase our training-dataset, our CNN will improve its performance and may serve as a useful clinical treatment-planning tool.

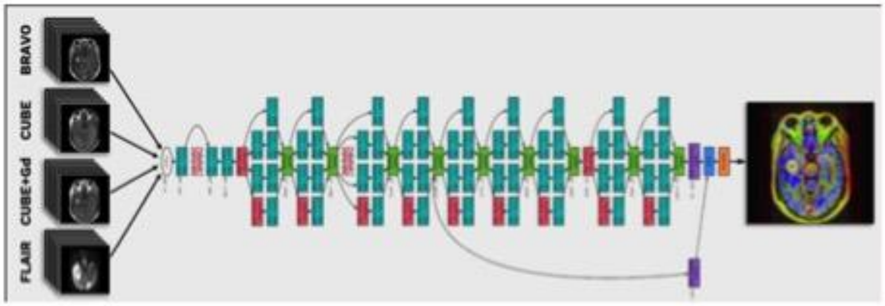

Figure 1. Flowchart of the convolutional neural-network showing four input sequences, modified GoogLeNet architecture, and color-coded prediction map.

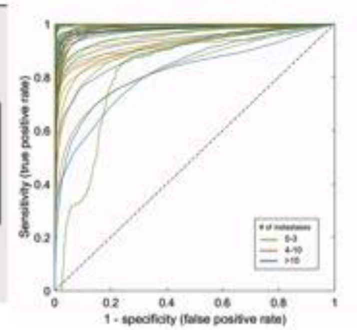

Graph 1. ROC curves for test-set. Average area under ROC curve was 0.96.

Subgroup (Num of Metastases)	Num of patients	Total num of metastases	Total num of miss
Few lesions (≤3)	17	37	3 (2 punctate lesions, 1 lesion >1cm)
Moderate (4-10)	17	119	20 (17 punctate lesions, 3 lesions >1cm)
Many lesions (>10)	17	>200	>40 (all are subcentimeter lesions)

Table 2. Results of 51 test patients, subdivided in 3 subgroups according to number of metastases in each individual: (1) fewer than 4 lesions, (2) between 4-10 lesions, and (3) above 10 lesions.

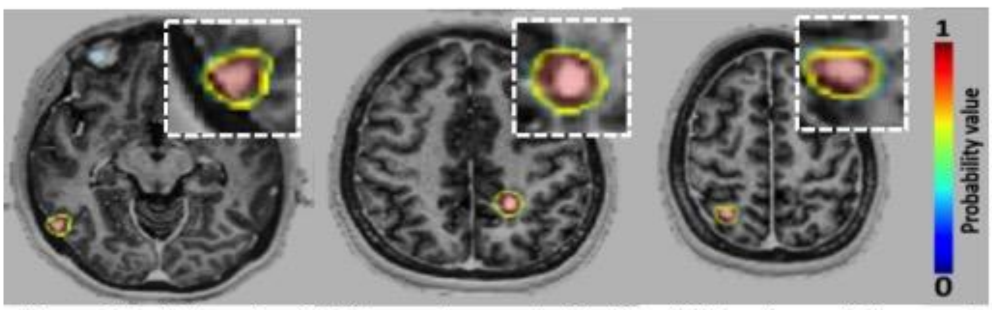

Figure 2. Predictions (probability-maps) generated by Neural-Network, overlaid on post-contrast BRAVO image in a female with three lung metastases. Yellow outline represents 'ground-truth' delineated by neuroradiologists

(Filename: TCT_3253_NewFigure.jpg)

2461

1:21PM - 1:28PM

Automated Detection of Acute Infarction in Multi-Parametric Brain MRI using an Artificial Intelligence 3D Pipeline

K Nael[1], B Odry[2], C Yang[3], A Doshi[4], B Georgescu[2], M Nadar[2], D Comaniciu[2], B Stoeckel[5], T Re[5], S Huwer[5], H Meyer[5], D Mendelson[6], Z Fayad[6]
[1]ICAHN SCHOOL OF MEDICINE AT MOUNT SINAI HOSPITAL, NEW YORK, NY, [2]Siemens Healthineers, Princeton, NJ, [3]Icahn School of Medicine at Mount Sinai, new york, NY, [4]MOUNT SINAI ICAHN SCHOOL OF MEDICINE, NEW YORK, NY, [5]Siemens Medical Solutions, Malvern, PA, [6]Icahn School of Medicine at Mount Sinai, New York, NY

Purpose
With rapid growth and increasing use of brain MRI, there has been a significant interest in automated image processing and classification of brain MRI scans to supplant human interpretation and improve workflow (1). In this study we aim to assess the diagnostic accuracy of an AI 3D pipeline in automated identification of acute infarction.

Materials and Methods
A total of 1,153 consecutive clinical brain MRI studies including sagittal T1W , T1W Post and axial FLAIR, ADC, B1000, T2W, GRE sequences were selected from our institution HIPAA compliant imaging registry. Brain MR studies were obtained using standardized protocol across multiple MR scanners from two manufacturers (GE and Siemens). Each sequence was reformatted to common resolution to accommodate for differences between vendors. Two board certified neuroradiologists assigned each case to acute infarction or none based on the review of clinical report of each case. Consequently, acute infarct was diagnosed in 486 cases, or 42% of the MRI scans. A 3D AI pipeline was developed: first, a deep reinforcement learning based landmark detection was used to estimate positioning and brain coverage. Brain was extracted using an adversarial dense image-to-image based technique then 7 sequence-independent dense convolutional networks were trained in a supervised way, with data augmentation (random rotation, translation and added noise at each iteration), and merged to flag acute infarction cases. Training was performed on1037 cases (232,288 images – 40% acute infarct) with class weights to address class imbalance, testing included 116 cases (25,984images – 39% acute infarct).
Results
Receiver operating characteristic (ROC) analysis showed that an area-under-the-curve (AUC) of 0.90 with accuracy of 85%, sensitivity of 94%, and specificity of 80% for our detection pipeline.
Conclusions
Our proposed intelligent pipeline accurately identifies acute infarction on brain MRIs from the individual patients. If its potential is realized, it can be used as a clinical tool to flag abnormal MRIs, allowing for improved triage and timely interpretation of abnormal scans in a busy and large clinical practice.

3469

1:28PM - 1:35PM

Clinical Feasibility of Multi-band Diffusion Tensor Imaging (DTI) Using Simultaneous Multi-slice Acquisition for Presurgical Slanning: Comparisons with Standard DTI in Patients with Brain Tumor

M Jenabi[1], M Gene[1], N Cho[2], R Young[1], A Holodny[3], K Peck[1]
[1]Memorial Sloan Kettering Cancer Center, New York, NY, [2]Memorial Sloan-Kettering Cancer Center, New York, NY, [3]MSKCC, DEMAREST, NJ

Purpose
Standard diffusion tensor imaging (s-DTI) is currently utilized during presurgical planning to visualize white matter tracts despite long scanning time. Multi-band DTI (mb-DTI) utilizes simultaneous multi-slice excitation, which greatly reduces scanning time and increases coverage1,2, but there has been limited assessment of clinical feasibility3,4. The purpose of this study is to qualitatively and quantitatively compare tractography results from s-DTI and mb-DTI in brain tumor patients for the arcuate fasciculus (AF) and corticospinal tract (CST), which are major tracts for language and motor function, respectively.
Materials and Methods
Forty-two brain tumor patients who underwent presurgical s-DTI and mb-DTI were analyzed. Fractional anisotropy (FA), tract volume, and tract length were determined in the AF and CST. Seed ROIs were set at the superior temporal gyrus and inferior frontal gyrus for the AF and at the pons and foot motor area for the CST. Two-tailed paired t-tests were used to assess differences between s-DTI and mb-DTI parameters.
Results
Scan time was 40% shorter with mb-DTI (3:02) over s-DTI (5:25). Both techniques produced visually similar whole-brain FA maps and whole-brain, AF, and CST tractography. Fiber length, fiber volume, and FA in the whole-brain, AF, and CST were slightly higher for nearly all subjects with mb-DTI. These differences were significant at the individual level for FA values in the whole-brain (mb-DTI/s-

DTI=0.48±0.02/0.47±0.02), AF (0.55±0.04/0.53±0.04), and CST (0.60±0.03/0.58±0.03), as well as fiber length (72±14/58±13) and fiber volume (2760±1280/2080±970) in the AF (all $p<0.0001$).
Conclusions
This study demonstrated the clinical feasibility and potential advantages of mb-DTI. S-DTI and mb-DTI produced very similar results for the fiber tractography of the AF and CST, two white matter tracts of critical importance during presurgical planning. However, mb-DTI provides a considerable reduction in scan time over s-DTI while preserving image quality and quantitative diffusion parameters, suggesting there may be clinical advantages for utilizing mb-DTI over current techniques.

3215

1:35PM - 1:42PM

Deep Learning-Based Imaging Classifier for Improving Differential Diagnosis Between Primary and Petastatic Brain Tumors with Highly Overlapping MRI Morphologies

M Maros[1], C Cho[2], A Förster[3], A Mansour[4], E Neumaier Probst[2], G Christoph[2], H Wenz[2]
[1]UNIVERSITY MEDICAL CENTER, MEDICAL FACULTY MANNHEIM, UNIVERSITY HEIDELBERG, GERMANY, HEIDELBERG, Germany, [2]University Medical Center Mannheim, Medical Faculty Mannheim of University Heidelberg, Mannheim, BW, [3]University Medical Center Mannheim, Medical Faculty Mannheim of University Heidelberg, Germany, Mannheim, Baden-Württemberg, [4]University Medical Center Mannheim, Medical Faculty Mannheim of University Heidelberg, Germany,, Mannheim, BW

Purpose
The solely radiological differentiation between glioblastoma multiforme (GBM) and metastases (META) at initial case presentation can be extremely challenging, due to highly overlapping imaging morphologies and scarce clinical data regarding a primary tumor. Here, we investigated the applicability of deep learning-based image classifiers combined with (always available) clinical data to improve this distinction and support neuroradiologists to provide more robust diagnoses.
Materials and Methods
We retrieved a retrospective cohort of 450 patients including 225 GBMs (102F / 234M, mean age 64years, range: 2-92 yrs) and 225 METAs (97F / 128M, mean age 62years, range: 23-86 yrs) undergoing cranial magnetic resonance imaging (cMRI) using institutional tumor protocol between 2015-2018. Three independent blinded readers reassessed all cases and selected the subset of tumors with highly overlapping cMRI morphologies (n=360; 168 GBM / 192 META). From each case the single most representative transversal FLAIR, DWI, ADC and contrast enhanced T1-weighted images (T1c) were selected and categorized based on histopathological findings. The subset was randomly split into training- (~68%; 115 GBM / 131 META), validation- (~19%; 32 GBM / 37 META) and test sets (~12%; 21 GBM / 24 META). We used data augmentation techniques and custom designed and fitted deep convolutional neural networks (CNN) for each MRI sequence. In the second stage we built an ensemble model on top of these CNN classifiers combined with imaging information (not necessarily available for CNNs from a single transversal slice) like supra- or infratentorial location and solitary or multifocal/centric tumor distribution along with clinical data including age and sex.
Results
Despite our lean approach and challenging data set the regularized sequence-specific CNNs achieved training accuracies between ~70-99% with corresponding validation accuracies of 65-75%, in the sense of weak classifiers. The most difficult sequence for CNNs to classify was T1c with training- and validation accuracies of 75% (185/246) and 69% (45/69) and test accuracy of 52% (24/45). Test set predictions of CNNs trained on DWI images were often complementary to CNNs trained on T1c. CNNs developed on ADC sequences had the highest test accuracy of 75% (34/45) while FLAIR- and DWI-based CNNs achieved 64% and 69% respectively. In the second stage we implemented an ensemble model that combined the best-performing CNN classifiers with clinical data using boosted decision trees. The

ensemble model achieved an over all test accuracy of 82% (37/45). In Figure 1 we present a random subset of 11 test cases (5 GBM; 6 META) on which the ensemble achieved 73% accuracy making only 3 mistakes (8/11).

Conclusions

Deep learning-based GBM and META differentiation using expert-guided MR-image selection can support neuroradiologists to increase initial diagnostic accuracy in challenging scenarios.

Figure 1: Test set images of supra- (A) and infratentorial (B) GBMs and METAs with challenging, highly overlapping MRI-morphologies in T1c.

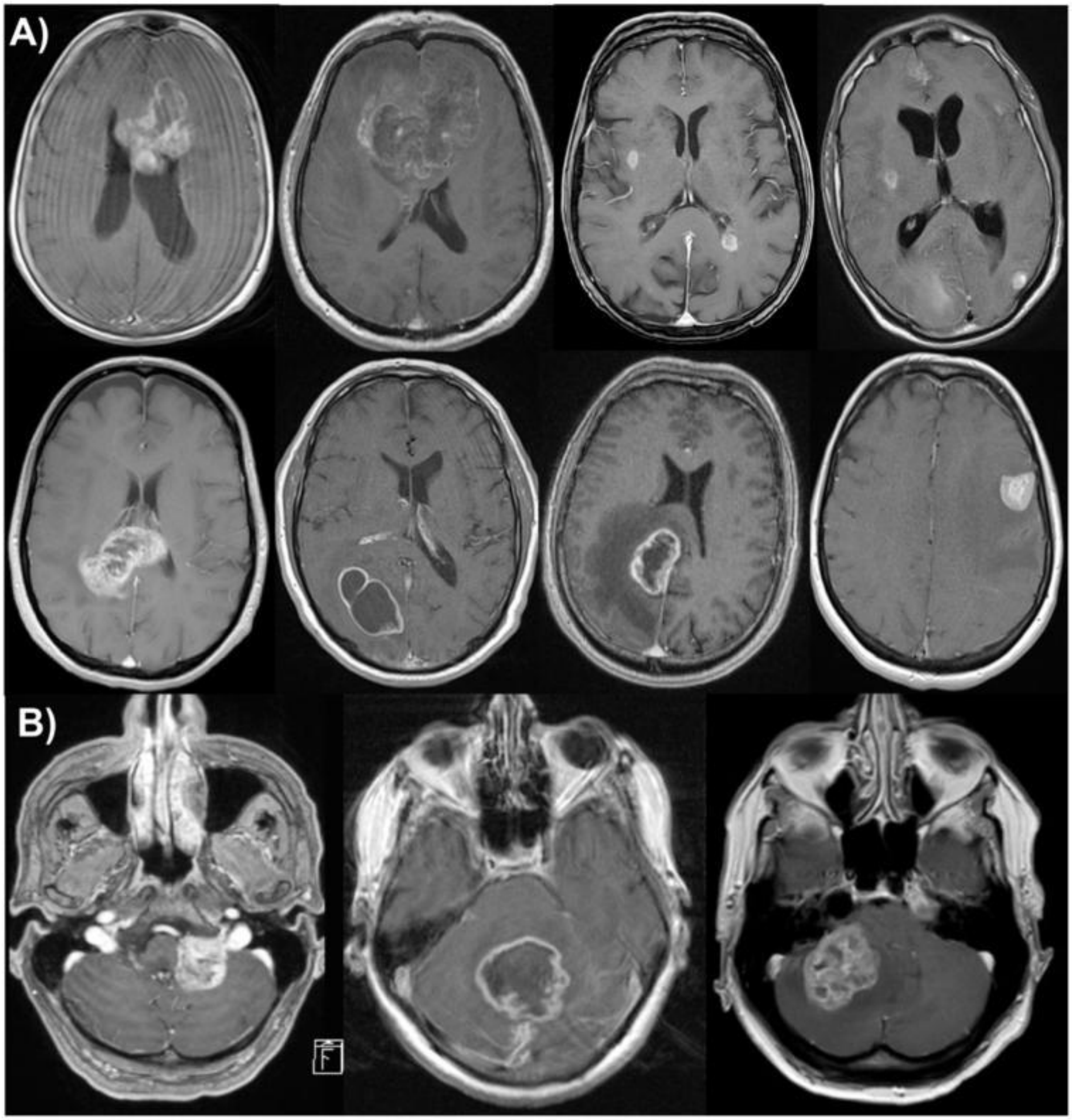

Solutions: (from left to right) → **(A)** META bronchial carcinoma, GBM, multifocal GBM, META esophagus ca. (2nd row) GBM, META bronchial ca., META mamma ca.; **(B)** GBM with extracranial intraforaminal (F. jugulare) extension; midline GBM; locotypico META from serous papillary peritoneal carcinoma

(Filename: TCT_3215_MarosME-ASNR-Figure1-GBMvsMETA.jpg)

2207

1:42PM - 1:49PM

Determining Whether Susceptibility Weighted Imaging (SWI) is Useful in Improving the Accuracy of DSC-MRI Parameters in Low-Grade Glioma

A Altokhis[1], M Borri[2], J U-King-Im[3], C Dudau[3], A Yamamoto[2], J Ashmore[4], T Booth[2]
[1]King's College London, London, England, [2]King's College Hospital NHS Foundation Trust, London, England, [3]King's College Hospital NHS Foundation Trust, London , England, [4]King's College Hospital NHS Foundation Trust, London, England

Purpose
Brain tumor perfusion evaluated with DSC-MRI provides information on grade and transformation during follow-up (1). During DSC-MRI analysis, an ROI is typically placed on the area with the highest perfusion (hot-spot method). However, the presence of vessels might be a confounding factor, giving a falsely high perfusion reading. In this work, we evaluate two different strategies for placing ROIs in DSC maps incorporating the presence of vessels.
Materials and Methods
35 patients with a diagnosis of low-grade glioma (LGGs, WHO II) were analyzed. Raw perfusion data was processed using OLEA sphere (La Ciotat, France) using oSVD deconvolution with an automatic AIF. The hot-spot method was employed to obtain the maximum cerebral blood volume (CBVmax) and nCBVmax (CBVmax normalized to contralateral white matter) (2). Then, the position of the ROIs was corrected to avoid vessels. For this purpose, two additional co-registered images sets were tested (Figure 1): 1) Scrolling raw perfusion data identified signal intensity change due to the presence of vessels (3). 2) SWI: in our novel approach small vessels were identified as they were dark due to the paramagnetism of venous blood. The Friedman test was used for comparison. Intra-class correlation coefficient (ICC) was used to test intra-observer and inter-observer (3 readers) reproducibility on a subset of 10 patients.
Results
The hot-spot method gave significantly higher median values of CBVmax and nCBVmax compared to SWI and scrolling; the values derived from SWI and scrolling were not significantly different from each other (Table 1). Regarding intra-observer reproducibility, CBVmax showed greater agreement than nCBVmax in all methods (Table 2) with SWI giving the highest ICC (> 0.9). Inter-observer results (Table 3) were only statistically significant in CBVmax.
Conclusions
This study demonstrates that small vessels could confound perfusion analysis. These findings highlight the importance of using a consistent ROI placement technique which avoids the vessels and thus, limits overestimation. SWI co-registration depicts vessels more clearly and leads to more reproducible results.

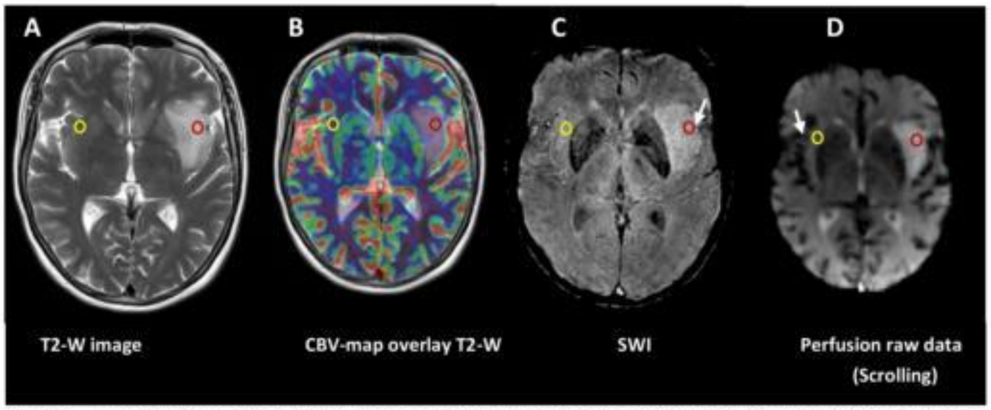

Figure 1 An example of the ROI placement on images of oligodendroglioma WHO grade II **(a)** T2-weighted image for tumor localisation **(b)** CBV map co-registered with T2-weighted image, where the circles point to the ROIs; red circle represents CBVmax, and yellow the contralateral white matter CBV. Adjustment of the ROI based on **(c) SWI** method (vessel highlighted by the white arrow in both sides) and **(d) Scrolling** method (the presence of vessel was found in one side of the brain in this case).

Table 1. Perfusion parameters by method of measurement

	Mdn (IQR)	Pair-wise comparison	
		SWI (p-value)	Scrolling (p-value)
CBV_{max}			
Hot spot	1.45 (1.2)	(.005)	(.018)
SWI	1.14 (0.96)	-	(1.000)
Scrolling	1.06 (0.81)	-	-
$nCBV_{max}$			
Hot spot	1.1 (0.9)	(.036)	(.846)
SWI	0.91 (0.73)	-	(.454)
Scrolling	1.03 (0.66)	-	-

Table 2. Intra-observer reliability and estimated bias with limits of agreement of perfusion analysis methods in diagnosing LGGs.

	Single measure ICC (95%CI)	Average measure ICC (95%CI)	Bias Estimated bias (LoA)
CBV_{max}			
Hot spot	0.75 (0.26,0.93)	0.86 (0.41,0.97)	0.09 (-0.13,0.3)
SWI	0.83 (0.47,0.95)	0.91 (0.64,0.98)	-0.08 (-0.55,0.4)
Scrolling	0.82 (0.43,0.95)	0.9 (0.6,0.98)	-0.03 (-0.35,0.29)
$nCBV_{max}$			
Hot spot	0.74 (0.23,0.93)	0.85 (0.37,0.96)	-0.01 (-0.57,0.54)
SWI	0.68 (0.1,0.91)	0.81 (0.17,0.95)	-0.24 (-0.84,0.36)
Scrolling	0.68 (0.17,0.91)	0.81 (0.29,0.95)	0.14 (-0.33,0.6)

Table 3. Inter-observer reliability and estimated bias with limits of agreement of perfusion analysis methods in diagnosing LGGs.

	Single measure ICC (95%CI)	Average measure ICC (95%CI)	Bias Estimated bias (LoA)
CBV_{max}			
Hot spot	0.75 (0.20,0.95)	0.86 (0.33,0.97)	0.10 (-0.18,0.37)
SWI	0.49 (-0.21,0.87)	0.66 (-0.54,0.93)	0.11 (-0.49,0.71)
Scrolling	0.73 (0.19,0.93)	0.84 (0.33,0.96)	0.08 (-0.26,0.41)
$nCBV_{max}$			
Hot spot	0.24 (-0.40,0.77)	0.39 (-0.13,0.87)	-0.26 (-1.36,0.84)
SWI	0.14 (-0.50,0.73)	0.25 (-2.03,0.84)	-0.26 (-1.42,0.91)
Scrolling	0.3 (-0.51,0.72)	0.23 (-2.13,0.83)	-0.27 (-1.48,0.95)

(Filename: TCT_2207_Figures.jpg)

2995

1:49PM - 1:56PM

Early Detection of Malignant Transformation in Non-Enhancing Low-Grade Gliomas Using Multiparametric MRI

M Bowen[1], M Patel[1], N Davies[1], R Flintham[1], R Wesolowski[1], J Kennedy[1], J Herbert[1], A Zisakis[1], A Kay[1], C Watts[1], V Sawlani[1]
[1]*University Hospitals Birmingham NHS Foundation Trust, Birmingham, West Midlands*

Purpose
New contrast enhancement is the established imaging feature used to identify malignant transformation in low-grade gliomas on conventional MRI. Multiparametric MRI including spectroscopy, diffusion and perfusion imaging is increasingly being utilised to predict malignant transformation in non-enhancing low-grade gliomas in an attempt to improve survival by facilitating earlier treatment.
Materials and Methods
A retrospective review of PACS and online clinical records identified cases over the last 5 years where multiparametric MRI had been used to assess non-enhancing low-grade gliomas prior to a biopsy being obtained. Parameters assessed included the lowest apparent diffusion coefficient (ADC) value, highest relative cerebral blood volume (rCBV) ratio and highest choline:creatine (Cho:Cr) ratio within each glioma.
Results
Of the 26 cases reviewed, 14 were classified as high-grade gliomas and 12 as low-grade gliomas using a combination of biopsy results and follow-up imaging. ADC was significantly lower (mean 930 x 10–6mm2/s vs 1397 x 10–6mm2/s; p=0.001) and rCBV ratio was significantly higher (mean 4.14 vs 1.96; p=0.02) in high-grade gliomas than low-grade gliomas. Whilst high-grade gliomas had a higher Cho:Cr ratio than low-grade gliomas, this was not statistically significant (mean 2.12 vs 1.92; p=0.27). High-grade gliomas generally had two or more positive parameters whereas low-grade gliomas often only had one positive parameter (mean 2.20 vs 0.91; p<0.001) when using cut-off values of ADC <1200 x 10–6mm2/s, rCBV ratio >2 and Cho:Cr ratio >2.
Conclusions
Multiparametric MRI can be used to detect malignant transformation in non-enhancing low-grade gliomas. A low ADC and high rCBV ratio are the best single predictors of malignant transformation. If more than one positive parameter is present then malignant transformation can be predicted with increased confidence.

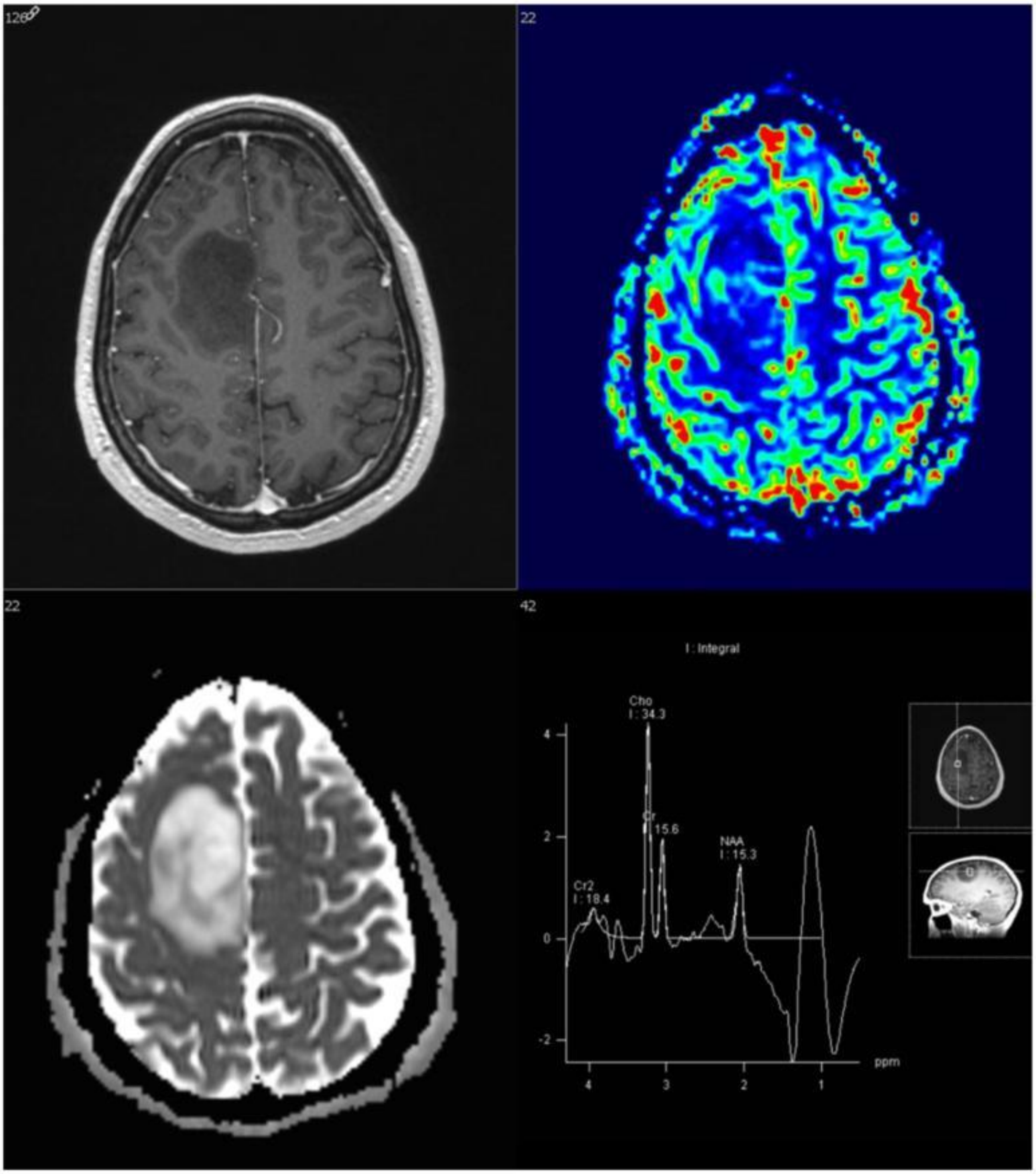

Non-enhancing right frontal glioma demonstrating low ADC, high rCBV ratio and high Cho:Cr ratio in keeping with malignant transformation.

(Filename: TCT_2995_MalignantTransformationGraphic.JPG)

3231

1:56PM - 2:03PM

Evaluation of AI-powered identification of LVOs in a Comprehensive Stroke Center

R Sivan Hoffmann[1], M Saban[2], E Abergel[2], A Eran[3]

[1]Rambam Health Care Campus, Haifa, Israel, [2]Rambam Healthcare Campus, Haifa, Israel, [3]Rambam Healthcare Campus, HAIFA, ISRAEL

Purpose
Large vessel occlusion (LVO) accounts for up to 40% of all acute ischemic strokes (AIS) and is associated with poor outcome. Fast, accurate identification of LVO and notification of relevant specialists is critical to maximizing the benefit of reperfusion therapies. Viz LVO (Viz.ai Inc. San-Francisco, CA, USA) is a medical product leveraging a convolutional neural network designed to detect LVOs in CTA scans and to notify a neurointerventional specialist within minutes via a dedicated mobile application. We report our evaluation experience of Viz LVO at Rambam Medical Center (RMC).
Materials and Methods
Viz LVO was installed and reviewed from May 2018. All CTA scans during that period were auto-forwarded to the system (including non-stroke protocols). Device sensitivity and specificity were evaluated in this non-standard setup. In addition, qualitative system usability feedback was collected.
Results
In 4 months, the system processed 1031 scans. Of those, 32 (3.1%) were positive for distal ICA/M1 occlusions, the target population of the Viz LVO device. Sensitivity and specificity were 84% and 98%, respectively. Six false positives were either due to a mass or trauma patients presenting a large intracerebral hemorrhage, and 2 due to chronic stenosis. After removal of these, the PPV increased to 69%. Median time interval from scan to LVO notification was under 3 minutes. The complete system provides early detection and enables fast, effective decision making in real time between multidisciplinary personnel.
Conclusions
Automatic LVO detection using artificial intelligence, coupled with notification and preliminary viewing via a mobile application has real potential for early, accurate identification of stroke patients, enabling quick decision-making for reperfusion therapies. Our experience evaluating Viz LVO suggests the system might qualify as a decision support tool.

2481

2:03PM - 2:10PM

Overall Survival Prediction of High-Grade Glioma Based on Deep Transfer Learning in Combination with Radiomics Features

w han[1], L Qin[2], C Bay[3], X Chen[1], K Yu[4], X Xu[1], G Young[5]
[1]Brigham and Women's Hospital, Boston, MA, [2]Dana-Farber Cancer Institute, Boston, MA, [3]Brigham and Women's Hospital, Boston, MA, [4]Harvard Medical School, Boston, MA, [5]Brigham and Women's, Boston, MA

Purpose
High grade gliomas(HGG) are the most common primary brain malignancy with low survival rate. Thus, accurate prognosis and survival prediction for glioma patients would provide essential treatment planning. Our study is aiming to predict overall survival of HGG patients based on deep transfer learning techniques in combination with radiomics models
Materials and Methods
We obtained 52 patients of high grade glioma as discovery data set and 128 additional magnetic resonance (MR) imaging scans from The Cancer Genome Atlas (TCGA) as validation data set. In this study, we investigated a model of combining both deep features extracted via transfer learning from Convolutional neural networks (CNNs) and the explicitly-designed hand-crafted features from radiomics models, then we tried three steps of unsupervised and supervised feature reduction methods to reduce the complexity of these features and employed them into elastic net-Cox model.

Results
We extracted 8192 deep features and 348 radiomics features from each cohort. After feature reduction and machine learning based statistical analysis, we were able to distinguish longer-term survivors from shorter-term survivors in 52 patients discovery set ($p < 0.0149$). Then we validated our prediction framework on 128 TCGA cohort ($p < 0.0227$).
Conclusions
Our approach demonstrated this model was able to distinguish longer-term survivors from shorter-term survivors of HGGs with good performance.

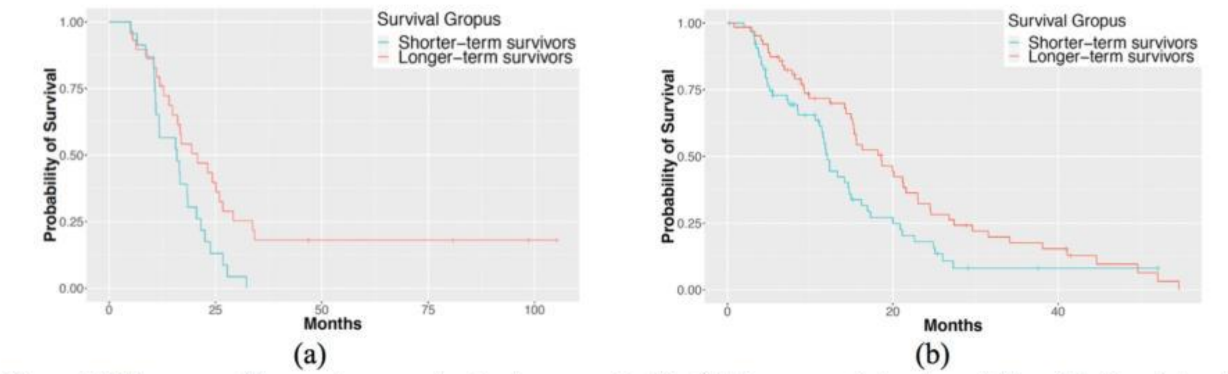

Figure 2 KM curves of longer-term vs shorter-term survival in (a) discovery datasets and (b) validation datasets

(Filename: TCT_2481_figure2.jpg)

2473

2:10PM - 2:17PM

Real-World Performance of Deep-Learning-based System for Intracranial Hemorrhage Detection

S Yune[1], H Lee[1], M Kim[1], S Do[1], S Pomerantz[1], S Kamalian[1], J Romero[1], M Lev[1], R Gonzalez[1]
[1]*Massachusetts General Hospital, Boston, MA*

Purpose
Recently, a few studies reported impressive performance in detection of intracranial pathology by using deep learning. To use such systems in clinical practice, it is critical to know their performance in the real world. Here, we evaluated the applicability of our intracranial hemorrhage (ICH) detection deep-learning system in the clinical setting by comparing the model performance on real-world cases to that on a selected dataset.
Materials and Methods
We trained and validated a deep learning system for ICH detection using a total of 904 cases of 5-mm, nonenhanced head CT scans with exclusion of cases with any history of brain surgery, intracranial tumor, intracranial device placement, skull fracture, or cerebral infarct. Six board-certified neuroradiologists annotated all 2D axial slices according to the presence of ICH based on consensus. For evaluating the model, we retrieved an additional, non-overlapping set of 200 cases - 100 with ICH and 100 without ICH - using the same exclusion criteria with the training dataset. For performance evaluation in the real-world setting, all nonenhanced head CT scans consecutively collected at a single emergency department for three months were obtained. Collected were 2,606 cases including 163 cases with ICH.
Results
Area under the receiver operating curve (AUC) was 0.993 for detecting the presence of ICH in the 200 selected cases with 98.0% sensitivity and 95.0% specificity. The same model achieved AUC of 0.834 on the real-world cases with 87.1% sensitivity and 58.3% specificity at the high sensitivity operating point.
Conclusions
The deep-learning-based ICH detection model achieved lower sensitivity and specificity when tested on

real-world data compared to when tested on the selected data that excluded potentially confusing cases. The performance of deep-learning based systems should be evaluated on real-world data before being used in clinical practice to assist clinicians in interpreting the automated output.

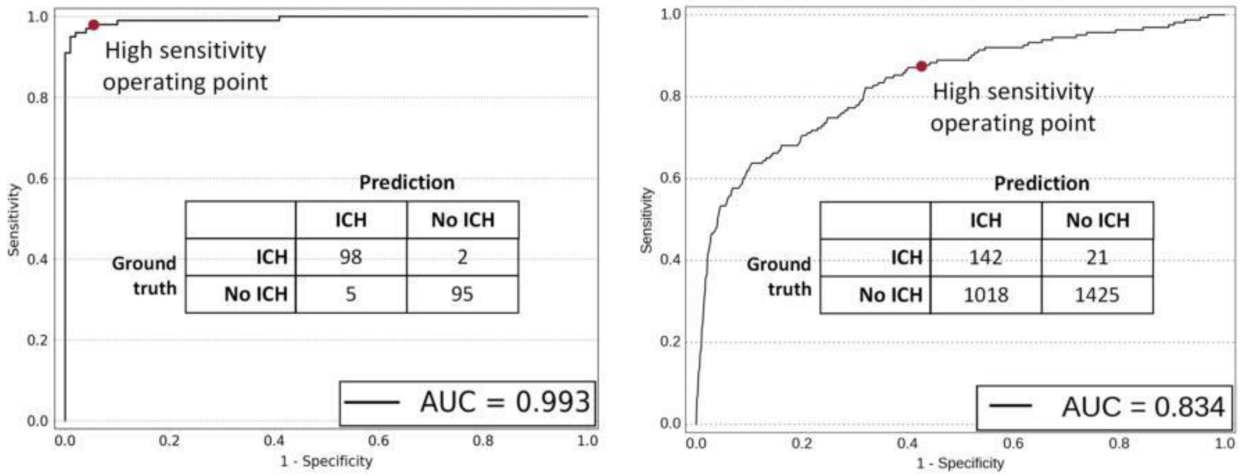

(a) Result on the 200 selected test dataset (b) Result on the real-world test dataset

(Filename: TCT_2473_Figure_300dpi.jpg)

3457

2:17PM - 2:24PM

Resting State Functional Connectivity of the Supplementary Motor Area to Motor and Language Networks in Patients with Brain Tumors

M Gene[1], G BATHLA[2], M Jenabi[1], K Peck[1], A Holodny[3]
[1]Memorial Sloan Kettering Cancer Center, New York, NY, [2]University of Iowa hospitals and Clinics, IOWA CITY, IA, [3]MSKCC, DEMAREST, NJ

Purpose
We studied the resting state functional connectivity (RSFC) of the supplementary motor area (SMA) in patients with brain tumors. The main objective was to compare the SMA subdivisions (pre-SMA, SMA proper, and central SMA [1]) in terms of functional connectivity projected from each region to the motor gyrus and language areas.
Materials and Methods
Fourteen brain tumor patients who underwent both task-based and resting-state fMRI, and who completed language and hand motor paradigms, were identified retrospectively. Task-based fMRI consisted of motor and language paradigms that activated the SMA proper and pre-SMA, respectively. Regions of interest (ROIs) obtained from the task-based fMRI were generated in both areas as well as in the central SMA to produce RSFC maps from each region. Degree of RSFC was measured from each subdivision to both Broca's area (BA) and the motor gyrus.
Results
All patients showed RSFC between the pre-SMA and the language centers as well as RSFC between the SMA proper and motor gyrus. 13/14 patients showed RSFC between the central SMA and both language and motor areas. There was no significant difference between regions in degree of RSFC to BA (pre-SMA, r=0.801; central SMA, r=0.803; SMA proper; r=0.760). However, the pre-SMA showed significantly reduced RSFC to the motor gyrus (r=0.732) compared to the central SMA (r=0.842, p=0.016) and the SMA proper (r=0.883, p=0.00142).
Conclusions
The region between the pre-SMA and SMA proper produces reliable RSFC to the motor gyrus and

language areas in brain tumor patients. This is the first study to examine the RSFC of the central SMA in this patient population. Consequently, our results provide further validation to previous control studies and support the existence of a central portion of the SMA with connectivity to both motor and language networks.

Monday, May 20, 2019
1:00PM - 2:30PM
CT Imaging in Stroke

2507

1:00PM - 1:07PM

Dual-Energy CT Iodine Map ASPECTS in Acute Ischemic Stroke Setting

A Honarmand[1], S Rotenberg[1], R Hayeri[1], F Brown[1], M Brooks[1], C Pedersen[1], O Teytelboym[1], J Mackey[1]
[1]*Mercy Catholic Medical Center, Darby, PA*

Purpose
Alberta Stroke Program Early CT Score (ASPECTS) has been widely used in acute ischemic stroke (AIS) patients for disease severity estimation, patient selection for reperfusion therapy, estimation of the response to recanalization, and prediction of final functional outcome. Although ASPECTS has been originally utilized in baseline routine non-contrast CT (NECT) studies, other modalities have been incorporated in using ASPECTS as well including DWI and CTA source image ASPECTS. Dual-Energy (DE) CT has provided potential helpful opportunities for simultaneous evaluation of cerebral parenchyma and vasculature in a single study which can potentially save time and reduce radiation exposure. We embarked on this study to evaluate the utilization of DECT angiography in AIS setting and compared NECT, DE virtual non-contrast (VNC), and DE Iodine Map (IMP) ASPECTS.
Materials and Methods
This is an IRB approved retrospective chart review of randomly selected patients presenting with AIS (NIHSS score >6) for whom stroke alert was called and NECT and brain DECT angiography were performed, consecutively. Two blinded observers assigned ASPECTS to NECT, VNC, and IMP images randomly. Demographic, presence of MRA/CTA verified vessel occlusion, presence of CT/MRI verified acute stroke, and effective dose of NECT and DECT images were obtained subsequently. Inter-observer agreement was evaluated by intra-class correlation coefficient (ICC). Appropriate parametric and nonparametric statistical tests were utilized. Two-tailed P value of <0.05 was considered to be significant.
Results
This is an ongoing study. Twenty patients (13F/7M, mean age: 63.6 years, SD ± 14.3) were recruited. Anterior circulation stroke with large or small vessel occlusions were present in 6 and 7 patient, respectively. Inter-observer agreement was good (ICC=0.7). Scores assigned by one observer were selected for data analysis. No significant difference was observed between NECT versus VNC ASPECTS (P=0.6) or NECT versus IMP ASPECTS (P=0.7). Both VNC and IMP ASPECTS correlated with NECT ASPECTS (P<.001), however IMP demonstrated stronger correlation compared to VNC (τ=0.8 versus τ= 0.6, respectively). Mean effective dose was significantly lower in DECT compared to NECT (0.7 mSV versus 1.6 mSV, P<0.001).
Conclusions
DECT provides exclusive opportunities in AIS setting for concurrent evaluation of parenchymal infarction and vascular occlusion in a single study. IMP ASPECTS can be utilized as an equivalent to routine NECT ASPECTS in DECT angiography studies.

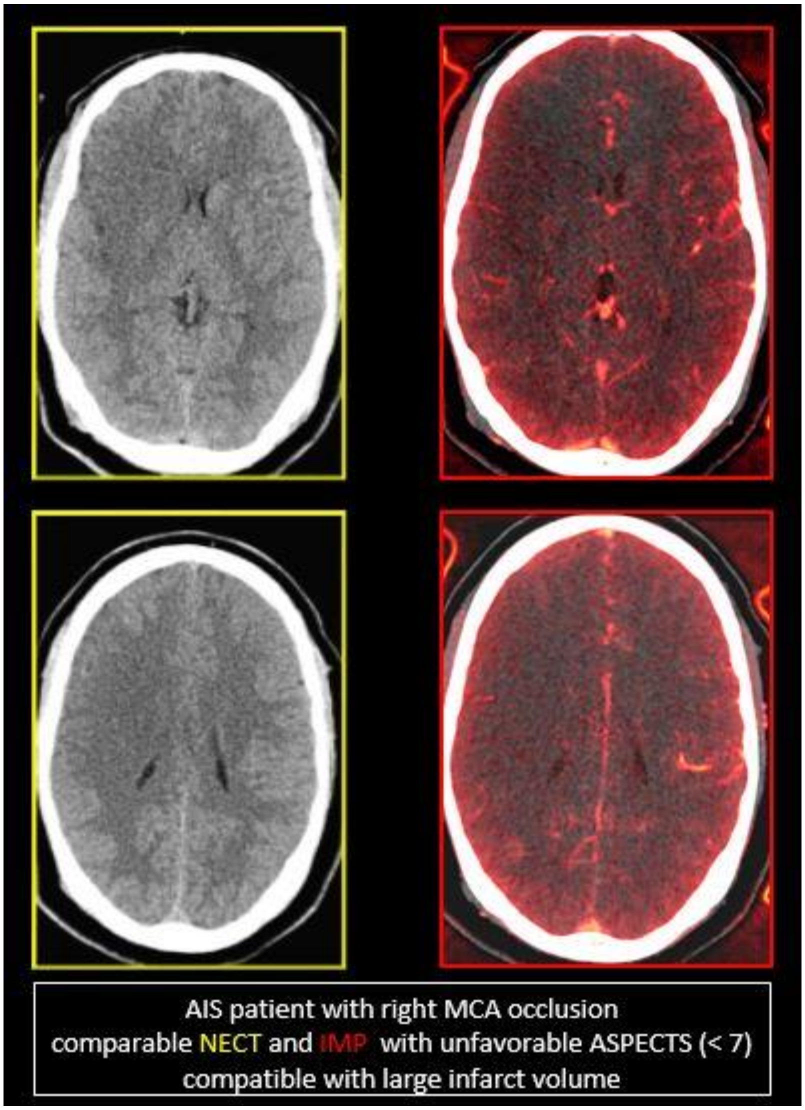

(Filename: TCT_2507_ASPECTS.JPG)

2370

1:07PM - 1:14PM

Accuracy of CT Perfusion-Defined Core in Large Vessel Occlusion Ischemic Strokes: A Stroke Registry Real World Experience

J Vidovich[1], S Voleti[1], B Corcoran[1], B Zhang[2], V Khandwala[1], E Mistry[1], P Khatri[3], S Gangatirkar[1], Z Smith[1], A Vagal[4]
[1]University of Cincinnati College of Medicine, Cincinnati, OH, [2]Cincinnati Children's Hospital Medical Center, Cincinnati, OH, [3]University Of Cincinnati Medical Center, cincinnati, OH, [4]UNIV. HOSP./UNIV. CINCINNATI COLLEGE OF MEDICINE, CINCINNATI, OH

Purpose
Recent endovascular trials have spurred a paradigm shift toward use of CT perfusion (CTP) for decision-making in acute ischemic stroke. The optimal relative cerebral blood flow (rCBF) threshold to estimate final infarct volume, however, remains uncertain. We compared the accuracy of CTP-defined cores at

various rCBF thresholds to predict final infarct volumes for large vessel occlusions (LVO) in a real-world setting.

Materials and Methods

Utilizing a single-institutional, retrospective registry of patients with acute LVOs (ICA, M1, and M2 occlusions) between May 2016 and May 2018, we included patients who underwent CTP within 6-24 hours of stroke onset and subsequently achieved successful reperfusion (TICI 2b/3). We recorded RAPID CTP cores at relative CBF thresholds of <30%, <34%, and <38%. Final infarct volumes (FIV) were calculated using follow up MRI and CT, obtained within 72 hours after stroke onset.

Results

Among the 161 patients in our registry who underwent CTP, 39 patients met our inclusion criteria. Table 1 displays characteristics of the group. At rCBF <30%, the mean CTP core was 23.8 ml (SD 20.8) and the mean difference between core and FIV was -29.3 ml (p= 0.001). At rCBF <34% the mean CTP core was 34.4 ml (SD 26.3), and the mean difference between core and FIV was -21.9 ml (p= 0.018). At rCBF <38%, the mean CTP core was 43.2 ml (SD 31.5), and the mean difference between core and FIV was -13.0 ml (p= 0.157). Correlation between CTP core volumes and FIVs at each threshold were as follows: rCBF<30%, r=0.38(p<0.018); rCBF<34%, r=0.35(p<0.038); and rCBF<38%, r=0.34, (p<0.043). Table 2 summarizes these results. Figure 1 presents the agreement between CTP-derived core volumes and FIVs.

Conclusions

Our real practice experience demonstrates that CTP significantly underestimates final infarct volume. With increased utilization of CTP in clinical decision making, future work is needed to improve CTP accuracy.

Table 1. Characteristics of study group

Variables	Total n = 39
Age (y), median (min - max)	65 (22-96)
Female, no (%)	18 (46.25%)
Atrial fibrillation, no (%)	11 (28.21%)
History of congestive heart failure, no. (%)	12 (30.77%)
History of hyperlipidemia, no. (%)	20 (51.28%)
History of hypertension, no. (%)	28 (71.79%)
Median NIH stroke score	16
Median time from last known well to CTP(hours)	10.6 (IQR 8.3-13.9)
M2 occlusions	8
M1 occlusions	19
ICA occlusions	12
Median final infarct volume (FIV)	34.5 ml (IQR 13.9-74.9)

Table 2. Comparison of CTP core and FIV at each rCBF threshold

CTP rCBF Threshold	Baseline CTP core mean ± SD (mL)	Difference between CTP predicted core and final infarct volume (mL)	Correlation of CTP core volume with FIV (r)
<30%	23.8±20.8	-29.3 (p = 0.001)	0.38 (p = 0.018)
<34%	34.4±26.3	-21.9 (p = 0.018)	0.35 (p = 0.038)
<38%	43.2±31.5	-13.0 (p = 0.157)	0.34 (p = 0.043)

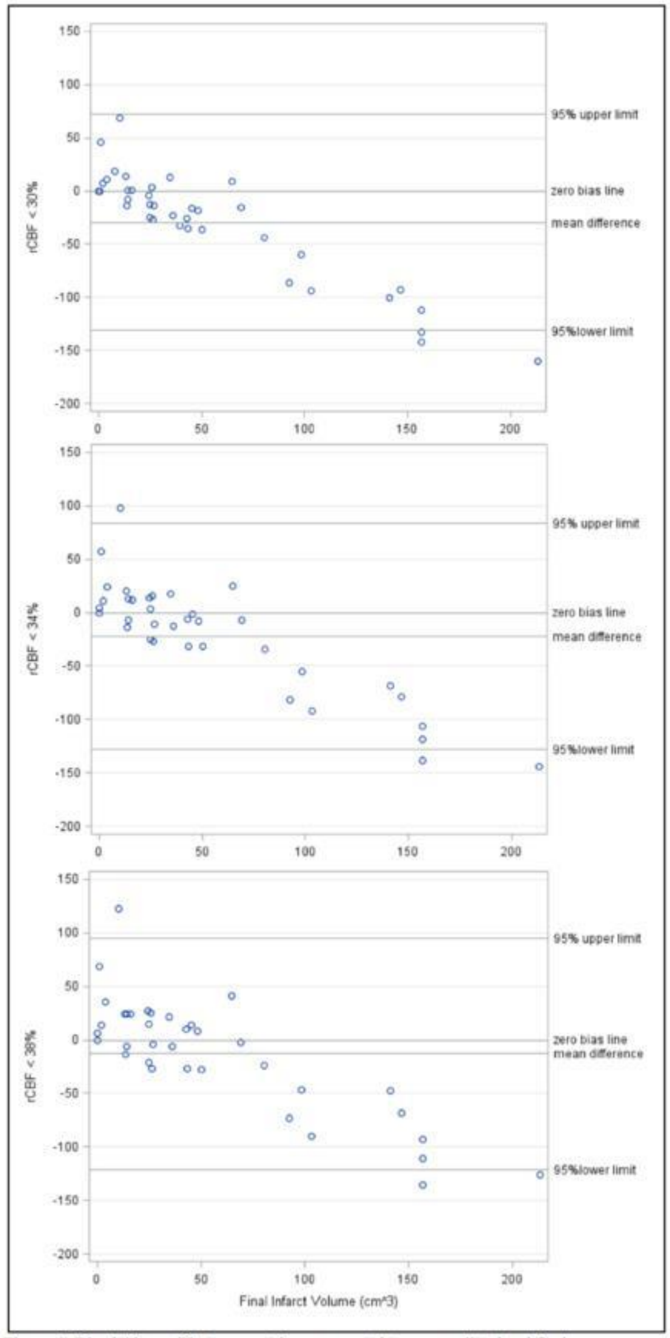

Figure 1. Bland-Altman Plots representing agreement between predicted and final infarct core volumes at rCBF <30%, <34%, and <38%.

(Filename: TCT_2370_LVOVolumesASNRGraphic.jpg)

2495

1:14PM - 1:21PM

Achieving Comparable Perfusion Results across Vendors: The Next Step in Standardizing Stroke Care

G BATHLA[1], B Policeni[2], E Klotz[3], M Juergens[3], C Derdeyn[4]
[1]University of Iowa hospitals and Clinics, IOWA CITY, IA, [2]University Of Iowa, Iowa City, IA, [3]Siemens Healthineers, Forchheim, Germany, [4]University of Iowa, St. Louis, MO

Purpose
We compared the outcomes of two commercial perfusion software packages to determine whether comparable Computed tomographic perfusion (CTP) results could be attained with modified post-processing.
Materials and Methods
Post IRB approval, 30 consecutive patients with suspected stroke were retrospectively selected. Data was acquired using the CTP protocol recommended by RAPID. One patient was excluded from the final analysis due to artifacts. Both software packages performed post-processing using the vendor specified parameters. Vendor recommended thresholds for RAPID are defined as non-viable tissue (NVT) with rCBF < 30%, and hypoperfused volume as tMax > 6s. The Syngo.via software was run at different rCBF thresholds between 20-30%, with increments of 2%.
Results
Mean patient age was 70.8 years. With RAPID, the mean core infarct volume was 43 cc and a mean hypoperfusion volume of 88 cc. Using Syngo.via at the predefined setting (NVT as rCBF<30%), the corresponding values were 66 cc and 95 cc respectively. Comparable results were achieved with rCBF threshold of 20%, giving a mean core of 43 cc and hypoperfusion volume of 88 cc. A Bland-Altmann analysis showed no statistical difference in 25 cases (86%). When analyzed using DEFUSE III definitions as a 'go-versus-no go' for mechanical thrombectomy, a concordant result was obtained in 27/29 cases (93%), with one false negative for both RAPID and syngo.via respectively. However, both cases involved M2 occlusions that would not be eligible for thrombectomy with either DEFUSE III or DAWN criteria.
Conclusions
A high concordance, both in terms of NVT and hypoperfusion volumes as well as therapeutic decision making is feasible between different CTP post-processing programs despite implementational differences and may not be a time or resource intensive task.

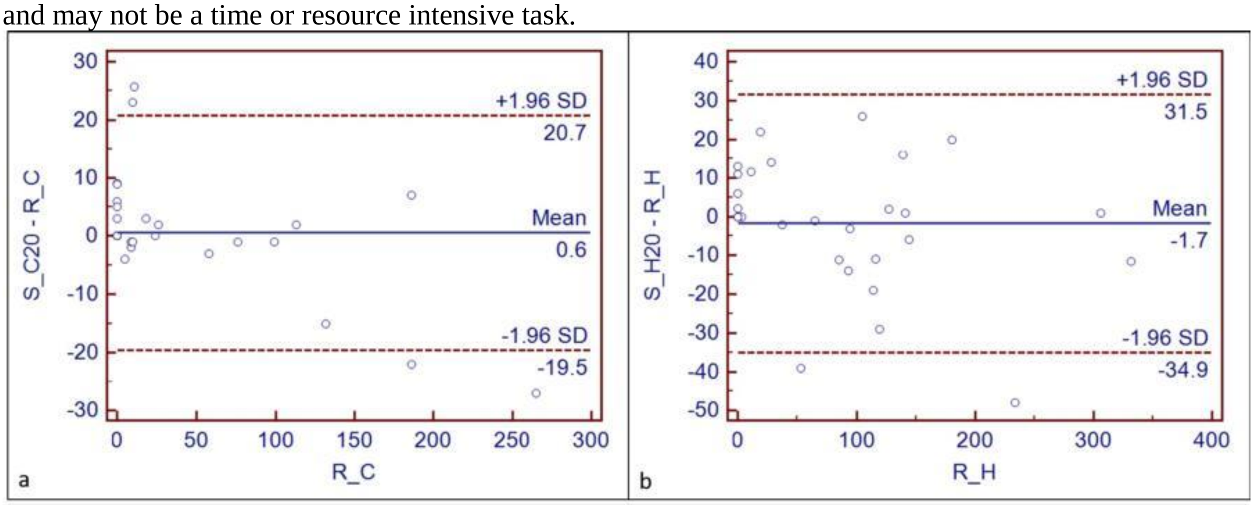

Bland-Altman plots for the NVT (a) and hypoperfusion (b) show correlation between the two software packages

(Filename: TCT_2495_Fig-1.jpg)

2686

1:21PM - 1:28PM

Dual Energy Computed Tomography (DECT) Evaluation of Dense Intracranial Artery Sign

S Mathur[1], P Mukherjee[1], J Walsh[1], N Murray[1], S Nicolaou[2]
[1]University of British Columbia, Vancouver, BC, [2]Vancouver General Hospital, Vancouver, British Columbia

Purpose

We aimed to determine the usefulness of dual energy computed tomography (DECT) technique in the evaluation of dense intracranial artery sign on non-contrast computed tomography (NCCT) head by using computed tomography angiography (CTA) as the gold standard.

Materials and Methods

In this retrospective study, consecutive NCCT head with CTA head studies performed using DECT technique in the last 10 years formed the study population. Two radiologists blinded to the findings on other imaging examinations reviewed this data starting from the most recent studies and identified asymmetrically dense MCA or dense basilar artery (BA) on NCCT head studies in consensus. Reader confidence before and after DECT interrogation of the NCCT study was recorded independently using likert scale. The readers reviewed both polychromatic and monoenergetic data sets. The readers were asked to note imaging features useful for detection of intra-arterial clot. Another radiologist correlated these findings with the gold-standard CTA. The review of NCCT studies was performed until 30 cases positive and 30 cases negative for MCA occlusion, and 5 cases positive and 10 cases negative for BA occlusion on CTA were found.

Results

There was significant improvement in the reader confidence in evaluation of intracranial dense artery sign ($p < 0.05$) after DECT interrogation was performed. Relatively high attenuation in the arterial lumen on high kV was found to be the useful imaging feature by the readers for detection of clot on DECT.

Conclusions

Assessment of the dense intracranial artery sign on DECT increases confidence of interpretation.

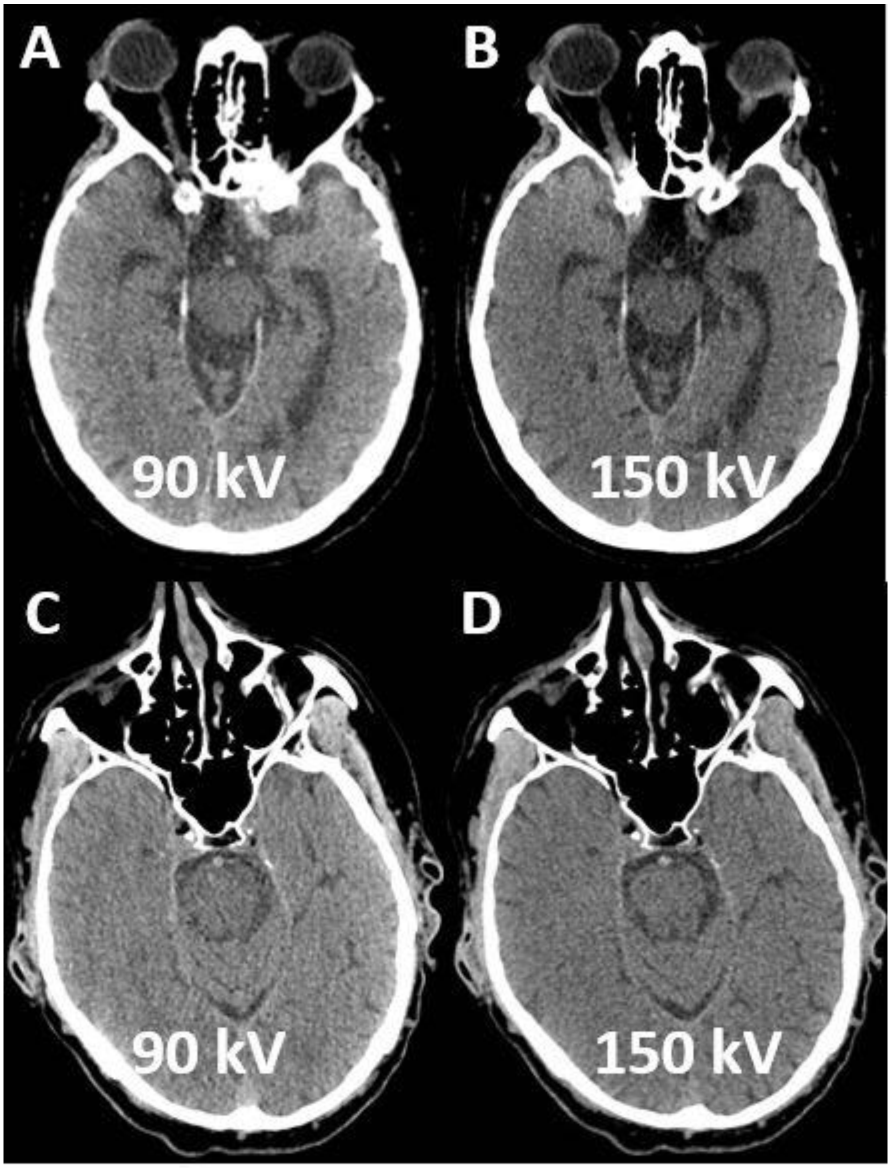

Figure 1. A & B: Relatively lower attenuation of basilar artery (BA) lumen on high kV on dual energy NCCT. CTA (not shown) was negative for BA clot. C & D: Relatively higher attenuation of basilar artery lumen on high kV on dual energy NCCT. CTA (not shown) was positive for BA clot.

(Filename: TCT_2686_DECT.JPG)

2323

1:28PM - 1:35PM

Iodine Staining on Post Thrombectomy Dual Energy Head CT: What is the Fate of the Iodine Stained Tissue?

S Thornton[1], G Avey[1]
[1]*UNIVERSITY OF WISCONSIN, MADISON, WI*

Purpose
There are limited data regarding the association between iodine staining and hemorrhagic conversion, the fate of the iodine stained tissue, and overall patient outcome.
Materials and Methods
This IRB approved retrospective review included all thrombectomy patients with a subsequent DECT from January 1st 2017 to December 31, 2017. The DECT was evaluated to determine whether iodine staining, hemorrhage (petechial vs. mass-like), or both were present. Software image fusion of the post treatment DECT and delayed imaging was performed to analyze the volume of iodine staining, hemorrhage and infarct size. The volume of iodine stained tissue, infarcted tissue and the overlap between the iodine stained tissue and infarct were recorded. Other potential associated variables were recorded, including the NIH Stroke Scale Score, the location of the stained tissue (cortical, deep or both), the occluded vessel, TICI score, time between the procedure and DECT, type of anesthesia, 90 day Modified Rankin Score, and use of a thrombolytic agent.
Results
69 patients met inclusion criteria. Iodine staining was present in the majority of cases (62/69, 89.8%). Mass like hemorrhage was rare (2/69, 2.9%), but petechial hemorrhage was found in 14/69 patients (20.2%). 47 patients had imaging follow-up suitable for determining eventual infarct size. The mean eventual infarct volume was 46.8 ml (range 0-197.3 ml). There were 53 independent locations of iodine staining, of which 30 contained infarcted tissue (57%). Within these 30 iodine stained lesions with associated infarct, 49.4% of the volume of the iodine stained tissue went on to infarct. There was a significant difference in the iodine concentration between iodine stained tissue which did and did not go on to infarct (10.9 vs 8.2 mg/dL, $p<0.01$).
Conclusions
Iodine staining is common following embolectomy. There is incomplete correlation between the volume of iodine stained tissue and infarcted tissue.

Figure 1. Fusion of the post thrombectomy DECT with iodine staining (Io), infarcted tissue on the diffusion weighted image (DWI) from the follow-up MRI (In), and the overlapping tissue (Ov).

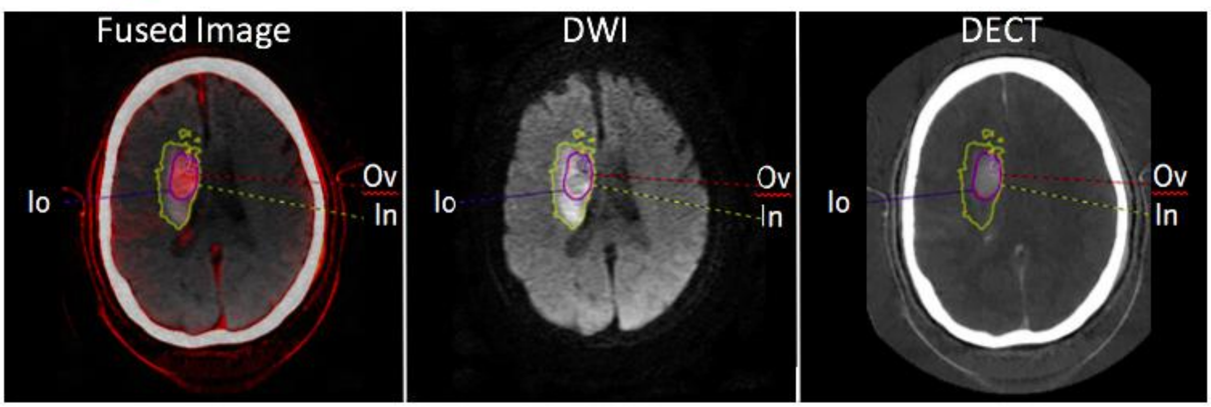

(Filename: TCT_2323_Picture1.jpg)

2719

1:35PM - 1:42PM

Changes in Automatically Thresholded CT Perfusion Volumes with Alterations in CT Perfusion Technique

G Avey[1], A Kuner[2], T Szczykutowicz[3]

[1]*UNIVERSITY OF WISCONSIN, MADISON, WI,* [2]*University of Wisconsin Hospitals and Clinics, Madison, WI,* [3]*University of Wisconsin School of Medicine and Public Health, Madison, WI*

Purpose
Automatically thresholded CT perfusion volumes have been used as a selection criterion for endovascular stroke therapy. There are large variations in perfusion protocols, and little is known regarding how changes in perfusion parameters affect these volumes.
Materials and Methods
CT perfusion examinations with large vessel occlusion were enrolled from 1/1/2017 through 8/1/2017. 43 exams met inclusion criteria. The reference protocol included a 40 ml injection of contrast (5 ml/s), a sampling rate of 3.2 seconds, and duration of 60 seconds. Alternative protocols were constructed, including sampling at ½ and 1/3rd rates, examinations truncated at 45 seconds, and increasing the sampling interval after 45. The rCBF <30% and Tmax > 6 second volumes were recorded. Clinical agreement was defined as a less than 10 ml or 10% change in rCBF and Tmax.
Results
rCBF volumes were consistent, with a 98% clinical agreement for exams truncated at 45 second. There was complete CBF agreement for exams with dynamic sampling after 45 seconds. Examinations sampled at ½ and 1/3rd rates showed rCBF clinical agreement of 91% and 84%. rCBF volumes were statistically different for the 5.6 second sampling rate (p=0.01). Tmax agreement was 70% for exams truncated at 45 seconds, increasing to 88% and 98% with dynamic sampling. Examinations sampled at ½ and 1/3rd rates showed poor Tmax agreement with 67% and 16% clinical agreement. Tmax volumes were statistically different for sparse sampling intervals (p<0.01), as well as the examination sampled every 8.4 seconds after 45 seconds (p=0.03).
Conclusions
Thresholded rCBF volume is consistent across variations in perfusion technique. Close adherence to recommended perfusion sampling rate and duration is required to maintain Tmax volumes. Dynamic perfusion sampling after 45 seconds remains a viable strategy to reduce CT dose while maintaining unchanged perfusion volumes.

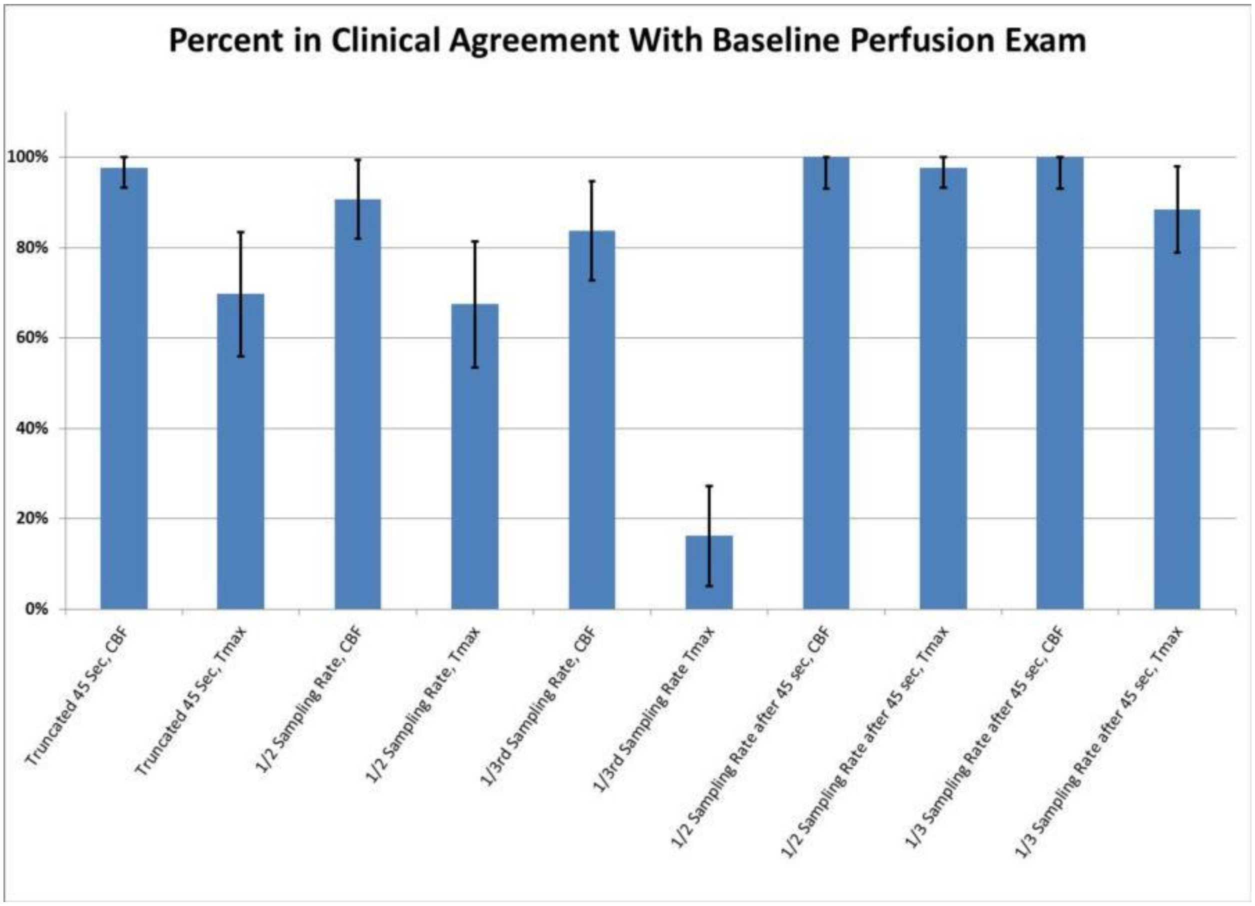

(Filename: TCT_2719_ASNRperfusion.jpg)

2956

1:42PM - 1:48PM

Low Dose Computed Tomographic Angiography (CTA) for Evaluation of Cerebral Vasculature

N Soni[1], S Deo[2], S Priya[2], G BATHLA[3]
[1]UIHC, iowa, IA, [2]UIHC, iowa city, IA, [3]University of Iowa hospitals and Clinics, IOWA CITY, IA

Purpose
CTA of cerebral vasculature is often performed in acute settings with no prior renal function information. Recent advancement in image acquisition and iterative reconstruction (IR) techniques have allowed scanning using lower tube voltage and radiation doses without image compromise. The authors present a subjective and objective comparison of image quality between different scanners, one using Advanced Modeled IR algorithm (ADMIRE) and normal contrast dose and the other using Sonogram Affirmed IR algorithm (SAFIRE), albeit with a low contrast dose.
Materials and Methods
We compared image quality of 15 cerebral CTA studies performed using low dose [LD] (50cc) contrast at 192 detector-row dual source scanner (SOMATOM Force) with 15 control performed at different scanner (SOMATOM definition) using normal dose contrast (100cc). Differences between the two groups were compared using the Mann-Whitney U test and $p<0.05$ was considered significant.
Results
Table-1 summarizes the patient characteristics, contrast and radiation dose parameters for both Groups. Contrast-to-noise (CNR) and signal-to-noise (SNR) ratios were measured at mid M1 segment of the

middle cerebral artery (MCA) on each side and the mid-basilar artery in both groups and found no significant difference (Table-2). Subjective image quality was measured using a semi-quantitative Likert-like scale in 17 different vascular segments (bilateral ICA'S, M1-MCA's, A1-ACA's, P1-PCA's, A2/A3 ACA, M2/M3 MCA, P2/P3 PCA, V4-VA segments and the basilar artery) and found no significant difference between the two groups.
Conclusions
The authors present a novel CTA technique utilizing low contrast dose yet maintaining diagnostic image quality. Previous studies have shown utility of newer IR techniques in reducing radiation dose. Our preliminary analysis also shows that the contrast dose could potentially be halved with next generation IR algorithms.

2748

1:48PM - 1:55PM

Maximum Intensity Projections from CTA are a better Predictor of Final Infarct Volume on MRI than CT Perfusion

V Ivanovic[1], Y Chang[1], R Bhadelia[1], X Yunyun[1], M Selim[2]
[1]Beth Israel Deaconess Medical Center, Boston, MA, [2]Beth Israel Deaconess Medical Center, Harvard Medical School, Boston, MA

Purpose
CT Perfusion (CTP) with fully automated analysis and MRI diffusion images have been used to estimate infarct volume in management of acute ischemic stroke. We hypothesized that maximum intensity projections (MIPs) from CTA source data may depict infarct size better than CTP. Our purpose was to correlate estimated infarct volume (EIV) from CTP, CTA-source and CTA-MIPs images with MRI-DWI demonstrated final infarct volume (FIV).
Materials and Methods
Sixty three consecutive patients with acute ischemic stroke undergoing CTA, CTP and MRI of the head were reviewed. CTA-source images (1.25-mm thickness, 0.25-mm overlap), CTA-MIPs (5-mm thickness, 4.5-mm overlap). CTP was processed on a commercially available, fully automated platform. EIV were assessed on CTA-source, CTA-MIPs and CTP maps; and FIV were assessed on MRI-DWI using ASPECTS. All ASPECT scores within each category were analyzed during separate sessions and were blinded to each other. Actual infarct volumes in milliliters (ml) were calculated using an independent workstation based on MRI-DWI data. Spearman's correlation was used to assess relationships between FIV on MRI-DWI with EIV obtained from CTA-source, CTA-MIPs and CTP. Logistic regression was used to test which of the CT methods was a better predictor of small or large infarcts (FIV >20-ml).
Results
Spearman's correlation between MRI-DWI FIV and CTA-source was (R=0.709), CTA-MIPs (R=0.875) and CTP (R=0.601). Additionally, MRI-DWI detected total of 14 infarcts outside MCA vascular distribution of which CTA- MIPs detected 7, CTA source images 5, and CTP 2 infarcts. Multiple regressions showed CTA-MIPs to be an independent predictor of MRI infarct volume >20 ml (odds ratio: 0.517, 95% confidence interval: 0.362-0.737).
Conclusions
EIV obtained from CTA-MIPs is an independent predictor and had strongest correlation with FIV on DWI. Our results suggest that CTA-MIPs ASPECT could be a valuable alternative to CTP in imaging evaluation of patients presenting with acute ischemic stroke.

2551

1:55PM - 2:02PM

Outcome in Patients with Contrast Staining After Endovascular Treatment for Acute Ischemic Stroke

E Portela de Oliveira[1], S Chakraborty[2], M Patel[3], S Finitsis[4], D Iancu[2]
[1]University of Ottawa - The Ottawa Hospital, Ottawa, Ontario, [2]The Ottawa Hospital, Ottawa, Ontario, [3]University of Ottawa, Ottawa , Ontario, [4]Aristotle University of Thessaloniki, Thessaloniki , Greece

Purpose
Hyperdense cerebral areas are commonly seen on head CT performed early after endovascular treatment and may be secondary to contrast extravasation or hemorrhage. The incidence and prognosis of these post interventional cerebral hyperdensities (PCHDs) on CT have been reported recently in few articles, however the imaging evolution and clinical significance is not completely understood. The goal of this study is to evaluate the imaging pattern of PCHDs in patients who underwent endovascular treatment for acute ischemic stroke in the last 7 years in our institution and their clinical outcome.
Materials and Methods
We retrospectively review a prospectively maintained database of patients who underwent Digital Subtraction Angiography (DSA) and/or interventional for treatment of acute ischemic stroke (AIS) over past 7-year period in our institution. PACS database search was performed for "contrast staining" to include any patients where hyperdensities were seen in acute stroke patients. Inclusion criteria for the study was acute stroke patients with a head CT examination within 72 hours following DSA. Information regarding patients' demographics, method of stroke intervention (intravenous rtPA, intraarterial rtPA, mechanical thrombectomy, complications and final outcome were obtained from electronic records (vOacis). Clinical evolution was evaluated by the preprocedural National Institutes of Health Stroke Scale (NIHSS) and Modified Rankin Scale for Neurologic Disability (mRS) scores and mRS score at discharge.
Results
Of approximately 750 thrombectomies performed, 29 patients met the inclusion criteria. The mean age was 66 years old (34-102); 17 (58,6%) females and 12 (41,4%) males; 17 (58,6%) patients had successful recanalization of the artery involved, 7 (24,1%) had partial recanalization and 5 (17,2%) unsuccessful recanalization. Average ASPECT was considered 8.3. Average NIHSS and MRS pre-procedure was 15 and 1, respectively. 10 patients received intra-arterial tPA and 21 received it intravenous, (6 patients received both). 23 patients (79,3%) had CT and/or MRI for follow up in less than 72h, 17 (58,6%) was considered essentially contrast staining and 6 (20%) a combination of contrast staining and hemorrhage. Overall mortality was about 20% (6 patients) and average mRS post procedure was 4.
Conclusions
Patients with AIS who underwent DSA for mechanical thrombectomies and presented contrast staining in the follow up CT demonstrated high mortality and high mRS post procedure.

2357

2:02PM - 2:09PM

Portable CT Head Exams May Overestimate Findings of Cerebral Edema in Neurosurgical ICU Patients.

V Sundaram[1], M Cedillo[2], C Liu[3], K Nael[4], B Delman[5], P Belani[6], N Dangayach[1], A Doshi[7]
[1]ICAHN SCHOOL OF MEDICINE AT MOUNT SINAI, NEW YORK, NY, [2]Mount Sinai Hospital, New York, NY, [3]Icahn School of Medicine at Mount Sinai, New York City, NY, [4]ICAHN SCHOOL OF MEDICINE AT MOUNT SINAI HOSPITAL, NEW YORK, NY, [5]Icahn School of Medicine at Mount Sinai, New York, NY, [6]MT. SINAI HOSPITAL, NEW YORK, NY, [7]MOUNT SINAI ICAHN SCHOOL OF MEDICINE, NEW YORK, NY

Purpose
Neurosurgical ICU (NSICU) patients are often not stable to leave their unit and therefore, when available, may undergo portable CT (PCT) head examinations for monitoring acute and chronic developments. PCT

scanners may produce artifacts and reduced quality of images, potentially resulting in overestimation of radiologic findings such as cerebral edema, to the detriment of the radiologist, ordering clinicians, and the patient. Recent studies demonstrate that PCT scanners result in poorer quality studies compared with fixed scanners [1], however to date no study has correlated findings such as cerebral edema with the clinical and laboratory data of a patient. The purpose of this study is to retrospectively review CT head examinations using PCT scanners to determine accuracy of findings of cerebral edema in comparison to clinical history and laboratory data. A better understanding of the benefits and risks of PCT head examinations will allow the radiologist and the ordering clinician to more safely judge the validity of potential findings in regards to patient management.

Materials and Methods

For our single institution retrospective study, after IRB approval, query of our hospital database yielded 200 portable CT head exams from 10/2014 to the 12/2017. These exams were cross-referenced with ICP measurements obtained by external ventricular drain, yielding 18 portable CT head exams with documented elevated ICP (20 mm Hg or above) on the day of the exam, and 27 exams with normal ICP. Three board-certified neuroradiology attendings then individually performed blind randomized re-reads of the 45 exams, answering scaled questions (no, maybe or yes) on the presence of the following categories: sulcal effacement; ventricular effacement; crowding of cisternal structures; presence of cerebral edema. At a later date, the three neuroradiologists also performed a consensus re-read of the 45 exams, answering the same scaled questions. Statistical analysis was performed using kappa and intraclass correlation. Sensitivity and specificity measures for detection of cerebral edema were calculated from the consensus read using ICP data as the reference of standard.

Results

Using data from the individual neuroradiologist re-reads, interobserver reliability was only 'fair' (0.4-0.59) amongst the three readers for presence of sulcal effacement and ventricular effacement, and was 'poor' (<0.4) for presence of crowding of cisternal structures and cerebral edema. Kappa with 95% CI were as follows: sulcal effacement kappa of 0.56 (95% CI: 0.40 to 0.70); ventricular effacement kappa of 0.53 (95% CI: 0.36 to 0.67); crowding of cisternal structures kappa of 0.39 (95% CI: 0.22 to 0.56); cerebral edema kappa of 0.40 (95% CI: 0.22 to 0.57). Using the consensus read data, the sensitivity for correctly detecting cerebral edema, with elevated ICP as the reference standard, was best for sulcal effacement, at 71%. However, the specificity was only 62%. For ventricular effacement, the sensitivity and specificity for detecting cerebral edema was 61% and 82% respectively. For crowding of cisternal structures, the sensitivity and specificity for detecting cerebral edema was 60% and 90% respectively. Overall, when the neuroradiologists considered the above three categories together in their consensus read when determining whether the patient had cerebral edema due to elevated ICP, the consensus read performed poorly, with a sensitivity of 56% and a specificity of 69%.

Conclusions

Portable CT head exams had poor interobserver reliability for calling presence of cerebral edema. Of the three categories used to determine presence of cerebral edema, the presence of sulcal effacement performed the best. However, during the consensus read, the neuroradiologists considered all factors together to make a judgment on the presence of cerebral edema. Overall, the consensus read demonstrated poor sensitivity and specificity for presence of cerebral edema in patients with elevated ICP. Portable CT head exams may therefore overestimate the presence of cerebral edema in NSICU patients, an important consideration for both the interpreting radiologist and the ordering clinician.

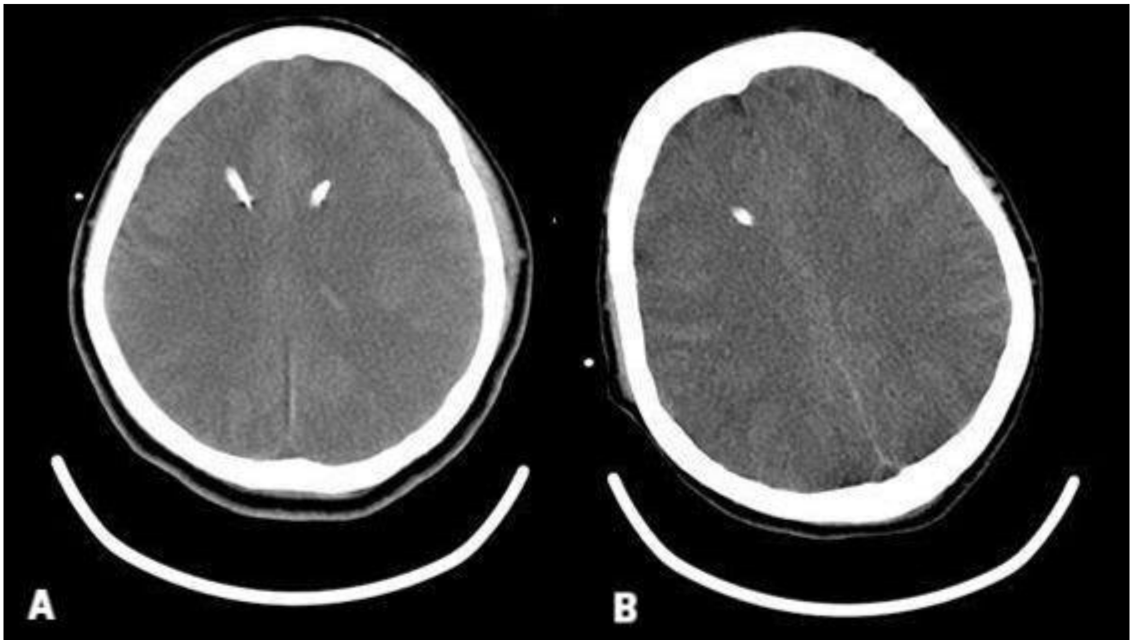

Figure 1A: Axial image from Portable CT Head Exam in patient with elevated ICP to 25 mm Hg and Glasgow Coma Scale between 3 and 5.
Figure 1B: Axial image from Portable CT Head Exam in patient with normal ICP to 7 mm Hg and Glasgow Coma Scale between 7 and 11.

(Filename: TCT_2357_Figure1.jpg)

2213

2:09PM - 2:16PM

Reconstruction of Perfusion CT Data in Acute Stroke Demonstrates High Diagnostic Yield for MCA M2 Occlusions

A Bryant[1], G BATHLA[2], B Policeni[3], C Derdeyn[4], K Limaye[1]
[1]University of Iowa, Iowa City, IA, [2]University of Iowa hospitals and Clinics, IOWA CITY, IA, [3]University Of Iowa, Iowa City, IA, [4]University of Iowa, St. Louis, MO

Purpose
CT angiography (CTA) reconstruction derived from CT perfusion (CTP) data has been proposed for detection of large vessel occlusion (LVO) in acute stroke patients. This technique obviates the need for an additional single-phase CTA, saving time and additional iodinated contrast. Previous studies have validated this technique for proximal LVO confined to M1 MCA. With advances in stroke management, the previously considered "distal" branches of MCA like M2 segments are now considered amenable to therapy. In this study, we test reliability of CTP-derived CTA for identifying M2 MCA occlusions.
Materials and Methods
A total of 34 patients who underwent CTP at presentation and had diagnosis of M2 occlusion confirmed with follow-up diagnostic cerebral angiograms (DSA) were retrospectively selected from our stroke database. An additional 10 patients with normal CTP and 24-hour follow-up MRI were randomized and included in interpretation as a control. CT perfusion protocol used 40 cc iodinated contrast and 60 seconds acquisition time, with slice thickness of 0.6 mm (perfusion images reconstructed at 10 mm). CTA data was reprocessed at 1 mm slice thickness. Three radiologists with differing levels of experience (1 neuroradiology fellow, 1 fellowship-trained attending, and 1 CAQ-certified attending) reviewed the

randomized CTP exams while blinded to presence or absence of occlusion. Scans were scored for subjective CTA image quality of the M1/M2 segments, as well as for presence and site of occlusion. Results were compared to the follow-up DSA read by an independent neurointerventionalist for cases that underwent endovascular intervention. Observed probability of agreement was computed to measure agreement.

Results

The image quality observed agreement for M1/M2 segments ranged from 96% (95% CI: 92-99%) for M1 segments to 77% (95% CI: 72-81%) for M2 segments. The observed agreements when comparing CTP-derived angiography to DSA in M2 patients (n=24) was 99% for identifying occlusion (95% CI 96-100%), 94% for identifying proximal M2 occlusion (95% CI 88-98%), and 96% for identifying distal M2 occlusion (95% CI 90-100%). There was 92% (95% CI 85-97%) and 90% (95% CI 83-96%) agreement for correctly identifying inferior and superior branch of M2 occlusion, respectively.

Conclusions

Angiographic reconstructions of arterial-phase CTP source images preserves high diagnostic yield for correctly identifying M2 MCA occlusion without the addition of dedicated single-phase CTA.

2754

2:16PM - 2:23PM

Initial Experience in the Analysis of Acute Stroke Utilizing RAPIDTM at a Major Stroke Center

B Laughlin[1], A Chan[2], E Dutweiler[3], A Iaia[4], B Reznikov[5], P Moftakhar[6]

[1]CHRISTIANA CARE HEALTH SYSTEM, MIDDLETOWN, DE, [2]CHRISTIANA CARE HEALTH SYSTEM, BEAR, DE, [3]Christiana Care Health System, Newark, DE, [4]Christiana Care, Newark, DE, [5]CHRISTIANA CARE HEALTH SYSYTEM, WEST CHESTER, PA, [6]Christiana Healthcare system, Newark, DE

Purpose

The adaptation of automated CT Perfusion analysis software, RAPIDTM (Ischemaview, Menlo Park, CA) at major stroke treatment centers has come with the promise of improved decision making in the acute stroke setting. To realize this achievement, Radiologists and Clinicians must understand and accurately interpret the CTP output information. The purpose of this presentation is to provide the audience our initial experience with RAPIDTM by utilizing a case-based format highlighting instances where RAPIDTM recognized subtle acute ischemia not detected by the Radiologist along with cases where technical and/or physiological pitfalls caused potentially clinically significant misinterpretations.

Materials and Methods

In a retrospective analysis of CT examinations performed utilizing RAPIDTM in the setting of acute stroke since March 2018, 63 CTP cases with RAPIDTM were performed at our center. We identified cases where RAPID detected acute ischemia not recognized by the Radiologist, and also cases with technical errors, physiologic errors, and other unexpected results.

Results

Of the 63 total cases identified in our retrospective analysis, 45/63 (79%) were determined to be normal given congruence of results between RAPIDTM, the Radiologist's read, as well as follow up imaging. Of the remaining 18 cases, 5/63 cases (8%) demonstrated that RAPIDTM detected acute ischemia not identified by the Radiologist. In the remaining 13 cases, 4 (6%) demonstrated physiologic errors, 6 (10%) demonstrated technical errors, and 3 (5%) demonstrated unexpected results. No cases demonstrated acute ischemia on the initial non-contrast head CT and CTA head and neck.

Conclusions

In our institution's initial 9 month experience with RAPIDTM in the acute stroke setting, the software was able to identify areas of acute ischemia not detected by the Radiologist, particularly in difficult imaging and clinical settings. Additionally, there were cases where RAPIDTM produced confounding results due to technical and physiological factors. The goal of this presentation will be to showcase examples highlighting advantages of RAPIDTM and to present cases that illustrate clinically significant pitfalls which may be recognized and avoided in the future.

Monday, May 20, 2019
1:00PM - 2:30PM
Adult Brain Excerpta 1

3146

1:00PM - 1:04PM

Anaplastic Meningioma Associated with Leptomeningeal Carcinomatosis

O Arevalo[1], S Galvis Vega[2], S Calle[1], C Soto[3], Y Esquenazi[4], L Ballester[5], A Blanco[4], R Riascos[1]
[1]Department of Diagnostic and Interventional Imaging. McGovern Medical School, UTHealth., Houston, TX, [2]Universidad el Bosque, Bogota, Colombia, [3]National University of Colombia, Bogota, Colombia, [4]Vivian L. Smith Department of Neurosurgery. McGovern Medical School, UTHealth., Houston, TX, [5]Department of Pathology and Laboratory Medicine. McGovern Medical School, UTHealth., Houston, TX

Purpose
To present a case of an anaplastic meningioma with leptomeningeal carcinomatosis.
Materials and Methods
36 years old woman complaining of six months of insidious onset of headache and blurry vision.
Results
Well-defined, avidly enhancing pineal region mass, associated with internal coarse calcifications and spoke-wheel configuration. Obstructive hydrocephalus was also identified. Diffuse seeding of the leptomeninges by tumor metastases was seen in the posterior fossa and within the thecal sac throughout the entire spine. Histopathologic examination was consistent with chordoid and rhabdoid features.
Conclusions
Anaplastic meningiomas are uncommon malignant meningeal neoplasms, accounting for less than 1% of all meningiomas. These tumors show aggressive local growth and high recurrence rate; however, to the best of our knowledge, leptomeningeal dissemination of an anaplastic meningioma is uncommon, and only few cases have been described in the literature. We intend to review the imaging manifestations and the differential diagnosis of leptomeningeal dissemination of malignant meningiomas.

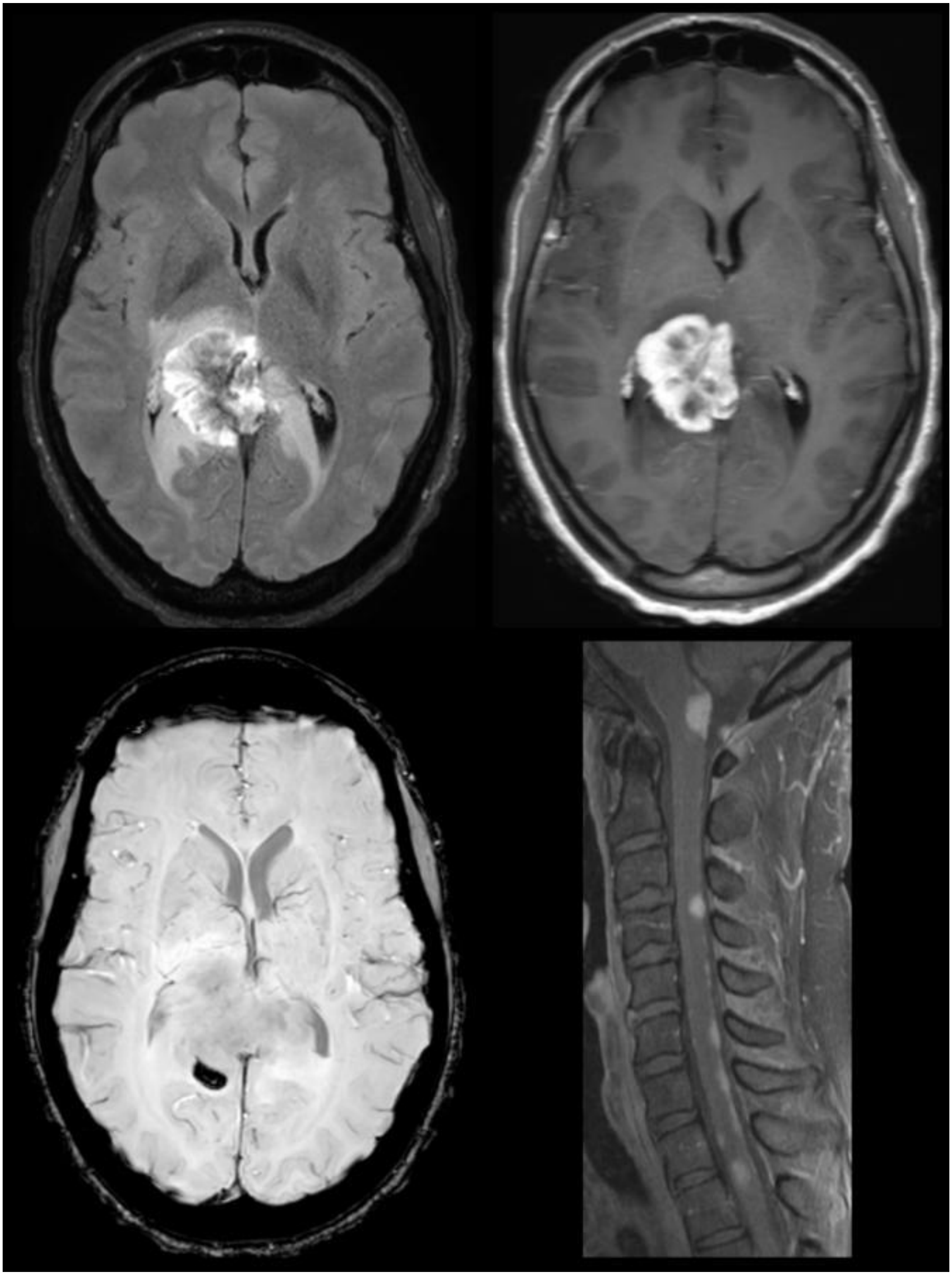

(Filename: TCT_3146_Anaplasticmeningioma.jpg)

2568

1:00PM - 2:30PM

Cervical Artery Dissection: Demythifying the Need of Axial T1 Fat Saturation Images

D Quiñones-Tapia[1], A Herrera Muñoz[2], E Vaño[3]
[1]RM Rosario, Madrid, Madrid, [2]Hospital NS del Rosario, Madrid, Madrid, [3]RM Rosraio, Madrid, Madrid

Purpose
During many years we have been recommended to use axial T1 fat saturated axial images of the neck to detect arterial dissection, but in fact many other sequences demonstrate the same findings of crescentic vessel wall lesion that lead to the radiologic diagnosis of arterial dissection.
Materials and Methods
We have revised all MR reports including the diagnosis of "dissection of neck vessels" from our center during the past 5 years. Axial T1 fat sat sequences were only obtained in a third of cases, where there was a strong clinical suspicion of dissection related to neck pain or Horner Syndrome.
Results
Thin section imaging and higher resolution of MRI equipment permit many sequences that are able to detect vessel wall hematoma/lesion that characterise vessel dissections. The vessel wall damage may be hyperacute, or chronic (both not hyperintense on T1) and can be depicted by other sequences routinely used such as Diffusion, T2 or FLAIR. The use of 3D brain imaging in our daily practice, has permitted us to detect unsuspected dissections in some cases. The "crescent sign" around the vessel lumen remains diagnostic for dissection with many sequences, even detecting some chronic cases where the wall lesion is no longer hyperintense on T1.
Conclusions
Nowadays, thin section imaging and higher resolution of MRI equipment allow us to detect vessel wall hematoma/lesion that identify and characterize dissections in many sequences (not only T1 fat sat). In many cases the vessel wall damage may be hyperacute, or chronic (both not usually hyperintense on T1) and can be depicted by other sequences routinely used for brain imaging such as Diffusion, T2 or FLAIR.

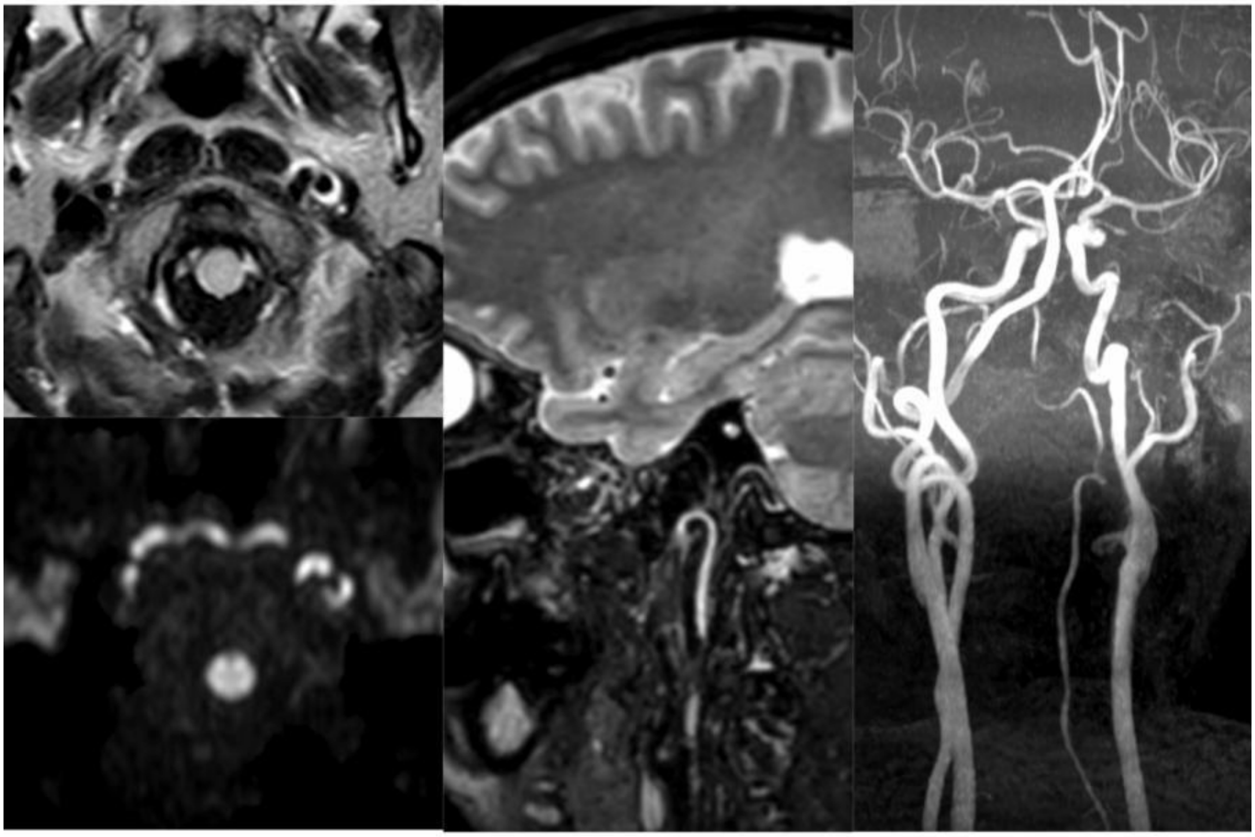

(Filename: TCT_2568_Diapositiva1.jpg)

3559

1:04PM - 1:08PM

A Precise Comparison of Heterogeneous Pathological Features of Glioblastoma at Autopsy to T1 Subtraction Maps

A Lowman[1], A Barrington[1], B Ellingson[2], S Bobholz[3], J Connelly[1], S McGarry[1], J Bukowy[1], A Nencka[1], P LaViolette[1]
[1]Medical College of Wisconsin, Milwaukee, WI, [2]University of California Los Angeles, Los Angeles, CA, [3]Medical College of Wisconsin, Wauwatosa, WI

Purpose
The heterogeneous nature of glioblastoma often makes it difficult to visualize subtly enhancing infiltrative glioblastoma. To mitigate this issue, T1-weighted subtraction maps are beginning to be adopted for determining the extent of tumor location. These maps are created by subtracting intensity normalized T1 weighted images from T1 post-gadolinium contrast images (T1+C). Tumor volume derived from T1 subtraction maps has been shown to predict patient prognosis and response to therapy. This study precisely correlates large format histology acquired at autopsy to a T1 subtraction map acquired in vivo to quantify pathological features responsible for enhancement.
Materials and Methods
One patient was recruited for this radiological-pathological (rad-path) study. At autopsy, the whole brain sample was sliced axially to match the T1+C MRI scan acquired 22 days prior to death (Figure 1). Large

specimens suspected to contain tumor were sectioned at autopsy, embedded on large format histology slides, H&E stained, then digitized. Each digital slide was then manually annotated to indicate regions of necrotic treatment effect, hypercellularity with pseudopalisading necrosis, and hypercellularity without pseudopalisading necrosis. The digital histology was then aligned and resampled into the MRI space using custom software previously published. A T1 subtraction map was generated by first performing a gaussian normalization of the T1 and T1+C images, linearly alignment, then performing a subtraction. Tumor regions annotated on the pathology samples were then compared to the values within the T1 subtraction map.

Results

A total of 8662 voxels were assessed with tissue from two large samples. Regions of pseudopalisading necrosis co-localized with heightened enhancement on the T1 subtraction map. The enhancement differed significantly ($p<0.00001$) from regions of infiltrative tumor, which showed enhancement levels much more similar to regions without tumor present (Figure 1). Regions of necrotic treatment effect enhanced subtly.

Conclusions

Regions of pseudopalisading necrosis are more evident on T1 subtraction maps than those of hypercellularity which are nonenhancing. Additional research is necessary to determine how well this pattern generalizes across patient populations.

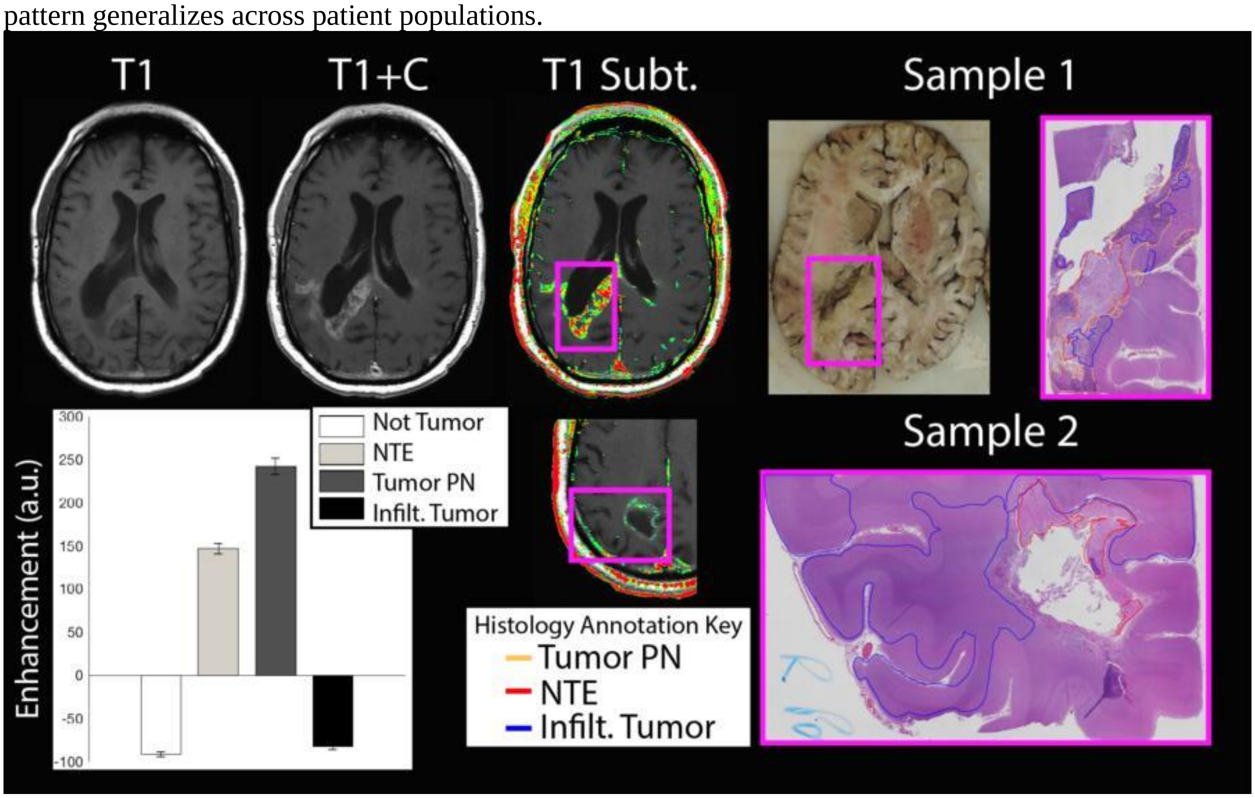

(Filename: TCT_3559_Figure1.jpg)

2254

1:08PM - 1:12PM

Atypical Presentation of Medulloblastoma

P Cogswell[1], S Messina[1]
[1]*Mayo Clinic, Rochester, MN*

Purpose
To illustrate an atypical presentation of medulloblastoma and problem in diagnosis when aggressive disease mimics a benign neoplasm.
Materials and Methods
A 29 year old male presented to an outside institution with progressive low back pain and diplopia and was referred with diagnosis of probable NF2. Repeat MR suggested a more aggressive process. Pathology from right cerebellar lesion biopsy showed medulloblastoma (SHH-activated and TP53-wildtype, WHO grade IV).
Results
The presumed diagnosis of NF2 was based on outside imaging that showed enhancing lesions along the bilateral CN3 and bilateral IACs as well as diffuse enhancing lumbar intradural tissue, thought to represent nerve sheath tumors. Repeat MR (Figure) two months later showed ill-defined, mildly enhancing, T2 hypointense tissue with restricted diffusion within the internal auditory canals (red arrow), along the oculomotor nerves (yellow arrow), Meckel cave (blue arrow), foramen ovale, and within the lumbar thecal sac that had progressed from the prior exam and nearly filled the thecal sac from L1 through the sacrum. Nodular enhancing right cerebellar lesions had increased in size and demonstrated associated restricted diffusion. In addition, new lesions with similar findings had developed in the left cerebellar hemisphere.
Conclusions
Multiple aspects of the case are unusual for medulloblastoma, including age, extent of leptomeningeal disease at presentation, and multiplicity of the cerebellar lesions. Most medulloblastoma are diagnosed by age 5 years, 75% by 10 years. About 1/3 of medulloblastomas have CSF seeding with drop metastases appearing as small nodules of enhancement along the cord or icing-like ("Zuckergrass") enhancement, rather than diffuse, confluent tissue filling the thecal sac in this case. Leptomeningeal disease along the cranial nerves is also uncommon, with rare cases of disease extension along cranial nerves or primary leptomeningeal disease. Additionally, the imaging was not consistent with NF2 for multiple reason, including interval progression, restricted diffusion, and infiltrative nature of the lesions.

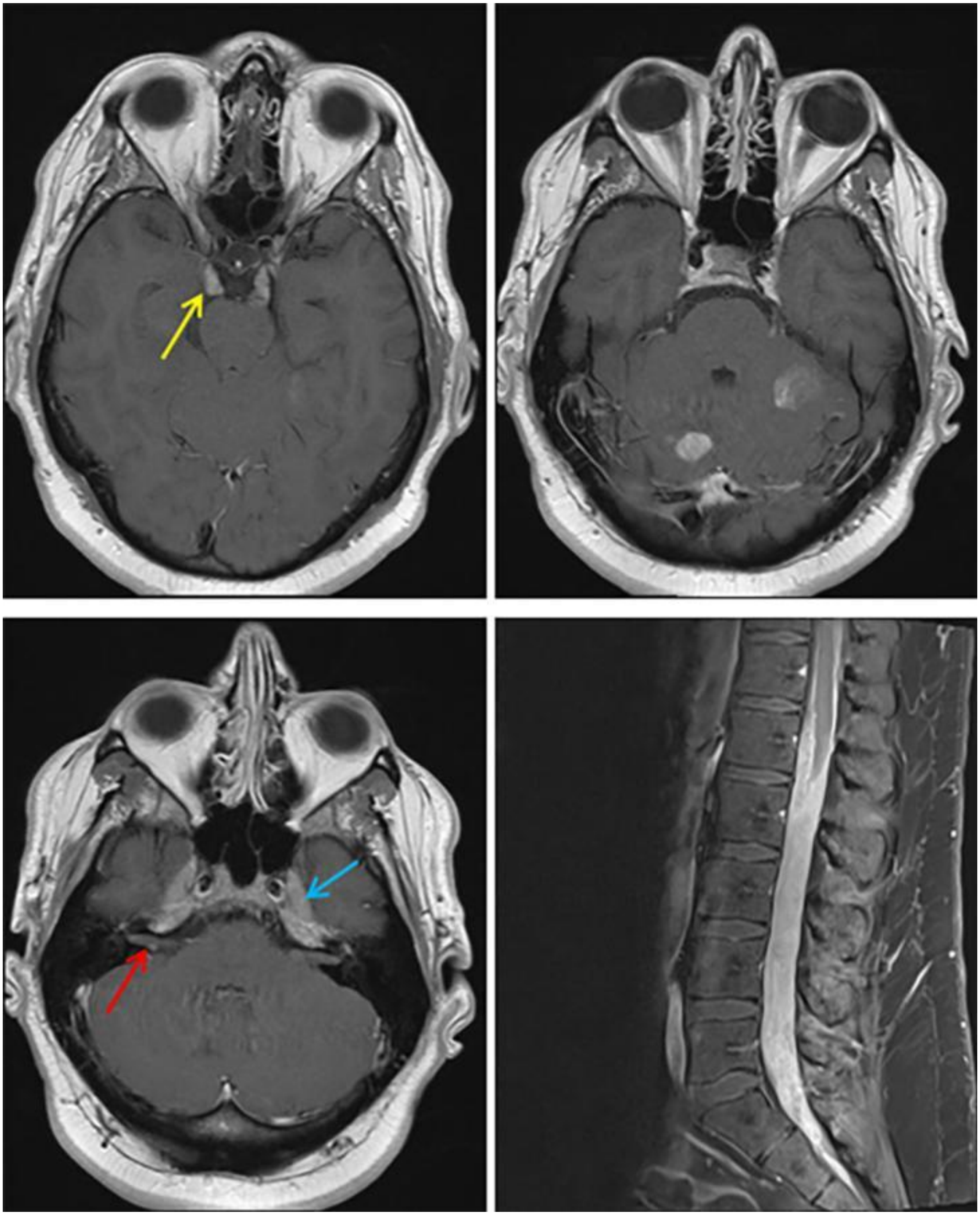

(Filename: TCT_2254_Medullo_ASNR.jpg)

3465

1:12PM - 1:16PM

Ferumoxytol: A Potential Neuroimaging Pitfall

J Rogers[1], C SITTON[2], L Ocasio[3]
[1]UNIVERSITY OF TEXAS HEALTH SCIENCES CENTER AT HOUSTOIN, Houston, TX, [2]UNIVERSITY OF TEXAS - HOUSTON MEDICAL SCHOOL, HOUSTON, TX, [3]Memorial Hermann Hospital Texas Medical Center, Houston, TX

Purpose
To illustrate the persistent T1-shortening effects of ferumoxytol seen on brain MR imaging studies
Materials and Methods
46 year old woman with history of right frontotemporal oligodendroglioma which was initially resected. She presented two years after resection with worsening seizures, which prompted imaging evaluation for recurrent tumor. She had additional history of iron deficiency anemia treated with serial doses of IV ferumoxytol, with the last dose administered one week prior to imaging. Clinical and imaging findings were consistent with recurrent tumor, and the patient was taken to the OR for re-resection. She has done well after surgery with her seizures well controlled.
Results
SPGR T1-weighted images obtained prior to contrast administration show enhancing intracranial vessels, curvilinear enhancement within the resection cavity, and enhancement of the overlying dura. In additon there is diffuse enhancement of the pituitary gland and nasal mucosa. Overall the images appear as if they were obtained after contrast administration. Susceptibility weighted images demonstrated susceptibility corresponding to several areas of enhancement, particularly in the dura. After gadolinium contrast administration, there is increased conspicuity of enhancement within the resection cavity and of the overlying dura. However, the degree of relative enhancement is diminished by the intrinsic T1-shortening effects of furomoxytol.
Conclusions
Parenteral ferumoxytol is an ultra-small superparamagnetic iron oxide currently FDA-approved to treat iron deficiency anemia in adults. ferumoxytol has a long blood-pool dwell time (plasma half-life of 14-21 hours), making it suitable for use both as an intravascular and a perfusion contrast agent. Beginning at around 24 hours, there is significant migration of ferumoxytol into the extracellular space, permitting use a parenchymal contrast agent. As it is ultimately internalized by tissue macrophages (and astroglial cells in the CNS), it can also be used as an imaging marker of inflammation. Several studies demonstrate that ferumoxytol produces local T1 shortening, which persists for several days after administration, as seen in our case. The T1 hyperintensity produced by ferumoxytol reduce the apparent degree of enhancement on T1WI after GBCA administration. Conversely, the increased susceptibility usually peaks by 3 days. During this period it may adversely impact dynamic susceptibility contrast (DSC) studies. There is increasing interest in ferumoxytol as a CNS contrast agent, particularly when there is contraindication to GBCA administration. Whether it is administered to treat anemia or as a contrast agent, neuroradiologists should be aware of these effects to avoid interpretative pitfalls. Depending on the indication, it may be prudent to delay the exam, allowing for clearance of the agent. Particularly if assessment of enhancement is critical to the diagnosis and management of the patient.

2226

1:16PM - 1:20PM

Lymphoma with Incomplete Ring Enhancement Mimicking Demyelination

J Bregni[1], A Mansour[2], C Zamora[3], M Castillo[3]
[1]Universidad Francisco Marroquin, Guatemala, Guatemala, [2]King Hussein Cancer Center, Amman, Jordan, [3]University of North Carolina, Chapel Hill, NC

Purpose
Ring enhancement can be seen in a variety of lesions and is most commonly caused by infection and

malignancy. Incomplete ring enhancement, particularly that which is frequently open toward the cortex has been described as highly specific for active or tumefactive demyelination. However, this sign is not pathognomonic. Here we present 2 patients with CNS lymphoma who presented lesions with incomplete ring enhancement on brain MRI.

Materials and Methods

The first patient is a 38-year-old woman treated for cutaneous large cell lymphoma (CD30+) with widespread lesions in the skin, lymph nodes and soft tissues. One year after diagnosis she presented with seizures. Brain MRI demonstrated a left frontal lobe lesion which was shown to be anaplastic large cell lymphoma on biopsy. The second patient is a 33-year-old male with known extra-CNS lymphoma who came to the Emergency Department after of loss of consciousness. MRI of the brain was performed with findings described below.

Results

Axial postcontrast T1 image in patient 1 at admission (Fig. A) shows a lesion with surrounding edema and incomplete ring-enhancement in the left frontal lobe (arrow). The lesion shows significant growth and appears masslike on a follow up study (Fig. B) where it also shows restricted diffusion (arrowhead in Fig. C). Sagittal postcontrast T1 image in patient 2 (Fig. D) shows a frontal lobe lesion with faint and incomplete ring enhancement (blue arrow). The lesion had restricted diffusion restriction (not shown).

Conclusions

Incomplete or open ring sign on postcontrast T1 has been largely associated with active or tumefactive demyelination. We present 2 cases of biopsy proven lymphoma which highlight the fact that this sign is not pathognomonic for demyelination.

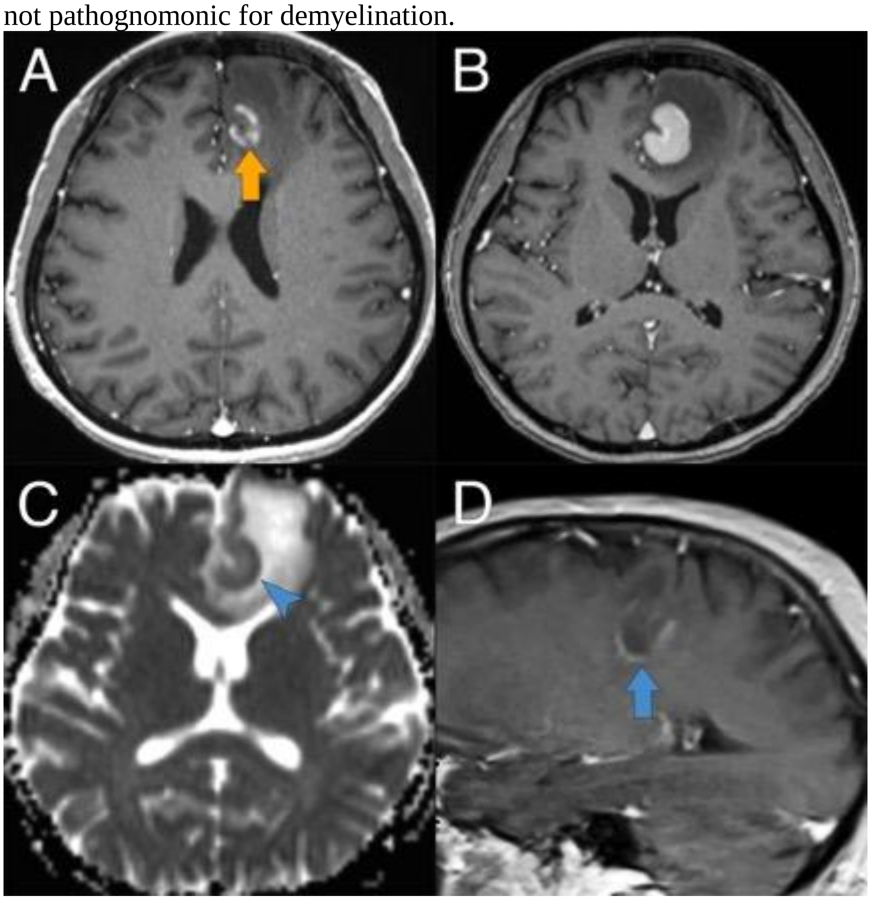

(Filename: TCT_2226_ASNR.jpg)

3166

1:20PM - 1:24PM

Persistence of Gadolinium in a Patient with Chronic Kidney Disease: Imaging Appearance of a Potential Diagnostic Pitfall

N Hyson[1], J Corrigan[2], H Marin[1], S Patel[3], B Griffith[1]
[1]HENRY FORD HEALTH SYSTEM, Detroit, MI, [2]HENRY FORD HOSPITAL, NORTHVILLE, MI, [3]HENRY FORD HOSPITAL, DETROIT, MI

Purpose
The appearance of gadolinium retention in the brain has become well recognized in recent years. However, in patients with poor renal function, gadolinium can also persist within various compartments, including the subarachnoid and subdural spaces, ventricles, and globes. Lack of familiarity with this latter phenomenon and its imaging appearance creates a potential diagnostic pitfall as it can be mistaken for pathologic processes. This excerpta demonstrates multi-compartmental persistence of gadolinium in a patient with chronic kidney disease (CKD) and reviews both the imaging appearance, as well as the pathophysiologic basis.
Materials and Methods
A 67-year-old female with a history of CKD and stage IV lung cancer underwent MRI of the brain. Of note, the patient had undergone a contrast enhanced MRI of the spine one day prior. Imaging demonstrated pre-contrast T1 hyperintensity within a known metastatic lesion, as well as hyperintense FLAIR signal within bilateral subdural collections raising suspicion for intralesional and subdural hemorrhage, respectively. FLAIR hyperintensity was also present within the globes, inner ear structures, and internal auditory canals. The possibility of gadolinium persistence was raised and a follow-up MRI 8 days later showed near complete resolution of these areas of signal abnormality.
Results
Axial FLAIR images demonstrates hyperintense signal within the anterior and posterior chamber of the right greater than left globe (A), bilateral inner ear structures and subarachnoid fluid of the internal auditory canals (B), and bilateral frontal and right parietal subdural collections (C). Axial pre-contrast T1-weighted image demonstrates hyperintensity within the right posterior frontal metastatic lesion (D).
Conclusions
Persistence of gadolinium is an under-recognized entity that can occur in patients with poor renal function. This case nicely demonstrates the various locations that this phenomenon can occur. This is an important entity for radiologists to be aware so as to ensure appropriate follow-up and avoid misdiagnosing more sinister pathologies.

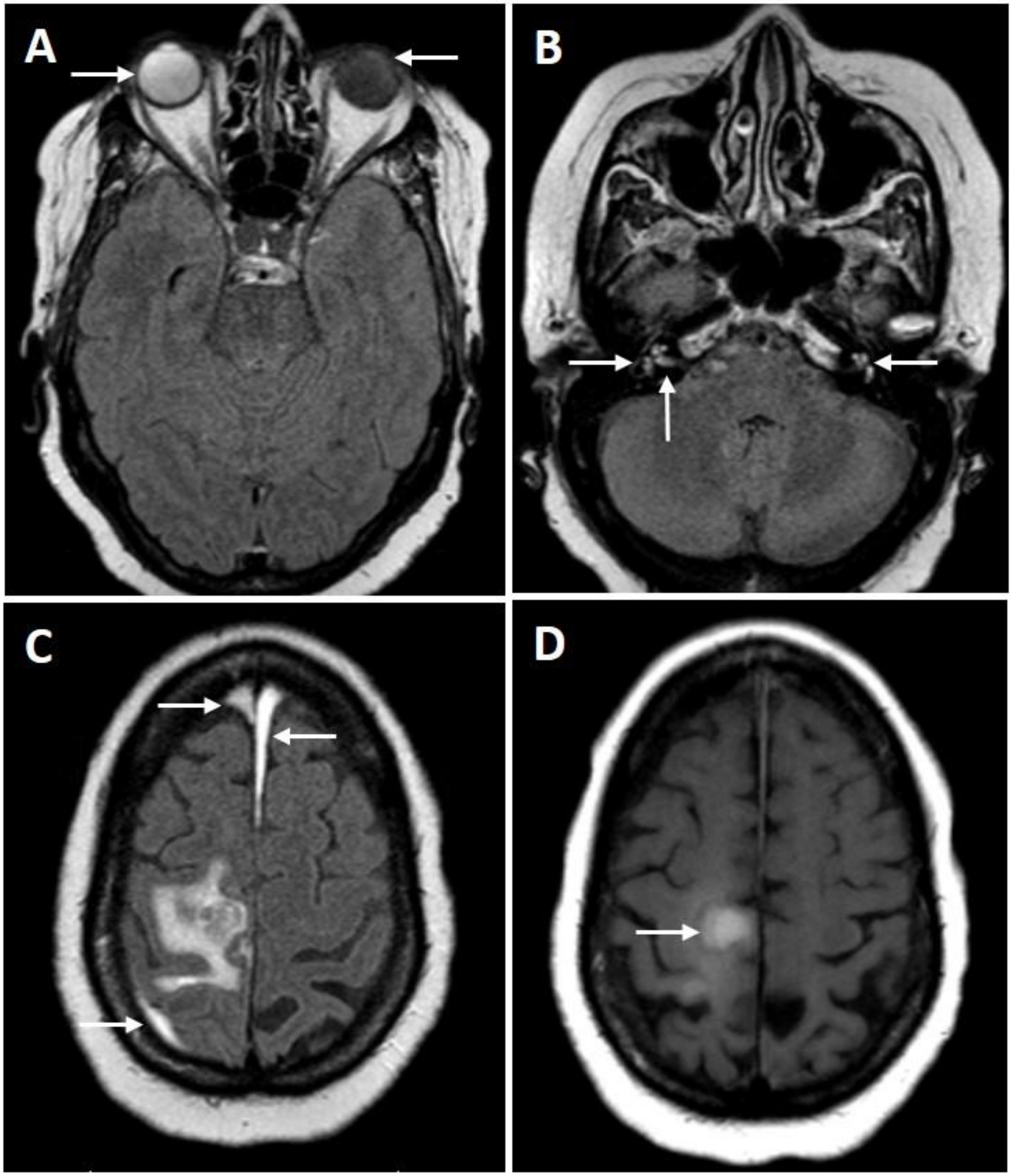

(Filename: TCT_3166_Gadretention.jpg)

2654

1:24PM - 1:28PM

Pilocytic Astrocytoma Manifesting as a Cystic Mass of the Third Ventricle

M Gao[1], O Arevalo[1], C Soto[2], S Khanpara[1], A Kamali[1], Y Esquenazi[3], L Ballester[4], A Blanco[3], R Riascos[1]

[1]*Department of Diagnostic and Interventional Imaging, McGovern Medical School. UTHealth., Houston, TX,* [2]*National University of Colombia, Bogota, Colombia,* [3]*Department of Neurosurgery, McGovern Medical School. UTHealth., Houston, TX,* [4]*Department of Pathology and Laboratory Medicine, McGovern Medical School. UTHealth., Houston, TX*

Purpose

To show an uncommon presentation of pilocytic astrocytoma (PA) as a cystic mass centered at the third ventricle.

Materials and Methods

A 19-year-old female, with no significant past medical history, presented to the emergency department for the insidious onset of worsening "tunnel vision" and headache. She had associated blurry vision, nausea, vomiting, and neck pain that was unrelieved by over-the-counter analgesics. She then started having numbness/tingling of the left upper extremity. On ophthalmologic exam, she was found to have bilateral papillary and disc edema associated with bilateral proptosis.

Results

A well-defined, lobulated, ring-enhancing cystic lesion is seen centered at the floor of the third ventricle, extending into the suprasellar cistern, without associated vasogenic edema calcifications, mural nodules or restricted diffusion. Dilatation of the supratentorial ventricular system, associated with periventricular T2/FLAIR hyperintensity consistent with obstructive hydrocephalus with transependymal edema.

Conclusions

PA are rare, slow-growing, highly vascular grade I gliomas according to the current WHO classification. They are the most common glial neoplasm in children and are usually seen in children and young adults. The most common locations for PAs are the cerebellum, optic nerve and chiasm, around the third ventricle, and in the region of the hypothalamus-thalamus. It can also extend into the brainstem and spinal cord. Depending on the size and location of the neoplasm, patients will have different signs and symptoms for several months. Prognosis is very good with a survival rate of 90% at ten years. Treatment of PA is usually by total resection unless the hypothalamic-optic chiasm region is involved in which case, chemotherapy and radiation are employed. Although the final diagnosis is obtained through pathology, imaging is characteristic and can help narrow the differential before a biopsy is performed.

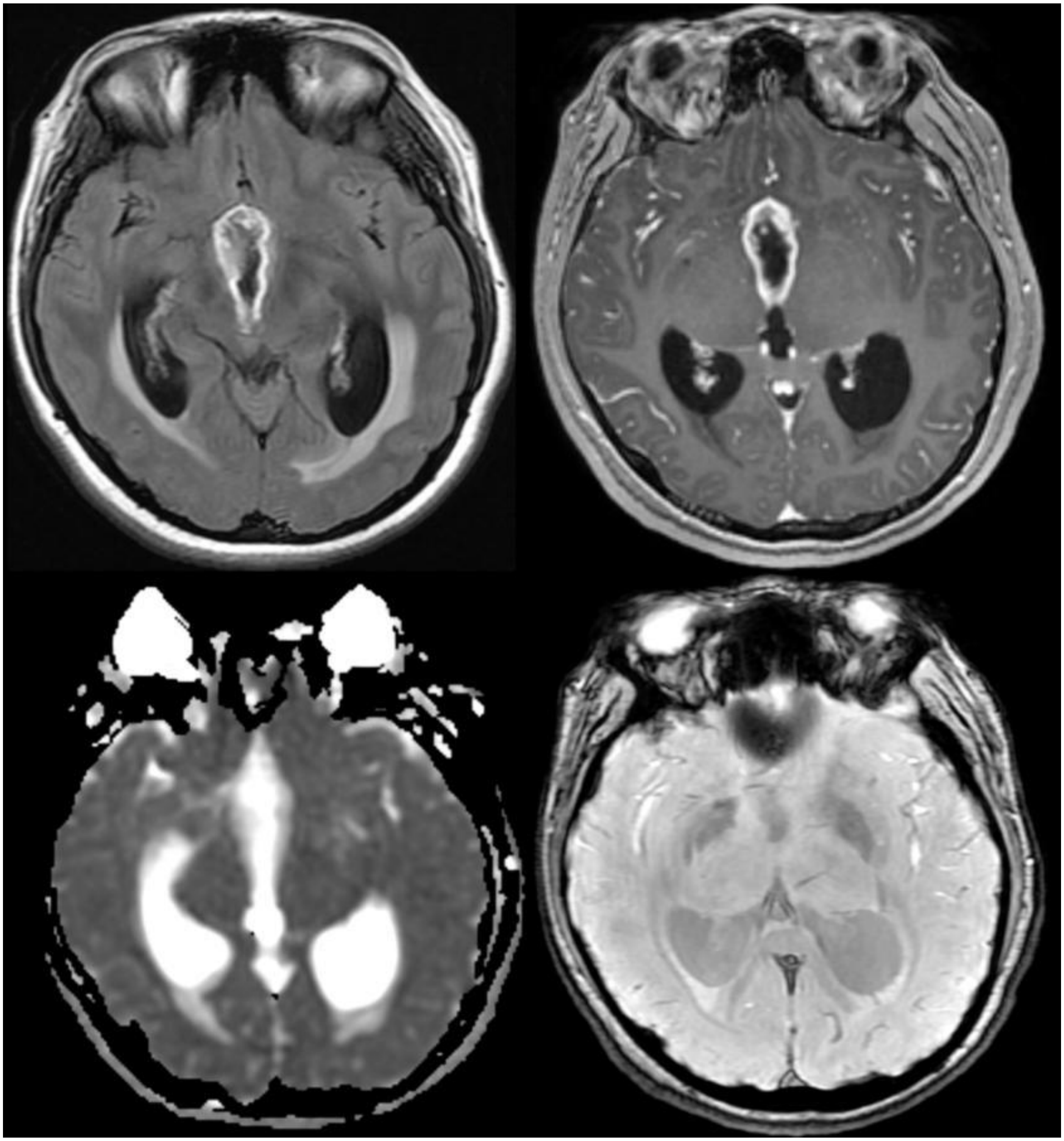
(Filename: TCT_2654_ThirdventricleJPA.jpg)

2125

1:28PM - 1:32PM

Pre-operative Diagnosis of Suprasellar Hemangioblastoma in a Patient without VHL Disease

Y Tong[1], D Sirhan[2], M Cortes[2]
[1]McGill University, Montreal, Quebec, [2]Montreal Neurological Institute, Montreal, Quebec

Purpose
- To describe the imaging features of sporadic suprasellar hemangioblastoma in a patient without VHL

disease, a rare diagnosis - To illustrate the importance of pre-operative suspicion for hemangioblastoma given the high risk of hemorrhage associated with surgical intervention

Materials and Methods

A 39-year-old woman presented to the emergency department with visual disturbances and headache for the past few months. Other than diabetes mellitus type II and hyperlipidemia, she was not known for any other diseases. Family history was also insignificant. She was found to have bitemporal hemianopsia, confirmed on formal visual field testing, but no other focal neurological deficits. Physical examination showed no other signs of VHL disease. Endocrinological profile was normal. The diagnosis of suprasellar hemangioblastoma was confirmed on pathology via a transsphenoidal biopsy. No resection was attempted due to the extent of post-biopsy bleeding and the lesion's proximity to the optic chiasm. The patient will undergo radiation instead.

Results

Initial CT of the head without contrast in a community hospital: 3.1 cm solid suprasellar mass with no cystic component and no mass effect. Diagnosed as pituitary adenoma. Repeated CT of the head with contrast after patient was referred to an academic center: The lesion extended superiorly into the third ventricle with no invasion of the cavernous sinuses or hyperostosis noted. It seemed separate from the normal-sized sella and normal-appearing pituitary gland: pituitary adenoma considered less likely given this feature. MRI recommended for further characterization. MRI with gadolinium, and MRA of the sella turcica: Solid, heterogeneous mass, T1 isointense, T2 hyperintense containing large flow voids, consistent with intratumoral vessels. The mass was avidly enhancing. Important bilateral internal capsule white matter edema is also noted, with important mass effect on the hypothalamus, the pituitary stalk and the third ventricle. Repeated MRI of the sella turcica one month later: new significant mass effect on the midbrain and pons is noted, as well as edema of the inferior frontal and mesial temporal regions. The mass was also noted to have very prominent vascular structures on its posterior and right lateral aspect and a very large vein posteriorly draining into the basal vein of Rosenthal. The optic chiasm, although not well visualized, was found to be likely superior to the mass, with lateral deviation of the optic nerves. CT angiography: marked curvilinear enhancement around the mass, most pronounced along its right lateral aspect, likely reflecting a combination of feeding arteries and prominent venous drainage, although the exact vessels of origin were not definitely identified due to tumor size.

Conclusions

Suprasellar hemangioblastoma is an extremely rare diagnosis, but should be on the list of differential diagnoses when encountering an avidly-enhancing suprasellar mass with prominent intratumoral and peritumoral flow voids on MRI. A CT angiogram can confirm the highly vascular nature of the lesion. Suprasellar location is especially common in patients with VHL disease, but can also occur sporadically. Pre-operative diagnosis of hemangioblastoma is important in assessing the surgical approach given the high risk of hemorrhage.

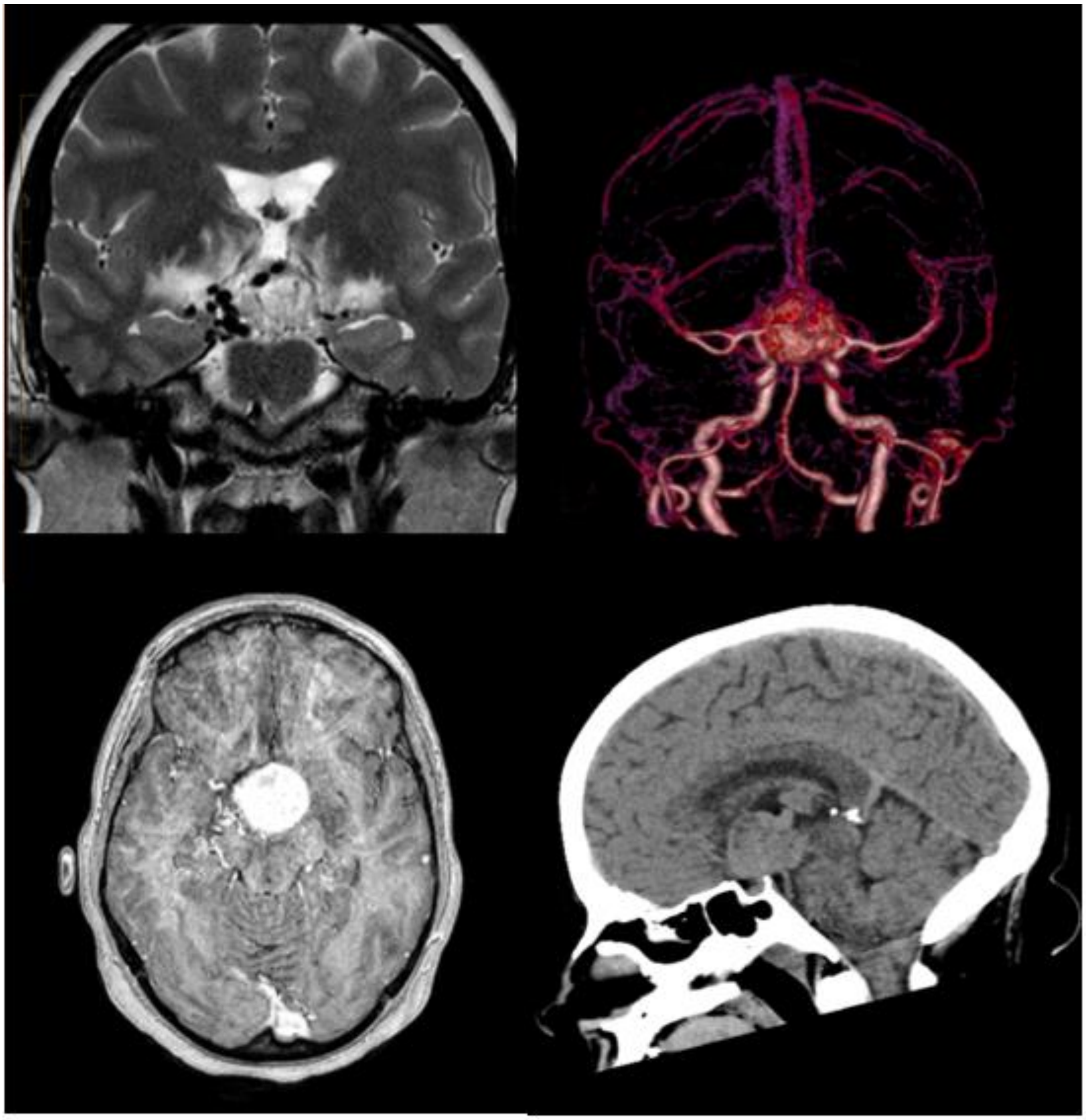

(Filename: TCT_2125_ScreenShot2018-10-30at135644.jpg)

2557

1:32PM - 1:36PM

Primary Intracranial Leiomyosarcoma in an Immunocompetent, EBV-Negative Patient

R Ward[1], M Burgess[2], A Weyer[2]
[1]University of Pittsburgh School of Medicine, Pittsburgh, PA, [2]University of Pittsburgh Medical Center, Pittsburgh, PA

Purpose
Primary intracranial leiomyosarcomas (LMS) are exceedingly rare and have almost exclusively been reported in patients with Epstein-Barr virus (EBV), in children, or in immunocompromised individuals, such as those with HIV. We present a case of an elderly woman with celiac disease who was found to have cerebellar LMS in the absence of immunosuppression and EBV infection.
Materials and Methods
A 71-year-old female with a history of celiac disease, Raynaud's syndrome, and Bowen's disease

presented to her physician for evaluation of "continual dizziness." The patient complained of a one-week history of a rushing sound in her left ear, the sensation of falling backward, fatigue, and nausea. Brain MRI was suspicious for posterior fossa meningioma. Neurosurgery performed a suboccipital craniotomy with near total resection of the mass. Pathology was consistent with a high-grade LMS. Over three months, the patient received adjuvant radiation in 29 fractions. A PET imaging study performed one month after initial presentation showed no evidence of extracranial malignancy. However, chest CT performed 10 months after initial presentation demonstrated multiple pulmonary nodules. Metastatic LMS of the right lower lobe was confirmed by fine needle aspiration of a 9 millimeter nodule. Thirteen months after her initial presentation, an abdominal CT showed a 1.5 centimeter hypoattenuating lesion in the right hepatic lobe which was presumed metastatic.

Results

Initial brain MRI demonstrated an extra-axial enhancing mass with central hypoenhancement in the posterior fossa with transosseous extension and involvement of the torcula. Preoperative catheter cerebral angiography revealed intense tumor blush of the mass supplied by the bilateral occipital arteries. Initial postoperative MRI demonstrated some enhancement at the resection site, but subsequent MRIs performed up to 20 months after presentation showed no evidence of tumor progression.

Conclusions

Primary intracranial leiomyosarcoma, although rare, can be on the differential for an extra-axial mass, even in the absence of EBV-positive status or a history of immunosuppression.

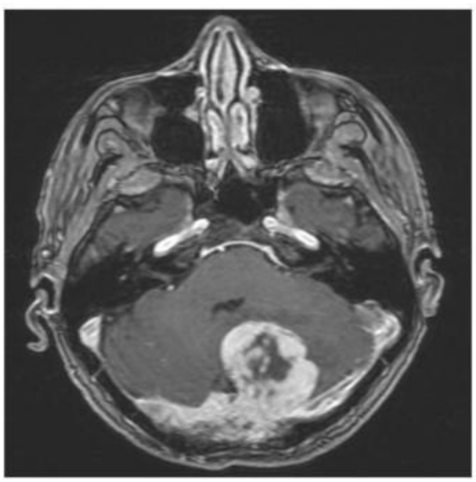

Figure 1. Post-contrast Axial FSPGR

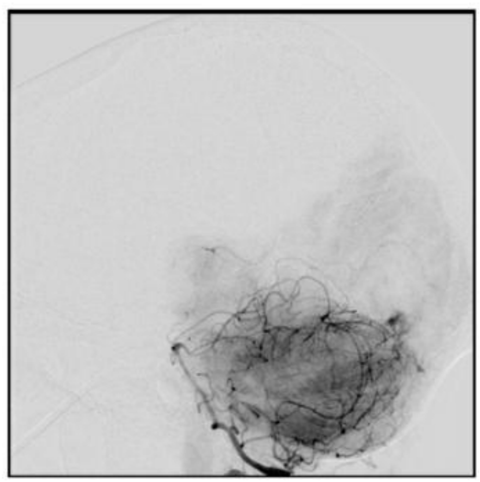

Figure 2. Lateral DSA, Left External Carotid Artery Injection

(Filename: TCT_2557_118ASNR.jpg)

2526

1:36PM - 1:40PM

Primary CNS Lymphoma Presenting as Enhancing Cortical Ribboning and Hemorrhage: Lessons from Atypical Presentation of a Usual Suspect.

H Morales[1], N Marko[1], A Kanfi[2], K Brannock[1], R Chaudhary[1]
[1]University of Cincinnati, Cincinnati, OH, [2]Arkansas Children's Hospital, Little Rock, AR

Purpose

Enhancing cortical ribboning on CT or MRI is rarely, if ever, considered a presenting feature of CNS lymphoma. Other lesions but lymphoma are usually included in the differential diagnosis. Hemorrhagic changes are also atypical and can further complicate the assessment. To our knowledge, only one prior case with similar imaging features has been reported.1

Materials and Methods

A 54-year-old male presented to the ER with acute onset of aphasia. CT and CTA of the head were performed to assess for an acute stroke. An enhancing left frontal lobe lesion was found, which prompted a subsequent MRI. Further clinical work-up revealed recent changes in personality and behavior, no history of immunosuppression and no evidence of primary malignancy. The morphology and imaging characteristics of the lesion were atypical and given the need for diagnosis and the extensive symptomatic frontal edema, the decision was made to take the patient to the operating room for biopsy with the possibility of resection. After three non-diagnostic intraoperative biopsies, the lesion was resected. Final pathology was consistent with a high-grade B cell lymphoma, not otherwise specified (WHO 2017 Revised Classification). The tumor was composed of sheets of intermediate to large-sized atypical lymphocytes with scattered macrophages imparting a "starry sky appearance." The lymphoma co-expressed BCL-2 and C-MYC by immunohistochemistry, consistent with a "double expressor" phenotype. The Ki-67 proliferation index was 90%. FISH studies were negative for rearrangement of MYC, BCL-2, and BCL-6. The cortical parenchyma adjacent to the lymphoma showed hemorrhage, chronic inflammation, and reactive gliosis.

Results

CT revealed prominent cortical enhancement in the left frontal lobe with associated moderate vasogenic edema. MRI imaging demonstrated an enhancing cortical ribbon-like lesion in the left superior frontal gyrus (Figure A) with gyral-like hemorrhagic changes (Figure B), as well as moderate vasogenic edema. There was prominent cortical restricted diffusion (not shown). Mild thickening and enhancement of the adjacent falx was also noted (Figure A). Differential diagnosis included a high-grade glioma or an infectious/inflammatory process. Given the hemorrhagic changes, a lymphoma was considered unlikely. On final pathology, as shown on Figure C: HGBL-40X- H&E 40X, High-grade B cell lymphoma, NOS, with adjacent cortical brain parenchyma. And Figure D: HGBL-100X- H&E 100X, Hemorrhage, chronic inflammation, and reactive gliosis adjacent to lymphoma.

Conclusions

The most common imaging presentation of lymphoma in immunocompetent patients is that of a solid enhancing mass in the white matter with extension into the subependymal regions.2, 3 Enhancing lesions in atypical locations, such as the cortex, can be difficult to distinguish from other neoplastic, infectious/inflammatory processes or vascular lesions. Hemorrhagic changes in CNS lymphoma are usually only seen in immunosuppressed patients, or previously treated lesions.4, 5 On intraoperative frozen-section pathology, lymphoma can be difficult to distinguish from oligodendroglioma, primitive neuroectodermal tumors (PNET) and metastatic small-cell carcinoma. Moreover, the infiltrated brain parenchyma typically shows reactive changes such as astrocytosis and activated mycroglia, which can lead to a misdiagnosis of an inflammatory rather than a neoplastic process, as occurred on one of the frozen samples of our case. On microscopy, the cells tend to invade the walls of small cerebral vessels and accumulate in perivascular spaces, which over time can lead to necrotic and hemorrhagic changes (Figure D). Our case demonstrates the need to keep a high index of suspicion for lymphoma in atypical lesions, even with hemorrhagic changes. It also illustrates the importance of biopsy and tissue sampling to assess for the most appropriate management. As the incidence of lymphoma has steadily increased since the 1980s, we need to also consider that previous rare or atypical imaging features of lymphoma may be on the rise as well.

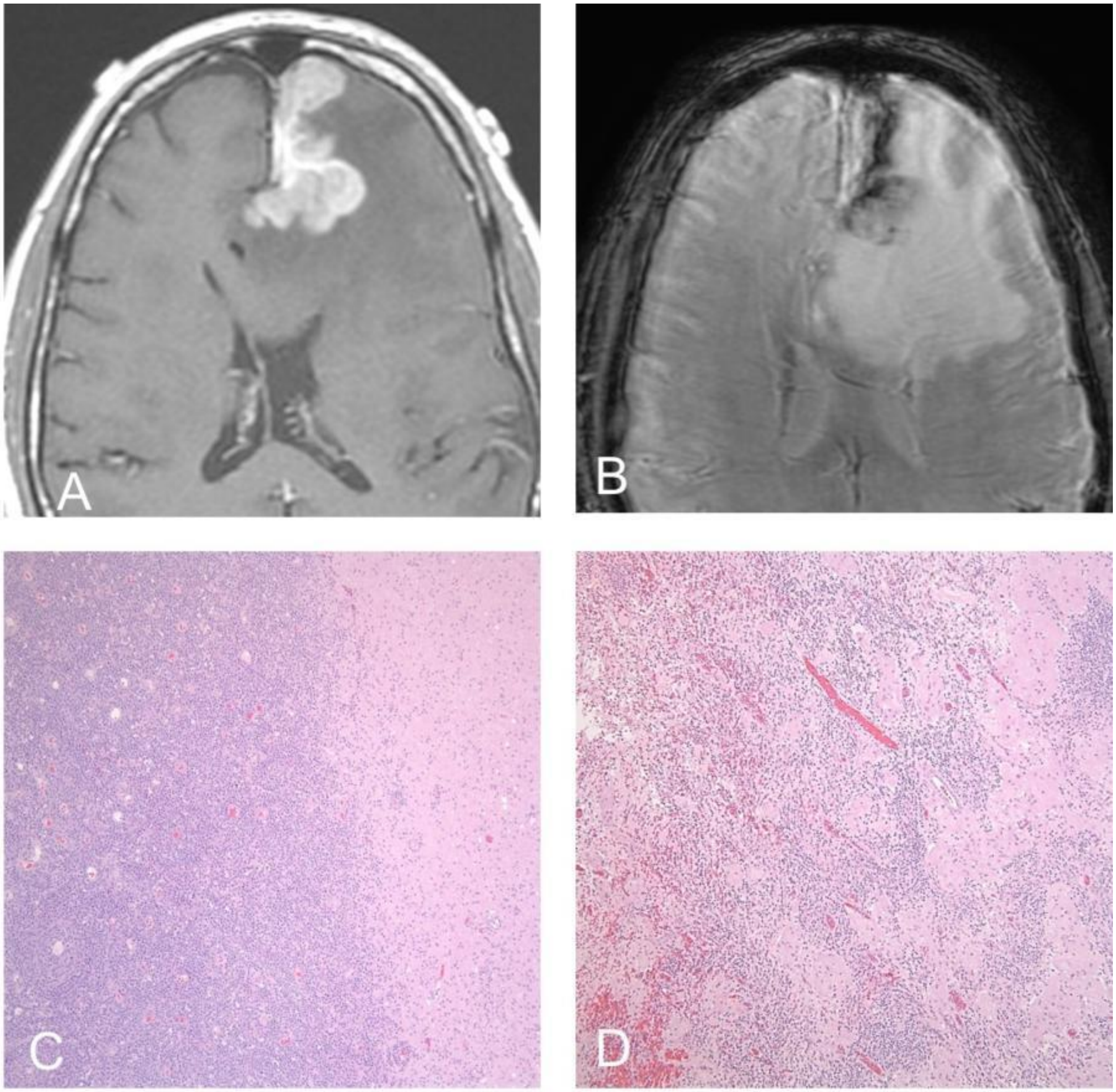

(Filename: TCT_2526_Picture1.jpg)

2396

1:40PM - 1:44PM

Pseudoresponse of Non-Small Cell Lung Cancer Brain Metastases to Corticosteroid Therapy

N Bansal[1], R Jain[1], S Kurz[1], E Raz[1], D Kondziolka[2]
[1]NYU Langone Health, New York, NY, [2]NYU Medical Center, New York , NY

Purpose
Intracranial lesions exhibiting spontaneous regression following corticosteroid therapy are colloquially referred to "vanishing tumors". Lesional response to steroids may complicate management decisions, especially when a definitive diagnosis is uncertain. While well-described in CNS lymphoma, vanishing

tumors may harbor an array of histopathologic entities and rarely include metastases from other primary malignancies.

Materials and Methods

A 64 year-old man with extensive smoking history and HIV on anti-retroviral therapy and no prior opportunistic illness presented with a simple motor seizure affecting his left hemibody. Initial MRI showed multiple ring enhancing intracranial mass lesions with associated edema. CT chest demonstrated a right upper lobe lung mass and pathology revealed poorly differentiated lung adenocarcinoma. Given the clinical presentation and edema associated with the brain masses, the patient was given IV dexamethasone and was scheduled for radiosurgery for the presumptive diagnosis of brain metastases. Pre-gamma knife planning MRI 15 days later showed marked regression of all the lesions and the procedure was halted, with the suspicion of an alternative diagnosis including lymphoma considering patient's history of HIV. Corticosteroids were tapered and a workup for possible lymphoma was unremarkable. Follow-up imaging at eight weeks showed interval re-growth of all lesions. Biopsy was performed which revealed metastatic lung adenocarcinoma.

Results

Brain MRI at the initial presentation demonstrated multiple thick-walled, irregularly-shaped, ring-enhancing lesions with peripheral reduced diffusion and surrounding interstitial edema. Serial followup evaluation demonstrated sequential decrease in size of lesions and improvement of edema while on steroid therapy. During steroid taper, multiple lesions increased in size with return of edema.

Conclusions

Lung cancer brain metastases can show marked regression or pseudo-response with corticosteroid therapy alone and should be considered in the differential diagnosis, especially if the patient has a known primary cancer.

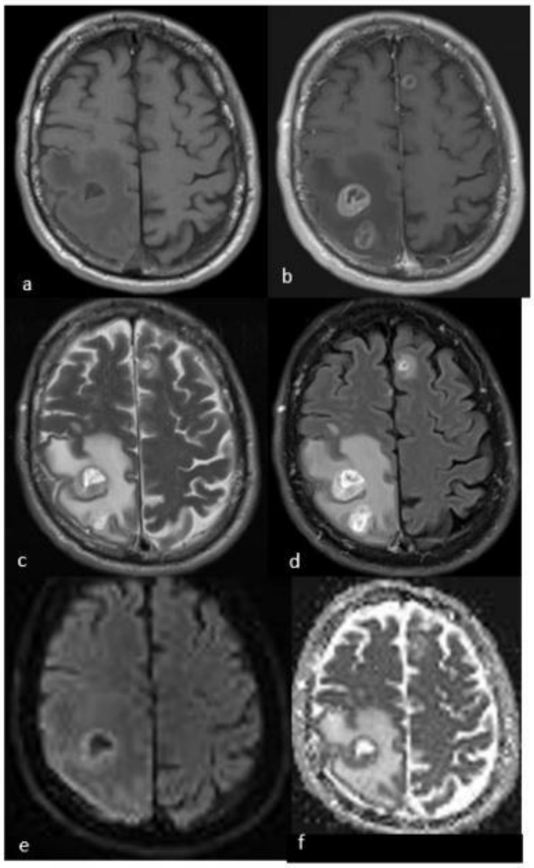

Figure 1 – Signal characteristics of representative brain lesion

Brain MRI at the initial presentation; axial T1 (a), T1 post contrast (b), T2 (c), FLAIR (d), DWI (e), and ADC (f) images showing multiple thick, irregular-walled ring enhancing lesions with surrounding edema.

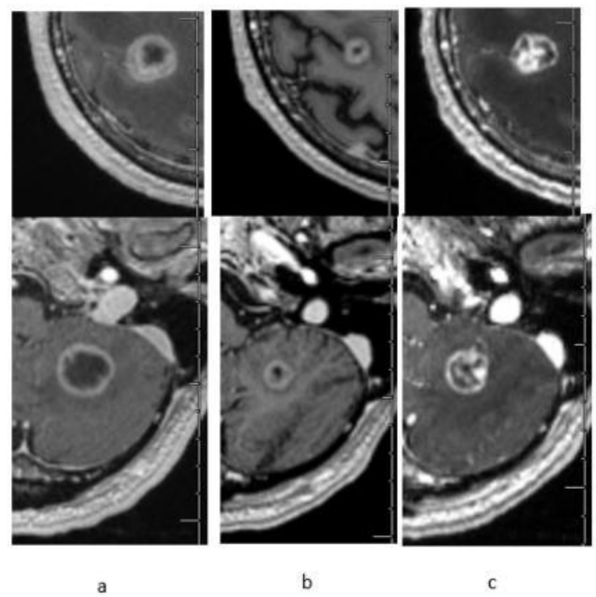

Figure 2 – Serial followup before, during, and following steroid therapy

Lesion size on sequential axial post-contrast T1 brain MRI sequences (top row right parietal lesion, bottom row left cerebellar lesion) performed on initial ED presentation (a), follow-up three weeks later on maintenance steroids (b), and 7 weeks after steroid taper (c).

(Filename: TCT_2396_paradoxicalregressionabstractfigure.JPG)

3062

1:44PM - 1:48PM

Septum Pellucidum Malignant Germinoma - a Rare Case Report

Y Munir[1], J Rogers[2], C SITTON[3], R Jordan[4]
[1]University of Texas-Houston, Houston, TX, [2]UNIVERSITY OF TEXAS HEALTH SCIENCES CENTER AT HOUSTOIN, Houston, TX, [3]UNIVERSITY OF TEXAS - HOUSTON MEDICAL SCHOOL, HOUSTON, TX, [4]University of Texas-Houston, HOUSTON, TX

Purpose
To illustrate a rare case of a septum pellucidum malignant germinoma.
Materials and Methods
19 year old woman with history of intermittent migraines that progressed to daily migraines. Presented after episode of right upper extremity numbness lasting 10 minutes followed by nausea and vomiting.

Results
CT findings: heterogeneous enhancing mass with solid components hyperdense relative to gray matter
MRI findings: Diffusion restriction in solid components Multiple small cysts best seen on T2 Avid enhancement
Conclusions
Germinoma is a tumor of primordial germ cells, histologically identical to gonadal or extragonadal seminoma and dysgerminoma. Intracranial germ cell tumors represent ~2% of primary intracranial tumors, predominately affecting children and young adults. These tumors classically occur in the pineal region (40-50%) with majority extending into bilateral thalami and/or 3rd ventricle. Suprasellar region is 2nd most common location (30-40%). CSF spread of metastasis is common (25-40%). A few case reports have described germinomas that arise from the septum pellucidum, however this is an extremely rare location for GCT. Important to image the entire CNS due to the high occurrence of CSF metastasis at the time of diagnosis.

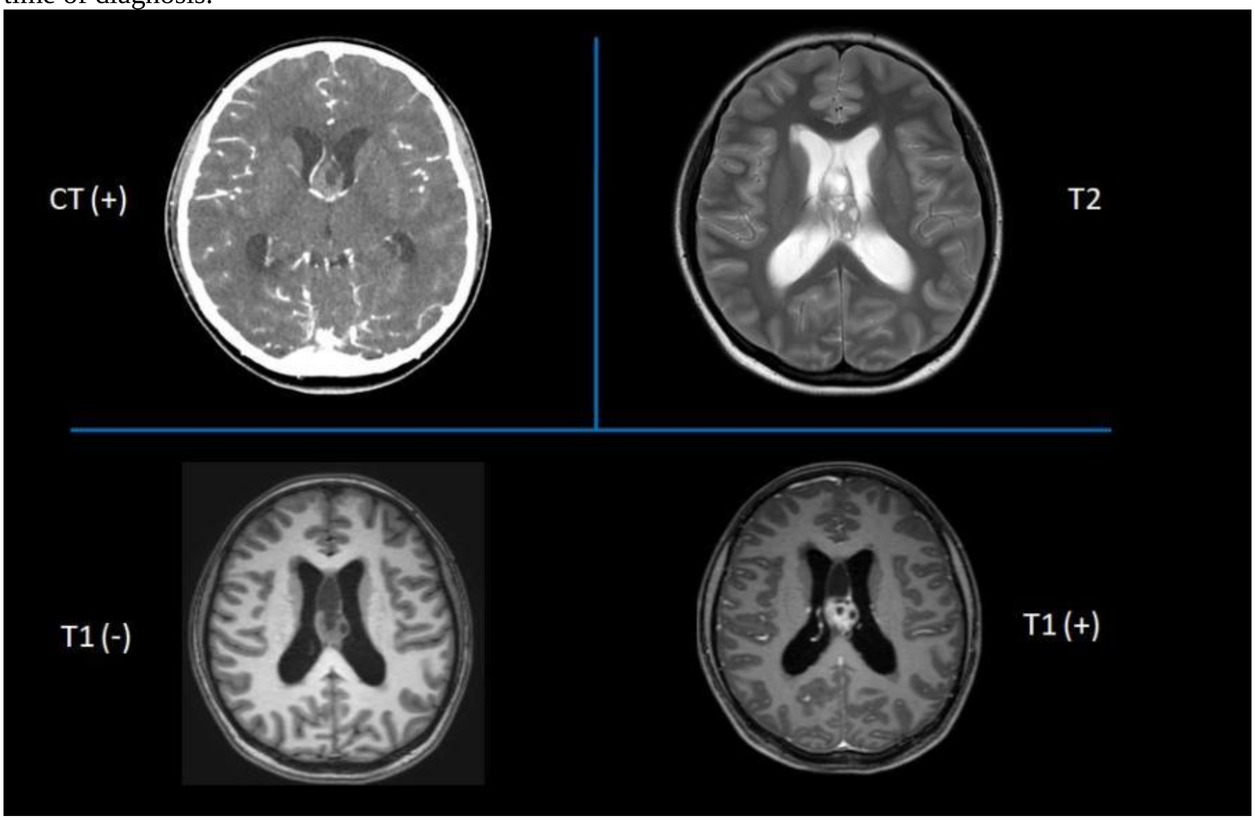

(Filename: TCT_3062_Imagesubmission.JPG)

2186

1:48PM - 1:52PM

Trigeminocardiac Reflex during Onyx Embolization of a Posterior Fossa Hemangioblastoma

A Kuhn[1], P Foreman[1], A Thomas[1]
[1]Beth Israel Deaconess Medical Center, Boston, MA

Purpose
To highlight the importance of dural innervation during embolization of a posterior fossa tumor involving the tentorium cerebelli.
Materials and Methods
A 40-year-old male with a recurrent posterior fossa hemangioblastoma presented electively for Onyx

embolization prior to re-resection of the tumor. During the interventional procedure, the middle meningeal artery was catheterized for embolization of a tumor feeder. During injection of Onyx, the patient became bradycardic with a subsequent several beat asystole. Onyx injection was stopped and shortly thereafter, the patient's heart rate normalized. Onyx injection was resumed and the same phenomenon was observed a second time. Intravenous atropine was administered and the embolization was completed without further bradycardic or asystolic episodes.
Results
There is a well-circumscribed and gently lobulated 3.9 x 2.6 x 2.3 cm (APxTRxSI) intensely enhancing mass in the left posterior fossa with involvement of the tentorium cerebelli, consistent with recurrent hemangioblastoma (Fig 1A). Left common carotid artery contrast injection shows arterial tumor feeders from the posterior auricular artery and middle meningeal artery (Fig 1B). Left external carotid artery injection following successful Onyx embolization of a branch of the middle meningeal artery (arrow) with small residual tumor blush (Fig 1C).
Conclusions
The trigeminocardiac reflex (TCR) is an autonomic brainstem reflex that results in bradycardia due to stimulation of the trigeminal nerve and its branches. Patients recover after cessation of the causative stimulus. The tentorium cerebelli is partially supplied by tentorial branches of the ophthalmic and maxillary divisions of the trigeminal nerve and the possibility of eliciting a TCR during embolization of tumors involving the tentorium cerebelli should be considered.

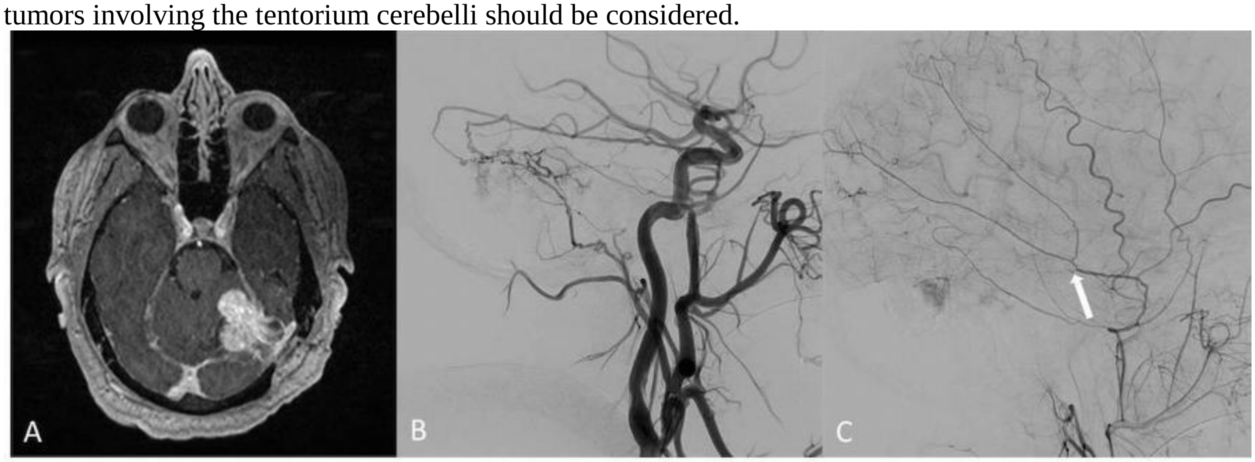

(Filename: TCT_2186_TCR_Figure1.jpg)

2476

1:52PM - 1:56PM

Unusual Presentation and Imaging Findings of a Rare Supratentorial Neurenteric Cyst

E Portela de Oliveira[1], V Tsehmaister-Abitbul[2], C Torres[3], N Zakhari[4]
[1]University of Ottawa - The Ottawa Hospital, Ottawa, Ontario, [2]University of Ottawa, Ottawa, Ontario, [3]UNIVERSITY OF OTTAWA, OTTAWA, ON, [4]The Ottawa Hospital/University of Ottawa, Ottawa, ON

Purpose
Neurenteric cysts or enterogenous cysts are rare benign endodermal lesions of the central nervous system. They more commonly present in the spine and posterior fossa, though rare supratentorial cysts have been reported. We will present a rare case of Supratentorial Neurenteric Cyst with unusual presentation. We will delineate the imaging spectrum of intracranial cysts described in the literature and we will briefly discuss basic embryogenesis, pathology, and differential diagnosis of these cysts.
Materials and Methods
We report an unusual presentation of a Neurenteric Cyst found incidentally in a 30-year-old gentleman

after head trauma. Post-concussion noncontract CT demonstrated a large right frontoparietal cyst with hyperdense material suspicious for hemorrhage. MRI was performed and remonstrated the cystic lesion in the right frontoparietal region with some focus of hemorrhage and minimal enhancement at the wall of the cyst. Serial imaging has revealed a subsequent decrease and increase in the size of the lesion over 3 years period and the patient remained asymptomatic. After this period, he started to experience headaches and paresthesia at the left hand. Following new component of hemorrhage, enlargement of the lesion and worsening of symptoms a craniotomy was performed for excision of the lesion. Histopathology confirmed Neurenteric Cyst.

Results

Serial brain imaging MRI and CT show a large right frontoparietal cystic lesion, areas of hemorrhage and enhancement of the walls.

Conclusions

We present imaging findings of a rare Supratentorial Neurenteric Cyst with unusual presentation.

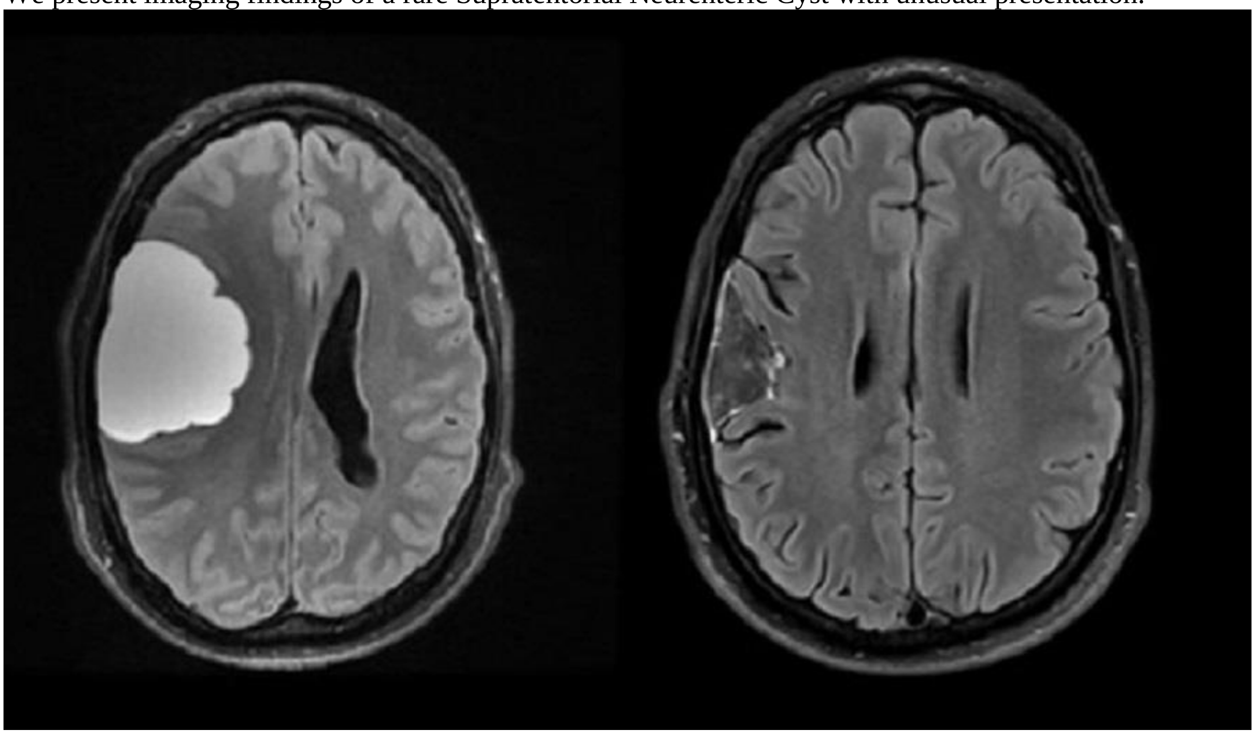

(Filename: TCT_2476_PictureNeurenteric300.jpg)

3583

1:56PM - 2:00PM

Multiparametric MRI Assessment of Response to Convection Enhanced Intratumoral Delivery of MDNA55, an Interleukin-4 Receptor Targeted Immunotherapy for Recurrent Glioblastoma

S Mohan[1], S Wang[2], S Chawla[3], K Abdullah[4], A Desai[2], E Maloney Wilensky[5], S Brem[2]
[1]University of Pennsylvania School of Medicine, Philadelphia, PA, [2]Hospital of the University of Pennsylvania, Philadelphia, PA, [3]Perelman School of Medicine at University of Pennsylvania, Wallingford, PA, [4]Perelman School of Medicine at the University of Pennsylvania, and the University of Pennsylvania He, Philadelphia, PA, [5]University of Pennsylvania, Philadelphia, PA

Purpose

Glioblastoma is the most common malignant brain tumor, and carries a dismal prognosis. Attempts to develop biologically targeted therapies are challenging as the blood-brain barrier can limit drugs from reaching their target when administered via conventional (intravenous or oral) routes. Furthermore, systemic toxicity of drugs often limits their therapeutic potential. To circumvent these problems, convection-enhanced delivery (CED) provides direct, targeted, intralesional therapy with a secondary objective to alter the tumor microenvironment from an immunologically "cold" (nonresponsive) to an inflamed (immunoresponsive) tumor. We describe our initial experience with multiparametric MRI to assess short term response to CED of a fusion protein MDNA55 (a targeted toxin directed toward the interleukin-4 receptor) in a patient with recurrent glioblastoma.

Materials and Methods

A 57-year-old female with right occipital recurrent glioblastoma, IDH-wild type and MGMT promoter methylated, was treated with MRI guided convection enhanced intratumoral delivery of MDNA55.

Results

The patient underwent serial MRI scans including a baseline and one-month follow-up MRI on a 3 T MRI scanner, (Tim Trio; Siemens, Erlangen, Germany) using a 12-channel phased array head coil. The imaging protocol included an axial 3D T1-weighted magnetization-prepared rapid acquisition of gradient-echo (MPRAGE) images; fluid attenuated inversion recovery (FLAIR) images; diffusion tensor imaging using 30 directions and dynamic susceptibility contrast (DSC) MRI perfusion. The corrected raw images were combined to compute mean diffusivity (MD) and fractional anisotropy (FA). Leakage corrected cerebral blood volume (CBV) maps were constructed using Nordic ICE program (nordicICE, Nordic Imaging Lab, Bergen, Norway). MD, FA, CBV maps and FLAIR images were co-registered to postcontrast T1-weighted images and a semi-automated routine was used to segment the contrast-enhancing region of tumor. The CBV values were normalized to the contralateral normal white matter to generate relative CBV (rCBV) values. Median values of MD and FA were computed from the enhancing region at each time point. The top 90th percentile rCBV values were measured from the enhancing region and reported as maximum rCBV (rCBVmax). On conventional imaging there was a significant reduction of contrast enhancement which was observed during this period which could be indicative of tumor necrosis. Increased MD along with decreased FA and rCBVmax were noted at 1 months relative to baseline consistent with tumor response, with reduced cellularity and vascular normalization (Figure 1). As there is no tissue immunophenotyping, it is unknown whether the favorable local response is due to a direct pharmacological effect or an induced immunomodulatory effect.

Conclusions

Monitoring of patients using MRI remains a challenge in immunotherapy-based clinical trials. Our preliminary findings indicate the potential of advanced multiparametric MRI to assess early response to convection enhanced intratumoral delivery of MDNA55 (a targeted toxin directed toward the interleukin-4 receptor) in glioblastoma patients.

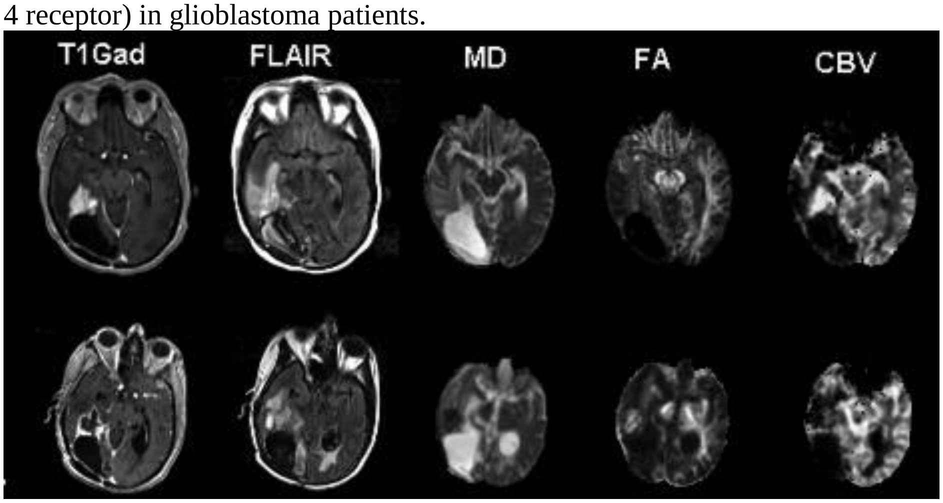

(Filename: TCT_3583_Figure1.jpg)

Monday, May 20, 2019
2:55PM - 4:25PM
AI/Advanced Imaging in Preoperative Planning and Beyond

3002

2:55PM - 3:02PM

Age-Related Microstructural Alterations in the Corpus Callosum Measured by High-Gradient Diffusion MRI

Q Fan[1], Q Tian[1], A Nummenmaa[1], T Witzel[1], S Tobyne[1], E Klawiter[1], B Rosen[1], L Wald[1], D Salat[1], S Huang[1]
[1]Athinoula A. Martinos Center for Biomedical Imaging, Massachusetts General Hospital, Boston, MA

Purpose
Cerebral white matter exhibits degenerative changes during the course of normal aging. Noninvasive approaches to probe microstructural alterations in white matter would be invaluable for understanding the substrate and regional variability of age-related white matter degeneration. Recent advances in diffusion MRI have leveraged high gradient strengths to increase sensitivity toward axonal size and density in the living human brain[1, 2]. The goal of this study is to explore age-related differences in apparent axon diameter and density in the corpus callosum estimated using high-gradient diffusion MRI.
Materials and Methods
A total of 36 healthy, cognitively normal adults (aged 22-72, 23F) participated in this study. Imaging data were acquired on the 3T Connectome scanner equipped with 300 mT/m maximum gradient strength.[3] Sagittal 2-mm isotropic resolution diffusion-weighted images were acquired with whole brain coverage: TR/TE = 4000/77ms, gradient duration=8ms, diffusion time=19/49ms, 8 diffusion gradient strengths between 30-290 mT/m per diffusion time, 32-64 diffusion directions per gradient strength. Corpus callosum masks were created from FreeSurfer labels and were further divided into five sub-sections. Correlation analyses were performed between age and the ROI-averaged axonal metrics.
Results
Apparent axon diameter and axon density were significantly correlated with age in the whole corpus callosum (Figure). Similar analyses in sub-regions of the corpus callosum showed the strongest age-related effects in the axonal metrics in the genu of the corpus callosum, but not in the splenium.
Conclusions
The regionally selective, age-related axonal alterations in the corpus callosum estimated from high-gradient diffusion MRI are consistent with previously reported findings on histology[4]. Our results support an anterior-to-posterior gradient of axonal degeneration with age, in keeping with previously reported age-related differences in FA within anterior versus posterior fiber bundles[5], suggesting that the underlying substrate of age-related white matter degeneration may relate to fiber size and packing density.

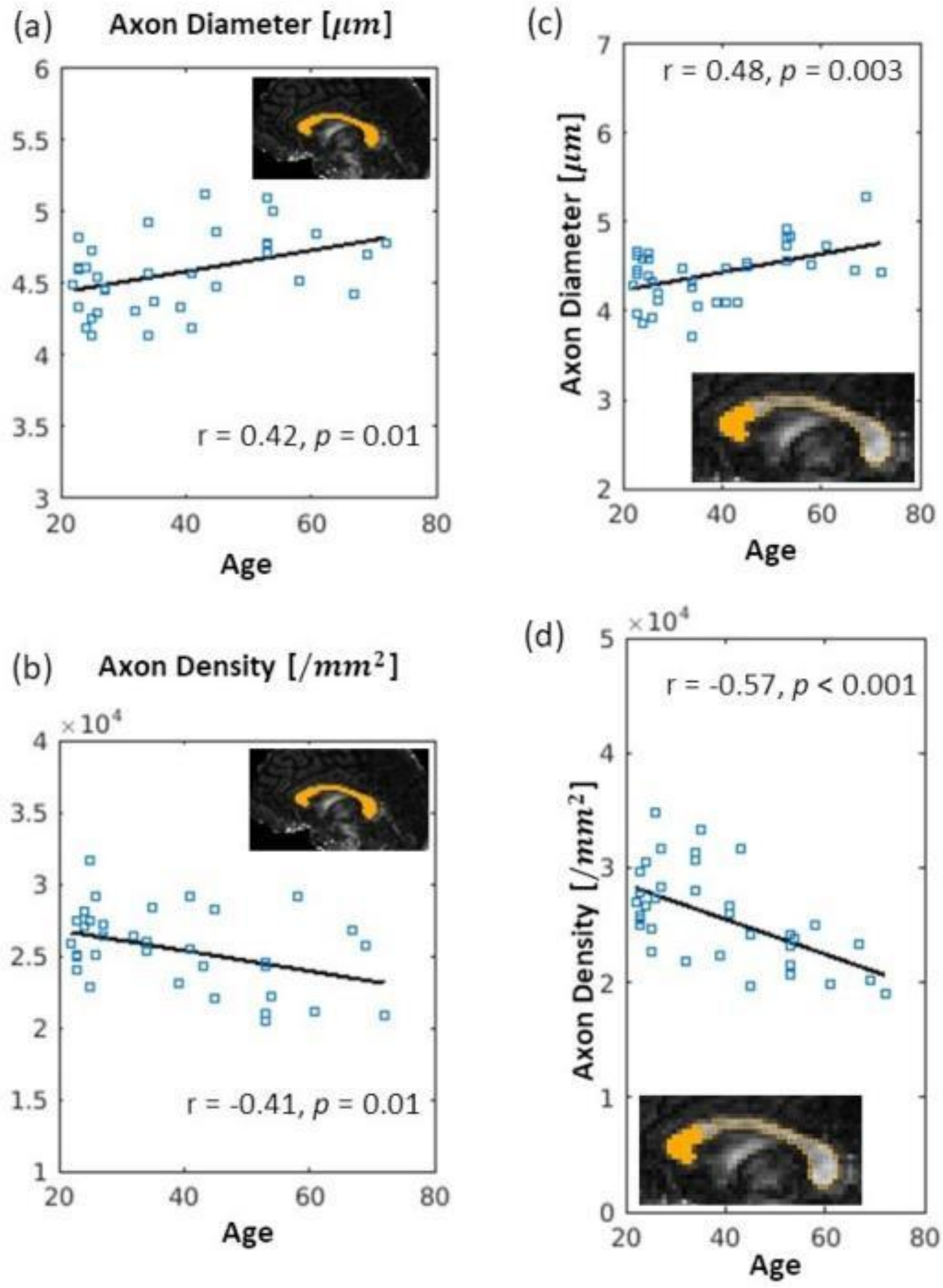

Figure. Correlations of axonal microstructural metrics in the corpus callosum with age. (a) Axon diameter increased with age, and (b) axon density decreased with age throughout the corpus callosum, (c,d) with the strongest correlation found in the genu of the corpus callosum. Pearson's linear correlation controlling for gender was used to report the correlation coefficients (r) and significance level (p).

(Filename: TCT_3002_Figure.jpg)

2910

3:02PM - 3:09PM

Bayesian Networks to Aid Spine MRI Interpretation

R Mattay[1], J Rudie[1], N Cross[2], S Mohan[1]
[1]Perelman School of Medicine at University of Pennsylvania, Philadelphia, PA, [2]University of Washington, Seattle, WA

Purpose
Accurate MRI diagnosis of spinal pathology (SP) requires integration of a variety of imaging features together with clinical and demographic factors. Bayesian networks (BN) can estimate the probability of multiple diagnoses based on these inputs and have the potential to improve clinical diagnostic accuracy (1). Here, we explore the utility of BNs in spine MRI interpretation to better differentiate a varied set of spine disorders.
Materials and Methods
A naive BN was generated consisting of 47 parent "disease" nodes connected to 14 child "feature" nodes including MR signal and spatial characteristics. Pre-test probabilities (PP) for each disease and the probability of a specific feature in the setting of each disease were generated from literature review and expert neuroradiologist input. 59 cases with varied SP were selected from the Picture Archiving and Communication System (PACS). Inclusion criteria included either a pathology report confirming the neuroradiologist's final diagnosis or a strong consensus agreement on the diagnosis by three expert radiologists. A radiologist identified distinguishing features from these cases, which were processed through the BN to determine the three highest-probability differential diagnoses. BN's performance with the top diagnosis and the top three diagnoses was evaluated with and without inclusion of pre-test probabilities.
Results
Accuracy for correct differential diagnosis (within top 3) was 44% and 31% for the exact correct diagnosis (with chance prediction at 6.4% and 2.1%; $p < .001$). When pre-test probabilities were included in the model this improved to 58% for correct differential diagnosis and 42% for exact correct diagnosis. The sensitivity for and specificity without pre-test probabilities was 0.36 and 0.99 (AUC = 0.71). The sensitivity and specificity with pre-test probabilities was 0.54 and 0.99 (AUC = 0.77)
Conclusions
These preliminary results demonstrate the potential utility of BNs for enhancing Spine MRI interpretation and show that inclusion of pre-test probability improves network output. Future work including a more robust validation set using real-world cases will further mitigate biases from textbooks and clinical resources on 'classic' appearance of pathology and emphasize intra-case variability.

2442

3:09PM - 3:16PM

Cross-Institutional Generalizability of a Deep Learning Model for Automated Stenosis Grading of Lumbar Spine MRI

W Wiggins[1], S Pomerantz[2], J Lu[3], B Canedo Bizzo[2], M Caton[4], N Tenenholtz[3], M Michalski[3], R Gonzalez[2], K Andriole[1]
[1]Brigham & Women's Hospital/Harvard Medical School, Boston, MA, [2]Massachusetts General Hospital, Boston, MA, [3]MGH-BWH Center for Clinical Data Science, Boston, MA, [4]Brigham and Women's Hospital, Boston, MA

Purpose
An important question in medical imaging AI is whether algorithms developed at one institution will generalize, i.e. perform equivalently on data from others. Algorithms trained on images from one set of equipment and acquisition protocols may perform differently on other images. Previously, we trained and validated DeepSPINE, a deep learning model for automated stenosis grading of lumbar spine MRI on data from one of the institutions ("Institution A") in our network. To evaluate its generalizability, we assessed performance on a large cohort from another ("Institution B").
Materials and Methods
DeepSPINE consists of separate convolutional neural networks for vertebral segmentation and stenosis grading. The data from "Institution A" used for training and validation included 4,075 cases (22,796 disc-levels) performed with various scanner models, manufacturers and imaging protocols. Segmentation results were subject to a quality control (QC) checkpoint prior to stenosis grading. Model generalizability was assessed by comparing performance between independent test sets of consecutive cases from each institution, including 800 cases and 3,415 disc-levels from "A", and 303 cases and 1,544 disc-levels from "B". Ground truth stenosis grades for training and validation were extracted from each cohort's associated free-text radiology reports by natural language processing.
Results
DeepSPINE generalized well, demonstrating similar performance for foraminal and central stenosis grading when applying the algorithm trained at "A" to cases from "B" (see Table). Segmentation performance was slightly lower (81% on "B" vs. 88% on "A") and successful QC identification of faulty segmentation was slightly higher (69% on "B" vs. 62% on "A").
Conclusions
Performance assessment on internal data is critical prior to clinical deployment of an AI algorithm developed at another institution. DeepSPINE demonstrated strong cross-institutional generalizability for segmentation and stenosis grading of lumbar spine MRI. Future work will evaluate the effect of transfer learning on performance by retraining the model on data from both institutions.

Accuracy	Normal	Mild/Moderate	Severe
Foraminal Stenosis			
Institution A **Institution B**	79.6% 75.8%	84.2% 84.1%	70.5% 67.8%
Central Stenosis			
Institution A **Institution B**	79.7% 85.4%	83.7% 74.1%	77.7% 81.3%

(Filename: TCT_2442_Table_ASNR.jpg)

2217

3:16PM - 3:23PM

Data Set Assembly

Z Guan[1], R Bruce[2], J Garrett[2]
[1]University of Wisconsin Hospital and Clinics, Madison, WI, [2]University of Wisconsin - Madison, Madison, WI

Purpose

Recent developments in machine learning and deep learning algorithms have raised significant interest in applications to radiology. Successful application of these techniques often requires a very large imaging dataset. For example, the DeepFace facial recognition system used 4.4 million labeled face images from Facebook to create an algorithm which approaches human-level performance. Assembling large, quality medical imaging datasets is laborious and time consuming. Indexed databases of radiology reports have been developed along with search software to identify studies of interest, but these must be sorted accurately into positive and negative cases to ensure quality. Irrelevant or duplicate studies also must be screened out. Newer software with natural language processing (NLP) features can automatically sort reports into positive and negative cases, but the performance of these systems has not been studied. The purpose of this paper is to review our experience using industry-designed software implementing NLP to assemble a dataset of 3,064 CT studies depicting spinal disorders and spinal anatomy for machine learning application.

Materials and Methods

Software An indexed database containing all radiology reports from 2001–2018 at an academic medical center was queried using an Apache Lucene-based search program with NLP features developed by an industry sponsor. This program identified studies of interest based on search terms and modality and automatically sorted the results into positive and negative categories. Search targets A list of 14 search targets including spinal disorders and anatomic variants was created in agreement with the industry sponsor. The targets are listed in the Table. Search terms and report categorization Appropriate search terms were generated for each target and the database was queried. Search results were limited to CT reports with unique accession numbers with a maximum of 500 reports. The search results were then manually categorized into positive and negative cases. A third category was used for reports which were obviously duplicated. For example, the same report might be used for CTs of the cervical, thoracic, and lumbar spine listed under different accession numbers. A fourth category was used for erroneous search results. For example, some of the search results did not contain the search term at all, and others were reports for studies of the wrong modality. Analysis The automatic sorting results were cross-tabulated with manual categorization to determine the software's performance. Search term performance was indirectly assessed by the total yield of positive cases and the fraction of search results which were positive cases.

Results

NLP performance The search terms used, search results, and categorization are summarized in the Table. A total of 6,532 search results were obtained, of which 4,975 were automatically sorted as positive (76%) and 1,557 negative (24%). This yielded, by the manual categorization, 3,064 positive cases (47%), 97 negative cases (1%), 239 duplicate cases (4%), and 3,132 (48%) erroneous cases. 2,480 (81%) of the 3,064 positive cases were correctly sorted as positive by the software and 21 (22%) of the 97 negative cases were correctly sorted as negative. Among the 4,975 search results sorted as positive, 2,480 (50%) were positive cases and 76 were negative cases (2%). Among the 1,557 search results sorted as negative, 584 (38%) were positive cases and 21 (1%) were negative cases. Search term performance The number of search results obtained by querying the search terms ranged from 428–497 with a median of 467. The yield of the search terms ranged from 0–454 positive cases with a median of 229.5 cases. The fraction of search results which were positive cases ranged from 0–97% with a median of 51%. H-shaped vertebra had the lowest yield and efficiency. Diffuse idiopathic skeletal hyperostosis had the highest yield and efficiency. Shorter search terms and those with fewer words yielded more positive cases at the expense of more negative cases. For example, we identified reports in which limbus vertebrae were variously referred to as limbus deformity, limbus body, limbus configuration, limbus fragment, or limbus in different reports. Using the search term limbus rather than limbus vertebra allowed us to identify these variants. However, this also identified reports which included limbus calcifications (arcus senilis) and a report describing a saddle limbus (saddle embolus).

Conclusions

Searching indexed databases of radiology reports is an effective way to identify large datasets for machine learning application, but the reports must be verified manually to ensure quality, making this a laborious process. Software implementing NLP may applied to assist with this process, but further refinement is needed to improve the performance of these systems. A more streamlined process for generating large, high-quality imaging datasets is needed to enable future work on machine learning applications in radiology.

Table: Targeted radiologic findings, search terms used, and search results by category

Search target	Search term	Automated categorization	Manual categorization (%)
Hemivertebra	hemivertebra	Positive: 335	Positive: 83 (25) Negative: 14 (4) Duplicate: 25 (7) Erroneous: 213 (64)
		Negative: 111	Negative: 2 (2) Positive: 6 (5) Duplicate: 1 (1) Erroneous: 102 (92)
Lumbarized S1	lumbarized	Positive: 391	Positive: 241 (62) Negative: 2 (1) Duplicate: 15 (4) Erroneous: 133 (34)
		Negative: 60	Negative: 1 (2) Positive: 41 (68) Duplicate: 3 (5) Erroneous: 15 (25)
Sacralized L5	sacralized	Positive: 358	Positive: 292 (82) Negative: 43 (12) Duplicate: 23 (6)
		Negative: 70	Negative: 7 (10) Positive: 52 (74) Duplicate: 11 (16)
Vertebra plana	plana	Positive: 345	Positive: 160 (46) Negative: 1(0) Duplicate: 6 (2) Erroneous: 178 (52)
		Negative: 98	Positive: 17 (17) Duplicate: 1 (1) Erroneous: 80 (82)
Dextroscoliosis	dextroscoliosis	Positive: 403	Positive: 357 (89) Duplicate: 46 (11)
		Negative: 74	Positive: 70 (95) Duplicate: 4 (5)
Levoscoliosis	levoscoliosis	Positive: 368	Positive: 346 (94) Duplicate: 22 (6)
		Negative: 97	Positive: 94 (97) Duplicate: 3 (3)
Ankylosing spondylitis	ankylosing	Positive: 370	Positive: 254 (69) Negative: 3 (1) Duplicate: 36 (10) Erroneous: 77 (21)
		Negative: 93	Positive: 50 (54) Duplicate: 10 (11) Erroneous: 33 (35)
Block vertebra	block vertebra	Positive: 353	Positive: 37 (10) Duplicate: 3 (1) Erroneous: 313 (89)
		Negative: 135	Erroneous: 135 (100)
Butterfly vertebra	butterfly vertebra	Positive: 353	Positive: 33 (9) Negative: 1 (0) Duplicate: 4 (1) Erroneous: 315 (89)
		Negative: 127	Positive: 3 (2) Duplicate: 1 (1) Erroneous: 123 (97)
Spinal decompression	spinal decompression	Positive: 360	Positive: 37 (10) Duplicate: 4 (1) Erroneous: 319 (89)
		Negative: 127	Erroneous: 127 (100)
Diffuse idiopathic skeletal hyperostosis	diffuse idiopathic skeletal hyperostosis	Positive: 347	Positive: 343 (99) Negative: 2 (1) Erroneous: 2 (1)
		Negative: 122	Positive: 111 (91) Erroneous: 11 (9)
Limbus vertebra	limbus	Positive: 295	Positive: 283 (96) Negative: 9 (3) Duplicate: 3 (1)
		Negative: 152	Negative: 3 (2) Positive: 139 (91) Duplicate: 10 (7)
Lumbar rib	l1 rib	Positive: 347	Positive: 14 (4) Negative: 1 (0) Duplicate: 7 (2) Erroneous: 325 (94)
		Negative: 144	Negative: 1 (1) Positive: 8 (6) Duplicate: 1 (1) Erroneous: 134 (93)
H-shaped vertebra	h-shaped vertebra	Positive: 350	Erroneous: 350 (100)
		Negative: 147	Erroneous: 147 (100)

(Filename: TCT_2217_table.jpg)

3570

3:23PM - 3:30PM

DeepSPINE: AI-Enhanced Lumbar-Spine MRI Interpretation & Reporting

S Pomerantz[1], J Lu[2], B Canedo Bizzo[1], W Wiggins[3], M Caton[4], N Tenenholtz[2], S Doyle[5], K Andriole[6], M Michalski[2], R Gonzalez[1]
[1]Massachusetts General Hospital, Boston, MA, [2]MGH-BWH Center for Clinical Data Science, Boston, MA, [3]Brigham & Women's Hospital/Harvard Medical School, Boston, MA, [4]Brigham and Women's Hospital, Boston, MA, [5]MGH & BWH Center for Clinical Data Science, Boston, MA, [6]MGH & BWH Center for Clinical Data Science, Brigham & Women's Hospital/Harvard Medical School, Boston, MA

Purpose
Spinal MRI is an expensive study performed at high volumes due to the prevalence of low-back pain. Radiologic interpretation, however, remains time-consuming with high inter-reader variability even among those with sub-specialty expertise. An automated system for spinal MRI analysis can help address these and other workflow and reporting issues. We report on the efficient methodology and performance of our deep learning-based system for automated lumbar stenosis grading with clinical integration.
Materials and Methods
Natural language processing (NLP) was utilized to efficiently extract per-level numerical stenosis grades from large-scale archival free-text radiology reports. Distinct stenosis grades for spinal canal and foramina for each of 6 levels per study were extracted from 4,075 free-text lumbar spinal MRI reports generated by 67 different radiologists from a recent 2 year period. Automated vertebral level segmentation on corresponding study images was performed using a U-Net convolutional neural network (CNN) which generated axial images obliquely-reformatted to each disc level. The NLP-extracted grades were applied as weakly-supervised labels to corresponding spinal level volumes to train a 3D ResNeXt-50 algorithm for stenosis grading. Automated quality control checkpoints are implemented in the pipeline for clinical integration to prevent faulty analysis from segmentation failures from being presented to radiologists. Saliency maps are generated to visualize localized regions of pathology to help readers validate stenosis grade inferences. Automatially-generated text from the algorithm's stenosis inferences is available for insertion into appropriate spinal-level fields within the radiology reports templates utilized in our institution's reporting software via a customized integration.
Results
DeepSPINE was evaluated on an independent test set of consecutive cases from multiple MR scanners and imaging centers within the same institution. Vertebral body segmentation was successful in 88% (705/800) of cases. Performance for stenosis grading was performed by comparing algorithm classification to original report text as ground truth labels. For Normal, combined Mild/Moderate, and Severe categories, the model achieves 84.4%, 74.9% and 77.0% accuracy for central canal stenosis and 80.3%, 79.9% and 74.6% for foraminal stenosis, respectively. DeepSPINE performed well across a range of challenging cases with varying degrees of disease severity and image artifact. Class-specific saliency maps for DeepSPINE adds further clarity and confidence for readers of algorithmic inferences.
Conclusions
DeepSPINE demonstrates the feasability of an AI-based system for automated lumbar vertebral segmentation and spinal stenosis grading. It achieved high performance utilizing NLP-derived weakly-supervised labels applied to automatically-segmented spinal imaging study data. Our quality control checkpoint failures identify potential areas for improvement in future model development as well as expanding model prediction capabilities to other imaging features of spinal degeneration. We will also further assess impact of clinical integration.

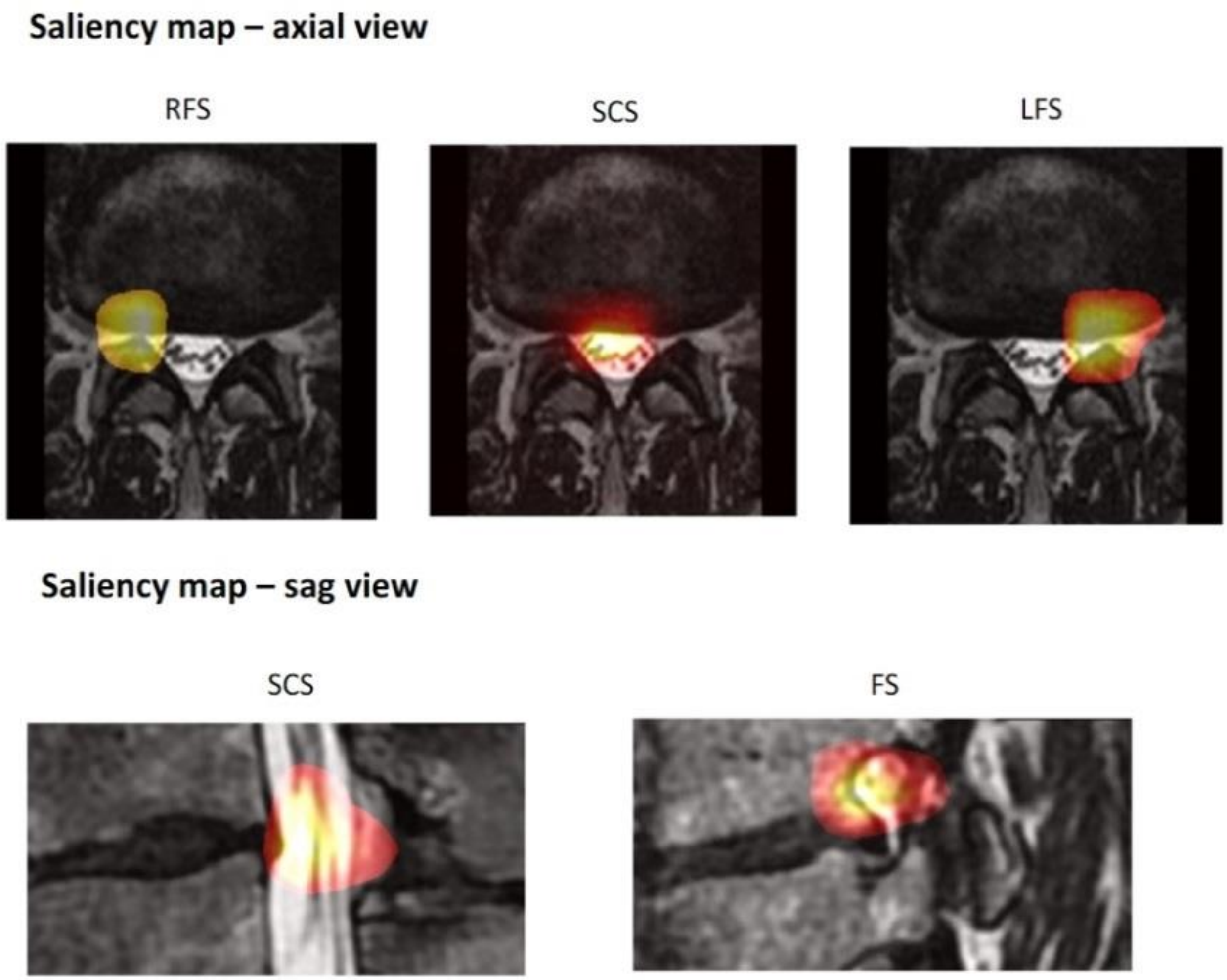

(Filename: TCT_3570_SaliencyMap.jpg)

2624

3:30PM - 3:37PM

Diagnostic Utility of 68-Gallium-DOTATATE PET in the Diagnosis and Management of Somatostatin Receptor Positive CNS Tumors

M Roytman[1], N Karakatsanis[1], R Magge[1], D Pisapia[1], J Osborne[1], T Schwartz[1], A Tassler[1], S Pannullo[1], J IVANIDZE[1]
[1]*New York-Presbyterian Hospital/Weill Cornell Medicine, New York, NY*

Purpose
68-Gallium-DOTATATE, a highly sensitive and specific PET radiotracer targeting somatostatin receptor 2 (SSTR2), has entered clinical practice for the management of gastrointestinal neuroendocrine tumors. SSTR2 positive CNS tumors, such as meningioma, esthesioneuroblastoma, and paraganglioma, are promising targets for 68-Gallium-DOTATATE PET. We present a pilot analysis of the diagnostic utility of 68-Gallium-DOTATATE PET in these entities compared to standard-of-care imaging.
Materials and Methods
IRB approval with waived consent was obtained for this retrospective case series. We evaluated a total of

14 patients with meningioma (PET/MRI), 3 patients with paraganglioma (PET/CT) and 3 patients with esthesioneuroblastoma (PET/CT). PET acquisition was performed in 3D list mode for 40 minutes; MR- and CT-based attenuation correction was performed according to manufacturer's specifications. Each meningioma and paraganglioma case was assessed for N(tumors) with PET compared to conventional imaging. In esthesioneuroblastoma, SUVmax measurements discriminated between metastatic and reactive lymph nodes; SUVmax of suspected metastatic nodes were compared to SUVmax of nodes that did not enlarge on follow-up imaging. Mann-Whitney-U-tests were performed to determine statistical significance.

Results

Conventional MRI demonstrated a total of 38 tumors in the meningioma and paraganglioma cohorts combined; DOTATATE PET revealed an additional 11 tumors in 5 patients that were not identified prospectively. The esthesioneuroblastoma cohort had a combined 18 significant lymph nodes described on CT; 4 nodes demonstrated initial average SUVmax 9.8 (range: 2.6 - 18.1), which, on 6-month follow up, demonstrated average SUVmax 35.0 (range: 7.5 – 84.5), suspicious for metastatic disease; 14 nodes demonstrated average SUVmax 2.8 (range: 1.2 – 5.2), which were decreased to unchanged on follow-up, suggesting no evidence of metastatic involvement.

Conclusions

68-Gallium-DOTATATE PET demonstrates diagnostic utility in the diagnosis and management of SSTR-positive CNS tumors by detecting additional lesions not otherwise identified on conventional MRI alone and identifying sites of suspected nodal metastases. These findings allow for targeted follow-up and the potential to improve disease monitoring and clinical outcomes. This pilot data lays the groundwork for future studies characterizing SUV thresholds for nodal metastases and distinguishing recurrent tumor from treatment-related change in patients post resection and/or radiation therapy. Limitations of this case series include a small patient cohort, the possibility of partial volume averaging errors based on lesion size and the absence of pathologic correlation. Future prospective studies with a larger patient cohort, longitudinal follow-up, and pathologic correlation will expand the fund of knowledge established in this pilot evaluation. In summary, DOTATATE PET is a promising tool improving initial diagnosis and monitoring for extent of disease in SSTR-positive CNS tumors.

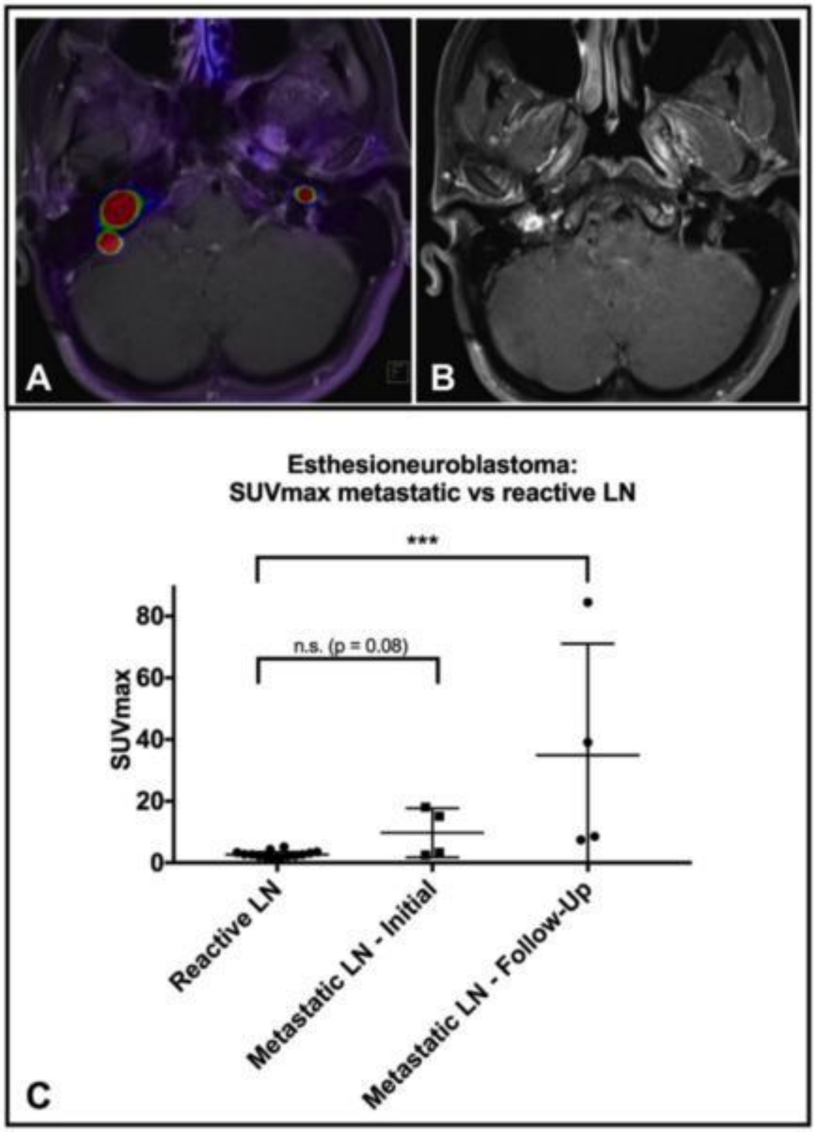

A and B – Axial 68-Gallium-DOTATATE PET/MRI (A) and Axial DIXON post-contrast MRI (B) demonstrate a heterogeneously enhancing soft tissue mass along the right posterolateral skull base, demonstrating intense associated DOTATATE avidity, SUVmax 236.3, consistent with known glomus jugulare. Additional intensely DOTATATE avid lesions are identified in the right petrous temporal bone and lateral to the left jugular foramen, not prospectively identified on conventional MRI alone, suspicious for additional paragangliomas.

C – Scatter plots comparing SUVmax of reactive lymph nodes, suspected metastatic lymph nodes on initial imaging and suspected metastatic lymph nodes on follow-up imaging. 18 significant lymph nodes were identified; 14 were reactive (SUVmax 2.8; range: 1.2 – 5.2); 4 nodes were suspicious for metastases, with initial average SUVmax 9.8 (range: 2.6 - 18.1), and 6-month follow up average SUVmax 35.0 (range: 7.5 – 84.5).

(Filename: TCT_2624_MichelleFigureASNR.jpg)

3343

3:37PM - 3:44PM

High-Resolution Whole Brain ASL Perfusion using Cartesian FSE and Compressed-Sensing

M Taso[1], L Zhao[2], D Alsop[1]
[1]Beth Israel Deaconess Medical Center, Harvard Medical School, Boston, MA, [2]Children's National Medical Center, Washington, DC

Purpose
While volumetric whole brain ASL perfusion is feasible and usually acquired using Stack-of-Spirals Fast-Spin-Echo (FSE) or GRASE as recommended by the ASL consensus paper for neuroradiological application(1), those sequences suffer from some off-resonance sensitivity and/or image degradation, mostly significant blurring. Here, we propose an alternative based on Cartesian 3D-FSE, which is a workhorse of MR volumetric imaging, accelerated with Compressed-Sensing (CS)(2) to make its acquisition time compatible with clinical translation.
Materials and Methods
We implemented a background-suppressed pseudocontinuous ASL labeling with a Cartesian volumetric Fast-Spin-Echo readout. For acceleration, we used a variable spatial (using a variable-density-Poisson-disk) and temporal (permutation of the pseudo-random outer k-space coverage) sampling for better incoherence required in the CS reconstruction. Four healthy volunteers were scanned on a 3T (GE Discovery MR750) scanner with a 32-ch head coil. Scanning included a 3D T1-w FSPGR volume, as well as standard 3D Stack-of-Spirals ASL (8 interleaves, 512 points, 3NEX, TR/TE=4635/10ms, 3.6x3.6x4mm3, 44 axial slices) and our VD-3D-FSE sequence (64 coronal slices, 4NEX, 128x128 matrix, 2x2x3mm3, TR/TE=6200/11ms). All ASL data were acquired with a 1.5/1.5s labeling/post-labeling delay in 4 minutes each. A 4D-Compressed-Sensing reconstruction was performed offline with the BART toolbox(3) for the VD-FSE and after qualitative assessment, a quantitative blurring metric was computed to assess difference between both sequences.
Results
Qualitative assessment of image quality shows an increase in image quality on the perfusion-weighted volume for a similar acquisition time and better definition of the cortical gray matter especially in the parietal/occipital regions (cf. figure), confirmed by quantitative blurring analysis (0.55±0.02 vs 0.38±0.03 for Spiral and Cartesian, $p<0.0001$).
Conclusions
While spiral trajectories offer better time-efficiency without further acceleration, our proposed Cartesian-FSE volumetric ASL represents a promising and valuable alternative to GRASE (although not explored in the current study) or SoS-FSE for high-resolution, high-quality whole-brain perfusion measurement using ASL. Early neuro-radiological applications for brain tumor or Alzheimer's should confirm those results in healthy volunteers.

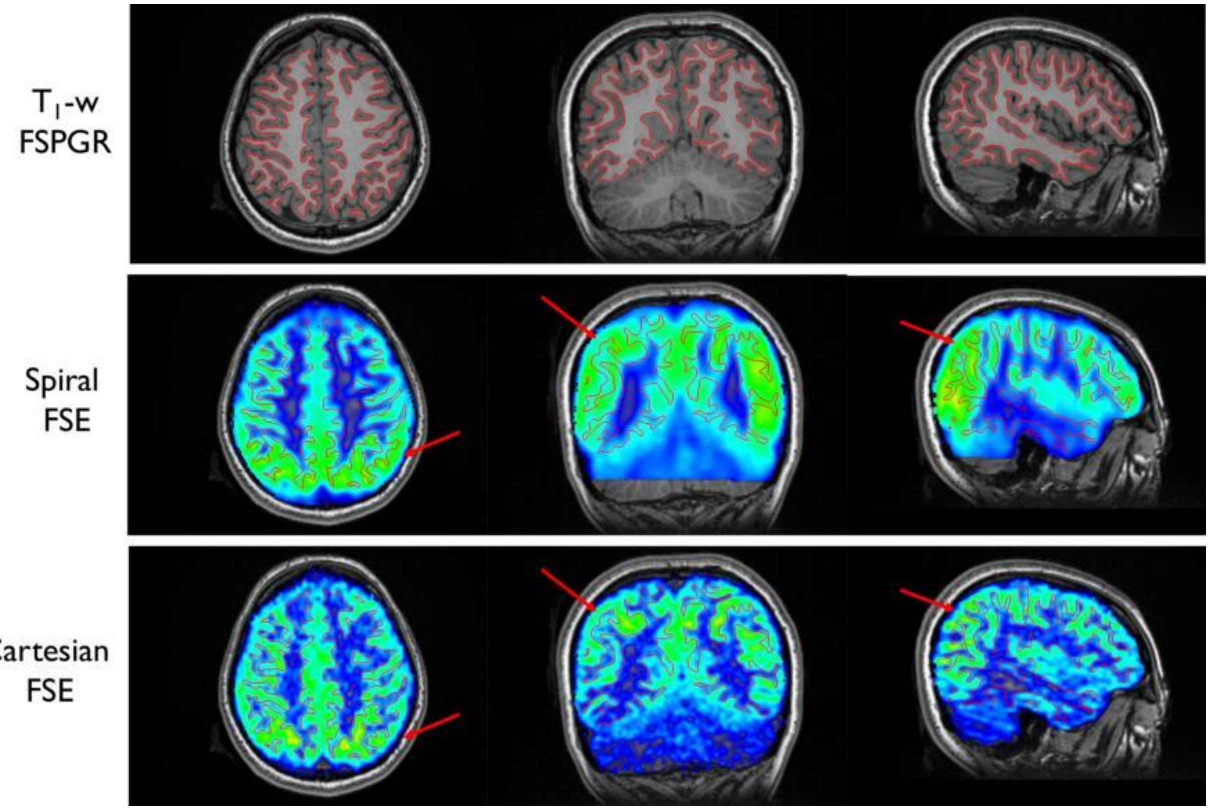

(Filename: TCT_3343_ASNR_figure.jpg)

2401

3:44PM - 3:51PM

Machine Learning Predicts Acuity of Compression Fracture on CT

A Doshi[1], J Schefflein[2], X Mei[3], J Song[3], K Nael[4], X Yang[3], A Fernandes[3], D Gorovoy[5]
[1]MOUNT SINAI ICAHN SCHOOL OF MEDICINE, NEW YORK, NY, [2]Icahn School of Medicine at Mount Sinai, New York, NY, [3]Mount Sinai Medical Center, New York, NY, [4]ICAHN SCHOOL OF MEDICINE AT MOUNT SINAI HOSPITAL, NEW YORK, NY, [5]Mount Sinai Hospital, New York, NY

Purpose
To evaluate the feasibility of using machine learning for determining whether a benign vertebral compression fracture is acute or chronic based on single computed tomography (CT) slice and various imaging features.
Materials and Methods
101 patients with 146 vertebral compression fractures on CT were evaluated. Patients with a history of malignancy or suspected malignancy on imaging were excluded. Fractures that either demonstrated edema on Short Tau Inversion Recovery (STIR) MRI imaging, or occurred within six weeks of prior normal imaging were classified as acute, while fractures with no STIR edema or prior imaging greater than six weeks demonstrating stability were classified as chronic. A single representative sagittal image of each fracture was captured from the corresponding CT, which were then evaluated by two radiologists based on the features of age, sex, presence of fracture cleft, fracture line, bone fragment, vertebral body air, and vertebral body density ("sclerosis") greater or less than 50%. Each fractured vertebrae was segmented. A normal adjacent vertebral body was captured to standardize gray-scale values. A novel machine learning algorithm was then generated using these labeled inputs and statistical modeling was performed to determine accuracy of the modeling in determining acuity and chronicity of fractures.

Separately, three readers (Neuroradiologist (NR), Emergency Radiologist (ER), and Senior Resident (SR)) independently assigned a label of acute or chronic fracture to the captured images only to their accuracy with that of the machine learning algorithm.

Results

Various machine learning classifiers were used for training, with XGBoost achieving the highest accuracy (86.6%) for determining whether a fracture is acute, with a sensitivity of 69.6%, specificity of 92.2%, and an Area Under the Curve of 87.4%. The combined accuracy of the three independent readers was 65.1%.

Conclusions

A novel machine learning algorithm, using various imaging features, may provide greater accuracy in the evaluation of benign vertebral compression fracture acuity on CT examination of the spine. This may assist the radiologist and treating physician in determining if additional imaging or evaluation is necessary.

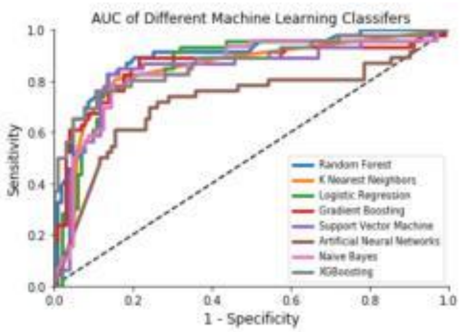
AUC of Different Machine Learning Classifers
Sensitivity
1 - Specificity
Random Forest
K Nearest Neighbors
Logistic Regression
Gradient Boosting
Support Vector Machine
Artificial Neural Networks
Naive Bayes
XGBoosting

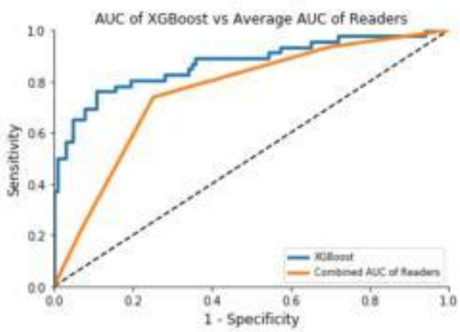
AUC of XGBoost vs Average AUC of Readers
Sensitivity
1 - Specificity
XGBoost
Combined AUC of Readers


Search Data
Accession ID:
Copy ID
Eraser
Load Status:
Search Status:
Age:
83
Gender:
f
Fracture:
Chronic
Fracture ID:
1
Search
Back
Next
Vertebra
Air
Soft tissue
undo
redo
Image Capture
Angle Code:
R
Save Image
Feature Description
Retropulsion
Mild
Fracture Line
Fracture Cleft
Bone Fragment
Vertebral Body Sclerosis
>50%?
Vertebral Body Air
Min:
Max:
Site:
Reference:
Doctor Name:

(Filename: TCT_2401_merge_from_ofoct.jpg)

2912

3:51PM - 3:58PM

Prediction of Chronological Age from Intracranial Time-of-Flight Magnetic Resonance Angiography Images by Deep Convolutional Neural Network

I Hwang[1], H Kim[1], J Kim[1]
[1]*Seoul National University Hospital, Seoul, Korea, Republic of*

Purpose
To investigate whether or not there are learnable features by a deep convolutional neural network (CNN) in the brain time-of-flight magnetic resonance angiography (MRA) images that might be associated with cerebrovascular aging.
Materials and Methods
There were 486 MRA data downloaded from the Information eXtraction from Images (IXI) repository. In addition, another 500 MRA data were collected from Health Promotion Center of our institution. All MRI scans in our institution were performed for routine check-up without evidence of brain disease. The range of age in the pooled dataset was 19 to 88 years, mean age was 52.0 years. The data were divided randomly into a training (n = 886) and a test (n = 100) sets. Each MRA volume data from source images was randomly scaled, translated, and rotated 10 times for data augmentation. The maximum intensity projection (MIP) images were obtained along the axial, coronal and sagittal directions, therefore, three orthogonal MIP images were fed to input layer of CNN. We built CNN consisted of 3 convolution blocks, 2 max pooling layers, 1 fully connected layer, and final regression layer. For the test set validation, the augmented data in the test set were individually predicted by the optimized CNN, and the mean predicted age over the 10 augmented images from the each MRA source image was used to evaluate the performance of the CNN. We performed correlation analysis between ground-truth age and MRA-predicted age.
Results
After optimization of hyperparameters of CNN, we conducted training for 50 epochs using batch size of 32. We calculated MRA-predicted age in the test set. The mean absolute error (MAE) between MRA-predicted age and ground-truth age was 8.40 years. The correlation coefficient between MRA-predicted age and ground-truth age was 0.79.
Conclusions
The MAE and correlation coefficient obtained in our study indicate that there might be learnable features by CNN in the MRA images in association with cerebrovascular aging.

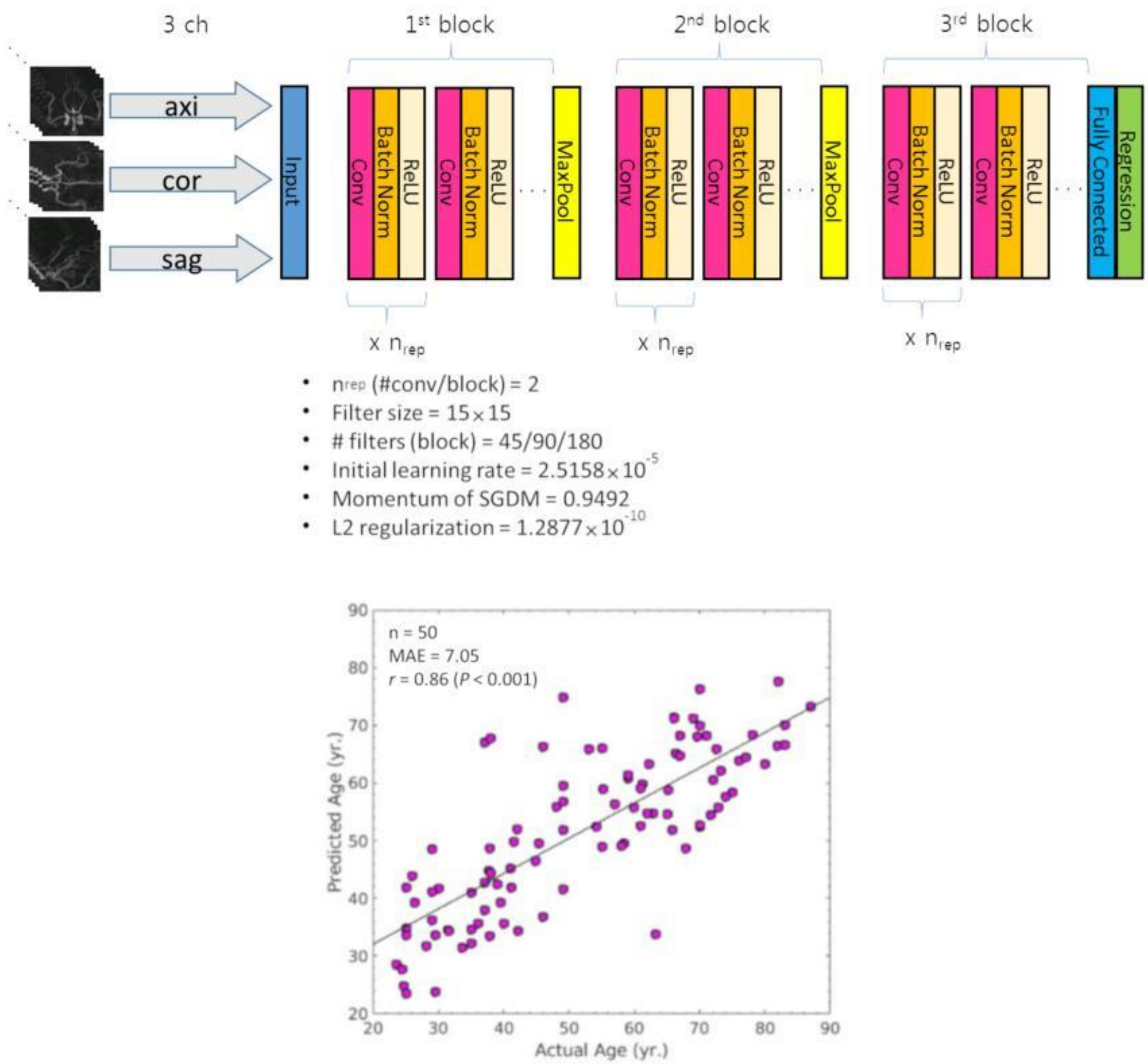

Figure. CNN architecture, optimized hyperparameters, and scatter plot showing correlation between the ground truth and the CNN-predicted brain ages in test sets

(Filename: TCT_2912_fig-mra-cnn.jpg)

3314

3:58PM - 4:05PM

SpineCloud: Image Analytics for Predictive Modeling of Spine Surgery Outcomes

T De Silva[1], S Vedula[1], A Perdomo-Pantoja[1], R Vijayan[1], S Doerr[1], A Uneri[1], R Skolasky[2], N Theodore[1], J Siewerdsen[3]
[1]Johns Hopkins University, Baltimore, MD, [2]Johns Hopkins Medical Institutions, Baltimore, MD, [3]Johns Hopkins University, BALTIMORE, MD

Purpose
We report a data-intensive analytic framework (called SpineCloud) that automatically extracts image features from medical image data in combination with patient demographic data as a basis for machine

learning-based prediction of patient-specific outcome, understanding outcome variability[1], improving patient selection, and guiding therapeutic pathways.
Materials and Methods
An IRB-approved retrospective pilot study was conducted involving 200 patients undergoing spinal neurosurgery at our institution. Image data included preoperative CT, intraoperative radiographs, and postoperative CT. Analytics intrinsic to SpineCloud included image-based features derived from automatic vertebral labeling, local/global spinal alignment, automatic surgical planning, and analysis of surgical instrumentation. Patient demographics from chart review included age, sex, BMI, smoking status, diabetes, hypertension, and prior spine surgery. Outcomes from chart review at 3 and 12 month follow-up were analyzed in terms of pain and function (mJOA[2] and Nurick[3]). A predictive model was developed using a Boosted Decision Tree classifier to predict outcome based on demographic and image-analytic features. The model was assessed using accuracy and area-under-the-curve (AUC) in leave-one-out-cross-validation in 84 surgeries.
Results
SpineCloud demonstrated 67.6% accuracy [AUC=0.69 (CI: 0.56-0.90)] and 68.3% [AUC=0.62 (CI:0.47-0.87)] for mJOA functional improvement at 3 and 12 months, respectively, compared to 53.5% [AUC=0.47 (CI:0.34-0.56)] and 38.3% [AUC=0.36 (CI:0.14-0.52)] for analysis based on demographics alone. The corresponding accuracy for Nurick functional improvement was 68.6% [AUC=0.55 (CI:0.45-0.68) (3 month)] and 67.2% [AUC=0.70 (CI:0.57-0.95) (12 month)] for SpineCloud compared to 62.8% [AUC=0.54 (CI:0.37-0.72) (3 month)] and 62.0% [AUC=0.60 (CI:0.46-0.74) (12 month)] for demographics alone. While both methods were predictive of pain improvement at 3 months, neither was predictive at 12 months.
Conclusions
SpineCloud analytics uses high-level image features combined with patient demographics as a novel foundation for machine learning-based predictive models. Initial studies demonstrated improved prediction of surgical outcome compared to analysis based on demographics alone, providing potential models for improved patient selection, surgical planning, and rehabilitative care.

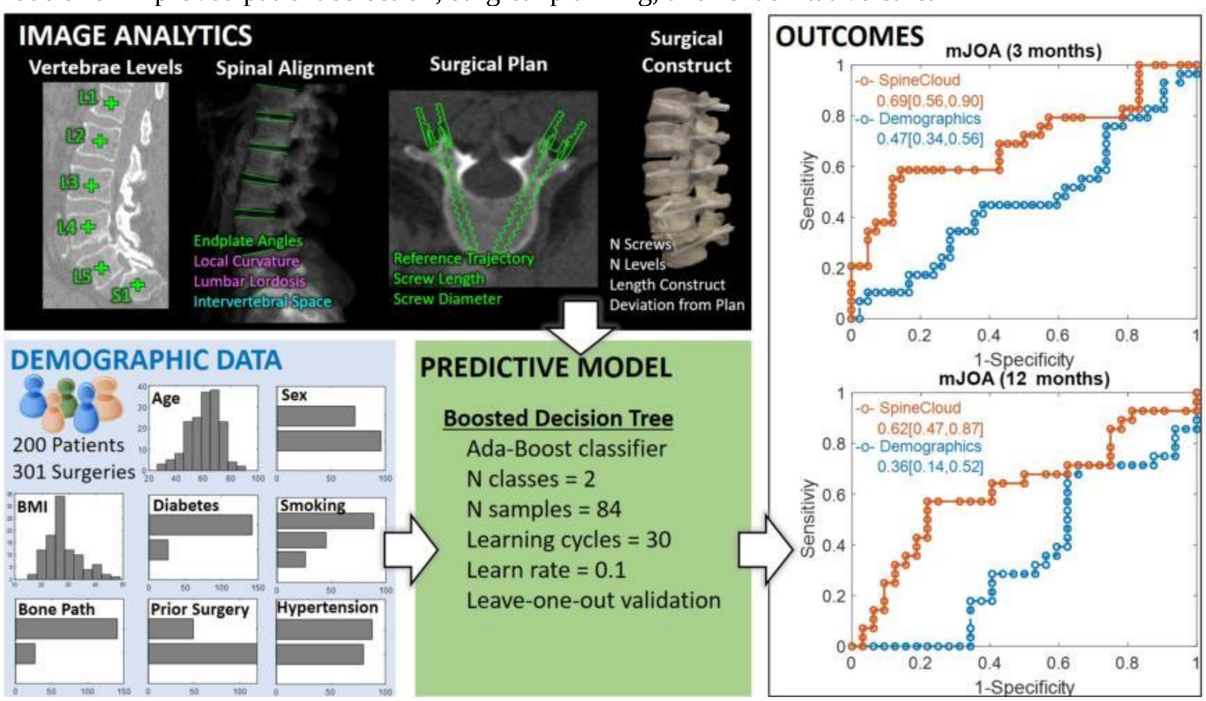

(Filename: TCT_3314_Figure3.jpg)

3677

4:05PM - 4:12PM

Temporal Hypometabolism in Athletes with Head Trauma: A Pilot FDG-PET/MRI Study

A Franceschi[1], C Michael[2], K Naser-tavakolian[3], D Franceschi[3], G Cruciata[4], L Bangiyev[5], A Franceschi[1]
[1]SUNY Stony Brook, New York, NY, [2]Stony Brook University Hospital, N/A, [3]Stony Brook University Hospital, Stony Brook, NY, [4]Stony Brook University Hospital, Brooklyn, NY, [5]Stony Brook University Hospital, Stony Brook , NY

Purpose
Animal models have demonstrated transient changes in glucose metabolism throughout the cerebral cortex in the setting of head trauma. These findings have not been validated to date in human subjects; however reports in the literature have suggested that transient changes in glucose metabolism can be visualized in the subacute phase following a concussion. Therefore, in this prospective pilot study, we assessed FDG uptake in division 1A-active college athletes following traumatic head injury and age-matched controls.
Materials and Methods
Six male college athletes (age range 18-22) currently enrolled in NCAA Division-1A Athletics underwent FDG PET/MRI brain imaging following a concussion during field play. Subjects were imaged within 94 hours of injury, and again at 3-month or longer follow-up interval. Three male age-matched controls were also imaged. The subjects were administered 3-5 mCi of 18F-FDG and following a 40-minute delay, underwent a 20-minute PET/MRI study including diagnostic quality and developmental brain MRI sequences. Data was analyzed using MIM software both qualitatively [2 readers; 1 board-certified neuroradiologist and 1 nuclear medicine physician] and semi-quantitatively utilizing Z-scores of abnormal uptake as compared to normal brain database.
Results
No structural brain abnormalities were noted on dedicated brain MRI sequences. All six athletes demonstrated relative temporal lobe hypometabolism [left greater than right] upon blinded review of PET surface maps, with 100% concordance between the 2 readers. Left greater than right temporal hypometabolism was confirmed upon semi-quantitative review demonstrating decreased Z-scores as compared to normal brain atlas. Follow-up imaging at 3 months or longer illustrated resolution of mild temporal lobe hypometabolism in all 3 athletes who underwent repeat PET/MR. No evidence of lobar-specific variation in FDG uptake was identified in the 3 control subjects upon both qualitative and semi-quantitative assessment. Statistical significance was not reached due to small dataset.
Conclusions
Preliminary data in our small pilot study demonstrated mild left dominant temporal lobe hypometabolism in the subacute setting following concussion injury in otherwise healthy college athletes as compared to age-matched controls. Continued imaging of athletes, and their normal counterparts, within the subacute concussion state will help guide clinical significance.

3483

4:12PM - 4:19PM

Using Deep Learning to Predict Age from CT Brains

J Seah[1], J Tang[2]
[1]Alfred Health, Melbourne, VIC, [2]ROYAL MELBOURNE HOSPITAL, MELBOURNE, VIC

Purpose
Radiologists make an intrinsic assessment of whether the features of a brain are age appropriate. There are many features that a radiologist looks at including the size of ventricles, gyri and sulci as well as the symmetry of the brain. The age appropriateness of a CT scan is very important in determining whether

there may be underlying pathology. The purpose of this study is assess whether a deep learning model is able to accurately predict patient age.

Materials and Methods

1008 non-contrast CT brain scans with 2.5mm slice thickness were extracted from a tertiary centre from 842 patients (Age range 19-98, median 65) . Age was determined from Digital Imaging and Communications in Medicine (DICOM) file information. 58,882 slices were used for training. A 100 layer convolutional Densenet network was used to process inputs of 16 contiguous 128x128 slices. 897 studies were used for training, 67 studies for testing and 44 for validation, split by patient.

Results

After training for 100 epochs, the algorithm converged with a training mean-squared error of 0.004 (with age reported in centiyears). Visual analysis of the predicted age demonstrates good agreement with actual age as seen in Fig 1. Bland-Altman analysis of the testing set shows a mean prediction difference of 1.4 +/- 22 years (95% limits of agreement).

Conclusions

The deep learning algorithm can accurately determine patient age which may be useful in determining the age appropriateness of a CT brain. Further work will look into the application of techniques such as generative visual rationales to identify what features the deep learning model is attributing to age.

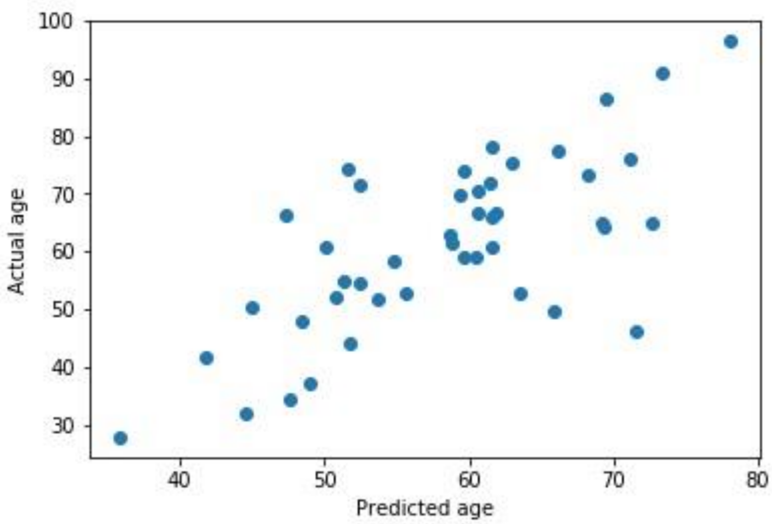

(Filename: TCT_3483_Fig1.jpg)

Monday, May 20, 2019
2:55PM - 4:25PM
Diagnostic Imaging of Brain Tumors for Characterization and Differentiation

2521

2:55PM - 3:02PM

"T2 FLAIR Mismatch" Sign and Radiomics in Lower Grade Gliomas

Y Choi[1], B Sohn[1], S Bae[2], S Lee[1], A Franceschi[3], S Patel[4], A Chi[5], R Jain[5]
[1]Yonsei University College of Medicine, Seoul, Korea, [2]National Health Insurance Service Ilsan Hospital, Goyang-si, Korea, Korea, [3]SUNY Stony Brook, New York, NY, [4]University of Virginia Health System, Charlottesville, VA, [5]NYU School of Medicine, New York, NY

Purpose

IDH mutation and 1p/19q co-deletion status are key molecular markers to classify gliomas. Our "T2 FLAIR mismatch" sign has been validated to be a robust and highly specific imaging biomarker that identifies a subgroup of IDH mutant astrocytomas. The purpose of this study was to investigate the correlation of radiomic features with T2 FLAIR mismatch sign and the incremental value of this sign over radiomic features in molecular classification of lower grade gliomas (LGGs).

Materials and Methods

A total 304 LGG patients from a single institution (n = 205) and a TCGA cohort (n = 99) were evaluated for T2 FLAIR mismatch sign by 2 independent neuroradiologists, and subjected to radiomic feature (n = 250) extraction from pre-operative MRI studies. T2 FLAIR mismatch sign for identifying IDH mutant and 1p/19q non-codeleted gliomas (IDHmut astrocytomas) was validated on the institutional cohort. Radiomic classifiers to predict the T2 FLAIR mismatch sign and IDH mutant astrocytomas were trained on the institutional cohort using random forest analysis, and validated on the TCGA cohort. Performance of the radiomic classifier was evaluated by using receiver operating characteristics (ROC) analysis. The incremental value of T2 FLAIR mismatch sign over radiomic classifier in the prediction of IDH mutant astrocytomas was assessed using continuous net reclassification index (NRI). The same analysis for radiomic classifier and incremental value of T2 FLAIR mismatch sign were conducted in the subgroups of all IDH mutant gliomas and all non-enhancing LGGs.

Results

T2 FLAIR mismatch sign showed substantial interrater agreement (kappa = 0.755), was present in 22 cases (12%), and showed and 100% positive predictive value for IDH mutant astrocytomas. Radiomics classifier for predicting T2 FLAIR mismatch showed excellent performance (AUC, 0.917 – 0.952). Radiomics classifier for identifying IDH mutant astrocytomas was fair to good (AUC = 0.825, 0.859 and 0.726 for the entire cohort, all IDH mutant glioma and nonenhancing LGG subgroups, respectively). Integration of T2 FLAIR mismatch sign to the radiomics classifier significantly improved accuracy of the radiomics classifer for identifying IDH mutant astrocytomas (AUC 0.825 vs. 0.839, 0.859 vs. 0.873, and 0.726 vs. 0.796 for entire cohort, all IDH mutant glioma and nonenhancing LGGs, respectively, and $P < 0.001$ for all).

Conclusions

T2 FLAIR mismatch sign showed a good correlation with radiomic features, and improved the radiomic classifier for molecular subtyping of LGGs. Our study suggests that radiologists' visual assessment for a robust imaging feature such as the T2 FLAIR mismatch sign can augment machine learning-based radiomics tools.

2987

3:02PM - 3:09PM

Amide Proton Transfer Weighted (APTw) Imaging Improves the Pre-Surgical Radiological Accuracy for Final Diagnosis in Brain Tumors

F Durmo[1], A Rydhög[2], F Testud[3], J Lätt[2], B Schmitt[4], A Rydelius[5], P van Zijl[6], L Knutsson[7], P Maly Sundgren[1]

[1]Lund University; Clinical Sciences, Department of Radiology, Lund, Sweden, [2]Skåne University Hospital, Center for Medical Imaging and Physiology, Lund, Sweden, [3]Siemens Healthcare AB, Malmö, Sweden, [4]Siemens Healthcare Pty. Ltd., Sydney, Australia, [5]Lund University Clinical Sciences, Department of Neurology, Lund, Sweden, [6]Johns Hopkins University School of Medicine, Baltimore, MD, [7]Lund University; Department of Medical Radiation Physics, Lund, Sweden

Purpose

To evaluate the use of amide proton transfer weighted (APTw) MRI for pre-surgical radiological diagnosis of brain tumors.

Materials and Methods
This MRI study consists of 22 patients with brain lesions (mean age 53 years, range 30-73 years) that underwent MRI with conventional images and APTw prior to surgery for suspected primary/secondary brain tumor. Patients were examined on a 3T scanner (MAGNETOM Prisma, Siemens Healthcare, Erlangen, Germany). APTw images were obtained using a CEST prototype sequence with 3D GRE (22 slices, 2x2x4 mm3) acquisition of the water saturation spectrum (Z-spectrum, B1=2 µT, 21 frequency offsets from -610 to 610 Hz, tsat = 600ms, 5 hyperbolic secant pulses, 60 ms interpulse delay, TA 6:50min), followed by B0 correction and processing optimized for APTw contrast at 3.5 ppm. The radiological pre-operative diagnosis was based on the conventional MRI. The maximum and mean % APTw signal were retrospectively evaluated to verify if the pre-surgical radiological diagnosis would have changed if the APTw measurements had been included in the initial radiological assessment
Results
Initial radiological diagnosis pre-operatively was glioblastoma (6 patients), low grade tumor (12 patients), and metastases (4 patients). When including the mean and maximum % in APTw signal in the pre-operative evaluation the diagnoses changed in 7 of the 22 patients. By using a cut-off value of mean 2 % APT signal all 3 of the suspected LGG would have been diagnosed as glioblastoma, which also was confirmed by final definitive histopathological diagnosis. The mean % APTw signal varied more (0.58-4.24) in the 4 metastases histopathologically confirmed as glioblastoma
Conclusions
Including APTw images and their % mean and % maximum in the lesion improved the pre-operative radiological evaluation and more accurately matched the radiological diagnosis with the final histopathological diagnostic confirmation.

2876

3:09PM - 3:16PM

Apparent Diffusion Coefficient Improves the Prediction of Low-Grade Glioma Subtype, IDH-Mutant with No 1p19q Codeletion: Added Value to the T2/FLAIR Mismatch Sign

M Lee[1], J Park[2], H Kim[3]
[1]Asan Medical Center, Seoul, Korea, Republic of, [2]N/A, Seoul, 05555, SOUTH KOREA, [3]Asan Medical Center, Seoul, NA

Purpose
Combining the T2/FLAIR mismatch sign and advanced imaging parameters may improve the differentiation of lower grade gliomas (LGGs). We tried to assess added diagnostic value of apparent diffusion coefficient (ADC) and cerebral blood volume (CBV) to the T2/FLAIR mismatch sign for determining the molecular subtype of LGGs.
Materials and Methods
Of 119 patients analysed, 46 had IDH mutation and 1p/19q codeletion (IDHmut-Codel), 45 were IDH wild-type (IDHwt) and 19 had IDH mutation and no 1p/19q codeletion (IDHmut-Noncodel). Preoperative MRI scans were reviewed to assess the T2/FLAIR mismatch sign and the apparent diffusion coefficient (ADC) and cerebral blood volume (CBV) values. Diagnostic models were constructed to distinguish IDHmut-Noncodel from other LGGs and from IDHwt, and the performance was compared with that of single parameters using the area under the receiver operating characteristics curve (AUC).
Results
IDHmut-Noncodel showed higher ADC and lower CBV values than other LGGs, using ADC50 (50th percentile of ADC,P=.002) and nCBV90 (90th percentile of normalized CBV,P=.017). Addition of the ADC50 to the T2/FLAIR mismatch sign significantly improved the distinction of the IDHmut-Noncodel group from other LGGs (AUC 0.88,P=.02), whereas addition of the nCBV was not helpful. The combination of ADC50 and T2/FLAIR mismatch also showed the best performance (AUC 0.92) for

distinguishing the IDHmut-Noncodel group from IDHwt, compared to nCBV90 (AUC 0.89) or T2/FLAIR mismatch (AUC 0.87) alone.

Conclusions

The combination of the T2/FLAIR mismatch sign and the ADC50 value can improve the identification of IDHmut-Noncodel LGGs, which can be easily applied in clinical practice.

2392

3:16PM - 3:23PM

Correlation of rCBV with Established and Novel Genomic Markers in Gliomas

R Jain[1], I Littig[2], C Wu[3], S Patel[4], M Snuderl[5], A Chi[1]
[1]NYU School of Medicine, New York, NY, [2]New York University, New York, NY, [3]Taipei Veterans General Hospital; School of Medicine, National Yang Ming University, Taipei, AK, [4]University of Virginia Health System, Charlottesville, VA, [5]Department of Pathology New York University Medical Center, New York, NY

Purpose

There is variability in survival within IDHmut gliomas determined by chromosomal events and it has been reported that copy number variation (CNV) abundance as well as CDKN2A/B (p16) homozygous deletion is associated with poor survival in low-grade gliomas. The purpose of this study was to determine whether rCBV values correlate with isocitrate dehydrogenase (IDH) mutation status, CDKN2A/B homozygous deletion status, genome-wide copy number variation (CNV) and patient overall survival in diffuse gliomas.

Materials and Methods

105 treatment naive diffuse gliomas with genomic data (IDH mutation and 1p19q co-deletion status) and DSC T2* perfusion data were included. rCBV was obtained from 4 regions of interests within the highest perfusion areas including enhancing and non-enhancing segments of each tumor, utilizing Olea Sphere software (v 3.0, Olea Medical, LaCiotat). Copy number (CN) plots obtained with Illumina Infinium 450k or Illumina EPIC methylation array were reviewed in 38 IDHmut astrocytomas for CNV as well as for CDKN2A/B status. Mean differences in rCBV were compared by ANOVA and t-test. Associations with overall survival, defined as the time from diagnosis to death or last follow-up, were estimated by Cox regression models and Kaplan-Meier methods.

Results

IDHwt gliomas (44.8%) demonstrated higher rCBV (rCBV = 6.87 ± 3.09) than IDHmut gliomas (55.2%, rCBV =2.21 ± 1.71 for 1p/19q codeleted gliomas and 2.09 ± 2.00 for non-codeleted gliomas, ANOVA, $p<0.0001$). rCBV was a significant predictor of overall survival either used alone (HR 1.23, $p<0.0001$) or added to a model with age of diagnosis (HR 1.21, $p<0.0001$). Gliomas with rCBV < 3.80 showed better survival (n = 54, median survival time unobserved) than gliomas with rCBV > 3.8 (n = 53, median 18 months; log-rank $p<0.0001$). IDHwt gliomas with high rCBV had the worst survival (10.6% surviving at 3 years, 95% CI (4%, 30%)). CNV-S (N=19) IDHmut astrocytomas demonstrated significantly lower mean rCBV (1.3 ± 1.2) than CNV-U (N=19) IDHmut astrocytomas (3.3 ± 2.3; t-test $p = 0.0027$; Wilcoxon $p = 0.0026$). IDHmut astrocytomas with CDKN2A/B homozygous deletion (N=9) showed higher rCBV (3.7 ± 2.1) as compared to CDKN2A/Bwt (N=28) IDHmut astrocytomas (1.8 ± 1.9; t-test $p=0.0375$; Wilcoxon $p = 0.0169$).

Conclusions

IDHwt gliomas show higher rCBV than IDHmut gliomas irrespective of the glioma grade. Higher rCBV measurements are associated with poorer survival in the entire cohort and also within IDHmut and IDHwt gliomas. IDHmut astrocytomas with higher degrees of genomic instability (CNV-U) and those with CDKN2A/B homozygous deletion also show higher rCBV and poor survival.

2346

3:23PM - 3:30PM

Detection of Brain Metastases: Comparison of DANTE prepared 3D T1-weighted TSE and 3D MP-RAGE Sequences

Y Heo[1], H Jeong[2], J Beak[3]
[1]INJE UNIVERSITY, BUSAN PAIK HOSPITAL, BUSAN, Busan, [2]INJE UNIVERSITY, BUSAN PAIK HOSPITAL, Busan, Busan, [3]Inje university Busan Paik hospital, Busan, Busan

Purpose
To compare a DANTE (delayed alternating with nutation for tailored excitation) prepared 3D T1-weighted TSE and a 3D magnetization-prepared rapid gradient echo (MP-RAGE) sequence for the detection of brain metastases.
Materials and Methods
Forty-six patients with brain metastases were enrolled in this retrospective study. Two neuroradiologists were evaluated the number of enhancing lesions (<=5mm, >5mm), false positive lesions, presence of artifact for DANTE prepared 3D TSE and MP-RAGE sequence. CNR (contrast-to-noise ratio) lesion/parenchyma and CNR WM/GM were also evaluated.
Results
Smaller than 5mm sized lesions were more significantly detected using DANTE prepared 3D TSE than MP-RAGE (ICC, 0.98). However, detection of larger than 5mm sized lesions were not significantly different between DANTE prepared 3D TSE and MP-RAGE (ICC, 0.99). Significantly more false positive lesions were detected using DANTE prepared 3D TSE than MP-RAGE and significantly more artifact were detected with MP-RAGE than DANTE prepared 3D TSE. Mean CNR lesion/parenchyma was higher for DANTE prepared 3D TSE (55.47±47.46 vs 17.07±19.78, <0.001) and mean CNR WM/GM was lower for DANTE prepared 3D TSE (-0.61±1.51 vs 2.73±1.44) than MP-RAGE.
Conclusions
DANTE prepared 3D TSE showed increased contrast of the lesions and significantly better detection of small brain metastases (<=5mm) compared with conventional 3D MP-RAGE.

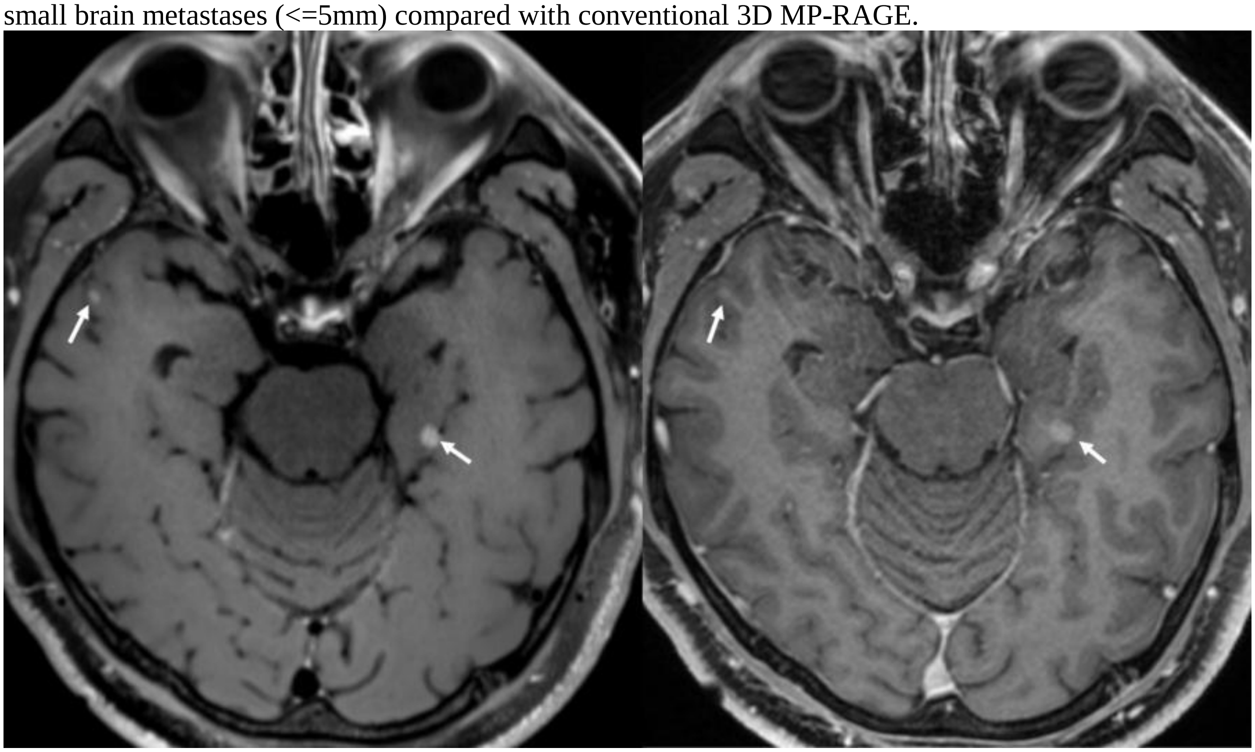

(Filename: TCT_2346_ASNR.jpg)

2120

3:30PM - 3:37PM

Development and Evaluation of a Matlab-Based Toolbox for Calculation of the Percentage of Signal Recovery (PSR) from Dynamic Susceptibility Contrast MR Perfusion Sequences (DSC-MR) for Classification of High-Grade Intra-Axial Brain Lesions

J Orejuela[1], A Granados[2], J Núñez[3], M Arango-Granados[2]
[1]University Hospital Fundación Valle del Lili, Cali, Valle del Cauca, [2]Fundación Valle del Lili, Cali, Valle del Cauca, [3]Universidad Autónoma de Occidente, Cali, Valle del Cauca

Purpose
Differentiating brain lesion by conventional MRI is sometimes challenging. Some techniques have been proposed to characterize brain lesions more accurately, but their use remains limited in some cases. Percentage Signal Recovery (PSR) seems to be a promising tool for this purpose. Our objective was to develop a Matlab-based toolbox to calculate the PSR from dynamic susceptibility contrast MR perfusion sequences (DSC-PWI), and to evaluate its utility to differentiate high-grade intra-axial brain lesions in a series of patients seen at a high-level University Hospital.
Materials and Methods
A Matlab-based toolbox was built to process and evaluate the PWI curves. PSR was defined as the ratio between the postcontrast signal intensity minus the minimum signal intensity, and the precontrast signal intensity minus the minimum signal intensity multiplied by 100. PSR maps were generated. Two ROIs were placed in both healthy and lesion tissues. Minimum, maximum, mean and standard deviation of PRS were calculated. Twelve patients (10 female, 2 male; mean age: 58.75±15.02 years-old) with high-grade brain lesions were included (glioblastoma, n=5; lymphoma, n=3; metastasis, n=4). All patients had pre-surgical MRI studies. PSR results were compared with the findings of the currently MR protocol, and with the histopathological results.
Results
Mean rCBV in glioblastoma was 2.96±0.96, metastasis 2.36±1.59, and lymphoma 2.30±0.30; no statistically significant differences was observed (p=0.633). Mean PSR in metastasis was 57.43±23.99, glioblastoma 95.36±39.86, and lymphoma 236.95±102.59; different statistically significant (p=0.015). The evaluation by pairs showed statistically significant differences between lymphoma and metastasis (p=0.046), lymphoma and glioblastoma (p=0.028), without observing statistically significant differences between metastasis and glioblastoma (p=0.258). Diagnostic accuracy was 41.67% based on currently MR protocol, and 91.67% using the PSR analysis.
Conclusions
A Matlab-based toolbox was developed for PSR evaluation. Our findings suggest that PSR measurement could improve the performance of the MRI studies in the characterization and classification of high-grade brain lesions.

2908

3:37PM - 3:44PM

False Positive Measurement on 2-Hydroxyglutarate Magnetic Resonance Spectroscopy in Isocitrate Dehydrogenase Wild-Type Glioblastoma: A Multifactorial Analysis

C Suh[1], H Kim[1], S Kim[1]
[1]Asan Medical Center, Seoul, Republic of Korea

Purpose
To investigate factors associated with false positive measurements of 2-hydroxyglutarate (2HG) on magnetic resonance spectroscopy in isocitrate dehydrogenase (IDH) wild-type glioblastoma.

Materials and Methods

This retrospective study was approved by institutional review board and informed consent was waived. Eighty-two consecutive histopathologically confirmed pre- and post-treatment glioblastoma patients were evaluated between December 2017 and August 2018. Spectroscopy parameters including 2HG measurements were obtained from single-voxel point-resolved spectroscopy, and apparent diffusion coefficient (ADC) values were obtained. To assess independent factors related to false positive 2HG measurements, univariate and multivariate logistic regression analyses were performed. Necrosis was graded according to the proportion of necrosis within a volume of interest. Subgroup analyses were performed according to treatment status.

Results

2HG measurement showed a false positive rate of 24% (17 of 71) in IDH wild-type glioblastoma. Multivariate analysis revealed that necrosis ($p=0.003$) and ADC value ($p=0.014$) were associated with an increased false positive rate in the 2HG measurement. Necrosis more than 20% showed significantly higher false positive 2HG measurements (OR, 11.355) compared to necrosis less than 20%. Although ADC value was a significant factor, the effect was small (OR, 0.997). The 2HG false positive rate was significantly higher in pretreatment (50%) than post-treatment glioblastoma (14%, $p=0.001$). Among 17 false positive, 15 patients (88%) showed a lactate concentration ≥2.0mM and 14 (82%) showed a lactate concentration ≥3.0mM.

Conclusions

The interpretation of 2HG measurement should be made with great care, as it is subject to a high false positive rate, especially in pretreatment large necrotic glioblastoma.

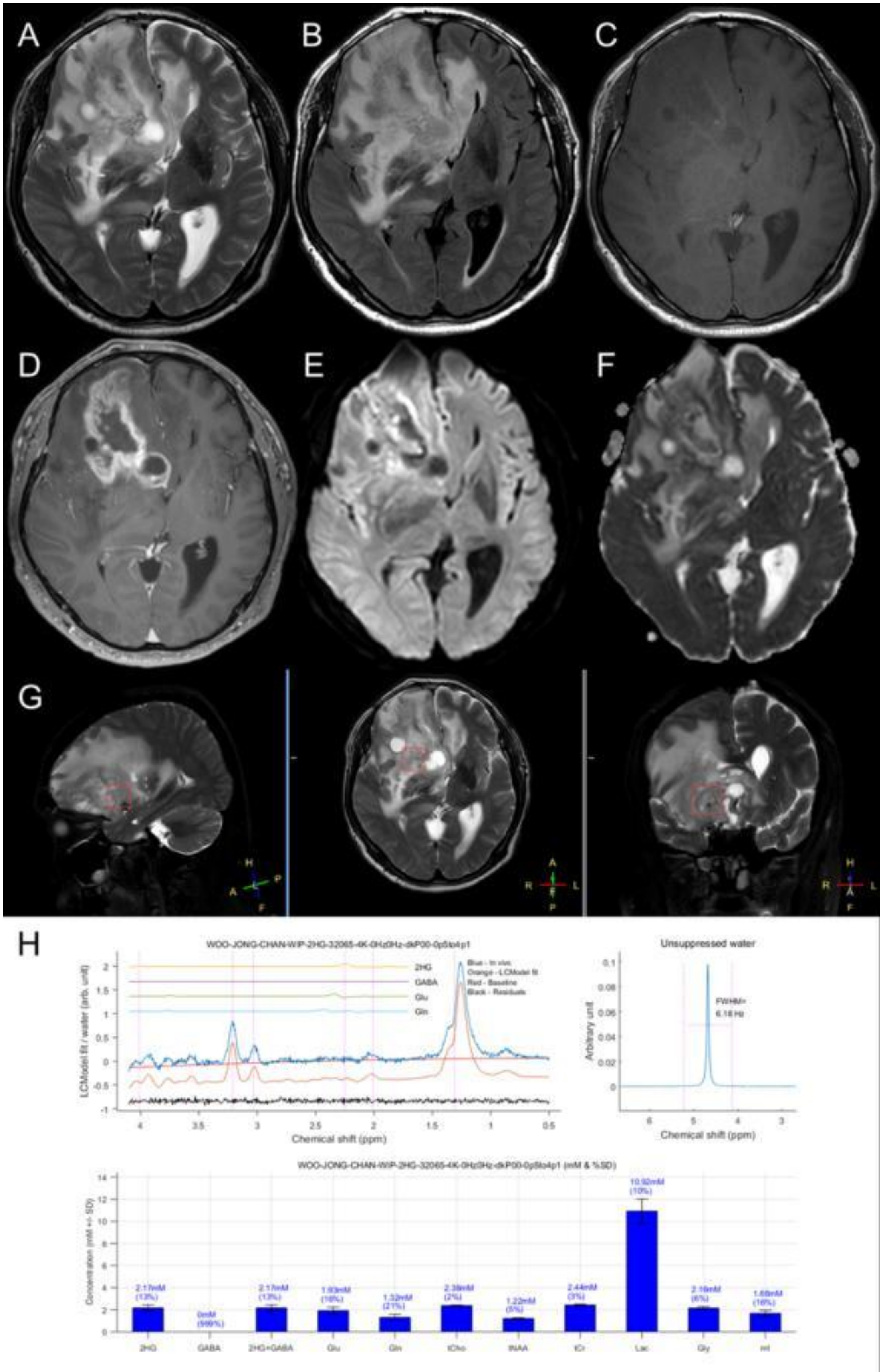
A
B
C
D
E
F
G
H
WOO-JONG-CHAN-WIP-2HG-32065-4K-0Hz0Hz-dkP00-0p5to4p1
2HG
GABA
Glu
Gln
Blue - In vivo
Orange - LCModel fit
Red - Baseline
Black - Residuals
LCModel fit / water (arb. unit)
Chemical shift (ppm)
Unsuppressed water
FWHM=
6.18 Hz
Arbitrary unit
Chemical shift (ppm)
WOO-JONG-CHAN-WIP-2HG-32065-4K-0Hz0Hz-dkP00-0p5to4p1 (mM & %SD)
Concentration (mM +/- SD)
2.17mM (13%)
0mM (999%)
2.17mM (13%)
1.93mM (16%)
1.32mM (21%)
2.38mM (2%)
1.22mM (5%)
2.44mM (3%)
10.92mM (10%)
2.16mM (6%)
1.68mM (16%)
2HG
GABA
2HG+GABA
Glu
Gln
tCho
tNAA
tCr
Lac
Gly
mI

(Filename: TCT_2908_Figure4.jpg)

2432

3:44PM - 3:51PM

Influence of First Pass Leakage Correction on Cerebral Blood Flow in Glioma Grading Using T1-Perfusion MRI

R Gupta[1], J Saini[2], A Ramaniharan[3], A Sengupta[4], D SASI S[4], A Singh[4], P Gupta[5], A Mohan Rao[6], A Awasthi[7]
[1]Fortis Memorial Research Institute, Gurgaon, India, Haryana , MA, [2]NATIONAL INSTITUTE OF MENTAL HEALTH & NEURO SCIENCES, BANGALORE, India, [3]Fortis Memorial Research Institute, Gurugram,, Others, [4]Indian Institute of Technology Delhi, Delhi, India, New Delhi, others, [5]Fortis Memorial Research Institute, Gurgaon, India, Gurgaon, others, [6]Philips India Limited,, Banglore, others, [7]Public Health Foundation of India, Delhi,, New Delhi, others

Purpose
Whenever there is break down in blood-brain barrier (BBB), there would be leakage of contrast into extravascular extra-cellular space (EES) and results in the erroneous estimate of hemodynamic parameters obtained using T1-perfusion MRI. The purpose of this study is to estimate the magnitude of leakage during first pass, perform first pass leakage correction in Cerebral Blood Flow (CBF) and to investigate its potential in glioma grading
Materials and Methods
This study has included 14 Grade-II, 12 Grade-III and 29 Grade-IV glioma patients for the analysis. Upon fitting Leaky tracer kinetic model to first pass, leakage contribution from first pass concentration-time curve C(t) was removed by subtracting contribution from EES and leakage compartments and is used to estimate leakage corrected CBF (CBF_Corr). Statistical analysis was performed on the obtained values for differentiating different grades of tumors.
Results
The amount of leakage contribution was observed as evident by values of tracer kinetic parameters during the first pass. The proposed methodology could perform leakage correction in CBF measure. rCBF_Corr was found to be statistically significant ($p < 0.001$) in the differentiation of high-grade tumors. However, no significant difference was observed in the differentiation of Grade-II from Grade-III tumors. The area-under-curve of rCBF_Corr was observed to be 0.98 and 0.99 for Grade-III vs Grade-IV and Grade-II+III vs Grade-IV respectively with high sensitivity and specificity (Fig. 1).
Conclusions
In the presence of blood-brain barrier breakdown, there is a contribution of leakage in the CBF quantification in the first pass analysis and its correction in CBF measure results in improvement in the discrimination of Grade-III vs Grade-IV and Grade-II+II vs Grade-IV glioma.

Table: 1. Results of ROC analysis

	Hemodynamic parameters	AUC	Cutoff	Sensitivity	Specificity
Grade-II versus Grade-III	rCBF	0.75	2.61	0.75	0.64
	rCBF_Corr	0.77	2.61	0.75	0.64
	rCBV	0.80	2.36	0.75	0.71
	rCBV_Corr	0.80	2.34	0.75	0.71
	Vp_FP	0.88	0.03	0.83	0.79
Grade-II versus Grade-IV	rCBF	1.00	4.20	1.00	1.00
	rCBF_Corr	1.00	4.07	1.00	1.00
	rCBV	1.00	3.60	1.00	1.00
	rCBV_Corr	1.00	3.40	1.00	1.00
	Vp_FP	0.98	0.03	0.93	0.86
Grade-III versus Grade-IV	rCBF	0.95	5.12	0.93	0.83
	rCBF_Corr	0.98	4.25	1.00	0.83
	rCBV	0.94	4.31	0.93	0.75
	rCBV_Corr	0.97	4.12	0.93	0.83
	Vp_FP	0.83	0.04	0.90	0.59
Grade-II+III versus Grade-IV	rCBF	0.98	4.65	0.97	0.89
	rCBF_Corr	0.99	4.25	1.00	0.92
	rCBV	0.97	3.61	1.00	0.85
	rCBV_Corr	0.98	3.42	1.00	0.85
	Vp_FP	0.91	0.03	0.93	0.62
Grade-II versus Grade-III+IV	rCBF	0.93	2.62	0.93	0.64
	rCBF_Corr	0.93	2.61	0.93	0.64
	rCBV	0.94	2.46	0.90	0.79
	rCBV_Corr	0.94	2.52	0.88	0.86
	Vp_FP	0.95	0.03	0.95	0.79

(Filename: TCT_2432_ROC_Table_CBF_correction.jpg)

2839

3:51PM - 3:58PM

Powassan Virus Rhombencephalitis and Poliomyelitis–Like Syndrome

V Tsehmaister-Abitbul[1], M Kontolemos[2], A Guarnizo[3], R Glikstein[1], C Torres[4]
[1]University of Ottawa, Ottawa, Ontario, [2]The Ottawa Hospital, Ottawa, Ontario, [3]UNIVERSITY OF OTTAWA, THE OTTAWA HOSPITAL, OTTAWA, ON, [4]UNIVERSITY OF OTTAWA, OTTAWA, ON

Purpose
Powassan virus (POWV) is a rare tick-borne agent of encephalitis in North America. We report a case of POWV rhomb encephalitis and anterior cord myelitis.
Materials and Methods
62 year-old man, travelling back from Newfoundland, Canada with sudden onset of fever, nausea and vomiting, followed by diplopia and ataxia. He progressively deteriorated over the following days, with progression of brain stem syndrome (increased ataxia, weakness, dysarthria) with eventual respiratory failure, leading to intubation. There was no clear preceding viral illness, no rashes or insect bites. There

was no prior history of rheumatologic, autoimmune or neurologic illness. CSF was negative for Cryptococcus, HSV 1/2, VZV and AFB stain. Serum investigations for HIV, Syphilis, Lyme Disease, West Nile Virus, Japanese Encephalitis and St. Louis Encephalitis were also negative. He was eventually diagnosed with Powassan virus infection by positive serum reaction.

Results

MRI at presentation showed superficial T1 hyperintesity and enhancement over the cerebellar vermis. There was diffuse sulcal FLAIR hyperintensity and subtle diffuse leptomeningeal enhancement after gadolinium administration. In addition, a linear area of T2 hyperintensity was seen along the ventral grey matter, extending between C3 and C6 levels. There was no associated enhancement.

Conclusions

Powassan virus is a tick-borne flavivirus that was first identified in 1958 in Powassan, Ontario, in a 5-year-old boy who died with encephalitis. Powassan virus encephalitis is a rare entity, with non- specific MRI findings, characteristically involving the brainstem, deep gray structures and cortex. We present a case of Powassan virus encephalitis, with involvement of the cerebellar vermis, ventral grey matter of the cervical cord as well as the supra and infratentorial leptomeninges. A High index of suspicion is needed for this rare however potentially fatal disease, especially in endemic areas.

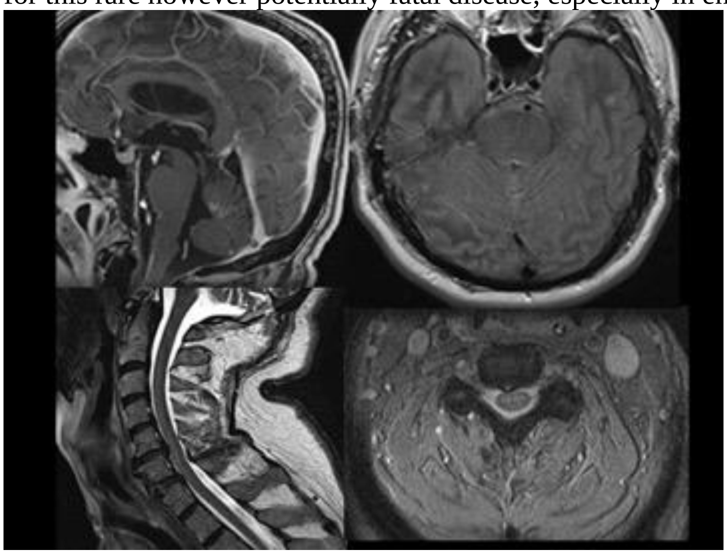

(Filename: TCT_2839_Powassanvirus.jpg)

2329

3:58PM - 4:05PM

Quantitative Features Extracted Based on Conventional MRI for Grading Diagnosis of Glioma

X Du[1]

[1]*Department of Radiology, Daping Hospital, Chongqing, Chongqing*

Purpose

To explore the value of quantitative features derived from conventional MRI in grading diagnosis of glioma.

Materials and Methods

Pre-operative MRI data of 153 patients with glioma were analyzed retrospectively. The quantitative image features were extracted from conventional MRI using the visually accessible Rembrandt images (VASARI) features (F1-F30). The stability of 30 features were evaluated with Kappa test. The image features with significant differences of different grades of gliomas were obtained, and their grading diagnostic value were evaluated with Binary Logistic regression.

Results
In all the 153 patients, 68 patients were of WHO II gliomas, 34 were of WHO III and 51 were of WHO IV gliomas. The stability of all the features were high (all Kappa>0.5). Ten features, including eloquent brain (F3), enhancement quality (F4), proportion enhancing (F5), proportion non-enhancing tumor (F6), proportion necrosis (F7), thickness of enhancing margin (F11), definition of the enhancing margin (F12), diffusion (F17), ependymal invasion (F19), non-enhancing tumor crosses midline (F22) showed significant differences among different glioma grades (all $P<0.01$). F3 was helpful to differentiating high and low grade (regression coefficient=-0.467, odd ratio=0.627, P=0.005) gliomas and WHO III and IV gliomas (β=-0.683, OR=0.505, P=0.006), while F22 had high value in differentiating WHO II and III gliomas (β=2.161, OR=8.682, P=0.008).
Conclusions
Quantitative image features extracted from conventional MRI are stable and helpful to pre-operative grading diagnosis of gliomas.

2472

4:05PM - 4:12PM

Sequential Acquisition of T1-Perfusion and T2*-Perfusion MRI for Comparative Evaluation of Cerebral Gliomas

J Saini[1], R Gupta[2], A Singh[3], M Kumar[4], V Santosh[5], M Beniwal[6]
[1]NATIONAL INSTITUTE OF MENTAL HEALTH & NEURO SCIENCES, BANGALORE, India, [2]Fortis Memorial Research Institute, Gurgaon, India, Haryana , MA, [3]Indian Institute of Technology Delhi, Delhi, India, New Delhi, others, [4]National Institute of Mental Health, Bangalore, others, [5]National Institute of Mental Health And Neuro Sciences, Bangalore, Karnataka, [6]National Institute of Mental Health and Neurosciences, Bengaluru, others

Purpose
The purpose of this study was to assess the inter-technique agreement of relative cerebral blood volume (rCBV) measurements obtained using T1 and T2* perfusion MR imaging.
Materials and Methods
T1- and T2*- perfusion imaging was performed in a single sitting in a total of 49 adult patients with histopathologically proven gliomas and voxelwise rCBV was estimated using both the techniques. Visual inspection of the conventional MRI and rCBV maps was done to look for the presence of significant susceptibility within a tumor. For qualitative analysis; two observers independently recorded rCBV values derived from T1 and T2* perfusion methods. Interobserver and Inter-technique rCBV measurement agreement were determined by using 95% Bland-Altman limits of agreement and the intra-class correlation coefficient (ICC) statistics.
Results
Qualitative analysis of the conventional and perfusion images showed that 16/49 (32.65%) patient T2*-perfusion study could not be completely evaluated due to the abundant susceptibility within the tumor arising from tumoral hemorrhage, calcification, and post-surgical changes or proximity of the tumor to the skull base or paranasal sinuses (Fig. 1). Bland-Altman plots revealed a significant agreement between two independent observers for both T1- and T2*- perfusion MRI. The intra-class correlation coefficient (ICC) demonstrating strong agreement between rCBV values recorded by two observers for DSC (ICC 0.96, p = 0.040), DCE (ICC 0.97, p = 0.125) imaging and between the rCBV estimated using the two methods (ICC 0.74, $P<0.001$). Grade IV Gliomas showed significantly higher rCBV values compared to grade III lesions (p = 0.037). On ROC analysis, rCBV values estimated using T1- and T2* perfusion techniques were able to discriminate between grade III and grade IV tumors with AUC of 0.723 and 0.767 respectively.

Conclusions
We conclude that T1- perfusion MRI with a single dose of contrast could be used as an alternative to T2*-perfusion to overcome the issues related to susceptibility in brain tumors evaluation.

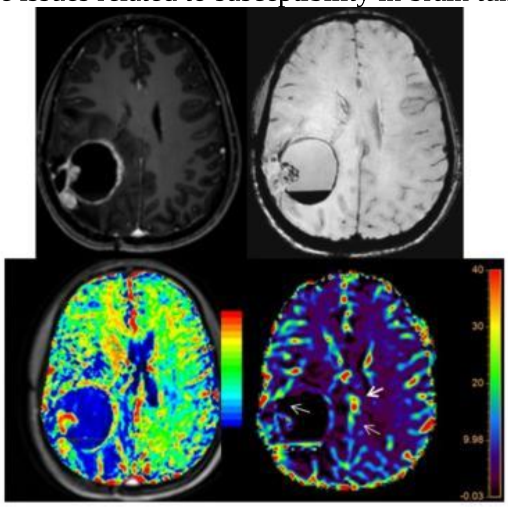

Figure 1: Patient with recurrent tumor with foci of susceptibility in the mural nodule as well as blood fluid level in the cystic component. The mural nodule is showing high CBV on T1- perfusion. Corresponding area shows relatively low CBV on T2* perfusion MRI. Another foci of increased CBV seen posteriorly detected well on both T2*- and T1- perfusion MRI. Artifactual increased CBV is seen within the cystic component of the tumor on T2*- perfusion.
(Filename: TCT_2472_Fig_1_Comp.jpg)

2318

4:12PM - 4:19PM

There is an Exception to Every Rule: T2 FLAIR Mismatch Sign in Gliomas

D Johnson[1], T Kaufmann[1], S Patel[2], A Chi[3], M Snuderl[4], R Jain[3]
[1]Mayo Clinic, Rochester, MN, [2]University of Virginia Health System, Charlottesville, VA, [3]NYU School of Medicine, New York, NY, [4]Department of Pathology New York University Medical Center, New York, NY

Purpose
The T2 - FLAIR mismatch sign, in which a well-circumscribed low-grade glioma is homogenously hyperintense on T2-weighted MR and centrally hypointense on FLAIR images, has been reported as having 100% positive predictive value for IDH-mutant, 1p/19q intact, astrocytoma in multiple recent studies. We now present examples of "false positive" T2 - FLAIR mismatch sign occurring outside the context of IDH-mutant astrocytomas and discuss how they inform interpretation of this sign in clinical practice.
Materials and Methods
Multi-institution retrospective analysis of cases of "false positive" T2 - FLAIR mismatch sign in the authors' clinical practices. MR imaging was performed per local protocols and interpreted by subspecialty certified neuroradiologists. All tumor cases were evaluated for IDH mutation and 1p/19q codeletion as applicable with final diagnoses by subspecialist neuropathologists.
Results
Five cases of "false positive" T2 - FLAIR mismatch sign were observed. Patient ages ranged from 12 to 44 years (median 14 years). Three cases were children or young adults with "pediatric type" glial tumors, and one case was a child with non-neoplastic pathology. Only one false positive T2 - FLAIR mismatch was observed in an adult with infiltrating glioma, a 44 year-old man with oligodendroglioma (IDH mutant and 1p/19q codeleted). Figure 1 depicts an example of T2 - FLAIR mismatch in a pediatric-type glioma without IDH mutation.

Conclusions

We present the first known examples of "false positive" T2 - FLAIR mismatch sign, previously reported to be 100% specific for IDH-mutant astrocytoma. The majority of these exceptions occurred in children and young adults, suggesting caution in the interpretation of the mismatch sign in the pediatric population.

Figure 1

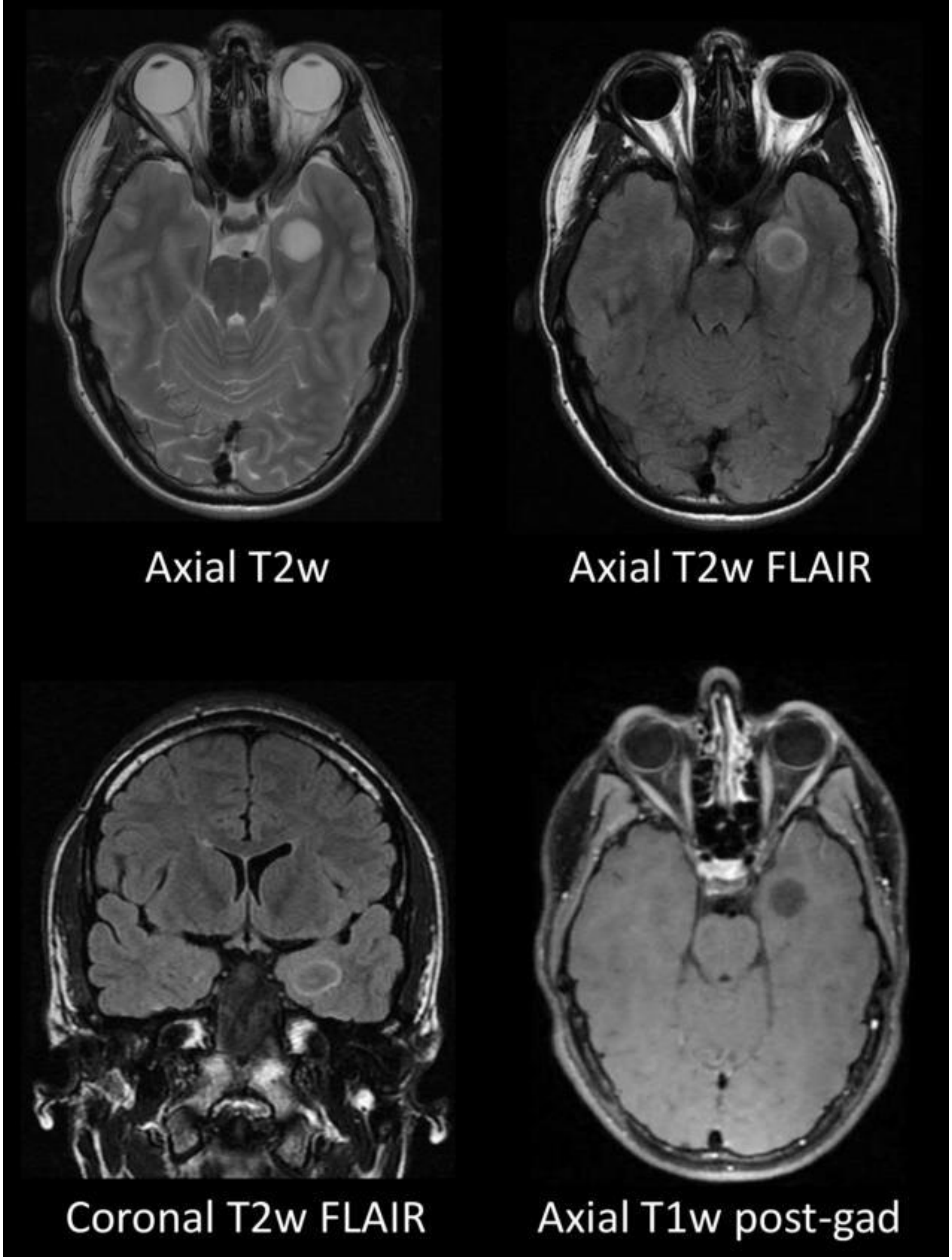
Axial T2w
Axial T2w FLAIR
Coronal T2w FLAIR
Axial T1w post-gad

(Filename: TCT_2318_AbstractFigureFinal.jpg)

2938

4:19PM - 4:25PM

Use of Quantitative Dynamic Susceptibility Contrast (DSC) MRI in Differentiating Between Glioblastoma and Primary Central Nervous System Lymphoma

O Arevalo[1], L Ocasio[2], M Bledsoe[1], X Zhang[3], A Lugo[1], C Soto[4], S Calle[1], Y Esquenazi[5], L Ballester[6], J Zhu[5], A Blanco[5], R Riascos[1], A Kamali[1]
[1]Department of Diagnostic and Interventional Imaging. McGovern Medical School, UTHealth., Houston, TX, [2]Memorial Hermann Hospital Texas Medical Center, Houston, TX, [3]Center for Clinical and Translational Sciences. University of Texas Health Science Center at Houston, Houston, TX, [4]National University of Colombia, Bogota, Colombia, [5]Vivian L. Smith Department of Neurosurgery. McGovern Medical School, UTHealth., Houston, TX, [6]Department of Pathology and Laboratory Medicine. McGovern Medical School, UTHealth., Houston, TX

Purpose
To determine whether the relative cerebral blood volume (rCBV) values by using hotspot technique can be used to discriminate glioblastomas (GBM) from Primary Central Nervous System Lymphomas (PCNSL)
Materials and Methods
MRIs and pathology records from thirteen and eight patients with pathology-proven GBM and PCNSL, respectively, were reviewed retrospectively. Patients underwent standard technique DSC MRI on a 3T magnet preoperatively. Patients included in the study had not initiated any therapy before imaging. Three blinded readers with different levels of experience acquired the mean rCBV values by placing free-hand region-of-interest (ROI) over the areas of greatest perfusion signal within the enhancing area of the tumor using a DynaSuite™ workstation. Control ROIs were placed in the normal-appearing contralateral white matter. The mean rCBV value and the ratio between the affected side and normal-appearing were compared between GBM and PCNSL by using Welch's t-test. The inter-rater variability was measured by the intra-class correlation coefficient (ICC) in the context of a two-way random effect model.
Results
The mean rCBV values in the GBM vs the PCNSL group were 253.1 ± 176.5 Vs. 131.8 ± 69.7 for rater 1 (p=0.041), 320.6 ± 255.4 Vs. 162.3 ± 75.6 for rater 2 (p=0.003), and 301.1 ± 190.5 Vs. 140.8 ± 81.9 for rater 3 (p=0.016). The ratio of mean rCBV between the lesion and the normal-appearing contralateral white matter in the GBM vs the PCNSL group were 4.35 ± 2.02 Vs. 2.13 ± 0.85 (p=0.003) for rater 1, 5.41 ± 4.10 Vs. 2.73 ± 1.51 for rater 2 (p=0.049), and 6.14 ± 3.18 Vs. 3.06 ± 1.39 for rater 3 (p=0.007). The readings among three raters were highly agreeable. The ICC value was 0.90 (95% CI 0.80 to 0.96, p<0.001) for mean rCBV value and was 0.70 (95% CI 0.48 to 0.85, p<0.001) for the ratio between the affected and normal-appearing side.
Conclusions
GBM shows higher mean rCBV values and CBV ratios than PCNSL. It is thought to be related to the angiogenic drive characteristic of GBM tumor biology.

Table 1. CBV evaluation between GBM and lymphoma (mean ± SD are shown in the table)

Rater	Variable	GBM (N=13)	Lymphoma (N=8)	P value
Rater 1	CBV mean	253.1 ± 176.5	131.8 ± 69.7	0.041
	CBV ratio	4.35 ± 2.02	2.13 ± 0.85	0.003
Rater 2	CBV mean	320.6 ± 255.4	162.3 ± 75.6	0.053
	CBV ratio	5.41 ± 4.10	2.73 ± 1.51	0.049
Rater 3	CBV mean	301.1 ± 190.5	140.8 ± 81.9	0.016
	CBV ratio	6.14 ± 3.18	3.06 ± 1.39	0.007

Ratio is the ratio of mean value between diseased side and control side.
Welch's t test was used to compare mean between GBM and lymphoma groups.

Table 2. Inter-rater variability evaluation based on data of three raters – intra-class correlation coefficient (ICC)

Variable	ICC estimate	95% CI	P value
CBV mean	0.90	0.80 to 0.96	<0.001
CBV ratio	0.70	0.48 to 0.85	<0.001

(Filename: TCT_2938_Tables.jpg)

Monday
2:55PM - 4:25PM
3rd Floor, Room 310

Stroke: Clinical Outcomes
2394

2:55PM - 3:02PM

Addition of MRI to the Neurologic Examination to Predict Outcome in Comatose Patients Following Cardiac Arrest

R Ward[1], J Mettenburg[2], N Siripong[3], J Rittenberger[3]
[1]University of Pittsburgh School of Medicine, Pittsburgh, PA, [2]UPMC, PITTSBURGH, PA, [3]University of Pittsburgh, Pittsburgh, PA

Purpose
Following resuscitation from cardiac arrest (CA), coma is common. In addition to the clinical examination, MRI has been proposed to prognosticate neurologic outcome. Locally, we characterize initial neurologic illness using the Pittsburgh Cardiac Arrest Category (PCAC). Increasing levels indicate more severe neurologic injury. We developed a model incorporating MRI results to predict neurologic outcome in patients with moderate neurologic injury (PCAC II and III).
Materials and Methods
Diffusion-weighted MRI images were available from 106 CA patients. The percentage of voxels below a specified ADC threshold (<750 x 10−6 mm2/sec, <700 x 10−6 mm2/sec, <675 x 10−6 mm2/sec, and <600 x 10−6 mm2/sec) was calculated for whole brain and the following regions: brainstem, caudate, cerebellum, frontal, insula, occipital, parietal, putamen, temporal, thalamus, & subcortical white matter. Good outcome was defined as discharge to home or acute rehabilitation facility. Because of the complex interactions among variables, classification and regression tree analysis was used to classify individuals into outcome categories. Ten sample folds were specified for crossvalidation.
Results
The root node underwent splitting into two subnodes. 89% of individuals with >10.85% of parietal voxels

<600 had a poor outcome. Of the individuals with >10.85% parietal voxels <600, 100% of patients with greater than 16.01% of voxels in the brainstem <675 had a poor outcome. 51% of patients with <10.85% of parietal voxels <600 had a good outcome. The model correctly predicted good and poor outcome 89.7% and 49.3% of the time, respectively.

Conclusions

CA patients with moderate coma and reduced ADC values in the parietal and brainstem regions are likely to have poor neurological outcomes. Further investigation into factors predictive of poor outcome in individuals with relatively preserved parietal lobes is needed.

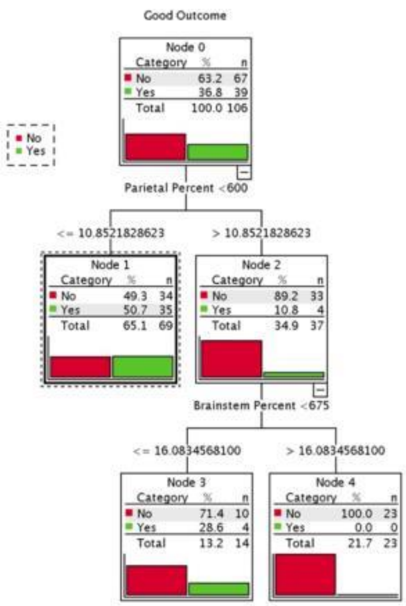

		Pittsburgh Cardiac Arrest Category			Total
		Coma (not following commands, intact brainstem responses)	Coma with moderate to severe cardiopulmonary dysfunction	Unknown	
Good Outcome	No	35	19	13	67
	Yes	33	6	0	39
Total		68	25	13	106

		Rhythm				Total
		Unknown	VF/VT	PEA	Asystole	
Good Outcome	No	14	25	21	7	67
	Yes	6	22	7	4	39
Total		20	47	28	11	106

(Filename: TCT_2394_Ward_ASNR_2019_JPEG300.jpg)

2902

3:02PM - 3:09PM

Effect of ACA Patency on mTICI 2a versus 2b/3 Reperfusion of ICA Terminus Occlusion in IMS III.

T Tomsick[1], Z Smith[2], J Carrozzella[3], P Khatri[4], J Broderick[2], D Liebeskind[5]

[1]University of Cincinnati Hospital, Cincinnati, OH, [2]University of Cincinnati College of Medicine, Cincinnati, OH, [3]University of Cincinnati, Cincinnati, OH, [4]University Of Cincinnati Medical Center, Cincinnati, OH, [5]Department of Neurology, Neurovascular Imaging Research Core, UCLA, Los Angeles, CA

Purpose

To study the effect of A2 occlusion on mTICI 2a vs 2b/3 reperfusion and clinical outcome for ICA terminus occlusion. 50% mTICI 2b/3 reperfusion has become the target for intracranial revascularization procedures. However, definition, application, and convention should not be similarly applied for MCA vs. ICAT occlusion. mTICI following ICAT EVT occlusion has been based on MCA reperfusion, ignoring distal A2 occlusion on reperfusion and clinical outcome measures.

Materials and Methods

IMS III DSA and available baseline CTA were reviewed for ipsilateral A2 segment flow prior to/following EVT of ICAT occlusion. Both A2 flow patency/occlusion and mTICI MCA reperfusion were compared to mRS 0-2 for EVT-treated ICAT occlusion.

Results

Results: 66 treated ICAT occlusions experienced similar mRS 0-2 for both mTICI 2a (6/19, 31.6%) and 2b-3 (8/25, 32%) reperfusion. No mRS 0-2 occurred with confirmed A2 occlusion prior to EVT (n=10, p=0.05,) following EVT (n=10, p=0.06), or both prior to and following EVT. No mRS 0-2 occurred in 10 subjects with pre- or post-EVT A2 occlusion and mTICI 2a or 2b/3, compared to 5/10 (50%) mTICI 2a and 5/12 (40%) mTICI 2b/3 reperfusion patients with A2 patency (p=0.01). 16 occluded A1 segments failed to recanalize, with no good outcomes and higher ASPECTS compared to 49 subjects with confirmed A1 patency (5.2 vs. 3.7, p=0.0002).

Conclusions

Conclusions: A2 occlusion was associated with poor outcome in ICAT occlusion for both mTICI 2a and 2b/3 reperfusion. A2 patency predicted better, yet equal, mRS 0-2 outcomes for both mTICI 2a and 2b/3. Further investigation of an ACA patency modifier to adjust mTICI score in ICAT occlusion should be considered.

3606

3:09PM - 3:16PM

EVT -v- Best Medical Therapy in LVO Patients with Low NIHSS

P Nicholson[1], J Schaafsma[2], V Mendes-Pereira[1]
[1]Toronto Western Hospital, Toronto, Ontario, [2]University Health Network, University of Toronto, Toronto, Ontario

Purpose

Purpose: The evidence for endovascular thrombectomy (EVT) in patients with large vessel occlusion (LVO) and mild strokes (e.g. those with National Institute of Health Stroke Score - NIHSS - <6) is limited, as most trial patients thus far have been patients with more severe strokes. There remains considerable uncertainty regarding the best treatment of these patients. We wished to evaluate the safety and efficacy of EVT in this patient cohort, as compared with those patients who instead received best medical therapy (BMT)

Materials and Methods

Using our prospectively maintained stroke database, we performed a retrospective assessment of our patients who presented with (1) an LVO and (2) an NIHSS of 6 or less. This was performed with ethics approval. In order to try and eliminate bias in this retrospective assessment, we performed a propensity score analysis, matching patients according to age, gender, NIHSS, ASPECTS, clot location, degree of collaterals and time since onset of symptoms. We looked at the safety of the procedure, and compared clinical outcomes between the two groups by using a modified Rankin score (mRS) assessment at 90 days as a primary outcome.

Results

66 patients were identified - 38 were male. Mean patient age was 67 years, while median NIHSS was 3. Median ASPECTS was 10, while median time since last seen well was 4.43 hours. 72.5 % of patients in the BMT group were functionally independent (mRS 0-2) at 90 days, compared with 76% in the EVT group. Despite these differences, EVT was not associated with a statistically significant increase in good outcomes as compared with best medical therapy (p=0.97). 3 deaths occurred in the EVT group, and none in the medical group. Following propensity score matching, EVT failed to show a statistically significant association with increased good outcomes (p=0.39). In terms of subgroups, EVT did not offer a benefit when looking at proximal clots (ICA+M1) versus more distal clots (M2,M3 and more distal). Similarly, there was no differences between outcomes when comparing anterior circulation with posterior circulation outcomes.

Conclusions

In our small, retrospective single centre study, there was no statistically significant benefit in terms of EVT over medical therapy with respect to mRS at 30 days. There remains a paucity of data in this subgroup of stroke patients, and we hope that our data will add to the growing body of evidence looking at EVT outcomes in patients with mild strokes.

2618

3:16PM - 3:23PM

Hypo-Perfusion Intensity Ratio Predicts Patient Eligibility for Thrombectomy

A Guenego[1], D Marcellus[1], B Martin[1], S Christensen[1], G Albers[2], M Lansberg[3], M Marks[4], M Wintermark[5], J Heit[3]
[1]Stanford University, Stanford, CA, [2]Stanford University Medical Center, Palo Alto, CA, [3]Stanford, Stanford, CA, [4]Stanford Univ. Med. Ctr., Stanford, CA, [5]Stanford, San Carlos, CA

Purpose
Hypoperfusion intensity ratio (HIR) correlates with collateral status in acute ischemic stroke (AIS). We assessed whether HIR is a marker of patient eligibility for mechanical thrombectomy (MT).
Materials and Methods
We performed a retrospective cohort study of consecutive AIS patients with large vessel occlusion (LVO) who underwent MT triage with CT or MRI perfusion imaging. Clinical data, ischemic core (mL), HIR (volume TMax>10 seconds / volume TMax>6 seconds), core/penumbra mismatch, and MT details were assessed. Primary outcome was favorable HIR score (HIR < 0.4) between patients who underwent MT (MT+) and those who did not (MT-) up to 24 hours after symptom onset. Secondary outcomes were favorable HIR score in MT- sub-groups (NIHSS70mL) and core-penumbra mismatch volumes.
Results
197 patients (145 MT+ and 52 MT-) were included. MT+ patients had a lower median HIR compared to MT- patients (0.4 [IQR 0.2-0.5] versus 0.6 [IQR 0.5-0.8], p<0.001) and a higher core/penumbra mismatch volume (96mL versus 27mL, p<0.001). Among MT- patients, 43 had a core >70 ml, and 9 had a NIHSS<6. MT- patients with NIHSS <6 had a lower HIR than MT- patients with core >70ml (0.2 [IQR 0.2-0.3] versus 0.7 [IQR 0.6-0.8], p<0.001), but their HIR was not significantly different that MT+ patients.
Conclusions
Patients who meet AHA thrombectomy guidelines are more likely to have favorable HIR (good collaterals). HIR may be a marker for MT eligibility and useful for MT triage.

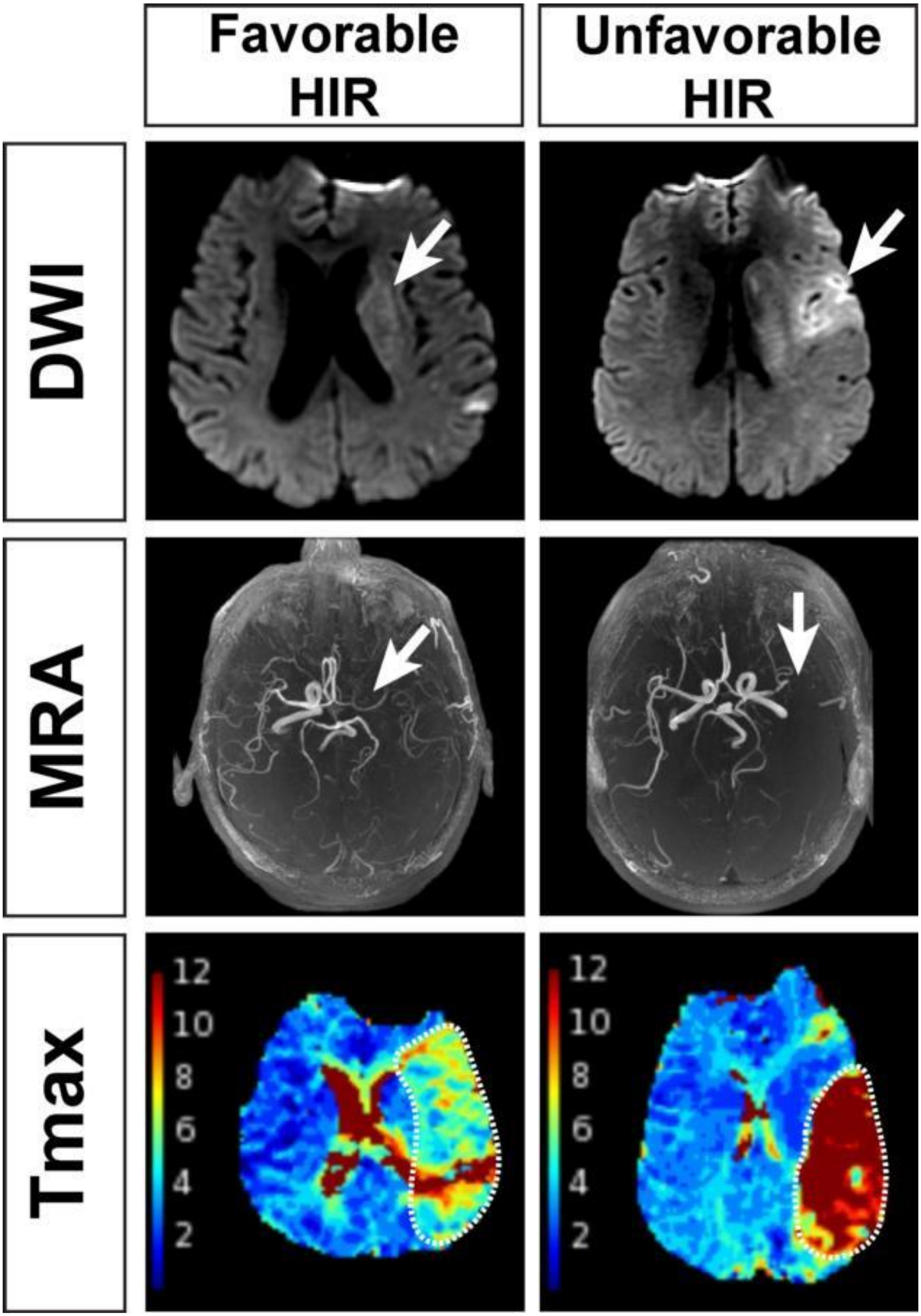
Favorable HIR
Unfavorable HIR
DWI
MRA
Tmax
12
10
8
6
4
2
12
10
8
6
4
2

(Filename: TCT_2618_Figure1v1.jpg)

3638

3:23PM - 3:30PM

Influence of Simultaneous Vasodilator and Inotropic Agents on the Evolution of Infarct Growth in Experimental Acute Middle Cerebral Artery Occlusion

N Saadat[1], G Christoforidis[2], Y Jeong[3], S Roth[4], M Niekrasz[2], K Kawaji[5], T Carroll[2]
[1]University of Chicago, chicago, IL, [2]University of Chicago, Chicago, IL, [3]Northwestern University, Chicago, IL, [4]University of Illinois, Chicago, IL, [5]Illinois Institute of Technology, Chicago, IL

Purpose
It has been previously shown experimentally that simultaneous administration of norepinephrine and hydralazine can overcome cerebral autoregulation. In the setting of acute ischemic stroke, we hypothesize that overcoming cerebral autoregulation may result in improved perfusion to the ischemic territory. This work assesses the influence of a combination of norepinephrine and hydralazine on the evolution of cerebral infarction during middle cerebral artery (MCA) occlusion in an experimental model while taking into account the effect of pretreatment pial collateral recruitment.
Materials and Methods
Sixteen mongrel canines (20-30kg) underwent cerebral angiography, and permanent endovascular occlusion of an M1 segment of MCA followed by MRI- based (3T Achieva, Philips Healthcare, Best, Netherlands) infarct volumes measurement. Six subjects received a continuous infusion of norepinephrine (0.1-1.5200 µg/kg/min; titrated to 50 mm Hg above baseline mean arterial pressure) and hydralazine (20mg) starting 15 minutes following MCA occlusion. Ten subjects were used in a control group. Anesthesia was chosen so as not to influence cerebrovascular reactivity (isoflurane (1%, 0.75 MAC), propofol (100-200 µg/kg/min), and rocuronium (0.4-0.6 mg/kg). Physiologic parameters were maintained in the normal range except during the induction of hypertension in the treatment group. The bilateral femoral arteries and one femoral vein were catheterized to measure the blood pressure and infuse norepinephrine respectively. Diffusion-weighted MR (DWI-MRI) imaging was acquired on 60, 90, 120, 180, 240 minutes post-MCA occlusion. Measured infarct volumes over time from DWI-MRI were compared to volumes predicted by 15 minutes collateral score evaluation based on previously published work. Differences between the predicted and measured values were compared based on the slope of a correlation plot and the mean difference between the measured and predicted values (i.e., residual).
Results
None of the subjects showed evidence of hemorrhagic conversion or herniation or signs posterior reversible encephalopathy. In the control group, our previously published parameterization of infarct growth was highly predictive of observed infarct volume (Measured=.94*predicted+228, r2=0.85). In the treatment group, the measured infarct volumes were found to be significantly lower than infarct volumes predicted by the model (Measured=0.44*predicted+2892, r2=0.71) in subjects with poor collateral recruitment. A point by point comparison of the difference between predicted and measured infarct volumes showed a smaller infarct volume in the treatment group (=-1842+/-4786 mm3) compared to the control group (469+/- 2549 mm^3), p<0.03).
Conclusions
Preliminary results in this experimental model demonstrate that a combination of norepinephrine and hydralazine administered in the acute phase of ischemic stroke mitigates infarct evolution especially in subjects with poor collateral recruitment. This may have implications for acute ischemic stroke treatment in patients with poor collaterals.

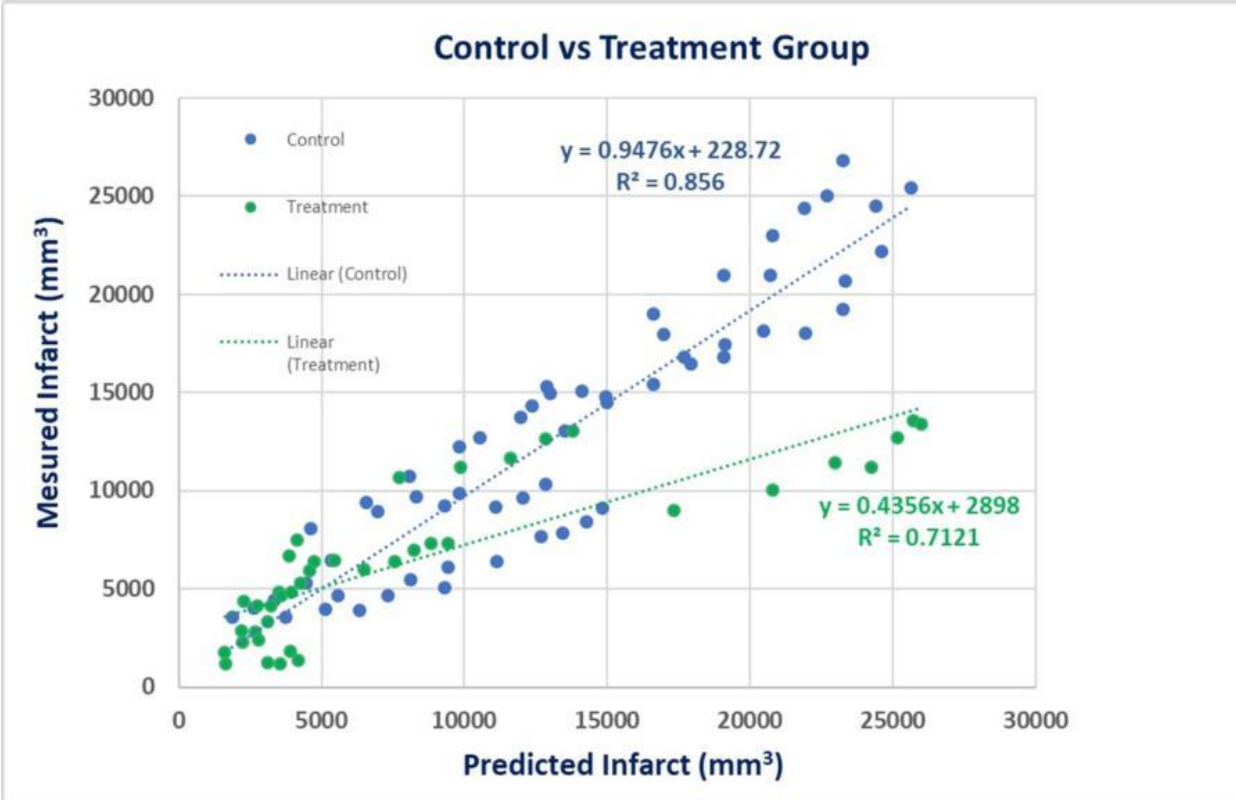

Figure 1. Correlation plot of predicted infarct volume versus measured infarct volume (mm^3) of cases with (green) and without (blue) treatment. Dotted line represents linear regression. High correlations were found, but in the treatment group, the measured volumes were much lower in general than the predicted outcome.

(Filename: TCT_3638_treatmentvscontrolgroup.jpg)

2354

3:30PM - 3:37PM

Initial Thrombocytopenia and Declines in Platelet Counts Are Associated with Mortality and Outcome in Acute Ischemic Stroke

S Mönch[1], T Boeckh-Behrens[2], K Kreiser[3], D Hedderich[4], C Maegerlein[5], M Lehm[5], S Wunderlich[5], B Friedrich[6]
[1]TECHNICAL UNIVERSITY MUNICH, KLINIKUM RECHTS DER ISAR, MUNICH, Germany, [2]Klinikum Rechts der Isar, TU München, München, Bavaria, [3]Klinikum rechts der Isar, Munich, Bavaria, [4]Klinikum rechts der Isar, Technical University of Munich, Munich, Germany, [5]Klinikum rechts der Isar, Technical University Munich, Munich, Bavaria, [6]Klinikum rechts der Isar, Technical University Munich, Munich, Germany

Purpose
Acute ischemic stroke (AIS) has several well-known risk factors. In the treatment of acute myocardial infarction with percutaneous coronary intervention, initial thrombocytopenia (TP) and a decline of platelets counts (DPC) are well-studied complications associated with increased mortality. In this study we investigated if TP and DPC are also relevant in AIS patients treated with mechanical thrombectomy (MT).

Materials and Methods
In a case-control study including all consecutive MT-stroke patients between 01/01/2017 and 31/05/2018, we analyzed the influence of TP and DPC on the outcome and mortality after MT as well on the rate of intracranial hemorrhages (ICH). A multivariate logistic regression model was used to test for good clinical outcome (mRS 90 days <= 2) and mortality adjusting for age, initial NIHSS, pretreatment with tPA, statins and platelet inhibitors, occlusion site, time from symptom onset to recanalization, initial TP (< 150 x 109/L) and DPC (> 26%).
Results
Of 353 patients included, 8.2% had an initial TP and 23.8% a DPC > 26%. The mortality rate in patients with normal platelet counts was 26.1% vs. 48.3% (p=0.002) in patients with initial TP with an aOR of 3.47 (CI 1.28 - 9.4, p=0.005). No difference regarding the rate of good clinical outcome and ICH (p=0.18) was observed. A DPC of more than 26% during the first five days of hospitalization predicted the rate of mortality (aOR 0.376 CI 0.175 - 0.79, p=0.01) and the chances of a good clinical outcome (aOR 3.19 CI 1.4 - 7.2, p=0.005) without significant differences of ICH rates (p=0.735).
Conclusions
We for the first time show that an initial TP and a marked DPC in AIS patients treated with MT are independently associated with higher mortality rates and poorer clinical outcomes. Abnormal platelet counts should therefore be closely monitored.

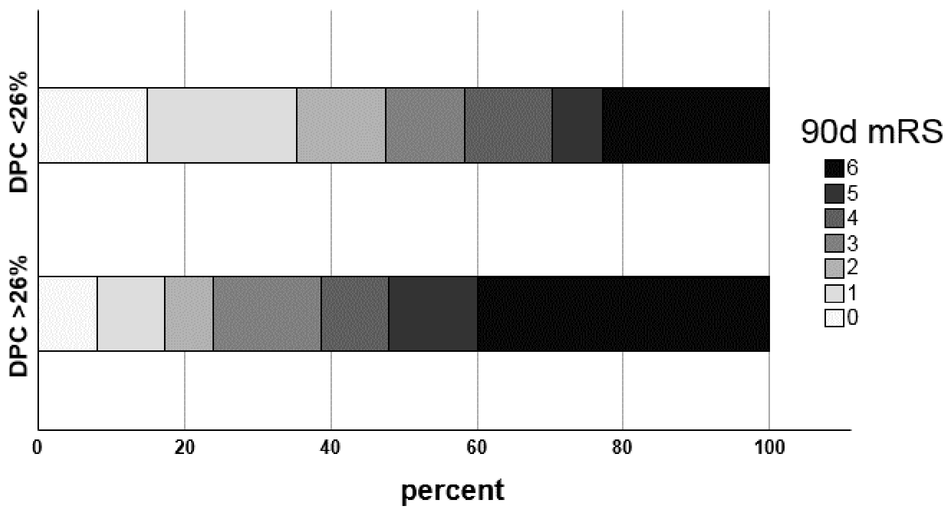

(Filename: TCT_2354_PDCandPatientMortality.gif)

2892

3:37PM - 3:44PM

Peripheral Emboli After Mechanical Thrombectomy on High Resolution DWI: Incidence, Predictors and Clinical Significance

M Schoenfeld[1], R Kabiri[1], H Kniep[1], G Broocks[2], U Hanning[3], M Bechstein[4], J Fiehler[5]
[1]University Medical Center Hamburg-Eppendorf, Hamburg, Hamburg, [2]University Medical Center Hamburg-Eppendorf, Hamburg, Germany, [3]University of Hamburg-Eppendorf, Hamburg, Germany, [4]UNIVERSITY MEDICAL CENTER - HAMBURG, HAMBURG, Germany, [5]University Medical Center Hamburg-Eppendorf, Hamburg, AK

Purpose
To analyze the incidence of small peripheral emboli after mechanical thrombectomy (MT), their impact on stroke severity, and their predictors.

Materials and Methods

Patients successfully treated with MT for a large vessel occlusion received a 1.5T MRI with diffusion-weighted imaging (DWI) in normal and high resolution on the day following the intervention. Punctuate DWI lesions distant to the continuous core were defined as peripheral emboli. Success of MT was assessed on DSA by eTICI score. Procedural details of MT (primary aspiration or stent retrieval with or without balloon occlusion, number of passes) as well as NIHSS before thrombectomy and upon discharge were collected and correlated with the number of peripheral emboli.

Results

In 28 consecutive patients, a total of 324 peripheral emboli were seen on DWI. 173 peripheral emboli (53.4%) were exclusively detected in high resolution DWI. The number of emboli correlated with eTICI score (Spearman's rho 0.605; $p<0.001$). In 8/9 patients with complete recanalization on DSA (eTICI 3) peripheral emboli were detected. Only 2 patients did not show any peripheral emboli. 21 peripheral emboli (6.5%) in 11 patients were classified as emboli into new territory. There was a tendency towards fewer peripheral emboli when recanalization was achieved using only one pass of the stent retriever or by a single distal aspiration ($p=0.68$) and when a balloon catheter was used ($p=0.94$). The number and the volume of peripheral emboli did not correlate with NIHSS upon discharge or the temporal course of NIHSS.

Conclusions

Using high resolution DWI peripheral emboli in the territory affected by a large vessel occlusion are commonly detected even after supposedly complete recanalization. These peripheral emboli are more common than emboli into new territory. Factors influencing the occurrence of peripheral emboli and their clinical relevance are still uncertain.

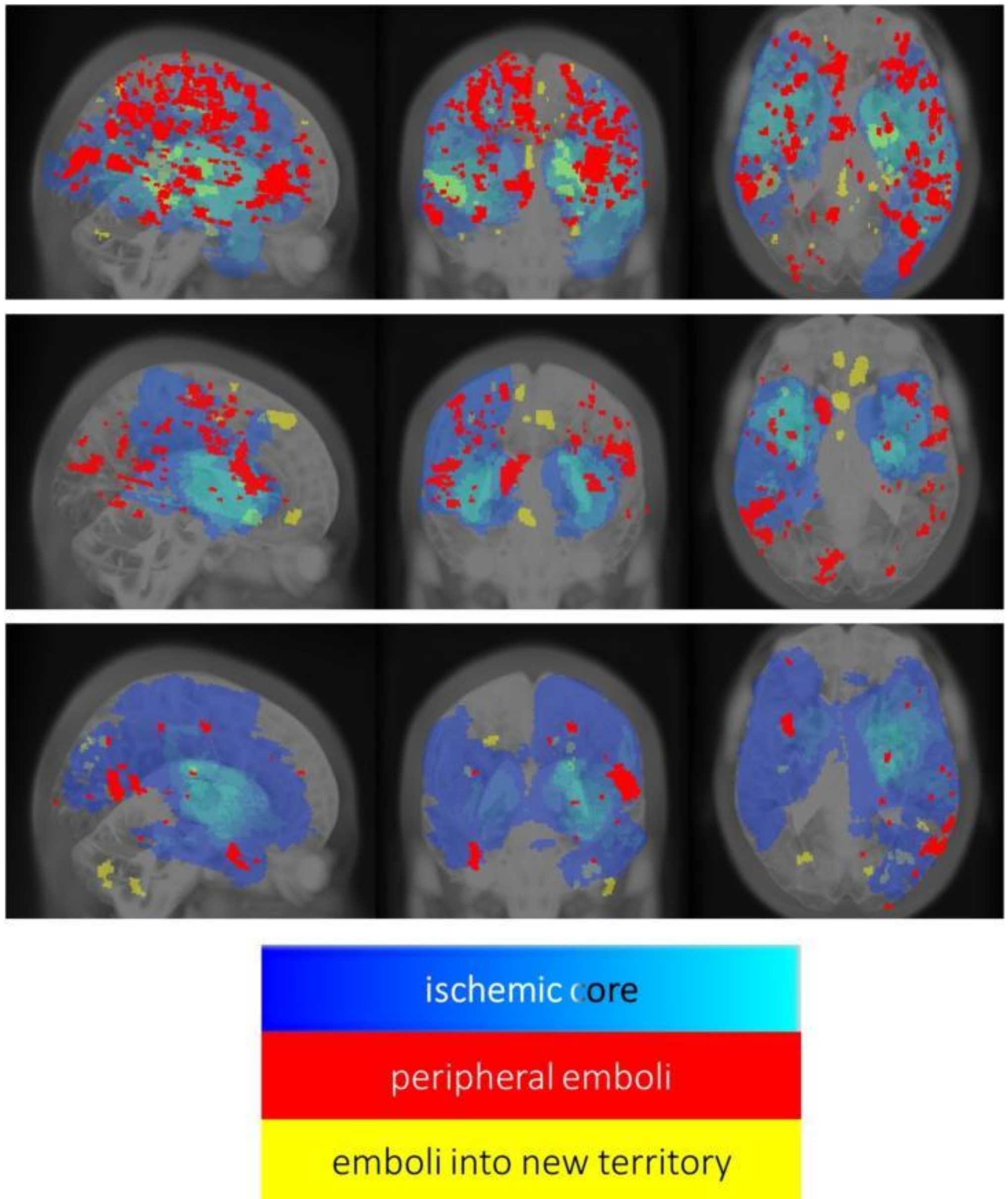

(Filename: TCT_2892_ASNR2019_Schoenfeld.jpg)

3041

3:44PM - 3:51PM

Recurrent MCA Infarction in a Patient with a Carotid Web: 2 Thrombectomies in a 24 hour period.

J Lavie[1], J Milburn[1], A Steven[2]
[1]Ochsner Clinic Foundation, New Orleans, LA, [2]OCHSNER HEALTH SYSTEM, NEW ORLEANS, LA

Purpose
Carotid webs are shelf-like filling defects found at the carotid bifurcation, thought to reflect intimal hyperplasia. These lesions have been increasingly recognized as a potential etiology of ischemic stroke, especially in young patients without traditional risk factors1-3. However, they may be overlooked, as the

disease is still not widely known and not typically associated with a hemodynamically significant stenosis1. Treatment options range from observation or medical therapy to more invasive procedures like carotid stenting and carotid endarterectomy.2 There are no consensus treatment guidelines in place for either symptomatic or asymptomatic patients. We present a case of recurrent ischemic stroke in a patient with a carotid web, requiring 2 thrombectomies in a 24 hour time period.

Materials and Methods

A 39 year old patient presented with right sided weakness and dysarthria. Imaging evaluation showed acute left middle cerebral artery(MCA) thrombus, prompting transfer to our comprehensive stroke center. Emergent thrombectomy was successfully performed, and the patient's right sided weakness and dysarthria improved. Approximately 12 hours after the procedure, the patient developed right hemiplegia and aphasia, and repeat CTA showed a recurrent left MCA occlusion. Thrombectomy was again performed with restoration of TICI 2B flow. The patient was discharged with complete right hemiplegia and moderate aphasia. Carotid endarterectomy was subsequently performed after discharge to mitigate risk of an additional recurrent embolic stroke.

Results

Coronal CT Angiogram image shows abrupt occlusion of the M1 segment of the left MCA (A). Lateral DSA projection of left common carotid injection (B) and sagittal CT Angiogram of the neck (C) demonstrate a shelf-like protrusion from the posterior aspect of carotid bulb, compatible with a carotid web.

Conclusions

Carotid webs are an increasingly recognized potential cause of ischemic stroke, but management guidelines are not yet well established. This case suggests that aggressive management of carotid webs may be warranted in acutely symptomatic patients.

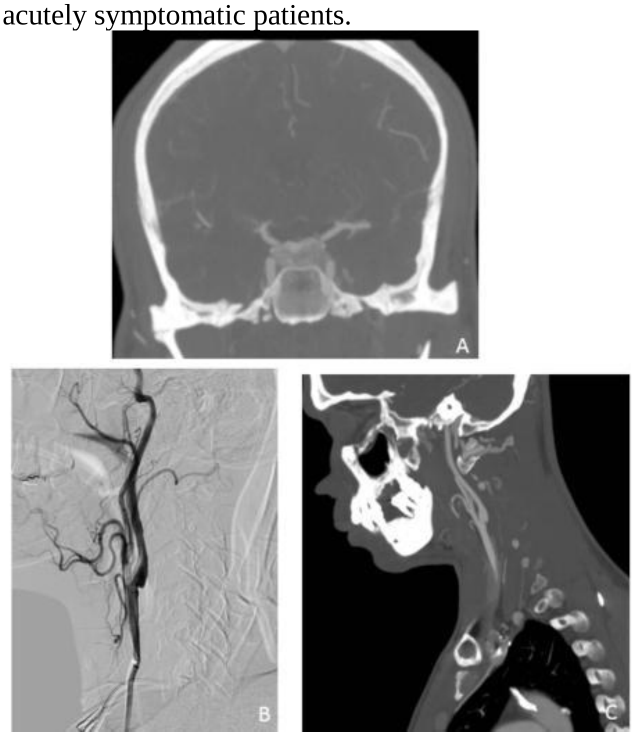

(Filename: TCT_3041_Slide1.JPG)

3196

3:51PM - 3:58PM

Safety and Efficacy of Adjuvant Endovascular Interventions in Refractory anterior Circulation Thrombectomies

R Abdalla[1], M Darwish[2], T Shokuhfar[3], M Hurley[3], A Shaibani[3], B Jahromi[4], M Potts[4], S ANSARI[5]
[1]Northwestern University, Chicago, IL, [2]northwestern university, chicago, IL, [3]Northwestern University Feinberg School of Medicine, Chicago, IL, [4]Northwestern University, Feinberg School of Medicine, Chicago, IL, [5]NORTHWESTERN UNIVERSITY, FEINBERG SCHOOL OF MEDICINE, CHICAGO, IL

Purpose
Emergent large vessel occlusion due to underlying vessel wall pathology might be refractory to the regular endovascular treatment with or without stent retrievers requiring further intervention to achieve successful recanalization. The aim of our study is to determine the prevalence of refractory thrombectomies requiring further intervention, compare their baseline characteristics and outcomes with patients undergoing regular endovascular treatment, and compare outcomes among different treatment modalities.
Materials and Methods
We retrospectively reviewed 148 patients treated endovascularly for anterior circulation ELVO from Nov 2016 till May 2018. Refractory thrombectomy was defined as patients requiring intracranial stenting, eptifibatide injection or patients suffering re-occlusion in the same artery within one day of the procedure. Baseline characteristics and outcomes were compared between the refractory and the regular treatment groups using Mann-Whitney and Fisher Exact test. Outcomes were compared within the refractory group undergoing different treatment modalities. Favorable outcome was defined as MRS ≤ 2 after 3 months.
Results
Refractory thrombectomies amounted to 19 cases (12.8%). No statistically significant difference between refractory and regular groups in baseline characteristics, median National institute of health stroke scale score (16 vs. 17, P=0.16), and percentage of favorable outcomes (41.2% vs 50.5%, P=0.6) respectively. Patients in the refractory cohort had a significantly higher prevalence of Diabetes (52.6% vs. 21.1%, P=0.008), while regular group patients had significantly higher rates of Atrial fibrillation (53.1% vs. 21.1%, P=0.013). Diabetes was the sole independent predictor of refractoriness with OR 4.757 (1.513-14.956; P=0.008). Within the refractory group, 11 patients were treated by intracranial stenting (52.6%), 6 received Intraarterial eptifibatide injection (31.6%), and 3 had silent re-occlusions (15.8%). No significant difference in favorable outcome between intracranial stenting vs eptifibatide (55.6% Vs. 33.3%, P=0.61).
Conclusions
Refractory thrombectomy is more common in Diabetics. Emergent intracranial stenting and eptifibatide injection are equally safe and effective adjuvant treatments in hyperacute strokes with underlying vascular pathology.

3649

3:58PM - 4:05PM

Simulation Training for Acute Ischemic Stroke Image Interpretation in a Comprehensive Stoke Center

R Javan[1], P Heidari[1], A Nelson[2], A Goyal[1], F Huda[3], M Osman[2], M Losee[4], C Leon-Guerrero[1]
[1]George Washington University Hospital, Washington, DC, [2]George Washington University School of Medicine and Health Sciences, Washington D.C. , DC, [3]The George Washington University Hospital, Washington, DC, [4]George Washington University Columbian College of Arts & Sciences, Washington D.C. , DC

Purpose
Recent clinical trials and imaging advancements have yielded significant changes in the management and triage of acute ischemic stroke, particularly the extension of the treatment window for acute therapy using 'tissue as oppose to time' based decision making. To create a tailored and active learning experience for radiology and neurology residents as well as neuroradiology fellows, and to evaluate their ability to

interpret acute stroke neuroimages, we utilized "Weasis," an open-source web-based Picture Archiving and Communication System (PACS) with an integrated reporting system.
Materials and Methods
We establish a new PACS teaching system by utilizing the open-source PACS system "dcm4chee" and integrating Weasis as imaging viewing browser, MySQL as database and JBOSS as application server. The developmental environment is MyEclipse, developmental language is JAVA. We use WADO (Web Access to Digital Imaging and Communications in Medicine (DICOM) Object) to achieve web-client DICOM images access. Java applets are used via a browser to serve as a DICOM viewer without special software required, and all functions (window width and level, zoom, measurement, etc.) are provided as controls within the server application.
Results
Twenty cases of varying diagnoses and clinical scenarios, each containing multiple neuroimaging studies, with findings ranging from normal to complex were used. Imaging modalities included non-contrast CT head, multiphase CTA, CT perfusion, MRI brain, MRA head and neck, and catheter angiography. Post-treatment neuroimages were used to demonstrate concepts such as hemorrhagic conversion or extravasation of contrast after neurointervention. The anonymized cases are accessible on any computer connected to the hospital's secure network. Trainees could simulate being a neuroradiologist and independently formulate an opinion and write up a brief report without the need for occupying an expensive PACS workstation. Trainees were asked to provide impression points for each of the reviewed studies. The length of time used by the trainee to review and complete the assigned cases was automatically recorded.
Conclusions
Using Weasis with a reporting system provides trainees with a real-time, easy-access, and novel imaging database for learning how to interpret stroke neuroimages. Trainees are able to personalize their learning experience and work through a wide breadth of real world clinical scenarios. Teaching cases are easily accumulated for learning, didactic and evaluation purposes. In summary, Wesasis with a reporting system is a novel educational tool useful for both teaching and evaluating radiology and neurology trainees in the interpretation of acute stroke neuroimages.

2640

4:05PM - 4:12PM

Thromboaspiration of Distal Emboli Caused by Mechanical Thrombectomy of Large Vessel Occlusions Leads to Improved mTICI Scores

F Settecase[1]
[1]*University of British Columbia, Vancouver, British Columbia*

Purpose
Higher angiographic revascularization scores after mechanical thrombectomy (MT) of large vessel occlusion (LVO) acute ischemic stroke (AIS) are correlated with improved functional outcomes. While mTICI 2B is generally considered a good revascularization score and/or procedural endpoint, higher revascularization score may be achieved by treatment of distal emboli (DE). The safety and efficacy of endovascular treatment of DE, however, is not well known.
Materials and Methods
Institutional review board approval was obtained. Eighteen consecutive patients at our center with LVO AIS undergoing MT, subsequently developing DE for which thromboaspiration was performed, were retrospectively reviewed. Demographic and clinical characteristics, procedural and angiographic data, and outcomes were collected for each patient.
Results
Eighteen patients with 18 distal emboli after LVO thrombectomy were treated. Locations of DE were the: distal M2 and M3 MCA, pericallosal and callosomarginal arteries, and P1 PCA (all arteries $\geq$ 1.5 mm in

diameter). Thromboaspiration of DE was successful in 13/18 (72%). Thromboaspiration resulted in improvement in the final mTICI score in 14/18 patients (78%) compared to initial mTICI score after LVO thrombectomy (Figure 1A-C). Initial mTICI score after LVO thrombectomy was 2A in 4/18 (22%) of patients and 2B in 14/18 (78%) of patients. Final mTICI score after DE aspiration improved to 2B in 7/18 (39%) patients, 2C in 3/18 (17%) patients, and 3 in 8/18 (44%) patients (Figure 1D). No procedural complications were noted. In 13 patients with successful DE thromboaspiration, 10 patients (77%) had a 90 day mRS of 0-2. In the 5 patients with unsuccessful DE aspiration, 3 patients (60%) had a 90 day mRS of 0-2.

Conclusions

Thromboaspiration of select DE is feasible and leads to improved final mTICI scores. Larger prospective studies are needed to establish the clinical benefit and safety of this approach.

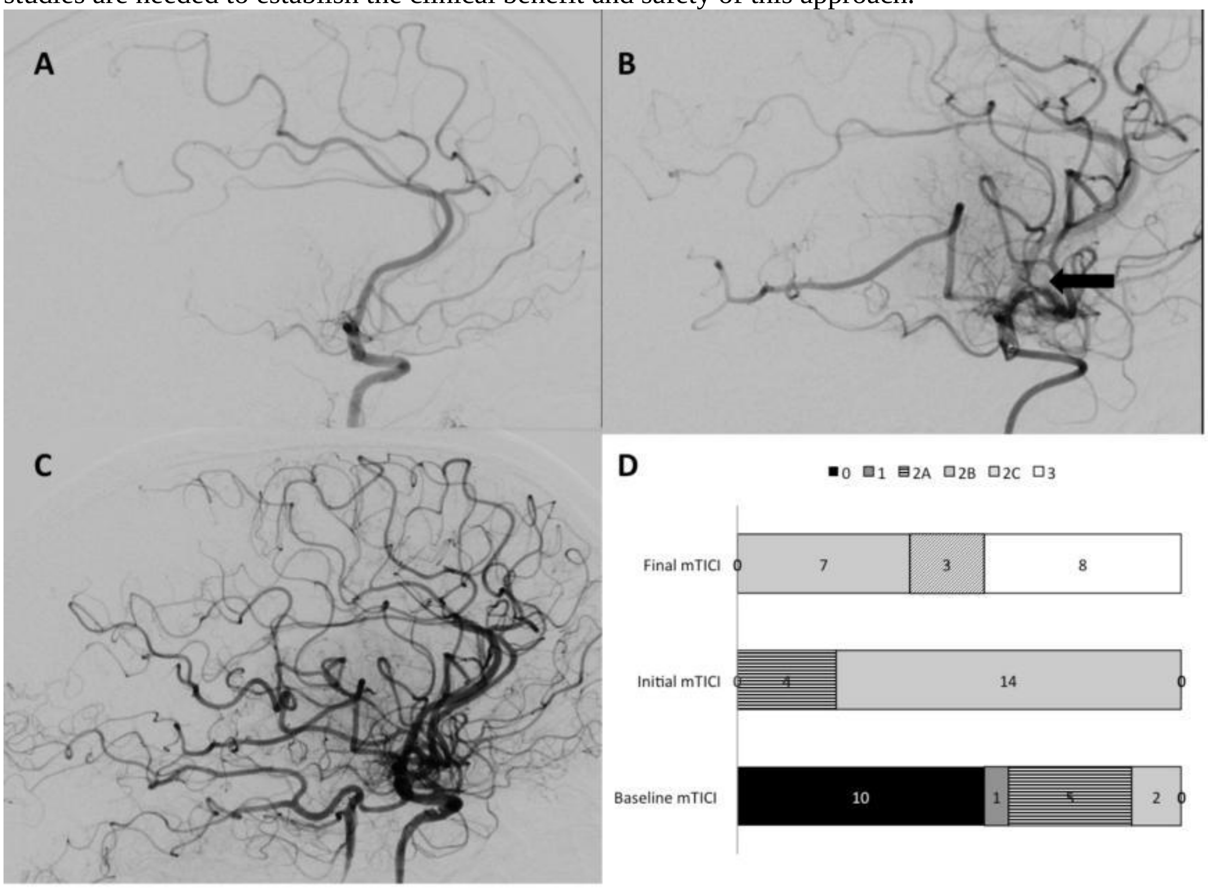

(Filename: TCT_2640_ASNR2019abstractDEFIGURE1.jpg)

2896

4:12PM - 4:19PM

Utility of Mechanical Thrombectomy for Isolated M2 Branch Occlusions

M Bhatt[1], F Memon[1], J Wilseck[1]
[1]Beaumont-Royal Oak (William Beaumont Hospital), Royal Oak, MI

Purpose

While mechanical thrombectomy was known to be an effective revascularization tool for acute ischemic stroke, the five major clinical trials demonstrated that mechanical thrombectomy for large vessel occlusions has impacted and improved clinical outcomes. However outcomes for isolated M2 occlusions have yet to be delineated. Our purpose is to add to available evidence that mechanical thrombectomy for M2 branch occlusions has clinical benefit.

Materials and Methods

Retrospective analysis of data set for patients at our single institution who underwent mechanical thrombectomy between January 2010 and August 2018. All patients to meet our inclusion criteria, which include: isolated M2 branch occlusion, comprehensive imaging evaluation (non-enhanced CT, CT-Angiography and CT-Perfusion), and underwent mechanical thrombectomy.

Results

Included patients will meet our inclusion criteria. Collected data to include patient demographics, right or left-sidedness, co-morbidities, National Institute of Health (NIH) stroke scale scores, radiologic findings (ischemic penumbra), symptom onset to canalization time, procedure time, thrombectomy device used, Thrombolysis in Cerebral Infarction Scale (TICI) scores, follow-up of modified Rankin Scale (mRS) scores and complications.

Conclusions

Lack of randomized control trials (RCTs) for isolated M2 branch occlusions adds relevance to the importance of retrospective analysis of outcomes in mechanical thrombectomy for M2 branch occlusions. This data set can be compared with similar studies to depict the positive radiologic and clinical outcomes of mechanical thrombectomy for isolated M2 branch occlusions.

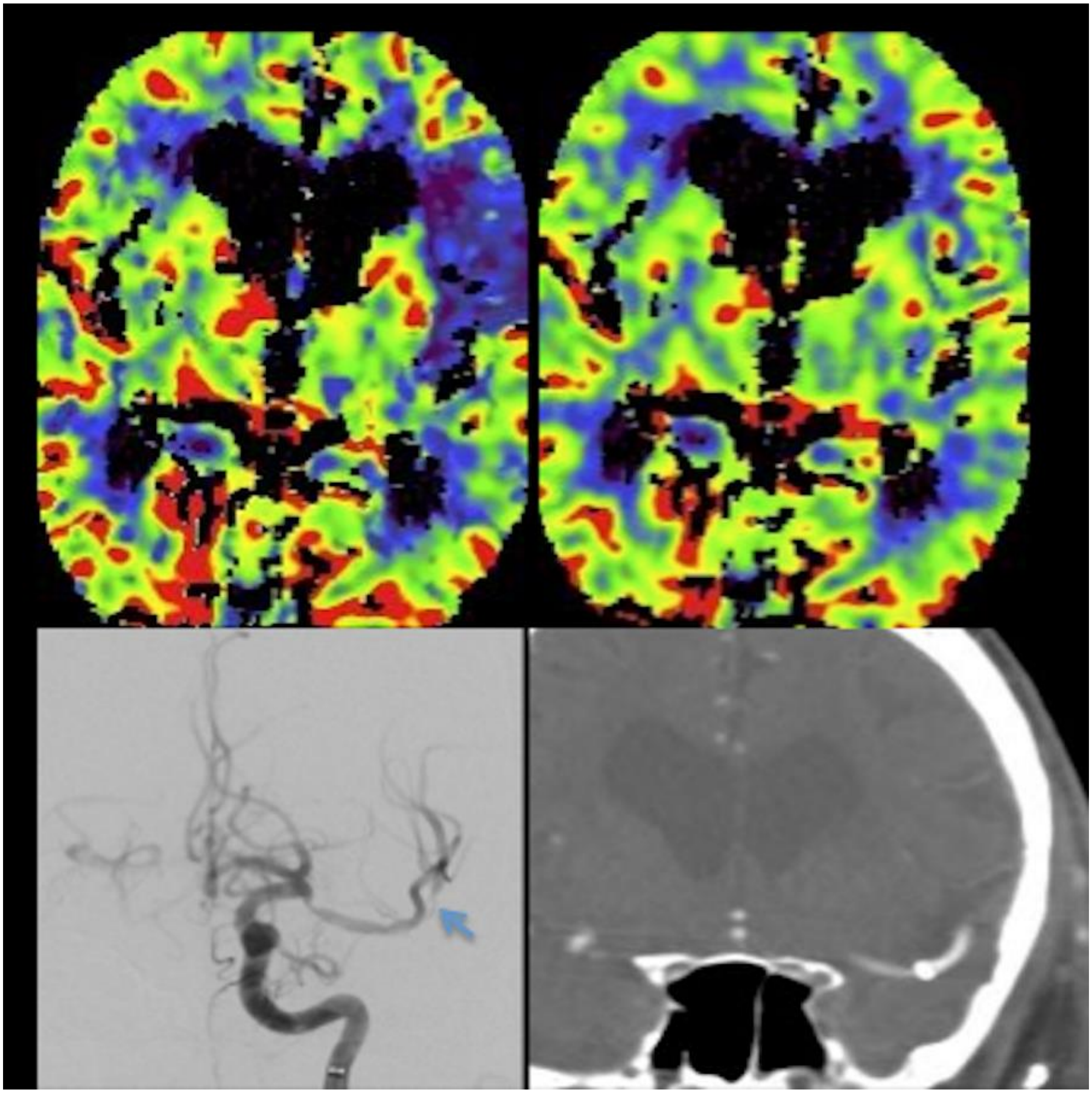

(Filename: TCT_2896_M2imagesabstractasnr.jpg)

Monday, May 20, 2019
2:55PM - 4:25PM
Vascular Malformations

3468

2:55PM - 3:02PM

A Frequent Yet Unreported Dural Venous Sinus Draining Into the Transverse Sinus

A Hedjoudje[1], D San Millán[2]
[1]Johns Hopkins University, Baltimore, MD, [2]Sion Hospital, Sion, Valais

Purpose
In the course of our routine angiographic activity, we have observed a frequent termination of the cortical veins draining the surface of the temporal and occipital lobes into a supratentorial dural venous sinus located in the dura mater overlying the occipital squama or parietal bone over the transverse sinus (TS). We hereby present the angiographic anatomy of this dural venous sinus, offer an embryological hypothesis, and describe possible clinical implications for transtemporal neurosurgical approaches.
Materials and Methods
The presence of a supratentorial dural sinus on the occipital squama (SDSOS) was prospectively sought in the venous phase of 100 routine adult diagnostic CTV (320 detector subtracted dynamic volume CT scanner performed in our institution. Patient presenting with intracranial venous malformation, venous thrombosis or pseudotumor cerebri were excluded from analysis. Tributaries of the SDSOS were noted and classified.
Results
We included 82 patients in this analysis. The mean age was 57 years (range 34-82). 18 patients were excluded from analysis. After careful examination of 82 venous phase we could identify a total of 9 SDSOS which corresponded to a prevalence of 11%. Tributaries of the SDSOS included lateral temporal veins, lateral parietal veins; lateral occipital veins; and internal occipital veins. Presence of a lesser anastomotic vein of Labbé (VL) draining into the SDSOS was also noted. The presence of a lesser anastomotic vein of Labbé draining into the SDSOS was noted in 2 cases.
Conclusions
This study presents a frequent yet undocumented type of drainage of the inferior temporal lobe through a supratentorial venous sinus draining into the transverse sinus. Embryological "ballooning" of the transverse sinus with rapid increase/decrease can results in the formation of pouch or pouches of the duralsinus that may extend from the transverse sinus into the convexity dura or the tentorial dura. This is the reason that, in some cases, a cortical vein or veins indirectly join the transverse sinus through a small tentorial sinus or a dural sinus over the convexity. A lesion or sacrifice of supratentorial veins joining the transverse sinus represents a hemorrhagic and ischemic hazard during supratentorial surgical approaches. A detailed venous documentation before undertaking this type of surgery is important to avoid potential complications. Figure legend : MR venograms showing different views of a left supratentorial dural sinus of the occipital squama draining into the transverse sinus.

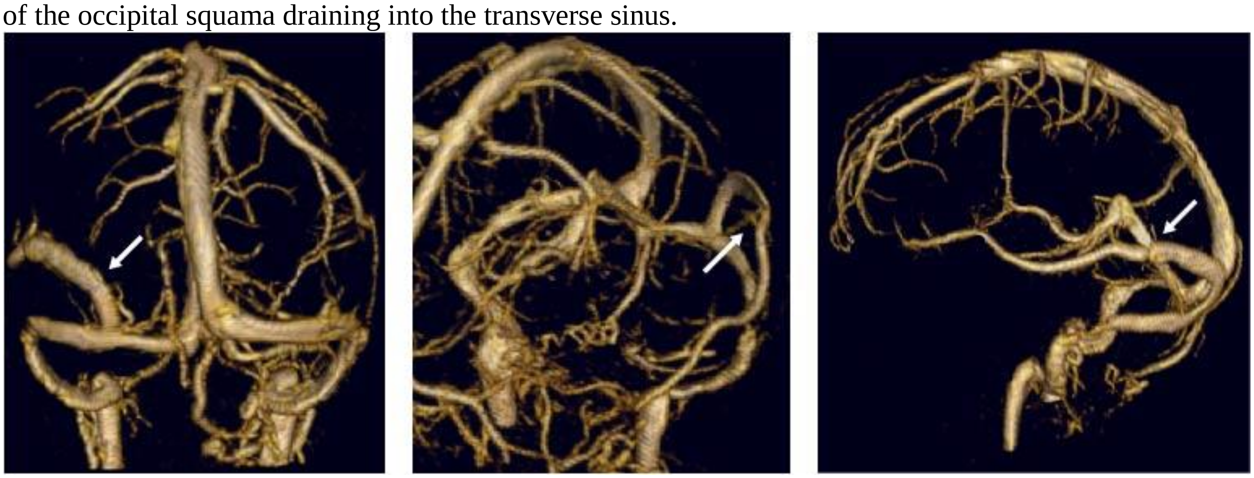

(Filename: TCT_3468_figure1.jpg)

3623

3:02PM - 3:09PM

An Update on Screening for Intracranial Aneurysms in patients with Thoracic Aortic Aneurysms

K Seifert[1], X Wu[2], V Kalra[3], L Tu[4], A Malhotra[5]

[1]*YALE NEW HAVEN HOSPITAL, NEW HAVEN, CT,* [2]*Yale University School of Medicine, New Haven, CT,* [3]*MCRG ORLANDO HEALTH, TAMPA, FL,* [4]*Yale School Of Medicine, New Haven, CT,* [5]*YALE UNIVERSITY SCHOOL OF MEDICINE, NEW CANAAN, CT*

Purpose
A higher incidence of intracranial aneurysms (ICA) has been reported in patients with ascending aortic aneurysms in previous retrospective reviews. The purpose of the current study was to provide an update on prospectively screened patients with ascending aortic aneurysms and the incidence of intracranial aneurysms.
Materials and Methods
Patients over the age of 18 with thoracic aortic aneurysms (TAA) were prospectively screened with CT angiography (CTA) and magnetic resonance angiography (MRA) over a 9-year period between 2009 and 2018. Each aneurysm was detailed according to its location and maximum diameter. Additional patient demographics were obtained, included pertinent comorbidities and smoking use. Follow-up imaging results in patients with ICAs were recorded when available.
Results
A total of 544 patients with TAA were prospectively screened for intracranial aneurysms and included in the study. 31 IAs were identified in 27 of the 544 patients for overall prevalence of 4.9%. The prevalence of IA in patients with ascending TAA was 4.51% and in descending TAA was 9.09%. 20/31 aneurysms were 2 mm in size, 6/31 were 3 mm and 5/31 were 4 mm in size. Hypertension was associated with an increased prevalence of IAs, especially in patients with descending TAAs. None of the patients with IA had rupture during the available follow up.
Conclusions
The prevalence of IAs in patients with thoracic aortic aneurysms may not be as high as previously described in other retrospective studies, and may not be significantly higher than in the general population. Further cost-effectiveness analysis is needed before routine screening for IAs in TAA patients can be justified.

3496

3:09PM - 3:16PM

Arterial Spin Labeling Versus Digital Subtraction Angiography in Differentiating Developmental and Transitional Venous Anomalies in Symptomatic Patients

J Mathieu[1], M Amans[1], M Barkovich[2]
[1]*UCSF, San Francisco, CA,* [2]*UNIVERSITY OF CALIFORNIA-SAN FRANCISCO, SAN FRANCISCO, CA*

Purpose
Developmental venous anomalies (DVAs) are considered benign vascular lesions, representing a normal anatomic variant and an essential parenchymal venous drainage pathway. However, DVAs with hemodynamic changes may lead to cavernoma formation, seizure and parenchymal changes (1, 3). DVAs with early arteriovenous shunting are termed "transitional venous anomalies" (TVAs) and are thought to have an increased risk of hemorrhage and symptomatology. Arterial spin labeling (ASL) abnormalities are uncommon in DVA, and high signal on ASL suggests the presence of a shunting transitional lesion (2, 4). We present a case series of patients presenting with neurological symptoms and ASL abnormalities in or around their DVAs; some had shunting on DSA and others did not.
Materials and Methods
This is a single-center retrospective review of four patients presenting with neurological symptoms and found to have elevated ASL within or around the DVAs. CT, MRI, and DSA were reviewed for anatomic information, location of ASL signal (within DVA vs parenchyma), and early filling on DSA.
Results
Two patients presented with seizures, one with and one without an adjacent cavernoma. Both had

elevated ASL, although the DVA with cavernoma did not shunt on post-operative DSA. Another patient with seizures had a TVA, intraventricular hemorrhage, and an adjacent aneurysm. A patient with vertigo, gait instability, and dementia had elevated ASL (fig1) and proven TVA (fig2), as well as a remote DAVF.
Conclusions
This series highlights the difficulties in identifying TVAs, particularly in symptomatic patients. Interestingly, the one patient with elevated ASL without shunting on DSA was post-operative at the time of DSA. The DVA itself was not manipulated during surgery, yet this introduces a potential confounding factor. This series illustrates the potential limitations of using ASL to diagnose TVAs.

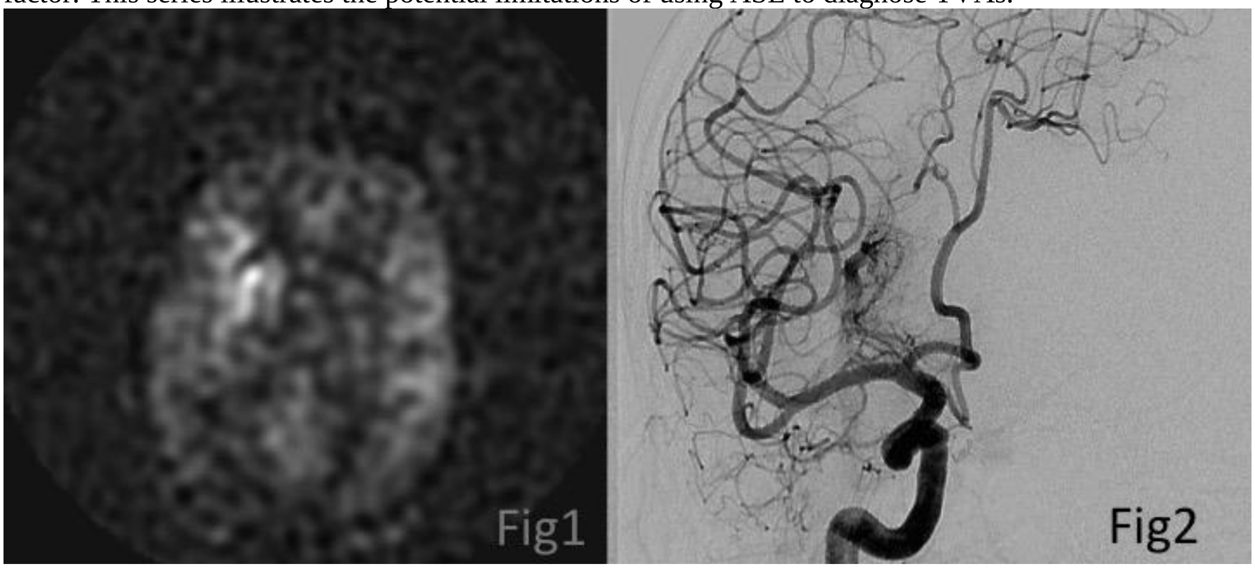

(Filename: TCT_3496_DVAAbstractImagesJPEG.jpg)

3336

3:16PM - 3:23PM

Carotid-Cavernous Fistula: Normal and Pathologic appearance of the Cavernous Sinus on Computed Tomography Angiography.

B Bussey[1], B Zhang[2], H Morales[1]
[1]University of Cincinnati, Cincinnati, OH, [2]Cincinnati Children's Hospital Medical Center, Cincinnati, OH

Purpose
Asymmetric enhancement (AE) of the cavernous sinuses (CS) on CT Angiography (CTA) is used as criteria for a probable Carotid-Cavernous Fistula (CCF), particularly when Hounsfield units (HU) values are near of those in the Internal Carotid Artery (ICA). To our knowledge, no prior work has estimated the normal AE of the cavernous sinus on CTA and the variability that could indicate pathology. We thought to investigate the appearance of the CS in a large sample, focusing on increasing the specificity in the diagnosis of CCF in the setting of trauma.
Materials and Methods
This will be a retrospective study of patients with prior CTA exams. Three groups will be included according to indication and radiology report: no trauma with reported normal findings (n=200), trauma with reported findings other than CCF (n=200), and trauma with reported findings suspicious for a CCF (n=50). Data analysis will include enhancement in HU of the CS, ICA, transverse sinuses (TS), and superior ophthalmic veins (SOV) as well as measuring the thickness of the CS. Subjective assessment of AE of the CS, superior petrosal sinus (SPS) and SOV engorgement will also be made. Confirmation of a CCF with angiogram will be recorded.

Results
Our preliminary analysis in a small sample of 25 patients indicates that there is no significant difference between the AE of the CS (numeric or subjective) in between the three groups. Enhancement of the CS compared with the ICA did not show a significant difference either. In fact, we noticed two cases, one with a confirmed CCF and the other without a confirmed CCF on conventional angiograms that had "arterialized" enhancement of the sinus. We will also analyze the data on the difference between CS enhancement and TS enhancement as a marker for a venous phase contaminating the CTA.
Conclusions
Our work will provide normative data of the appearance of the CS on CTA, focusing on AE. We hypothesized that no difference exists in the AE between groups. We believe that the AE of the CS in trauma patients should not be used as criteria to suggest a CCF. This could prompt an invasive cerebral angiography in an already critically ill patient. Additional variables such as contrast phase (arterial versus venous) or central skull base fractures would likely provide insights about the normal versus pathologic appearance of the CS. Secondary signs such as engorgement of the SOV, might also be helpful. Unfortunately, they might be absent in the acute setting, making the diagnosis of CCF more challenging. An angiogram in a patient with high clinical suspicion for a CCF (including symptoms such as endangering vision), or a follow-up CTA in the arterial phase (with close monitoring of the bolus timing) in doubtful cases, would be reasonable approaches.

2980

3:23PM - 3:30PM

Connecting The Metameres: Facial Venous Malformations and Intracranial Developmental Venous Anomalies

I Mark[1], J Guerin[2], P Morris[3], W Brinjikji[3]
[1]MAYO CLINIC - ROCHESTER, MN, ROCHESTER, MN, [2]CINCINNATI CHILDREN'S HOSP. MED. CTR., CINCINNATI, OH, [3]Mayo Clinic, Rochester, MN

Purpose
A number of studies have demonstrated the existence of segmental vascular disorders affecting soft tissues of the head and neck along with the intracranial vasculature. The purpose of this study was to determine whether there is an association between cerebral developmental venous anomalies and venous malformations of the face, head, and neck.
Materials and Methods
A consecutive series of patients with head and neck venous malformations who underwent MR imaging of the brain with postcontrast T1-weighted imaging were included. Developmental venous anomaly prevalence in this patient population was compared with an age- and sex-matched control group without venous malformations at a ratio of 1:2. All images were interpreted by a neuroradiologist. Data were collected on venous malformation location, developmental venous anomaly location, developmental venous anomaly drainage pattern, and metameric location of venous malformations and developmental venous anomalies. Categoric variables were compared using $\chi 2$ tests.
Results
Forty-two patients with venous malformations were included. The mean age was 41.1 ± 25.1 years, and 54.8% of patients were female. The prevalence of developmental venous anomalies in this patient population was 35.7% (15/42). The control population of 84 patients had a mean age of 40.0 ± 5.9 years, and 78.6% of patients were female. The prevalence of developmental venous anomalies in this patient population was 9.5% ($P = .01$). In 86.7% of cases, developmental venous anomalies were ipsilateral to the venous malformation, and in 66.6% of cases, they involved the same metamere.
Conclusions
Our case-control study demonstrated a significant association between brain developmental venous

anomalies and superficial venous malformations. These findings suggest that there may be a similar pathophysiologic origin for these 2 entities.

3114

3:30PM - 3:37PM

Cost-Effectiveness of CT Angiography in Management of Tiny UIAs

X Wu[1], A Malhotra[2], K Seifert[3], V Kalra[4], D Gandhi[5], P Sanelli[6]
[1]Yale University School of Medicine, New Haven, CT, [2]YALE UNIVERSITY SCHOOL OF MEDICINE, NEW CANAAN, CT, [3]YALE NEW HAVEN HOSPITAL, NEW HAVEN, CT, [4]MCRG ORLANDO HEALTH, TAMPA, FL, [5]University of Maryland School of Medicine, Baltimore, MD, [6]NORTHWELL HEALTH NSUH, MANHASSET, NY

Purpose
To evaluate the cost-effectiveness of CTA for surveillance of tiny unruptured intracranial aneurysms (UIAs) and the impact of CTA radiation induced brain tumor on the overall utility of CTA
Materials and Methods
A Markov decision model was constructed from a societal perspective starting with patients 30, 40 or 50-year-old, with incidental detections of UIA ≤ 3 mm and no prior history of subarachnoid hemorrhage. Five different management strategies were assessed- annual CTA surveillance, biennial CTA, CTA follow-up every 5 years, coiling and follow-up and, no preventive treatment or routine follow-upannual follow-up for the first 2 years and follow-up every 5 years subsequently. Probabilistic, one-way, and two-way sensitivity analyses were performed.
Results
The base case calculation shows follow-up every 5 years to be the most cost-effective strategy in all 3 age groups. Follow-up every 5 years remains the dominant strategy when the annual growth risk is varied from 0-30%, the rupture risk of growing aneurysms is <55.3%, and rupture risk of nongrowing aneurysms is <2.61%. The radiation-induced brain cancer risk is relatively low and sensitivity analysis shows that the radiation-induced cancer risk has mininal influence on the conclusions.
Conclusions
Given the current literature, no preventive treatment or routine surveillancevery 5 year follow-upe imaging follow-up is the cost- effective strategy in patients with aneurysms ≤ 3 mm, resulting in better health outcomes and lower healthcare spending. Patients with aneurysms at high risk of rupture might need more aggressive management.

	30 years of age at aneurysms discovery		40 years of age at aneurysms discovery		50 years of age at aneurysms discovery	
	Cost	Effectiveness (QALY)	Cost	Effectiveness (QALY)	Cost	Effectiveness (QALY)
Annual followed by every 5 year	$80,587	20.62	$66,960	19.88	$52,532	18.29
Annual CTA follow-up	$115,896	23.66	$94,161	21.52	$70,689	18.66
Biennial CTA follow-up	$68,362	23.64	$75,522	21.16	$55,004	18.36
CTA every 5 years*	$91,639	24.20	$75,814	22.65	$59,526	20.71
Coiling	$226,526	22.11	$200,012	19.98	$169,123	17.24

(Filename: TCT_3114_Table2.jpg)

3494

3:37PM - 3:44PM

Ganglionic Eminence Abnormalities in Fetal Hydrocephalus

G Kasprian[1], G Dovjak[1], M Cardoso Diogo[1], D Prayer[1]
[1]*Medical University of Vienna, Vienna, Austria*

Purpose
Recent neuropathology studies have reported abnormal neuronal migration in the setting of fetal hydrocephalus. This study aims to assess the ganglionic eminence (GE) to detect migrational alterations of this specific brain compartment in fetuses with conditions complicated by abnormal cerebrospinal fluid circulation using the technique of fetal MRI.
Materials and Methods
This retrospective observational single center 1.5 Tesla MR study included 72 cases with normal brain imaging findings, 64 fetal myelomeningocele/Chiari II cases and 71 aqueductal stenosis (AS) cases imaged between 18 and 34 gestational weeks (GW). T2-w fetal MRI sequences were reviewed and the following features were assessed: -morphology of the GE, - width of the internal and external CSF spaces. The frequency of GE abnormalities was documented. In 12 cases (6 chiari II and 6 AS) postmortem MRI was available.
Results
Up to 25 GW, the appearance of the normal ganglionic eminence was rated as "large" in 39/42 cases (92.5%) and "moderate" in 3/42 cases (7.5%). Between 26 and 31GW, the ganglionic eminence was rated as large in 0/24 (0%), "moderate" in 6/24 (25%) and minimal in 18/24 cases (75%). In 6/12 (50%) of post mortem cases finger like structures radiating from the ganglionic eminence could be identified. In 0/72 fetuses this change could be seen. "Ganglionic eminence fingers" were found in vivo in 22/64 (34.4%) of Chiari II cases and in 18/71 (25.4%) of AS cases. No statistically significant difference of the presence of ganglionic eminence fingers in dependency of ventricular size (p=.266 Chiari 2 and p=.323 AS) or insular width (p=.621 Chiari 2 and p=.181 acqueductal stenosis) was detected.
Conclusions
Abnormalities of the ganglionic eminence can be frequently detected by in vivo and post mortem MRI in cases of acqueductal stenosis and chiari II. These changes may indicate early migrational abnormalities linked to ependymal pathologies in fetal hydrocephalus.

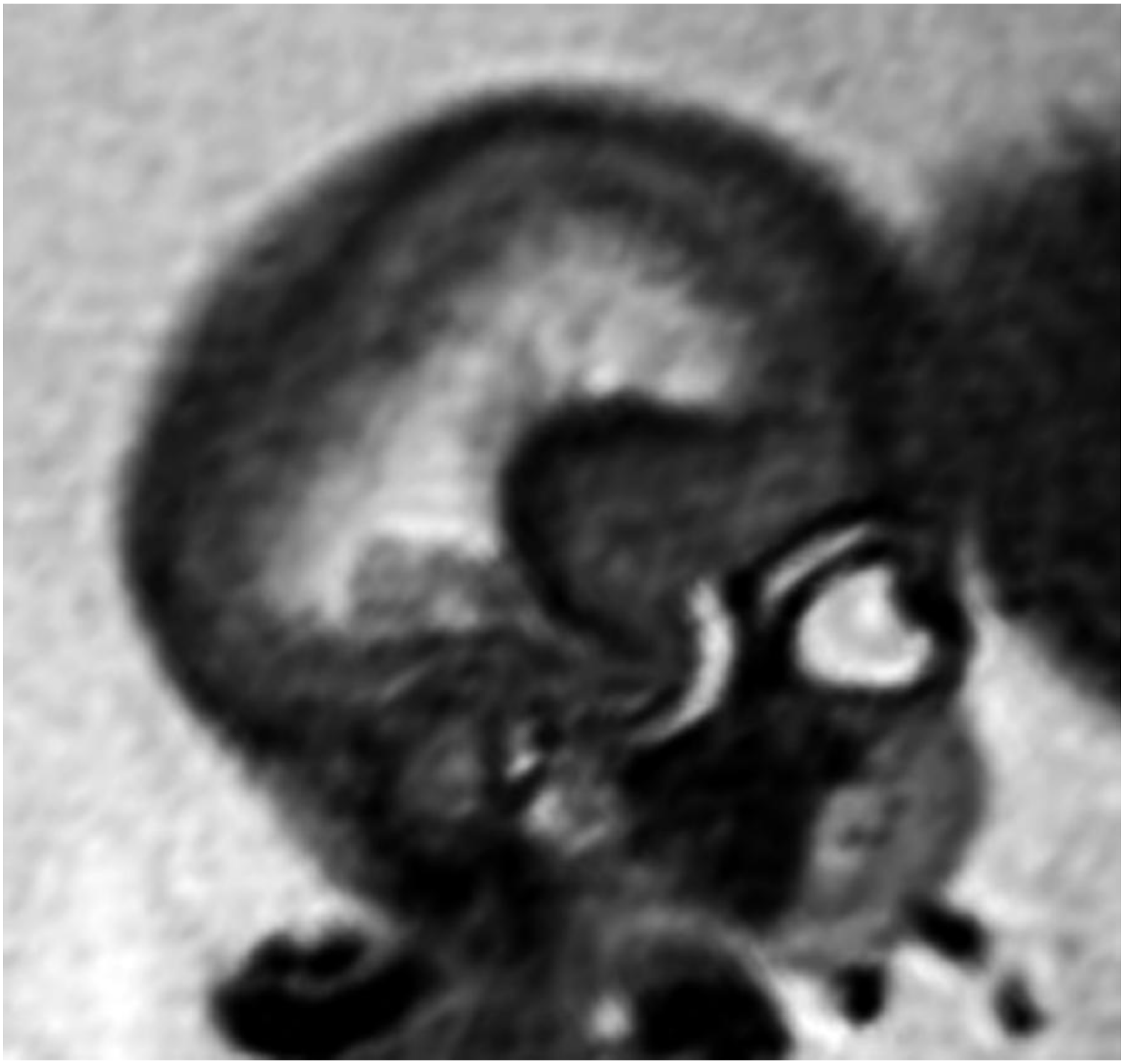
(Filename: TCT_3494_Figure1.jpg)

2459

3:44PM - 3:51PM

MR Characteristics of Unruptured Intracranial AVMs Associated with Seizure As Initial Clinical Presentation

J Benson[1], S Chiu[1], K Flemming[1], D Nasr[1], G Lanzino[1], W Brinjikji[1]
[1]*Mayo Clinic, Rochester, MN*

Purpose
Patients with intracranial AVMs are at increased risk for epileptic seizures. The aim of this study was to assess if MR imaging characteristics of unruptured intracranial AVMs are predictive of presentation with seizure.
Materials and Methods
A retrospective review was completed of all patients found to have an unruptured intracranial AVM on

MRI at our institution between 1/1/2000 and 12/31/2016. A blinded reviewer assessed the architectural characteristics of AVMs and surrounding parenchyma; findings were statistically analyzed for correlation with epilepsy.

Results

Of 165 included patients, 89 were female (53.9%). 57/165 (34.5%) patients were imaged as part of a work up for seizures. Of 27 assessed AVM MRI characteristics, 9 were found to be positively or negatively correlated with seizures. Patients imaged as part of a workup for seizures more commonly had peri-AVM edema (36.8%, compared to 11.1% of other patients, $p<0.0001$), peri-AVM T2* (27.3% versus 8.0%, $p=0.028$), a venous pouch/varix (61.4% versus 31.5%, $p=0.0003$), long draining vein (91.2% versus 55.6%, $p<0.0001$), and larger size based on Spetzler-Martin grade categorization ($p=0.006$). By location, AVMs located in the frontal lobe, motor cortex, and sensory cortex were associated with seizures ($p=0.004$, $p=0.001$, and $p=0.006$, respectively).

Conclusions

Certain MR imaging characteristics of unruptured intracranial AVMs are associated with seizures. Such correlations may assist in identifying the pathophysiological mechanisms by which AVMs cause seizures.

	Seizure presentation	Other presentation	P value
Patient characteristics		-	
Gender (% Female)	47.4%	57.4%	0.252
Average age	35.9	42.5	**0.011**
AVM characteristics		-	
Gliosis	66.7%	58.3%	0.318
Peri-AVM edema	36.8%	11.1%	**<0.0001**
Venous pouch/varix	61.4%	31.5%	**0.0003**
Thrombosed venous pouch	7.0%	1.9%	0.183
Long draining vein (>3 cm)	91.2%	55.6%	**<0.0001**
*Peri-AVM T2**	27.3%	8.0%	**0.029**
Feeding artery aneurysm	15.8%	14.4%	0.820
Intranidal aneurysm	5.3%	4.8%	1.000
Spetzler-Martin		-	
Deep venous drainage	35.1%	46.2%	0.186
Involvement eloquent cortex	73.2%	57.7%	0.060
Size:			**0.006**
<3 cm	45.6%	71.2%	
3-6 cm	43.9%	24.0%	
>6 cm	10.5%	4.8%	
SM grade			0.170
1	17.9%	24.0%	
2	26.8%	36.5%	
3	35.7%	24.0%	
4	8.9%	11.5%	
5	10.7%	3.9%	
SM grade 3+	53.6%	38.5%	0.094

(Filename: TCT_2459_ASNRtablefigure.jpg)

2192

3:51PM - 3:58PM

Quantification of Hemodynamics of Cerebral Arteriovenous Malformations after Stereotactic Radiosurgery using 4D Flow MRI

S Srinivas[1], T Retson[1], A Simon[1], J Handwerker[1], A Hsiao[1], J Hattangadi-Gluth[1], N Farid[1]

[1]*University of California, San Diego, La Jolla, CA*

Purpose

For cerebral arteriovenous malformations (AVM) not amenable to complete surgical resection, stereotactic radiosurgery (SRS) is often used as a primary or adjunctive treatment modality. SRS causes fibrointimal damage of the endothelium of the arteries supplying the AVM, eventually leading to nidus obliteration (1). However, complete obliteration can take 3 years or longer to be visualized on structural MRI and MRA. This study utilizes 4D flow imaging to quantify early hemodynamic changes following treatment of AVMs with SRS.

Materials and Methods

This was a retrospective, observational study with serial measurements performed before and after SRS using a 3T GE Discovery 750 MRI scanner. A total of 6 patients were included with both pre-SRS and post-SRS imaging, with the post-SRS imaging obtained at 4-9 months after SRS. 4D flow MRI was performed with velocity encoding of 150-200 cm/s. Specifically, flow was measured for the dominant feeding artery, the draining vein, and the corresponding contralateral artery as a control. Differences in flow between the feeding artery and the contralateral control artery were assessed both before and after SRS using a 2 tailed paired t-test. Additionally, differences in flow and circumference of the feeding artery and draining vein before and after SRS were assessed using a 2 tailed paired t-test.

Results

Before SRS, arterial flow (L/min) was higher in the AVM primary feeding artery (mean: 0.393, sd: 0.230) than in the contralateral arterial control (mean: 0.080, sd: 0.018) ($p = .024$, $df = 5$) (Fig. 1). After SRS, the flow differential between the feeding artery (mean: 0.223, sd: 0.168) and the control artery (mean: 0.093, sd: 0.025) was much less pronounced (Fig. 1). Arterial flow decreased in the feeding artery after SRS (mean: 0.223, sd: 0.168) compared to before (mean: 0.393, sd: 0.230) ($p = 0.040$, $df = 5$). Circumference of the feeding artery, however, did not significantly decrease after SRS (mean: 14.160, sd: 6.117) compared to before (mean: 17.212, sd: 3.770) ($p=0.176$, $df = 5$). Similarly, flow decreased in the draining vein after SRS (mean: 0.105, sd: 0.110) compared to before (mean: 0.205, sd: 0.151) ($p = 0.019$, $df = 5$) (Fig. 2). Circumference of the draining vein, however, did not significantly decrease after SRS (mean: 13.817, sd: 8.452) compared to before (mean: 19.345, sd: 7.882) ($p = 0.107$, $df = 5$). Figure 3 and Figure 4 depict time-of-flight MRA and 4D flow MRI images respectively for a patient with an AVM before and after SRS.

Conclusions

We demonstrate hemodynamic changes measurable by 4D flow within 4-9 months following SRS. Specifically, 4D flow showed a reduction of flow within the AVM primary feeding artery as well as reduction of flow within the draining vein. Interestingly, the circumference of the feeding artery and draining vein did not change significantly within 4-9 months after SRS, confirming that hemodynamic changes occur prior to visible structural changes within the vessels of the AVM. Therefore, 4D flow has the potential to serve as an early biomarker of treatment response in AVM's following SRS and may serve as an adjunct to routine MRI/MRA.

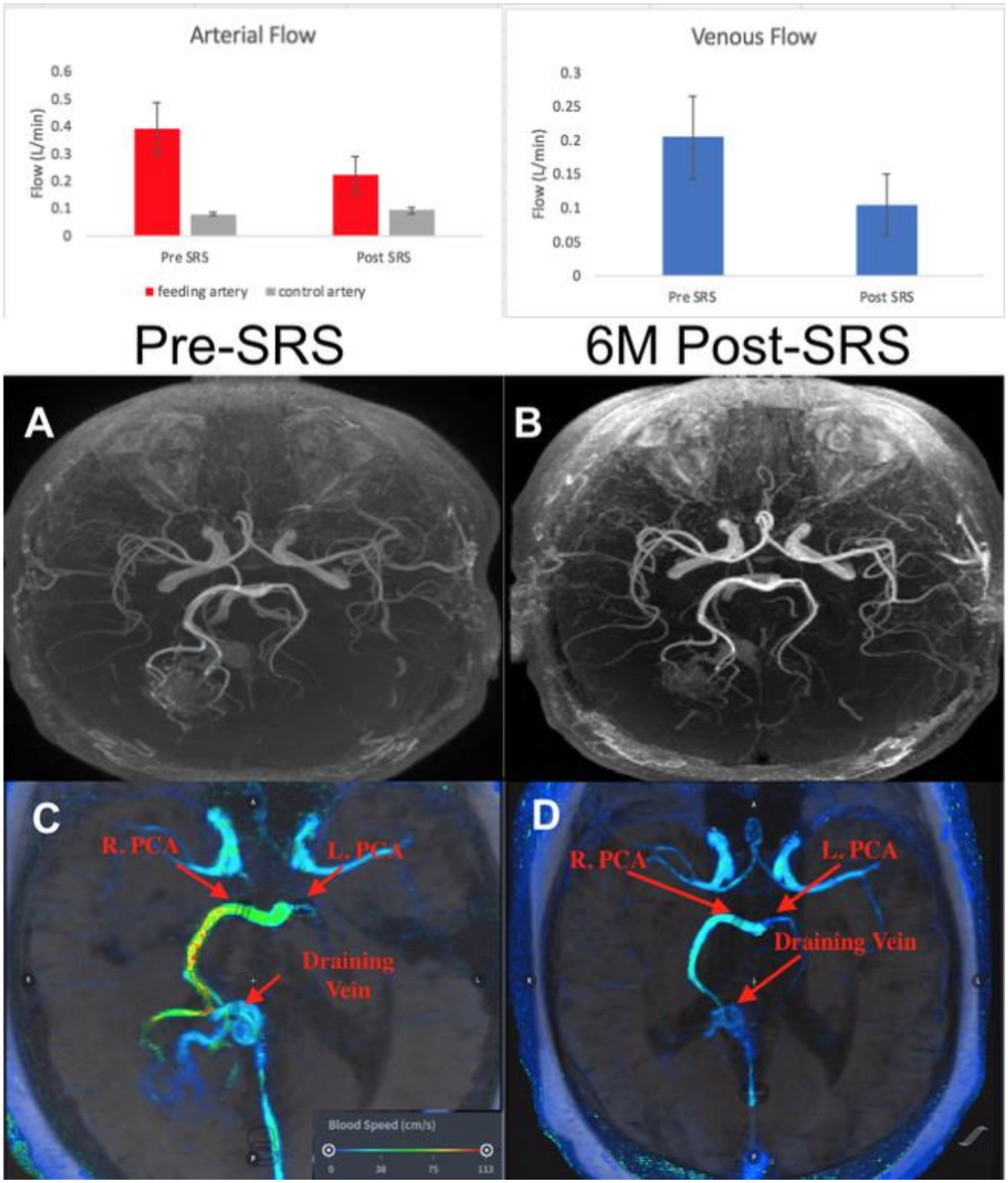

(Filename: TCT_2192_ASNR_Figure_Final.jpg)

3110

3:58PM - 4:05PM

Risk of Radiation-Induced Cancer from CT Angiography Use in Imaging Surveillance for Unruptured Cerebral Aneurysms

X Wu[1], A Malhotra[2], K Seifert[3], P Sanelli[4], D Gandhi[5]
[1]Yale University School of Medicine, New Haven, CT, [2]YALE UNIVERSITY SCHOOL OF MEDICINE, NEW CANAAN, CT, [3]YALE NEW HAVEN HOSPITAL, NEW HAVEN, CT, [4]NORTHWELL HEALTH NSUH, MANHASSET, NY, [5]University of Maryland School of Medicine, Baltimore, MD

Purpose
Although CTA is an excellent, non-invasive imaging modality for surveillance of intracranial aneurysms, radiation concerns have been cited to restrict its use in surveillance imaging. The goal of this study was to estimate distributions of radiation-induced CNS cancer incidence from CTA surveillance for intracranial aneurysms, and the impact of frequency and duration of surveillance imaging using follow-up CTAs.
Materials and Methods
Simulation-modeling approach was performed using data on CT angiography associated radiation risk. We used the RadRAT risk assessment tool, based on the data using the BEIR VII report. Each CTA was assigned as a separate exposure event. Men and women respectively starting surveillance imaging at 30, 40 and 50 years and receiving annual CTAs were considered as separate sub-groups. As a comparison, we also calculated the radiation-induced cancer risk in the same groups of patients but receiving CTAs every 2 and 5 years respectively.
Results
CTA-associated excess cancer risk per exposure increases relatively more rapidly with the first 10 exposures and plateaus after the 44th exposure. On average, per CTA incurs approximately 0.0026% in excess lifetime cancer risk. Receiving CTA follow-up at a younger age, more frequent follow-up, longer surveillance period, and male gender are the major factors contributing to an elevated excess lifetime risk. In the highest risk group, male patient receiving annual CTA follow-ups from age 30, the excess lifetime risk is 0.115% at age 81.
Conclusions
Radiation-induced brain cancer incidence associated with UIA surveillance strategies using CTA is very low relative to the risk for aneurysmal rupture. Further cost-effectiveness/utility analyses might help assess this risk in the context of aneurysmal ruptures prevented by surveillance imaging.

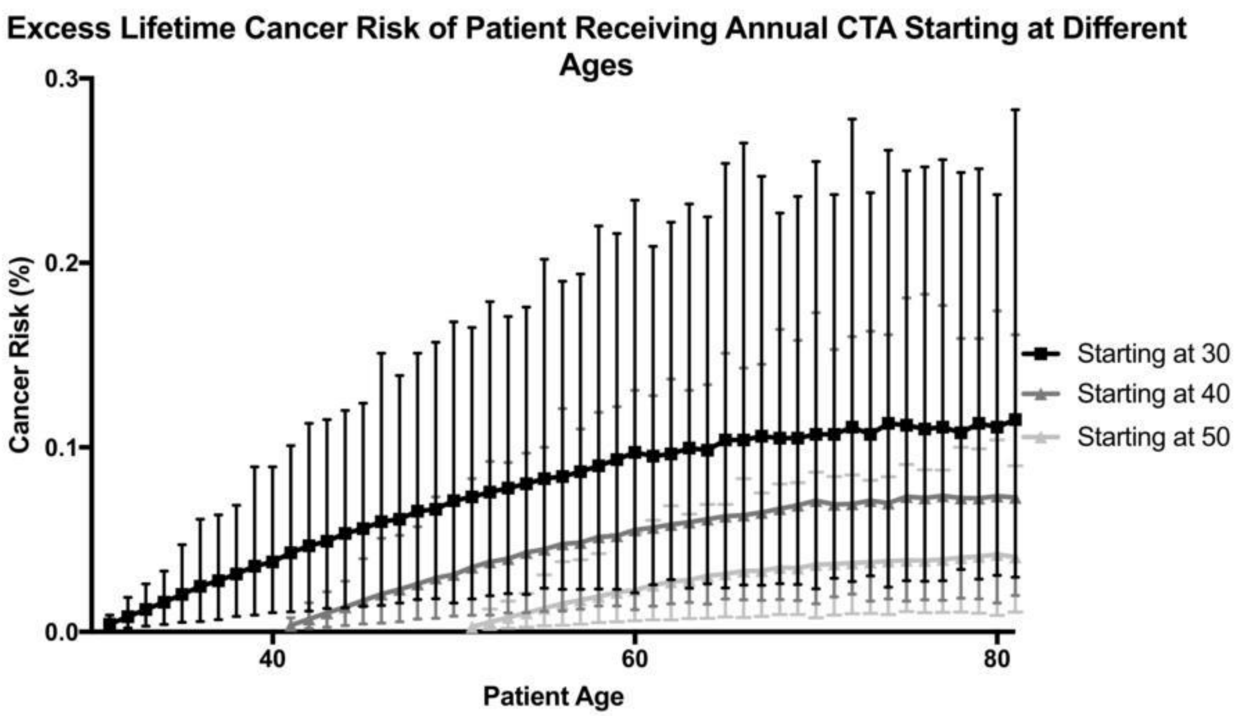

(Filename: TCT_3110_Final_figure4.jpg)

2796

4:05PM - 4:12PM

Seeing an Opening: Features of Vertebral Artery Fenestration

A D'Sa[1], M Alvin[2], R Brody[1], S Javed[1], S Faro[1], R Nadgir[2]
[1]Johns Hopkins School of Medicine, Baltimore, MD, [2]Johns Hopkins Hospital, Baltimore, MD

Purpose
Vertebral artery fenestration (VAF) is a rare congenital vascular anomaly which has been associated with intracranial aneurysm. VAF has similar imaging appearance to vertebral artery dissection (VAD), which can confound diagnosis of the latter on CT and MR angiography. The purpose of this investigation is to assess which imaging features of VAF are distinct from VAD.
Materials and Methods
Using keyword search on CTA and MRA head and neck imaging reports performed from 2010-2017, cases of VAD and VAF were identified and imaging was re-reviewed. Imaging features including laterality, cervical level, length of affected segments, presence, number and caliber of lumens, and presence of other vascular abnormalities were recorded for all cases.
Results
Of 64,888 studies reviewed, VAF was identified in 67 (0.1%) and VAD in 54 (0.1%) Compared with VADs, VAFs were found to have shorter segments ($p<0.001$), were more likely to occur in the V3/V4 segments ($p<0.001$), less likely to present post-trauma ($p<0.001$), and more likely to have two distinct lumens rather than one ($p<0.001$). 9% of those with VAF also had an intracranial aneurysm.
Conclusions
Vertebral artery fenestrations, although rare, can be distinguished from dissections on angiographic imaging. Diagnosis should prompt review for intracranial aneurysm.

2466

4:12PM - 4:19PM

Utility of Routine Brain MRI Sequences in Differentiating Transverse Dural Sinus Hypoplasia from Thrombosis on Non-contrast MRV

A Kuhn[1], N Porbandarwala[1], R Bhadelia[1], R Rojas[1], Y Chang[1]
[1]Beth Israel Deaconess Medical Center, Boston, MA

Purpose
Differentiating hypoplasia of a Transverse Dural Sinus (TDS) from Transverse Sinus Thrombosis (TST) can be a diagnostic conundrum on non-contrast MRV (NC-MRV). Therefore, routine use of contrast enhanced MRV or 3D-T1 GRE sequences has been recommended. However, gadolinium may be contraindicated in many patients, requiring an alternative strategy. Our purpose was to determine whether non-contrast brain MRI sequences can help differentiate hypoplasia from TST on NC-MRV.
Materials and Methods
A retrospective review was made from 2014-2017 for NC-MRV (phase-contrast MRV with VENC 30 cm/s) studies with additional spin-echo (sagittal T1, axial T2, FLAIR), GRE and post-contrast MPRAGE performed within 24 hours of the NC-MRV. MPRAGE served as the reference gold standard for the presence of TST, characterized by a central filling defect. NC-MRV signal in the TDS was categorized as normal or abnormal (> 50% non-visualization of the TDS). TDS spin-echo signal was categorized as hypo/isointense or hyperintense relative to the brain parenchyma and GRE for presence of T2* artifact. Sensitivity and specificity of T1, T2/FLAIR and T2* signal abnormality for the detection of TST was calculated.

Results
Of 182 NC-MRVs, 134 (73.6%) had normal and 48 (26.4%) had abnormal signal. 0/134 normal NC-MRV demonstrated TST. 9/48 abnormal NC-MRV showed thrombus on MPRAGE. 1/39 abnormal NC-MRVs without TST (hypoplastic TDS) showed T2/FLAIR hyperintensity but without T1 hyperintensity or T2* abnormality. A combination of T2/FLAIR and T1 hyperintensity or T2* artifact was 78% sensitive and 100% specific for TST in abnormal NC-MRV. A combination of only T2/FLAIR high-signal or T2* artifact was 100% sensitive and 97% specific.
Conclusions
Our results show that routine brain MRI sequences can help differentiate hypoplasia from TST on NC-MRV in most cases, limiting the use of gadolinium to a selected few patients.

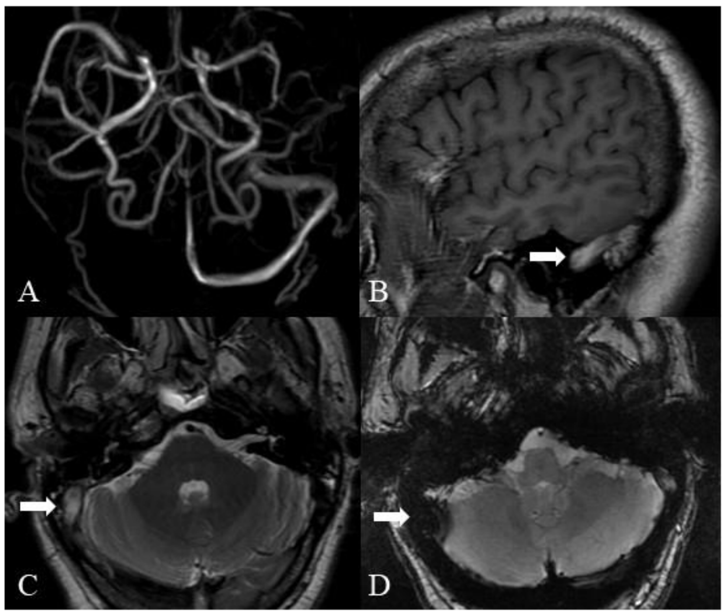

Transverse Dural Sinus Thrombosis: A) Phase Contrast MRV demonstrating non-visualization of the right TS confirmed to be thrombosis on post contrast MPRAGE (not shown). There is corresponding hyperintense signal of the right TS on T1 (B) and T2 (C) as well T2* artifact on GRE (D).

(Filename: TCT_2466_Slide1.JPG)

2506

4:19PM - 4:25PM

Wall Shear Stress Patterns and Flow Morphology for Risk Stratification of Intracranial Aneurysms Assessed using High Resolution 4D Flow MRA

W Chang[1], C Li[1], M Goldberg[1], J Villablanca[2]
[1]Allegheny Health Network, Pittsburgh, PA, [2]UCLA, Los Angeles, CA

Purpose
Intracranial aneurysms have high prevalence (~3%) and carry high mortality (~50%) and neurologic morbidity (~75%) with rupture. The PHASES study found that 5 year rupture risk varies greatly (0.4-

>20%). Treatment of aneurysms carries 2-10% mortality and 5-20% neurologic morbidity. Therefore, risk stratification of aneurysms has high clinical utility. 4D Flow MRA can analyze flow morphology and wall shear stress (WSS) hemodynamics, as long as there is adequate spatial resolution. Helical flow patterns are associated with relative stability, while inflow-jet morphology and focally elevated impact zone WSS are associated with increased risk of aneurysm growth/rupture. In this study, we examine flow patterns and WSS with 4D Flow at 0.5 mm isotropic spatial resolution.

Materials and Methods

Informed consent was obtained from patients for acquisition of experimental sequences. Studies were performed under the supervision of the local IRB. Six patients with seven aneurysms were scanned on a Siemens Prisma 3.0T MRI scanner using 4D Flow MRA at 0.5 mm isotropic spatial resolution. VENC was 80 cm/s. Scan time was 12 minutes. Images were reconstructed using a custom MATLAB environment and custom mesh was created to acquire 3D WSS maps and streamline plots.

Results

Two aneurysms demonstrated inflow jet patterns with focally elevated WSS at the impact zone (4.50 and 5.49 N/m2). In contrast, the other aneurysms demonstrated helical flow patterns with normal WSS within the aneurysm dome (0.68 to 1.46, mean 1.01 N/m2). The difference in WSS was statistically significant ($p < 0.0001$).

Conclusions

4D Flow MRA was used to evaluate flow and hemodynamic patterns in six patients with seven aneurysms. Two aneurysms demonstrated inflow jet morphology with significantly higher WSS ($p < 0.0001$), suggesting increased risk of aneurysm growth/rupture compared to five aneurysms with helical flow patterns and normal WSS within the aneurysm dome, suggesting stability. Flow patterns and WSS analysis may assist in risk stratification of aneurysms and help guide treatment planning.

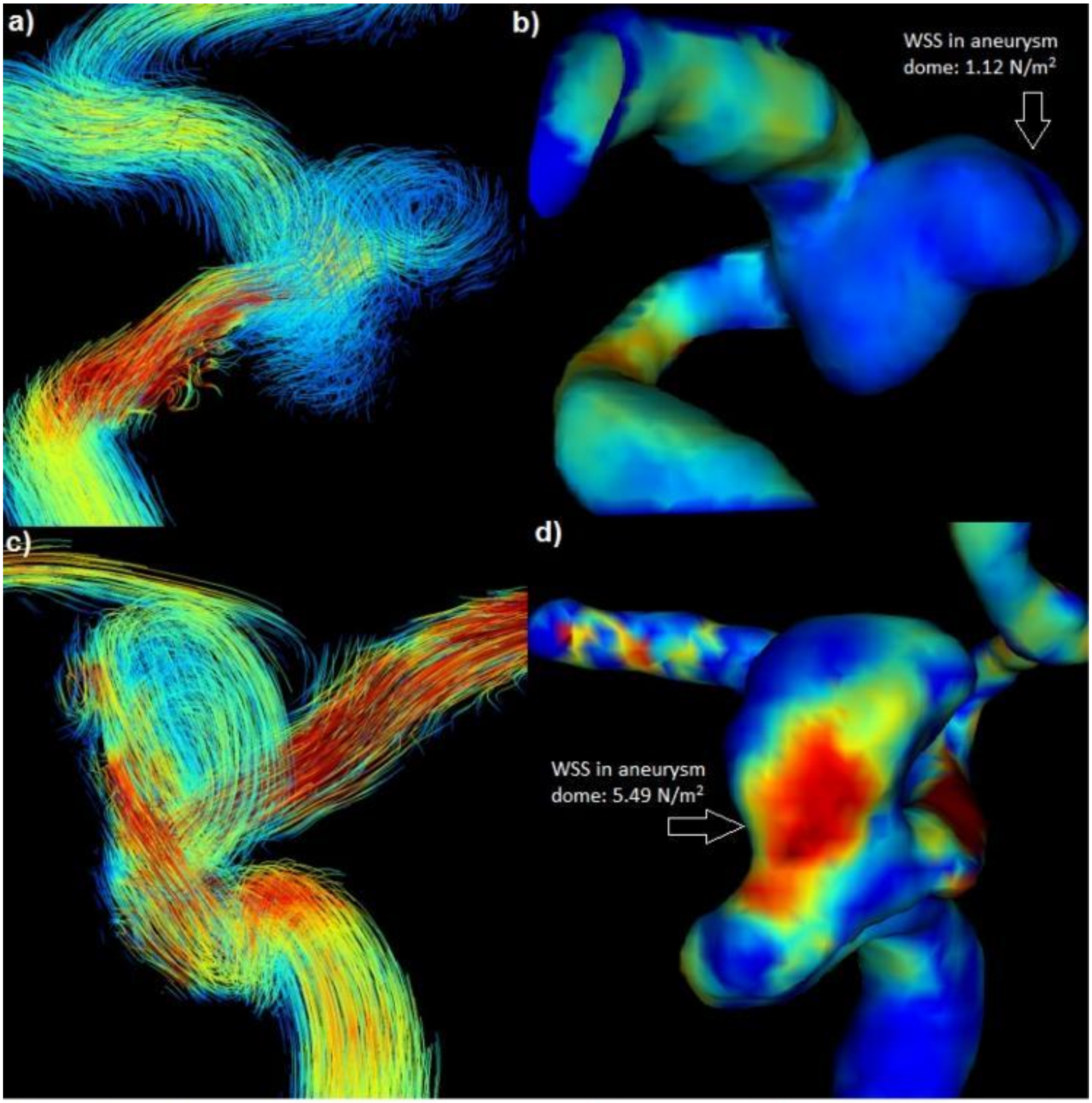

Figure 1: a) Streamline map of an aneurysm demonstrating helical flow pattern in the aneurysm dome. **b)** WSS map of the same aneurysm with normal WSS within the dome. These findings are associated with relative stability. **c)** Streamline map of an aneurysm demonstrating an inflow jet contacting the aneurysm dome. **d)** WSS map of the same aneurysm showing focally elevated WSS at the impact zone. These findings are associated with increased risk of growth and rupture.

(Filename: TCT_2506_4dflow.jpg)

3651

4:30PM - 4:37PM

A 3D Printed Apparatus of the Ventricular and Cisternal System: Color-Coded Using Light Sources

R Javan[1], C Fleming[2], P Shahid[2], N Mostaghni[3], F Huda[4], T Arusoo[1]
[1]George Washington University Hospital, Washington, DC, [2]George Washington University School of Medicine and Health Sciences, Washington, DC, [3]University of California, Irvine, Irvine, CA, [4]The George Washington University Hospital, Washington, DC

Purpose
One of the difficulties with using three-dimensional (3D) printed models for teaching purposes is the limitation of labeling and color-coding. Full color 3D printing is limited to a material that is somewhat fragile and has many design limitations (Z-corp technology). PolyJet technology is expensive, has certain design limitations, and there is a limit of usually 3 or at the most 6 colors. An alternative method for color-coding subcomponents of a 3D printed model may be through using light sources. We showcase this possibility in the ventricular and cisternal system as a part of neuroanatomy where this is possible.
Materials and Methods
Initially DICOM images of a FIESTA MRI of the whole brain was used in Materialise InPrint 3.0 where segmentation of the lateral and third ventricles as well as the foramina of Monro was performed. Additionally FIESTA MRI of the region of the internal auditory canals was used to segment the cerebral aqueduct, fourth ventricle, and foramina of Luschka and Magendi, as well as the cisternal system. This task was performed with the use of the 'Threshold' and 'Split' tools with eventual manual correction and addition in some areas where artifact was present. The 'Hollow Outward' function was subsequently used with 2.5 mm thickness to create a number of stereolithography (STL) files. The 3D models were then imported into Autodesk 3D studio Max, where necessary design modifications were made, such as creating attachment and support structures. The STL files were then sent for 3D printing through an online service with polyamide material. The resulting physical models were then assembled and wired from inside with Light-Emitting Diode (LED) strips measuring 3 x 30 mm were embedded into designated sites and glued to their appropriate undersurfaces of the model.
Results
A lightweight hollow 3D model of the ventricular and cisternal system was created with dedicated sites for placement of LED strips from inside with the ability to show up to 12 different colors. The thin polyamide material constituting the walls of the model is thin enough to allow passage of some colored light while remaining durable. The ideal condition to use the model is in dim lighting conditions.
Conclusions
The main use of this model is for teaching purposes. It highlights the potential for utilizing light sources as a labeling and identification technique for complex 3D anatomic models. Other examples may include the brain surface anatomy, liver segmental anatomy, circle of Willis branch anatomy, the pterygopalatine fossa with its surrounding connections. If connected to an electronic controller, possibly even with voice command, this technique may present an effective interactive method for more extensive and expansive color-coding of customized 3D printed anatomic models.

3102

4:37PM - 4:44PM

Brain Extraction Method for Multi-Institutional FLAIR MRI

J DiGregorio[1], G Arezza[1], A Moody[2], A Khademi[1]

[1]*Ryerson University, Toronto, ON - Ontario,* [2]*University of Toronto, Toronto, ON - Ontario*

Purpose

Fluid Attenuation Inversion Recovery (FLAIR)-weighted MRI is gaining momentum for neurodegenerative disease detection and analysis. FLAIR MRI are advantageous over T1- and T2-weighted MRI because the CSF signal is nulled, which allows white matter lesions (WML) to be better visualized. Unfortunately, manual analysis of medical images is subjective and inefficient, which ultimately effects diagnostic accuracy and the ability to conduct large research studies. Image analysis and machine learning techniques offer a better alternative since they automatically measure image properties in a quantitative and reproducible manner. Although FLAIR MRI have many advantages, only few algorithms exist, and novel methods are much needed. Critical to the automated analysis of neurological FLAIR MRI is a step known as brain extraction (BE). BE removes non-brain tissue from the images (i.e. skull, eyes) and can be used to measure brain volumes. BE is also a critical pre-processing technique for many downstream processes such as WML or ventricle segmentation. Many BE tools exist for T1- and T2 MRI [1]. These methods may not be adequate for FLAIR MRI due to differences in contrast and the presence of WML. Few works have been developed to specifically handle BE for FLAIR [2]; but these works have been designed for small datasets from a single centre. To enable large-scale research studies, BE tools must be developed and validated on multicentre data. Multicentre data poses challenges for automated approaches since differences in scanning equipment and parameters creates variation in intensities, noise and contrast – even for the same patient. In this work, we apply a standardization methodology to correct for intensity variation and then apply thresholding and morphological processes for automated BE in multicentre FLAIR MRI. It is validated on 150 subjects (~7000 images) from 30 international centres representing one of the largest FLAIR MRI datasets used for BE validation.

Materials and Methods

An existing FLAIR MRI standardization method that has been validated on >350,000 images from 60 imaging centres is used to correct for multicentre variability [3]. Figure 1 shows the intensity histograms before and after standardization. Before standardization, there is wide variability in the intensities. After standardization, there is alignment of tissue intensities across the multicentre datasets for all patients. Since there is a consistent intensity interval for tissues, a constant threshold is applied for all patients to isolate the brain. Morphological processing is applied to tidy up the segmentation result, which consisted of dilation, erosion, hole filling and connectivity analysis. The result is a 3D binary mask that corresponds to the detected brain tissue for each patient. The dice similarity coefficient (DSC) and extra fraction (EF) which measures segmentation overlap and false positives, respectively, is computed between automated BE and expert generated manual segmentations. The BE scheme was tested on two multi-institutional FLAIR MRI datasets from the Canadian Atherosclerosis Imaging Network (CAIN) [4] and the Alzheimer's Disease Neuroimaging Initiative (ADNI) [5]. In CAIN, TR is between 8000-11000ms, TE 117-150ms, TI 2200-2800ms, pixel spacing .4266-1mm and slice thickness 3mm. In ADNI, TR is between 650-11900ms, TE 90-193ms, TI 2000-2800ms, pixel spacing .7813-1.01mm and slice thickness 5mm. The scanner vendors are GE, Siemens and Philips. To generate validation data, 129 CAIN volumes (~6000 images) from 9 centres and 21 ADNI volumes (~700 images) from 21 centres were randomly sampled to get equal representation across centres, and in the case of ADNI, across disease classifications as well. Each of these volumes have manual ground truth generated by an expert rater for validation purposes. These datasets are an excellent representation of a multicentre dataset and represent one of the largest FLAIR MRI datasets used for BE validation.

Results

Figure 2 shows sample brain extractions for CAIN and ADNI volumes. These visually demonstrate a close agreement between automated and manual segmentations despite the presence of WML or diverse tissue compositions that reside in upper and lower slices. Figure 3 shows the DSC and EF across all the volumes. The average DSC is 88% +/- 6, and average EF is 9% +/- 7, indicating high overlap and a low number of false positives. Many of the observable false positives resided in the region between the brain and skull where the intensity range corresponding to brain tissue begins to taper off. To test the algorithm's robustness to multicentre effects, Figure 4 shows DSC and EF as a function of scanner vendor. This shows the proposed methodology performing consistently regardless of the scanner vendor. Typically, scanner vendors use different reconstruction algorithms and vary in their imaging parameters for FLAIR MRI, which can create large variabilities in the intensity scale. This would traditionally create difficulties in automated approaches, since algorithms have trouble generalizing to wide, unpredictable variabilities in intensities. In large multicentre, retrospective studies, this becomes especially important. Therefore, intensity standardization followed by a robust threshold holds promise for automated brain extraction techniques for multicentre FLAIR MRI. No complex models or training data is required; which allows these algorithms to be run real-time in a clinical environment. These tools also enable large volumetric research studies that examine total brain volume as a function of clinical variables. This BE scheme can also be used as a preprocessing tool to permit for robust WML segmentation in multicentre datasets, allowing insights to be gleaned about neurodegenerative and vascular diseases. In the future, we will investigate the use of spatial context and unsupervised machine learning models to further improve performance of the proposed BE method.

Conclusions

FLAIR MRI are routinely collected for the examination of neurodegenerative diseases, and are being used increasingly for research into ischemic, vascular and dementia diseases. Therefore, the design and development of automated tools for FLAIR MRI would have large clinical value for the diagnosis and treatment of neurodegenerative diseases. However, intra-modality intensity non-standardness makes the development of multi-institutional segmentation algorithms difficult. This work highlights that intensity standardization is a powerful preprocessing tool for overcoming this obstacle. By pairing standardization with simple image processing techniques, it was possible to replicate expert generated brain extractions to a high degree in real-time. The extracted brain images can be used to compute features such as brain volume which serve as useful biomarkers for monitoring neurological disease progression and can be paired with metadata parameters such as patient age and sex and other clinical variables related to cognition.

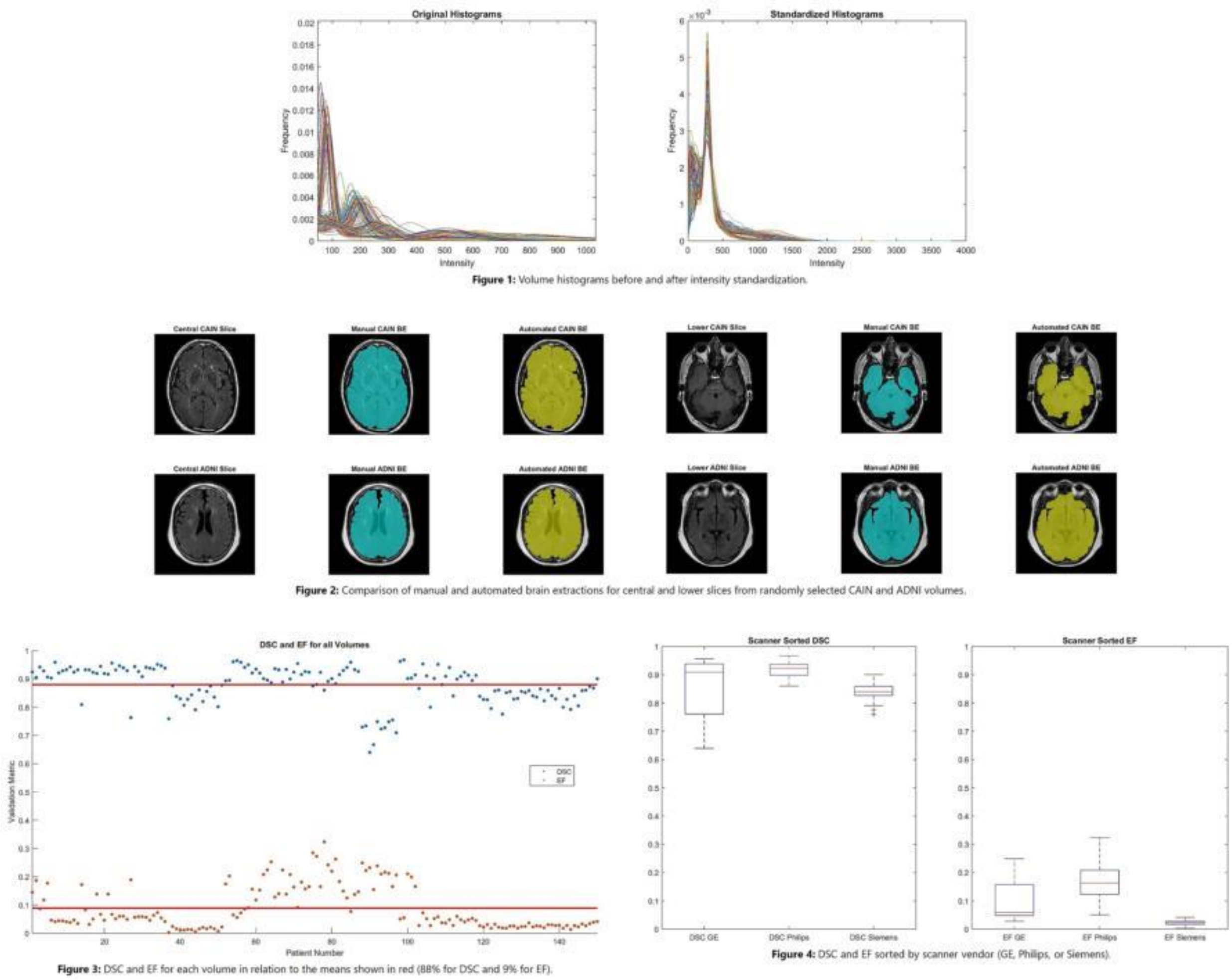

Figure 1: Volume histograms before and after intensity standardization.

Figure 2: Comparison of manual and automated brain extractions for central and lower slices from randomly selected CAIN and ADNI volumes.

Figure 3: DSC and EF for each volume in relation to the means shown in red (88% for DSC and 9% for EF).

Figure 4: DSC and EF sorted by scanner vendor (GE, Philips, or Siemens).

(Filename: TCT_3102_GraphicsFile300.jpg)

3594

4:44PM - 4:51PM

Common Data Elements (CDE) Reporting Quality Assurance Initiative for MRI Pituitary Macroadenoma Prior to Implementing ASNR-ACR- RSNA Templates/Macros

M Lee[1], A Malhotra[2], I Ikuta[3]
[1]Yale University - School of Medicine, Norwalk, CT, [2]YALE UNIVERSITY SCHOOL OF MEDICINE, NEW CANAAN, CT, [3]YALE UNIVERSITY-SCHOOL OF MEDICINE, MILFORD, CT

Purpose
This retrospective study was performed as part of a quality assurance initiative to evaluate the completeness of neuroradiology reports for the evaluation of pituitary macroadenoma for MRI pituitary studies. The ASNR-ACR-RSNA Common Data Elements (CDE) Neuroradiology Working group has produced a number of report templates in an effort to promote best-practice reporting, standardize reports and facilitate research. Our hypothesis is that there are components of the reporting templates that may not be reported consistently. By identifying report deficiencies, we can educate and improve reporting consistency when our group implements the CDE reporting templates.
Materials and Methods
The PACS was queried for all MRI pituitary exams performed between 1/1/18 to 9/31/18. Reports were excluded for the following reasons: 1) biopsy proven non - adenoma lesions, 2) if no biopsy was

available, then image characteristics typical for non-adenoma lesions, 3) normal MRI pituitary study, 4) patient was status post pituitary resection. Reports were reviewed for the explicit inclusion of each of the reporting fields in the ASNR-ACR-RSNA CDE MRI pituitary macroadenoma template. The primary outcome was the frequency of CDE reporting and lack of reporting. Secondary outcome was the percentage of the 26 CDE fields explicitly reported in each report. A review of reporting deficiencies for the root cause was also performed.

Results

From the study period, 160 reports were reviewed with 138 meeting the exclusion criteria. Of the 22 reports, the most frequently reported CDE were: contrast administration route (100%), AP dimension (100%) and focal mass (97%). The least consistently reported CDE were: borders (5%), T2 intensity (5%) and sphenoid sinus extension (5%). The reporting of CDE fields in each report averaged 52%, ranging from 32 to 69%.

Conclusions

In general, reports conveyed the relevant imaging findings but often times made broad general statements for normal findings or even omitted negative findings all together. Although this tendency quickens reporting time and makes the reports more digestible for the reader it often introduces some ambiguity. For example the ASNR-ACR-RSN CDE template includes elements related to extension of tumor. These include suprasellar, cavernous, sphenoid and clivus extension. In some reports, sella contained lesions often omitted these elements from the report. As a result this potentially hinders quality assurance checks and in the domain of artificial intelligence hinders the use of natural language processing and machine learning. In addition, some CDE were omitted because they were detailed in prior reports. For example the T1 and T2 enhancement elements were often missing from reports unless they happened to be the index case. While the overall core concepts of the relevant anatomy and disease states are conveyed with follow up reports, details of certain CDE are variable. The goal of the ASNR-ACR-RSNA CDE templates were to provide a starting point for best-practice reporting. Although some aspects of the templates are debatable for their clinical relevance as it pertains to each study the decision to keep or discard elements will ultimately be decided by the radiology group. Within our institution, which consists of academic radiologists an average of 50% CDE field reporting is the threshold for implementing templates. As the need for AI data for natural language processing and machine learning begin to develop the reasons to standardize reporting is that much more compelling.

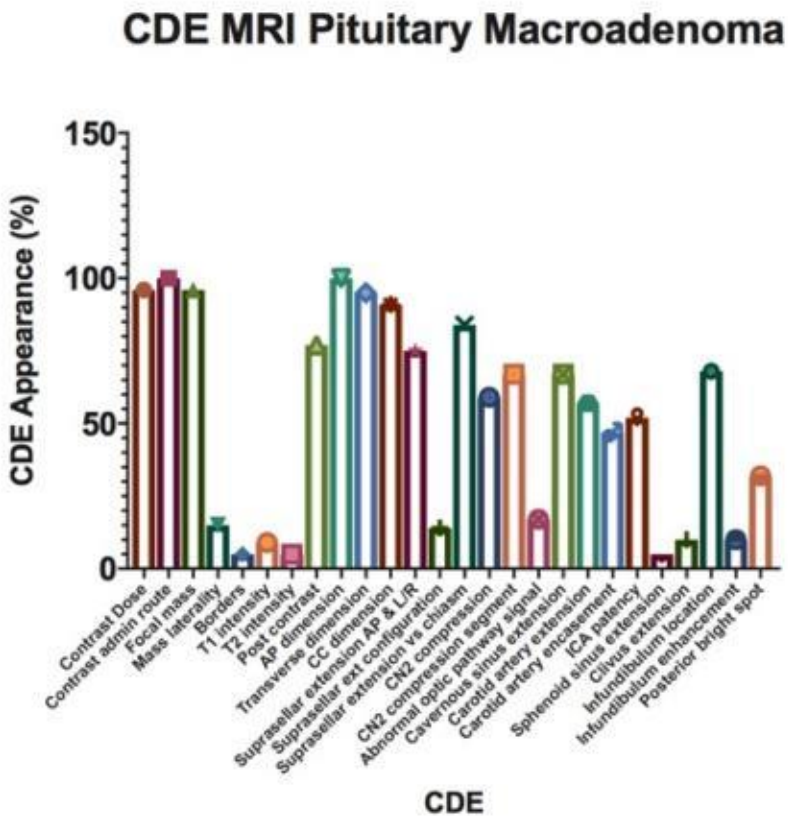
CDE MRI Pituitary Macroadenoma
CDE Appearance (%)
150
100
50
0
Contrast Dose
Contrast admin route
Focal mass
Mass laterality
Borders
T1 intensity
T2 intensity
Post contrast
AP dimension
Transverse dimension
CC dimension
Suprasellar extension AP & L/R
Suprasellar ext configuration
Suprasellar extension vs chiasm
CN2 compression
CN2 compression segment
Abnormal optic pathway signal
Cavernous sinus extension
Carotid artery extension
Carotid artery encasement
ICA patency
Sphenoid sinus extension
Clivus extension
Infundibulum location
Infundibulum enhancement
Posterior bright spot
CDE

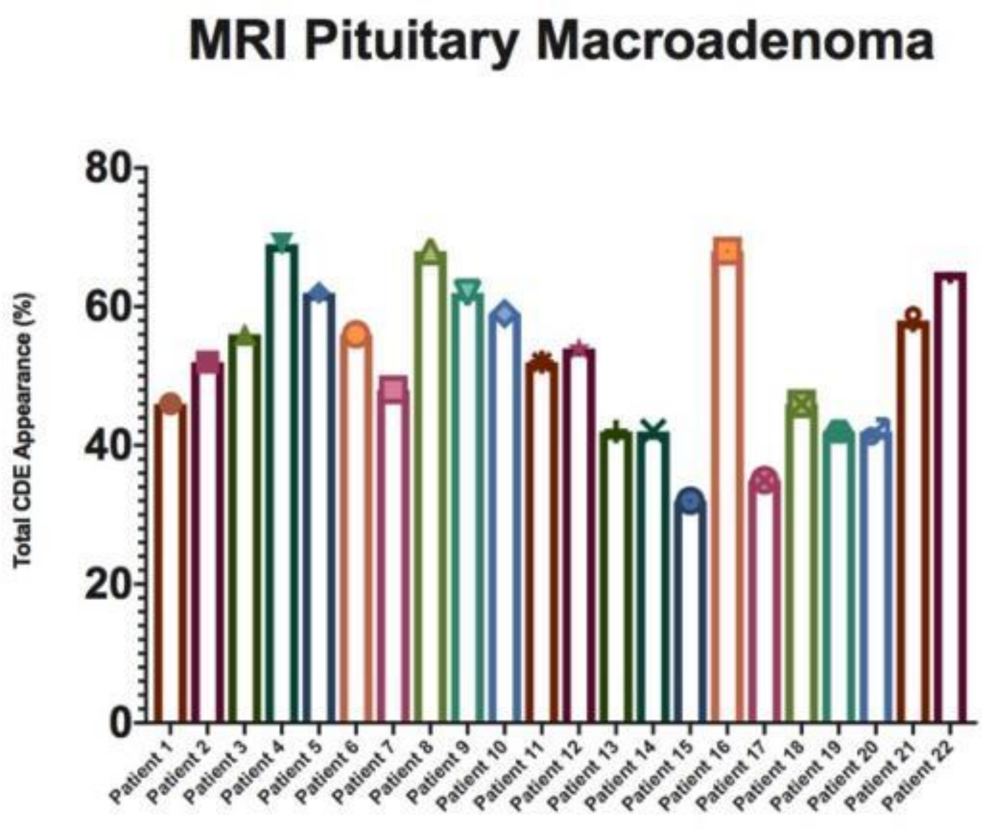
MRI Pituitary Macroadenoma
Total CDE Appearance (%)
80
60
40
20
0
Patient 1
Patient 2
Patient 3
Patient 4
Patient 5
Patient 6
Patient 7
Patient 8
Patient 9
Patient 10
Patient 11
Patient 12
Patient 13
Patient 14
Patient 15
Patient 16
Patient 17
Patient 18
Patient 19
Patient 20
Patient 21
Patient 22

(Filename: TCT_3594_Macro_layout.jpg)

2586

4:51PM - 4:58PM

Convergent Structural Alterations to White Matter and Neurite Density Across Multiple Genetic Models of Schizophrenia and Autism Spectrum Disorder

J YU[1]
[1]*University of Wisconsin School of Medicine and Public Health, Madison, WI*

Purpose
Neuroimaging studies of neuropsychiatric disease have revealed a wide spectrum of structural and functional perturbations that are attributable to the complex genetic heterogeneity underpinning these disorders. These previously observed perturbations were identified in both preclinical genetic models and patients when compared to control populations; however, few studies have directly explored intrinsic similarities or differences between the models themselves. Recent work has demonstrated strong evidence for the unanticipated genetic, molecular, and neurostructural convergence of several psychiatric diseases including autism spectrum disorder (ASD), schizophrenia, bipolar disorder, and major depression including recent work from our laboratory demonstrating strong convergence in neural microstructure in preclinical genetic models of autism spectrum disorder. To expand our work beyond ASD and to mirror advances in our understanding of the genetic and biochemical similarities between ASD and schizophrenia, the purpose of this study was to compare the similarities in neural microstructure in preclinical genetic models of ASD and schizophrenia (Disc1svΔ2, Fmr1, Nrxn1, and Pten) with diffusion tensor imaging (DTI) and neurite orientation dispersion and density imaging (NODDI).
Materials and Methods
Fmr1, Nrxn1, and Pten genetic knockout rat models of ASD were generated via zinc finger nuclease genome editing yielding a hemizygous, homozygous, and heterozygous genotype, respectively. Utilizing the CRISPR-Cas9 genome-editing technique, the second coding exon of the rat Disc1 gene encoding amino acids 19-342 was targeted to generate a nonsense mutation. Ex-vivo DTI imaging was then performed with 4.7-T Agilent MRI system with multi-slice, diffusion-weighted, spin echo images. Data were preprocessed with raw data files converted to NIfTI format and corrected for eddy current artifacts. Spatial normalization with DTI-TK provided a study-specific tensor template to which each subject tensor volume was then spatially normalized. Tract-based spatial statistics were then performed with a FA threshold of 0.2, corrected for multiple comparisons and threshold-free cluster enhancement was implemented with FSL's Randomize to compare each of the experimental groups to the control group as well as to each other with $p < .05$ as a threshold for significance. After image acquisition and preprocessing, volumetric parameter maps were constructed with output volumes corresponding to neurite density and the orientation dispersion index.
Results
TBSS results comparing the Fmr1, Nrxn1, and Pten models of ASD to wild-type controls reveal widespread changes in white matter microstructure, specifically decreased fractional anisotropy (FA) bilaterally in neocortex, external capsule, and corpus callosum. In contrast to the variation in white matter microstructure observed when comparing genetic models to control animals, TBSS identified very few areas of difference in FA between the genetic models. TBSS did not reveal any significant FA differences between individual pairwise comparisons of Fmr1, Nrxn1, and Pten models. Strikingly, TBSS comparing Disc1svΔ2 animals to Fmr1 and Nrxn1 models only identified very minimal FA differences in left neocortex. Cluster analysis was then performed within six regions of interest: neocortex, internal capsule, external capsule, corpus callosum, hippocampus, and basal ganglia. Following automated volumetric segmentation of the brain, mean values of both diffusion and neurite indices were computed within each ROI (left and right hemisphere). Principal component analysis of this data set was exhaustively screened for separation of each experimental group by k-means clustering with $k = 5$, repeated for $n = 1000$

iterations. The top 4 combinations with the most frequent clustering of controls are shown. Cluster analysis matches results from our TBSS results with only the wild-type control group demonstrating reliable separation (clustering) from the other groups, which were indistinguishable from each other.

Conclusions

High-resolution diffusion tensor imaging of transgenic models of psychiatric illness can provide insight into the relationship between genetic variants and aberrant white matter microstructure and neurite density and ultimately highlights the structural convergence in genetic models of complex neuropsychiatric disorders. Our findings demonstrate unexpected convergence in brain structures across all four genetic models investigated herein and buttresses an emerging understanding of neurostructural phenotypic convergence in psychiatric disease. Future work with other genetic variants of ASD and genetic models of psychiatric illness will continue to shed light on the impact of genotype on global measures of neural microstructure and will help refine our understanding of the shared neuroimaging features in psychiatric illness.

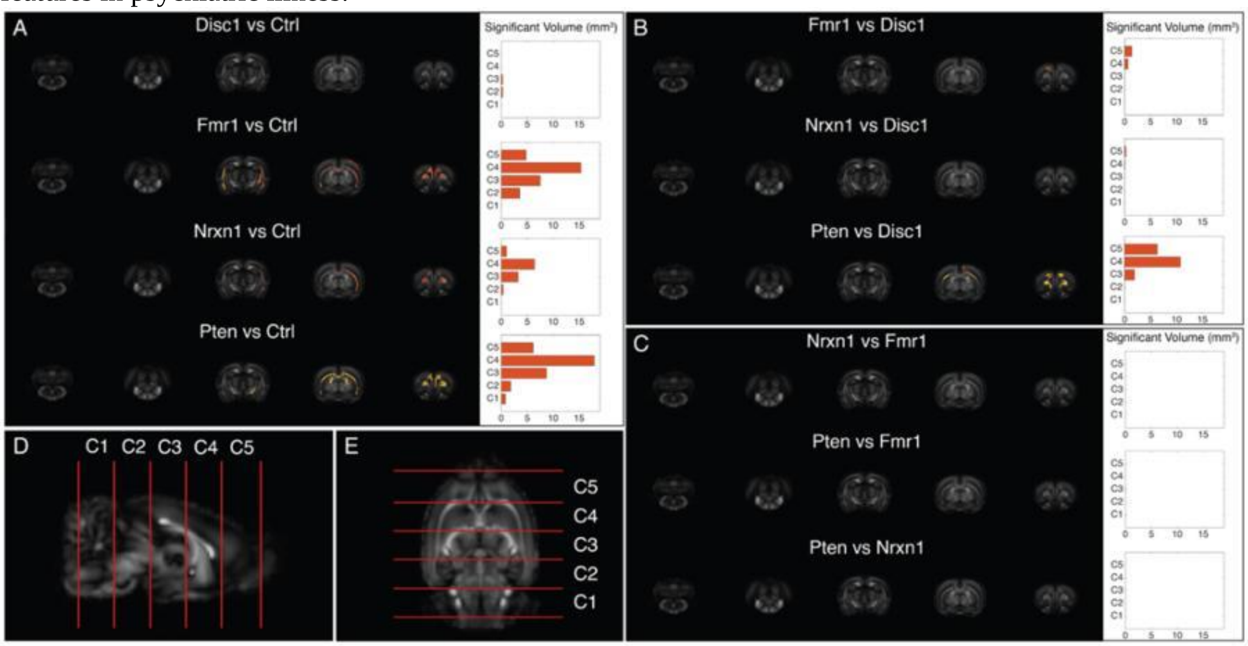

(Filename: TCT_2586_Yu2019.jpg)

3524

4:58PM - 5:05PM

Diffusion MRI Connectome Subnetworks in 16p11.2 Deletion Syndrome Reveals Differential Structural White-Matter Alterations

A Chung[1], B Ahtam[1], P Grant[1], K Im[1]
[1]*Boston Children's Hospital, Boston, MA*

Purpose

Copy number variants of the chromosomal locus 16p11.2 have been associated with several neurodevelopmental disorders including autism and epilepsy with ~71% of patients going on to experience delays and deficits in speech and language acquisition (1). Diffusion MRI studies on children with 16p11.2 deletion syndrome have found widespread (2), abnormal brain white-matter structure with selective involvement of language pathways. Here we extend the analysis onto DTI tractography-based connectomes, and employ network theoretical principles to understand the brain as an organized, inter-connected system. We utilize the network topological principle of the rich-club (RC), a core 'backbone' integral for effective brain function (3). We investigate the network topology between 16p11.2 deletion patients and controls in terms of global network measures, and within RC, feeder and seeder subnetworks as defined by partitioning the brain regions according to their connection to core RC nodes (4).

Materials and Methods

Data were from Simons VIP Consortium (5). Subjects: Twenty-one 16p11.2 deletion patients (aged 10.91+/-2.09 years, 11 males, 11 right-handed), and 18 controls (12.58+/-1.99 years, 10 males, 11 right-handed). MRI: Data acquired on a 3T Tim Trio Siemens included a T1-Weighted MPRAGE (TE/TR/TI=1.64/2530/1200ms; flip angle=7°; voxel size=1mm^3; FOV=256mm) and a DWI sequence (30 gradient directions at b=1000s/mm^2; one b=0s/mm^2; TR/TE=10s/80ms; voxel size=2mm^3; FOV=256mm). Processing (Fig1): T1-Weighted cortical surface was parcellated into 68 regions and mapped to b0 space. DWI were motion-corrected and co-registered to the b0 volume. Following whole brain, white-matter seeded interpolated streamline tractography a 68x68 connectome, W, was computed and weighted by number of tracts connecting pairwise nodes, and normalized by the total number of streamlines in the brain. Global network analysis: Network measures (mean transitivity, global efficiency, and nodal density, degree and strength) were calculated from W. Subnetwork analysis: Group connectomes, Wgroup, were computed separately for patients and controls where edges present in at least 90% of each group were retained and averaged. RC coefficients were computed from Wgroup, then normalized, Φnorm, by 1000 random degree-, strength- and density-distribution preserved networks, Φrand. RC nodes were initially chosen when their corresponding Φnorm was >1 and significantly differed from Φrand. RC nodes were finalized by choosing the 13 nodes (20% of total connectome regions) with the highest mean ranking of degree and strength. W was then divided into an 1) RC subnetwork of 13 RC nodes and their inter-connections; 2) feeder subnetwork of non-RC nodes which 'feed' into the RC; and 3) seeder subnetwork of non-RC nodes connected to other non-RC regions. Global network measures were also calculated for each subnetwork. All network measures between groups were compared with unpaired t-tests.

Results

Global network analysis: No significant group differences in network measures were found (Table2). Subnetwork analysis: An RC regime was observed from k=8 and 9 for patients and controls, respectively, yielding 19 and 22 regions. The 13 RC nodes were largely similar in both groups, with the exception of left precentral appearing for controls, and left supramarginal gyrus for patients (Fig1, Table 1), suggesting a preserved RC topology in 16p11.2. Significant group differences were found in all subnetworks and across network measures (Table 2). RC subnetwork density and degree as well as seeder subnetwork density, degree and strength were significantly decreased in patients. These findings suggest lower structural connectivity in compartments that are central (RC) and peripheral (seeder) to brain organization. These structural alterations align with the distributed changes found from tract-based diffusion analysis (2). In contrast feeder subnetwork transitivity, efficiency and strength were significantly increased in patients, possibly indicative of a support or mediating network compensating for a deficit in the RC (although not significant, equivalent measures in the RC were lower in patients).

Conclusions

We demonstrate that subnetwork analysis by RC stratification has the potential to reveal differential alterations in brain organisation with greater group differences in 16p11.2 deletion syndrome that could not be detected by whole brain connectome analysis. Whilst RC regions are largely preserved in location, patients exhibit significant reduction in structural connectivity with differential changes in network topology within its subnetworks which may be indicative of underlying compensatory mechanisms. Future work will ascertain the implications of these network aberrations in relation to language deficits that are characteristic of 16p11.2 deletion.

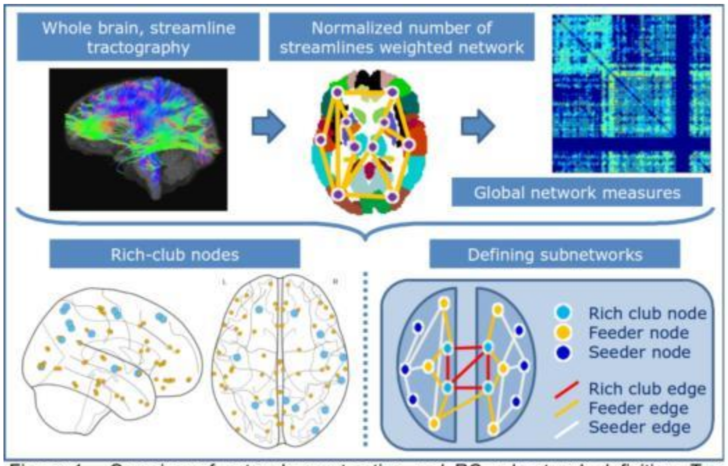

Figure 1 - Overview of network construction and RC subnetwork definition. Top panel: Depicts post-processing steps following tractography. Bottom panel: RC nodes are identified (circles in light blue) and top 20% are retained. Having defined 13 RC nodes, edges and remaining nodes in the network are subsequently grouped into RC, feeder and seeder subnetworks according to their relationship to the RC.

Rank		Controls		16p11.2 Patients
1	R	Superior Frontal	R	Superior Frontal
2	R	Precentral	R	Precentral
3	R	Supramarginal	R	Supramarginal
4	R	Superior Parietal	R	Superior Parietal
5	R	Inferior Parietal	R	Inferior Parietal
6	R	Precuneus	R	Precuneus
7	R	Lateral Occipital	R	Lateral Occipital
8	R	Superior Temporal	R	Superior Temporal
9	R	Insula	R	Insula
10	L	Superior Frontal	L	Superior Frontal
11	L	Precentral	L	Supramarginal
12	L	Superior Parietal	L	Superior Parietal
13	L	Precuneus	L	Precuneus

Table 1 (Above) - Top 13 RC nodes derived from control and patient group-averaged connectomes. Control RC nodes are depicted in Figure 1.

	Group *t*-test, *p*-values				Mean network measure values					
	W	Subnetwork			Controls			Patients		
		RC	F	S	RC	F	S	RC	F	S
Transitivity	0.2808	0.8849	**0.0004***	0.2793	0.0046	0.001	0.0009	0.0045	0.0011	0.001
Global Efficiency	0.3003	0.3118	**0.0007***	0.0986	0.0055	0.0006	0.0004	0.0053	0.0008	0.0004
Density	0.8868	**0.0045***	0.2298	**0.0324***	0.6574	0.2142	0.2765	0.6178	0.2079	0.2516
Degree	0.9058	**0.0043***	*0.0516*	**<0.0001***	6.8889	6.625	4.345	6.4176	6.9939	3.2292
Strength	0.8781	0.51	**<0.0001***	**0.0053***	0.0508	0.0128	0.0059	0.0497	0.0153	0.0046

Table 2 (Left) - Statistical *p*-values from unpaired *t*-tests comparing network measure between controls and 16p11.2 deletion patients. Network measures were computed from the subject's connectome, **W**, and from rich-club defined subnetworks of the connectome. Mean network measure values from subnetwork analysis are also presented Significant group differences ($p < 0.05$) are denoted by '*' in bold.

(Filename: TCT_3524_FIG.jpg)

2194

5:05PM - 5:12PM

Functional MRI Study of Language Organization in Left-handed and Right-handed Trilingual Subjects

C Atat[1], R Moussa[1], J Abdel Hay[1], S Yazbek[1]
[1]Hotel Dieu de France Hospital, Beirut, Lebanon

Purpose
fMRI has replaced WADA testing for the preoperative assessment of language lateralization and localization. In our country, most people are trilingual. Selecting the appropriate language to test is therefore intricate. Our objective is to compare fMRI maps for all 3 languages in left-handed and right-handed trilingual subjects.
Materials and Methods
We included 15 right-handed and 15 left-handed healthy adult volunteers, fluent in three languages. We performed fMRI for each volunteer with a visual responsive naming task paradigm repeated for every language. Maps were generated using the same threshold at P<0.001and we compared the areas of activation.
Results
Language lateralization was identical for the 3 languages in 87% of patients. The 4 subjects who demonstrated different lateralization were all left-handed and showed left lateralization or codominance.

Left-handed volunteers have lower odds of left lateralization of language (OR 0.176, 95% CI: 0.046-0.669; P =0.011), higher odds of codominane (OR 1.184, 95% CI: 1.045-1.342; P = 0.012) and higher but not significant odds of right lateralization of language (OR 2.154, 95% CI: 0.504-9.208; P = 0.485). Broca and Wernicke's areas demonstrated bilateral activation in 88% of the cases, and presented the same anatomical localization for all 3 languages whereas the number and localization of the accessory language areas were different. Correlation between the global activation index and the chronology of language acquisition in right-handed subjects tended towards statistical significance (rs = .275, p = .068) with the last language learned inducing a higher degree of activation.

Conclusions

In right-handed trilinguals, fMRI performed for a single language can accurately determine language lateralization, whereas in left-handed all languages need to be tested. To determine the anatomical localization of accessory language areas, it is preferable to study all 3 languages. If the duration of the fMRI study was to be shortened, a study of the last language learned in right-handed patients could be considered.

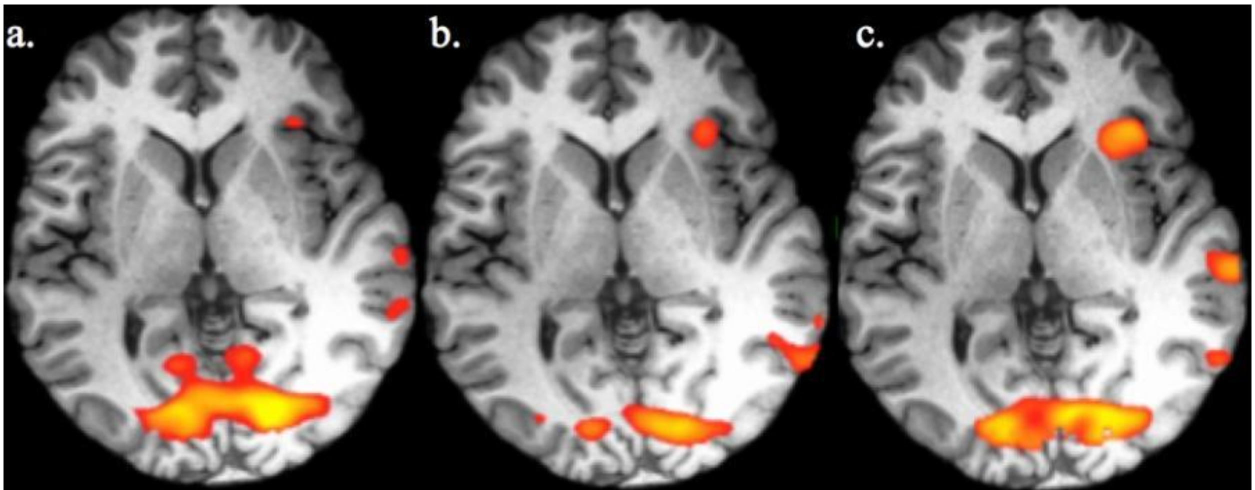

Figure 1 Axial fMRI maps in a right-handed trilingual subject demonstrating Broca and Wernicke's activation as well as visual areas of activation.
Fig 1 (a) language maps for L1 , first language acquired at 1 year of age
Fig 1 (b) language maps for L2 , second language acquired at 5 years of age
Fig 1 (c) language maps for L3, third language acquired at 8 years of age

The maps demonstrate left lateralization for all 3 languages with overlapping localization for Broca and Wernicke's areas . The last language learned (Fig 1c) shows the highest degree of activation (the same threshold at $P<0.001$ was applied for all 3 languages)

(Filename: TCT_2194_fig1.jpg)

2510

5:12PM - 5:19PM

Higher Temporal Resolution Multiband fMRI Provides Improved Presurgical Language Maps

I Mark[1], D Black[1], M Ho[1], D DeLone[1], T Passe[1], I Parney[1], T Burns[1], K Welker[1]
[1]*Mayo Clinic, Rochester, MN*

Purpose
We investigated if increasing fMRI temporal resolution using a multiband gradient echo-echo planar imaging (GRE-EPI) pulse sequence provides language maps of higher statistical quality compared to a traditional GRE-EPI sequence.
Materials and Methods
This prospective study enrolled 11 consecutive patients receiving language fMRI prior to a potential brain resection for tumor, AVM, or epilepsy. Among clinically indicated fMRI runs, a 4 minute rhyming task (40 second blocks x 6) was performed at 3.0 Tesla with a traditional GRE-EPI pulse sequence (TR=2000, TE=30, Matrix=64/100%, Slice=4/0, FOV=24, Slices=30 Time points = 120). With informed consent, an additional 4 minute run of the same rhyming task was performed using a multiband GRE-EPI pulse sequence with an acceleration factor of 6 (TR=333, TE=30, Matrix 64/100%, Slice=4/0, FOV=24, Time points = 720). The order of tasks was randomized. fMRI runs were processed using Prism Clinical Imaging software and spatially filtered t-statistical maps were generated. A neuroradiologist drew ROIs around activations at Broca's, dorsolateral prefrontal cortex, Wernicke's, and the visual word form areas. The t-value maxima was measured for the overall brain as well as each of the ROIs. A paired t-test was performed for the corresponding traditional and multiband GRE-EPI measurements.
Results
The mean age of subjects was 39 years old (18-62). 73% were male. The average overall brain t-value maxima for the multiband pulse sequence (t=16.99) was higher than for the traditional pulse sequence (t=8.92, $p<.001$). This also held true for Broca's area ($p< 0.001$), Wernicke's area ($p<.001$) , dorsolateral prefrontal cortex ($p<.001$), and the visual word form area ($p=.002$).
Conclusions
A multiband GRE-EPI fMRI pulse sequence employing high temporal resolution provides fMRI language maps of greater statistical significance than those obtained with a traditional GRE-EPI sequence.

3194

5:19PM - 5:26PM

Identifying Language Laterality via Functional Connectomes

C Liu[1], M Nelson[1], B Tamrazi[1]
[1]*Children's Hospital Los Angeles and University of Southern California Keck School of Medicine, Los Angeles, CA*

Purpose
To evaluate if resting-state functional connectomes can identify the language laterality in the pediatric population. Rather than performing whole-brain independent component analysis to calculate a laterality index [1], we hypothesize that the number of connections to hemispheric language centers can determine laterality.
Materials and Methods
Nine right-handed subjects (mean age = 16.1 years, 4:5 male:female) had undergone resting-state fMRI with 3T MRI (Philips Healthcare, Cleveland, Ohio) utilizing the following echo planar imaging parameters: TE = 30 ms, TR = 3 s, flip angle = 90 degrees, 200 frames (10-minute acquisition). High-resolution T1-weighted gradient-echo sequence was performed for the structural data. The data was analyzed utilizing CONN [2] with the default preprocessing steps. Denoising of the functional data was then performed with linear regression of the following confounding effects: white matter, CSF, realignment, imaging outliers. Bandpass filtering (0.008Hz, 0.09 Hz) was then applied after linear regression (RegBP). Region-of-interest to region-of-interest (ROI-to-ROI) analysis was then performed for the group using the following sources (with standard coordinates): left (-51,26,2) and right (54,28,1) inferior frontal gyrus (e.g. Broca area); left (-57,-47,15) and right (59,-42,13) posterior superior temporal gyrus (e.g. Wernicke area). ROI-to-ROI connections threshold was set at a two-sided false discovery rate (seed-level) of $p < 0.05$.

Results
There were 42 connections to the left inferior frontal gyrus, with extensive connections between the left-sided Broca and Wernicke areas as well as to other regions of the left temporal lobe. Connections to the contralateral language centers were also seen. In contrast, there were only 24 connections to the right inferior frontal gyrus (Figure 1). There were 57 connections to the left posterior superior temporal gyrus, with 56 connections to the right posterior superior temporal gyrus.
Conclusions
Differences in the number of connections to Broca area between the two cerebral hemispheres could help identify the dominant language hemisphere.

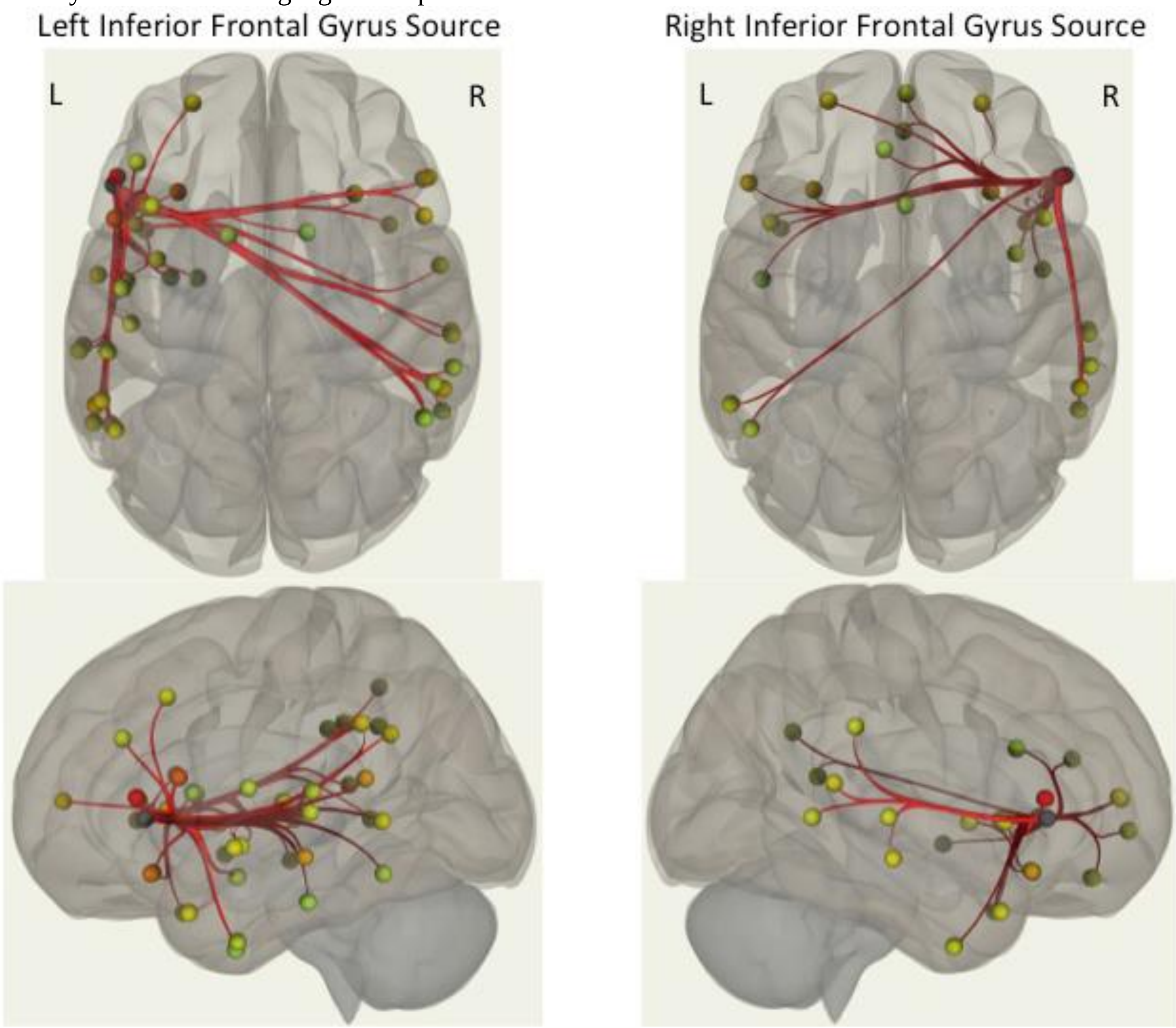

(Filename: TCT_3194_asnr_2019_figure1.jpg)

3569

5:33PM - 5:40PM

Increasing MRI Safety for Patients with Implanted Medical Devices: Comparisons of a 0.5 T Head-Only MRI to 1.5 T and 3 T

I Connell[1], A Panther[2]
[1]The University of Western Ontario, London, ONTARIO, [2]Synaptive Medical, Toronto, Ontario

Purpose

Patients with implanted medical devices are traditionally excluded from MR imaging or are imaged under highly rigorous FDA safety regulations that can severely limit the clinical utility of the resultant image potentially resulting in insufficient field-of-view (FOV) coverage and several-fold increases in scan duration in clinical 1.5 T scanners [1]. Implants in the presence of an external radio-frequency (RF) field pose the risk of tissue heating due to induced electric currents on implanted devices [2]. Implants of concern include electrically conductive neuro-stimulator leads that have the potential to resonate at or near the Larmor frequency, resulting in a high local specific absorption rate (SAR) that exceeds the FDA regulation of 10 W/kg [3]. Neuro-stimulators in MRI present two common problems: (1) achieving a resonant length due to lead geometry (including inductance due to lead coiling, etc.) and (2) orientation with-respect-to the externally applied RF field. SAR is proportional to the square of the main magnetic field strength. While imaging at lower field strengths (< 1.0 T) reduce patient risk due to device RF heating, historically such mid-field scanners have suffered from lower achievable signal-to-noise ratio (SNR) compared with higher-field scanners. However, as demonstrated in the presented MR images obtained with our 0.5 Tesla scanner, recent strides in mid-field technology have increased the clinical utility of a mid-field head-only scanner to be comparable to currently available 1.5 T scanners. Thus, studies on safety for patients with implanted devices are warranted for mid-field systems.

Materials and Methods

This study investigates the resonant lengths corresponding to 21.3 MHz, 64 MHz, and 128 MHz, for a head-only birdcage coil. Parametric simulations were performed with CST Microwave Studio 2018 using the full-wave time-domain solver with a 12-leg 'high-pass' birdcage volume coil: 39.7-cm in diameter and 35-cm long. A phantom (dimensions: 9 x 35 x 35 cm) was placed inside the birdcage coil ($\varepsilon r = 80$). Embedded in the phantom was a 0.254-mm perfect electrical conducting (PEC) rod with an overall length ranging from 5-cm to 80-cm. Two simulation studies were performed: (1) Rod lengths were stepped between 5-cm to 35-cm in 5-cm increments, with additional lengths selected around $\lambda/2$ resonances corresponding to 64 MHz and 128 MHz. The rod length of 72.5-cm corresponding to the $\lambda/2$ resonance of the rod at 21.3 MHz extended outside the FOV of the birdcage. For this simulation, phantom dimensions were 6 x 35 x 85 cm. This physically represented an implant extending into the torso. (2) A total rod length of 30-cm plus two 3.2 uH in-series inductors - corresponding to an effective 21.3 MHz resonant length enclosed in the birdcage FOV. Rod placement was determined according to the ASTM F2182011a guidelines whereby the area of worst-case implant orientation, located at least 2-cm from phantom boundaries, was determined. Mesh density located 2-cm around the rod was fixed for all simulation runs, ensuring equal discretization of the rod when comparing individual simulations. All simulations were normalized to produce a B1+ rms =1 µT at the isocenter of the phantom.

Results

Visible in the presented figure is a demonstrably lower 10-g local SAR for 21.3 MHz across all lengths - resonant and non-resonant. According to the simulations, 10-g local SAR at 21.3 MHz does not suffer the same fractional increase in power deposition as is visible at 1.5 T and 3.0 T. We hypothesize the reduced electric field present at 0.5 T is a proportionally greater effect than the reduction in reactance occuring at resonance. A representative 35-cm birdcage coil, operating at clinical 1.5 T and 3.0 T field strengths, is amenable to exciting $\lambda/2$ resonant lengths for 64- and 128-MHz conductors. However, the ~ 75 cm long rod could not be 'folded' into the entire 35-cm FOV. Therefore, reducing rod exposure to tangential electric fields results in reduced power deposition, even when the rod is resonant. Interestingly, even when resonance was enforced via lumped element placement on the rod at 21.3 MHz, maximum 10-g SAR at 21.3 MHz was appreciably lower than non-resonant lengths for 1.5 and 3.0 T, respectively. Nominal safety precautions for DBS implants come in several forms: 0.1 W/kg whole-brain SAR and average B1+ field maximums [4]. The authors note that the 2.0 µT average field metric would cause both 1.5 T and 3.0 T scanners to exceed the 10 W/kg local SAR limits, however the 0.5 T scanner would appear to be able to run at ~ 10 µT average. Considering low RF duty cycles used during routine pulse sequences, this could allow for substantial increases in peak B1+. Further experiments will test this hypothesis.

Conclusions
The mid-field system studied here demonstrates reduced maximum 10-g SAR when performing RF excitation around resonant lead lengths as well as a total reduction in SAR consistent with the reduction in main magnetic field strength. In comparison to 1.5 T and 3 T clinical scanners, mid-field scanners provide unique opportunities to obtain diagnostically relevant information with a commensurate increase in safety for patients with implanted devices.

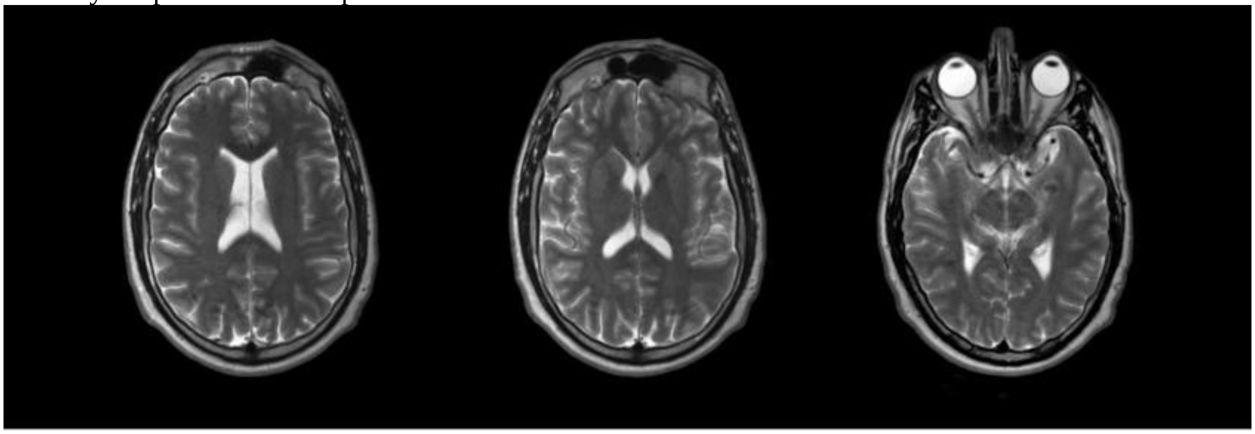

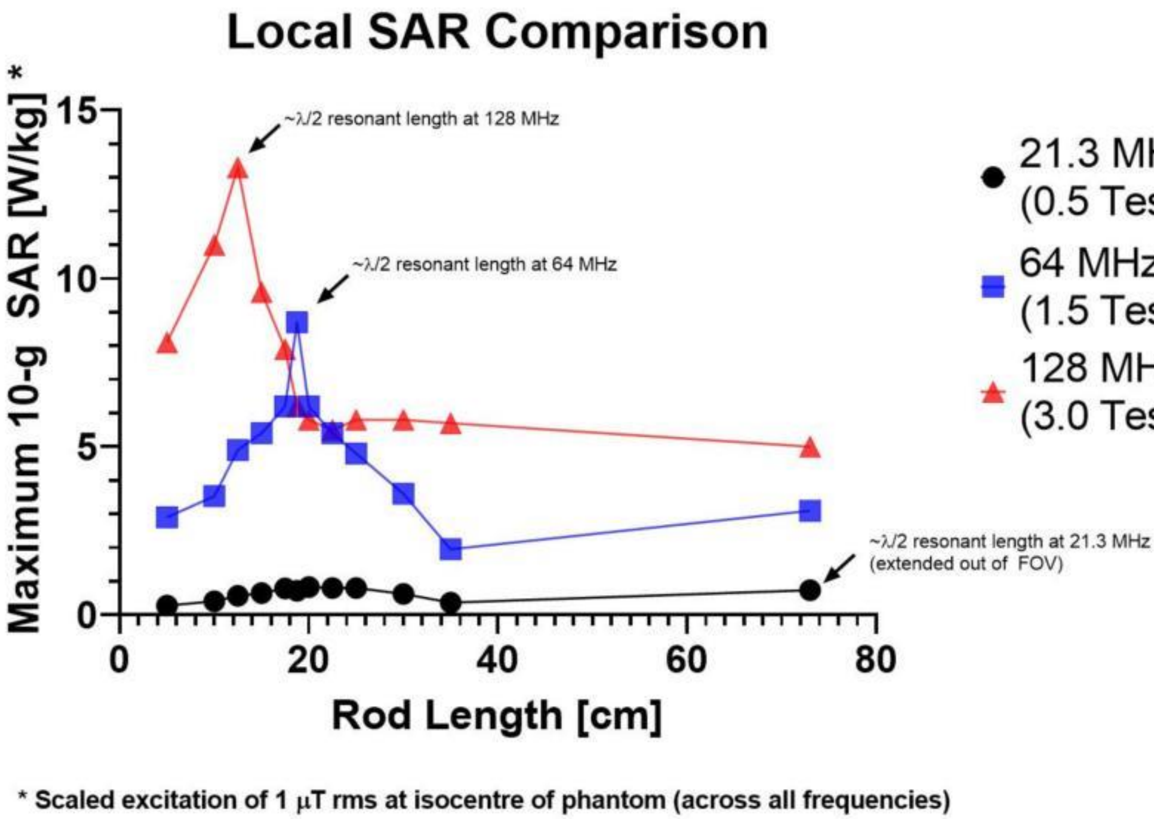

(Filename: TCT_3569_ajnr.jpg)

3011

5:40PM - 5:47PM

Prolonged Microgravity Affects Human Brain Structure and Cognition

D Roberts[1], T Brown[2], D Asemani[3]
[1]Medical University of South Carolina, Charleston, SC, [2]Medical University of Soth Carolina, Charleston, SC, [3]MUSC, Charleston, SC

Purpose
The long-term influences of spaceflight on the human brain are unknown but must be understood prior to establishing a lunar colony or sending humans to Mars. We have previously shown in astronauts following missions aboard the International Space Station, there is an upward shift of the brain, crowding of eloquent brain tissue at the vertex, and enlargement of the ventricular system. However to what extent, if any, these structural changes may impact cognitive function has not been previously studied.
Materials and Methods
We perform detailed quantitative analyses of brain MRI scans of International Space Station astronauts obtained before and following spaceflight and correlated the results with astronaut performance on cognitive testing.
Results
We found that long-duration spaceflight resulted in a 10.7% increase in total ventricular volume (%ΔVV) and a significant global displacement of the brain in reference to the skull including an upward translational shift (+0.56mm, $P=0.03$), inferior-superior stretching (+0.78%, $P=0.002$) and a transverse compression (-0.37%, $P=0.002$) of the brain parenchyma. There was a significant association between %ΔVV and mission duration ($r = 0.72$, $P = 0.001$) but a negative association with astronaut age ($r = -0.48$; $P = 0.048$). Our results suggest gender may also play a role in structural brain changes during spaceflight, however this hypothesis will need to be tested in a larger female astronaut cohort. The %ΔVV predicted significant changes in cognitive function, including accuracy for a memory-related code substitution learning test ($r = -0.60$, $P<0.05$) and reaction times for math ($r = -0.58$, $P<0.05$) and continuous performance test ($r = -0.62$, $P<0.05$). Local changes in brain structure were assessed using the Jacobian determinant and three white matter regions emerged as significant predictors of altered reaction time on the continuous performance test (bilateral optic radiations and splenium of the corpus callosum).
Conclusions
Here we show that alteration of brain structure during spaceflight is progressive based on mission duration, varies based on astronaut demographics, and predicts postflight changes in cognitive performance. The variation in structural adaptation of the brain in response to spaceflight in our cohort may reflect differences in the mechano-elastic properties of the brain. For example, previous investigators have demonstrated brain elasticity differs among normal subjects depending on gender and age. Additional studies are needed to further investigate this hypothesis. These findings may inform plans for long-term human exploration missions to the Moon or Mars and need for artificial gravity as humanity considers future colonization of the solar system.

3565

5:47PM - 5:54PM

Unexpected Clinical Outcomes After Deep Brain Stimulation for Essential Tremor: When Established Targeting Methods Fail

M Achilleos[1], J Waugh[1], J McDaniel[1], D Imphean[1], B Wagner[2], J Maldjian[3], B Shah[4]
[1]University of Texas Southwestern Medical Center, Dallas, TX, [2]UT Southwestern Medical Center, Dallas, TX, [3]University of Texas Southwestern, Dallas, TX, [4]UT Southwestern Medical Center, Irving, TX

Purpose
To compare atlas and landmark-based (Guiot's) methods of identifying the ventral-intermediate nucleus (VIM) in patients status post Deep Brain Stimulation (DBS) surgery for essential tremor and correlate them with clinical outcomes.

Materials and Methods
20 patients who received DBS targeting the VIM for essential tremor were reviewed. Pre-operative planning and post-operative imaging studies (CT and MRI) were obtained and 2 established methods of VIM localization were performed. First, Guiot's method was performed to predict the expected location of the VIM. Second, the expected location of the VIM was mapped with atlases using the Lead-DBS toolbox. The predicted location of the VIM was then compared to the actual location of the DBS leads on post-operative imaging studies. Volume of tissue activated (VTA) calculations surrounding the leads were also performed using the Lead-DBS program.
Results
The majority of the patients receiving DBS for their essential tremor experienced some improvement in their symptoms, and the final lead positions largely corresponded to the predicted locations of the VIM. Three patients (15%) were identified who had optimal lead positions on imaging analysis but did not have a sustained clinical response. One of these patients experienced continued breakthrough tremors requiring frequent reprogramming. Another developed parkinsonian symptoms secondary to stimulation. In the third tremor improvement could not be achieved despite multiple reprogramming sessions, and they ultimately required lead revision surgery.
Conclusions
These findings provide additional evidence that current methods for targeting the VIM are suboptimal and further functional and connectivity analysis is required to optimize surgical strategies in patients undergoing DBS surgery. Previously described variability in the location of neurons contributing to tremor may potentially account for some of these clinical manifestations.

Monday, May 20, 2019
4:30PM - 6:00PM
Machine Learning, Automated Processing and Lesion Segmentation Brain Applications
3537

4:30PM - 4:37PM

A Deep Learning Pipeline for Automated Brain Tumor Segmentation

C Bangalore Yogananda[1], B Wagner[1], G Murugesan[1], S Nalawade[1], A Madhuranthakam[2], J Maldjian[1]
[1]University of Texas Southwestern, Dallas, TX, [2]UT Southwestern Medical Center, Dallas, TX

Purpose
The purpose of this study is to describe a method for automatic brain tumor segmentation using patch-based 3D Dense-Unets and multi-modal brain MRI.
Materials and Methods
Multi-modal brain MRI data from the BraTS2018 [1, 2] challenge consisting of 210 High Grade Glioma (HGG) and 75 Low Grade Glioma (LGG) subjects were used including 4 sequences (Flair, T1, T1C and T2) and ground truth labels for enhancing-tumor, non-enhancing tumor including necrosis, and edema. 265 subjects (198 HGG and 67 LGG) were used for training and 20 (12 HGG and 8 LGG) were held-out for testing. Data preprocessing included 1) Co-registration 2) Skull-stripping, 3) N4BiasCorrection [3] and 4) Intensity normalization to 0-mean and unit-variance. The pipeline was also tested on 66 studies from the BraTS2018 validation dataset. It was also fine-tuned on 25 subjects and tested on 15 subjects from a clinical dataset from Oslo, Norway. Three separate 3D-Dense-Unets were designed. EN-net was trained to segment the enhancing tumor, TC-net to segment the tumor core (consisting of enhancing tumor, non-enhancing tumor and necrosis) and WT-net to segment whole tumor (tumor core + edema). Each network's predicted volume was fused together in the post-processing step called Multi-Volume Fusion (MVF).

Results
We evaluated the pipeline's performance and reliability in segmenting brain-tumors on the BraTS challenge data and clinical data. Our method obtained similar results as the top performers [5] of the BraTS2017challenge and outperformed the BraTS2018 participants using similar model architectures [4].
Conclusions
We demonstrate a deep learning pipeline for brain tumor segmentation which performs well on the BraTS2018 challenge data as well as clinical data. The Oslo dataset was acquired as part of clinical evaluations with variations in sequences acquired and orientations. These were acquired as 2D images with larger slice thickness and high in-plane resolution. Our pipeline performed well not only on the challenge dataset, but also on real world clinical data that is challenging to work with.

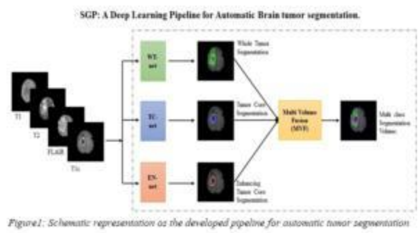

Figure1: Schematic representation os the developed pipeline for automatic tumor segmentation

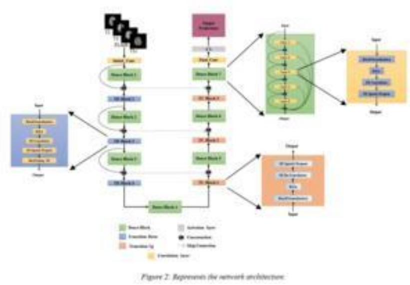
Figure 2: Represents the network architecture

	Before MVF	After MVF
Whole Tumor	0.889	0.901
Tumor Core	0.821	0.842
Enhancing Tumor Core	0.782	0.800

Table 1 represents the quantitative evaluations on held out dataset

	Before MVF	After MVF
Whole Tumor	0.870	0.900
Tumor Core	0.780	0.800
Enhancing Tumor Core	0.749	0.780

Table 2: Represents the quantitative evaluations on BraTS 2018 validation data

	Before MVF	After MVF
Whole Tumor	0.70	0.731
Tumor Core	0.76	0.767
Enhancing Tumor Core	0.68	0.70

Table 3: Represents the quantitative evaluations on the clinical brain tumor dataset

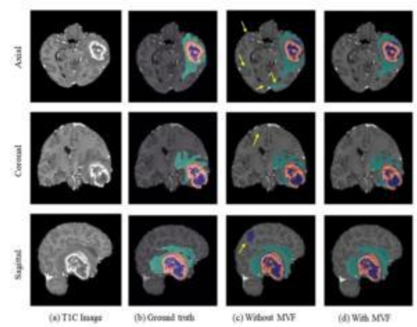

Figure 3: Comparative segmentation result of a High Grade Glioma (HGG) in all the three views. (a) A 2D slice of the post-contrast image. (b) Ground truth (c) Network output without MVF. (d) Network output with MVF.
Color COde -
Red = Enhancing tumor
Blue = Tumor core (enhancing tumor + non-enhancing tumor + necrosis)
Green = Edema
Red + Blue + Green = Whole tumor (enhancing tumor + Non-enhancing tumor + necrosis + edema)

(Filename: TCT_3537_Results_Figure.jpg)

2726

4:37PM - 4:44PM

A Quasi-conformal Mapping-based Data Augmentation Technique for Improving Deep Learning Techniques on Brain Tumor Segmentation

M Zhang[1], D An[2], X Gu[2], G Young[1], X Xu[1]
[1]Brigham and Women's Hospital, Boston, MA, [2]Stony Brook University, Stony Brook, NY

Purpose
We aimed to develop a data augmentation technique tailored to brain tumor images for improving deep learning approaches on tumor segmentation. We designed a novel differential geometry-based quasi-conformal mapping processing to augment brain tumor MRI.
Materials and Methods
We used the high-grade glioblastoma (GBM/HGG) dataset of the BRATS2015 [1,2]. We divided 220 expert-marked HGG volume data into training set (187), validation set (11), and testing set (22). We applied our quasi-conformal mapping technique to augment the 187 training data to 374. Our data augmentation scheme was based on the quasi-conformal. We randomly generated a complex-valued function on the image domain, the so-called Beltrami coefficient, to obtain a homeomorphic mapping by solving the Beltrami equation [3]. The mapping wrapped the input image to augment the training set. Figure 1 shows an example of augmented data. We then applied an existing deep learning method, DeepMedic [4], to the augmented data set for training. As a comparison, we applied the same deep

learning method on the original 187 training data. We compared the two approaches to the same validation and testing sets.

Results

The experimental result showed that the model trained by augmented data has better performance than the original data. For the deep learning model trained on the augmented data, the Dice coefficients of the complete tumor, necrosis, edema, non-enhancing tumor, and enhancing tumor on the test data set were 0.9128, 0.5551, 0.7989, 0.3211, and 0.8197, respectively, substantially higher than the corresponding Dice coefficients of 0.6892, 0.4697, 0.4788, 0.1542, and 0.7737 obtained by the model trained on the un-augmented data set.

Conclusions

We proposed a new data augmentation technique by exploring an important differential geometry concept. Our experimental results showed that the technique can effectively improve the performance of deep learning on brain tumor segmentation.

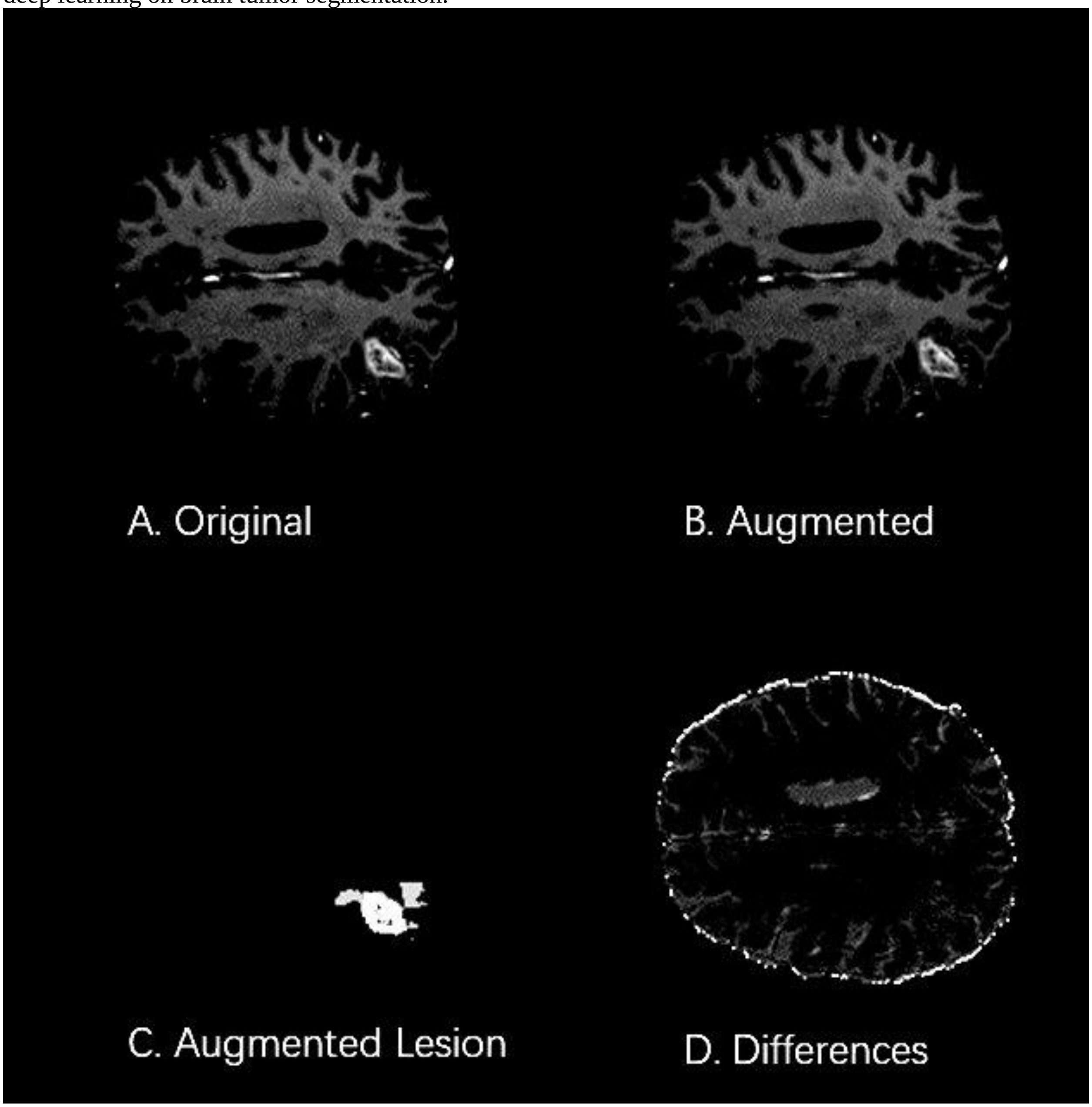

(Filename: TCT_2726_fg1_2.jpg)

3149

4:44PM - 4:51PM

Amygdala Volume in Pulmonary Hypertension: A Pilot Study Comparing to Human Connectome Project Normative Population

J Zhang[1], J Mettenburg[1], S Chan[1]
[1]*University of Pittsburgh Medical Center, Pittsburgh, PA*

Purpose
Pulmonary arterial hypertension (PAH) is a complex multifactorial vascular disease characterized by increased pulmonary vascular resistance and elevated pulmonary arterial pressure, resulting in functional limitations and eventual heart failure. Consequences include cognitive deficiencies and psychiatric disorders in approximately 50% of patients, which are not adequately explained by severity of heart failure. Previous studies have shown correlation between elevated amygdala activity, arterial inflammation, and cardiovascular event risk. This study's purpose is to find evidence of neural re-wiring in patients with PAH by analyzing amygdala volumes, using methodologies developed through the Human Connectome Project, a publicly available normative database of brain structure, function, and connectivity.
Materials and Methods
Eight subjects with PAH (ages 26-61, nonsmokers, earlier stage of disease, no other cardiovascular or autoimmune conditions) were scanned using optimized HCP MRI protocols. Four age matched HCP controls per patient were selected. Amygdala volumes were measured for patients and controls and compared using the unpaired one-tailed t-test, assuming equal variance.
Results
Average volume of the patient population was 3253.96 mm3 and average volume for the control population was 2986.9 mm3, with standard deviation 619.1 (p=0.03).
Conclusions
Amygdala volumes in subjects with PAH were greater than those of the control population, with preliminary statistical significance p=0.03, although small population size limits power. This finding suggests alterations in amygdala activity in the PAH disease state and supports further investigation of other regional differences as well as analysis of functional MRI, DTI, and perfusion acquired using the optimized HCP protocol.

2617

4:51PM - 4:58PM

Application of Machine Learning-based Iterative Image Reconstruction Algorithms for MRI Scan Time Reduction in Brain and Spine

L Tanenbaum[1], W Gibbs[2], B Johnson[3], I Varaganov[4], J Gomori[5], A Pais[6], T Aharoni[6], R Shreter[7]
[1]*RadNet, Inc., New York, NY,* [2]*Kech School of Medicine, University of Southern California, Los Angeles, CA,* [3]*Center for Diagnostic Imaging, St. Louis Park, MN,* [4]*Rambam Health Care Campus, Haifa, Israel,* [5]*Hadassah Medical Organization, Jerusalem, Israel,* [6]*Medic Vision Imaging Solutions Ltd., Tirat-Carmel, Israel,* [7]*Hillel Yaffe Medical Center, Hadera, Israel*

Purpose
To investigate whether accelerated brain and spine MR protocols enhanced with a machine-learning based algorithm (iQMR by MedicVision) can serve as a possible alternative to routine protocols.
Materials and Methods
Under multi-site IRB approval, seventy three patients (mean age 47+/-16 years) were scanned on clinical

1.5T MR scanners (Philips-Ingenia, n=30; Siemens-Aera, n=19; General Electric Signa-HDxt, n=10 and Optima 450w, n=14). Each patient was imaged using the site's clinical routine brain, cervical spine and lumbar spine protocols and with ~30% shorter variants with scan time trading off signal to noise ratio by modifying acquisition parameters. Images acquired with the accelerated protocols were processed with the iQMR algorithm and compared with images acquired with the corresponding routine protocols (153 brain, 43 lumbar spine and 48 cervical spine sets). Blinded, side-by-side comparisons of diagnostic quality, visual image quality, presence of artifacts and for brain, grey-white (GW) matter differentiation were performed by five experienced neuroradiologists using a 5-point Likert-scale (3= equal, >3 processed-short image is superior).

Results

The overall image quality, diagnostic quality, artifacts appearance and brain GW-matter differentiation of the short protocols were equal or better than those of routine protocols (P(brain)<0.01, n=614 reads, 5 readers; P(lumbar spine)<0.001, n=129 reads, 3 readers; P(cervical spine)<0.001, n=192 reads, 4 readers; one-sample t-test for noninferiority; noninferiority margin=0.25, alpha=0.05). Figure 1 shows comparable T2- and T2-FLAIR weighted imaging of routine and processed short protocols for cervical spine and brain, respectively.

Conclusions

Novel machine learning-based algorithms may allow the use of 30% faster MRI brain and spine protocols while maintaining image quality and diagnostic value. Significant reductions in scan time can improve the patient experience, minimize motion artifacts and repeat scan rate.

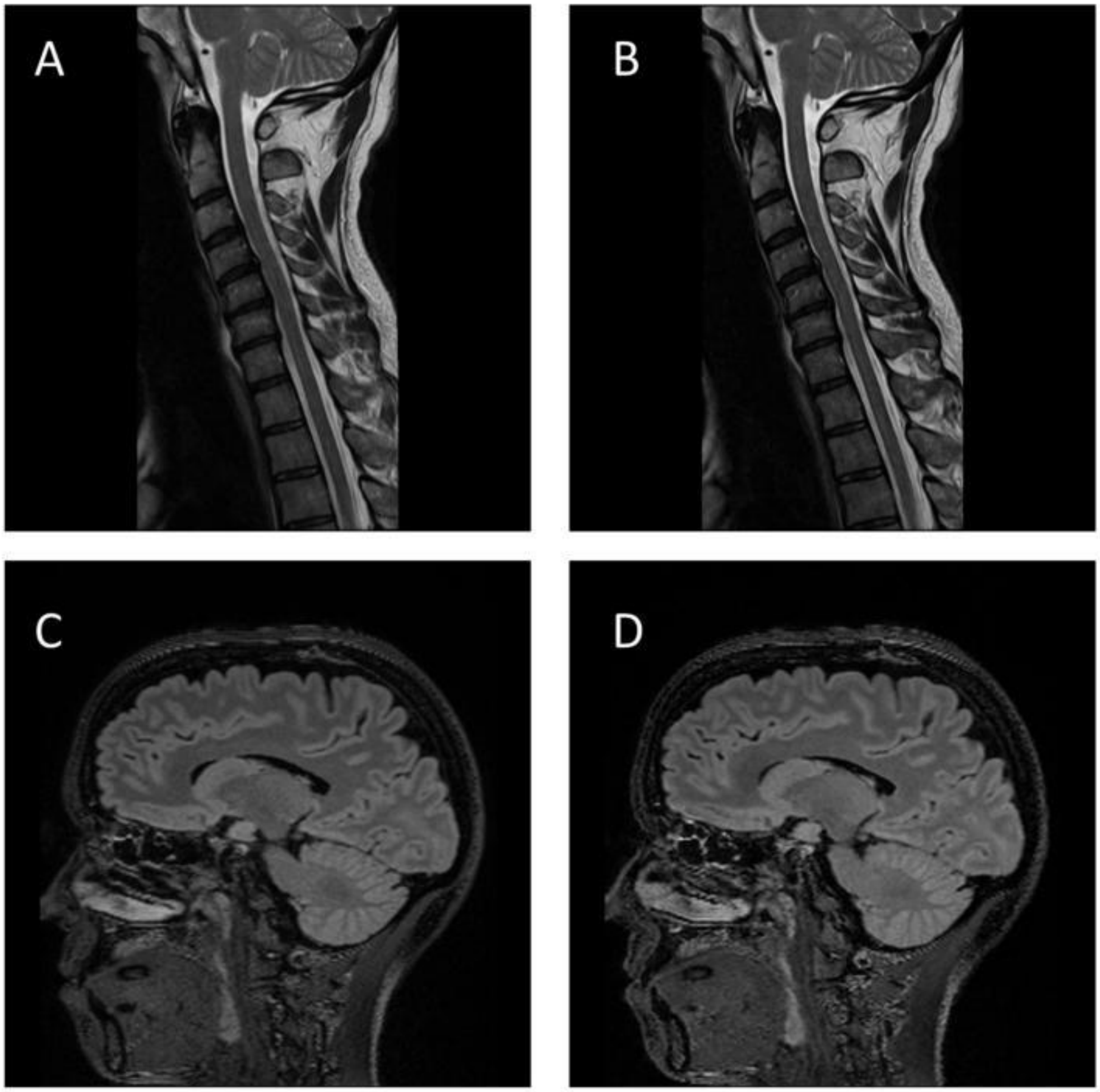

Figure 1. Conventional and processed-short protocols of cervical spine and brain 1.5T imaging. Conventional cervical spine T2w imaging (A) and brain T2 FLAIR 3D imaging (C) and the corresponding processed-short protocol variants (B and D, respectively), demonstrating comparable image quality and diagnostic suitability. Scan time of variants was reduced by 32% for cervical spine and 29% for brain.

(Filename: TCT_2617_FigureForAbstractwithtext-Final.jpg)

2170

4:58PM - 5:05PM

Automated versus Manual Imaging Assessment of Early Ischemic Changes in Acute Stroke - Comparison of two Software Packages and Expert Consensus

F Austein[1]

[1]UNIVERSITY HOSPITAL SCHLESWIG-HOLSTEIN, KIEL, KIEL, Germany

Purpose
The purpose of our study was to compare the accuracy of both the total Alberta Stroke Program Early CT Score (ASPECTS) and region-based scores from two automated ASPECTS software packages and an expert consensus reading (EC) in patients who had prompt reperfusion from endovascular thrombectomy (EVT).
Materials and Methods
ASPECTS were retrospectively and blindly assessed by two software packages and EC on baseline non-contrast enhanced computed tomography (NCCT) images. All patients had multimodal CT imaging including NCCT, CT-angiography and CT-perfusion which demonstrated an acute anterior circulation ischemic stroke with a large vessel occlusion. Final ASPECTS on follow-up scans in patients who had EVT and achieved complete reperfusion within 100 min from NCCT served as ground truth and were compared to total and region-based scores.
Results
Fifty-two patients met our study criteria. Good agreement was obtained between the software packages and EC for total ASPECTS but the two software packages differed significantly with respect to regional contribution. EC and one software package achieved a better agreement for region-based scoring and both were superior to the other software. One software more commonly identified cortical areas as abnormal and less often identified deep structures, while the other software more frequently identified deep structures as abnormal and less commonly identified cortical areas; P<0.0001.
Conclusions
Using the follow-up ASPECTS as ground truth, significant differences in accuracy were documented between the software programs.

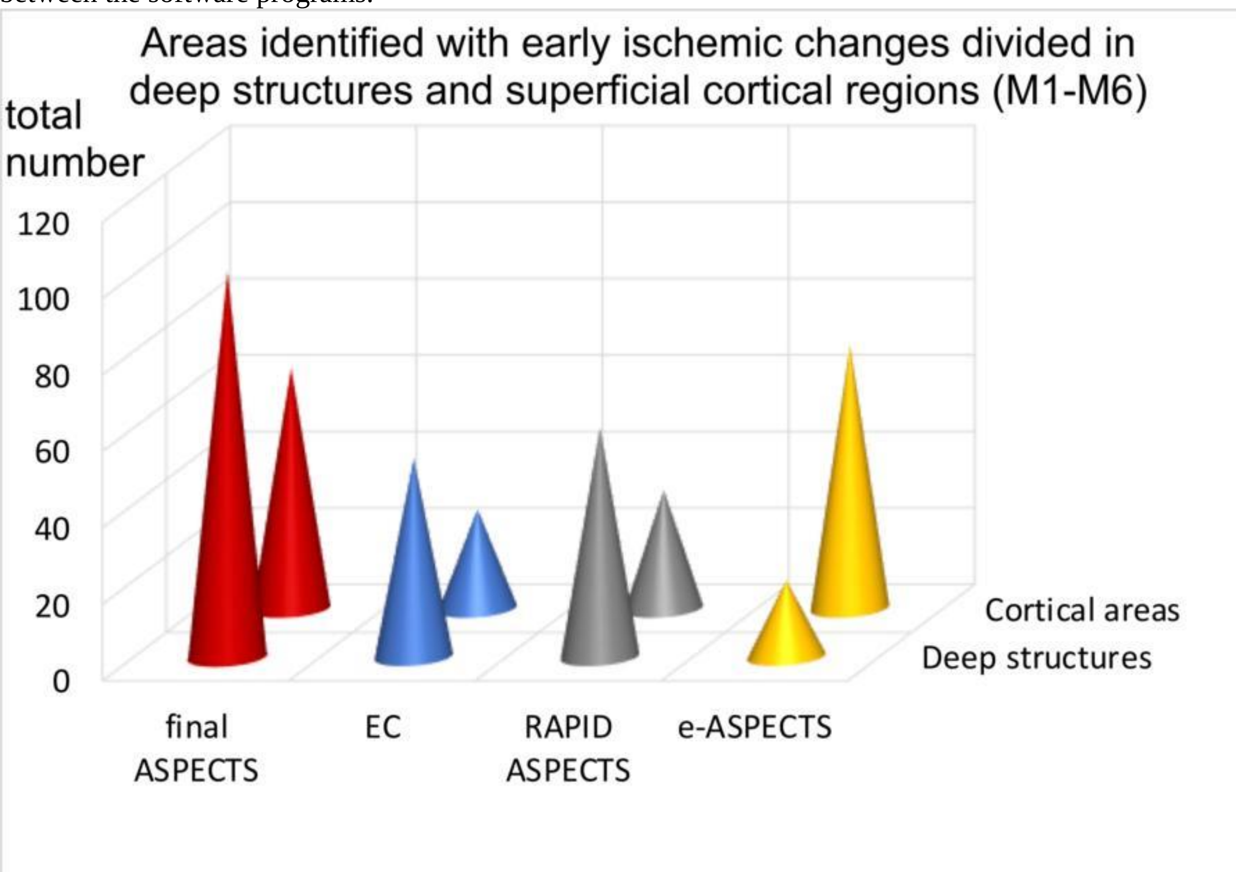

(Filename: TCT_2170_Figure4C.jpg)

2361

5:05PM - 5:12PM

Automated-ASPECTS vs. Conventional ASPECTS in Acute Ischemic Stroke: A Comparative Analysis with CBV-ASPECTS

V Sundaram[1], J Goldstein[2], D Wheelwright[3], A Aggarwal[3], P Pawha[3], A Doshi[4], J Fifi[5], R De Leacy[1], J Mocco[3], K Nael[6]

[1]ICAHN SCHOOL OF MEDICINE AT MOUNT SINAI, NEW YORK, NY, [2]Florida Atlantic University, NEW YORK, NY, [3]Icahn School of Medicine at Mount Sinai, New York, NY, [4]MOUNT SINAI ICAHN SCHOOL OF MEDICINE, NEW YORK, NY, [5]Mount Sinai Hospital, New York, NY, [6]ICAHN SCHOOL OF MEDICINE AT MOUNT SINAI HOSPITAL, NEW YORK, NY

Purpose

There is interobserver variability for ASPECT score in determination of infarct extent in patients with acute ischemic stroke (AIS). In this study using automated software trained on deep learning algorithm, we compare the performance of automated ASPECTS and conventional ASPECTS obtained from head non-contrast CT (NCCT) and compare them with concurrent CT perfusion (CTP)-based CBV ASPECTS.

Materials and Methods

In this single institutional retrospective study, patients with AIS and MCA occlusion who had baseline NCCT and CTP were included. NCCT were reviewed by 2 board certified neuroradiologists independently to assign an ASPECT score. Discrepancies were resolved by consensus. CTP-CBV maps were used for assignment of ASPECT score [1] by a different neuroradiologist. The automated ASPECTS analysis was performed using e-ASPECTS software (Brainomix, Oxford, United Kingdom), which uses a machine-learning algorithm to calculate ASPECTS from DICOM data. All ASPECT scores were also trichotomized (1: ASPECT 7-10, 2: ASPECT 4-6, 3: ASPECT 0-3). Kappa test and intraclass correlation coefficient analysis were performed between raw and trichtomized ASPECTS.

Results

A total of 59 patients (32 female, age [mean, range]: 70, 38-91) were included. The spread of trichomotized ASPECT scores were: ASPECT 7-10 (n=45), ASPECT 4-6 (n=12), and ASPECT 1-3 (n=2). Interobserver agreement between two neuroradiologists was moderate (k 0.46, 95% CI: 0.31-0.61) and slightly improved when trichomotized ASPECTS were used (k 0.56, 95% CI 0.32-0.80). Using neuroradiologists' consensus ASPECTS against CBV-ASPECTS, there was fair agreement (k 0.23, 95% CI 0.07-0.39), however this was improved to moderate when trichomotized ASPECTS were used (k 0.55, 95% CI 0.37-0.72). Using automated ASPECTS against CBV-ASPECTS, there was fair agreement (k 0.33, 95% CI 0.14-0.52), however this was significantly improved to excellent when trichomotized ASPECTS were used (k 0.75, 95% CI 0.5-1). There was good reliability across all 3 ratings (consensus neuroradiologists ASPECTS, automated-ASPECTs and CBV-ASPECTS) with intraclass correlation coefficients of 0.87, 95% CI 0.80-0.92 and of 0.80, 95% CI 0.68-0.87 for the trichomotized and raw ASPECTS respectively [2].

Conclusions

In comparison to CBV-ASPECTS, the described e-ASPECT software provides automated ASPECTS in patients with AIS with acceptable reliability and slightly improved agreement over the human interpretations. Automated ASPECTS may be used to provide standardized ASPECTS to minimize interpretation variability if its potential is realized in a larger prospective study.

	CBV-ASPECTS	
	Raw scores	Trichotomized scores
Human ASPECTS	k 0.23 95% CI 0.07-0.39	k 0.55 95% CI 0.37-0.72
Automated ASPECTS	k 0.33 95% CI 0.14-0.52	k 0.75 95% CI 0.5-1

(Filename: TCT_2361_Table1.jpg)

2766

5:12PM - 5:19PM

Comparative Study of Human Observations and Machine Learning in the Differentiation of Biopsy-Proven Pseudoprogression and True Progression in High-Grade Gliomas

S Turk[1], N Wang[2], J Kim[2], R Lobo[2], T Ma[2], T Johnson[2], A Rao[2], J Bapuraj[2], A Srinivasan[2]
[1]Ege University Hospital, Izmir, TR, [2]University of Michigan, Ann arbor, MI

Purpose
Patients undergoing treatment for high-grade gliomas may exhibit indistinguishable MRI findings of true tumor progression from pseudoprogression. We employed to shape and texture features on a machine learning algorithm to make accurate predictions compared to human observations.
Materials and Methods
Three consecutive studies prior to a definitive biopsy in 50 high-grade glioma patients who underwent treatment were evaluated. The last study before revision surgery with a known pathology result (12 pseudoprogression and 38 true progressions) was chosen as the final time point. Pre-post-contrast T1, T2, FLAIR, ADC, CBV, CBF, K2, MTT maps were reviewed by 2 neuroradiologists. Patterns of enhancement, ADC maps, CBV, CBF, MTT, K2 values, perifocal FLAIR signal intensity changes were recorded. Odds ratios (OR) for each statement, raters' success of predicting true and pseudoprogression and inter-observer reliability were calculated with R statistics software. To compare the texture parameters and histogram parameters of pseudo and true progression groups, the unpaired Student's t-test and receiver operating characteristic (ROC) analysis were applied. All first-order and second-order image texture features and shape features were used for training and testing Random Forest classifier (RFC).
Results
For the first visit, none of the observers could identify true progression. For the first and second visits, the rater's success of prediction for the visits before biopsy were %72 and %62. The AUC for the same visits with RFC was %81, the success by using first order texture analysis alone was between %61 and %68. For the first visit, the AUC of the RFC model was %70 where second-order texture analysis could distinguish the groups between %65 and %67.
Conclusions
Radiologists success by using both conventional MRI and perfusion maps was lower than RF classifier success using conventional MRI images alone. Second order texture features were useful to make better predictions than human raters.

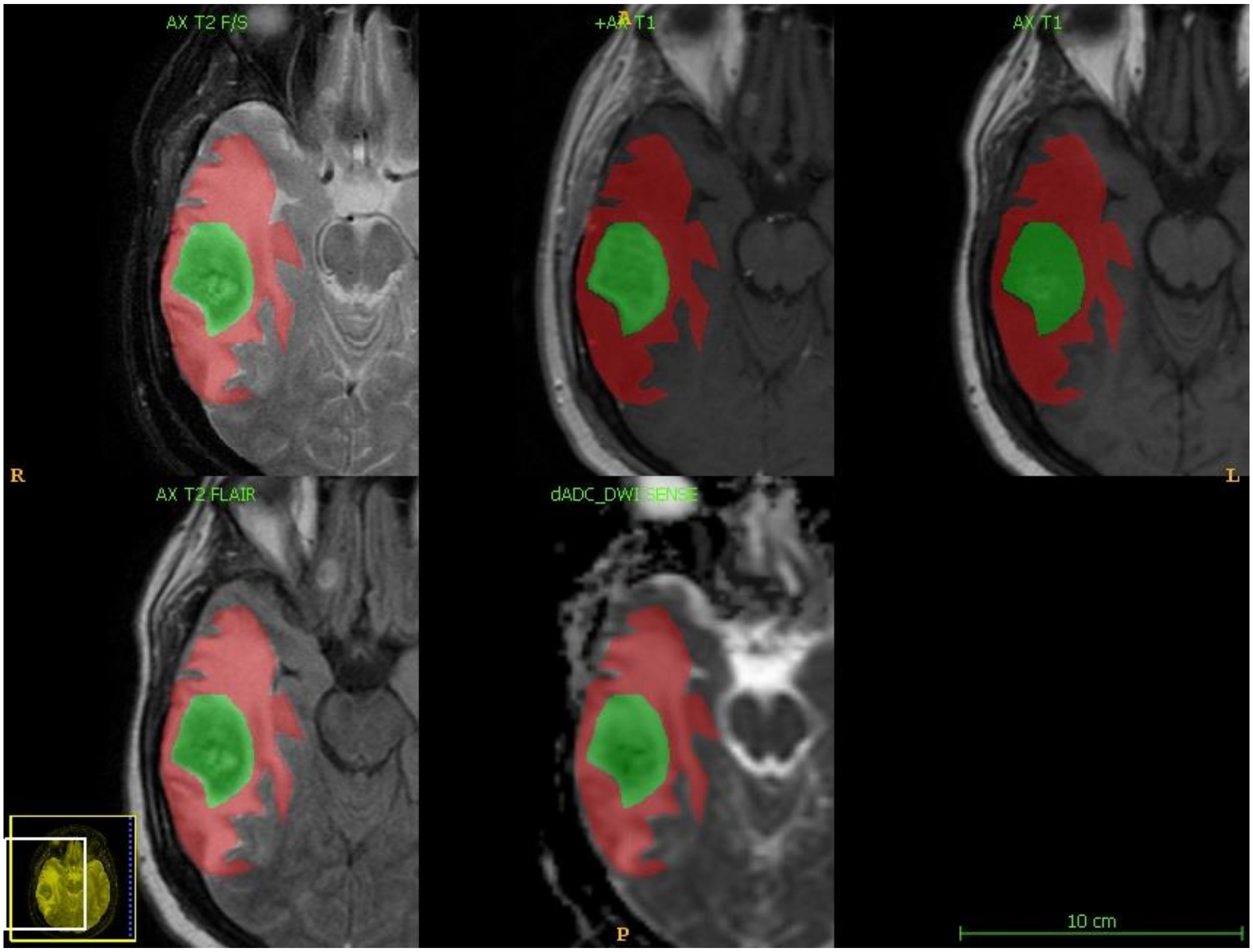

(Filename: TCT_2766_102.jpg)

3571

5:19PM - 5:25PM

Deep Learning For Ischemic Core Prediction With CT Perfusion

P Chang[1], D Chow[2], K Nael[3]
[1]UNIVERSITY OF CALIFORNIA IRVINE, IRVINE, CA, [2]UNIVERSITY OF CALIFORNIA, IRVINE, IRVINE, CA, [3]ICAHN SCHOOL OF MEDICINE AT MOUNT SINAI HOSPITAL, NEW YORK, NY

Purpose
CT perfusion (CTP) is critical in selection of stroke patients for revascularization. Traditional CTP analysis is based on deconvolution of raw data with an arterial input function (AIF) however rely on single value decomposition which is sensitive to image noise and artifacts. In addition, the calculated maps only indirectly reflect underlying tissue infarct. This study evaluates the use of convolutional neural networks (CNN) directly on raw CTP data to derive predictions maps for final core infarct.
Materials and Methods
After IRB approval, patients with proximal arterial occlusion (carotid/MCA) stroke were identified with: (1) baseline CTP; (2) successful recanalization defined by TICI ≥ IIb via mechanical thrombectomy; (3) follow-up DWI within one-week. Final DWI core infarct volumes were nonlinearly coregistered to raw CTP. AIF curves were derived using ICA/MCA masks generated by a previously described CNN algorithm. All CTP data was motion-corrected, normalized and resampled to 27 time points. 13x13 voxel

CTP patches with AIF curves were together used as input into a 5-layer 3D CNN for prediction of final core infarct (Figure 1A).

Results

A total 200,000 CTP patches originating from 28 stroke patients (70.0 ± 66.4 years old) were obtained. The median National Institute of Health Stroke Scale (NIHSS) was 15 (10-21) and time from CTP to recanalization was 1.7 hours (1.3-2.5). Upon five-fold cross-validation, the CNN predicted final core infarct volume with a median Dice score on 0.631 (0.518-0.694) and Pearson correlation of 0.877 (0.835 to 0.920). By comparison, threshold-based rCBF<30% demonstrated a Pearson correlation of 0.755 (0.610 to 0.851). The trained algorithm required 150,000 iterations for convergence (6.4 hours) but just 5.8 seconds for inference per new patient on a GPU optimized workstation.

Conclusions

Deep learning generated infarct maps derived from raw CTP outperform standard rCBF-threshold methods for estimation of core infarct (Figure 1B-C).

Figure 1. Deep Learning Based CT Perfusion Ischemic Core Maps

(A) Final core infarct on DWI is coregistered to original raw CT perfusion volume. Voxel-by-voxel time series data are concatenated with arterial input function derived from CNN-generated distal ICA and proximal MCA masks. An 27-channel 13 x 13 input patch is used as input into a custom 3D CNN for prediction of final core infarct. (B) and (C) Raw original CT perfusion data (left column), deep learning generated ischemic core prediction maps (middle column) and final core infarct on DWI (right column) are shown for representative large volume (B) and small volume (C) areas of ischemia.

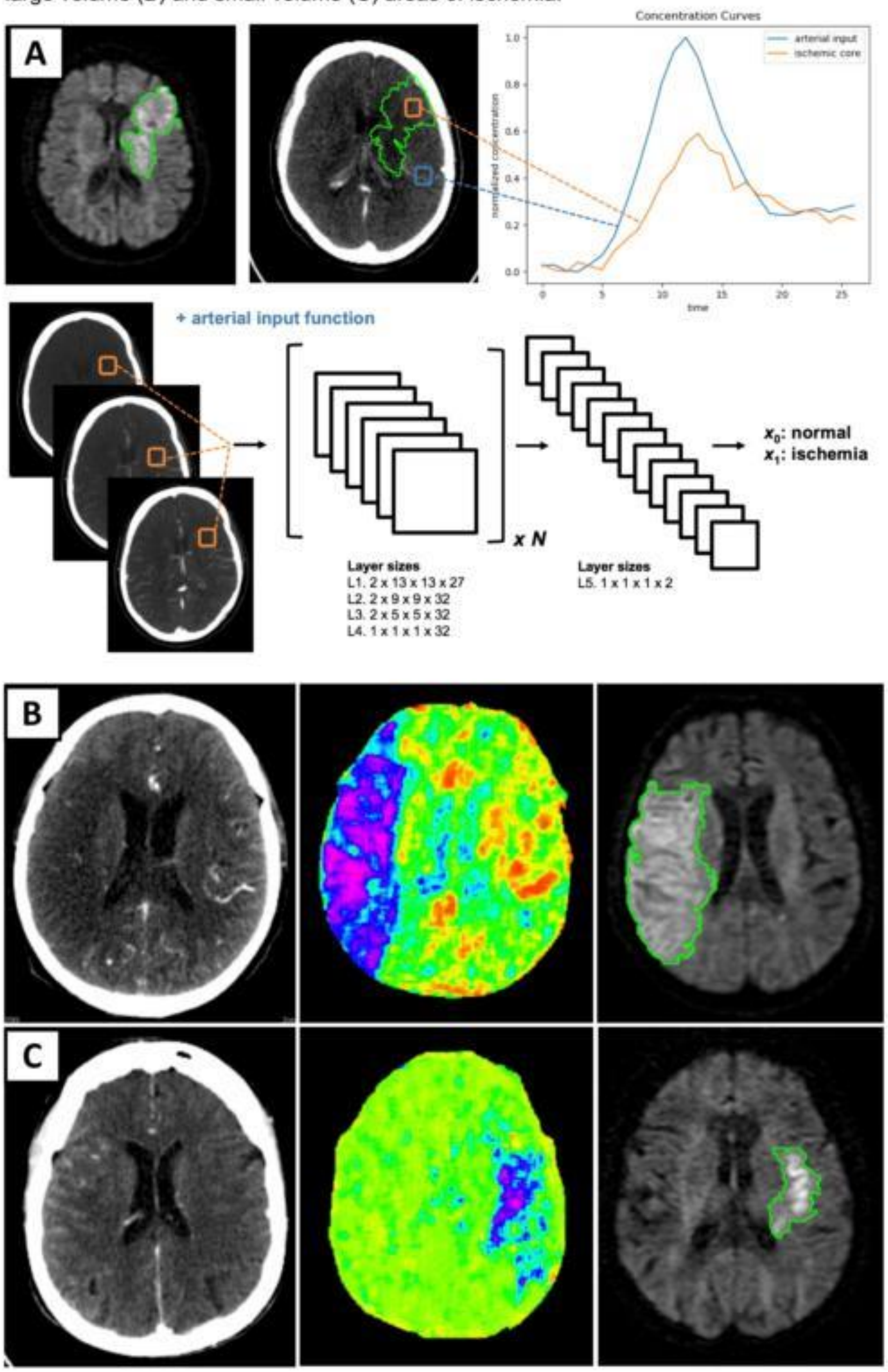

(Filename: TCT_3571_compiled.jpg)

2411

5:25PM - 5:32PM

Detecting Brain Metastases on MRI Using a Combined Deep Learning and Support Vector Machine Approach

M Zhang[1], X Wu[2], X Cao[3], L Qin[4], X Xu[1], G Young[1]
[1]Brigham and Women's Hospital, Boston, MA, [2]Tsinghua University, Beijing, Beijing, [3]Boston Children's Hospital, Boston, MA, [4]Dana-Farber Cancer Institute, Boston, MA

Purpose
This work aims to develop a deep learning technique to assist the detection of brain metastases on MRI for improving accuracy in diagnosis.
Materials and Methods
We retrospectively extracted 200 brain metastasis cases from our PACS and manually marked the lesions on T1-weighted contrast-enhanced MRI as the ground-truth. We then randomly separated the cases into training, validation, and test sets for developing and optimizing the deep learning neural network. Our proposed approach was based on a fast region-based convolutional neural network (R-CNN) as the main step of metastasis detection followed by SVM as a post-processing step to improve the results of R-CNN [1]. We used the VGG16 model that had been pre-trained on the ImageNet database as the main structure, which consists of several convolution layers and pooling layers to generate feature maps. The window of the region proposal network slid on the feature map to obtain the proposals. The results given by the neural network were then post-processed by an SVM based on multiple features to further improve the overall performance of the whole pipeline by reducing false positives.
Results
We trained our approach on 80 brain scans and then tested its performance on 20 brain scans. Our results, as shown in Figure 1, proved that the proposed deep learning approach achieved 82% recall and 67% precision rates. Testing results also showed that the approach can detect individual and multiple metastases, even when they were of very small sizes and weak intensities.
Conclusions
Brain metastases can be very challenging to detect in practice due to their varying sizes, intensities, and locations on different slices [2,3,4]. In the current work, our approach missed some metastatic lesions and sometimes created false positives in differentiating between metastases and small blood vessels. Our future work focuses on improving the approach through data augmentation.

(Filename: TCT_2411_BrainMetFigure1.jpg)

2885

5:32PM - 5:39PM

Fully Automated CT-based Prediction of pc-ASPECTS in Patients with Basilar Artery Occlusion

H Kniep[1], G Broocks[2], J Nawabi[3], H Leischner[4], F Flottmann[5], M Bechstein[6], M Schoenfeld[1], T Faizy[6], A Kemmling[7], J Fiehler[8], P Sporns[9], U Hanning[10]
[1]University Medical Center Hamburg-Eppendorf, Hamburg, Hamburg, [2]University Medical Center Hamburg-Eppendorf, Hamburg, Germany, [3]UNIVERSITY MEDICAL CENTER HAMBURG-EPPENDORF, HAMBURG, Germany, [4]University Hospital Hamburg, Hamburg, HH, [5]UKE Hamburg, Hamburg, HH, [6]UNIVERSITY MEDICAL CENTER - HAMBURG, HAMBURG, Germany, [7]University Hospital Münster, Münster, NRW, [8]University Medical Center Hamburg-Eppendorf, Hamburg, AK, [9]University Münster, Münster, NRW, [10]University of Hamburg-Eppendorf, Hamburg, Germany

Purpose
Acute occlusion of the basilar artery is often associated with adverse functional outcome or death. Posterior-circulation Alberta Stroke Program Early CT Score (pc-ASPECTS) allows objective quantification of ischemic changes and was shown to have predictive value for the patient's prognosis and final infarct size (1,2). However, visual assessment of pc-ASPECTS on non-contrast enhanced computed tomography (NCCT) images suffers from strong inter- and intra-reader variability and may be complicated due to artifacts and reduced imaging quality in the posterior circulation areas. We propose a machine learning approach to predict the final infarct extend based on acute NCCT images for patients with suspected ischemic posterior circulation stroke.
Materials and Methods
The analysis includes NCCT brain scans from 69 patients with acute posterior circulation ischemia and 63 healthy patients. Follow-up CT scans served as ground truth for the final infarct extend. In total, the dataset comprises 125 pc-ASPECTS areas with definite infarction in the follow-up imaging and 836 areas without infarction (Table 1). Standardized pc-ASPECTS areas (thalamus, pons, midbrain, territory of the

posterior cerebral artery, cerebellum) were derived by registering and averaging manual segmentations performed on NCCT images of the healthy subgroup. 787 quantitative image features (3) of each standardized pc-ASPECTS area were evaluated utilizing random forest algorithms with 5-fold model-external cross-validation (Figure 1).

Results

ROC AUCs of the test sets for predicting definitive infarction were 0.68 for midbrain to 0.78 for thalamus; all P-values <0.01. Specificities reached 80% at sensitivities of 60% for all pc-ASPECTS areas except for midbrain, which showed lower specificities of 60% (Figure 2).

Conclusions

Quantitative features of acute NCCT images provided high discriminatory accuracy in predicting definitive infarction in pc-ASPECTS areas. The proposed approach could facilitate reproducible analysis in research and may allow standardized pc-ASPECTS ratings for prognosis prediction and therapy planning in clinical routine.

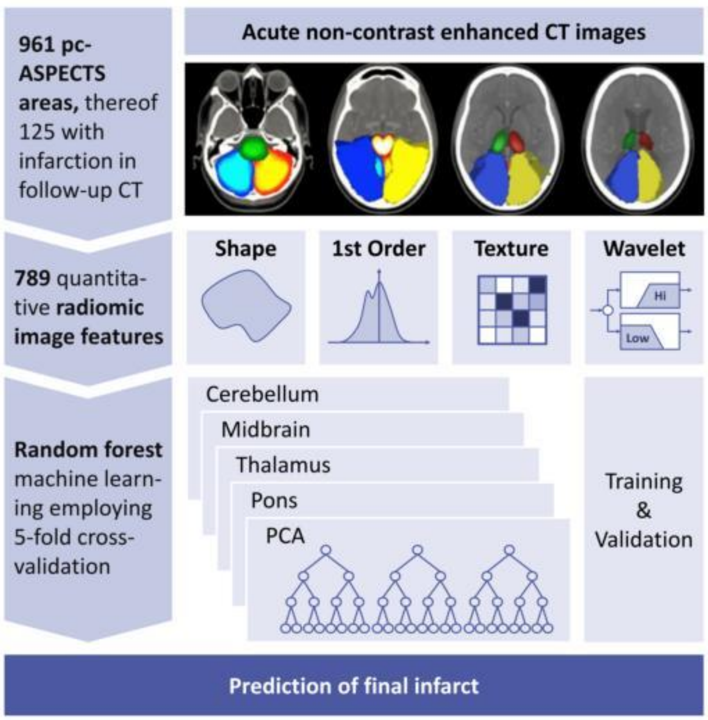

Figure 1: Conceptual overview of proposed random forest machine learning prediction of the final infarct extend based on acute non-contrast enhanced CT images of patients with suspected ischemic posterior circulation stroke. PCA: posterior cerebral artery

	FU-CT infarction		
Area	no	yes	Total
Cerebellum	147	23	170
Midbrain	111	21	132
PCA	231	33	264
Pons	108	23	131
Thalamus	239	25	264
Total	836	125	961

Table 1: Study data set. FU: follow-up; PCA: posterior cerebral artery

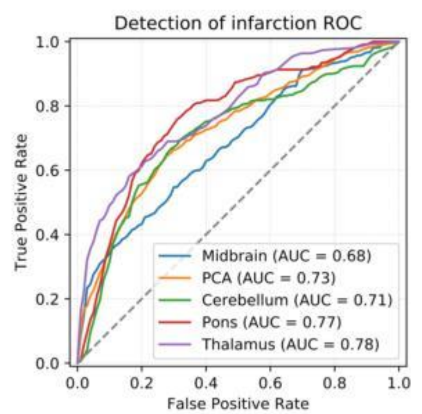

Figure 2: Test set receiver operating characteristics (ROC) of the machine learning classifiers. AUC: Area-under-the-curve; PCA: posterior cerebral artery

(Filename: TCT_2885_Figures_pcASPECTS.jpg)

2513

5:39PM - 5:46PM

Reliable Automated Segmentation of Meningiomas Using a Specially Adapted Deep Learning Model on Multiparametric MRI

Laukamp, K.
University Hospitals Cleveland
Cleveland, OH

2964

5:46PM - 5:53PM

Tumorous and Non-Tumorous Acute Intracerebral Hemorrhage in CT brain scans: Machine Learning-based Prediction of Dignity using Radiomic Image Features

H Kniep[1], J Nawabi[2], G Broocks[3], H Leischner[4], F Flottmann[5], T Faizy[6], P Sporns[7], M Bechstein[6], M Schoenfeld[1], J Fiehler[8], U Hanning[9]
[1]University Medical Center Hamburg-Eppendorf, Hamburg, Hamburg, [2]UNIVERSITY MEDICAL CENTER HAMBURG-EPPENDORF, HAMBURG, Germany, [3]University Medical Center Hamburg-Eppendorf, Hamburg, Germany, [4]University Hospital Hamburg, Hamburg, HH, [5]UKE Hamburg, Hamburg, HH, [6]UNIVERSITY MEDICAL CENTER - HAMBURG, HAMBURG, Germany, [7]University Münster, Münster, NRW, [8]University Medical Center Hamburg-Eppendorf, Hamburg, AK, [9]University of Hamburg-Eppendorf, Hamburg, Germany

Purpose
Intracerebral hemorrhage (ICH) encompasses a number of entities, of which tumors account for 10% of all ICH cases (1). Early triage of patients according to the suspected cause of hemorrhage could optimize clinical work-flows and facilitate the selection of subsequent follow-up imaging diagnostics and therapy regimes. Differentiation of tumorous and non-tumorous bleedings is often complicated due to potential masking of the underlying malignant lesion by acute ICHs (2,3). We propose a machine learning approach to predict the dignity of acute ICHs based on quantitative radiomic image features extracted from acute NCCT brain scans.
Materials and Methods
The analysis includes NCCT brain scans from 62 patients with acute ICH, thereof 40 non-tumorous and 22 tumorous bleedings. ICH and edema regions of interest were defined using semi-automatic delineation. Radiomic features including shape, histogram and texture markers were extracted from the original images and from respective wavelet filterings. A total of 3935 quantitative features (4) were evaluated utilizing random forest algorithms with 5-fold model-external cross-validation (Figure 1).
Results
Receiver operating characteristic area-under-the-curve of the test sets for predicting tumorous vs. non-tumorous ICHs was 0.89 (95% CI: 0.68-0.99; P-value <0.001). Specificities reached 86% at sensitivities of 83% at the classifier's minimum-distance operating point (Figure 2). Analyses of the 100 most important predictors showed that only 5 markers were pure ICH features, 95 of the features related to edema characteristics. 32 features were first order histogram metrics, 12 were shape metrics and 56 were texture markers. 28 features were derived from the original images, 72 from wavelet filtered inputs, thereof 41 from pure low-passes.
Conclusions
Quantitative features of acute NCCT images provided high discriminatory accuracy in predicting non-tumorous vs. tumorous ICHs. The proposed approach could facilitate early and sensitive detection of tumorous ICHs and might optimize triaging of patients for appropriate follow-up diagnosis and treatment in clinical routine.

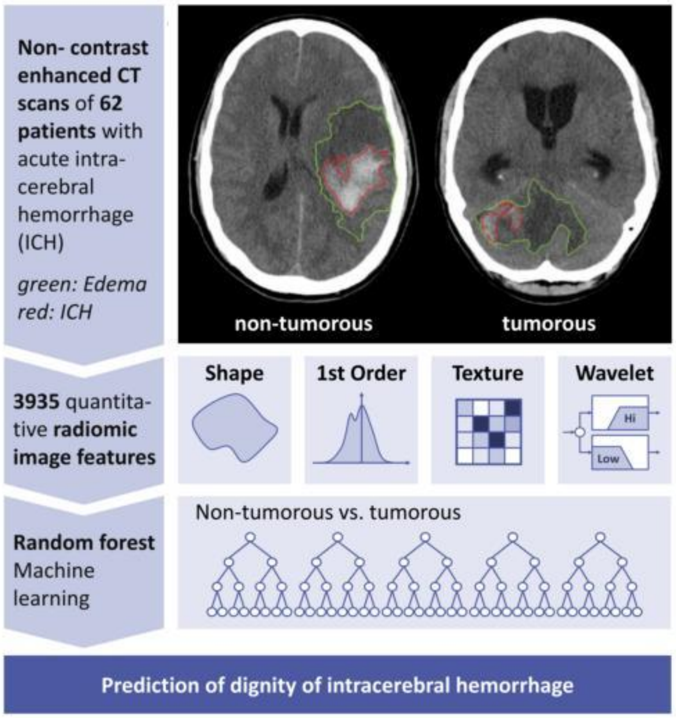

Figure 1: Conceptual overview of proposed random forest machine learning prediction of the intracerebral hemorrhage dignity (tumorous vs. non-tumorous) based on acute non-contrast enhanced CT images of patients with acute intracerebral hemorrhage

		Mean vol [mm³]		**Mean int** [HU]	
Dignity	**No**	**ICH**	**Edema**	**ICH**	**Edema**
non-tumorous	40	16,621	28,699	56.4	33.2
tumorous	22	15,119	47,903	52.1	28.5

Table 1: Study data set. No: number of patients; ICH: intracerebral hemorrhage; vol: volume; int: intensity

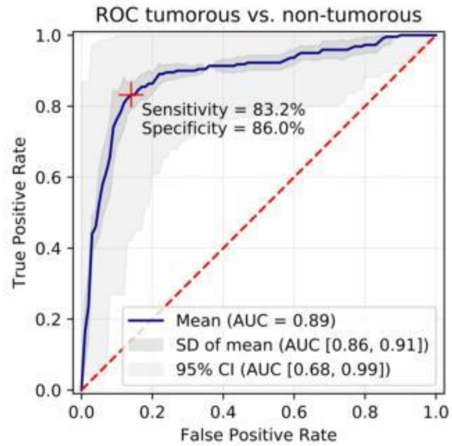

Figure 2: Test set receiver operating characteristics (ROC) of the machine learning classifier. AUC: Area-under-the-curve; SD: standard deviation; CI: confidence interval

(Filename: TCT_2964_Figure_v1.jpg)

Monday, May 20, 2019
4:30PM - 6:00PM
Neuroimaging in Brain Tumor Prognostication

3193

4:30PM - 4:37PM

2-Hydroxyglutarate/Lactate Ratio as a Biomarker Using 2-Hydroxyglutarate MR Spectroscopy: Improved Prediction of IDH Mutation Status in Glioma with Necrosis

C Suh[1], H Kim[1], S Kim[1]
[1]Asan Medical Center, Seoul, Republic of Korea

Purpose
When 2-hydroxyglutarate (2HG) MR spectroscopy (MRS) is used to predict isocitrate dehydrogenase (IDH) mutation status in glioma patients, the presence of other metabolites including lactate may present a diagnostic challenge. We assessed the incremental value of the 2HG/lactate ratio over 2HG concentration in the prediction of IDH mutation status in glioma patients.
Materials and Methods
The study population consisted of 62 consecutive histopathologically confirmed pretreatment glioma patients (WHO grades 2–4; 20 IDH mutant, 42 IDH wild-type) presenting between July 2016 and August 2018. 2HG concentration and other MRS parameters were obtained from single-voxel point-resolved

spectroscopy. The sensitivities, specificities, and areas under the curve (AUCs) of 2HG concentration and 2HG/lactate were calculated. Improvements in predictive accuracy over 2HG were determined by calculation of the net reclassification improvement (NRI) and integrated discrimination improvement (IDI). Subgroup analyses were performed on glioblastomas and lower-grade gliomas.

Results

The sensitivity, specificity, and AUC of 2HG cin the prediction of IDH mutant glioma were 95.0%, 52.4%, and 0.761, respectively, while those of 2HG/lactate were 70.0%, 95.2%, and 0.886. According to the NRI and IDI, 2HG/lactate significantly improved prediction of IDH mutation compared with 2HG alone. In glioblastoma, the sensitivity, specificity, and AUC of 2HG/lactate were 100.0%, 60.0%, and 0.767, while 2HG concentration were 83.3%, 60.0%, and 0.610, with significantly improved prediction of IDH mutant glioblastoma ($p=0.015$). In lower-grade glioma, 2HG/lactate showed comparable diagnostic performance to 2HG.

Conclusions

For noninvasive prediction of IDH mutation status, the 2HG/lactate ratio shows incremental value over 2HG, especially in glioblastomas with substantial necrosis.

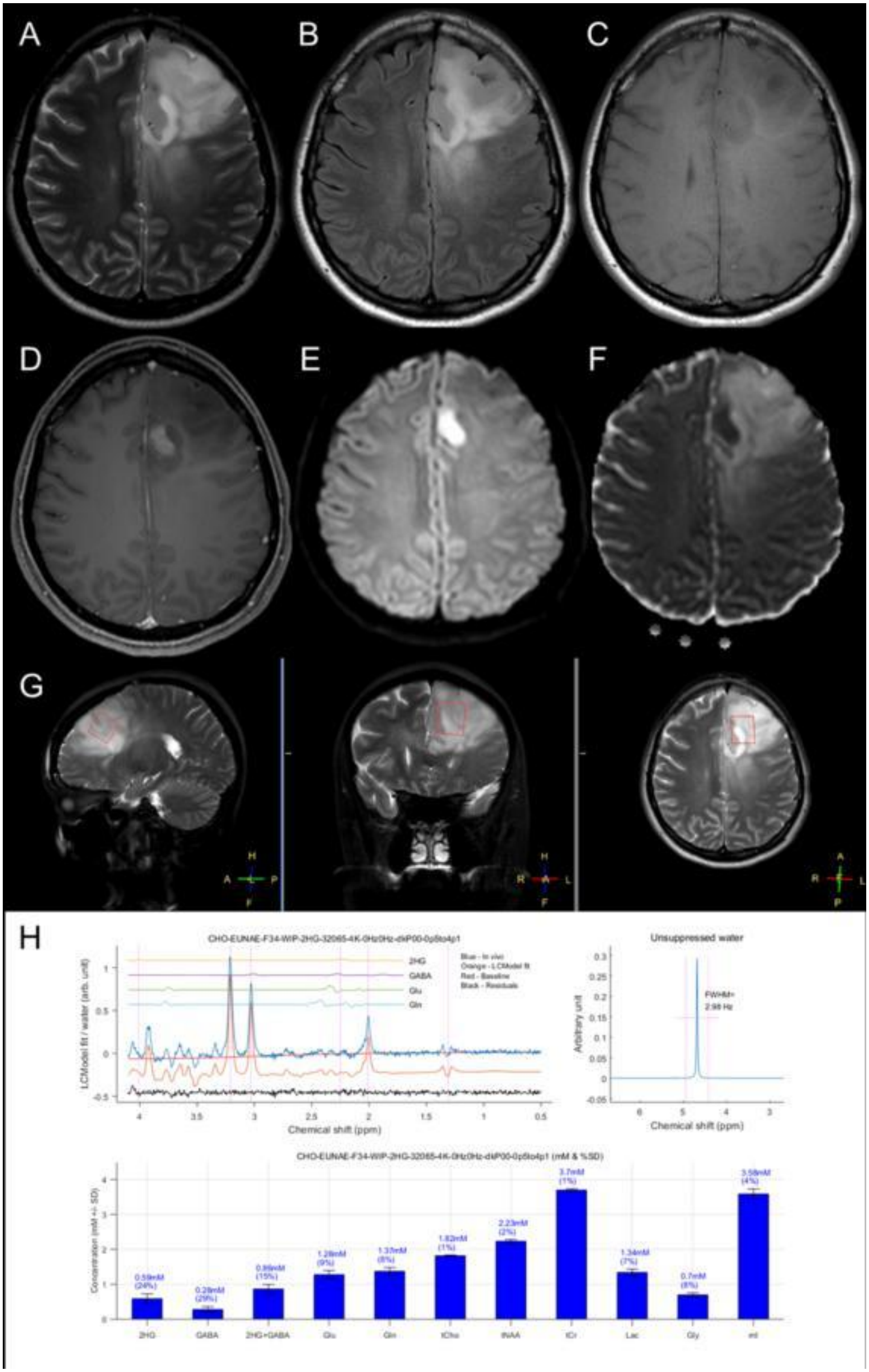
A
B
C
D
E
F
G
H
CHO-EUNAE-F34-WIP-2HG-32065-4K-0Hz0Hz-dxP00-0p5to4p1
Blue - In vivo
Orange - LCModel fit
Red - Baseline
Black - Residuals
2HG
GABA
Glu
Gln
LCModel fit / water (arb. unit)
Chemical shift (ppm)
Unsuppressed water
FWHM=
2.98 Hz
Arbitrary unit
Chemical shift (ppm)
CHO-EUNAE-F34-WIP-2HG-32065-4K-0Hz0Hz-dxP00-0p5to4p1 (mM & %SD)
Concentration (mM +- SD)
0.59mM (24%)
0.28mM (29%)
0.86mM (15%)
1.28mM (9%)
1.37mM (8%)
1.82mM (1%)
2.23mM (2%)
3.7mM (1%)
1.34mM (7%)
0.7mM (8%)
3.58mM (4%)
2HG
GABA
2HG+GABA
Glu
Gln
tCho
tNAA
tCr
Lac
Gly
mI

(Filename: TCT_3193_Figure3.jpg)

2948

4:30PM - 6:00PM

Using Brain Tumor MRI Structured Reporting to Quantify the Impact of Brain Tumor Board

S Abidi[1], M Hoch[2], R Hu[3], B Weinberg[2]
[1]Emory University School of Medicine, Atlanta, GA, [2]Emory University Hospital, Atlanta, GA, [3]Emory University, Atlanta, GA

Purpose
Tumor boards (TBs) are essential components of NCI-designated cancer centers with radiological findings being one of the major factors determining TB recommendations for management. Using a newly implemented structured reporting system for stratifying brain tumor MRIs, the brain tumor reporting and data system (BT-RADS), we prospectively assessed the association between initial radiological interpretation, its concordance with the TB consensus interpretation, and their impacts on management strategies.
Materials and Methods
Primary brain tumor cases presented at TB by three board certified neuroradiologists were prospectively collected over six months. Structured report scores were assigned as described previously and summarized in Figure 1A. Lower scores indicated a favorable ("better") interpretation with improving imaging findings whereas higher scores indicated an unfavorable ("worse") interpretation with imaging findings concerning for disease progression. Each study was assigned three scores: one on the initial radiology report, one on second review by the radiologist presenting at TB, and a third based on the TB consensus. Management recommendations were recorded.
Results
98 cases were presented. The original radiology report scores agreed with the TB consensus 78% of the time, with the consensus being better in 8% and worse in 14% of cases (Figure 1B). Scores based on the presenter's second review agreed with TB consensus 88% of the time, with the consensus being better in 5% and worse in 7% of cases (Figure 1C). The TB recommended significant management changes (new chemotherapy, radiation, surgery, or palliative care) at higher rates with higher TB consensus scores (Figure 1D).
Conclusions
TBs are critical parts of cancer care, but their impact on imaging interpretation and patient outcomes is incompletely studied. Use of a structured reporting system allowed for quantification of how frequently secondary radiologist review and tumor board consensus changed MRI interpretation and patient management. Future efforts will attempt to further characterize how these changes affect patient outcomes.

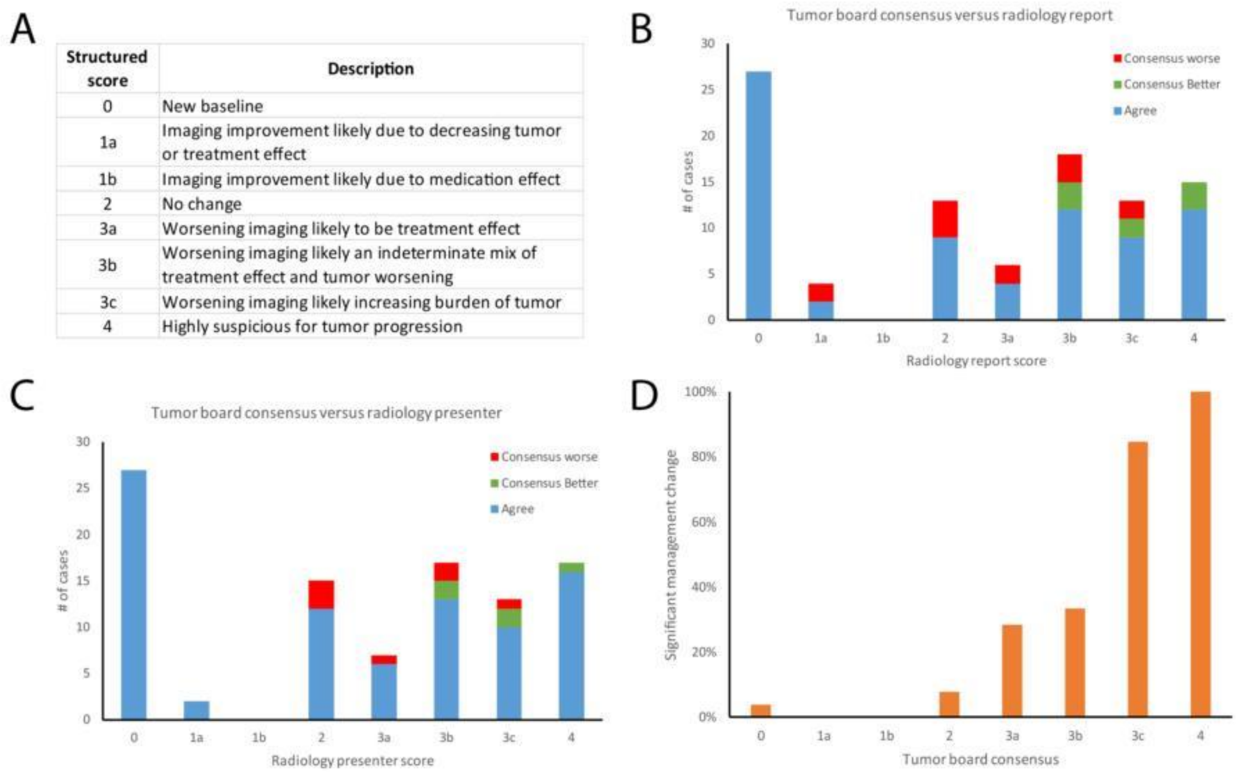

Figure 1. (A) Structured scoring categories for MRI reports. Scores assigned in the radiology report (B) or by tumor board presenting radiologist (C) with differences between tumor board consensus noted. (D) Frequency of significant management change by tumor board score.
(Filename: TCT_2948_TBabstractfigure1.jpg)

2914

4:37PM - 4:44PM

A Prospective Trial of Texture Analyses of Contrast-Enhanced T1-Weighted MRI and Dynamic Contrast-Enhanced MRI Perfusion to Predict Survival in Patients with Suspected Pseudoprogression

P Yao[1], K Nevel[2], K Beal[3], F Tixier[3], K Peck[3], C Nolan[3], H Um[3], A McKenney[4], T Kaley[3], Y Choi[3], I Gavrilovic[3], H Veeraraghavan[3], R Young[3]
[1]Weill Cornell Medical College, New York, NY, [2]Indiana University Health, Indianapolis, IN, [3]Memorial Sloan Kettering Cancer Center, New York, NY, [4]NewYork-Presbyterian Hospital/Weill Cornell Medical Center, New York, NY

Purpose
Pseudoprogression may present as transient new or increasing enhancing lesions that mimic tumor progression in brain tumors treated with radiation therapy (RT). Pseudoprogression portends a better prognosis, which is likely related to accelerated and more efficient tumor cell killing [1]. Accurate differentiation between pseudoprogression and tumor progression is essential for optimal treatment. We hypothesize that texture analyses of contrast-enhanced T1-weighted MRI (ceT1WI) and dynamic contrast-enhanced (DCE)-MRI perfusion will help identify pseudoprogression and predict patient survival.
Materials and Methods
Patients with indeterminate enhancing brain lesions on conventional MRI after RT underwent brain DCE-

MRI in a prospective trial. Lesion outcomes were determined by histopathology or follow-up. Using in-house software, we extracted 147 texture features from volumes of each lesion on 3 sequences: ceT1WI and volumetric plasma volume (Vp) and time-dependent leakage constant (Ktrans) maps calculated from DCE-MRI. The most relevant textures were sorted using LASSO analysis and correlated with lesion outcome and patient survival. Significance was set to p=0.05.
Results
We analyzed 91 lesions: 41 (45%) lesions were pseudoprogression and 50 (55%) lesions were tumor progression. 48 lesions were gliomas and 43 were brain metastases. Four of the 16 features selected by LASSO correlated with patient survival: standard deviation of Sobel ceT1WI (p=0.001), skewness of Gabor Ktrans (p=0.03), standard deviation of Laplacian of Gaussian (LoG) Vp (p=0.04), and skewness of LoG Vp (p=0.04). The standard deviation of Sobel ceT1WI remained significant after false discovery rate correction for multiple comparisons. None of the features were able to differentiate pseudoprogression from tumor progression (p>0.16).
Conclusions
A texture feature derived from ceT1WI, the standard deviation of Sobel ceT1WI, was correlated with overall survival in patients with indeterminate enhancing brain lesions after RT and remained significant after multiple comparison correction. This suggests a role for texture analysis to help inform patient prognosis.

3381

4:44PM - 5:51PM

A UK Survey of Neuro-Oncology Imaging Practices in the Management of Glioblastoma

A Luis[1], A Pandey[2], K Ashkan[3], L Brazil[4], T Booth[3]
[1]St George's University Hospitals NHS Foundation Trust, London, United Kingdom, [2]Peterborough City Hospital, North West Anglia NHS Foundation Trust, Peterborough, United Kingdom, [3]King's College Hospital NHS Foundation Trust, London, United Kingdom, [4]Guy's and St Thomas' NHS Foundation Trust, London, United Kingdom

Purpose
MRI remains the imaging investigation of choice for the management of glioblastoma. Once treatment is initiated, appropriate and timely neuroimaging in the follow up period is believed to be crucial in making subsequent management decisions. On review of current UK, European and international guidelines [1-5], there is a lack of evidence-based consensus on the optimal frequency, timing and type of neuroimaging during the post-treatment follow up period. The aim of this study was to determine the current neuro-oncology imaging practices following treatment for glioblastoma in the UK.
Materials and Methods
We invited each lead oncologist, neuroradiologist and neurosurgeon providing the neuro-oncology expertise in every neuro-oncology centre within the UK to complete an online survey using evidence-based methodology to maximise yield. Participants were asked about current imaging practices at their institution following initial treatment for glioblastoma and ideal practice (defined as practice without time or cost constraint).
Results
Ninety-two participants (100%; one expert covered two centres) from all 31 neuro-oncology centres completed the survey. Almost all the centres (94%, 29/31) stated that they routinely perform an early post-operative MRI (EPMRI) on patients after debulking surgery. Half the centres (15/31, 48.4%) reported performing an MRI prior to commencing radiotherapy. Most centres (20/31, 64.5%) reported a standard imaging protocol during adjuvant temozolomide (TMZ) treatment, whilst few centres reported that they avoided scanning during this period altogether (3/31, 9.7%). The first MRI examination following completion of concomitant radiotherapy and TMZ was performed at one month in 38.7% (12/31) of centres. Following completion of adjuvant TMZ, scans were conducted at three-monthly

intervals for the initial 1-2 years, before increasing to longer intervals thereafter in fifteen centres (15/31, 48.4%).
Conclusions
Significant variations in imaging practices exist in the frequency and timing of interval scanning after initial treatment of glioblastoma within the UK. There is a clear need to standardise this with direct benefit to the patients as well as potential significant cost savings to the NHS.

2911

4:51PM - 4:58PM

Lower Grade Diffuse Gliomas: Diagnostic and Prognostic Value of 500 Gene Panel Assay and Associated Imaging Phenotypes

M Chan[1], S Cha[2]
[1]University of California, San Francisco, Toronto, Ontario, [2]University of California San Francisco, San Francisco, CA

Purpose
Diffuse gliomas represent a heterogeneous group of brain tumors associated with various genetic mutations and imaging phenotypes. While IDH-status has become a defining diagnostic and prognostic marker for diffuse gliomas, predicting outcomes in this group of tumors remains challenging. We hypothesize that a combination of genetic and imaging factors may aid in predicting survival in patients with diffuse gliomas.
Materials and Methods
We performed a retrospective review of patients with a histopathologic diagnosis of grade II or III diffuse gliomas who underwent tissue based 500 gene panel assay, a cutting-edge sequencing tumor DNA and the patient's germline (inherited) DNA. The prevalence of genetic mutations and quantitative and qualitative imaging patterns were examined and correlated with 6-month progression-free survival. All patients had brain MR imaging without and with contrast including susceptibility-weighted, diffusion-weighted and perfusion-weighted imaging.
Results
The most common mutations associated with IDH-wildtype diffuse gliomas include TERT promotor (15/32, 47%), CDKN2A/B (12/32, 38%), and combined whole chromosome 7 gain and whole chromosome 10 loss (10/32, 31%). The most common mutations associated with IDH-mutation diffuse gliomas include TP53 (34/49, 69%), ATRX (24/49, 49%), and 1p/19q codeletion (18/49, 37%). No significant difference in imaging features – including ADC values, cerebral blood flow, enhancement, susceptibility – was noted between IDH-wildtype and IDH-mutant tumors. Several genetic mutations showed a statistically significant correlation with 6-month progression free survival, including IDH, CDKN2A/B, PIK3CA, and EGFR. Enhancement was positively correlated with 6-month progression (p=0.031 for IDH-wildtype; p=0.045 for IDH-mutant). Amongst IDH-wildtype diffuse gliomas, the minimum measured ADC value was significantly lower in tumors that progressed at 6-months (791x10-6 mm2/s) compared to progression-free tumors (990x10-6 mm2/s).
Conclusions
Predicting outcomes in lower grade diffuse gliomas requires consideration of multiple genetic mutations as well as imaging features. Imaging features are not useful for predicting the molecular status of diffuse gliomas; however, tumor enhancement is a predictor of survival, independent of IDH-status. In addition, a lower ADC value is associated with progression at 6-months amongst IDH-wildtype diffuse gliomas.

2330

4:58PM - 5:05PM

MRI Derived Radiomics Features Predicts STAT3 Expression in GBM and Indicates Survival

X Du[1]
[1]*Department of Radiology, Daping Hospital, Chongqing, Chongqing*

Purpose
To build a reliable radiomics model from multiregional and multiparametric magnetic resonance imaging (MRI) for pretreatment prediction of signal transducer and activator of transcription 3 (STAT3) status in glioblastoma multiforme (GBM).
Materials and Methods
In this retrospective study, 92 GBM patients were included and 1,705 multiregional radiomics features were automatically extracted from multiparametric MRI. A radiomics model with a minimal set of all-relevant features and a radiomics model with univariately predictive and non-redundant features were built for STAT3 prediction from a primary cohort. Predictive models combing clinical factors were built and evaluated. Both radiomics models were assessed on subgroups stratified by clinical factors.
Results
The radiomics model with six all-relevant features allowed pretreatment prediction of STAT3 (AUC=0.88, accuracy=80%), which significantly outperformed the model with eight univariately-predictive and non-redundant features (AUC=0.76, accuracy=70%). Combing clinical factors with radiomics features did not benefit the prediction performance. The all-relevant model achieved significantly better performance in stratified analysis.
Conclusions
Radiomics model built from multiregional and multiparameter MRI may serve as a potential imaging biomarker for pretreatment prediction of STAT3 in GBM. The all-relevant features have the potential of offering better predictive power than the univariately-predictive and non-redundant features.

2349

5:05PM - 5:12PM

Perfusion Permeability Mismatch: A New Prognostic Factor for Glioblastoma, But Not Useful in Lymphoma

T Abe[1], M Otomo[1], M Harada[1]
[1]*Tokushima University, Tokushima, Tokushima*

Purpose
ASL offers non-invasive measurement of cerebral blood flow. Hyperintensity on ASL generally represent at contrast-enhanced (CE) area in brain tumor, but sometimes outside the CE area; we previously reported that finding was related to glioma and lymphoma, not metastasis. We studied the relationship of this finding (perfusion permeability mismatch, PPM) and prognosis of the cases with glioblastoma and primary central nervous system lymphoma (PCNSL).
Materials and Methods
This retrospective institutional review board approved study included consecutive 26 untreated cases with glioblastoma and 7 untreated cases with PCNSL who received MRI scan (GE, Discovery 750, 3-tesla) including ASL and CE-T1WI. We compared the prevalence of PPM findings and prognosis (Figure, at the bottom is MR images of glioblastoma with PPM. Arrows indicated PPM finding).
Results
The prognosis of the cases with glioblastoma showing PPM finding is better than another group (Figure, $p = 0.038$: Kaplan-Meier, log-rank test), but the cases with lymphoma didn't ($p = 0.68$). Clinical factors including sex, age, PS, KPS, eloquent area invasion, resection rate, treatment were not different ($p > 0.05$) between the two groups. Currently, IDH1 R132H immunostaining is added, and IDH 1 status of each group is also reported.
Conclusions
The combination of ASL and CE-MRI offers a useful information for the cases with glioblastoma.

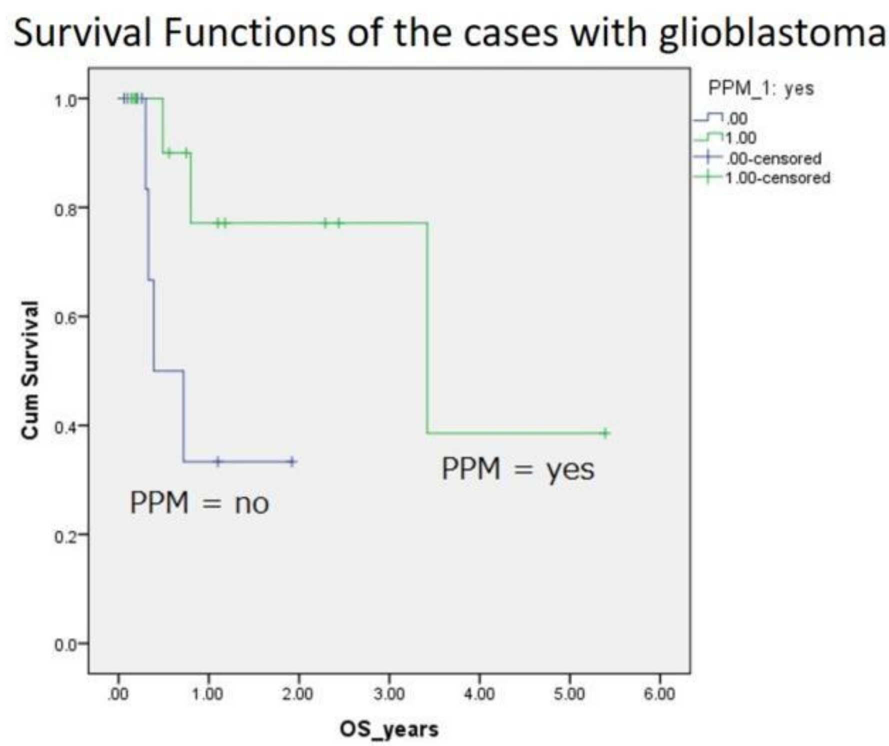

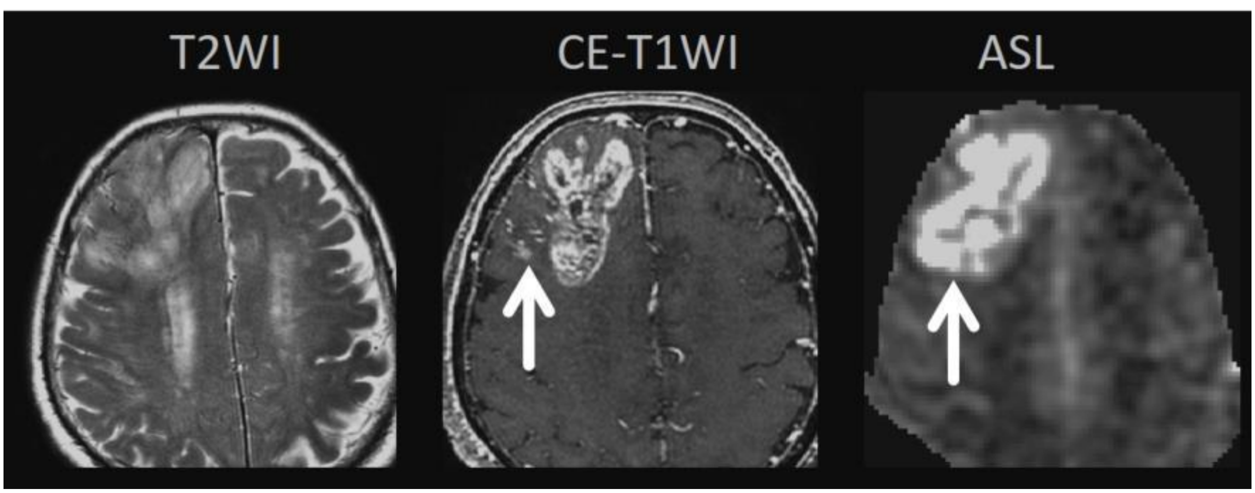

(Filename: TCT_2349_GBsurvivalPPM_.jpg)

2124

5:12PM - 5:19PM

Texture Analysis to Predict Survival in Patients with Glioblastomas Receiving Immunotherapy

E Wang[1]
[1]*Memorial Sloan Kettering Cancer Center, New York, NY*

Purpose
Immunotherapy is emerging as a successful method to treat some cancers, including glioblastomas. Enlarging lesions after immunotherapy may, however, arise from avid immune or inflammatory effects

(pseudoprogression) rather than worsening tumor. We aim to use texture analysis to improve prediction of survival in patients with glioblastomas.
Materials and Methods
We retrospectively analyzed data on 16 patients with recurrent disease who had pembrolizumab immunotherapy. Contrast-enhancing lesions were manually segmented (3D Slicer) on dynamic contrast enhanced T1-weighted perfusion magnetic resonance images (MRI) acquired before and after immunotherapy. Lesion volumes were transferred onto calculated Ktrans and plasma volume maps from corresponding MRIs. 49 texture features were extracted from an in-house software. The 3 most relevant texture features were selected using least absolute shrinkage and selection operator (LASSO) regression, segregated by median values and correlated with progression-free survival (PFS) and overall survival (OS) by Kaplan-Meier analysis, with $p<0.05$ significant
Results
Among these 16 patients, median number of glioblastoma recurrences per patient was 3 (range, 1-5); median number of immunotherapy doses was 4 (range, 2-22). Median age was 51.5 years (range, 33-77); 9 (56%) patients were female and 7 (44%) were male. Median PFS from start of immunotherapy was 2.5 (range, 0.8-5.6) months; median OS was 5.7 (range, 1.5-13.8) months. All tumors were successfully segmented. 13 (81%) of 16 patients had increased lesion volume with average volume increase of 39%. 2 of the 3 texture features extracted by LASSO selection, ("mean Gabor8" and "correlation VP") significantly correlated with survival with $p<0.03$.
Conclusions
Our series suggests that texture analysis has potential to predict survival in patients with glioblastomas. Larger prospective studies are needed to further evaluate this promising technique, including its ability to distinguish progression from pseudoprogression in immunotherapy patients with glioblastomas.

3572

5:19PM - 5:26PM

The Hemodynamic Evaluation of Arterial Spin Labeling and Dynamic Susceptibility Contrast Perfusion Weighted Imaging in Patients with Malignant Brain Tumors

X Liu[1], W TIAN[2], A hussain[3], H Wang[4]
[1]University of Rochester Medical Center, Pittsford, NY, [2]University of Rochester medical Center, Rochester, NY, [3]University of Rochester Medical Center, Rochester, NY, [4]University of Rochester Medical Cente, Rochester, NY

Purpose
The immune checkpoint blockade therapy is a novel treatment in the malignant brain tumors. However, it is reported that dramatic imaging change on conventional MRI is common in such patients after immunotherapy, which is a dilemma for accurate evaluation of treatment response. The purpose of this study is to assess changes of relative cerebral blood volume (rCBV) derived from DSC-PWI in patients with malignant brain tumors treated with immunotherapy.
Materials and Methods
MRI images of 35 patients with malignant brain tumors treated with immunotherapy were reviewed, and 13 patients with new or enlarged enhancing lesions were enrolled in this study. Pathology result or serial follow-up MRI examinations were acquired to conform the final diagnosis. The rCBV maps with contrast leakage correction were generated using FDA-approved NordicICE program. Two neruoradiologists measured the maximal rCBV ratio in these lesions suspected tumor progression, and compared the maximal rCBV ratio between the true tumor progression lesions and necrosis/pseudo-progression changes using Mann–Whitney U test.
Results
There were 22 true tumor progression lesions and 4 necrosis/pseudo-progression lesions were evaluated.

The mean maximal rCBV ratio of rCBV with contrast leakage correction of true tumor progression lesions (1.68±1.357) was higher than rCBV without contrast leakage correction (0.94 ± 0. 82, p<0.001).
Conclusions
The MR imaging changes after immunotherapy in patients with malignant brain tumors are complex, and may be mixed with active tumor component and necrosis/pseudo-progression changes. The rCBV derived from MR DSC-PWI is useful in differentiating true tumor progression lesions with necrosis/pseudo-progression in such patients treated with immunotherapy.

2847

5:26PM - 5:33PM

Tumor Genetics and Ventricular Contact as Predictors of Progression and Survival in WHO Grade II and III Gliomas

G Chiang[1], D Pisapia[2], R Magge[2], I Kovanlikaya[3]
[1]Weill Cornell Medicine, New York, NY, [2]NewYork-Presbyterian Hospital - Weill Cornell, New York, NY, [3]Weill Cornell Medical Collage, New York, NY

Purpose
Gliomas that contact the ventricular margin have a poor prognosis, possibly due to involvement of the subventricular zone. The purpose of this study was to evaluate whether ventricular contact or tumor genetics better predict progression and survival among lower-grade, WHO grade II and III, gliomas (LGG).
Materials and Methods
Forty-five patients with LGG, who had preoperative imaging and underwent next generation sequencing, were included in this study. Distance from the ependymal margin and regional ventricular contact were assessed on MRI. Progression was determined by RANO criteria. Kaplan-Meier curves and Cox regression analyses were used to determine the hazard ratios (HR) for ventricular contact and tumor genetics in predicting progression and survival.
Results
Mutations were found in 25 distinct genes. IDH1 mutation was associated with decreased risk of tumor progression (HR=0.25, p=0.001), whereas PTEN (HR=6.6, p=0.001) and EGFR (HR=3.1, p=0.011) mutations predicted increased risk. Ventricular contact in the parietal (HR=2.9, p=0.027), occipital (HR=43.5, p=0.008), and brainstem (HR=3.8, p=0.037) regions also predicted tumor progression, whereas contact in the frontal and temporal lobes and distance to the ependymal margin did not. In multivariate analysis, PTEN mutation was the strongest predictor of progression (HR=3.7, p=0.033). PTEN (HR=33.2, p=0.005), CDK4 (HR=11.2, p=0.017), and CDKN2AB (HR=13.0, p=0.006) mutations were associated with decreased survival, but ventricular contact was not. Tumor grade was not associated with progression or survival (p>0.05).
Conclusions
Both tumor genetics and regional ventricular contact were predictive of tumor progression, but tumor genetics were a stronger predictor of progression and survival.

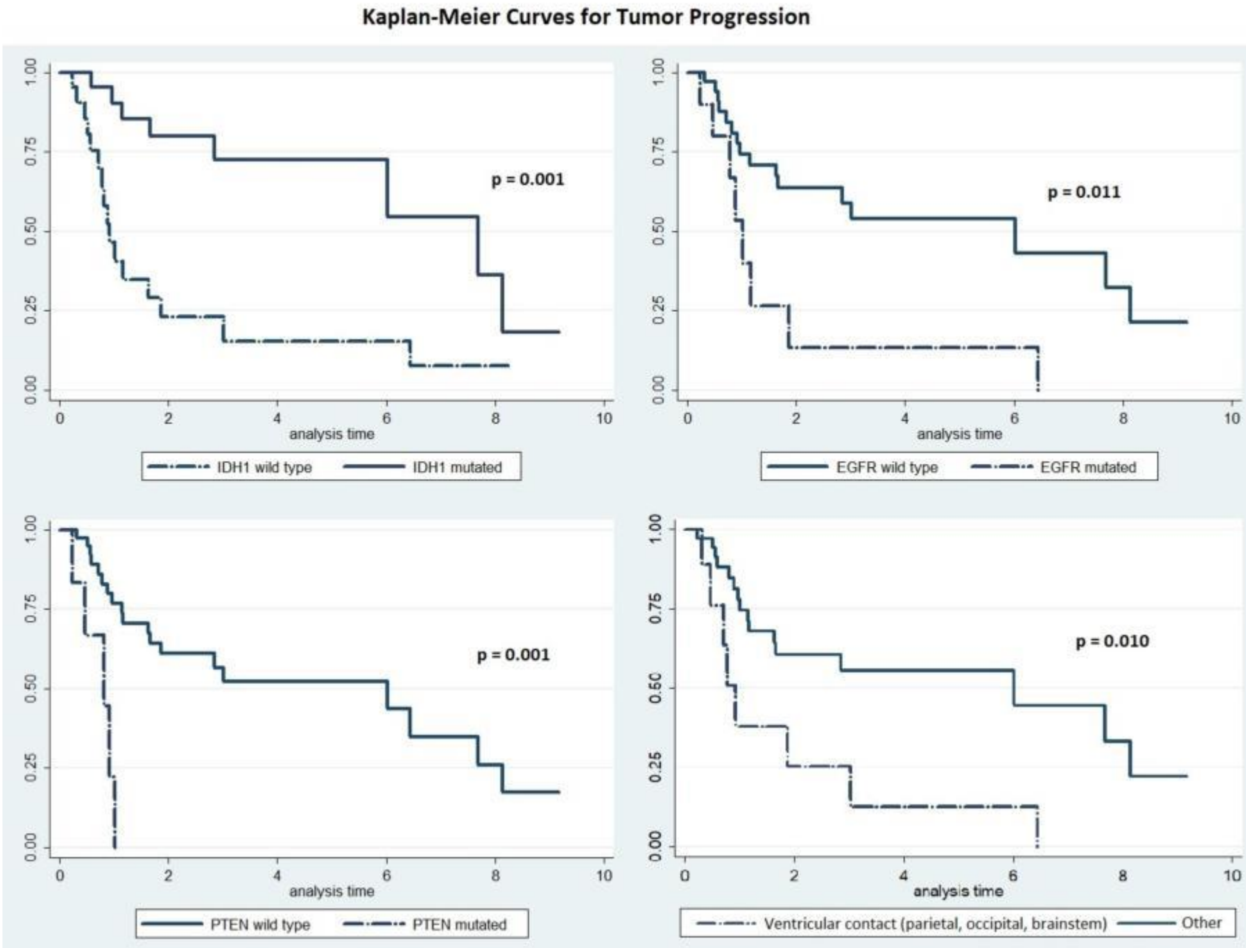

(Filename: TCT_2847_Fig1-300dpi.jpg)

2514

5:33PM - 6:00PM

Tumor Histogram Analysis with Co-Registered Diffusing-Weighted and T1 Post-Contrast MRI in Primary Central Nervous System Lymphoma Predicts Tumor Biomarkers and Outcome

I Chong[1], B Khan[1], Q Ostrom[1], A Kotrotsou[2], F Moron[1]
[1]Baylor College of Medicine, Houston, TX, [2]The University of Texas MD Anderson Cancer Center, Houston, TX

Purpose
Treatment of primary central nervous system lymphoma (PCNSL) is complicated as PCNSL in immunocompetent patients and in patients living with HIV (PLWH) are two distinct entities. The degree of Ki-67 expression, a marker of tumor proliferation, may have prognostic importance in PCNSL (1). Early studies investigating the relationships between apparent diffusion coefficient (ADC) values, Ki-67, and patient prognosis have been limited by a lack of PLWH, sample size, and the use of a single tumor region of interest rather than whole tumor segmentation (2-5). Our study aims to use a larger patient sample to investigate the correlation between ADC values and Ki-67 and the relationship between ADC values and patient prognosis.
Materials and Methods
Patients diagnosed with PCNSL at The University of Texas MD Anderson Cancer Center between Mar

2000 and Jul 2016 and at Ben Taub General Hospital between Jan 2012 and Dec 2016 were retrospectively studied. The ADC maps were co-registered with T1 post-contrast images and were analyzed by performing whole tumor segmentation using 3D Slicer. ADC values and ADC values normalized by utilizing a ratio with normal white matter (WM) were analyzed. Association between ADC measures and clinical outcomes (overall survival and response to treatment) were assessed using Cox proportional hazards models.

Results

Selection criteria yielded 56 patients, 20 PLWH and 36 immunocompetent. Higher ADC99 and ADC99/WM99 correlated with poorer survival ($p=0.0021$, $p=0.0013$) after adjusting for age, gender, HIV status, ECOG, and deep brain involvement. Ki-67 information was available on a subset of patients ($N=13$). In these patients, ADCMax/WMMax negatively correlated with Ki-67 expression ($p=0.0383$). When analyzing patients without intralesional hemorrhage ($N=8$), additional negative correlations between ADC75/WM75, ADC95/WM95, and Ki-67 expression were found ($p=0.0039$, $p=0.0073$).

Conclusions

These results confirm that radiologists can use ADC values to predict the degree of PCNSL proliferation and patient survival in both immunocompetent patients and PLWH.

3334

5:46PM - 5:53PM

Volumetric Analysis of Post-Operative Residual MR Enhancement in Glioblastoma as a Predictor of Time to Death and Time to Recurrence

M Hsieh[1], J Yu[1], F Khan[2], A Lignelli[1], V Gangaram[2], M Banu[1], B Gill[1], H Bagce[1], J Bruce[1], F Iwamoto[3], P Utukuri[1]

[1]Columbia University Medical Center - NYPH, New York, NY, [2]Columbia University College of Physicians and Surgeons, New York, NY, [3]Columbia University Medical Center - NYPH, New York City, NY

Purpose

Correlate residual enhancing MR volume after initial gross total resection and at 3 months in Glioblastoma patients with time to clinical recurrence and time to death.

Materials and Methods

An IRB-approved retrospective review from 3/2012 to 2/2017 identified 40 patients [age 24-82] with glioblastoma who underwent standard treatment with gross total resection and adjuvant temozolomide/radiation therapy. Each patient received a preoperative MRI, immediate postoperative MRI (within 24-72 hours), and follow-up surveillance MRI at 3 months post-op. T1 post-contrast enhancement volumes were segmented using 3D Slicer. The volume of residual enhancing tumor was correlated with time to recurrence and time to death.

Results

There was a negative correlation between residual enhancing MR volume after initial gross total resection to time to death ($r=-0.46$; $r2=0.21$, $p=<0.05$) and enhancing tumor volume at 3 months to time to death ($r=-0.26$; $r2=0.07$, $p<0.05$). Residual enhancing MR tumor was a poor predictor of clinical recurrence. Increase in enhancing residual tumor volume when comparing postoperative MRI to follow-up 3 month MRI volume showed a negative correlation with both time to recurrence ($r=-0.62$; $r2=0.39$; $p<0.05$) and time to death ($r=-0.25$; $r2=0.07$; $p<0.05$). The percent of tumor resection showed a positive correlation with time to death ($r=-0.26$; $r2=0.66$; $p<0.05$) but no statistically significant correlation to time to recurrence.

Conclusions

In this small cohort, residual volume of enhancing tumor after initial gross total resection and percentage of tumor resection are predictive of overall survival; however, both variables were poor predictors of time to clinical recurrence.

Monday, May 20, 2019
4:30PM - 6:00PM
Stroke: Technical Outcomes

3455

4:30PM - 4:37PM

Beyond the First Pass: Revascularization Remains Critical in Stroke Thrombectomy

G Jindal[1], H Carvalho[1], A Wessell[1], E Le[1], T Miller[1], D Gandhi[1]
[1]*University of Maryland Medical Center, BALTIMORE, MD*

Purpose
The first pass effect has been recently reported as a predictor of good clinical outcomes after stroke thrombectomy. The influence of revascularization status on these results has not been previously reported. We evaluate first pass effect on outcomes and the influence of revascularization in these and other patients.
Materials and Methods
We performed a retrospective analysis of a prospectively maintained database on anterior cerebral circulation stroke thrombectomy cases from April 2012 through April 2018. Data compiled included patient demographics, presenting NIHSS, site of vessel occlusion, thrombectomy procedural details, and 90 day mRS scores.
Results
A total of 205 patients were included. The numbers of patients who underwent 1, 2, 3, 4, 5, and 6 passes were 69, 70, 55, 9, 1, and 1, respectively. Successful revascularization was achieved in 87%, 83%, and 64% of patients in the 1, 2, and 3 or more passes groups, respectively (P=0.002). Good functional outcomes were more likely in the first pass group versus the non-first pass group (54% vs 36%; P=0.016). Good functional outcomes were more likely when comparing the 1, 2 and 3 or more passes groups (54%, 43%, 29%; P=0.014). In patients with revascularization, there was no significant difference in good functional outcomes between the 1, 2, and 3 or more passes groups (57%, 50%, 40%; P=0.274). In patients with full revascularization, there was no significant difference in good functional outcomes between the 1, 2, and 3 or more passes groups (64%, 65%, 50%; P=0.432). The number of passes was not an independent negative predictor of good clinical outcome (OR 1.66, 95% CI 0.82-3.39; P=0.165).
Conclusions
First pass thrombectomy patients have better functional outcomes compared with non-first pass patients. This effect may be related to a higher rate of revascularization in first pass patients. Revascularization beyond the first pass should continue to be the goal of stroke thrombectomy.

Table 5. Multivariate predictors of poor functional outcome (mRS >2) at 90 days in patients undergoing mechanical thrombectomy for treatment of anterior cerebral circulation occlusion.

Variable*	Multivariate Odds Ratio	95% Confidence Interval	p-value
Age	1.04	1.01-1.07	0.010
History of A-fib	1.57	0.72-3.43	0.261
Smoking History	0.77	0.39-1.51	0.441
NIHSS	1.11	1.04-1.19	0.002
TICI			
TICI 0	Reference	-	-
TICI 1	0.93	0.06-14.86	0.956
TICI 2A	0.65	0.09-4.66	0.669
TICI 2B	0.31	0.06-1.61	0.165
TICI 2C	0.04	0.01-0.24	<0.001
TICI 3	0.09	0.02-0.46	0.004
No. Thrombectomy Passes			
1 pass	Reference	-	-
≥2 passes (BFP)	1.66	0.82-3.39	0.165

Area under the curve for final multivariate logistic regression model: 0.83

* Variables achieving p-value ≤0.15 in univariate analysis were included in final logistic regression model.

Abbreviations: A-fib, atrial fibrillation; NIHSS, National Institutes of Health Stroke Scale; TICI, thrombolysis in cerebral infarction; BFP, beyond-first pass.

(Filename: TCT_3455_Table5.gif)

2702

4:37PM - 4:44PM

Clinical Implementation of Fast Markerless Motion Correction in K-Space of Structural 3D MR-Images of the Brain

J Slipsager[1], S Glimberg[2], D Gallichan[3], R Paulsen[1], L Højgaard[4], O Olesen[2]
[1]Technical University of Denmark, Kgs. Lyngby, Denmark, [2]TracInnovations, Ballerup, Denmark, [3]Cardiff University, Cardiff, Wales, [4]Rigshospitalet, Copenhagen, Denmark

Purpose
In this work, we demonstrate the combination of retrospective k-space correction using motion data recorded with an external marker-less motion tracker to demonstrate its potential for clinical use.
Materials and Methods
The markerless head motion tracking system "Tracoline" TCL 3.1 (TracInnovations)[1,2] was set up on a Siemens mMR Biograph 3T scanner to give precise head motion estimates of a healthy volunteer who has given written informed consent for participation. A 3D-MPRAGE scans of the volunteer's head were acquired with a 16-channel head-coil. During the scan, the volunteer was instructed to perform slow continuous head rotation. Retrospective correction was implemented using a freely available software package[3]. Each line of raw k-space data was temporally matched to the nearest motion-estimate available from the TCL system. Rigid-body correction was applied by additional phase-ramps to account for translations and using a non-uniform FFT implementation to account for rotations.
Results
Figure 1 shows the estimated head motion of the volunteer performing the slow head rotations. Image reconstruction from the raw data, with correction takes 2 minutes on a desktop PC with an Intel® Core™ i7-8700K running at 5GHz with 16GB RAM. The resulting images are in shown Figure 1, where the left and middle image are reconstructed without and with motion correction (MoCo), respectively. The image to the right shows the difference between the original and the corrected image.
Conclusions
We have demonstrated retrospective MoCo in the k-space domain using an external markerless motion tracker. The image quality of the motion corrected images is significantly improved, and can be

implemented on a clinical scanner without changing the existing pulse sequence or acquisition protocol. The low reconstruction time of 2 minutes allows the radiologist to be presented with the motion corrected image in the scan session.

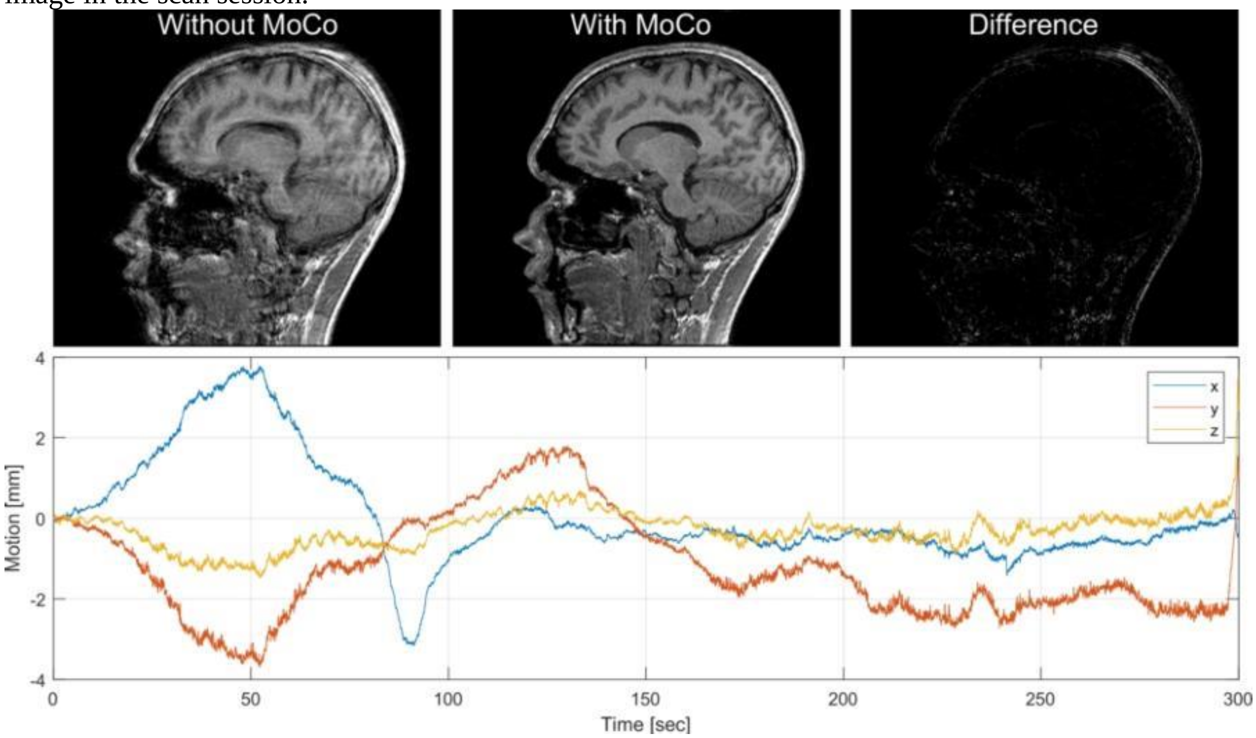

(Filename: TCT_2702_Figure1.jpg)

3441

4:44PM - 4:51PM

Effect of Endovascular Revascularization on Neutrophil-Lymphocyte Ratio and Its Relationship to 90 Days Clinical Outcome

R Abdalla[1], M Darwish[2], M Aly[1], A Muzaffar[1], A Shaibani[3], M Potts[4], M Hurley[3], B Jahromi[4], S ANSARI[5]

[1]Northwestern University, Chicago, IL, [2]northwestern university, chicago, IL, [3]Northwestern University Feinberg School of Medicine, Chicago, IL, [4]Northwestern University, Feinberg School of Medicine, Chicago, IL, [5]NORTHWESTERN UNIVERSITY, FEINBERG SCHOOL OF MEDICINE, CHICAGO, IL

Purpose

Admission Neutrophil-lymphocyte ratios (NLR) is significantly correlated with 90 days functional outcome in Acute ischemic strokes. The aim of our study is to detect post thrombectomy changes in NLR over 1 week with different degrees of revascularization and identify relationship between NLR changes and 90-day functional outcome.

Materials and Methods

We retrospectively reviewed our stroke data base from Nov 2016 till May 2018 for patients who underwent endovascular thrombectomy for anterior circulation large vessel occlusions, with an admission NLR (NLR 1) and 72 hours follow-up NLR (NLR 2) . We measured stroke severity by National Institute of Health Stroke Scale (NIHSS), degree of recanalization by modified Thrombolysis in Cerebral Infarction (mTICI) score, and outcomes by modified Rankin Scale (mRS). Univariate analysis was conducted between age, NLR1, NLR2, Change in NLR (NLR2-NLR1), NIHSS, mTICI and mRS using correlation coefficient. Change in mean NLR was assessed using Wilcoxon rank sum test. Logistic

regression models were developed to identify effect of NLR 2 on favorable outcome (mRS≤2) while controlling for age, NIHSS and IV rtPA utilization.
Results
Eighty eight patients met our inclusion criteria. Median NIHSS at admission was 18 (4-32), and 90 days mRS was 3 (0-6). 75% of patients had an increase in NLR following endovascular thrombectomy. Mean NLR 2 was significantly higher than NLR 1 (5.5 vs 3.1, p<0.001). There was a significantly negative correlation between TICI and change in NLR (p=0.002), and a significantly positive correlation between change in TICI and 90-day mRS (p=0.034), as well as NLR2 and mRS (p<0.001). High NLR2 was an independent predictor of poor functional outcome (OR=1.34, p=0.002).
Conclusions
NLR is a readily available biomarker that changes significantly with different degrees of revascularization; better recanalization is associated with lower F/U NLR. Follow up NLR is an independent predictor of good functional outcome.

3323

4:51PM - 4:58PM

Histological Clot Composition is Associated with Pre-Interventional Clot Migration in Acute Stroke Patients

U Hanning[1], A Kemmling[2], H Kniep[3], J Nawabi[4], A Jeibmann[5], J Fiehler[6], G Broocks[7], G Schön[8], W Heindel[5], P Sporns[9]
[1]University of Hamburg-Eppendorf, Hamburg, Germany, [2]University Hospital Münster, Münster, NRW, [3]University Medical Center Hamburg-Eppendorf, Hamburg, Hamburg, [4]UNIVERSITY MEDICAL CENTER HAMBURG-EPPENDORF, HAMBURG, Germany, [5]University of Muenster, Muenster, North Rhine Westfalia, [6]University Medical Center Hamburg-Eppendorf, Hamburg, AK, [7]University Medical Center Hamburg-Eppendorf, Hamburg, Germany, [8]University Hamburg, Hamburg, HH, [9]University Münster, Münster, NRW

Purpose
The introduction of stent retrievers allows for a complete extraction and histological analysis of human clots. Initial studies describe an impact of pre-interventional clot migration on technical and clinical success of thrombectomy and an association with worse clinical outcome. We therefore performed a large study of consecutive patients whose clots have been histologically analyzed and tried to determine whether clot composition influences the rates of clot migration and thereby interventional and clinical outcome.
Materials and Methods
We retrospectively evaluated data of a prospectively collected cohort of 198 consecutive patients with occlusion of the middle cerebral artery. We investigated the relationship between clot histology expressed as percentage of the main components (fibrin, erythrocytes (RBC), and white blood cells (WBC)), the pre-interventional CT attenuation of the emboli, embolus length and clot migration. We defined a binary outcome (clot migration versus no clot migration). The impact of embolus composition and CT features were assessed in univariable and multivariable logistic regression models.
Results
163 patients fulfilled the inclusion criteria, of which 36 (22.1%) showed a clot migration. Patients with proven clot migration had significantly higher levels of RBC than patients without clot migration (median 50% vs. 26%, P<0.001). Lower amounts of fibrin were significantly more often observed in patients in the clot migration group as compared to the no clot migration group (43.5% vs. 62.0%, P<0.001). Stroke etiology did not differ between migrated and stable emboli. Multivariable analysis identified a higher amount of erythrocytes (adjusted odds ratio (OR) 1.03 per median percentage, P<0.001) and a shorter embolus length (adjusted OR 0.90 per mm, P<0.008) as independent predictors of clot migration.

Conclusions
Erythrocyte-rich clots and a shorter embolus length are independent reliable predictors for clot migration. This finding is clinically important as clot migration might have negative impact on technical and clinical outcomes of patients suffering from emergent vessel occlusions of the middle cerebral artery undergoing endovascular therapy.

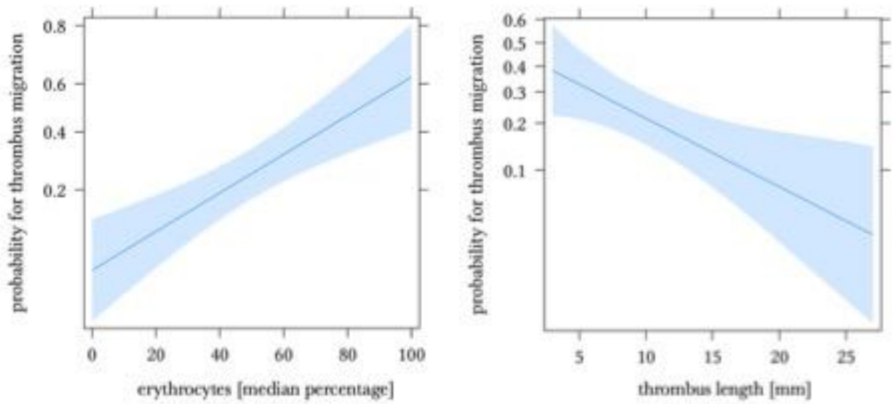

(Filename: TCT_3323_effectsoferythrocytesandclotmigration.jpg)

3228

4:58PM - 5:05PM

Impact of Vascular Anatomy on Clinical and Radiological Outcome of Endovascular Treatment of Acute Ischemic Stroke Patients

G Holswilder[1], M Stuart[1], T Dompeling[1], N Kruyt[1], M Wermer[1], M VAN WALDERVEEN[2]
[1]Leiden University Medical Centre, Leiden, Zuid-Holland, [2]LUMC, Leiden, South-Holland

Purpose
To investigate to what extent aortic arch and carotid artery anatomy relate to clinical and radiological outcome after EVT of acute ischemic stroke (AIS) patients.
Materials and Methods
CTA images of 891 patients included in the MR CLEAN Registry, a large prospective Dutch registry of AIS patients treated with EVT, were evaluated with regard to aortic arch configuration (variants and elongation), carotid artery tortuosity (number and degree of angles) and atherosclerosis. Logistic prediction models were developed including patient characteristics and baseline radiological findings. Subsequently, added value of vascular parameters for prediction of clinical and radiological outcome was assessed using likelihood ratio test for increase in area under the curve (AUC). Effect estimates were used to create risk prediction charts.
Results
Regarding clinical outcome, the AUC of 0.79 (95% CI, 0.76-0.82) of the baseline model slightly increased with addition of vascular parameters (AUC of 0.80 (95% CI, 0.77-0.83; $p<0.05$)). For reperfusion, adding vascular parameters increased AUC from 0.54 (95% CI, 0.50-0.58) to 0.60 (95% CI, 0.57-0.64)($p<0.05$). For EVT discontinuation (target occlusion not reached) AUC of 0.72 (95% CI, 0.65-0.79) was improved to 0.82 (95% CI, 0.77-0.88)($p<0.001$). The risk prediction chart for EVT discontinuation showed that predicted probability increased substantially in the presence of vascular characteristics; this increase was most pronounced in the elderly patient (> 80 years of age) where predicted probability increased from 0.02 to 0.86 in the presence of complex aortic arch configuration, carotid artery tortuosity and ≥70% carotid artery stenosis.
Conclusions
Clinical outcome of AIS patients after EVT is largely predicted by patients' baseline characteristics.

Prediction of reperfusion is improved with addition of vascular characteristics, but remains poor. Impact of vascular anatomy is most pronounced for prediction of EVT discontinuation. This latter finding could have implications for treatment decision in patients with complex vascular anatomy.

2930

5:05PM - 5:12PM

Intraprocedural Time Accounts for Majority of Door to Reperfusion Time During Endovascular Thrombectomy

M Gusman[1], D Cross[1], C Moran[1], J Osbun[1], A Kansagra[1]
[1]*Washington University School of Medicine, St. Louis, MO*

Purpose
Patient outcomes in acute ischemic stroke depend on time to reperfusion. Conventional quality improvement efforts have focused heavily on door to puncture time, with less emphasis on puncture to reperfusion time. We sought to understand the duration and variability of puncture to reperfusion time in order to better understand targets for ongoing quality improvement efforts.
Materials and Methods
Neurointerventional nursing staff contemporaneously recorded clinical data for all endovascular thrombectomy cases at our comprehensive stroke center (CSC) in 2017. Cases included a mix of transfer patients, primary ED patients, and inpatients. We divided patient workflow time into three stages: stage 1, arrival (for transfer patients with outside imaging) or CTA completion to table; stage 2, table to puncture; and stage 3, puncture to reperfusion. Stage 1 and stage 2 intervals are based on all patients in whom thrombectomy was intended, while stage 3 intervals are based on patients in whom thrombectomy was attempted.
Results
Of 106 patients taken to the interventional suite for thrombectomy, 86 proceeded to thrombectomy attempt and 20 underwent only diagnostic angiography. Reasons for not attempting thrombectomy included both spontaneous reperfusion and thrombus that did not appear amenable to thrombectomy. The demographics of the 86 thrombectomy patients and 20 angiography-only patients did not significantly differ from the overall group, which was: 48% were male, average age was 69 +\- 15, average NIHSS was 17 +\- 6. Median time was 40.5 min (IQR 19-67.5) for stage 1, 11 min (IQR 8-16.75) for stage 2, and 51.5 min (IQR 35-73.5) for stage 3. The median percentage of total time spent in stage 3 was 52.7% (IQR 39.5-67.1%). In a multivariate linear regression to predict the duration of stage 3, patient co-morbidities and procedure characteristics were not significant after controlling for a combination of device used, proceduralist, and anesthesia type.
Conclusions
Overall, intraprocedural time accounts for the majority of total door to reperfusion time. The magnitude of variability in intraprocedural time is comparable to that of pre-procedural time. Although pre-procedural workflows and metrics have been the traditional focus of quality improvement efforts, our data suggest that intraprocedural aspects of care represent a rich target for future study.

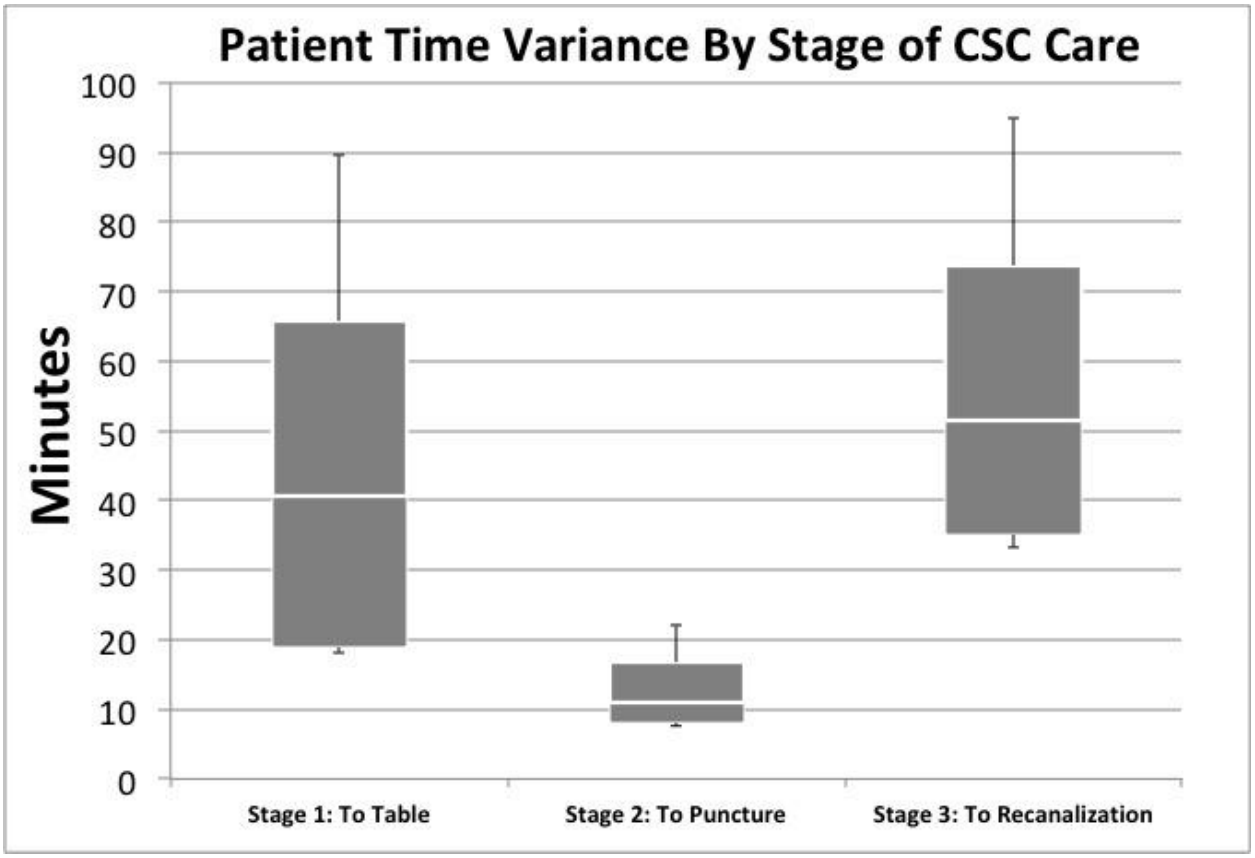

(Filename: TCT_2930_TimeVariancebyStage.jpg)

2883

5:12PM - 5:19PM

Live Streaming Technology in the Angiography Suite: Description of a Setup to Remotely Supervise and Instruct Thrombectomy

M Bechstein[1], J Buhk[2], A Frölich[2], J Fiehler[3], E Goebell[2]
[1]UNIVERSITY MEDICAL CENTER - HAMBURG, HAMBURG, Germany, [2]University Medical Center Hamburg-Eppendorf, Hamburg, Germany, [3]University Medical Center Hamburg-Eppendorf, Hamburg, AK

Purpose
Stroke patients are detained from expeditious endovascular recanalization in regions lacking neurointerventional specialists (ref. 1). We tested modern streaming technology capable of transmitting video and voice data in real time to deliver neurointerventional expertise to a distant angiography suite.
Materials and Methods
The system consists of a 360-degrees moveable and 180-degrees tiltable network camera system installed on a moveable bar in an angiography suite, capable of filming the suite and zoom in to the angiography monitor in high resolution (1080 pixel). The camera is connected to a server, which streams the video and voice data to an online platform. Using a conventional desktop computer connected to the platform via a VPN tunnel, a neurointerventional specialist not present inside the angiography suite controls the camera and interacts with the interventionalist using two-way communication.
Results
In a simulated thrombectomy scenario, the neurointerventional specialist located at a separate building was able to follow all actions inside the angiography suite in real time. Filming and streaming of the

angiography monitor was not associated with significant loss of picture quality, as the specialist could easily identify the smallest elements of the inserted endovascular devices.

Conclusions

Video and voice data in an angiography suite can be streamed successfully to a remote working space of a neurointerventional specialist, who is then able to supervise and instruct thrombectomy performed by a local interventionalist. Further studies will clarify, if application of this streaming technology facilitates stroke therapy in distant hospitals, where residing interventionalists would otherwise not be able to perform emergency thrombectomy.

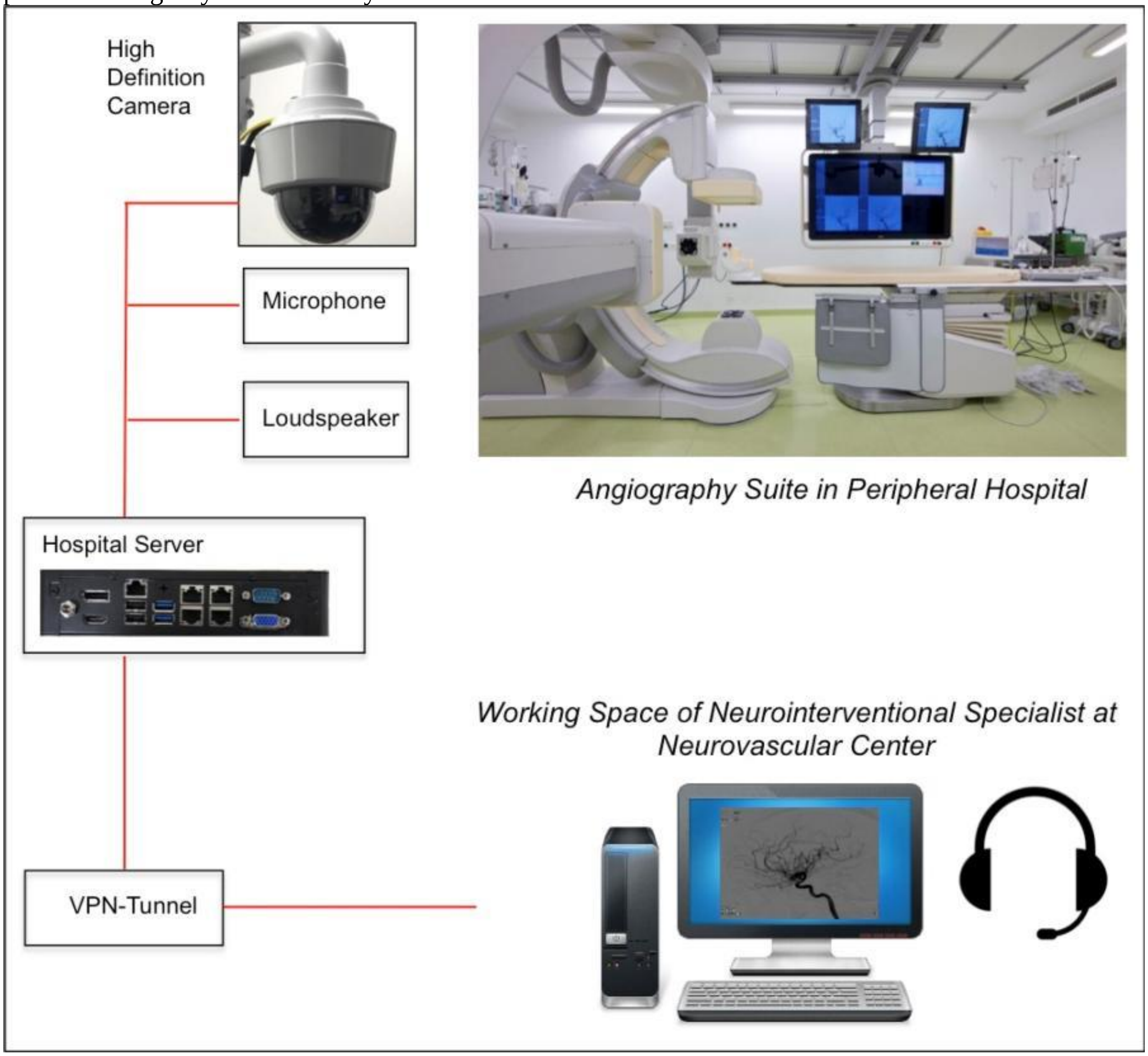

(Filename: TCT_2883_fig_setup_remote_streaming_support.jpg)

3357

5:19PM - 5:26PM

Predictors of Hemorrhagic Transformation after Successful Endovascular Recanalization of Acute Ischemic Stroke

J Nawabi[1], G Broocks[2], A Kemmling[3], F Flottmann[4], H Kniep[5], H Leischner[6], G Schön[7], G Thomalla[7], J Fiehler[8], U Hanning[9]

[1]UNIVERSITY MEDICAL CENTER HAMBURG-EPPENDORF, HAMBURG, Germany, [2]University Medical Center Hamburg-Eppendorf, Hamburg, Germany, [3]University Hospital Münster, Münster, NRW, [4]UKE Hamburg, Hamburg, HH, [5]University Medical Center Hamburg-Eppendorf, Hamburg, Hamburg, [6]University Hospital Hamburg, Hamburg, HH, [7]University Hamburg, Hamburg, HH, [8]University Medical Center Hamburg-Eppendorf, Hamburg, AK, [9]University of Hamburg-Eppendorf, Hamburg, Germany

Purpose
The aim of this study was to identify predictors for intracerebral hemorrhage (ICH) and subsequent symptomatic ICH (SICH) or asymptomatic ICH (aSICH) in patients with acute ischemic stroke undergoing successful mechanical recanalization.
Materials and Methods
107 patients with ischemic stroke with MCA occlusion fulfilled all inclusion criteria and were analyzed. All patients received successful ET (thrombolysis in cerebral infarction scale 2b/3) and subsequent follow-up CT (FCT) 24 hours later. ICH was diagnosed on non-enhanced CT and classified according to the Heidelberg Bleeding Classification. A binary outcome (ICH versus no ICH) was defined. We assessed the effect of selected demographic characteristics, clinical and imaging factors on the prediction of ICH in univariable and multivariable logistic regression models. The correlation on functional outcome at 90 days was also assessed.
Results
107 patients fulfilled the inclusion criteria, of which 37 (34.6%) showed an ICH within 24 hours after ET. According to Heidelberg Bleeding Classification 19 (17,8%) patients were diagnosed with symptomatic ICH (SICH) and 18 (48.6%) with asymptomatic ICH (aSICH). Multivariate regression analyses identified low ASPECTS (adjusted odds ratio (OR) 1.95, 95%CI: 1.4-3.63, P<0.037), low collateral score (adjusted OR 0.12, 95%CI: 0.03-0.49, P<0.003) and high Net Water Uptake (adjusted OR 1.56, 95%CI: 2.34-1.03, P <0.007) as independent predictors of HT after successful ET. Based on univariate receiver operating characteristic curve analysis, NWU above 8% predicted ICH with the highest discriminative power (area under the curve [AUC]: 0.90, 95%CI: 0.83-0.95, P <0.0001).
Conclusions
Elevated Net Water Uptake, a novel marker for ischemic brain edema, a low collateral score and low ASPECTS are independent reliable predictors for ICH after successful recanalization. This finding is clinically important, as the risk of SICH after endovascular treatment for acute ischemic stroke is significantly higher in real-world practice than reported by clinical trials. Further prospective studies are needed.

3424

5:26PM - 5:33PM

Relationship Between Device Type and Duration of Endovascular Thrombectomy is Influenced by Physician Device Preferences

M Gusman[1], D Cross[1], C Moran[1], J Osbun[1], A Kansagra[1]
[1]*Washington University School of Medicine, St. Louis, MO*

Purpose
Outcomes in patients with acute ischemic stroke depend heavily on time to acute reperfusion therapies. Several endovascular thrombectomy trials have demonstrated shorter door to reperfusion time with aspiration than with stent retrievers, but confounders of these relationship are not well studied. Here, we examine the influence of physician device preference on the relationship between device type and duration of endovascular thrombectomy.
Materials and Methods
Neurointerventional nursing staff contemporaneously recorded clinical data for all endovascular

thrombectomy cases at our comprehensive stroke center (CSC) in 2017. These prospectively recorded data were aggregated into a dedicated stroke quality database. Neurointerventional physicians freely chose thrombectomy devices as dictated by their preferences and by patient factors. Devices types were categorized as aspiration, stent retriever, or combined.

Results

Of the 86 patients who underwent thrombectomy, 47% were male, average age was 69 +\- 15, and average NIHSS was 17 +\- 6. Median procedure time was 51.5 min (IQR 35-73.5). Two of four staff used aspiration in the majority of cases (74% and 59%, respectively), while two used stent retrievers in the majority of cases (75 and 91%). A combined technique was used in a minority of cases (5-24%). Overall, aspiration produced the shortest procedure times, with a median median procedure time of 40 min (IQR 31-53). However, aspiration use by staff that were predominant users of stent retrievers had a mean procedure time of 68 minutes. Similarly, stent retriever procedure times were faster in the hands of those who preferred to use them (mean procedure times of 58 vs 80 min).

Conclusions

The relationship between thrombectomy device and overall puncture to reperfusion time is dramatically influenced by use history of staff physicians. Thus, device preference and experience may be important confounders of device type in overall time to reperfusion. These factors may thus be important to consider in observational studies and quality improvement efforts.

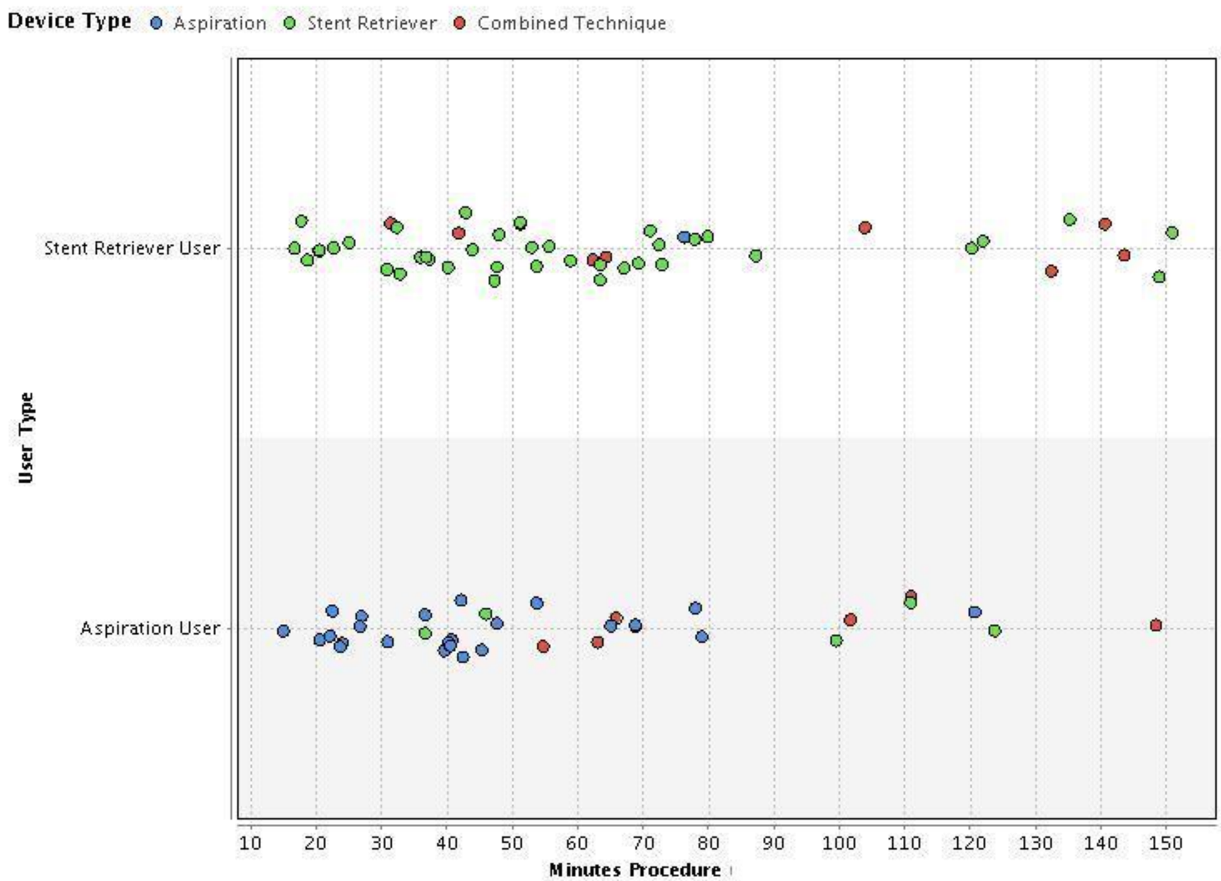

(Filename: TCT_3424_UserPreferences.jpg)

2893

5:33PM - 5:40PM

Supervision and Training of Thrombectomy by Remote Real Time Streaming Support: a Randomized Comparison Using Simulated Interventions

M Bechstein[1], J Buhk[2], A Frölich[2], J Fiehler[3], E Goebell[2]
[1]UNIVERSITY MEDICAL CENTER - HAMBURG, HAMBURG, Germany, [2]University Medical Center Hamburg-Eppendorf, Hamburg, Germany, [3]University Medical Center Hamburg-Eppendorf, Hamburg, AK

Purpose
Stroke patients are detained from expeditious endovascular recanalization in regions lacking neurointerventional specialists (ref.1). We tested a real-time on-demand streaming system, allowing a neurointerventional specialist located at a neurovascular center to supervise and instruct a thrombectomy (TE) performed at a distant hospital without being physically present (remote streaming support, RESS).
Materials and Methods
In total, 36 TE procedures were performed on a Mentice® endovascular simulator by 6 radiologists not specialized in neurointervention. Each radiologist was challenged with a TE under alternating conventional local support and remote streaming support (LOS vs. RESS). RESS was performed with a dedicated state-of-the-art online platform for visual and acoustic streaming.
Results
Both support modes lead to an average of 2 (SD +-0,4) attempts until successful recanalization. There was no difference in time from first catheter insertion to recanalization between LOS (median 1495 sec, IQR 1257-1890) and RESS (1435 sec, IQR 1301-1723). The percentage of thrombus covered by the stent-retriever was equal in both groups, as well as the average speed when retrieving the stent-retriever (3.7 mm/sec , IQR 3.25-5.35 vs. 3.6 mm/sec, IQR 2.5-4.7). Fluoroscopy time did not differ (1141 sec, IQR 1013-1411 vs. 1191 sec, IQR 954-1410) while a trend towards increased median amounts of injected contrast medium was observed under RESS (62.9 ml vs. 43.1 ml under LOS).
Conclusions
Our study proofs function of RESS in TE procedures performed in a simulated environment. Further analysis is needed to verify if this technology will facilitate continuous support of interventionalists with limited TE experience in remote areas.

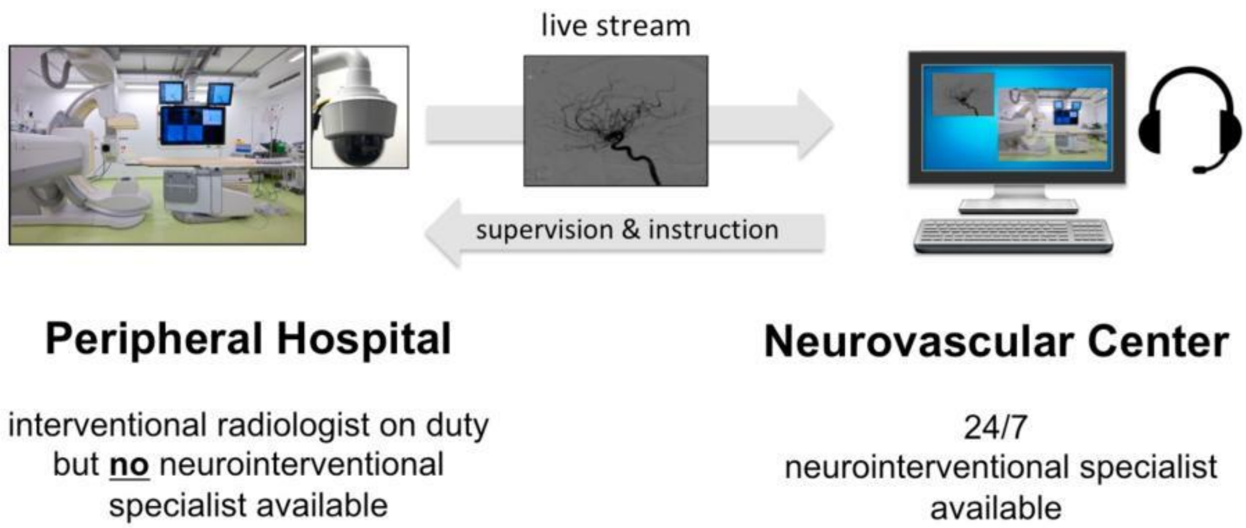

(Filename: TCT_2893_fig_concept_remote_streaming_support.jpg)

Tuesday, May 21, 2019
11:00AM - 12:00PM
Adding Value with Advanced Imaging

2807

11:00AM - 11:07AM

Added Value of Diffusion-Weighted Imaging in Magnetic Resonance Imaging of the Lumbar Spine

J Deutsch[1], D Charles[2], V Sundaram[3], K Zhong[1], A Aggarwal[2], B Delman[2], A Doshi[4]
[1]Mount Sinai Hospital, New York, NY, [2]Icahn School of Medicine at Mount Sinai, New York, NY, [3]ICAHN SCHOOL OF MEDICINE AT MOUNT SINAI, NEW YORK, NY, [4]MOUNT SINAI ICAHN SCHOOL OF MEDICINE, NEW YORK, NY

Purpose
Diffusion-weighted imaging (DWI) has previously demonstrated benefit in spine imaging. We aim to evaluate the impact of DWI on common indications for imaging of the lumbar spine.
Materials and Methods
Following IRB approval, MRI studies of the lumbar spine performed at our institution between 1/2015 - 12/2017 were retrospectively reviewed in patients with suspected osteomyelitis/discitis, metastatic osseous disease, or acute back pain. Studies with artifact secondary to orthopedic hardware were excluded. All studies were performed on a GE Optima MR450w 1.5T scanner. For each MRI study of the lumbar spine, sagittal T1, T2, STIR, and T1 post-contrast sequences when performed were evaluated, in consensus, by three neuroradiologists. The group provided a consensus opinion with regard to whether or not DWI impacted the final interpretation of the study.
Results
A total of 74 MRI lumbar spine studies were evaluated, 59 of which included the use of contrast. The average age of the patients evaluated was 53 years (range 19 - 85; STD 16.2). Overall, DWI influenced the final reading in 22% (16/74) of the cases. Subdivided by clinical indication, DWI impacted the final interpretation in 17% (4/24) of studies ordered to evaluate for osteomyelitis or discitis, in 25% (6/24) of studies ordered to evaluate for metastatic osseous disease, and in 23% (6/26) of studies ordered to evaluate for acute back pain. In studies with osteomyelitis or discitis as the clinical indication, DWI confirmed an abscess in 1 study and excluded an abscess in 3 cases. In studies performed to evaluate for osseous metastatic disease, DWI helped identify a metastatic lesion that would have otherwise been missed in 3 instances, as well as increased the conspicuity of a metastatic lesion in 3 cases. In studies performed to evaluate acute back pain, DWI better characterized a tumor in 1 case, helped exclude an abscess or osteomyelitis in 4 cases, and confirmed both osteomyelitis and an abscess in 1 case. In no instance did DWI negatively impact the final consensus interpretation.
Conclusions
DWI positively impacted the final interpretation in 22% of MRI studies of the lumbar spine performed to evaluate for osteomyelitis or discitis, metastatic osseous disease, or acute back pain.

3414

11:07AM - 11:14AM

Can T2 SPACE Differentiate Active Lesions of Multiple Sclerosis in the Spinal Cord from Chronic Lesions?

R RATAKONDA[1], C Lee[2], E Makariou[2]
[1]MEDSTAR GEORGETOWN UNIVERSITY HOSPITAL, WASHINGTON, DC, [2]Medstar Georgetown University Hospital, Washington, DC

Purpose
Active demyelinating cord lesions in multiple sclerosis typically show T1 contrast enhancement. T2

SPACE sequence is a single slab 3D TSE sequence with excellent spacial resolution, best used in evaluating relationship between the diameter of the spinal canal and its contents. This sequence, thought unable to provide adequate signal contrast in the cord especially for demyelinating lesions; however, does demonstrate lesions with high water content. We hypothesize T2 SPACE sequence can demonstrate edema in active enhancing demyelinating lesions, and hence can help differentiate an active lesion in multiple sclerosis versus a chronic lesion.

Materials and Methods

We conducted a retrospective study of consecutive cases of multiple sclerosis with MR cervical or thoracic spine from 10/2017 to 10/2018. We reviewed T2 SPACE, STIR and post contrast T1 sequences of the cord. T1 contrast enhancing lesions were considered active lesions; while non enhancing STIR lesions were considered chronic lesions. Comparison was made between T2 SPACE sequence and post contrast T1 sequences to evaluate sensitivity of T2 SPACE on enhancing active cord lesions. Simple correlative statistics was applied.

Results

152 studies were reviewed. 13 cases show active lesions with T1 contrast enhancement. All 13 cases show T2 SPACE hyperintense signal intensity. One case shows lesions with T2 SPACE signal but no contrast enhancement. One case has motion artifacts on post contrast T1. The remaining cases show chronic changes on STIR without contrast enhancement or T2 SPACE hyperintensity.

Conclusions

T2 SPACE is typically not used to evaluate MS cord lesions. In our study, we show that active MS lesions visible with T1 contrast enhancement show bright signal on T2 SPACE. T2 SPACE sequence can thus be used to evaluate for active MS lesions, and potentially avoid using gadolinium contrast.

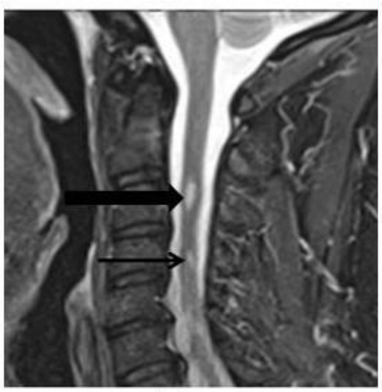

(a)

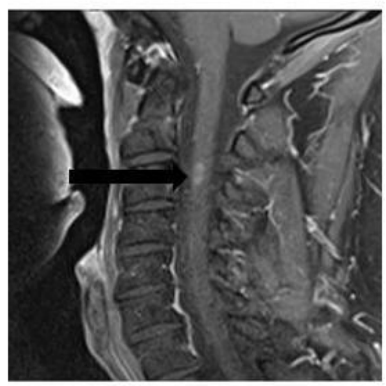

(b)

(c)

Fig : 45 years female with MS. MR of cervical spine shows two cord hyperintense lesions in STIR(a) at C3 (bold arrow)and C4 (thin arrow) level. T1 contrast study (b) shows an enhancing lesion in cord at C3 level representing the active lesion. T2 SPACE show hyperintensity at C3 level corresponding to T1 enhancing active on (bold arrow). Non-enhancing chronic MS lesion is not seen in T2 SPACE(c)

(Filename: TCT_3414_asnr.jpg)

2558

11:14AM - 11:21AM

Shoulder Artifact Reduction on Cervical Spine CT: Is There a Role for DECT?

U Erdenebold[1], N Zakhari[1], R Chatelain[1], C Torres[1]
[1]*University of Ottawa, The Ottawa Hospital Civic and General Campus, Ottawa, Ontario*

Purpose
Shoulder artifact is commonly encountered during CT cervical spine assessment limiting spinal canal evaluation. Dual energy CT (DECT) is used to reduce the metallic artifact secondary to spinal hardware. Our purpose is to evaluate the role of DECT in reducing shoulder artifact.
Materials and Methods
Post processing of retrospectively collected 50 neck DECT generated virtual monoenergetic images (VMI) at 50, 70, 100, 140 keV. Two neuroradiologists blinded to the energy level separately assessed the images. Five-point scale was used to assess the degree of artifact. Regions of interest (ROI) were placed within the spinal canal for objective noise measurement (HU standard deviation). Statistical analysis included repeated measures analysis of variance and intraclass correlation coefficient (ICC).
Results
Quantitative measurement: Lowest noise level mean was noted for 140 keV VMI (28.83 HU, 95%CI 21.08-36.59), followed by 100 keV (32.89 HU, CI 23.34-42.45), 70 keV (42.51 HU, CI 28.24 to 56.79) and 50 keV (74.01 HU, CI 51.14-96.88). Subjective assessment: 100 keV VMI was the most frequently ranked best image quality (88% reader 1 and 80% reader 2) and 50 keV VMI was the most frequently rated worst image quality (92% reader 1 and 90% reader 2). The interobserver agreement was substantial for 50 keV, good for 70 & 100 keV and fair for 140 keV VMI (ICC =0.78, 0.67, 0.62 and 0.48). Significant effect of the energy level was noted on the noise measurement and the subjective artifact assessment ($p<0.0001$). Post-hoc pairwise comparison revealed significant differences between VMI pairs on objective and subjective analysis ($p < 0.0001$) except for 70 and 140 Kev VMI pair on qualitative analysis ($p=0.38$).
Conclusions
VMI with high keV (100 and 140) show improved image quality compared with lower keV. DECT with high keV VMI might be useful in reducing shoulder artifact in routine cervical spine CT assessment.

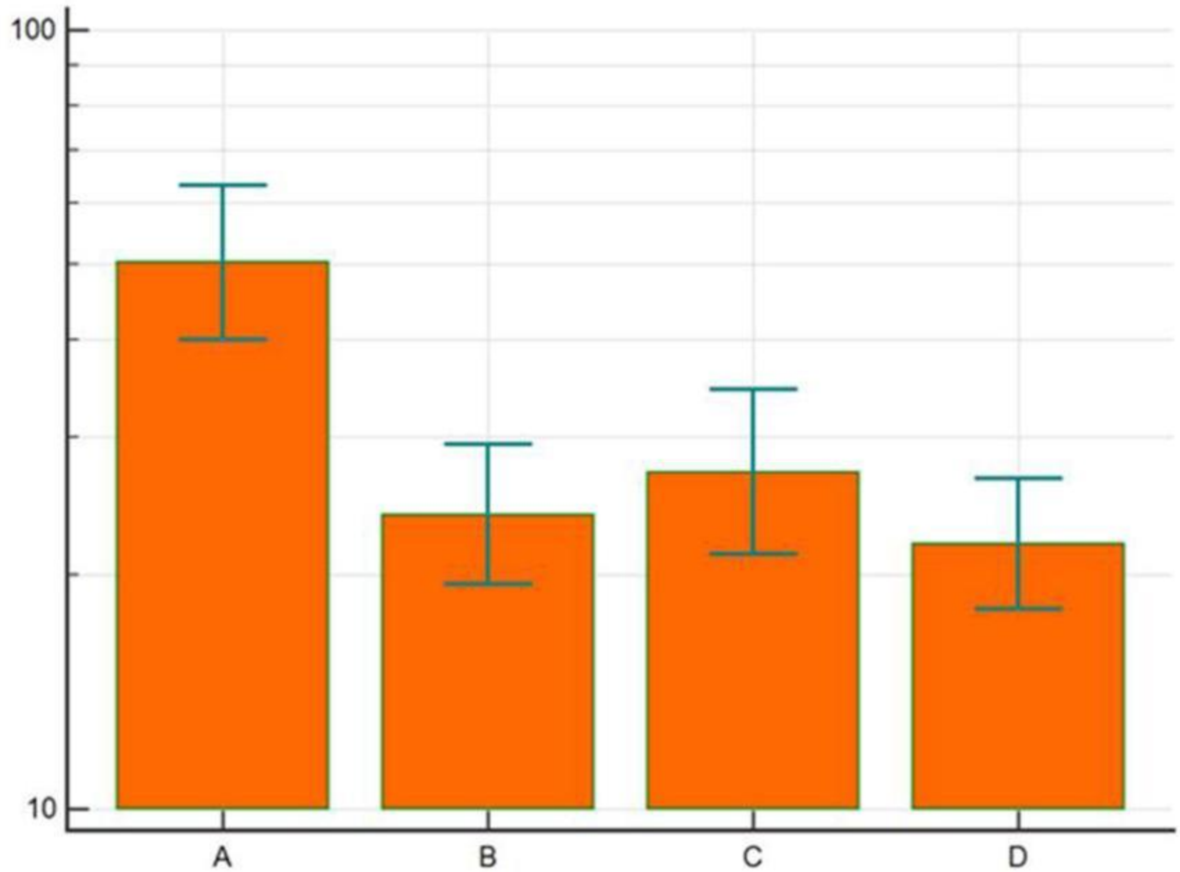

Fig 1: Comparison of the noise mean between the different VMI (A= 50 keV, B= 100 keV, C= 70 keV and D= 140 keV)

(Filename: TCT_2558_DECTimage.jpg)

2535

11:21AM - 11:28AM

Spinal Cord Perfusion MR Imaging Implicates Ischemia and Hypoxia in Cervical Spondylotic Myelopathy

B Ellingson[1], N Salamon[1], L Holly[1]
[1]*University of California Los Angeles, Los Angeles, CA*

Purpose

Despite being hypothesized as a critical pathophysiological mechanism in cervical spondylotic myelopathy (CSM), spinal cord ischemia and hypoxia have not been directly observed or quantified in vivo in CSM patients. A number of studies have documented histological changes and angiography data in CSM consistent with ischemia, and experimental work using animal or preclinical models has demonstrated indirect evidence of ischemia. However, quantification of ischemia and hypoxia in CSM remains elusive, and the potential role of spinal cord ischemia and hypoxia on disease progression and severity is prime for investigation. In the current study we assessed spinal cord perfusion and oxygenation in 22 patients with CSM and examined the relationship between perfusion, degree of spinal cord compression, and neurological status.

Materials and Methods

We used dynamic susceptibility contrast (DSC) perfusion MRI and a novel spin-and-gradient echo echoplanar (SAGE-EPI) acquisition before, during, and following gadolinium-based contrast injection. Estimation of relative spinal cord blood volume (rSCBV), the reversible relaxation rate (R2'), and relative oxygen extraction fraction (rOEF=R2'/rSCBV) was performed at the site of compression and compared with anterior-posterior spinal cord diameter and modified Japanese Orthopedic Association score (mJOA), a measure of neurological impairment.

Results

Results showed a linear correlation between rSCBV and both anterior-posterior cord diameter (R2=0.4667, P=0.0005) and mJOA (R2=0.2274, P=0.0248). R2' was linearly correlated with mJOA (R2=0.3998, P=0.0016). Estimates of rOEF were correlated with both cord diameter (R2= 0.3440, P=0.0041) and mJOA (R2=0.4699, P=0.0004).

Conclusions

These results support the concept that spinal cord compression results in both ischemia and hypoxia, the degree of which appears to be proportional to the amount of neurological impairment.

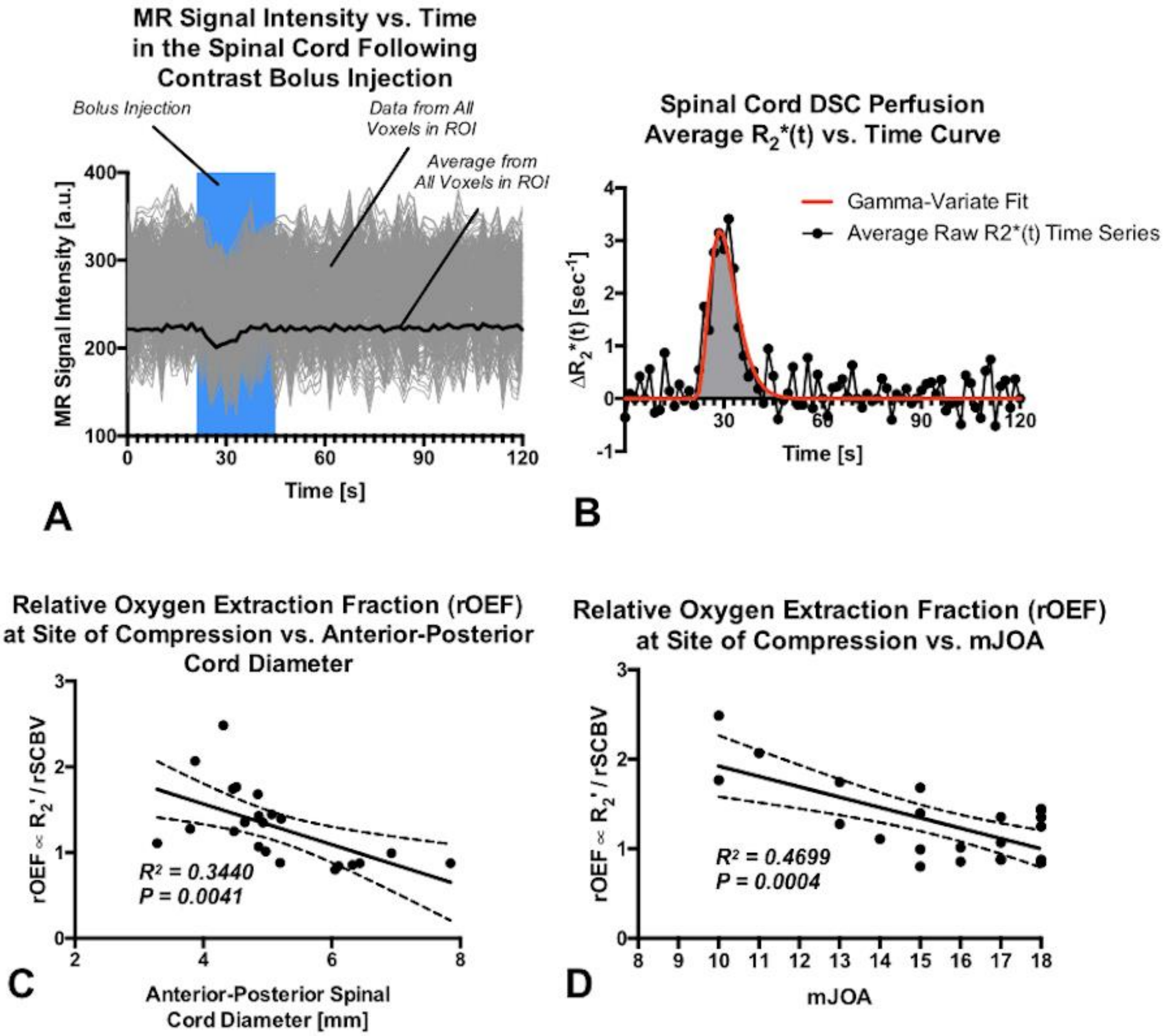

(Filename: TCT_2535_Figure.jpg)

2209

11:28AM - 11:35AM

Spinal Metastases from Neuroendocrine Neoplasm: Imaging Detection and Characterization with Simultaneously Acquired Ga-68 DOTATATE PET-MR

J Bai[1], K Naser-tavakolian[1], R Matthews[2], L Bangiyev[3]
[1]Stony Brook University Hospital, Stony Brook, NY, [2]Stony Brook University Medical Center, Stony Brook , NY, [3]Stony Brook University Hospital, Stony Brook , NY

Purpose
Evaluation of spinal metastases from neuroendocrine tumor (NET) is important for staging and assessment of treatment response. Ga-68 DOTATATE PET-MR imaging combines high somatostatin receptor affinity of DOTA peptides with advanced signal characterization of MRI for NET evaluation. The purpose of the study is to evaluate imaging characteristics of spinal metastases from NET with simultaneously acquired Ga-68 DOTATATE PET-MR.
Materials and Methods
We retrospectively identified 35 patients with NET (mean age 65 +/- 15, 19 male, 16 female) underwent combined Ga-68 DOTATATE PET-MRI for tumor staging between January 2016 and June 2018. Each PET-MRI was evaluated in consensus by a nuclear radiologist, a neuroradiologist, and a body radiologist. 37 spinal lesions from 6 patients (mean age 69, 4 male, 2 female) demonstrated abnormal osseous uptakes of DOTA consistent with metastases. MR sequences included axial T1 radial vibe fat suppressed, axial T2 haste, and sag T1 Dixon sequences.
Results
Of the 37 lesions, 33 lesions (89 %) were detected on Dixon, which demonstrated consistent abnormal signal characteristics with hyperintensity on water sequence, hypointensity on fat sequence, and signal decrease on in-phase comparing to out-of-phase (Mean SUV 23.1 for MR positive lesions vs Mean SUV 8.7 for the MR negative lesions). 1 cervical spinal lesion from the patient with concurrent prostate cancer demonstrated mild DOTA uptake (SUV 8.2), but prominent MR abnormalities. 1 lumbar spinal lesion from a patient with rectal carcinoid cancer also demonstrated mild DOTA uptake (SUV 5), but suspicious MRI features.
Conclusions
In this study Ga-68 DOTATATE was shown to be a highly sensitive molecular marker that can detect spinal metastases from NET before signal abnormalities could be identified on simultaneously acquired MRI sequences. Dixon sequences have shown consistent signal abnormality in spinal metastases from NET. The multi-sequential MRI provides incremental diagnostic value to distinguish bone metastases from NET versus bone metastases from other neoplasm and to identify potential complication from spinal metastases which would help in clinical management. In lesions with low DOTA uptake and prominent MRI signal abnormality, alternative diagnoses such as poorly differentiated NET or spinal metastases from other primary neoplasms may be considered.

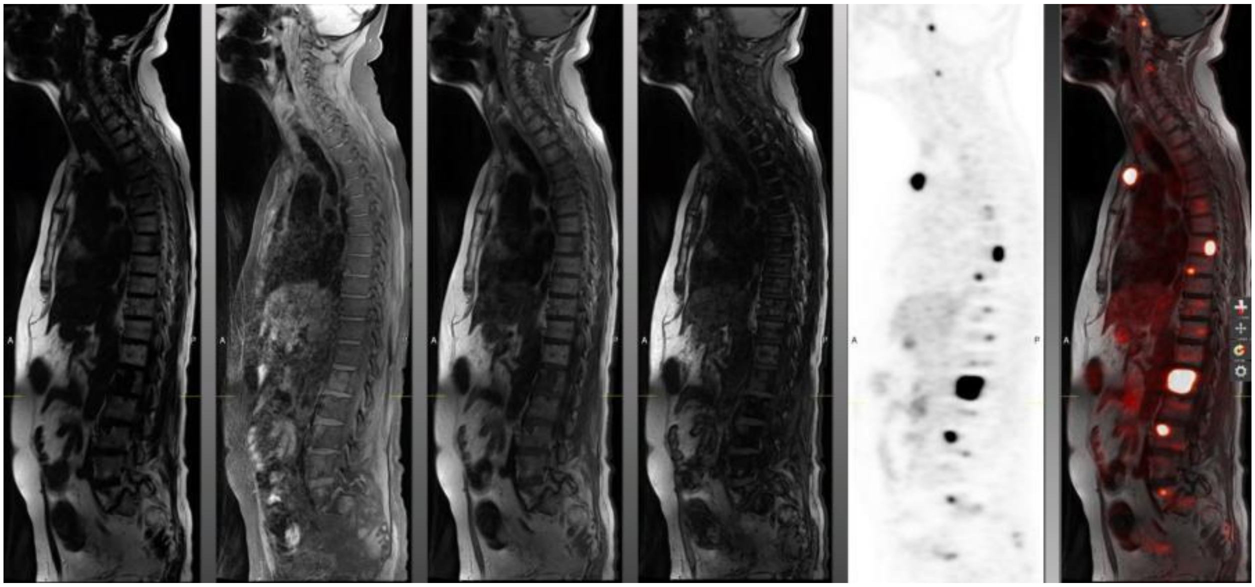
(Filename: TCT_2209_PETDIXONpt1new.JPG)

2206

11:35AM - 11:42AM

T-1 Weighted Dynamic Contrast-Enhanced MR Perfusion Imaging Correlates with Histopathology Findings: A Noninvasive Approach to Assess Malignancy in Spine

Y GUAN[1], J Lyo[1], E Lis[1], J Arevalo Perez[1], J Tisnado[1], A Holodny[1], S Karimi[1], K Peck[1]
[1]*Memorial Sloan Kettering Cancer Center, New York, NY*

Purpose
Biopsies are often performed in patients with cancer to confirm malignancy of spinal lesions, especially in those with inconclusive radiology imaging evidence. We investigated the correlation between Vp, a perfusion parameter derived from dynamic contrast-enhanced magnetic resonance (DCE-MR) perfusion imaging and histopathologic diagnosis. We hypothesized that Vp will be significantly different between non-neoplastic and malignant spinal metastases, providing additional information for distinguishing between the two groups.
Materials and Methods
In this retrospective study, we included 103 patients (male=53, female=50) who completed a DCE-MR perfusion imaging study followed by biopsy within 30 days after DCE-MR imaging between 2015 and 2018. A total of 141 lesions were separated into a non-neoplastic group (n=58) and a malignant group (n=83) according to histopathological evidence. A single investigator manually defined regions of interest on the vertebrae. We calculated the DCE-MR perfusion imaging parameter Vp using the Tofts pharmacokinetic two-compartment model. Vp was quantified, normalized, and compared between the two groups. A two-tailed t-test, and receiver operating characteristic analysis was performed to verify the statistical significance of the difference in Vp between the two groups.
Results
Vp was significantly different between the two groups ($p<0.00001$). Vp alone had a sensitivity of 92.8%, specificity of 79.3%, positive predictive value of 84.7%, negative predictive value of 90.6%, and overall accuracy was 87.0%. Upon including additional radiology images from routine scans, the statistics increased to a sensitivity of 93.3%, specificity of 95.1%, positive predictive value of 96.5%, and negative predictive value of 90.6%; the overall accuracy was 94.0%.

Conclusions
The DCE-MR perfusion imaging parameter Vp is strongly correlated with histopathologic diagnosis, and it can differentiate non-neoplastic spinal lesions from malignant lesions.

Figure. Box and Whisker plot of Vp ratios by group. The average Vp ratio in the non-neoplastic group was 1.6815, and the average Vp ratio in the malignant group was 4.1813. Lesions originating from hematologic malignancies and from solid tumors showed a similar distribution of Vp ratios, with an average of 3.60 for the former and 4.34 for the latter. There was a significant difference in Vp ratio between the non-neoplastic group and malignant group as evidenced by a two-tailed t test ($p<0.00001$).

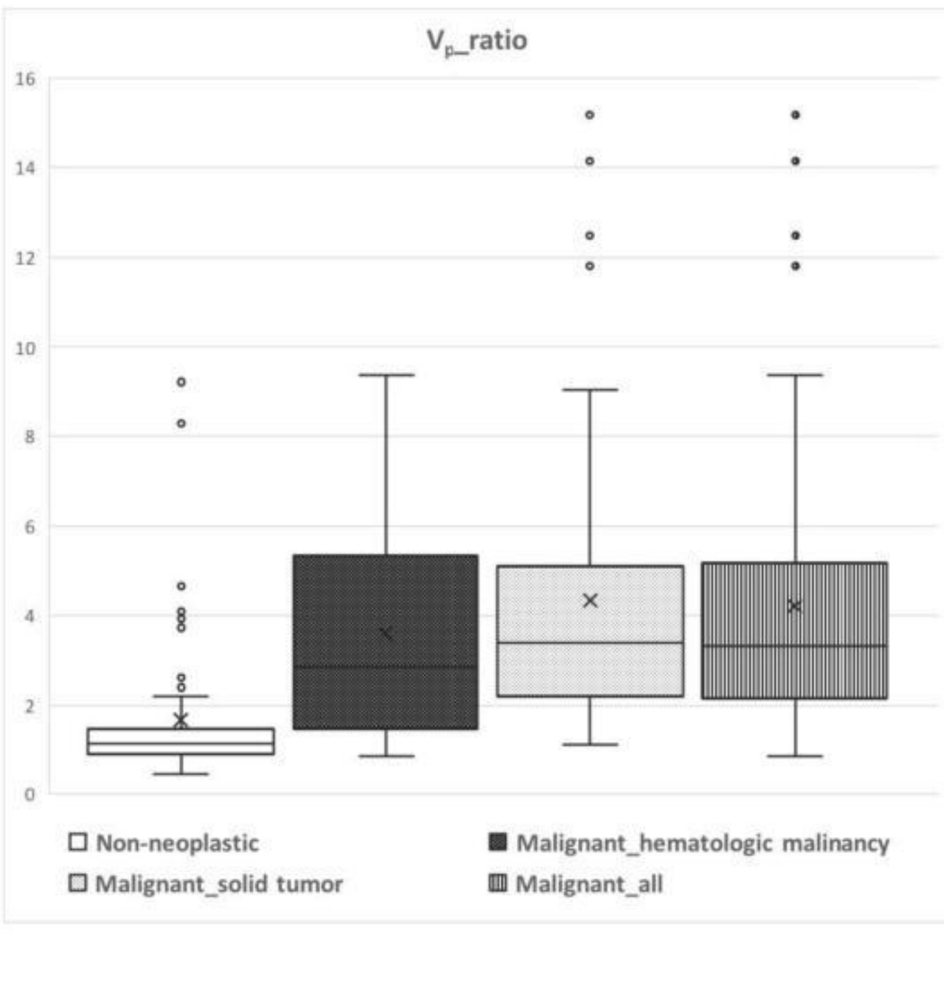

(Filename: TCT_2206_Figure.jpg)

Tuesday, May 21, 2019
11:00AM - 12:00PM
Cerebral Perfusion to Spine Diffusion

3653

11:07AM - 11:14AM

ASL Perfusion Abnormalities on Acute MR Imaging Following Focal Onset Pediatric Seizures

N Stence[1], I Neuberger[1], D Mirsky[2], J Maloney[1], L Fenton[1], M Barry[1], C Press[1]
[1]Children's Hospital Colorado, Aurora, CO, [2]CHILDRENS HOSPITAL COLORADO, AURORA, CO

Purpose
Many investigators have reported findings on ASL imaging in patients with seizure disorders, but only a few have described brain perfusion abnormalities on acute imaging in children suffering from focal onset seizures (1-3). We describe our institutional experience in acute ASL imaging of children with focal onset seizures imaged for persistent neurologic deficits.
Materials and Methods
Methods and Materials: A search of brain MRI radiology reports at our institution was performed using the keywords "perfusion" or "ASL". Inclusion criteria were: age <18 years, MR imaging performed for persistent neurological deficit following witnessed seizure activity, available MR sequences of ASL, MRA, DWI and SWI, and a clinical diagnosis of focal onset seizure. All imaging was analyzed by two pediatric neuroradiologists (IN and NS). The affected cerebral hemisphere was determined by lateralized clinical symptoms and neurological examination. Perfusion imaging was scored as either hypoperfusion (Fig 1A) or hyperperfusion (Fig 1B), and then further classified as affecting either the entire cerebral hemisphere (holohemispheric) or only a part of the hemisphere.
Results
Results: 15 MRI studies from 13 patients met inclusion criteria, 10 female, with mean age 5.6 years (range 1-14 years). The left hemisphere demonstrated abnormal perfusion in 10 exams. Perfusion abnormality was classified as holohemispheric in 5 patients. Hyperperfusion was present in 8 exams and hypoperfusion in 7. Mean time between symptom onset and MRI for all exams was 21.9 hours (range 2-65 hours). Among those exams with hypoperfusion the mean time was 6.6 hours, while those with hyperperfusion had a mean time of 35.3 hours (unpaired t test p=0.0057). All patients with ongoing neurologic abnormalities lasting greater than 24 hours demonstrated hyperperfusion. Abnormalities were found on MRA in 9 exams, on SWI in 1 and on DWI in 8. EEG confirmed corresponding focal electrographic abnormalities in 12 patients. Figure 1A depicts ASL imaging from a 13 year old girl obtained 1.5 hours after onset of right arm numbness and weakness, showing patchy left hemisphere hypoperfusion. Figure 1B shows ASL imaging in the same patient from a different episode of right sided hemiplegia 44 hours after onset of symptoms depicting marked diffuse hyperperfusion.
Conclusions
Our cohort of 15 acute imaging studies in pediatric patients with focal onset seizures demonstrated a clear temporal correlation to perfusion abnormalities, with those patients having a longer duration of ongoing symptoms most often demonstrating corresponding hyperperfusion, even in imaging performed days after symptom onset. Further study is needed to determine the exact time course of perfusion abnormalities in this setting.

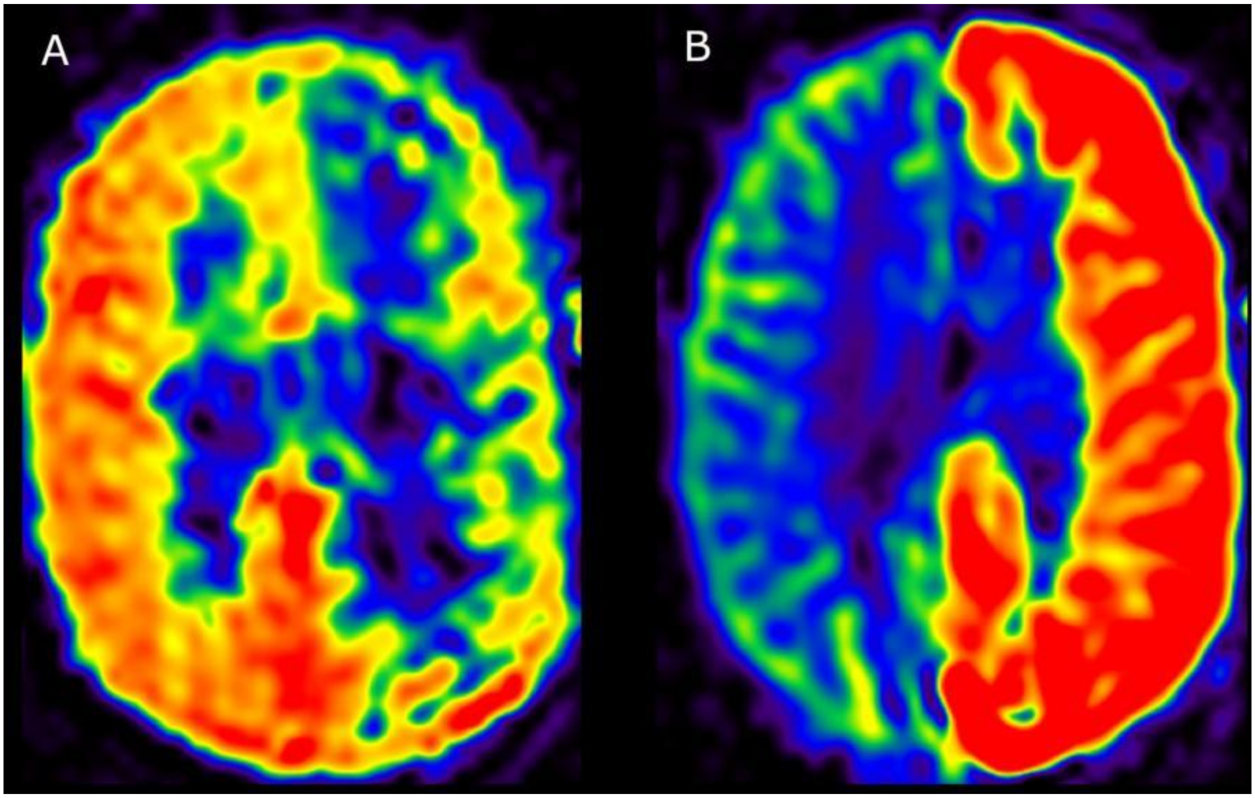

(Filename: TCT_3653_aslseizureperfusion.jpg)

3191

11:14AM - 11:21AM

Can SWI Determine Brain Oxygen Saturation in Neonates with Congenital Heart Disease?

S Teixeira[1], J Lynch[2], H Kristina[1], D Licht[1], A Vossough[3]
[1]Children's Hospital of Philadelphia, Philadelphia, PA, [2]University of Pennsylvania, Philadelphia, PA, [3]UNIVERSITY OF PENNSYLVANIA - CHOP, PHILADELPHIA, PA

Purpose
Susceptibility weighted imaging (SWI) is a powerful magnetic resonance imaging (MRI) sequence that takes advantage of the susceptibility differences between oxygenated and deoxygenated hemoglobin. This differences can be potentially manifest in the appearance of the cerebral veins, but is also affected by cerebral blood flow and blood transit times. Independent direct concurrent validation of SWI in assessment of focal cerebral oxygen saturation by non-MR-susceptometry based methods is limited and mostly lacking in diseased populations. Various forms of congenital heart disease (CHD) affect these various physiologic parameters. The purpose of this study is to evaluate and validate if SWI can be used as a method of gross estimation blood oxygenation in neonates with CHD using non-MRI-based near infra-red spectroscopy (NIRS).
Materials and Methods
This is a retrospective review of prospectively collected data in a study of neonatal congenital heart disease immediately prior to surgery performed from 2009 to 2014. Study was approved by the IRB and informed consent had been obtained from parents or legal guardians. Inclusion criteria were neonates with CHD, available diffuse optical spectroscopy (DOS) data (cerebral tissue oxygen saturation [SpO2], total cerebral hemoglobin concentration [THC], cerebral blood flow index [BFL]) obtained within one hour of pre-operative SW-MRI. SWI was qualitatively graded according to the visualization of the cerebral veins

as three grades (0=normal, 1=mild, 2=severe). Differences in NIRS-derived physiologic parameters among the SWI groups were assessed using one-way analysis of variance with post-hoc testing.
Results
In total, 163 patients met inclusion criteria (male=95 (55.8%). Patients age at the time of examinations was 4.52±3.2 days. Primary cardiac diagnoses were hypoplastic left heart syndrome (n=62; 38%), d-transposition of great arteries (n=52; 32%), and other malformations (N=49; 30%). Fifty (30.6%) neonates were categorized as grade 0, 92 (56.4%) grade 1, and 21 (12.8%) grade 2. Mean (95% confidence intervals) for SpO2 was 51.5% (48.1-55.05), 45.5% (42.9-48.1), and 41.5%(36.3-46.6), respectively. There was a statistically significant difference between mild and moderate (p=0.0047) and mild and severe (p=0.018) SWI categories, but no difference was found between moderate and severe (p=0.3564) categories. THC and BFL were not different across the SWI categories (p=0.5572 and p=0.4977, respectively).
Conclusions
SWI can be a non-invasive, gross method of estimating blood oxygenation in neonates with CHD when compared to ground truth NIRS measurements. Increased venous contrast in SWI in neonates with CHD can reflect decreased blood oxygenation. In this study, no direct independent relationship between SWI and total cerebral hemoglobin concentration or blood flow index was found beyond the relationship with SpO2. Quantitative susceptibility weighted imaging evaluation may determine more accurate cut-off values in the future.

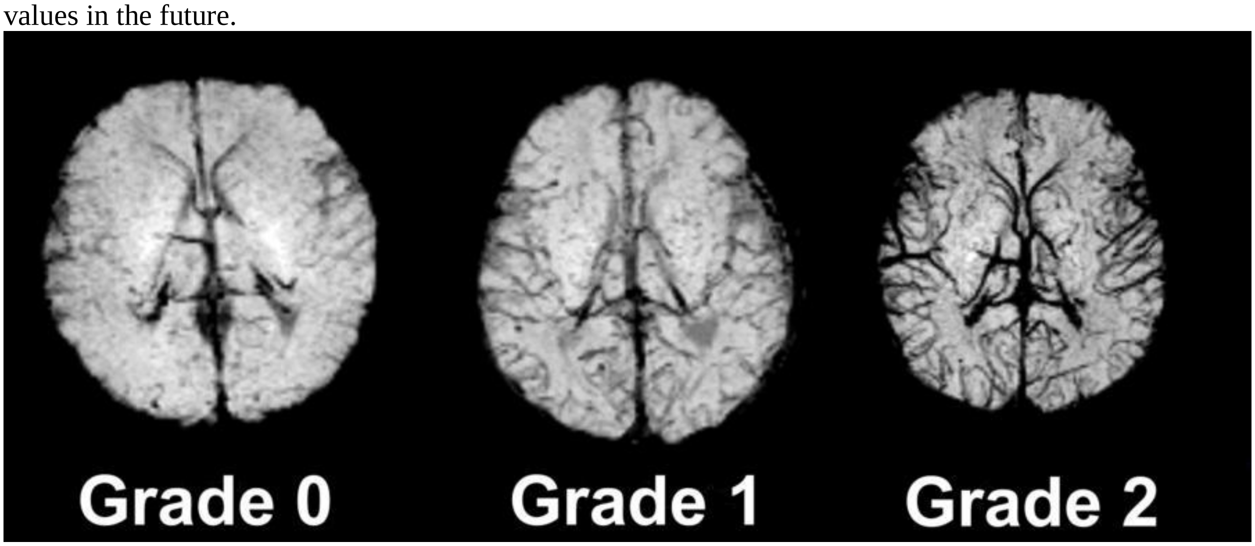

(Filename: TCT_3191_SWIgradingimage.jpg)

3349

11:21AM - 11:28AM

Deep Medullary Venous Thrombosis in Neonates Correlates Highly with Development of Shunt-Dependent Hydrocephalus

K Buch[1], S Rincon[1], P Caruso[2]
[1]Massachusetts General Hospital, Boston, MA, [2]MGH, Boston, MA

Purpose
Deep medullary venous thrombosis (DMVT) in neonates may lead to shunt dependent hydrocephalus (ShDH). While 10% of newborns with IVH from germinal epithelial bleeds (GEB) eventually require intraventricular shunts, the frequency of ShDH in neonates with IVH from DMVT remains unknown. Our purpose is to study a cohort of neonates with DMVT to determine if DMVT is a risk factor for ShDH.
Materials and Methods
Between 2006-2016, 27 neonates were found to have DMVT by MRI. DMVT was scored as mild

involving 1-3 central veins, moderate 4-6, or severe, greater than 6. The extent of DMVT, presence of hydrocephalus, IVH, seizures, and frequency of progression to ShDH were recorded.
Results
17 males and 10 females with a mean gestational age of 37 weeks (range 26-41 weeks) were included. The majority of neonates were scanned at 1-10 days of life (average = 10.2 days, range 0-66 days). 12 patients had mild DMVT; 10, moderate, and 5, severe. 21 patients had IVH that ranged from trace to severe. Hydrocephalus was observed in 13/27 (48%) patients. 5/27 (19%) of neonates developed ShDH and 5/21 (24%) of the neonates with DMVT and IVH developed ShDH.
Conclusions
The frequency of ShDH in neonates with IVH and DMVT is 24%, over twice as high as the frequency of ShDH in neonates with IVH from GEB. Awareness of this increased risk may indicate closer imaging surveillance in this group of neonates.

3137

11:28AM - 11:35AM

Development of a Standardized Normative Pediatric Spinal Cord structural template: Demonstration of an automatic estimation of Spinal Cord Cross Sectional Area measurements (SCCSA).

S Shahrampour[1], B De Leener[2], D Middleton[3], K Jonnavithula[4], M Alizadeh[5], H Pediyakkal[6], L Krisa[3], A Flanders[7], S Faro[8], J Cohen-Adad[9], F Mohamed[3]
[1]Temple University, Philadelphia, PA, [2]NeuroPoly Lab, Institute of Biomedical Engineering, Polytechnique Montreal, Montreal , QC, [3]Thomas Jefferson University, Philadelphia, PA, [4]University of California, Irvine, Irvine, CA, [5]Thomas Jeffesron University, Philadelphia, PA, [6]Boston University, Boston, MA, [7]THOMAS JEFFERSON UNIVERSITY HOSPITAL, PHILADELPHIA, PA, [8]Johns Hopkins School of Medicine, Baltimore, MD, [9]NeuroPoly Lab, Institute of Biomedical Engineering, Polytechnique Montreal, Montreal, QC

Purpose
The purpose of this work is to create a structural MRI based template of the normal pediatric spinal cord by combining T2w MR scans of several typically developing (TD) subjects and show its utility.
Materials and Methods
T2w 3D images from 30 TD subjects (6-16 yrs) were acquired in two slabs and stitched using a 3.0T MRI. Parameters: voxel size = 1 mm3, TR=1500ms, TE=122ms. The following pre-processing steps were performed on all subjects before the actual template generation: (I) spinal canal centerline extraction. (II)Semi-automatic identification of intervertebral discs using a template-matching detection algorithm [1]. (III) Slice-based intensity normalization: to normalize image intensity of the inside of spinal cord to the average intensity of the entire dataset. After successful preprocessing, following steps were performed: (I) the spinal cord centerline and the intervertebral discs positions were semi-automatically extracted on all images using tools from Spinal Cord Toolbox [2]. (II) The cord was then straightened and vertebral levels were aligned using a Non-Uniform Rational Bezier Spline based nonlinear transformation [3]. (III) An unbiased left-right symmetric template was constructed using a hierarchical group-wise nonlinear image-registration method (Automatic Nonlinear Image Matching and Anatomical Labeling) [4,5]. The template generation algorithm computes the average of all subjects iteratively and registers the images to this average nonlinearly. As a demonstration of the utilization of this template, spinal cord cross sectional area (SCCSA) was computed at disc levels in all the subjects.
Results
Fig (1) shows sagittal and coronal view of the template along with the labeled vertebral bodies and segmented cord. Axial views illustrate probabilistic map of white and gray matter and Cerebrospinal Fluid (CSF) as well as cord segmentation. Fig(2) top window shows the SCCSA of the produced pediatric template (average across levels: 46.5 mm2 ±12.5) and the bottom window shows the average SCCSA

across all 30 subjects (average across levels: 47 mm2 ±9.6). The similarity in the shapes of the plots suggests the intactness of the overall structure of the cord after straightening and deformation process.
Conclusions
To our knowledge this work is the first to create a standardized template of spinal cord in pediatric subjects. Utility of this template in automatically estimating the SCCSA is also demonstrated. Future work with a larger cohort is warranted.

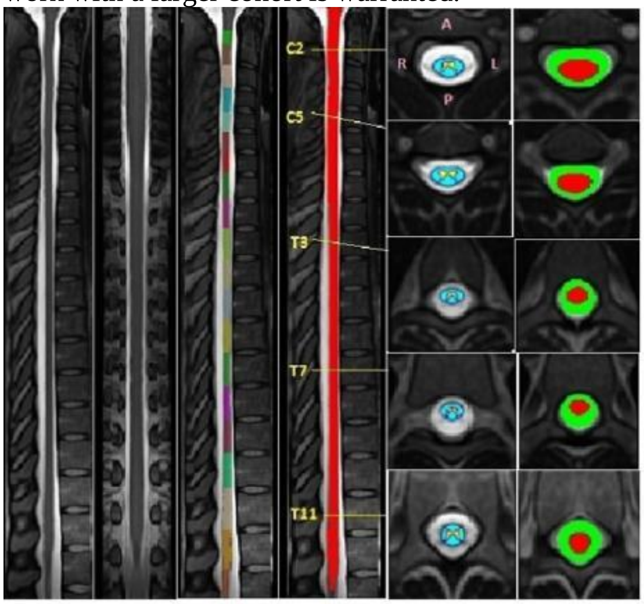

Figure (1): The left four images show the sagittal and coronal view of the template along with the vertebral labels and segmented cord in red. The right two images show probabilistic map of white and gray matter as well as Cerebrospinal Fluid (CSF) and cord segmentation.

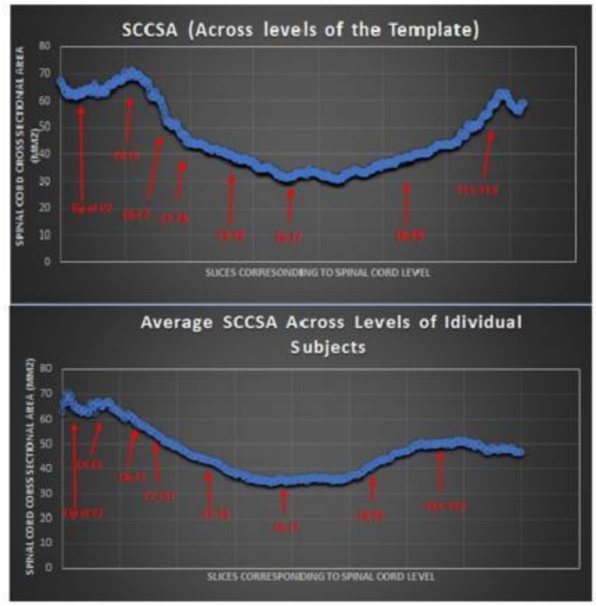

Figure 2: Top window shows the SCCSA of the pediatric template (average across levels: 46.5 mm2 ±12.5). The bottom window shows average SCCSA across all 30 subjects (average across levels: 47 mm2 ±9.6). This suggests that SCCSA is preserved between native subjects' space and the template.

(Filename: TCT_3137_ASNR19.jpg)

2445

11:35AM - 11:42AM

Imaging Cerebral Focal Increase of Deoxygenation in Pedatric Patients with Migraine with Aura

V Lehmann[1], F Kellner-Weldon[1], P Breiding[1], L Grunder[1], A Scutelnic[1], R Muri[1], M Pastore-Wapp[1], M El-Koussy[1], N Slavova[1]
[1]*University Bern, Bern, Switzerland*

Purpose
Migraine with aura (MwA) in pediatric patients is a clinically frequent phenomenon, but magnetic resonance (MR) imaging features have only been reported in small case series. Diagnosis of MwA in children is challenging, as patient history and clinically complex symptoms need to be differentiated to exclude mimicking conditions. We suspected that cortical spreading depression is relevant to MwA in children. We sought to find a structural correlate of focally increased deoxygenation (FID) in susceptibility imaging (SWI) and increased time to peak (TTP) on perfusion maps in the acute phase of MwA.
Materials and Methods
Between 2010 and 2018, we evaluated symptoms and MR imaging of pediatric patients with MwA attacks (< 7 days after onset of symptoms). Focal abnormal SWI and perfusion TTP imaging was visually scored in 10 ROIs on both hemispheres distributed on 3 slices. The scores were zero for normal, one for discrete, two for distinct, and three for severely abnormal FID. The distribution was noted as either asymmetric left versus right hemispheric or bilateral anterior versus posterior gradient. The TTP images were rated in the same fashion, with a window adjusted manually to depict maximum contrast.

Results
99 patients (69 female, 69.7%), mean age 14.07 y, (range 7.5-17.9 ± 2.8) were included. FID in SWI was present in 61.6% (61/99). Laterality of FID on SWI was left hemispheric in 60.7% versus right hemispheric in 31.1% (difference significant, $p < .001$). In 8.2% the distribution of FID was bilateral symmetric. The association between reported side of aura symptoms and contralateral hemispheric imaging alterations in patients with FID was highly significant ($p = .002$, n=45). 61 of 99 patients had perfusion MR and 59.0% showed focal increase of TTP. Age correlated significantly with FID in SWI and increase of TTP in perfusion (SWI: $r = -.248$, $p = .013$; perfusion: $r = -.252$, $p = .05$). On both SWI and TTP maps, areas most often abnormal were inferior and medial temporal lobe, parietal and occipital lobe. Focal abnormalities correlated significantly between SWI and TTP maps.
Conclusions
This study provides confidence in linking FID in SWI to acute MwA in pediatric patients. Additionally, we found that the FID phenomenon had a left hemispheric significant dominance. We firstly report bilateral occurrence of FID.

3119

11:42AM - 11:49AM

MR Vessel Wall Imaging in Pediatric Arterial Stroke Due to Focal Cerebral Arteriopathy

F Perez[1], G Oesch[1], C Amlie-Lefond[1]
[1]*Seattle Children's Hospital, Seattle, WA*

Purpose
Focal cerebral arteriopathy (FCA) of childhood is a cause of pediatric arterial stroke characterized by focal, unilateral stenosis or irregularity of a large anterior circulation artery presumed to be inflammatory (1). Arterial wall enhancement on MR Vessel Wall Imaging (VWI) has been advocated as a biomarker to identify an active inflammatory arteriopathy for predicting clinical course and guiding appropriate therapy, such as steroids or antivirals (2, 3). To determine the prevalence of vessel wall enhancement in FCA, we conducted a retrospective review of VWI findings in cases of pediatric arterial stroke related to FCA.
Materials and Methods
Suspected cases of FCA, as identified by a pediatric stroke specialist, where VWI was obtained as part of conventional stroke MRI evaluation between January 2009 and July 2018 were retrospectively reviewed for enhancement pattern as well as conventional MRA and brain MRI findings by a pediatric neuroradiologist. VWI was performed on a 1.5 or 3T MRI using high-resolution 3D dark blood T1 sequences (T1 SPACE) following intravenous gadolinium contrast administration.
Results
Fifteen cases of FCA were identified, nine of which had VWI near the time of stroke. The mean age of onset of stroke among these nine patients was 8.6 years with a range of six months to 16 years. The average time of VWI from stroke onset was 5.6 days, ranging from 0 to 14 days. 1/9 cases demonstrated definite evidence of arterial wall enhancement at site of arterial stenosis/irregularity on VWI; 2/9 cases demonstrated equivocal enhancement; and 4/9 cases demonstrated no evidence of enhancement. In 2/9 cases, long segment petrous and cavernous internal carotid artery wall enhancement was observed.
Conclusions
Not all cases of FCA in our cohort demonstrated arterial wall enhancement which may reflect the heterogeneity of FCA etiologies. Future work is needed to assess the reliability of VWI as a biomarker in FCA.

3036

11:49AM - 11:56AM

Spinal Cord Lesions in Mitochondrial Disorders

C Alves[1], S Teixeira[1], F Gonçalves[1], J Martin-Saavedra[1], A Goldstein[1], G Zuccoli[2]
[1]Children's Hospital of Philadelphia, Philadelphia, PA, [2]CHOP, Philadelphia, PA

Purpose
Mitochondrial cytopathies (MC) are a heterogeneous group of genetic diseases being the central nervous system (CNS) the most affected one. Although brain imaging findings in MC have been already described and also few characteristic patterns have been recognized in some specific mutations, there is a lack of information linking spinal cord involvement in MC in the scientific literature. Therefore, this study aims to assess the prevalence and imaging phenotype of spinal cord lesions in MC.
Materials and Methods
In this retrospective IRB approved study, the magnetic resonance imaging (MRI) database was queried for patients with MC (2000-2018). Patients with a confirmed molecular diagnosis of MC and spinal cord imaging were evaluated. Spinal cord lesions (SCL) were classified based on location, extension (less or more than 2 vertebral bodies), and imaging features. Imaging phenotype was associated with the molecular genotype.
Results
Out of 105 patients, 23 had spinal cord imaging, at least from the cervical segment. Thirteen patients (53.5%), showed SCL. Ten patients had lesions at the cervical level (76.9%) while 3 (23.1%) at the thoracolumbar level. Eight (61.5%) SCL were short and 5 (38.5) were long in extension. In 4 (30.8%) patients the lesions reached the area postrema. Furthermore, three different patterns of SCL were identified; Group A: 7 (54%) tumefactive lesions; Group B: 2 (19,5%), B12 vitamin deficiency-like lesions; Group C: 4 (30%) spinal cord infarct-like lesions.
Conclusions
SCL are not infrequent in patients with MC. MC-related SCL may mimic demyelination, stroke, and vitamin B12 deficiency.

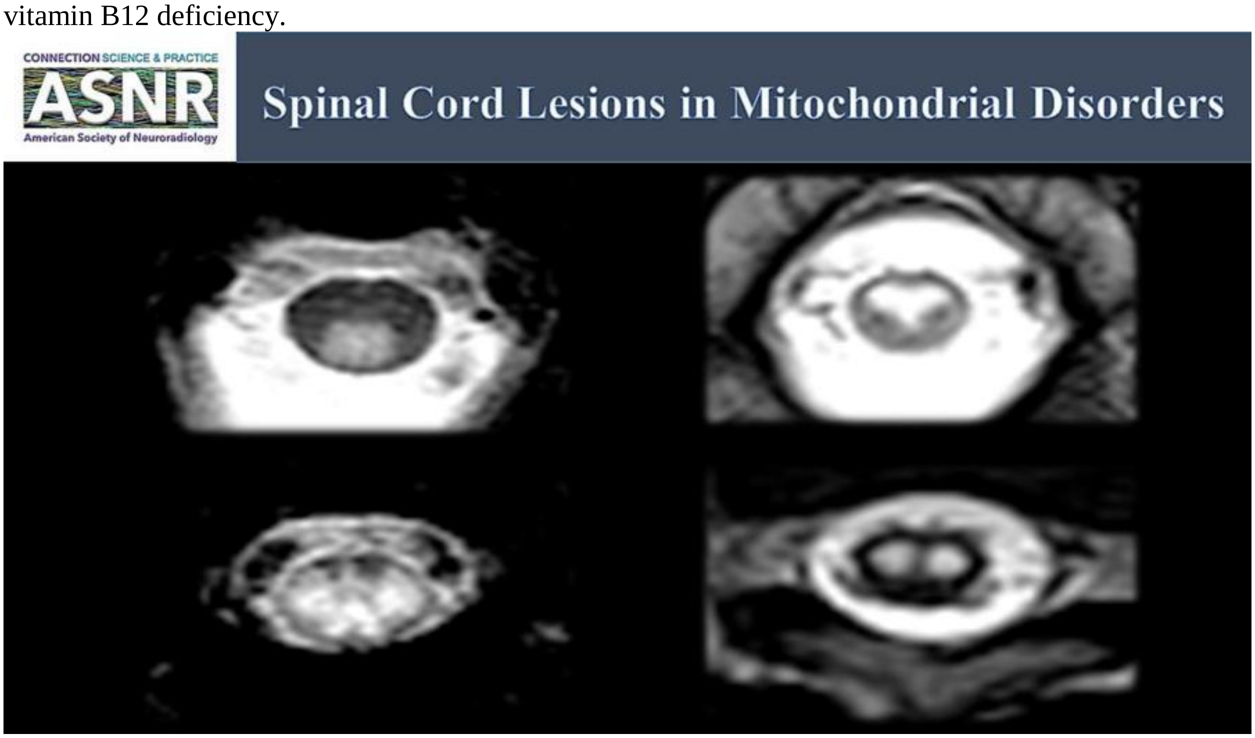

(Filename: TCT_3036_SPINEABSTRACTSC300.jpg)

2148

11:00AM - 12:00PM

Brain Core Temperature of Patients Before and After Orthotopic Liver Transplantation Assessed by DWI-Thermometry

G Sparacia[1], B Laughlin[2], G Sparacia[1], R Cannella[1], V Lo Re[3], A Iaia[4], G Mamone[3], K Sakai[5], K Yamada[5], R Miraglia[3]
[1]University of Palermo, Palermo, Italy, [2]CHRISTIANA CARE HEALTH SYSTEM, MIDDLETOWN, DE, [3]IRCCS-ISMETT (Mediterranean Institute for Transplantation and Advanced Specialized Therapies), Palermo, Italy, [4]Christiana Care, Newark, DE, [5]Kyoto Prefectural University of Medicine, Kyoto, Japan, Kyoto, Kamigyo-ku

Purpose
The brain produces heat as a result of cerebral metabolism, and the heat is removed mainly through circulation of the intracranial blood vessels and cerebrospinal fluid (CSF). The aim of this study was to assess the brain core temperature of adult patients with end stage liver disease before and after orthotopic liver transplantation (OLT) using a noninvasive temperature measurement technique based on the diffusion coefficient of the cerebrospinal fluid.
Materials and Methods
This retrospective study used the data collected from January, 2014 to January, 2017. The study group comprised 19 patients (16 men, 3 women, mean age 57.9 ± 7.4 years) with a MELD score 23.7 who underwent magnetic resonance (MR) imaging before OLT and within 30 days after OLT. The etiology of end stage liver diseases was determined as follow: drug-related fulminant hepatic failure (n=1), nonalcoholic steatohepatitis (n=3), hepatocellular carcinoma (n=8), HCV/HBV/HDV infection (n=3), primary biliary cholangitis (n=1), acute liver failure on chronic sclerosing cholangitis (n=1), cryptogenic cirrhosis (n=1) and liver cirrhosis (n.=1). MR imaging studies were performed with a 1.5T MR scanner. Brain core temperature (T: °C) was calculated using the following equation from the diffusion coefficient (D) in the lateral ventricular (LV): CSF: $T = 2256.74/\ln(4.39221/D) - 273.15$ using a standard DWI single-shot echo-planar pulse sequence (b value 1000 s/mm2). Statistical analysis was performed using a nonparametric Mann-Whitney U test.
Results
Brain core temperature measurements were successfully performed in all patients before and after OLT. Mean (± standard deviation) measured LV temperature was 38.67 ± 1.76 °C before OLT and 38.60 ± 0.99 °C after OLT, showing no significant difference ($P = 0.643$).
Conclusions
Brain core temperature was stable in patients undergoing OLT. Brain core thermometry using DWI-based MR imaging may provide a supplementary brain biomarker to confirm that cerebral blood flow and cerebral metabolism are stable during OLT.

2984

11:00AM - 11:07AM

Characterization of Perivascular Spaces in Healthy Subjects

G Barisano[1], N Sheikh-Bahaei[2], F Sepehrband[1], M LAW[3], A Toga[1]
[1]University of Southern California, Los Angeles, CA, [2]University of Southern California, Los Angeles , CA, [3]Keck Medical Center of USC, Los Angeles, CA

Purpose

Perivascular spaces (PVS) have recently attracted significant attention from the scientific community working on degenerative brain disease partly due to discovery of the glymphatic system(1). Enlargement of PVS has been associated not only with aging, but also with a number of pathophysiological conditions(2). However, their physiological associations and variability in healthy young subjects are still not clear.

Materials and Methods

In this study, we analyzed PVS in a large sample of normal subjects from the Human Connectome Project(3). PVS were independently rated by two expert readers on axial T2W images at 3T MRI using a validated 5-point visual rating scale(2) in basal ganglia (PVS-BG) and centrum semi-ovale (PVS-CS) (0:no PVS, 1:1-10, 2:11–20, 3:21–40, and 4=>40 PVS) and also in the midbrain (PVS-MB) (0=no PVS, 1=PVS visible). The total PVS score (PVS-tot) for each subject was calculated as the sum of the single scores.

Results

One hundred healthy subjects (53 females, 47 males; mean age 28.3, range 22-36) were randomly selected from the HCP database. The mean number of PVS-CS and PVS-BG were 34.7 (range 11-78) and 9.2 (range 3-20), respectively. 35% of these subjects presented with grade 4 PVS and 58% had enlarged PVS in their midbrain. There was significant correlation between PVS-CS and PVS-BG ($p<0.001$). Moreover, PVS-BG was significantly correlated with subjects' height ($p=0.01$), brain volume ($p=0.005$), and brainstem volume ($p=0.005$).

Conclusions

Identifying the physiological factors affecting PVS in normal subjects is fundamental in order to better understand the significance of PVS in pathological states and, ultimately, PVS function. This study demonstrates that a high inter-subjects variability of enlarged PVS is detectable in a healthy young population, and more than 1/3 of them presented with what is considered as abnormal level of PVS. We also found that some morphological factors may affect PVS particularly in basal ganglia in normal subjects. These results are relevant for all future studies investigating the role of PVS in pathological conditions and across different groups.

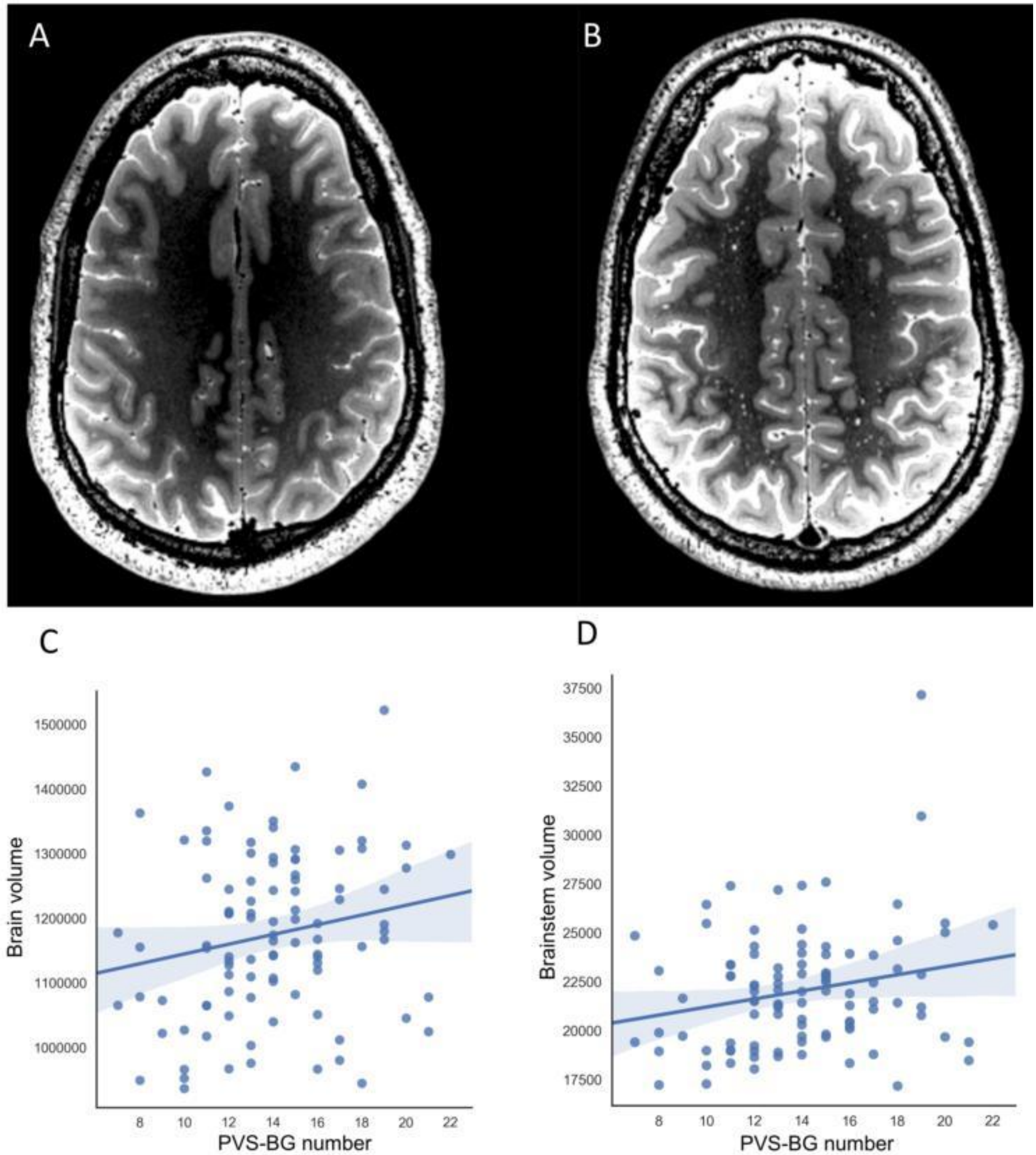

Figure 1: (A and B) Axial T2-weighted MRIs of two healthy subjects showing a significantly different number of PVS in centrum semiovale. (C and D) Scatterplots depicting the statistically significant relationship between PVS in basal ganglia and brain volume (C) and brainstem volume (D).

(Filename: TCT_2984_Fig1_caption.jpg)

2917

11:07AM - 11:14AM

Dose Finding Study of Gadopiclenol, a New Macrocyclic Gadolinium-Based Contrast Agent, in MRI of the Central Nervous System

D Roberts[1], M Bendszus[2], V Brakni[3]
[1]Medical University of South Carolina, Charleston, SC, [2]Heidelberg University Hospital, Heidelberg, Baden-Wuerttemberg, [3]Guerbet, Villepinte, France

Purpose
To determine a safe and effective dose of gadopiclenol, a new high relaxivity macrocyclic GBCA, based on the Contrast-to-Noise Ratio (CNR) as compared to gadobenate dimeglumine.
Materials and Methods
This double-blind, randomized, dose-parallel group and cross-over study included patients with known or highly suspected focal areas of disrupted blood brain barrier. Patients were randomized to one of the four doses of gadopiclenol (0.025, 0.05, 0.1, 0.2 mmol/kg) and to one series of two MRIs: gadopiclenol and then gadobenate dimeglumine at 0.1 mmol/kg or vice versa. Three independent blinded readers performed the signal intensity measurements off-site. Three other readers assessed overall diagnostic preference in a matched-pairs fashion. Adverse events were collected up to one day post second MRI.
Results
The study population included 272 patients (58.5% females) with a mean±SD age of 53.8±13.6 years. The superiority of gadopiclenol over gadobenate dimeglumine was statistically demonstrated at 0.2 and 0.1 mmol/kg for all readers with an increase in the CNR >30%. At 0.05 mmol/kg, gadopiclenol showed a similar CNR as gadobenate dimeglumine at 0.1 mmol/kg. A linear relationship between CNR and dose of gadopiclenol was demonstrated for all readers. Similar results were observed for the other quantitative assessments (lesion to brain ratio and contrast enhancement percentage). When comparing paired images for diagnostic preference, at the same dose of 0.1 mmol/kg, the readers mostly prefer gadopiclenol (45.2% to 86.8% of cases) or express no preference (9.4% to 49.1%). With gadopiclenol at a dose of 0.05 mmol/kg, all readers predominantly reported no preference between GBCAs (46.5% to 77.6%). Similar rates of adverse reactions were reported with gadopiclenol (11.7%) and gadobenate dimeglumine (12.1%).
Conclusions
When compared to gadobenate dimeglumine at the standard dose of 0.1 mmol/kg, the doses of 0.05 and 0.1 mmol/kg can be considered as effective and safe clinical doses of gadopiclenol.

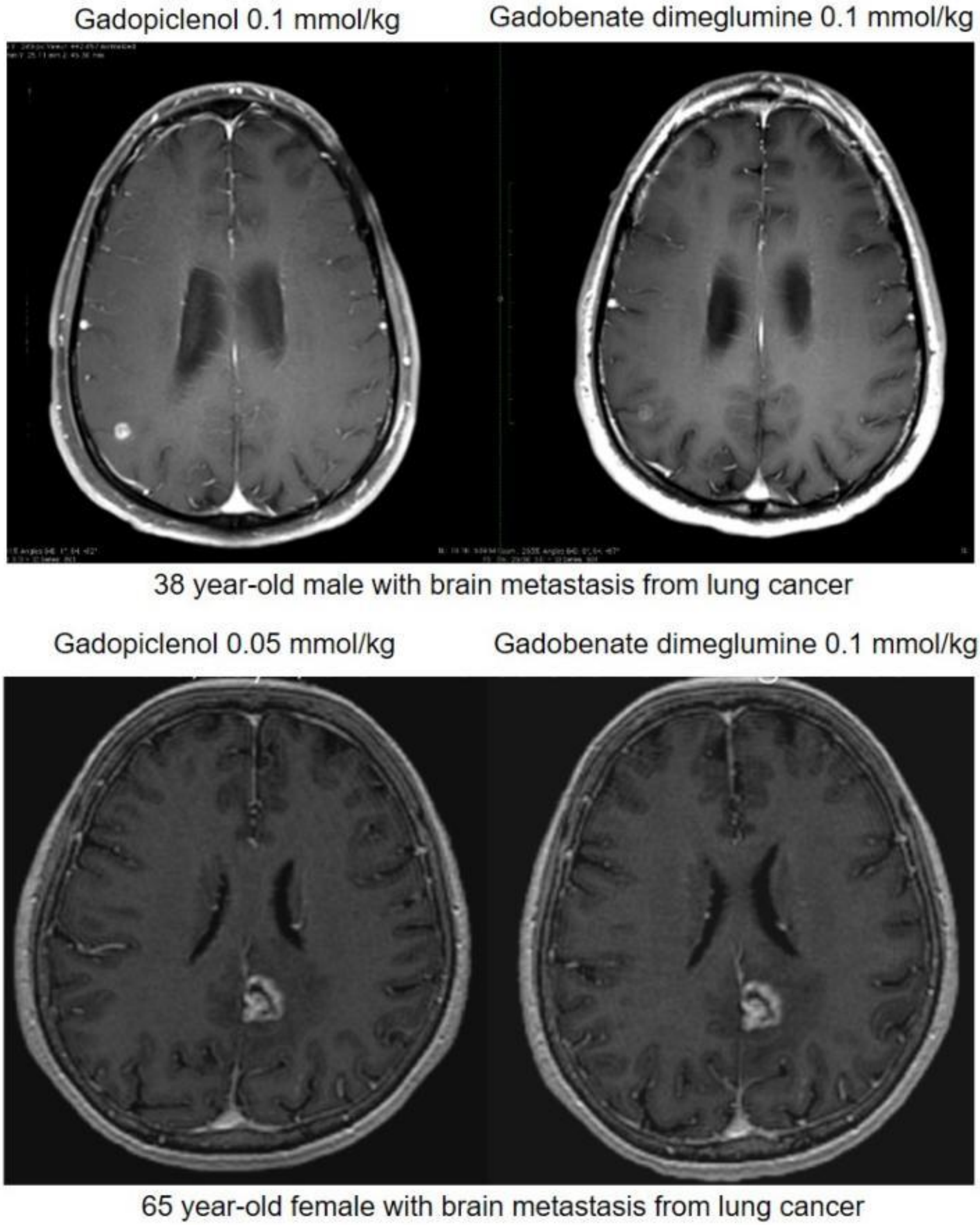

(Filename: TCT_2917_Figure_gadopiclenol_MultiHance_01_005_v2.jpg)

3232

11:14AM - 11:21AM

Glymphatic Pathway of Gadolinium-Based Contrast Agents through the Brain: Overlooked and Misinterpreted

K Deike-Hofmann[1], J Reuter[1], R Haase[1], D Paech[1], R Gnirs[1], S Bickelhaupt[1], M Forsting[2], C Heußel[3], S Heinz-Peter[1], A Radbruch[1]
[1]German Cancer Research Center, Heidelberg, Germany, [2]Institute of Diagnostic and Interventional Radiology and Neuroradiology, University Hospital Essen, Essen, Germany, [3]Thorax Clinic at Heidelberg University Hospital, Heidelberg, Germany

Purpose
The "glymphatic system" (GS), a brain-wide network of cerebrospinal fluid microcirculation[1-3], supplies a pathway through and out of the central nervous system (CNS); malfunction of the system is implicated in a variety of neurological disorders[4,5]. In this exploratory study, we analyzed the potential of a new imaging approach that we coined delayed T2-weighted gadolinium-enhanced imaging to visualize the GS in vivo.
Materials and Methods
Heavily T2-weighted fluid-attenuated inversion recovery MRI (hT2w-FLAIR) was obtained before, 3h and 24h after intravenous gadolinium-based contrast agent (GBCA) application in 33 neurologically healthy patients and 7 patients with an impaired blood-brain barrier (BBB) due to cerebral metastases. Signal intensity (SI) was determined in various cerebral fluid spaces and white matter hyperintensities (WMHs) were quantified by applying the Fazekas scoring system (FS).
Results
Delayed hT2w-FLAIR showed GBCA entry into the CNS via the choroid plexus and the ciliary body, with GBCA drainage along perineural sheaths of cranial nerves, and along perivascular spaces of penetrating cortical arteries. In all patients and all sites, a significant SI increase was found for the 3h and 24h time point compared to baseline. While no significant difference in SI was found between neurologically healthy patients and patients with an impaired BBB, a significant positive correlation between FS and SI increase in the perivascular spaces 3h post injection was shown.
Conclusions
Delayed T2-weighted gadolinium-enhanced imaging can visualize the GBCA pathway into and through the GS. Presence of GBCAs within the GS might be regarded as part of the natural excretion process and should not be mixed up with gadolinium deposition. Rather, the found correlation between deep WMH, an imaging sign of vascular dementia, and GS functioning demonstrated feasibility to exploit the pathway of GBCAs through the GS for diagnostic purposes.

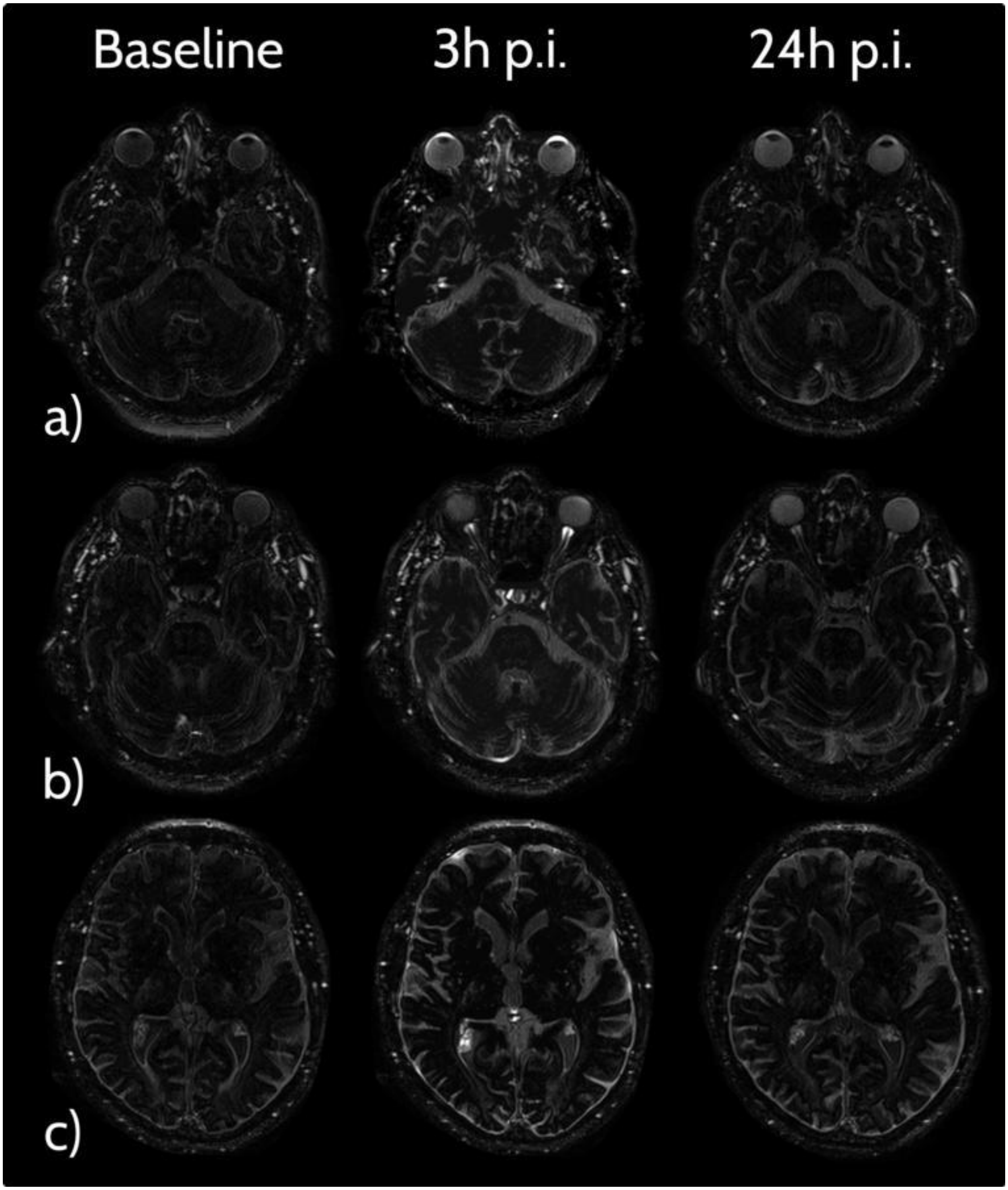

(Filename: TCT_3232_Fig.jpg)

3169

11:21AM - 11:28AM

Methemoglobinemia Mimics Contrast Enhancement on T1-Weighted Sequences and Represents a Potential Alternative to Gadolinium

J Mcnally[1], J Jaffey[2], C Larson[3], M Alexander[3], K Shumway[2], L Cohn[2], D Parker[3], R Day[3]
[1]UNIVERSITY OF UTAH, SALT LAKE CITY, UT, [2]University of Missouri College of Veterinary Medicine, Columbia, MO, [3]University of Utah, Salt Lake City, UT

Purpose
Gadolinium based contrast agents (GBCA) allow evaluation of enhancement and perfusion in the workup of many diseases including stroke, vascular disease, tumors and infectious/inflammatory states. Recently, gadolinium deposition has been noted in a variety of tissues including brain, raising safety concerns and the need to investigate alternative contrast agents. Our goal was to determine the feasibility of modulating methemoglobin levels in a canine CYB5R deficiency model as an alternative to GBCA.
Materials and Methods
Institutional Animal Care and Use Committee (IACUC) approval and consent of the canine's owner was obtained prior to this study. Magnetic resonance imaging was performed at 3T with T1-weighted sequences including 3D TOF, T1-weighted FSE and MPRAGE. Images were obtained without and with intravenous methylene blue (1 mg/kg) and analyzed via qualitative visualization and quantitative techniques. Tissue contrast was obtained by normalizing signal of vascular structures to adjacent muscle in multiple regions of interest per sequence.
Results
This canine CYB5R deficiency model with baseline methemoglobinemia of 19.5% decreased to 4.9% after methylene blue administration. Venous structures demonstrated higher tissue contrast between pre vs. post methylene blue on TOF (1.64 ± 0.14 vs. 1.09 ± 0.11, $p<0.001$), T1 TSE (1.71 ± 0.23 vs. 1.05 ± 0.22, $p<0.001$), and MPRAGE (1.34 ± 0.09 vs. 0.83 ± 0.05, $p<0.001$), and arterial structures demonstrated higher tissue contrast only on MPRAGE (1.23 ± 0.10 vs. 0.81 ± 0.12, $p<0.001$). Figure: Representative MPRAGE images demonstrate increased vascular signal between baseline and methylene blue administration. Comparing baseline methemoglobinemia (A) and post methylene blue (B), there was high T1 signal within epidural venous plexus (arrowheads) and in the basilar artery (arrow) that decreased after methylene blue treatment. Similarly, baseline methemoglobinemia (C) resulted in high T1 signal within the dural venous sinuses (arrowheads) that decreased after methylene blue treatment (D).
Conclusions
Modulating intracellular methemoglobin results in qualitative and quantitative signal changes on a variety of clinically applicable T1-weighted sequences. These occur within a range of methemoglobin concentration that could be used in humans. Techniques that induce mild methemoglobinemia deserve further study and may represent an alternative to GBCA.

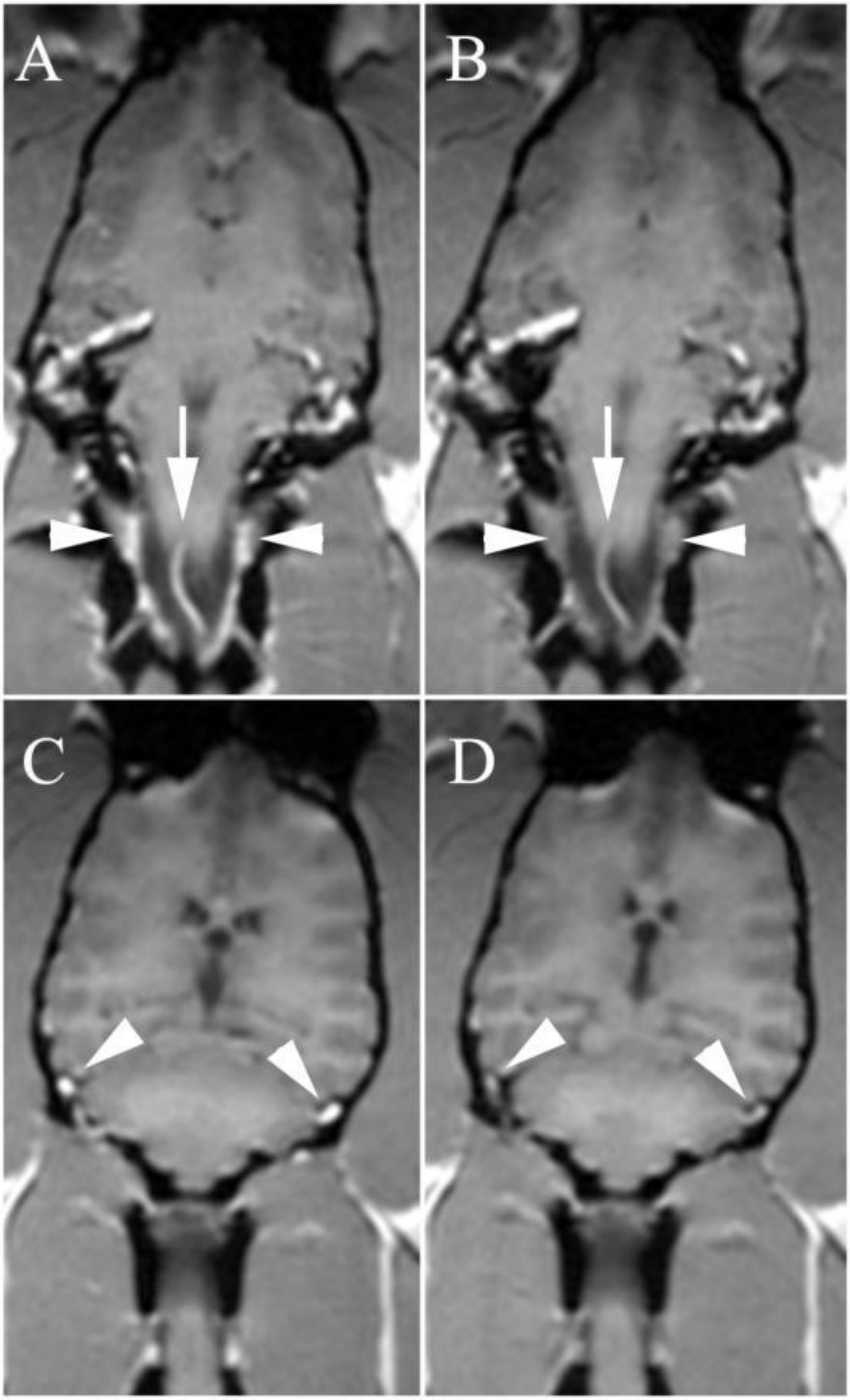
A
B
C
D

(Filename: TCT_3169_dogmethb110618copy.jpg)

3330

11:28AM - 11:35AM

Multi-shell, Multi-direction Diffusion Imaging as a Biomarker of Parenchymal Glymphatic Flow

J Andre[1], E Peskind[2], R Hendrickson[2], M Raskind[2], S Rane[1]
[1]University of Washington, Seattle, WA, [2]VA Puget Sound Health Care System, Seattle, WA

Purpose
The recently defined glymphatic system (GLS), which clears toxic cerebral solutes, is comprised of cerebrospinal fluid (CSF) flow around the subarachnoid and periventricular spaces through the paravascular brain parenchyma (interstitial fluid [ISF]/bulk flow), draining into the nasal lymphatics and dural venous sinuses[1]. We investigate the use of noninvasive Multi-Shell, multi-direction Diffusion Imaging (MSDI) to measure bulk GLS parenchymal flow (via the pseudo-diffusion coefficient, D*)[2], while leveraging the validated effect of prazosin, an α1-adrenergic antagonist to significantly increase ISF volume and GLS flow[3,4].
Materials and Methods
Eight adults (5F, 47-75 years old) were consented per IRB protocol, under HIPAA compliance, and scanned before administration of prazosin and after 9-12 weeks of titrated prazosin administration. To date, 6 subjects completed both time points. Acquisition: MSDI parameters: 6 directions + b0, 12 b-values (10, 20, 40, 80, 110, 140, 170, 200, 300, 500, 800, and 1000 s/mm2), resolution = 1×1×5 mm3, 30 slices, TR/TE=3000/62ms. Processing: Conventional diffusion, D, was calculated using standard mono-exponential decay for high b-values (500, 800, and 1000 s/mm2). Capillary volume, f, and pseudo-diffusion coefficient, D*, were derived in MATLAB 2016a as previously described[2]. Parameter maps before and after prazosin administration were co-registered. D, D*, and f were compared using a whole-brain region of interest. In 4 healthy controls, MSDI was performed twice within the same imaging session to obtain intra-scan variability, and performed at 10 week follow-up in 3 of these 4 controls to assess inter-scan variability.
Results
RESULTS: In 6 individuals undergoing prazosin therapy, mean ΔD* was 4.97±9.44% while mean ΔD was 0.08±3.39%. Mean ΔD* (4.97±9.44%) was notably greater than intra-scan (-0.25±1.95%) and inter-scan (0.47±10.8%) D* variability, respectively. Corresponding change in D was 0.08±3.39% with prazosin, -1.46±2.72% within a session, and 3.06±3.78% between scan sessions. Here D represents slow diffusion but fast transport over short distances, and D* represent fast diffusion but slow transport over long distances. Figure 1 depicts percent change in D (left chart) and D* (right chart) before and after 9-12 weeks of prazosin therapy (yellow bars; units of D, D* = mm2/s), intra-scan variability in D and D* (black bars), 10-week inter-scan variability in D and D* (blue bars). These data suggest that prazosin effects are greater than measurement variability and are detectable using D*. Following prazosin therapy, f changed by 5.44±8.47%, by -0.66±5.97% within a session, and by 2.63±5.90% between scan sessions. Noting the similar behavior of f and D* post prazosin, Spearman's correlation (ρ) was calculated at baseline for all 6 participants, which was 0.39 (p=0.47). Change in f (Δf/f) was also correlated with change in D* (ΔD*/D*), which revealed that ρ for Δf/f to ΔD*/D* was 0.96 (p=0.005).
Conclusions
Leveraging known effects of prazosin to increase ISF volume and GLS flow, we show that MSDI is a potential marker to detect increases in parenchymal ISF flow. While the exact physiological basis is unclear, D* is known to have contributions from perfusion, as well as ISF and CSF flow[2]. The latter are believed to comprise GLS flow. Although at baseline, a weak correlation was observed between f and D*, Δf/f was strongly correlated with ΔD*/D*, suggesting the possible mechanistic coupling of the vascular system to GLS when using prazosin, as suggested by prazosin's effect on syntrophins[5] and aquaporin 4

water channels[1]. Future work will involve validation using contrast-based, invasive, gold-standard markers of GLS as well as testing advanced models for evaluation of D*.

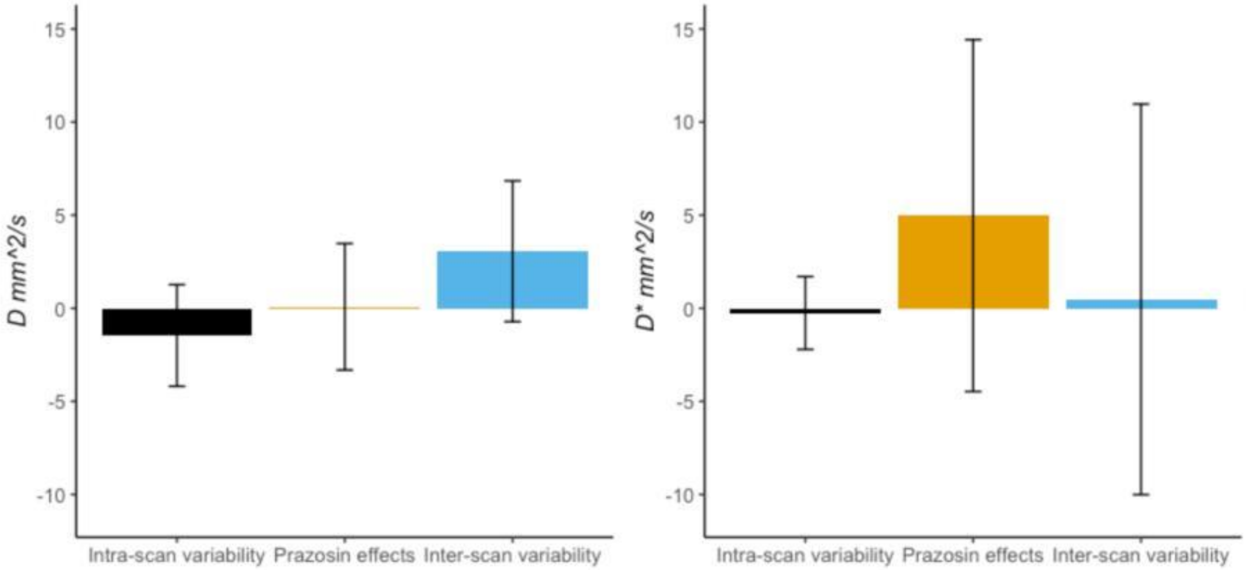

(Filename: TCT_3330_Figure1GlymphASNRabstract.jpg)

2863

11:35AM - 11:42AM

Perivascular Spaces – a Marker of Atrophy? An Exploratory Study in Patients with Frontotemporal Lobe Dementia

M Larvie[1], S Shams[2], J Pillai[3]
[1]Cleveland Clinic, Cambridge, MA, [2]Stanford, Menlo Park, CA, [3]Cleveland Clinic, Cleveland, OH

Purpose
Perivascular spaces (PVS) have been considered a normal finding in the brain and are typically overlooked. Recent data shows that PVS, when numerous, may be a marker of cerebral small vessel disease. We hypothesized that PVS may represent a third space of atrophy, in addition to the ventricles and subdural spaces, and that PVS would be numerous in areas of atrophy. To date, there is no computational method to reliably quantify and assess PVS and their relation to atrophy, and therefore manual measurements were used for assessment. We performed an exploratory assessment using a cohort of patients with a clinical diagnosis of frontotemporal dementia to test to the correlation between PVS and atrophy.
Materials and Methods
This is a cross-sectional study performed with a cohort of 18 patients with a clinical diagnosis of frontotemporal dementia, as established at a specialty behavioral neurology clinic. All patients underwent 3.0T MRI imaging. PVS were counted for each brain lobe, in each hemisphere. Regional atrophy was assessed through the global cortical atrophy scale for each brain lobe, also in each hemisphere.
Results
Patients with frontotemporal lobe dementia had the highest number of perivascular spaces in the frontal lobe (median 9, interquartile range 6-15). Similarly, cortical atrophy was highest in the frontal lobes. There was a moderate correlation between number of perivascular spaces and regional atrophy in the occipital lobe (r=0.5, P=0.001). No other association between perivascular spaces and regional atrophy was found.
Conclusions
PVS are common and frequent in the frontal lobe in patients with frontotemporal lobe dementia. The total

number of frontal PVS are not associated with frontal cortical atrophy, which may be due to the imprecision of visual assessment of atrophy in this study. Atrophy of the occipital lobe was associated with an increased number of PVS, which may reflect the predilection of small vessel disease for the occipital lobe. Further assessment of the correlation between PVS and atrophy will focus on quantitative assessment using brain segmentation techniques. Additionally, we will undertake visual assessment of PVS in other patient cohorts, including patients with Alzheimer disease, to further test the performance of such an approach.

3278

11:42AM - 11:49AM

The Anterior Chamber of the Eye: An Overlooked Entry of the Natural Excretion Pathway of Gadolinium Based Contrast Agents?

A Radbruch[1], K Deike-Hofmann[2], E Stenzel[1], M Forsting[3]
[1]University Hospital Essen, Essen, Germany, [2]German Cancer Research Center, Heidelberg, Baden-Württemberg, [3]Institute of Diagnostic and Interventional Radiology and Neuroradiology, University Hospital Essen, Essen, Germany

Purpose
Previous studies provided evidence that gadolinium can be found in the anterior chamber (AC) of the eye several hours after injection of gadolinium-based contrast agents (GBCAs). In the current study, we analyzed if gadolinium can be detected immediately after injection of a macrocyclic GBCA on contrast-enhanced T1 weighted images in the AC of children.
Materials and Methods
This retrospective study was approved by the ethical committee of the University Essen and healthy eyes of fifty children treated for retinoblastoma of the contralateral eye were assessed with an orbital coil. Difference of signal intensity (SI) ratios of the AC and vitreous chamber (VC) were determined on pre and post contrast-enhanced T1 weighted images.
Results
47 of 50 patients showed an increase of the AC-to-VC ratio immediately after GBCA injection (median SI ratio difference = 0.09, interquartile range 0.06-0.17; $p < 0.001$) and spearman correlation revealed a negative association between patient age and SI ratio difference ($\varrho = -0.44$, $p = .001$).
Conclusions
The current study provides evidence that gadolinium can be found in the AC of the eye immediately after GBCA injection. A possible pathway to the AC might be the excretion through the ciliary body and the negative correlation between patient age and SI increase might be explained by a maturation process of the blood ocular barrier impeding the excretion of GBCAs with increasing age. Future studies should assess the duration as well as possible side effects and potential diagnostic applications of this new imaging finding.

Tuesday, May 21, 2019
1:00PM - 2:30PM
Adult Brain Potpourri Topics 2

2556

1:07PM - 1:14PM

An Atypical Case of Fulminant Hemorrhagic Neuromyelitis Optica

M Mitsunaga[1], O Raslan[1], A Ozturk[1], J Chang[1], M Bobinski[1], J Ziegler[1], B Dahlin[1], N Pham[1]

[1]*University of California Davis Health, Sacramento, CA*

Purpose
To report a rare case of rapidly progressive, hemorrhagic, tumefactive brain lesions associated with neuromyelitis optica (NMO).
Materials and Methods
A 59-year-old African-American woman presented with paresthesias and lower extremity weakness. Initial MRI of her total spine showed a long-segment T2 hyperintense, non-enhancing lesion extending from C7 to T6. Initial brain MRI showed T2 prolongation in the left cerebellar peduncle without diffusion abnormality or enhancement. Cerebrospinal fluid studies were negative for infection but positive for aquaporin-4 autoantibody, and she was diagnosed with NMO. Her disease progressed over the course of several years with worsening symptoms of optic neuritis, lower extremity weakness, and worsening back pain, despite aggressive treatment with steroids, immunosuppressants, and plasma exchange. She continued to decline, ultimately to a Glasgow Coma Scale of 3, requiring a tracheostomy and gastrostomy tube.
Results
Sequential brain MRIs showed progression of white matter signal abnormalities. Brain MRI with contrast (not shown) at the beginning of the most recent hospitalization showed FLAIR signal hyperintensity and enhancement involving the periventricular white matter and posterior limb of the right internal capsule. Repeat MRI just nine days later shows multiple new FLAIR signal hyperintense lesions (Figures A and B) including a confluent cortical and subcortical lesion in the left parieto-occipital lobe demonstrating restricted diffusion (Figure C), leptomeningeal enhancement (not shown), and susceptibility artifact (Figure D), consistent with cytotoxic edema and petechial hemorrhage.
Conclusions
Hemorrhagic leukoencephalitis is a rare and severe complication of demyelinating diseases such as acute disseminated encephalomyelitis and multiple sclerosis; however, it has never been described in association with NMO. We report a rare case of hemorrhagic leukoencephalitis in the setting of NMO, suggesting that perivascular and vascular hemorrhagic necrosis can be part of the pathophysiology of this disease process.

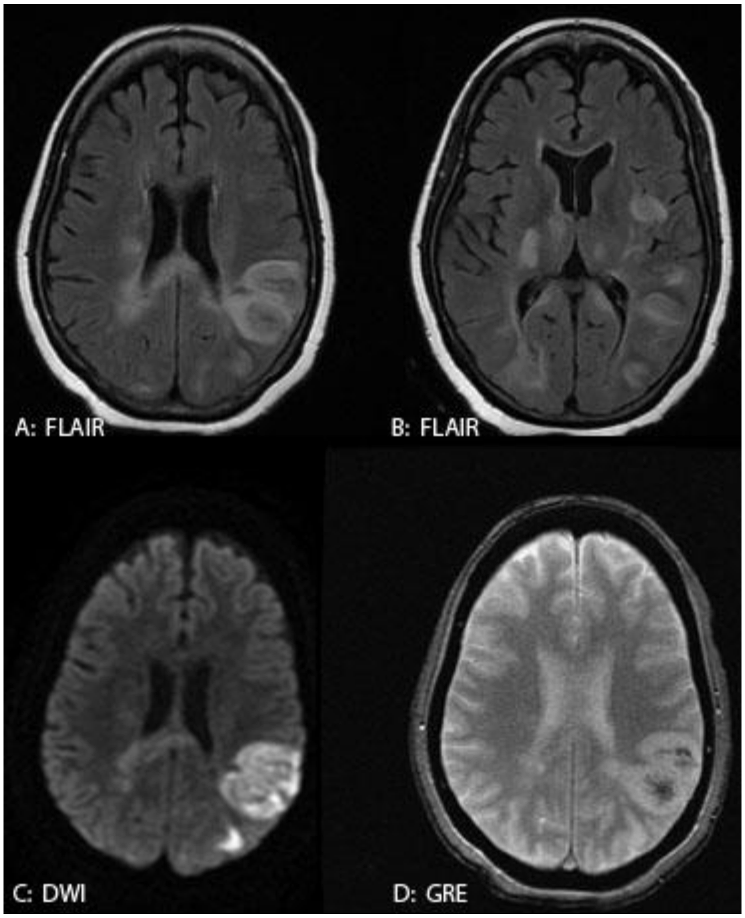

(Filename: TCT_2556_NMOhighrescopy2.jpg)

2276

1:14PM - 1:21PM

An Unusual Presentation of Posterior Reversible Encephalopathy Syndrome

C Gemmell[1], J Thiessen[1], C MacMillan[1], J Sadler[2], J Pollock[3]
[1]Oregon Health and Science University, Portland, OR, [2]Salem Radiology Consultants, Salem, OR, [3]Oregon Health & Science University, Portland, OR

Purpose
Posterior reversible encephalopathy syndrome (PRES) is frequently seen in clinical practice with symmetric cortical/subcortical T2 and FLAIR hyperintense signal most commonly involving the parietooccipital region. We present a rare case of PRES mimicking a diffuse midline brainstem glioma with hemorrhage.
Materials and Methods
A 44-year-old man with a past history of tobacco dependence and methamphetamine use disorder presents with acute left hemibody and right facial weakness, paresthesias, and double vision. CT from the Emergency Department demonstrated intraparenchymal pontine hemorrhage. The patient was admitted to the Neuro ICU for management. An MRI was obtained, for which differential diagnostic considerations included a midline glioma. Radiation oncology and neurosurgery were consulted and recommended a biopsy to direct treatment planning, however the patient deferred. Steroids were administered and hypertension treated and over 10 days the patient's left-sided weakness improved, with stable left hemibody sensory loss and partial right cranial nerve III palsy. He was discharged 4 days later in stable

condition. At 2-week follow-up visit he continued to suffer from diplopia and left-sided paresthesias. Follow-up imaging was ordered which demonstrated near complete resolution of previously seen T2/FLAIR signal within the brainstem and evolving residual pontine blood products; findings consistent with an atypical presentation of posterior reversible encephalopathy syndrome (PRES).

Results

Initial CT of the head revealed right-sided pontine hemorrhage and significant vasogenic edema. Subsequent CTA of the head and diagnostic cerebral angiogram without evident nidus of hemorrhage. Brain MRI showed susceptibility within the right pons and middle cerebellar peduncle with surrounded mass-like T2/FLAIR hyperintense signal expanding the pons and involving the cerebellum and medulla without evident enhancement (Figure 1). Based on initial appearance, differential considerations favored diffuse midline glioma with hemorrhage; PRES was suggested as an alternative consideration. Follow up MRI 4 weeks later showed complete resolution of T2 hyperintensity with evolving residual blood products.

Conclusions

Isolated involvement of the brainstem with hemorrhage is extremely rare in PRES. In a hypertensive patient with otherwise unexplained symmetric T2 hyperintensity that resolves on follow-up, this rare variant of PRES should be considered.

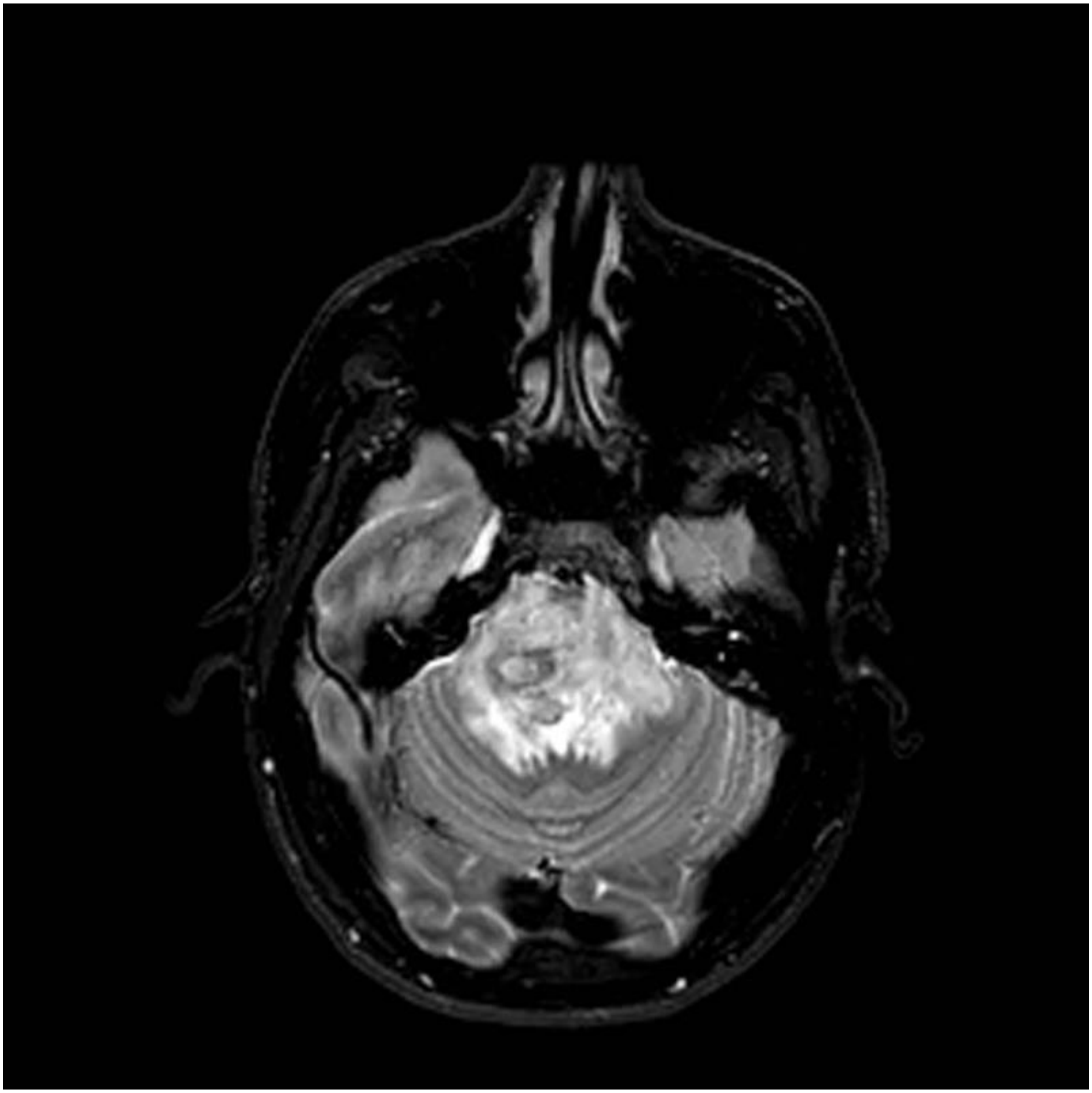

(Filename: TCT_2276_Figure1.jpg)

2996

1:21PM - 1:28PM

Combination Immune Checkpoint Inhibitor-Induced Hypophysitis: A case report and review of the clinical and imaging findings.

N Hyson[1], B Griffith[1], J Corrigan[2], H Marin[1], S Patel[3]
[1]HENRY FORD HEALTH SYSTEM, Detroit, MI, [2]HENRY FORD HOSPITAL, NORTHVILLE, MI, [3]HENRY FORD HOSPITAL, DETROIT, MI

Purpose
Immune checkpoint inhibitors have emerged as a promising new class of anti-cancer drugs. Unfortunately, while potentiating the immune system's response to cancer cells, these drugs also place the

patient at risk for the development of immune-related adverse events (irAEs). Although most commonly involving the gastrointestinal tract and skin, involvement of the endocrine system also occurs, with hypophysitis one of the most frequent complications. This excerpta describes a case of immune checkpoint inhibitor-induced hypophysitis in a patient with metastatic melanoma undergoing combination therapy.

Materials and Methods

A 60-year-old male undergoing combination immune checkpoint therapy with nivolumab and ipilimumab for metastatic melanoma developed headaches. An MRI of the brain was obtained and demonstrated new enlargement of the pituitary. The patient was also found to be hypothyroid. Further endocrinological evaluation revealed evidence of pituitary insufficiency, including low testosterone, low random cortisol level, and low TSH. At this time, the checkpoint inhibitor therapy was held and the patient was treated with prednisone with excellent clinical response, including resolved headaches and improved energy. Follow-up MRI demonstrated resolution of the pituitary enlargement.

Results

Sagittal pre-contrast MR images demonstrate a normal appearance of the pituitary prior to initiation of the combination checkpoint inhibitor therapy (A) and interval enlargement of the pituitary approximately three months later near the end of the combination therapy (B). A sagittal post-contrast MR image following checkpoint inhibitor therapy discontinuation and steroid treatment demonstrates near resolution of the pituitary enlargement (C).

Conclusions

As new cancer therapies emerge, radiologists must remain aware of the potential for unique adverse effects – such as those occurring with immune checkpoint inhibitor therapies, including hypophysitis. In addition, as the imaging appearance of hypophysitis is nonspecific, understanding the clinical context in which it occurs can aid in recognizing it as a possible diagnosis and help guide appropriate clinical management.

(Filename: TCT_2996_Hypophysitis.jpg)

2744

1:28PM - 1:35PM

DECT Comparison with MR SWI Following Acute Stroke Management

K Peters[1], A Khanna[1]

[1]*University of Florida, Gainesville, FL*

Purpose

Case report demonstrating the specificity of DECT in evaluation of hemorrhage relative to MR Susceptibility Weighted Imaging.

Materials and Methods
73yo male presented with acute onset of right sided hemiparesis, facial droop, and aphasia found to have short segment Left ICA occlusion on CTA with relative preserved CBV on CT perfusion imaging in the setting of elevated TTP. Patient was treated with IV tPA and taken for mechanical thrombectomy. Patient suffered a rapid decline during the procedure requiring emergent intubation. Procedure was completed with TICI 3 reperfusion.
Results
Immediate post procedure CT was performed with Dual Energy Technique. 120KeV equivalent imaging demonstrated high attenuation material in the region of the left basal ganglia (Image A) which correlated with the Iodine map (Image B). No areas of high attenuation were noted in the region of question on the Virtual Subtraction Images. One day later the patient was taken to MR and these areas were intensely dark on SWI (Image C), raising concern for potential underlying hemorrhage. DECT was repeated demonstrating clearing of the high attenuation material (Image D), confirming this did not represent a focus of hemorrhage.
Conclusions
DECT was accurate in defining that the area of high attenuation did not represent a focus of hemorrhage as confirmed on short term follow-up CT. Therefore the area of signal dropout on MR SWI was not secondary to hemorrhage. Potential etiologies of the SWI findings are chemical shift artifact related to calcium or the effect of parenchymal contrast staining. Review of the literature suggests that areas of contrast staining should not produce alteration of SWI. This case highlights both the specificity of DECT in the detection of iodine staining vs hemorrhage and the need for further work in the imaging findings of post stroke intervention on MRI.

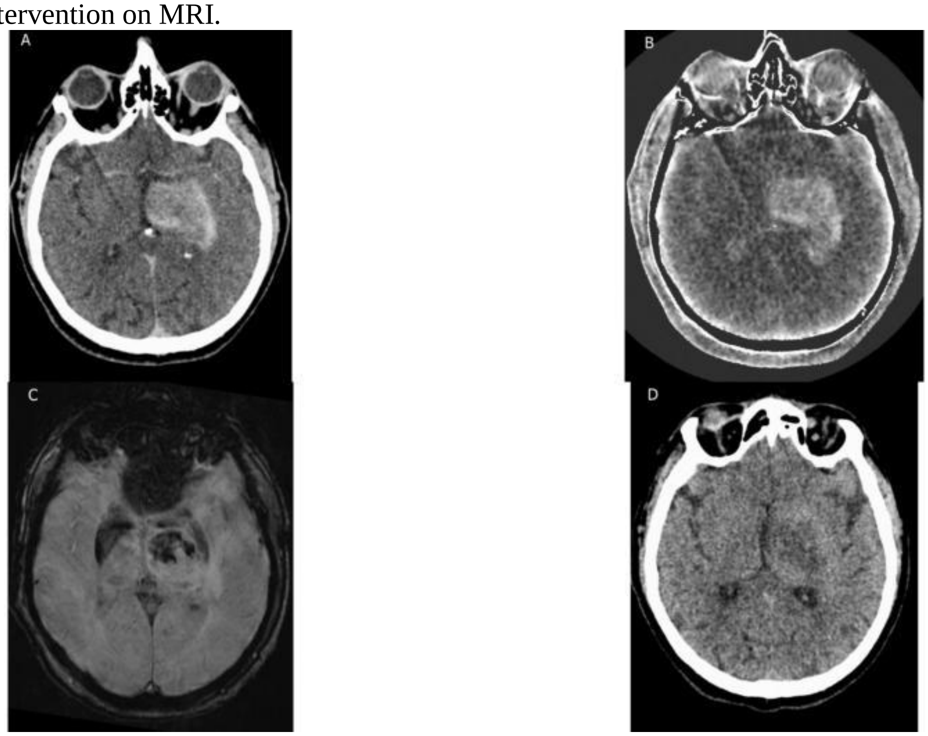

(Filename: TCT_2744_asnr_2019_krp_dect.jpg)

3631

1:35PM - 1:42PM

Do NOT Make A MoVemeNT on MVNT: Multinodular and Vacuolating Neuronal Tumor

I Ikuta[1]
[1]YALE UNIVERSITY-SCHOOL OF MEDICINE, MILFORD, CT

Purpose

Sometimes a patient with seizures not controlled by anti-epileptic drugs may need neurosurgery. Epilepsy imaging is a key part of the evaluation for patients with seizures, as it may locate a lesion amenable to neurosurgical cure. Multinodular and vacuolating neuronal tumor (MVNT), however, has been felt to be a lesion that may not be responsible for epileptogenesis, and may be more incidental and unrelated. We provide one such case to illustrate the characteristic imaging findings, and to stress the need for further epilepsy work-up if resection is to be considered.

Materials and Methods

A 16-year-old male presented with a long history of partial-complex seizures controlled with anti-epileptic drugs, but recently initially starting with right hand tremors and quickly evolving to generalized seizures. He underwent neuroimaging to determine if there was an epileptogenic focus amenable to neurosurgical intervention.

Results

MRI brain demonstrated an area of punctate T2/FLAIR hyperintensities within centered within the right frontal subcortical white matter, with possible punctate foci of intrinsic T1 hyperintensity, and without definite enhancement. A preliminary concern for dysembryoplastic neuroepithelial tumor (DNET) or other cortically-based tumor was raised. However, prior to going to epilepsy board review, a neuroradiologist that regularly attends epilepsy board review recognized the bubbly pattern and appearance of T2, FLAIR, and T1 sequences (see Images).

Conclusions

Multinodular and Vacuolating Neuronal Tumor (MVNT) is a lesion that should be recognized by its characteristic imaging appearance. While a differential diagnosis may be needed for any atypical appearance of MVNT, a classic lesion should not be resected as it is possibly a hamartoma instead of a true neoplasm. MVNT may not be the source of epileptogenesis (possibly more of an incidental finding). It has been studied by imaging and by pathology, and with recent recognition by the World Health Organization (WHO). As more cases are identified, it will be more thoroughly understood. Recognizing and understanding this lesion is key to preventing unnecessary neurosurgery, which would be an unnecessary risk for the patient and could worsen the patient's condition. For this case, the patient improved with anti-epileptic drug regimen adjustments, and imaging will be performed only if symptomatic.

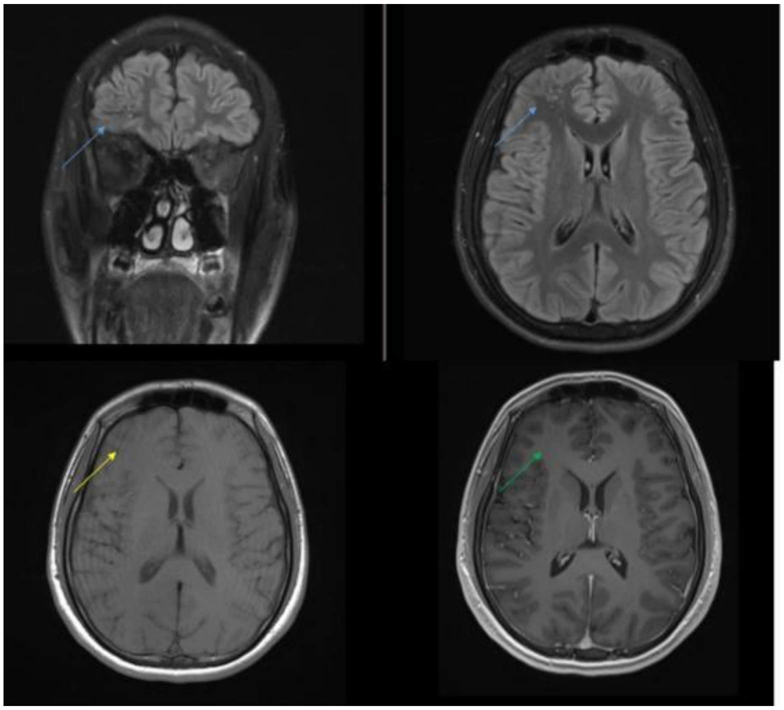

(Filename: TCT_3631_MVNT_ASNR19.jpg)

2629

1:42PM - 1:49PM

Hashimoto's Encephalopathy

B Hastings[1], V Ivanovic[1]
[1]*Beth Israel Deaconess Medical Center, Boston, MA*

Purpose
Review MRI features of Hashimoto's encephalopathy.
Materials and Methods
69-year-old woman with history of hypothyroidism, currently off medications for several months, presented with new onset of altered mental status and seizures. MRI of the brain demonstrated multiple cortical and subcortical FLAIR hyperintensities , with associated mild contrast enhancement, without restricted diffusion. Laboratory studies were significant for TSH > 100 uIU/mL (nl <4.2) and elevated thyroid peroxidase antibodies at 696 IU/mL (nl <35). Lumbar puncture was negative for infection and neoplasm; 14-3-3 protein was elevated favoring inflammatory process. Work-up for demyelinating process was negative. Because of worsening clinical condition, the patient underwent brain biopsy. Biopsy was consistent with Hashimoto's encephalopathy. Therapy with steroids and autoimmune agents was initiated. Our patient has had a mixed response over time with improved seizure control, persistent episodes of altered mental status and waxing and waning MR abnormalities.
Results
MRI of the brain demonstrated multiple cortical and subcortical FLAIR hyperintensities , with associated mild cortical and leptomeningeal contrast enhancement, without restricted diffusion.
Conclusions
Hashimoto's encephalopathy is a rare and poorly understood disorder with variable MR appearance. This condition should be a diagnostic consideration in a poorly controlled or untreated hypothyroid patients presenting with acute to subacute neurologic symptoms. Early diagnosis is important, as some of imaging findings may be reversible with treatment.

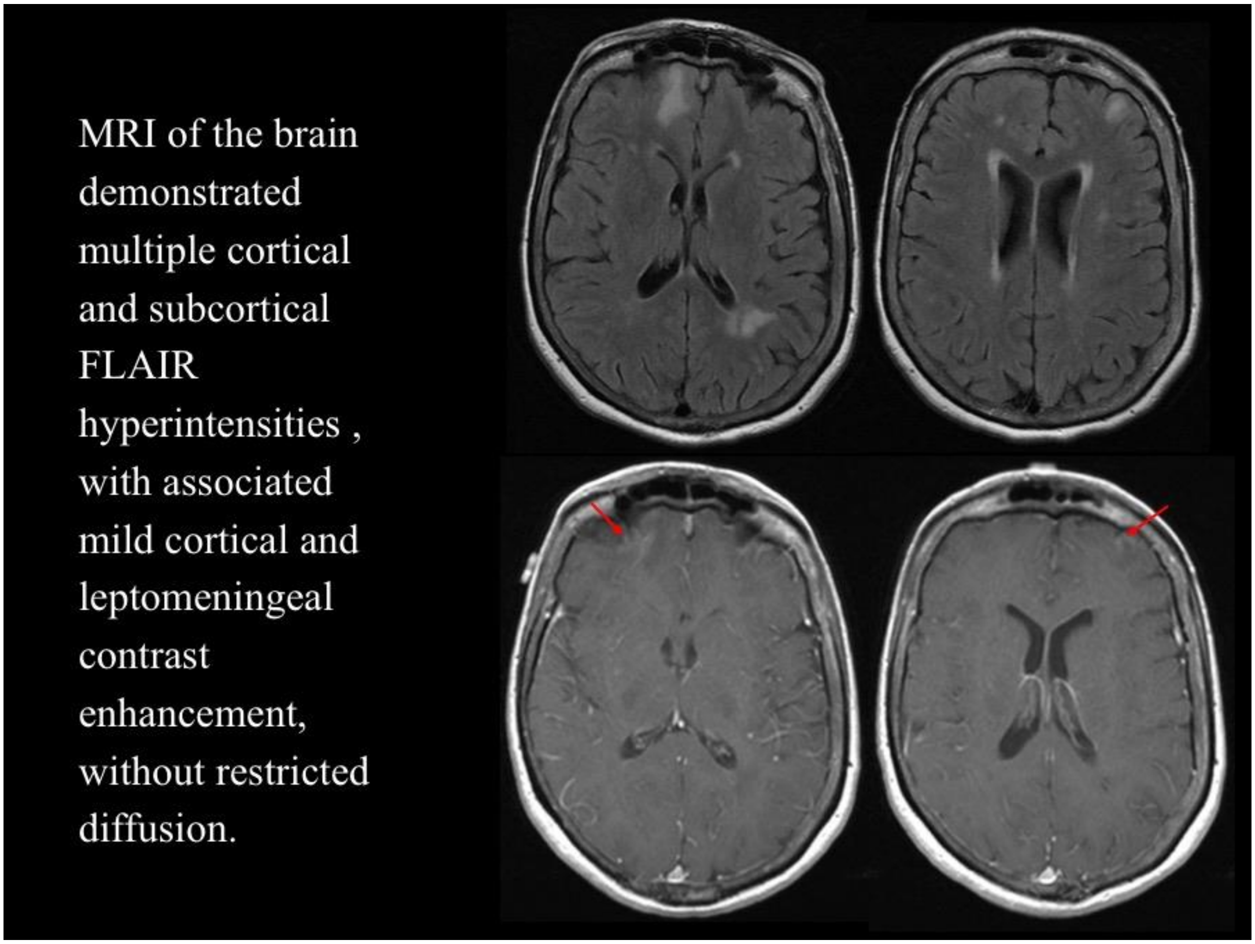

(Filename: TCT_2629_HashimotosASNR.jpg)

2797

1:49PM - 1:56PM

Influenza B Virus Encephalitis with Associated Reversible Restricted Diffusion in the Splenium of the Corpus Callosum "Boomerang Sign"

S Kamalian[1], M Lake[1], S Kamalian[2], S Teoh[1], P Sasson[1]
[1]Mount Auburn Hospital, Cambridge, MA, [2]Massachusetts General Hospital, Boston, MA

Purpose
Influenza-B virus is a rare but well-known cause of encephalitis in adults with variable neurological symptoms and imaging findings, making it a challenging diagnosis. Our purpose is to review the imaging features of influenza B virus encephalitis with associated reversible and irreversible restricted diffusion.
Materials and Methods
A 40 year-old right-handed man presented to our ED with sudden onset of left sided numbness, diplopia, nausea and diaphoresis; last known well time was 2 hours before arrival. The initial examination was notable for gaze evoked right horizontal nystagmus and left hemisensory loss (NIHSS=1). The initial imaging was normal. Approximately 8 hours after admission, the patient developed severe left hemiplegia, left facial droop, and dysarthria. Laboratory studies were notable for leukocytosis, positive nasal-swab rapid influenza-B antigen test, and elevated ESR and CRP. Treatment with Oseltamivir was initiated. He underwent lumbar puncture, which revealed CSF-WBC count of 6. All other relevant laboratory studies were negative.

Results
The initial head-CT, head and neck CT-angiogram and brain MRI were unremarkable. The repeat MRI 2 days after admission shows restricted diffusion in the splenium of the corpus callosum ("boomerang sign"), and bilateral centrum semiovale, which resolved on the follow up imaging (day 6) after treatment. In addition, there was a new area of restricted diffusion in the right pons, which persisted on follow up imaging, representing infarction (Figure).

Conclusions
Influenza-B virus associated encephalitis has variable neurological symptoms and imaging findings, making it a challenging diagnosis. It is important to consider Influenza-B virus associated encephalitis in the differential diagnosis of reversible restricted diffusion in the splenium of corpus callosum. Influenza infection is also associated with increased risk of ischemic stroke. Therefore, it should be considered in the differential diagnosis, particularly during the influenza season. Familiarity with the constellation of possible imaging findings and related interval changes is essential for radiologists to guide patient management.

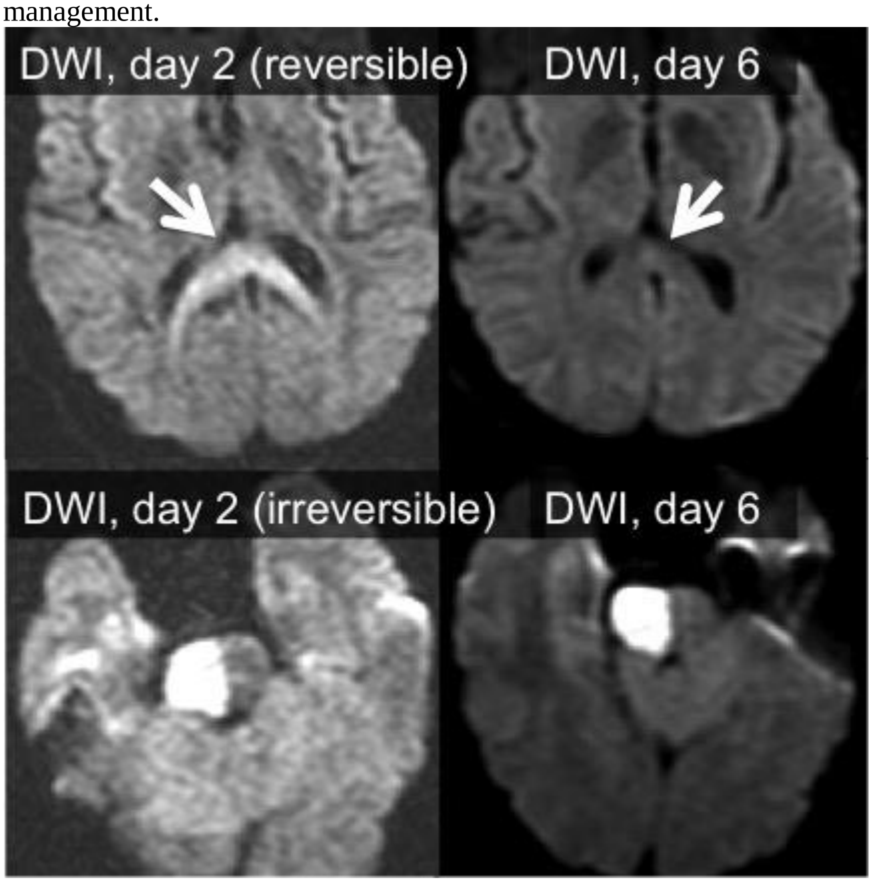

(Filename: TCT_2797_ASNRinfluenza.jpg)

3090

1:56PM - 2:03PM

Lymphohistiocytosis: A Case Report

C Dixon[1], A Nemeth[2]
[1]Northwestern University, Chicago, IL, [2]Northwestern University / Feinberg School of Medicine, Chicago, IL

Purpose

To discuss hemophagocytic lymphohistiocytosis (HLH) and how it may pose a diagnostic dilemma at brain imaging.

Materials and Methods

A 23-year-old pregnant female at 7 weeks, 4 days gestational age presented following multiple seizures. She experienced upper respiratory symptoms and fevers in the days leading up to admission. She was initially alert and oriented at admission but subsequently became more confused requiring ICU admission and intubation. The patient was found to be in thyroid storm and started on antithyroid and antiepileptic medications with no initial change in mentation. She had multiple brain studies that showed cerebral white matter abnormalities with a wide differential diagnosis. Hospitalization was complicated by persistent fevers, multifocal pneumonia, pulmonary hemorrhage, and a missed abortion. She met the clinical diagnostic criteria for the diagnosis of HLH.

Results

Head CT obtained at presentation showed hypoattenuation involving the cerebral white matter and the corpus callosum. Initial noncontrast MRI showed areas of restricted diffusion/abnormal signal in the cerebral white matter and splenium. Subsequent contrast-enhanced MRI showed worsening restricted diffusion/abnormal signal involving the cerebral white matter and splenium with a small focus of enhancement within the splenium. PET scan showed no evidence for hyper-metabolism. Subsequent MRI showed a decrease in restricted diffusion/abnormal signal involving the cerebral white matter and splenium with resolution of enhancement. While the differential diagnosis was wide and initially included entities such as posterior reversible encephalopathy syndrome, acute disseminated encephalomyelitis, and lymphoma, after excluding these entities, findings may be compatible with HLH.

Conclusions

Hemophagocytic Lymphohistiocytosis (HLH) is a rare entity of which neuroradiologists should be aware as it can be fatal or lead to long term morbidity if not treated promptly.

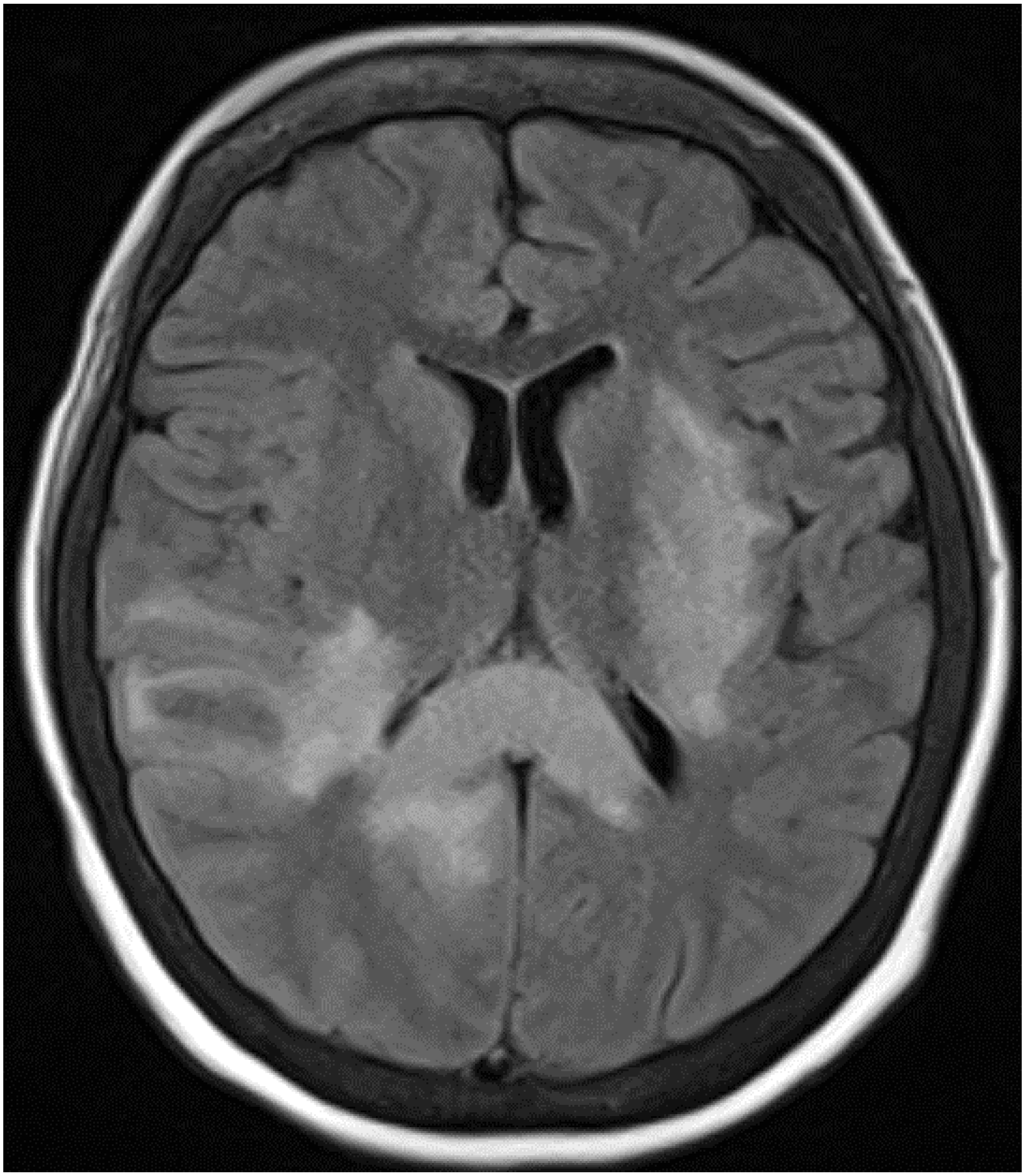

(Filename: TCT_3090_FLAIR.gif)

3448

2:03PM - 2:10PM

PET and Diffusion-Weighted MRI Features in Creutzfeldt-Jakob Disease

R Taylor[1], N Patel[1], R Fisher[1], E Lai[1], S Fung[1]
[1]*Houston Methodist Hospital, Houston, TX*

Purpose
Creutzfeldt-Jakob disease(CJD) is a transmissible spongiform encephalopathy characterized by rapidly progressive dementia, myoclonus and ataxia. We present a case series of four patients with CJD, emphasizing one clinical course, in order to correlate 18FDG-PET patterns of hypometabolism with hyperintense signal on DW-MRI.

Materials and Methods

A 58 year-old male presented with gait ataxia and confusion. Initial labs and imaging showed no acute findings. Two weeks later, worsening ataxia, behavioral changes, and limb rigidity were observed despite treatment. CSF analysis revealed negative 14-3-3 and elevated tau. Sharp wave EEG discharges were recorded. His condition progressively deteriorated, and death occurred 3 months after presentation. Autopsy revealed spongiform changes and positive prion protein monoclonal antibody immunostaining consistent with CJD

Results

Although initial MRI was interpreted as negative, retrospectively, increased DWI signal was present in the right basal ganglia. MRI one month later showed progressive conspicuity and extent of DWI signal with reduced ADC involving the right basal ganglia and patchy involvement in the right frontal, temporal, parietal lobes and insula. 18FDG-PET showed markedly reduced uptake throughout the right cerebral cortex, basal ganglia, and right thalamus in similar but more extensive distribution to DWI.

Conclusions

CJD is characterized on DW-MRI by reduced diffusion in the cortex and basal ganglia; however, early findings can be subtle and mimic other conditions such as hypoxic-ischemic encephalopathy, infectious and autoimmune encephalitis. On 18FDG-PET, CJD is associated with reduced uptake in the cortex, basal ganglia, and thalami. Aside from corticobasal ganglionic degeneration, other neurodegenerative diseases typically spare basal ganglia and thalami. Encephalitis can present with increased or decreased 18FDG uptake. In CJD, each method alone may be subtle or non-specific, but involved regions on DW-MRI and PET are correlated. DW-MRI and PET in conjunction may increase sensitivity, specificity, and earlier detection of CJD.

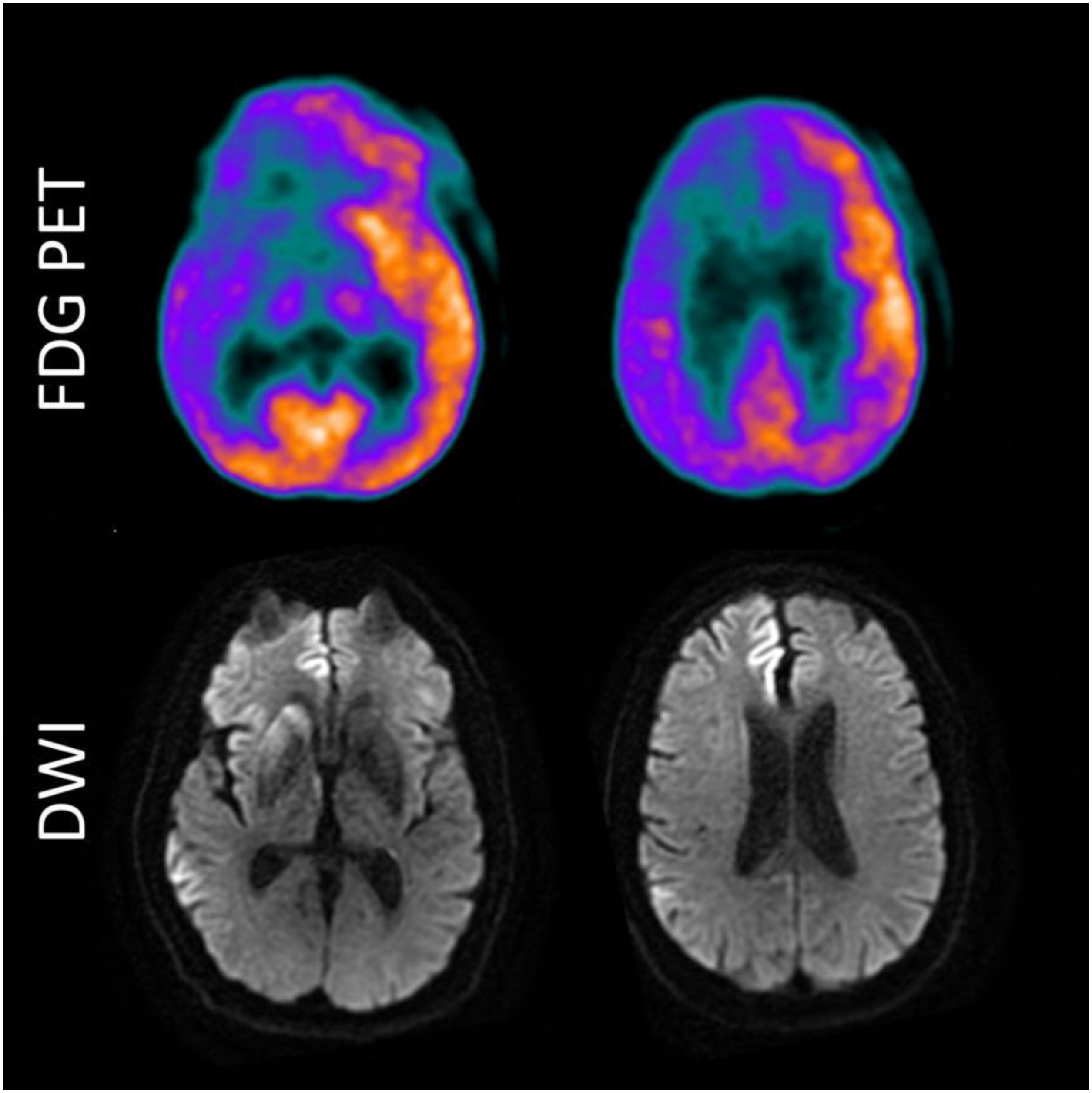

(Filename: TCT_3448_BLCJD.jpg)

3604

2:10PM - 2:17PM

Recurrent Encephalitis due to anti-NMDA Receptor Antibody Encephalitis in a Patient with HIV CSF Escape

A Cervantes-Arslanian[1], J Post[2]
[1]Boston University School of Medicine/ Boston Medical Center, Boston, MA, [2]Boston University School of Medicine / Boston Medical Center, Winchester, MA

Purpose
To educate about the differential diagnosis in HIV Encephalitis

Materials and Methods

A man with well controlled HIV (serum viral load suppressed) developed sub-acute decline in cognitive functioning with behavioral changes. He rapidly deteriorated into akinetic mutism then coma complicated by non-convulsive status epilepticus. CSF revealed a lymphocytic pleiocytosis and CSF HIV viral load >15,000. He was diagnosed with HIV encephalitis due to CSF escape. His anti-retrovirals were changed to a regimen with increased CNS penetrating effectiveness. After many months he returned to close to his neurologic baseline. Two years later, he relapsed with decline in functioning, aphasia, automatisms, and tremor. CSF again showed pleiocytosi but suppressed viral load. He was treated with steroids. An autoimmune encephalitis panel revealed the presence of anti-NMDA receptor antibodies. The patient improved on high dose steroids but eventually needed discontinuation due to adverse effects. Months later he developed severe agitation, paranoia, and wide fluctuations in consciousness. CSF showed a pleiocytosis and HIV was absent. NMDA receptor antibodies were again present. He was given a steroid pulse and initiated on rituximab with gradual improvement.

Results

Initial MRI (a) demonstrated diffuse bilateral confluent slightly asymmetric white matter FLAIR hyperintensity involving the periventricular white matter extending to subcortical regions. After his first relapse, MRI showed FLAIR lesions within the left frontal and parietal lobes. At the time of his second relapse, MRI revealed new non-enhancing T2 FLAIR signal abnormality within the left temporo-occipital white matter and within the right corona radiata. Following rituximab his MRI (b) demonstrated resolution of the majority of the parenchymal abnormalities.

Conclusions

Imaging findings suggestive of HIV encephalitis may be the product of uncontrolled HIV within the CNS even in the presence of serum suppression (known as CSF escape). This uncontrolled HIV expression in the CNS may be causally linked to the anti-NMDA receptor antibody encephalitis seen in our patient.

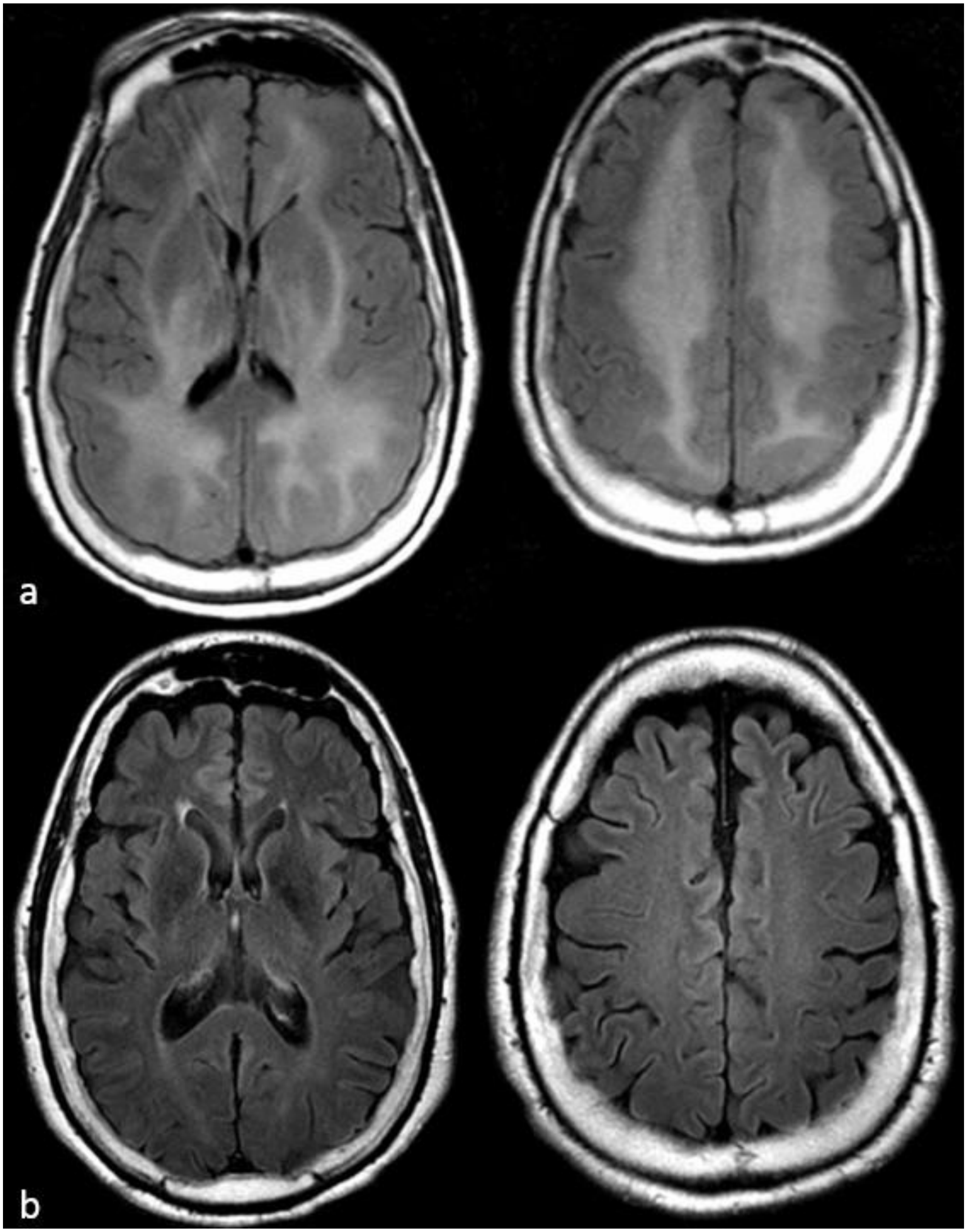

(Filename: TCT_3604_JDASNRAbstractImage.jpg)

3654

2:17PM - 2:24PM

Rheumatoid Meningitis with Communicating Hydrocephalus

C Krumpelman[1], C Cankurtaran[1], B Liu[1]
[1]*Northwestern University Feinberg School of Medicine, Chicago, IL*

Purpose

This abstract describes a case of rheumatoid meningitis with communicating hydrocephalus, a previously unseen association.

Materials and Methods

The patient was a 52-year-old man who presented to the ED with a seizure and left-sided weakness. His medical history was significant for a 33-year history of rheumatoid factor positive rheumatoid arthritis, unresponsive to disease-modifying anti-rheumatic drugs, which had been managed with long-term steroid therapy. At presentation, a non-contrast CT head examination showed a small right frontal acute subarachnoid hemorrhage. A subsequent brain MRI revealed a small right frontal lesion suspicious for a cavernous malformation with nearby leptomeningeal enhancement presumed to be related to subarachnoid blood products. Seizures were controlled medically. Follow-up MRI after one month confirmed stability of the right frontal lesion, which was subsequently resected and confirmed pathologically to be a cavernous malformation. Increased leptomeningeal enhancement in the right frontal region on the preoperative MRI was again presumed to relate to subarachnoid blood products. Anti-epileptic medications were discontinued four months after surgery and the patient experienced no further seizure activity. Two years later, the patient presented with memory decline, urinary incontinence, and gait disturbance. A brain MRI revealed new communicating hydrocephalus and new diffuse leptomeningeal enhancement. Extensive imaging, hematologic, and CSF evaluation found no evidence of metastatic disease or an infectious process. Neurosurgery placed a ventriculoperitoneal shunt and performed a dural biopsy with pathology interpreted as "dura with reactive changes". Neuro-oncology and rheumatology evaluations found the clinical evidence compatible with rheumatoid meningitis, and a steroid taper was initiated. After discharge, the patient's functional status improved on subsequent visits with neuro-oncology. A follow up MRI five months after discharge showed stable hydrocephalus and stable diffuse leptomeningeal enhancement.

Results

Image A: Postcontrast axial T1 image from initial presentation. Leptomeningeal enhancement confined to the right frontal lobe (arrow) was presumed to be associated with subarachnoid hemorrhage from the nearby cavernous malformation (not shown). Image B: Postcontrast axial T1 MPRAGE image from two years after initial presentation, when the patient presented with altered mental status, gait abnormalities, and urinary incontinence. There has been interval development of marked hydrocephalus and diffuse leptomeningeal enhancement (arrows). The right frontal cavernous malformation has been resected (not shown). Image C: Postcontrast axial T1 MPRAGE image acquired shortly after image B, following placement of a left parietal approach ventriculoperitoneal shunt catheter. Inflammatory changes associated with the catheter placement are visible in the right parietal lobe. Hydrocephalus has decreased. Diffuse leptomeningeal enhancement persists (arrows). New pachymeningeal enhancement is compatible with shunting. Image D: Postcontrast axial T1 MPRAGE image acquired five months after images B and C. Inflammation related to shunt placement has resolved. Hydrocephalus and shunt-related pachymeningeal enhancement are stable. Diffuse leptomeningeal enhancement persists (arrows).

Conclusions

Rheumatoid leptomeningeal involvement is rare, and is classically seen in adults with long-standing, poorly-controlled rheumatoid disease. These patients often have been on long-term immunosuppressive or steroid therapy and thus have increased risk of infection and lymphoma. Rheumatoid meningitis is therefore a diagnosis of exclusion. In the presented case, extensive workup found no evidence of a metastatic or infectious etiology, and the clinical picture was compatible with rheumatoid meningitis. The co-occurrence of rheumatoid meningitis and communicating hydrocephalus presenting with normal pressure hydrocephalus syndrome has not been previously reported. While this patient also had a cavernous malformation, there was very little associated subarachnoid hemorrhage. The development of hydrocephalus two years after resection of the cavernous malformation is likely attributable to the gradual occlusion of the arachnoid villi by accumulation of debris related to the chronic leptomeningeal inflammation.

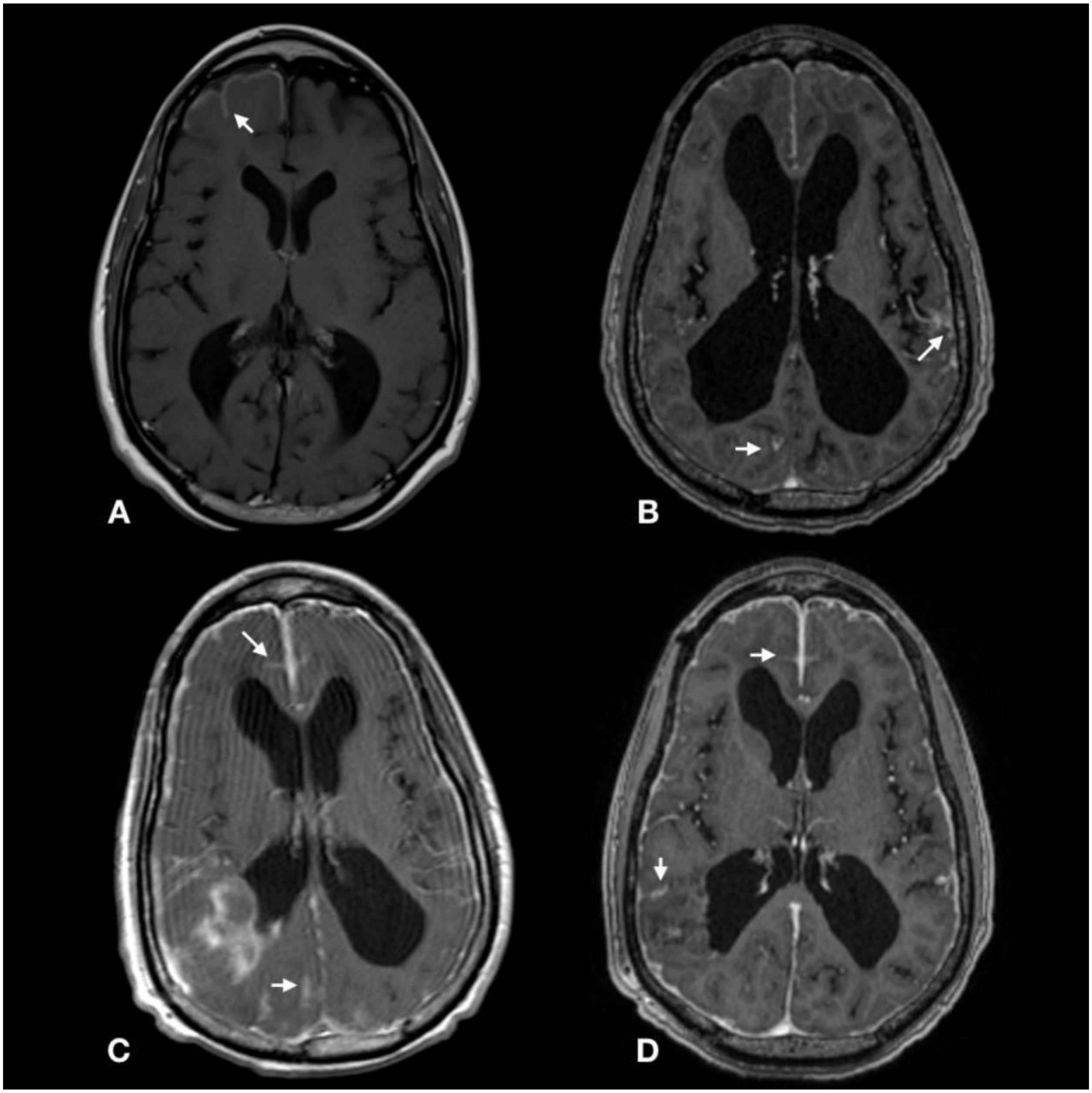

(Filename: TCT_3654_krumpelman_asnr_2019_graphic.jpg)

Tuesday, May 21, 2019
1:00PM - 2:30PM
Aneurysms Interventional

3505

1:00PM - 1:07PM

A Case of Early Rupture Following Flow-Diversion with Quantification of Hemodynamics and Aneurysmal Wall Stress using Additive Manufacturing and Particle Tracking Velocimetry

A Willis[1], N Mehta[2], R Mejia-Alvarez[3], D Chason[4]

[1]San Antonio Military Medical Center, San Antonio, TX, [2]IVC Northwest, Wilsonville, OR, [3]Michigan State University, East Lansing, MI, [4]University of Texas Southwestern, Dallas, TX

Purpose

Early rupture following treatment is a rare but devastating complication of flow-diversion in giant aneurysms. Computational models have been performed to explain the mechanisms by which flow-diversion could lead to early rupture, but fluid mechanical experiments have demonstrated computational models fail to accurately predict flow through flow-diverting stents (FDS). We present a case of early rupture in a 56-year-old female following treatment with a FDS for a left ophthalmic aneurysm of size 24mm x 20mm x 22mm. We perform fluid mechanical experimental analysis to quantify the changes of wall stress and hemodynamics following flow diversion in a three dimensional model of this patient's aneurysm.

Materials and Methods

Clinical imaging of aneurysm was acquired from angiography data during routine clinical treatment of patient. Angiographic reconstructions were exported as DICOMs (see Figure a) and model silicone vessel were fabricated by BDC Laboratories – www.bdclabs.com (see Figure b). Model aneurysm was submerged in deionized water and glycerol was added to fluid to match the refractive index of the silicone model and reduce optical distortion. Rhodium B coated microparticles (10 microns) will be suspended in model blood and pumped through the aneurysm using pulsatile blood pump (Harvard Apparatus 55-3305). The heart rate and blood pressure will be matched to that of the patient. Time dependent flow within the aneurysm is quantified using the three-dimensional particle tracking velocimetry technique termed "Shake the Box" (STB) (see Figure c) which reconstructs the flow vectors within the aneurysm (see Figure d). This experimental technique will provide the information to calculate the wall shear stress at high spatial and temporal resolution on the surface of the aneurysm.

Results

The three-dimesional unsteady hemodynamics and aneurysmal wall stress both before and after flow-diversion will be quantified and presented.

Conclusions

New, patient specific insights into the cause of early rupture following flow diversion can be obtained using additive manufacturing techniques and advanced experimental engineering analysis.

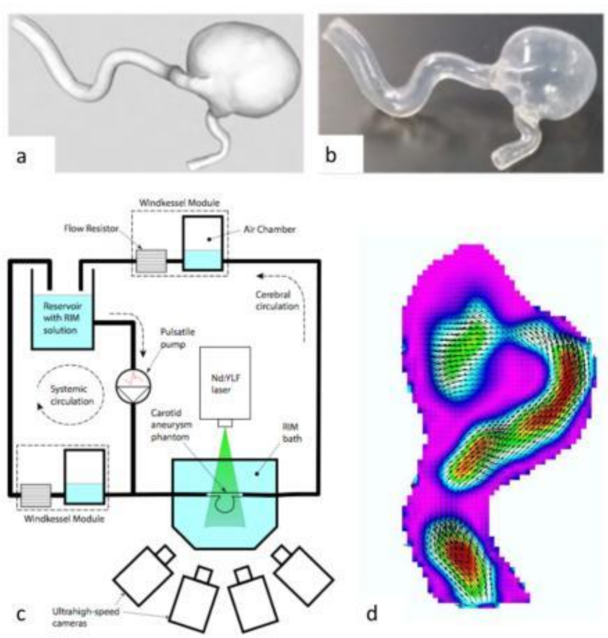

(Filename: TCT_3505_graphics.jpg)

2968

1:07PM - 1:14PM

Early Versus Late Establishment of Full Dual Antiplatelet Therapy after Emergency Carotid Artery Stenting in Tandem Occlusions.

A Haussmann[1], R Mühl-Benninghaus[2], A Simgen[2], W Reith[1], U Yilmaz[1]
[1]Saarland University Hospital, Homburg, Germany, [2]Saarland University Hospital, Homburg, Saarland

Purpose
Currently emergency carotid artery stenting is having a renaissance since a series of randomized trials demonstrated the benefit of mechanical thrombectomy in acute large vessel occlusions of the anterior circulation and 30% of those are accompanied by an additional occlusion or high grade stenosis of the extracranial ICA that requires PTA and/or stenting in order to gain access to the intracranial clot. However emergency stenting bears the risk of acute stent occlusions due to the emergency setting with an insufficient preparation with antiplatelet medication and on the other hand the risk of hemorrhagic complications due to the application of antiplatelet medication in combination with iv-thrombolysis. The purpose of this study was to compare occlusion rates and hemorrhagic complications when dual antiplatelet therapy is started within 24 hours after endovascular treatment or thereafter.
Materials and Methods
Patients with acute tandem occlusions of the anterior circulation who were endovascularly treated at our institution were identified from our registry of neuroendovascular interventions. Clinical, angiographic and neuroimaging data was analyzed. Endpoints included acute occlusions of the carotid stents and symptomatic ICH.
Results
36 patients were included. Full dual antiplatelet therapy was established within 24 hours after intervention in 18 patients. Rates of acute stent occlusions did not differ between patients who received antiplatelet therapy within 24h and those who did not (n = 2 in either group).
Conclusions
Late establishment of full dual antiplatelet therapy after emergency carotid artery stenting in tandem occlusions did not have a higher risk of acute stent occlusion in this retrospective analysis.

2741

1:14PM - 1:21PM

First National Outcome Study of the Pipeline Embolization Device With Shield Technology

D Atasoy[1], N Kandasamy[2], J Hart[2], S Yang[3], D Walsh[2], C Tolias[2], T Booth[2]
[1]Karadeniz Technical Unıversity Farabi Hospital, Trabzon, Turkey, [2]King's College Hospital NHS Foundation Trust, London, London, London, [3]Wan Fang Hospital, Taipei Medical University, Taipei, Taiwan

Purpose
Flow diverting devices (FDDs) have been used for the treatment of cerebral aneurysms for nearly 10 years. Pipeline Flex Embolization Device with Shield Technology (Pipeline Shield) is the third generation of Pipeline FDDs. We show our initial safety and efficacy outcomes using Pipeline Shield from a single UK institution.
Materials and Methods
The electronic patient records, diagnostic and procedural images and written procedural records of Pipeline Shield treatments between March 2016 and January 2018 were evaluated. TOF MRA was

performed for follow-up after 6 and 12 months from treatment. The mortality, morbidity rates and radiographic outcomes were analyzed and compared with other FDD and PED studies.
Results
A total of 44 attempted Pipeline Shield procedures were performed on 41 patients with 44 target aneurysms (total 52 aneurysms treated). Forty-nine (94.2%) aneurysms were saccular, 1 (1.9%) was fusiform. One aneurysm was an iatrogenic pseudoaneurysm and one was a dissecting aneurysm. 70% (35/50) of the saccular aneurysms were wide-necked (neck >4 mm), 36.5% (19/52) were large (≥ 10 mm), 2% (1/52) were giant (≥ 25 mm). The majority, 88.5%, of aneurysms were located in the anterior circulation and 11.5% in the posterior circulation. The mean aneurysm sac maximal diameter was 9 mm, and mean neck width was 5 mm. The overall mortality and morbidity rates were 2.3% and 2.3%, respectively. Our complete occlusion rate was 67% at 6 months and 79% at 18 months.
Conclusions
Our retrospective, pragmatic study is the first safety and efficacy study of the Pipeline Shield device either in a single center or in a single country. Our results demonstrated that occlusion rates and safety outcomes are similar with previously published studies with FDDs and previous generation PEDs. Follow-up with TOF MRA seemed to show similar PED occlusion results when compared to those acquired with DSA from other studies.

2471

1:21PM - 1:28PM

Flow Diversion Treatment of Anterior Communicating Artery Region Aneurysms

K Amuluru[1], F Al-Mufti[2], C Romero[1]
[1]University of Pittsburgh Medical Center - Hamot, Erie, PA, [2]Westchester Medical Center at New York Medical College, Valhalla, NY

Purpose
Flow diverter devices, such as the Pipeline Embolization Device (PED), were initially developed for the treatment of large, wide-necked, unruptured aneurysms originating from the petrous to superior hypophyseal segments of the internal carotid artery. Treatment options for these complex aneurysms remain limited using traditional microsurgery or coil embolization, even with adjunctive techniques. Recently, the off-label uses of PED flow diversion have expanded to include the treatment of ruptured aneurysms, posterior circulation aneurysms, carotid-cavernous fistulas, pseudoaneurysms and distal aneurysms. Few reports describe PED flow diversion treatment of cerebral aneurysms distal to the Circle of Willis, the vast majority of which involve middle cerebral artery locations. Reports on flow diversion of anterior communicating artery region aneurysms are even more scarce. We present a single center series of patients with anterior communicating artery region aneurysms who were treated with PED flow diversion.
Materials and Methods
Patient Selection: Our institutional, prospectively maintained cerebral aneurysmal database was retrospectively reviewed to identify patients with aneurysms located around the anterior communicating artery (AcomA) treated with the PED between November 2016 and December 2018. Patient and aneurysm-specific data were recorded. Endovascular Procedure: Patients were treated with daily aspirin 325 mg and Plavix 75 mg for 10 days prior to the procedure. Verify Now P2Y12 assay testing (Accumetrics, San Diego, CA) was performed to ensure sufficient platelet inhibition. All procedures were performed under general anesthesia. Patients received intravenous heparinization to achieve an activated clotting time >250 seconds. A 6-French Neuron MAX (Penumbra, Alameda, CA) guide catheter was placed in the ipsilateral proximal ICA. Through this, an intermediate catheter (Navien 058; Covidien Neurovascular, Irvine, CA or AXS Catalyst 5; Stryker Neurovascular, Fremont CA or Phenom Plus; Medtronic Neurovascular, Irvine, CA) was positioned in the distal ICA or in the A1 segment. Finally, the PED was deployed from the A2 segment to the ipsilateral A1 segment through a 0.027-inch ID delivery

microcatheter (Marksman; Covidien/ev3, Irvine, CA, USA or Phenom 027; Medtronic Neurovascular, Irvine, CA). Concomitant coil embolization was performed at the operator's discretion. Post procedure management: Dual antiplatelet therapy was continued for a minimum of 6 months, at which time a follow-up angiogram was performed and the antiplatelet regimen was re-evaluated depending on angiographic and clinical status. Clinical and Imaging Follow-Up: Procedural data, complications, and clinical and angiographic follow-up details were recorded. A neurological assessment along with a Modified Rankin Score (mRS) was performed before and after the treatment, and at all follow-up encounters. The O'Kelly Marotta grading (OKM) scale was used to angiographically evaluate aneurysm occlusion.

Results

Population Eleven AcomA region aneurysms in 10 patients were treated with the PED. 7 aneurysms were unruptured, 2 had recurred after prior rupture and embolization, and one was acutely ruptured. Angiographic Results One PED was successfully deployed in all cases with concurrent coil embolization performed in one case. Among the 10 aneurysms treated with PED alone, all demonstrated immediately diminished filling (B2 to C3 per OKM Scale). In 7 cases, the PED covered a side-branch vessel (70%). Angiographic follow-up (mean 6.2 months; range 4-8) was available for 10 aneurysms in 9 patients (90%), with 10/10 (100%) aneurysms showing occlusion. Two patients developed asymptomatic in-stent stenosis. Of the 7 patients with PED covering side-branches, none developed ischemic complications. Complications Two instances of intra-procedural PED retraction occurred, which caused long-term neurological morbidity in one patient (10%). In case #6, the spontaneous PED retraction into the carotid terminus caused intraluminal thrombus and right MCA occlusion, which was successfully treated with stent-retriever thrombectomy. The patient developed a left hemiparesis. In case #9, proximal PED retraction resulted in uncovering of the aneurysm neck, which necessitated coil embolization. The patient did not suffer neurological morbidity. There were no deaths, no cerebral hemorrhagic events, and no delayed neurological deficits. One patient (10%) developed a reversible left lower extremity paresis on post-procedure day #1 due to a punctate right frontal infarct. The patient's Plavix was switched to Ticagrelor, and the symptoms resolved in 8-weeks. Two non-neurological complications were encountered (20%), both involving retroperitoneal hemorrhage, one of which was treated with operative closure. At the last clinical follow-up, one patient had a worse mRS score changed from 0 (pretreatment) to 2. Two patients had stable pre-procedure mRS of 2, and all others had mRS 0.

Conclusions

In this series, flow diversion of 11 anterior communicating artery region aneurysms with the PED showed high rates of aneurysm occlusion and low complication rates. Complete occlusion was achieved in 100% of patients at 6.2 months. Hemorrhagic complications occurred in 0%. Symptomatic ischemic complications occurred in 2 patients (20%), one with completely reversible symptoms, and one who sustaining permanent neurological deficit (10%). Although 70% of cases involved covering perforator lenticulostriate vessels, no ischemic complications resulted. These results are comparable to large studies of PED treatment of carotid aneurysms, despite the smaller vessel size, manipulation of smaller, distal vasculature, and increased density of small perforator arteries.

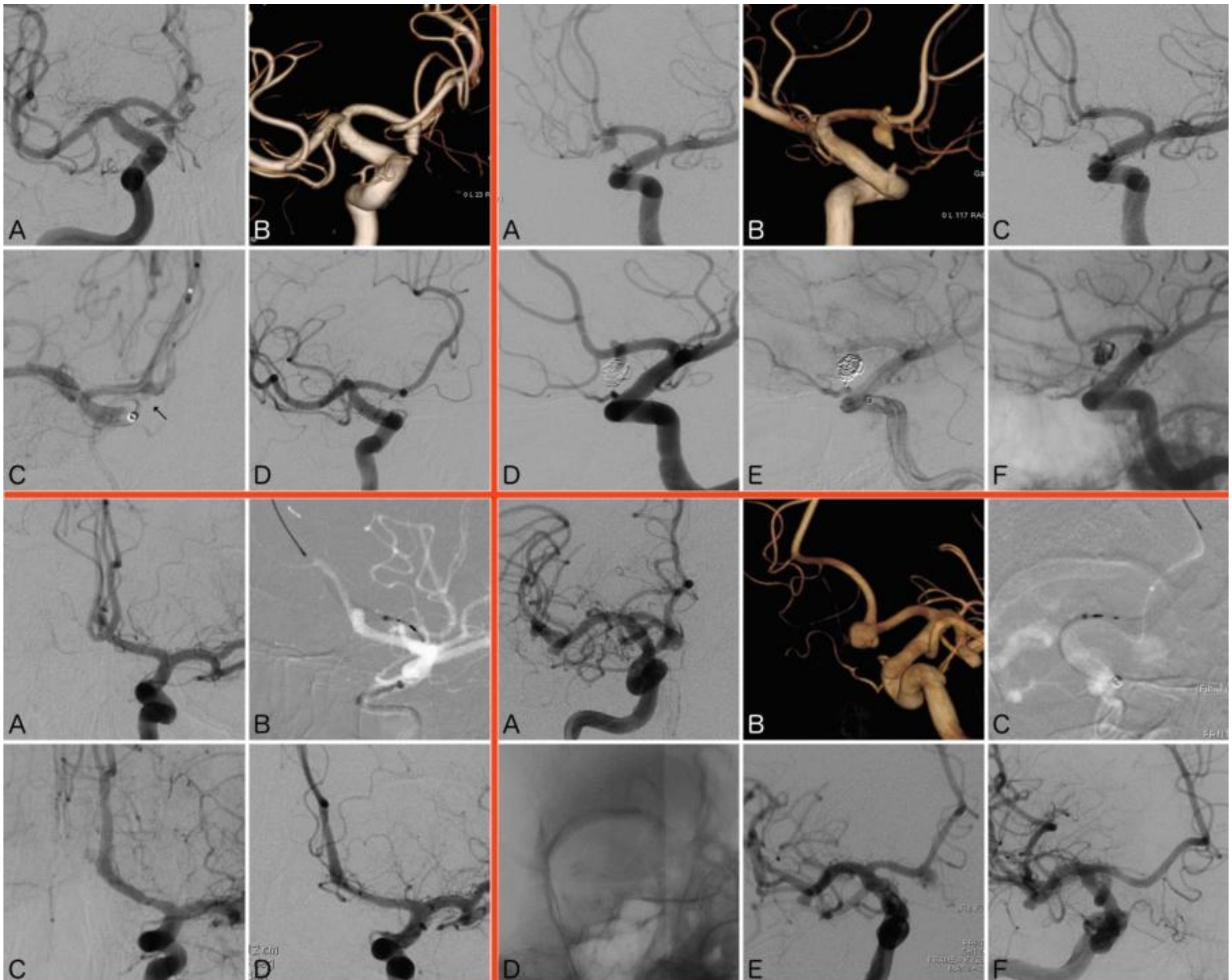

Patient Number	Aneurysm Number	Sex	Age	Smoker (Y N, Prior)	Aneurysm Location	Aneurysm Type (fusiform, saccular, dissecting)	Aneurysm Size (mm)	Aneurysm Neck (mm)	Dome:Neck	Distal ACA Size (mm)	Proximal ACA Size (mm)	Prior SAH	Prior Treatment	PED Size	Occlusion of side branch? immediate flow (NA, patent, moderate reduction, occlusion)	Concomitant Coiling?	Aneurysm filling pre-PED (OKM scale, A-D)	Immediate aneurysm filling (OKM scale)	Last DSA (mos)	Occlusion of side branch at F/U? (patent, moderate reduction, occlusion)	Aneurysm F/U (OKM Scale)	Intra/Peri-procedural complications	Non neuro Complication	Hemorrhagic Complications	Ischemic Complications	In-stent stenosis on follow-up	mRS at Last F/U
1	1	F	62	Y	AcomA	Saccular	4x4	3	1.3	1.5	1.9	0	0	3x12	Y, patent	0	A1	B2	6	NA	D	0	0	0	0	0	0
2	2	M	60	Y	A1/A2	Saccular	7x6	4	1.5	1.7	2	0	0	3x16	Y, patent	0	A2	B2	8	patent	D	0	0	0	0	0	0
3	3	F	49	Y	A2	Saccular	4x4	3	1.3	1.8	2.3	0	0	3x12	Y, MR	0	A1	B3	7	patent	D	0	0	0	0	Y	0
4	4	M	57	Y	AcomA	Saccular	6x4	4	1.5	1.7	1.9	1	1; primary coil embolization 9 mos prior to PED	2.5x10	Y, patent	0	A1	B3	6	patent	D	0	0	0	0	Y	1
	5				AcomA	Blister	2x1	1	2.0	1.7	1.9	1	0	2.5x10	Y, patent	0	A1	B2	6	patent	D	0	0	0	0	Y	1
5	6	F	65	N	AcomA	Saccular	3x3	1	3.0	2	2.4	1	0	2.5x12	N	0	A1	C2	6	NA	D	1	0	0	1	0	2
6	7	F	68	Y	AcomA	Saccular	4x4	3	1.3	1.7	1.9	0	0	2.5x10	Y, patent	0	A1	B3	6	NA	D	0	1	0	0	0	0
7	8	F	72	P	AcomA	Saccular	5x4	2	2.0	1.7	2.1	0	0	2.5x14	Y, patent	0	A2	A3	7	patent	D	0	0	0	1	0	0
8	9	F	74	P	A2	Saccular	6x4	4	1.5	2.5	2.5	0	0	2.75x14	N	1	A1	D	4	patent	D	0	1	0	0	0	0
9	10	M	61	P	AcomA	Saccular	5x5	3	1.7	2	2	0	0	2.75 x 14	Y, MR	0	A1	B1	6	NA	D	0	0	0	0	0	0
10	11	F	55	Y	AcomA	Saccular	5x5	2	2.5	1.6	2	1	1; primary coil embo 22 mos prior to PED	2.5x12	N	0	A1	B1	6	NA	NA	0	0	0	0	NA	1

(Filename: TCT_2471_ASNRAbstract_300dpi.jpg)

3363

1:28PM - 1:35PM

High-Frequency Optical Coherence Tomography for Interventional Neuroradiology

A Puri[1], M Marosfoi[2], G Ughi[2], R King[2], E Langan[2], M Gounis[1]
[1]University of Massachusetts, Worcester, MA, [2]University of Massachusetts Medical School, Worcester, MA

Purpose
Intravascular optical coherence tomography (OCT) has a well-established role for the diagnosis and image guided treatment of coronary artery disease (1). The profile, design, and technology are unsuitable for neurovascular use due to the diameters and tortuosity of the cerebral vasculature. A high-frequency

OCT (HF-OCT) device has been developed and tested for imaging of tortuous vessels representative of the human cerebrovasculature and neurointerventional devices.
Materials and Methods
In patient-specific cerebrovascular phantoms, we investigated the ability to clear a blood-like fluid from the image field-of-view. In vivo imaging in elevated tortuosity was tested in a total of 16 swine brachial arteries (2) in 8 subjects. Additionally, 16 flow-diverting stents were implanted in the internal maxillary arteries. The HF-OCT device was delivered via a standard 0.027-inch microcatheter and blood clearing obtained using routine contrast injection protocols (0.058-inch intermediate). Volumetric images of 6-cm vessel segments were acquired in 2-3 seconds. Three raters analyzed the presence of clot along the flow-diverters surface and malapposition to the vessel wall across three imaging modalities: digital subtraction angiography (DSA), high-resolution cone beam CT (CBCT), and HF-OCT (Figure).
Results
In the phantoms, the device was successfully delivered and adequate blood clearance with an injection of contrast (3-5 ml/s, depending on target location) was obtained in all cases, using a standard 0.058-inches intermediate catheter. In each brachial artery, the device was able to successfully acquire high-resolution image volumes. In assessing the clot formation at 3 locations along the flow diverters, the agreement between the reviewers (Fleiss' kappa) was 0.49, 0.67 and 0.90 for DSA, CBCT, and HF-OCT, respectively. The agreement in diagnosing malapposition was 0.18, 0.67, and 0.87 for DSA, CBCT and HF-OCT, respectively.
Conclusions
A novel device for high-resolution endovascular imaging (HF-OCT) has been developed and tested for neurovascular intervention. HF-OCT holds promise for overcoming the limitations of existing intravascular imaging tools and for a successful translation to the clinic.

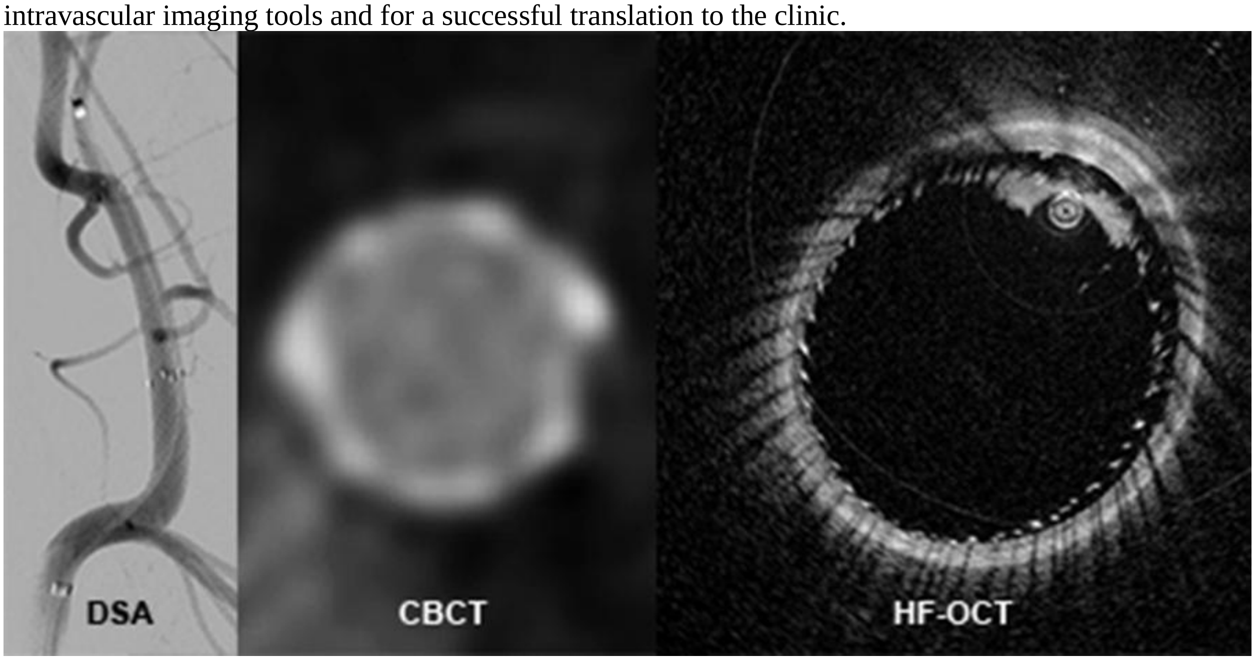

(Filename: TCT_3363_ASNR-fig.jpg)

2844

1:35PM - 1:42PM

In-Stent Stenosis in Patients with Stent Assisted Coiling: Incidence, Clinical Significance and Long-Term Follow-Up

V Tsehmaister-Abitbul[1], S Finitsis[2], F Essbaiheen[3], E Cora[4], B Drake[3], M Kassab[5], D Iancu[3]

[1]University of Ottawa, Ottawa, Ontario, [2]Aristotle University of Thessaloniki, Thessaloniki , N/a, [3]The Ottawa Hospital, Ottawa, Ontario, [4]OTTAWA UNIVERSITY, OTTAWA, ON, [5]The Ottawa hospital, Ottawa, Ontario

Purpose
Ongoing improvements in the flexibility, maneuverability, and effectiveness of intracranial neurovascular stents, have led to growing increase in their use in endovascular aneurysm embolization. The incidence of In-stent stenosis in mid-term follow up has been previously published, However, long-term follow-up and clinical implications of in-stent stenosis have not been well assessed.
Materials and Methods
Retrospective review of patients treated with stent-assisted coiling in our center between January 2013 to June 2017. Only cases with short-term (4 +/- 2 months) and long-term follow ups with digital subtraction angiograms were included. In-stent stenosis was graded as mild (<25%), moderate (25-50%) or severe (>50%). The following predictors for ISS were assessed: gender, age, the presence of SAH, aneurysm size, location, occlusion status and post-stenting angioplasty.
Results
29 patients met the inclusion criteria, with a total of 37 stents deployed. At mid-term follow-up, Mean time post procedure= 3.6 months, (2.5 - 6 months, SD= 0.9), ISS was observed in 7/37 stents (23.3%). Vast majority 85.71% was mild (6/7) , 1 was moderate(14.28%). No severe ISS was observed. All patients were maintained on dual antiplatelet therapy. At long-term follow-up (Mean time post procedure= 15.9 months, 10 - 33 months, SD= 5.1), there were three cases of mild in-stent stenosis (3/37, 8.1%), and complete ISS resolution was seen in the remaining 4 cases. No case of de novo ISS was observed. Univariate analysis showed association of ISS development with stent mis-deployment. (4/7, 57.1%, p value= 0.007). No association was found with any of the other evaluated factors.
Conclusions
In-stent stenosis following stent- assisted coiling is a common, asymptomatic finding on mid-term angiographic follow-up. Complete resolution or improvement at long-term follow-up is seen in patients who are maintained on dual anti-platelet therapy.

3439

1:42PM - 1:49PM

Magnetic Resonance Imaging Follow Up of Posterior Inferior Cerebellar Artery Aneurysms Treated with Flow Diversion

C PARADA[1]
[1]INSTITUTO MEDICO ENERI, BUENOS AIRES, Argentina

Purpose
To evaluate the efficacy of flow diverter stents in the management of posterior inferior cerebellar artery (PICA) aneurysms and the performance of magnetic resonance imaging (MRI) for follow up after treatment.
Materials and Methods
We retrospectively review our institutional database and identify 13 patients with PICA aneurysm who underwent endovascular treatment with flow diverters and were followed up with MRI and digital subtraction angiography (DSA). Demographic, clinical data and imaging findings pre-treatment and follow up were recorded and analyzed.
Results
We identified 13 patients that met our inclusion criteria. 9 (69%) were female and 4 (31%) male with an average age of 61 (33 –72) years old. Risk factors were encountered in 10 (77%) patients and twelve (77%) were symptomatic with the majority suffering from mass effect symptoms (46%) prior to treatment. Nine (69%) aneurysms were saccular and four (31%) fusiform, their average size was 14 mm

(1,6 – 39 mm). MRI follow up studies were available for all patients during the first 24 months after treatment, 11 (85%) aneurysm show decrease in size while 2 (15%) remain unchanged. Complete occlusion was found in 4 cases (31%) and 9 (69%) show remnants. There were no intraoperative vessel or aneurysm ruptures and no mortalities

Conclusions

PICA aneurysms are rarely encountered and like any other intracranial aneurysm are prone to rupture if not treated. Our results with MRI showed for the majority of the cases decrease in size of the aneurysm sac with small remnants within the first 24 months following endovascular management. We report our experience as a referral center for the treatment of intracranial aneurysm and support endovascular treatment of PICA aneurysms with flow diverters as an efficient therapy. MRI is an useful noninvasive imaging modality for follow up of both intracranial aneurysms after treatment and adjacent parenchyma.

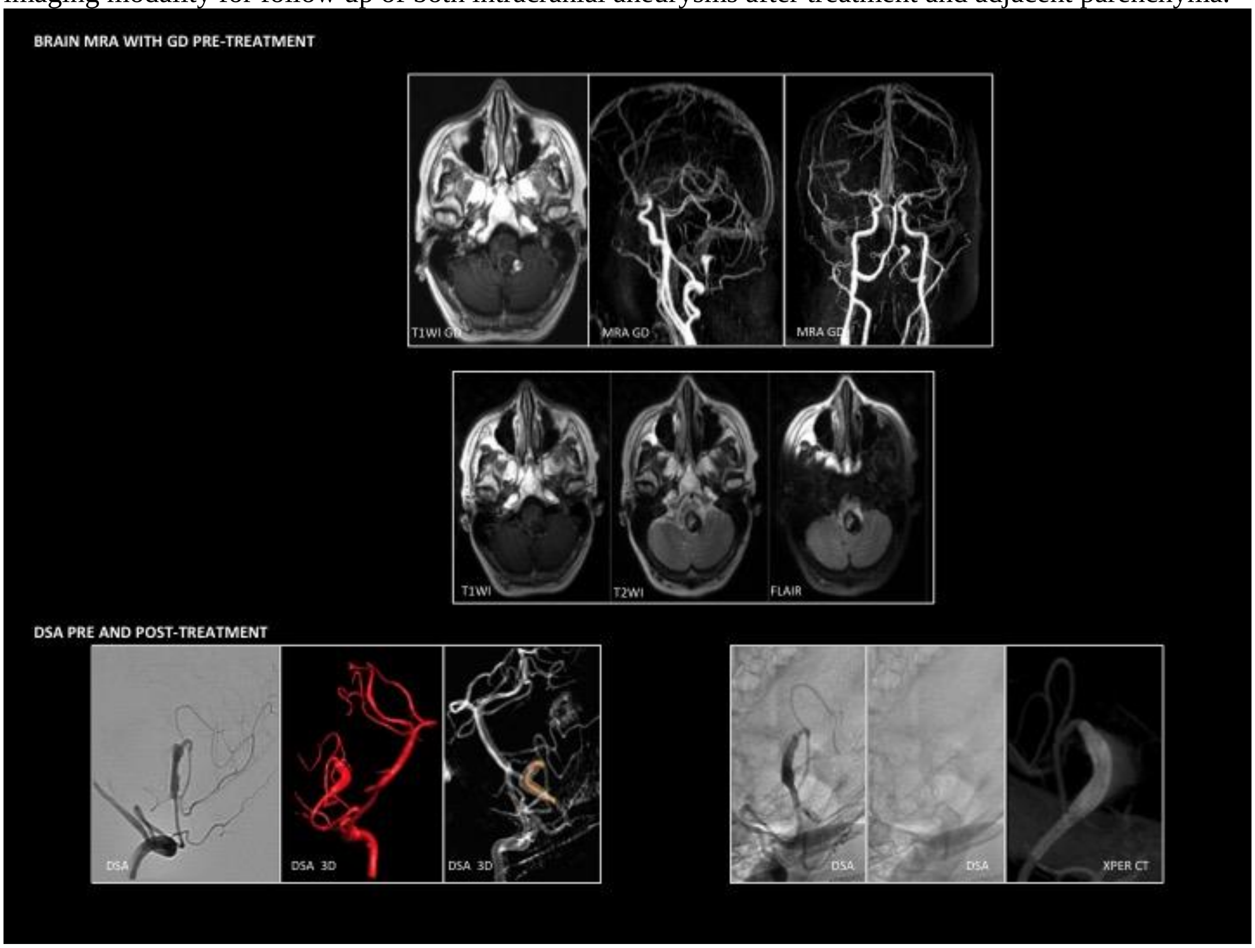

(Filename: TCT_3439_Slide1.jpg)

3312

1:49PM - 1:56PM

Pipeline Endovascular Device versus Stent-Assisted Coiling in Small Unruptured Aneurysms: A Cost-Effectiveness Analysis

A Malhotra[1], X Wu[2], P Sanelli[3], D Gandhi[4]

[1]YALE UNIVERSITY SCHOOL OF MEDICINE, NEW CANAAN, CT, [2]Yale University School of Medicine, New Haven, CT, [3]NORTHWELL HEALTH NSUH, MANHASSET, NY, [4]University of Maryland School of Medicine, Baltimore, MD

Purpose
Both stent-assisted coiling and flow diversion with the Pipeline Embolization device (PED) have been shown to be safe and clinically effective for treatment of small (<10 mm) unruptured aneurysms. However, the economic impact of these different techniques has not been established. We conducted a cost-effectiveness analysis between stent-assisted coiling and flow-diversion using PED, including procedural costs as well as long term outcomes and aneurysm recurrence, to compare their benefits.
Materials and Methods
A decision-analytical study was performed with Markov modeling methods to simulate patients undergoing stent-assisted coiling (SAC) or PED for treatment for unruptured aneurysms of sizes 5 and 7 mm. Input probabilities were derived from prior literature, and one-way, two-way and probabilistic sensitivity analyses were performed to assess model and input parameter uncertainty.
Results
In base case calculation, PED was the dominant strategy for both the size groups, with and without consideration of indirect costs. With 10,000 iterations in probabilistic sensitivity analysis, PED was the better option in 8,006 of them. One-way sensitivity analyses show that the conclusion remained robust when varying the retreatment rate of SAC from 0 to 40%, and only changes when the retreatment rate of PED exceeded 35.8%. PED remained the more cost-effective strategy when the morbidity and mortality of PED increased by less than 41%, and when the morbidity and mortality of SAC decreased by less than 31%. SAC only became cost-effective relative to PED when the total cost of PED is at least $40,000 more expensive than the total cost of SAC.
Conclusions
With the increasing use of PED for treatment of small unruptured anterior circulation aneurysms, our study indicates that PED is cost-effective relative to stent-coiling irrespective of aneurysm size. This is due to lower aneurysm recurrence rate, as well as better health outcomes.

3066

1:56PM - 2:03PM

Readmission after Elective Treatment of Unruptured Cerebral Aneurysm: A Nationwide Readmission Database Analysis

P Golnari[1], P Nazari[1], S Ansari[2], A Shaibani[1], M Hurley[3], M Potts[4], B Jahromi[4]
[1]Northwestern University, Chicago, IL, [2]NORTHWESTERN UNIVERSITY, FEINBERG SCHOOL OF MEDICINE, CHICAGO, IL, [3]Northwestern University Feinberg School of Medicine, Chicago, IL, [4]Northwestern University, Feinberg School of Medicine, Chicago, IL

Purpose
Mortality rates following treatment of unruptured cerebral aneurysm (UA) have decreased over the past decades, which may be due to use of modern microsurgical and endovascular techniques as well as overall increased volumes of UA treatment. However, treatment of UA harbors a small but finite risk, and resulting readmission rates have not been well described.
Materials and Methods
Adult patients who underwent elective coiling or clipping of UA were extracted from the Nationwide Readmission Database (2014). Primary diagnosis for non-elective readmission within 30 and 90 days were identified and readmission rates for coiling vs clipping were compared. Poisson regression was performed using generalized estimating equations and adjusted risk ratio (aRR)s were obtained for factors associated with 30 and 90 day readmission. The adjusted model included terms for patient- and hospital-specific factors, comorbidity scores and disease severity.
Results
Of 10179 UA patients treated and discharged alive, 670 (6.6%) patients were readmitted within 30 days (516 non-elective and 154 elective), and 1238 (14.8%) patients were readmitted within 90 days (747 non-elective and 491 elective). The most common primary diagnoses for non-elective readmission within 30

and 90 days, respectively, were cerebral infarction (4.8%, 6.1%), septicemia (4.1%, 3.4%), headache (4.4%, 2.5%), subdural hemorrhage (2.8%, 4.0%), ICH (4.1%, 2.3%), SAH (3.3%, 2.0%), TIA (1.9%, 3.2%) and UTI (2.3%, 2.9%). The 30 and 90 day non-elective readmission rate for coiling vs clipping was 4.2% vs 7.2% (p<0.0001) and 8.1% vs 10.8% (p=0.0002), respectively. Patients undergoing clipping had a higher adjusted risk of non-elective 30 and 90 day readmission than patients having coiling (aRR=1.49; 95%CI, 1.26-1.76; p<0.001 and aRR=1.16; 95%CI, 1.05-1.28; p=0.003).
Conclusions
The most common reasons for 30 and 90 day non-elective readmission after treatment of UA were cerebral infarction and septicemia. Adjusted risk and rates of non-elective readmission after 30 and 90 days were higher after clipping than coiling.

3023

2:03PM - 2:10PM

The Safety and Efficacy of Ticagrelor or Prasugrel in Intracranial Flow-diverting Stents – a Systematic Review and Meta-analysis.

A Podlasek[1], A Al Sultan[2], M Goyal[2], M Almekhlafi[2]
[1]Southend University Hospital, Southend-on-Sea, Essex, UK, [2]University of Calgary, Calgary, AB, Canada

Purpose
Thromboembolic complications are not uncommon in patients undergoing neuro-interventional procedures. The use of flow-diverting stents is associated with higher risks of these complications despite current dual antiplatelet regimens (DAPT). This systematic review and meta-analysis aim to present contemporary evidence for the consequences other than ASA+clopidogrel antiplatelet regimens used for flow-diverting stenting procedures.
Materials and Methods
We identified relevant articles by searching electronic databases and reviewing relevant references. Studies reporting on the effectiveness and/or complications of ASA+ticagrelor or ASA+prasugrel compared to ASA+clopidogrel in flow-diverting stenting procedures were included.
Results
Out of 451 potentially relevant studies, we identified 4 with a total of 934 patients, which reported on the effectiveness and/or safety of ticagrelor or prasugrel. DAPT with clopidogrel was as effective as with prasugrel (ischemic events OR 0.80, 95% CI 0.30-2.10; P = 0.800) and with ticagrelor (OR 0.58, 95% CI 0.15-2.28; P = 0.436). DAPT with ticagrelor was not associated with a higher risk of hemorrhagic complications (OR 1.57, 95% CI 0.14-17.01; P = 0.711).
Conclusions
Current evidence suggests that antiplatelet regimens including ticagrelor or prasugrel are effective and safe for patients undergoing flow-diversion procedures.

3347

2:10PM - 2:13PM

Woven Endobridge (WEB) Device as a Re-treatment Strategy After Unsuccessful Trial of Surgical Clipping: Feasibility, Safety, and Efficacy

C Parra-Farinas[1], R Scott[2], N Kandasamy[2], T Booth[3]
[1]St. Michael's Hospital, Toronto, Canada, Toronto, Ontario, [2]King’s College Hospital NHS Foundation Trust, London, England, London, London, [3]Kings College Hospital NHS Foundation Trust, London, England, London, United Kingdom

Purpose

A drawback of aneurysm coiling and clipping is the risk of recurrence or treatment failure. We aimed to determine the procedural feasibility as well as the safety and efficacy of using the Woven Endobridge (WEB) device to treat wide-necked residual aneurysms after unsuccessful surgical clipping.

Materials and Methods

We reviewed the electronic patient records, diagnostic and procedural images, and written procedural records from four United Kingdom hospitals with WEB treatments following an unsuccessful trial of surgical clipping, between January 2014 and January 2016. All patients had clinical follow-up and imaging follow-up using DSA, or TOF MRA. To determine safety, we used the peri-procedural and follow-up modified Rankin Scale (mRS). Any complications such us ischemia and hemorrhage were also recorded. To determine efficacy, we used a peri-procedural and follow-up 3-grade scale: complete occlusion, neck remnant and sac remnant (we also used the Web Occlusion Scale).

Results

Four middle cerebral artery and two anterior communicating artery complex aneurysms were treated with WEB after unsuccessful surgical clipping. Prior to clipping two aneurysms had ruptured. The mean time between surgical clipping and WEB re-treatment was 37 days. In all cases 6/6/ (100%) the WEB placement was satisfactory with no peri-procedural complications. There were no delayed complications; the mRS at 18 months remained the same as the pre-procedural mRS (0 in four 4 patients, 1 in one patient, and 2 in one patient). At 18 months follow-up 5/6 (83%) aneurysms showed adequate occlusion (complete occlusion and neck remnant) and 1/6 (17%) showed a sac remnant.

Conclusions

Following an unsuccessful trial of surgical clipping, we have shown for the first time that the WEB device provides a feasible treatment option for wide-necked intracranial aneurysms with low complication rates and high adequate occlusion rates. A limitation of this study is that the series is small with relatively short-term follow-up.

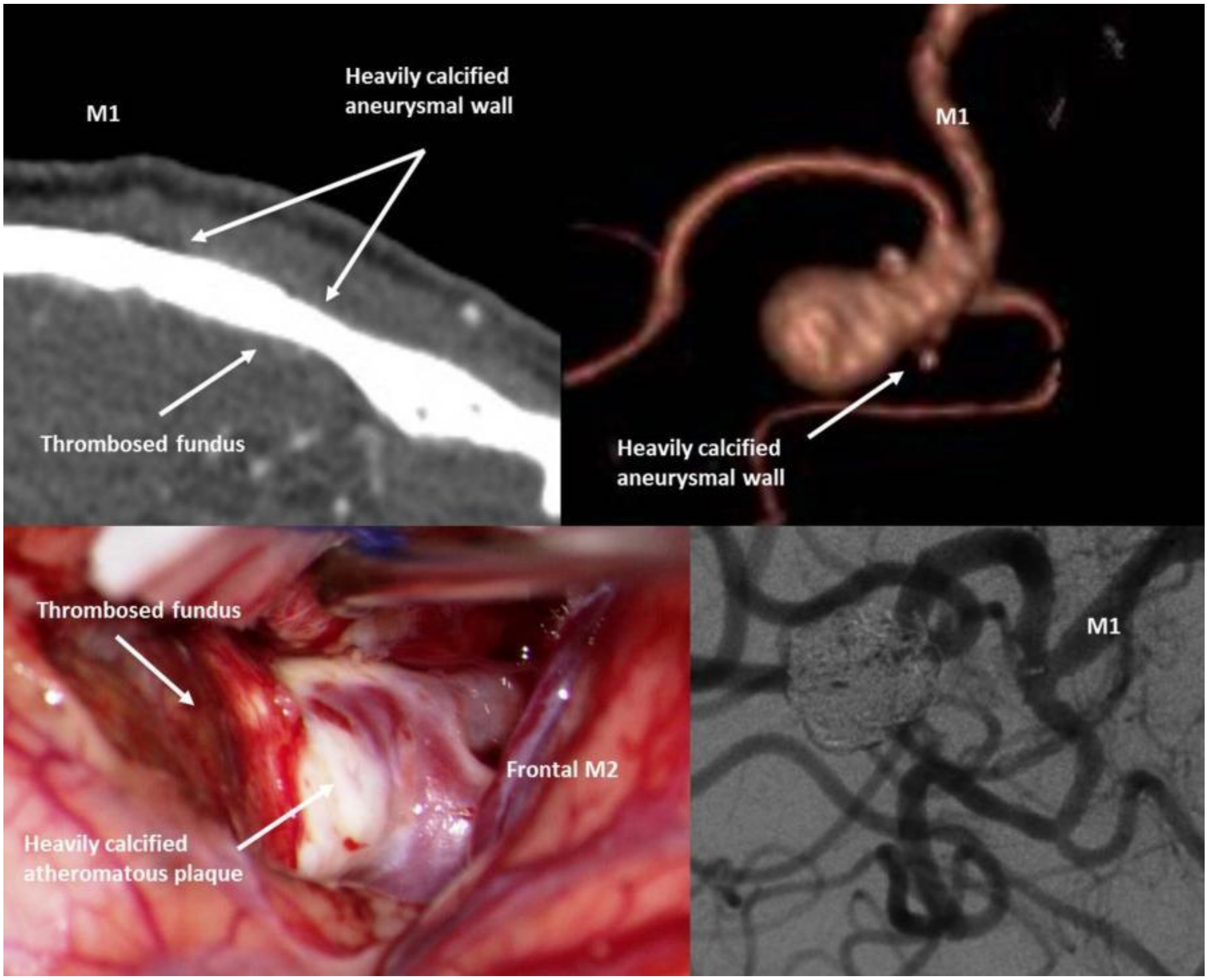

(Filename: TCT_3347_CPF_ASNR_2019.jpg)

Tuesday, May 21, 2019
1:00PM - 2:30PM
Breaking the Mold in Pediatric Neuroimaging

3134

1:00PM - 1:07PM

Development of an Express MRI Protocol for Pediatric Brain Imaging

C Schwartz[1], P Quarterman[2], A Lignelli[3]
[1]Columbia University Medical Center/New York Presbyterian Hospital, New York, NY, [2]GE Healthcare, Brooklyn, NY, [3]Columbia Presbyterian, New York, NY

Purpose
To develop an "express" MRI protocol for routine pediatric brain imaging which will consistently provide diagnostic quality images, comparable to that of current industry standard protocols, but in just one-quarter of the scan time. A significantly lower scan time will be most beneficial for a pediatric population

that frequently requires sedation, and will also increase patient throughput. The use of sedation increases the cost and time required for each examination, and exposes subjects to potential risks.

Materials and Methods

MR imaging of the brain was performed on 20 pediatric patients, using both a standard routine brain protocol, and our investigative "express" brain protocol. The examinations were performed on 3T 70cm bore MR scanners (Discovery MR750w, GE Healthcare, USA) using a GE Signa MRI Brain Array Coil (8 channel, High Resolution). All sequences were performed without the use of intravenous contrast and focused on the core imaging sequences of a non-contrast MR exam. Imaging parameters, slice coverage, and scan time for the "express" and routine protocols are shown in Figure 1. Two radiologists (one senior and one junior) independently performed blind ratings of diagnostic quality, artifacts, uniformity, noise level, and soft tissue contrast using a 5-point scoring scale (with 5=Excellent Image Quality: suitable for diagnostic use, and 1=Unacceptable Image Quality: not suitable for diagnostic use). Inter-rater reliability was evaluated using Cohen's kappa statistic, with an inter-rater kappa score of 0.81.

Results

Average score for the standard brain protocol was 4.8 (Excellent Image Quality), while average score for the "express" brain protocol was 3.8 (Good Image Quality). The "express" protocol scored lower in resolution, especially on the T2* GRE and T1 sequences. The average scan time decreased from 15m47s using the standard protocol to 4m19s using the "express" protocol, for an approximately 73% reduction in overall scanning time.

Conclusions

This novel "express" brain protocol for pediatric patients can provide a significant reduction in scan time as compared to a standard brain protocol, while consistently providing diagnostic image quality. This reduction in scan time may allow for increased scanner utilization and operational efficiency, and a decreased need for patient sedation.

Figure 1. Imaging parameters, slice coverage, and scan time for the "express" and standard brain imaging protocols.

Express Brain Imaging Parameters						
Sequence	**Scan Plane**	**TE (msec)**	**TR (msec)**	**TI (msec)**	**Voxel Size**	**Scan Time**
T1 FLAIR	Sagittal	22.8	2900	857	0.8 x 1.1 x 4	55s
T2 FSE	Axial	88	5800	N/A	0.7 x 0.9 x 4	34s
T2 FLAIR	Axial	89	9000	2500	0.8 x 1.0 x 4	1m 21s
T2* GRE	Axial	13	580	N/A	0.8 x 1.0 x 4	1m 4s
DW-EPI	Axial	79	5300	N/A	1.8 x 1.8 x 4	25s
						Total - 4m 19s

Standard Brain Imaging Parameters						
Sequences	**Scan Plane**	**TE (msec)**	**TR (msec)**	**TI (msec)**	**Voxel Size**	**Scan Time**
SPGR	Sagittal	2.6	7.3	450	1 x 1 x 1	3m
T2 FSE	Axial	121	8500	N/A	0.5 x 0.5 x 4	2m 38s
T2 FLAIR	Axial	83	9000	2500	0.8 x 1.0 x 4	3m 45s
GRE SWI	Axial	23	51	N/A	0.7 x 0.8 x 3	4m 46s
DW-EPI	Axial	79	10000	N/A	1.7 x 1.6 x 3.6	1m 38s
						Total - 15m 47s

Figure 2. Images from the same patient using the "express" protocol (A) and the standard protocol (B). The use of an "express" protocol with reduced scan time can produce images of similar diagnostic quality to that of standard protocols for many sequences (T2, FLAIR, DW-EPI).

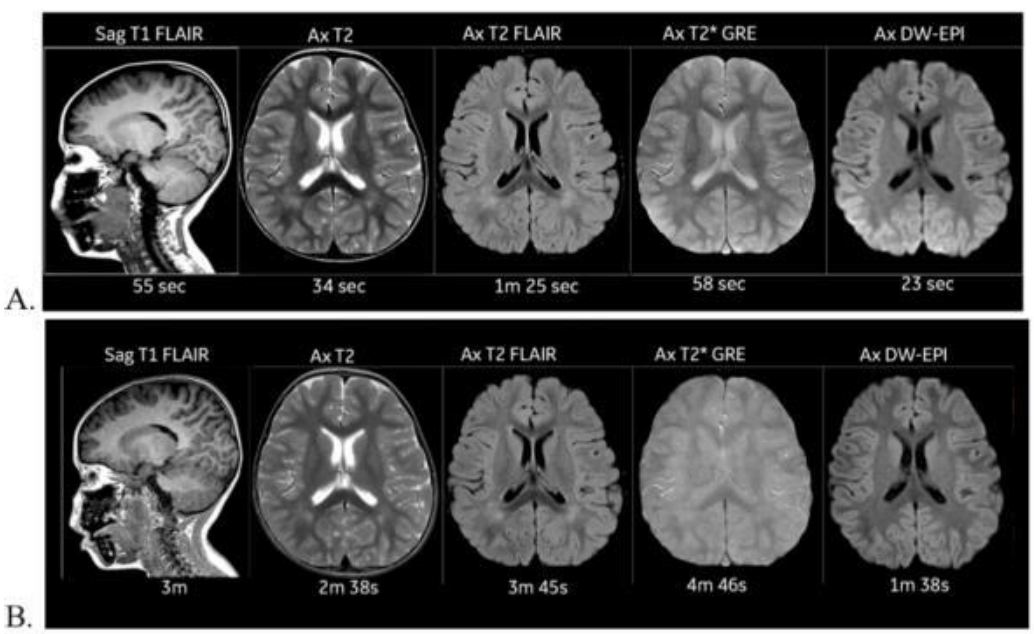

(Filename: TCT_3134_Figures1and2.jpg)

2949

1:07PM - 1:14PM

Effects of Pharmacological Sedation on Resting State Functional Connectivity in Pediatric Epilepsy

V Nair[1], N Tellapragada[2], V Prabhakaran[3], R Ahmed[4]
[1]University of Wisconsin School of Medicine and Public Health, Madison, WI, [2]UW Madison, MADISON, WI, [3]University of Wisconsin-Madison, Madison, WI, [4]University of Wisconsin Madison, MADISON, WI

Purpose
Functional neural networks may be inferred from measurements of synchronous BOLD signal fluctuations at rest. These neural connectivity patterns may have clinical applications in epilepsy by offering insights into mechanisms of seizure propagation and determining eloquent function localization. Pharmacological sedation during imaging of pediatric patients may however, affect background hemodynamic fluctuations through alterations in ongoing brain activity and regional cerebral metabolism (ref 1). We investigated differences in resting functional connectivity (rsFC) in pediatric patients scanned under awake versus sedated conditions during their epilepsy evaluation.
Materials and Methods
Resting-state data from 10 awake (AW; range 10-17 years, 3 males) and 10 sedated epilepsy patients (SED; range 5-6 years, 6 males) were analyzed. After standard rsFC preprocessing (SPM12; Matlab; DPABI toolbox), RSFC maps were computed with seed regions in left somatomotor cortex (sensory-motor network), left inferior frontal gyrus (language), and right precuneus (default-mode network). Fisher-z transformed maps were used. An analysis of covariance was used to test for group differences with age, gender, intracranial volume, scanner type, and framewise motion displacement as covariates (statistical significance set at $p < .05$; FWE corrected).
Results
There were no significant differences in rsFC maps with seed regions in the left inferior frontal gyrus, and the left somatomotor cortex. There were significant differences in rsFC computed with right precuneus seed region. AW patients showed significantly stronger connectivity between right precuneus and bilateral regions of the putamen, as well as the right superior and inferior parietal regions.
Conclusions
Our pilot results in pediatric patients, indicate reduced rsFC in brain regions involved in higher order executive processes and subcortical circuits as previously reported in adult subjects. Neural activity in primary sensory cortices is unaffected by sedation. Accurately characterizing sedation effects on spontaneous hemodynamic fluctuations is important to minimize potential confounding effects on estimation of functional connectivity during clinical work flow.

2541

1:14PM - 1:21PM

Fast Imaging Protocol: Can It Be Used to Evaluate the Pediatric Brain?

A Taori[1], J Davila[1], V Bijelic[1], B Smith[1], C Kapoor[1], E Miller[1]
[1]CHEO, Ottawa, Ontario

Purpose
Implementation of pediatric fast imaging techniques can shorten scan times, decrease motion-related artifacts, and more importantly reduce the need for sedation in children. The fast 5-minute brain MRI protocol provides the basic clinical sequences including sagittal T1-weighted, axial T2-weighted, axial T2 TSE Dark Fluid (FLAIR), axial diffusion-weighted (DWI), and axial T2*-weighted sequences. The aim of this study was to evaluate the image quality and diagnostic accuracy of the fast MR protocol for the detection of clinically relevant imaging findings in pediatric patients.
Materials and Methods
Institutional research ethics board approval was obtained. This is a retrospective study of 105 pediatric patients that underwent a fast MR protocol between January 1, 2015 and July 30, 2017. Two pediatric

radiologists, blinded to patient information and protocol assignments, independently reviewed the 5-minute brain MR protocol. Image quality was assessed using a three-point scale (1=non-diagnostic, 2=diagnostic, substantial artifacts, 3=diagnostic, no artifacts). The diagnostic performance of each fast sequence was assessed for the detection and quantification of intracranial pathologies. Analysis was performed with R statistical software version 3.5.1. Quantification of the degree of agreement between the two reviewers was assessed with weighted Kappa. Overall agreement is also provided.

Results

Diagnostic concordance between readers for the fast MR sequences with regards to image quality was best on Axial T2 (kappa=0.66) and Sag T1 (kappa=0.56) sequences. Intracranial pathologies were detected by both readers with Kappa values suggesting moderate to substantial diagnostic concordance on the various imaging sequences, best on Axial T2WI (kappa=0.73). No significant differences were seen in regards to detection of clinical important intracranial mass-like lesion, intracranial hemorrhage, ischemia, congenital malformation and hydrocephalus.

Conclusions

This study suggests that fast 5-minute brain MRI protocol is of sufficient diagnostic quality and has the potential to be included in clinical pediatric brain MR exams as a fast diagnostic tool or adjuvant in lengthy protocols. Further studies with larger patient populations, specific disease processes, patients undergoing MRI with anaesthesia and neonatal age groups are warranted.

Table 1. Diagnostic Concordance for Image Quality

Sequence	Weighted Kappa	Overall Agreement
Sagittal T1	0.56	96.6 %
Axial T2	0.66	98.7 %
Axial FLAIR	*	96.6 %
Axial Diffusion	0.31	95.1 %
T2* Axial	0.10	79.3 %

* Due to sparseness of the data, there were no cases where both raters identified a substantial artifact. The resulting kappa is not reliable.

Table 2. Diagnostic Concordance in Detection of Pathologies

Sequence	Weighted Kappa	Overall Agreement
Sagittal T1	0.52	75.9 %
Axial T2	0.73	77.3 %
Axial FLAIR	0.67	73.6 %
T2* Axial	0.67	92 %

(Filename: TCT_2541_ASNRTables.jpg)

3331

1:21PM - 1:28PM

Improved Pediatric MRI with Motion Robust Acquisition and Reconstruction Strategies

S Warfield[1], T Wallace[1], A Pour Yazdanpanah[1], O Afacan[1]
[1]*Boston Children's Hospital, Boston, MA*

Purpose

MRI of children, for both clinical care and for research, is limited by the motion sensitivity of current MRI acquisition sequences. We have explored faster imaging with high undersampling factors, as well as the use of both hardware tracking and intrinsic navigators to characterize the motion pattern the child is undergoing. We have assessed strategies for retrospectively correcting motion artifacts, and for prospectively steering the acquisition field-of-view, and demonstrate a capability to obtain excellent quality images through the elimination of motion artifact in pediatric MRI.

Materials and Methods

One way to deal with motion is to acquire faster images. Conventional parallel imaging exploits spatially varying coil sensitivities to enable undersampling of data acquisition. The extent of undersampling that preserves high quality images is limited in part by the total reduction in signal associated with undersampling, as well as an additional geometry factor that arises from the position of the coil array with respect to the anatomy being imaged. We propose to further constrain the image reconstruction by using the spatial gradients of the sensitivity information. (Fig 1.a) We propose using free induction decay navigators (FIDnavs) as a motion correction strategy in pediatric populations. FIDnavs are sensitive to head motion and can be rapidly acquired (in microseconds) using standard scanner hardware, making them an attractive approach for motion detection in pediatric MRI. We present a new approach that uses simulation of the acquisition physics and the effect of motion on the measured FIDnav from each coil to estimate motion parameters every 25ms. We also investigated the feasibility of using an electromagnetic (EM) tracker to estimate rigid-body motion parameters. Our EM trackers consist of 6 RF coils and the system uses a mapping of the gradients to estimate position and orientation of each sensor by analyzing the induced currents on these coils due to motion. We then use these position and orientation measurements to retrospectively and prospectively correct for motion in real time.

Results

Our reconstructions of T2w TSE acquisitions with an acceleration factor of 4 have lower reconstruction error than conventional parallel imaging with an acceleration factor of 2. For 3D acquisitions, even higher acceleration factors provide satisfactory images. For motion measurement and correction with FID navigators, sub-millimeter and sub-degree tracking accuracy (Fig 1.b) was achieved across all volunteers, demonstrating the efficacy of this approach for real-time head motion measurement. Our results using external trackers (Fig 1.d) show that retrospective and prospective correction using EM tracker motion data can be used to reduce effects of motion in both research and clinical imaging scenarios.

Conclusions

In this work, we show that motion-robust pediatric imaging can be accomplished by faster imaging and real-time motion measurements from navigators and external trackers. We show improved image quality using a variety of motion correction strategies.

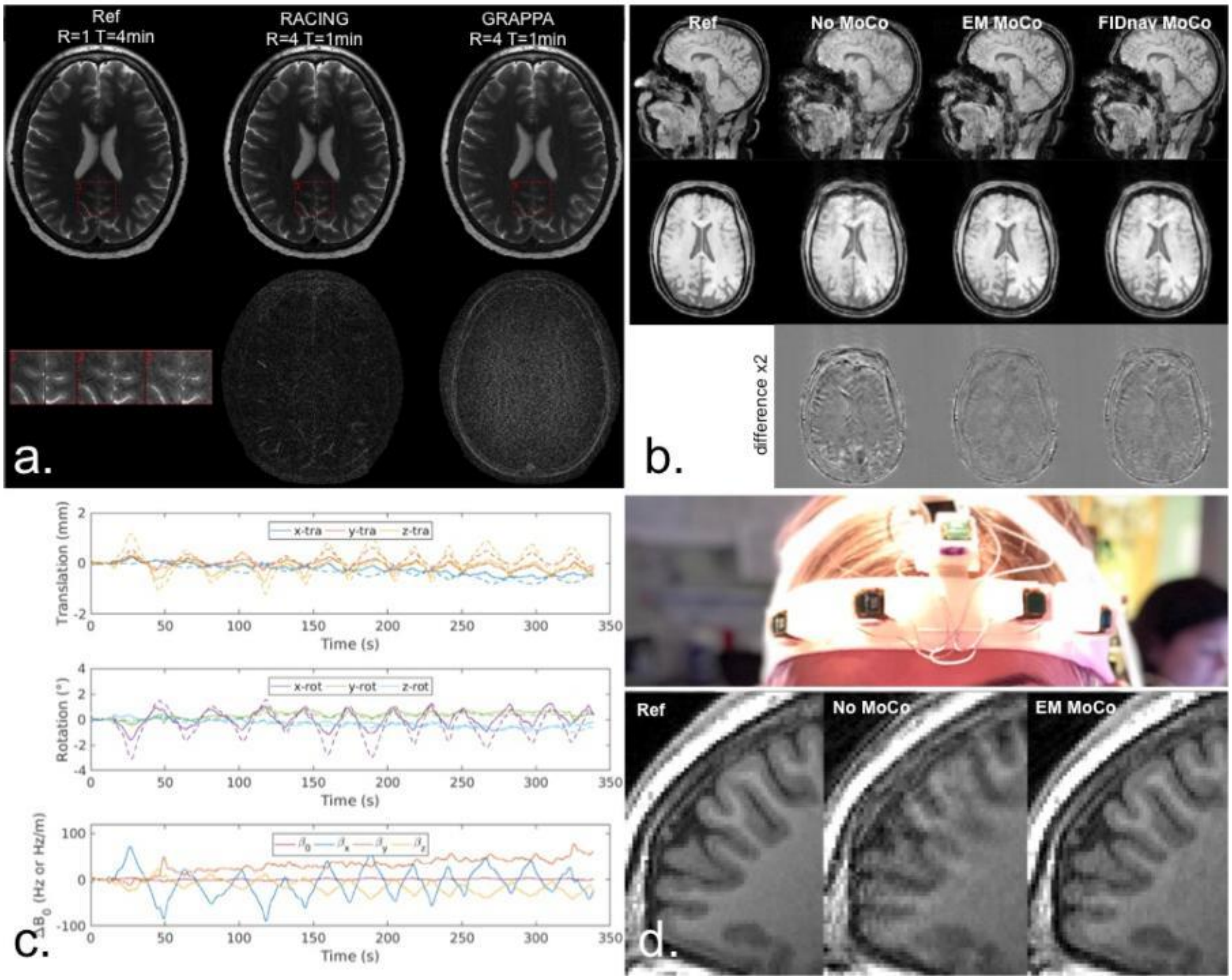

(Filename: TCT_3331_asnr_figure.jpg)

2855

1:28PM - 1:35PM

Modified Fast Trauma Brain MRI as a Follow Up Imaging Modality in Pediatric Traumatic Brain Injury: Higher Percentage of Injury Detection without Radiation and Anesthesia

J Wen[1], C Robertson[2], S Suskauer[3], S Kannan[2], T Ruddy[2], A Tekes-Brady[1]
[1]Johns Hopkins Hospital, Baltimore, MD, [2]Johns Hopkins, Baltimore, MD, [3]Kennedy Krieger Institute and Johns Hopkins, Baltimore, MD

Purpose
Traumatic brain injury (TBI) is a common cause of pediatric emergency room encounters and hospitalizations. CT is the first line of imaging given fast acquisition and wide availability. MRI has greater sensitivity for detecting extra-axial hemorrhage and additional parenchymal injuries, however in young children it may require sedation or anesthesia for adequate imaging quality. Fast brain MRI protocols were first introduced for evaluation of shunted hydrocephalus; more recent indications have included evaluation of macrocephaly and arachnoid cyst follow up. The goal of our study is to evaluate the modified fast trauma brain MRI (MFTB-MRI) compared to initial head CT in patients admitted to the PICU with mild, moderate, and severe TBI.

Materials and Methods

Our institution's modified fast trauma brain MRI (MFTB-MRI) includes axial, sagittal, and coronal HASTE images, DWI and ADC maps, SWI, and a T1 gradient echo black bone sequence. No patients received anesthesia for MFTB-MRI. Sedatives, if used, were administered per PICU providers and as part of the patient's ongoing care. Patients were retrospectively identified from a database of PICU admissions. Inclusion criteria were mild, moderate or severe TBI, age ranging from 0-18 years, and acquisition of a head CT on initial presentation followed by a MFTB-MRI within 36 hours of initial head CT. Presence or absence of the following findings were recorded for each imaging study: calvarial fracture, extra-axial hemorrhage, intraparenchymal hemorrhages, parencyhmal focal arterial ischemic injury, cortical contusion, and diffuse axonal injury (DAI).

Results

Our cohort consisted of 20 patients ranging from ages 10 days to 14 years of age. 19/20 patients had MFTB-MRI within 24 hours of initial head CT; 1 patient received MFTB-MRI within 30 hours of head CT. Mechanisms of TBI were variable and included fall, motor vehicle collisions, pedestrian struck by vehicle, direct penetrating head trauma, and NAT. CT imaging detection of findings by category was as follows: 17 out of 20 cases of calvarial fractures; 5 out of 20 cases of epidural hemorrhage; 14/20 cases of subdural hemorrhage; 14/20 cases of subarachnoid hemorrhage; 0 cases of subpial hemorrhage; 1/20 cases of posterior fossa hemorrhage; 1/20 cases of arterial ischemic injury; 6/20 cases of cortical contusions; 1/20 cases of DAI. MFTB-MRI imaging detection of findings by category was as follows: 14/20 calvarial fractures identified using black bone sequence; 5/20 cases of epidural hemorrhage; 16/20 cases of subdural hemorrhage; 16/20 cases of subarachnoid hemorrhage; 3/20 cases of subpial hemorrhage; 5/20 cases of posterior fossa hemorrhage; 1/20 cases of parenchymal arterial ischemic injury; 10/20 cases of cortical contusions; 7/20 case of DAI. Additional in-depth analysis was performed categorizing the laterality and location of each of the abnormal findings for each case. MRI outperformed CT by identifying additional areas of subdural hemorrhage in 10 out of 20 cases, and subarachnoid hemorrhage in 8 out of 20 cases. MRI was also able to detect an additional 4 out of 5 cases of posterior fossa subarachnoid hemorrhage compared to 1 of 5 cases on CT. No subpial hemorrhage was detected on CT, but 3 cases were identified by MRI. MRI was also more sensitive in detecting DAI in 7 cases, compared to 1 case by CT. The 3 cases of calvarial fractures seen on CT were not detected on MRI secondary to motion artifact (2 cases) and blood products in the mastoid air cells obscuring the fracture line (1 case).

Conclusions

MFTB-MRI is a radiation and anesthesia free MR protocol which is highly effective for initial diagnosis and follow-up of imaging findings in pediatric patients with TBI during their PICU admission. A higher percentage of parenchymal injury and extra-axial hemorrhage was detected on MRI, particularly subpial hemorrhages and subarachnoid hemorrhage in the posterior fossa. In cases where extra-axial hemorrhage was already identified, MRI was able to detect greater extent of hemorrhage in 50% of cases. MFTB-MRI also detected more cases of diffuse axonal injury and cortical contusions compared to CT. Improved injury detection helps to characterize the full extent of TBI in pediatric patients; this in turns has a high impact on patient management and prognostication. Our data will be validated with a larger cohort, and future data analysis will aim to correlate the imaging findings with the clinical severity of brain injury and evaluate the prognostic ability of early imaging for longer term clinical outcomes.

	Total Cases	CT +	MFTB-MRI +	CT + /MFTB-MRI -	CT - /MFTB-MRI +
Calvarial Fracture	17	17	14	3	0
Epidural Hemorrhage	5	5	5	0	0
Subdural Hemorrhage	16	14	16	0	2
Subarachnoid Hemorrhage	16	14	16	0	2
Subpial Hemorrhage	3	0	3	0	3
Posterior Fossa Hemorrhage	5	1	5	0	4
Diffuse Axonal Injury	7	1	7	0	6
Cortical Contusion	10	6	10	0	4

(Filename: TCT_2855_CTvMFTBMRI.jpg)

3086

1:35PM - 1:42PM

Pediatric Brain Ultrasonography with Shear Wave Elastography: Parenchymal Disease Detection and Evaluation of Progression

A El-Ali[1], J Squires[2], S Subramanian[3]
[1]University of Pittsburgh Medical Center, Pittsburgh, PA, [2]CHILDREN'S HOSPITAL OF PITTSBURGH UPMC, Pittsburgh, PA, [3]CHILDREN'S HOSPITAL OF PITTSBURGH UPMC, PITTSBURGH, PA

Purpose
Conventional ultrasound imaging (grayscale and color doppler) can assess a range of intracranial pathology in neonates and young infants; however, there are recognized limitations including relatively low sensitivity and specificity compared to CT and MRI. Early reports have suggested that Ultrasound (US) Shear Wave Elastography (SWE) is a feasible method in neonatal brain US imaging and one report identified abnormal stiffness in preterm infants. We describe our initial experience with brain SWE and report preliminary data suggesting its utility in detecting white matter disease.
Materials and Methods
SWE has been a part of the standard head US protocol at our institution since September 2018. SWE velocity measurements were obtained using a GE Logiq E9 machine with a C1-6 transducer and were recorded in meters per second (m/s). Regions of Interest (ROI) were placed by an US technologist with additional measurements by the supervising physician, for consistency. In order to establish normal anatomic stiffness, ROIs were attempted for each patient in the following areas: periventricular white matter, lateral ventricular cerebrospinal fluid (CSF), and basal ganglia (thalamus and/or caudate head). SWE was also attempted in patients with dural sinus venous thrombosis. ROIs were pooled for analysis. Statistical analysis performed in the R software package included unpaired two tailed Student's t-test and one-way ANOVA.
Results
A total of 74 SWE studies were attempted and 53 (72%) were successfully performed. The most common

reason for failure was excessive patient motion. Almost all studies were completed independently by ultrasound technologists (94%). Most patients were less than 30 days old (n=30, 57%) with an age range of 0-197 days. All patients less than 30 days old were born at >33 weeks gestational age. 50 patients (93%) had normal head ultrasounds or only minor intracranial pathology that did not affect SWE analysis. 3 patients (8%) demonstrated significant WM abnormalities including extensive bilateral venous infarction and intraparenchymal hemorrhage . SWE demonstrated reliable differences in mean velocity between the lateral ventricle (0.82 m/s), WM (1.11 m/s), and basal ganglia (1.43 m/s) ($p<0.001$). Direct comparison between WM and basal ganglia was also significant (t-test, $p<0.001$). Mean velocity for normal WM (1.11 m/s) also significantly differed from abnormal WM (2.49 m/s) (t-test, $p<0.001$). Preliminary data from two patients with dural sinus venous thrombosis demonstrate that SWE velocity measurements change independent of Hounsfield unit (HU) measurements on serial CT images (see Figure). Relative to normal brains there is increased WM stiffness and decreased BG stiffness.

Conclusions

Results from our prospective study demonstrate that SWE is a feasible technique for evaluation of brain parenchyma as significantly different stiffness was found in various normal intracranial structures ($p<0.001$). Additionally, we demonstrate the utility of SWE in the evaluation of WM disease as significant differences in stiffness between normal and pathologic white matter were found ($p<0.001$). Finally, our study is the first published report of institutional level exploration of this technique in North America. Scans were generally (94%) performed by ultrasound technologists, in contradistinction to prior studies which were performed by single experienced pediatric radiologists.

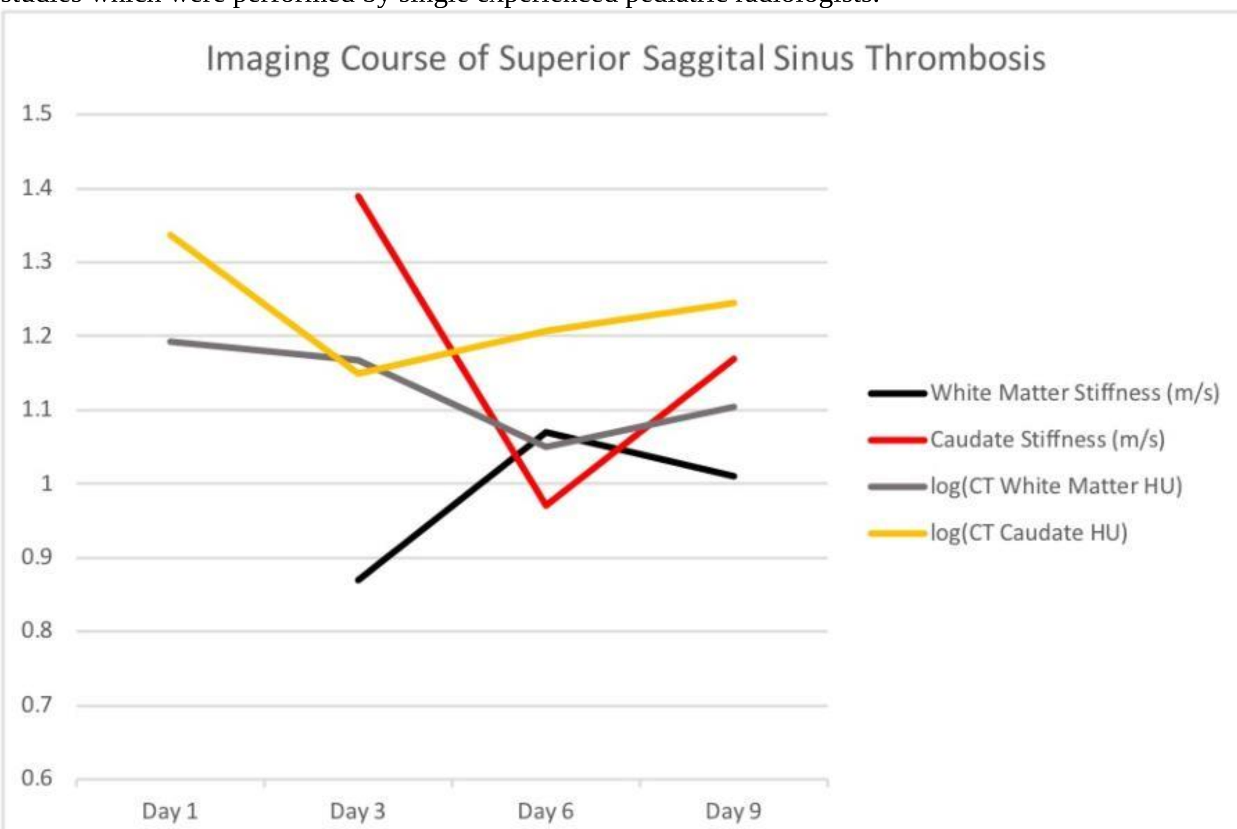

(Filename: TCT_3086_superiorsaggitalsinus.jpg)

3306

1:42PM - 1:49PM

Quick Brain MRI for Evaluation of First-time Afebrile Seizures in Children

T Tsai[1], W Mehan[1], P Caruso[1]
[1]*Massachusetts General Hospital, Boston, MA*

Purpose
MRI is the preferred imaging modality for the investigation of pediatric patients presenting with afebrile seizures to investigate for an underlying acute lesion or brain malformation1. Our goal was to evaluate the accuracy of quick brain MRI (qbMRI) for the detection of such pathology.
Materials and Methods
A retrospective analysis was performed of consecutive pediatric patients presenting to our Institution with first-time afebrile seizures who underwent a quick brain MRI (qbMRI) protocol between January 2010 and August 2018. The imaging and medical records were reviewed for patient demographics, clinical characteristics, and MRI findings. Children were divided into two groups: those with no second seizure during the study period (Group A) and those with a second seizure (Group B). The timing and findings of any follow-up complete, epilepsy protocol MRI brain studies were catalogued.
Results
A total of 30 children met the inclusion criteria. 12 children underwent a subsequent complete epilepsy MRI (40%). Overall, three MR studies (10%) had acute, actionable findings including venous hemorrhagic infarction, ADEM and HSV encephalitis. Group A consisted of 27 patients. There were zero acute or actionable findings missed on qbMRI that were detected on follow-up complete, epilepsy MRI. There were 2 patients with non-acute, non-actionable findings missed by initial qbMRI (7.4%), including hippocampal dysplasia. Group B contained 3 patients, none of whom had missed acute, actionable findings on the initial qbMRI. There was a single patient (33.3%) with a non-actionable finding of a punctate occipital lobe infarction missed on initial qbMRI.
Conclusions
Quick brain MRI may be a useful strategy in the evaluation of pediatric patients presenting with new-onset afebrile seizures. This approach could help rapidly triage children for more dedicated complete, epilepsy MR studies or potentially obviate the need for additional MR imaging in patients with reassuring clinical exams in the setting of a normal qbMRI.

2658

1:49PM - 1:56PM

Review of Neck CTA Examinations for Pediatric Soft Palate Injury and Proposal of a New Targeted CTA Protocol

J Choi[1], C Burton[1], S Voss[1], A Danehy[1]
[1]*Boston Children's Hospital, Boston, MA*

Purpose
Neck CTA is commonly requested for patients with soft palate injuries to exclude vascular injury. Debate exists regarding which imaging studies, if any, are indicated in this setting. Standard neck CTA protocols, extending from thoracic inlet to skull base, result in considerable radiation to the neck. The purpose of this study is to review the yield of neck CTA following oropharyngeal trauma and to propose a new reduced dose targeted CTA protocol for this indication.
Materials and Methods
Neck CTA's obtained between 2008-2018 for evaluation of soft palate and oropharyngeal injury were retrospectively reviewed. Study variables included age at presentation; mechanism of injury; otolaryngology consultation; presence of vascular or neurologic injury; and any other clinically significant findings. All neck CTA exams were performed from the thoracic inlet to skull base per standard institutional protocol. Effective dose was estimated using CTDIvol and tissue weighting conversion factors from ICRP 60 and ICRP 13, with calculations based on sagittal CTA reconstructions, using the z-axis of the patient from skull base to thoracic inlet (full neck CTA) and skull base to hyoid

bone (targeted neck CTA), to provide an estimate of organs at risk. Dose reduction for the targeted neck CTA was defined as the % decrease in effective dose compared to full neck CTA.

Results

Between 2008-2018, 98 neck CTA's were ordered in the setting of oropharyngeal trauma. Average patient age was 5.1 ± 3.3 yrs. Otolaryngology consultation was obtained in 98% of cases. The most common indication was fall with foreign object in mouth (toothbrush, straws, and toys). 1 study was excluded due to contrast extravasation. No studies were positive for either neurologic injury or injury to the carotid arteries. 1 study was positive for minor small vessel injury. Clinically significant nonvascular findings were present in 5/97 (5%) cases and included: retained toothbrush foreign body (1/97); phlegmonous change (2/97); retropharyngeal/upper mediastinal air (1/97); and minimally displaced medial pterygoid process fracture (1/97). With exception of mediastinal air, all vascular and non-vascular findings would have been included in a targeted neck CTA extending from hyoid bone to skull base. Mean effective dose was 8.63 ± 3.98 mSv per ICRP 60 and 8.44 ± 3.95 mSv per ICRP 130 for standard neck CTA. For the proposed targeted neck CTA extending only from skull base to the hyoid bone, the effective dose estimate was 2.25 ± 0.96 mSv, resulting in significant dose reduction of ~72% ± 8% ($p<0.01$).

Conclusions

Based on the low yield of routine neck CTA for evaluation of vascular injury following oropharyngeal trauma, a new targeted neck CTA protocol is proposed that results in significantly less dose to the neck, while preserving the diagnostic yield for both vascular and non-vascular findings.

3530

1:56PM - 2:03PM

Screen-time is Linked to Decreased Cortical Surface Area and Lower Cognitive Performance in Early Adolescence

A Rauschecker[1], M Olaru[2], R Nillo[2], R Desikan[1], L Sugrue[1]

[1]UCSF, San Francisco, CA, [2]University of California San Francisco, San Francisco, CA

Purpose

Screen-time has been linked to decreased cognitive performance in children (Walsh et al., 2018). However, no recommendations regarding screen-time exist for adolescents. We sought to study the link between screen-time and cognition by examining its effects on measures of brain anatomy, such as cortical area and cortical thickness.

Materials and Methods

This cross-sectional study examined data from 4,077 children (ages 9-10) who participated in the Adolescent Brain Cognitive Development study (Volkow et al., 2018), with data collected across 21 study sites in the US. Subjects self-reported average weekday duration of TV/movie watching. Using a multivariable linear mixed-effects model, we examined the associations between this measure of screen-time and brain anatomy, as measured by MRI (cortical surface area and cortical thickness across 66 regions of interest). We also examined the relationship between duration of TV/movie watching and cognitive scores, as measured by the NIH Toolbox composite score.

Results

There was a significant association between screen-time and global cognition ($p<10^{-6}$), despite accounting for race/ethnicity, sex, age, parental education level, parental income, and parental marital status, familial relationships, and imaging site with a mixed effects linear model. There was also a significant association between screen-time and total cortical area ($p<0.05$) and total cortical volume ($p<0.01$), but not with mean cortical thickness ($p>0.05$). Examining the spatial distribution of these effects across the brain revealed a diffuse distribution, suggesting global effects (Figure).

Conclusions

By leveraging a representative sample of over 4,000 normally developing adolescents across the US, we report a definitive link between screen-time, anatomical brain development, and cognitive performance in early adolescence. Specifically, larger average durations of TV watching were associated with decreased cognitive scores and with decreased global cortical surface area. Future studies will explore additional anatomical and functional neural correlates of screen-time in this cohort and evaluate changes in regional specificity as these children are followed longitudinally through adolescence.

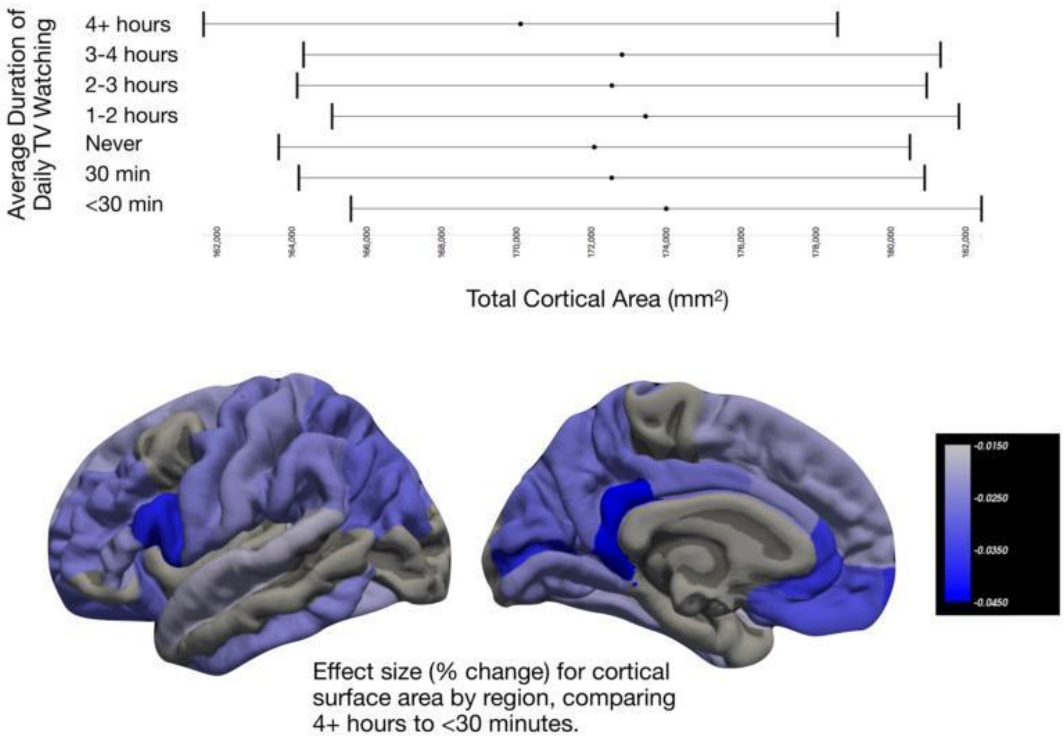

(Filename: TCT_3530_Rauschecker_Figure.jpg)

3557

2:03PM - 2:10PM

Snoring is Linked to Decreased Cortical Surface Area and Lower Cognitive Performance in Early Adolescence

M Olaru[1], A Rauschecker[2], R Nillo[1], R Desikan[2], L Sugrue[2]
[1]University of California San Francisco, San Francisco, CA, [2]UCSF, San Francisco, CA

Purpose
Snoring has been linked to adverse behavioral outcomes in children (Bonuck et al., 2012). However, little is known about the impact of snoring on global cognition and/or anatomical brain development. We sought to study the link between snoring and both cognition and anatomical measures of cortical area in a large cohort of normally developing adolescents.
Materials and Methods
This cross-sectional study examined data from 4,077 children (ages 9-10) who participated in the Adolescent Brain Cognitive Development study (Volkow et al. 2017), with data collected across 21 study sites in the US. The parents of subjects self-reported the average frequency with which the subject snores. Using a multivariable linear mixed-effects model, we examined the associations between this measure of snoring and brain anatomy, as measured by MRI cortical surface area. We also examined the relationship between frequency of snoring and cognition, as measured by the NIH Toolbox composite score.
Results
There was a significant association between snoring and global cognition ($p<0.05$), despite accounting for

race/ethnicity, sex, age, parental education level, parental income, and parental marital status, familial relationships, and imaging site with a mixed effects linear model. Using a similar mixed effects linear model, there was also a significant association between snoring and total cortical area ($p<0.05$). Examining the spatial distribution of these effects across the brain, revealed a distribution of effects most pronounced in the frontal and parietal association cortices (Figure).

Conclusions

By leveraging a representative sample of over 4,000 normally developing adolescents across the US, we report a definitive link between snoring, anatomical brain development, and cognitive performance in early adolescence. Specifically, a higher frequency of snoring was associated with decreased composite cognitive scores and with decreased total cortical surface area. Regionally the pattern of brain effects was selective for frontal and parietal association cortex. Future studies will explore additional anatomical and functional neural correlates of snoring frequency in this cohort and evaluate how the regional specificity of these effects changes as these children are followed longitudinally through adolescence.

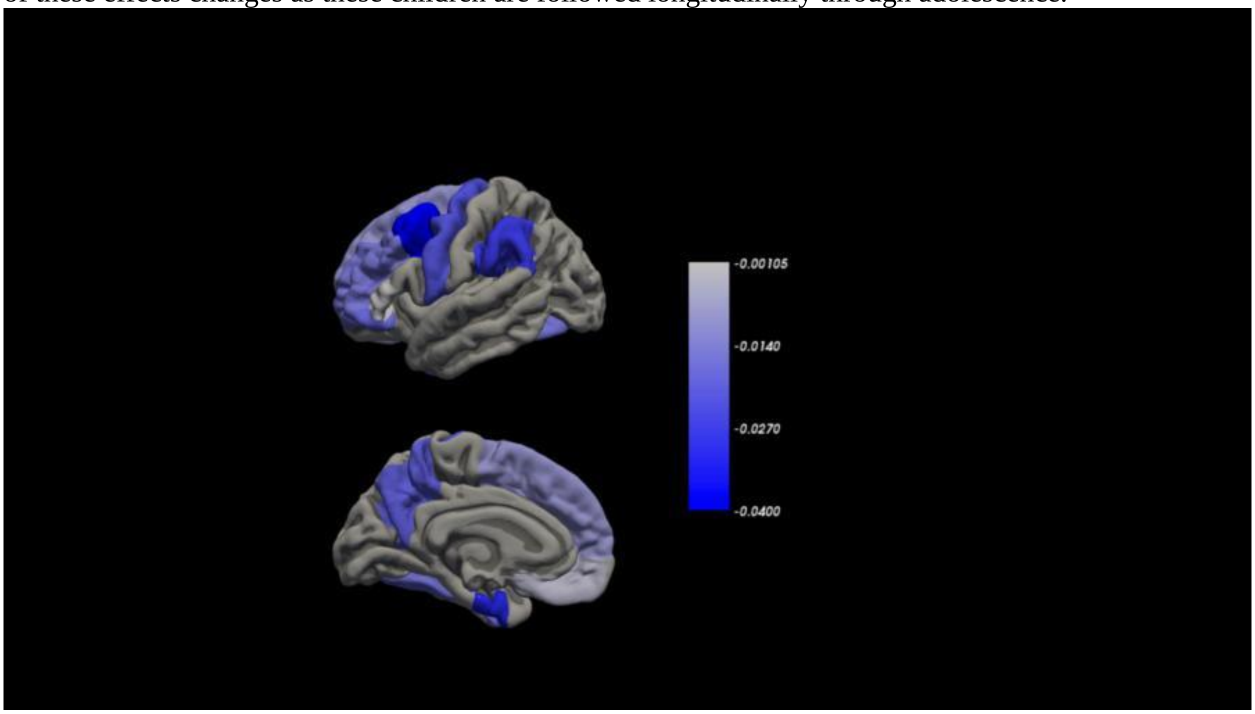

(Filename: TCT_3557_lhCAsnore.jpg)

2856

2:10PM - 2:17PM

Subfields in Children with Non-Lesional Focal Epilepsy

M Wagner[1], J Skocic[1], E Widjaja[2]
[1]The Hospital for Sick Children, Toronto, ON, [2]Diagnostic Imaging, Toronto, Ontario

Purpose

Animal studies have shown that recurrent seizures result in cumulative neuronal loss. However, it is not clear if this occurs in human. The aim of the study was to determine if seizure control influenced the hippocampal subfield volumes longitudinally in children with focal epilepsy.

Materials and Methods

37 patients with focal epilepsy and normal MRI underwent volumetric T1-weighted imaging at two time-points. We assessed the total hippocampal and hippocampal subfields including CA1, CA3, CA4, subiculum, presubiculum, parasubiculum, molecular layer, and dentate gyrus volumes using FreeSurfer.

Seizure frequency at baseline and follow-up were assessed, and seizure control was determined using Engel classification. Patients were grouped into Engel I/II (Group 1), i.e. those who were seizure-free or with rare disabling seizures, and Engel III/IV (Group 2), i.e. those with some or no seizure reduction. Linear regression was used to evaluate if there were group differences in total or subfield hippocampal volumes, adjusting for baseline total or subfield hippocampal volumes, age, total brain volume, and time interval between the MRIs.

Results

The mean age of patients at baseline was 9.86±3.74 years, and there were 12 females. The median number of antiepileptic drugs at baseline was two. The interval between the two MRIs was 2.59±1.27 years. The right parasubiculum volume at follow-up was smaller in Group II than Group I (62.89±12.03 mm^3 and 75.77±21.36 mm^3, respectively), controlling for baseline parasubiculum volume, age, total brain volume, and time interval between the MRIs ($p=0.022$). There were no significant differences in total hippocampal, CA1, CA3, CA4, subiculum, presubiculum, molecular layer, and dentate gyrus volumes between the two groups (all $p>0.05$).

Conclusions

Reduced volume in the parasubiculum, one of the subiculum complex that is located between the hippocampus and parahippocampus, suggests that spread of seizures to the hippocampus may contribute to neuronal loss in this region.

2895

2:17PM - 2:24PM

Synthetic-MRI Detects Delayed Myelination in Preterm-Neonates

V Schmidbauer[1], G Geisl[1], K Goeral[1], D Prayer[1], G Kasprian[1]
[1]*Medical University of Vienna, Vienna, Austria*

Purpose

"Synthetic-MRI" generates different MR-contrasts and characterizes tissue properties based on one Multi-Dynamic-Multi-Echo-FLAIR-sequence (MDME). The aim of this study is to assess the feasibility of "Synthetic-MRI" in the assessment of myelination in term-born- (TN) and preterm-neonates (PN).

Materials and Methods

30 PN and TN were examined at the approximate due date [gestational-age + days to MRI= corrected gestational-age (CGA)] using a standardized neonatal MRI-protocol (1.5 Tesla / T1 SE- / T2 SE- / DWI- / DTI-sequence). MDME-sequence (FOV: 200 x 165 x 109mm / Voxel: 0.9 x 1 x 4mm / Matrix: 224 x 158 x 22 slices / TE: 13ms / TR: 3309ms / Acquisition-time: 5min. 22sec.) based post-processing was performed using "Synthetic-MRI" (Synthetic MR AB, Storgatan 11, Linköping, SWEDEN. Version 8.0.4). Myelination was assessed by scoring seven brain-regions on T1- / T2-maps generated by "Synthetic-MRI" and on standard T1- / T2-images, acquired separately. Analysis of covariance (ANCOVA / Covariate: CGA at MRI) was used for group-comparison.

Results

In 25/30 (83.33%) cases [18 PN (mean gestational-age: 178.17 d / SD= 12.56) and 7 TN (mean gestational-age: 279.14 d / SD= 8.86)] myelination assessment could be performed. T1- / T2-maps generated by "Synthetic-MRI": ANCOVA results showed significantly lower myelination-scores in PN compared to TN [T1: $F(1, 22)= 7.420$ / $p= 0.012$; T2: $F(1, 22)= 5.658$ / $p= 0.026$]. The myelination-score showed a positive correlation with the CGA at MRI (T1: $r= 0.662$ / $n= 25$ / $p\leq 0.001$; T2: $r= 0.676$ / $n= 25$ / $p\leq 0.001$). The myelination-score based on standard T1- / T2-images did not correlate with the CGA at MRI. No significant differences between PN and TN were detectable.

Conclusions

Substantial differences concerning the myelination in TN and PN are detectable on T1- / T2-maps generated by "Synthetic-MRI". The method allows detecting myelination differences more sensitively and rapidly than standard MR-sequences.

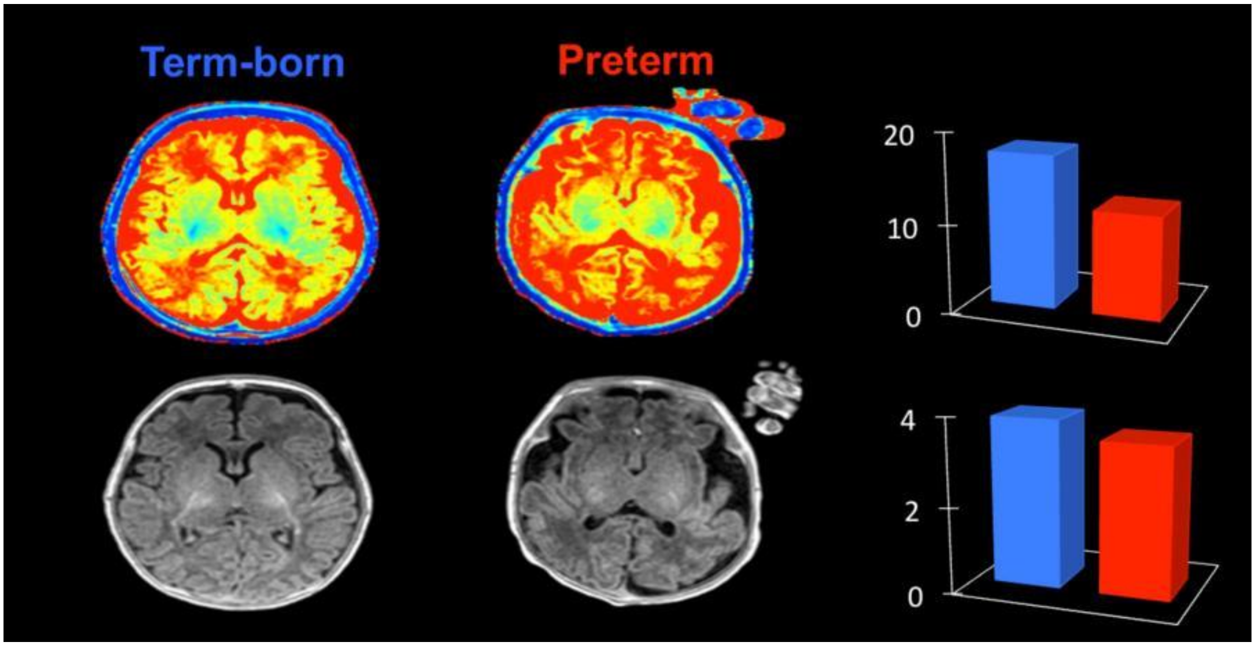

(Filename: TCT_2895_Synthetic_vs_Conventional.jpg)

Tuesday, May 21, 2019
1:00PM - 2:30PM
Let's Talk Techniques in H&N

3675

1:00PM - 1:07PM

PET Taupathology: Novel Direction of PET/MRI Imaging

A Franceschi[1], M Clifton[2], K Naser-tavakolian[3], D Franceschi[3], G Cruciata[4], L Bangiyev[5], A Franceschi[1]
[1]SUNY Stony Brook, New York, NY, [2]Stony Brook University Hospital, N/A, [3]Stony Brook University Hospital, Stony Brook, NY, [4]Stony Brook University Hospital, Brooklyn, NY, [5]Stony Brook University Hospital, Stony Brook , NY

Purpose
Postmortem examination has demonstrated that neurodegenerative disease progression correlates more specifically with neurofibrillary tangle burden rather than Amyloid βeta (AB) plaque load. Presently, imaging techniques rely heavily on qualitative characteristics such as decreased parenchymal volumes or hypometabolism within disease specific cortex. Novel PET radiotracers (18F-T807) targeting the neurofibrillary tangle, hyperphosporylated tau protein, demonstrate closer association with clinical severity and neurodegeneration on postmortem analysis compared to amyloid PET. As tau tangle burden increases, symptom severity should follow. We report on the effectiveness of 18F-T807 PET/MRI imaging in human subjects with neurodegenerative disease due to suspected underlying tau accumulation.

3168

1:14PM - 1:21PM

Shock Thyroid in a Patient with Hypovolemic Shock Complex

M Shroads[1], P Manning[1], E Bergman[2], M McDonald[1], J Chen[2]

[1]UC San Diego Health System, San Diego, CA, [2]San Diego Veterans Administration Medical Center/UC San Diego Health System, La Jolla, CA

Purpose
A number of imaging findings can be identified in patients with hypovolemic shock complex, regardless of cause. To our knowledge, there are only two previously published reports to date of imaging in cases of "shock thyroid." The purpose of this excerpta is to present a rare case from our institution, highlighting key imaging features of "shock thyroid" and additional imaging clues to suspect a hypoperfused state.
Materials and Methods
A 58-year-old male was found down after an unknown duration of time by his roommates. He was altered in mental status, hypothermic, and in multiorgan failure due to massive upper gastrointestinal hemorrhage. After undergoing hemodynamic resuscitation, his hospital course was complicated by abdominal compartment syndrome requiring decompressive laparotomy, ischemic colitis, and multifactorial shock requiring multiple vasopressors and causing end-organ damage.
Results
As part of the trauma protocol, CT angiography of the neck was obtained, which revealed an enlarged, heterogeneous thyroid gland with fluid surrounding and tracking around the gland, most pronounced anteriorly. There was also an overall diminutive appearance of the cervical arteries, with the carotid arteries appearing even smaller than the foramen transversarium, suggestive of a low cardiac output/vasoconstricted state. No vascular wall thickening or mural hematoma was present in the visible arteries.
Conclusions
Reflex thyrotoxicosis and cell death in the setting of the hypovolemic shock complex can be reflected in a characteristic abnormal CT appearance of the thyroid gland, which, in addition to other sequelae of hypoperfusion, should be recognized and reported to avoid confusion with primary thyroid or vascular injury.

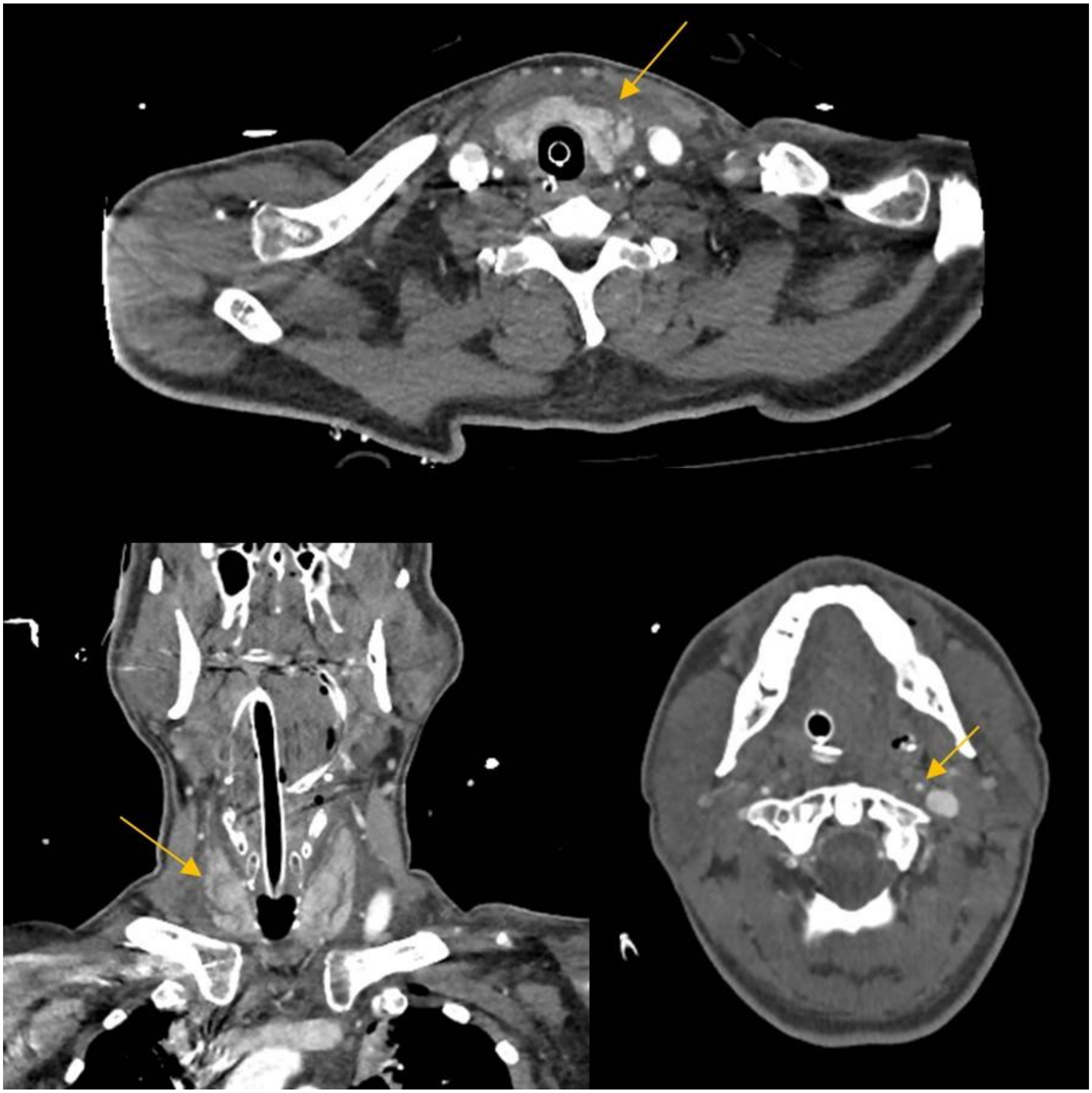

(Filename: TCT_3168_Shockthyroid.jpg)

2810

1:21PM - 1:28PM

3D Double-Echo Steady-State with Water Excitation MR Imaging: Evaluation of Intraparotid Facial Nerve in Patients with Deep-Seated Parotid Tumors

H Kim[1], Y Kim[2], M Seong[3], Y Kim[3]
[1]SAMSUNG MEDICAL CENTER, SEOUL, none, [2]Samsung Medical Center, Sungkyunkwan University School of Medicine, Seoul, none, [3]Samsung Medical Center, Seoul, none

Purpose
Preoperative imaging identification of the intraparotid facial nerve is a critical issue to prevent nerve injury during surgery. The purpose of this study was to assess the utility of 3D double-echo steady-state

with water excitation (3D DESS-WE) sequence for the evaluation of the intraparotid facial nerve in patients with deep-seated tumors in the parotid gland.

Materials and Methods

Twenty-five patients with deep-seated tumor in the parotid gland were prospectively enrolled and underwent MR imaging with 3D DESS-WE sequence. The visibility of the intraparotid facial nerve was independently assessed by 2 neuroradiologists. Based on a consensus interpretation, we compared the diagnostic accuracy of 3D DESS-WE imaging for predicting the tumor location with those of 2 conventional methods employing the retromandibular vein and facial nerve line, with surgery as the reference standard. We also evaluated the pattern of relationship between the tumor and the main trunk of the intraparotid facial nerve on DESS-WE images.

Results

According to a consensus interpretation, DESS-WE imaging could visualize the main trunk, the temporofacial division, and the cervicofacial division of the intraparotid facial nerve in 100% (25/25), 48% (12/25), and 36% (9/25), respectively. With the surgery as the reference standard, the diagnostic accuracy of 3D DESS-WE imaging for predicting the tumor location was 92% (23/25), which was statistically significantlybetter than those of the retromandibular vein method (60% [15/25]; P = .021) and the facial nerve line method (52% [13/25]; P = .006). 3D DESS-WE imaging correctly predicted the pattern of relationship between the tumor and the main trunk of the facial nerve in 92% (23/25).

Conclusions

By direct visualization of the facial nerve, 3D DESS-WE imaging can provide valuable information on the localization of deep-seated tumors in the parotid gland. This information is considered crucial to minimize the risk of injury of the facial nerve during parotid surgery.

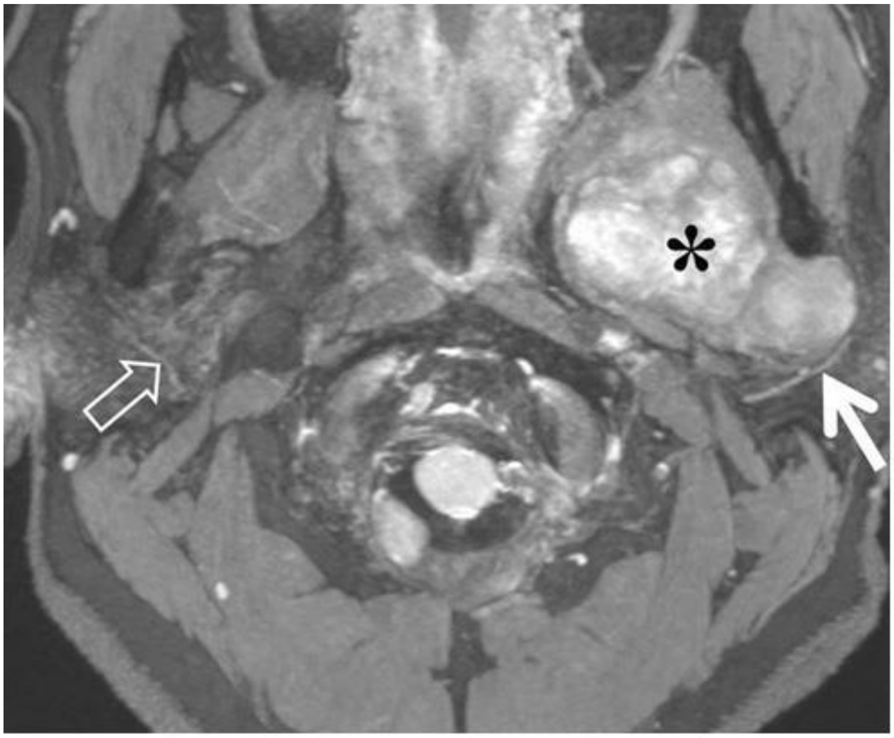

Table: Localization of the parotid tumors

Surgery $n = 25$	DESS-WE			RMV Method			FNL Method		
	SL	DL	BL	SL	DL	BL	SL	DL	BL
SL, $n = 11$	10	0	1	3	0	8	2	0	9
DL, $n = 3$	0	3	0	0	2	1	0	1	2
BL, $n = 11$	1	0	10	0	1	10	0	1	10
Accuracy	92% (23/25)			60% (15/25)			52% (13/25)		
P Value	–			.021			.006		

(Filename: TCT_2810_Fig.jpg)

3632

1:28PM - 1:35PM

Accelerated Simultaneous Acquisition of QSM and MTV for in Vivo Susceptibility and Myelin-Sensitive Imaging

F Yu[1], S Huang[2], B Bilgic[3]

[1]UT Southwestern Medical Center, Dallas, TX, [2]Massachusetts General Hospital / Athinoula A. Martinos Center for Biomedical Imaging, Boston, MA, [3]A. A. Martinos Center for Biomedical Imaging, Bldg. 149, 13th St., MA

Purpose

There has been growing interest in quantitative MR imaging markers for the evaluation of neurological diseases. We previously devised a novel strategy for simultaneously acquiring co-registered whole-brain COSMOS (Calculation of Susceptibility through Multiple Orientation Sampling) quantitative susceptibility mapping (QSM; a measure of magnetic susceptibility that has been shown to correlate with tissue iron content) and macromolecular tissue volume (MTV; a myelin-sensitive metric) at the scan cost of only one of these contrasts by exploiting their inherent redundancies (1). In addition to QSM and MTV, the multi-echo acquisition also allowed us to provide T1, proton density, and R2* parameter maps. However, this protocol still required approximately 15 minutes to acquire. Therefore, to further enhance its clinical feasibility, we propose the use of Joint Virtual Coil (JVC-) generalized autocalibrating partially parallel acquisitions (GRAPPA) to further accelerate the acquisition (2). This method jointly reconstructs multi-echo images by treating data from other echoes as extra coils, allowing the creation of additional channels to improve parallel imaging and acceleration capability. For example, assuming Nc coils and Ne echoes, the total number of coils available for joint reconstruction would be increased by 2 x Nc x Ne, where the additional factor of 2 is coming from the Virtual Coil concept which uses image phase for extra encoding. This subsequently allows for reductions in artifact as well as scan time. We demonstrate that JVC-GRAPPA enables R=9-fold acceleration with scan quality that is comparable to the slower, R=6-fold accelerated GRAPPA acquisition. With this, we provide a 6-min protocol for simultaneous QSM, MTV, T1, T2* and PD mapping at 1mm3 isotropic resolution with whole-brain coverage.

Materials and Methods

Comparing the retrospectively undersampled MTVF maps to the fully-sampled ground truth MTVF maps, the R=3x3 accelerated GRAPPA demonstrated an root-mean-squared error (RMSE) of 6.1%. The R=3x3 accelerated JVC-GRAPPA MTVF map performed similarly with an RMSE of 6.8%. Since there was no fully-sampled reference data for the prospectively undersampled acquisitions, we compared R=3x3 JVC-GRAPPA with R=3x2 GRAPPA reconstruction. For the magnitude data at each of the 3 flip angles, R=3x3 JVC-GRAPPA showed RMSE of approximately 2 x 10-5 % compared to R=3x2 GRAPPA. The processed MTVF maps showed a larger deviation between the two techniques at 8% which was partly attributed to slight differences in brain extraction results in the posterior fossa (Figure 1). COSMOS susceptibility maps demonstrated an RMSE of 0.14% when comparing JVC-GRAPPA to GRAPPA (Figure 2). Regions-of-interest (ROIs) were placed in the bilateral deep frontal white matter, globus pallidi, and internal capsule posterior limbs for the prospectively undersampled susceptibility and MTVF maps (Table 1). GRAPPA demonstrated minimally lower absolute values but similar standard deviations for susceptibility compared to JVC-GRAPPA. No consistent differences were observed between JVC-GRAPPA and GRAPPA for MTVF. Additional T1, proton density, and R2* maps were also generated from the multi-echo data as previously described, with representative images shown in Figure 3 (1).

Results

Comparing the retrospectively undersampled MTVF maps to the fully-sampled ground truth MTVF maps, the R=3x3 accelerated GRAPPA demonstrated an root-mean-squared error (RMSE) of 6.1%. The R=3x3 accelerated JVC-GRAPPA MTVF map performed similarly with an RMSE of 6.8%. Since there was no fully-sampled reference data for the prospectively undersampled acquisitions, we compared R=3x3 JVC-GRAPPA with R=3x2 GRAPPA reconstruction. For the magnitude data at each of the 3 flip angles, R=3x3 JVC-GRAPPA showed RMSE of approximately 2 x 10^-5 % compared to R=3x2 GRAPPA (Figure 1). COSMOS susceptibility maps demonstrated an RMSE of 0.14% when comparing JVC-GRAPPA to GRAPPA (Figure 2). The processed MTVF maps showed a larger deviation between the two techniques at 8% which may be partly attributed to slight differences in brain extraction results in the posterior fossa (Figure 3). Regions-of-interest (ROIs) were placed in the bilateral deep frontal white matter, globus pallidi, and internal capsule posterior limbs for the prospectively undersampled susceptibility and MTVF maps (Table 1). GRAPPA demonstrated minimally lower absolute values but similar standard deviations for susceptibility compared to JVC-GRAPPA. No consistent differences were observed between JVC-GRAPPA and GRAPPA for MTVF.

Conclusions

Our implementation of JVC-GRAPPA allowed for a 9-fold reduction in acquisition time for MTVF and QSM. The image quality and artifacts from this method were comparable to GRAPPA with 6-fold acceleration as well as the fully sampled non-accelerated acquisition. As previously described, this method also allows for the generation of three additional quantitative maps (T1, proton density, and R2*) for a total of five (1). It should be noted that although we acquired the data at different head positions to facilitate COSMOS QSM, a single orientation approach can also be adopted to further broaden its clinical utility. We believe that this rapid protocol will facilitate detailed studies of a variety of neurological diseases, particularly those that undergo disturbances in myelin (demyelination, dysmyelination) and iron content, such as multiple sclerosis as well as neurodegenerative disorders.

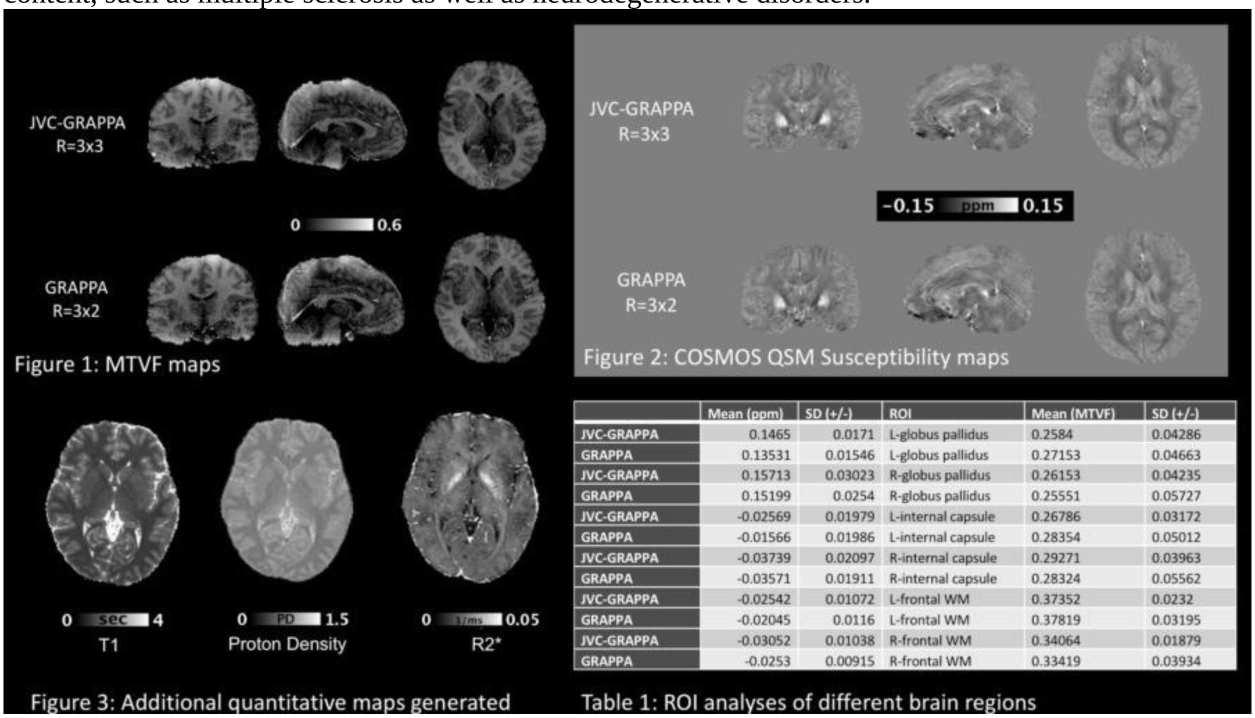

Figure 1: MTVF maps

Figure 2: COSMOS QSM Susceptibility maps

Figure 3: Additional quantitative maps generated

	Mean (ppm)	SD (+/-)	ROI	Mean (MTVF)	SD (+/-)
JVC-GRAPPA	0.1465	0.0171	L-globus pallidus	0.2584	0.04286
GRAPPA	0.13531	0.01546	L-globus pallidus	0.27153	0.04663
JVC-GRAPPA	0.15713	0.03023	R-globus pallidus	0.26153	0.04235
GRAPPA	0.15199	0.0254	R-globus pallidus	0.25551	0.05727
JVC-GRAPPA	-0.02569	0.01979	L-internal capsule	0.26786	0.03172
GRAPPA	-0.01566	0.01986	L-internal capsule	0.28354	0.05012
JVC-GRAPPA	-0.03739	0.02097	R-internal capsule	0.29271	0.03963
GRAPPA	-0.03571	0.01911	R-internal capsule	0.28324	0.05562
JVC-GRAPPA	-0.02542	0.01072	L-frontal WM	0.37352	0.0232
GRAPPA	-0.02045	0.0116	L-frontal WM	0.37819	0.03195
JVC-GRAPPA	-0.03052	0.01038	R-frontal WM	0.34064	0.01879
GRAPPA	-0.0253	0.00915	R-frontal WM	0.33419	0.03934

Table 1: ROI analyses of different brain regions

(Filename: TCT_3632_ASNR_19_fig_v2.jpg)

2976

1:35PM - 1:42PM

Accurate Non-Invasive Eye Vitreous Temperature Measurement and Mapping using Diffusion-Based Thermometry MRI

J Derakhshan[1], L Loevner[2], F Wehrli[2], N Parvin[1], R McKinstry[1]
[1]Washington University School of Medicine, Saint Louis, MO, [2]University of Pennsylvania, Philadelphia, PA

Purpose

Prior non-invasive measurements of vitreous temperature using diffusion-based thermometry MRI (1) showed variability within and between subjects and was different based on choice of b-values (2-4). The effect of eye motion and b-value were studied using data from prospective temperature measurements in ten healthy volunteers and a phantom experiment.

Materials and Methods

Sets of 10 measurements of diffusion coefficient in 10 healthy human volunteers using two sets of b-

values (b=0,200,400,600 and b=0,500,1000 s/mm^2) were analyzed in Matlab. Motion was identified as elevation in temperature near the periphery of the globe. Linear regression of globe temperature as a function of motion was performed. The intercept was used to determine temperature in the absence of motion. A phantom experiment was performed (Siemens Prisma) with vials of 2, 5 and 10mL distilled water and 2mL human vitreous from an unrestricted autopsy within 48 hours of death. ADC was measured using both sets of b-values above as well as a full dataset (b=0:100:1500 s/mm^2, 16 b-values).
Results
Phantom experiments revealed a -28x10^-6 mm^2/s offset in ADC compared to distilled water (-1.3%, p=0.02), corresponding to a -0.5°C temperature offset (Fig. A). Compared to the full diffusion dataset, vitreous temperature estimated with the 3 (higher) and 4 (lower) b-values had a -0.1°C (p=0.67) and -0.9°C (p<0.001) temperature offsets, respectively, which are inherent to the fitting technique. In-vivo, temperature maps without significant motion confirmed a predicted -2.5°C temperature gradient from the retina to the lens (Fig. B) (5). The intercept of the regression analysis showed a temperature of 33.7°C using 3 b-values (Fig. C) and 32.9°C using 4 b-values (Fig. D) (relative temperature offset -0.8°C, the same as the phantom experiment).
Conclusions
Eye vitreous temperature in healthy volunteers is determined to be 33.7°C. Even in the presence of motion, a globe temperature difference of 0.8°C can be used as a biomarker of pathology.

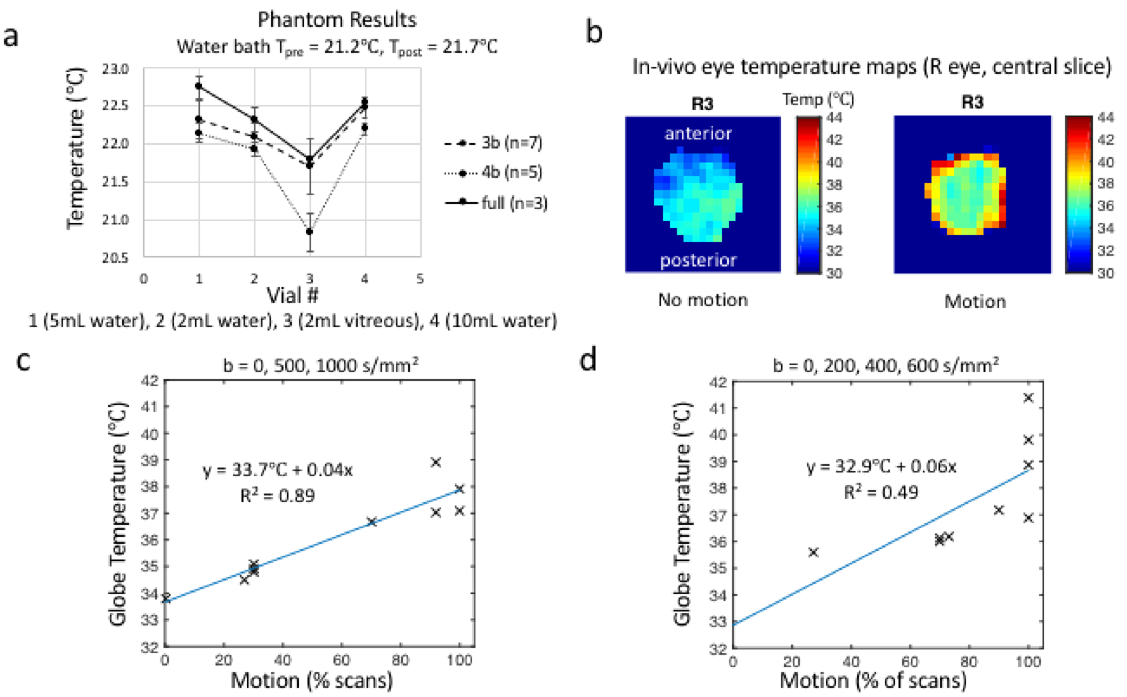

(Filename: TCT_2976_Slide1.gif)

3251

1:42PM - 1:49PM

Comparison of Fat Saturated Coronary Turbo-Spin-Echo vs Short-Tau-Inversion-Recovery Sequences in the Diagnostic Workup of Optic Nerve Neuritis

T Faizy[1], G Broocks[2], C Thaler[3], F Flottmann[4], H Leischner[5], J Nawabi[6], M Schoenfeld[3], J Fiehler[7], U Hanning[8]
[1]UNIVERSITY MEDICAL CENTER - HAMBURG, HAMBURG, Germany, [2]University Medical Center Hamburg-Eppendorf, Hamburg, Germany, [3]University Medical Center Hamburg-Eppendorf, Hamburg, Hamburg, [4]UKE Hamburg, Hamburg, HH, [5]University Hospital Hamburg, Hamburg, HH, [6]UNIVERSITY

MEDICAL CENTER HAMBURG-EPPENDORF, HAMBURG, Germany, [7]University Medical Center Hamburg-Eppendorf, Hamburg, AK, [8]University of Hamburg-Eppendorf, Hamburg, Germany

Purpose
Coronary fat-saturated (fs) T2 Short-Tau-Inversion-Recovery (STIR) sequences are broadly used to evaluate optic nerve morphology, e.g. in patients with clinical suspicion of neuroinflammatory diseases. However, T2w fs coronal Turbo-Spin-Echo (TSE) sequences may also be used for the detection of pathological signal abnormalities of the optic nerve, but their utilization is less common. TSE sequences may provide a higher spatial resolution of the optic nerve, however in exchange for a lower spatial depiction of other brain regions at the same time. For the time being, no rater-based clinical studies exist investigating the diagnostic capabilities of coronary fat-saturated TSE sequences in comparison to the well-established STIR technique. Moreover, for conditions such as neuromyelitis optica spectrum disease (NMOSD), special characteristics and lesion patterns affecting the optic nerve exist, which may be useful for an early discrimination of NMOSD from other inflammatory processes. The aim of this study was to compare imaging findings of fs T2 STIR and TSE sequences in patients with the clinical suspicion of acute optic nerve neuritis in a rater-based clinical imaging investigation.
Materials and Methods
52 patients underwent 3T MRI examination including coronary fs STIR and TSE sequences. All patients underwent ophthalmologic examination prior to the MRI scan and were clinically in suspicion of acute optic nerve neuritis. Images were assessed by two neuroradiologists, blinded to the subjects´ identity, in random order on diagnostic workstations. The raters scored the images based on a standardized rating-sheet that was designed prior the investigation. The number and extent of optical lesions (OL), as well as their localization (retroorbital, passage of optic canal and involvement of optic chiasm) were assessed. Moreover, NMOSD-specific lesion characteristics were investigated on both sequences, namely: 1) If ≥ 50% of the length of optic nerve showed a hyperintense signal abnormality and 2) if the posterior part of the optic nerve including the optic chiasm was affected by a lesion. Furthermore, a "certainty-rating" was established and raters had to indicate, whether they were "sure", "pretty certain" or "unsure" about any of their rating and the assessability of the sequences.
Results
Higher numbers of OLs were detected on TSE (49/52) compared to STIR (43/52) sequences ($p=0.01$). OLs appeared brighter on TSE sequences ($p=0.02$). Lesions located retroorbitally ($p<0.001$), in the passage of optic canal ($p=0.03$) and optic chiasm ($p=0.01$) appeared hyperintense in more consecutive slices and thus indicated a more extensive involvement of optic nerve on TSE sequences. 11 patients were diagnosed with NMOSD during the conduct of the study. In the group of NMOSD patients, a significantly higher number of NMOSD-specific OL criteria was detected on TSE sequences (10/11) compared to STIR sequences (4/11) ($p<0.001$). Overall reader scoring certainty was higher for TSE compared to STIR sequences ($p=0.01$).
Conclusions
Coronary fat-saturated TSE sequences detected a higher number of optic nerve lesions compared to STIR sequences in patients with the suspicion of acute optic nerve neuritis. NMOSD-specific optic lesion criteria were detected in a higher number of NMOSD patients on TSE compared to STIR sequences, while overall rater certainty was also superior for the TSE sequence. We conclude that coronal TSE sequences may add valuably to the diagnostic work-up of optic nerve neuritis.

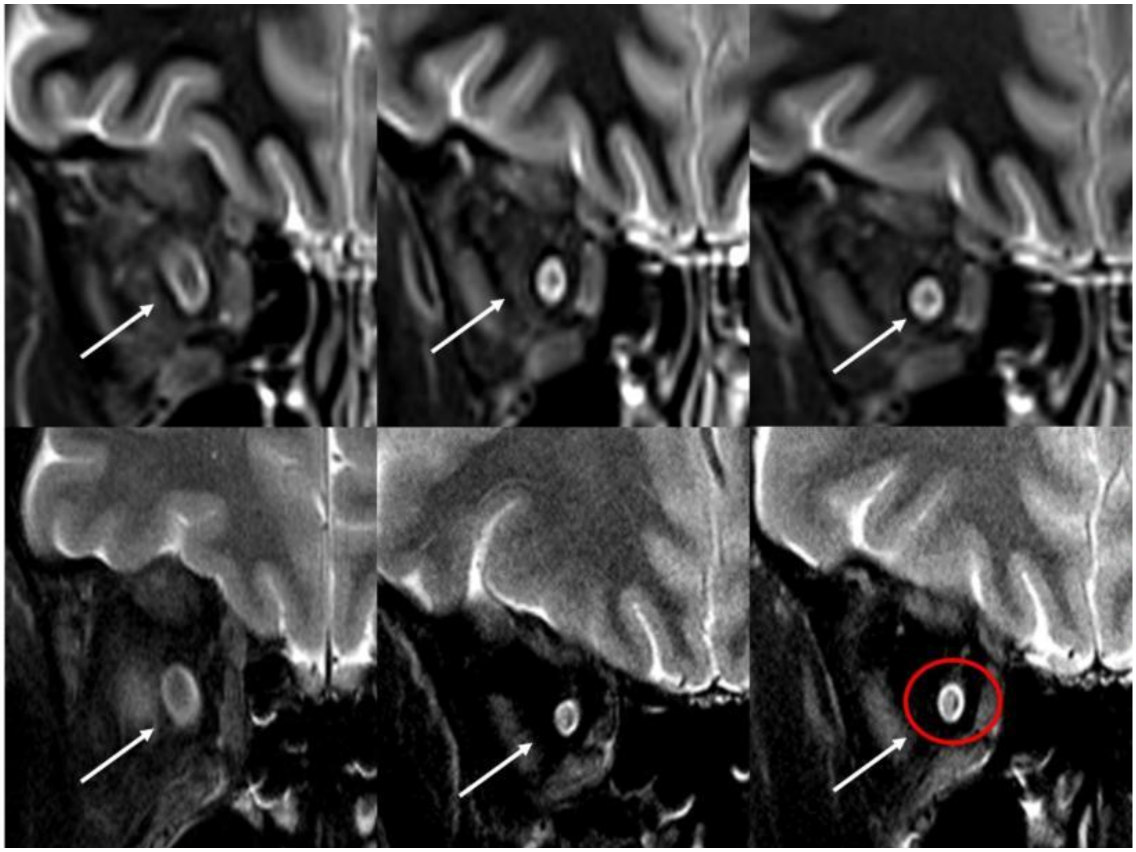

(Filename: TCT_3251_Figure1.jpg)

3373

1:49PM - 1:56PM

Correlation between Dual-Energy CT Iodine Quantification and Perfusion CT in Patients with Head and Neck Squamous Cell Carcinoma

Y Lee[1]
[1]*Korea University Ansan Hospital, Ansan-si, Gyunggi-do*

Purpose
Recently, dual-energy CT(DECT)-derived iodine quantification has been recognized as alternative for CT perfusion(CTP), which previously used to measure tumor vascular physiology and hemodynamics. So, we compared the parameters derived from both DECT and CTP taken in the patients with pathologically proven Head and Neck Squamous Cell Carcinoma(HNSCC).
Materials and Methods
Institutional review board approval and written informed consents were obtained for this single institutional study. We prospectively enrolled the patients suspicious for HNSCC who consecutively underwent 80kVP-CTP immediately followed by DECT during the recent 1 year. So, we determined to correlation between the iodine concentration(IC) derived from DECT and CTP parameters [blood volume(BV),blood flow(BF) and peak enhancement(PE)] after obtaining time-attenuation curves of the pathologically proven Head and Neck Squamous Cell carcinoma(HNSCC) by drawing the region of interests. Pearson R and linear correlation and paired t-test were used.
Results
A total of 24 patients with HNSCC diagnosed in oral cavity and oropharynx who underwent CTP and single-phase DECT using a dual-layer detector DECT scanner. On the analysis of their time-attenuation

curves, all regions of HNSCC reached the peak attenuation just immediately after ipsilateral arterial peak and sustained plateau of elevated CT attenuations. All CTP parameters (BV,BF,PE) and IC were significantly higher in regions of HNSCC as compared to their contralateral normal tissue($p<0.05$), however we did not observe the significant correlation between IC and CTP parameters ($p>0.05$).
Conclusions
To understand hemodynamic status of patients with HNSCC, a more dedicated study should be conducted for CTP- and DECT-parameters.

3454

1:56PM - 2:03PM

Detection of Bone Marrow Edema in the Head and Neck with DECT: Ready to Use?

V Timmer[1], W Henneman[1], A van Kroonenburgh[1], L Vaassen[1], E Roele[1], L Poort[1], A Jacobi-Postma[2]
[1]MUMC+, Maastricht, [2]MAASTRICHT UNIVERSITY MEDICAL CENTRE, MeHNs, MAASTRICHT

Purpose
Dual Energy CT (DECT) is one of the recent developments in CT-applications. Using DECT, calcium containing structures can be virtually subtracted from the image, creating a virtual non-calcium image (VNCa). This makes it possible to visualize bone marrow edema (BME). BME can be a sign for fractures, infections or oncologic bone invasion. DECT has already been used for BME detection in the musculoskeletal system, but it's potential in the human head and neck region has not previously been investigated. The aim of this study is to evaluate the capability of DECT to identify BME in the head and neck region in comparison to magnetic resonance imaging (MRI) as the standard of reference.
Materials and Methods
This retrospective study included 33 patients who underwent DECT and MRI of the head and neck between February 2016 and February 2018. Two radiologists visually evaluated the presence of bone marrow edema with VNCa reconstructions using color coded maps. MRI was used as the standard of reference. Furthermore, quality assessment and presence of metal artefacts were evaluated on both imaging modalities.
Results
BME was detected by DECT in 18 patients. DECT VNCa images had a sensitivity, specificity, positive predictive value and negative predictive value of 85%, 92%, 94% and 80% respectively compared to MRI. Quality assessment of DECT imaging was rated as excellent to moderate in 94% compared to 84% of the MR images, with no significant difference.
Conclusions
DECT VNCa images are able to detect bone marrow edema in the head and neck region.

2833

2:03PM - 2:10PM

Generation of Panoramic Dental Images from Non-dental CT Scans for Improved Visualization of Dental Pathology

J Stember[1], C Silva[2], M Maher[3], G Moonis[3], S Jambawalikar[3]
[1]Columbia University Medical Center - NYPH, NEW YORK, NY, [2]Columbia University Medical Center - NYPH, NY, NY, [3]Columbia University Medical Center, New York, NY

Purpose
Dental pathology can be missed by neuroradiologists while interpreting CT scans of the head, neck or facial bones / sinuses. In order to decrease false negatives, we propose incorporating reconstructed panoramic views of the teeth to accompany standard axial, coronal and sagittal images.

Materials and Methods
Multidetector CT scan volumes were downloaded from The Cancer Imaging Archive (TCIA) (www.cancerimagingarchive.net/). The panoramic images were generated using In Vivo 6 software (Anatomage Inc., San Jose, CA). Images were extracted from the CT scans using InVivo's Pano module. The Pano module allows for the focal trough to be manipulated to conform to the arch form, which allows a panoramic image to be extracted even when the patient is not orthogonally-correct. Whenever desired, the InVivo program offers a realignment module whereby the image can be rearranged into ideal orthogonal display.
Results
The reconstructed panoramic images provided a better and more readily apparent demonstration of dental pathology than the axial / sagittal / coronal image data. An example of such pathology that is well illustrated with this reconstructed view is shown in Figure 1, which displays a panoramic image of the teeth reconstructed from a neck CT. Of note is the presence of a lateral periodontal cyst on tooth # 21 (mandibular left first premolar, red arrow).
Conclusions
Panoramic images to accompany CT scans including part or all of the teeth should be considered for incorporation into the sequences of images available for radiologist review. Particularly because this consists of a single image slice, we anticipate that interpreting the panoramic image would not significantly hinder workflow. Future work will employ deep learning to automate the time-consuming process of manually delineating the arch form, which should facilitate panoramic image inclusion in standard reconstructions.

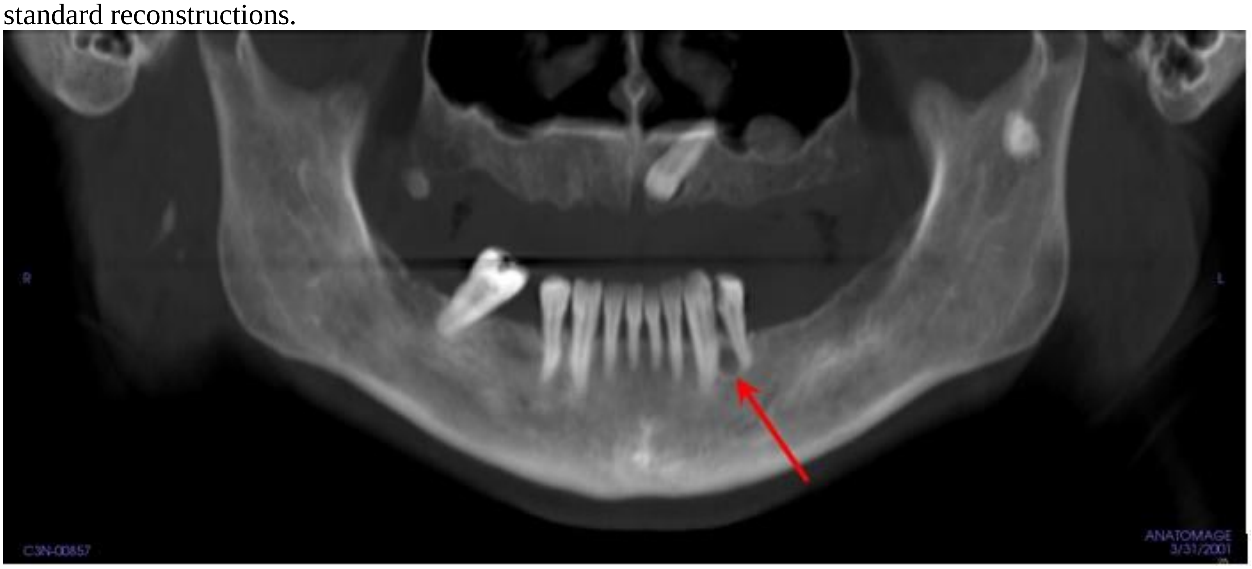

(Filename: TCT_2833_ScreenShot2018-11-06at71508AM.jpg)

2512

2:10PM - 2:17PM

The Combination of Metal Artifact Reduction Algorithms and Virtual Monoenergetic Images from Spectral-Detector CT Can Reduce Even Strongest Artifacts from Large Oral Implants

Laukamp, K.
University Hospitals Cleveland
Cleveland, OH

3443

2:10PM - 2:17PM

Virtual Non-Contrast Reconstructions Derived from DECT Cannot Replace True Native Scans in Head and Neck Imaging

A van Kroonenburgh[1], S van Kuijk[1], A Jacobi-Postma[2]
[1]MUMC+, Maastricht, [2]MUMC+, MeHNs, MAASTRICHT

Purpose
Virtual non-contrast (VNC) scans from Dual energy CT are thought to reflect True non-contrast (TNC) images and could therefore be used as a substitute to lower radiation dose. The general accepted difference in HU measurement between VNC and TNC is 15 HU points in order to accept VNC as a substitute for TNC. We investigated whether VNC reflects TNC in the head and neck region.
Materials and Methods
From November 2016 until June 2018 forty-seven patients underwent a DECT scan as part of their regular diagnostic work up for primary hyperparathyroidism with TNC, 30 s and 50 s postcontrast DECT scan of the neck. VNC images were calculated from postcontrast scans. Best fit ROIs were placed in thyroid tissue, parathyroid adenoma, lymph node, carotid artery, jugular vein, fat and sternocleidomastoid muscle. VNC densities were compared to TNC. Also difference in VNC 30sec densities and VNC 50sec densities were compared.
Results
Differences in mean density between TNC and VNC of the organs were as follows: Thyroid 54,1 HU ($p<0{,}001$); Parathyroid adenoma 20,2 HU ($p<0{,}001$); Lymph node 22,3 HU ($p<0{,}001$); Carotid artery 15,5 HU ($p<0{,}001$); Jugular vein 14,4 HU ($p<0{,}001$); Fat 61,2 HU; $p<0{,}001$); Muscle 11,8 HU ($p<0{,}001$). The HU value between 30 sec and 50 sec did not differ more than 5 HU.
Conclusions
The mean difference in density measurements exceeds far the limit of 15 HU in thyroid tissue, this reflects possibly the intrinsic iodine of the thyroid. Thus VNC cannot replace TNC in head and neck imaging.

3185

2:17PM - 2:24PM

The Incremental Value of MRI 3D-STIR-SPACE Enhanced Sequence for the Diagnosis of Mild Postganglionic Brachial Plexus Damage

Y Li[1], Y Wang[2], L Yin[1]
[1]Sichuan Provincial People's Hospital, CHENGDU, other, [2]Sichuan Provincial People's Hospital, Chengdu, China

Purpose
Mild postganglionic brachial plexus damages that generally do not require surgical intervention can be under-diagnosed with routine imaging sequences and are often diagnostic challenges. This study aims to investigate the incremental value of 3T MRI 3D-STIR-SPACE (3DSS) enhanced sequence for diagnosis of these conditions.
Materials and Methods
Thirty-eight consecutive patients in our clinical database from 2016 to 2018 (24 male, 14 female; age 18-65 years) with mild postganglionic brachial plexus lesions confirmed by electromyogram of the upper extremity, lab results and clinical follow-up were identified. These conditions included mild trauma without laceration (n=15), posterior disc protrusion (n=7), intervertebral joint disorder (n=3), herpes virus infection (n=6), compression from surrounding lesions (n=6), and diabetic peripheral neuropathy (n=1). The routine sequences included T1W, T2W, T2W with fat saturation, DWI, and enhanced T1W. Images of 3DSS sequence were reconstructed using maximum intensity projection (MIP). The diagnostic performance of routine sequences and routine plus 3DSS sequences were compared.

Results
Seventy-eight postganglionic lesions were identified, amongst which 50 lesions were accompanied with preganglionic abnormalities. Forty-three lesions involved single trunk (33 upper trunks and 10 lower trunks), and 35 lesions involved multiple trunks. According to the experienced radiologist's overall impression, 3DSS enhanced sequence depicted mild abnormalities of postganglionic brachial plexus structures with more details than the routine sequences. The sensitivity, specificity and accuracy of routine sequences compared to routine plus 3DSS sequences were 70.5% vs. 91.0%, 80% vs. 90%, 72.7% vs. 89.8%, respectively. The main positive findings on 3DSS sequence included nerve edema with thickening (51.3%), thinning (10.3%), deviation of nerve course (10.3%), and abnormal signal intensities of corresponding nerves. The gradation of abnormal nerves presented as mild hyperintensity (n=65, 83.3%, including 5 lesions with mild enhancement), isointensity (n=8, 10.3%, including 5 with mild enhancement) and mild hypointensity (n=5, 6.4%, including 1 with mild enhancement).
Conclusions
MRI 3D-STIR-SPACE (3DSS) enhanced sequence showed significant incremental diagnostic value for mild postganglionic brachial plexus damages over routine sequences with improved sensitivity. It has potential to facilitate the detection of mild postganglionic lesions in clinical practice.

(Filename: TCT_3185_Figures.jpg)

Tuesday, May 21, 2019
2:55PM - 4:25PM
Adult Brain and Head and Neck Mixed Session

2280

2:55PM - 3:02PM

A Rare Case of Central Posterior Reversible Encephalopathy Syndrome

K Sullivan[1], J Rogers[2], R Riascos[3], R Patel[3], A Kamali[4]
[1]University of Texas Houston Medical School, Houston, TX, [2]UNIVERSITY OF TEXAS HEALTH SCIENCES CENTER AT HOUSTOIN, Houston, TX, [3]The University of Texas Health Science Center at Houston, Houston, TX, [4]UT HEALTH, HOUSTON, TX

Purpose
Posterior Reversible Encephalopathy Syndrome (PRES) is characterized by reversible vasogenic edema of the brain that presents with a wide range of clinical manifestations and is diagnosed through clinical

findings and imaging. In most cases the parieto-occipital regions of cortical and subcortical white matter are involved, the pathogenesis which is not well understood. About 9 percent of the cases with diagnosis of PRES maybe hemorrhagic. Involvement of the basal ganglia, brain stem, and cerebellum are sometimes seen in conjunction with parieto-occipital regions in patients with PRES, but these central regions rarely show isolated involvement. Only a rare number of individual cases have been described to show isolated involvement of the central areas of the brain (basal ganglia, brainstem, and cerebellum) which are called Central PRES, lacking cortical and subcortical edema. A 2013 study found that only 5 of 124 patients with diagnosis of PRES studied (4%) had MRI findings consistent with Central PRES syndrome. A hemorrhagic central PRES is even a more rare scenario. We present a very rare case of hemorrhagic central PRES in a young patient.

Materials and Methods

A 36 year old Male presented to the ER after a fall from an 8 foot fence with an initial GCS of 8. The patients blood pressure was 225/147, HR 128, and SpO2 93%. Physical exam showed increased work of breathing, bowel incontinence, inability to speak, and no focal neurologic deficits. The patient was intubated to protect the airway. History was limited due to patient's mental status and lack of family at bedside. Neurologic exam at the time of MRI showed a GCS of 3. Patient was started on IV Nicardipine infusion for blood pressure control. At this time the differential diagnosis included a brain tumor, metabolic derangements, inflammatory conditions, autoimmune disorder, or a demyelinating process, ruling out a stroke. Two days post admission patient recovered consciousness and was able to provide some historical information, including a long history of hypertension with medication noncompliance and myocardial infarction in 2017. Four days after admission LP results showed a CSF protein of 62, IGG 5.9, albumin 40.8, prompting treatment with IV methylprednisolone. Patient was seen by ophthalmology and revealed past issues with right eye, reporting seeing shadows and current worsening vision with new onset finger to nose ataxia. Ophthalmology diagnosed hypertensive retinopathy of both eyes with mild non-proliferative diabetic retinopathy in both eyes. Persistently elevated blood pressure prompted changing hypertensive medications to Clonidine 0.1 mg BID, Labetalol 300 mg PO Q8.

Results

Initial imaging with AP CXR showed CHF with possible underlying pneumonia. Brain CT w/o contrast showed no evidence of acute hemorrhage. Hypodensity concerning for acute ischemia along the left thalamus, midbrain, and pons, along with a 7mm hypodensity in the corona radiata. CT Head and Neck held due to initial concerns for renal failure. Tomography revealed bilateral aspiration of vomitus in the lower lung fields. MRI w/o contrast of the brain revealed onfluent signal abnormality with increased FLAIR/T2 signal in pons, midbrain, and the left thalamus with scattered areas of microhemorrhages, localized mass effect and edema. Initial analysis was concerning for a primary glial neoplasm with a second area of abnormality in the anterior temporal lobe concerning for a second glioma. Given the presence of microhemorrhages, a low grade glioma deemed less likely. No increased perfusion (hypervascularity) was identified, on the perfusion scan to represent a high grade tumor. Given the absence of diffusion restriction, lymphoma is unlikely.

Conclusions

Repeat Brain MRI taken after a week post admission revealed significantly decreased T2 and FLAIR hyperintense signal in the rhombencephalon and mesencephalon with marked signal improvement, leading to the diagnosis of central PRES given response after adequate blood pressure treatment on intensive regimen.

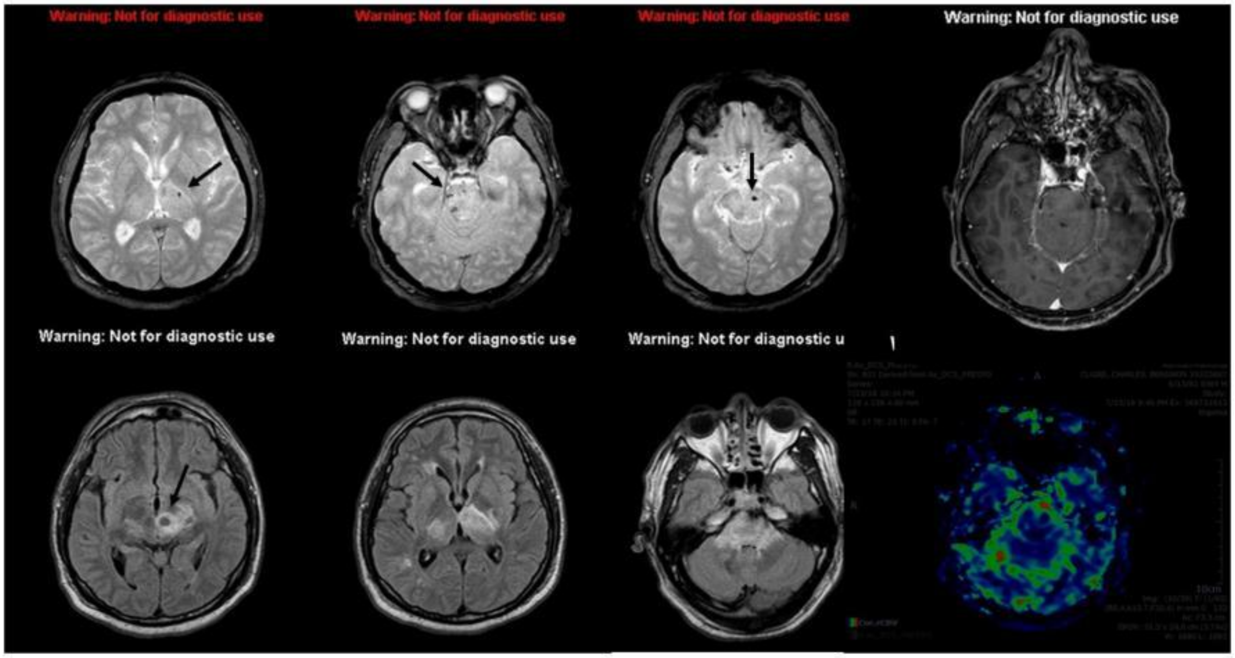

(Filename: TCT_2280_Images.jpg)

3417

3:02PM - 3:09PM

CT Angiography (CTA) for Evaluation of Acute Stroke in Elderly (Patients >80 Years)

A Malhotra[1], M Lee[2], X Wu[3], K Seifert[4], L Tu[5]
[1]YALE UNIVERSITY SCHOOL OF MEDICINE, NEW CANAAN, CT, [2]Yale University - School of Medicine, Norwalk, CT, [3]Yale University School of Medicine, New Haven, CT, [4]YALE NEW HAVEN HOSPITAL, NEW HAVEN, CT, [5]Yale School Of Medicine, New Haven, CT

Purpose
Strokes in patients aged ≥ 80 years are common and advanced age is associated with relatively poor post-stroke functional outcome. Several recent trials have demonstrated efficacy of endovascular thrombectomy (EVT) to improve outcomes in acute stroke patients with large-vessel occlusion (LVO). This has resulted in increasing use of CTA in Emergency Department (ED) to assess LVO in patients with suspected acute stroke. The purpose of this study is to assess the utilization of CTA in acute stroke for elderly patients above age 80 years from ED, its trend over time, and correlation with outcomes.
Materials and Methods
After IRB approval, a retrospective search was performed through PACS database for CTAs performed from the Emergency Department for acute stroke evaluation from 1/1/2012 through 10/31/2018. The temporal trends of CTA use were recorded. The percentage of patients undergoing intravenous thrombolysis and/ or subsequent endovascular thrombectomy were also noted.
Results
A total of 2572 CTAs were performed in 2005 patients over this time period.1814 of these studies were performed in 80-89-year age group and 736 in the 90-99 age groups. A significant increase in the number of CTAs performed was noted over time (Figure) The volume of CTAs performed per month in this age-group has doubled from 2015 to 2018. However, a very small percentage of these patients underwent systemic thrombolysis or thrombectomy.

Conclusions
The use of CTA for acute stroke evaluation through the ED in elderly patients (>80 years) has increased significantly over time. However, its utility and effectiveness needs further evaluation in terms of low percentage of these patients being candidates for mechanical thrombectomy.

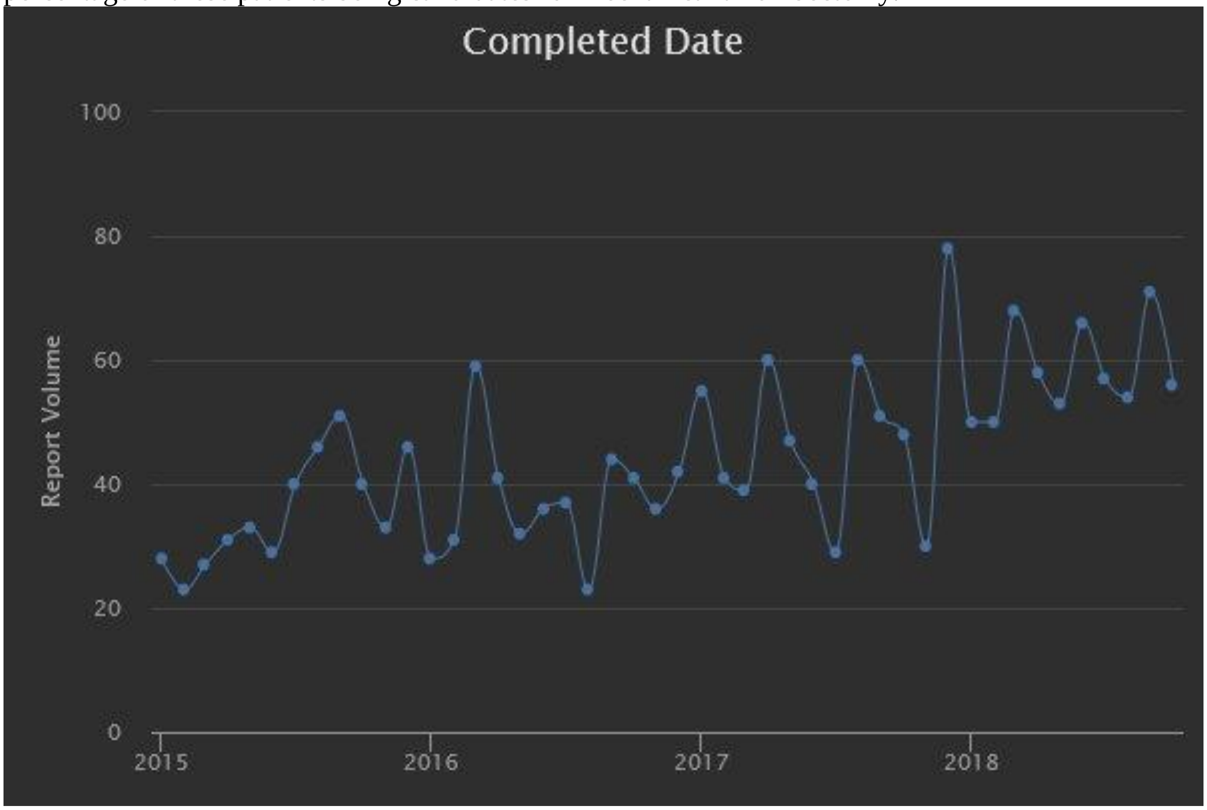

(Filename: TCT_3417_chart.jpg)

3399

3:09PM - 3:16PM

Hearing Aid Use Preserves Left Superior Temporal Gyrus Volume

H Bagce[1], G Moonis[1], A Lalwani[1]
[1]*Columbia University Medical Center, New York, NY*

Purpose
Correlation of age-related hearing loss with cerebral atrophy is well-established (Qian et al 2017). The purpose of the current study is to elucidate the functional benefit and anatomic changes following hearing aid (HA) placement.
Materials and Methods
Retrospective search yielded 70 patients who presented with a history of age-related hearing loss. Pure-tone air conduction thresholds in both high (HFPTA) and low (LFPTA) frequency domains were calculated in both ears and averaged. Sagittal T1 MRI data for each patient was obtained; following manual slice selection at the level of the lateral temporal lobe, the minimum width of the right ('rSTG') and left ('lSTG') superior temporal gyrus was automatically calculated utilizing custom-designed MATLAB edge-detection algorithms. Of the 70 patients, 24 had HA at the time of audiometry evaluation. Of these 24 patients, 10 ('PreHA') had the MRI performed prior to placement of the HA, while 14 ('PostHA') had imaging performed after HA placement. 46 patients did not have hearing aids ('NoHA').

Clinical and radiological data were analyzed and compared between subsets utilizing standard two-tailed independent-sample t-tests.

Results

On audiometry analysis, there was a significant difference in LFPTA between PreHA-vs-NoHA (t=2.62,p=0.011) and PostHA-vs-NoHA (t=2.34,p=0.023) [Mean±SE: NoHA=45.9±1.9 Hz; PreHA=58.2±5.2; PostHA=54.8±3.1]. There was a significant difference in HFPTA for PreHA-vs-NoHA (t=3.17,p=0.003) but only a trend towards significance for PostHA-vs-NoHA (t=1.82,p=0.07) [NoHA=59.4±2.5 Hz; PreHA=77.4±4.4; PostHA=68.1±3.0]. On MRI analysis, there was a significant difference in lSTG width for PreHA-vs-NoHA (t=-3.28,p=0.002) but not for PostHA-vs-NoHA (t=0.95,p=0.35) [LEFT STG: NoHA=5.2±0.1 mm; PreHA=4.2±0.3; PostHA=5.4±0.2]. There was no significant difference in rSTG width for either PreHA-vs-NoHA (t=1.64,p=0.11) or PostHA-vs-NoHA (t=-0.31,p=0.75) [RIGHT STG: NoHA=5.1±0.2 mm; PreHA=5.3±0.4; PostHA=5.2±0.4].

Conclusions

Findings suggest that earlier placement of HA may be protective against left-sided superior temporal gyrus volume loss, which may manifest clinically as preservation of high-frequency tone detection. Findings support prior functional literature demonstrating high-frequency lateralization of human auditory processing to left superior temporal gyrus (STG) activation (Devlin et al 2003, Eckert et al 2012).

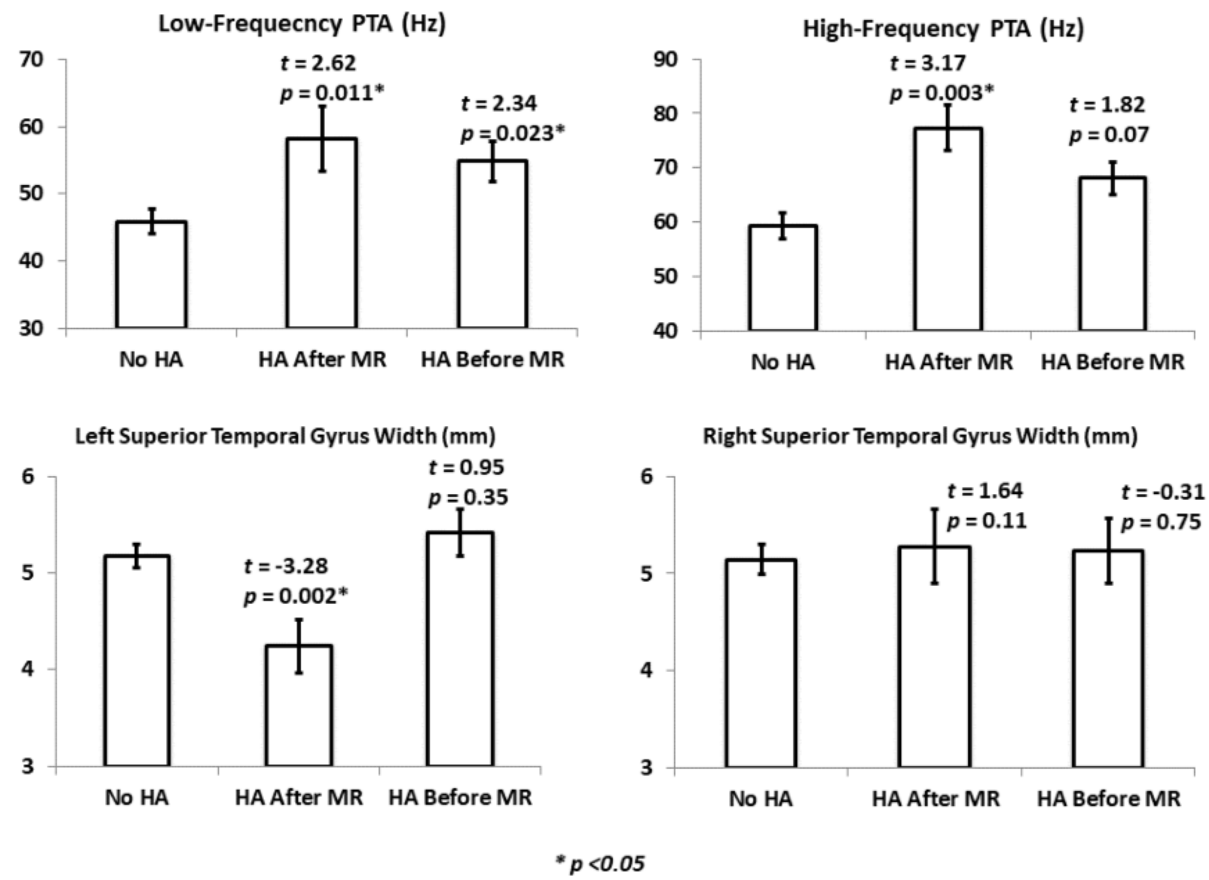

(Filename: TCT_3399_ASNR2019abstractfigv2.gif)

3445

3:16PM - 3:23PM

Intracranial Subarachnoid Fat Arising From An Occult Pelvic Fracture

T Retson[1], P Manning[2], M McDonald[3], J Handwerker[4], N Farid[5]
[1]UC SAN DIEGO RADIOLOGY, SAN DIEGO, CA, [2]UCSD - UNIVERSITY OF CALIFORNIA SAN DIEGO, SAN DIEGO, CA, [3]University of California at San Diego, San Diego, CA, [4]University of California, San Diego, San Diego, CA, [5]UC San Diego Med. Ctr., San Diego, CA

Purpose
Fat in the subarachnoid space has been described due to rupture of an intracranial or spinal dermoid (1,2). However, a less well known cause for fat in the subarachnoid space is pelvic trauma (3). We describe a case of fat in the subarachnoid space due to a previously unrecognized sacral fracture.
Materials and Methods
An 86 year old woman with mild dementia presented to the emergency department after a fall at her nursing facility with questionable loss of consciousness. She reported low back tenderness, hand and wrist pain. Initial trauma workup was negative; however, she tested positive for a UTI and was admitted for antibiotics. On day 2 of admission she reported new onset blurriness in her left eye, prompting additional imaging.
Results
Trauma plain films of the pelvis, hand and wrist were negative at the time of admission. Initial CT scan of the cervical spine, chest, and head showed no acute findings. Repeat head CT at the time of vision changes demonstrated several new foci of fat density in the subarachnoid space (Image A and B, arrowheads). As there was no etiology for these findings within the head or imaged spine, a pelvic CT was recommended which demonstrated a displaced sacral fracture with extension into the sacral ala (Image C, arrow), the likely source of subarachnoid fat.
Conclusions
Here we present a case of fat in the subarachnoid space, an unusual phenomenon in the absence of a ruptured dermoid. When this finding is seen in a trauma patient, pelvic trauma should be considered as a potential cause.

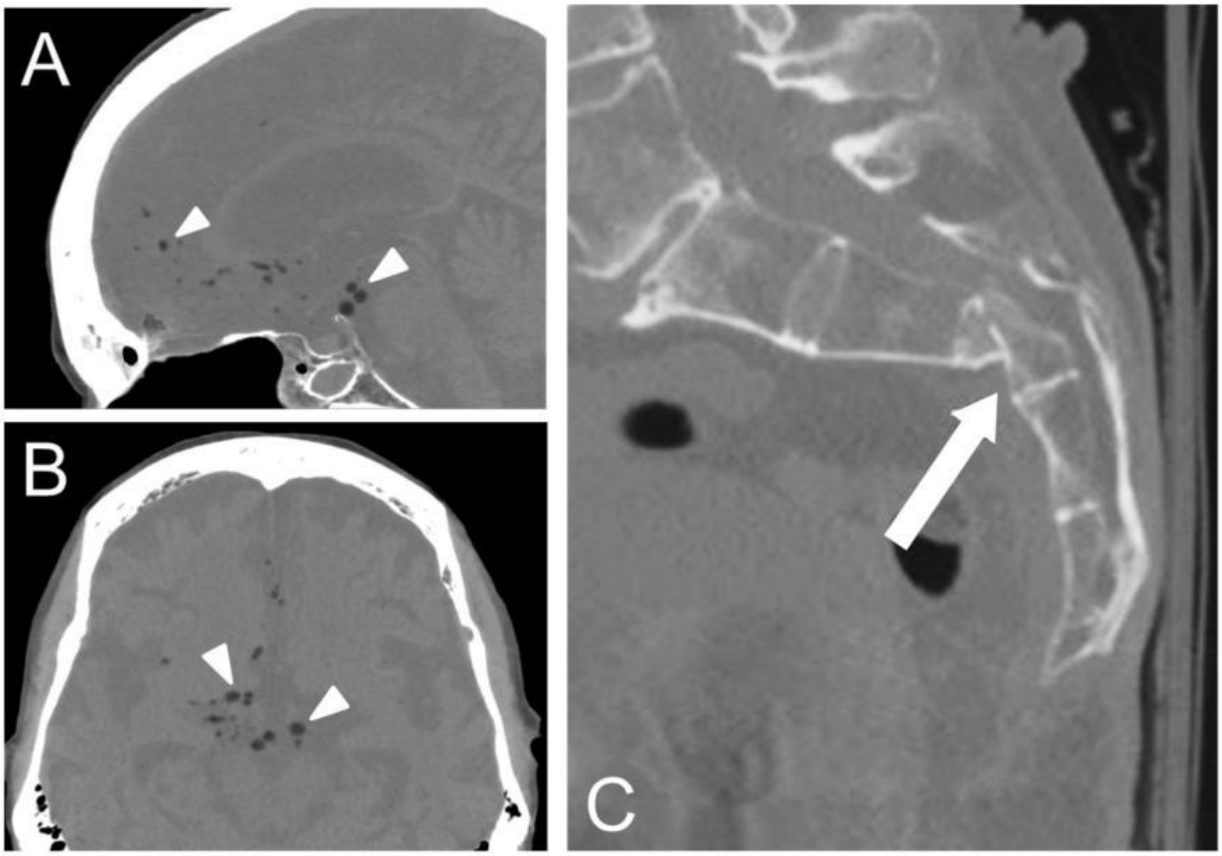

(Filename: TCT_3445_ASNR2019FigureJPG.jpg)

3105

3:23PM - 3:30PM

Mass Casualty and Human Trafficking: Raising Radiologists Concerns for Heatstroke

S Emamzadehfard[1], V Eslami[1], Z Fulton[2], K Clark[1], J Kim[3]
[1]University of Texas Health Science Center, San Antonio, TX, [2]University of Texas Health Science Center San Antonio, San Antonio, TX, [3]San Antonio Military Medical Center, San Antonio, TX

Purpose
Heat stroke is a critical illness characterized by hyperthermia with failure of the thermoregulatory mechanism. The immediate complications of severe heat stroke include shock, ARDS, electrolyte disturbances, DIC, and rhabdomyolysis. The central nervous system is particularly sensitive to heat injury. If homeostatic compensatory mechanisms are overwhelmed, several neurologic complications can occur: cerebral edema, increased intracranial pressure, decreased cerebral blood flow, and hemorrhage.
Materials and Methods
The University of Texas at San Antonio is a Level 1 tertiary referral center with a referral base that includes south Texas and portions of Northern Mexico. In July of 2017, a tractor-trailer smuggled 100 people from Mexico into the United States. Due to high ambient temperatures, failure of the truck's refrigeration component, and lack of access to water, those trapped inside were exposed to a homogeneous hostile environment. We conducted a retrospective analysis of the victims involved with the specific interest in the neurologic effects of heat exposure. Eight people were found dead at the scene. Approximately 24 were taken to area hospitals, 10 patients were referred to our hospital.

Results
Age ranges of the patients were 19-43. Of the 10 patients referred to our hospital, 5 obtained neurologic imaging. Glasgow coma scales ranged from 3-15. Of those 5 patients, all 5 had normal initial head CTs. Two patients underwent MR imaging. One patient had positive MR findings with a predilection to the basal ganglia. All 5 patients survived.
Conclusions
We present data from 100 people exposed to a uniform toxic heat insult in order to underscore the variability of this disease process and to identify areas where radiologists can offer value. Patients suffering from heat stroke may present clinically unresponsive with normal initial imaging. Positive findings may be delayed in onset and require advanced neurologic imaging (e.g. MR+DTI+MRS) to identify. Awareness of the heterogeneous clinical presentation and imaging findings related to this type of trauma can allow radiologists to more readily identify compromised patients.

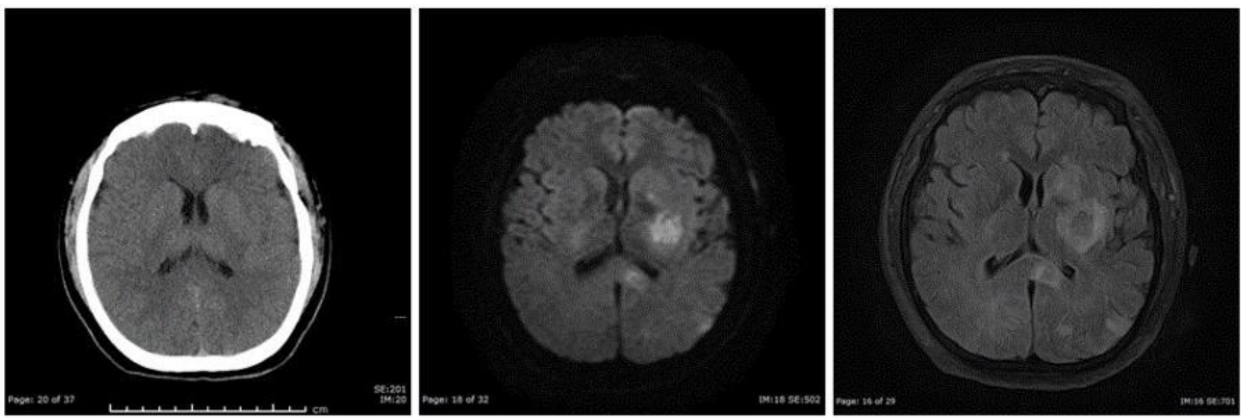

(Filename: TCT_3105_figureheatstroke.jpg)

2433

3:30PM - 3:37PM

Optimizing CT Angiography of the Neck: Does the Side of Injection Influence Vascular Opacification?

C Freeman[1], K Davtyan[2], A Mamourian[2]
[1]*HOSPITAL OF THE UNIVERSITY OF PENNSYLVANIA, PHILADELPHIA, PA,* [2]*University of Pennsylvania, Philadelphia, PA*

Purpose
To determine if injection side affects the opacification of the common carotid arteries on computed tomography angiography (CTA) of the neck.
Materials and Methods
200 adult patients, 100 injected in the right upper extremity and 100 injected in the left upper extremity, who underwent a CTA of the neck at the University of Pennsylvania Health System between the years of 2015 and mid-2018 were retrospectively, randomly selected. The studies were reviewed in PACS, and using a region of interest tool placed in the center of the vessel, the attenuation of the patient's left and right distal common carotid arteries, approximately 1 cm inferior to the carotid bifurcation, were recorded. Side of injection was determined by the appearance of the subclavian vein and patients with central line injections were excluded. Using these measurements, a mean vascular attenuation value for each patient was calculated. The effects of patient age, sex, and injection side were determined using ANOVA and ANCOVA.
Results
Injection side and patient sex had significant effects on opacification of the common carotid arteries.

Right-sided injections produced approximately 8% greater opacification, and female patients demonstrated 23.1% greater vascular opacification than males. There was a poor correlation between the post-contrast attenuation of the common carotid arteries and patient age.
Conclusions
Right-sided injections are associated with greater common carotid opacification on CTA of the neck and should be the preferred side of venous access for these studies. This seems likely to reflect anatomic differences between the left and right venous pathways rather than the effect of retrosternal narrowing from atherosclerotic aortic dolichoectasia based on the poor correlation of carotid opacification with patient age.

3165

3:37PM - 3:44PM

Risk of Thyroid Cancer in Lung Cancer Risk Patients According to the Presence of Incidental Thyroid Nodules Detected on Screening Low Dose Chest CT: A Retrospective Study

J Kim[1]
[1]Seoul National University Hospital, Seoul, Seoul

Purpose
To evaluate risk of thyroid cancer in lung cancer risk patients according to the presence of incidental thyroid nodules (ITN) detected on screening Low Dose Chest CT (LDCT)
Materials and Methods
2375 consecutive subjects with high risk of lung cancer (current or former smoker with cessation within 15 years, > 30 pack-year and, $55 \leq$ age < 75) underwent both screening LDCT and thyroid ultrasonography (US) from January 2004 to May 2013. Incidence of ITN on LDCT in whole population, incidence of US and risk of thyroid cancer in whole population and comparison were evaluated according to the presence of ITN on LDCT.
Results
The incidence of ITNs on LDCT was 4.8% (115/2375). The incidence of ITN on US, incidence of thyroid nodule indicative for FNA, incidence that FNA or CNB performed, risk of thyroid nodules cytohistopathologically reported as being indicative for surgery, and incidence of surgically proven thyroid cancer were 51.1% (1048/2050), 4.8% (99/2050), 5.3% (109/2050), 0.9% (19/2050) and 0.5% (11/2050), respectively. The aforementioned incidences in LDCT -ITN positive group [99/115, 50/115, 48/115, 7/115, 3/115] were significantly higher than those in the patients in LDCT-ITN negative group [949/2260, 49/2260, 61/2260, 12/2260, 8/2260] of ($P < 0.05$). Thyroid surgery was performed at 11 patients in whole group, 3 patients in ITN + group and 8 patients in ITN – group. All of them are papillary thyroid microcarcinomas with very low pathologic stage (T1aN1a).
Conclusions
In the subjects with high risk of lung cancer, the incidence of thyroid nodule on US was high up to 50% and the risk of thyroid cancer was higher in group with ITN on CT than the group without ITN. However, irrespective of the presence of ITN, the incidence of thyroid cancer was low and the proven cancers were staged as being low.

Table 2. Thyroid US charateristics of NLST population

Subjects	USG 2050	CT ITN + 105	CT ITN - 1945	P value
US nodule	1048 (51.1%)	99 (94.2%)	949(48.8%)	<0.01
US nodule size (mm)	6.40±5.17	14.72±8.73	5.53±3.69	<0.01
FNA/CNB	109	48	61	0
KSTHR guideline				<0.01
1 Spongiform >2cm	0	0	0	
2 Low suspicion> 1.5cm	36	23	13	
3 Intermediate suspicion>1cm	56	26	30	
4 High suspicion > 1cm	7	1	6	
ATA guideline				<0.01
1 Very low suspicion > 2cm	3	3	0	
2 Low suspicion > 1.5cm	45	25	20	
3 Intermediate suspicion >1cm	32	14	18	
4 High suspicion >1cm	10	1	9	
FNA B4/5/6	19	7	12	0.014
Surgery	11	3	8	0.016

*NLST: National Lung Cancer Trial, *ITN: Incidental Thyroid Nodule
(Filename: TCT_3165_2.JPG)

2335

3:44PM - 3:51PM

SMART Syndrome: A Rare Complication of CNS Radiation Therapy

A Foust[1], J Fritz[2], E Bourekas[3], C Fetko[4]
[1]The Ohio State University Wexner Medical, Columbus, OH, [2]Wexner Medical Center at The Ohio State University, Columbus, OH, [3]THE OHIO STATE UNIVERSITY, COLUMBUS, OH, [4]The Ohio State University Wexner Medical Center, Columbus, OH

Purpose
To demonstrate the imaging features of stroke-like migraine attacks after radiation therapy (SMART).
Materials and Methods
The patient is a 40 year old male who was transferred to our institution due to concern for possible stroke. The patient reported symptoms of migratory headaches, blurred vision, difficulty with word finding and slowed speech intermittently over the prior week. The patient had a past medical history of a seizure disorder, an AVM (surgically treated in 1980s), and a posterior fossa astrocytoma which was managed with surgical resection, chemotherapy, and radiation therapy when the patient was 5 years old. At the time of presentation, neurologic exam was positive for a partial gaze palsy, partial hemianopsia, mild aphasia, and mild dysarthria resulting in an NIH stroke scale score of 4. EEG during his hospitalization demonstrated left hemisphere slowing, however no epileptiform discharges. The patient was managed medically and reported improvement in his symptoms over the next few weeks.

Results
MRI of the brain with contrast demonstrated expected post-surgical changes of prior suboccipital craniotomy and surgical resection within the cerebellum, consistent with reported resected posterior fossa astrocytoma. New abnormal FLAIR signal abnormality and dot-like gyriform cortical enhancement was identified within the left occipital parenchyma adjacent to the surgical cavity. On DWI, there are several punctate foci of restricted diffusion within the same region of the left occipital lobe.
Conclusions
SMART syndrome is a rare delayed complication of CNS radiation therapy which should be considered in the differential diagnosis of patients with history of CSN neoplasm presenting with stroke like symptoms.

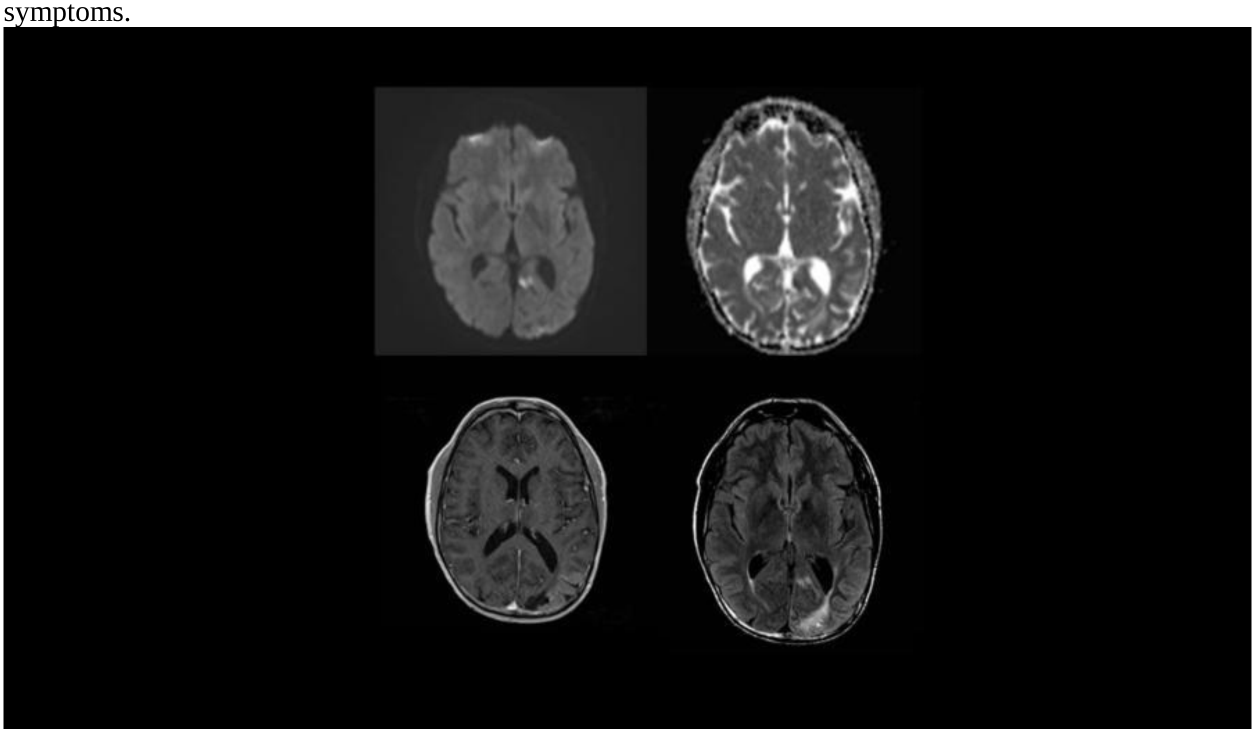

(Filename: TCT_2335_SMARTcomposite-300DPI.jpg)

2678

3:51PM - 3:58PM

Sporadic Creutzfeld-Jacob Disease: An Unusual Presentation of a Rare but Increasingly Prevalent Entity

S Montoya[1], A Bhatt[2], H Wang[1], J Almast[3]
[1]University of Rochester Medical Center, Rochester, NY, [2]Mayo Clinic, Jacksonville, FL, [3]Univeristy of Rochester, Rochester, NY

Purpose
Sporadic Creutzfeldt-Jacob disease (sCJD) is the most common human spongiform encephalopathy, and seems to be on the rise. The estimated incidence is 1 case per 1 million people, however diagnosed cases have been on the rise nationally. The radiologist may help in detection by recognizing the spectrum of imaging abnormalities, if given the appropriate clinical context. Here we present a case of confirmed sCJD with an unusually rapid time course and atypical imaging findings involving the bilateral heads of the caudate nuclei, contrasted with a more typical case of sCJD, in order to emphasize the possible variations in presentation.

Materials and Methods

Case 1: A previously healthy 52-year-old woman was admitted for work-up of dizziness after several ED visits within a month for the same complaint. She was noted to be neurologically normal upon admission, but developed altered mental status which worsened during her hospital course. A brain MRI obtained for encephalopathy was initially reported as normal, but rapid decline from independent to nonverbal and bed-bound over 3 weeks prompted transfer to our institution for more exhaustive work-up. CSF was found to have elevated 14-3-3, and re-review of imaging noted subtle caudate signal abnormalities. Case 2 (companion): A previously healthy 60-year-old woman presents with gait disturbance and cognitive decline over several months, leading to fall with resulting mandibular fracture and subsequent superimposed infection requiring hospitalization. A brain MRI was obtained to evaluate delirium and revealed classic imaging findings for sCJD; this was confirmed with elevated 14-3-3 in CSF.

Results

Case 1: DWI (a) and T2 FLAIR (b) images reveal subtle diffusion restriction and corresponding edema of the caudate heads bilaterally (arrows). This was missed on initial report and only detected upon transfer to our institution. Involvement of the basal ganglia is not unusual for sCJD, however isolated caudate involvement with sparing of the lentiform nuclei is highly uncommon. Case 2 (companion): DWI (c) and T2 FLAIR (d) images reveal a cortical pattern of diffusion restriction with corresponding edema, with sparing of the perirolandic region (oval). This is the most common imaging pattern for sCJD.

Conclusions

Both of these cases - one atypical and one classic - presented to our institution this year and represent only a portion of the cohort of patients at our institution found to have sCJD. We propose that the apparent rising incidence of sCJD is attributed to the growing aging population and increased premortem detection by imaging and laboratory testing. sCJD should not be thought of as a "zebra" but instead should be included in the differential diagnosis for those who present with progressive cognitive decline. By keeping in mind the various imaging findings in sCJD, radiologists may be able to aid in earlier diagnosis of this entity. Future investigation involves exploration of post-processing imaging correction to aid in detection of subtle findings.

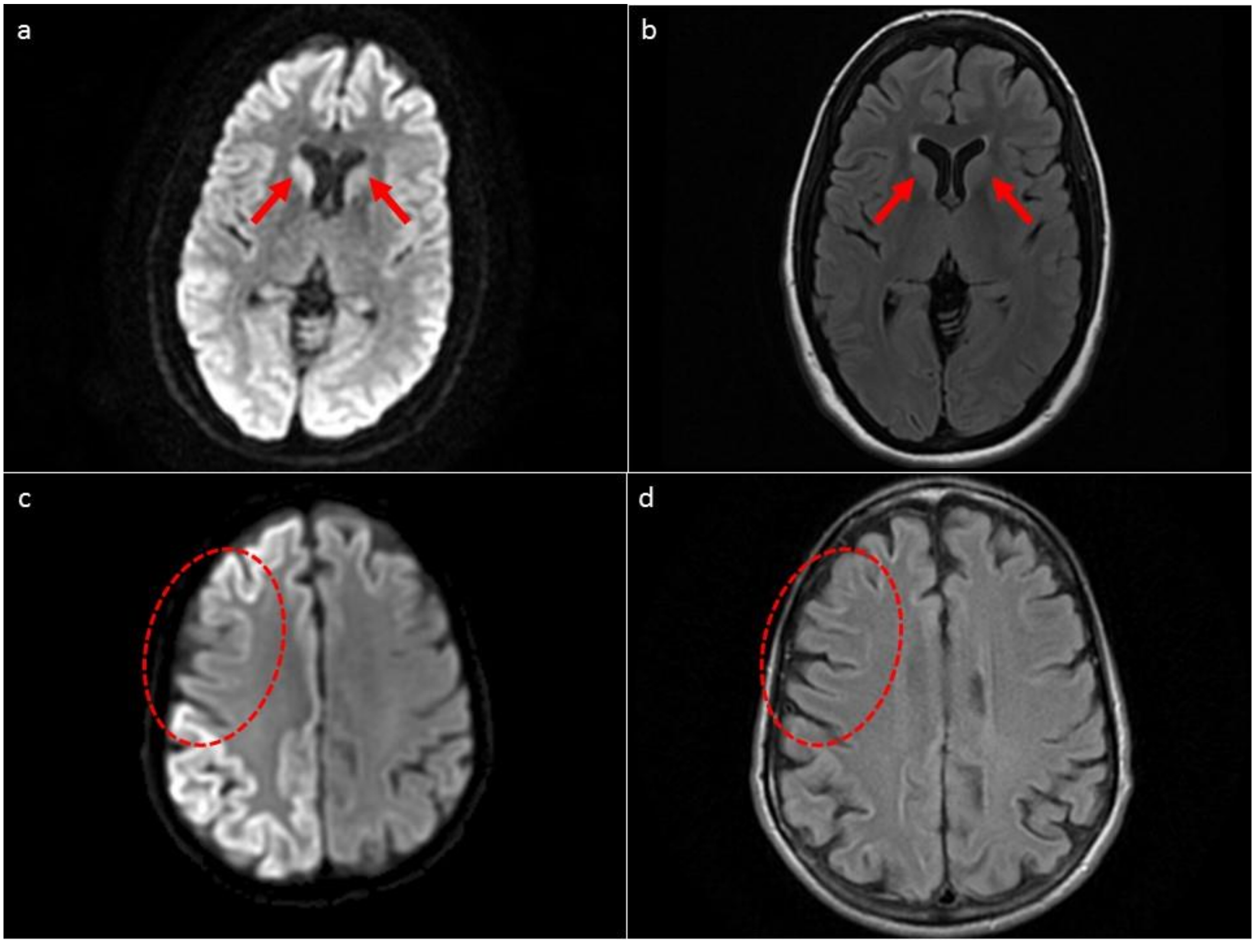

(Filename: TCT_2678_ASNR19_CJD300.jpg)

2867

3:58PM - 4:05PM

Systemic and Craniospinal Rosai-Dorfman Disease with Intraparenchymal, Intramedullary and Leptomeningeal Disease

Y Li[1], A Bollen[1], D Solomon[1], S Cha[1]
[1]*University of California San Francisco, San Francisco, CA*

Purpose
To present the clinical features, imaging findings and pathology results of a rare case of systemic and craniospinal Rosai-Dorfman Disease with intraparenchymal, intramedullary and leptomeningeal involvement.
Materials and Methods
A 26-year-old female patient presented initially to an outside institution with a 2 years of systemic complaints including fatigue, joint aches, nausea/vomiting, polyuria, and extreme thirst. An urgent MR brain was obtained after an ophthalmologist noted a left visual field deficit. MRI brain with contrast at the outside institution demonstrated a solidly enhancing hypothalamic mass, which was biopsied, with a pathologic diagnosis of "astrocytic neoplasm," which could not be further characterized. The patient then presented to our institution for further evaluation. Repeat MRI brain demonstrated a large, homogeneously-enhancing hypothalamic mass with mass effect on the optic chiasm. Additionally, leptomeningeal dissemination was noted, with multiple, scattered, small enhancing leptomeningeal

masses. Repeat biopsy at our institution demonstrated Rosai-Dorfman disease, with molecular sub-typing demonstrating BRAF positivity. Further evaluation after histologic diagnosis revealed disseminated intramedullary and leptomeningeal disease in the spine, as well as hypermetabolic lymphadenopathy throughout the neck, mediastinum and retroperitoneum.

Results

Initial MRI brain demonstrated a large, homogeneously-enhancing hypothalamic mass without reduced diffusion, with mass effect on the optic chiasm. Additionally, leptomeningeal dissemination was noted with multiple, scattered, small, enhancing leptomeningeal masses throughout the supratentorial brain. Subsequent imaging after diagnosis revealed small enhancing intramedullary and leptomeningeal masses throughout the spine. These lesions were hypermetabolic. Additionally, PET/CT demonstrated hypermetabolic lymphadenopathy throughout the neck, mediastinum and retroperitoneum.

Conclusions

We present a rare case of systemic and craniospinal Rosai-Dorfman disease with intraparenchymal, intramedullary and leptomeningeal involvement. Of particular interest, there was no sinus or dural-based involvement, making preoperative diagnosis challenging. Additionally, we present histopathology and molecular sub-typing of this lesion, with radiologic-pathologic correlation. There is one previously published case reports of hypothalamic Rosai-Dorfman disease with similar imaging characteristics. (1) A few case reports of craniospinal disseminated Rosai-Dorfman and intramedullary Rosai-Dorfman disease also exist in the literature. (2–4)

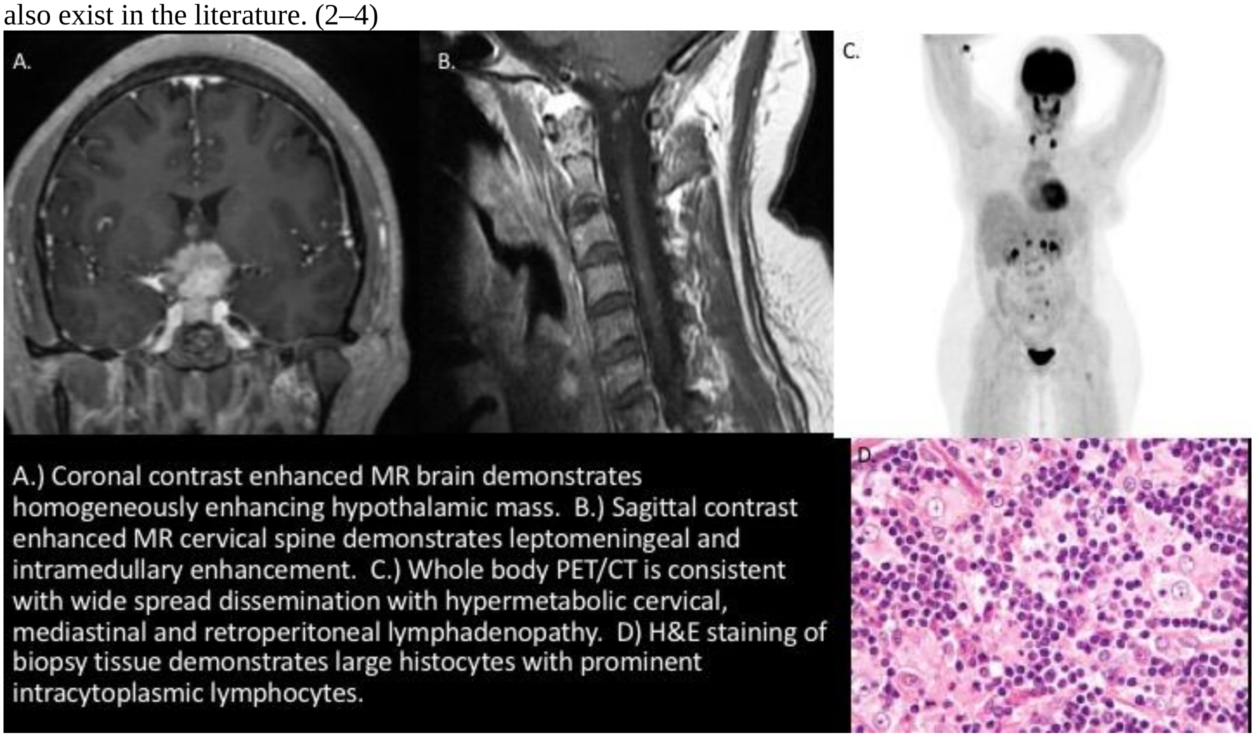

A.) Coronal contrast enhanced MR brain demonstrates homogeneously enhancing hypothalamic mass. B.) Sagittal contrast enhanced MR cervical spine demonstrates leptomeningeal and intramedullary enhancement. C.) Whole body PET/CT is consistent with wide spread dissemination with hypermetabolic cervical, mediastinal and retroperitoneal lymphadenopathy. D) H&E staining of biopsy tissue demonstrates large histocytes with prominent intracytoplasmic lymphocytes.

(Filename: TCT_2867_RDDexcerpta.jpg)

3017

4:05PM - 4:12PM

Temporal Progression of Imaging Findings in a Case of Pathology-Proven Adult Rabies Encephalitis

V Babatunde[1], M Nasrallah[2], E Lee[3], S Prokop[2], R Kurtz[4]
[1]Univeristy of Pennsylvania, Philadelphia, PA, [2]Hospital of the University of Pennsylvania, Philadelphia, PA, [3]University of Pennsylvania, Philadelaphia, PA, [4]University of Pennsylvania, Berwyn, PA

Purpose

Data regarding progression of imaging findings of rabies encephalitis is sparse due to typical history of animal bite followed by fulminant disease and no effective therapy. This presentation will focus on the progression of imaging findings in a case of rabies encephalitis and clues that may help to distinguish rabies from other encephalitides.

Materials and Methods

A 69-year-old woman presented with progressive decline in neurologic function, emesis, diarrhea, and fever. Her clinical course deteriorated; eventually becoming comatose with loss of brain stem reflexes. Serum and cerebrospinal fluid samples were later found to have rising titers of anti-rabies IgG, consistent with rabies encephalitis. The patient had a fulminant encephalitic course resulting in death.

Results

MRI of the brain at presentation was normal. At hospitalization day 10 (image A), there was bilateral symmetric T2 prolongation in the hippocampi (image A). On day 30 (images B and C), there was bilateral symmetric T2 prolongation in the insula, basal ganglia, medial thalami, periaqueductal grey matter, and midbrain. Also involved were the cingulate gyri, dorsal pons, medulla and cervical cord (not shown). Autopsy (image D) showed few viable neurons in the brain stem, cerebellum, cortex and hippocampal formation with eosinophilic cytoplasmic inclusions, Negri bodies and lyssa bodies (arrows). Throughout the brain, severe loss of neurons with reactive gliosis, lymphocytic inflammation, accumulation of macrophages, and infarction were noted.

Conclusions

Human rabies, caused by Lyssavirus infection, is considered one of the most feared communicable diseases as it is virtually fatal. Rabies is a zoonotic infection transmitted to humans primarily through the bite of an infected animal. MRI may be used as a tool for diagnosis of rabies encephalitis, particularly when there is no known exposure. The predilection of rabies for the brainstem, thalami and medial temporal lobes/hippocampi coupled with the absence of hemorrhage should raise suspicion for this rare but fatal infection.

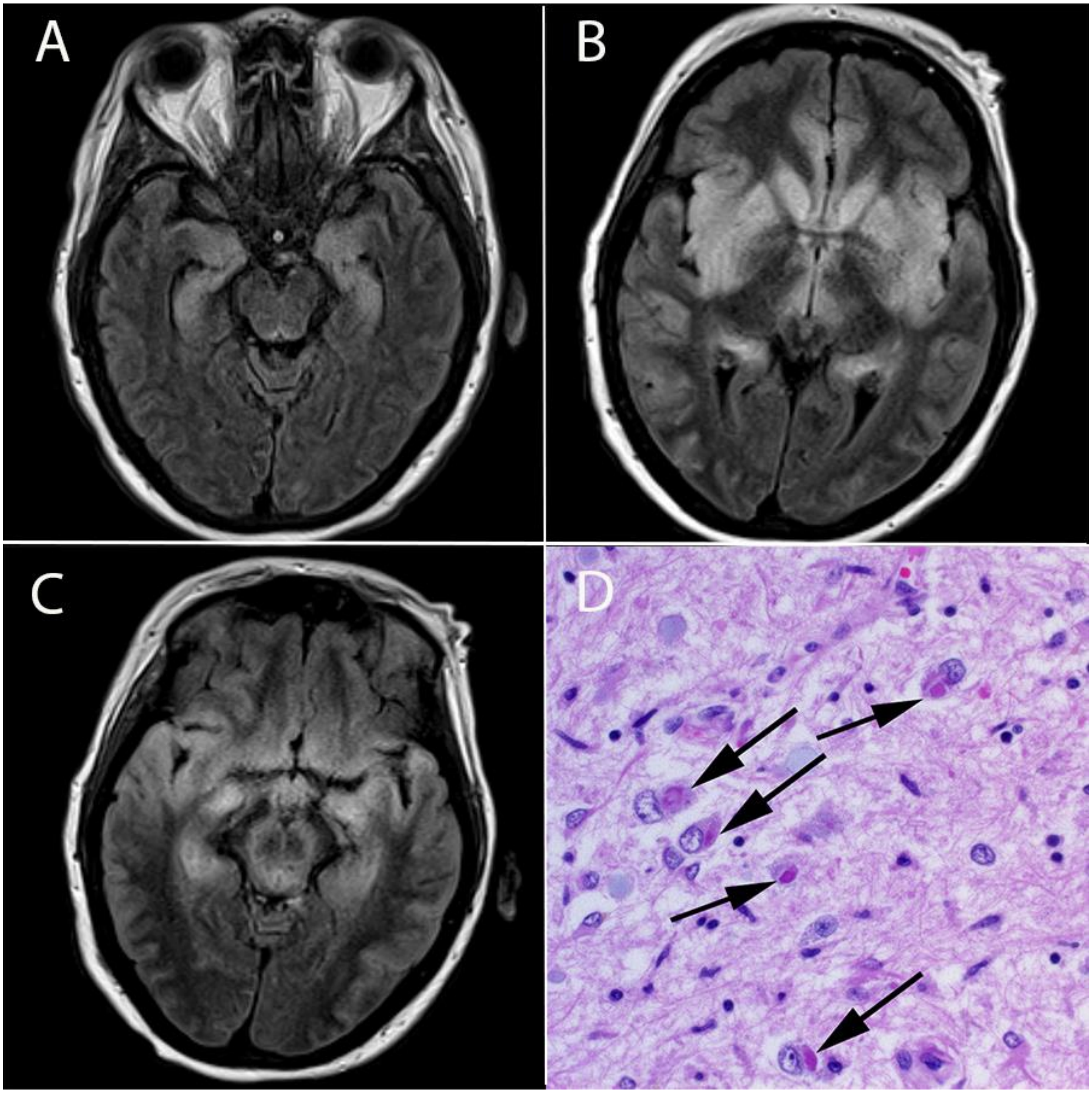

(Filename: TCT_3017_Rabies20abstract20figure.jpg)

3248

4:12PM - 4:19PM

Unconventional Imaging Characteristics of a Tumefactive Demyelinating Lesion Masquerading as a High-Grade Glioma

V Kuttappan[1], H Mazin[1], P Shah[1], A Tsimpas[1]
[1]*Advocate Illinois Masonic Medical Center, Chicago, IL*

Purpose
Tumefactive demyelinating lesions can often present as an imaging conundrum demonstrating mass effect and contrast enhancement comparable to high grade gliomas. Given these neuroimaging features, clinical

manifestations are often similar further obfuscating distinction. We present a case demonstrating this complexity with discordant radiologic and histopathologic findings.
Materials and Methods
We present a 20-year-old female with a two-week history of headache, nausea and vomiting and no neurological deficits. A head CT demonstrated a 4.6 cm paramedian left frontal lobe mass with perilesional edema. Subsequent MRI demonstrated callosal involvement, uninterrupted peripheral enhancement, internal restricted diffusion and hemorrhage, and mass effect on the right frontal lobe. Imaging findings were most consistent with a high-grade glial neoplasm. A stereotactic needle biopsy and corresponding histopathology revealed hypercellular tissue with reactive astrocytosis and minimal mitotic activity. In conjunction with a positive Luxol Fast Blue stain, histopathologic findings were indicative of CNS demyelination. Based on these biopsy findings, the patient underwent a dexamethasone taper with a follow-up MRI to assess interval change. Thereafter, the patient's symptoms improved. Follow-up MRI three months later revealed marked improvement of lesion size as well as associated edema and mass effect on adjacent structures.
Results
A) Noncontrast CT demonstrating a mass in the left frontal lobe with internal calcification. B) T2 image showing perilesional edema of this mass with extension into the genu of the corpus callosum. C) Postcontrast T1 image demonstrating uninterrupted peripheral enhancement of this lesion. D) Postcontrast T1 image three months later showing significant reduction in lesion size, edema, and mass effect.
Conclusions
Distinguishing tumefactive demyelinating lesions and high-grade gliomas present an imaging challenge as both can share similar morphologic and enhancement characteristics. Relatively specific for demyelination, the "open ring sign" can be used to provide further clarity. However, absence of this sign does not exclude a tumefactive demyelinating lesion especially when considering younger patients and nonspecific clinical symptoms as evidenced in this case. Additional tools as MR perfusion and spectroscopy can be used for further discrimination to potentially avoid unwarranted neurosurgical intervention and unnecessary removal of viable brain tissue.

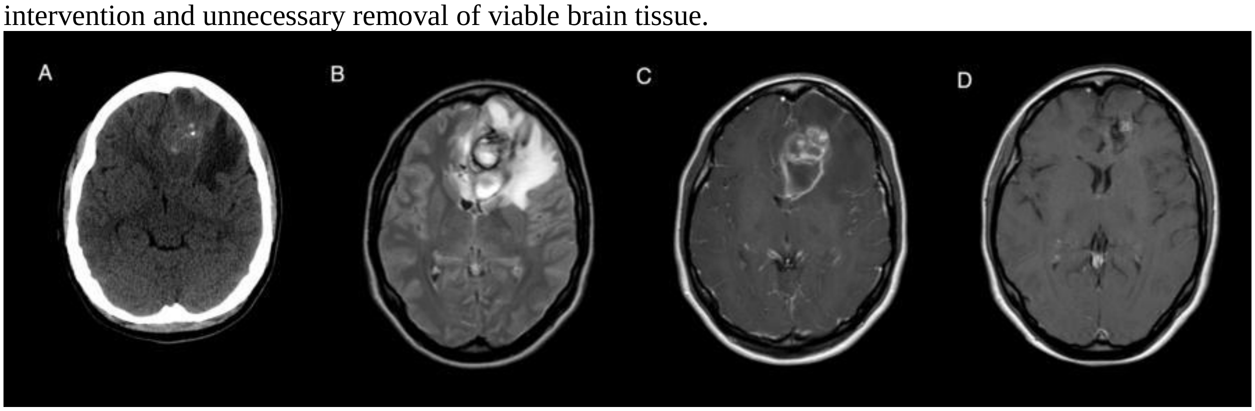

(Filename: TCT_3248_TDL-GBM_compiled.jpg)

2671

4:19PM - 4:25PM

Unique Imaging Manifestations of Ventriculoperitoneal Shunt Malfunction

S Joseph[1], A Tesfay[2], M Chakko[2]
[1]Providence/Providence Park Hospital, Royal Oak, MI, [2]Providence/Providence Park Hospital, Southfield, MI

Purpose
Though ventriculoperitoneal (VP) shunting is the mainstay for the emergent treatment of hydrocephalus,

shunt malfunction is common. This case highlights a unique and important presentation of VP shunt dysfunction with uncommon imaging findings.

Materials and Methods

A 43 year-old female with history of idiopathic intracranial hypertension who presented with headache and new onset fever status post recent ventriculoperitoneal shunt revision. Cross-sectional imaging was performed on POD 2 demonstrating discontinuity of the VP shunt catheter at the reservoir. Additionally, there was development of a hypoattenuating fluid collection adjacent to the ventriculostomy catheter with surrounding vasogenic edema. Multiple new small hypoattenuating lesions were seen along the catheter which were difficult to differentiate between fat and post operative gas.Given the patients symptoms, findings were concerning for abscess. Subsequent MRI redemonstrated the fluid collection adjacent to the VP catheter without abnormal enhancement. The periventricular hypoattenuating lesions on prior imaging were found to be T1 bright and consistent with fat droplets. The patient was then taken to the operating room for VP shunt revision where it was found that the fluid collection was sterile.Given the pertinent imaging findings including catheter discontinuity and T1 bright fluid collections in combination with the history of fever, the etiology of shunt malfunction resulting in the retrograde intracranial migration of fat droplets was confirmed.

Results

Cross-sectional imaging was performed on POD 2 demonstrating the development of a hypoattenuating fluid collection adjacent to the ventriculostomy catheter with surrounding vasogenic edema. Multiple new small hypoattenuating lesions were seen along the catheter which were difficult to differentiate between fat and post operative gas. Subsequent MRI redemonstrated the fluid collection adjacent to the VP catheter without abnormal enhancement. The periventricular hypoattenuating lesions on prior imaging were found to be T1 bright and consistent with fat droplets with associated vasogenic edema.

Conclusions

The presence of intracranial fat is a nonspecific imaging finding frequently related to incidental lipomas. This may be also seen in rare cases such as a ruptured dermoid cyst resulting in the dissemination of intracranial fat manifesting as aseptic meningitis. As our case demonstrates, in the setting of VP shunt placement, catheter complications must be considered.

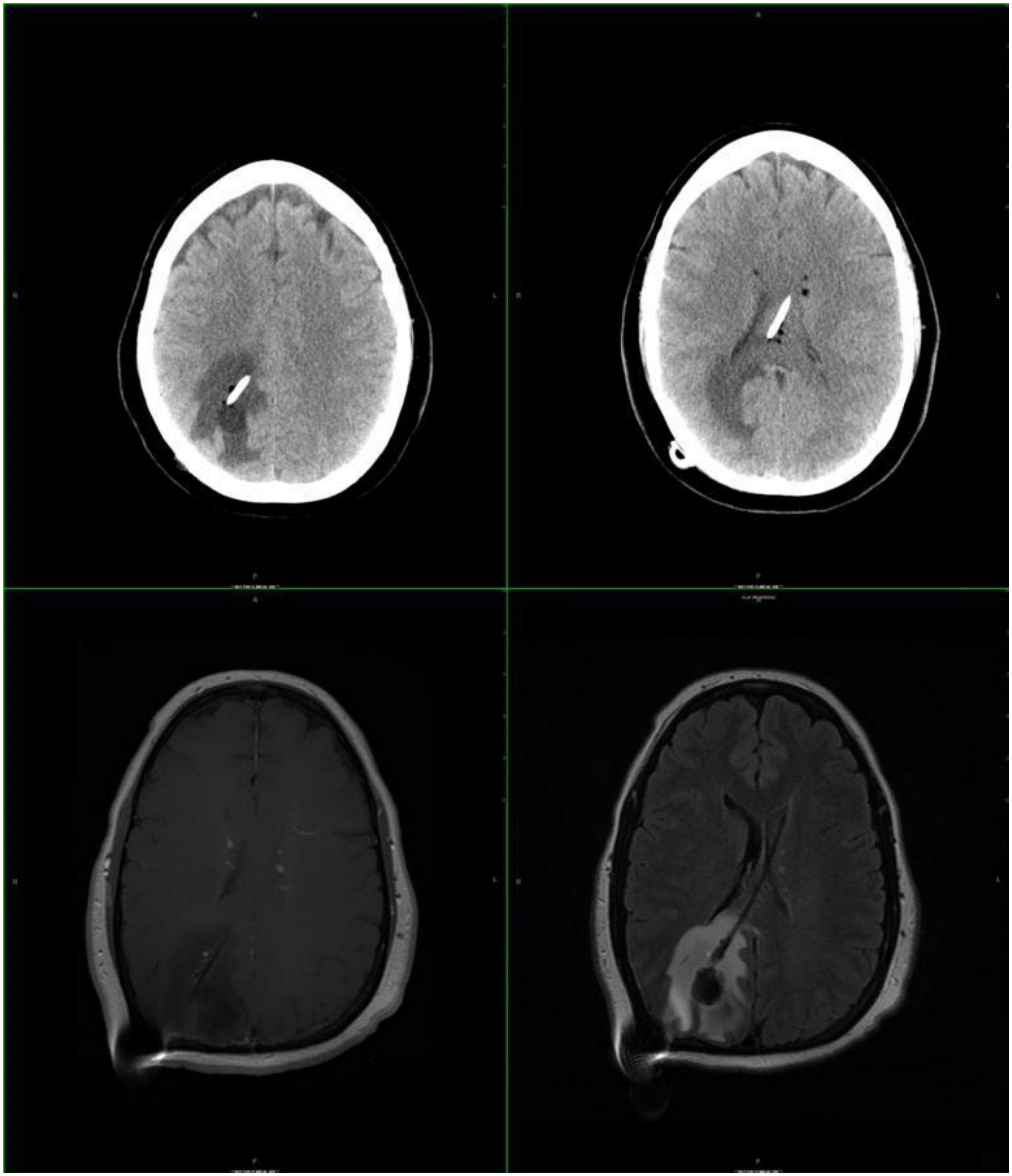

(Filename: TCT_2671_1image.jpg)

2353

2:55PM - 3:02PM

Anatomy of the Great Posterior Radiculomedullary Artery

J Small[1], V Perez Perez[2]
[1]Lahey Clinic, Burlington, MA, [2]Instituto de Ciencias Forenses, Mexico City, Mexico City

Purpose
Purpose: A variable number of radiculomedullary arteries contribute arterial supply to the anterior spinal artery as well as the paired posterior spinal arteries. Although significant variability exists as to the overall caliber of radiculomedullary arteries, dominant radiculomedullary arteries such as the artery of Adamkiewicz (AKA) exist. The existence of a great posterior radiculomedullary artery has attracted little attention and has been a matter of debate in the literature. The aim of this anatomic study was to determine the presence or absence of the great posterior radiculomedullary artery. In addition, we set out to analyze its morphometric characteristics and branching pattern.
Materials and Methods
Materials and Methods: We studied 50 (49 male and 1 female) unembalmed cadaveric specimens. The cadavers ranged in age from 20 to 70 years (median age 40). We performed microsurgical dissection on formaldehyde fixed human spinal cords, red colored natural latex was injected into arterial structures and blue colored latex was injected into venous structures. Two weeks after fixation, the spinal cord specimens were studied with surgical loupes (5x). We identified and measured the artery of Adamkiewicz (AKA) as well as the major posterior radicular arteries. In particular, we searched for the presence or absence of a Great Posterior Radiculomedullary Artery (GPRA). Its course, diameter and location were documented.
Results
A Great Posterior Radiculomedullary Artery (GPRA) was identified in 35 spinal cord specimens (35/50 or 70%). In 11 specimens, bilateral GPRAs were present (22%). A unilateral left sided GPRA was present in 14 cases (28%). A unilateral right sided GPRA was present in 10 cases (20%). Although the caliber of the GPRAs did not approximate that of the AKA, the vessels were truly dominant and easily distinguished from the tiny caliber of the radicular arteries which accompany posterior spinal nerves. The GPRAs varied in caliber between 0.120 microns to 0.678 microns on the left and 0.260 to 0.635 on the right. On average, the GPRAs measured 0.44 microns.
Conclusions
The results of this study demonstrate that in most individuals there is a posterior medullary artery in the region of the lumbar spine which distinguishes itself from other posterior medullary arteries due to its size. This prominent posterior artery supplying the spinal cord may be considered the great posterior radiculomedullary artery (GPRA), and our findings conclusively describe its presence. The definitive identification of a GPRA in 70% of our cases corroborate the disputed findings of Gillian 1958, Jellinger 1966, and Thron 2016, and refute the findings of Corbin 1961, and Piscol 1972. Our study adds new information highlighting the importance of a dominant posterior radiculomedullary artery to the arterial supply of the posterior distal spinal cord. Understanding this intricate anatomy and its variations is critical for addressing vascular malformations of the spinal cord. A better understanding of the spinal cord circulation will lead to reduced risk of surgical and endovascular spinal and aortic procedures.

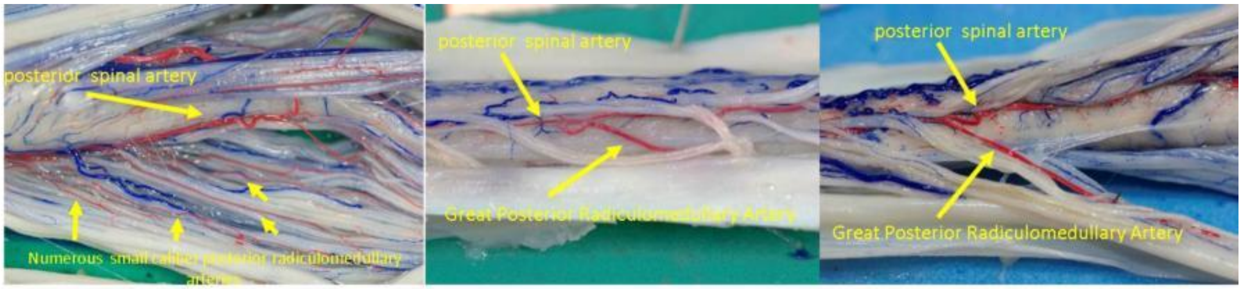

(Filename: TCT_2353_ASNR2019.jpg)

2757

3:02PM - 3:09PM

Are Anatomic Measurements an Effective Predictor of Cough-Associated Headache in Chiari I malformation (CMI)?

C Huang[1], I Chiali[1], A Bezuidenhout[1], R Bhadelia[1]
[1]*Beth Israel Deaconess Medical Center, Boston, MA*

Purpose
While headache is a common symptom of CMI, cough-associated headache-CAH is the most distinctive symptom indicating clinically significant disease, and better outcome after surgery (1). Our purpose was to investigate if previously described anatomic measurements at the cranio-cervical junction correlate with presence of CAH in CMI patients.
Materials and Methods
47 patients with CMI who had MRI with high resolution 3D-T2W images as part of their protocol were included. 3D-T2W images were used to measure: amount of tonsillar herniation, length of the clivus and supra-occiput, McRae line, Twining line, pB-C2 line, clivus-canal angle, odontoid retroversion angle, skull base angle, and the ratio of neural tissue to total area of foramen magnum (foramen magnum index) (2-4).Clinical notes were reviewed to determine presence of CAH. Spearman's correlation was used to determine relationships between the presence of CAH and anatomic measurements. Each anatomic measurement with significant relationship was further investigated, using median as divider, to test their sensitivity and specificity in predicting CAH in a CMI patient.
Results
40/47 (85.1%) CMI patients reported headaches of which 26/47 (55.3%) were CAH. A significant but weak correlation between CAH and degree of tonsil herniation (CC=0.303; p=0.04), and clivus-canal angle (CC=-0.346; p=0.02) was noted. Tonsillar herniation ≥10-mm showed sensitivity and specificity of 65.38% and 61.90% respectively for predicting CAH. A clivus-canal angle of ≤ 150° showed sensitivity and specificity of 65.38%and 61.90 % for predicting CAH. Other anatomic measurement did not show any association with CAH.
Conclusions
Of the numerous anatomic measurements described in the setting of CMI, only the amount of tonsillar herniation and clivus-canal angle show significant but weak correlation with CAH with low sensitivity and specificity in predicting its presence in a CMI patient. Our findings suggest that anatomical measurements cannot be used in isolation to predict characteristic CMI symptomatology.

3047

3:09PM - 3:16PM

Conventional MRI Findings in 92 Consecutive Cases of Symptomatic Low-Flow Spinal Arteriovenous Fistulas

A Hedjoudje[1], P Gailloud[2]
[1]Johns Hopkins University, Baltimore, MD, [2]THE JOHNS HOPKINS HOSPITAL, BALTIMORE, MD

Purpose
Low-flow spinal arteriovenous fistulas (SAVFs) include spinal dural arteriovenous fistulas (SDAVFs), low-flow spinal epidural arteriovenous fistulas (SEAVFs) and low-flow perimedullary arteriovenous fistulas (PmAVFs). Low-flow SAVFs with intradural venous drainage typically present in older patients with a progressive myelopathy. They represent a diagnostic challenge as MRI, the primary screening tool for myelopathies, is often nonspecific: many cases are initially misdiagnosed, notably as transverse myelitis (1). This work retrospectively analyzes the prevalence of 3 findings classically associated with low-flow SAVFs, i.e., abnormal parenchymal signal, flow-voids and pial/parenchymal enhancement after gadolinium administration, in a cohort of patients with angiographically confirmed lesions.
Materials and Methods
Conventional MRI studies obtained in 92 consecutive cases of symptomatic low-flow SAVFs with intradural drainage treated at our institution between 2009 and 2018 were reviewed. The following features were recorded: (i) parenchymal anomalies on T2-weighted images (focal, longitudinally extensive, absent), (ii) flow voids on T2-weighted images (subtle, prominent, absent), (iii) pial and/or parenchymal enhancement on T1-weighted images after gadolinium administration (focal, diffuse, absent).
Results
The reviewed cases included 49 SDAVFs, 37 SEAVFs and 6 PmAVFs. (i) T2 parenchymal anomalies were noted in 89 cases (96.7%, 82 extensive, 7 focal), (ii) flow voids were present in 57 cases (62%). They were subtle in 17 (18.5%), prominent in 40 (43.5%). (iii) pial enhancement was found in 70 of the 86 patients who received gadolinium (81.4%) while parenchymal enhancement was noted in 62 (72.1%).
Conclusions
Longitudinally extensive parenchymal anomalies on T2-weighted images are the most reliable MRI finding in patients with symptomatic low-flow SAVFs. Prominent flow-voids – a finding commonly considered as the disease's hallmark – were present in 43.5 % of patients; they were subtle (18.5%) or absent (38%) in a majority of cases. Parenchymal enhancement, a finding often considered as indicative of an inflammatory myelopathy – was present in 72.1% of patients with low-flow SAVFs. Figure legend: Sagittal T2-weighted image in 3 patients with symptomatic low-flow SAVFs with intradural venous drainage, illustrating absent (left), subtle (center) and prominent (right) flow voids.


(Filename: TCT_3047_Figure1.jpg)

2159

3:16PM - 3:23PM

Differentiation Between Tuberculosis and Pyogenic Spondylodiscitis: The Role of the Ventral Meningovertebral Ligament in Patients with Anterior Epidural Abscess

S Strauss[1], S Gordon[2], J Burns[2], J Bello[2], S Slasky[2]
[1]Weill Cornell Medical Center, Manhattan, NY, [2]Montefiore Medical Center, Bronx, NY

Purpose
Differentiation between pyogenic and tuberculous spondylodiscitis is a diagnostic challenge, as few imaging reliably distinguish between the two entities and percutaneous biopsies are often culture negative. The purpose of this study is to determine if violation of the anterior meningovertebral ligament in the setting of epidural abscess discriminates between these two infectious entities.
Materials and Methods
This was a retrospective cohort study of all patients with anterior epidural abscess diagnosed on spinal MRI between 1/1/2005 and 3/16/2018 and final diagnosis of TB spondylodiscitis or pyogenic spondylodiscitis. 6 cases of TB spondylodiscitis (mean age of 44, 83.3% male) and 32 cases of pyogenic spondylodiscitis were included in the final analysis (mean age of 58, 53.1% male). Cases were evaluated for presence or absence of anterior meningovertebral ligament destruction on MRI. Additional features examined were vertebral height loss, number of contiguous vertebral bodies, paraspinal abscess, endplate

destruction and segmental location. Chi-squared test of independence and independent sample t-tests were performed to test for significance of difference between the groups.
Results
6/7 (85.7%) cases of TB anterior epidural abscess had intact anterior epidural septum (Figure 1) and only 3/32 (9.4%) cases of pyogenic associated abscess demonstrated intact septum (p=0.00001). The presence of an intact septum had 85.7% sensitivity and 90.6% specificity with 66.7% positive predictive value and 96.7% negative predictive value for TB spondylodiscitis. Additional imaging features studied did not significantly differ between the two groups.
Conclusions
The presence of an intact meningovertebral ligament has high sensitivity and specificity for TB spondylodiscitis associated epidural abscess.

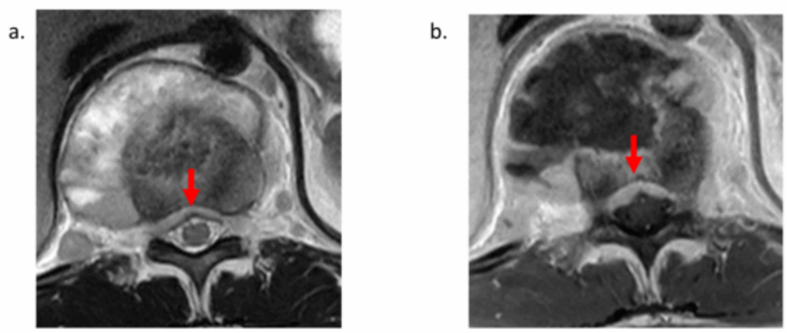

Figure 1. Preserved anterior meningovertebral ligament in a patient with TB epidural abscess.
Axial T2WI (a) and contrast enhanced T1WI (b) shows a bilobed appearance of epidural abscess. The central indentation (arrow) represents the preserved anterior meningovertebral ligament.

(Filename: TCT_2159_TB_Figure.gif)

2672

3:30PM - 3:37PM

Renal Excretion of Contrast on CT Myelogram: A Specific Marker of Cerebrospinal Fluid Leak?

S Behbahani[1], J Raseman[2], A Sharma[3], r el daya[4]
[1]Mallinckrodt Institute of Radiology, Washington University School of Medicine, St Louis, MO, [2]Mallinckrodt Institute of Radiology, Washington University School of Medicine, St. Louis, MO, [3]WASHINGTON UNIV. SCHOOL OF MEDICINE, MALLINCKRODT INSTITUTE OF RADIOLOGY, ST. LOUIS, MO, [4]Mallinckrodt Institute of Radiology, Saint Louis, MO

Purpose
To study the sensitivity and specificity of renal/ureteric opacification on post-myelogram CT as a sign of CSF leak.
Materials and Methods
In this retrospective IRB approved case-control study, post-myelogram CT images of 49 consecutive patients (mean age 48 years; 15 M, 34 F) seen at a tertiary care hospital with imaging and/or clinical findings related to intracranial hypotension between January 2008 and August 2018 were reviewed for

presence of contrast in the renal excretory system. We also performed similar assessment for 90 consecutive controls (mean age 58 years; 33 M, 57 F) in whom myelogram had been performed for indications other than suspected CSF leak. Patients who had received intravenous iodinated or gadolinium-based contrast within 48 hours preceding myelogram were excluded.

Results

Cases included 21 with (group 1) and 28 without (group 2) overt CSF leak on CT myelogram. Renal/ ureteric opacification was seen 14.3% (7/49) of all cases. In group 1, 24% (5/21) exams had renal/ ureteric opacification. Three of these cases had spontaneous spinal CSF leak, one had post-traumatic CSF leak, and one case had CSF-venous fistula. Renal/ureteric opacification was also present in 7% (2/28) of group 2 patients. Both these cases had evidence of CSF hypovolemia on brain MRI and both responded to epidural blood patch. None (0%) of 90 controls had renal/ ureteric opacification on post-myelogram CTs.

Conclusions

Renal/ ureteric opacification was exclusively seen in the presence of CSF leak. Given its 100% specificity, identification of this finding should prompt a closer "second look" for subtle myelographic contrast extravasation or an underlying CSF-venous fistula. Our results suggest that this sign may be considered as an additional diagnostic criterion for CSF leak in absence of an identifiable leak.

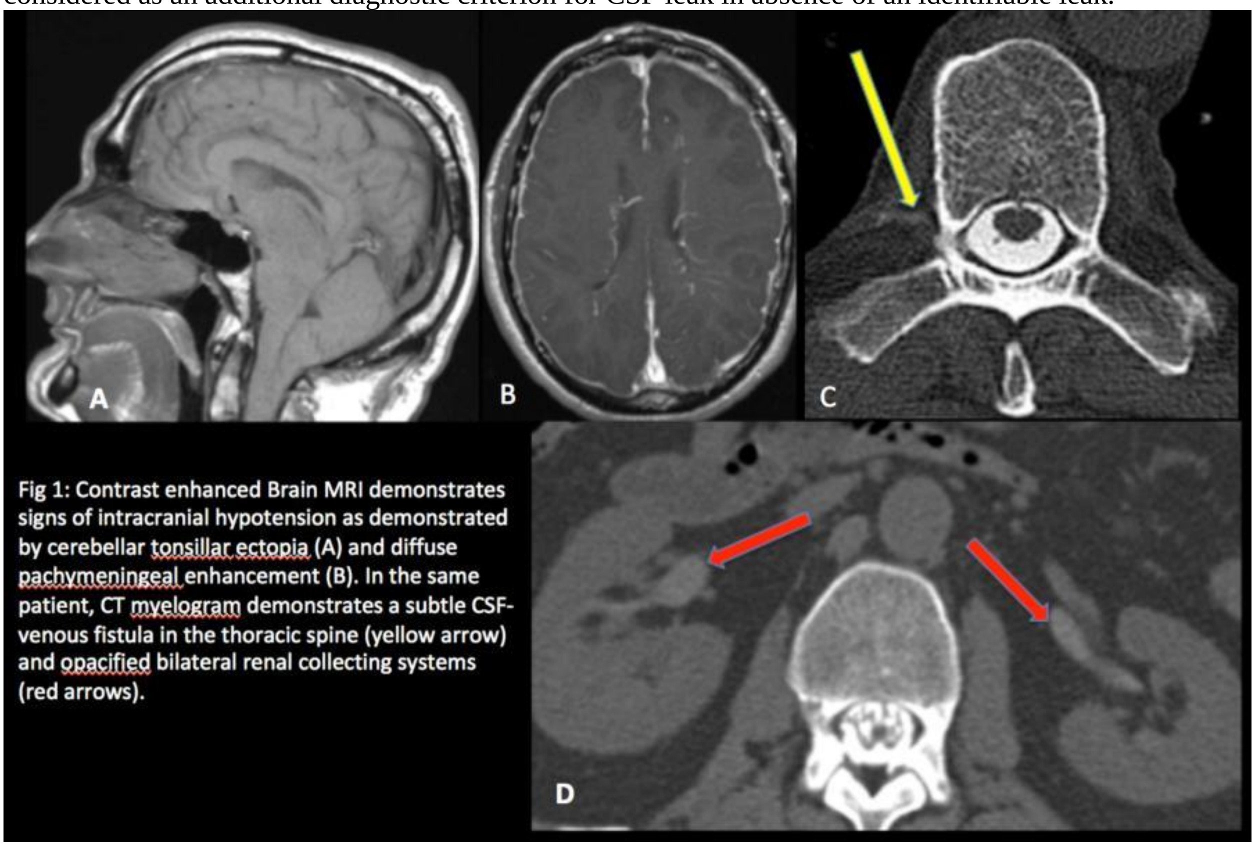

Fig 1: Contrast enhanced Brain MRI demonstrates signs of intracranial hypotension as demonstrated by cerebellar tonsillar ectopia (A) and diffuse pachymeningeal enhancement (B). In the same patient, CT myelogram demonstrates a subtle CSF-venous fistula in the thoracic spine (yellow arrow) and opacified bilateral renal collecting systems (red arrows).

(Filename: TCT_2672_csfleakmyeloabstract.jpg)

2755

3:37PM - 3:43PM

Safety and Efficacy of Embolization of Low-Flow Spinal Arteriovenous Fistula with Intradural Venous Drainage Using NBCA: Technical Outcome in 21 Consecutive Cases

P Gailloud[1]

[1]*THE JOHNS HOPKINS HOSPITAL, BALTIMORE, MD*

Purpose

To evaluate the safety and efficacy of embolization of low-flow spinal arteriovenous fistulas (SAVFs) with intradural drainage using n-butyl-cyanoacrylate (NBCA).

Materials and Methods

21 lesions embolized over a 33-month period were prospectively analyzed, including 12 spinal dural arteriovenous fistulas, 8 spinal epidural arteriovenous fistulas and 1 perimedullary arteriovenous fistula. The lesions were thoracic (5), lumbar (14) or sacral (2); 8 had multiple feeding arteries. All lesions were embolized with NBCA. Adjunct methods included coiling in 5 cases and 5%-dextrose push in 11 (1). One NBCA injection was performed in 19 cases, 2 injections in 2 of the 8 cases with multiple feeders. Embolization was considered successful when the liquid embolic agent reached the proximal segment of the draining vein. Follow-up angiography, due in 11 patients at time of submission (minimum 6-month interval), was obtained in 10 and declined by 1.

Results

Immediate technical outcome: NBCA embolization addressed the draining vein in 19 patients. In 2 cases of SDAVFs with multiple feeders, embolization of a residual feeding artery from an adjacent level was not attempted as a radiculomedullary artery arose from the targeted branch; both patients were referred for surgical therapy. Technical complications: No NBCA-related event was noted. Self-limited minor extravasation (attributed to microwire perforation) occurred in one case without preventing successful embolization. Clinical complications: Sudden worsening of leg weakness was noted in one of the 2 patients with incomplete embolization 12 hours after treatment; perimedullary venous thrombosis was suspected and confirmed angiographically. Surgery was postponed and the patient went on to develop deep venous thrombosis 2 months later while on dual antiplatelet therapy. The weakness was improved compared to pre-treatment baseline at the 3-month follow-up visit. Follow-up angiography: no residual or recurrent lesions was noted in the 10 cases with follow-up angiography.

Conclusions

Embolization of low-flow SAVFs with NBCA is safe and shows long-lasting efficacy. It offers a valid alternative to surgical therapy. Figure legend: Right L3 spinal epidural fistula (*) draining into a left L5 radiculomedullary vein (arrowheads) via a partially thrombosed epidural pouch (arrows) (left – selective DSA, middle – superselective DSA, right – NBCA cast)

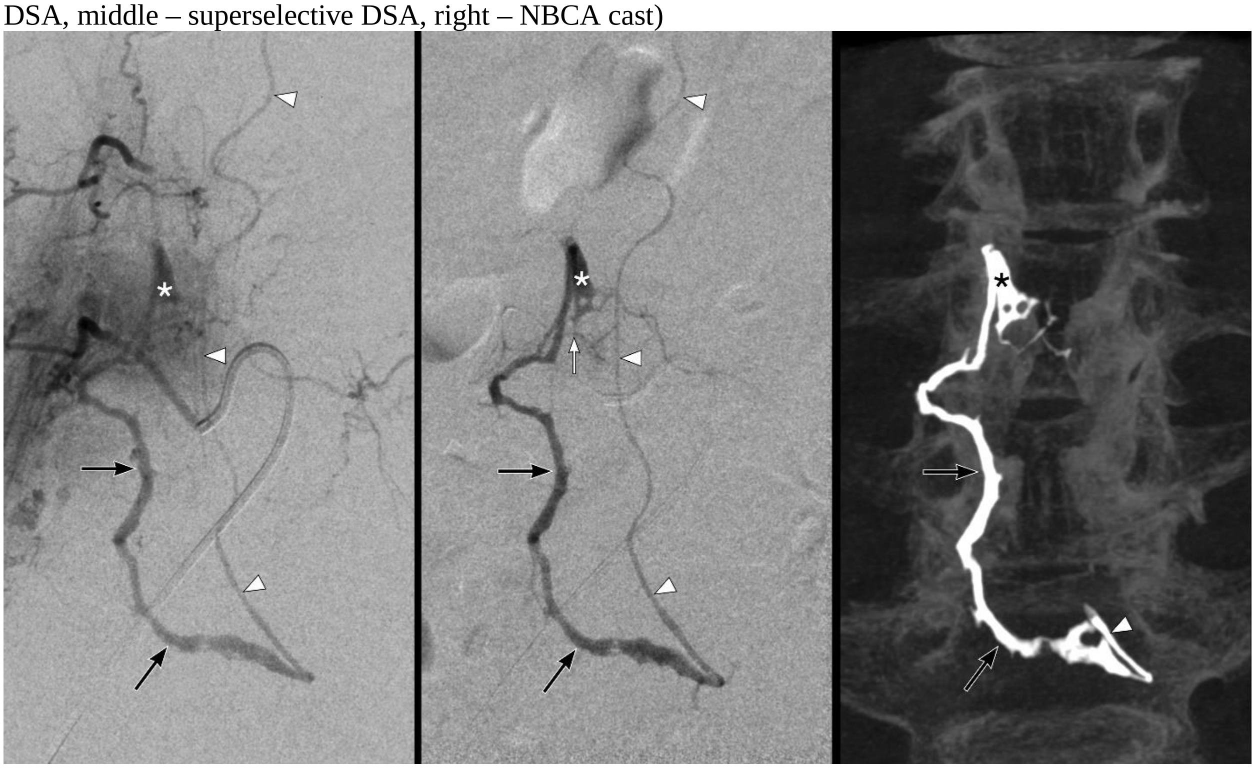

(Filename: TCT_2755_Figure1.jpg)

2857

3:43PM - 3:50PM

Spinal Cord Herniation: A Lack of Syringomyelia to Assist in Differentiation from Arachnoid Webs and Cysts

L Eisenmenger[1], A Chan[1], C Dalle Ore[1], A Clark[1], C Chin[1]
[1]*UCSF, San Francisco, CA*

Purpose
Spinal cord herniation (SCH), arachnoid webs, and arachnoid cysts are uncommon abnormalities affecting the spinal cord that can result in significant neurological morbidity. Differentiating between these entities on the basis of radiological findings remains challenging but is essential in planning a surgical approach. Our purpose was to examine SCH cases on MRI and CT myelography to improve diagnostic confidence prior to surgery.
Materials and Methods
A search of medical charts between 10/1/1998 through 10/1/2018 was performed for patients with surgically proven spinal cord herniation. 9 cases were found with preoperative MRI with 8/9 cases having preoperative myelograms. Two neuroradiologists recorded the level of the dural defect, the morphology of the spinal cord (nature of dorsal cord indentation), visualization of a complete plane of CSF ventral to the deformity, and the presence or absence of cord signal abnormality or syringomyelia.
Results
Of the nine SCH cases, seven were female and two were male ranging in age from 35 to 75 with a mean age of 52-years-old. Four patients presented with myelopathy, three with back pain, and two with radiculopathy. All nine SCH cases occurred between T3-T6 in the kyphotic curvature of the thoracic spine. 6/9 cases occurred at the disc level with 3/6 of those cases having a small osseous spur/disc complex. All cases had a "C"-shaped dorsal cord indentation (yellow arrow) with a lack of CSF (orange arrow) ventral to the cord deformity. No cases had the "scalpel sign." No cases had cord signal abnormality or syringomyelia.
Conclusions
This is one of the largest known case series of surgically confirmed SCH. This study confirmed previously found SCH characteristics including the lack of ventral CSF at the level of the cord deformity and "C"-shaped dorsal cord indentation; however, unlike cases of arachnoid web/cysts that have a high association with cord signal abnormality and syrinx formation (green arrow), this is the first study to document the lack of cord signal abnormality and/or syringomyelia in cases of SCH, an additional imaging feature to assist in accurate diagnosis.

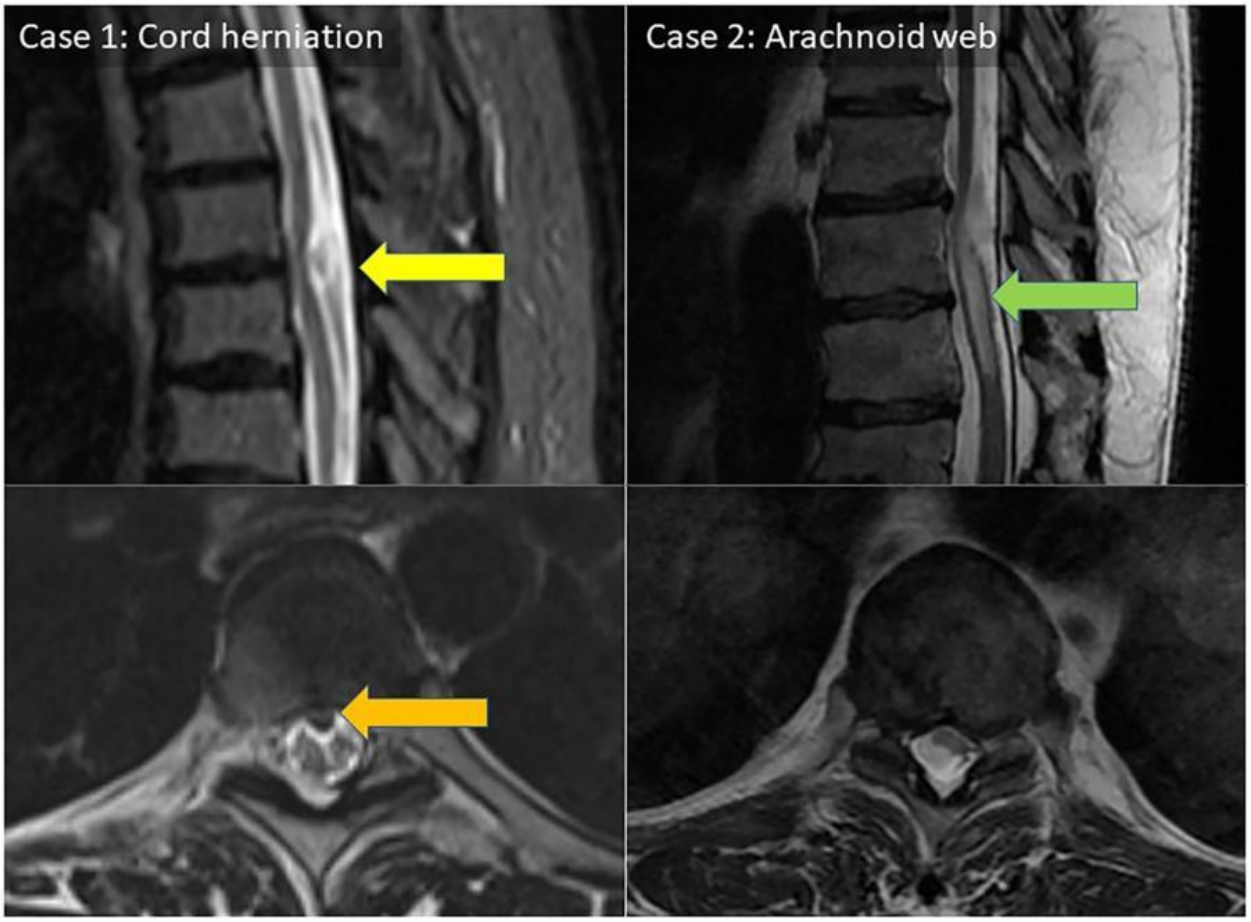

(Filename: TCT_2857_ASNRSCHfigure110118-final.jpg)

2137

3:50PM - 3:57PM

Tectorial Membrane Injury in the Acute Trauma Setting: Examining Disparities Between the Adult and Pediatric Populations

E Soule[1], P Fiester[2], P Natter[2], D Rao[2]
[1]University of Florida College of Medicine - Jacksonville, Jacksonville , FL, [2]University of Florida College of Medicine - Jacksonville, Jacksonville, FL

Purpose
To study and classify the different types of tectorial membrane (TM) injuries that occur in the adult and pediatric populations in the setting of craniocervical trauma.
Materials and Methods
Patients who suffered TM injury were identified retrospectively using the keyword 'tectorial membrane' included in radiology reports between 2012 and 2018 using Nuance Powershare software. All relevant imaging studies were reviewed by two CAQ certified neuroradiologists. Detailed descriptions of TM injury were recorded along with any relevant additional findings including clinical history.
Results
10 adults and 6 pediatric patients were identified with acute traumatic injuries involving the TM. Ninety percent of the adult patients demonstrated a disruption of the TM. All adult patients demonstrated a TM injury inferior to the clivus (subclival) with 22% of subclival tears at the level of the basion and 78% at

the level of the odontoid tip. In contrast, 83% of pediatric patients suffered a stripping injury of the TM located posterior to the clivus (retroclival). All stripping injuries were associated with retroclival epidural hematoma (REH). Stretch injuries of the TM were identified in 10% of adults and 17% of pediatric patients.
Conclusions
A classification system for TM injuries is proposed based on this data: type 1 - retroclival stripping injury (more common in pediatric patients; associated with REH); type 2a - subclival disruption at the basion; type 2b - subclival disruption at the odontoid (both more common in adult patients); and type 3 - stretching injury of the TM.

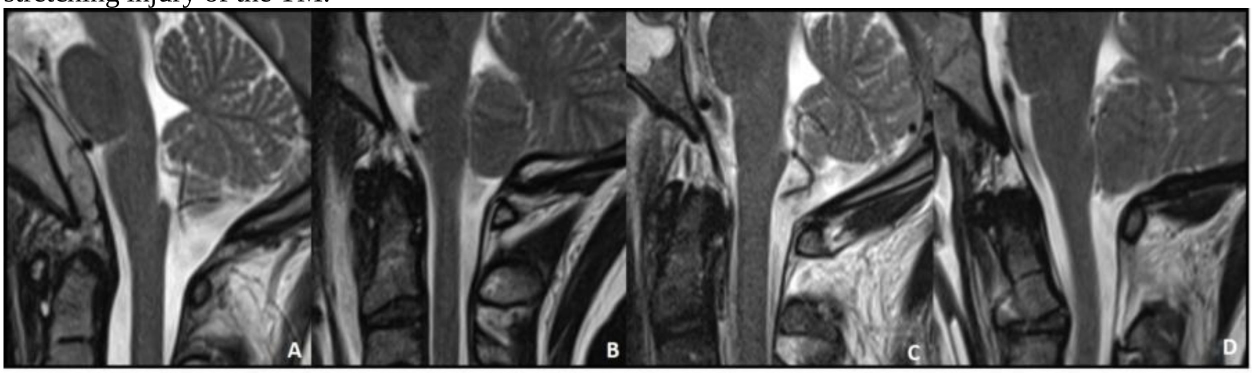

Figure 1A: sagittal T2-weighted MRI of pediatric stripped tectorial membrane (type 1 TM injury) with retroclival location and REH
Figure 1B: sagittal T2-weighted MRI of adult disrupted tectorial membrane with clival location (type 2A TM injury)
Figure 1C: sagittal T2-weighted MRI of adult disrupted tectorial membrane with odontoid location (type 2B injury)
Figure 1D: sagittal T2-weighted MRI of pediatric stretched tectorial membrane (type 3 injury)

(Filename: TCT_2137_ASNR_figure.jpg)

2492

3:57PM - 4:04PM

The Relationship between Magnetic Resonance Imaging Features of Discitis/Osteomyelitis and the Diagnostic Yield and the Result of Biopsy

B Kang[1], A Radmanesh[1]
[1]NYU, New York, NY

Purpose
Many imaging features have been described to suggest discitis/osteomyelitis. The relative value of these imaging features is still not agreed upon as it relates to the diagnostic yield of biopsy. In addition, one aspect that has not received as much attention is the relationship between MRI appearance of discitis/osteomyelitis and the causative organism. Evaluation of how variable infectious organisms can progress in the process of erosion of vertebrae, liquefaction of discs, and involvement of paraspinal soft tissue, may provide further sensitivity and specificity to treating these etiologies at an earlier stage. One contention that we would like to propose, by virtue of our anecdotal observations and understanding of endotoxin role, is that those infections which are due to gram negative bacteria will tend to cause a much more aggressive process in comparison to gram positive bacteria, and can contributes to associated phlegmon and abscess formation. The overarching goal of this project is to determine the imaging features seen on cases that were biopsied for suspicion of discitis/osteomyelitis. Our objective is to determine if certain features can predict a positive biopsy result and a particular type of causative organism.

Materials and Methods
Sets of anonymized imaging data were retrospectively reviewed (MRI of the cervical, thoracic, and lumbar spine). These were evaluated by a neuroradiology fellow and a neuroradiology faculty for the pertinent imaging finding with respect to infectious etiology. The study procedures involved evaluation of the imaging findings and attempted to correlate those imaging findings with the etiology of infection. Different imagining features were catalogued and a statistical analysis was performed to determine if the features can be tied to the infectious species found on culture of the biopsy sample.
Results
Utilizing the Pearson Chi-square test of Independence, the features which demonstrated significant correlation with a positive culture/laboratory result were aggressive endplate erosion and paraspinal component. Significant negative correlation was seen with symmetric edema/enhancement on both sides of the affected disc. The imaging findings of disc edema and effacement of the nuclear cleft were not significantly correlated with a positive culture/laboratory result. When the imaging findings were correlated to the etiology of infection, a trend was noted between paraspinal soft tissue involvement and gram negative organisms ($p = 0.08$). The remaining imaging findings did not correlate with etiology of infection.
Conclusions
Our results demonstrate that certain features of imaging can be utilized to predict the yield and utility of biopsy. Specifically when the imaging findings demonstrate aggressive erosions without symmetric marrow edema and presence of paraspinal collections, there is a higher likelihood of a positive culture/laboratory result confirming infection. Paraspinal soft tissue involvement was noticed more frequently in association with gram negative organisms than with gram positive ones. Presence of a statistically significant correlation should be tested with a larger sample size.

3534

4:04PM - 4:11PM

The Effect of Pre-procedure Spinal Magnetic Resonance Angiography on Digital Subtraction Angiography Fluoroscopy Times in Patients with Suspected Spinal Dural Arteriovenous Fistulas

A Chu[1], K Davtyan[1], A Mamourian[1]
[1]*University of Pennsylvania, Philadelphia, PA*

Purpose
Spinal dural arteriovenous fistulas (SDAVFs) can cause debilitating and progressive neurological deficits [1]. The gold standard for the diagnosis and localization of feeding vessels of SDAVFs is digital subtraction angiography (DSA) [2]. However, spinal DSA is often challenging and more often than not time consuming due to the extensive and variable arterial supply to the spinal cord vasculature. Contrast enhanced spinal magnetic resonance angiography (MRA) is frequently performed in patients with suspected SDAVFs prior to DSA in an attempt to establish the diagnosis and, when possible, localize feeling vessels to the fistula. The purpose of this study was to determine if identification of the supplying vessels on spinal MRA is effective in shortening the procedure time of the subsequent DSA.
Materials and Methods
Retrospective data collection was performed in accordance with our institution's IRB. All patients who had both a spinal MRA and subsequent DSA were included, as long as they had no prior demonstration of an SDAVF on DSA. DSA fluoroscopy times were recorded, as well as the presence/absence of an SDAVF and the vertebral level of any feeding vessels. A total of 38 patients were included, 19 of which had available DSA fluoroscopy times. The 19 patients with fluoroscopy times were divided into Group 1 and Group 2, where Group 1 consisted of 6 patients where the MRA correctly identified the feeder location within 2 vertebral levels of the feeder location on DSA, and Group 2 consisted of 13 patients where the MRA indicated that the feeders were beyond 2 levels from those found on DSA, suggested

there was a SDAVF when there was none on DSA, or identified no SDAVF when there was no SDAVF on DSA. A 2-sided, 2-sample t-test, along with a power analysis, was performed on the two groups.
Results
Using all 38 patients, MRA resulted in a sensitivity of 0.82, specificity of 0.75, positive predictive value of 0.82, and negative predictive value of 0.75. Using the 19 patients with available DSA fluoroscopy times, the mean fluoroscopy time of Group 1 was 16.9 minutes, the mean time of Group 2 was 32.0 minutes, the t-test p-value was 0.2474, the 95% confidence interval was -41.7 to 11.5 minutes, and the statistical power was 0.20.
Conclusions
We found that that the positive predictive value of MRA for the diagnosis of SDAVF in our experience (38 cases) was 0.82. Although the mean fluoroscopy time was substantially shorter in patients when MRA correctly identified the supply within 2 vertebral levels (16.9 minutes versus 32.0 minutes), the difference did not reach statistical significance. This may well be a reflection of the small size of the study group of patients with this uncommon disease.

Tuesday, May 21, 2019
2:55PM - 4:25PM
Keys to Understanding the Developing CNS

3170

2:55PM - 3:02PM

Diffusion Tensor Imaging Indices of the Pediatric Spinal Cord in Myelomeningocele Repair Patients Compared to Normal

A Bhatia[1], B Reynolds[2], C Tong[3], S By[4], A Witt[5], J Martus[5], D Clayton[3], M Adams[6], S Smith[3]
[1]Monroe Carell Jr Children's Hospital at Vanderbilt, Nashville, TN, [2]Vanderbilt University Medical Center, Franklin, TN, [3]Vanderbilt University Medical Center, Nashville, TN, [4]Philips Healthcare, Baltimore, MD, [5]vanderbilt University Medical Center, Nashville, TN, [6]Vanderbilt Childrens' Hospital, Nashville, TN

Purpose
The purpose of the study is to evaluate diffusion tensor imaging (DTI) indices of the pediatric spinal cord (SC) in myelomeningocele (MMC) repair patients and compare to normal SC based on age and cord level.
Materials and Methods
A retrospective analysis was performed from 2016-2018 on DTI acquired in a pediatric population of myelomeningocele repair at Vanderbilt Children's Hospital. MMC repair patients were separated into stable and unstable groups based on urologic testing. Diffusion weighted images (15 directions) were acquired on a 3.0T Philips Achieva in the cervical and/or thoracolumbar SC as well as conus (By et al., 2016). Volumes of interest (VOI) were manually drawn for each axial slice to include whole cord, excluding CSF. Mean DTI metrics (AD, RD, MD, and FA) were calculated across all voxels within each slice and across all slices containing cord (3D VOI). The 3D VOI in MMC repair groups were compared to previously acquired normal age matched population. Statistical analysis was made using Wilcoxon rank-sum test assuming nonparametric distribution.
Results
There were 11 MMC repair patients (mean age: 4.6 years), three had worsening urologic testing (circles) while eight had stable urologic studies (x) (Figure 1). Axial diffusivity demonstrated statistically significant difference in the thoracolumbar region compared to controls for both unstable and stable

groups (1.4 vs. 0.98, p=0.03 and 1.17 vs. 0.98, p=0.04). Mean diffusivity was statistically significant different in unstable MMC patients compared to controls (0.80 vs. 0.55, p=0.02).
Conclusions
DTI indices in the SC of MMC repair patients demonstrate the potential to differentiate which patients might be urologically unstable, providing an objective biomarker for clinicians to manage this complex patient population. Further studies are needed in larger patient populations and with additional correlation with clinical testing.

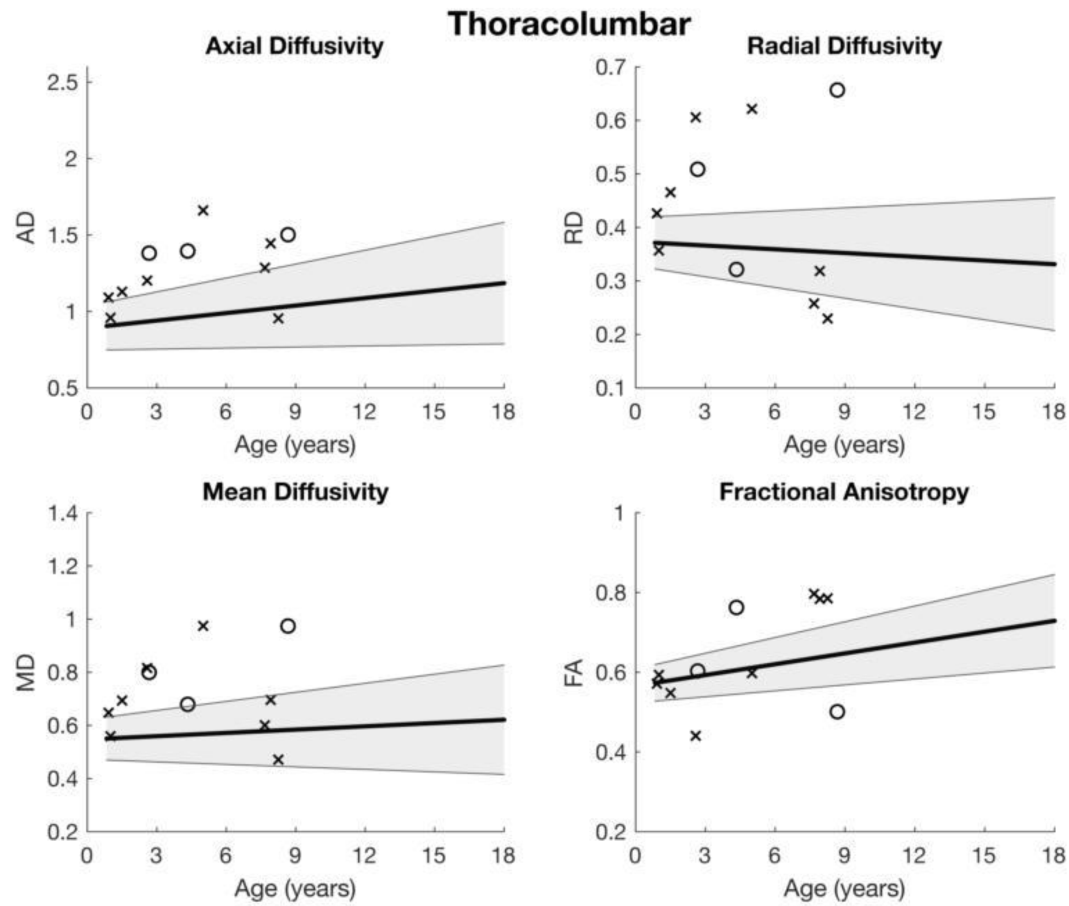

(Filename: TCT_3170_GU_MMC_Thoracolumbar_102918.jpg)

2204

3:02PM - 3:09PM

Dural Venous Sinuses and Subarachnoid Spaces in Fetuses with MMC Correlate with Sac Morphology

Shelef, I.
Soroka University Medical Center
Beer-Sheva

2539

3:09PM - 3:16PM

Impact of Craniocervical Junction and Cervical Spine Anatomy on Syringohydromyelia in Pediatric Patients with Chiari 1 Malformation

A Hsu[1], M Paldino[1], N Desai[2], M Kukreja[1], S Kralik[1]
[1]*Texas Children's Hospital, Houston, TX,* [2]*Texas Children's Hospital Baylor College of Medicine, Houston, TX*

Purpose
Syringohydromyelia is a common complication of Chiari 1 malformation. Why some patients develop syrinx while others do not remains poorly understood. Differences in cervical spinal canal anatomy measurements have been reported to differ between adults with Chiari I malformation with and without syrinx, but whether similar differences are present in children has yet to be investigated. The purpose of this study is to quantify anatomic differences of the craniocervical junction and cervical spine associated with syrinx formation in children with Chiari I malformation.
Materials and Methods
Following IRB approval, a retrospective review from 2010-2017 was performed among pediatric patients (age ≤ 18) with Chiari I malformation defined as ≥ 5 mm cerebellar tonsil herniation below McRae line. A syrinx was defined as well-defined central spinal cord T2-hyperintensity ≥ 2 mm in diameter on axial images. Anatomic measurements of the craniocervical junction included: pB-C2 line, odontoid retroflexion angle, odontoid retroversion angle, clivus length, supraoccipital length, clivus supraoccipital angle, and clivus spine angle. Anatomic measurements of the cervical spine included anteroposterior diameter of the spinal canal at each level from C1 to C7 (Fig 1 and 2). Taper ratios using the cervical spine canal diameters were calculated for C1-7, C1-4, and C4-7 segments using the slope from a least squares method for the line of best fit. A multivariate analysis was performed using a statistical learning algorithm (Random Forest approach) to measure the independent contribution of each anatomic variable to the prediction of syrinx development. This analysis was performed for all patients as well as for two subgroups - patients aged 0-8 years and patients 9-18 years - given that anatomy of the cervical spine is expected to be similar to the mature adult form at approximately 9 years of age. Individual variable(s) demonstrating importance to prediction greater than noise were considered significant and reported from greatest to least significance. A separate Random Forest analysis and Pearson correlation coefficient (r) analysis were performed between anatomic measurements and syrinx size; $p < 0.0026$ considered statistically significant when accounting for multiple comparisons.
Results
A total of 186 patients were included with mean age 6.77 years and SD 4.59 (range 0-18 years). 91 (49%) were females. 78 (42%) had syrinx (mean syrinx diameter = 6.47 mm; SD =4.17). There was no statistically significant difference in mean age between the two groups (Chiari with syrinx mean age 7.02 years, SD = 4.51; Chiari without syrinx mean age 6.59 years, SD = 4.66; P = 0.45). Random Forest analysis for all ages of patients demonstrated that cervical spine measurements (smaller C1-7 taper ratio, larger C6 spinal canal diameter, and larger C5 spinal canal diameter) were found to be associated with syrinx formation (Fig 3). Random Forest analysis for age 0-8 years also demonstrated that cervical spine measurements (larger C4-7 taper ratio, smaller C1-4 taper ratio, and smaller C1-7 taper ratio) were found to be associated with syrinx formation. Random Forest analysis for age 9-18 years however demonstrated both cervical spine and craniocervical measurements (larger odontoid retroversion and retroflexion angles, and larger C6 spinal canal diameter) were found to be associated with syrinx formation. Among Chiari I patients with a syrinx, a larger C7 spinal canal diameter was found to have a positive correlation to the syrinx size ($r=0.37$; $p = 0.0008$) and was also the most significant factor for syrinx size by Random Forest analysis.
Conclusions
Among pediatric patients with Chiari I malformation, both craniocervical junction and cervical spine anatomy may contribute to the formation and size of the spinal cord syrinx.

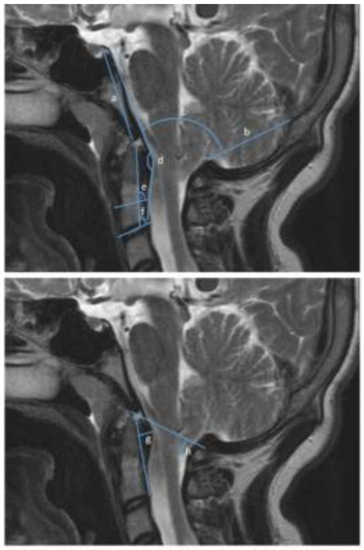

Fig 1. Craniocervical junction measurements: a) clivus length, b) supraoccipital length, c) clivus supraoccipital angle , d) clivus spine angle, e) odontoid retroflexion angle, f) odontoid retroversion angle, g) pB-C2 line, h) tonsillar position

Fig 2. Cervical spinal canal diameters at C1 through C 7 levels

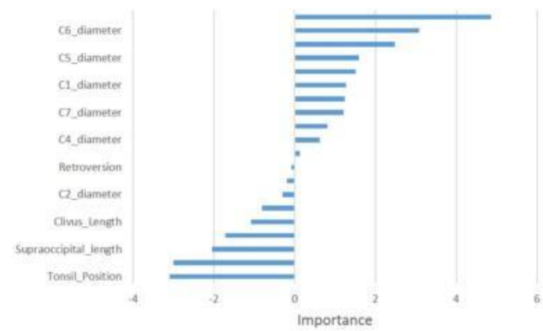

Fig 3. Importance levels of anatomic measurements for presence of syrinx by Random Forest analysis: one out of 500 runs performed is presented here.

(Filename: TCT_2539_Chiaripicture.jpg)

2531

3:16PM - 3:23PM

Increased notching of the corpus Callosum in Fetal Alcohol Spectrum Disorder: A Callosal misunderstanding?

E Schneble[1], C Lack[2], M Zapadka[2], J Cagley[3], O Obayashi[1], D Howard[1], D Pettersson[1], R Barajas[1], D Ross[1], J Pollock[1]
[1]Oregon Health & Science University, Portland, OR, [2]Wake Forest School of Medicine, Winston Salem, NC, [3]University of Wisconsin-Madison, Madison, WI

Purpose
Fetal alcohol spectrum disorders (FASD) have historically been associated with abnormalities of the corpus callosum (CC). In the medico-legal literature, notching of the CC has been claimed to be associated with FASD. We sought to compare the prevalence of notching of the CC in a FASD population and compare it to a radiographically normal population to determine if notching occurs with increased frequency in the FASD population.
Materials and Methods
We performed a multi-center medical record search for cases of fetal alcohol syndrome disorders (FASD) and included all patients who had a sagittal T1 weighted brain MRI. Any patients with concomitant intracranial pathology were excluded. The CC was examined for notches using a standard method developed with the normal population. Data from each center was anonymous and combined. A Fisher's exact test was used to compare the FASD and normal groups.
Results
23 FASD patients (ages 0-32 years) with MRI imaging were identified that met all inclusion and exclusion criteria. Two notches of the anterior CC were identified in the FASD group (prevalence 8.7%). Six patients had a posterior CC notch (prevalence 26%). In the normal population, the anterior notch prevalence was (117/778) 15%, and the posterior notch prevalence was (337/778) 43%. There was no significant difference between the anterior (p=0.5582) and posterior (p=0.1338) notch prevalence in the

FASD and normal groups. Normal patients were 95% more likely to have a posterior notch and 80% more likely to have an anterior notch than the FASD group.
Conclusions
In our multi-center study population, there is no significant difference in notching of the corpus callosum between patients with FASD and a normal population. Although historically thought to be a marker of FASD, notching of the corpus callosum should not be viewed as a specific finding associated with FASD.

3433

3:23PM - 3:30PM

Nodular Heterotopia: Prevalence and Significance in Typically Developing Adolescents

Y Li[1], R Nillo[1], M Olaru[1], R Tanikella[1], R Desikan[1], A Pfefferbaum[2], L Sugrue[1]
[1]*University of California San Francisco, San Francisco, CA,* [2]*SRI International, Menlo Park, CA*

Purpose
The Adolescent Brain and Cognitive Development (ABCD) study, the largest longitudinal study of brain development and child health in the united states, offers a unique opportunity to define the true prevalence of incidental findings in brain structural MRI in a representative cross section of typically-developing children. Moreover, the rich data set collected about these study subjects allows us to explore the significance of such findings with respect to health and developmental history, neurocognitive performance, and quantitative measures of brain structure and function. Here we apply this approach to the most common malformation of cortical development – periventricular nodular heterotopia – whose prevalence and significance in normally developing children is poorly understood.
Materials and Methods
We evaluated 4,512 structural brain MRIs of typically developing children aged 9-10 years enrolled in the ABCD study. Imaging consisted of 3D T1 and T2 sequences acquired at 3T using a standard protocol, reformatted in 3 planes, and anonymized to patient demographic factors. Each study was reviewed by a board certified, fellowship-trained neuroradiologist for incidental findings, such as periventricular nodular heterotopia (PVNH). Using data from the ABCD baseline medical and developmental questionnaires, we determined each subject's history of seizures and prenatal substance exposure. Using the FreeSurfer software package (version 5.3) we calculated the cortical volume, thickness, and area of 33 regions in each hemisphere for each subject. We subsequently used multivariate regression models to examine the relationship between each of our measures – seizure history, developmental exposure, and regional cortical morphology – with the presence or absence of PVNH while controlling for age, sex, and other confounding factors.
Results
In the 4,512 subjects contained within the first ABCD data release, we found 44 cases (1% prevalence) of PVNH. There was no increased history of seizures in subjects with PVNH compared to those without. However, subjects with PVNH did have a significantly increased risk of maternal exposure to alcohol or tobacco in early pregnancy. Moreover, subjects with PVNH showed statistically significant differences in cortical volume and thickness in multiple areas including: left inferior parietal lobule, right middle temporal gyrus, right parahippocampal gyrus, right pars opercularis and right post central gyrus ($p<0.05$). These regions corresponded to the areas of cortex overlying the ventricular regions where PVNH was most likely to occur.
Conclusions
In a large sample of over 4,512 typically developing 9- and 10-year old children representing a broad cross section of the US population we identified a 1% prevalence of PVNH. Interestingly, at this age, the presence of PVNH was not associated with an increased history of seizures. However, PVNH was associated with prenatal exposure to alcohol and tobacco in the first trimester and with subtle systematic variations in brain morphology, such as differences in the volume and thickness of multiple cortical regions. Our approach revels the power of large comprehensive neuroimaging studies such as ABCD to

determine the significance of common gross structural imaging findings through their association with developmental history, health/neurocognitive factors, and quantitative structural and functional brain imaging measures.

2482

3:30PM - 3:37PM

Postnatal Intracranial Findings Following Fetal Repair of Spinal Dysraphisms: A Retrospective Review

S Calle[1], E Bonfante-Mejia[2], G Simmons[3], J Rogers[4], C SITTON[5], K Hughes[6], S Fletcher[7], R Riascos[8], R Patel[9]

[1]The University of Texas Health Science Center at Houston, Houston, TX, [2]UNIV. OF TEXAS HEALTH SCIENCE CENTER, HOUSTON, TX, [3]UT Houston, Houston, TX, [4]UNIVERSITY OF TEXAS HEALTH SCIENCES CENTER AT HOUSTOIN, Houston, TX, [5]UNIVERSITY OF TEXAS - HOUSTON MEDICAL SCHOOL, HOUSTON, TX, [6]The University of Texas Health Science Center at Houston UTHealth, Houston, TX, [7]University of Texas Health Science Center at Houston, Mischer Neuroscience Institute, Houston, TX, [8]UTHSC-Houston, Houston, TX, [9]THE UNIVERSITY OF TEXAS HEALTH SCIENCE CENTER, HOUSTON, HOUSTON, TX

Purpose

Studies have documented that patients that undergo fetal repair of spinal dysraphisms demonstrate improvement in hindbrain herniation relative to those with postnatal repair(1,2). However, other classic features of Chiari II malformation persist despite reversal of the tonsillar herniation. This contradictory appearance represents an obstacle for the radiologist. Our objective is to document the imaging appearance in the intracranial compartment at the time of the infants' first postnatal brain MR imaging, with an emphasis on the evolution with respect to the fetal MRI.

Materials and Methods

IRB-approved retrospective evaluation of patients having undergone fetal repair for open spinal dysraphism at our institution. 29 patients had both fetal MRI and at least one postnatal brain MRI available for review. The fetal MRI and the infants' postnatal brain MRI were reviewed for features of Chiari II malformation.

Results

Tonsillar ectopia on fetal MRI ranged from C1 to C6. On postnatal brain imaging, 16/29 infants had resolution of the ectopia. 18 infants showed an outpouching of the thecal sac between the opisthion and the posterior arch of C1. On postnatal imaging, 27/29 patients had a prominent massa intermedia, 27/29 of infants had tectal beaking, 16/29 had a towering cerebellum, 26/29 showed flattening of the fourth ventricle, 28/29 had a low-lying torcula, 19/29 had a heart-shaped incisura, and 17/29 had tonsillar atrophy.

Conclusions

The combination of normally-positioned or minimally descended, oftentimes atrophic cerebellar tonsils in the presence of a posterior fossa configuration typical of Chiari II, can be considered characteristic of infants following fetal repair. An additional feature that may alert the radiologist is an outpouching of the dorsal thecal sac between the opisthion and the posterior arch of C1. To our knowledge, this feature has not previously been described and was present in 62% of our patients.

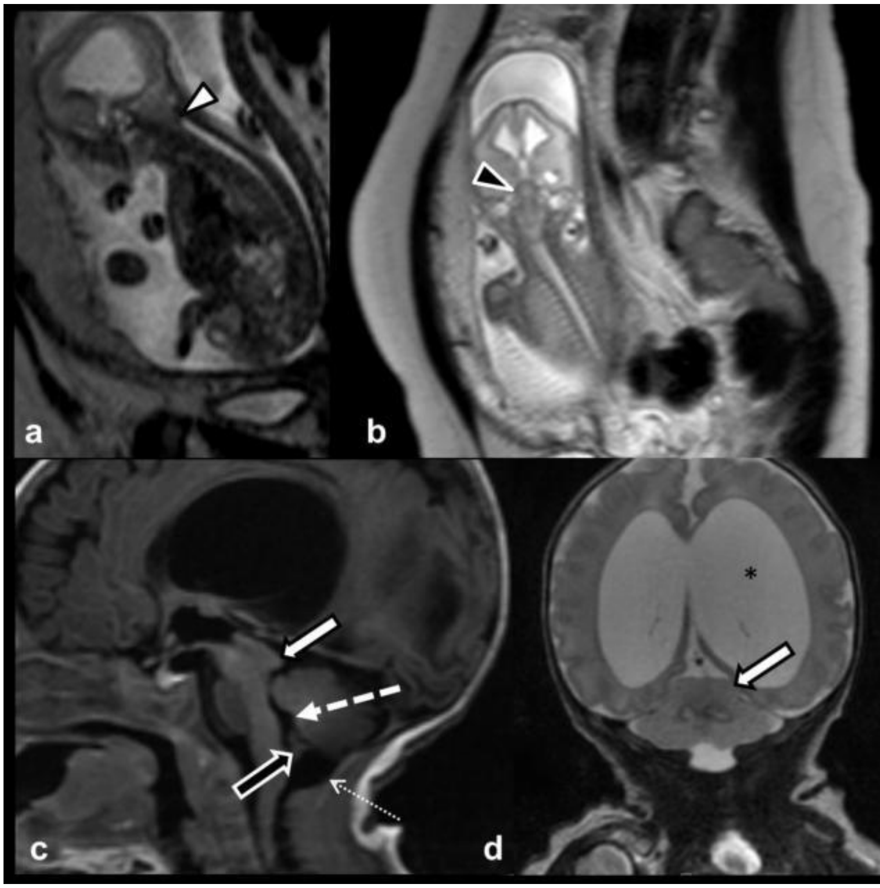

(a) Fetal MRI, sagittal T2WI of the fetus shows tonsillar herniation at the level of C6 (white arrowhead). **(b)** Fetal MRI, coronal T2WI of the fetus demonstrates a towering cerebellum (black arrowhead). **(c)** Sagittal T1WI of the brain of the same patient after delivery shows tectal beaking (white block arrow), flattening of the fourth ventricle (white dashed arrow) and normally-positioned atrophic tonsils (black block arrow). A small CSF-containing outpouching of the dorsal thecal sac is seen between the opisthion and the posterior arch of C1 (dotted arrow). **(d)** Coronal T2WI shows persistence of the towering cerebellum (white block arrow) as well as enlargement of the ventricular system (asterisk).

(Filename: TCT_2482_FigureforASNR.JPG)

2981

3:37PM - 3:44PM

Postnatal Spine Findings Following Fetal Repair of Spinal Dysraphism: A Retrospective Review

J Rogers[1], C SITTON[2], G Simmons[3], S Calle[4], K Hughes[5], S Fletcher[6], R Riascos[4], R Patel[7], E Bonfante-Mejia[8]
[1]UNIVERSITY OF TEXAS HEALTH SCIENCES CENTER AT HOUSTON, Houston, TX, [2]UNIVERSITY OF TEXAS - HOUSTON MEDICAL SCHOOL, HOUSTON, TX, [3]UT Houston, Houston, TX, [4]The University of Texas Health Science Center at Houston, Houston, TX, [5]The University of Texas Health Science Center at Houston UTHealth, Houston, TX, [6]University of Texas Health Science Center at Houston, Mischer Neuroscience Institute, Houston, TX, [7]THE UNIVERSITY OF TEXAS HEALTH SCIENCE CENTER, HOUSTON, HOUSTON, TX, [8]UNIV. OF TEXAS HEALTH SCIENCE CENTER, HOUSTON, TX

Purpose
In utero repair for open neural tube defects is becoming increasingly common, but most imaging studies have focused on changes in the posterior fossa. We present post-natal spine imaging findings observed post in-utero repair of open NTD, relating findings to the pre-repair morphology.
Materials and Methods
IRB-approval was obtained to perform retrospective evaluation of 73 consecutive patients having undergone in utero neural tube defect closure at our institution. 25 had both fetal MRI and at least one postnatal spine US (3) or MRI (22) for review. A consensus read of 18 myelomeningoceles and 7 myeloschisis was obtained between one neuroradiology fellow and one faculty with 15 years of

experience. Fetal MRI was reviewed for the type, level, and span of spinal dysraphism and checked against the operative report. Postnatal imaging was evaluated for the position of the conus, syrinx, tethering, and miscellaneous findings.

Results

For small MMC with relatively little neural tissue contained in the sac, imaging was often characterized by adhesion of the conus to the repair with a small area of direct contact or thin bands. The conus often had a bulbous appearance with some thinning of the cord proximally. There was a low incidence and severity of syrinx and complicating cysts. In patients with more extensive MMC defects, containing larger amounts of neural tissue, there was often multi-focal and broad-based physical contact of the cord/conus to the patch itself. Cysts of variable complexity were frequently present within the filum and/or the conus. On those patients with follow-up examinations, these cysts increased in size. Associated syringomyelia tended to be more severe and progress over time. Myleoschesis patients tended to look more similar to those with severe MMC. Several of them had a distinctive series of hemosiderin lined cysts replacing the conus with tethering to the distal sacral canal.

Conclusions

The post-natal appearance in these patients can be quite variable depending on the type of defect originally present. Radiologists should be aware of the range of imaging findings, in order to facilitate the identification and communication of unexpected findings.

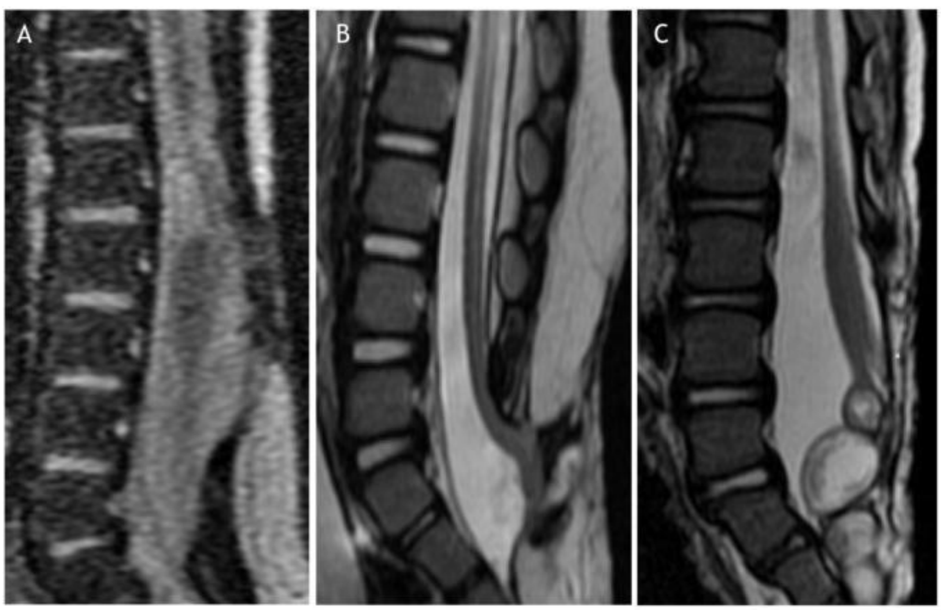

Figure 1. Three distinct imaging patterns seen in patients status-post in utero repair of spinal open neural tube defect.
A. Post-natal MRI s/p fetal repair of a small MCC showing an enlarged and bulbous conus with thinning of the adjacent cord. Thin T2 hypointense band tethering the cord was seen on axial images.
B. Post-natal MRI showing broad-based tethering of the dorsal conus/neural placode to the patch and adjacent repaired tissues.
C. After in utero myeloschisis repair post-natal MRI showing complex cysts in the filum and near the conus, which grew on follow-up.

(Filename: TCT_2981_FetalRepairSpine.jpg)

3122

3:44PM - 3:51PM

Structural and Functional Alterations in Language-related Brain Regions for Children with Non-syndrome Cleft of Lip with or without Palate (NSCL/P)

H Cheng[1], B Rao[2], Y Fan[3], W Zhang[4], Y Peng[2]

[1]*Beijing Children's Hospital ,Captital Medical University, Beijing, beijing,* [2]*Beijing Children's Hospital, Capital Medical University, Beijing, Beijing,* [3]*MR Research China, GE Healthcare, Beijing, Beijing,* [4]*Beijing Stomatological Hospital, Capital Medical University, Beijing, Beijing*

Purpose
To explore whether the aberrant phonology cognition and articulation behavior may induce the neuroplastic changes[1] in language-related regions for NSCL/P children using multimode MR imaging.
Materials and Methods
A total of 25 children with NSCL/P and 25 gender- and age-matched healthy controls underwent 3D T1w images and rs-fMRI examinations. Preprocessing steps were conducted using the CAT12 and DPARSFA software. The parameters of surface-based morphometry and local spontaneous brain activities were computed and between-group differences were assessed using two-sample t-tests (corrected $p < 0.05$). Besides, the correlations between values of all those parameters and Chinese language clear degree scale (CLCDS) were calculated.
Results
Both structural related parameters (CT: cortical thickness and GI: gyrification index) and functional related parameter (ALFF: amplitude of low frequency fluctuations) showed significant between-group differences in distributed cortical regions (see Fig.1). Increased CT values were demonstrated in left IFG, PreCG, PostCG, SFG, MOG, LO, STG, planum polare and fusiform (Fig.1 a). Moreover, increased GI values were found in left PreCG, PostCG, insula, IFG, PMC (Fig.1 b). For functional parameters, decreased ALFF were detected in left MTG, OC, PostCG, PC and TC, fusiform and increased ALFF values were found in left ITG and fusiform (Fig.1 c). Besides, right TC and cuneus showed decreased ALFF values. There was a significant negative correlation between the ALFF values of bilateral frontal poles and CLCDS (Fig.2, $r=-0.66$, $p<0.05$). These regions are mainly in the dorsal stream of language network responsible for phonological processing[2] and the frontal pole guided goal-directed behavior effectively[3].
Conclusions
Multimode MR imaging could be used to detect the aberrant structural and functional alterations in the language-related brain regions for NSCL/ P children. The CT, GI and ALFF values could be the potential imaging biomarkers for the plastic changes of language network for children with NSCL/ P.

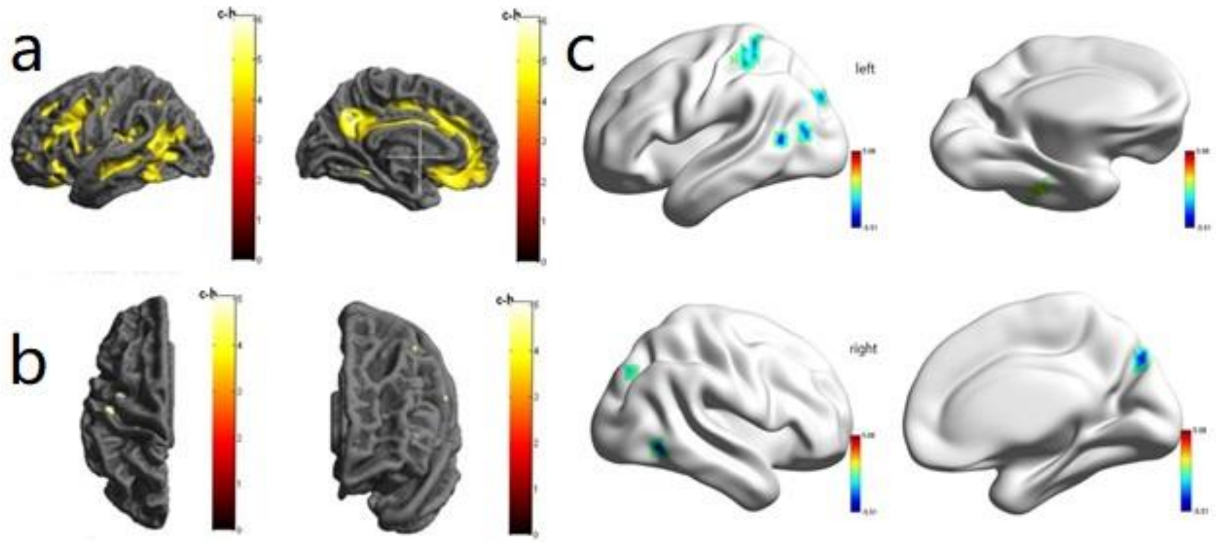

Figure.1 Cortical regions revealed significant between-group differences of CT (a), IG (b) and ALFF (c) (GRF corrected $p < 0.05$).

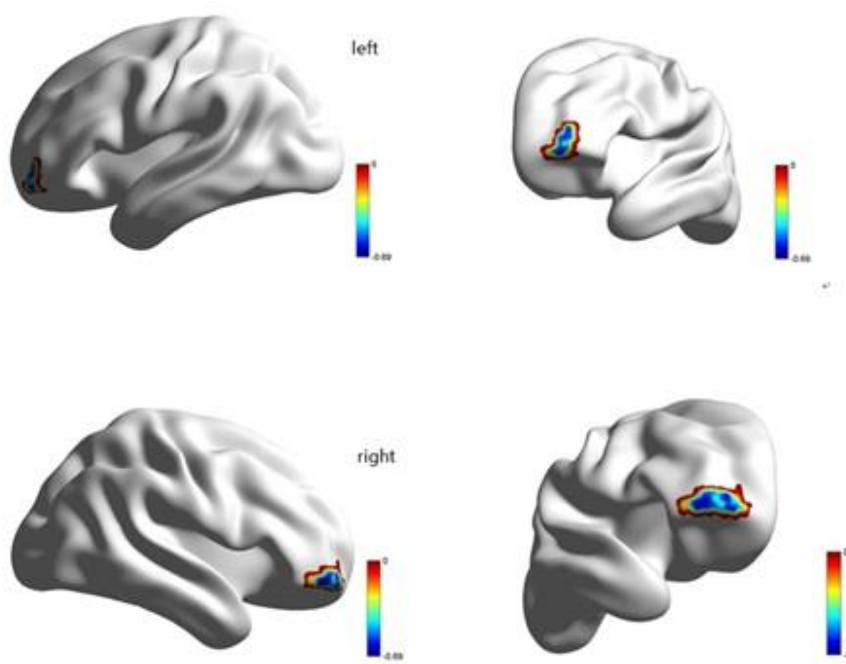

Figure.2 Significant negative correlation between the ALFF values of the bilateral frontal pole and CLCDS ($r=-0.66$, GRF corrected $p < 0.05$).

(Filename: TCT_3122_558693676132873303.jpg)

3350

3:51PM - 3:58PM

Structural Imaging Phenotype of XYY Chromosomal Aneuploidy

S Sotardi[1], L Bloy[2], T Roberts[3]

[1]The Childrens Hospital of Philadelphia, Philadelphia, PA, [2]Childrens Hospital of Philadelphia, Philadelphia, PA, [3]THE CHILDREN'S HOSP. OF PHILADELPHIA, PHILADELPHIA, PA

Purpose

XYY syndrome is a sex chromosome aneuploidy, with affected individuals frequently demonstrating cognitive and behavioral deficits, as well as high rates of autism spectrum disorder (ASD), (1). The relationship between structural imaging abnormalities and patients with XYY has not been previously comprehensively investigated. In this work, we investigate imaging alterations of patients with XYY chromosomal aneuploidy.

Materials and Methods

This study was performed with IRB approval. Thirteen patients with XYY chromosome aneuploidy without ASD diagnosis (mean age 12.8 years), and nineteen patients with XYY chromosome aneuploidy and with ASD diagnosis (mean age 13.5 years), as well as nineteen unaffected noncarrier control participants (mean age 12.9 years), were imaged on a 3T Siemens MRI machine. For the purposes of this study, our analysis was constrained to the structural T1 weighted sequence and multiplanar reconstructions. Statistical analysis was performed using the Chi-square test in Excel (Microsoft).

Results

The corpus callosum (CC) demonstrated an abnormal morphology in 38.5% ($p \leq 0.018$) of patients with XYY chromosome aneuploidy and without ASD diagnosis, when compared with healthy controls. We also found that the CC, particularly the body of the CC, was thin in 23.1% ($p \leq 0.028$) of patients with XYY chromosome aneuploidy and without ASD diagnosis. These findings are depicted in Figure 1.

Conclusions

We demonstrate alterations in the corpus callosum associated with XYY aneuploidy, when compared with healthy controls. These changes in the corpus callosum have important implications for interhemispheric connectivity. Abnormalities in white matter development, particularly within the corpus callosum, have been previously described in autism spectrum disorders (2-4). However, the relationship of an atypical CC in our XYY population does not appear related to the presence or absence of the ASD diagnosis and may be related to the genetics of XYY. Future work will investigate the electrophysiological and cognitive outcomes in the XYY group.

Figure 1.

	Abnormal CC	p value	Thin CC	p value
Healthy Controls	5.3%	-	0%	-
XYY without ASD	38.5%	0.0181	23.1%	0.0278
XYY with ASD	31.6%	0.0364	21.1%	0.0344
XYY with & without ASD	34.4%	0.0178	21.9%	0.0281

(Filename: TCT_3350_Presentation1.jpg)

2903

3:58PM - 4:05PM

The role of fetal MRI for evaluating brain pathology in fetuses with Abnormal Chromosomal Microarray Analysis

Y Weissbuch[1], E Katorza[2], C Hoffmann[2], S Shrot[1]
[1]Sheba Medical Center, Ramat-Gan, Israel, [2]Sheba Medical Center, Ramat-Gan, AK

Purpose
Chromosomal microarray analysis (CMA) is rapidly increasing as fetal chromosomal assessment tool, resulting in an increasing demand for fetal MRI in search of brain abnormalities. Our objective was to assess the value of fetal brain MRI (fbMRI) over detailed fetal sonography for detection of brain pathology in fetuses with CMA abnormalities.
Materials and Methods
Records of pregnant women referred to fbMRI due to CMA abnormalities were retrospectively reviewed for imaging findings on fbMRI and brain ultrasonography and for CMA results. CMA findings were classified as either high probability (i.e. associated with known clinical significance) or variant of unknown significance (VOUS). Patients with abnormal karyotype were excluded from our study.
Results
Fifty fbMRI studies were performed following abnormal CMA results between 2012-2018 (1.5% of all studies). In 5 fetuses (10%), novel findings were found on fbMRI, i.e. white matter T2-hyperintensities (3), dysplastic corpus callosum (1), facial abnormalities (1) and delayed gyration pattern (1). Of these, only one CMA was classified as high probability and 4 were classified as VOUS. In 13 fetuses (26%), fbMRI findings matched known sonography findings, i.e. dysplastic corpus callosum, enlarged cisterna magna, asymmetric ventricular size or mild ventriculomegaly. In 32 fetuses (64%), fbMRI was found to be normal. None of the fetuses showed cortical migration or organization abnormalities.
Conclusions
FbMRI confirmed known sonographic findings and discovered novel findings in fetuses with CMA abnormalities. The most common novel findings were non-specific white matter signal hyperintensities. Further studies are needed to quantify and correlate these imaging findings with long term outcomes.

Tuesday, May 21, 2019
2:55PM - 4:25PM
Radiomics and Extra-Axial Lesions

3555

2:55PM - 3:02PM

Comparison of MRI and Histology Radiomics in Glioblastoma

S Bobholz[1], A Lowman[2], J Connelly[2], S McGarry[2], J Bukowy[2], A Nencka[2], A Barrington[2], P LaViolette[2]
[1]Medical College of Wisconsin, Wauwatosa, WI, [2]Medical College of Wisconsin, Milwaukee, WI

Purpose
Radiomic features of MR images have recently been shown to be predictive of prognosis and phenotypic variation in glioblastoma. However, little is known about the underlying tissue properties that manifest as macroscopic textures measurable with radiomics. This study compares MRI derived radiomic features to large tissue samples acquired at autopsy to quantitatively establish a histological basis.

Materials and Methods

Two patients recruited for brain donation following treatment for glioblastoma were included in this study. The whole brain samples were sliced in the same orientation as the axial clinical imaging using patient specific 3D-printed slicing jigs. Large tissue specimens were acquired from regions suspicious of tumor. H&E stained histology slides images were registered to MR space and down-sampled to the MRI resolution. Pyradiomics v2.1.0 was used to calculate first order statistics, gray level co-occurrence matrix features, gray level run length matrix features, gray level size zone matrix features, neighboring gray tone difference matrix features, and gray level dependence matrix features for both the down-sampled histology and for the T1+C image. Features were calculated for tiles of the ROI (8 voxels by 8 voxels with 2 voxel overlap in each direction) in addition to the whole ROI in order to observe the preservation of radiomic features at different scales. Kendall's tau rank correlations between the histological and MR radiomic feature were calculated.

Results

Tile-based results showed widespread correlations between the histology and MR radiomic features across all feature sets, with nearly all features demonstrating correlation. ROI-based results also demonstrated several correlations between histology and MR radiomic features, though less ubiquitously than with the tile-based results.

Conclusions

These findings indicate that histological radiomic features of glioblastoma tissue are reflected in the radiomic features of T1+C MRI, suggesting that the MR radiomic features capture histological information, potentially relevant to prognostic predictions.

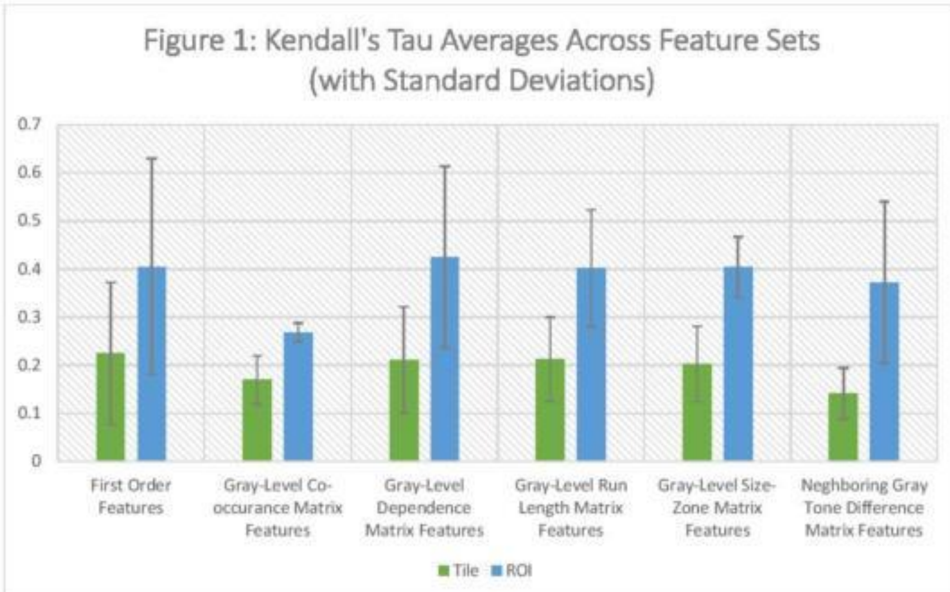

Figure 1: Kendall's Tau Averages Across Feature Sets (with Standard Deviations)

Feature Set	Tile-Based Correlations	ROI-Based Correlations
First Order	17 of 19	9 of 19
Gray-Level Co-Occurrence Matrix	15 of 24	7 of 24
Gray-Level Dependence Matrix	12 of 16	6 of 16
Gray-Level Run Length Matrix	14 of 16	7 of 16
Gray-Level Size Zone Matrix	14 of 16	7 of 16
Neighboring Gray Tone Difference Matrix	4 of 5	2 of 5

Table 1: Proportion of Tile-Based and ROI-Based radiomic features with significant correlation between MR and histology.

(Filename: TCT_3555_Figures_for_HistRad-page-001.jpg)

3272

3:02PM - 3:09PM

Utility of Microhemorrhage as a Diagnostic Tool in Distinguishing Vestibular Schwannomas from Other Cerebellopontine Angle (CPA) Tumors

L Pisani[1], J Aristizabal[2], F Contreras[3], R Bhatia[1], C Sidani[1], G Saigal[1]
[1]University of Miami Miller School of Medicine, Miami, FL, [2]University of Antioquia, Medellin, South America, [3]Jackson Memorial Hospital, Miami, FL

Purpose
Although a majority of tumors in the Cerebellopontine Angle (CPA) are vestibular schwannomas (VS), other masses can also be seen in the region and differentiation of various CPA tumors can be difficult on imaging alone. Treatment options may vary based on the specific pathology of the CPA tumor. In this study, we evaluate to see if the presence of microhemorrhage can serve as an useful tool in differentiating VS from other CPA masses.

Materials and Methods
Retrospective review of all Cerebellopontine Angle (CPA) masses in the last 3 years in a single institution was performed. All tumors included had pathology-proven diagnosis and at least 1 pre-treatment MRI. The studies were reviewed by three blinded neuroradiologists and the statistical analysis was done using SPSS and Fischer Exact Test. Depending in the availability, either T2-weighted gradient-echo (GRE) or susceptibility weighted imaging (SWI) was used to assess presence of microhemorrhage within the mass. All cases without a GRE or SWI were excluded from the analysis.
Results
There were a total of 37 CPA masses, of which 20 patients were females as 17 were males. Vestibular Schwannoma (VS) was diagnosed in 25 cases (67.5%). Other CPA masses, which were seen, were meningiomas, metastasis, lipomas, epidermoid tumors, paragangliomas and chondrosarcomas. The percentage of Schwannomas which demonstrate microhemorrhage (sensitivity) was 64.0%. All masses, however, which demonstrated microhemorrhage were pathologicaly proven as VS (specificity of 100%). The results were significant at $p<.01$(statistic value of .0002).
Conclusions
Although difficult to differentiate CPA tumors on imaging alone, presence of microhemorrhage can serve as an extremely useful tool for the noninvasive diagnoses of VS. When seen, microhemorrhage was found to be 100% specific for VS.

3288

3:09PM - 3:16PM

Comparison of Signal Changes in Cochlea on Fluid-Attenuated Inversion Recovery (FLAIR) and 3D Constructive Interference in Steady State (CISS) Imaging in Patients with Cerebellopontine Angle (CPA) Masses with Internal Acoustic Canal (IAC) Component

G Saigal[1], L Pisani[2], J Aristizabal[3], F Contreras[4], R Bhatia[2], C Sidani[2]
[1]University of Miami/Jackson Memorial Hospital, Miami, FL, [2]University of Miami Miller School of Medicine, Miami, FL, [3]University of Antioquia, Medellin, South America, [4]Jackson Memorial Hospital, Miami, FL

Purpose
The correlation between alterations of signal intensity in the cochlea and the degree of hearing loss in patients with Vestibular Schwannomas (VS) has been described in literature. High signal intensity on FLAIR and low T2 signal on 3D CISS have been associated with a decreased prognosis in hearing. The cause of the hearing loss has been hypothesized to be due to an increase in protein concentration caused by stasis in the perilymph within the cochlea. Our purpose is to compare the signal changes on FLAIR and 3D CISS sequences within the cochlea in patients with CPA masses with an IAC component.
Materials and Methods
Retrospective review of pathology-proven tumors located on the Cerebellopontine Angle (CPA), in a single institution. All tumors had pathology-proven diagnosis and at least 1 pre-treatment MRI. The studies were reviewed by three blinded neuroradiologists. FLAIR and 3D CISS sequences were used to assess the signal changes within the cochlea on the affected side. Comparison was made with the signal within the cochlea on the normal contralateral side.
Results
There were 47 patients with a CPA tumor, 39 of whom had an IAC component and eight were extra meatal. High FLAIR signal in the cochlea was seen in 30 of the 39 patients (76.9%) and low T2 CISS signal was seen in only 11 of these 39 cases (28.2%). All cases of CPA tumors with an IAC component and low signal intensity on CISS (11 in number) also had high signal intensity on FLAIR. Of the CPA masses with the extra meatal component, only 1 case showed high FLAIR signal intensity and without low T2 signal on the CISS sequence, within the cochlea.

Conclusions
In patients with CPA masses with an IAC component, FLAIR imaging has a higher sensitivity than CISS imaging in assessing signal changes within the cochlea.

3284

3:16PM - 3:23PM

Incidence of Microhemorrhage in Cystic Vestibular Schwannomas in the Cerebellopontine angle.

L Pisani[1], J Aristizabal[2], F Contreras[3], R Bhatia[1], C Sidani[1], G Saigal[1]
[1]University of Miami Miller School of Medicine, Miami, FL, [2]University of Antioquia, Medellin, South America, [3]Jackson Memorial Hospital, Miami, FL

Purpose
It has been reported that presence of microhemorrhage is a highly specific indicator for the diagnosis of a Vestibular Schwannoma (VS). Cystic schwannomas are a subtype vestibular schwannomas with a dominant cystic components within the mass. The purpose of the study is to evaluate for the incidence of microhemorrhage in cystic subtype of VS.
Materials and Methods
Retrospective review of all Cerebellopontine Angle (CPA) masses in the last 3 years in a single institution was performed. All tumors included had pathology-proven diagnosis of VS and at least 1 pre-treatment MRI. The studies were reviewed by three blinded neuroradiologists. Depending on the availability, T2-weighted gradient-echo (GRE) or susceptibility weighted imaging (SWI) was used to assess the presence of microhemorrhage. All cases without a GRE or SWI were excluded from the analysis
Results
There were a total of 37 CPA masses, of which 20 patients were females as 17 were males. Vestibular Schwannoma (VS) was diagnosed in 25 cases. Of the VS's, there were 9 Cystic VS. Seven (77.7%) of these presented with underlying microhemorrhage. No hemorrhage was noted in two of the VS's (22.3%).
Conclusions
When seen, presence of microhemorrhage is highly predictive of a Vestibular Schwannoma. It is important to note however, that not all Vestibular Schwannomas, show microhemorrhage. In this study, greater than 20% of the cystic subtype of VS did not show the presence of microhemorrhage.

3568

3:30PM - 3:37PM

Comparison of MRI Radiomics and Histological Features in Glioblastoma

S Bobholz[1], A Lowman[2], J Connelly[2], S McGarry[2], J Bukowy[2], A Nencka[2], A Barrington[2], P LaViolette[2]
[1]Medical College of Wisconsin, Wauwatosa, WI, [2]Medical College of Wisconsin, Milwaukee, WI

Purpose
Recent studies of glioblastoma radiomics have found that specific features and radiomic features of gadolinium enhanced T1-weighted MRI (T1+C) possess predictive utility regarding prognosis and phenotype. However, there has been little research investigating a biological candidate for the pathologically relevant information the radiomic measures are able to capture. Therefore, this study tested the hypothesis that radiomic features of T1-weighted MR images would be predictive of histological tissue features in glioblastoma tissue.
Materials and Methods
Two glioblastoma patients recruited for brain donation were included in this study. The whole brain samples were sliced axially to match T1+C clinical imaging using patient specific 3D-printed slicing jigs. Tissue specimens were acquired from regions suspicious of tumor, H&E stained, and registered to MR space. After registration of the histological slices to MR space, manually drawn regions of interest (ROI)

were used to highlight the areas of the tissue with relevant histological information. The masked ROIs were also split into tiles (8 voxel by 8 voxel with 2 voxel overlap) in order to compare the relationship between radiomic and histological features at different scales. Pyradiomics v2.1.0 was used to generate radiomic features for each tile and each ROI, and the voxelwise average of the extracellular fluid (ECF) and cellularity of the ROIs/tiles were calculated. Kendalls' tau rank coefficients were used to evaluate the correlation between the histological statistics and radiomic features using a significance threshold of $p < 0.001$.

Results

The tile-based results demonstrated several histological statistics correlating with radiomic features across feature sets, with stronger correlations in ECF than cellularity. The ROI-based results mirrored the tile-based results, with the exception of no significant correlations between ROI-based radiomics and cellularity observed, though several factors trended towards significance.

Conclusions

These results suggest that the prognostic utility of MR radiomics may be a result of its ability to capture histologically relevant features. The absence of cellularity correlations in ROI-based analysis could be a result of texture heterogeneity of the ROI, as well as a matter of sample size, as the trending factors had tau coefficients similar to the tile-based results.

Figure 2: Kendall's Tau Averages Across Feature Set Correlations with Cellularity (with Standard Deviation)

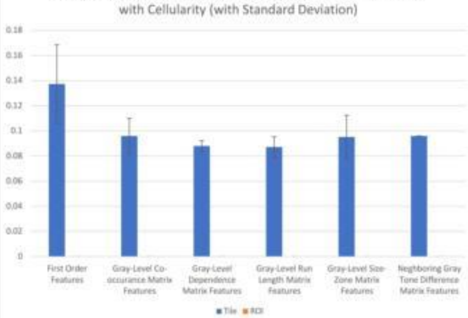

Feature Set	Tile-Based Correlations	Tile-Based Trends	ROI-Based Correlations	ROI-Based Trends
First Order	10 of 19	6 of 19	0 of 19	6 of 19
Gray-Level Co-Occurrence Matrix	6 of 24	3 of 24	0 of 24	2 of 24
Gray-Level Dependence Matrix	2 of 14	4 of 14	0 of 14	2 of 14
Gray-Level Run Length Matrix	5 of 16	4 of 16	0 of 16	2 of 16
Gray-Level Size Zone Matrix	3 of 16	3 of 16	0 of 16	3 of 16
Neighboring Gray Tone Difference Matrix	2 of 5	2 of 5	0 of 5	1 of 5

Table 2: Proportion of Tile-Based and ROI-Based radiomic features with significant and trending correlation with cellularity. Trending is defined as $0.01 < p <= 0.001$.

Figure 1: Kendall's Tau Averages Across Feature Set Correlations with ECF (with Standard Deviation)

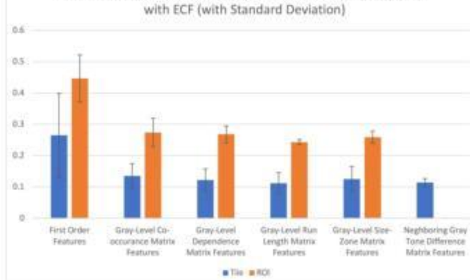

Feature Set	Tile-Based Correlations	Tile-Based Trends	ROI-Based Correlations	ROI-Based Trends
First Order	16 of 19	0 of 19	8 of 19	3 of 19
Gray-Level Co-Occurrence Matrix	17 of 24	0 of 24	2 of 24	5 of 24
Gray-Level Dependence Matrix	7 of 14	4 of 14	2 of 14	3 of 14
Gray-Level Run Length Matrix	13 of 16	1 of 16	3 of 16	3 of 16
Gray-Level Size Zone Matrix	12 of 16	1 of 16	3 of 16	2 of 16
Neighboring Gray Tone Difference Matrix	2 of 5	1 of 5	1 of 5	0 of 5

Table 1: Proportion of Tile-Based and ROI-Based radiomic features with significant and trending correlation with ECF. Trending is defined as $0.01 < p <= 0.001$.

(Filename: TCT_3568_merge_from_ofoct.jpg)

3293

3:37PM - 3:44PM

DTI Assessment of Optic Pathway Function in Patients with Anterior Visual Pathway Compression

K Kang[1], E Choi[2], W Jung[3], J Lee[3], S Choi[1], Y Kim[1]

[1]Seoul National University Hospital, Seoul, Seoul, [2]Laboratory for Imaging Science and Technology, Department of Electrical and Computer Engineering, Seoul, Seoul, [3]Seoul National University, Seoul, Seoul

Purpose
To investigated diffusion tensor imaging (DTI) features in the optic radiation according to the degree of visual disturbance in patients with masses around the anterior visual pathways
Materials and Methods
This study included fifty-six patients with mass around the anterior visual pathways. Participants were divided into patients with visual disturbance (23 males and 21 females, 50.45±14.87years) and patients without (4 males and 8 females, 36.50±15.80 years). Preoperative visual tract impairment score (VTIS) indicating the defected visual field was measured. A score range was zero to eight. If all part of unilateral optic tract became visual field defect, the score would be eight. All participants were scanned on a 3T including the multi-shell DTI. Regions of interest (ROIs) were drawn on each side of optic radiation. The ROI mask from the fractional anisotropy (FA) map was applied to mean diffusivity (MD), axial diffusivity (AD), and radial diffusivity (RD) maps. Analysis of covariance was used to compare the DTI features between patients with presence and absence of visual disturbance adjusting for age. Partial correlation analysis was used to assess the relationship between VTIS and DTI features in patients with visual disturbance adjusting for age.
Results
The FA, MD, and RD in optic radiations were significantly different between patients with and without visual disturbance. The FA was significantly decreased in patients with visual disturbance ($p<0.001$), while the MD and RD were significantly larger in patients with visual disturbance compared to patients without ($ps<0.05$). The FA demonstrated a significant negative correlation with VTIS ($p< 0.001$), while the MD and RD showed a significant positive correlation with the VTIS (MD $p<0.018$ and RD < 0.001).
Conclusions
DTI might be useful to evaluate the effects of mass around the anterior visual pathway on the white matter microstructural changes in the optic radiation.

2591

3:44PM - 3:51PM

Gallium-68-DOTATATE PET-MRI in Recurrent Meningioma: Correlation with DCE Perfusion Parameters

W Feltus[1], M Roytman[1], N Karakatsanis[1], R Magge[1], D Pisapia[1], J Osborne[1], T Schwartz[1], S Pannullo[1], J Ivanidze[1]
[1]New York Presbyterian Hospital/Weill Cornell Medicine, New York, NY

Purpose
Contrast-enhanced MRI is the gold standard in postoperative meningioma treatment planning and response assessment, especially in WHO-2 and -3 disease. However, MRI can have limited sensitivity in infiltrative or invasive lesions, and in the presence of posttreatment scarring. Pilot studies have found DCE perfusion MRI to have utility in meningioma. Meningiomas express high levels of somatostatin receptor 2. Ga-68-DOTATATE PET-CT has shown promise in the evaluation of meningiomas. Our purpose was to correlate Ga-68-DOTATATE PET-MRI findings to DCE perfusion parametric maps in patients with meningioma.
Materials and Methods
We performed a retrospective analysis in patients with suspected meningioma recurrence who underwent Ga-68-DOTATATE PET-MRI with DCE perfusion. Tumor volumes were segmented on volumetric T1-postcontrast sequence and superimposed transposed onto parametric DCE maps. PET acquisition was performed in 3D list mode for 40 minutes, and MR-based attenuation correction was applied. Perfusion parameters including, area under curve (AUC), rate efflux constant (KEP), transfer constant (KTRANS), time of peak enhancement (TME), volume fraction of the extravascular extracellular space (VE) in tissue, volume fraction of plasma in tissue (VP), (WASHIN), (WASHOUT) were recorded. Pearson's correlation

analyses were performed to assess correlation between Ga-68-DOTATATE PET-MRI SUVmax and DCE-derived perfusion parameters.
Results
8 patients (WHO-I, N=3; WHO-II, N=2; WHO-III, N=3) with a total of 11 meningiomas were included in this retrospective study. Ga-68-DOTATATE SUVmax values demonstrated a strong positive correlation with Vp ($r = 0.8779$; $p = 0.0004$) and WASHIN ($r = 0.8411$; $p = 0.0012$), and a moderate positive correlation with WASHOUT ($r = 0.6296$, $p = 0.0379$).
Conclusions
We present the first evaluation of Ga-68-DOTATATE PET-MRI and DCE perfusion imaging in meningioma. Limitations include the pilot character and small sample size of our study. Our future work will focus on exploring the clinical significance of this multimodal imaging approach to recurrent meningioma.

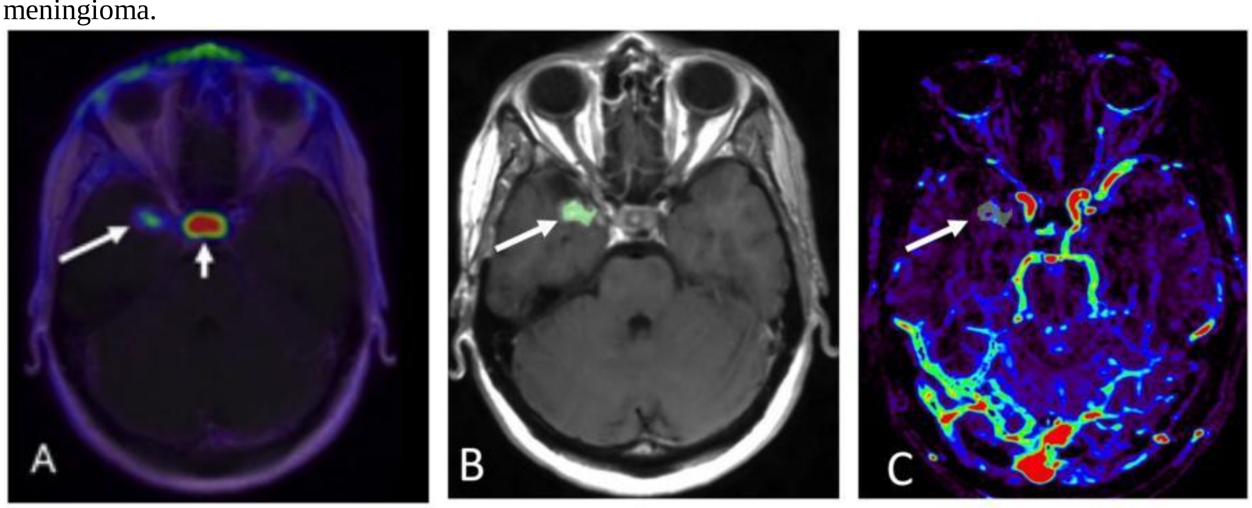

Ga-68-DOTATATE PET-MRI correlates to DCE perfusion/ permeability parameters. A. PET/MRI demonstrating a focus of Ga-68-DOTATATE avidity in the right middle cranial fossa (long arrow); physiologic uptake is noted in the pituitary gland (short arrow). B. Conventional T1-postcontrast MRI with volumetric segmentation of nodular enhancement (green overlay and arrow). C. VP DCE perfusion MRI parametric map with superimposed postcontrast-T1-derived segmentation overlay (green) for subsequent measurement of permeability parameters. Preliminary analysis in 11 meningiomas from 8 patients demonstrated a strong positive correlation between Ga-68-DOTATATE PET and DCE parameters (Pearson r for VP I SUVmax was 0.88, p = 0.0004).

(Filename: TCT_2591_Whitney_Figure1.jpg)

2929

3:51PM - 3:58PM

Predicting Intraoperative Blood Loss in Meningioma: Application of DSC MR imaging

Y Kang[1], C Toh[1]
[1]*Chang Gung Memorial Hospital, Linkou, Taipei, Taiwan*

Purpose
To investigate vascularity and vascular permeability of meningiomas and its correlation with predicting estimated blood loss (EBL) using preoperative DSC perfusion MR imaging, we proposed an index reflecting an inherent bleeding tendency of meningioma, i.e., EBL/cm3, which is EBL per unit volume of meningioma. The purpose of our study was to evaluate the potential of quantitative DSC perfusion MR imaging parameters as imaging biomarkers for predicting EBL in meningioma.
Materials and Methods
This retrospective study included 57 histopathologically confirmed non-embolized meningioma patients. All patients underwent preoperative DSC perfusion MR imaging at our institution. The corrected cerebral

blood volume (CBV) and leakage coefficient K2 of the entire enhancing tumor were obtained through leakage correction. The corrected CBV were normalized by dividing their values by the values in the contralateral normal-appearing white mater. Tumor volume, location, grade, and other clinical variables were also investigated. Simple regression was done to identify predictors of EBL/cm3, all variables with a p-value less than 0.1 were considered relevant and included into the multiple linear regression analysis.
Results
On univariate analysis, EBL/cm3 correlated with CBV ($r = 0.672$; $p < 0.001$), K2 ($r = 0.238$; $p = 0.075$), and tumor volume ($r = –0.240$, $p = 0.072$) on univariate analysis. EBL/cm3 was not correlated with age ($p = 0.828$), sex ($p = 0.329$), tumor location ($p = 0.371$), and the histologic grade ($p = 0.424$). On multiple linear regression, CBV [$\beta = 0.666(0.470\text{-}0.857)$, B=1.392(0.966-1.817), $p<0.001$] and K2 [$\beta = 0.214(0.018\text{-}0.405)$, B=2.044(0.078-4.009), $p=0.042$) were only independent predictors of EBL/cm3.
Conclusions
We found that CBV and K2 were significant explanatory factors of EBL/cm3, which could be an index indicating the bleeding tendency of the meningioma. DSC perfusion MR imaging may provide useful information for meningioma characterization and serve as feasible tools for clinicians to predict EBL and facilitate surgical planning.

3161

3:58PM - 4:05PM

Profiling of Glioblastoma During Chemoradiation Therapy: A Pilot Study

F Salehi[1], S Myrehaug[2], A Sahgal[2], A Chan[3], P Maralani[3]
[1]*Sunnybrook Health Science Centre, Toronto, ON,* [2]*Department of Radiation Oncology, Sunnybrook Health Sciences Centre, Toronto, ON, Canada., Toronto, Ontario,* [3]*Sunnybrook Health Science Centre, Toronto, Ontario*

Purpose
Glioblastoma is the most common primary brain tumor in adults. Despite advances in treatment, overall prognosis remains poor. Radiation planning and post-treatment response assessment utilize magnetic resonance imaging (MRI). The aim of this study was to establish non-contrast enhanced MRI sequences equivalent to gadolinium enhanced sequences in the delineation of glioblastoma multiforme; to examine if changes in fluid attenuated inversion recovery (FLAIR) abnormality during radiotherapy correlate to symptoms and dexamethasone dose; and to examine if MRI changes during radiation treatment can predict tumor response.
Materials and Methods
The study included 20 patients with GBM who underwent MRIs before and during chemoradiation at days 0, 10 , 20, and 30. MRI sequences included T1 with and without contrast, DWI, ADC maps and FLAIR. Regions of interest containing the lesions were drawn on ADC maps and volume-based data of tumor were constructed. Texture and first order features including entropy, skewedness and kurtosis were obtained, and compared at different time points using a student t-test.
Results
Preliminary results included analysis of 5 of 20 patients. Trends were exhibited in radiomic features, including decreased volume and kurtosis during treatment, with increasing skewedness, elongation and entropy. Although the trends did not reach statistical significance (likely related to small preliminary sample size), they provide information on the dynamic quantitative imaging changes that occur during chemoradiation of GBM. Statistically significant results are expected upon completion of the study with inclusion of all patient data points.
Conclusions
To our knowledge, this is the first study to investigate the utility of radiomics analysis in GBM patients during chemoradiation. An understanding of the evolution of dynamic imaging features in tumors during treatment may provide clinicians with tools to undertake adaptive chemoradiation therapy, with potential

implications including adjustment of radiation dose, corticosteroid therapy and temozolomide regimen to minimize harmful effects and optimize response to therapy.

2688

4:05PM - 4:12PM

Radiomic Features and Multilayer Perceptron Network Classifier: A Robust MRI Classification Strategy for Distinguishing Glioblastoma from Primary Central Nervous System Lymphoma

S Cho[1], H Kim[1], J Park[2]
[1]University of Ulsan College of Medicine, Asan Medical Center, Seoul, Korea, Republic of, [2]Asan Medical Center, Seoul, 05555, Korea, Republic of

Purpose
To establish a high-performing and robust classification strategy, using magnetic resonance imaging (MRI), along with combinations of feature extraction and selection in human learning, machine learning, and deep learning by employing a small dataset.
Materials and Methods
Diffusion and contrast-enhanced T1-weighted MR images obtained from 153 patients with glioblastomas and primary central nervous system lymphomas and randomized into a training set (123 MR image sets, 50 PCNSLs, and 73 glioblastomas) and an internal validation set (30 MR image sets, 12 PCNSLs, and 18 glioblastomas). An external validation set with 42 MR image sets (14 PCNSLs and 28 glioblastomas) was collected from another tertiary hospital to test the effect of different acquisition protocols on model performance. Classification task was assigned to a combination of radiomic features and supervised machine learning after feature selection (metric 1) or multilayer perceptron network (MLP, metric 2); or MR image input without radiomic feature extraction to two neuro-radiologists (metric 3) or an end-to-end convolutional neural network (CNN, metric 4). The performance was compared using the area-under-the receiver operating characteristic curve (AUC).
Results
The MLP was optimized with 100-10 layer. Combination of radiomic features and MLP (metric 2, AUC 0.991) showed better performance than machine learning (metric 1, AUC 0.931), metric 3 (AUC 0.833-0.875), or metric 4 (AUC 0.879) in the internal validation set. The MLP network remained robust (AUC0.947) in the external validation set obtained using different MRI protocols compared to metric 1 (AUC 0.811) or 4 (AUC 0.496).
Conclusions
A combination of radiomic features and MLP network classifier serves a high-performing and generalizable model for classification task for a small dataset with heterogeneous MRI protocols.

3427

4:12PM - 4:19PM

Radiomic Analysis Differentiates Between Uveal and Cutaneous Melanoma Brain Metastases.

S Ahmed[1], A Kotrotsou[1], T Haboub[1], D Gombos[1], S Patel[1], R Colen[1]
[1]The University of Texas MD Anderson Cancer Center, Houston, TX

Purpose
Uveal melanoma is considered the most common primary malignant intra-ocular tumor. Although the uveal and cutaneous melanoma share the same cellular lineage, melanocytes, they don't exhibit the same etiology, clinical features, and cytogenetics abnormalities and show different metastatic behavior. This study will be focusing on using radiomic analysis to outline the differences between uveal and cutaneous melanoma brain metastases (MBMs).

Materials and Methods
The study included 15 patients with uveal melanoma BM and 65 patients with cutaneous MBM. Conventional MR images were used tp delineate four tumor phenotypes (ROIs), namely edema/invasion, necrosis, enhancing tumor, and hemorrhage (3D slicer 4.3.1). A total of 310 features (10 histogram-based and 300 second-order features) were calculated from each ROI. Second-order features were calculated using the Grey Level Cooccurrence Matrix (GLCM) resulting in 20 Haralick features. To account for directionality, the mean, variance and range of the features across different directions were calculated. Finally, different number of gray levels were also considered in the analysis (N=8, 16, 32, 64, 256). Accounting for the different phenotypes and MR sequences a total of 3100 radiomic features were extracted for each patient. Core features were obtained using a feature selection approach based on Least Absolute Shrinkage and Selection Operator (LASSO). Selected features were used to build a classification model for prediction of uveal vs cutaneous MBM (XGboost). To evaluate the robustness of the estimates, Leave-One-Out Cross-Validation (LOOCV) was conducted on the patient set.
Results
Overall, we found that XGboost-based classification of radiomic features is a promising approach for differentiating uveal and cutaneous MBM. The prediction of uveal MBM using LOOCV was significant with p-value<0.0001; area under the curve, sensitivity and specificity were 98.41%, 100%, 80% respectively.
Conclusions
Our results demonstrate that radiomics were able to identify imaging differences between uveal and cutaneous MBMs resulting from the variance in the metastatic behavior of the primary tumors.

Tuesday, May 21, 2019
4:30PM - 6:00PM
Advanced Neuroimaging of Neurodegenerative Diseases and Aging

3111

4:30PM - 4:37PM

Clinical Benefit of Nigrosome 1 Detection at 3T MRI for Diagnosis of Neurodegenerative Parkinsonism

J Lee[1], A Lee[1]
[1]Soonchunghyang univ hospital, Puchun, Select One

Purpose
To evaluate the clinical benefit of nigrosome 1 detection on SWI of 3T MRI for diagnosis of primary Parkinsonism.
Materials and Methods
This retrospective study was enrolled patients with suspected Parkinsonism (n=48) or other intracranial pathologies (n=31) who underwent brain MRI including SWI. All suspected Parkinsonism patients was underwent N-3-fluoropropyl-2--carbomethoxy-3--(4-iodophenyl) nortropane (FP-CIT) PET and clinical diagnosis was made by neurologist in clinical follow up. The nigrosome 1 detection findings by using the SWI were rated as 'normal', and 'abnormal' by 2 independent reviewers without clinical information and followed by consensus reading. Agreement between the SWI and FP-CIT PET was examined by using the Cohen's kappa test. The diagnostic sensitivity, specificity, accuracy, positive predictive value (PPV), and negative predictive value (NPV) were calculated. According to clinical diagnosis, the AUC of FP-CIT PET and SWI were analyzed and compared using delong test.
Results
The study included 79 subjects (28 iPD, 6 atypical PD, 14 disease control, 31 healthy control). Of the 34

patients with primary Parkinsonism, 25 patients were positive on SWI. We identified 11 false positive cases and 9 false negative cases. The measured diagnostic sensitivity, specificity, accuracy, PPV, and NPV are as follows (0.74, 0.76, 0.69, 0.79, 0.75). Among the suspected Parkinsonism patients, the agreement between nigrosome 1 detection on SWI and FP-CIT PET imaging was moderate (kappa=0.41). And there was no significant difference in AUC between SWI and FP-CIT PET(0.83, 0.91, P=.11)
Conclusions
Although nigrosome 1 detection on SWI showed lower diagnostic performance than FP CIT PET, but it is in an acceptable range. So we recommend to add to the Parkinson MR screening protocol because of its better assessibility than FP-CIT PET and no raditaion.

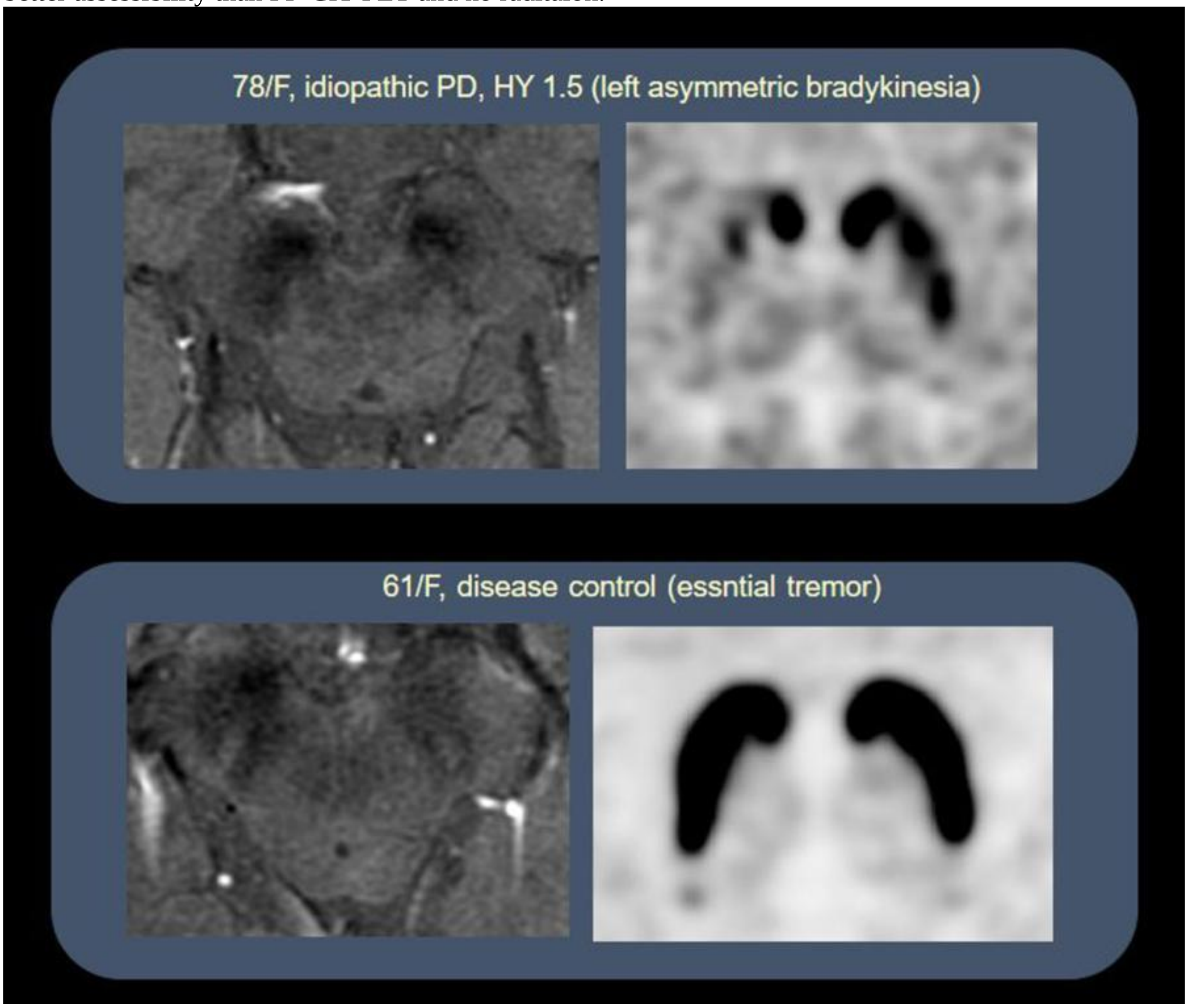

(Filename: TCT_3111_fig2.JPG)

3597

4:37PM - 4:44PM

Comparative Study of Susceptibility Map Weighted Image (SMWI) with Susceptibility Weighted Image (SWI) in the Substantia Nigra to Diagnose of Idiopathic Parkinson Disease

J Choi[1], M Han[2], W Jung[3]
[1]Ajou University School of Medicine, Suwon-si, Gyeonggi-do, [2]Ajou University Medical Center, Suwon-si, Gyeonggi-do, [3]Ajou University Hospital, Suwon, Korea, Republic of

Purpose

Several MR sequences have been introduced to detect change in the substantia nigra (SN) for diagnosis of parkinson disease (PD). Histologic studies in PD have reported that depletion of dopaminergic neurons in the nigrosome-1. Signal changes in the nigrosome-1 have shown in PD on SWI at 7T MRI, but at 3T, this structure was seen with substantially reduced contrast. Recently, new methods have been introduced SMWI which utilized susceptibility weighted mask derived from QSM for the magnitude images. The purpose of this study is to compare the image quality and diagnostic performance of SMWI with SWI of signal changes in the SN to diagnose of idiopathic Parkinson disease (IPD).

Materials and Methods

48 patients clinical proved IPD patients and 30 normal control were included in this study. They were assessed by using H&Y, UPDRS III and underwent 18F-FP-CIT PET for initial diagnosis. All patients were obtained 3D multiecho spoiled gradient echo sequence at 3T (750W; GE Healthcare). To observe the nigrosome-1, oblique coronal imaging plane oriented perpendicular to the midbrain structure was selected with high spatial resolution (0.5X0.5X1.0mm3). SMWI and SWI were generated from acquired data. Postprocessing were performed using MatLab(MathWorks, Natik, MA). To compare the visibility, the contrast-to-noise ratios (CNR) of the nigrosome-1 were calculated at the level of substantia nigra using the following formula: CNRN1 = │mean of N1 region) – (mean of SN region) │/(standard deviation of SN region), where N1, Nigrosome-1; SN, nigrosome-1 and the neighboring substantia nigra. For visual assessment, the nigrosome-1 images were classified into three grades: normal (iso- or hyperintensity in the central portion of the presumed nigrosome 1 area), possibly abnormal (hypointensity in less than 50% of the presumed nigrosome-1 area, and definitely abnormal (hypointensity in equal to or more than 50% of the presumed nigrosome-1. Diagnostic performance was evaluated in SMWI and SWI.

Results

The average CNRN1 of SMWI and SWI in all control subjects were 1.91±0.43 and 1.50±0.52, respectively. When the average CNR of nigrosome-1 for the SMWI and SWI from normal control were compared quantitatively, CNRN1 of SMWI was better than SWI with a statistically significant difference ($p= 0.002$). The interrater agreement on the abnormality of nigrosome-1 finding was excellent (κ, SMWI vs SWI, 0.873 vs 0.783). After consensus agreement, the sensitivity, specificity and diagnostic accuracy were 91.6%, 86.3% and 88.2% in SMWI, whereas 86.6%, 71.6% and 75.0 % in SWI, respectively. ROC curve showed that SMWI was better diagnosis performance than SWI (AUC, 0.890 vs 0.714).

Conclusions

Our study showed that SMWI is better image quality and diagnostic performance than SWI for the diagnosis of IPD at 3T. SMWI at 3T can be used to screen patients who need further diagnostic imaging modality in patients who were suspected early stage IPD.

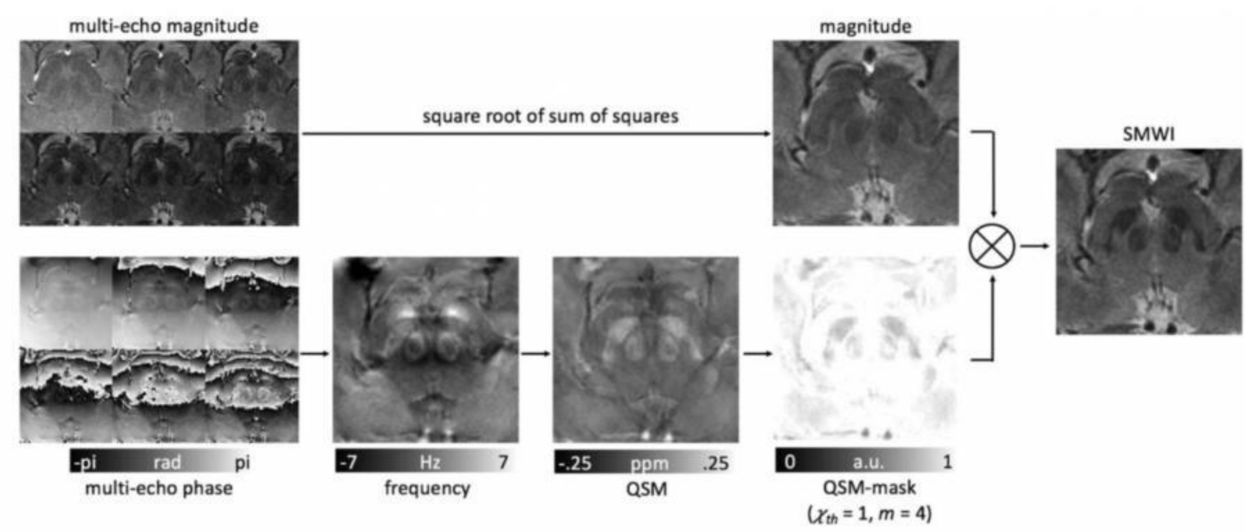

(Filename: TCT_3597_Fig1.jpg)

3435

4:44PM - 4:51PM

Correlation of Motor Outcome in Early Wallerian Degeneration Using Synthetic MRI in Patients with Recent Stroke

V Andreu Arasa[1], H Jara[2], K Takumi[3], O Sakai[4]
[1]BMC, BOSTON, MA, [2]Boston University/Boston Medical Center, Boston, MA, [3]Boston Medical Center, Boston University School of Medicine, BOSTON, MA, [4]BOSTON UNIVERSITY SCHOOL OF MEDICINE, BOSTON, MA

Purpose
Wallerian degeneration is a progressive antegrade disintegration and demyelination of axons after an insult to the proximal axon or cellular body. Signal abnormalities on diffusion-weighted imaging (DWI) and on diffusion tensor imaging within the corticospinal tract are a marker of underlying parenchymal atrophy, gliosis, and myelin loss, and a predictor of poor outcome. White matter fibrography (WMF) is a recently developed imaging technique based on synthetic MRI with which the global brain connectome can be rendered in three dimensions at high spatial resolution with the anatomic accuracy of the turbo spin echo (TSE) pulse sequence. The purpose of this study is to correlate early motor outcome from early Wallerian degeneration using synthetic MRI with WMF in patients with recent infarct.
Materials and Methods
In this IRB approved retrospective study, the Tri-TSE 3T-MRI scans of 15 patients with recent infarct during the first 7 days after onset of symptoms, were processed with a synthetic-MRI program that permits to create weighted images of the four principal qMRI parameters: T1, T2, PD and correlation time diffusion coefficient. Imaging parameters: 36 contiguous slices, voxel=0.5x0.5x5mm3, TRs=475&3500ms, TEs=10&90ms. Areas of recent infarcts were identified as hyperintensities on DWI, and then compared to the raw images of the heavily 1/T1 weighted synthetic images of the connectome. ROIs were placed in the cerebral peduncles; both on the affected and contralateral sides and then parameters were compared.
Results
Decreased signal and loss of white matter fiber integrity of the corticospinal tract in 1/T1 maps was seen on patients with recent infarcts with motor deficits at presentation and at the time of discharge.
Conclusions
WMF is sensitive to loss of myelin water and could be used to identify changes in the corticospinal tracts during the first week post stroke onset and predict the early stage motor outcome.

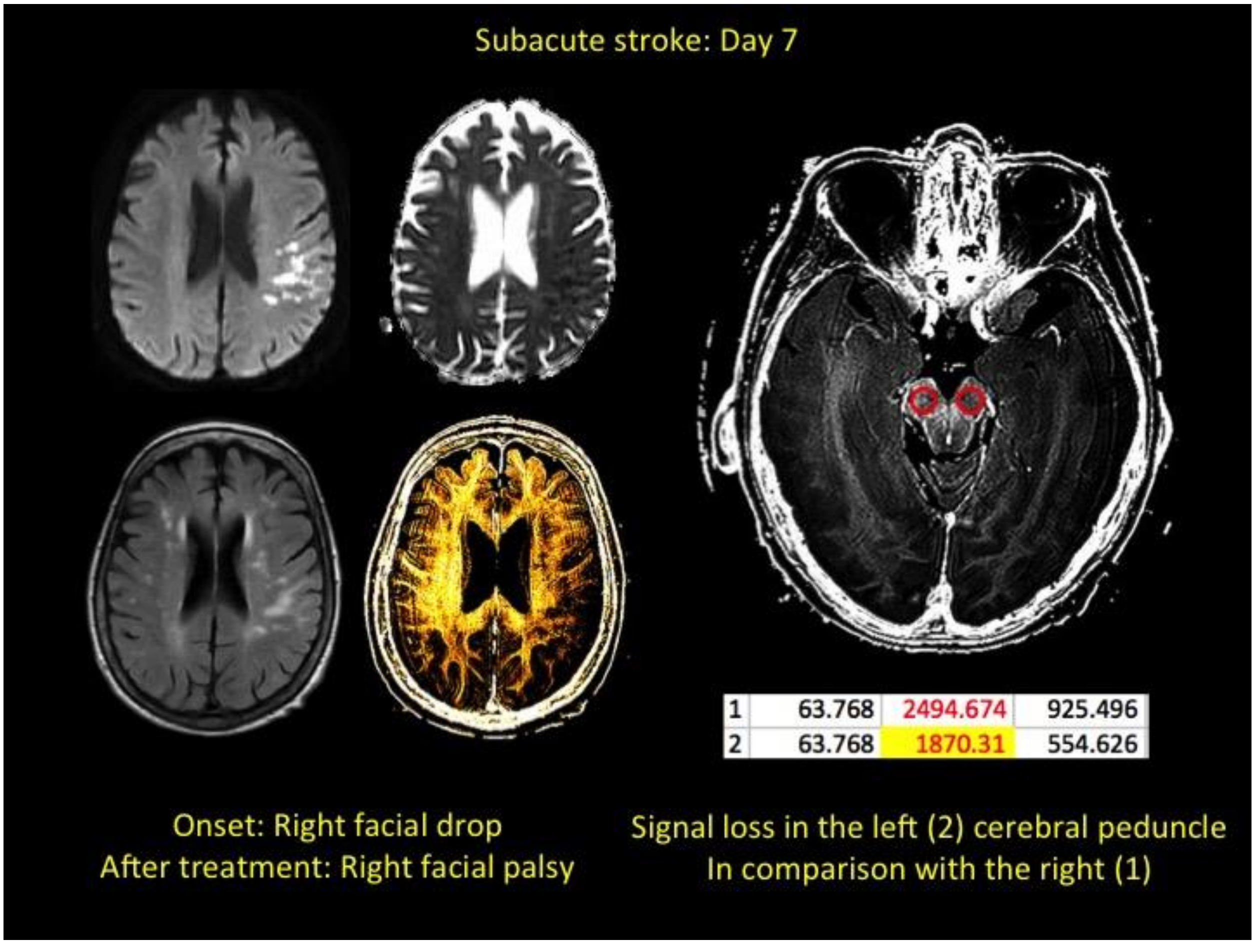

(Filename: TCT_3435_Diapositiva1.jpg)

3333

4:51PM - 4:58PM

Discrimination Of Intra-thalamic Nuclei Using Magnetic Susceptibility Mapping At 3T MRI

S Chung[1], J Jang[2], T Shepherd[1], Y Lui[1]
[1]NYU School of Medicine, New York, NY, [2]Seoul St. Mary's Hospital, The Catholic University of Korea, Seoul, NA

Purpose

The thalamus is a heterogenous structure composed of several functionally specific nuclei which play critical roles in a range of neurological functions and the target for functional neurosurgery in some conditions such as Parkinson's disease and essential tremor. Visualization of the thalamic nuclei boundaries continues to allude us and has been a major challenge due to low intrinsic contrast between adjacent nuclei on conventional imaging. In current clinical practice, gross indirect targeting is done based on geometry and relative location gleaned from pathologic atlases. Here, we develop a new method for subject-specific thalamic nuclei parcellation based on quantitative susceptibility mapping (QSM)[1] which takes advantage of the intrinsic susceptibility differences between thalamic nuclei to achieve personalized segmentation and preoperative mapping. Best contrast for delineation of thalamic nuclei boundaries was achieved by optimizing regularization parameters during post-processing (named here, Thalamic Nuclei-specific Susceptibility Mapping [TN-SM]).

Materials and Methods
High resolution, isotropic, 3D multiple gradient echo (MGRE) sequence was performed on 15 healthy individuals (mean age,31y.o) using 3T MR scanner (Skyra, Siemens). Imaging parameters include: FOV=220x170x75mm3, voxel size=1.25mm isotropic, flip angle=22deg, TR=92ms, 20 TEs=1.90:2.32:45.98ms. TN-SM maps were calculated with a high regularization parameter (lambda) that would trade data fidelity with sharpness to get best contrast (MEDI toolbox, Cornell MRI Research Lab). The boundaries of nuclei were manually drawn on TN-SM maps by a radiologist.
Results
Figure 1 shows (left) a representative TN-SM map (41 y.o, female) and (right) corresponding 13 thalamic nuclei, including Lamella medialis oralis(Lao), N.lateropolaris(Lpo), Adhaesio interthalamica(Ai), N.ventrooralis medialis(Vom), N.ventrooralis(Vo), Substantia periventricularis(Spv), N.parafascicularis(Pf) & N.centralis thalami(Ce), N.limitans(Li), N.ventrointermedius(Vim), Fasciculus retroflexus meynertii(FM), N.pulvinaris medialis(Pum), N.ventrocaudalis(Vc), N.pulvinaris laterale(Pul).
Conclusions
Our TN-SM method is able to delineate the boundaries of thalamic nuclei in a subject-specific way for neurosurgical planning and has a potential to help guide personalized targeting to the VIM using MR-guided focused ultrasound or gamma knife irradiation in patients with essential tremor.

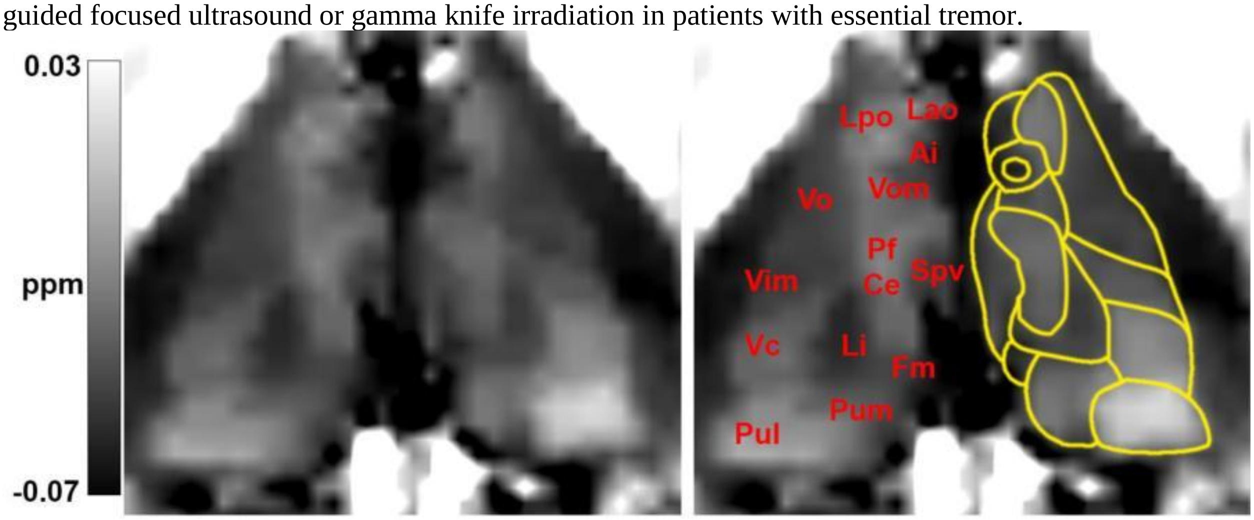

Figure 1. (left) A representative thalamic nuclei-specific susceptibility map (TN-SM) and (right) corresponding 13 thalamic nuclei.

(Filename: TCT_3333_figure1_new.jpg)

2315

4:58PM - 5:05PM

Effects of Alcohol and Acetate on Brain Perfusion: A Pilot Study

J Tanabe[1], D Yamamoto[1], M Regner[1], B Sutton[1], M Brown[1], P Hoffman[1], B Tabakoff[1], D Glueck[1]
[1]*University of Colorado, Aurora, CO*

Purpose
Alcohol affects mood and behavior likely through neurotransmission, brain metabolism and blood flow. Acetate, a metabolic byproduct of alcohol, rises in the circulation and in the brain, where it can be used as an energy source. Acetate may alter cerebral blood flow (CBF) by altering brain metabolism or by driving the production of the vasodilator adenosine. No previous studies have separated the effect of acetate from that of alcohol on CBF. We hypothesized that compared to placebo, alcohol and acetate would increase CBF in cortical and subcortical regions.

Materials and Methods

Design: Prospective, single-blinded, within-person, two-arm non-randomized study comparing intravenous acetate or oral alcohol to placebo, on CBF. Methods & Material: Twenty-four healthy controls were non-randomly assigned to receive either .6 g/kg oral alcohol jello shots (n=12) or intravenous acetate (n=12). Plasma acetate was measured at baseline, following placebo, and after drug. Cerebral blood flow was measured using a pulsed arterial spin (PASL) labeling sequence on a 3T MR scanner. Whole brain CBF maps were compared between placebo and drug using a paired t-test, set at a threshold of $p<0.05$ cluster-corrected for multiple comparison, voxel level $p<0.005$.

Results

Plasma acetate levels increased significantly following alcohol and acetate (main effect time $F(1,14)=14.76$, $p<0.001$), but did not differ between the alcohol and acetate arms (main effect group, $F(1,16)=.113$, ns) (group x time ($F(1,14) = 0.643$, ns). Alcohol and acetate both increased CBF in the medial thalamus. Alcohol increased CBF in the right medial prefrontal cortex, cingulate cortex and hippocampus, but acetate did not.

Conclusions

Our findings suggests that thalamic blood flow response after drinking may be mediated by acetate. The thalamus may have an enhanced ability to utilize acetate as an energy substrate. As acetate is a preferred energy source for certain cell types, including cells of immune system, astrocytes and microglia in the CNS, our results may provide insight into the acute and chronic effects of alcohol. The increase in CBF in prefrontal and limbic regions seen with alcohol is consistent with prior studies and may be related to the behavioral effects alcohol.

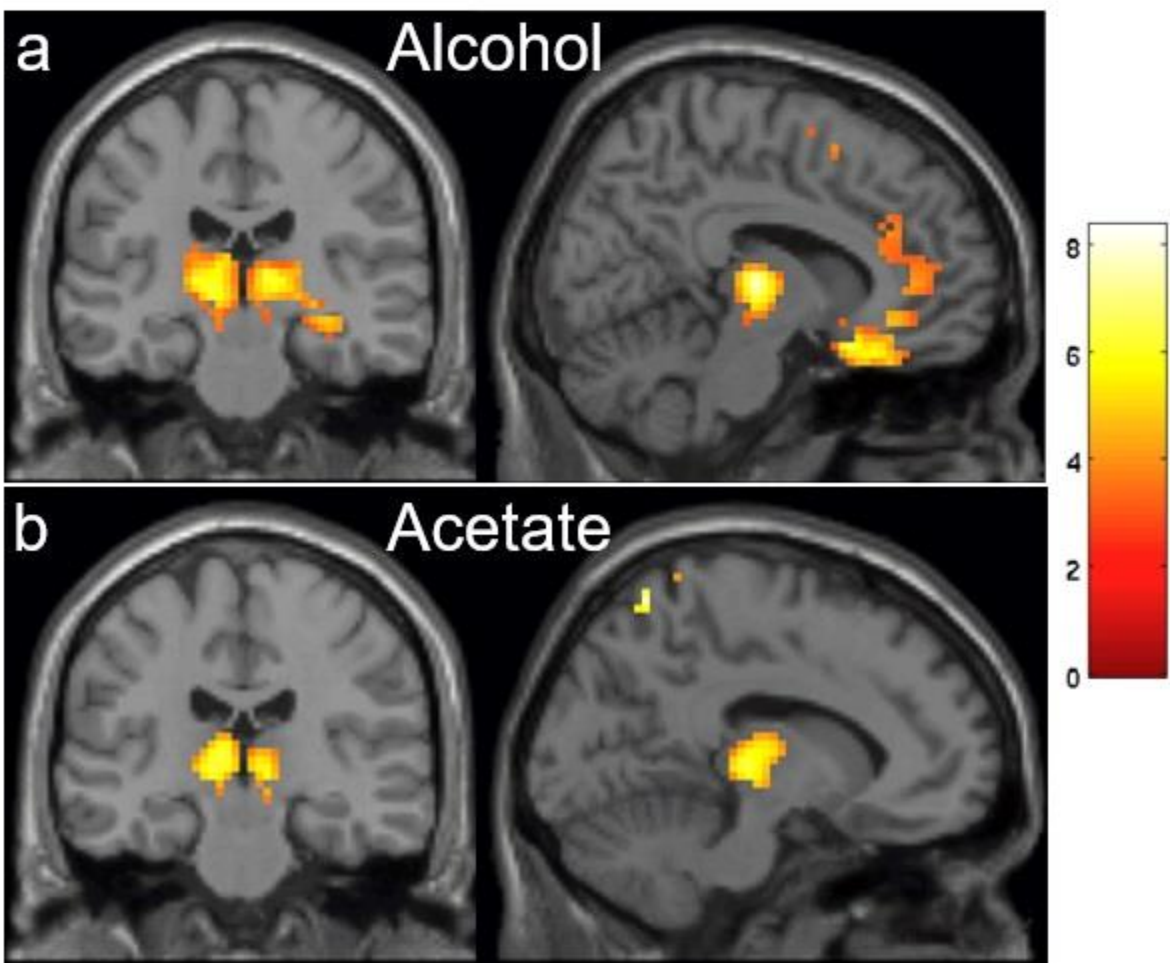

(Filename: TCT_2315_Figure3.jpg)

3340

5:05PM - 5:12PM

Fully-Automatic Quantitative Susceptibility Mapping of the Precentral Gyrus in Motor Neuron Disease

G Conte[1], V Contarino[1], E Scola[2], C Morelli[3], S Calloni[4], L Sanmiguel Serpa[5], F Trogu[6], V Silani[7], F Triulzi[8]
[1]Fondazione IRCCS Ca Granda Ospedale Maggiore Policlinico, Milano, ITALY, [2]Fondazione IRCCS Ca Granda Ospedale Maggiore Policlinico, Milano, Italy, [3]Istituto Auxologico Milano, Milano, ITALY, [4]University of Milan, Milan, MI, [5]Politecnico di Milano, Milano, ITALY, [6]Università degli Studi Milano, Milano, ITALY, [7]IRCCS Istituto Auxologico Italiano, University of Milan, Milano, MI, [8]Università degli Studi Milano, MILANO, Italy

Purpose
Aim: to develop and apply a fully-automatic image processing pipeline to investigate the susceptibility properties of the precentral gyrus in MND. Background: Motor Neuron Disease (MND) is a group of neurodegenerative disorders primarily affecting motor neurons. MND exhibits different phenotypes and can present with a widely variable involvement of upper and lower motor neurons. Moreover, regional variants restricted to the arms, legs or bulbar region as well as different patterns of clinical expression (distal or proximal, symmetric or asymmetric) are well-known [1]. Amyotrophic Lateral Sclerosis (ALS) is the most common MND and is characterized by degeneration of both upper and lower motor neurons. Precentral gyrus susceptibility changes have been investigated in ALS with T2*-weighed imaging, Susceptibility-weighted imaging (SWI) and Quantitative susceptibility mapping (QSM) based on hand-drawn ROIs and/or visual inspection [2,3,4]. Susceptibility increase is observed in both cortex and subcortical white matter probably due to iron overload and myelin content decrease respectively. However, hand-drawn ROIs-based measures and visual inspection-based scoring are strongly user-dependent and time consuming.
Materials and Methods
51 MND (61.21 ±9.63 y) and 25 Healthy Controls (HC, 57.32 ±7.30 y) were enrolled and scanned at IRCCS Istituto Auxologico Italiano-San Luca Hospital, Milan (Italy). A 3D sagittal FSPGR BRAVO T1w (TR=8.7ms, TE=3.2ms, TI=450ms; Pixel 0.5x0.5mm, thickness=1mm, spacing=1mm, FA=12°, matrix 256x256) and a spoiled gradient-echo multiecho (TR=39ms, 7 equally spaced echoes centered at 24ms, Pixel 0.47x0.47mm, thickness=1.4mm, spacing=0.7mm, FA=20°, matrix 416x320) whole-brain sequences were acquired at 3T General Electric (GE) SIGNA unit. Images were visually assessed and processed at Neuroradiology Deparment of Fondazione IRCCS Ca' Granda Ospedale Maggiore Policlinico, Milan (Italy). FSL Brain Extraction Tool provided the brain mask from magnitude image. Phase image and mask image were used to calculate the QSM by using the Matlab toolbox STI Suite [5]. Streaking artifacts reduction (STAR) QSM algorithm was adopted [6]. QSM was coregistered to T1w image with a mutual information-based rigid transformation in SPM12 and automatic segmentation of brain regions was performed in Freesurfer (Fig.1). Precentral gyrus cortex (PreGC) and subcortical white matter (PreGSubcWM) ROIs were extracted (Fig.2). Mean susceptibility and skewness of the susceptibility distribution were calculated in the PreGC and PreCSubcWM ROIs and statistically analyzed in SPSS.
Results
In PreGC, mean susceptibility was higher in MND but not statistically different from HC (p=0.139) while skewness was statistically significantly higher (p=0.002) in MND compared to HC. In PreGSubcWM, mean susceptibility (p=0.005) and skewness (p=0.039) were significantly higher in MND compared to HC. Mean susceptibility in PreGSubcWM showed a significant correlation with disease duration (Sig=0.033, r=0.26) and ALS Functional Rating Scale (ALSFRS, Sig=0.026, r=−0.42).

Conclusions
The skewness of susceptibility distribution in PreGC is sensitive to susceptibility changes in MND measured on the automatically-segmented bilateral PreGC. On the contrary, the metric of susceptibility mean calculated on this large automatic cortical ROI may lose significance: the values of the voxels with increased susceptibility are indeed averaged with all the other voxels compounding the bilateral PreGC. In addition, cortical voxels largely suffer from partial volume effects especially in standard resolution scans. In PreGSubcWM, which is less affected by partial volume effects, automatically-measured mean susceptibility is able to highlight white matter anomalies in MND likely linked to degeneration of myelinated fibers. In conclusion, for the first time, a fully-automatic pipeline have been applied to quantitatively study the susceptibility properties of the precentral gyrus in MND. The skewness of susceptibility distribution in PreGC is sensitive to susceptibility changes in MND. An automatic non-invasive tool able to quantify the susceptibility properties of precentral gyrus cortex and subcortical white matter would be beneficial in building a biomarker of pathology in MND, as the diagnosis of MND is a complex process with clinical and neurological examinations during a long period of time and there is no single definitive test.

2337

5:12PM - 5:19PM

Improved Targeting of the Globus Pallidus Interna Using Quantitative Susceptibility Mapping Prior To MR-Guided Focused Ultrasound Ablation in Parkinson's Disease

E Ebani[1], M Kaplitt[1], J Chazen[1]
[1]*Weill Cornell Medicine, New York, NY*

Purpose
The last two decades have seen a resurgence in the performance of surgical interventions for the treatment of Parkinson's Disease. Historically, the most commonly utilized surgical treatments have included radiofrequency ablation and deep brain stimulation techniques. However, both of these procedures have significant limitations including complications related to device implantation, electrical stimulation, uncontrollable lesion size with subsequent irreversible side effects, and the need for continuous, long term follow-up. Recently, MR-guided focused ultrasound (MRgFUS) ablation has emerged as a minimally invasive/nonincisional neurosurgical technique with favorable clinical outcomes reported in several trials involving patients with essential tremor, obsessive-compulsive disorder, intractable pain, and Parkinson's Disease. Specifically, MRgFUS of the globus pallidus interna (GPi) has shown promising results in the treatment of drug-resistant Parkinson's Disease in small clinical trials. However, direct visualization and precise targeting of the GPi is challenging with traditional MR imaging sequences. Quantitative susceptibility mapping (QSM) is a novel MR technique which has shown promise in depicting the deep brain nuclei. The purpose of this study was to compare various preoperative MR imaging techniques in the depiction of the GPi prior to MRgFUS ablation as part of a pivotal ongoing clinical trial of the management of medically refractory dyskinesia symptoms or motor fluctuations of advanced idiopathic Parkinson's Disease.
Materials and Methods
Four patients with medication refractory Parkinson's Disease were enrolled as part of an ongoing clinical trial and referred for preoperative navigation MR imaging prior to MRgFUS ablation of the GPi. Traditional MR sequences including T1 and T2-weighted as well as Fast Gray Matter Acquisition T1 Inversion Recovery (FGATIR), an imaging sequence currently recommended by the clinical trial sponsor, InSightec (Haifa, Israel), were acquired. Quantitative Susceptibility Mapping (QSM) sequences were also generated for GPi depiction. These sequences were all performed with a 3 mm slice thickness and zero gap technique. In addition, postprocessing of a 60 direction diffusion tensor imaging (DTI) acquisition was used to generate tractograms in order to better delineate the optic and corticospinal tracts, which form the inferior and posteromedial borders of the GPi. The optic tract was generated by placing seeds at the

optic chiasm and calcarine gyrus. The corticospinal tract was generated by placing seeds at the precentral gyrus and cerebral peduncle. DTI imaging data was imported into the Brainlab iPlan Cranial software package and eddy current correction was performed. Postprocessing was performed with a minimum fiber length of 90 mm and fractional anisotropy value of 0.3. All imaging sequences were independently reviewed and compared by both a neuroradiologist and neurosurgeon in multiple preoperative planning sessions after which a consensus target for ablation was selected.

Results

Image quality was satisfactory for all patients despite a resting tremor. Successful fiber tracking of the optic and corticospinal tracts was also achieved in all patients. The borders of the GPi and medial medullary lamina between the GPi and GPe were difficult to delineate with traditional T1 and T2-weighted imaging sequences (Figures 1A and 1B). FGATIR, a sequence recommended by the clinical trial sponsor, also provided suboptimal depiction of the GPi (Figure 1C). Both independent reviewers found the combination of QSM and DTI tractography to be superior to both the traditional and currently recommended sequences for the depiction of the GPi (Figure 1D). Successful ablation was achieved in all patients without any significant adverse effects.

Conclusions

QSM and DTI tractography are complementary in yielding superior depiction of the GPi prior to MRgFUS ablation in Parkinson's Disease compared with the traditional and currently recommended imaging techniques including FGATIR, which provided suboptimal visualization in this patient cohort. Precise targeting of the GPi is critical in order to maximize potential clinical benefit and mitigate possible damage to neighboring structures, which can result in potentially irreversible side effects. QSM should be considered as part of all preoperative planning MR imaging protocols prior to MRgFUS ablation of the GPi.

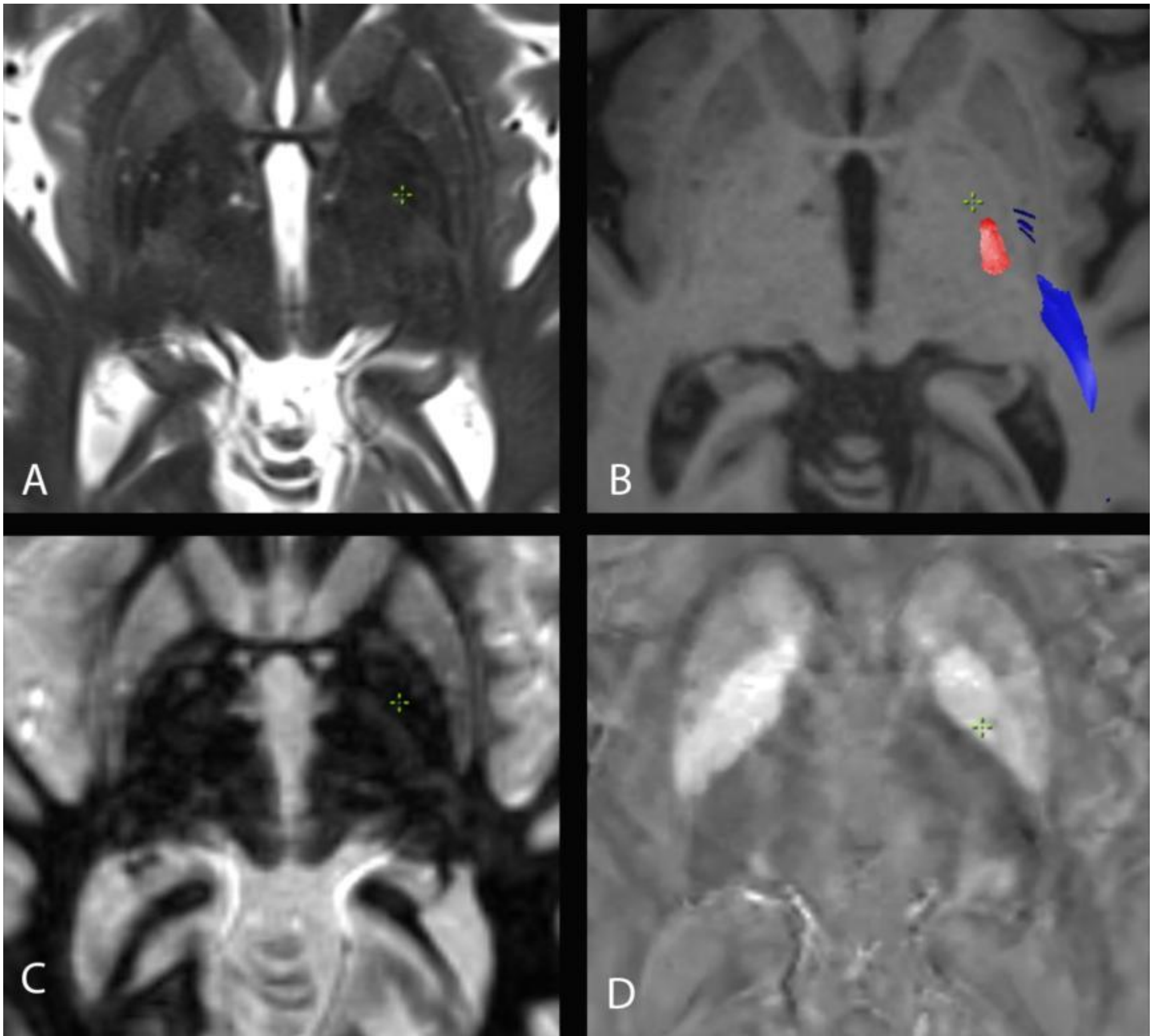

Figure 1: Axial T2 (A), T1 (B), FGATIR (C), and QSM (D) images through the GPi with final ablation target overlaid (green crosshairs). Axial T1 image (B) demonstrates corticospinal (red) and optic radiation (blue) tractograms.

(Filename: TCT_2337_ASNRFig1Final.jpg)

2340

5:19PM - 5:26PM

Neuropsychological and Functional Neuroimaging Changes Following Bariatric Surgery

A Saindane[1], D Qiu[1], J Wu[1], A Singh[2], D Drane[1]
[1]Emory University School of Medicine, Atlanta, GA, [2]Emory University, Atlanta, GA

Purpose
Obesity has been associated with cognitive deficits and increased risk for dementia. Weight loss through bariatric surgery may result in improved cognitive function, however, the anatomic and functional brain

correlates are unknown. This study explores the hypothesis that specific brain regions and networks underlie cognitive changes and can be altered through weight loss from bariatric surgery.
Materials and Methods
Nine obese patients undergoing bariatric surgery, and eight age-, sex-, and education level-matched healthy non-obese controls were enrolled in this prospective study. All subjects underwent a standardized battery of neuropsychological testing along with structural and functional MRI testing on a 3T unit including sequences for assessment of cerebral blood flow and resting state connectivity. Bariatric patients underwent MRI and neuropsychological testing both prior to and six months following bariatric surgery. Differences in MRI and neuropsychological testing between bariatric patients and controls, and longitudinal changes within bariatric patients were assessed.
Results
At baseline, bariatric patients demonstrated deficits in executive function relative to controls (p=0.01). On repeat testing following significant weight loss (mean 15 kg; p=0.05) there was significant improvement in these deficits. Diminished connectivity in the left executive control network was found in patients prior to bariatric surgery (p=0.03), which significantly improved following bariatric surgery to be statistically comparable to that of controls. No significant differences in regional brain volume or cerebral blood flow were detected between patients and controls, or longitudinally within patients. Bariatric surgery was not associated with changes in number of T2-hyperintense white matter lesions.
Conclusions
Obese individuals undergoing bariatric surgery exhibit deficits in executive function and specific alterations of the brain networks underlying this cognitive domain, however, those deficits and networks can be altered through weight loss from bariatric surgery.

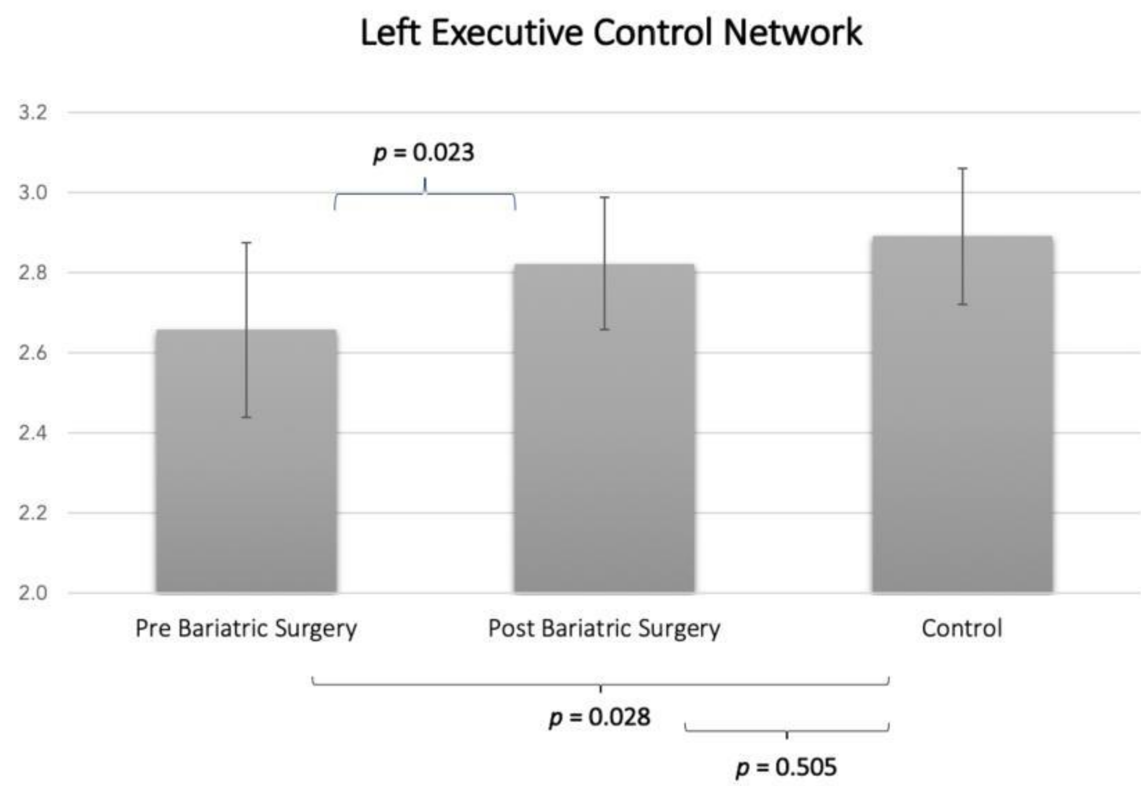

(Filename: TCT_2340_ScreenShot2018-10-28at90732PMcopy.jpg)

2243

5:26PM - 5:33PM

Symmetric Parieto-Occipital Hypoperfusion on Arterial Spin Labeled MRI is Associated with Major Depressive Disorder and Parkinson's Disease.

S Kihira[1], K Nael[1], P Belani[1]
[1]*Mount Sinai Hospital, New York, NY*

Purpose
To investigate comorbidities and visual-spatial symptoms associated with hypoperfusion of the parieto-occipital lobes as captured on Arterial Spin Labeling MRI.
Materials and Methods
This was a retrospective single center IRB approved study. Pseudo-continuous arterial spin labeling (pCASL) MRI was utilized for cerebral flow imaging and added on for non-contrast brain MRIs performed in the inpatient and emergency setting in a large tertiary care hospital. pCASL was utilized with a post-labeling imaging delay of 2025 ms. Adult patients with symmetric reductions in cerebral flow in the parieto-occipital lobes were identified. Age and gender matched patients with no perfusion defect were concurrently collected for normal control. Patients with evidence of prior parieto-occipital strokes on MRI were excluded. Comorbidity data was collected from EMR including major depressive disorder (MDD, diagnosed per DSM-5), dementia, Parkinson's disease, hypertension, diabetes mellitus type II, coronary artery disease, and chronic kidney disease. Data on visual symptoms, cataract history, smoking history, and prior history of strokes were also collected. A Pearson's Chi Square test was performed to assess for comorbidities and visual symptoms associated with hypoperfusion of the occipital lobes.
Results
Our patient cohorts consisted of 93 patients with symmetric hypoperfusion in the parieto-occipital lobes and 93 patients with no perfusion defect based on pCASL. Demographic comparison of the two cohorts revealed no statistical difference in gender, age, or history of prior strokes. The mean ± standard deviation of age (years) was 75 ± 13 with median of 76 for the cohort with occipital hypoperfusion and 75 ± 11 with a median of 76 for the normal control. Among the comorbidities assessed, there was a statistically significant association between hypoperfusion of the parieto-occipital lobes and MDD ($p=0.004$) and Parkinson's disease ($p=0.044$). Specifically, there were 29 patients with MDD in the cohort with parieto-occipital lobe hypoperfusion compared to 13 in the normal control, and 10 patients with Parkinson's disease compared to 3 in the normal control. There was no statistically significant association for dementia, diabetes, hypertension, coronary artery disease, chronic kidney disease, cataracts, visual symptoms, or smoking history.
Conclusions
These results indicate that clinically diagnosed MDD and Parkinson's disease associates with hypoperfusion of the parieto-occipital lobes. This may be explained by visual spatial deficit that has been observed in patients with these comorbidities in prior studies and its relation to the functionality of the parietal and occipital lobes. We plan to further explore this association in the setting of treatment response and disease severity.

2861

5:33PM - 5:40PM

Symmetric Hypoperfusion of Parieto-Occipital Lobes as it Relates to Aging.

S Kihira[1], K Nael[1], P Belani[1]
[1]*Mount Sinai Hospital, New York, NY*

Purpose
To investigate the correlation between symmetric parieto-occipital lobe hypoperfusion and advancing age.

Materials and Methods

This was a retrospective single center IRB approved study. Pseudo-continuous arterial spin labeling (pCASL) sequence was added on as a routine sequence for non-contrast brain MRIs performed in the inpatient and emergency setting in a large tertiary care hospital and was utilized to measure symmetric reductions in cerebral flow in the parieto-occipital lobes. pCASL was utilized with a post-labeling imaging delay of 2025 ms. Adult patients with pCASL within a 1 year time frame were analyzed based on age, gender, stroke history, and cerebral perfusion characteristics. Patients with evidence of acute or chronic occipital strokes on MRI were excluded. A Pearson's correlation coefficient and scatter plot analysis was performed to assess prevalence of parieto-occipital hypoperfusion to advancing age. A Fisher's Z test was performed to assess for gender predisposition when comparing correlation coefficients.

Results

A total of 120 patients with symmetric parieto-occipital hypoperfusion without an anatomic correlate were identified among 625 consecutive patients who had undergone a routine non-contrast MRI with addition of a pCASL sequence. The mean ± standard deviation of age (years) was 62 ± 18 with a median of 64 in the total enrolled population, and the mean age was 75 ± 12 with median of 76 in the sample with symmetric parieto-occipital hypoperfusion. There was a significant positive correlation between hypoperfusion of the parieto-occipital lobes to advancing age (Pearson correlation coefficient = 0.933, $P = 0.0007$). A scatterplot (Figure) revealed age-related increase in prevalence ratio of parieto-occipital hypoperfusion with hypoperfusion found in up to 50% of the population with age > 90. Assessment for gender predisposition by comparing gender-adjusted correlation coefficients through Fisher's Z test revealed no significant difference ($P > 0.05$).

Conclusions

These results indicate that symmetric parieto-occipital hypoperfusion correlates with advancing age with no significant gender predisposition. Many factors may be contributory and confounding such as longer transient delay of tagged protons (a delay between the time arterial blood is tagged and the time it reaches the ROI), age-related atrophy of the brain, and comorbidities associated with advanced age. We plan to further explore this correlation by evaluating for associated comorbidities and assessing for risk factors that may contribute to early onset parieto-occipital hypoperfusion.

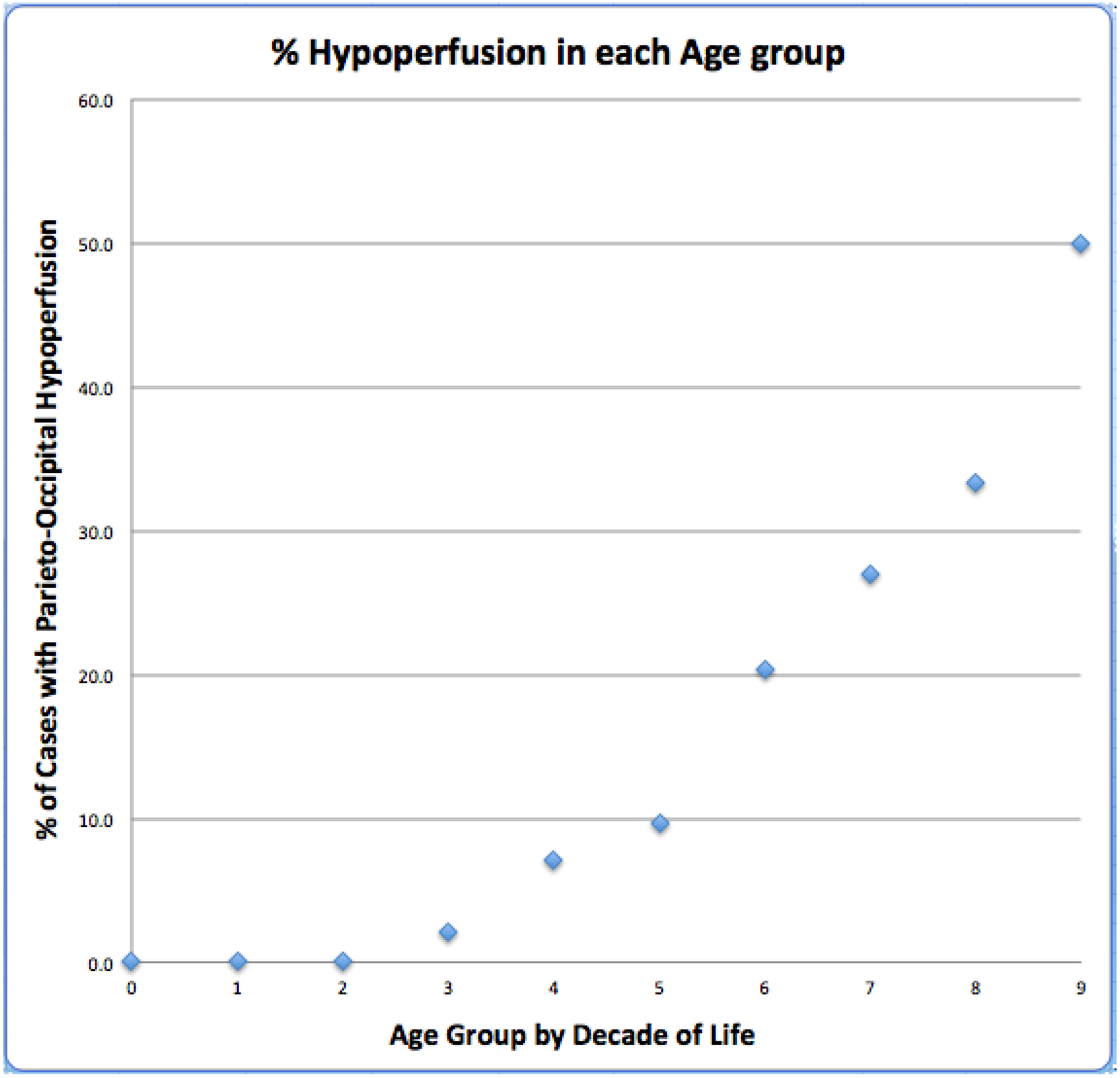

(Filename: TCT_2861_FigureASNR.jpg)

3297

5:40PM - 5:47PM

Tractographically-defined Targets for Tremor Reduction in Parkinson's Disease Patients Treated with Focused Ultrasound

W Wagstaff[1], J Elias[2], T Druzgal[2]
[1]Emory University, Atlanta, GA, [2]University of Virginia, Charlottesville, VA

Purpose
MR-guided focused ultrasound in Parkinson's disease patients treats tremor by ablating the ventral intermediate (VIM) nucleus in the thalamus. Because the VIM is indiscernible on current imaging modalities, indirect targeting methods, including coordinate-based or atlas-based, have been developed to direct therapy. Because these approaches can be inaccurate by as much as 5mm, we hypothesized that the tremor reduction circuit can be directly and more accurately targeted using probabilistic tractography.
Materials and Methods
A retrospective analysis was performed on 17 patients who underwent unilateral thalamotomy for tremor-

dominant Parkinson's disease. Responders (n=9), patients with greater than the median tremor response, were compared to nonresponders (n=8). All patients had pre-treatment MP-RAGE and 64-directional diffusion weighted imaging as well as day one post-treatment T2 imaging. Cortical segmentations were calculated with Freesurfer, tracks were generated with constrained spherical deconvolution (CSD) tractography using MRtrix, and lesions were manually segmented. Final targets were analyzed on the AC-PC plane and correlated with tremor reduction using Pearson's coefficients.
Results
Significant differences between responders and nonresponders were found in distances from lesions to the precentral gyrus hand-face area (1.94mm vs 3.67mm, p=0.01), the post-central gyrus upper-limb-hand-face area (1.92mm vs 3.65mm, p=0.04), and the primary motor cortex caudal-dorsolateral area (2.01mm vs 4.16mm, p=<0.01). In responders, tremor response significantly correlated with distance from the lesion to the primary motor cortex caudal-dorsolateral area (r^2=0.81), the caudal-middle-frontal gyrus (r^2=0.56), and the entire primary motor cortex (r^2=0.47). No difference was found between responders and nonresponders in distance from lesion to the coordinate-based VIM (2.55mm vs 2.47mm, p=0.91).
Conclusions
CSD tractography effectively generated tracks whose lesion distances correlated with tremor reduction, specifically in tracks that terminated in the caudal-dorsolateral area of the primary motor cortex. Lesioning this area, a prime location in the tremor circuit, had greater tremor reduction correlation than coordinate-based approaches, suggesting a new method for VIM targeting.

2793

5:47PM - 5:54PM

Validation of Ultrafast Wave-CAIPI Magnetization Prepared Rapid Gradient-Echo (MPRAGE) for Quantitative Evaluation of Brain Tissue Volume in the Workup of Suspected Neurodegenerative Disease

M Longo[1], J Conklin[1], Q Tian[2], S Cauley[3], K Setsompop[3], J Kirsch[4], W Liu[5], R Gonzalez[1], P Schaefer[6], O Rapalino[1], S Huang[7]
[1]Massachusetts General Hospital, Boston, MA, [2]Athinoula A. Martinos Center for Biomedical Imaging, Massachusetts General Hospital, Boston, MA, [3]Harvard Medical School, Boston, MA, [4]Massachusetts General Hospita (MGH), Boston, MA, [5]Siemens Healthineers, Erlangen, Erlangen, [6]MASS GENERAL HOSPITAL, WAYLAND, MA, [7]Massachusetts General Hospital / Athinoula A. Martinos Center for Biomedical Imaging, Boston, MA

Purpose
Evaluation of brain atrophy with 3D anatomical MRI plays a central role in the workup of neurodegenerative diseases. However, these sequences suffer from long acquisition times, and may be degraded by artifacts in motion prone elderly patients. We evaluated the use of an ultrafast MPRAGE sequence using Wave-CAIPI (Wave-MPRAGE) compared to standard MPRAGE for quantitative evaluation of brain volumes in a clinical setting.
Materials and Methods
This study was approved by the IRB and was HIPAA compliant. Eleven consecutive patients (including 8 being evaluated for suspected neurodegenerative disease) underwent 3T brain MRI (MAGNETOM Prisma; Siemens Healthcare GmbH, Erlangen) using 20 or 32-channel multiarray receiver head coils. In addition to the clinical protocol, each scan included a standard MPRAGE sequence (R=2, acquisition time TA=5.2min) and a resolution-matched prototype Wave-MPRAGE sequence (R=9, TA=1.15 min for the 32-channel coil; R=6, TA=1.75 min for the 20-channel coil). Each anatomical dataset was automatically processed using the FreeSurfer longitudinal stream, and volumes were co-registered using the linear registration tool in FSL. Dice similarity coefficients and the percentage of volume change between the sequences were calculated.

Results
Wave-MPRAGE showed a subjective increase in image noise compared to standard MPRAGE, more pronounced in the central brain. However, quantitative evaluation of brain tissue volumes showed excellent agreement between the two sequences, suggesting that the mild increase in image noise had minimal impact on quantitative brain tissue segmentation (Figure Panel A). The Dice coefficient for the brain regions evaluated varied from 0.88 to 0.95 (Figure Panel B). For all brain regions, the relative difference in volume was less than 10% between the two sequences, and was less than 5% for all regions other than the occipital lobes and cerebellum (Figure Panel C).
Conclusions
Brain volumes estimated using ultrafast Wave-MPRAGE show excellent agreement with standard MPRAGE in patients undergoing evaluation for suspected neurodegenerative diseases. Rapid high-resolution anatomical imaging of this population could result in reduced motion artifacts, reduced patient anxiety, and improved utilization of valuable MRI resources, and further clinical evaluation and validation is recommended.

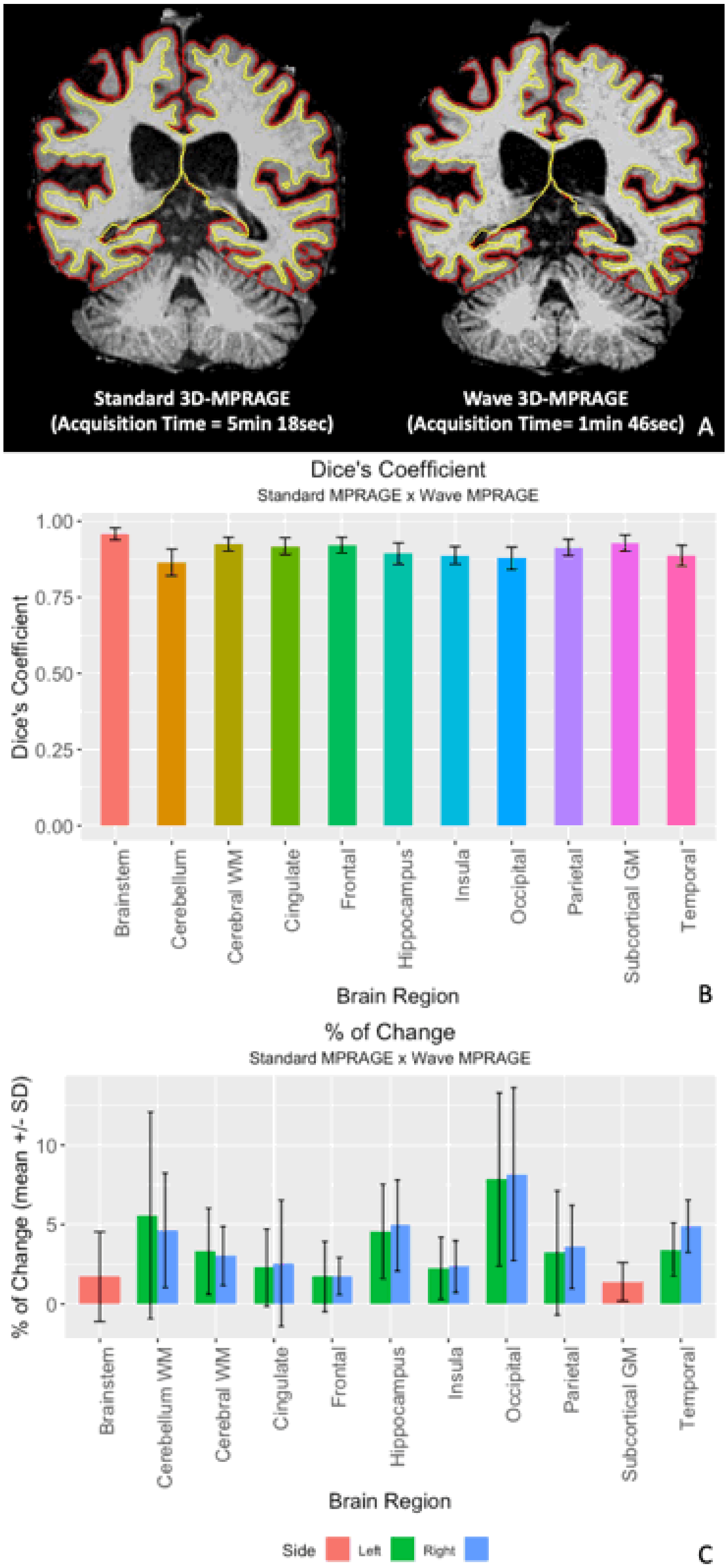

(Filename: TCT_2793_wave_mprage.gif)

2253

4:30PM - 4:37PM

Age, but Not Repeated Exposure to Gadoterate Meglumine, Is Associated with T1- And T2-Weighted Signal Intensity Changes in the Deep Brain Nuclei of Pediatric Patients

P Pozeg[1], R Meuli[1], J Forget[1], P Maeder[1]
[1]*Lausanne University Hospital, Lausanne, Switzerland*

Purpose
The studies on signal intensity (SI) changes in brain magnetic resonance images (MRI) and multiple exposures to macrocyclic gadolinium-based contrast agents (GBCA) in children are scarce, inconclusive(1–4), and possibly confounded with the effects of radiotherapy(1) and brain maturation processes(2). We have evaluated longitudinal SI changes of T1- and T2-weighted MRI of pediatric patients exposed to multiple administrations of gadoterate meglumine (Dotarem, Guerbet, France); and assessed correlations between the SI change and relevant clinical covariates, including age and radiotherapy. The study was followed-up with a cross-sectional control cohort of pediatric patients, naïve to any GBCAs to validate the effects of brain maturation on the SI changes.
Materials and Methods
Retrospective MRI data of 24 patients (1-20 years), who received at least 10 doses of exclusively gadoterate meglumine, were included in the longitudinal study, and the data of 190 GBCA naïve patients in the control, cross-sectional study. We measured SI (native, T1-weighted GRE and T2-weighted TSE) of 12 deep brain nuclei. The regions of interest (ROI) were measured at each of the first 11 MRI examinations of the contrast exposed patients, and at the first control patients' MRI. ROIs SI, normalized by the pons, were analyzed with mixed-effects models.
Results
The number of gadoterate meglumine administrations, radiotherapy or chemotherapy had no effect on the T1- or T2 weighted SI changes in any of the ROIs (all $p>0.05$), but age significantly correlated with increased SI in T1-weighted globus pallidus (GP) ($p<0.01$) and caudate ($p<0.05$), and decreased SI in T2-weighted GP ($p<0.001$) and dentate nucleus ($p<0.005$). The cross-sectional analyses of the control cohort showed a significant age-dependent SI increase in multiple ROIs, including T1-weighted GP and caudate, and decrease in T2-weighted GP and DN ($p<0.05$).
Conclusions
Age, but not repeated exposure to gadoterate meglumine, radiotherapy or chemotherapy, was associated with the SI changes in the pediatric brain.

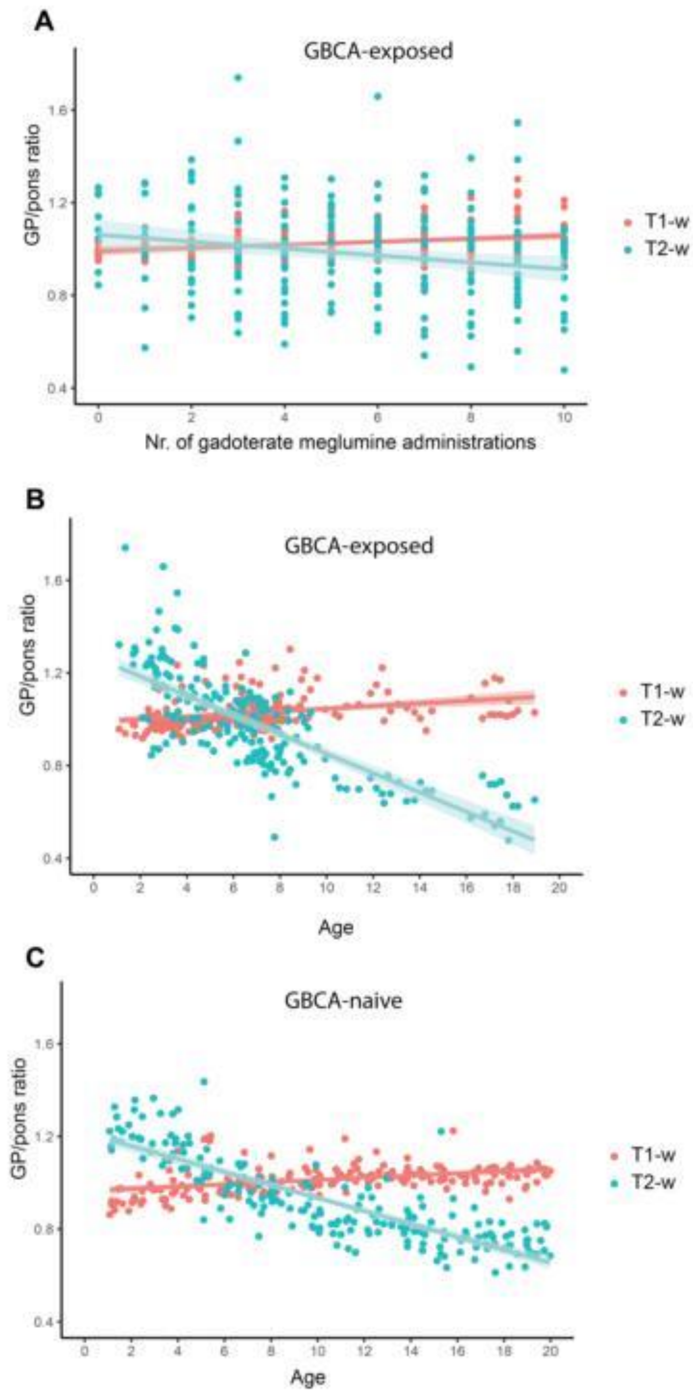

Figure1. GP/pons ratios for T1-weighted (GRE) and T2-weighted (TSE) signal intensities **(A)** across the first 10 gadoterate meglumine injections and **(B)** across age in GBCA -exposed patients, and across age in the control sample **(C)**. The shaded areas represent a 95% confidence interval of the regression line.

(Filename: TCT_2253_ANSRfigurecolor.jpg)

3539

4:37PM - 4:44PM

Biomechanical Accelerations Associated with Concussion and the Development of Microhemorrhages in High School Football

J Holcomb[1], B Shah[2], E Davenport[3], J Maldjian[4]
[1]UT SOUTHWESTERN MEDICAL CENTER, Dallas, TX, [2]UT Southwestern Medical Center, Irving, TX, [3]UNIVERSITY OF TEXAS SOUTHWESTERN, DALLAS, TX, [4]University of Texas Southwestern, Dallas, TX

Purpose
Previous literature has shown that rotational accelerations are associated with acquiring concussion, while linear inertial forces correlate with peak pressures within the brain. This study sought to identify specific types of accelerations unique to the acquisition of concussion and microhemorrhages in high school football.
Materials and Methods
91 high school football players were instrumented with the Head Impact Telemetry System during all practices and games to record linear and rotational head accelerations for each impact. Each subject underwent pre and post-season MRI including susceptibility-weighted imaging. Scans were reviewed by 2 board-certified neuroradiologists to quantify susceptibility lesion counts for each subject to estimate the number of microhemorrhages acquired during their season. None of the concussed subjects showed evidence of microhemorrhage. Subjects were separated into a microhemorrhage group (MH) (n=9), a concussed group (CG) (n=8), and a non-hemorrhaged, non-concussed group (NHNC) (n=74). Wilcoxon rank sum tests were used to compare peak rotational accelerations and peak linear accelerations between groups. CG was expected to show significantly greater peak rotational accelerations than MH and NHNC, while it was expected that MH would show significantly greater peak linear accelerations than MH and NHNC.
Results
Statistical analysis revealed significantly greater peak rotational accelerations in CG than in NHNC and MH (p-value=0.01572 and p-value=0.003949, respectively). There were no significant differences in peak rotational acceleration between the NHNC and MH. There were also no significant differences in peak linear accelerations between groups.
Conclusions
These findings suggest that concussion in high school football is associated with elevated peak rotational accelerations, but not peak linear accelerations. Additionally, development of microhemorrhage was not shown to be directly influenced by peak linear or peak rotational accelerations. These results suggest that even low peak accelerations over a season of high school football can lead to microhemorrhage. Location of impact may provide an unexplored risk factor for microhemorrhage development.

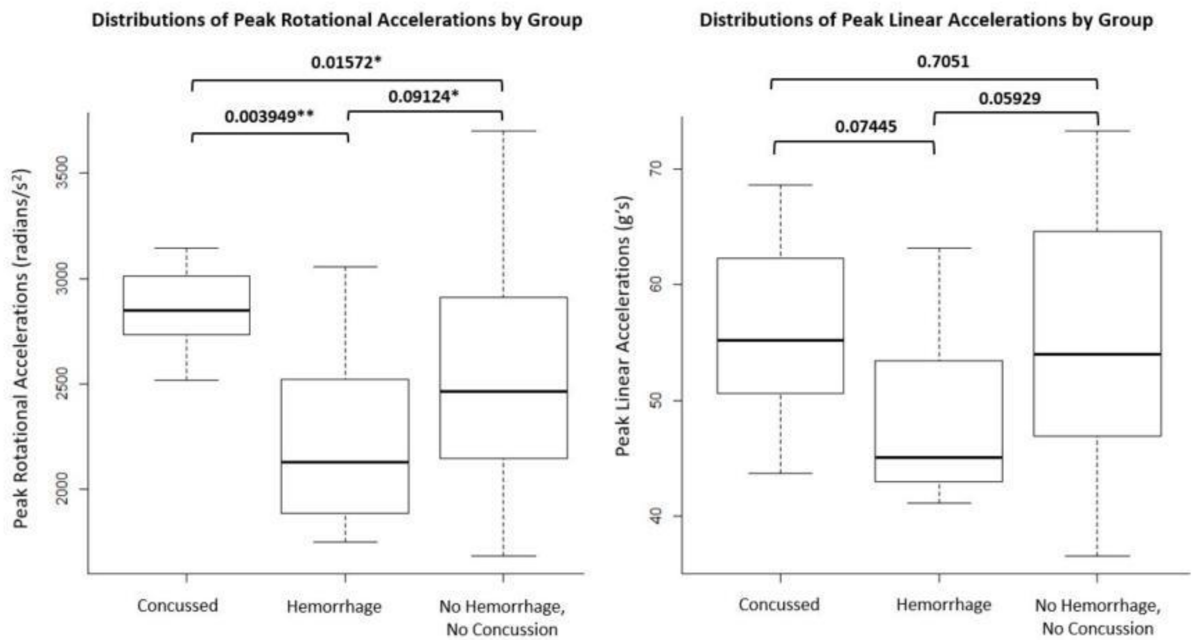

(Filename: TCT_3539_ASNR_2019_CONC_MICRO.JPG)

2528

4:44PM - 4:51PM

Clinical Utility of Diffusion Weighted Imaging of the Brain on Fetal MRI in Monochorionic Twin Gestation

M Kocaoglu[1], U Nagaraj[2], M Habli[3], B Kline-Fath[4]
[1]Cincinnati Children's Hospital Medical Center, Cincinnati, OH, [2]CINCINNATI CHILDREN'S HOSPITAL MEDICAL CENTER, CINCINNATI, OH, [3]Cincinnati Children's Hospital, Cincinnati, OH, [4]CINCINNATI CHILDREN'S HOSP. MED. CTR., CINCINNATI, OH

Purpose
Monochorionic twin pregnancies are associated with increased risk of cerebral injury when twin-twin transfusion syndrome (TTTS) occurs through the placental anastomosis. Selective fetoscopic laser photocoagulation (SFLP) of abnormal placental anastomosis has been considered the best method in moderate stages of TTTS. Our aim is to define the cerebral diffusion weighted (DW) and conventional magnetic resonance (MR) imaging abnormalities of monochorionic diamniotic fetuses before the SFLP.
Materials and Methods
An IRB-approved retrospective review of DW/MR images of fetal brains in 199 twin pairs and their electronic medical records from January 2014 to December 2015 performed. Fetuses with diagnostic quality of DW/MR studies before the SFLP were included. Axial DWI of each fetal brain was performed on a 1.5 T clinical magnets with a spin-echo echo-planar DWI sequence in the axial plane with b-values 0, 350 and 700 s/mm3 in 3 orthogonal directions, by using a phased array abdominal coil. Visibility of abnormal signal or structural changes on DW and conventional MR sequences (T2-SSFSE) were noted.
Results
A total of 144 monochorionic diamniotic twins with gestational ages 15-26 weeks and diagnostic quality of DW imaging were included. Abnormalities identified only by DW imaging include diffusion restriction in 5 donors (n=3 diffuse, n=2 focal) and focal diffusion restriction in 2 recipient fetuses. Additional abnormalities such as ventriculomegaly (n=5), germinal matrix hemorrhage (n=3) and encephalomalacia (n=1) were observed both on DW and conventional MR sequences.

Conclusions
DW imaging is feasible in fetuses. Cerebral damage in TTTS can be detected in both donor and recipient fetuses before the SFLP. DW imaging can show acute, subacute and chronic changes. It helps to obstetrician in deciding to proper therapeutic approach and also counseling the parents for possible outcomes of these injuries.

2517

4:51PM - 4:58PM

Diffusion Weighted MR Imaging in a Prospective Cohort of Children with Cerebral Malaria Offers Insights into Pathophysiology and Prognosis

S Mohajeri Moghaddam[1], G Birbeck[2], T Taylor[3], K Seydel[3], S Kampondeni[4], M Potchen[2]
[1]University of Rochester Medical Center, Rochester, NY, [2]University of Rochester Medical Center, Rochester , NY, [3]Michigan State University, East Lansing, MI, [4]University of Malawi College of Medicine, Blantyre , Blantyre

Purpose
Cerebral malaria (CM), the most severe form of malaria illness, primarily affects young children and despite antimalarial treatment carries significant morbidity and mortality. In the past decade, imaging studies have uncovered new insights into the pathophysiology of the syndrome. Our group has previously described the range of MRI abnormalities, generated by a 0.35T MRI in Malawi, during the acute phase of CM. Findings from diffusion-weighted sequences were initially excluded due to concerns regarding the validity of the diffusion weighted imaging (DWI) data from this machine. These data have now been validated, and we reviewed various patterns of diffusion restriction in this large cohort of children with CM (n = 269). There was one unusual pattern of isolated white matter diffusion restriction, and given the limited understanding of coma etiology in pediatric CM, we further evaluated risk factors for and outcomes associated with this unique imaging pattern.
Materials and Methods
From 2009-2014, comatose children admitted to the Pediatric Research Ward of Queen Elizabeth Central Hospital in Blantyre, Malawi who met inclusion criteria for CM underwent brain MRI. Inclusion criteria required evidence of P. falciparum parasitemia, coma, and no other etiology for coma evident. Imaging data were interpreted independently by two fellowship trained neuroradiologists and compiled into NeuroInterp, a searchable RedCap database. Specific patterns of diffusion restriction were identified for categorization. 'Isolated White Matter Diffusion Restriction' included study participants who demonstrated isolated subcortical DWI abnormality on MRI without concurrent basal ganglia and cortical diffusion restriction using established norms. Clinical information collected included temperature, whole blood lactate and glucose levels, systolic blood pressure, HIV status, history of seizures prior to admission, histidine-rich protein (HRP-II) levels (a molecular marker of parasite burden), anticonvulsant administration upon admission, and overall coma duration (a combination of coma prior to admission, and coma after the onset of antimalarial treatments). Outcomes were categorized as death, neurologic sequelae at discharge, or full recovery.
Results
A total of 269 consecutive pediatric patients with CM were imaged on the 0.35 Tesla GE MRI. Mean age was 51.4 months. Of these, 194/269 (72.1%) demonstrated at least one area of diffusion restriction. The most common pattern observed was bilateral subcortical white matter involvement (112/269, 41.6%). Other patterns included cortical gray matter (48/269, 17.8%) deep gray matter (99/269, 36.8%), corpus callosum (101/269, 37.5%) and posterior fossa (24/269, 8.9%) involvement. Sixty-one (22.7%) CM children demonstrated the unusual pattern of isolated subcortical white matter diffusion restriction. Children with isolated subcortical white matter restricted diffusion had significantly lower whole blood lactate levels (OR 0.9, 95% CI 0.85-0.98), and were less likely to have required anticonvulsant medication upon admission, (OR 0.6, 95% CI 0.30-0.98). All but one of the 61 children with isolated

subcortical white matter diffusion restriction survived (OR 11.3, 95% CI 1.5-83.9). Among survivors, 55 (90%) fully recovered without evidence of neurologic sequelae at discharge (OR 3.7, 95% CI 1.5-9.1).
Conclusions
Restricted diffusion is an extremely common finding on MRI in Malawian children with CM. Among specific patterns of diffusion restriction in this cohort, we observed an unusual pattern of isolated white matter diffusion restriction not often seen in Western settings. This pattern is associated with a less severe form of the disease and carries a good prognosis for full recovery. It may represent selective vulnerability of the white matter to the deleterious reversible physiologic changes that occur with CM. MRI DWI may offer a biomarker for risk stratification in cerebral malaria clinical trials.

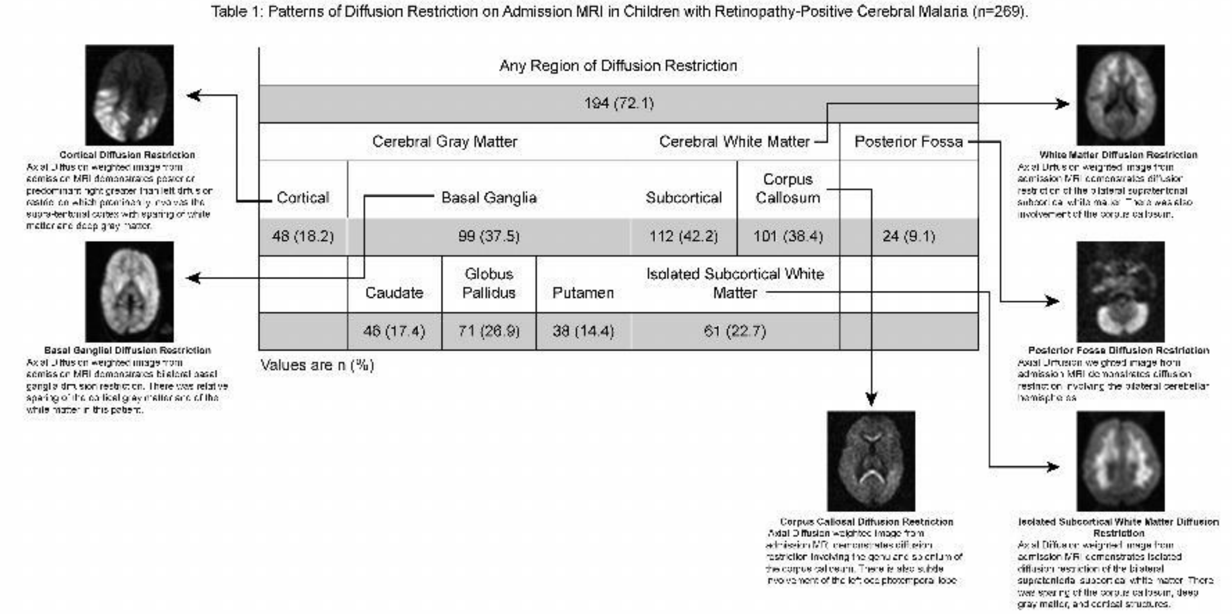

Table 1: Patterns of Diffusion Restriction on Admission MRI in Children with Retinopathy-Positive Cerebral Malaria (n=269).

Any Region of Diffusion Restriction						
194 (72.1)						
Cerebral Gray Matter				Cerebral White Matter		Posterior Fossa
Cortical	Basal Ganglia			Subcortical	Corpus Callosum	
48 (18.2)	99 (37.5)			112 (42.2)	101 (38.4)	24 (9.1)
	Caudate	Globus Pallidus	Putamen	Isolated Subcortical White Matter		
	46 (17.4)	71 (26.9)	38 (14.4)	61 (22.7)		

Values are n (%)

(Filename: TCT_2517_Table1-95by5.jpg)

3554

4:58PM - 5:05PM

Early Brain Findings in Cerebral Adrenoleukodystrophy: Are We Missing Subtle Disease?

D Nascene[1], A Swenson[1]
[1]*University of Minnesota, Minneapolis, MN*

Purpose
To review the earliest findings of cerebral Adrenoleukodystrophy on brain MRI and to review the accuracy of radiologist interpretations. We also explored the age of onset of cerebral disease, location of cerebral disease, and the impact of screening intervals on disease progression.
Materials and Methods
From a database of 222 ALD patients, we identified 30 patients with a reported normal MRI on initial presentation. We reviewed the MRI studies to identify the spectrum of subtle abnormalities and volume of involvement. We also noted whether or not the earliest disease was identified on initial interpretation. We then subdivided those 30 patients into four groups: 1-Patients with true negative MRI studies throughout the follow-up interval (n=8), 2-Initial normal MRI where early findings of ALD were recognized (n=6), 3- Initial normal MRI where early findings of ALD were unrecognized (n=9), and 4- Initial MRI true positive for ALD but reported normal (n=7). The 22 patients with disease progression were further

characterized by screening interval to determine whether the screening interval was associated with greater extent of disease.

Results

The mean age of disease onset of the 20 pediatric patients in this study was 5.25, range 3-9 years. Two adults were 26 and 46 years old. The splenium of the corpus callosum was involved in 19 of the 22 patients (86%). One 5-year-old boy had genu involvement. Interestingly, neither of the adult patients had involvement of the splenium at diagnosis, with one having genu involvement and another with brainstem involvement. Early, subtle signs of cALD were missed in 73% of cases despite the onset of disease in common areas of involvement. However, we did note that in many cases the earliest involvement of the corpus callosum was at the edges rather than centrally within the splenium. In regards to Loes scores, there was not a large difference in Loes scores at disease onset in the 6 or less vs 12 or more month groups. However, the average increase in Loes score from scans prior to disease onset to follow up after first sign of disease was greater in the 12 or more month screening interval group. When initial findings were missed, the volume of diseased white matter was less at 6 months screening than at 12 or more months. One patient from the 6 month group had a very large increase in volume of brain matter involvement (34.5 cm3) at 6 month follow up. Differences in volume of affected diseased brain matter in the 6 or less vs 12 month screening interval groups were not found to be statistically significant (p=.45).

Conclusions

The purpose of this study was to better characterize early radiologic findings in cerebral X-ALD patients so that treatment can begin and overall outcomes can improve. Area of involvement from our review of first abnormal MRI correlates well with the findings by Loes [4]. Despite affecting commonly known areas, early MRI changes can be extremely subtle and may easily be missed. In our study, 73% of cases of initial onset of cALD were missed. However, whether early disease was recognized or not did not seem to have a significant effect on the majority of patients disease progression. However, one patient had severe disease progression in the group where early findings of ALD were not recognized. Such extreme outliers in a low sample size makes data interpretation more difficult. In regards to screening, the patients screened at 6 month intervals had lower volume of disease brain matter upon post cALD follow up compared to those screened every 12 or more months also shown in Figure 4. Patients treated with a Loes score <10 have a much higher 5 year survival rate than those with higher scores [5]. Therefore, if we can recognize disease early enough, patients are likely to have better outcomes. Time of cALD onset varied but the majority were ages 3-7 when initial disease was identified, which is consistent with current literature. In conclusion, we believe it would be appropriate to start screening X-ALD patients every 6 months from ages 2-10 with careful attention to common areas of involvement. Gadolinium administration may not be necessary in screening for early cerebral ALD.

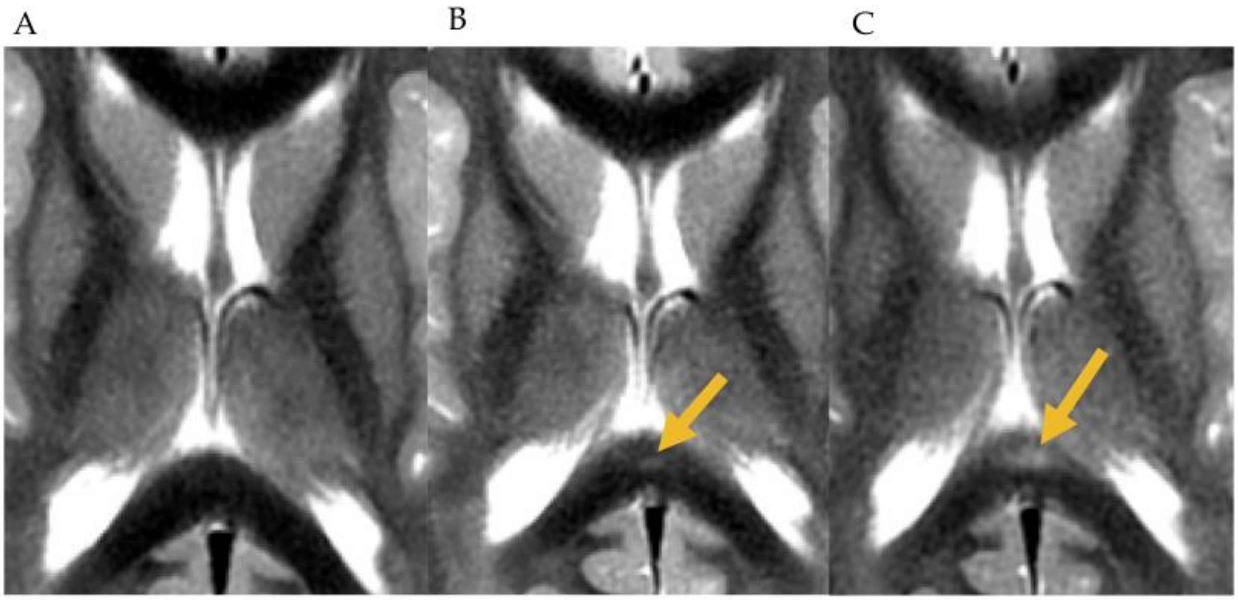

Figure 3 shows the subtle progression of disease in the central splenium. Image A shows normal splenium before disease onset. Image B shows subtle T2 signal indicated by orange arrow at 6 month follow up. Image C shows worsened T2 signal indicated by white arrow at 12 month follow up.

(Filename: TCT_3554_ALDposter-FINAL-FINAL.jpg)

3328

5:05PM - 5:12PM

Effect of Early MRI in the Management of Pediatric Traumatic Head Injury

K Buch[1], P Caruso[2]
[1]*Massachusetts General Hospital, Boston, MA,* [2]*MGH, Boston, MA*

Purpose
CT is traditionally considered standard of care for the assessment of pediatric traumatic brain injury (TBI). MRI offers improved detection of pediatric TBI but remains underutilized in this setting. Our purpose is to describe the effect of early MRI findings in the management of a cohort of children admitted to the PICU with TBI.
Materials and Methods
We retrospectively identified patients admitted to the PICU with an acute head injury between September 2010 and May 2018 and who underwent head CT and MRI within the first 96 hrs. We compared MRI with CT findings, using the NIH Common Data Elements definitions of injury type. We determined by chart review whether and how MRI findings led to a change in PICU management, defined as either an escalation or a de-escalation of care.
Results
MRI identified additional lesions in 60/94 (64%) of patients who had first undergone head CT. 49/60 (82%) patients had intra-parenchymal lesions, 22/60 (37%) had extra-axial lesions, and 11/60 (18%) had both intra-parenchymal and extra-parenchymal lesions identified by MRI. The most frequent lesions were contusions and traumatic or diffuse axonal injury. Acute management was influenced by MRI in a majority, leading to a de-escalation of care in 50%, and an escalation of medical or surgical management in 33%.

Conclusions
Early MRI may have a beneficial role in the acute management of pediatric TBI. MRI frequently identified lesions not appreciated on CT. Using MRI in acute TBI frequently impacts management decisions.

2786

5:12PM - 5:19PM

Iron Deposition in Deep Gray Matter Nucleus on Pediatric Patients with MCT8 Transporter Deficiency: Can MRI Identify Disrupted Neuronal Processes?

M Beasley[1], M Beasley[1], C McGill[2], L Bonilha[2], M Matheus[3]
[1]MUSC, Charleston, SC, [2]Medical University of South Carolina, Charleston, SC, [3]MEDICAL UNIVERSITY OF SOUTH CAROLINA, MT. PLEASANT, SC

Purpose
MCT8 transporter deficiency (MCT8) is a rare X-linked neurogenetic disorder. It occurs from a mutation in the monocarboxylate transporter 8 gene encoding a thyroid hormone transporter. The affected boys present early in life with significant neurodevelopmental delays, hypotonia, and involuntary movements, most often dystonia. Abnormal levels of iron in the basal ganglia, substantia nigra (SN) and red nucleus (RN) have been implicated with movement disorders and disrupted neuronal processes including dopaminergic abnormalities. Our hypothesis is that iron levels in the deep gray matter structure of pediatric MCT8 patients may be altered and could be detected by brain MRI studies
Materials and Methods
Pediatric patients with MCT8 (n=11), age 2-13 years, were recruited with an almost symmetrical distribution to reflect 12 years of childhood. Age and gender matching normal controls were also recruited (n=17). Brain MRI volumetric T1-weighted and proton transverse relaxation rate (R2*) pulse sequences were acquired. Deep gray matter structures were segmented and R2* values were measured in the caudate, putamen, SN and RN in both groups. An independent samples t-test was used for comparison between groups.
Results
Comparison of R2* values between MCT8 patients and age-matched control subjects showed significantly lower R2* values on MCT8 patients in the caudate nucleus=4.76E-06 ($p<0.01$), putamen=0.00015 ($p<0.01$), and RN=0.04 ($p<0.05$). No statistical difference was noted in the SN=0.42.
Conclusions
The results reveal lower R2* in some of the selected deep gray matter structures (caudate, putamen, RN) of MCT8 patients which can be extrapolated to abnormal iron accumulation. Investigation in other neurological diseases reported the association of low brain iron to disrupted neuronal process and dopaminergic abnormalities. This finding has never been reported with MCT8 and may reflect a new biomarker for disrupted neuronal processes, or at least a starting point for additional investigation.

3548

5:19PM - 5:26PM

Microstructural Changes in Multipotent Neural Stem Cell Niche Associated with Subconcussive Impacts in High School Football

J Holcomb[1], B Shah[2], E Davenport[3], J Maldjian[4]
[1]UT SOUTHWESTERN MEDICAL CENTER, Dallas, TX, [2]UT Southwestern Medical Center, Irving, TX, [3]UNIVERSITY OF TEXAS SOUTHWESTERN, DALLAS, TX, [4]University of Texas Southwestern, Dallas, TX

Purpose
The subventricular zone (SVZ) is a brain region known to contain multipotent neural stem cells1,3. The purpose of this study was to use mean diffusivity (MD), to investigate structural changes in the SVZ related to subconcussive impacts in high school football.
Materials and Methods
16 high school football players were instrumented with the Head Impact Telemetry System (HITS) during all practices and games to record number of head impacts and head impact magnitude. HITS data were used to compute the combined probability risk weighted cumulative exposure (RWECP) for each subject2. Each subject underwent a pre and post-season MRI, including diffusion tensor imaging (DTI). Six controls also underwent the same scanning protocol. SVZ masks were generated on structural images using FreeSurfer by multiplying the caudate nucleus segmentation with the lateral ventricle segmentation dilated using the morpholocial dilation operator and applied to coregistered and normalized DTI data using VBM8. Average MD values were extracted using the normalized mask for each scan. Linear regression analysis was performed comparing RWECP with percent changes in SVZ-MD. Peak linear and rotational accelerations were included as covariates in the model. The subject population was divided by RWECP into tertiles, with the percent change in SVZ-MD of the highest and lowest impact subjects compared against those of controls.
Results
Regression analysis demonstrated a significant inverse relationship between RWECP and percent change in SVZ-MD (p-value=0.000204, R2=0.6386). Peak accelerations did not demonstrate any significant relationships with changes in SVZ-MD. The high impact group showed significantly greater decreases in SVZ-MD than controls (p-value=0.01358). The low impact group did not show a significant difference in SVZ-MD changes than controls (p-value=0.4546).
Conclusions
This study demonstrates that significant decreases in MD in the SVZ are associated with the subconcussive, cumulative impact exposure experienced in high school football. Reduced MD may indicate neural stem cell activation and proliferation following trauma1,3.

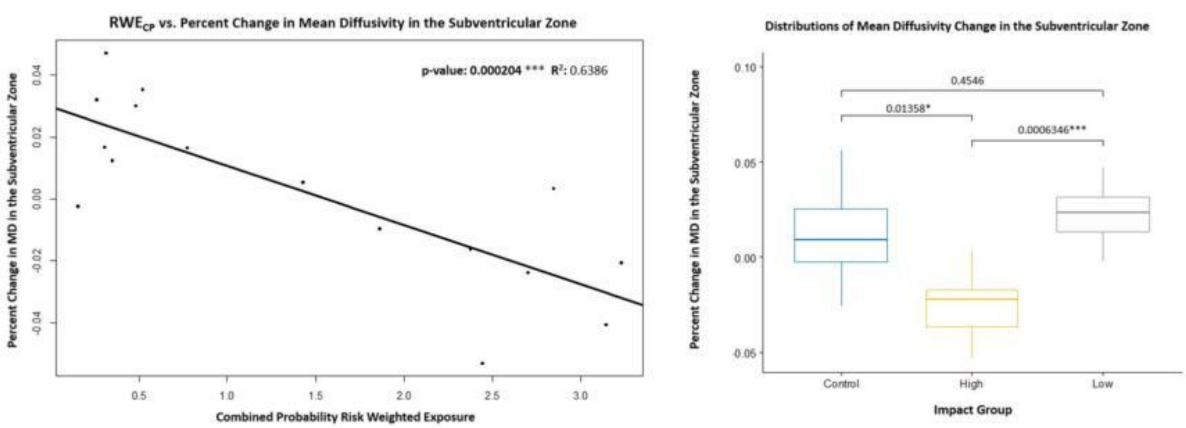

(Filename: TCT_3548_SVZ_img_ASNR_2019.JPG)

3546

5:26PM - 5:33PM

MRI Findings in a Pediatric Population with Neurologic Disease and Enterovirus A71 Infection

J Maloney[1], I Neuberger[1], D Mirsky[2], N Stence[1], K Reddy[3], K Messacar[1], L Fenton[1]
[1]Children's Hospital Colorado, Aurora, CO, [2]CHILDRENS HOSPITAL COLORADO, AURORA, CO, [3]UNIVERSITY OF COLORADO ANSCHUTZ MED CTR, DENVER, CO

Purpose

In the summer and fall of 2018, the state of Colorado experienced an outbreak of hand, foot and mouth disease (HFMD) associated with enterovirus A71 (EV-A71). We characterized MRI findings in a cohort of patients presenting to our institution during this period with neurological disease and EV-A71 infection.

Materials and Methods

Patients presenting to our institution between 3/1/2018 and 9/30/2018 who tested positive for enterovirus on nasal, throat, or rectal swab had EV-A71 subtyping performed by the Centers for Disease Control. Inclusion criteria were: age 1 month-18 years, neurologic complaints following febrile illness, positive EV-A71 testing, and MRI of the brain and spinal cord performed while symptomatic. Chart and neuroimaging review was performed by two pediatric neuroradiologists (JAM and NVS).

Results

Twenty brain MRIs and 19 spine MRIs were analyzed, from eighteen patients meeting inclusion criteria (16 males; mean age 34.4 months). Neurologic manifestations included meningitis (16 of 18 patients), encephalitis (17), myoclonus (16), and ataxia (16). Seven patients met CDC clinical criteria for acute flaccid myelitis (AFM). Intracranial sites of MRI abnormalities included the dorsal pons (15), dentate nuclei (15), medulla (11), supratentorial lesions (4) and leptomeningeal enhancement (5). Fourteen spinal cord lesions were identified, average length 11.6 vertebral segments, involving central gray matter diffusely (11) or focally in the anterior horns (3). Four patients had normal neuroimaging. Spinal cord lesions were seen in all 7 AFM patients and in 5 patients without limb weakness. No deaths or cardiopulmonary collapse occurred. Neurologic symptoms completely or nearly completely resolved.

Conclusions

Our findings match prior descriptions of enterovirus-related neurologic disease, including EV-A71 (1-3). In contrast to AFM in the setting of enterovirus D68 infection, we found poor correlation between spine MRI findings and limb weakness, and clinical outcomes were less severe. This study adds to descriptions of clinical and neuroimaging findings in EV-A71 infection.


(Filename: TCT_3546_EVA71spine.JPG)

3411

5:33PM - 5:40PM

Neuroimaging and Natural History of FIRES in a Pediatric Population

J Hunter[1]
[1]*TCH/BAYLOR, HOUSTON, TX*

Purpose
To describe the imaging and natural history of febrile infection-related epilepsy syndrome presenting to a tertiary referral pediatric center over the past 4 years.
Materials and Methods
A word engine search of the PACS system at a tertiary referral pediatric hospital was performed using the term FIRES. Seven children were identified who fulfilled clinical criteria for FIRES. Their imaging and clinical course were studied and are reported.
Results
Seven children (5 females and 3 males) age range 5-19 y.o. (mean = 8 years) who fulfilled clinical criteria for FIRES were identified. All children had long hospital stays, 4 of the 7 requiring phenobarbital coma for intractable epilepsy as defined by the use of 3 or more AEDs. One child spent 90 days in the ICU. Outcomes correlated with length of hospital stay. There was a range of imaging findings .All

children sustained a degree of diffuse cerebral volume loss. The most severely affected children (n =2) sustained periventricular gliosis. Four of the seven children demonstrated evidence for hippocampal damage by imaging, presumed related to a "kindling" effect. All children had some degree of cognitive impairment on follow-up after their discharge from the hospital.

Conclusions

FIRES can be a devastating illness requiring prolonged hospital stays and with longterm cognitive sequelae. While there is a range of outcomes, in this small cohort outcome appeared to correlate with duration of hospitalization and the need for therapeutically induced coma to control the intractable epilepsy syndrome.

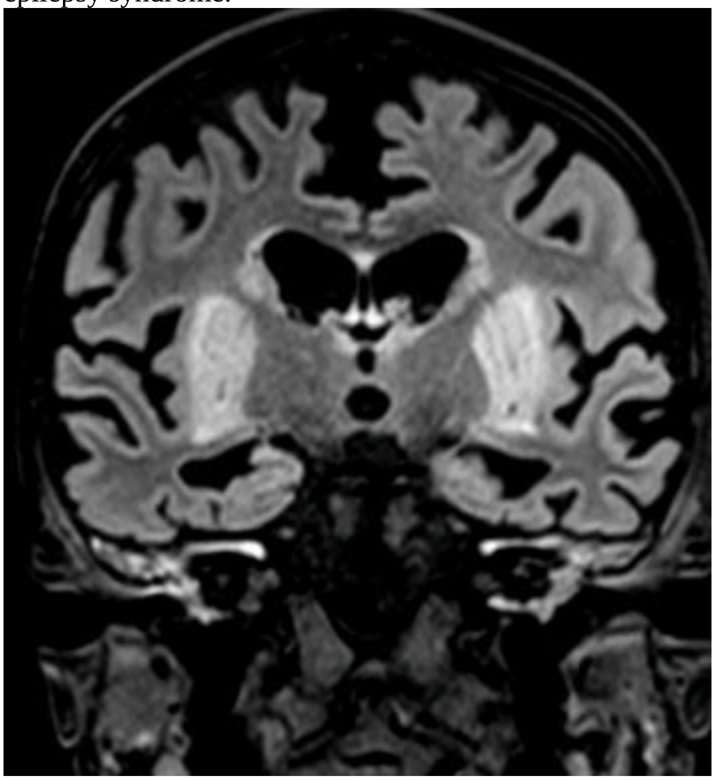

(Filename: TCT_3411_asnr_2019fig1.jpg)

2272

5:40PM - 5:47PM

White Matter Tract Development in Autistic Toddlers by Diffusion Tensor Imaging and Correlation with Ongoing Therapies

R Hourani[1], S Saaybi[2], S Hannoun[3], R Tutunji[4], N ALArab[1], M saade[5], C Zeeni[6], R Shbarou[2], R Boustany[2]

[1]Department of Diagnostic Radiology, American University of Beirut Medical Center, Beirut, Lebanon, [2]Department of Pediatrics and Adolescent Medicine, American University of Beirut Medical Center, Beirut, Lebanon, [3]Biomedical and Molecular Genetics, American University of Beirut Medical Center, Beirut, Lebanon, [4]Donders Institute for Brain, Cognition and Behaviour, Department of Cognitive Neuroscience,RUMC, Nijmegen, Netherlands, [5]Special Kids Clinic,American University of Beirut Medical Center, Beirut, Lebanon, [6]Department of Anesthesiology, American University of Beirut Medical Center, Beirut, Lebanon

Purpose

Autism spectrum disorders (ASDs) are neurodevelopmental disorders characterized by social, communication and behavioral symptoms. Early intervention including speech, occupational and psychomotor therapies, in addition to Applied Behavior Analysis (ABA) have improved the outcome in affected children, as confirmed by the following assessment battery (Verbal Behavior Milestones Assessment and Placement Program or VB-MAPP). Given that aberrancies in white matter (WM) development may play a role in the pathogenesis of ASDs, this study aims to identify culprit WM tracts through diffusion tensor imaging (DTI) indices, as well as to correlate these radiological findings with clinical improvement after therapies.

Materials and Methods

DTI scans were acquired for 17 toddlers diagnosed with ASD (median age 2.9 years); 10 of whom had a follow up MRI one year after institution of early intervention and ABA programs and 7 age-matched controls (medium age 3 years) on a 3T MRI system. VB-MAPP scores of ASD subjects are determined at diagnosis and one year after initiation of therapies. In addition, DTI indices including fractional anisotropy, mean diffusivity, radial diffusivity and axial diffusivity, are measured and recorded by TBSS (Tract-Based Spatial Statistics).

Results

There was significant improvement in VB-MAPP scores as early as 6 months following ABA and early intervention therapies. TBSS analysis showed significant decrease in Regions Of Interest (ROIs) in FA and increase in RD when comparing ASD patients at baseline to the control group; and increase in AD in treated ASD patients compared to control subjects. When comparing ASD patient scans pre- and post-therapies, a significant increase in ROIs FA is noted.

Conclusions

These findings highlight several WM abnormalities detected in brain of ASD subjects at diagnosis, and further confirm the benefits of ABA programs. DTI is suggested as an objective tool to clinical assessments that aids in monitoring response of ASDs patients to therapies.

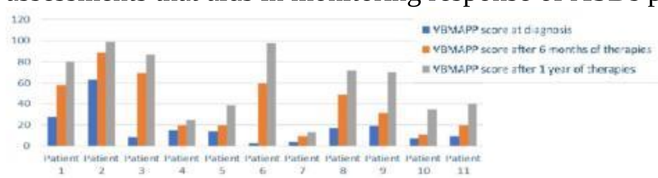

Graph showing the VBMAPP scores among treated ASD patients at diagnosis, after 6 months and after 1 year of therapy

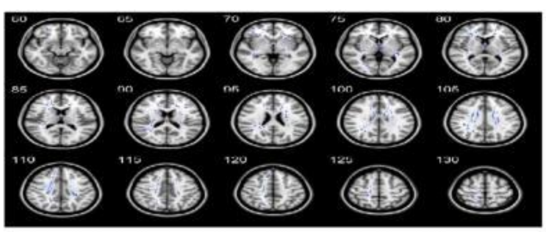

White matter tracts showing significantly higher values (>5%, p<0.05) in fractional anisotropy (FA) in brain scans of normotypical controls compared to brain scans of ASD patients at diagnosis, based on TBSS.

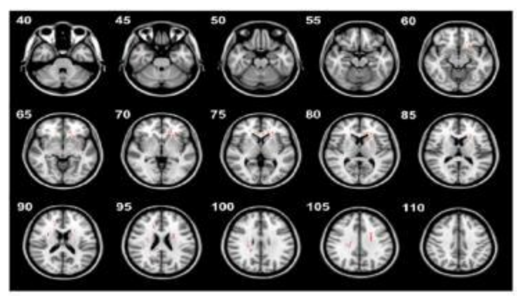

White matter tracts showing significantly lower values (>5%, p<0.05) in radial diffusivity (RD) in brain scans of normotypical controls as compared to brain scans of ASD patients at diagnosis, based on TBSS

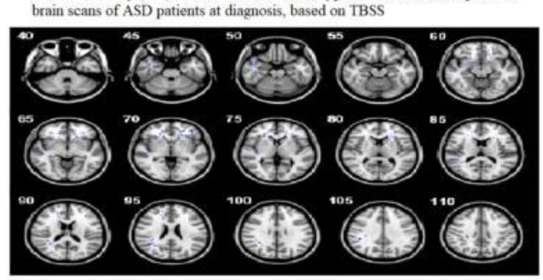

White matter tracts showing significantly higher values (>5%, p<0.05) in fractional anisotropy (FA) in brain scans of ASD patients following one year of therapies as compared to brain scans of ASD patients at diagnosis, based on TBSS.

(Filename: TCT_2272_DTIstudyfile.jpg)

2175

4:30PM - 4:37PM

A Comprehensive Clinical Care Pathway for the Appropriate Management of Vertebral Fragility Fractures

O Clerk-Lamalice[1], J Hirsch[2], D Beall[3], M Chambers[4], T Andreshak[5], A Brook[6], B Bruel[7], H Deen[8], P Gerszten[9], D Kreiner[10], C Sansur[11], S Tutton[12], P van der Meer[13], H Stoevelaar[14]
[1]University of Alberta, Edmonton, Alberta, [2]MASSACHUSETTS GENERAL HOSPITAL, BOSTON, MD, [3]Spine Fracture Institute, Edmond, OK, [4]University of Alabama at Birmingham, Birmingham, AL, [5]Consulting Orthopaedic Associates, Toledo, OH, [6]Montefiore Medical Center, Bronx, NY, [7]Baylor College of Medicine- McNair Campus, Houston, TX, [8]Mayo Clinic, Jacksonville, FL, [9]University of Pittsburgh Medical Center, Pittsburgh, PA, [10]Ahwatukee Sports & Spine, Phoenix, AZ, [11]University of Maryland Medical Center, Baltimore, MD, [12]Medical College of Wisconsin, Milwaukee, WI, [13]Southern New Hampshire Radiology Consultants, Belford, NH, [14]Ismar Healthcare, Belgium, Lier

Purpose
Vertebral fragility fractures (VFF) are very common and associated with significant morbidity and mortality. There is a lack of consensus on the appropriate management of patients with or a suspected VFF. This study aimed at developing a comprehensive Clinical Care Pathway (CCP) for VFF.
Materials and Methods
The RAND/UCLA Appropriateness Method (RUAM) was used to develop patient-specific recommendations for the various components of the CCP. A multidisciplinary expert panel (orthopedic and neurosurgeons, interventional radiologists and pain specialists) assessed the importance of signs and symptoms for the suspicion of VFF, the relevance of diagnostic procedures, the appropriateness of vertebral augmentation versus non-surgical management in a variety of clinical scenarios, and the adequacy of follow-up care.
Results
The panel identified ten signs and symptoms to be relatively specific for VFF. In patients suspected of VFF, imaging was considered mandatory, with MRI being the preferred diagnostic modality. Vertebral augmentation was considered appropriate in patients with positive findings on advanced imaging and in whom symptoms had worsened and in patients with 2 to 4 unfavorable conditions (e.g. progression of height loss, severe impact on functioning), dependent on their relative weight. Time since fracture was considered less relevant for treatment choice. Follow-up should include evaluation of bone mineral density and treatment of osteoporosis.
Conclusions
Using the RUAM, we present a multidisciplinary expert panel established a comprehensive CCP for the management of VFF. The CCP may be helpful to reduce practice variations and thus to improve quality of care.

3531

4:37PM - 4:44PM

Combined Percutaneous Radiofrequency Ablation and Vertebroplasty (CRAV) for Vertebral Tumors: A Prospective Single Center Study with Longitudinal MRI Follow-Up

A Hedjoudje[1], D San Millán[2]
[1]Johns Hopkins University, Baltimore, MD, [2]Sion Hospital, Sion, Valais

Purpose
There is an increasing body of literature that suggests that combined percutaneous RFA and vertebroplasty (CRAV) is a safe and efficacious procedure offering pain management, vertebral stabilization and local tumor control. The purpose of this study, was to prospectively evaluate the local antitumoral effect of CRAV in the treatment of vertebral metastatic or primary tumors, to analyze local antitumoral effect of CRAV with respect to systemic progression.
Materials and Methods
This is a single institution prospectively conducted study. A standard pre- and post- treatment imaging protocol including dynamic contrast enhanced MRI (DCE-MRI) was established and conducted for all patients undergoing CRAV. A set of specified pre-procedure imaging characteristics were assessed for each lesion and used for comparison with post procedures follow up MRI (degree of vertebral body tumor invasion, degree of epidural involvement (grade 1-3: 1 = bulging not extending behind the anterior surface of the thecal sac; 2 = extension circumferentially or hemi-circumferentially with persistent CSF around the spinal cord; 3 = no CSF around spinal cord), tumor enhancement characteristics on DCE-MRI). The same MRI protocol performed in the same MRI scan was obtained before CRAV, at day 0 and at 1, 3, 6, 12 months. At each follow-up exam tumor status was classified as "local control" ("avascular zone" and tumor volume residue insignificant compared to initial tumor volume on day 0 MRI, or enhancement with DEC-MRI curves consistent with inflammatory or fibrosis on follow-up MRI) or "local control failure" (significant tumor residue on day 0 MRI or tumor progression at any time point) based on morphological criteria and contrast enhancement patterns of the tumor on DCE-MRI. Non-treated (by CRAV) additional remote bone lesions at the time of CRAV were considered as "control lesions" on follow-up MRIs.
Results
A total of 25 patients were included in the study, 8 males and 17 females, aged 51-81 years (mean age : 62). A total of 44 lesions (42 metastasis, 2 primary tumors) were treated. Primary site of metastasis were : breast 24%, prostate 16%, lung 12%, cholangiocarcinoma and kidney 8%.4/44 lesions were located in the iliac bone, the remaining 40 lesions were in the vertebras. Primary bone tumors were 1 B-cell lymphoma and 1 plasmocytoma (initially thought to be a gastric carcinoma metastasis). 36/ 40 vertebral lesions had epidural space involvement (50% with extensive grade 2 or 3). Mean time of follow-up was 244 days (range 27-423 days). No radiological or clinical procedural complications were observed. All patients underwent chemotherapy. 12/44 lesions underwent adjuvant radiation therapy (RT). Over the entire study period, radiological "local control" of lesions was observed in 36/44 (81%) including 24 /36 lesions that showed "local control" on day 0 MRI, 2 lesions that showed "local control failure" at day 0 MRI and remained stable on follow-up MRIs (no progression) and 10 lesions that showed "local control failure" on day 0 MRI and subsequently regressed. Over the entire study period, "local control failure" with tumor progression was observed in 8/44 (19%), including 1 lesion that showed "local control" on day 0 MRI and progressed on MRI at 1 month, and 7 lesions which showed "local control failure" on day 0 MRI. Of the 36 lesions with "local control", there were 5 lesions (without RT) associated with remote bone lesion regression, 5 lesions (2 without RT, 3 with RT) associated with remote bone lesion stability, 13 lesions (11 without RT and 2 with RT) associated with remote bone lesion progression. Overall, systemic disease progression (mean time to systemic progression 139 days, range 26– 423 days) occurred in all non-controlled lesions (8/8, 100%) and in 18 of the 36 (50 %) locally controlled lesion (50 %).
Conclusions
Over the entire study period, local tumor control was obtained in 86% of lesions treated with CRAV even in cases of systemic disease progression. "Local tumor control" observed at day 0 MRI after CRAV was highly predictive of sustained "local tumor control" with only one case of subsequent local tumor progression. RT likely had a minor impact on local tumor control in most lesions. CRAV is safe, with no clinical complications observed during and after treatment. CRAV, in addition to providing rapid pain relief and bone stabilization, offers local tumor control in a high proportion of lesions. These results contribute to the growing argument for a multidisciplinary approach to the management of metastatic bone disease that incorporates percutaneous ablation for pain palliation and local tumor control. For the

vast majority of patients, local tumor progression was found less frequently than systemic progression and epidural tumoral involvement was often decreased. CRAV may allow curative resection which is of particular importance of patient with oligo metastatic disease. Figure legend : MRI follow up of of 56 year old male with isolated L5 metastasis from oesophagus carcinoma treated with CRAV before treatment (A), at 1 month (B), 3 months (C) and 11 months (D) after treatment.

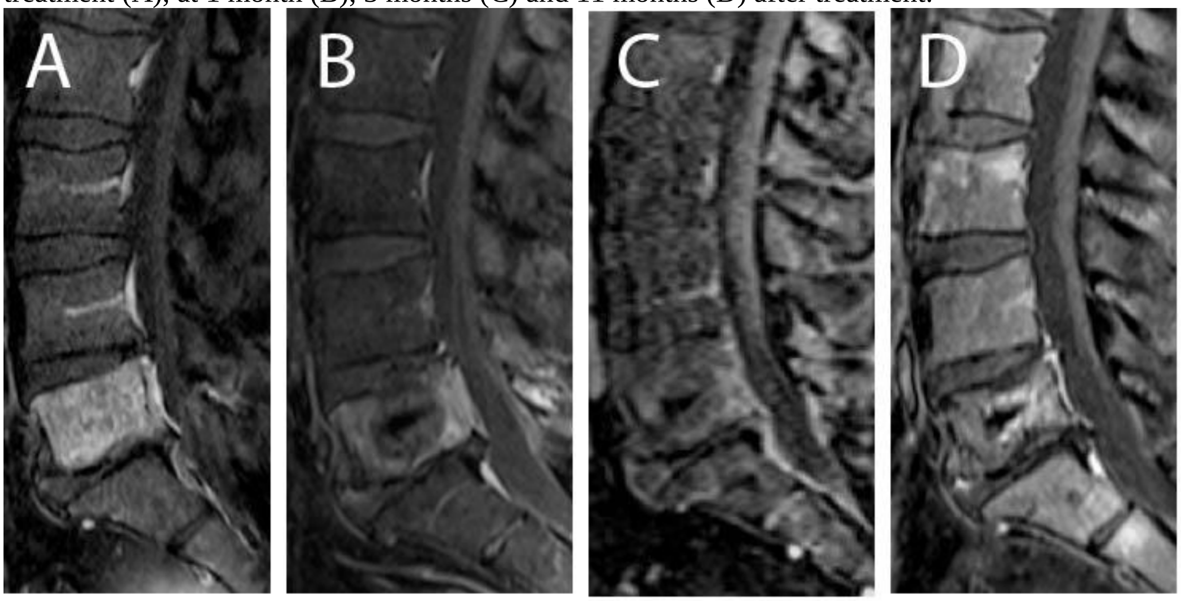

(Filename: TCT_3531_Figure4.jpg)

2166

4:44PM - 4:51PM

Comparison of Powered Drill & Manual Bone Biopsy Systems: Does the Diagnostic Yield Justify the Cost?

E Huh[1], M Khan[1], F Hui[2], D Ray[3], P Yi[1], M Thomas[1]
[1]Johns Hopkins Hospital, Baltimore, MD, [2]Johns Hopkins University, Baltimore, MD, [3]University of Mississippi Medical Center, Jackson, MS

Purpose
Bone biopsies are traditionally performed using manual drill devices. More recently, powered drill biopsy systems have been developed, ostensibly to improve diagnostic yield. This study compared the diagnostic yield and costs of the powered drill biopsy system to traditional manual needle devices on the basis of diagnostic yield, specimen size and material costs.
Materials and Methods
We reviewed 309 consecutive bone biopsy procedures from a single academic institution over a 25 month period. 221 cases (72%) were performed using a manual needle device, and 88 (28%) using the powered drill device. Biopsies were performed with fluoroscopic or CT guidance by Diagnostic (Neuroradiology and Musculoskeletal) and Neurointerventional Radiology services. We compared the following variables between cases performed using the manual and powered drill devices: specimen diagnostic adequacy, qualitative interpretation of diagnostically inadequate specimens, aggregate specimen volume and material costs. T-tests and Fisher's Exact tests were used, as appropriate.
Results
All 309 biopsy cases were technically successful. Diagnostic yield was significantly higher in the powered drill group, with 86% of cases yielding adequate biopsy specimens versus 67% of cases using the manual method (p<0.001). Average core specimen volume was higher with the powered drill device

(164 mm3 versus 72 mm3, p<.0001). The materials cost associated with the powered drill device was higher than those of any of the manual needle devices with an average difference of $270.19 per case.
Conclusions
Powered drill devices result in a significantly higher yield of diagnostically adequate bone biopsy specimens compared to manual needles. Bone biopsy specimens obtained with the powered drill device were larger, possibly improving diagnostic adequacy. However, the powered drill device carries a higher materials cost. Future studies could evaluate the cost-effectiveness of using a powered drill vs. manual bone biopsy system.


Figure 1 – Teleflex Arrow® OnControl® powered drill bone biopsy system (https://www.teleflex.com/la/product-areas/oncology/bone-access-system/oncontrol-biopsy-driver.jpg)


Figure 2 – AprioMed Bonopty® coaxial bone biopsy system (http://apriomed.com/wp-content/uploads/2018/05/penetration-set-14g-300x200.png)


Figure 3 – Cook Medical Osteo-Site® bone biopsy needle set http://www.chsltd.com/DATA/PRODUIT/249_original.jpg

	Powered Drill System	Manual Needle System
Diagnostic adequacy rate	86% (76/88)	67% (148/221)
Qualitative assessment of inadequate specimens		
Crush/fragmentation	5	24
Scant tissue	3	14
No lesion present	2	13
Blood products only	1	11
Other	1	11
Average biopsy specimen volume (mm^3)	163.6	72.1
Average materials cost (USD)	421.27	151.08

Table 1 – Comparison of bone biopsy cases performed by the powered drill system versus manual needle systems

(Filename: TCT_2166_Graphic.jpg)

2548

4:51PM - 4:58PM

Correlation Between Findings of Facet Arthropathy or Synovitis on MRI and Pain Score Response from Therapeutic Lumbar Facet Joint Injections

K Kazmi[1], M Van Hal[2], M Onimus[2], c snell[2], M Green[2], V Potigailo[1], W Prokop[3]
[1]Hahnemann University Hospital, Drexel University College of Medicine, Philadelphia, PA, [2]Drexel University College of Medicine, Philadelphia, PA, [3]Hahnemann University Hospital, Philadelphia, PA

Purpose
The purpose of this study is to determine if there is a correlation between MRI findings of facet arthropathy or synovitis and pain score response following therapeutic lumbar facet joint injection.
Materials and Methods
156 patients who had bilateral facet joint injections at L4-L5 were screened retrospectively. Of those, 91 subjects met inclusion criteria. MRI's were reviewed for the presence of facet arthropathy and/or facet synovitis at L4-L5. Preprocedural and postprocedural average pain scores were recorded using 0-10 scale. The reduction in pain score was compared between different subgroups and T-test was utilized to assess statistical significance (p=0.05).
Results
16 patients had facet synovitis, 7 of which were bilateral. 49 patients had facet arthropathy, including 36 with bilateral facet arthropathy. For all patients, the mean preprocedural and postprocedural pain scores

were 8.2 and 6.5, respectively. While no comparisons showed statistical significance at $P<0.05$, there was nearly a statistically significant difference in mean pain score improvement between those patients who had bilateral facet synovitis and those who did not have synovitis ($P=0.06$).
Conclusions
Although the number of patients with bilateral facet synovitis was small, our data did show a trend towards greater pain score response from therapeutic lumbar facet injections among these patients compared with those patients without synovitis. Additional prospective controlled study would be helpful to validate our results in a larger population of patients as well to study whether patients with unilateral facet synovitis have improved response to ipsilateral therapeutic injection.

2193

4:58PM - 5:05PM

Early Experience of High Volume Blood Patch in the Management of Refractory Intracranial Hypotension.

D Johnson[1], S Islam[2]
[1]ST GEORGE'S HOSPITAL LONDON UK, LONDON, United Kingdom, [2]Imperial College London, London, United Kingdom

Purpose
To demonstrate the effectiveness of high volume blood patch in refractory Idiopathic intracranial hypotension and the potential implications for future management and investigation of this disorder.
Materials and Methods
A retrospective review of large volume blood patches that were performed in our institution from 2015 to 2018 for refractory Idiopathic Intracranial Hypotension (IIH). 18 patients were identified who were referred to the department with failed conservative management for low pressure headache syndrome which included a small volume blood patch in most cases.Conservative management included bed rest, fluids and caffeine supplements. Symptoms had been present for at least 2 months and varied up to 18 months. All cases had MRI imaging of the brain and most had MR imaging of the spine. No further imaging was requested. The imaging at presentation was abnormal in 15 cases and normal in 3 cases. All patients were referred by senior clinicians experienced in IIH. All patients underwent fluoroscopically guided blood patch with the deliberate intention of introducing a large volume to the point of tolerance.The procedures were performed by one experienced operator at one or two levels using 18 gauge Tuohy needles. Needle position was checked with iodinated contrast. Most patients received light sedation from an anaesthetist. Blood was injected until pain or an impending vasovagal event terminated the procedure. If possible patients were tilted head down after the procedure for 20 minutes. MRi scanning of the spine was performed post procedure in some cases. No CT guided procedures were performed. No myelography or other studies were performed preoperatively. Autologous blood was the only therapeutic substance injected into the epidural space. Empirical antibiotics were administered.
Results
18 patients underwent the procedure. 15 had abnormal imaging and 3 had normal imaging. 17-83 mls of blood were injected. 13/18 patients who had classical imaging findings on MRI were cured of their symptoms at the first attempt. 2/18 patients required repeat treatment and were cured. Therefore overall (13+2) 15/18 were cured of symptoms. 2/18 patients with normal MRI felt better after blood patch 1/18 with normal MRI felt worse and complained. Most patients had back pain or headache that terminated the procedure. 4 patients had a vasovagal event that terminated the procedure. 1 prolonged vasovagal episode/pseudoseizure that terminated the procedure.. 1 overnight stay post blood patch for pain control. No other complications
Conclusions
Large volume blood patch is a highly effective treatment for refractory IIH as long as the injection continues to the point close to intolerance; either pain or vasovagal event. I believe in nearly all cases

adjunct imaging investigations searching for leaks are unnecessary. In this series no CT guided procedures or other therapeutic substances were injected. I would suggest caution using this procedure for patients with normal imaging.

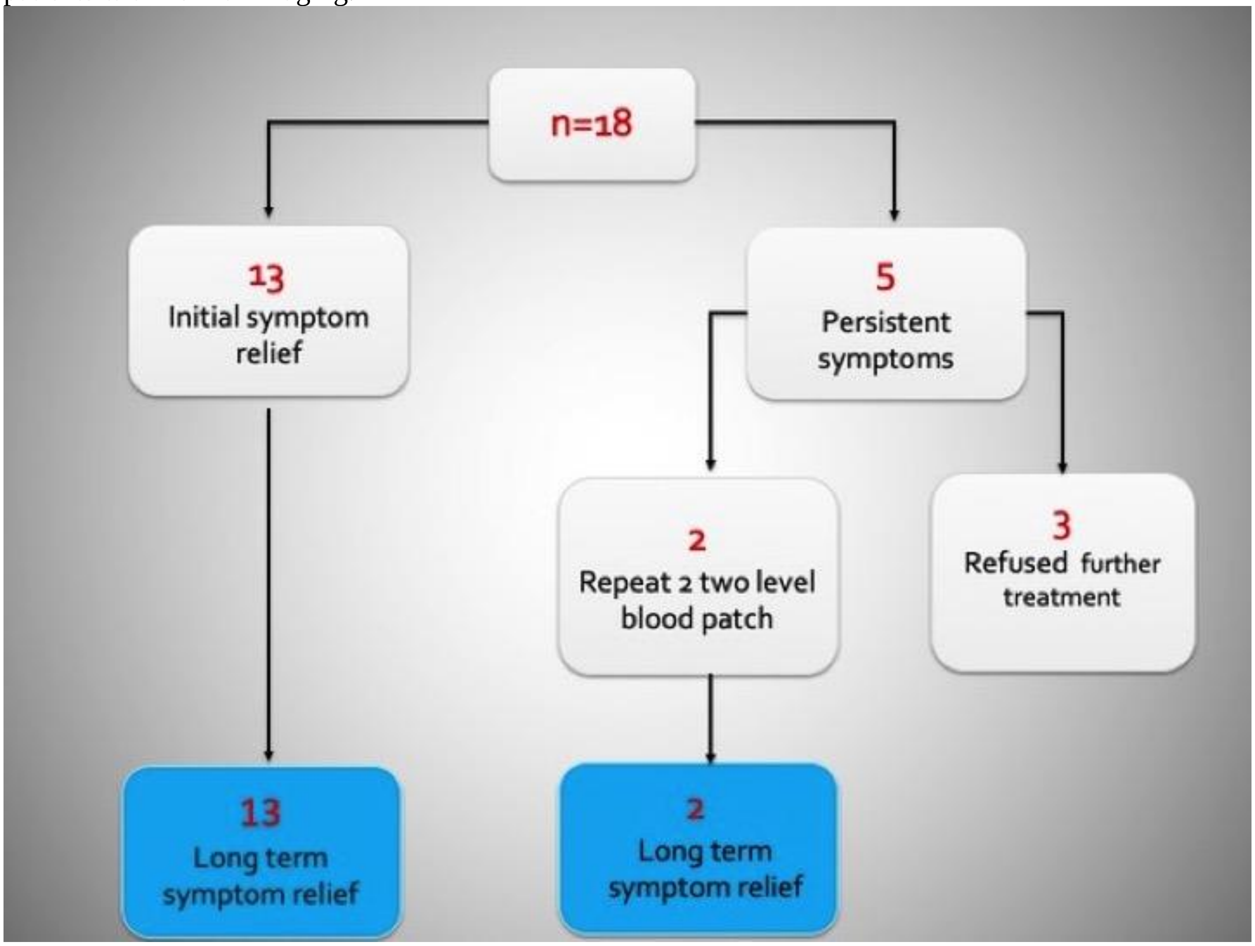

(Filename: TCT_2193_Slide14.jpg)

2767

5:05PM - 5:12PM

Examination of Lifetime Risk of Cancer by Organ, Age and Sex in CT-Guided Interventional Nusinersen Administrations for Young Patients with Spinal Muscular Atrophy

N Guberina[1], D Oldenburg[1], A Radbruch[1], B Stolte[2], K Kizina[3], T Hagenacker[3], C Kleinschnitz[3], M Forsting[4], C Mönninghoff[1]
[1]Institute of Diagnostic and Interventional Radiology and Neuroradiology, University Hospital Essen, Essen, NRW, [2]Department of Neurology, University Hospital Essen, Essen, NRW, [3]Department of Neurology, Essen, NRW, [4]Institute of Diagnostic and Interventional Radiology and Neuroradiology, University Hospital Essen, Essen, Germany

Purpose
The purpose of this study was to examine life-time risk of radiation induced cancer by organ, age and sex in CT-guided interventional nusinersen (Spinraza, Biogen Switzerland AG) administrations for young adult patients with spinal muscular atrophy (SMA) at a large multicenter institute.
Materials and Methods
In a retrospective study design altogether 56 consecutive, computed-tomography (CT)-guided intrathecal

nusinersen administrations were included in this study for the time period from 08/2017 to 10/2018. Patient cohort comprised 14 young adult patients with SMA (8 female and 6 male). All interventions were performed with second generation of dual-source CT-scanner generations SOMATOM Definition Flash and third generation of dual-source CT-scanner generations SOMATOM Force (both Siemens Healthcare, Forchheim, Germany). Technical features including tube voltage, tube-current-time product, collimation, scan length and number of series were recorded for each intervention. Life-time risk of cancer was assessed as a function of organ (I), age (II) and sex (III) following recommendations of the UK Health Protection Agency (HPA-CRCE-028, 2011).

Results

Life-time risk of cancer for female patients (III) (age range 19-48 years, mean age 33.9 (II)) is summarised as follows: (I) (a) adrenals 0.0006%, (b) colon 0.0047%; (c) gallbladder 0.0045%; (d) red bone marrow 0.0013%; (e) gonadal organs 0.0013%; (f) stomach 0.0021%; (g) overall 0.023%. Life-time risk of cancer for male patients (III) (age range 25-47 years, mean age 31.0 (II)) is distributed as follows: (I) (a) adrenals 0.0013%, (b) colon 0.0091%; (c) gallbladder 0.0076%; (d) red bone marrow 0.0029%; (e) gonadal organs 0.0003%; (f) stomach 0.0014%; (g) overall 0.093%.

Conclusions

The present data acquisition allows a life-time cancer risk calculation by organ, age and sex in CT-guided intrathecal nusinersen administrations. This is essential for an individual risk stratification of cancer for patients with SMA.

3076

5:12PM - 5:19PM

Intraprocedural MRI Monitoring During Percutaneous Cryoablation Procedures of the Head, Neck, and Spine: A Single Institution Experience

P Schaefer[1], J Guenette[1], T Lee[1]
[1]*Brigham and Women's Hospital, Boston, MA*

Purpose

Evaluate whether intraprocedural MRI monitoring of percutaneous cryoablation of head, neck, and spine lesions is effective for avoiding iatrogenic neurovascular and mucosal injury.

Materials and Methods

We retrospectively reviewed 60 consecutive percutaneous head, neck, and spine cryoablation procedures with intraprocedural MRI guidance performed on 41 patients (mean age 58 years, range 17 – 91 years). Ablation goals were either complete local control of primary or metastatic lesions or pain relief.

Results

The technical success rate was 98%. The complication rate was 13% with only 3 complications (5%) requiring further intervention. There were no neurological or vascular complications. Subsequent cryoablation in the same location was performed in 20 of these cases (34%). Subsequent surgical intervention in the same location was performed in 7 of these cases (12%) for progressive disease or worsening symptoms.

Conclusions

MRI provides excellent visualization of the ice ball during percutaneous cryoablation procedures. Accurate intraprocedural visualization of the ice ball allows for adjustment of cryoablation parameters to avoid damage to adjacent vital neurovascular structures or mucosal surfaces. Intraprocedural MRI is thus a novel and highly effective method that allows a high rate of technical success for cryoablation in the head, neck, and spine while avoiding iatrogenic injury.

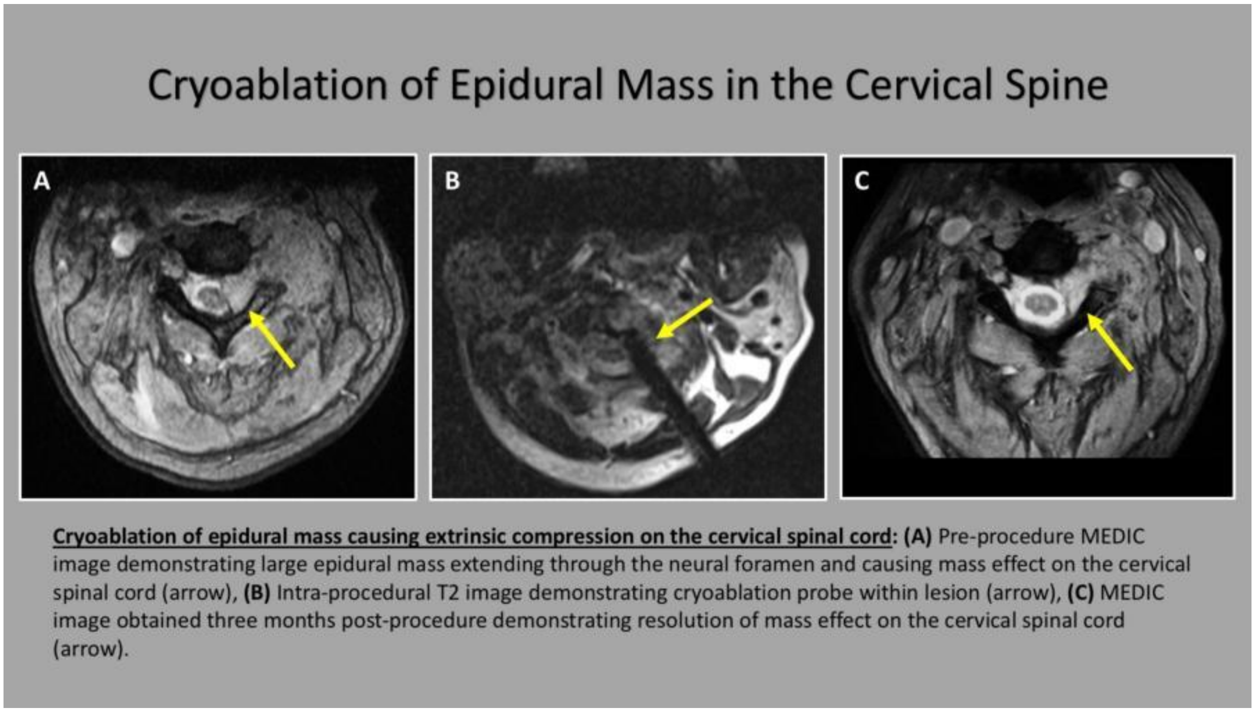

Cryoablation of epidural mass causing extrinsic compression on the cervical spinal cord: (A) Pre-procedure MEDIC image demonstrating large epidural mass extending through the neural foramen and causing mass effect on the cervical spinal cord (arrow), **(B)** Intra-procedural T2 image demonstrating cryoablation probe within lesion (arrow), **(C)** MEDIC image obtained three months post-procedure demonstrating resolution of mass effect on the cervical spinal cord (arrow).

(Filename: TCT_3076_ASNR_cryo_figure.jpg)

2784

5:19PM - 5:26PM

Transforaminal Lumbar Puncture for Injection of Spinraza is Adult & Pediatric Patients with Spinal Muscular Atrophy

T Shokuhfar[1], S Ansari[2], P Nazari[1], R Abdalla[1], S Azmi[3], B Jahromi[4], M Hurley[1], A Shaibani[5]
[1]Northwestern University Feinberg School of Medicine, Chicago, IL, [2]NORTHWESTERN UNIVERSITY, FEINBERG SCHOOL OF MEDICINE, CHICAGO, IL, [3]Northwestern University Feinberg School of Medicine, Chicago, IL, [4]Northwestern University, Feinberg School of Medicine, Chicago, IL, [5]Northwestern University, Chicago, IL

Purpose
To assess the safety and efficacy of transforaminal lumbar puncture (LP) for the injection of Nusinersen (Spinraza®)in the subset of patients who had extensive spinal fusion and/or scoliosis which precluded the standard interlaminar approach.
Materials and Methods
This is a single-center study approved by our institutional review board. Retrospective chart reviews of all patients requiring fluoroscopically-guided intrathecal Nusinersen injections were performed. Demographic and procedural details and related complications were obtained from the electronic medical records. All transforaminal intrathecal injections were conducted under fluoroscopic guidance and patients were evaluated immediately and within two weeks follow up for complications.
Results
Between September 2017 and April 2018, we performed 85 Nusinersen injections in patients who were previously diagnosed with Spinal Musclar Atrophy (SMA). Fluoroscopic-guided transforaminal injections were successfully performed 27 times (31.7% of these injections) in 5 pediatric patients (3 male and 2 female) aged between 4 to 17 years (Mean = 12 years) and 5 adult patients (4 female and 1 male) aged between 24 to 38 years (Mean= 29 years). One pediatric patient had SMA type 1 and nine had SMA type 2. Details regarding each procedures are presented in the table. Out of five pediatric patients, four

had chronic respiratory failure, three were BiPAP dependent, and three had osteoporosis. One patient had morbid obesity (BMI=33.8) but the rest had a BMI within the normal range (Mean= 21.4). In adult patients, three out of five had chronic respiratory failure and one had local osteoporosis. Complications such as post-LP headache, back pain, bleeding, radicular pain and/or paresthesia were evaluated whether immediately after procedures or at 1-2 days and 2 weeks follow up. One adult patient (patient A1) reported a severe progressive bilateral radicular pain initiating from the lower lumbar region to the right foot 1 week after the first injection which was not responsive to NSAID. CT scan ruled out any evidence of spinal/epidural hematoma or other abnormality and hydrocodone was administered with the possible diagnosis of nerve inflammation. The patient reported significant decrease in pain on the next day follow up. No other complication such as post-LP headache, back pain, bleeding, radicular pain and/or paresthesia were noted immediately after procedure or at 1-2 days and 2 weeks follow up.
Conclusions
Transforaminal lumbar puncture is a safe and effective method for delivering intrathecal Nusinersen in children with spinal muscular atrophy and complex spinal fusions that preclude the use of the standard interlaminar route however attention must be paid to the technical nuances of and indications for its use in order to avoid potential complications.

Table: Demographic and procedural details of Nusinersen injections:

Pediatric patients	Age	Gender	BMI	Level	Side	Anesthesia
P1 (4 sessions)	11	F	17.8	L2/3	L	LA
P2 (4 sessions)	13	F	22.5	L3/4	R	GA
P3 (3 sessions)	17	M	24.1	L2/3	L	GA
P4 (4 sessions)	13	M	21.3	L2/3	R	GA
P5 (4 sessions)	15	M	33.8			
S 1 and 2				T12/L1	R	GA
S 3 and 4				L1/2	R	GA
Adult patients						
A1 (4sessions)	38	F	19.5	L3/4	R	LA
A2	29	F	19.4	L2/3	L	LA
A3	25	F	25.5	L2/3	R	LA
A4	30	F	29.8	L3/4	R	LA
A5	24	M	14.65	L2/3	R	LA

Abbreviations:
F=Female, M=Male, L=Left, R=Right, LA=Local Anesthesia, GA= General Anesthesia, S= Sessions

(Filename: TCT_2784_Demographicandresults.jpg)

2715

5:26PM - 5:33PM

Metastatic Spinal Tumors Management: Combined OsteoCool RF Ablation and Vertebral Augmentation Treatment

F Massari[1], K de Macedo Rodrigues[1], A Kuhn[2], A Puri[1]
[1]University of Massachusetts, Worcester, MA, [2]Beth Israel Deaconess, Boston, MA

Purpose
The purpose of the study is to evaluate the efficacy and safety of combined use of the new OsteoCool ™

RadioFrequency Thermal Ablation devices and Kyphoplasty for the palliative treatment of spinal bone metastases.

Materials and Methods

Hybrid Treatments have been widely and efficiently used in pain management of terminally ill or not surgical candidate patients with spinal bone metastases. Our Institution is the only medical center in the Northeastern United States to be part of an International Trial regarding the use of the new generation of spinal RF Ablation devices for metastatic spinal tumors management. Patients referred to our institution for symptomatic malignant fractures were treated, during the same session, with bipolar RFA, performed with the OsteoCool RF ablation system (Medtronic), able to generate a constant temperature of 70 C° within the core of the neoplastic lesion, followed by cement injection. Clinical outcomes were evaluated by review of the electronic medical record (EMR) and clinical visit F/U. Pre and post-procedural pain scores were documented in order to determine the degree of pain relief.

Results

Patients clinical data and procedural technical aspects were retrospectively reviewed. All were technically successful without morbidity or mortality. There was a significantly reduced rate of posterior and venous cement leaks when RFA was used prior to KP. Pain scores in the RFA assisted group decreased significantly post procedure with no unanticipated neuropathic events.

Conclusions

The new generation of RadioFrequency Thermal Ablation devices (OsteoCool) using a bipolar device, coupled with Vertebral Augmentation, have demonstrated an increased efficacy in achieving pain relief and VB stabilization in spinal metastases management, allowing a controlled injection of cement into a preformed thermal cavity with a significant decrease in venous and posterior cement leaks.

2874

5:33PM - 5:40PM

The 'Stent-Screw Assisted Internal Fixation' (SAIF) Technique to Reconstruct the Vertebral Body in Severe Osteoporotic Spinal Fractures with Middle Column Involvement

D Distefano[1], P Scarone[1], M Isalberti[1], M Reinert[2], L La Barbera[3], T Villa[3], J Hirsch[4], G Bonaldi[5], A Cianfoni[6]

[1]Neurocenter of Southern Switzerland, Lugano, Switzerland, [2]Neurocentro della Svizzera Italiana, Lugano, Ticino, [3]Politecnico di Milano, Milan, Italy, [4]MASSACHUSETTS GENERAL HOSPITAL, BOSTON, MD, [5]ospedale papa giovanni XXIII bergamo, Bergamo, Italy, [6]Institute for Clinical Neurosciences of Southern Switzerland, Lugano, Ticino

Purpose

The treatment of highly fragmented osteoporotic/traumatic vertebral fractures (VFs) with middle-column (MC) involvement is controversial, especially in neurologically-intact patients. Surgery offers immediate stability but it is invasive whereas vertebral augmentation (VA) might represent an undertreatment as the MC, represented by the posterior third of the VB and pediculo-somatic junction, is rarely reinforced and rather left as a non-augmented "bare area". The "Stent-Screw Assisted Internal Fixation" (SAIF) technique is a new percutaneous image-guided procedure combining use of vertebral-body-stents (VBS) and percutaneous fenestrated cement-augmented screws, intended to restore axial-load capability of the VB. The stents reconstruct the anterior-column, and screws strengthen the MC, bridging pedicular fractures, and anchor VBS to the posterior elements, avoiding their mobilization. A finite element (FEM) analysis supports the SAIF technique.

Materials and Methods

Retrospective analysis of 36 consecutive levels with severe osteoporotic VFs (grade II and III McCormack and/or Genant) with MC involvement treated with SAIF in 33 patients. VB-reconstruction independently evaluated on post-procedure CT by one neurosurgeon and one neuroradiologist. Clinical and radiological follow-up performed.

Results

SAIF was performed at 26 lumbar and 10 thoracic levels. VB-reconstruction was satisfactory in 96% of levels. Cement leaks visible in 14% of levels, all asymptomatic. Follow-up at 1 month available in 35/36 levels, beyond 6 months in 29 levels (mean 8.6 months). Pain amelioration observed in 31/33 patients (mean VAS 8.56 on admission and 2.54 at 6 months). Target-level stability maintained in all cases during follow-up. FEM proved SAIF more effective than VA in reducing the strains on the MC.

Conclusions

SAIF might represent a minimally invasive and safe option to obtain VB-reconstruction in severe osteoporotic VFs with MC involvement.

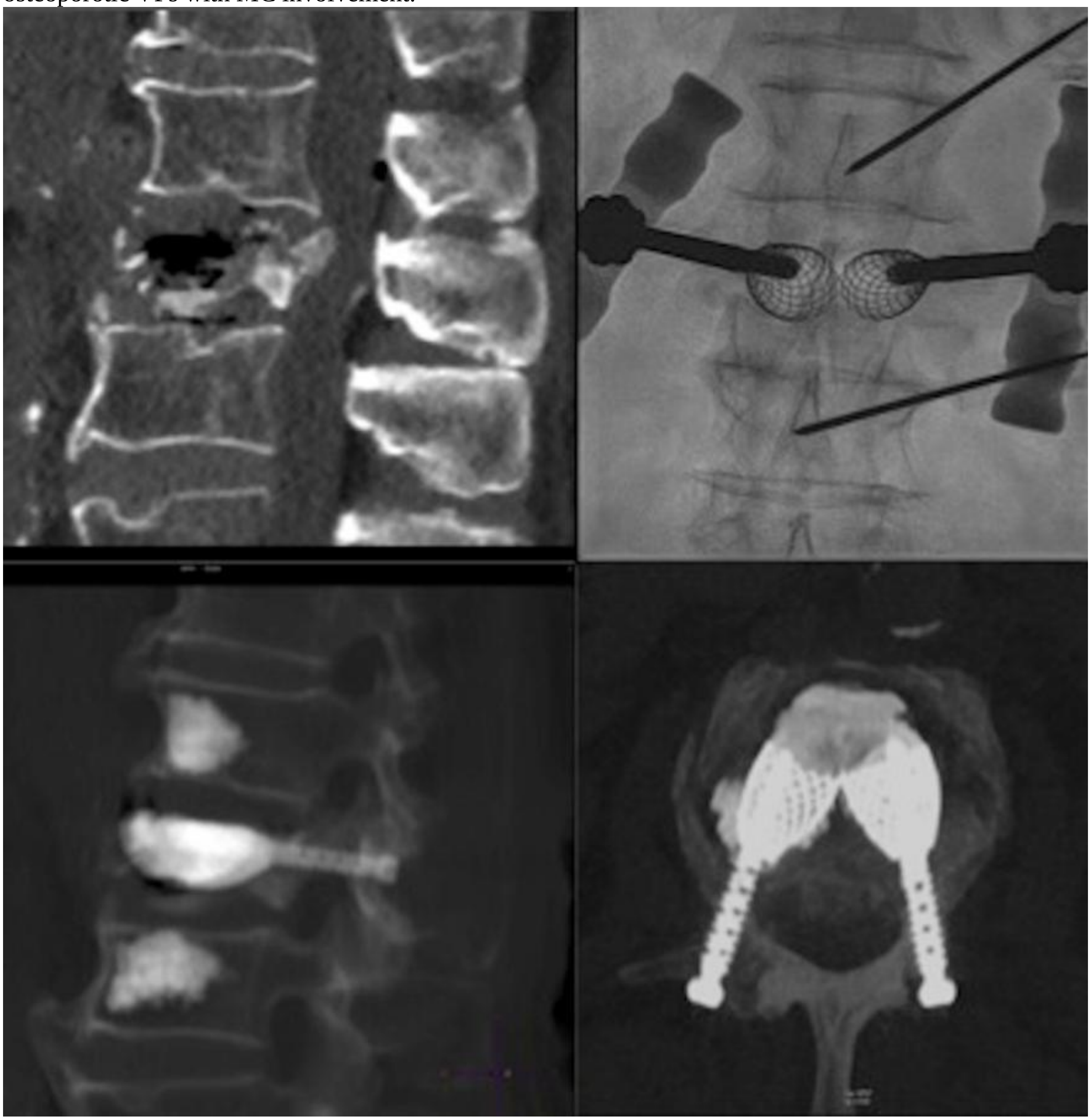

(Filename: TCT_2874_FigASNROP2019.jpg)

2781

5:40PM - 5:47PM

The Stent-Screw Assisted Internal Fixation (SAIF) Technique to Reconstruct the Vertebral Body in Neoplastic Extreme Osteolysis

D Distefano[1], P Scarone[1], M Reinert[2], G Pesce[3], L La Barbera[4], T Villa[4], G Bonaldi[5], J Hirsch[6], A Cianfoni[2]
[1]Neurocenter of Southern Switzerland, Lugano, Switzerland, [2]Neurocenter of Southern Switzerland, Lugano, Ticino, [3]Oncology Institute of Southern Switzerland, Bellinzona, Switzerland, [4]Politecnico di Milano, Milan, Italy, [5]ospedale papa giovanni XXIII bergamo, Bergamo, Italy, [6]MASSACHUSETTS GENERAL HOSPITAL, BOSTON, MD

Purpose
In extensive lytic lesions of the vertebral body (VB) stability-restoration requires anterior and posterior instrumentation. The anterior approach to stabilise the anterior column carries significant invasiveness and morbidity. Standard vertebral augmentation might represent an undertreatment. The "Stent-Screw Assisted Internal Fixation" (SAIF) technique is a new percutaneous image-guided procedure combining use of vertebral-body-stents (VBS), cannulated fenestrated percutaneous pedicle screws, and cement-augmentation, intended to restore axial-load capability of the VB. VBS scaffolds the VB and help cement-containment while screws anchor the stents to the posterior elements reducing the risk of their mobilization, bridging the middle column. The purpose of this study is to retrospectively assess feasibility, safety and clinical outcome of VB reconstruction through SAIF technique in 'extreme' lytic lesions considered unstable or potentially unstable according to SINS score. A finite element (FEM) simulation supports SAIF technique.
Materials and Methods
Retrospective analysis of 28 consecutive levels with extensive lytic VB destruction (Tomita 4-6), in 27 patients, treated with SAIF under fluoroscopy-guidance. VB-reconstruction was independently evaluated on post-procedure CT by one neurosurgeon and one neuroradiologist. Clinical and radiological follow-up was performed.
Results
SAIF was performed at 12 lumbar and 16 thoracic levels. VB-reconstruction was satisfactory in 94% of levels. Cement-leak caused transient radicular pain in 1 patient, and required surgical decompression with no permanent deficit in 1 patient. Follow-up at 1 month was available in 23/27 patients, beyond 3 months in 18 patients (mean 8.9 months). Target-level stability were observed in all cases during follow-up. FEM proved SAIF more effective than short posterior instrumentation.
Conclusions
Our preliminary results support off-label use of SAIF as a minimally invasive procedure of stabilization in patients with extensive lytic VB lesions.

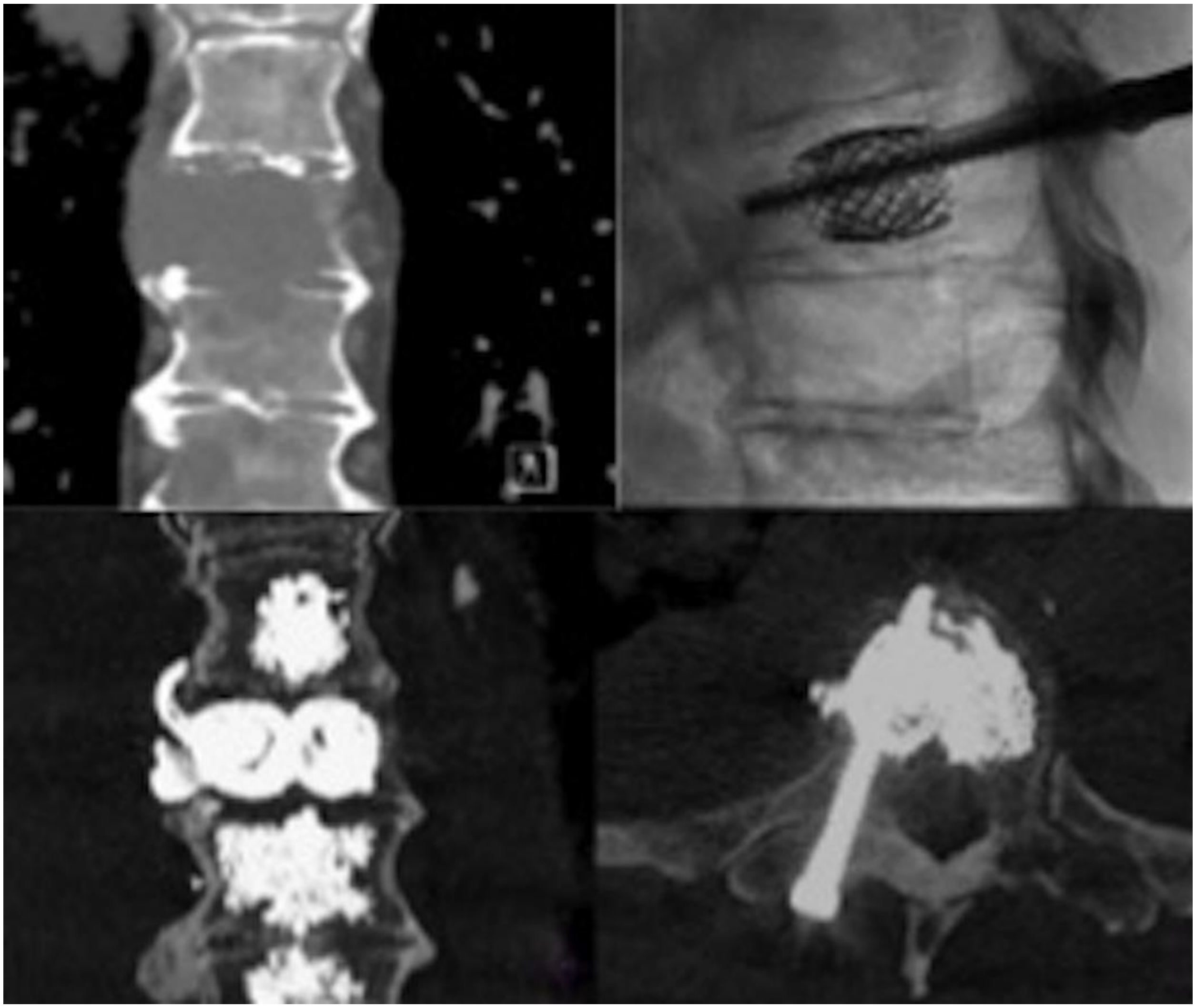

(Filename: TCT_2781_Fig1ASNR2019.jpg)

2564

5:47PM - 5:54PM

Waiting Is the Hardest Part: Patience Could Reduce Disc Biopsies for Discitis-Osteomyelitis

S Johnson[1], L Shah[2], E Ryals[3], G Noda[3], M Peckham[4], T Hutchins[5]
[1]UNIVERSITY OF UTAH HEALTH SCIENCES, MURRAY, UT, [2]University Of Utah, Salt Lake City, UT, [3]University of Utah, Salt Lake City, UT, [4]UNIVERSITY OF UTAH HEALTH SCIENCE CENTER, SALT LAKE CITY, UT, [5]University of Utah, Neuroradiology, salt lake city, UT

Purpose
Biopsy of the disc/endplate is often requested when there is clinical or imaging concern for discitis-osteomyelitis (DOM). Although biopsy is a second-line option if blood cultures fail to identify an organism per Infectious Disease guidelines, not uncommonly, some patients are biopsied prematurely or unnecessarily. Our objective was to identify the percentage of biopsies that could have been avoided by adhering to the current guidelines.
Materials and Methods
The institutional database for the billing codes corresponding to biopsy from 2010-2018 were reviewed. Inclusion criteria were any patient receiving a disc/vertebral biopsy for suspected spinal infection.

Patients undergoing other infection-related procedures such as paraspinal abscess aspiration, facet joint aspiration, or paraspinal soft tissue biopsy were excluded. Clinical information including sepsis, blood culture results, white blood cell count (WBC), C-reactive protein (CRP), and erythrocyte sedimentation rate (ESR) were also collected. Descriptive and regression statistics were performed.

Results

Database review identified 140 disc/vertebral biopsies performed for suspected infection. Seventy-seven biopsies were positive. Forty-one biopsies (29%) were performed in the setting of ultimately positive blood cultures. Biopsy was 53% sensitive (95% confidence interval (CI): 28-77%) and 45% specific (95% CI: 35-56%). There was no statistically significant association between positive biopsy results and sepsis, WBC, ESR, or CRP either individually or in aggregate. Length of stay was statistically correlated with positive biopsy and culture (p=.02).

Conclusions

Given the coin-flip chance of positivity and that almost 30% were performed in the setting of positive blood cultures, we question the necessity of routine spinal biopsies for DOM. Additionally, clinical factors such as sepsis, WBC, CRP, or ESR may not have predictive value for positive biopsy results. These results reinforce the current published recommendations and the value of patience in reducing unnecessary procedures.

2713

5:54PM - 6:00PM

Disc Surround Sign: A Static CT Myelogram and MRI Finding for Rapid CSF Leak Localization

J Costello[1], L Shah[2], M Peckham[3], T Hutchins[4]
[1]University of Utah, Salt Lake City, UT, [2]University Of Utah, Salt Lake City, UT, [3]UNIVERSITY OF UTAH HEALTH SCIENCE CENTER, SALT LAKE CITY, UT, [4]University of Utah, Neuroradiology, salt lake city, UT

Purpose

Spontaneous intracranial hypotension secondary to spinal CSF leaks has become a well-recognized disease entity. Imaging localization of spinal CSF leaks is critical for diagnosis and targeted treatment. Rapid spinal CSF leaks are most commonly related to dural tears from ventral disc-osteophyte complexes (DOC), have associated ventral spinal subdural fluid collections, and are typically evaluated with dynamic CT myelogram or digital subtraction myelography (DSM). However, in the setting of multiple DOCs it can be difficult to target these diagnostic studies. We propose a reliable sign identified on conventional CT myelogram and fluid sensitive MR sequences, the "disc surround sign (DSS)," which can be used for localization of rapid CSF leaks.

Materials and Methods

CT myelogram and MRI performed for evaluation of CSF leak within the past year were retrospectively reviewed. Of these, only cases with subsequent confirmation of leak site by surgery or DSM were included. Criteria for the DSS included: (1) subdural fluid collection surrounds greater than 50% of each side of the DOC and (2) angle at the dura-disc interface is between 80-100 degrees. The DOC was measured for maximum axial dimension and assessed as calcified or non-calcified. Literature review was also performed to identify whether prior reported surgically or DSM proven cases met criteria for DSS.

Results

Six cases met criteria for evaluation. Of these, 26 DOCs were identified within the region of the subdural collection. However, only one DOC met criteria for DSS in each of the six cases, each of which corresponded to site of CSF leak at surgery or DSM. Three DOCs meeting criteria for DSS were non-calcified. Mean DSS anterior-posterior DOC length was 3.4 mm. Mean dura-disc angle was 90.8 +/- 3.4 degrees for DSS, and 157.2 +/- 20.3 degrees for extradural DOCs (p < 0.001). Of the 5 DSS cases where both CT myelogram and MRI were available, 3 were better visualized on CT myelogram and 2 were

better visualized on MRI. Comprehensive literature review revealed 19 additional surgically or DSM proven cases meeting criteria for the DSS.
Conclusions
"Disc surround sign" is a helpful CT myelogram and MRI feature to localize the site of CSF leak in the setting of ventral spinal subdural fluid collections and can direct targeted DSM or surgical evaluation.

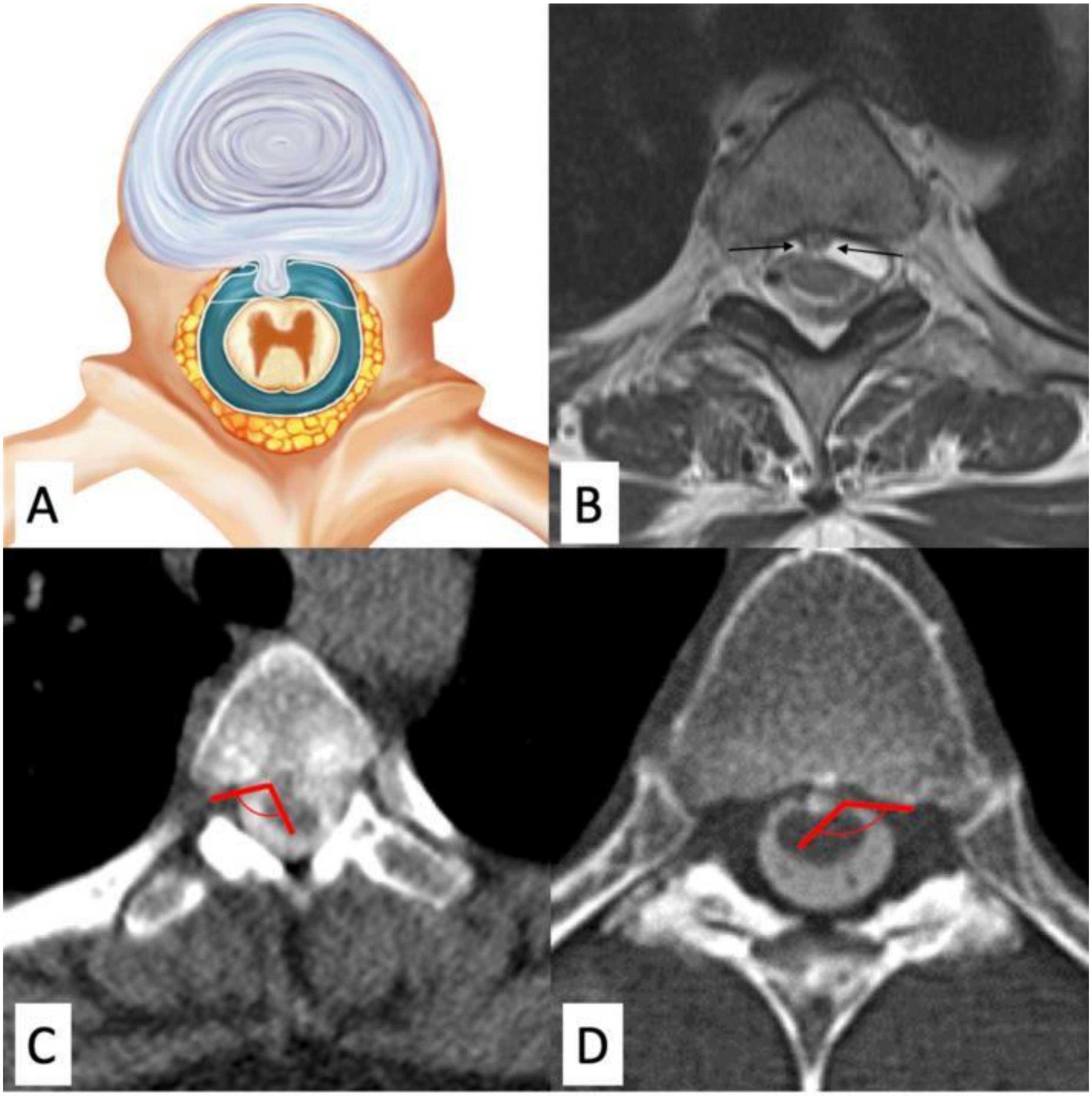

(A) Axial illustration of intradural disc herniation resulting in dural tear and ventral subdural fluid collection, a source of rapid CSF spinal leaks. “Disc surround sign” can be used to identify indradural disc herniations associated with ventral subdural fluid collections and is defined as (B) CSF surrounding greater than 50% of each side of the disc (black arrows) and (C) a dura-disc angle of 80 to 100 degrees. Extradural disc herniations (D) will demonstrate a dura-disc angle of greater than 100 degrees.

(Filename: TCT_2713_DSSfigures.jpg)

Wednesday, May 22, 2019
11:00AM - 12:00PM
Adult Brain - Stroke

2698

11:00AM - 11:07AM

A Retrospective Investigation of the Relationship Between Cerebral Microbleeds and White Matter Hyperintensities in Patients with Systemic Lupus Erythematosus: Cerebral Microbleeds as an Imaging Biomarker of Vasculitis

J Lee[1], Y Lee[2], D Park[3], T Kim[4], H Jung[5]
[1]Hanyang University Hospital, Seoul, Korea, Republic of, [2]Hanyang University Hospital, Seoul, Seoul, [3]Hanyang University Guri Hospital, Guri, Gyeonggi-do, [4]Hanyang University Guri Hospital, Guri, Gyeonggido, [5]Korea University Guro Hospital, Korea University College of Medicine, Seoul, Korea, Republic of

Purpose
White matter hyperintensities (WMH) and cerebral microbleeds (CMBs) are known to be associated with small vessel diseases (SVD) and neuroinflammation. The purpose was to investigate the relationship between CMBs and WMH in patients with systemic lupus erythematosus (SLE).
Materials and Methods
Thirty-one SLE patients with WMH and 27 SLE patients with normal brain MRI were compared. The presence, location, and grading of CMBs were assessed using susceptibility-weighted images. WMH volume was quantitatively measured. Clinical characteristics and serologic markers were compared. We also performed two separate subgroup analyses after 1) dividing WMH into inflammatory lesion vs. SVD subgroups and 2) dividing WMH into those with vs. without CMBs subgroups.
Results
The WMH group showed more frequent CMBs than the normal MR group ($p < 0.001$). The WMH group showed higher SLE disease activity index, longer disease duration, and a higher incidence of antiphospholipid syndrome than the normal MR group ($p = 0.02$, 0.04, and 0.04, respectively). There was a moderate correlation between WMH volume and CMBs grading ($r = 0.49$, $p = 0.006$). Within the WMH group, the inflammatory lesion subgroup showed more frequent CMBs and larger WMH volume than the SVD subgroup ($p < 0.001$ and 0.02, respectively). The WMH with CMBs subgroup had larger WMH volume than the WMH without CMBs subgroup ($p = 0.004$).
Conclusions
In patients with SLE, CMBs could be related to large-volume WMH and inflammatory lesions. CMBs along with severe WMH could be used as an imaging biomarker of vasculitis in patients with SLE.

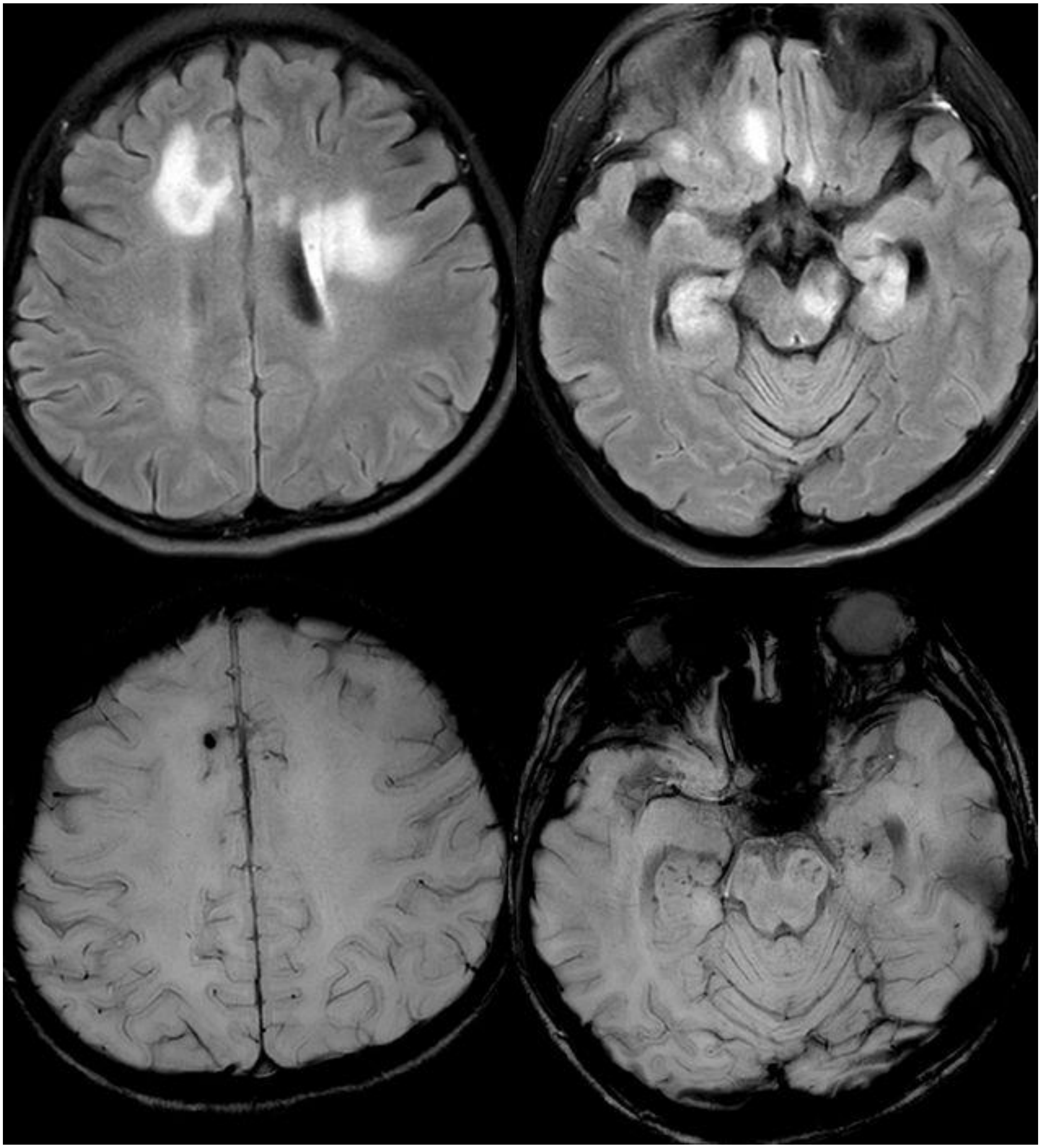

(Filename: TCT_2698_K-121.jpg)

2496

11:07AM - 11:14AM

CT Perfusion Collateral Index for Prediction of Recanalization in Patients with Acute Ischemic Stroke

K Nael[1], J Goldstein[2], J Deutsch[3], J Larson[4], P Pawha[5], A Aggarwal[5], J Fifi[3], A Doshi[6], G Yaniv[5], H Shoirah[5], J Mocco[5]

[1]*ICAHN SCHOOL OF MEDICINE AT MOUNT SINAI HOSPITAL, NEW YORK, NY,* [2]*Florida Atlantic University, NEW YORK, NY,* [3]*Mount Sinai Hospital, New York, NY,* [4]*Icahn School of Medicine at Mount Sinai, new york, NY,* [5]*Icahn School of Medicine at Mount Sinai, New York, NY,* [6]*MOUNT SINAI ICAHN SCHOOL OF MEDICINE, NEW YORK, NY*

Purpose
Good collateral flow correlates with improved functional outcome and reperfusion in patients with acute ischemic stroke (AIS) (1). Perfusion collateral index (PCI) has been recently defined as a promising measure of collateral flow (2). We aim to assess CT-based PCI in determination of functional outcome and recanalization status in patients presenting with AIS and large vessel occlusion.
Materials and Methods
AIS patients with anterior circulation large vessel occlusion who had baseline CT perfusion and underwent endovascular treatment were included. CT perfusion data were processed by Bayesian method to generate arterial tissue delay (ATD), CBV and CBF maps. Ischemic core was calculated using rCBF<30% with region of ATD> 2sec. In addition previously defined perfusion collateral index (PCI) (2) was calculated from volume of hypoperfusion defined by (2sec < ATD < 6sec) multiply by its rCBV: (Vol-ATD 2-6sec x rCBV). Final recanalization after endovascular treatment was rated by TICI scoring. Final functional outcome were determined by 90-day mRs and dichotomized (poor: ≥3, good: ≤2). The association of PCI was assessed against clinical/demographic data, recanalization status and final functional status by repeated measure of analyses and receiver operating characteristic (ROC).
Results
A total of 38 patients met out inclusion criteria: 20 female, age (mean ± SD: 69.8 ± 12.4 years), median NIHSS: 14, ischemic core volume (mean ± SD: 36.8 ± 44 mL), PCI (mean ± SD: 96.1 ± 65.2). TICI scores were: ≤ TICI2B (n=11), TICI2C (n=6), and TICI3 (n=21). Functional outcome: good (n=16), poor (n=22).After controlling for age, sex, baseline NIHSS and infarction volume by multivariate logistic regression analysis, PCI remained as as independent (p=0.018) predictor of excellent recanalization (≥TICI2C) (AUC:0.85, 95%CI: 0.70-0.95, overall diagnostic accuracy of 80% at threshold of 88.8). For determination of functional outcome, baseline PCI was higher in patients with good functional outcome, although this didn't not reach statistical significance (p=0.07) (AUC: 084, 95%CI: 0.68-0.93, overall diagnostic accuracy of 75.6% at threshold of 72).
Conclusions
CT-based perfusion collateral index (PCI) predicts excellent recanalization (≥TICI2C) in AIS patients with large vessel occlusion. PCI also tends to be higher in patients who will have better functional outcome. Our results need to be validated in a larger prospective cohort.

2211

11:14AM - 11:21AM

Influence of Spatial Resolution on Error of Stroke Infarct Core Volume Measurement in DWI-MRI

J Ospel[1], V Schulze-Zachau[2], K Blackham[3], S Kozerke[4], C Federau[5]
[1]*UNIVERSITY HOSPITAL BASEL, BASEL, Switzerland,* [2]*University Hospital of Basel, Basel, Basel-Stadt,* [3]*University Hospital of Basel, Basel, BS,* [4]*ETH Zürich, Zürich, Zürich,* [5]*University Hospital Basel, Basel, Basel*

Purpose
To compare the extent of error in stroke infarct core volume measurement using standard and high-resolution DWI-MRI and to evaluate how often this error might lead to changes in interventional therapy decision making.
Materials and Methods
483 DWI-MRI exams of acute stroke patients with a spatial resolution of 2.0x2.0x4.0 mm were manually segmented and the infarct volume calculated. Since partial volume effects occur in surface voxels only,

the volume of surface is an established measure of error. Surface volume was calculated for the standard resolution, and after virtually doubling and quadrupling spatial resolution, and was then compared between the 3 resolution dimensions. In addition, the number of cases for each resolution, in which 70 ml - the established endovascular therapy threshold – was contained within the margin of error, was extracted.

Results

Mean infarct core volume was 23.5 ml (SD 49.1). Mean volume of surface was 12.2 ml (SD 18.6) for 2.0x2.0x4.0 mm resolution, 8.7 ml (SD 12.6) for 1.0x1.0x2.0 mm resolution and 5.2 ml (SD 7.4) for 0.5x0.5x1.0 mm resolution. With standard resolution, in 52 cases (10.8%), 70 ml were within the margin of error, with double resolution this was the case in 39 cases (8.1%) and with fourfold resolution in 22 cases (4.6%).

Conclusions

With DWI imaging in standard resolution, a maximum error of 12 ml could have occurred due to partial volume effects, and this potentially would have affected endovascular therapy decision in 52/483 patients (10.8%). Doubling the resolution reduced this inaccuracy by approximately 30% and fourfold resolution by 50%. High resolution DWI sequences can be obtained in 4 minutes as opposed to 1 minute that is necessary for standard resolution DWI and should be considered to accurately measure infarct cores and come to a solid endovascular therapy decision.

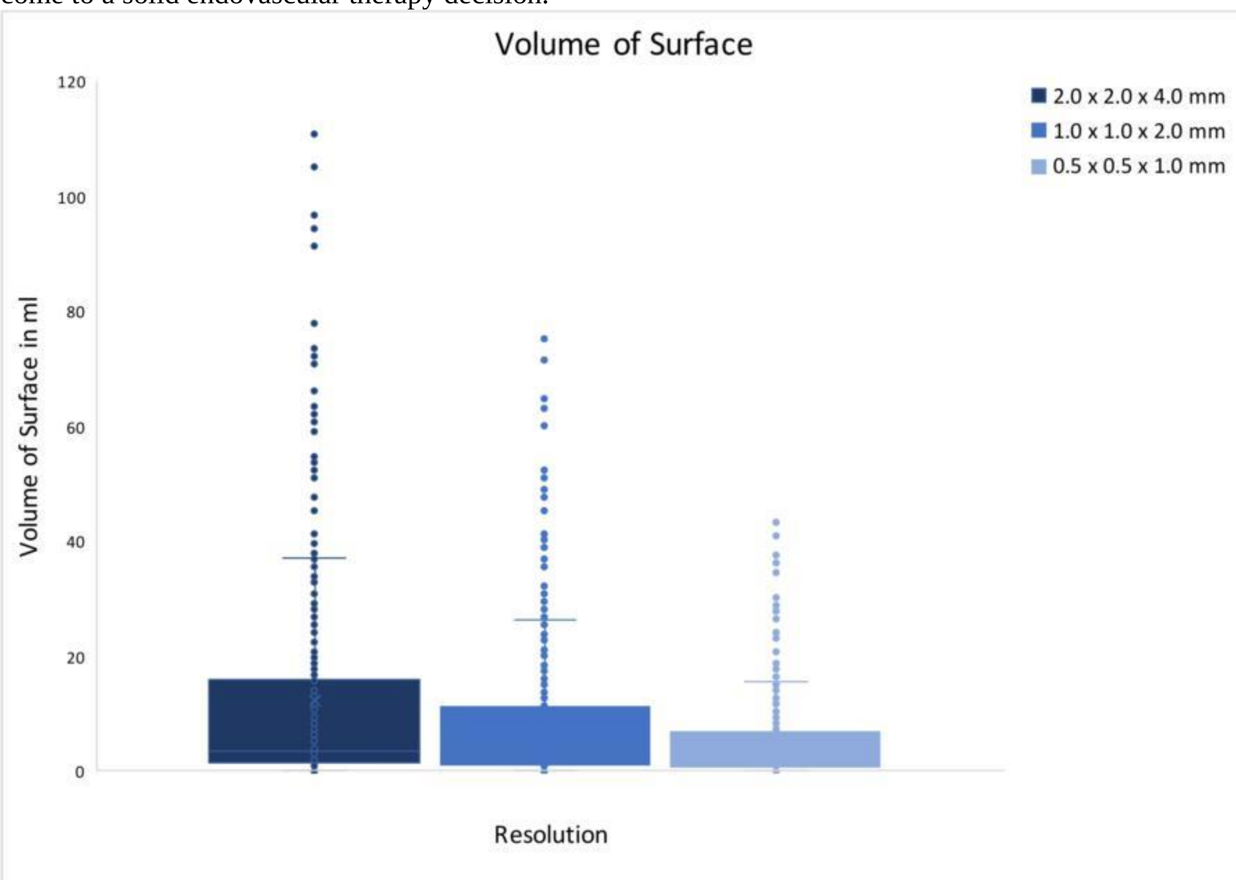

(Filename: TCT_2211_VOS.jpg)

2689

11:28AM - 11:35AM

Sensitivity and Inter-Rater Reliability of Stroke Protocol CT in the Early Detection of Stroke Mimics

a Emira[1], A Schmitt[2], A Al Busaidi[3], A Qureshi[4], H Jager[5]
[1]Lincoln County Hospital, Lincoln, uk, [2]Queen Square, London, london, [3]QUEEN SQUARE, LONDON, LONDON, United Kingdom, [4]Kings College Hospital, London, United Kingdom, [5]ION Institute of Neurology, London, United Kingdom

Purpose
Stroke mimics (SM) are common, especially at the earliest stages of the acute ischemic stroke (IS) pathway, occurring in up to a third of patients with clinically suspected IS. Computed tomography (CT) is a valuable early diagnostic measure that may demystify doubt over the clinical diagnosis of IS, though the added value of CT/CT angiogram (CTA) in identifying stroke mimics has not been measured. Our aim was to investigate the diagnostic benefit of CT/CTA in the early detection of stroke mimics by measuring its sensitivity and the inter-rater reliability.
Materials and Methods
A total of 86 patients who presented to accident and emergency with early stroke-like symptoms were recruited. The cohort comprised of patients with stroke (n= 22), stroke mimics (n=42), and patients without stroke or a mimic (n=22). The final clinical diagnoses were taken as the reference standard. Two neuroradiology fellows retrospectively reviewed the CT/CTA scans individually, blinded to the CT report findings and the final clinical diagnosis. The reviewers indicated their diagnosis (IS, SM or normal) and scored their diagnostic confidence of stroke on a scale of 1-5. The inter-rater reliability was also measured.
Results
The sensitivity of CT/CTA in diagnosing a SM was around 33%. The inter-rater reliability was moderate with a Kappa= 0.634 (95% CI 0.465 to 0.803), (P <0.001). The total number of SM identified by both readers was 19 out of 42 (45%); 14 of which were correctly diagnosed.
Conclusions
Given the low sensitivity and the moderate inter-rater reliability, additional imaging such as MRI is recommended to ensure early and accurate diagnosis in cases where stroke is clinically doubtful or where a stroke mimic is suspected. Further studies comparing CT and MRI may illustrate the added value of a second modality.

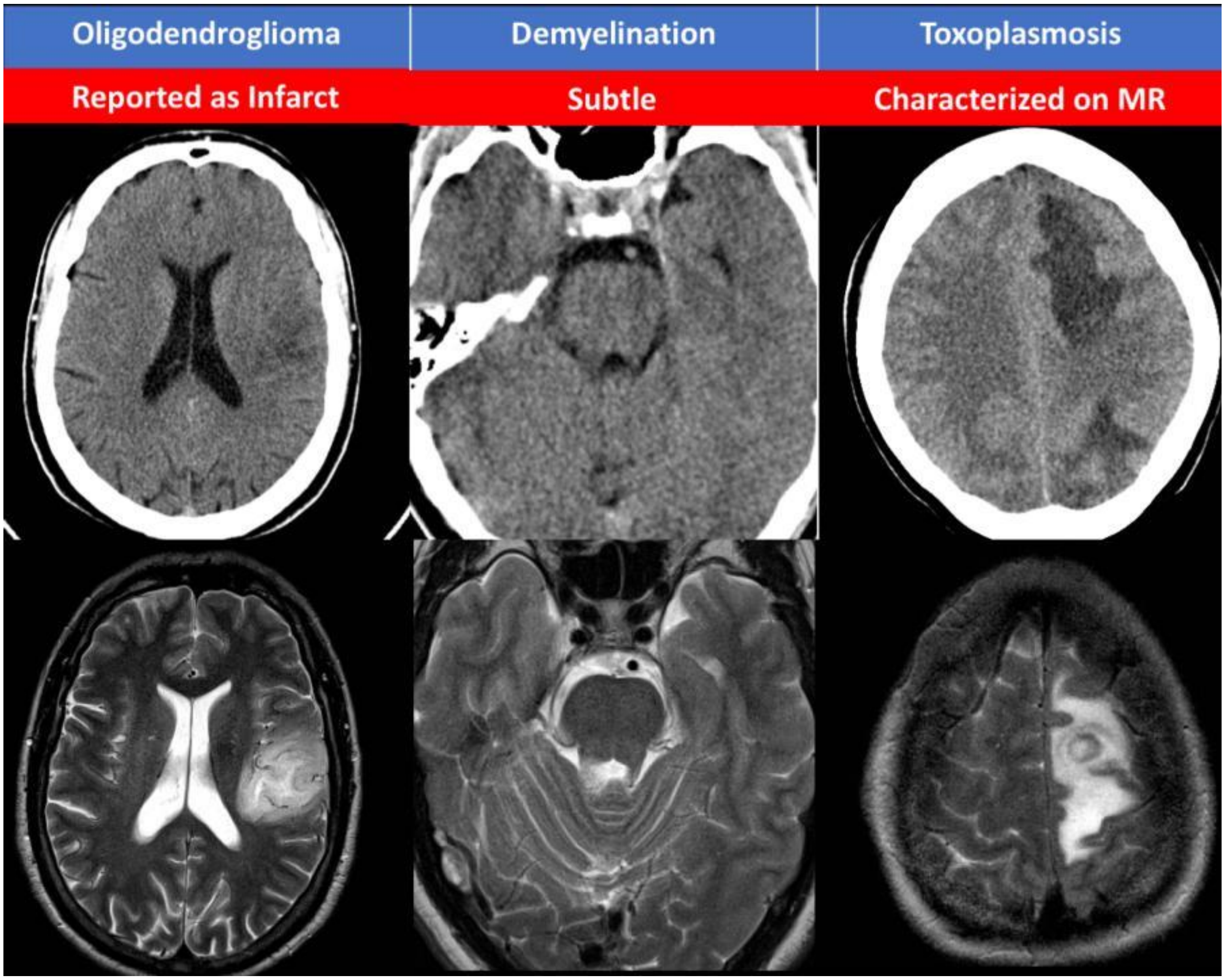

(Filename: TCT_2689_ASNRCTabstractimagecopy.jpg)

2348

11:35AM - 11:42AM

Time to Imaging Does Not Affect Intracranial Collateral Circulation Score in Acute Large Vessel Embolic Stroke

G Vilanilam[1], E McCoy[1], M Badi[1], C D'Souza[1], T Becker[1], L Okromelidze[1], N Gopal[1], V Gupta[1]
[1]*Mayo Clinic, Jacksonville, FL*

Purpose
The presence of intracranial collaterals is a strong predictor of salvageable neurological function in acute stroke; however, factors affecting the ability to recruit collaterals are poorly understood, especially in stroke with unknown time of onset. We aimed to study the relationship between time to imaging and collateral circulation in acute embolic large vessel stroke.
Materials and Methods
From 2008 to 2018, adults with acute embolic large vessel stroke confirmed on CT angiography (CTA) were identified. Collateral scores (CS) were calculated on CTA using the modified Tan scale (0-4) by two trained independent investigators and confirmed by a neuroradiologist. Time to imaging was calculated as the time of stroke onset to time of CTA. Baseline NIH stroke scale (NIHSS), systolic and diastolic blood

pressures, and blood glucose levels were abstracted from medical records. Spearman ρ was used to calculate the relationship between CS and continuous variables. All tests were significant at $P<0.05$.
Results
A total of 372 patients (mean age 70±15 years, 45%[169/372] women) satisfied the inclusion criteria. Median NIHSS was 16 (range, 0 – 32) and time to imaging was 210 minutes (range, 15 – 4320 minutes). Admission glucose was 134±51 mg/dL. The means of systolic and diastolic blood pressures were 148±29 mmHg and 83±18 mmHg respectively. There was no statistically significant relationship between time to imaging and CS ($\rho=0.02$, $P=0.68$). However, admission blood glucose showed significant negative correlation with CS ($\rho=-0.23$, $P=0.008$). NIHSS, systolic or diastolic blood pressure did not exhibit statistically significant association with CS.
Conclusions
In a setting where time of stroke onset is unknown, the status of collateral flow on CTA may not be indicative of the true collateral recruitment after large vessel occlusion. Correspondingly, our results indicate that time to imaging does not significantly affect CS in patients with acute embolic large vessel stroke. Larger populations with longer imaging follow-up are warranted.

2127

11:42AM - 11:49AM

Stroke-like Migraine Attacks After Radiation Therapy (SMART) Syndrome: A Unique Post-Treatment Complication or Manifestation of Status Epilepticus?

V Yedavalli[1], M Iv[2]
[1]Stanford University, San Francisco, CA, [2]STANFORD UNIVERSITY, LOS ALTOS, CA

Purpose
Emerging treatments of intracranial neoplasms give us growing optimism in improving prognosis of these conditions. However, short- and long-term complications of such therapies are now being recognized with increased utilization of neuroimaging. One such rare and perplexing complication, commonly associated with seizures and/or abnormal EEG findings, is stroke like migraine attacks after radiation therapy (SMART), reported in only 40 cases to date. Although steroids are a treatment mainstay, studies haven shown complete recovery with administration of only antiepileptics. We present a patient with presumed SMART syndrome that resolved after alteration of seizure medications.
Materials and Methods
A 58-year-old male diagnosed with a right parietal glioblastoma was treated with gross total resection and chemoradiation. He was doing well clinically until presenting with gait instability and arm weakness thirteen years later. CT head showed no acute abnormality. MRI demonstrated gyral enhancement adjacent to the resection cavity, findings reported with SMART. EEG showed four subclinical seizures within thirty minutes, localized to the right posterior brain. The patient's symptoms then resolved three days after alteration of only his seizure medications.
Results
A) Axial contrast-enhanced T1W BRAVO demonstrates gyral thickening and enhancement lateral to the resection cavity. B) DWI shows corresponding diffusion restriction. C) Arterial Spin Labeling (ASL) perfusion demonstrates focal hyperperfusion in the same region. D) Axial contrast-enhanced T1W BRAVO performed six months later shows complete resolution of gyral enhancement and thickening.
Conclusions
SMART syndrome is increasingly being recognized as a post radiation complication following treatment of brain tumors. However, given the efficacy of antiepileptics alone in this patient, SMART syndrome may be a manifestation of status epilepticus rather than a separate entity. Nonetheless, these two entities should be included on the differential as to not misinterpreted the findings as recurrence.

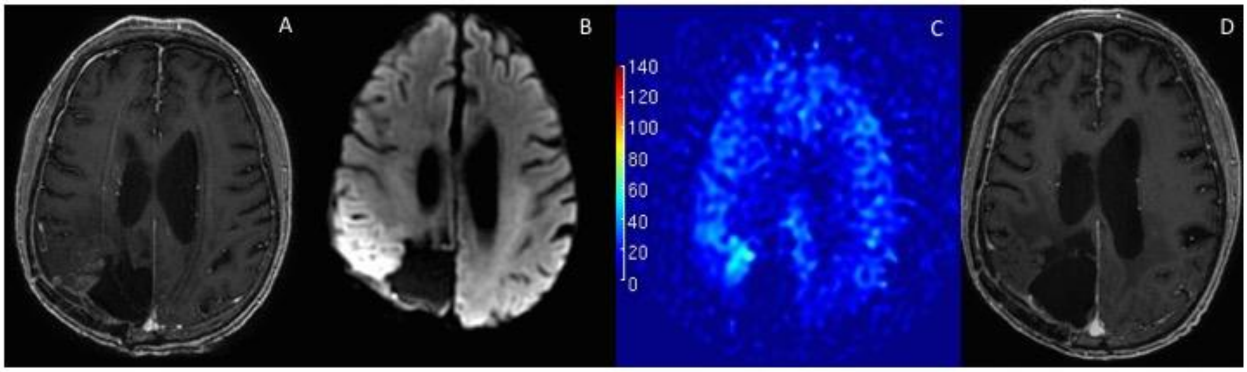

A) Axial contrast-enhanced T1W BRAVO demonstrates gyral thickening and enhancement lateral to the resection cavity. B) DWI shows corresponding diffusion restriction. C) Arterial Spin Labeling (ASL) perfusion imaging demonstrates focal hyperperfusion in the same region. D) Axial contrast-enhanced T1W BRAVO performed six months later shows complete resolution of gyral enhancement and thickening.

(Filename: TCT_2127_SMARTsyndrome.jpg)

2508

11:49AM - 11:56AM

The Effects of Peripheral Vascular Disease on Acute Ischemic Stroke

C Heiberger[1], D Sandhu[2], J Kim[2], G Sandhu[1]
[1]University of South Dakota, Sioux Falls, SD, [2]University of Minnesota, Minneapolis, MN

Purpose
Chronic limb hypoperfusion induced by PVD can produce a neuroprotective effect in acute ischemic stroke, resembling other models of remote ischemic preconditioning (RIPC). To determine how the degree of prolonged peripheral hypoperfusion affects stroke outcomes we compared populations with and without PVD existing prior to stroke and categorized PVD patients by ankle-brachial-index (ABI) values.
Materials and Methods
Retrospectively gathered stroke populations with and without PVD were compared by clinical outcomes (admission NIHSS, 3 month mRS) and stroke volume within 24 hours on diffusion weighted imaging (DWI). The PVD population was categorized by ABI values to further delineate outcomes.
Results
A total of 109 patients, 53 with PVD and 56 as control were collected. Included were 18 mild, 22 moderate, and 13 severe cases of PVD. A higher incidence of comorbidities were present in those with PVD. Stroke volumes as measured in cubic centimeters were significantly lower in the PVD population (PVD: 4.18±8.75, Control: 19.12±43.93, P = 0.0167). A trend towards good outcomes at 3 months (mRS < 3) in the PVD group was evident (PVD: 94.3%, Control: 83.9%, P = 0.0826). No significant difference was found in admission NIHSS (PVD: 4.17±4.38, Control 4.96±5.02, P = 0.38). Severe PVD tended to have lower stroke volumes than mild and moderate disease (Severe: 0.59±0.71, Mild-Moderate: 5.34±9.81, P = 0.0889).
Conclusions
Increasing degrees of hypoperfusion related to PVD have a potential neuroprotective effect in acute ischemic stroke as seen in other preclinical models of RIPC.

Wednesday, May 22, 2019
11:00AM - 12:00PM
Imaging of Neurodegenerative Diseases and Aging

3273

11:07AM - 11:14AM

Imaging Findings Associated with Gamma Knife Thalamotomy for Essential Tremor

D Monks[1], V Agarwal[1], J Mahajan[2], E Monaco[1], A Niranjan[1], L Lunsford[1]
[1]University of Pittsburgh Medical Center, Pittsburgh, PA, [2]University of Pittsburgh, Pittsburgh, PA

Purpose
Gamma Knife Thalamotomy (GKT) has been described as an effective treatment for Essential Tremor and Parkinson's Disease in the neurosurgical literature(1,2). However, neuroradiological literature describing the associated post-surgical imaging findings is lacking. We therefore aim to characterize the evolution of post-surgical imaging related to GKT.
Materials and Methods
A retrospective review of pre-GKT and post-GKT imaging of 40 patients (53% female), average age 69.3 years (range 46-92) with essential tremor treated with gamma knife radiosurgery from 2001 through 2015 was performed. Mean imaging follow-up was 10.7 months (range 2.5-63).
Results
The most common initial post-GKT imaging finding was round or ring enhancement with concordant thalamic T2 signal abnormality (47.5%, n =19). Several patients demonstrated widespread thalamic T2 signal abnormality with adjacent streaking (n=14), streaking without widespread signal abnormality (n=4), susceptibility (n= 12), and restricted diffusion (n=1). Widespread thalamic T2 signal abnormality and streaking decreased on subsequent imaging. In all patients followed for 18 months or longer, enhancement and T2 signal abnormality became concordant (n=7; Figure 1). Figure: T1 postcontrast (A,C) and T2-weighted (B,D) images demonstrate initial left thalamic ring enhancement (A) and widespread T2 signal abnormality (B) 3 months post-GKT (A-B). Subsequent imaging at 20 months (C-D) demonstrates a concordant small focus of enhancement (C) and T2 signal (D).
Conclusions
Following GKT, immediate imaging findings of ring enhancement and surrounding T2 signal abnormality are expected. While a minority of patients initially demonstrated widespread T2 signal abnormality, this became concordant with enhancement by 18 months post-procedure. This suggests that imaging findings lag behind clinical improvement, which reportedly averages 3-4 months (1,2). As always, clinical symptomatology should determine follow-up imaging. However, familiarity with the evolution of post-GKT changes is essential for any neuroradiologist interpreting studies on these patients, so that expected changes are not misinterpreted as pathologic processes.

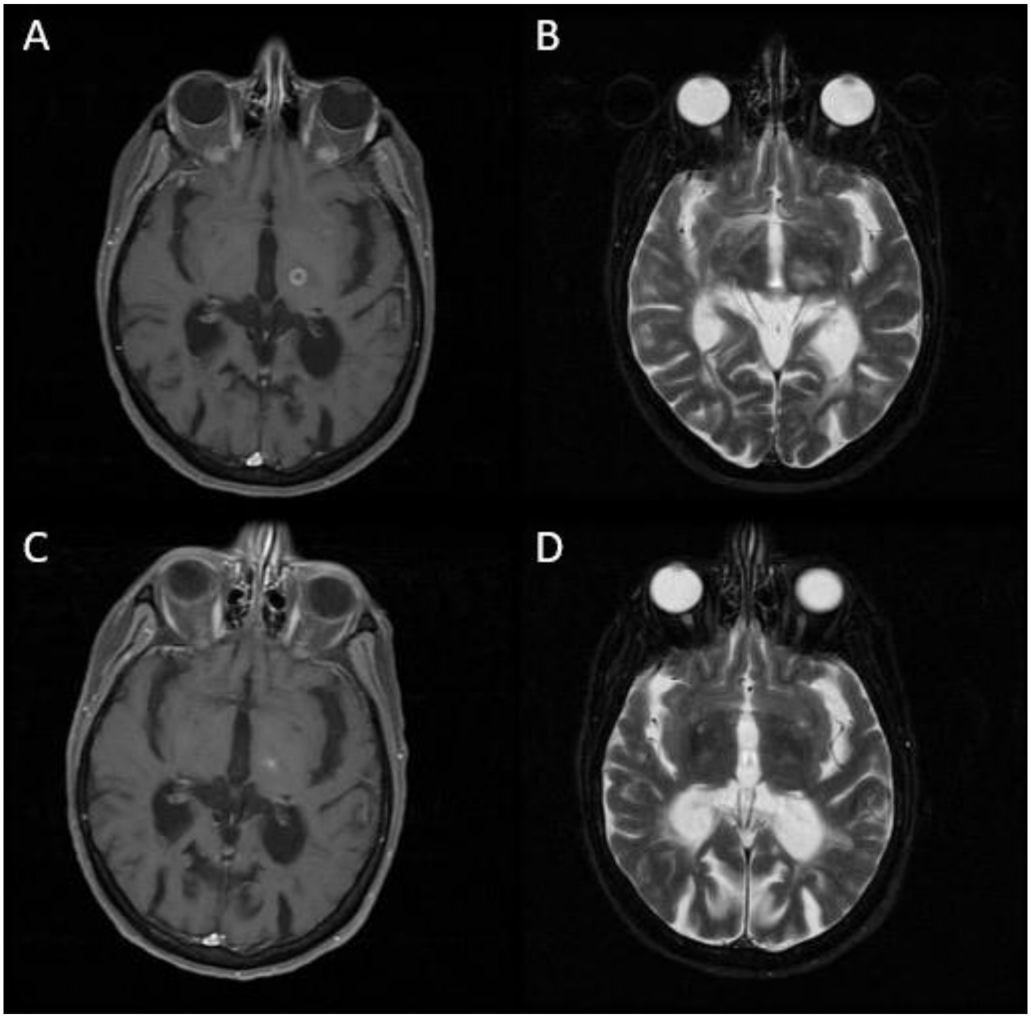

(Filename: TCT_3273_Slide1300.jpg)

2814

11:14AM - 11:21AM

Intra-Individual Correlations Between Quantitative THK5351 Positron Emission Tomography Measurement and MRI-Derived Cortical Volume Across the Alzheimer's Disease Spectrum

S Cho[1], J Park[2]
[1]University of Ulsan College of Medicine, Asan Medical Center, Seoul, Korea, Republic of, [2]Asan Medical Center, Seoul, 05555, Korea, Republic of

Purpose
To assess in vivo whole-brain relationship between uptake of [18F]THK-5351 and cortical atrophy on structural magnetic resonance according to the presence and severity of Alzheimer's disease (AD).
Materials and Methods
Sixty-five participants (21 normal controls, 32 mild cognitive impairment [MCI], and 12 AD patients) were enrolled from a prospective multicenter clinical trial (NCT02656498). Structural MRI and [18F] THK-5351 PET were performed within a 2 month interval. Cortical volume and standardized uptake value ratio (SUVR) were calculated from MRI and PET images, respectively, for 35 FreeSurfer-derived regions-of-interests (ROIs). Pearson's correlation coefficients between SUVR and cortical volume were

calculated for the same ROIs, and correlated regions were compared according to disease severity and β-amyloid PET positivity.
Results
No significantly correlated regions were found in the normal controls. Negative correlations between SUVR and cortical volume were found in MCI and AD groups, mainly in limbic locations in MCI and isocortical locations in AD. The AD group exhibited stronger correlations (r=−0.576–0.781) than the MCI group (r=0.368–0.571). Hippocampal atrophy did not show any correlation with SUVR in the β-amyloid PET-negative group, but negatively correlated with SUVR (r=−0.494, P=.012) in the β-amyloid PET-positive group.
Conclusions
Regional THK-5351 uptake correlated more strongly with cortical atrophy in patients further along the AD spectrum, which demonstrates a close relationship between neuro-pathologic process and cortical atrophy. Hippocampal atrophy was associated with both β-amyloid and THK-5351 uptake, possibly reflecting an interaction between β-amyloid and tau deposition in the neurodegeneration process.

3416

11:21AM - 11:28AM

Recognition of Underlying Neurodegeneration on Emergency Head CT Scans

N Bansal[1], T Shepherd[2]
[1]NYU Langone Health, New York, NY, [2]NYU Medical Center, New York, NY

Purpose
The prevalence of dementia in the elderly US population will double in the next 25 years. Patients with underlying dementia require more frequent visits to emergency clinics, but often present with falls, dizziness or suspected strokes. The underlying neurodegenerative process often goes unrecognized by the patient, caregiver, treating physician and radiologist. We assessed radiology assessment of dementia on emergent CTs and review lobar-specific atrophy patterns that can improve early recognition of underlying neurodegeneration.
Materials and Methods
We searched our institutional records for the last 1600 non-contrast head CTs performed in our Emergency Department. Reports were analyzed to assess demographic data, study indications and percentage reporting morphologic changes attributed to neurodegeneration. We then selected representative cases from our institution with such morphologic changes to illustrate CT findings which support further evaluation for previously unrecognized dementia.
Results
Of the last 1600 noncontrast head CT examinations performed in our ED, 49% of patient were age 65 or older (where dementia prevalence is 10%). The five most common indications included trauma (33%), altered mental status (17%), headache (14%), stroke (11%), and vertigo/dizziness (9%). Excluding NPH and significant white matter disease, dementia was suggested in less than 1% of all reports. Lobar specific atrophy patterns were easy to recognize on noncontrast CT especially when coronal and sagittal reformats are provided to the interpreting radiologist.
Conclusions
Underlying neurodegeneration in patients is under-recognized clinically in the Emergency Department, but suspicious lobar-specific atrophy patterns can be detected by radiologists using noncontrast head CT scans with reformats. This may result in the initial diagnosis of dementia, accelerate patient enrollment in appropriate treatment and decrease medical utilization.

3591

11:28AM - 11:35AM

Regionally Specific Variation in Brain Structure in Behavioral Variant Frontotemporal Dementia Compared to Alzheimer's Dementia

S Meysami[1], C Raji[2], D Merrill[3], M Mendez[1]
[1]David Geffen School of Medicine at UCLA, Los Angeles, CA, [2]Washington University in St. Louis, ST LOUIS, MO, [3]UCLA Medical Center, Los Angeles , CA

Purpose
The purpose of this study was to evaluate patterns of brain atrophy as measured on volumetric Magnetic Resonance (MR) neuroimaging in behavioral variant frontotemporal dementia (bvFTD)[1] compared to Alzheimer's dementia (AD). There is limited application of quantitative techniques for the assessment of clinical brain images in neurodegenerative disorders. Early assessment of quantitative differences on MR neuroimaging could be extremely helpful in distinguishing bvFTD from AD.
Materials and Methods
We evaluated ten comparably demented patients, 4 meeting International Consensus Criteria for clinically probable bvFTD[2] and 6 meeting diagnostic criteria for with Alzheimer's dementia (AD) of early onset. The clinical diagnosis in both groups was supported by changes on flurodeoxyglucose positron emission tomography. We then analyzed their volumetric MRI scan 3 Tesla with MP-RAGE sequences. Each MRI had quantification of 45 brain structures with a program called Neuroreader[3]. Each volume was adjusted for the head size, age, and gender and compared to a normative database to compute Z-scores and percentiles. Partial correlation analysis was done to determine the variation in brain structure between the groups.
Results
There were no statistically significant differences between age and gender in between the bvFTD and AD groups. In the total sample, 70% were women. Persons with AD on average were age 63 ± 3.4 years and those with FTD were 68 ± 7.1 years. Persons with bvFTD had significantly smaller left thalamic volumes ($r = -.73$, $p = .03$), ventral diencephalon volumes ($r = -.73$, $p = .03$) and were more likely to have cerebrospinal fluid ventricular expansion particularly in the lateral ventricles ($r = .75$, $p = .03$). Persons with AD were more likely to have asymmetric hippocampal atrophy but this finding only trended towards statistical significance ($r = .68$, $p = .06$). Those with bvFTD showed trends towards statistical significance for right cerebellar atrophy ($r = -.67$, $p = .06$). There are no statistically significant differences in frontal, temporal, or parietal lobar volumes.
Conclusions
We conclude that the regionally specific variations in brain structure between bvFTD and AD patients can be detected on quantitative MRI. For example, hippocampal asymmetry is more pronounced in AD and this has been reported previously[4]. This work can be applied towards better diagnostic differentiation of bvFTD from AD early in their course, when current and future interventions may be most effective.

3607

11:35AM - 11:42AM

Role of Multiparametric Imaging in Unravelling Pathogenic Pathways in Hepatic Encephalopathy

J CHAGANTI[1]
[1]St Vincent's Hospital, Sydney, UNSW

Purpose
Hepatic encephalopathy (HE) represents a diverse spectrum of complex neuropsychiatric disturbance resulting from liver disease. It is characterized by deficits in cognitive, psychiatric, and motor function and can range in severity from minimal (or covert) hepatic encephalopathy (MHE) to overt hepatic encephalopathy (OHE), coma, and death. It's well known that there are diverse factors that are associated with the HE and most conspicuous of them include immunological and metabolic derangements that

accompany this syndrome. Regardless of the multifactorial causes, the underpinning mechanism is hyperammonemia and the cascade of pathogenic pathways include blood brain barrier disruption, neuroinflammation and Glutaminergic pathways disruption and conduction abnormalities. To understand such diverse pathway of neuropathogenesis, we employed volumetric imaging, spectroscopy, functional connectivity and blood brain barrier imaging to measure each of these independent pathways and assumed that this approach could lead us to identify a biomarker or diagnostic pathway which could lead us to unravel the true extend of HE impact on the central nervous system.

Materials and Methods

We have recruited 16 patients with mild HE and used 9 controls of equal age and sex and measured the resting state connectivity (in6 known networks using conn tool box) and BBB disruption (using DCE imaging and derived k-trans) as well as single voxel short TE spectroscopy in the high parietal cortex. All the patients underwent neuropsychological examination and the psychometric hepatic encephalopathy sores (PHES). The optimal diagnostic cut-offs and the description of their sensitivity and specificity for the final diagnosis of recurrence were derived from the receiver operating characteristic (ROC) analysis with the area under the ROC curve (AUC) for distinguishing between the two diagnostic groups (HE vs normal controls). We compared the differences in metabolites, k-trans and between patients and controls using Wilcoxon rank-sum test. To explore multivariable relationships, generalised linear models (GLM) were then built with K-trans as response variable and group (patients vs controls) and the MRS derived metabolite (glutamates) as explanatory variables.

Results

As compared to the normal controls resting state connectivity showed attenuation in the connectivity in the salience and attentional networks as well as attenuation of pallidum and Putaminal networks and cerebello-cerebral networks ($p= <0.001$ p Uncorrected, Cluster size p-FDR corrected, Cluster treshold- 0.05). The DCE imaging demonstrated increased K trans as compared to the normal controls in parietal white matter and basal ganglia. ($p= 0.001$) MR spectroscopy showed elevation of glutamates in the parietal cortex region (compared to the normative data obtained from the literature as we could not get enough controls for the MR spectroscopy). The volumetry showed moderate volume loss in the parietal cortex while rest of the areas did not show any significant differences ($p= 0.004$).

Conclusions

Currently, there is no golden standard for the diagnosis and possible prediction of HE in cirrhosis patients. The combination of different analysis methods is vital for comprehensive mapping of functional neurological deficits underlying cirrhosis. It's also unclear if there is any correlation of the neurocognitive decline in these patients had any imaging correlates. In this study, we have shown that the complex cascade of neuroinflammatory events results in disrupting the BBB and which leads to blood oxygen dependent changes in the salience networks of brain that are necessary for organisation of execution of complex commands. Spectroscopic derived Glutaminergic pathway disruption is likely contributor to this neuroinflammation.

3516

11:42AM - 11:49AM

Signature of Preclinical Alzheimer's Disease in a Longitudinal Cohort

N Sheikh-Bahaei[1], G Barisano[2], F Sepehrband[2], J Acharya[3], A Rajamohan[4], P Kim[5], M Law[6], H Chui[7], A Toga[2]

[1]University of Southern California, Los Angeles , CA, [2]University of Southern California, Los Angeles, CA, [3]UNIVERSITY OF SOUTHERN CALIFORNIA, KECK SCHOOL OF MEDICINE, Monrovia, CA, [4]UNIVERSITY OF SOUTHERN CALIFORNIA, KECK SCHOOL OF MEDICINE, LOS ANGELES, CA, [5]Keck School of Medicine of USC, La Crescenta, CA, [6]Keck Medical Center of USC, Los Angeles, CA, [7]Keck school of medicine of USC, Los Angeles , CA

Purpose
A growing body of evidence has shown that the role of microvascular changes in Alzheimer's disease (AD) is far more pivotal than what was previously believed. In this study we investigated the microvascular changes of cognitively normal subjects who developed AD to identify potential MRI biomarkers for diagnosis of preclinical AD, which can be used in the clinical setting particularly when PET is not available.
Materials and Methods
25 subjects who converted from normal cognition to dementia and 25 age- and sex-matched stable controls from Alzheimer's Disease Neuroimaging Initiative (ADNI) cohort were investigated. Their baseline (when all clinical examinations were normal) T2, FLAIR and T2*W images were scored by expert readers. The number and grade of PVS, severity of deep and periventricular white matter changes (DWM and PVWM) and presence of lobar cerebral micro bleeds (LCMB) were recorded according to 5-point visual-scale (0-4)1, Fazekas scoring (0-3)2 and MARS grading system3 respectively and compared between two groups. JMP pro 13 was used to analyze the data.
Results
Both number (p=0.003) and grade (p=0.002) of PVS were significantly higher in the initial MRI of the subjects who developed AD over the time. They also had more LCMB (p=0.02) and higher grade of PVWM (p=0.01) but not DWM (p=0.4) changes. In logistic regression model adjusted for age, both PVS number (p=0.01) and PVWM changes (p=0.02) had significant associations with conversion from normal cognition to AD.
Conclusions
Presence of enlarged PVS and severe PVWM changes could potentially be valuable imaging biomarkers for identifying preclinical subjects who will develop AD in the future. These microvascular changes could be easily detected on T2w and FLAIR images and might help clinicians to stratify cases for future screening and treatment.

2751

11:49AM - 11:56AM

The Role of Volumetric Analysis in the Preoperative Assessment of Parkinson's Disease Patients Undergoing Deep Brain Stimulation

K Atcheson[1], R Richardson[2], J Mettenburg[3]
[1]University of Pittsburgh School of Medicine, Pittsburgh, PA, [2]University of Pittsburgh Medical Center, Pittsburgh, PA, [3]UPMC, PITTSBURGH, PA

Purpose
Patients with Parkinson's Disease (PD) electing to undergo Deep Brain Stimulator (DBS) implantation undergo an evaluation prior to surgery, including UPDRS On/Off assessment, optimization of medications, and MRI with volumetric structural imaging. We propose that volumetric analysis may correlate with pre-operative disease severity and provide information regarding DBS efficacy.
Materials and Methods
A retrospective analysis of 53 patients with PD who underwent DBS implantation from 2012-2018 was performed. All patients had UPDRS Part III On and Off scores recorded in addition to pre-operative brain MRI. Quantitative volumetric analysis was completed using NeuroReader (Horsens, Denmark). Regional brain volumes were analyzed for correlation with pre-operative UPDRS scores, and subgroup analysis of regional brain volumes using UPDRS Scores greater than 25 and post-operative medication regimens were completed.
Results
Higher UPDRS On/Off scores pre-operatively correlated with decreased brain volumes, notably with whole brain (On: r = -0.487 [p = 0.000], Off: r = -0.366 [p = 0.007]), gray matter, (On: r = -0.427 [p = -0.001], Off: r = -0.312 [p = 0.023]), and thalamus (On: r = -0.534 [p = 0.000], Off: r = -0.451 [p =

0.001]). Patients with a UPDRS On scores greater than 25 had significantly smaller brain volumes than those with lower scores in whole brain (54.88% vs. 54.12%, p = 0.009), gray matter (25.91% vs. 29.06% [p = 0.023]), and thalamus (0.91% vs. 0.98% [p = 0.007]). Lower total gray matter was observed in patients with unchanged or increased dopamine medication post-operatively (n = 37; 25.639% vs. 29.461% [p = 0.026]).
Conclusions
Patients with PD undergoing DBS implantation with higher UPDRS Part III On/Off scores correlate with decreased whole brain volume as well as in specific brain regions, most notably the thalami. Moreover, pre-operative gray matter volume may influence dopaminergic medication requirements following implantation.

Patient Demographics

Demographic	Median ± SD
Patients	53
Male	47
Female	6
Age (range)	68 (44-82)
UPDRS Part III Score	
On (range)	18 ± 8.22 (2-36.5)
Off (range)	40 ± 13.95 (10-75)

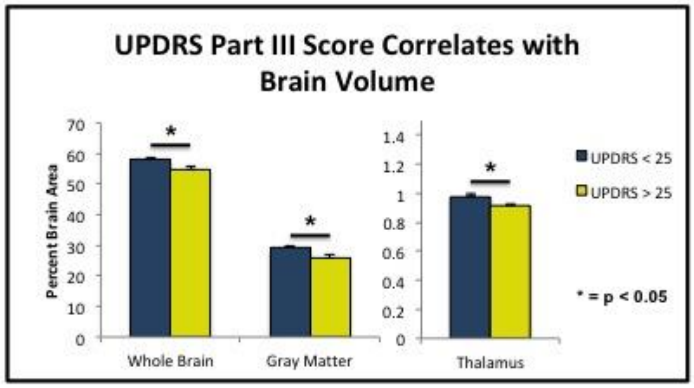

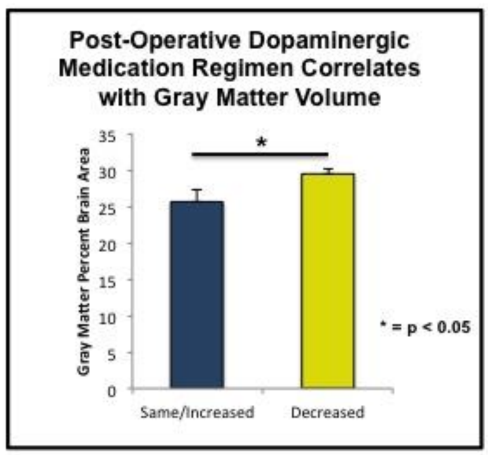

(Filename: TCT_2751_Slide1.jpg)

Wednesday, May 22, 2019
11:00AM - 12:00PM
Pediatrics Potpourri Topics

2901

11:00AM - 11:04AM

ASL Perfusion of Pediatric Hemangiomas

S Dyer[1], M Ho[2]
[1]Mayo Clinic, Rochester, MN, [2]MAYO CLINIC, ROCHESTER, MN

Purpose
To illustrate the diagnostic utility of arterial spin labeling (ASL) perfusion for imaging evaluation of pediatric hemangiomas.
Materials and Methods
5 patients presenting with infantile hemangiomas (IH) and 2 patients with congenital hemangiomas (CH) were seen in the vascular anomalies clinic at our institution over the past year. Diagnoses were confirmed based on consensus clinical history and examination by a pediatric dermatologist and pediatric neuroradiologist. Patients were imaged by MRI using standard anatomic and postcontrast sequences, as well as arterial spin labeling (ASL) perfusion.
Results
All hemangiomas showed similar anatomic imaging characteristics with smooth lobulated margins, T2-hyperintense signal, avid homogeneous enhancement, and internal flow voids. Congenital hemangiomas (CH) demonstrated central areas of hypoperfusion on ASL, which corresponded clinically to progressive ulceration and involution. Infantile hemangiomas (IH) in the proliferative phase demonstrated diffuse hyperperfusion on ASL, which corresponded clinically to subsequent lesion proliferation. In one patient with IH who was imaged following propanolol therapy, follow-up imaging showed treatment response with decreased lesion size and perfusion. For patients with concurrent ultrasound (US) examinations, patterns of lesion vascularity appeared similar between ASL and US Doppler images.
Conclusions
Arterial spin labeling perfusion is a useful noncontrast imaging technique that provides added value over conventional imaging sequences for the characterization of pediatric vascular anomalies. For pediatric hemangiomas, use of ASL improves diagnostic workup, management, and follow-up.

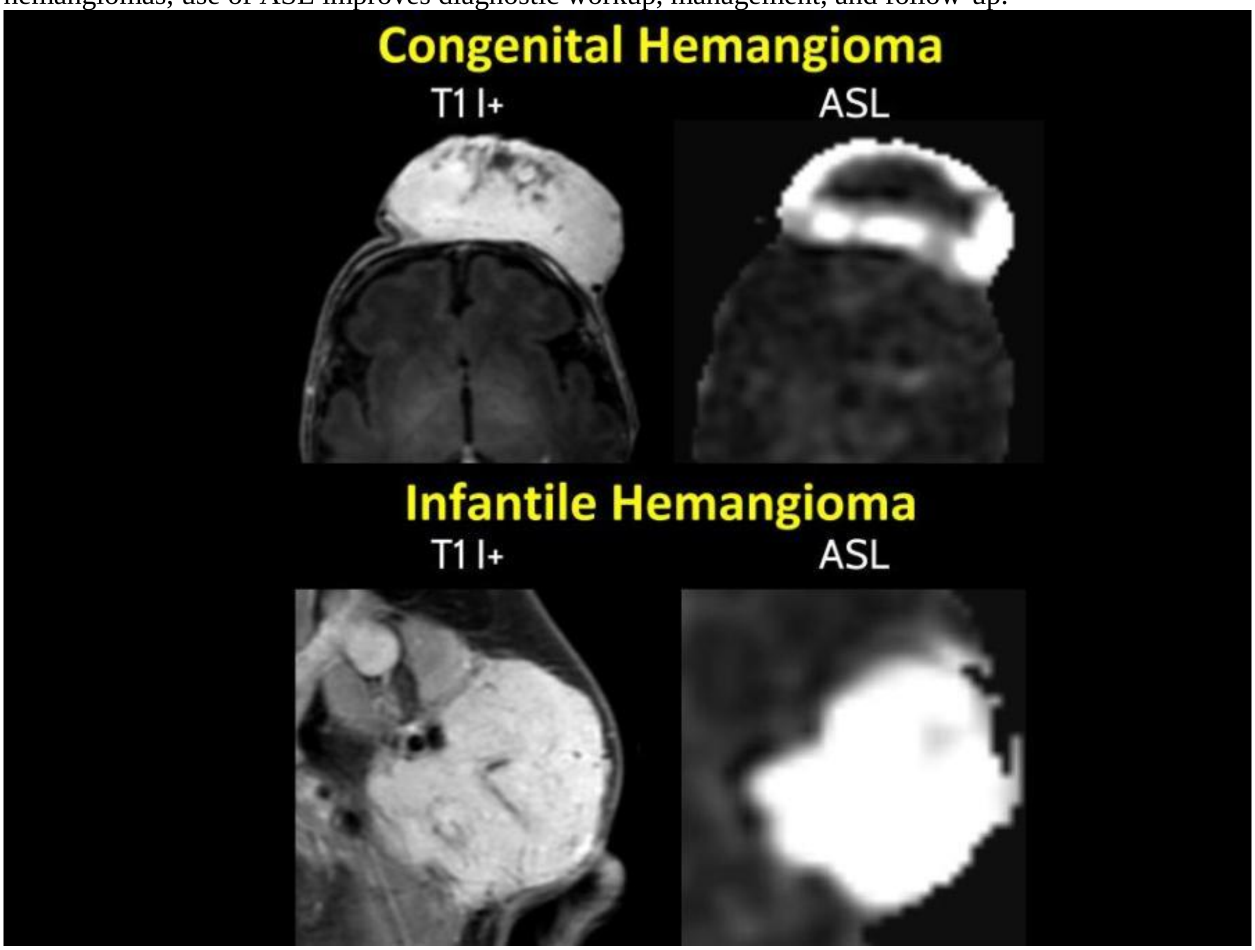

(Filename: TCT_2901_Figure300.jpg)

2683

11:04AM - 11:11AM

CNS Involvement of Hemophagocytic Lymphohistiocytosis in a Pediatric Patient

M Kumar[1], J Chang[1], A Ozturk[1], O Raslan[1], M Bobinski[1], B Dahlin[1], J Ziegler[1], N Pham[1]
[1]*University of California, Davis Health, Sacramento, CA*

Purpose
To present a severe pattern of central nervous system hemophagocytic lymphohistiocytosis (HLH) involvement.
Materials and Methods
The patient is a 16-year-old male presenting with fevers, cough, jaundice, weight loss, night sweats, and lymphadenopathy for one month. Labs were notable for pancytopenia, hyponatremia, and elevated liver enzymes. Bone marrow biopsy revealed iron laden macrophages, suggesting HLH, and plasma cells, suggesting Epstein-Barr viral (EBV) infection. Patient began chemotherapy, but developed episodes of confusion, aphasia, and headache. MRI was obtained at symptom onset and at one-month follow-up.
Results
Initial brain MRI (not shown) demonstrated lesions within the deep white matter, including corpus callosum, periventricular white matter, and temporal lobe white matter, but without involvement of the leptomeninges. A subsequent MRI revealed progression of disease with increasing size, number, and distribution of white matter lesions, with restricted diffusion (not shown), foci of internal hemorrhage, and postcontrast leptomeningeal and parenchymal enhancement, consistent with stage II CNS involvement (1).
Conclusions
HLH is characterized by diffuse infiltration of activated lymphocytes affecting multiple organs. CNS disease has been categorized into three neuropathological stages: stage I with leptomeningeal inflammation, stage II with perivascular infiltration, and stage III with extensive tissue infiltration, blood vessel destruction, and tissue necrosis. HLH-associated CNS involvement is often progressive and one of the main contributors of mortality, but is treatable (2). Findings include diffuse white matter lesions, hemorrhage, restricted diffusion, and enhancement. Leptomeningeal enhancement suggests infiltration with histiocytes and lymphocytes, while parenchymal enhancement, which is seen in our case, suggests compromised blood-brain barrier and active demyelination, consistent with a higher stage of CNS involvement (3, 4). We present a pediatric case of at least stage II CNS involvement of HLH likely secondary to EBV infection and its imaging characteristics on contrast enhanced MRI. This case demonstrates the important role of imaging and suggest that brain MRI should be performed routinely at diagnosis and follow-up (5).

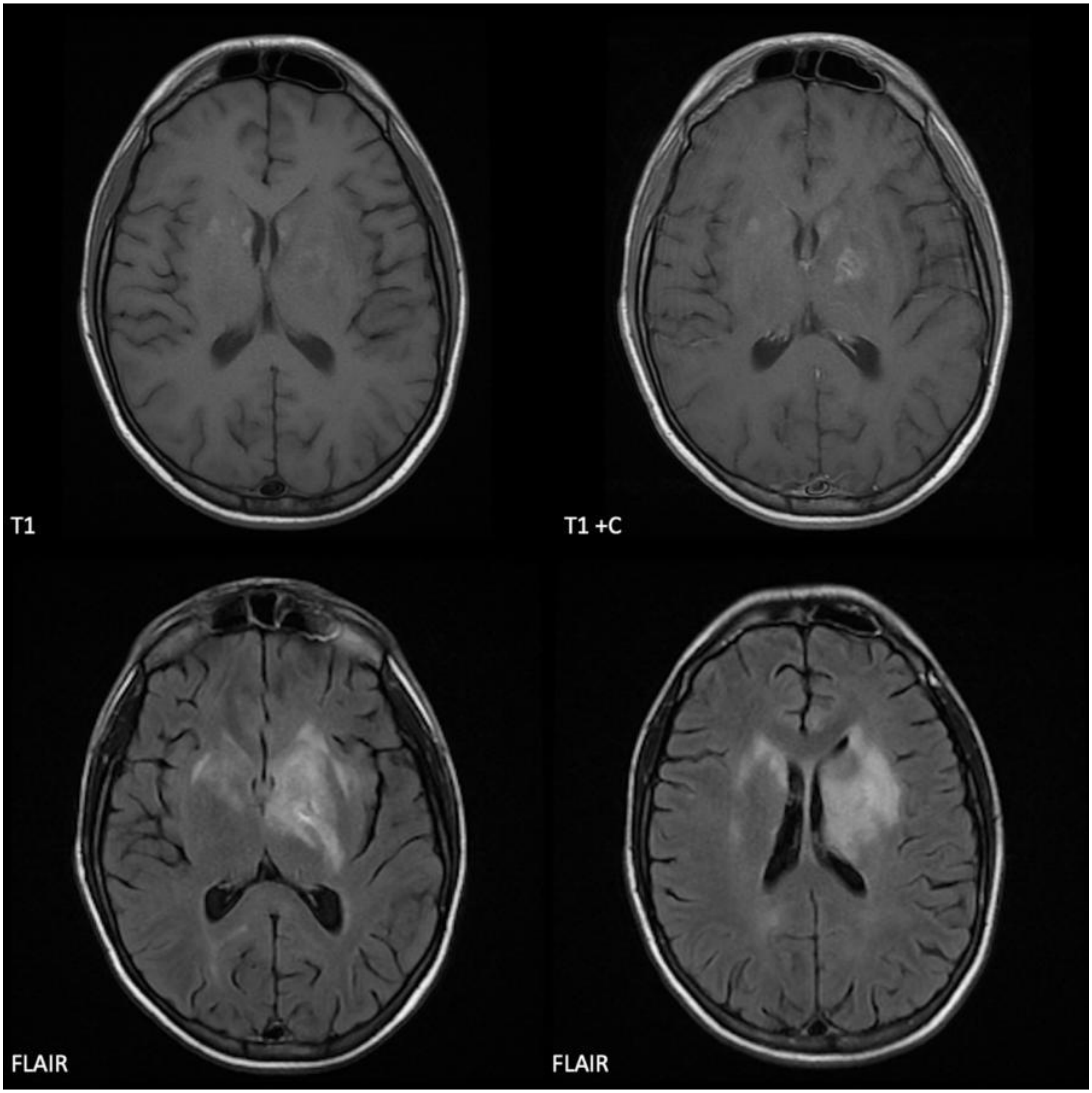

(Filename: TCT_2683_Final4HLH.jpg)

3326

11:11AM - 11:18AM

DTI of Spinal Cord Lesions of Varying Severity Based on MRI in the Entire Pediatric Spinal Cord

S SAKSENA[1], F Mohamed[1], D Middleton[1], L Krisa[1], M Alizadeh[2], S Shahrampour[3], A Flanders[4], S Faro[5]
[1]Thomas Jefferson University, Philadelphia, PA, [2]Thomas Jeffesron University, Philadelphia, PA, [3]Temple University, Philadelphia, PA, [4]THOMAS JEFFERSON UNIVERSITY HOSPITAL, PHILADELPHIA, PA, [5]Johns Hopkins School of Medicine, Baltimore, MD

Purpose
In patients with spinal cord injury (SCI), secondary injury may involve the development of necrosis, glial scarring and cavitation. These secondary injuries develop through a multi-factorial process, including

infiltration of astrocytes, microglia, macrophages, fibroblasts, chemokines and their receptors as well as chronic axonal injury such as Wallerian degeneration1. These processes interfere with spinal cord (SC) recovery by preventing axonal regeneration2. Examining the perilesional areas distant from the injury site may provide valuable insights into the full extent of injury. A recent DTI study has shown changes in the SC white matter regions remote from the lesion in chronic SCI children3. In this study, we classified the pediatric SCI subjects into five groups of varying severity based on the type of SC lesion seen on MRI. The purpose of this study was two-fold: a) to determine whether DTI at sites cephalad and caudal to the MRI lesion provides measures of cord abnormalities in different SCI groups (ranging from SCIWORA to focal atrophy with associated hemorrhage) compared to typically developing (TD); b) any correlation between the varying severity of MRI abnormality and DTI abnormalities cephalad and caudal to the MRI lesion.

Materials and Methods

A total of 36 TD (mean age, 11.72±3.12years) without evidence of SCI or pathology and 23 subjects with chronic SCI (mean age, 11.91±3.03years) were included in the study. The lesion in subjects with SCIWORA was based on ISNCSCI examination. Written informed assent and consent was obtained and approved by IRB. Imaging: Subjects underwent scans using 3T Verio MR scanner. The protocol: T1, T2, axial DTI scans based on the iFOV4 to cover the cervical and thoracic SC8. The imaging parameters: 20 diffusion directions, 6 b0, b=800s/mm2, voxel=0.8x0.8x6mm3, axial slices=40, TR=7900ms, TE=110ms, TA=8:49min. Data analysis: After motion correction5 and tensor estimation5, ROIs were manually drawn, by a board-certified pediatric neuroradiologist to extract information from the whole cord along the entire SC. DTI metrics; FA, MD, AD and RD were quantified at each intervertebral disk level and at the mid-vertebral body level of the entire SC. The cord was separated into proximal, middle and distal thirds cephalad and caudal to the MRI lesion. The five SCI groups included; 1= SCIWORA (n=6); 2=Syringohydromyelia (n=4); 3=Atrophy+Syringomyelia (n=7); 4=Atrophy+Myelomalacia (n=3); 5=Atrophy+Hemorrhage (n=3). Groups 1 to 5 represent a progressive measure in cord abnormality. Among these groups, we looked at concordant DTI correlation which is defined as the expected change in DTI metrics with increasing cord severity. Statistical analysis: To detect differences in DTI metrics between TD and different SCI groups in the segments of the cord, a one-way analysis of variance with pooled t-test was performed, $p<0.05$.

Results

In group 1, FA showed a decrease and RD showed an increase in the middle segment of the cephalad cord, all the three segments of the caudal cord showed FA decrease and RD increase compared to TD (Tables 1 and 2). In group 3, FA was decreased in all three segments of the cephalad and caudal cord compared to TD. Cephalad to the lesion, FA was decreased in distal and middle segments in group 2 and middle and proximal segments in group 4 respectively, however, FA was decreased in proximal segment of the caudal cord. In group 5, FA decreased in the proximal segment of the cephalad cord and proximal and middle segment of the caudal cord (Table 1). RD was increased in all segments of the cephalad and caudal cord in group 3 except for middle segment of cephalad cord. In group 4, RD showed an increase in middle and proximal segments of the cephalad cord and only in the proximal segment of caudal cord (Table 2). For each SCI group 1 to 5, we also examined those segments showing statistically significant changes in DTI metrics compared to TD. For all groups 1 to 5, FA showed the greatest number of abnormal segments followed by RD, MD and AD (Table 3). A concordant correlation between abnormal DTI values and different SCI groups is shown in Table 4. Overall, FA showed the greatest concordant correlation among the groups 1 to 5 for both cephalad and caudal cord (Table 4).

Conclusions

In this study, SCIWORA showed DTI abnormality at segments of the cephalad and caudal cord with the caudal cord more affected consistent with the anterograde degeneration. FA showed the greatest total number of segments in the cephalad and caudal cord that showed abnormal DTI values in comparison to the other DTI metrics. We also found that FA showed the most concordant correlation among the SCI groups 2 to 4 indicating a trend that may show a correlation between pathology and FA. Overall, FA appears to be the most sensitive and consistent DTI metric and a potential imaging biomarker in evaluating pediatric SCI patients. DTI might be useful in the detection of various types of SC lesions which may establish a therapeutic strategy and prognosis.

Table 1: Summary of changes of FA in segments of the cord cephalad and caudal to the level of MRI lesion in SCI groups 1, 2, 3, 4 and 5 and TD subjects.

Groups based on type of MR abnormality		Cephalad DTI Parameters			Caudal DTI Parameters		
		FA_{distal}	FA_{middle}	$FA_{proximal}$	$FA_{proximal}$	FA_{middle}	FA_{distal}
Group 1	TD	0.59±0.09	0.58±0.07	0.53±0.09	0.54±0.09	0.59±0.09	0.51±0.11
	SCI	0.60±0.07	**0.47±0.09**	0.50±0.12	**0.47±0.09**	**0.48±0.07**	**0.45±0.09**
Group 2	TD	0.59±0.08	0.55±0.08	0.53±0.09	0.59±0.10	0.57±0.10	0.50±0.12
	SCI	**0.53±0.12**	**0.50±0.12**	0.51±0.13	**0.46±0.13**	0.52±0.11	0.47±0.12
Group 3	TD	0.59±0.08	0.55±0.08	0.53±0.09	0.56±0.09	0.59±0.09	0.50±0.11
	SCI	**0.52±0.10**	**0.52±0.06**	**0.47±0.07**	**0.44±0.09**	**0.42±0.14**	**0.44±0.08**
Group 4	TD	0.59±0.08	0.53±0.09	0.56±0.09	0.60±0.09	0.52±0.09	0.48±0.14
	SCI	**0.62±0.06**	**0.45±0.12**	**0.37±0.13**	**0.32±0.05**	0.54±0.05	0.46±0.07
Group 5	TD	0.59±0.08	0.55±0.08	0.53±0.09	0.59±0.10	0.57±0.10	0.50±0.12
	SCI	0.57±0.12	0.51±0.09	**0.48±0.11**	**0.42±0.11**	**0.46±0.12**	0.54±0.09

Bold indicates that the DTI value is significantly different in subjects with SCI compared to the TD subjects.

Table 3: Summary of the total number of segments of the cephalad and caudal cord showing abnormal DTI values in different SCI groups 1 to 5.

Groups based on type of MR abnormality	FA_{cep}	FA_{cau}	FA_{tot}	MD_{cep}	MD_{cau}	MD_{tot}	AD_{cep}	AD_{cau}	AD_{tot}	RD_{cep}	RD_{cau}	RD_{tot}
Group 1	1	3	4	0	3	3	0	2	2	1	3	4
Group 2	2	1	3	2	0	2	1	0	1	2	0	2
Group 3	3	3	6	1	0	1	0	0	0	2	3	5
Group 4	2*	1	3	1	1	2	1	1	2	2	1	3
Group 5	1	2	3	1	0	1	0	0	0	1	0	1

Cep=Cephalad; Cau=Caudal; Tot=Total
*Distal segment was not included as it showed discordant FA value (increase).

Table 2: Summary of changes of RD in segments of the cord cephalad and caudal to the level of MRI lesion in SCI groups 1, 2, 3, 4 and 5 and TD subjects.

Groups based on type of MR abnormality		Cephalad DTI Parameters			Caudal DTI Parameters		
		RD_{distal}	RD_{middle}	$RD_{proximal}$	$RD_{proximal}$	RD_{middle}	RD_{distal}
Group 1	TD	0.62±0.18	0.67±0.14	0.73±0.22	0.59±0.21	0.62±0.26	0.57±0.25
	SCI	0.66±0.14	**0.74±0.20**	0.71±0.30	**0.81±0.16**	**0.82±0.15**	**0.75±0.22**
Group 2	TD	0.64±0.17	0.70±0.20	0.59±0.21	0.66±0.26	0.59±0.24	0.54±0.24
	SCI	**0.82±0.28**	0.78±0.24	**0.87±0.30**	0.74±0.28	0.64±0.25	0.64±0.25
Group 3	TD	0.64±0.17	0.70±0.17	0.63±0.23	0.64±0.23	0.61±0.26	0.55±0.23
	SCI	**0.74±0.29**	0.71±0.16	**0.7560.23**	**0.69±0.20**	**0.79±0.34**	**0.66±0.27**
Group 4	TD	0.64±0.16	0.68±0.21	0.62±0.23	0.57±0.02	0.60±0.24	0.52±0.25
	SCI	0.58±0.14	**0.84±0.29**	**1.19±0.61**	**0.78±0.08**	0.62±0.08	0.68±0.10
Group 5	TD	0.64±0.17	0.70±0.20	0.59±0.21	0.66±0.26	0.59±0.24	0.54±0.24
	SCI	0.66±0.21	0.76±0.15	**0.73±0.25**	0.86±0.51	0.55±0.29	0.47±0.24

Bold indicates that the DTI value is significantly different in subjects with SCI compared to the TD subjects.

Table 4: Concordant correlation between the different SCI groups 1 to 5 and those segments showing the abnormal DTI values in both cephalad and caudal cord.

	Cephalad DTI Parameters				Caudal DTI Parameters			
	FA	MD	AD	RD	FA	MD	AD	RD
Group 1	0.47±0.10			0.74±0.21	0.47±0.09	1.09±0.21	1.64±0.39	0.79±0.19
Group 2	0.52±0.12	1.21±0.26	1.93±0.29	0.85±0.30	0.47±0.14			
Group 3	0.51±0.08	1.05±0.28		0.75±0.26	0.44±0.11			0.72±0.29
Group 4	0.41±0.13	1.47±0.62	2.01±0.63	1.03±0.52	0.31±0.06	0.93±0.10	1.41±0.17	0.78±0.08
Group 5	0.48±0.11	1.02±0.23		0.74±0.25	0.44±0.12			

$FA_{cephalad}$: Group 2 vs Group 4: p<0.0001; Group 3 vs Group 4: p<0.0001; Group 1 vs Group 4: p=0.0197
FA_{caudal}: Group 2 vs Group 4: p=0.0008; Group 3 vs Group 4: p=0.0022; Group 1 vs Group 4: p=0.0001; Group 1 vs Group 3: p=0.0457
$MD_{cephalad}$: Group 4 vs Group 3: p<0.0001; Group 4 vs Group 2: p=0.0031
$RD_{cephalad}$: Group 4 vs Group 1: p=0.0005; Group 4 vs Group 3: p<0.0001; Group 4 vs group 2: p=0.0096

(Filename: TCT_3326_Image-File.jpg)

3181

11:18AM - 11:25AM

Reaching the Limit: Specific Absorption Rate (SAR) MRI Threshold in Pediatric Spine Imaging

A Saha[1], I Ikuta[1]
[1]Yale University School of Medicine, New Haven, CT

Purpose
We describe a case to highlight safety mechanisms in place to monitor the potential thermal effects of MRI via specific absorption rate (SAR) and strategies to minimize reaching the limit. Radiofrequency (RF) power deposition results in potential heating of patients' tissues. The power delivered during a MRI examination is referred to as the SAR and is expressed in watts per kilogram (W/Kg) (1). Radiofrequency pulses consist of oscillating electromagnetic fields that results in patients' tissues conducting electrical currents while in the magnetic field, which generates heat. The RF energy depends on the pulse sequence utilized, coil type used to transmit energy to the body, size, shape and electromagnetic and thermodynamic properties of the body (2). RF exposure safety during clinical MRI is regulated by the FDA, and the International Electrotechnical Commission provides guidelines via standard 60601-2-33 which defines two operating modes that allows MRI scanners to enforce SAR limits during the scan: normal operating mode (whole body SAR ≤ 2 W/kg) and first level controlled operating Mode (whole body SAR ≤ 4 W/kg) (3).
Materials and Methods
A 16-year-old female with a past medical history significant for spina bifida and scoliosis presented to orthopedic surgery for possible operative correction. Physical exam was notable for 5 degrees thoracic rotation on the right and 8 degrees of lumbar rotation on the left. An outpatient MRI Total Spine with and without intravenous contrast was ordered to evaluate for tethered cord, spina bifida, and hydromyelia. The study was incidentally protocolled by the musculoskeletal radiology service to include sagittal thin-

section T2-SPACE in addition to the normal protocol on a Siemens 3T Verio MRI. The study was interpreted by the neuroradiology service.

Results

MRI of the total spine demonstrates the scoliotic curvature of the thoracolumbar spine on corona, Half-Fourier Single Shot Turbo Spin Echo (HASTE) sequence (A) and previously described on prior radiographs (not shown). Sagittal (B) and axial (C) T2 sequences re-illustrate myelomeningocele involving the sacral posterior elements measuring up to 5.0 cm in greatest dimension. Prior to the administration of intravenous contrast, a warning was given by the scanner stating that continuation of the examination may lead to increased thermal stress with the advice to discontinue the exam (D). Upon review of the obtained images, it was felt that a diagnosis could be made without the administration of intravenous contrast, and thus the exam was terminated. The patient successfully underwent corrective surgery one month later.

Conclusions

It is important to note techniques that can prevent reaching the SAR limit. There may be utility in ensuring targeted MRI acquisition is made of interested anatomy rather than global acquisition, particularly when long sequences are utilized or large areas of imaging coverage are involved (such as total spine imaging). Other techniques include reducing flip angles of RF pulse when using fast spin-echo sequence, decreasing the number of slices in an acquisition, or reducing number of echoes in multiecho sequence (1,4). Advanced planning and implementation of reduced SAR techniques can facilitate quicker completion of studies and reduce thermal effects on tissues.

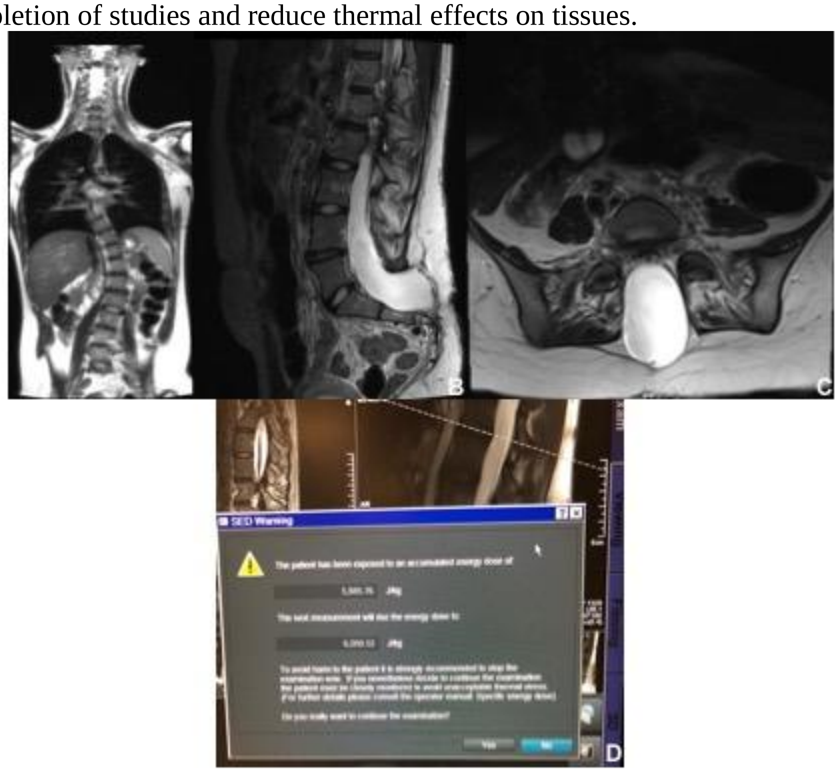

Figure 1: MRI-Total Spine Coronal HASTE (A), sagittal T2 (B), axial T2 (C), Thermal limit warning (D).

(Filename: TCT_3181_Figure1.jpg)

2630

1:00PM - 1:07PM

Uncommon Site for an Uncommon Disease of the Temporal Bone: Chondroblastoma of the Jugular Foramen

P Patel[1], K See[2], S Ceglar[3], J Go[4]
[1]LAC+USC Medical Center, Los Angeles, CA, [2]University of Southern California, Pasadena, CA, [3]LAC+USC, Los Angeles, CA, [4]UNIVERSITY OF SOUTHERN CALIFORNIA, KECK SCHOOL OF MEDICINE, LOS ANGELES, CA

Purpose
The purpose of this abstract is to discuss a case of chondroblastoma of the temporal bone, a rare tumor on its own in an even rarer location, the jugular foramen. The case will be discussed initially with the clinical history followed by radiologic findings associated with the case and ending with the classic appearance on pathology to make the diagnosis of chondroblastoma. With this case we hope that this entity is included in the differential of jugular foramen masses when other possibilities have been exhausted.
Materials and Methods
This is a case of a 61 year old male who presented with two year history of progressive left pulsatile tinnitus, vertigo, left hearing loss, and 30 pound weight loss. The patient recently developed hoarseness.
Results
CT: There is a large lytic expansile mass centered in the jugular foramen extending to the petrous apex encasing the left petrosal internal carotid artery superiorly. The mass extends inferiorly causing erosion of the inner ear including the cochlea, vestibule, and semicircular canals as well as extension into the middle ear causing ossicular chain erosion. The mass also erodes the mastoid portion of the temporal bone posteriorly. There is resultant left mastoid effusion. MRI: There is a large T1 isointense and T2 hypointense enhancing mass centered in the left jugular foramen with erosion/destruction of the temporal bone structures as described above in the CT findings. There is again seen encasement of the petrosal left internal carotid artery. The mass extends inferiorly going through the jugular foramen to the level of C1. This mass also extends intracranially along the left temporal lobe in the middle cranial fossa. The mass demonstrates reduced diffusion on diffusion weighted imaging. Indium-111 somatostatin receptor scintigraphy or octreotide scan: There is asymmetric radiotracer uptake in the region of the left temporal bone anteriorly. Pathology Slides: Chondroblastoma tumor demonstrated by chondrocytes in a background of hyaline cartilage material with chicken wire appearance due to calcifications within the matrix.
Conclusions
The left temporal bone mass centered in the jugular foramen was unusual given its size, location, and extensive osseous destruction and encasement of left petrous internal carotid artery. However, given statistical probability based on location, positivity on octreotide scan, and hypervascularity paraganglioma or meningioma were initially favored. However, the pathology demonstrated chondroblastoma. The location is highly unusual for chondroblastoma as most of them arise from squamosal portion and supraglenoid region of the temporal bone given cartilaginous rests in these regions. However, on imaging and during surgery the mass appeared to primarily arise from the jugular foramen extending into adjacent structures as far superiorly as middle cranial fossa and inferiorly to the level of C1 below the jugular foramen. In addition, this mass demonstrated T2 hypointensity whereas chondroblastomas typically demonstrate T2 hyperintensity on MRI. The pathology for chondroblastoma usually shows classic chicken wire appearance due to calcification within background of hyaline cartilage and chondrocytes.

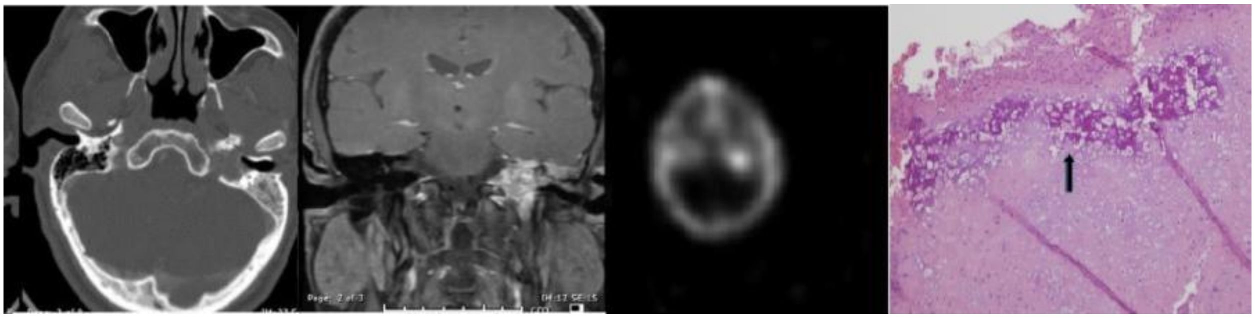

(Filename: TCT_2630_a.jpg)

2516

1:07PM - 1:14PM

Acquired Silent Sinus Syndrome of the Sphenoid Sinus

A Zlochower[1], G Parnes[1], W Mallon[2], R Zampolin[1], S Roknsharifi[1], J Bello[1], K Shifteh[1]
[1]Montefiore Medical Center, Bronx, NY, [2]Montefiore Medical Center, New York, NY

Purpose
We present a case report of acquired sphenoid sinus atelectasis, which to our knowledge has not been previously described in the literature. Our case report is important not only due to its unique nature, but also its impact on patient management.
Materials and Methods
A 48-year-old female with past medical history of prior endoscopic sinus surgery presented for repair of an anterior right skull base defect with subsequent right sphenoid sinusitis, requiring endoscopic sphenoidotomy. The patient continued to experience right sided refractory headache. Nasal endoscopy demonstrated the right sphenoid sinus ostium to be scarred and closed. The patient underwent Sinus CT to determine whether right sphenoid sinusitis required further intervention, such as revision of right sphenoid sinusotomy.
Results
CT Sinuses on 9/2018 compared to prior scan in 2016 showed interval atelectasis of the right sphenoid sinus with complete opacification. The carotid canal, optic canal, foramen rotundum and Vidian canal are border forming with the right sphenoid sinus. The 2016 Sinus CT demonstrated a well-developed right sphenoid sinus.
Conclusions
Sinus atelectasis is a well-known entity involving the maxillary sinus, whereby the affected maxillary sinus undergoes volume loss and wall retraction. This can lead to the clinical picture of facial asymmetry, hypoglobus and enophthalmos which is knows as "silent sinus syndrome". Although our case of sphenoid sinus atelectasis did not involve a facial deformity, it still had major clinical implications. Our patient had recurrent right sphenoid sinusitis and was planned for functional endoscopic sinus surgery for right sphenoid sinusotomy. Endoscopic sinus surgery is generally well tolerated with low complication rates. The complications of surgery are significantly increased with anatomic variations. It was crucial for the surgeon to understand the anatomic distortion that was caused by the atelectasis since vital structures including the internal carotid artery, optic nerve, foramen rotundum and Vidian canal are border forming with the sphenoid sinus. While the exact mechanism for sinus atelectasis is not completely understood, it is believed to involve obstruction of the sinus outflow tract resulting in a chronic hypoventilated state and negative pressure which subsequently leads to wall retraction and volume loss. The etiology is generally idiopathic; however, prior sinus surgery has been implicated as occurred in our case. .

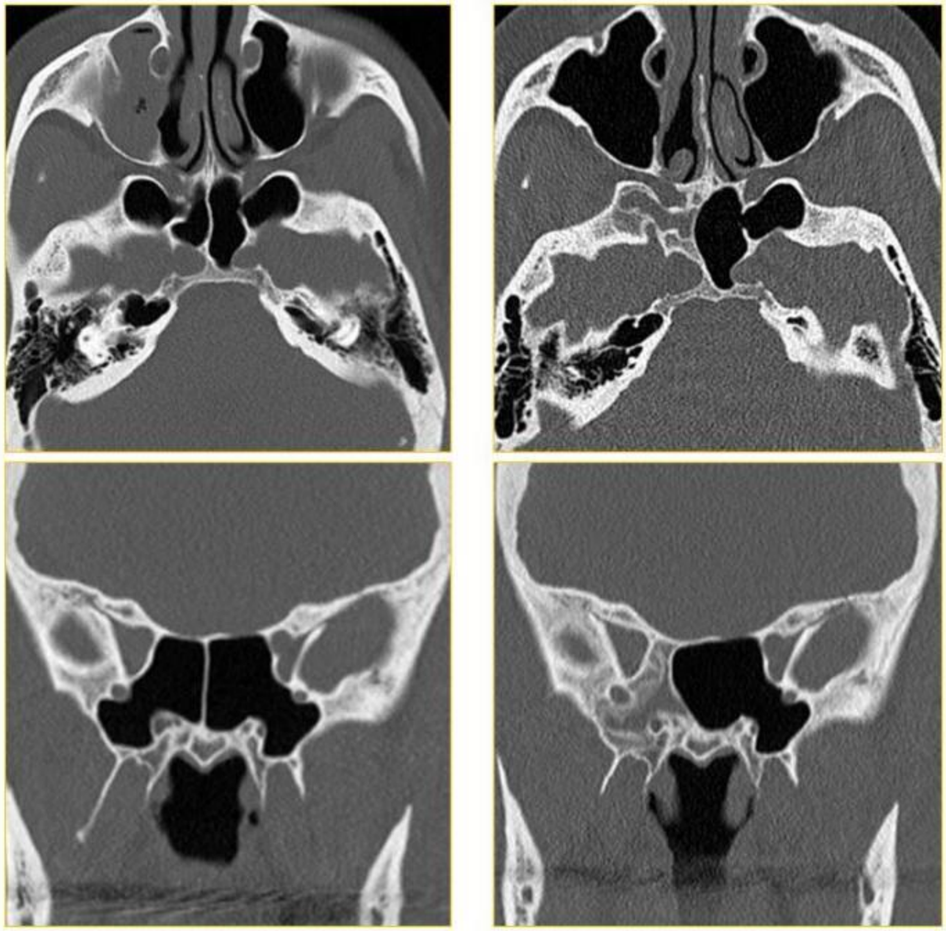

(Filename: TCT_2516_Presentation2.jpg)

3305

1:14PM - 1:21PM

An Unusual Presentation of Orbital Inflammation

S Veeraraghavan[1], G Avey[2], T Kennedy[3]
[1]University of Wisconsin Hospitals and Clinics, Madison, WI, [2]UNIVERSITY OF WISCONSIN, MADISON, WI, [3]THE UNIVERSITY OF WISCONSIN-MADISON, MIDDLETON, WI

Purpose
To illustrate an unusual cause of unilateral orbital inflammation, we present the case of a 72 year old male with metastatic prostate cancer who presented to urgent care with 1 day history of right eye chemosis, and right periorbital pain.
Materials and Methods
A 72 year old male with past medical history of metastatic prostate cancer presented to urgent care with one day history mild right blurry vision, right eye chemosis and ptosis, associated right retro-orbital pain and headache, and nausea and vomiting. His symptoms were exacerbated by superior and lateral right gaze. He was sent to the emergency room for further evaluation, ophthalmologic consultation and MRI of the orbits. The differential diagnosis prior to imaging was broad and included idiopathic orbital pseudotumor, orbital cellulitis, metastatic disease, and cavernous sinus thrombosis amongst other inflammatory processes. Four days prior to presentation, he had received an infusion of zoledronic acid as part of his treatment for bone metastasis. The imaging findings, acute presentation, and history with

response to treatment with IV steroids allowed for a presumptive diagnosis of bisphosphonate induced orbital inflammation, which is a rare but well documented side effect of bisphosphonate therapy. This side-effect usually begins within in hours to days after initiation of therapy. The exact mechanism is still unclear but it has been suggested that this is via a T-cell mediated response. He was discharged home on PO steroids, and while his eye pain did not return, he continued to have chemosis on follow up outpatient visit.

Results

MRI of the orbits with MRA and MRV were performed which demonstrated edema within the right pre and post septal soft tissues, extending into the intraconal fat. Enhancement of the right extraocular muscles is noted, particularly of the lateral and superior rectus muscle bellies. There is enhancement and inflammatory changes in the intraconal fat, along the optic nerve sheath and Tenon's capsule along the posterior margin of the globe. There is resultant 6 mm of proptosis. The ipsilateral superior ophthalmic vein and cavernous sinuses are patent. The imaging findings are nonspecific and the differential diagnosis included inflammatory, infectious, and neoplastic etiologies including idiopathic orbital pseudotumor and orbital cellulitis. Orbital lymphoma, thyroid orbitopathy, and cavernous sinus thrombus were considered by excluded by the acute painful presentation, lack of known thyroid disease, and the presence of patent flow on vascular imaging. The presumptive diagnosis of bisphosphonate induced orbital inflammation was made based on the patient's history, presenting symptoms and time course, and improvement with steroid therapy.

Conclusions

We present an unsusual cause of ipsilateral orbitial inflammation where the history played a key role in making the diagnosis of bisphosphonate induced orbital inflammation, while the imaging helped rule out other potentially more life threatening conditions such as cavernous sinus thrombosis.

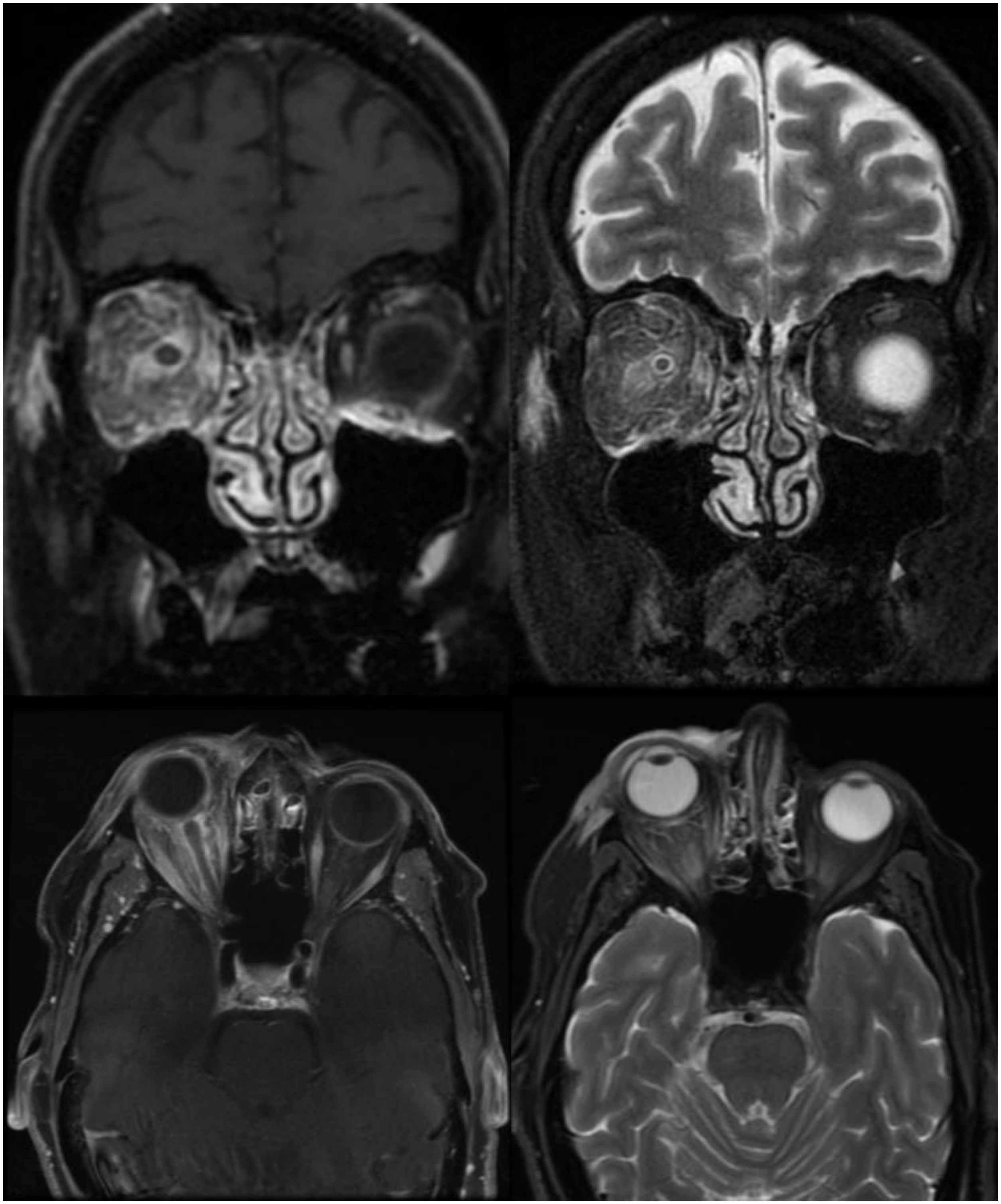

(Filename: TCT_3305_asnr2018.jpg)

2794

1:21PM - 1:28PM

Clival Lesion: Not Always Chordoma or Chondrosarcoma

A Guarnizo[1], N Zakhari[2], E Portela de Oliveira[3], T Nguyen[4], C Torres[5]
[1]UNIVERSITY OF OTTAWA, THE OTTAWA HOSPITAL, OTTAWA, ON, [2]The Ottawa Hospital/University of Ottawa, Ottawa, ON, [3]University of Ottawa - The Ottawa Hospital, Ottawa, Ontario, [4]The Ottawa Hospital University of Ottawa, Ottawa, Ontario, [5]UNIVERSITY OF OTTAWA, OTTAWA, ON

Purpose
1. To describe a pathology to consider in the differential diagnosis of lesions of the clivus.
Materials and Methods
A 63 old year woman presented with history of headaches and pulsatile tinnitus. Physical examination was unremarkable. CTA of the head and neck showed an expansile soft tissue mass involving the left petroclival junction and the left sphenoid sinus, the medial aspect of the left carotid canal was dehiscent. MRI of the brain showed interval increase in size in the soft tissue mass in the left petroclival region with iso signal on T1 and T2 and associated heterogeneous enhancement; differential considerations included chordoma and chondrosarcoma. Endonasal endoscopic trans – sphenoidal surgery was performed for resection of the lesion. The pathology showed sinusoid blood vessel spaces with reactive changes of the connective tissues. The endothelium lining the channels was positive for CD-34 and CD-31. The marker D2-40 was also positive which is the most specific marker consistent with lymphatics/ lymphangioma.
Results
Axial T1WI (A), T1WI post gad (B), T2WI (C) showing a soft tissue lesion centered in the left petroclival region with iso signal on T1/T2 and heterogeneous enhancement. Axial head CT (D) shows the expansile lesion and the focal dehiscence of the medial aspect of the left carotid canal
Conclusions
Lymphangiomas are congenital malformations of the lymphatics most of them diagnosed and treated in childhood, 75% develop in the head and neck. 10% of the cases are discovered in adulthood; patients are usually asymptomatic and the slow growing of the lesion is mostly related to fluid retention. Lymphangiomas in the clivus and nasopharynx are extremely rare with few cases reported in the literature. Surgical excision is the treatment of choice.

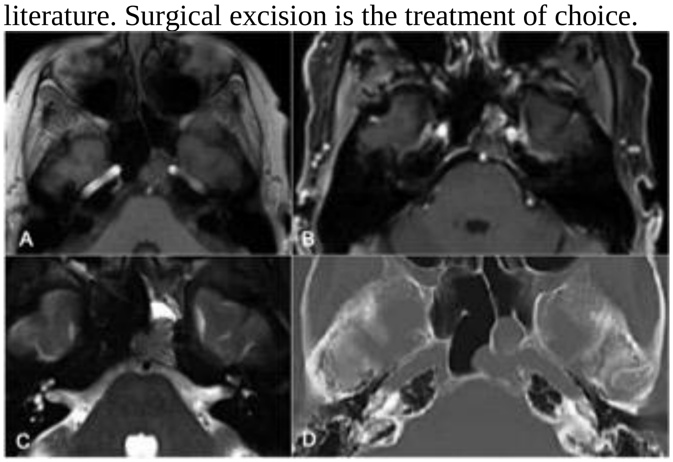

(Filename: TCT_2794_Lymphangioma.jpg)

2657

1:28PM - 1:35PM

CT-Guided Stellate Ganglion Blockade as Last Resort Treatment for Refractory Ventricular Tachycardia

L Lin[1], A Alhajeri[1]
[1]University of Kentucky, Lexington, KY

Purpose
Ventricular tachycardia (VT) is a cause of sudden cardiac death, and survivors may experience recurrent life-threatening arrhythmias during hospitalization. Although ablation of arrhythmogenic centers by electrophysiologists is common, some patients are too unstable for that procedure. Stellate ganglion blockade has been described in the literature as an acute therapy, however, it is done rarely. A recent metanalysis cites only 35 cases of stellate ganglion blockade reported between the years 1960 and 2017. We describe successful treatment of a patient with VT refractive to medical therapy.
Materials and Methods
61 year old male with history of coronary artery disease presented with uncontrolled VT and multiple defibrillations from lifevest. His ED course included multiple defibrillations and he was started on continuous infusion of amiodarone. He was intubated and transferred to the CV ICU and started on lidocaine infusion due to recurrent VT and fibrillation. We were consulted to do stellate ganglion blockade because the patient was not able to be weaned from his lidocaine infusion. Two days post procedure, the lidocaine infusion was successfully discontinued and the patient was ultimately discharged in stable condition after placement of ICD.
Results
The patient was placed supine on the CT table and CT angiography of the neck was performed (figure 1A). The track to the stellate ganglion posterior to the vertebral artery V1 segment between T1 body and transverse process was mapped. Under CT fluoroscopic guidance, a 25 gauge spinal needle was inserted to the target area and small volume contrast was injected. Subsequently, combination of 3 mL bupivacaine 0.35% and 1 mL lidocaine 1% was injected (figure 1B). Post procedure CT was preformed to confirm location of injection (figure 1C).
Conclusions
Stellate ganglion blockade is effective and can be performed with CT guidance for accurate targeting of the ganglion for refractory VT.

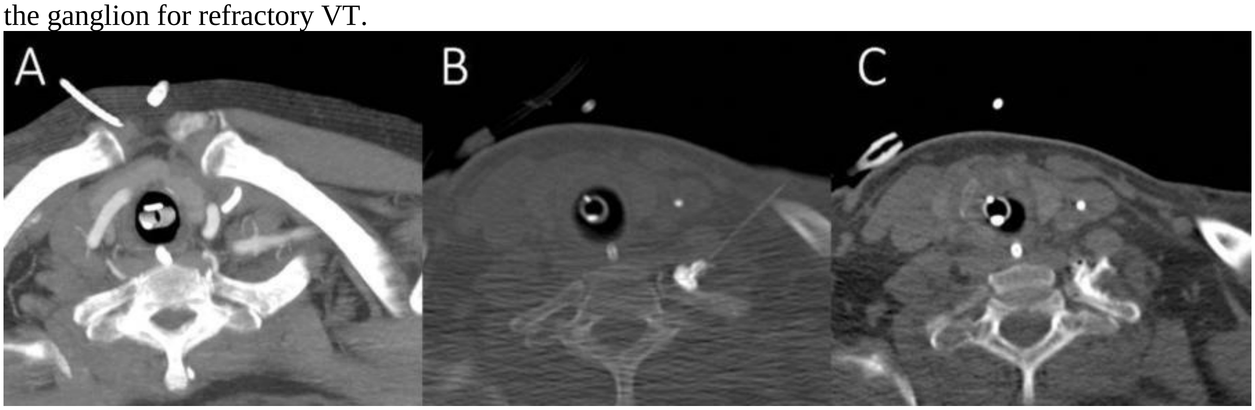

(Filename: TCT_2657_figures.jpg)

3549

1:35PM - 1:42PM

Diagnostic Dilemma and Pathologic Confirmation: Pediatric Cerebellopontine Angle Mass Versus Encephalocele.

W Caywood[1], E Quigley[2], R Wiggins[3], K Moore[4]
[1]University of Utah, Salt Lake City, UT, [2]University Of Utah, Salt Lake City, UT, [3]UUHSC, SALT LAKE CITY, UT, [4]Primary Children's Hospital, UT, UT

Purpose
Demonstrate an unusual case of pediatric cerebellopontine angle lesion extending into the internal auditory canal, examine the imaging findings, and consider an anatomically-based differential diagnosis.

Materials and Methods
MW, a two-year-old female patient with no past medical history initially presented for evaluation at pediatric emergency department due to fever, irritability, and emesis and was found to have left cranial nerve VI palsy. On imaging, patient was found to have a right cerebellopontine mass extending into the right internal auditory canal.
Results
MR imaging demonstrated a right cerebellopontine angle non-enhancing mass lesion which extended into the right IAC. Mass abutted the basal turn of the cochlea, without significant osseous expansion. There was clinical concern for ganglioglioma, ATRT, or encephalocele. After multiple consultation, the patient went for right retrosigmoid craniectomy. At surgery, the mass was found to be continuous with the brainstem. This was resected at the cerebellopontine angle.
Conclusions
We present an unusual case of right cerebellopontine lesion with extension into the adjacent right internal auditory canal which, after surgical biopsy and resection, was found to be gliotic or cicatrized brain parenchyma extending from the right pons. This case demonstrates the importance of recognizing encephaloceles in unusual locations.

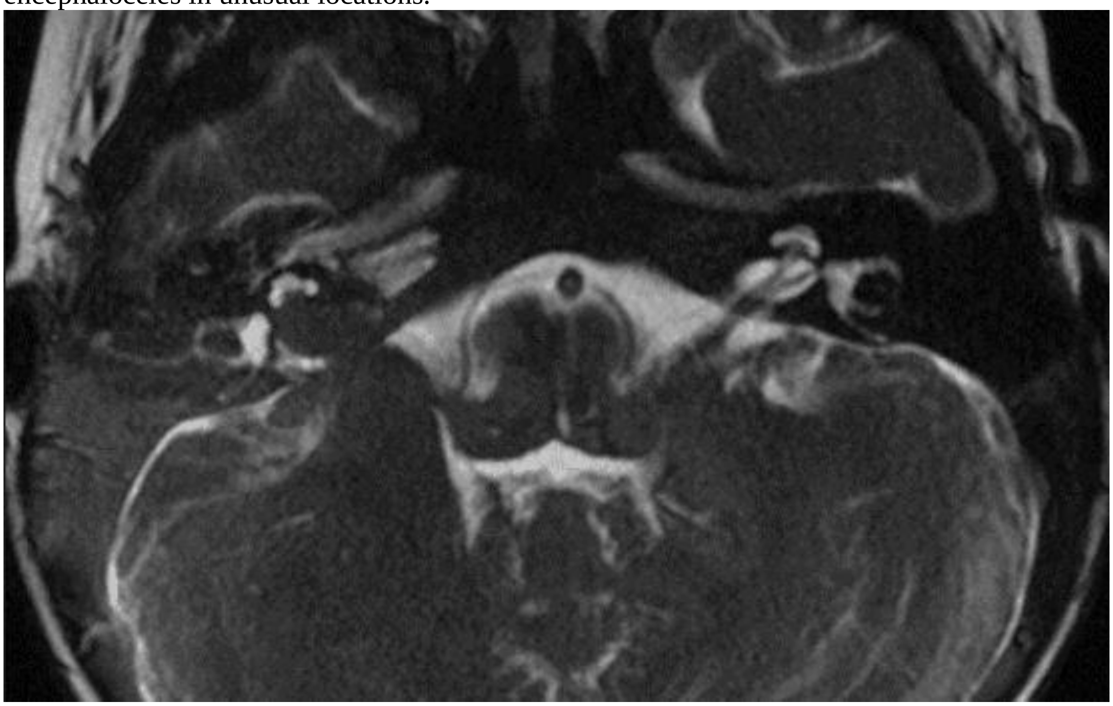

(Filename: TCT_3549_axialt2.JPG)

3517

1:42PM - 1:49PM

Fibromatosis Colli as a Uncommon Cervical Dystonia Mimic in Young Adults: MR, Ultrasound, Clinical and Radiopathological Correlation

A Mallik[1], J McCool[2], M Mahan[3], C Aquino[4]
[1]Loyola University Medical Center, University of Utah, Maywood, IL Salt Lake City, UT, [2]Loyola University Medical Center, Maywood, IL, [3]Universtity of Utah, Salt Lake City, UT, [4]University of Utah, Salt Lake City, UT

Purpose
Our goal is to present the MR, ultrasound, clinical exam and pathological presentation of fibromatosis colli in young adults, a recently described uncommon cervical dystonia mimic.
Materials and Methods
A 17 year old female with longstanding neck tightness was treated for cervical dystonia with multiple courses of botulinum toxin injections, with suboptimal benefit. A movement disorders neurologist noted facial asymmetry, consistent with a longstanding process. Further history elicited that the patient experienced symptoms since she was 4 years old, too early for cervical dystonia. Neuroradiology review of a recent MRI of the cervical spine demonstrated a small cord like right sternocleidomastoid (SCM) without fatty atrophy. A revised diagnosis of fibromatosis colli was made. The patient was referred to Neurosurgery for evaluation, and surgical release of the right SCM was planned. A preoperative ultrasound demonstrated a small right SCM with a focal hypoechoic cord-like appearance anteriorly. During surgery, the right SCM was identified and photographed, with preservation of the spinal accessory nerve using neurostimulation. The SCM was then divided using bipolar coagulation and resected portions of the SCM were sent to pathology. Surgical pathology demonstrated scattered dense fibroconnective tissue with normal skeletal muscle. Six weeks status post resection, the patient is very pleased with the results of surgery, estimating 90% improvement overall. She is able to hold her head in a nearly neutral position, has improved neck range of motion and continues physical therapy with progressive improvement.
Results
Patient photographs (presented with permission) demonstrate facial asymmetry and skew deviation of the eyes. MRI of the cervical spine demonstrates a small cord like right sternocleidomastoid (SCM) without fatty atrophy. Asymmetrically small right anterior and middle scalenes are also seen. The left SCM is normal. Ultrasound of the neck demonstrates a small right SCM, with a focal hyperechoic cordlike appearance of its anterior portion. Partially imaged small right scalene musculature is again seen. The left SCM is normal. Pathology demonstrates scattered dense fibroconnective tissue mixed with normal skeletal muscle.
Conclusions
Fibromatosis colli is a recently better described, uncommon cervical dystonia mimic in adults. This disorder can be misdiagnosed by primary care and movement disorders specialists, resulting in potential morbidity from inappropriate and suboptimal treatment, and delay in definitive treatment. Ultrasound is the modality of choice to evaluate pediatric fibromatosis colli, favored for its cost effectiveness and lack of ionizing radiation. Here, we present comprehensive multi-modality evaluation of adult fibromatosis colli, including ultrasound, correlated with previously described clinical exam, operative and pathological findings.

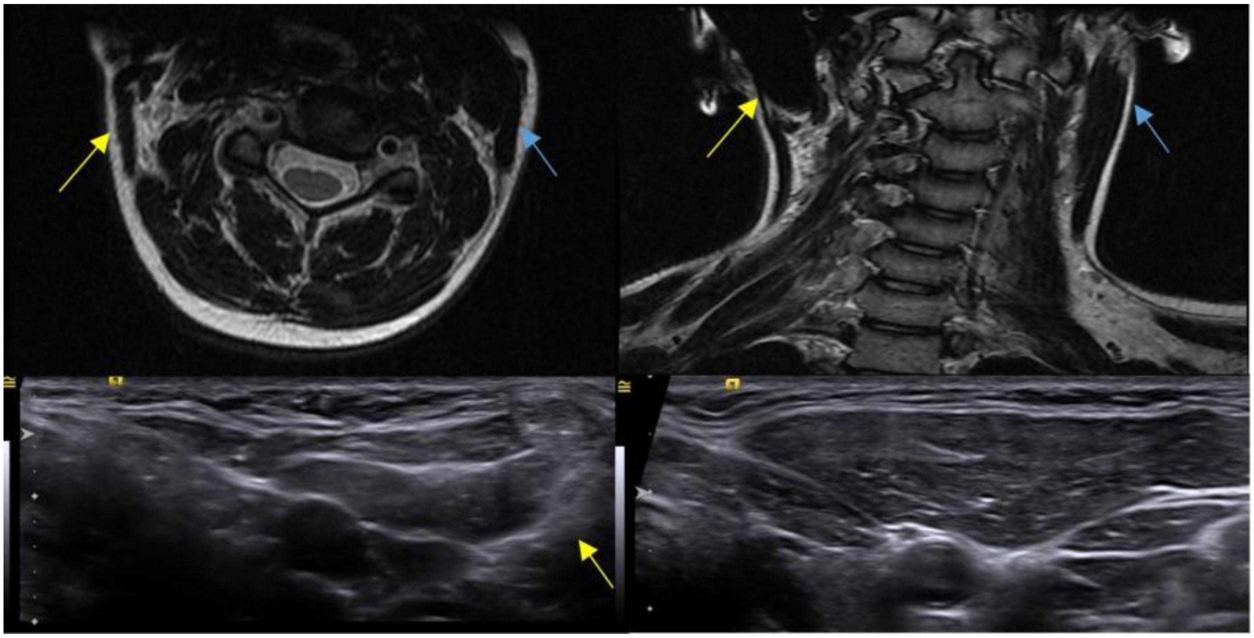
(Filename: TCT_3517_fc300.JPG)

3398

1:49PM - 1:56PM

Giant Dental Calculus Presenting as a Calcified Mandibular Mass on CT

J Bregni[1], J Phero[2], C Zamora[2]
[1]Universidad Francisco Marroquin, Guatemala, Guatemala, [2]University of North Carolina, Chapel Hill, NC

Purpose
Calculus or tartar refers to hardened dental plaque that arises from progressive deposition of calcium phosphate in and around a bacterial mass or biofilm in the oral cavity. It has been associated with severe periodontitis and poorly controlled type 2 diabetes. Our purpose is to present the unusual case of a patient with a giant, masslike dental calculus simulating a mandibular tumor on CT.
Materials and Methods
A 50-year-old male without significant past medical history presented to the emergency department with weakness, fever, and worsening dental pain for several weeks. He was diagnosed with sepsis due to Fusarium infection (presumed skin source) and admitted to the intensive care unit for treatment. Maxillofacial CT on admission showed a large calcified mass along the anterior mandible. On clinical exam the patient was found to have necrotizing periodontitis and a large calculus that encased the dorsal aspect of mandibular teeth. The patient underwent resection of the calculus as well as extraction of mandibular teeth and was discharged to a skilled nursing facility once sepsis was controlled.
Results
Sagittal (A) and axial (B) CT show a large calcified mass (orange arrows) along the dorsal aspect of mandibular teeth which are partially encased. A color photograph in a different patient (C) shows the typical appearance of a dental calculus (black arrows).
Conclusions
Dental calculus or tartar is a common finding in the oral cavity but the formation of large deposits is unusual. In rare occasions there can be excessive buildup and the lesion can present as a calcified mass on CT.

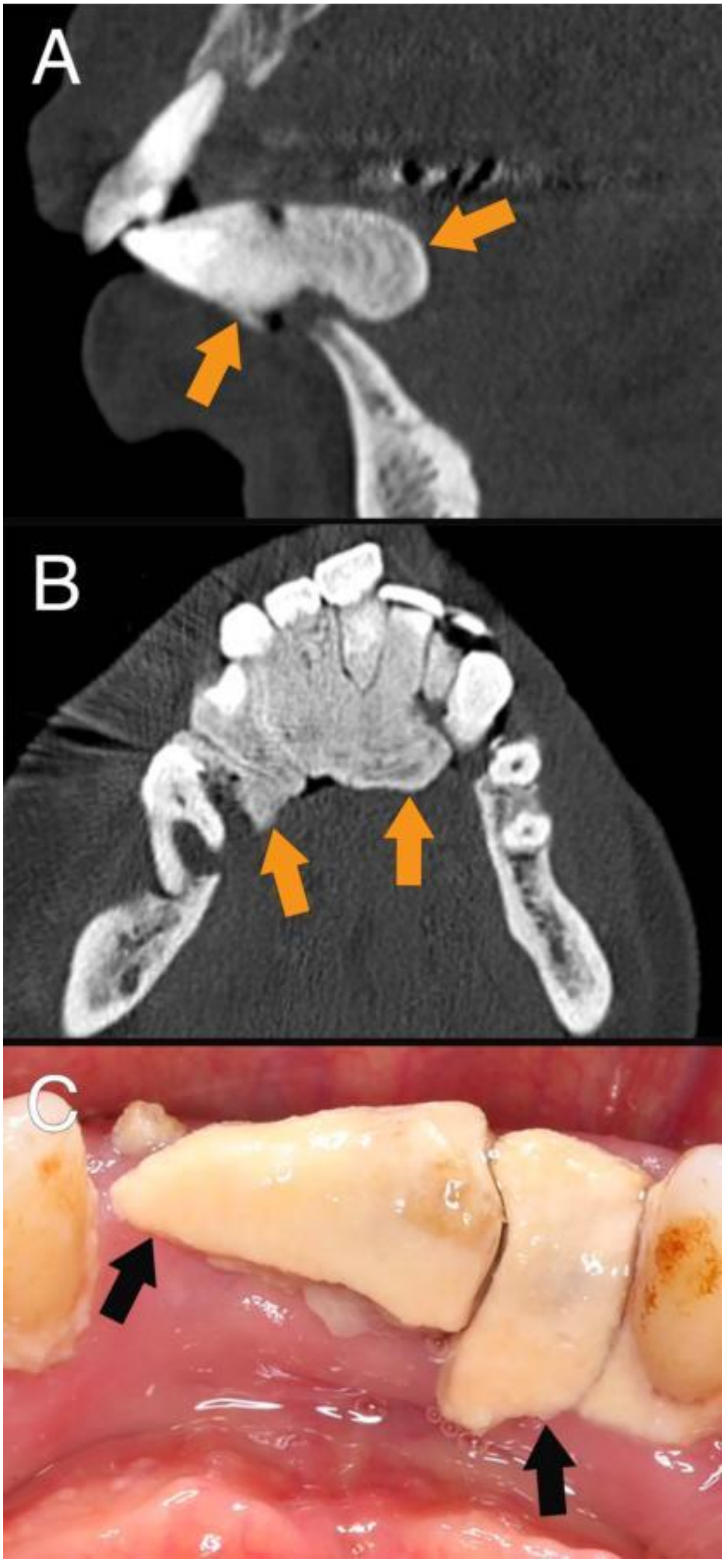
A
B
C

(Filename: TCT_3398_composite.jpg)

3676

1:56PM - 2:03PM

Hybrid Imaging in Dementia: Semi-quantitative PET/MRI Approach

A Franceschi[1], K Naser-tavakolian[2], C Michael[3], G Cruciata[4], D Franceschi[2], L Bangiyev[5], A Franceschi[1]
[1]SUNY Stony Brook, New York, NY, [2]Stony Brook University Hospital, Stony Brook, NY, [3]Stony Brook University Hospital, N/A, [4]Stony Brook University Hospital, Brooklyn, NY, [5]Stony Brook University Hospital, Stony Brook , NY

Purpose
Neurodegenerative disorders are known to demonstrate typical lobar and regional patterns of parenchymal volume loss with corresponding decreased glucose metabolism, which is depend-ent of dementia subtype. Currently, no data exist to correlate semi-quantitative volumetric in-formation with degree of reduced [F18] flurodeoxyglucose (FDG) uptake on metabolic brain imaging. In this retrospective study, we aim to correlate volumetric changes utilizing Neu-roquant morphometric analysis and corresponding decreased FDG uptake brain atlas Z-scores on hybrid FDG PET/MRI brain imaging to further characterize neurodegenerative disorders.
Materials and Methods
28 patients (19 female and 9 male, average age 70) with neurodegenerative disorders underwent [F18]-FDG PET/MRI brain imaging. Patients were categorized by dementia subtype as follows: Alzheimer's disease (8), Frontotemporal dementia (12), Lewy Body Dementia (7), and Corti-cobasal degeneration (1). NeuroQuant software was utilized for semi-quantitative assessment of intracranial volumetric information. Lobar-specific patterns of volume loss were recorded and compared to normal age-matched controls. MIM software was utilized to provide semi-quantitative FDG uptake data. Z-score patterns of abnormal decreased FDG uptake, as com-pared to standardized age-matched normal brain atlas uptake data. Volumetric and metabolic data (Z scores) were then correlated for statistical significance.
Results
8 patients with suspected AD (7 female, 1 male, average age 69) had mean temporal and parie-tal lobe volumes in 10th and 22nd percentile, respectively. Z-score values in the temporal and parietal lobes were -2.1 and -3.15, as compared to normal age-matched controls. 12 patients with suspected FTD (7 female, 5 male, average age 72) had mean frontal and temporal lobe volumes in 11th and 9th percentile, respectively. Z-score values in the frontal and temporal lobes were -1.14, and -1.17. 7 patients with suspected LBD (4 female, 3 male, average age 67) had mean parietal, occipital and temporal lobe volumes in 13th, 14th, and 6th percentile, re-spectively. Z-score values were -1.93, -2.20, and -1.02, respectively. Single patient data was available for CBD, with superior parietal lobule volumes in1st percentile and corresponding Z-score of -2.14.
Conclusions
Our semi-quantitative approach to recognizing lobar-specific patterns of volume loss and cor-responding brain hypometabolism in patients with cognitive impairment demonstrates compat-ibility of Neuroquant morphometric percentiles with FDG Z-score values. This combined ap-proach to neuroimaging volumetric and metabolic data interpretation may add precision and accuracy to the clinical radiologist in diagnosing lobar specific neurodegenerative disease.

2331

2:03PM - 2:10PM

Intracranial Rosai-Dorfman Disease: A Diagnostic Dilemma

A Foust[1], C Fetko[2], D Boulter[2], E Bourekas[3], J Fritz[4]

[1]*The Ohio State University Wexner Medical, Columbus, OH,* [2]*The Ohio State University Wexner Medical Center, Columbus, OH,* [3]*THE OHIO STATE UNIVERSITY, COLUMBUS, OH,* [4]*Wexner Medical Center at The Ohio State University, Columbus, OH*

Purpose
To demonstrate the diagnostic challenge encountered in intracranial Rosai-Dorfman disease.
Materials and Methods
The patient is a 63 year old female with past medical history of hypertension, who initially presented to an outside hospital with symptoms of sinusitis, headache, photophobia, and a third cranial nerve palsy. At the time, she was diagnosed with an optic nerve meningioma and underwent empiric ciberknife radiation treatment. A few months later, the patient developed an erythematous skin rash which was biopsy proven to be cutaneous Rosai-Dorfman disease. Six months later the patient presented to our institution complaining of worsening headache and blurred vision. She underwent a repeat MRI of the brain which demonstrated progression of a large extra-axial mass centered along the right anterior and middle skull base. Given the patient's prior cutaneous manifestation of histiocytosis, a differential diagnosis of intracranial involvement of Rosai-Dorfman disease was suggested. This consideration changed the surgical approach and, with pathological confirmation at surgery, led to a shorter and less extensive procedure.
Results
MRI of the brain with and without contrast demonstrated a large T1 isointense T2 hypointense homogenously enhancing infiltrative extra-axial dural based mass centered in the right cavernous sinus extending posteriorly along the clivus into the sella, laterally along the anterior wall of the right middle cranial fossa, and anteriorly into the right orbit and pterygopalatine fossa. CTA of the brain re-demonstrated the large extra-axial mass in the anterior skull base and confirmed complete encasement and narrowing of the right intracranial internal carotid artery. Significantly, there was no evidence of hyperostosis adjacent to the mass.
Conclusions
Rosai-Dorfman disease is a rare cause of dural based mass which can often be mistaken for a meningioma leading to delayed or inappropriate treatment. This entity should be considered in the differential diagnosis in patients with systemic manifestations of histiocytosis.

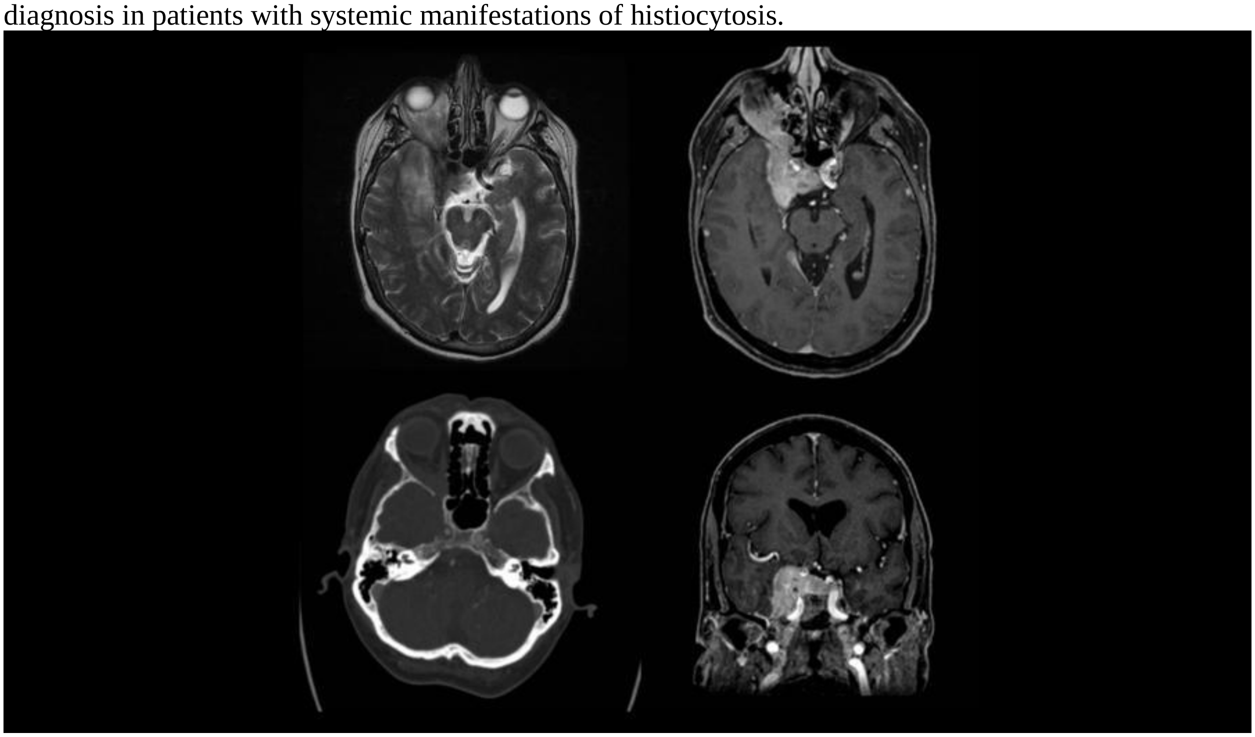

(Filename: TCT_2331_Rosai-DorfmanImages300DPI.jpg)

2375

2:10PM - 2:17PM

Isolated Ocolomotor Neuropathy: A Case Report

R Jordan[1], J Rogers[2], S Khanpara[3], R Patel[4], R Riascos[4], A Kamali[5]
[1]University of Texas-Houston, HOUSTON, TX, [2]UNIVERSITY OF TEXAS HEALTH SCIENCES CENTER AT HOUSTOIN, Houston, TX, [3]The University of Texas Health Science Center at Houston, Houston , TX, [4]The University of Texas Health Science Center at Houston, Houston, TX, [5]UT HEALTH, HOUSTON, TX

Purpose
To illustrate a case of isolated oculomotor neuropathy and differential diagnoses to consider.
Materials and Methods
A 58 year old woman with history of left facial nerve palsy in 1984, type 2 diabetes, hypertension, hyperlipidemia, and myocardial infarction in 2008 presents with: Acute onset of left upper eyelid drooping followed by diplopia and retrobular headache three weeks prior to presentation Diplopia gradually worsened over 3 days and has not improved since onset Physical exam Mild left upper eyelid ptosis with decreased levator excursion Limited upward and downward gaze in left eye Pupils equally round and reactive without afferent pupillary defect The CSF tap demonstrated increase in WBC count. The patietn was treated by steroid and she recovered completely in few weeks. The diagnosis of viral neuropathy was made after rouling out other causes of neuropathy such as demyelinating disease.
Results
Post-contrast images demonstrate enhancement of the oculomotor nerve in the precavernous, cavernous, fissural, and intraorbital segments of the 3rd nerve.
Conclusions
The diagnosis of oculomotor nerve palsy can often be made clinically. Imaging is necessary to determine the cause of the nerve palsy, some of the causes may be life threatening, such as stroke and aneurysm Patient history may also be helpful to determine the cause of neuropathy such as in diabetes, recent viral illness, multiple sclerosis, etc.

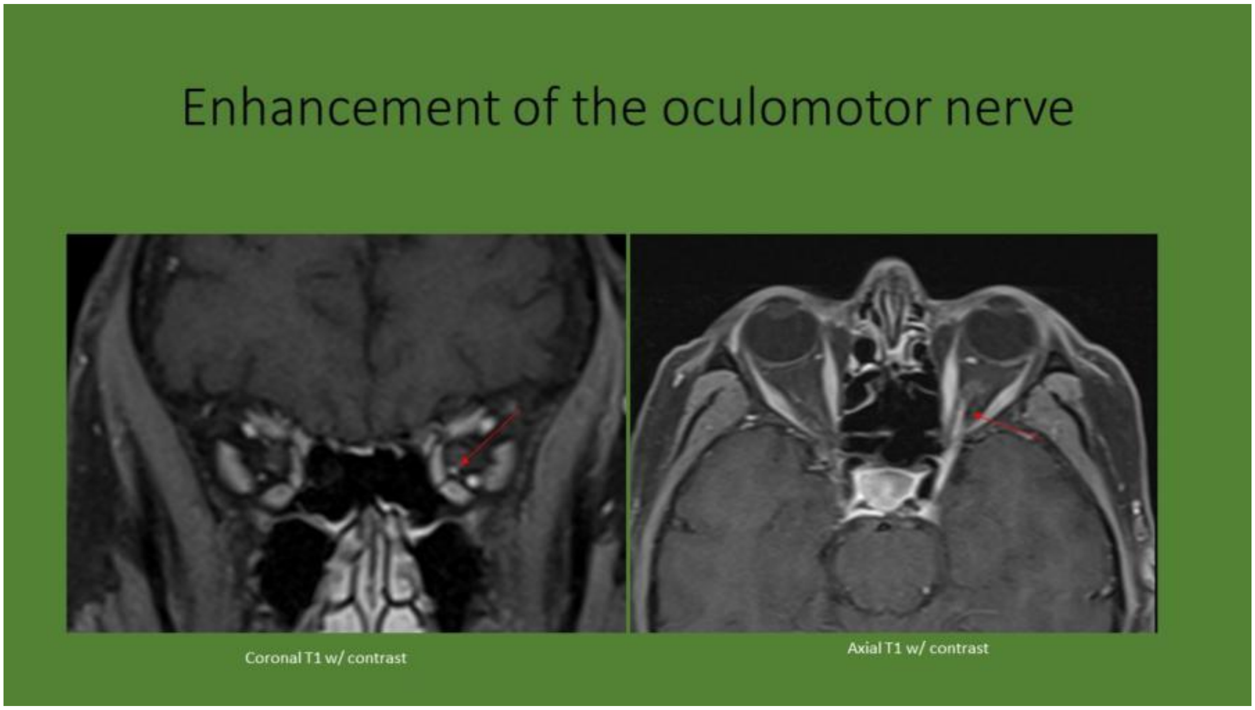

(Filename: TCT_2375_Image1.jpg)

2694

2:17PM - 2:24PM

Isolated Unilateral Small Trigeminal Nerve and Meckel's Cave in a Patient with Trigeminal Neuralgia.

M Peterson[1], G Kwan[1], C Hsu[1]
[1]*Gold Coast University Hospital, Australia*

Purpose
Small trigeminal nerve and Meckel's cave in isolation is exceedingly rare with only a few reported cases. More commonly, small trigeminal nerve and Meckel's cave are due to developmental hypoplasia as a clinicoradiologic manifestation of craniofacial developmental anomalies such as Goldenhar syndrome. Herein, we present a case of isolated small left trigeminal nerve and Meckel's cave in an adult patient and discuss the pathophysiologic mechanism for this rare condition.
Materials and Methods
We present a 47 year-old female with a protracted history of left trigeminal nerve neuralgia. Her symptomatology included hyperaesthesia in the mandibular (V2-V3) distributions of the trigeminal nerve with frequent intermittent exacerbations of lancinating pain. Neurological and ophthalmological examination findings were unremarkable. Specifically, there was no corneal hypoesthesia or loss of facial sensation. Past medical history was significant for breast cancer and medication controlled hypertension. Despite long term treatment with Amitriptyline (25mg nocte) and Pregabalin (225mg BD) there was minimal symptomatic relief especially during exacerbative episodes.
Results
Magnetic Resonance Imaging (MRI) brain high resolution T2-weighted sequence showed an asymmetrically small cisternal segment of the left trigeminal nerve with a hypoplastic ipsilateral Meckel's cave which was collapsed with absence of normal cerebrospinal fluid (CSF) signal. No neurovascular conflict was identified. No abnormal enhancement of the Meckel's cave or the trigeminal nerve was evident. Muscles of mastication on the left side were also subtly smaller in volume compared to the right.

Conclusions
Isolated small unilateral trigeminal nerve and Meckel's cave hypoplasia is an exceedingly rare clinicoradiologic entity. In adulthood it is debatable if it is an acquired or developmental anomaly, although the clinical manifestation in our illustrated case would support the latter. Nevertheless, we recommend a comprehensive MRI skullbase protocol with gadolinium to exclude other pathologies before arriving at the diagnosis.

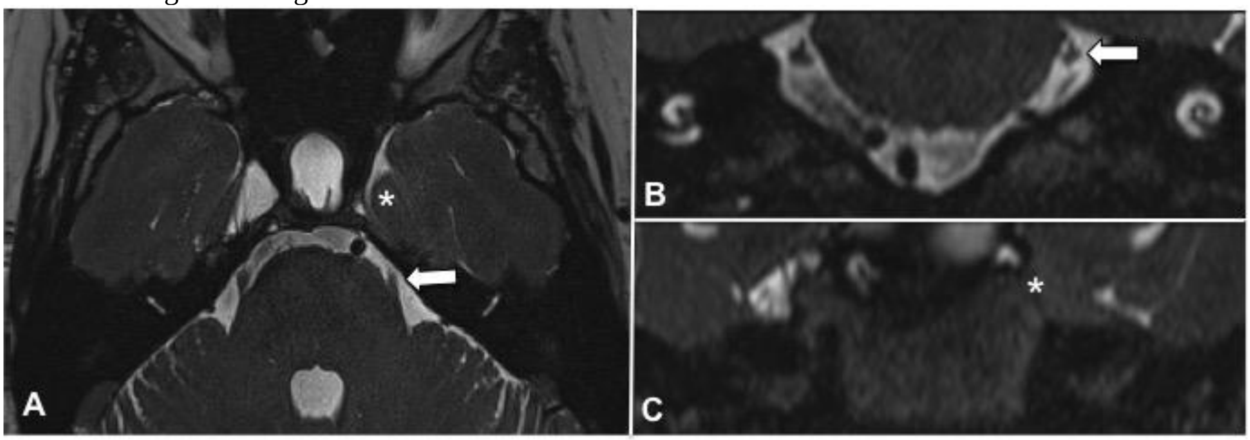

(Filename: TCT_2694_MeckelsCave300.jpg)

2960

2:24PM - 2:30PM

Lift Your Head out of the Fog: It's Anti-MOG!

M Maher[1], J Odel[2], G Moonis[1]
[1]Columbia University Medical Center, New York, NY, [2]Edward S. Harkness Eye Institute Columbia University Medical Center, New York, NY

Purpose
The purpose of this case is to discuss the presentation of anti-myelin oligodendroglioma protein (anti-MOG) optic neuritis and review the difference in presentation of optic neuritis caused by multiple sclerosis (MS) and neuro-myelitis optica (NMO).
Materials and Methods
A 28 year-old woman presented pain with left eye movement. On physical exam, visual acuity was 20/20 OU with intact color perception. She has a history of anti-MOG syndrome since December 2016. At that time, she presented with 90% bilateral vision loss. She was admitted optic neuritis and after a course of intravenous solumedrol, she was discharged on a steroid taper. On the steroid taper, she regained complete vision restoration bilaterally. Etiology was presumed to be multiple sclerosis until anti-MOG antibodies returned positive. Since that time, she has experienced 12 relapses of optic neuritis. Between episodes of optic neuritis, she had full visual fields and acuity; she noted mild reduction in red color perception on the right. She is currently on azithroprine 100 mg daily and intravenous immunoglobulin 0.4 mg/kg q5 weeks. An MRI orbit with contrast was ordered to evaluate for disease recurrance. The MRI demonstrated enlargement of the left orbital optic nerve and avid enhancement. Steroids were immediately initiated for control.
Results
MRI orbit with contrast demonstrated diffuse enlargement (A) and enhancement (B and C) of the orbital left optic nerve. No flattening of the globe is seen. There is no proptosis. There is no involvement of the chiasm or post-chiasmal tracts. There is a single high T2/FLAIR signal focus in corona radiata of the left frontal lobe.

Conclusions

Anti-myelin oligodendrocyte glycoprotein (MOG) syndrome is an autoimmune disease which results in optic neuritis (ON). New antibody assays have allowed differentiation of anti-MOG from multiple sclerosis and neuromyelitis optica ON. Anti-MOG NO is frequently bilateral. Multiple sclerosis typical affects a single optic nerve.The orbital and pre-chiasmal optic nerves are longitudinally enlarged and enhancing. In comparison, neuromylitis optica often affects the retrochiasmal optic tracts. Anti-MOG usually has not more than 3 poorly-circumscribed lesions in the infratentorial brain. Neuromyelitis optica is more commonly seen in the cervical spine. Multiple sclerosis typically has periventricular white matter lesion. Flattening of the posterior globe is more specific to anti-MOG from the engorgement and enlargement of the optic nerves. On physical exam, cotton wool spots and hemorrhage can be seen in anti-MOG and neuromyelitis optica but never in multiple sclerosis. Differentiation of NO is important for prognosis as well as treatment. Treatment is centered on steroids in the acute setting of anti-MOG. Anti-MOG relapses but does not often cause sustainable visual loss. Neuromyelitis optica causes more sustained and severe vision loss. Patient with anti-MOG do not progress to multiple sclerosis.

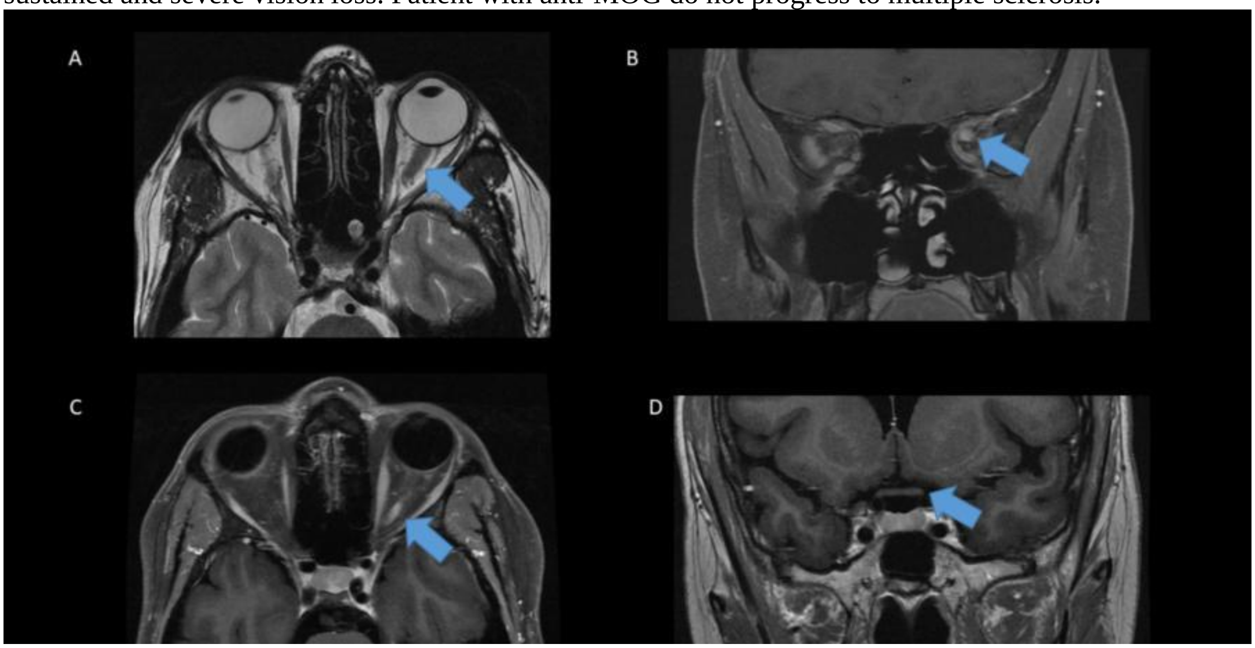

(Filename: TCT_2960_ASNRMOG.jpg)

Wednesday, May 22, 2019
1:00PM - 2:30PM
Tackling Tumors of the Pediatric CNS

3648

1:00PM - 1:07PM

Characterizing the Growth of Subependymal Nodules and Subependymal Giant Cell Tumors in Tuberous Sclerosis Complex

J Barnett[1], K Buch[2], E Thiele[3], P Caruso[4]
[1]Massachusetts General Hospital, Boston , MA, [2]Massachusetts General Hospital, Boston, MA, [3]MGH, Anytown, MA, [4]MGH, Boston, MA

Purpose
Surveillance imaging with MRI is routinely performed in patients with tuberous sclerosis (TSC) to monitor for the development of subependymal giant cell astrocytomas (SGCTs) many of which occur at the foramen of Monro, carry a risk for obstructive hydrocephalus, and are thus indications for surgical resection. SGCTs, however, occur in the same locale as subependymal nodules (SENs) that typically remain stable and are not associated with a risk of obstructive hydrocephalus. Currently MRI poorly distinguishes between early SGCTs and SENs. The purpose of our study was to characterize the growth curves of SENs and SGCTs and to determine if the rate of growth may serve as an early discriminator between these two types of lesions.
Materials and Methods
This retrospective IRB approved study consisted of 26 non-mTOR treated TSC patients who had MRI evidence of nodules at the foramen of Monro with at least three MRIs over a minimum period of 1.5 years available for analysis. The nodules were divided into 3 groups: SENs, SGCTs, and symptomatic SGCTs. SENs were defined as nodules at the foramen of Monro less than 10 mm. SGCTs, in keeping with the traditional definition, were considered to be any nodule at the foramen of Monro with a diameter greater than or equal to 10 mm. Symptomatic SGCTs were defined retrospectively as lesions that eventually required surgical resection because of obstructive hydrocephalus. Cubic volumetric analysis of the nodules were performed on all MRIs of the 26 patients from the earliest MRI to the most recent MRI or for symptomatic SGCTs, from the earliest MRI until surgical resection.
Results
26 patients, 13 M, 13 F, were included. The average age of participant at baseline was 5.4 years, and the average age of participant at most recent scan was 13.6 years. The average MRI surveillance period from baseline scan to most recent scan was 8.8 years. 73 lesions (range 1-7 lesions per patient) were measured at a total of 159 MRI time points (average 6.4 timepoints per patient). 53 of the lesions measured were SENs, 12 SGCTs, and 8 symptomatic SGCTs. The average rates of growth for the three different groups were SENs 5.9 mm^3/year (ST DEV 11.0): SGCTs,113.9 mm^3/year (ST DEV 133.8), and symptomatic SGCTs, 807 mm^3/year (ST DEV 414.2). The differences in average growth rates of SEN vs. SGCT (p<.003), SEN vs. symptomatic SGCTs (p<.0001), and SGCT vs. symptomatic SGCTs (p<.0001) were significant.
Conclusions
There is a significant difference in rate of growth of SENs, SGCTs defined traditionally as nodules at the foramen of Monro greater than 10 mm, and SGCTs that become symptomatic. These preliminary results suggest that growth rate may serve as an early discriminator between those foramen of Monro nodules at greater risk for progression and obstructive hydrocephalus

3016

1:07PM - 1:14PM

DTI and Volumteric Anlayses of Pediatric Patients Post Proton Radiotherapy

N Desai[1], Z Chu[1], A Hsu[1], S Kralik[1], M Kukreja[1], L Kahalley[1], E Wilde[2], D Grosshans[3], M Chintagumpala[1], M Okcu[1], W Whitehead[1], M Paldino[1]
[1]Texas Children's Hospital, Houston, TX, [2]Baylor College of Medicine/ MEDVAMC, Houston, TX, [3]UT MD Anderson Cancer Center, Houston, TX

Purpose
Chemo- and radiation therapies are associated with altered trajectories of cognitive development in children with brain tumors. The purpose of this study was to quantify supratentorial volumetric and diffusion tensor metrics in pediatric posterior fossa brain tumor patients undergoing chemotherapy and proton beam irradiation compared with those undergoing resection-only.
Materials and Methods
Following IRB approval, a retrospective review of neuro-oncology patients included patients diagnosed

with medulloblastoma post chemotherapy and proton beam irradiation who had also undergone a 3T MRI examination containing diffusion tensor imaging within 6 months of a neuropsychological evaluation. Patients with pilocytic astrocytoma post resection-only (no chemoradiation) with identical imaging were also included. Automated segmentation and parcellation of the 3DT1 image volumes were performed using FreeSurfer. White matter FA values and cortical thickness were calculated over each hemisphere and each parcel. ANCOVA was used to assess differences between groups.

Results

The study group included 11 patients with medulloblastoma who underwent chemotherapy and craniospinal proton beam irradiation (chemoradiation group) and 9 patients with posterior fossa pilocytic astrocytoma (resection-only group). Mean (SD) age at MRI was 11 (3.7) years in the chemoradiation group and 8 (3.7) years in the resection-only group. Mean (SD) age at completion of therapy was 6 (2.94) years. Widespread differences in the trajectory of both volumetric and diffusion metrics were observed between groups. In particular, whereas the resection-only group demonstrated increasing cortical thickness and white matter FA with age, these metrics consistently diminished with age in the chemoradiation group. Representative relationships are presented in Figure 1; the observed differences were statistically significant (cortical thickness: $p<0.002$; white matter FA: $p<0.004$).

Conclusions

Chemoradiation was associated with decreasing cortical thickness and white matter FA with age in multiple segments of the brain. Future work will correlate the presented data with a battery of neuropsychological data and dosimetry fields.

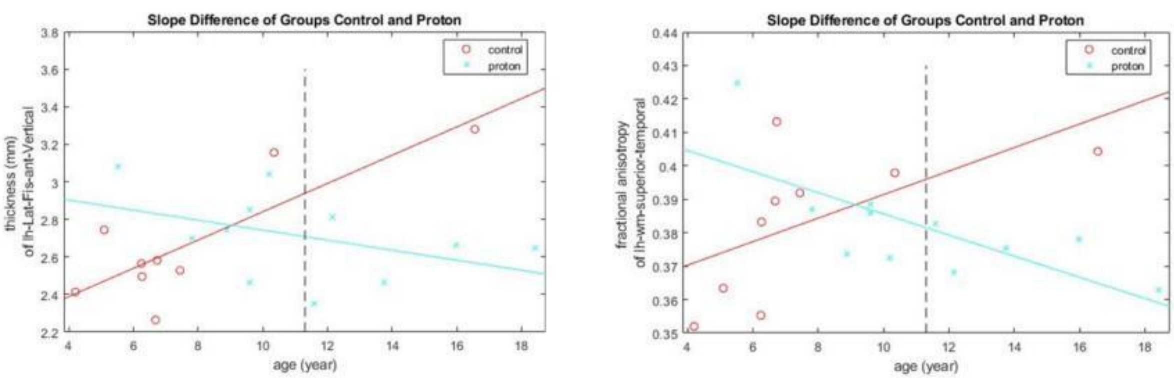

(Filename: TCT_3016_Figure1.jpg)

3332

1:14PM - 1:21PM

Frequency of Optic Nerve Involvement in Pediatric Intracranial Germ Cell Tumors

K Buch[1], O Rapalino[1], Y Torunn[1], P Caruso[2]
[1]Massachusetts General Hospital, Boston, MA, [2]MGH, Boston, MA

Purpose
Of the three most common pediatric sellar/suprasellar brain tumors (germ cell tumors, craniopharyngiomas, and optic pathway hypothalamic gliomas), optic nerve (ON) involvement is traditionally thought to be associated more specifically with optic pathway hypothalamic gliomas. ON involvement may, however, rarely be observed in intracranial germ cell tumours (GCT). ON involvement thus may influence need for biopsy and may impact radiation planning as targeted imaging of the ONs may not be routinely included in pretreatment planning of GCTs. The purpose of this study is to determine the frequency of ON involvement in a large cohort of patients with intracranial GCTs.
Materials and Methods
All patients with intracranial pure germinoma and nongerminomatous germ cell tumors (NGGCTs) treated at our institution with proton radiotherapy between 1998 and August 2018 were reviewed. Pre-treatment brain MRIs were evaluated for the presence of ON involvement.
Results
101 patients were identified with intracranial GCTs, including 61 pure germinoma and 40 NGGCTs. Of these patients, six (6%) demonstrated ON involvement. In those with CN involvement, the median age at diagnosis was 15.5 years, most were female (n = 4), and the majority had histologically proven pure germinoma (n = 5).
Conclusions
ON involvement may be seen in pediatric GCTs and thus should not be considered a specific feature of optic pathway hypothalamic gliomas. Dedicated orbital and ON sequences should be considered for radiation planning as it is important to identify ON involvement prior to treatment and to adjust radiotherapy field appropriately to ensure full radiation dose.

2970

1:21PM - 1:28PM

Imaging of Spinal Drop Metastasis in Pediatric Central Nervous System Tumors: Comparison of Balanced Fast Field Echo Sequence with T1-weighted Contrast Enhanced Sequence and Correlation with Cerebrospinal Fluid Cytology

K Koral[1], K Urgun[2], L Klesse[3], L Gargan[4], D Bowers[3]
[1]Donald and Barbara Zucker School of Medicine at Hofstra/Northwell, Queens, NY, [2]University of California, Irvine, Orange, CA, [3]University of Texas Southwestern Medical Center and Children's Health, Dallas, TX, [4]Children's Health, Dallas, TX

Purpose
The diagnosis of spinal drop metastasis (DM) is critical in the management of pediatric CNS tumors. Magnetic resonance imaging (MRI) of the whole neuroaxis and spinal cerebrospinal fluid (CSF) cytology are the primary methods in the diagnosis of DM. MRI and CSF cytology are complementary diagnostic tools. In children with intracranial CNS tumors, routine screening of the spine is performed by the acquisition of gadolinium-enhanced T1-weighted (T1W+C) images in the sagittal and axial planes. The purpose of this study is to compare the balanced fast field echo (BFFE) sequence with T1W+C sequence and spinal CSF cytology in the diagnosis of DM.
Materials and Methods
The institutional Neuro-Oncology database was reviewed from January 2011 and through December 2016 for newly diagnosed intracranial CNS tumors. Patients who underwent preoperative MRI including both T1WC+ images and BFFE images were included. A board-certified radiologist with additional qualification in neuroradiology and 15 years of experience evaluated the T1WC+ and BFFE images for the presence of LMD. The images were presented in a fashion that did not include any brain imaging and the radiologist did not know the pathology and CSF cytology results. Medical records were reviewed for the availability of the CSF cytology performed within 30 days of MRI examinations. Chi-square test was used to compare the DM rates diagnosed with T1WC+ and BFFE.

Results
Fifty-six patients (24F, 32M; mean age 80.8 months) were included. The tumors were infratentorial in 34 and supratentorial in 22 patients. There were 23 medulloblastomas, 6 pilocytic astrocytomas, 6 germinomas, 5 atypical teratoid rhabdoid tumors, 3 pilomxyoid astrocytomas, 2 ependymomas and 11 other tumors. T1W+C and BFFE sequences of the lumbosacral spine were obtained in 56 patients whereas the entire spine was examined with both sequences in 22 patients. Thirty-two patients had CSF cytology available performed within 30 days of the MRI. In 7 (12.5%) patients DM was visualized on both T1W+C and BFFE images. In 12 (21.4%) patients DM was present on BFFE but not on T1W+C. In 1 (1.8%) patient DM was present on T1W+C, but not on BFFE. CSF cytology was positive in 1 (1.8%) patient who had DM on both T1W+C and BFFE images. There was a statistically significant improvement in the diagnosis of DM with utilization of the BFFE sequence [19 patients (33.9%)] versus T1W+C sequence [8 patients (14.3%)] (p=0.001).
Conclusions
Addition of BFFE sequence to the T1W+C sequences significantly improved the spinal DM diagnosis in pediatric patients with newly diagnosed brain tumors.

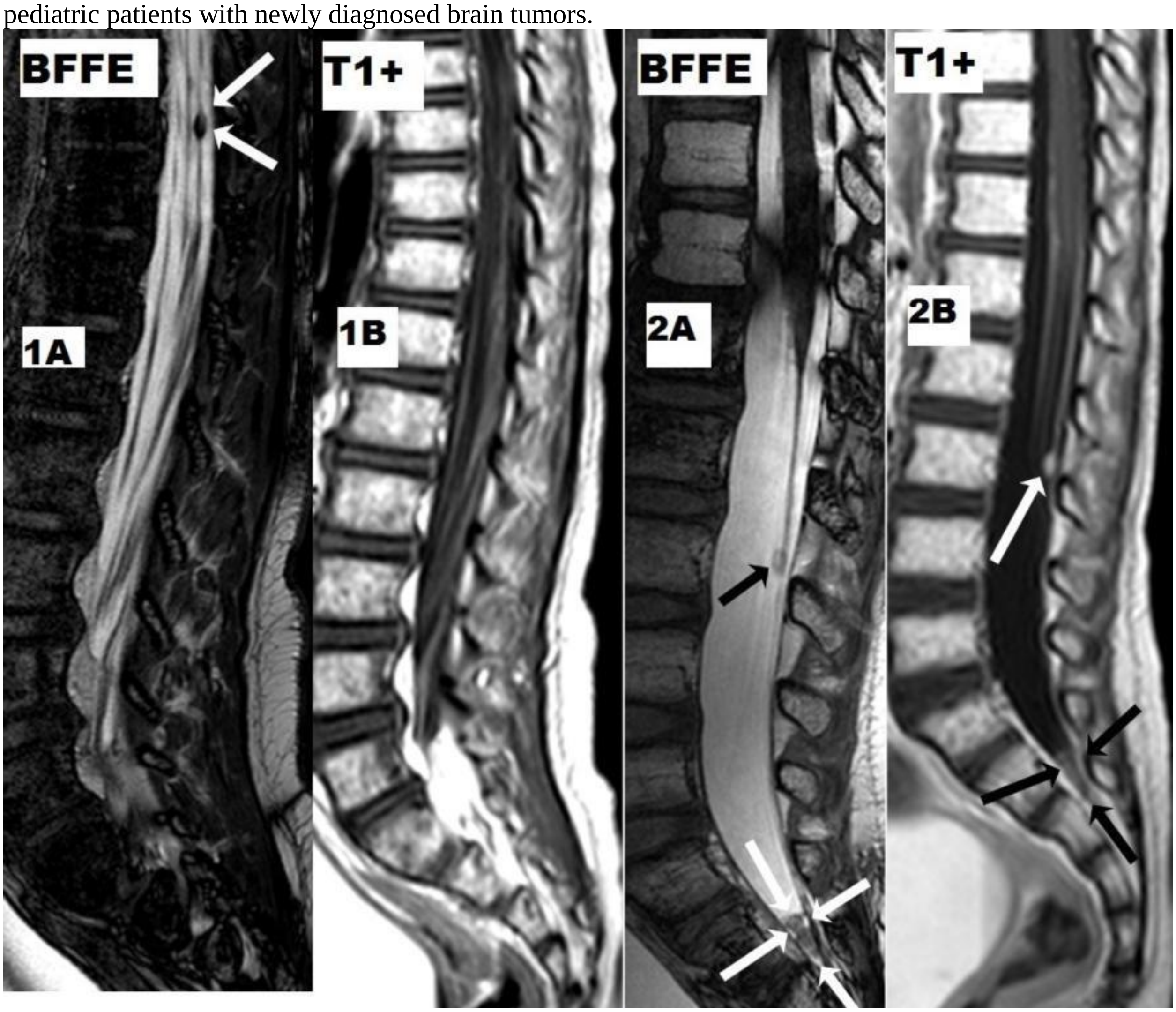

(Filename: TCT_2970_Figure.jpg)

3635

1:28PM - 1:35PM

Leukoencephalopathy, Quantitative MR Imaging and Neurocognitive Performance in Adult Survivors of Childhood Hodgkin Lymphoma

N Sabin[1], W Reddick[1], P Banerjee[1], W Liu[1], J Glass[1], D Srivastava[1], L Robison[1], M Hudson[1], K Krull[1]
[1]*St. Jude Children's Research Hospital, Memphis, TN*

Purpose
To estimate the prevalence of leukoencephalopathy (LE) and examine associations of LE with quantitative imaging measures and neurocognitive performance in adult survivors of childhood Hodgkin lymphoma (HL) compared to age, sex and race/ethnicity matched community controls.
Materials and Methods
163 survivors of childhood HL and 170 controls underwent brain MR imaging which was reviewed for leukoencephalopathy. Isotropic 3D MR imaging was obtained to assess white matter volume (WMV) and cortical thickness. Diffusion tensor imaging (DTI) was acquired and processed for standard DTI parameters. Neurocognitive testing was conducted for measures of attention, processing speed, memory and executive function. Chi-Square compared frequency of LE between survivors and controls. General linear models (GLM) compared imaging and neurocognitive measures between survivors and controls, with adjustment for age and stratified by sex. For imaging and neurocognitive measures that differed between survivors and controls, associations between imaging measures and neurocognitive outcomes in survivors were modeled using GLM.
Results
The prevalence of LE was greater in survivors than controls in females (53 vs 37%, p=0.03) but not in males (47 vs 40%, p=0.33). LE was not associated with neurocognitive performance. There were no significant differences in DTI parameters and WMV between survivors and controls. Compared to same sex controls, male survivors demonstrated thinner cortices in the right entorhinal cortex (mean[SD] 3.51[0.52] vs. 3.64[0.53], p=0.02) and left temporal pole (3.56[0.41] vs. 3.68[0.49], p=0.02), while female survivors demonstrated thinner bilateral middle temporal cortices (2.93[0.16] vs. 3.00[0.19] on left and 2.94[0.15] vs. 3.04[0.18] on right), p's<0.002). Survivors performed worse than controls on multiple neurocognitive measures. In males, a thinner left temporal pole cortex was associated with lower cognitive flexibility (Estimate[SE] 0.69[0.31], p=0.03).
Conclusions
Sex-specific differences exist in survivors of childhood Hodgkin lymphoma with respect to leukoencephalopathy, cortical thickness and neurocognitive performance. Elucidating the causes of these differences may require a focus on sex-specific disease and treatment effects.

2840

1:35PM - 1:42PM

Longitudinal Evaluation of Abnormal Cortical and Subcortical Cerebral Morphology in Neurofibromatosis Type 1

M Barkovich[1], A Barkovich[2], R Desikan[3]
[1]*UNIVERSITY OF CALIFORNIA-SAN FRANCISCO, SAN FRANCISCO, CA,* [2]*UNIVERSITY OF CALIFORNIA, SAN FRANCISCO, SAN FRANCISCO, CA,* [3]*UCSF, San Francisco, CA*

Purpose
Children with Neurofibromatosis Type 1 (NF1) have non-neoplastic overgrowth of both the cortex and deep grey nuclei, many of which occur in the same regions where the characteristic T2 hyperintensities of NF1 also occur. Longitudinal quantitative evaluation of these temporal course of these morphologic abnormalities may reveal associations with other clinical and imaging manifestations of NF1 and could provide biomarkers for alterations in NF1 associated molecular pathways at different developmental stages.

Materials and Methods

Subcortical volumes and cortical thicknesses were quantitatively assessed in 14 children with NF1 longitudinally. Each child with NF1 was imaged 2-4 times over approximately 2 years. The subcortical volumes and cortical thicknesses of these children were compared to 245 age- and sex-matched normal controls across 10 subcortical and 34 cortical regions of interest (ROIs)5. Using linear models and correcting for intracranial volume (ICV), quantitative differences between subcortical volumes and cortical thicknesses in NF1 patients and controls were assessed, covarying for gender and correcting for multiple comparisons.

Results

NF1 patients have larger ICV corrected subcortical volumes than controls but, when evaluated longitudinally, ICV corrected subcortical volumes in NF1 patients decrease with increasing age, particularly in the thalami and pallida. Differences in ICV corrected cortical thickness between NF1 patents and controls trend towards normalization when evaluated longitudinally.

Conclusions

The non-neoplastic morphologic abnormalities seen in children with NF1 are, at least in part, age dependent. Similar to other manifestations of NF1, such as the characteristic T2 hyperintensities attributed to myelin vacuolization, increased volumes of the thalami and pallida are seen during the first decade of life and resolve by the end of the second. Although our longitudinal cohort is not yet large enough fully evaluate the temporal course of cortical abnormalities in NF1, these findings suggest that the CNS effects of NF1 manifest differently in childhood when compared to young adulthood.

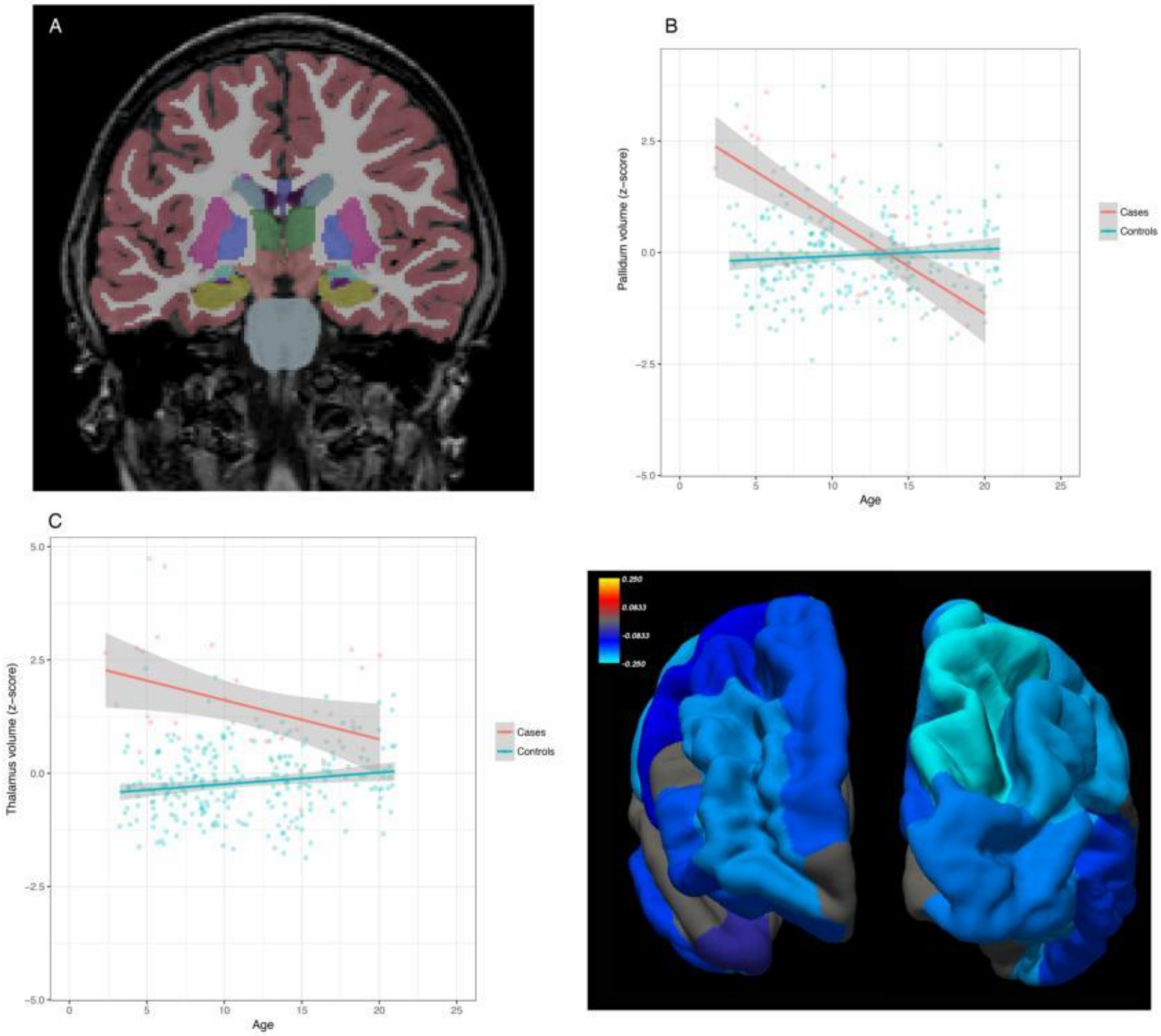

Subcortical segmentation (A) overlaid on non-contrast coronal T1 weighted image. Scatterplots of the subcortical pallidum (B) and thalamus (C) regions of interest, showing decreasing relative subcortical volumes in NF1 patients with increasing age. Heat map of slope of age verses cortical thickness in NF1 patients (D) painted over a surface rendering of the brain (showing the dorsal and ventral surfaces). Regions without significant effects are grey. Note that the slopes are all negative.

(Filename: TCT_2840_nf1fig.jpg)

3242

1:42PM - 1:49PM

MR Imaging Correlates for Molecular and Mutational Analyses in Children with Diffuse Intrinsic Pontine Glioma

T Poussaint[1], S Vajapeyam[1], D Brown[1], C Ma[2], P Kao[2], K Wright[2]
[1]Boston Children's Hospital, Boston, MA, [2]Dana Farber Cancer Institute, Boston, MA

Purpose
To explore MR imaging correlates with molecular and mutational analyses in DIPG.
Materials and Methods
A DIPG clinical trial (DIPG-Biology and Treatment Study) was instituted prior to commencement of therapy. Baseline MR imaging studies included standard pre and post contrast MR sequences. Retrospective imaging analyses of the tumors included FLAIR/T2 tumor volume, tumor volume

enhancing and cyst/necrosis, median, mean mode, skewness, kurtosis of apparent diffusion coefficient (ADC) tumor volume based on FLAIR and enhancement at baseline. Histone mutations were identified through whole-genome and RNA-sequencing. Univariate Cox proportional-hazards regression was used to test the association of imaging predictors with overall (OS) and progression-free survival (PFS). Wilcoxon rank-sum, Kruskal-Wallis, and Fisher's exact tests were used to compare imaging measures between groups.

Results

Fifty patients had biopsy and MR studies. Median age at trial registration was 6 years (range=3.3-17.5 years); 52% were female. Forty-eight patients were assigned to molecular subgroups: 28 in MGMT-/EGFR-, 14 in MGMT-/EGFR+, 3 in MGMT+/EGFR-, and 3 in MGMT+/EGFR+. Twenty-three patients had histone mutations in H3F3A, 8 in HIST1H3B, and 3 in HISTH3C. Median follow-up time was 11 months (range=0.4-33 months). Increased enhancing tumor volume was significantly associated with poorer OS ($p=0.01$) and PFS ($p=0.001$). Enhancing tumor volume was significantly different across molecular subgroups ($p=0.047$). Tumor enhancement, mode, skewness, and kurtosis ADC-FLAIR were significantly different ($p\leq0.048$) between patients with H3F3A and HIST1H3B mutations. Tumor enhancement, median, mode, skewness, and kurtosis ADC-FLAIR were significantly different ($p\leq0.048$) between patients with H3F3A and HIST1H3B or HISTH3C mutations.

Conclusions

MR imaging features including enhancement and ADC histogram parameters are correlated with molecular subgroups and mutations in children with DIPG. Future studies are required to verify these findings in a larger cohort.

3533

1:49PM - 1:56PM

MRI Features of 'Supratentorial PNET' in the Light of Molecular Diagnoses and the New WHO Classification: A Report From the Children's Oncology Group Randomized ACNS0332 Trial

A Jaju[1], E Hwang[2], D Capper[3], L Chavez[4], S Brabetz[5], C Billups[6], Y Li[6], R Packer[7], J Olson[8], L Heier[9]
[1]Ann and Robert H Lurie Children's Hospital of Chicago, Chicago, IL, [2]Children’s National Medical Center, Washington, D.C. , DC, [3]Charité Universitätsmedizin Berlin, Berlin, AK, [4]University of California, San Diego, San Diego, CA, [5]German Cancer Research Center, Heidelberg, AK, [6]St. Jude Children's Research Hospital, Memphis, TN, [7]Children’s National Medical Cent, Washington, DC, [8]Fred Hutchinson Cancer Research Center, Seattle, WA, [9]NYP - CORNELL, NEW ROCHELLE, NY

Purpose

To describe the MRI findings of a cohort of histologically diagnosed supratentorial primitive neuroectodermal tumors (CNS-PNET) which were subsequently reassigned by methylation analysis.

Materials and Methods

Histologically diagnosed supratentorial PNET were enrolled as a subset on the Children's Oncology Group ACNS0332 trial, and retrospective methylation analysis was performed. After excluding pineoblastomas, there were 29 CNS-PNET with complete imaging and methylation data available which were included in this analysis. MRI of the brain and spine were retrospectively reviewed by two neuroradiologists, and multiple parameters including location, size, margins, edema, diffusion restriction, T1/T2 signal, cysts/necrosis, calcification/hemorrhage, enhancement and metastatic status were systematically recorded. Based on methylation results, the tumors were divided into embryonal and non-embryonal groups per the 2016 WHO classification. Statistical and subjective comparison of the imaging features between the two subgroups was performed.

Results

Retrospective methylation analysis revealed a large number of discrepant entities. There were 19 (66%) non-embryonal tumors, which were not intended for trial inclusion, and only 10 embryonal tumors. For all tumors combined, parenchymal location was most common (76% hemispheric, 7% deep nuclei, 7%

pineal region and 10% intraventricular). Frontal lobe involvement was most common followed by parietal. The median size was 6 cm; 79% had well-defined margins and 66% had surrounding edema. All tumors enhanced post contrast although the degree and extent was variable. 90% had cystic/necrotic change and 62% had calcification/hemorrhage. None of the 29 patients had intracranial or spinal metastasis detectable by MRI, although 1 patient had positive CSF cytology. 55% had gross total or radical subtotal (>95%) resection, while the rest had subtotal resection. None of imaging parameters correlated significantly when compared between embryonal and non-embryonal subgroups.
Conclusions
'Supratentorial PNET' are typically large, necrotic, enhancing parenchymal tumors, with a small subset centered in ventricles. Based on molecular analyses, only a minority of those in our cohort belonged to the embryonal category. It was not possible to definitely distinguish embryonal from non-embryonal tumors by MRI.

2522

1:56PM - 2:03PM

Pediatric Intracranial Tumor Grading: Multiparametric Comparison Including ADC, IVIM, APT, ASL, and Stretched Exponential DWI with Histogram Analysis

K Kikuchi[1], A Hiwatashi[1], O Togao[1], K Yamashita[1], D Momosaka[1], H Honda[1]
[1]Kyushu University, Fukuoka, Fukuoka

Purpose
To investigate the utility of MR metrics by a histogram analysis for pediatric intracranial tumor grading.
Materials and Methods
Between April 2013 and June 2017, seventeen children (10 boys, 7 girls; 1–17 years; median 4 years) with 5 high- and 12 low-grade intracranial tumors were retrospectively evaluated. MRI was performed with a 3.0-T unit. Apparent diffusion coefficient (ADC) was calculated by b-values with 0 and 1000 s/mm2. Intravoxel incoherent motion (IVIM) parameters were calculated using 13 b-values with a biexponential model. Amide proton transfer (APT) was acquired with presaturation of 2 µT and 2 s. Arterial spin labeling (ASL) was obtained with label duration of 1650 ms and post-label delay of 1525 ms. Stretched exponential DWI were calculated using the same 13 b-values. ADC, perfusion fraction (f), pseudo-diffusion coefficient (D*), true diffusion coefficient (D), APT, APT with water suppression (APTws), cerebral blood flow (CBF), distributed diffusion coefficient (DDC), and α (alpha, intravoxel heterogeneity index) were measured and analyzed using a histogram in high- and low-grade tumors. These values were compared by Mann-Whitney U-test between the tumors. Receiver operating characteristic (ROC) analysis was used to evaluate diagnostic performance.
Results
D, ADC, DDC, and α were lower in high-grade tumors than in low-grade tumors with the 10th, 20th, 25th, and 50th percentiles ($P < 0.05$ for all). The f was higher in high-grade tumors than in low-grade tumors with 25th, 50th, 75th, and 80th percentiles ($P < 0.05$ for all). There were no statistically significant differences among D*, APT, APTws, and CBF. ROC analysis found D as well as combined f+D had the best diagnostic performance for tumor grading with 10th percentile (AUC = 0.967, respectively).
Conclusions
IVIM imaging may be the best method to evaluate pediatric intracranial tumors.

2465

2:03PM - 2:10PM

Post-RT Changes in ADC Histogram Metrics May Help Identify Pseudoprogression in Newly Diagnosed DIPG: A Report from the Pediatric Brain Tumor Consortium

S Vajapeyam[1], D Brown[1], C Billups[2], M Shiroishi[3], M Law[4], P Baxter[5], A Onar[2], I Dunkel[6], T Poussaint[1]

[1]*Boston Children's Hospital, Boston, MA,* [2]*St. Jude Children's Research Hospital, Memphis, TN,* [3]*KECK SCHOOL OF MEDICINE, USC, SOUTH PASADENA, CA,* [4]*Keck Medical Center of USC, Los Angeles, CA,* [5]*Texas Children's Hospital, Houston, TX,* [6]*Memorial Sloan Kettering Cancer Center, New York, NY*

Purpose
To explore using DSC perfusion, DCE permeability and ADC histogram metrics to identify pseudoprogression in newly diagnosed diffuse intrinsic pontine glioma (DIPG).
Materials and Methods
A PBTC protocol consisting of administering PARP-inhibitor ABT-888 concurrently with radiation therapy, followed by maintenance therapy with ABT-888 and temozolomide (TMZ) in children with DIPG was implemented. Standard MR imaging, diffusion, DSC perfusion and DCE perfusion were performed at baseline and approximately every 2 months throughout treatment. DSC perfusion, as well as DCE permeability and ADC histogram metrics of T2-FLAIR and enhancing tumor were generatedas described previously(1,2). Patients with suspected pseudoprogression that had subsequent imaging were compared to those with true early progressive disease. Only patients with documented radiological progression or clinical progression within 6 months of starting therapy were included in this analysis. In all 25 perfusion and diffusion metrics were used to compare the 2 groups.
Results
53 children were included in the Phase II trial. 7 patients had suspected pseudoprogression with subsequent imaging and were compared with 20 patients identified as true progression. No differences were found between the groups for any of the DSC perfusion or DCE permeability metrics. No difference was found in ADC histogram metrics of enhancing tumor. Post-RT change in the mode of the ADC histogram of tumor on T2-FLAIR was much smaller for pseudoprogression than for true early progression (-26.11 vs -268.15, p=0.0099). Due to low sample size and high number of comparisons, this was not statistically significant but the striking difference between groups is evident in Figure 1. Examining ADC histogram metrics in a larger cohort is warranted.
Conclusions
Post-RT changes in ADC histogram metrics may help differentiate RT-induced pseudoprogression from true early progression in DIPG.

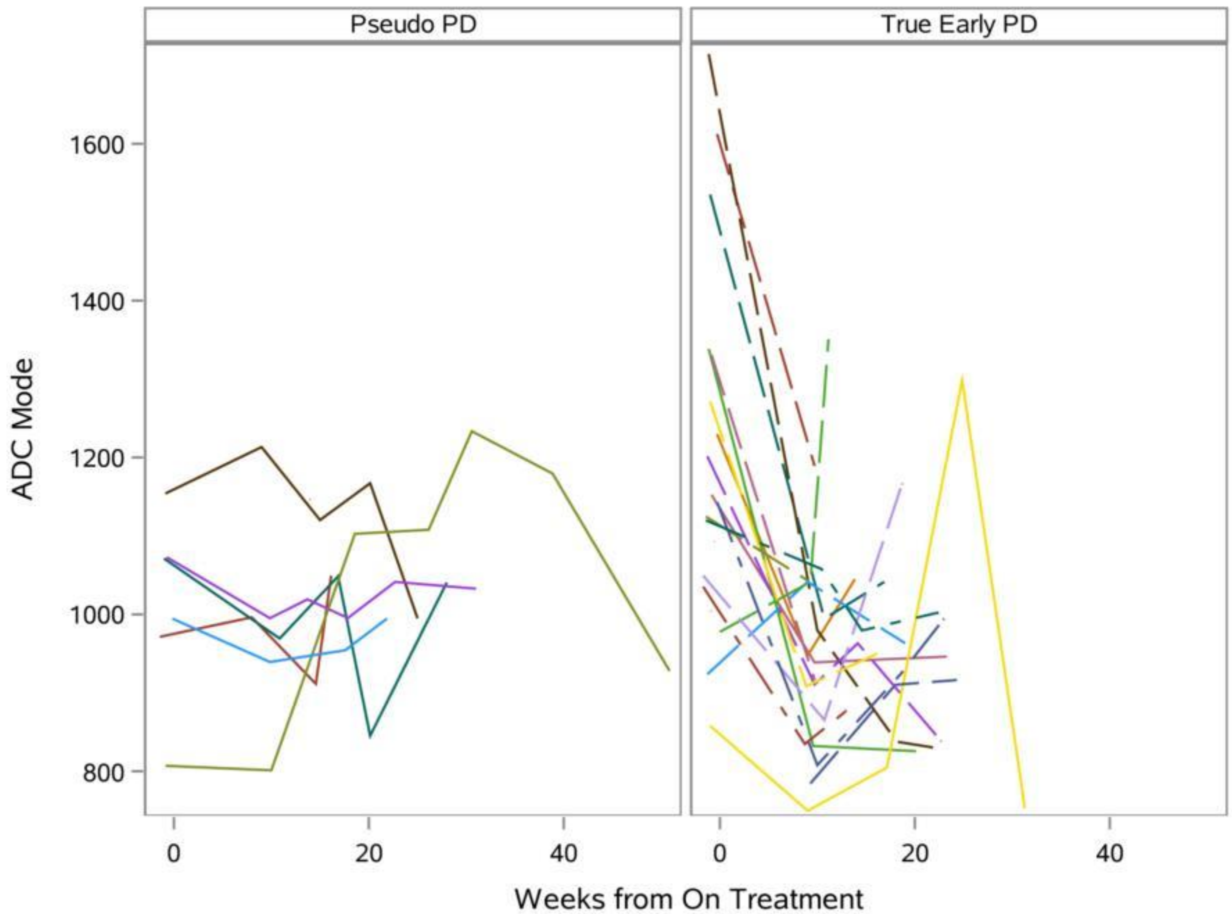

(Filename: TCT_2465_ADC_FLAIR_mode.jpg)

2991

2:10PM - 2:17PM

Response of Pediatric Brainstem Tumors to Proton Radiotherapy

K Buch[1], S Rincon[1], N Joshipura[2], P Caruso[2], Y Torunn[1]
[1]Massachusetts General Hospital, Boston, MA, [2]MGH, Boston, MA

Purpose
Brainstem gliomas are tumors of glial origin arising in the brainstem and include various histologies such as diffuse intrinsic pontine glioma and pilocytic astrocytoma. Diagnosis is often solely based on imaging assessment due to the inherent location posing a challenge for biopsy. Proton radiotherapy is an effective modality for the treatment of pediatric brainstem tumors and offers the advantage of high conformal control that limits radiation dose to the developing brain. The purpose of our study was to assess the volumetric response of pediatric brainstem tumors to proton radiotherapy on serial MRI exams.
Materials and Methods
Following IRB approval, a retrospective clinical database search was performed for patients with brainstem tumors. Patients 0-19 years with brainstem tumors who underwent proton radiotherapy were included. Patients with tumors previously treated with surgical resection were excluded. Volume measurements were obtained using a VitreaWorkstation™ to manually contour the tumor using FLAIR or T2 sequences at all available timepoints. To assess tumor response to treatment, the RANO criteria for the

assessment of low-grade gliomas was used. A partial response was defined as a greater than or equal to 50% decrease in tumor volume, per the RANO criteria.

Results

Nine patients met inclusion criteria with 2 females and 7 males, and an average age of 10.8 years (range 7 months-19 years). Follow-up evaluation ranged from 7-months to 13.9-years, with a mean follow-up period of 4.5 years. Median proton therapy treatment was 52.3Gy¬RBE (range 50.4-54.9GyRBE). 6/9 (67%) patients demonstrated a partial response to treatment at the end of the follow-up period (average follow-up 28 months; range 7.4-35.5 months). On average, partial response first occurred in this group at 14.2 months (range 1.3-35 months). These 6 patients all had initial tumor volumes less than 18 cc, and were confined to the brainstem. 3/9 (33%) patients never met criteria for partial response. 2 of these 3 patients developed progressive disease per the RANO criteria with a 25% increase in tumor volume by the end of the follow-up period (average follow-up 21 months; range 18.9-23.6 months). On average, disease progression first occurred in this group at 9 months (range 4-14 months). The 2 patients with disease progression had an initial tumor volume greater than 20 cc. One of these patients had a tumor which also involved the cerebellum, and was found to be a glioblastoma on autopsy. The other patient had a tumor which involved both the brainstem and cervical spinal cord. The last of these 3 patients met the RANO criteria for disease progression at 4-months, but subsequently returned to baseline and did not meet RANO criteria for disease progression at the end of the follow-up period. Therefore, this lesion was considered radiographically stable.

Conclusions

Brainstem gliomas, in our small cohort of 9 patients, demonstrated a varied response to proton radiotherapy. Disease progression was associated with large tumors volumes (greater than 20cc) and extension of tumor beyond the brainstem. A partial response to proton radiotherapy occurred on average at 14 months, and disease progression first occurred on average at 9-months. Therefore, early MRIs (earlier than 9 months) may not be predictive of eventual tumor response.

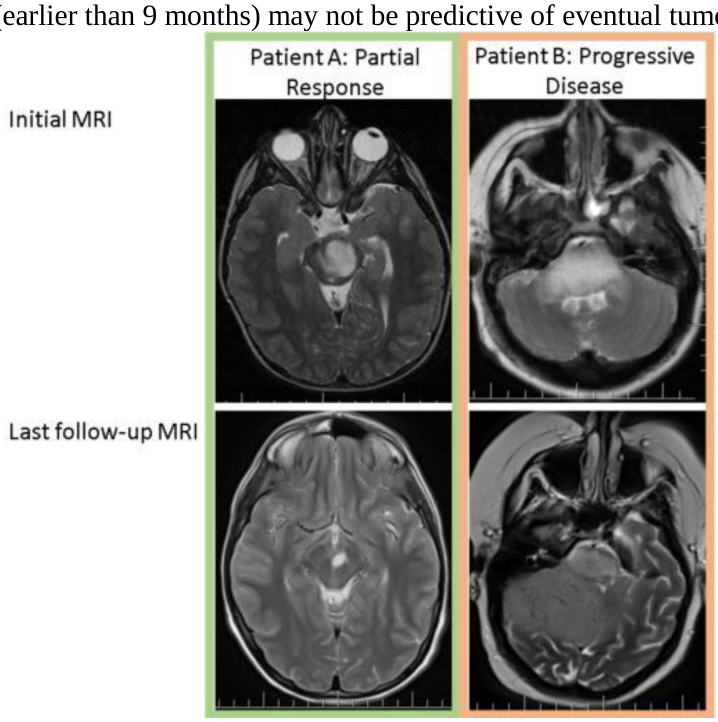

Axial T2 weighted sequences of two patients with brainstem tumors. Patient A (left column) was a 2-year old male followed for 8.8 years, who demonstrated a partial response per the RANO criteria. Patient B (right column) was a 19 year old female followed for 1.6 years, who demonstrated progressive disease with extension of disease into the right cerebellar hemisphere.

(Filename: TCT_2991_ASNR_bstem.jpg)

2467

2:17PM - 2:24PM

Use of Advanced Diffusion and Perfusion MR Metrics to Predict Survival in Newly Diagnosed DIPG: A Report from the Pediatric Brain Tumor Consortium

S Vajapeyam[1], D Brown[1], C Billups[2], M Shiroishi[3], M Law[4], P Baxter[5], A Onar[2], I Dunkel[6], T Poussaint[1]
[1]Boston Children's Hospital, Boston, MA, [2]St. Jude Children's Research Hospital, Memphis, TN, [3]KECK SCHOOL OF MEDICINE, USC, SOUTH PASADENA, CA, [4]Keck Medical Center of USC, Los Angeles, CA, [5]Texas Children's Hospital, Houston, TX, [6]Memorial Sloan Kettering Cancer Center, New York, NY

Purpose
To use advanced diffusion and perfusion MR metrics to predict survival in children with newly diagnosed diffuse intrinsic pontine glioma (DIPG).
Materials and Methods
A PBTC protocol consisting of administering PARP-inhibitor ABT-888 concurrently with radiation therapy, followed by maintenance therapy with ABT-888 and temozolomide (TMZ) in children with DIPG was implemented. Standard MR imaging, diffusion, DSC perfusion and DCE perfusion were performed at baseline and approximately every 2 months throughout treatment. ADC histogram metrics of T2-FLAIR and enhancing tumor were generated as described previously(1). DCE permeability metrics as described previously (2) were calculated for enhancing tumors whereas DSC perfusion was characterized by the rCBV ratio of tumor to normal-appearing white matter ROI. Baseline values, post-RT changes and longitudinal trends for all metrics were evaluated for association with survival.
Results
50 children were evaluable for survival analysis. There was no significant association between baseline ADC histogram metrics and outcome. Baseline perfusion ratio was significantly associated with survival (p=0.006) and PFS (p=0.017). Baseline mean k_trans was significantly associated with overall survival (p=0.027) and PFS (p=0.030). Higher perfusion ratio and mean k_trans at baseline led to shorter survival. Post-RT change in skewness_ADC_FLAIR was associated with PFS (p=0.026) - tumors with a smaller increase in skewness had longer PFS. Post-RT change in mean_ADC_enhancing was associated with PFS (p=0.049) - larger change in mean_ADC_enhancing had longer PFS. Post-RT change in max v_e was significantly associated with overall survival (p=0.041) as well as PFS (p=0.044), with a greater increase associated with worse outcome. When analyzed as time-dependent variables, median v_e and mean v_e were significantly associated with overall survival (p=0.046 and p=0.030, respectively) and max k_trans and mean v_e were significantly associated with PFS (p=0.026 and p=0.028, respectively). Higher increases were associated with worse outcomes.
Conclusions
Baseline, post-RT changes and longitudinal analyses of ADC histogram, DSC perfusion and DCE permeability metrics in DIPG are useful in predicting survival.

Wednesday, May 22, 2019
1:00PM - 2:30PM
Trauma Neuroimaging

2727

1:00PM - 1:07PM

Coupling: A Unifying Theory for Post-Concussion Syndrome Treatment and Functional Neuroimaging

M Allen[1], M Johnson[1], C Epps[1]
[1]Cognitive FX, Provo, UT

Purpose
Post-concussion syndrome (PCS) occurs in a significant percentage of concussion patients and is defined as having a history of traumatic brain injury with persistence of three or more symptoms. Standard structural clinical neuroimaging studies show no abnormal findings for the majority of PCS patients as opposed to functional MRI, which often reveals irregularities in the blood-oxygen level dependent (BOLD) signal. This suggests that dysregulation of neurovascular coupling (NVC), which causes abnormal BOLD signals, plays a significant role in PCS pathology. However, compared to the pathophysiologic mechanisms occurring in acute concussion, the underlying neuropathophysiology of chronic concussive sequelaeor PCS is less understood, though becoming clearer with emerging research. We present a treatment approach grounded in the physiological theory presented here called Enhanced Performance in Cognition (EPIC), which has shown strong clinical success. Dysregulation of neurovascular coupling (NVC), along with disruptions in cerebrovascular reactivity (CVR) and autonomic nervous system (ANS) dysregulation are the targets of EPIC treatment.
Materials and Methods
270 concussed patients underwent EPIC Treatment--a five day program of multidisciplinary rehabilitation. They participated in a standardized form of fMRI called functional Neurocognitive Imaging (fNCI) at the beginning and end of treatment to measure irregularities in NVC. The results from this study were combined with emerging research to propose a novel theory about PCS, its pathology, and treatment.
Results
After the completion of EPIC treatment the fNCI measurements of NVC improved 73.7 percent from their pre-treatment scan. Over the course of EPIC treatment, patients reported 65.8 percent improvement on conventional post-concussion symptom scale (PCSS) scores. EPIC treatment and its continuing results provide support that NVC is affected in PCS pathology. Success of EPIC treatment tentatively supports the hypothesis that dysregulation of NVC figures prominently in the neuropathophysiology of PCS.
Conclusions
Due to the promising results of EPIC treatment, along with extensive research on PCS pathology, we propose this novel theory concerning the mechanisms by which NVC dysregulation is normalized. It is intended that both the theory and treatment approach are presented explicitly enough to generate empirical studies with clear hypothetical predictions from the theory as well as clinical innovations with significant relevance to improve current practices.

3204

1:00PM - 2:30PM

Volumetric MR Imaging as a Biomarker for Cognitive Decline in Mild Traumatic Brain Injury

O Ashour[1], V Agarwal[2], J Mettenburg[3], A Puccio[2], S Beers[2], D Okonkwo[2]
[1]University of Pittsburgh Medical Center, Pittsburgh , PA, [2]University of Pittsburgh Medical Center, Pittsburgh, PA, [3]UPMC, PITTSBURGH, PA

Purpose
The study aims to identify whole brain and regional volumetric variables that correlate with abnormal neuropsychological testing in patients with chronic mild traumatic brain injury (mTBI).
Materials and Methods
70 mTBI patients were identified retrospectively with at least 6 months since the date of injury. Patients were matched with 42 healthy controls. Both groups underwent a battery of neuropsychological tests (previously validated for use in TBI patients), assessing for attention, learning, memory, and executive functioning. Simultaneously, subjects underwent MR imaging at 3.0 Tesla. Automated volumetric analysis was performed using Neuroreader (Horsens, Denmark). Volumetric parameters tested included whole brain grey matter, white matter, and segmented individual regions. Each volume was evaluated as a

ratio of total brain volume (Vol/TIV), and index scores for each individual regional volume were derived by comparison to normalized populations (NR index).
Results
Mean age for mTBI group was 36.9 years, and 32.4 years for the control group. Mean years of education at testing was 14.9 for the mTBI group, and 15.8 for the control group. Different volumetric measures were correlated against the validated neuropsychologic tests. Mean hippocampal Vol/TIV was 0.416 vs 0.433 for mTBI vs control groups. Mean white matter Vol/TIV was 28.5 vs 27.4 for mTBI vs control groups. Mean hippocampal Left/Right asymmetry NR index was 1.22 vs 2.04 for mTBI vs control groups. Mean white matter NR index was -1.56 vs -2.84 for mTBI vs control groups. There was a significant variation ($p<0.05$) of hippocampal and white matter Vol/TIV and white matter NR index between the mTBI and control groups, which correlated with lower scores in the mTBI group on the California Verbal Learning Test II Short delay and Long delay free recall as well as the WAIS IV PSI test.
Conclusions
Automated volumetric analyses are gaining traction in several areas of neurodegenerative diseases. The ability to utilize such tools as clinical biomarkers for the functional status of mTBI patients can further our understanding of this condition's clinical course. They can serve as a noninvasive tools for monitoring functional recovery or decline over time, and possibly to direct rehabilitation efforts.

3018

1:07PM - 1:14PM

Distinct Features of Traumatic vs Radiation Induced Microhemorrhage on Ultra-High Resolution Susceptibility Weighted Imaging

J Butman[1], H Ravi[2], D Pham[3], W Wang[2]
[1]Clinical Center of the NIH, Bethesda, MD, [2]Center for Neuroscience and Regenerative Medicine, Bethesda, MD, [3]Center for Neuroscience and Regenerative Medicne, Bethesda, MD

Purpose
Microhemorrhages (µh) are commonly thought of as having a stereotypical punctate appearance on susceptibility weighted imaging (SWI), independent of the underlying patholophysiology. We sought to characterize the fine structure of cerebral µh using ultra-high resolution SWI, and so determine whether the structure of traumatic µh is distinct from that of µh resultant from other pathologic processes.
Materials and Methods
High resolution susceptibility weighted images were obtained in 8 patient volunteers (under IRB approved portocol clinicaltrials.gov NCT00001711), 4 with traumatic brain injury (TBI) and 4 with radiation microangiopathy. Scanner: 3.0 Philips Achieva R5.3.0.0. Sequence: 3D multishot EPI GRE [1], 120 second acquisition. Geometry: FOV=256 mm, matrix 640 × 640, 463 sagittal slices, 0.4 mm thick. Contrast: TR 60, TE 29, FA 22°. Acceleration: EPI ETL 15, 9×SENSE (3×phase, 3×sense). This represents135-fold acceleration vs single echo 3D GRE often used for SWI. This was repeated 20 times (total 40 minutes) and each acquisition was coregistered and combined (sum-of-squares) to obtain single high resolution 400 µ isotropic data. The total number of microhemorrhages was counted, and were classified as "dot"-like or "chain"-like, and classified as the latter when µh were adjacent to each other and difficult to distinguish as separate puncta.
Results
In the 4 patients with radiation microangiopathy, a total of 677 µh (mean 169±68) were identified. Only one was classified as a "chain". Only 3 involved GM. In the 4 patients with a history of moderate to severe TBI, a total of 175 µh (mean 44±25) were identified. Of these, 78 were classified as "dots" and 97 as "chains". Cortical GM involvement was identified in 39 µh.
Conclusions
Traumatic microhemorrhages have distinct characteristics which distinguish them from those induced by

other pathologies (e.g. radiation microangiopathy) which undoubtedly reflect differences in the underlying mechanism of injury. yet been Whether these features represent a useful clinical diagnostic marker has yet to be established. Whether or not these patterns have different clinical implications is also yet to be established.

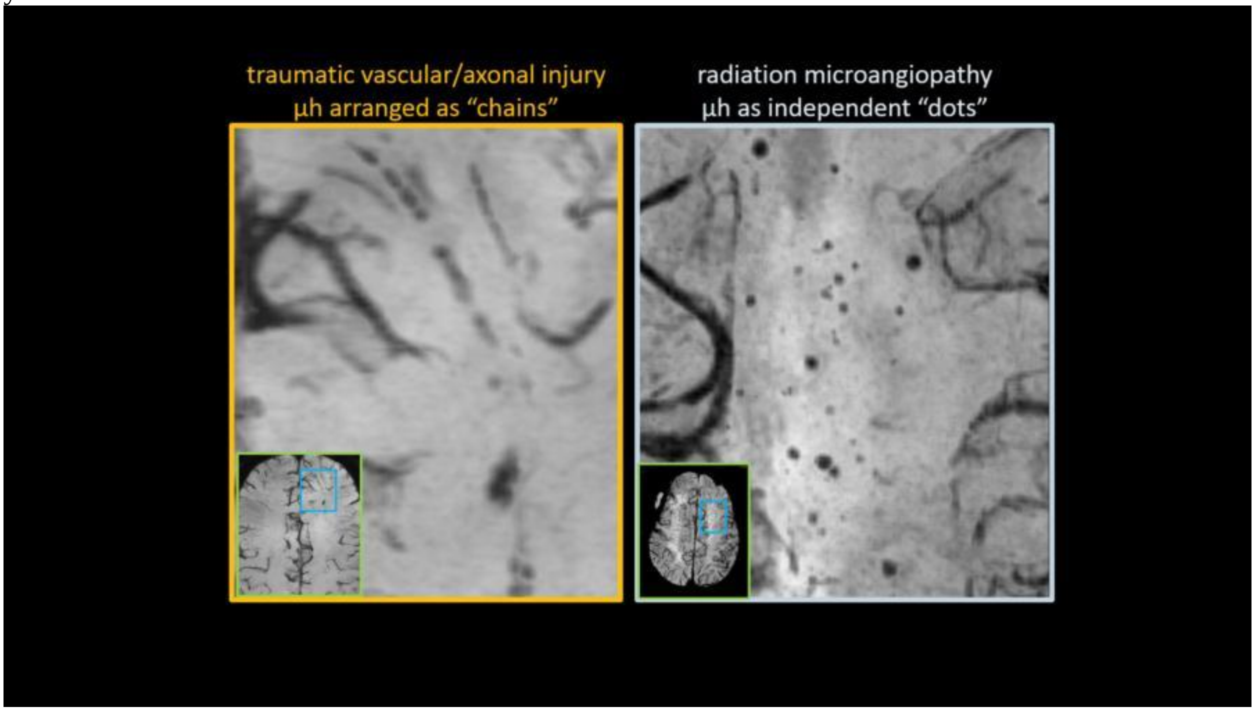

(Filename: TCT_3018_2018ASNRswi.jpg)

2161

1:14PM - 1:21PM

Early Dramatic Improvement on the National Institutes of Health Stroke Scale Predicts Favorable Outcome 90 Days After Thrombectomy in the DEFUSE 3 Study

J Heit[1], M Mlynash[2], S Kemp[3], M Lansberg[1], S Christensen[4], M Marks[5], P George[6]
[1]Stanford, Stanford, CA, [2]Stanford, Palo Alto, CA, [3]Stanford University, Palo Alto, CA, [4]Stanford University, Stanford, CA, [5]Stanford Univ. Med. Ctr., Stanford, CA, [6]Stanford University Medical Center, Palo Alto, CA

Purpose

Thrombectomy in late time windows leads to improved outcomes in patients with ischemic stroke due to large vessel occlusion (LVO). We determined if patients with a dramatic improvement in their National Institutes of Health Stroke Scale (NIHSS) score 24 hours (24h) after thrombectomy were more likely to have a favorable clinical outcome than patients without a dramatic change in NIHSS in the DEFUSE 3 study.

Materials and Methods

All patients who underwent thrombectomy in DEFUSE 3 were included. Dramatic improvement (DI) was defined as a reduction of ≥8 NIHSS or NIHSS 0-1 24h after thrombectomy. Clinical outcomes were assessed by an ordinal analysis modified Rankin Scale (mRS) score and a dichotomous analysis for functional independence (mRS 0-2) at 90 days. Pre- and post-thrombecotmy core infarction was quantified by the DEFUSE 3 core laboratory.

Results

91 patients in DEFUSE 3 underwent thrombectomy with follow up data; 31 patients (34%) experienced

DI (DI+) after thrombectomy and 60 patients (66%) did not (DI-). There were no differences in age, medical comorbidities, right sided infarction, LVO location, presentation NIHSS, treatment with intravenous tPA, or time of thrombectomy treatment between DI+ and DI-. Presentation ASPECTS and baseline infarct core and penumbra volumes were similar between these groups. Reperfusion (TICI IIB-III) after thrombectomy was achieved in 26 (84%) DI+ and 43 (72%) DI- (p=0.2). Symptomatic intracranial hemorrhage occurred in no DI+ and 8% of DI- patients (p=0.2). DI was associated with a favorable mRS shift at day 90 (OR 3.8 [CI 1.7-8.6]; p=0.001) and higher rates of mRS 0-2 (61% vs 37%) OR 2.7 [CI 1.1-6.7]; p=0.03. Mortality was 3% in DI+ vs 18% in DI- (p=0.05). DI+ patients has lower median 24h NIHSS (5 [IQR 1-7] vs 13 [IQR 7.5-21]; p<0.001), smaller 24h infarction volume (21 ml [IQR 5-32] vs 65 [IQR 27-145]; p<0.001), and less 24h infarct growth (8 ml [IQR 1-18] vs 37 [IQR 16-105]; p<0.001) compared to DI- patients. Hospital stay was shorter in DI+, 3.7 days [IQR 2.9-7.1] vs 7.4 [IQR 5.2-12.1] in DI-, p<0.001.

Conclusions

DI following thrombectomy correlates with favorable clinical and radiographic outcomes and reduced hospital length of stay. DI was a favorable prognostic sign following late window thrombectomy in the DEFUSE 3 cohort.

2653

1:21PM - 1:28PM

Functional Connectivity Alterations in Subacute Post-Concussive Visual Motion Sensitivity Using a Novel Task-Based Functional MRI Vestibular Paradigm

A Trofimova[1], V Ahluwalia[2], P Frias[3], C Foster[3], C Appleberry[4], R Gore[4], J Allen[1]
[1]Emory University, Atlanta, GA, [2]GSU/GT Center for Advanced Brain Imaging, Atlanta, GA, [3]Emory University School of Medicine, Atlanta, GA, [4]Shepherd Center, Atlanta, GA

Purpose

Patients with subacute post-concussive visual motion sensitivity (PCVMS) frequently report symptoms in complex visual environments1,2. We hypothesize that this results from increased activation/weighting of visual input into the parieto-insular vestibular cortex (PIVC). We sought to define these alterations in functional activation in PCVMS using a novel vestibular paradigm task-based functional MRI (t-fMRI).

Materials and Methods

Prospective IRB approved study. Study group:12 subjects with subacute (2-10 weeks) PCVMS; control group: 10 age-matched subjects without history of concussion or vestibular impairment. Both groups underwent clinical vestibular assessment which included objective and subjective vestibular and balance measures. Exclusion criteria: age younger than 18 or older than 50, peripheral vestibular dysfunction, moderate or severe TBI, seizure disorder, CNS surgery, peripheral neuropathy, developmental delay, drug/alcohol use chronic or in the last 24 hours. MRI was acquired on 3.0 T Siemens Trio, 12-channel head coil. Vestibular paradigm t-fMRI with block design included randomly presented 30 sec videos that were either neutral (n=5) or have been shown to provoke symptoms in patients with PCVMS (n=5) based on optic flow characteristics. Immediately after each video, subjects rated the presence of symptoms/intensity on a 5-point Likert scale using MRI-compatible device. fMRI data analysis included standard preprocessing and time series regression using FSL3,4. Group-level analysis was performed for 'provocative-neutral' condition. Z-statistic images were thresholded non-parametrically using clusters determined by Z>2.3 and a corrected cluster significance threshold of p=0.05.

Results

Study group had significantly more abnormalities on Vestibular/Ocular-Motor Screening5 (a quantitative measure of vestibular function) and significantly more symptoms while viewing provocative videos. Both groups showed robust mean activation in primary and secondary visual areas, parietal lobe, parieto-insular vestibular cortex (PIVC), and cingulate gyrus. Selective increased activation was demonstrated in the study versus control group for the 'provocative-neutral' contrast in the parietal operculum, insular cortex, central operculum, middle temporal gyrus, postcentral gyrus, posterior parietal cortex, frontal pole, anterior cingulate gyrus, lateral occipital cortex, and juxtapositional lobule cortex (supplementary motor area). Control>Study group contrast did not reveal any statistically significant activation.

Conclusions

Subjects with subacute PCVMS, a common subgroup of concussion patients at risk for prolonged recovery, have increased activation of primary vestibular cortex, visual association, and visual working memory areas while viewing visually provocative videos, suggesting that 'over-activation' of visual input may underlie PCVMS symptoms. To our knowledge, this is the first demonstration of altered functional activation in post-concussive visual motion sensitivity, allowing for better understanding of symptoms persistence.

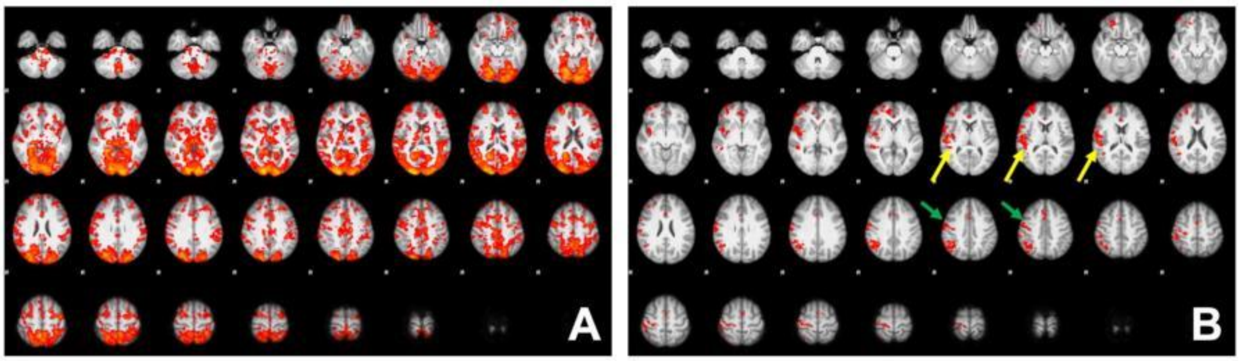

Figure 1. t-fMRI activation in novel visual-vestibular block-design paradigm. (A) Robust activation is seen in both hemispheres in patients with subacute PCVI when comparing watching visually provocative versus neutral videos. Increased activation is present in the bilateral occipital and parietal lobes including primary and secondary visual areas and parieto-insular vestibular cortex (PIVC). (**B**) Selective increased activation is present in several right hemisphere regions when comparing patients with PCVI to healthy controls watching provocative versus neutral videos including in the parietal operculum [*Z=3.3, MNI(mm)=54,-28,16*], insular cortex [*Z=2.9, MNI(mm)=46, 0, 0*], central operculum [*Z=3.1, MNI(mm)=54,-12,8*], middle temporal gyrus [*Z=3.0, MNI(mm)=44,-38, 2*], postcentral gyrus [*Z=3.3, MNI(mm)=30,-28,62*], posterior parietal cortex [*Z=3.3, MNI(mm)=66,-48,34*], frontal pole [*Z=3.1, MNI(mm)=16,68,24*], anterior cingulate gyrus [*Z=2.8; MNI(mm)= 0, 36, 10*], lateral occipital cortex [*Z=2.9; MNI=42,-60, 36*], juxtapositional lobule cortex [Z=2.9; MNI(mm)=2,-4, 54]. Yellow arrows indicate selective increased activation in the PIVC and green arrows indicate selective increased activation in the frontal eye field.

(Filename: TCT_2653_t-fMRIFigure1.jpg)

2458

1:28PM - 1:35PM

Maximum AmbiGuity Distance for Phase Imaging (MAGPI) in Detection of Traumatic Cerebral Microbleeds: An Improvement Over Current Imaging Practice

K Nael[1], J Dagher[2], M Downs[2], M Fine[2], E Brokaw[2], D Millward[3]
[1]ICAHN SCHOOL OF MEDICINE AT MOUNT SINAI HOSPITAL, NEW YORK, NY, [2]The MITRE Corporation, McLean, VA, [3]University of Arizona, Tucson, AZ

Purpose

By adopting a rigorous mathematical framework (maximum-likelihood), MAGPI has been recently developed as a promising phase imaging technique providing optimal phase SNR with no phase-wrapping and reduced susceptibility artifacts [1]. In this study, we hypothesize that the improved phase image quality of MAGPI has the potential to uncover ambiguities associated with the susceptibility-weighted imaging (SWI) process. We test this hypothesis clinically in the context of detection of traumatic cerebral microbleeds (TCMB) in athletes diagnosed with mild traumatic brain injury (mTBI).

Materials and Methods

Ten athletes diagnosed with mTBI were enrolled in this prospective longitudinal study. All subjects were scanned using a 3T MRI (Skyra, Siemens) at 2 days, 2 weeks and 2 months post head trauma. The imaging protocol included whole brain T1 MPRAGE, T2 FLAIR, standard SWI sequence (TE=30ms, TR=40ms, FA = 15deg) and the MAGPI Multi-Echo sequence (TR = 40ms, TE = 9.34, 17.29, 22.19, 27.09, 32.12, 37.56ms, FA = 15deg). All subjects had routine neuropsychological assessment (ImPACT exam) and Visuo-Motor Tests (VMT) performed by a physician. Phase images resulting from the MAGPI protocol were subsequently put through the SWI process described in [2]. We refer to this process as MAGPI SWI. Images were assessed by a board certified neuroradiologist for presence of contusions and TCMB.

Results

All study participants (18-22 years old, 3 females and 7 males) were diagnosed with mTBI by a trained clinician. Participants had an average Post-Concussion Symptom Scale (PCSS) score of 25.1 ± 18.5 and four of the participants were symptomatic based on a visuomotor tracking task [3] at the initial assessment within 3 days of injury. Two weeks post injury participants have an average PCSS score of 3.0 ± 6.0 with the majority (6 of 10) becoming asymptomatic at that time. Review of FLAIR images showed evidence of contusions in 4 patients (40%). Three out of these 4 patients had TCMBs on MAGPI-SWI confined to the region of gyrus rectus. The TCMBs were persisted on all 3 time-points, however in one patient TCMB was smaller on the third examination. None of these TCMBS were identified confidently on conventional SWI due to significant distortion and susceptibility artifact in the region of gyrus rectus (Figure).

Conclusions

Higher SNR and optimal unwrapping with reduced susceptibility in MAGPI-SWI can clarify small microbleeds that can go undetected with routinely used conventional SWI.

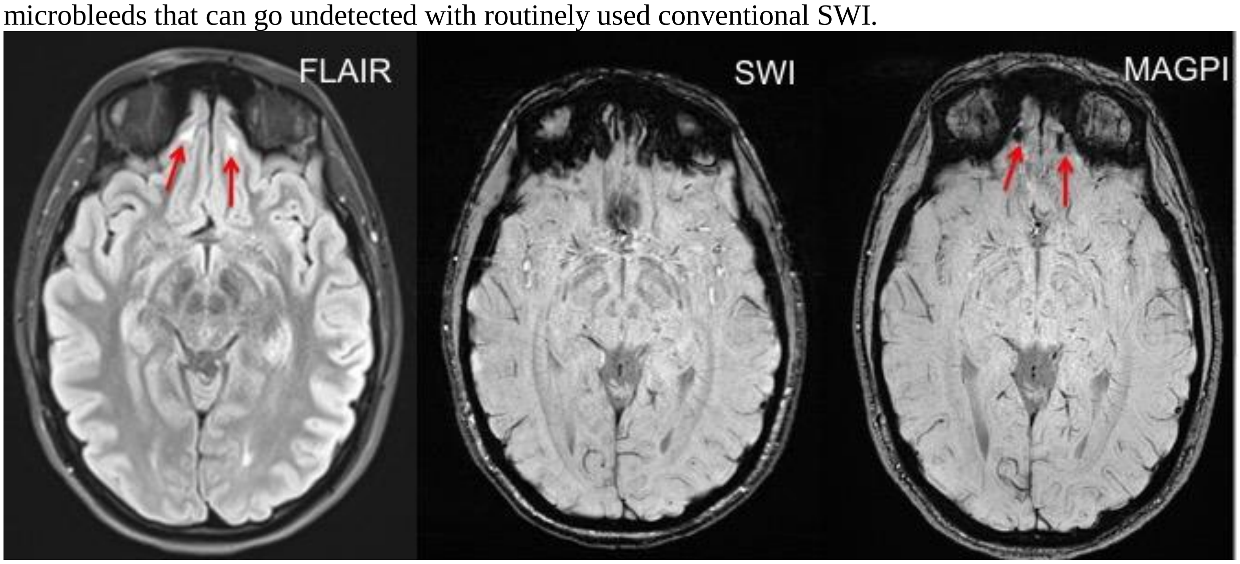

(Filename: TCT_2458_MAGPI.jpg)

2155

1:35PM - 1:42PM

Monitoring Small Subdural Parafalcine and Paratentorium Hemorrhages. Is it Beneficial?

K Seifert[1], X Wu[2], L Tu[3], A Malhotra[4]
[1]YALE NEW HAVEN HOSPITAL, NEW HAVEN, CT, [2]Yale University School of Medicine, New Haven, CT, [3]Yale School Of Medicine, New Haven, CT, [4]YALE UNIVERSITY SCHOOL OF MEDICINE, NEW CANAAN, CT

Purpose

As imaging in the emergency department increases, the incidence of intracranial hemorrhage has increased, including detection of small subdural hemorrhages. The management and monitoring of subdural hemorrhage is based on data from convexity subdural hemorrhages, with concern for mass effect and midline shift causing clinical decline. However, a subset of small subdural hemorrhages, along the falx and tentorium, may not require such rigorous monitoring, thus reducing patient cost and radiation. A review of literature reveals few small studies regarding patients with small parafalcine and paratentorial subdural hemorrhages, with no enlargement on follow up imaging. The purpose of this study was to evaluate patients with small parafalcine and paratentorial hemorrhages to evaluate the findings of the small studies on a larger scale and to provide recommendations for monitoring these patients on future imaging studies.

Materials and Methods

This study evaluated all patients over a three year period that had small parafalcine and paratentorial hemorrhages with multiple imaging studies. We assessed the change in each patients' subdural hemorrhage, as well as collected data regarding clinical course and intervention.

Results

A total of 94 patients were included. Our results reveal a small increase of subdural hemorrhage in 4% of the patients. All patients remained asymptomatic and stabilized without requiring intervention. There was no correlation with anticoagulation use and increasing hemorrhage, as none of our patients with an increase in hemorrhage were on anticoagulation.

Conclusions

Our study shows that most small isolated parafalcine and paratentorial hemorrhages do not increase on repeat imaging. This is the first study that evaluates patients with an increase in their parafalcine/paratentorium hemorrhage, and shows these hemorrhages stabilize without intervention. Therefore, we recommend that patients with asymptomatic small isolated subdural parafalcine and/or paratentorial hemorrhages do not require repeat imaging. The use of anticoagulation does not necessitate the need for repeat imaging in this subset of patients.

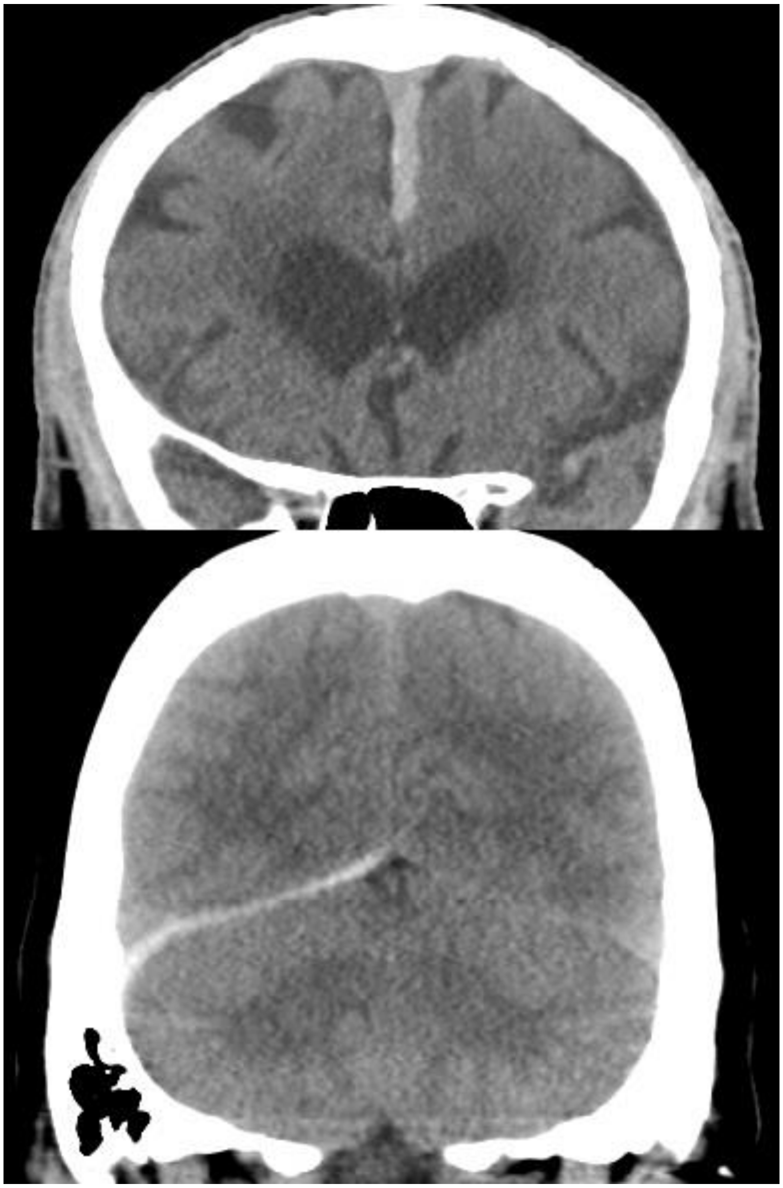

(Filename: TCT_2155_paratentfalxhem.jpg)

2739

1:42PM - 1:49PM

PH-Weighted Molecular MRI in Acute Traumatic Brain Injury Using Amine Proton Chemical Exchange Saturation Transfer Echoplanar Imaging (CEST EPI)

B Ellingson[1], J Yao[2], C Raymond[1], A Chakhoyan[2], J Villablanca[2], C Real[2], D McArthur[2], N Salamon[2]
[1]University of California Los Angeles, Los Angeles, CA, [2]UCLA, Los Angeles, CA

Purpose
Cerebral acidosis is a consequence of secondary injury mechanisms following traumatic brain injury (TBI), including excitotoxicity and ischemia, with potentially significant clinical implications. However, there remains an unmet clinical need for technology for non-invasive, high resolution pH imaging of human TBI for studying metabolic changes following injury. Thus, the purpose of the current project was to explore the use of pH-weighted molecular MR imaging in patients with TBI.

Materials and Methods

The current study utilized a combination of MR physics simulations, phantom experiments, and clinical scans in 17 patients with acute TBI using amine chemical exchange saturation transfer echoplanar imaging (CEST EPI) on a clinically available 3T MR scanner to obtain pH-weighted molecular MR images sensitive to areas of cerebral acidosis. Phantom experiments involving CEST EPI using 50mM vials containing glutamine and glutamate exhibited distinct contrast at lower pH, consistent with previous studies.

Results

The estimated pH-dependent exchange rate, in Hz, for glutamine and glutamate of kex(Gln) = 163.2+1.562×10[pH-3] and kex(Glu) = 781+2.522×10[pH-4], respectively. In support of the hypothesis that amine CEST EPI may be valuable in identifying tissue at risk of acidity due to excitotoxicity, MR simulations confirmed measures of CEST magnetization transfer ratio asymmetry (MTRasym) at 3ppm from bulk water (amine protons) for both glutamine and glutamate demonstrated sensitivity to pH, concentration, and T2 relaxation time. In patients with acute TBI, pH-sensitive CEST EPI showed significantly elevated pH-weighted image contrast (MTRasym at 3ppm) in areas of T2 hyperintensity or edema ($P<0.0001$), and a strong negative correlation with Glasgow Coma Scale (GCS) at the time of the MRI exam ($R2=0.4777$, $P=0.0021$), Glasgow Outcome Scale - Extended (GOSE) at 6 months from injury ($R2=0.5334$, $P=0.0107$), and a non-linear correlation with the time from injury to MRI exam ($R2=0.6317$, $P=0.0004$).

Conclusions

The evidence in the current study suggests clinical feasibility and potential value of pH-weighted amine CEST EPI as a high-resolution imaging tool for identifying tissue most at risk for long-term damage due to cerebral acidosis.

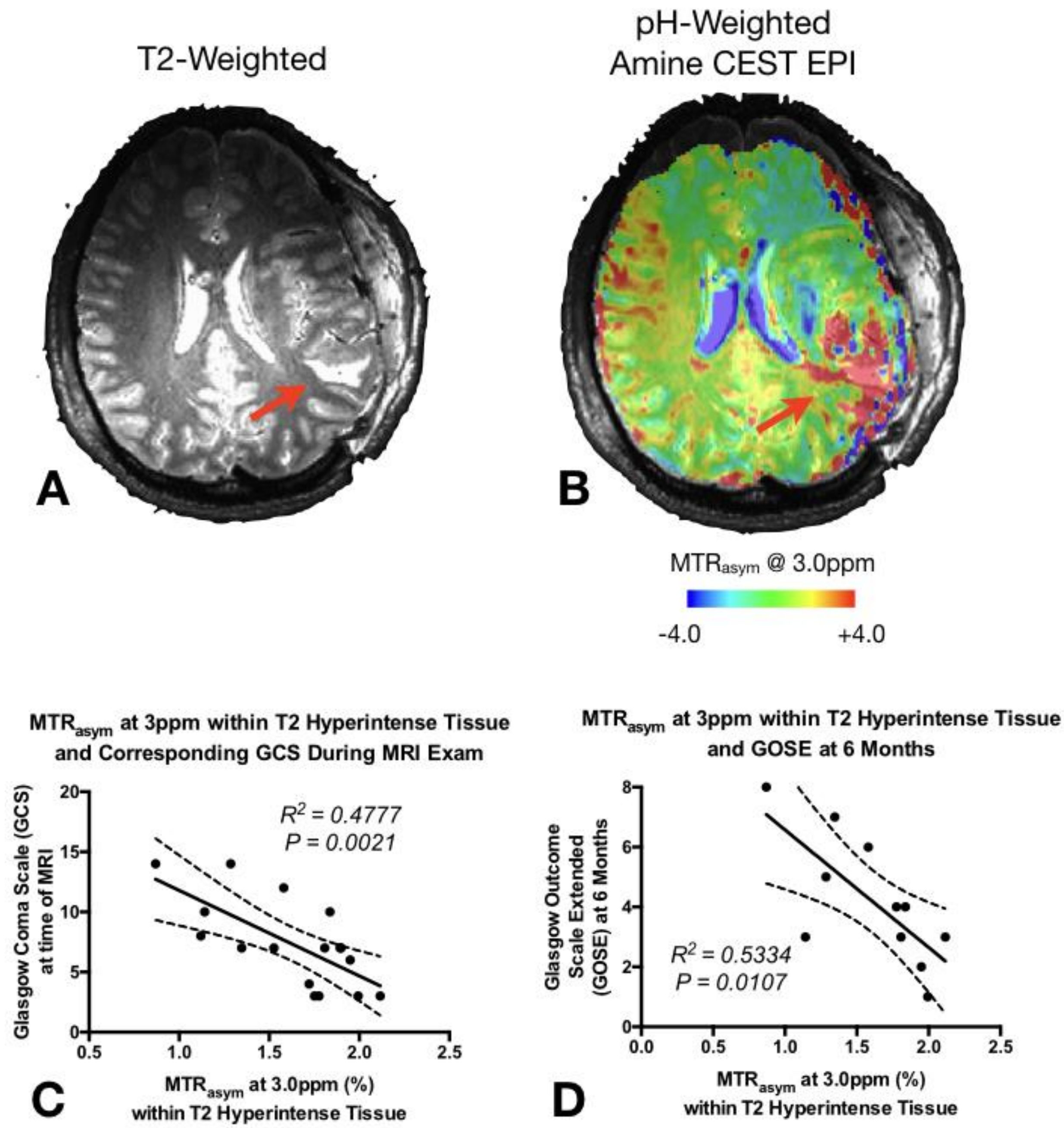

(Filename: TCT_2739_Fig1001.jpg)

2945

1:49PM - 1:56PM

Quantitative Perfusion-Weighted Imaging in Neuroimaging: ASL-PWI & DCE-PWI

R Yoo[1], S Choi[2]
[1]SEOUL NATIONAL UNIVERSITY HOSPITAL, SEOUL, Seoul, [2]Seoul National University Hospital, Seoul, Seoul

Purpose
To explore the utility of 2D FSE Multi- Dynamic, Multi-Echo (MDME) sequence for quantification of myelin content in mild traumatic brain injury (mTBI) patients with post-concussion syndrome (PCS).
Materials and Methods
Forty-one consecutive patients with PCS after mTBI and 29 controls, who had undergone MR imaging including Multi- Dynamic, Multi-Echo (MDME) sequence at our institution between October 2016 and April 2018, were included in this retrospective study. Myelin maps were derived from the MDME sequence using a dedicated software. After performing 3D T1-based brain segmentation with the FreeSurfer software package, mean myelin percentage and total myelin volume were analyzed at bilateral cerebral white matters, bilateral cerebral gray matters, corpus callosum, and brainstem. The Mann-Whitney U-test was performed to compare mean myelin percentage between mTBI patients and controls. Total myelin volume was correlated with neuropsychological test scores in mTBI patients using Spearman rank correlation test.
Results
The mean myelin percentage at bilateral cerebral white matters was significantly lower in mTBI patients with PCS than in controls (median, 25.2 [interquartile range (IQR), 22.6-26.4] vs. median, 26.8 [IQR, 25.6-27.8]; P=.004). Myelin percentages at bilateral cerebral gray matters, corpus callosum, and brainstem did not significantly differ between the two groups. The total myelin volume at bilateral cerebral white matters had borderline correlations with card sorting test (perseverative response) (r = 0.369; P = .063), VLT (delayed recall) (r = 0.373; P = .061), and VLT (delayed recognition) (r = 0.36; P = .071).
Conclusions
Myelin percentage, calculated from 2D FSE Multi- Dynamic, Multi-Echo (MDME) sequence, was significantly lower in mTBI patients with PCS than in controls. Total myelin volume at bilateral cerebral white matters had borderline correlations with neuropsychological test scores in the patients.

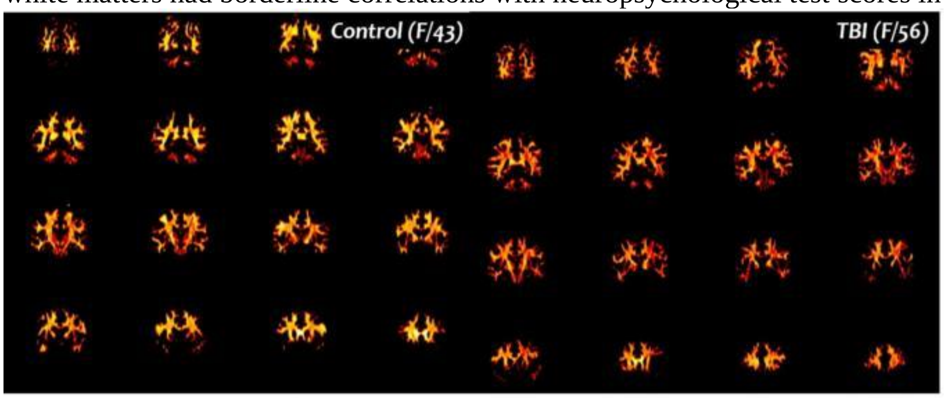

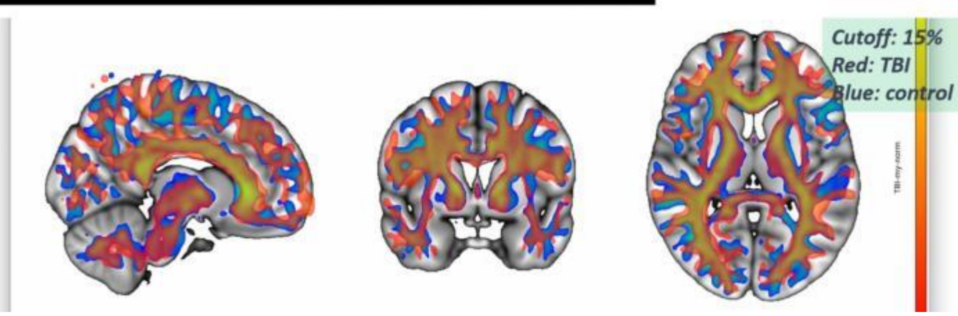

(Filename: TCT_2945_Picture11.jpg)

2805

1:56PM - 2:03PM

Resting-State fMRI Brain Connectivity Alterations in Subacute Post-Concussive Visual Motion Sensitivity

A Trofimova[1], V Ahluwalia[2], P Frias[1], C Foster[1], C Appleberry[3], R Gore[3], J Allen[1]
[1]*Emory University, Atlanta, GA,* [2]*GSU/GT Center for Advanced Brain Imaging, Atlanta, GA,* [3]*Shepherd Center, Atlanta, GA*

Purpose
Patients with subacute post-concussive visual motion sensitivity (PCVMS) frequently report symptoms in complex visual environments1,2. The purpose of this study was to define the alterations in functional connectivity in subacute PCVMS using resting-state fMRI (rs-fMRI).
Materials and Methods
Prospective IRB approved study. Study group: 9 subjects with subacute (2-10 weeks) PCVMS; control group: 8 age-matched subjects without history of concussion or vestibular impairment. Both groups underwent clinical vestibular assessment. Exclusion criteria: age younger than 18 or older than 50, peripheral vestibular dysfunction, moderate or severe TBI, seizure disorder, CNS surgery, peripheral neuropathy, developmental delay, drug/alcohol use chronic or in the last 24 hours. MRI was acquired on 3.0 T Siemens Trio,12-channel head coil. Whole brain rs-fMRI was performed with the following parameters: 3x3x3.5 mm3 resolution; TR/TE=2000/30 ms, flip angle=90°, acquisition time 10 min. Subjects were instructed to lie quietly with their eyes open and relax, to engender a neutral affective and attentional state. rs-fMRI data analysis included standard pre-processing after which group-level independent component analysis (ICA) via FSL MELODIC3,4 was performed. MELODIC can pick out different resting state networks (RSN) and artefactual components without any explicit time-series model being specified. Group differences between RSNs of interest were calculated using the 'dual regression' method. The resultant group difference maps were corrected for multiple comparisons using family-wise error correction ($p<0.05$).
Results
Patients with PCVMS demonstrated significantly more abnormalities on Vestibular/Ocular-Motor Screening (a quantitative measure of vestibular function) in comparison to controls. Using group-level ICA, regularly reported resting state networks (RSN) such as the default mode network (DMN) were identified. We also identified an RSN that included vestibular and somatosensory areas. In comparison to controls, patients with PCVMS had significantly increased connectivity between DMN and a focus in the right frontal eye field (right middle frontal gyrus), between DMN and foci in the right post-central gyrus, and between vestibular/sensorimotor network and a focus in the right frontal pole.
Conclusions
While alterations in DMN have been previously seen in patients with concussion5, patients with PCVMS have abnormal increased connectivity between the frontal eye field and DMN suggesting a pathologic link between oculomotor function and attention to external stimuli. In addition, patients with PCVMS also have increased connectivity between the right frontal pole and the vestibular network that may represent over-weighting of input into the primary vestibular cortex, even at rest. To our knowledge, this is the first report of abnormal resting functional connectivity in patients with PCVMS, which supports our hypothesis of potentially maladaptive post-concussive plasticity underlying PCVMS symptoms.

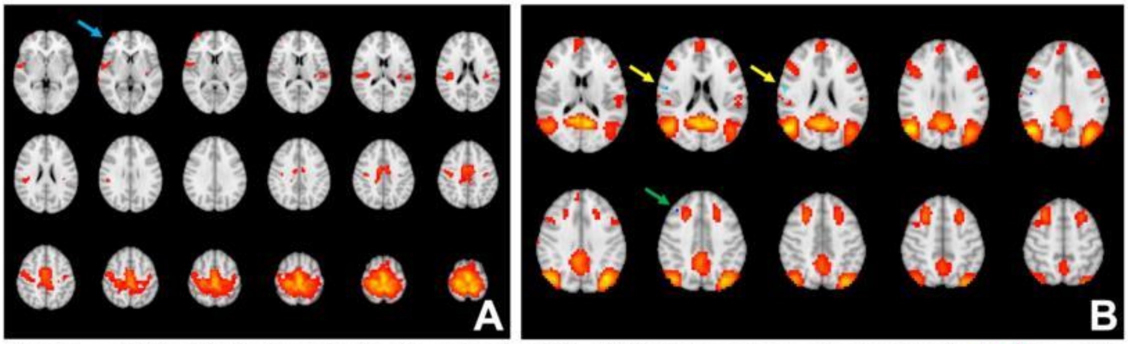

Figure 1. rs-fMRI activation in patients with subacute PCVI. (A) Vestibular and sensorimotor networks (**red**) are easily identified. Selective significantly increased connectivity between these networks and a focus in the right frontal pole (**blue arrow**; 44,46,4; p=0.042) is seen in patients with PCVI compared to controls. (**B**) Robust activation is seen within the DMN (**red**). Selective significantly increased connectivity is present between the DMN and a focus in the right eye field (**green arrow**; 37,30,40, p=0.046) as well as between the DMN and foci in the right post-central gyrus (**yellow arrow**; 50,-14,32; p = 0.043 and 59,- 6,2; p = 0.013) in patients with PCVI compared to healthy controls.

(Filename: TCT_2805_rs-fMRIFigure1.jpg)

3055

2:03PM - 2:10PM

Subcallosal Hemorrhage as a Sign of Diffuse Axonal Injury in Patients with Traumatic Head Injury.

S Chakraborty[1], A Guarnizo[2]
[1]The Ottawa Hospital, Ottawa, Ontario, [2]UNIVERSITY OF OTTAWA, THE OTTAWA HOSPITAL, OTTAWA, ON

Purpose
Diffuse axonal injury (DAI) develops due to rotational acceleration forces and differences in motion of some regions of the brain causing shearing strain with respect to the adjacent region. The corpus callosum is frequently injured due to its rigid attachment to the falx and its relation to the more mobile cerebral hemispheres. The purpose of this research is to identify the relationship between the subcallosal hemorrhage and the degree of diffuse axonal injury.
Materials and Methods
A retrospective review of CT scans of patients with traumatic head injury performed from January 1, 2012 to December 31, 2017 was conducted using the key words: diffuse axonal injury, DAI. Patients were divided in subcallosal hemorrhage positive or negative groups. The relationship between the subcallosal hemorrhage and the presence of DAI grade on CT and subsequent brain MRI was established. The modified ranking scale (MRS) was obtained for clinical follow-up.
Results
1150 patients were found with the search criteria, a total of 301 patients with history of head injury and imaging findings positive on CT and/or MRI for diffuse axonal injury were enrolled, 17 patients were excluded due to incomplete data, 20% (n=61) of the patients with DAI were positive for subcallosal hemorrhage on CT, 24% (n= 15) showed isolated subcallosal hemorrhage. In the positive group 52% showed severe (<8) initial GCS, in the negative group 42%. The most frequent degree of DAI was grade

2 (53%) in the positive group, in the negative group was grade 1 (56%). In the clinical follow up 37% of the patients in the positive group showed good clinical outcome, in the negative group 72%.
Conclusions
The subcallosal hemorrhage is a sign that could predict DAI grade 2 or 3 in patients with traumatic head injury.

3586

2:10PM - 2:17PM

Subdural Effusion/Hygroma (SDEH) as the Patho-Anatomic Basis for Traumatic Meningeal Enhancement (TME)

J Butman[1], M Cota[2], D Pham[3], L Latour[2]
[1]Clinical Center of the NIH, Bethesda, MD, [2]NINDS/NIH, Bethesda, MD, [3]Center for Neuroscience and Regenerative Medicine, Bethesda, MD

Purpose
Traumatic meningeal enhancement (TME) is seen with high conspicuity on post contrast Fluid Attenuated Inversion Recovery (FLAIR) MRI. Recently, TME has been recognized as a surprisingly common manifestation of head trauma [1,2]. Because the MRI findings of TME share features of the subdural enhancement seen in CSF hypovolemia/hypotension, we hypothesized that TME represents the acute development of a post-traumatic subdural effusion or subdural hygroma. Therefore, we sought to directly demonstrate separation of arachnoid from the dura in patients with TME using a fast high resolution BFFE sequence inserted into an acute imaging protocol.
Materials and Methods
Patients presenting with acute head trauma (n=42) were enrolled in an IRB approved study to perform a research MRI within 48 h of injury. This MRI included both pre- and post-contrast FLAIR and balanced fast field echo (BFFE) sequences. The 3D BFFE was adjusted to provide whole head coverage, high resolution (0.5 mm isotropic) rapidly (imaging time 180 s), as completion of the MRI within 30 minutes was a requirement of the IRB approved study. Pre- and post-contrast FLAIR with a gadolinium based contrast agent (GBCA) was used to assess for TME. TMR was identified as high signal along the dura seen on post contrast FLAIR without extension into the subarachnoid space. High signal on pre-contrast FLAIR in a similar distribution was considered evidence of subdural hematoma (SDH). BFFE was used to assess for subdural effusion/hygroma (SDEH) which was identified as a separation of the subarachnoid membranes from the inner table of the skull at locations initially identified with TME. Such visualization was possible using BFFE due to the combination of high spatial resolution (~500 µm isotropic) and high image contrast between CSF (high signal) and arachnoid membranes (low signal).
Results
Interpretable and complete data was obtained in 36 cases. TME was present in 12 of 36 cases (33%). TME was highly associated with the presence of SDEH ($p<0.001$, Fisher's exact test). In total, 10 of the 12 cases (83%) showed SDEH co-localizing with the site of TME (figure) Of the remaining two cases, one was complicated by a SDH, possibly obscuring the SDEH, and one was relatively small and confined to the falx.
Conclusions
Using high resolution BFFE sequences to directly visualize separation of the subarachnoid membranes from the dura of the inner table of the skull, we have shown a clear anatomic correspondence of TME and SDEH. Normally the blood brain barrier of the pia-arachnoid prevents the diffusion of GBCA into subarachnoid space, so that there is no enhancement of the CSF in the subarachnoid space which remains dark on both pre and post contrast FLAIR. However, this barrier does not exist for the dura. Normally, the subdural space is a non-existent "potential" space, so that the GBCA which permeates the interstitial space of the dura remains confined to the dura. TBI may cause a traumatic separation of the arachnoid from the dura, widening the subdural space. The fluid that fills this space is contiguous with the

interstitial space of the dura, hence the term "subdural effusion". Because the fluid of the effusion represents a transudate of the interstitial fluid of the dura, GBCA may freely diffuse into this space and result in the phenomenon of TME. Such injuries may represent the milder end of a spectrum of meningeal injury, with subdural hematoma representing a more severe injury, or simply the coincidence of a subdural vascular injury with the meningeal injury.

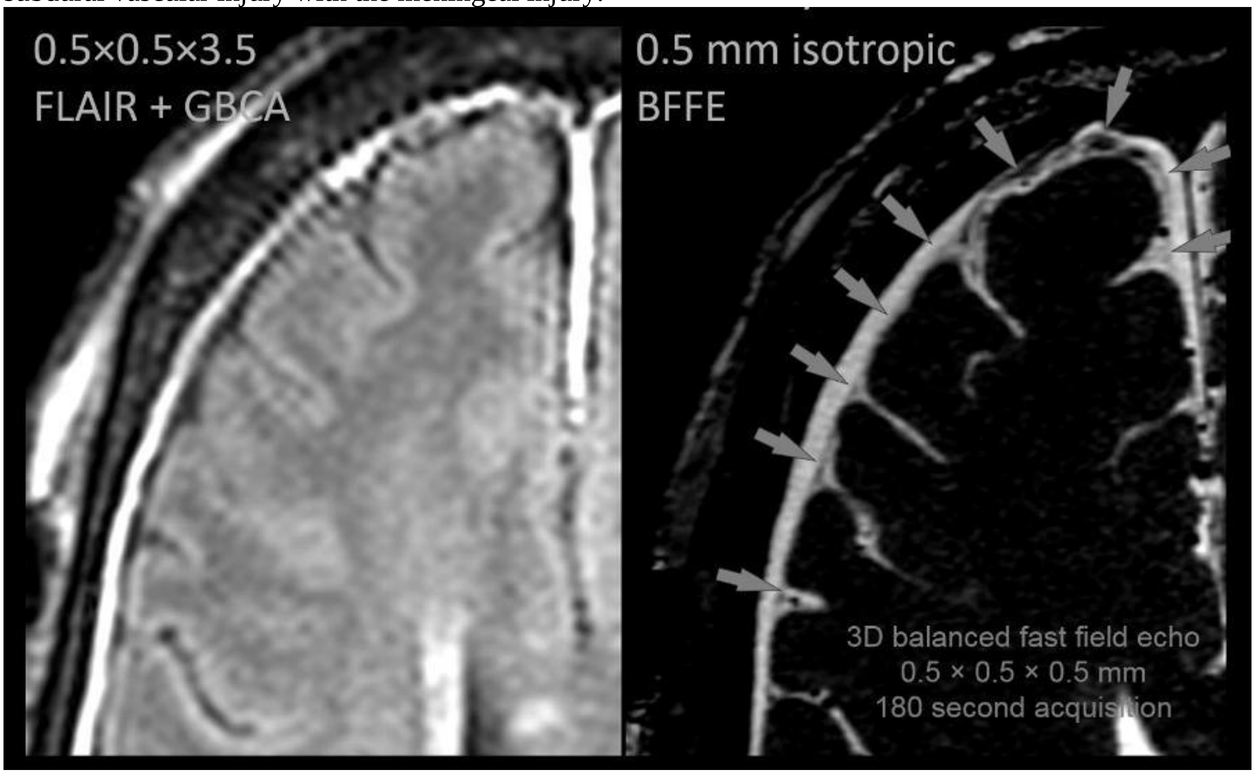

(Filename: TCT_3586_2018ASNRTME.jpg)

2344

2:17PM - 2:24PM

Thrombectomy for Acute Ischemic Stroke in Nonagenarians Compared to Octogenarians

J Heit[1], B Martin[2], D Marcellus[2], E Sussman[2], M Mlynash[3], R Dodd[2], H Do[4], M Lansberg[1], G Albers[5], M Marks[6]
[1]Stanford, Stanford, CA, [2]Stanford University, Stanford, CA, [3]Stanford, Palo Alto, CA, [4]Stanford Univ Medical Center, Menlo Park, CA, [5]Stanford University Medical Center, Palo Alto, CA, [6]Stanford Univ. Med. Ctr., Stanford, CA

Purpose
Thrombectomy leads to improved outcomes in patients with acute ischemic stroke (AIS) due to large vessel occlusion (LVO). Thrombectomy is beneficial in octogenarians (age 80-89), but thrombectomy effectiveness in nonagenarians (age 90-99) remains uncertain. We compared thrombectomy efficacy in octogenarians and nonagenarians.
Materials and Methods
We performed a retrospective cohort study of all thrombectomy patients at our neurovascular center. Inclusion criteria were: LVO, core infarct <70mL based on DWI or CBF<30% on CT-perfusion-weighted imaging, target mismatch between core and penumbra, age 80-99 years. Patients were grouped by age into octogenarians (age 80-89) and nonagenarians (age 90-99). Primary outcome was ordinal score on the

modified Rankin Scale at 90-days. Secondary outcomes included successful revascularization, symptomatic reperfusion hemorrhage, and mortality.
Results
97 patients met inclusion criteria: 70 octogenarians (72%) and 27 nonagenarians (28%). Median octogenarian age was 84 (IQR 82-86) versus 92 (IQR 91-93) in nonagenarians. Nonagenarians were more likely to be female (85% vs. 59%; p=0.02). There were no other differences in demographics, medical comorbidities, LVO location, presentation NIHSS, intravenous tPA administration, or time of thrombectomy treatment. Presentation infarct core and penumbra volumes were similar between these groups. Median mRS at 90-days was 5 in octogenarians and 6 in nonagenarians (p=0.2). The frequency of independence at 90-days (mRS≤2) was similar between octogenarians (13%) and nonagenarians (18%; p=0.7). Mortality was 64% in nonagenarians vs 43% in octogenarians (p=0.1). Reperfusion (TICI IIB-III) after thrombectomy was achieved in 20 (74%) nonagenarians and 53 (76%) octogenarians (p=1). Symptomatic intracranial hemorrhage after thrombectomy occurred in 6 (22%) nonagenarians and 6 (9%) octogenarians (p=0.03).
Conclusions
Thrombectomy results in similar reperfusion rates and clinical outcomes in nonagenarians and octogenarians, but symptomatic intracranial hemorrhage is more common in nonagenarians. However, overall rates of favorable outcome are low in these groups.

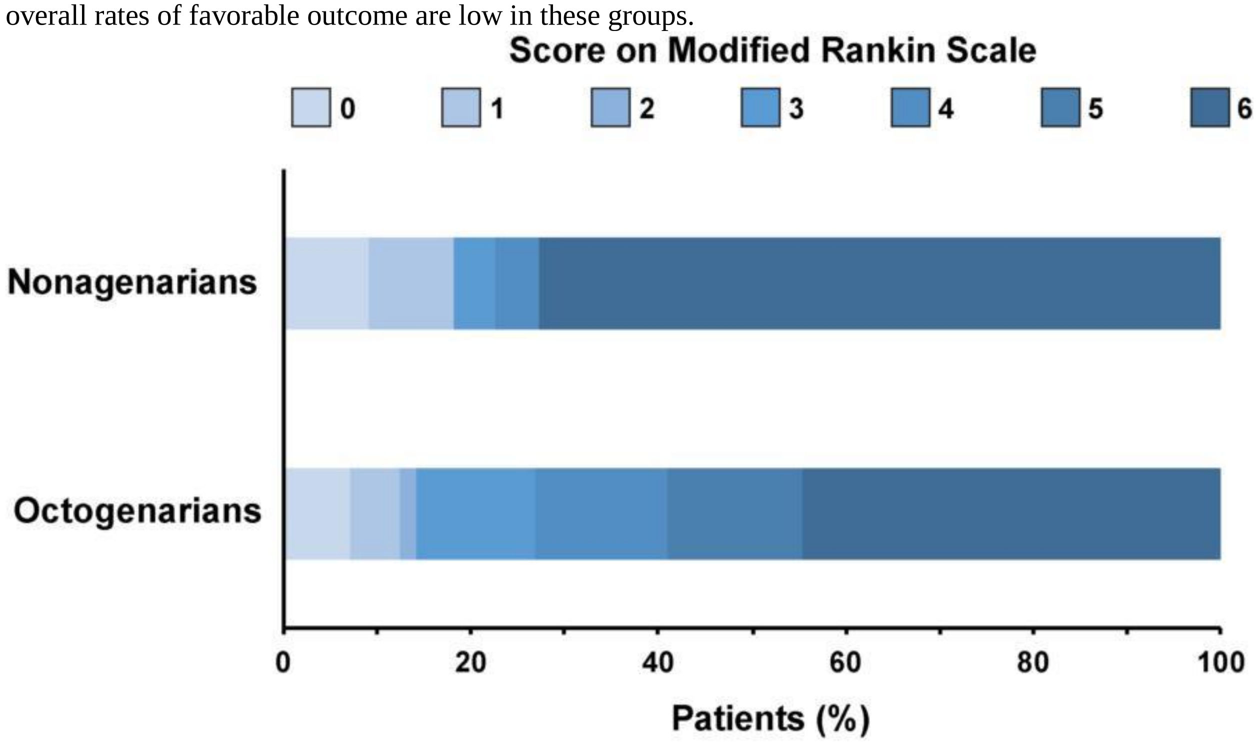

(Filename: TCT_2344_mRSFigure.jpg)

3625

2:24PM - 2:30PM

Variations in Blunt Trauma of the Head, Spine and Facial Injury Patterns in Elderly Patients

K Foryoung[1], A Malhotra[2], D Nuñez[3]
[1]Yale, Hamden, CT, [2]YALE UNIVERSITY SCHOOL OF MEDICINE, NEW CANAAN, CT, [3]Brigham & Women's Hospital/Harvard Medical School, Boston, MA

Purpose
- Establishing a variation in injury patterns in the setting of blunt trauma in Elderly patients (greater than

65 years old) - Examining variations in the mechanism of blunt trauma injury, differences in CNS anatomy and physiology and other ancillary factors which explain these injury variations

Materials and Methods

Trauma CT Scans of the brain, face and cervical spine of adults performed in the Emergency Department between 2014 and 2015 were retrieved from the electronic medical records. Studies with critical findings were selected and the images, reports and associated medical record were manually reviewed. Clinical history of pertinent ancillary findings were also listed. Data was stratified into two age groups for analysis; 18-65 and greater than 65. The following parameters were evaluated: Fractures (head, spine and face); hemorrhage (type and anatomic location) and collateral factors.

Results

Our initial results for total of 384 studies with patients above the age of 65 and 518 studies with patients aged between 18 and 65 with critical results were identified for manual review. Only 37% of the 18-64 years old met the inclusion criteria (194) and 57% of the 65 year old and older (217). For patients Greater than 65 years old: - The most common traumatic bleed above the age of 65 was an acute subdural bleed which occurred 26% of the time. - The predominant cranial area of fracture was the face in 30% of all studies above 65. - High velocity mechanisms of injury in the elderly were present in only 6% of the cases. - Diffuse axonal injuries, parenchymal hemorrhage and arterial epidural collections were rare. For patients 18-64 years old: - While epidural and subarachnoid hemorrhage remained a relatively rare finding in the younger age group, the preponderance of subdural hemorrhages decreased to 12.3%. - Similarly, high velocity injury mechanisms occurred about 10% of the time and a second predominant mechanism of injury, assault, occurred 12% of the time.

Conclusions

The elderly suffer specific injury patterns closely associated with their typical mechanisms of injury and anti-coagulation state.

Wednesday, May 22, 2019
2:55PM - 4:25PM
Brain Tumors: Post-Treatment Imaging

2978

2:55PM - 3:02PM

Assessing Glioblastoma Therapy Mediated Inflammatory Pseudoprogression with Delayed Ferumoxytol Iron Oxide Enhanced Magnetic Resonance Imaging In a Pre-Clinical Rat Model

R Barajas[1], R Woltjer[2], S Han[3], L Muldoon[3], E Neuwelt[3]
[1]*OREGON HEALTH & SCIENCE UNIVERSITY, PORTLAND, OR,* [2]*OREGON HEALTH & SCIENCE UNIVERSITY, Portland, OR,* [3]*Oregon Health & Science University, Portland, OR*

Purpose

Neuroinflammation plays a critical role in the response of glioblastoma (GBM) to temozolomide-based chemoradiotherapy (CRT). Progressive enhancement on gadolinium enhanced magnetic resonance imaging (Gd-MRI) is a manifestation of inflammation mediated therapeutic response (pseudoprogression; Psp)(1). Diagnosing Psp is critical as significantly prolonged survival suggests an effective therapeutic regimen. Unfortunately, Psp cannot be differentiated from recurrence by Gd-MRI. A preclinical animal model of Psp that specifically induces neuroinflammation is a critically unmet need. Macrophage infiltration plays a role in treatment-mediated Psp, and can be induced by Amphotericin B (Amp B)(2). Macrophage influx is noninvasively assessed by 24 hour delayed iron oxide nanoparticle Ferumoxytol-enhanced MRI (Feraheme®) (Fe-MRI)(3). The purpose of our study was to develop Fe-MRI as a biomarker of macrophage response to CRT in GBM.

Materials and Methods
Adult female athymic nude rats underwent intracerebral U87 GBM xenograft placement. Pre-therapeutic Gd-MRI (Gadodiamide, 70 mg/kg) was performed 7-10 days afterwards. Three treatment groups were studied; 1) control (N= 5), 2) CRT only (irradiation [5 Gy] and temozolomide [20 mg/kg, PO x1] (N=4), or 3) CRT with Amp B (0.2 mg/kg, IP QD x 3-7 days) (N=4). Post-therapeutic Gd- and Fe-MRI (ferumoxytol, 25 mg/kg IV) was performed 3 days following therapy. 7 day post-therapy Gd-MRI was performed to establish treatment efficacy. Semi-automated enhancement segmentation was performed with Horos software(4). Significance was evaluated using Students T-test with unequal variances.
Results
The ratio of Fe- to Gd-MRI enhancing volume at the 3 day time point was found to be significantly elevated within the CRT with Amp B group (1.8 +/- 0.77) when compared to the CRT alone (0.62 +/- 0.11; P=0.05) and control groups (0.43 +/- 0.11; P= 0.04) (Figure 1). The ratio of Gd-MRI volumes (post-/pre-therapy) tended to be elevated at the 3 day time point within the CRT (0.95 +/- 0.24) and CRT with Amp B (1.02 +/- 0.45) groups when compared to controls (0.89 +/- 0.38), however, this did not reach statistical significance (P= 0.78 and 0.79). At the 7 day post treatment time point, the ratio of Gd-enhancement was significantly decreased within the CRT with Amp B group (0.87 +/- 0.13) when compared to CRT alone (0.38 +/- 0.04; P< 0.01).
Conclusions
Preliminary results suggest that our treatment paradigm tend to replicate the Fe-MRI characteristics of Psp5. Fe- to Gd-MRI enhancement ratio may serve as a GBM Psp imaging model by capturing the modulatory effects of Amp B. Finally, we present preliminary data that CRT combined with Amp B increases tumor therapeutic efficacy that is only captured by dual Fe- and Gd-MRI at the 3 day post therapy time point.

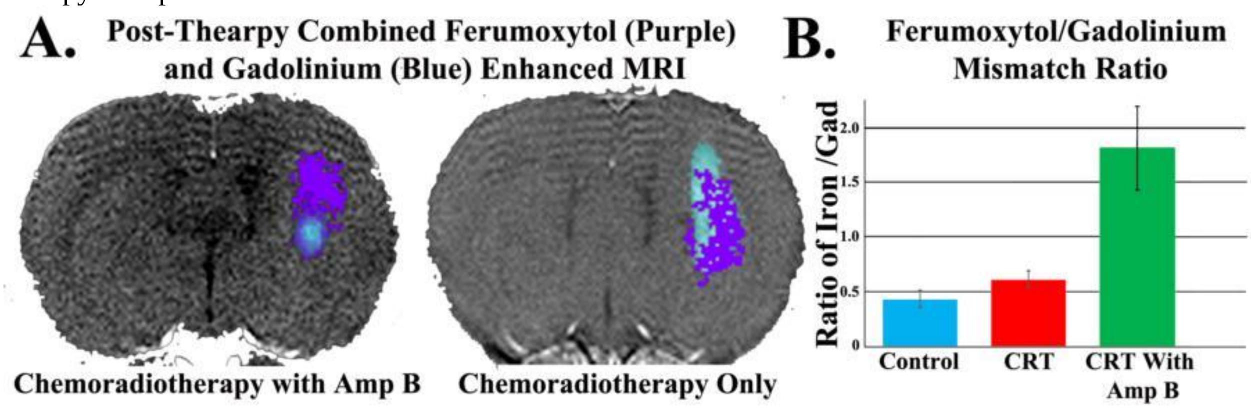

(Filename: TCT_2978_Figure1.jpg)

2383

3:02PM - 3:09PM

Assessing the Utility of Advanced DWI-MRI Parameters Using Multi-B Values Acquisition and a Histogram Approach for Assessment of Early Therapeutic Response in Glioblastoma

S Islam[1], M Morrison[1], A Waldman[2]
[1]Imperial College London, London, United Kingdom, [2]Univeristy of Edinburgh, Edinburgh, United Kingdom

Purpose
Imaging biomarkers to assess early treatment response in gliomas are important for guiding optimal clinical decision-making for individual patients, and as platforms for multi-institutional clinical trials of novel therapies. Current Response Assessment in Neuro-Oncology (RANO) criteria, rely on subjective, semi quantitative measurements with limited sensitivity and specificity in the early treatment phase.

Previous diffusion imaging studies have indicated early sensitivity to treatment response, however optimum acquisition and analysis approaches have yet to be established. The purpose of this study is to assess the utility of advanced quantitative diffusion MRI derived from multi B-value acquisitions in the assessment of treatment response, using a spatially independent approach.

Materials and Methods

We used least-square fitting to model six diffusion parameters from mono-, bi-, and stretch-exponential models, and performed a histogram analysis of voxels located within ROIs defined by enhancing tumour and increased signal on FLAIR sequences. Histograms were generated for 20 patients with GBM at 3 time-points before, at 6 weeks, and 3 months treatment with standard-of-care regimen (RT with concomitant and adjuvant temozolomide). Changes in the histogram percentile profiles were evaluated across the various time-points, back-projected onto MRI images for spatial correspondence, and compared with RANO assessment from structural MRI at the latest timepoint.

Results

Percentile profiles changed over the course of therapy, reflecting known biological changes in the tumour microenvironment in response to radiotherapy and chemotherapy.

Conclusions

These preliminary data suggest differential changes in diffusion parameters early in treatment. Spatially-independent diffusion parameter comparisons abrogate the confound of voxel misregistration due to tumour growth/shrinkage. Further assessment of this dataset, augmented by on-going patient recruitment across multiple centres, will provide insight to the prognostic value of advanced diffusion MRI as a standardized method for treatment response assessment.

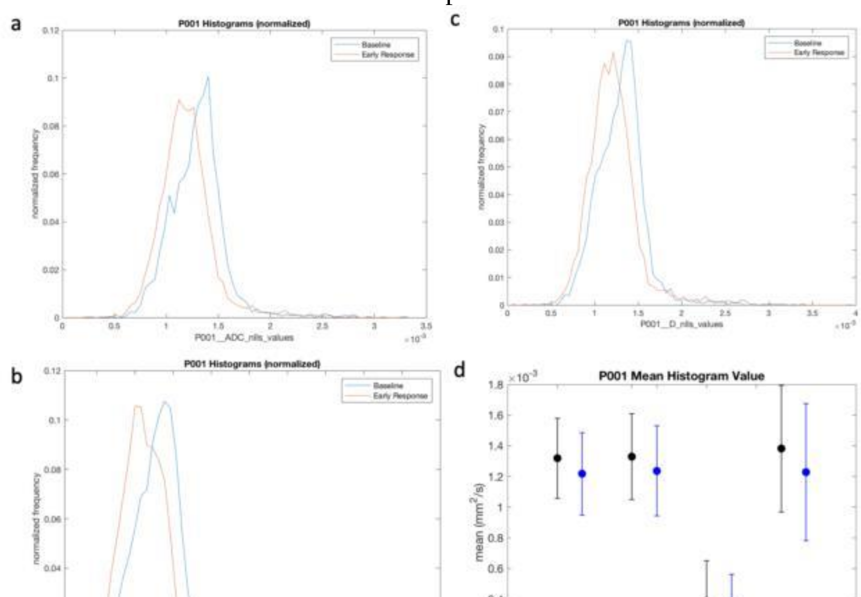

Figure 1- shows histograms of different diffusion parameters within abnormal FLAIR regions of interest in patients with resected GBMs at two time points; baseline (blue) and Mid treatment (red). (a) ADC histogram calculated using a mono-exponential, (b) DDC histogram from the stretched exponential model and (c) D histogram from a bi exponential model. (d) Shows the mean histogram changes for each model. The mid treatment histograms all show a shift to the left in keeping increased cellularity and progressive disease which was confirmed against RANO criteria following completion of treatment. This is an example of how histogram analysis can detect progressive disease sooner than conventional MRI.

(Filename: TCT_2383_Screenshot2018-11-04at222818.jpg)

2457

3:09PM - 3:16PM

Effect of Immune Checkpoint Inhibitors on MR Perfusion in Recurrent Glioblastoma

p aouad[1], S Prakkamakul[2], C Cankurtaran[3], A Korutz[4], B Liu[5]
[1]northwestern university, chicago, IL, [2]King Chulalongkorn Memorial Hospital the Thai Red Cross Society, Chulalongkorn University, Bangkok, Thailand, [3]Einstein Healthcare Network, Philadelphia,

PA, [4]Northwestern University, Feinberg School of Medicine, Chicago, IL, [5]Northwestern University Feinberg School of Medicine, Chicago, IL

Purpose
To understand perfusion effect of immune checkpoint inhibitor (ICI) therapy in recurrent glioblastoma. An animal study has shown that increased tumor vessel perfusion by immune checkpoint blockade is positively correlated with its therapeutic efficacy. We sought to determine 1)CBV change in tumor before and after ICI treatment 2) relationship of MR perfusion (MRP) to conventional MRI and clinical course using iRANO.
Materials and Methods
An IRB-approved, HIPAA-compliant, retrospective study in 14 glioblastoma patients who underwent dynamic-susceptibility contrast MRP at 1.5 or 3 Tesla before and after the initiation of ICI between April 2015 to September 2018 was performed. Seven patients who received concurrent other therapies were excluded. A total of 7 patients were analyzed (mean age±SD; 51±14). IDH mutation, MGMT status, Karnofsky clinical performance status, steroids use, types of ICI were recorded. Two neuroradiologists independently placed 4 ROIs within the recurrent glioblastoma and 3 ROIs within normal-appearing white matter (NAWM) to measure signal intensity on rCBV map on pretreatment and post-treatment MRP studies. Discrepancies were resolved by consensus. The highest tumoral rCBV intensity and average rCBV intensity in NAWM were used for modified nrCBV calculation. Modified nrCBV on pretreatment and post-treatment studies were compared using Wilcoxon signed rank test. Tumor response was assessed using iRANO criteria.
Results
All patients showed tumor progression and significantly increased modified nrCBV. The mean and standard deviation of pretreatment and post-treatment modified nrCBV were 2.09±1.07 and 6.36±2.98, respectively ($p<0.018$). Mean time to progression is 64 days. The majority of patients were IDH wild type, MGMT unmethylated, Karnofsky score ≥ 80 and received no/minimal steroid treatment at baseline.
Conclusions
In this cohort of recurrent glioblastoma patients who underwent MRP before and after the initiation of ICI, early progression was seen. Modified nrCBV increased concordantly with iRANO tumor progression.

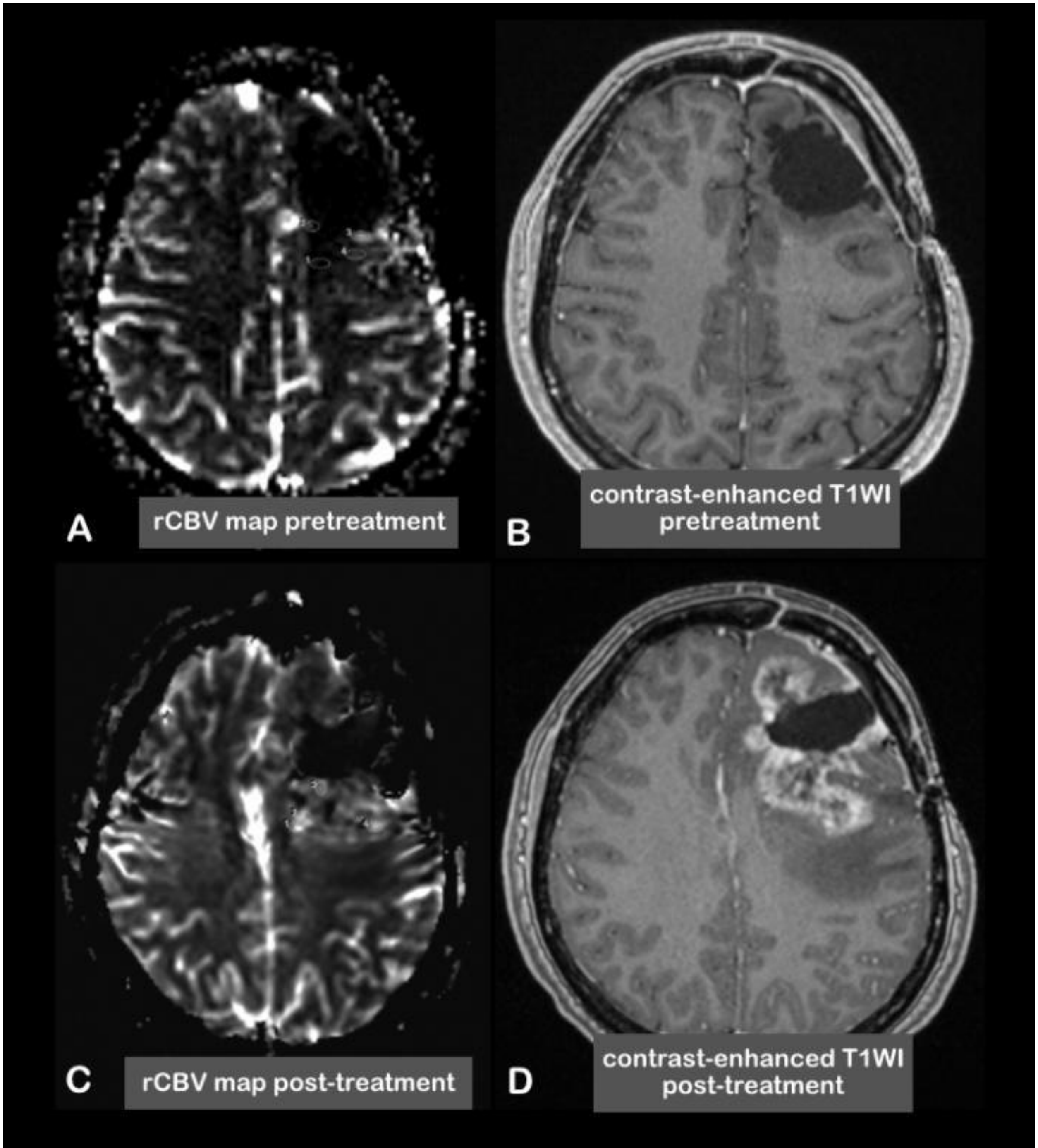

Figure1 exemplifies the location of ROI measurements on rCBV maps in pretreatment (A) and post-treatment (B) MR perfusion study

(Filename: TCT_2457_MRP_ICI_figureforASNR2019abstract1.jpg)

2218

3:16PM - 3:23PM

Enhancement Characteristics of the Brain Tumor Resection Cavity on 3T-MRI: Optimizing the Imaging Window

N Miskin[1], P Unadkat[1], M Carlton[1], A Golby[1], G Young[1], R Huang[1]
[1]*Brigham and Women's Hospital, Boston, MA*

Purpose
To determine the enhancement patterns after brain tumor resection on intraoperative MRI, and early postoperative MRI within 72 hours of surgery, on high field 3-Tesla MRI.
Materials and Methods
We performed a retrospective search for intraoperative post-contrast brain MRI (IO-MRI) in patients post brain tumor resection (N = 66), with a subset with an early postoperative MRI (EP-MRI) performed within 72 hours post-surgery (N = 43), and a subset of patients also with a late post-operative MRI (LP-MRI) available (N=35). Lesion pathology consisted of high-grade glial tumors, low-grade glial tumors, metastases, and vasculitis. Three radiologist readers evaluated the presence of new enhancement on the EP-MRI and LP-MRI studies, and if present, assessed how it change on subsequent EP-MRI or LP-MRI if available by the workflow demonstrated in Figure 1. The consensus assessment for presence of enhancement was determined by the majority response. Inter-rater agreement was assessed percent agreement, given prior work demonstrating erroneous kappa values for binary ordinal data with multiple raters, which this study utilizes.
Results
EP-MRI were performed on average 36 hours post-surgery, with a standard deviation of 11 hours. Agreement was 76% for the assessment of new enhancement on the IO-MRI. Agreement was 82% for the assessment of new enhancement on the EP-MRI. 15% (10/66) of the IO-MRI demonstrated new enhancement. Of those 10 IO-MRI, 7 EP-MRI were available to assess change in enhancement, all of which had either decreased or resolved. 2% (1/43) of the EP-MRI demonstrated new enhancement, performed 49 hours after surgery, which decreased on the LP-MRI.
Conclusions
Based on our data, a study during the 24-48 hour window after surgery is optimal to minimize the likelihood of manipulation-related enhancement. Our findings indicate the opportunity for further study to optimize the postoperative imaging window.

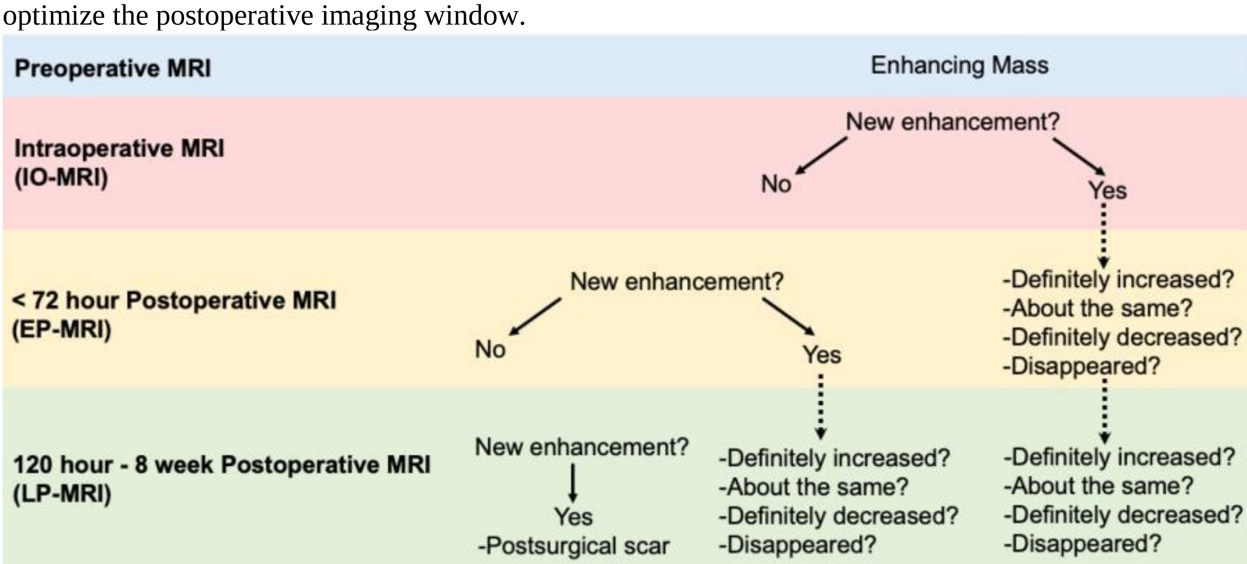

(Filename: TCT_2218_Figure1.jpg)

2993

3:23PM - 3:30PM

Multiparametric MRI for Prediction of Treatment Response in Patients with Recurrent Glioblastoma Treated With Programmed Death (PD)-1 Immunotherapy

J Song[1], P Kadaba[1], A Kravitz[2], A Hormigo[3], J Friedman[1], V Sundaram[4], P Belani[5], C Hadjipanayis[6], A Doshi[7], B Delman[3], K Nael[8]

[1]Mount Sinai Medical Center, New York, NY, [2]Charles E. Schmidt College of Medicine, Boca Raton , FL, [3]Icahn School of Medicine at Mount Sinai, New York, NY, [4]ICAHN SCHOOL OF MEDICINE AT MOUNT SINAI, NEW YORK, NY, [5]MT. SINAI HOSPITAL, NEW YORK, NY, [6]Mount Sinai Hospital, New York, NY, [7]MOUNT SINAI ICAHN SCHOOL OF MEDICINE, NEW YORK, NY, [8]ICAHN SCHOOL OF MEDICINE AT MOUNT SINAI HOSPITAL, NEW YORK, NY

Purpose

Physiologic changes quantified by MR diffusion and perfusion have been used to predict treatment response in patients with glioblastoma treated with cytotoxic (temozolomide) therapy. In this study we aimed to identify whether quantitative changes of MR perfusion and diffusion before and after Nivolumab- immunotherapy can predict treatment response.

Materials and Methods

The inclusion criteria for this retrospective study were: 1) patients with diagnosis of recurrent glioblastoma who were treated with Nivolumab; 2) availability of MR perfusion and diffusion before and after Nivolumab treatment, and 3) follow up MRI up to 6 months from the Nivolumab treatment to determine the final tumor volume and treatment response. Using coregistered images, mean values of the ADC, Ktrans Vp, Ve and CBV were calculated from a volume-of-interest of the enhancing tumor in pre and post immunotherapy scans. Final assignment of stable/improved vs. progressive disease was determined on up to 6-month follow-up clinical and imaging findings using RANO criteria. The trend of imaging biomarkers was compared between stable and progressed patients using Fisher's exact test.

Results

Fifteen patients (8M, 7F, mean age 60.13) met inclusion criteria. Interval time between 2 MRI studies was 2.76 ± 1.09 months. The mean ± SD of enhancing tumor volume were 8.0 +16.2 mL and 5.8 ± 5.7 mL in pre and post Nivolumab scans and 10.1 ± 11.8 mL in final 6-months follow up MRI. Seven patients were determined to have progression and 8 patients remained stable or showed decrease in final tumor volume. The value (mean ± SD) of imaging biomarkers in pre / post Nivolumab therapy were (2.1 ± 1.7 / 1.8 ± 1.1 for CBV), (0.1 ± 0.2 / 0.1 ± 0.1 min-1 for Ktrans), (0.3 ± 0.1 / 0.3 ± 0.2 for Ve), (0.1 ± 0/ 0.1 ± 0.1 for Vp) and (1108.0 ± 376.5 / 1075.3 ± 347.2 for ADC). None of our studied imaging biomarker were able to predict treatment response with statistical significance (table).

Conclusions

Unlike cytotoxic-based treatment, interval changes in ADC, CBV or permeability measures such as Ktrans, Vp, and Ve cannot confidently predict treatment response in patients with recurrent glioblastoma who are treated with Nivolumab. There is potentially a different mechanism and pathophysiology for treatment changes related to PD-1-mediated immunotherapy, which should be considered in interpretation of advanced imaging in clinical trials using Nivolumab.

Table. Sequential ADC, K^{trans}, Ve, Vp, and CBV pattern matched with number of lesions in stable/improved vs. progressive disease.

		Stable/improved ($n = 8$)	Progressive disease ($n = 7$)	Fisher's exact test
ADC	Interval increase	6/8	5/7	p=0.80
	Interval decrease	2/8	2/7	
K^{trans}	Interval increase	1/8	3/7	p=0.28
	Interval decrease	**7/8**	4/7	
CBV	Interval increase	4/8	2/7	p=0.60
	Interval decrease	4/8	5/7	
Ve	Interval increase	2/8	5/7	p=0.31
	Interval decrease	**6/8**	3/7	
Vp	Interval increase	2/8	1/7	p=0.85
	Interval decrease	6/8	6/7	

(Filename: TCT_2993_Table.JPG)

3551

3:30PM - 3:37PM

Mutation Status of IDH and TP53 and Correction of rCBV Derived from MR Perfusion Weighted Imaging in Early Diagnosis of Tumor Progression in Patients with High Grade Gliomas after Chemoradiation Treatment

X Liu[1], W TIAN[2], A hussain[1], H Wang[3]
[1]University of Rochester Medical Center, Rochester, NY, [2]University of Rochester medical Center, Rochester, NY, [3]University of Rochester Medical Cente, Rochester, NY

Purpose
Radiotherapy with concomitant and adjuvant temozolomide after surgical resection is the standard treatment regimen for patients with high grade gliomas (HGGs). Therefore, early diagnosis of tumor progression is critical important for such patients. MR dynamic susceptibility contrast (DSC)-perfusion weighted imaging (PWI) has been widely used in the treatment response evaluation. In this study, we compared the relative blood volume (rCBV) values without and with contrast leakage correction, as well as mutation status of IDH and TP53, in the early diagnosis of tumor progression in patients with HGGs after chemoradiation treatment.

Materials and Methods
We retrospectively reviewed 110 MR DSC-PWI examinations with pathology confirmed or RANO based tumor progression in patients with HGGs after chemoradiation treatment. The rCBV maps without and with contrast leakage correction were generated using FDA-approved GE BrainStat and NordicICE programs. Two neruoradiologists measured the rCBV values and percentage of signal intensity recovery (PSR) in the "hot" ROIs. The difference of maximal rCBV ratio between rCBV without contrast leakage correction and rCBV with contrast leakage correction was compared with Mann–Whitney U test, their association with mutation status of IDH and TP53 was assessed.
Results
The inter-operator analysis between two neuroradiologists showed that the intra-class correlation coefficient (ICC) was 0.917. The mean maximal rCBV ratio of rCBV with contrast leakage correction (2.26±1.88) were significantly higher than rCBV without contrast leakage correction (1.15±1.27, $p<0.001$) of all lesions. There were 42 tumor progression lesions be visible on both rCBV images with and without contrast leakage correction. The other 68 could be visible only on rCBV images with contrast leakage correction, these lesions had significantly higher PSR (1.175±1.4) than those 42 tumor progression lesions (0.77±0.26, $p<0.001$). There was no significant difference of mutation status of IDH and TP53 between these two groups, ($p>0.05$).
Conclusions
The hemodynamic change of tumor progression lesions in patients with HGGs after chemoradiation treatment was underestimated based rCBV images without contrast leakage correction. The rCBV with contrast leakage correction is a useful imaging biomarker for early diagnosis of tumor progression of HGGs, and independent to mutation status of IDH and TP53.

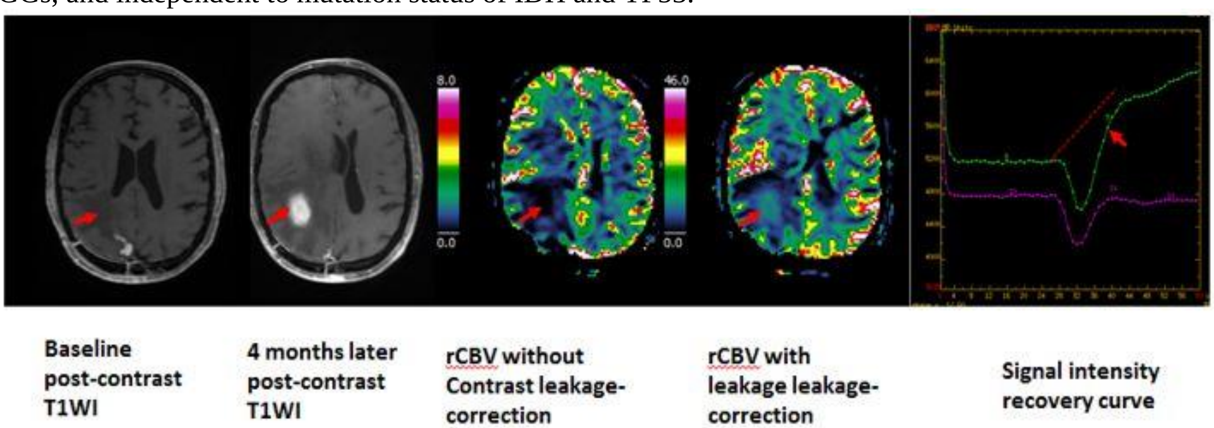

Illustration:

This new nodular enhancing tumor progression lesion in a patient with anaplastic astrocytoma showed higher rCBV value on rCBV image with contrast leakage correction, and high PSR.

(Filename: TCT_3551_XiangliuASNR2019_1.JPG)

2367

3:37PM - 3:44PM

Predictive Value of Magnetic Resonance Spectroscopic Imaging during Anti-angiogenic Treatment in Recurrent Glioblastoma

E Ratai[1], D Kim[2], J Dietrich[3], E Gerstner[3], O Rapalino[3], J He[3], M Vangel[3], M Fu[1], M Wenke[1], I Arrillaga-Romany[3], D Forst[3], A Ovidiu[1], Y Yen[1], J Kalpathy-Cramer[1], B Rosen[4], T Batchelor[3], R Gonzalez[3], E Ratai[1]

[1]*Massachusetts General Hospital, Charlestown, MA,* [2]*Massachusetts General Hospital, Charlesown, MA,* [3]*Massachusetts General Hospital, Boston, MA,* [4]*Athinoula A. Martinos Center for Biomedical Imaging, Charlestown, MA*

Purpose

Glioblastomas are challenging cancers to treat, and long term favorable clinical outcomes in patients with recurrent glioblastoma (rGBM) continue to be difficult to achieve. One of the main characteristics of glioblastoma is the presence of intratumoral neoangiogenesis. Therefore, patients with rGBM are often treated with anti-angiogenic agents such as bevacizumab [1]. Treatment with bevacizumab has shown promise in prolonging progression free survival and improving the quality of life for such patients [2]. However, not every patient with rGBM benefits from anti-angiogenic therapy. Detecting early failure of bevacizumab can protect the patients from potentially toxic and inefficacious treatments and can also divert the medical care costs. MR Spectroscopic Imaging (MRSI) is able to non-invasively provide biochemical information about the microenvironment of a tumor. N-Acetylaspartate (NAA) is considered a neuronal metabolite and is reduced or completely absent in malignant brain tumors. Choline (Cho) is a marker for increased glial proliferation and membrane synthesis, and an elevation of Cho is a hallmark of neoplasms. Lactate (Lac) is produced by enhanced glycolysis, it promotes cancer cell survival and proliferation. Furthermore, Lac may also stimulate angiogenesis and may be a marker for hypoxia. Because the use of bevacizumab is frequently associated with substantial reduction in contrast enhancement on T1-weighted MR imaging, as shown in Figure 1, it is often difficult to distinguish a true favorable tumoral response from pseudo-response using conventional MRI. Preliminary data from the clinical trial RTOG 0625/ACRIN 6677 suggested that MRSI may be a useful modality to predict the efficacy of bevacizumab-based treatment [3]. We here examine whether MRSI is clinically reliable to identify true responders from non-responders.

Materials and Methods

Thirty-five patients with rGBM were enrolled after obtaining informed consents. MRSI datasets were acquired on a 3T Siemens scanner using a LASER (Localized Adiabatic Selective Refocusing) sequence for localization and 3D spiral readout or on a 1.5T GE scanner using a PRESS (Point Resolved Spectroscopy) sequence for localization and 2D phase-encoding. Acquisition parameters for both vendors included TR/TE = 1700/135 ms, voxel size=0.7 – 1.7 cm3, acquisition time = 5-6.5 min. Figure 2 shows an example of a 3D MRSI voxel placement in a subject with rGBM. Collected MRSI data were analyzed using LCModel to quantify metabolites N-acetylaspartate (NAA), Creatine (Cr), choline (Cho), and lactate (Lac) in regions of interest at baseline and subsequent time points. Normalized Creatine (nCr) values were collected by measuring the Creatine level in the contralateral normal white matter. Voxels within enhancing areas were identified by visual inspection using the corresponding T1-weighted post-contrast images. Voxels identified as 'tumor' voxels in the baseline was followed up throughout the visits as previously described [3]. The average metabolite concentrations were calculated from the selected voxels. We then examined the percent changes in the metabolic ratios Cho/nCr, Lac/nCr, Cho/NAA, and Lac/NAA from baseline (pre-treatment) to three subsequent timepoints: 1-3 days, 4 weeks, and 8 weeks after starting treatment. Statistical data analysis was performed using JMP and R. Receiver operating characteristic (ROC) curves for these spectroscopic markers were constructed for a binary outcome, overall survival at 9 months (OS-9) [4]. A marker was considered effective in classification of an outcome status when its lower 95% confidence interval (CI) was at least 0.50.

Results

To date, 17 (12M/5F, mean age 60 ± 13, mean Karnofsky Performance Scale (KPS) 82 ± 8) of the 31 subjects had reached the endpoint of the study for data analysis. All subjects were treated with bevacizumab-based therapy (4 received bevacizumab mono-therapy, 7 received bevacizumab+lomustine, 5 received bevacizumab+temozolomide, 1 received bevacizumab+pembrolizumab). Six of these 17 subjects were alive at 9 months. Cho/NAA changes were chosen a-priori as preliminary data from the clinical ACRIN 6677 trial suggested that Cho/NAA predicted the efficacy of bevacizumab-based treatment [3]. Analysis of the areas under the ROC curves (AUC) revealed that %-Change in Cho/NAA from the baseline to 1-3-days, 4-weeks, and 8-weeks after treatment was predictive for OS-9 (AUC = 0.90 (CI: 0.70 – 1), 0.89 (CI: 0.69 – 1), and 0.97 (CI: 0.87 – 1), respectively). Figure 3 shows that subjects who survived at 9 months had a significant decrease in %-changes of Cho/NAA from the baseline. Thus, Cho/NAA percent changes in the tumor are associated with OS-9. Percent changes in the ratio of Lac/NAA was another marker that showed a significant predictive value at the three time-points (AUC=0.90 (CI: 0.68 – 1), 0.93 (CI: 0.80 – 1) and 0.83 (CI: 0.57 – 1), respectively). As Figure 4 demonstrates, lactate remarkably increased for those patients with poor OS-9 outcomes.

Conclusions

The MRSI data demonstrated that early changes in Cho/NAA and Lac/NAA and can be useful markers for predicting therapeutic response and overall survival in rGBM. The association between decreases in Cho/NAA ratios and positive OS-9 is also in agreement with many previous studies that showed direct links between increases in choline-containing compounds with tumoral recurrence. The increase in lactate concentration associated with worse outcomes may be reflective of true tumoral growth with intratumoral areas of acidosis, glutaminolysis, and hypoxia. Other studies have examined the use of MRSI to monitor the response to anti-angiogenic therapy [3, 5]. However, our additional data shows that MRSI can identify the response earlier than previous reported time points. The ability to predict outcomes with the described changes in Cho/NAA and Lac/NAA ratios demonstrates the potential value of MRSI for monitoring response during treatment with bevacizumab. Future steps include 1) additional subject accrual (In fact, we have enrolled 15 additional patients who have not reached the endpoint of the study (OS-9). 2) Examine the predictive values of MRS towards progression-free survival (PFS). 3) Compare MRSI to other imaging modalities including Dynamic Susceptibility contrast (DSC). And 4) Build statistical classifiers (e.g., Linear Discriminant Analysis) to assess the relative discriminant and predictive capabilities of MRS in combination with other markers.

Fig.1

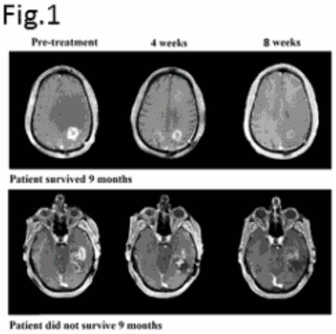

Fig.2

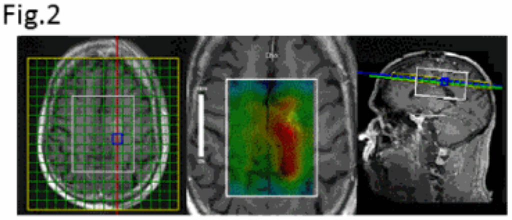

Fig.3

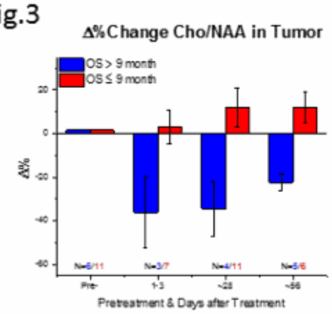

Fig.4

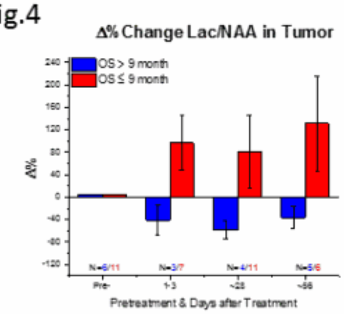

Figure 1. It is challenging to distinguish tumor response and pseudo-response on T1 weighted post contrast MR images. Both patients show a marked reduction in contrast enhancement.

Figure 2. Example of a 3D MRSI in a patient with rGBM.

Figure 3. The relative changes (%) in Cho/NAA separately grouped by the subjects' 9-months overall survival (OS-9) at three subsequent post-treatment time points.

Figure 4. The relative changes (%) in Lac/NAA separately grouped by the subjects' 9-months overall survival (OS-9) at three subsequent post-treatment time points.

(Filename: TCT_2367_Figures.gif)

3393

3:44PM - 3:51PM

Radiotherapy Treatment May Affect Quantitative MRI Assessment of Brain Tumour Treatment Response

H Shuaib[1], L Brazil[2], T Booth[3]
[1]King's College London, London, UK, [2]Guy's and St Thomas' NHS Foundation Trust, London, UK, [3]King's College Hospital NHS Foundation Trust, London, UK

Purpose
Functional diffusion map (fDM) analysis has been shown to be potentially useful in accurately categorising treatment response in glioma patients (1,2). Such fDMs are created using subtracted longitudinal ADC images, which are segmented and thresholded to quantify regions of significant increases and decreases in ADC values. Thresholds demarcating significant change have been defined in the literature by sampling longitudinal changes in contralateral normal appearing brain tissue (NABT) in the patient population that was studied (1,2). A recent publication has shown that the use of contralateral NABT to aid absolute quantification of CBV and CDF values due to radiation induced changes to DSC parameters is inappropriate (3). We have investigated how the radiotherapy dose response of contralateral NABT influences ADC measurements.
Materials and Methods
30 patients with gliomas were included in this study and had undergone an intervention regimen of surgical resection, radiotherapy treatment and temozolomide chemotherapy. In patients, postoperative MRI was performed at approximately quarterly intervals, follow-up scans were excluded if there was presence of significant displacement of contralateral NABT due to the effects of surgery or evidence of pathology in the contralateral hemisphere. The MRI images included in this study for each patient consisted of a high resolution isotropic T1W image and an ADC map. The MRI images were affine registered to the radiotherapy planning CT scan using the FLIRT program published by FSL (4, 5). A mask of the whole brain tissue (including necrotic and tumour tissue) was created using the 3dSkullStrip program published by AFNI. A 3-tissue segmentation was performed on the masked T1W volume using probabilistic tissue segmentation (via the Atropos algorithm). The segmentation was applied to both the RT Dose volume and the ADC map and then each volume was split into hemispheres with the hemisphere containing the pathology being discarded from the data analysis. Each voxel-wise pair from every patient's respective RT Dose and ADC map was then collected into intervals of 2 Gy between 0-10 Gy for final analysis.
Results
The lowest mean ADC value in NABT was measured for tissue that absorbed less than 2 Gy of dose during radiotherapy treatment, whilst the highest value of mean ADC was measured for tissue that absorbed between 8-10 Gy of dose during radiotherapy treatment. A strong, positive correlation can be seen between absorbed dose and ADC measured after treatment.
Conclusions
These findings suggest that the definition of significant change in ADC to create fDMs should not be calculated using NABT in patient data. More generally, attempts in using quantitative diffusion imaging in patients who have undergone treatment, which could affect the diffusivity , globally or in nonpathological areas, would be confounded by the effects of treatment. There is evidence that radiotherapy treatment may affect quantitative MRI parameters such as CBF, CBV and, as presented here, ADC. This could have a negative impact in accurate quantitative assessment of brain tumour patients. A more appropriate method would be to define normal variation in NABT by sampling from a healthy population and only. This change may have a positive impact in improving sensitivity and specificity of fDM analysis in its use in categorising treatment response in glioma patients.

3484

3:51PM - 3:59PM

RSI-Derived Neurite Density Can Differentiate True Progression from Immunotherapy-Related Pseudoprogression

S Daghighi[1], W Tom[2], N Bahrami[3], N Farid[4], C McDonald[3]
[1]University of California, San Diego, San Diego, CA, [2]UNIVERSITY OF CALIFORNIA, SAN DIEGO, SAN DIEGO, CA, [3]University of California, San Diego, La Jolla, CA, [4]UC San Diego Med. Ctr., San Diego, CA

Purpose
In recent years, immunotherapy has increasingly become one of the treatment modalities used in patients with glioblastoma (GBM) following treatment with standard chemoradiation. However, pseudoprogression (PsP) following immunotherapy remains poorly characterized and may delay treatment decisions for up to six months following administration. In this study, we evaluate whether an advanced diffusion imaging model, restriction spectrum imaging (RSI), can differentiate true progression (TP) from PsP in patients with GBM following immunotherapy. Specifically, we evaluate two measures derived from RSI: i.e., "cellularity" (RSI-CELL) and "neurite density" (RSI-ND), which provide surrogate measures of tumor cellularity and peritumoral tissue integrity, respectively.
Materials and Methods
RSI and ADC maps were available for 19 patients with high-grade glioma who were treated with immunotherapy. Fifteen patients received an immunotherapeutic vaccine, while 4 patients received an immune checkpoint inhibitor. Cases were classified as TP if pathology demonstrated recurrent tumor or if death occurred within one year of the MRI demonstrating imaging progression. The remainder of the cases were classified as PsP. Histogram values within regions of contrast enhancement (CE) and FLAIR hyperintensity (FLAIR-HI) were calculated for RSI-CELL, RSI-ND, and ADC. Wilcoxin Rank Sums Tests were used to compare RSI, ADC, and conventional imaging metrics for patients with TP versus PsP. A linear classifier was used to determine which imaging values best classified patients.
Results
Thirteen patients showed TP and six showed PsP. Patients did not differ in their CE or FLAIR volumes. Neither RSI-CELL nor ADC differentiated patients with TP from PsP. Rather, patients with TP showed lower RSI-ND (minimum ND; $p = .036$) in the FLAIR-HI region compared to those with PsP. RSI-ND correctly classified 73.3% of the sample ($p = .042$), with all 6 PsP cases and 8 of 13 TP cases correctly classified.
Conclusions
Lower RSI-ND within the FLAIR-HI region may reflect disruption of tissue microstructure (i.e., tumor infiltration), providing an imaging marker of tumor infiltration in patients with TP.

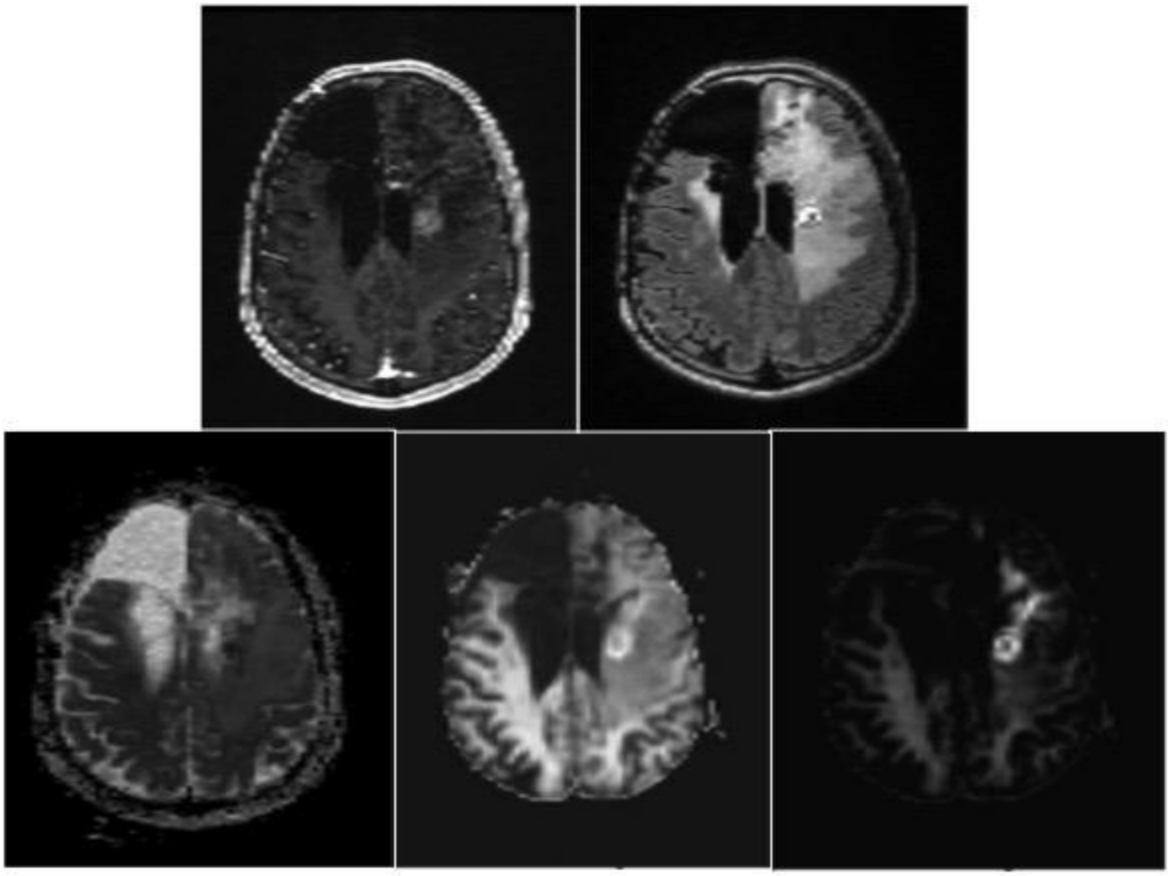

(Filename: TCT_3484_RSIImmunontherapy.jpg)

2738

3:59PM - 4:06PM

Treatment related lesions in Glioblastoma patients treated with Heat Shock Protein vaccine and Chemoradiation.

P Alcaide-Leon[1], T Luks[1], J Lupo[1], M Lafontaine[1], S Chang[1], J Clarke[1], J Villanueva-Meyer[1]
[1]*UCSF, San Francisco, CA*

Purpose
The goal of immunotherapy is the induction of an inflammatory response in the tumor which can mimic tumor progression. Treatment related lesions (TRL) represent a significant dilemma in the management of glioblastoma patients. The presence of centrally restricted diffusion has been recently described as a useful sign to recognize TRL in high grade glioma patients. The aims of this study were, first, to define the incidence of TRL in glioblastoma patients treated with heat shock protein (HSP) vaccine and chemoradiation and, second, to differentiate TRL from true tumor progression by using DWI.
Materials and Methods
Serial imaging was evaluated in 27 newly diagnosed adult glioblastoma patients treated with HSP vaccine and chemoradiation. New or worsening enhancing lesions were classified as TRL or tumor progression based on pathology or evolution on follow-up imaging. Ring-enhancing lesions without blood products were selected for analysis. The ratio between the ADC of the peripheral enhancing area and the ADC of the central non-enhancing region was calculated. Statistical analyses included Mann-Whitney U test and ROC curves.

Results
Nine patients (30%) developed TRL: 4 within 3 months after completion of radiotherapy; 3 at the 3-6 months period; 1 at 8 months; and 1 at 3.5 years. Eight progressive lesions and 8 TRL were included for analysis after exclusion of lesions with blood or without central non-enhancing area. ADC ratio was higher in TRL than in tumor progression (mean ADC ratio of TRL, 1.103 [95% CI, 1.006-1.199]; mean ADC ratio of tumor progression, 0.969 [95% CI, 0.937-1.002]; p=0.028). Area Under the ROC curve was 0.828 and the best cutoff value was 1.060.
Conclusions
TRL are common in patients treated with HSP vaccine and chemoradiation, particularly during the first 6 months after radiotherapy. The periphery/central ADC ratio is useful for differentiation between TRL and tumor progression in patients treated with HSP vaccine.

2597

4:06PM - 4:13PM

Tumor Recurrence versus Radiation Necrosis in Patients with Treated GBM: A Prospective Study Using DCE Perfusion MR

E Portela de Oliveira[1], N Zakhari[2], M Taccone[3], C Torres[4], S Chakraborty[5], J Woulfe[6], G Jansen[5], G Cron[6], N Majtenyi[7], T Nguyen[6]
[1]University of Ottawa - The Ottawa Hospital, Ottawa, Ontario, [2]The Ottawa Hospital/University of Ottawa, Ottawa, ON, [3]University of Toronto, Surgeon-Scientist Training Program, Toronto, Ontario, [4]UNIVERSITY OF OTTAWA, OTTAWA, ON, [5]The Ottawa Hospital, Ottawa, Ontario, [6]The Ottawa Hospital University of Ottawa, Ottawa, Ontario, [7]University of Ottawa, Ottawa, Ontario

Purpose
Glioblastoma (GBM) are aggressive high-grade primary brain tumors that remain with poor outcome and a low rate of long term survival. Post treatment imaging assessment is essential for the evaluation of tumor recurrence and radiation effects. MRI perfusion techniques may become an important tool distinguishing treatment-related changes from recurrent tumors. Objective: To evaluate the diagnostic accuracy of dynamic contrast-enhanced (DCE) MRI in differentiating tumor recurrence and radiation necrosis in patients with a new indeterminate enhancing lesions after standard treatment.
Materials and Methods
Twenty-nine patients with histologically diagnosed GBM who underwent surgery and radiation therapy were prospectively examined at 3.0 T MRI. Dynamic contrast-enhanced (DCE) were performed. Plasma volume (Vp) and volume transfer constant (Ktrans) were estimated from 3 different methods: (1) using a magnitude derived vascular input function (VIF) without T1 measurements; (2) using phase-derived vascular input function (VIF) and T1 mapping using variable-flip angle(VFA), and (3) using phase-derived VIF and T1 mapping using modified Look-Looker inversion (MOLLI). ROIs were placed over the solid part of the tumor and quantitative analysis of the largest area were performed. Patients were classified as having treatment-related changes or recurrent tumors based on pathological results from surgery or from clinical/radiological follow up. Differences in parameters between tumour recurrence and radiation necrosis were assessed by Mann-Whitney U tests. Diagnostic accuracy was assessed by using receiver operating characteristic (ROC) analysis.
Results
The study included 29 patients, progression was determined in 21/29 (72.41%) of indeterminate lesions and radiation necrosis in 8 (27.59%) lesions. Median Ktrans using phase-derived VIF and T1 mapping from MOLLI was x (interquartile range) group of tumor recurrence and y (interquartile range), which was statistically significant p=0.0454). ROC analysis showed a sensitivity of 81% and a specificity of 75% using a Ktrans cutoff of 0.0104 min-1 (p=0.0164).
Conclusions
The study included 29 patients, progression was determined in 21/29 (72.41%) of indeterminate lesions

and radiation necrosis in 8 (27.59%) lesions. Median Ktrans using phase-derived VIF and T1 mapping from MOLLI was x (interquartile range) group of tumor recurrence and y (interquartile range), which was statistically significant p=0.0454). ROC analysis showed a sensitivity of 81% and a specificity of 75% using a Ktrans cutoff of 0.0104 min-1 (p=0.0164).

2324

4:13PM - 4:20PM

Usefulness of MR Spectroscopy in Addition to Perfusion MRI in Differentiating Tumor Progression from Treatment Related Changes in High Grade Gliomas

U Erdenebold[1], N Zakhari[1], T Nguyen[1], M Taccone[2], C Torres[1], S Chakraborty[1], J Woulfe[1], G Jansen[1], G Cron[1]
[1]University of Ottawa, The Ottawa Hospital Civic and General Campus, Ottawa, Ontario, [2]University of Toronto, Surgeon-Scientist Training Program, Toronto, Ontario

Purpose
New enhancement after high grade glioma (HGG) treatment is a common diagnostic dilemma. We evaluated the diagnostic accuracy of MRS in combination with DCE and DSC MR for differentiating tumor recurrence (TR) from radiation necrosis (RN).
Materials and Methods
Prospective consecutive enrollment of HGG patients with new enhancement on post-treatment MR. TR and RN classification was based on histopathology or follow-up. Each patient underwent 3T MR examination including MRS, DCE, and DSC sequences. MRS used 2D or 3D CSI (TE=135) over the enhancement. Hot spot analysis of the perfusion maps was obtained (Olea Sphere 2.3, Olea Medical). Differences in Choline (Cho), N-acetyl aspartate (NAA), creatine (Cr), Cho/Cr, Cho/NAA and NAA/Cr as well as perfusion parameters between TR and RN were assessed via Mann-Whitney U test. Logistic regression analysis and ROC curve analysis were also performed.
Results
Sixty-two lesions had MRS, 36 TR and 26 RN. Significant differences between TR and RN were as follow: MRS: NAA, Cho/NAA and NAA/Cr (p 0.0034, 0.0425, 0.0425); Perfusion: CBV, CBVratio, corrected CBV, corrected CBVratio, AUCratio and VPratio (p= 0.0038, 0.014, 0.0128, 0.0238, 0.0159, 0.0175). After Bonferroni correction NAA (p 0.02) and (CBV (p 0.034) with AUROC 0.72 and 0.71 (p=0.002 and 0.001). The median NAA was higher for RN than TR in cases with high CBV optimal cutoff > 7.07 (13.9 Vs 0.39, p= 0.045) and cases with low CBV <7.07 (24.7 Vs 0.33, p=0.043). On logistic regression a combination of NAA, CBV and AUCratio as well as NAA and AUCratio improved diagnostic accuracy (p < 0.0001 and 0.0005 with AUROC 0.86 (CI 0.74-0.94) and 0.91 (CI 0.81 to 0.97)).
Conclusions
MRS is useful in differentiating TR from RN and the combination of MRS and perfusion improves the diagnostic accuracy. MRS can be useful in identifying RN with increased perfusion and TR with low CBV.

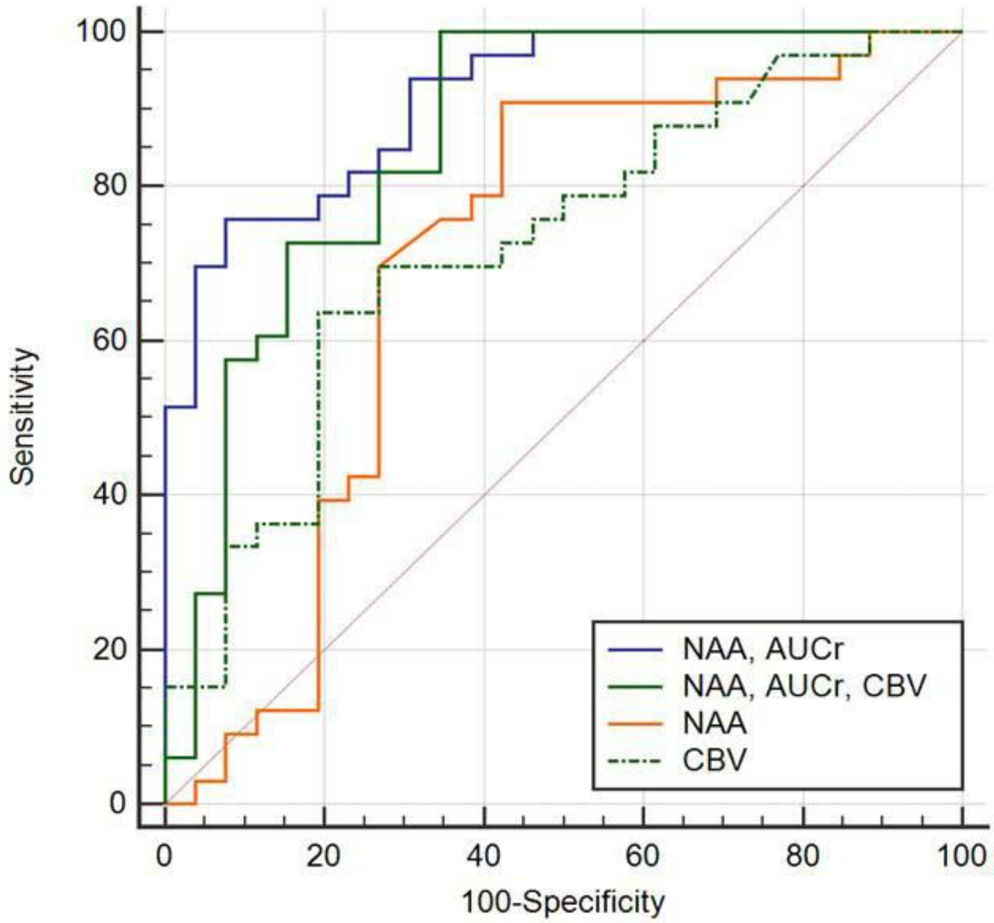

Fig 1: comparison of ROC curve analysis for CBV and NAA as well as MRS, DSC and DCE parameters combination.

(Filename: TCT_2324_Image2.jpg)

Wednesday, May 22, 2019
2:55PM - 4:25PM
Neurovascular Imaging Adult Brain

2583

3:02PM - 3:09PM

Imaging Neurovascular Uncoupling in Acute Migraine Attack with Susceptibility Weighted and Perfusion Imaging

F Kellner-Weldon[1], M Jossen[1], P Breiding[1], L Grunder[1], C Schankin[1], A Scutelnic[1], R Muri[1], M Pastore-Wapp[1], R Wiest[1], P Klinger-Gratz[2], R Verma[1], M El-Koussy[1]
[1]University Bern, Bern, Switzerland, [2]University Basel, Basel, Switzerland

Purpose
Migraine with aura (MwA) in the emergency setting is common and sometimes difficult to distinguish from mimicking conditions. Our study aimed at evaluating the frequency of regions of prominent focal veins (PFV) on susceptibility imaging (SWI) as a marker of increased deoxygenation in the acute phase and to study the underlying brain perfusion on dynamic susceptibility contrast enhanced magnetic resonance (MR).
Materials and Methods
Between 2011 and 2018 we evaluated symptoms and MR imaging of adult patients with MwA attacks (< 5 days after onset of symptoms). Abnormal SWI and perfusion TTP imaging was visually scored in 10 ROIs on both hemispheres distributed on 3 slices. The scores were zero for normal, one for discrete, two for distinct, and three for severely abnormal increase of PFV. The distribution was noted as either asymmetric left versus right hemispheric, or bilateral anterior versus posterior gradient. The time to peak (TTP) perfusion images were rated in the same fashion, with a window adjusted manually to depict maximum contrast.
Results
638 patients (436 female, 68.3 %) mean age 37.39 y, (range: 18-90 ± 14.47) were included. SWI and perfusion TTP was abnormal in 18.8% and in perfusion in 16.9% of patients. The same ROIs on both SWI and TTP maps were most often affected, this being the inferior and posterior medial temporal and the occipital lobe. SWI was superior to TTP in identifying abnormal regions and had fewer artefacts. Focal abnormality in 9 of 10 ROIs correlated significantly ($p < .001$) between SWI and TTP maps. The frequency of symptoms was 24.5 % for aphasia /dysarthria, 62.2% for visual disturbances, 50.5% for sensory symptoms, and 11.9% for motor disturbances. The association between side of aura symptoms and hemispheric imaging alteration in patients with abnormal SWI was highly significant ($p < .001$).
Conclusions
In acute attacks of MwA, SWI and perfusion imaging can show a combination of increased deoxygenation and delayed arterial supply. This study provides confidence in linking PFV to acute MwA.

3596

3:09PM - 3:16PM

Enhanced Perivascular Space Contrast Using T1-T2 Fusion and Adaptive Spatial Filtering

Sepehrband, F.
University of Southern California
Los Angeles, CA

3368

3:16PM - 3:23PM

Extreme Prominence of Deep Medullary Vein Score Correlates with Absent Cerebral Blood Flow on Nuclear Medicine Exams in Suspected Brain Death

E Peters[1], S Tedla[1], T Dowers[1], J Jacobson[1], S Harder[1], U Oyoyo[1], P Kim[1]
[1]*Loma Linda University Medical Center, Loma Linda, CA*

Purpose
Brain death is often suspected after a Magnetic Resonance Image (MRI) is performed. It is presumed that subjects without flow on a nuclear medicine cerebral blood flow exam (CBF) will have prominent deep medullary veins or possibly absent deep medullary veins on Susceptibility Weighted Images (SWI) compared with those that have blood flow on CBF.
Materials and Methods
52 subjects were retrospectively identified which had both a CBF exam and MRI within 10 days of each

other. Subjects were stratified by CBF exam result and timing of the MRI exam. SWI deep medullary vein scores were determined using two experienced neuroradiologists and a previously published scoring scale. SWI score was compared between subgroups ranging from 1 to 7.

Results

Nine subjects without flow on CBF had the MRI after the CBF exam (M:F 6:3; median age: 0.58 years [IQR 025,9]). Nine subjects had flow on the CBF (M:F 3:6; median age: 22 years [IQR 14,34]), when the MRI was completed before the CBF exam. The remaining subjects did not fit these strict criteria. There was a difference in deep medullary vein score between the CBF with no flow and MRI after CBF group, and the CBF with flow and MRI before CBF group, with high scores in the subjects with absent flow. ($p = 0.011$). When plotting all CBF without flow subjects' vein scores versus timing of the MRI before or after the CBF exam, there was a positive Spearmen's Rho correlation (0.500, $p = 0.002$) with trend of scores increasing over time.

Conclusions

High deep medullary vein scores predict the absence of cerebral blood flow in subjects with suspected brain death. Earlier identification of brain death patients may reduce unnecessary medical work up, increase availability of organ donation, and reduce cost associated with expensive intensive care unit hospitalizations.

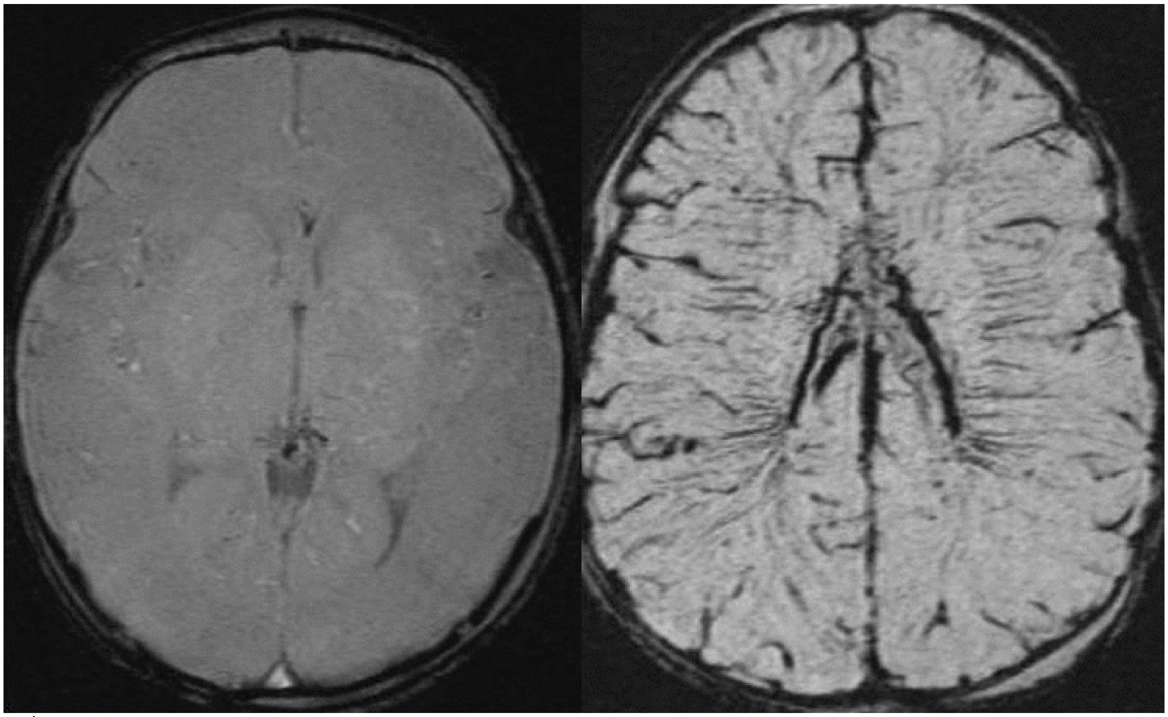

(Left) SWI score 1.   (Right) SWI score 7

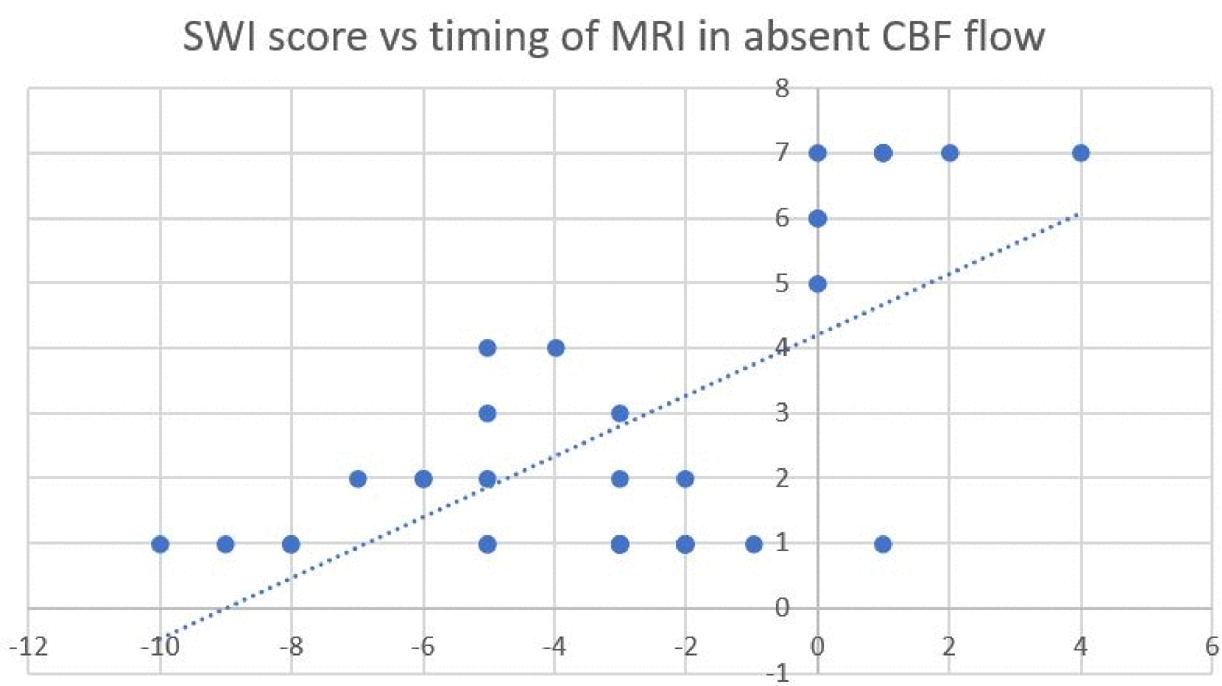

(Filename: TCT_3368_Imagesforupload.gif)

2899

4:01PM - 4:08PM

Imaging Biomarkers of Intracranial Arterial Disease: Comparing 7 Tesla MRI with CT

C Lucci[1], R Takx[2], A van der Kolk[1], A Harteveld[1], M Geerlings[3], P de Jong[1], J Hendrikse[1]
[1]*Utrecht University Medical Center, Utrecht, Netherlands,* [2]*University Medical Center Utrecht, Utrecht, Utrecht,* [3]*Julius Center for Health Sciences and Primary Care, Utrecht, Netherlands*

Purpose
Intracranial arterial disease (IAD) is a major cause of ischemic stroke. Arterial calcifications on CT and vessel wall lesions on MRI are often used interchangeably to describe the extent of IAD (graphics A); however, they depict different features of pathologic arterial remodeling. The aim of this study was to investigate the distribution and the correlation of these two imaging biomarkers in patients with a history of cerebrovascular disease.
Materials and Methods
Data from two ongoing prospective cohort studies of patients ≥18 years of age presenting with ischemic stroke or transitory ischemic attack in the anterior or posterior cerebral circulation, were used. A whole-brain 3D T1-weighted magnetization-prepared inversion recovery turbo spin echo vessel wall sequence pre-/post- contrast, was performed on a 7 Tesla MRI system within 3 months after symptom onset. Non-contrast CT scans performed for stroke work-up were retrieved from the hospital archive. Presence and burden of vessel wall lesions, and presence of intracranial artery calcifications and calcification severity (mild, moderate, severe) in the internal carotid artery (ICA) were visually assessed in the main arteries of the Circle of Willis.
Results
78 patients with both CT and MRI data available were analyzed. Of these, at least one vessel wall lesion or arterial calcification was assessed in 69 (88%) patients. The vessel wall lesion burden significantly increased with severity of ICA calcification (Jonckheere-Terpstra test statistics = 1.263, $p = 0.013$). Anterior, posterior and middle cerebral arteries presented almost exclusively vessel wall lesions. ICA showed mostly calcification while in the basilar and vertebral arteries vessel wall lesions were predominant (graphics B).
Conclusions
Although related, we found remarkable differences in the distribution pattern of vessel wall lesions on MRI and arterial calcifications on CT in the anterior versus posterior circulation. Our results suggest that CT and MRI provide complementary information for assessing the extent of IAD.

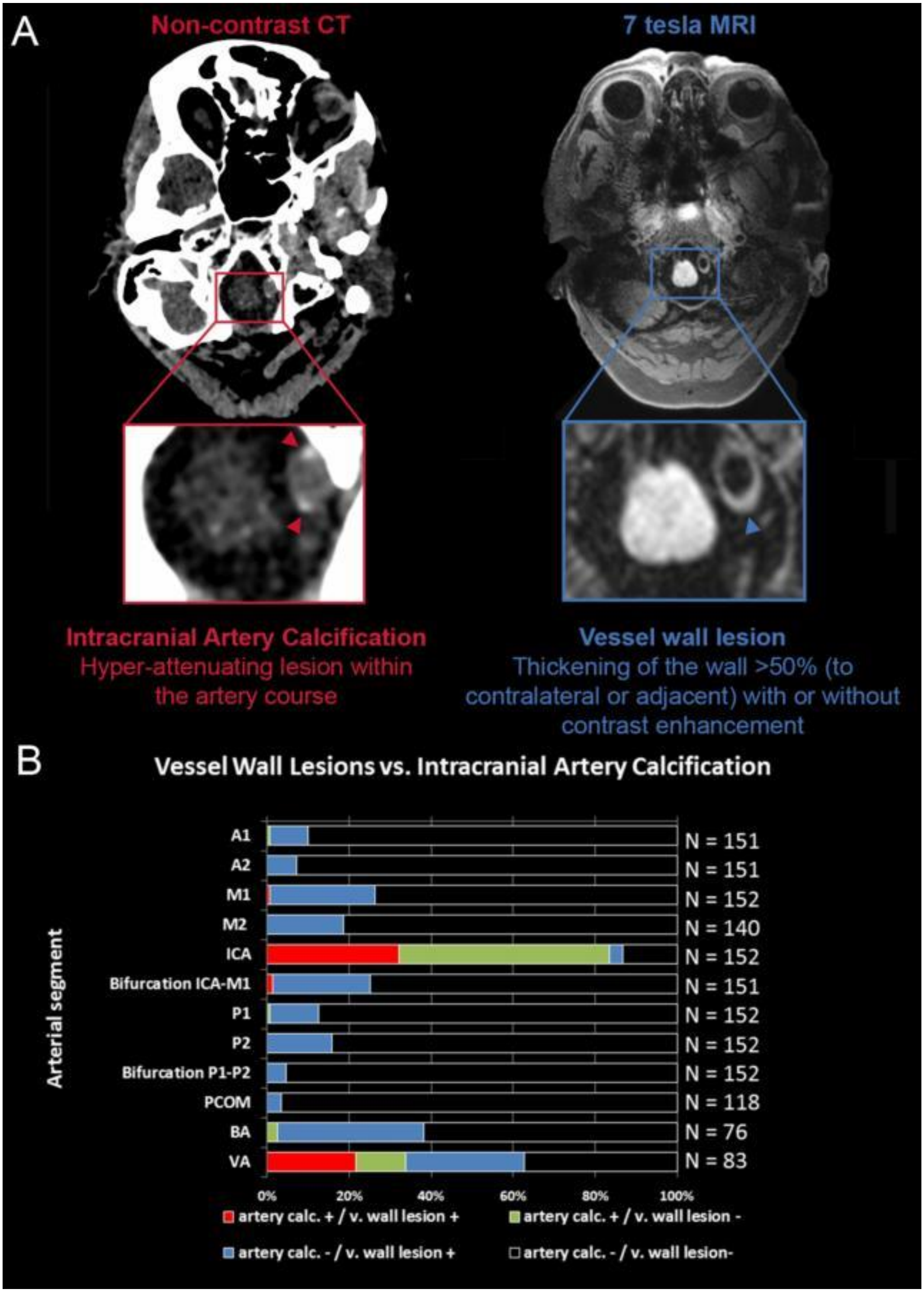
A
Non-contrast CT
7 tesla MRI
Intracranial Artery Calcification
Hyper-attenuating lesion within the artery course
Vessel wall lesion
Thickening of the wall >50% (to contralateral or adjacent) with or without contrast enhancement
B
Vessel Wall Lesions vs. Intracranial Artery Calcification
Arterial segment
A1
A2
M1
M2
ICA
Bifurcation ICA-M1
P1
P2
Bifurcation P1-P2
PCOM
BA
VA
N = 151
N = 151
N = 152
N = 140
N = 152
N = 151
N = 152
N = 152
N = 152
N = 118
N = 76
N = 83
0%
20%
40%
60%
80%
100%
artery calc. + / v. wall lesion +
artery calc. + / v. wall lesion -
artery calc. - / v. wall lesion +
artery calc. - / v. wall lesion-

(Filename: TCT_2899_graphics_ASNR_final.jpg)

2389

4:08PM - 4:15PM

Measurement of the transverse diameter of the meckel's cave, a very specific finding for diagnosis of the idiopathic intracranial hypertension/pseudotumor cerebri

A Kamali[1], K Sullivan[2], P Rabiei[3], R Patel[3], A Sahihi[2], R Riascos[3]
[1]UT HEALTH, HOUSTON, TX, [2]University of Texas Houston Medical School, Houston, TX, [3]The University of Texas Health Science Center at Houston, Houston, TX

Purpose
Idiopathic intracranial hypertension (IIH; pseudotumor cerebri) is a commonly missed diagnosis which may result in loss of vision in young adults. We propose an additional imaging criteria for diagnosis of the IIH by measuring the transverse diameter of the Meckel's caves on the coronal T2 weighted MRI sequences.
Materials and Methods
We examined 40 MRI brain of the patients with retrospectively confirmed diagnosis of the IIH. We selected 40 MRI imaging of age/sex matched healthy controls retrospectively. We measured the transverse diameter of the Meckel's caves on the coronal T2 weighted MRI in both groups.
Results
Our results showed that 35 out of 40 patients with diagnosis of IIH demonstrated enlarged Meckel's caves diameter with transverse diameter of the Meckel's caves measuring 6m or more as opposed to only one out of 40 healthy controls which demonstrated increased diameter of the Meckel's caves. The specificity of this imaging finding for diagnosis of IIH is bout 97 % and sensitivity about 87%.
Conclusions
Enlarged transverse diameter of the Meckel's caves is a very sensitive and specific imaging finding to diagnose the IIH or pseudotumor cerebri.

Diameter of Meckel's cave	N	IIH	HC	p-value
6m or above	40	35	1	
< 6m	40	5	39	0.099

Two-sample t test was used for pairwise comparisons

(Filename: TCT_2389_image1.jpg)

Wednesday, May 22, 2019
2:55PM - 4:25PM
Stroke

2953

2:55PM - 3:02PM

A Novel Rabbit Thromboembolic Occlusion Model

Y Ding[1], S Fitzgerald[1], D Jakaitis[1], D Dai[1], W Brinjikji[1], D Kallmes[1], R Kadirvel[1]
[1]*Mayo Clinic, Rochester, MN*

Purpose
To develop a preclinical thromboembolic occlusion model for studying revascularization strategies.
Materials and Methods
Radiopaque clot analogs were created by mixing rabbit blood with 10% barium sulfate. Three distinct clot analogs types were created; fibrin rich, red blood cell (RBC) rich and whole blood clots. The clots analogs were injected into the distal abdominal aorta using 3 cc plastic syringe via right common carotid access in 6 different rabbits. Locations of arterial occlusion were compared among fibrin-rich (n = 2) or RBC-rich (n = 2) or whole blood clots (n = 2) from digital subtraction angiography (DSA). Diameter of distal abdominal aorta and right common iliac artery were measured.
Results
The aortic bifurcation was occluded after a single delivery (clot length 1 cm) of fibrin-rich clot in one case (Figure 1). All the RBC-rich and whole blood clots and another fibrin rich clot occluded distal abdominal aorta and bilateral iliac arteries after multiple injections. Fragmentation of RBC-rich clots occurred during clot injection in both of the two cases. Distal aorta occlusion was achieved in every case. Mean diameter of distal abdominal aorta and right common iliac artery was 3.2 ± 0.3, and 2.3 ± 0.3 mm, respectively.
Conclusions
Consistent vessel occlusion at the bifurcation of distal abdominal aorta can be achieved with robust clot analogs. Diameter of distal abdominal aorta in rabbits is similar in size to that of human middle cerebral arteries. The rabbit aortic bifurcation model can be potentially used for thrombectomy devices and pharmaceutic drugs testing.

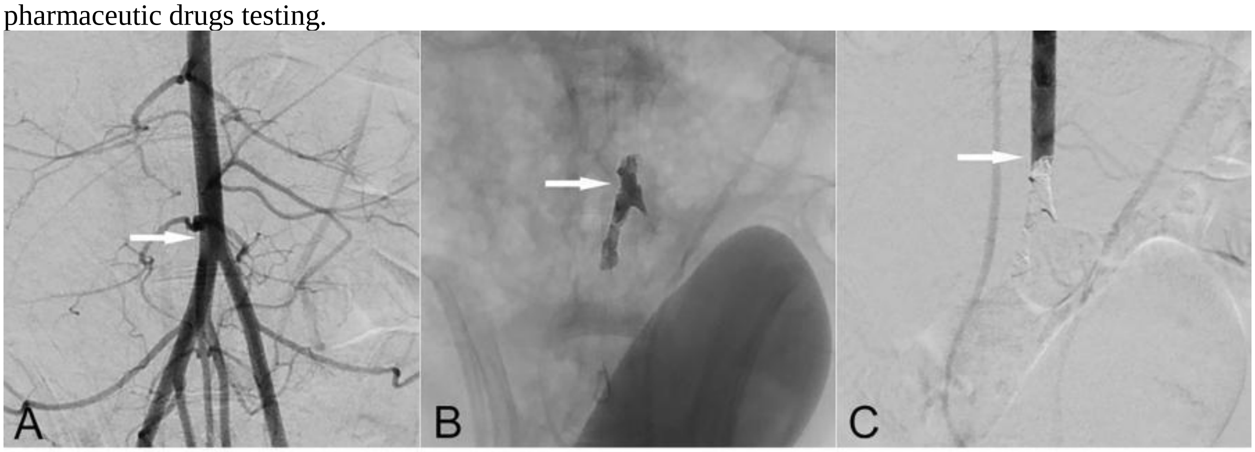

Figure 1. A. DSA before clot injection, showing distal aorta and its bifurcation (white arrow); B. Plain film after clot injection, indicating clot at the bifurcation of distal aorta (white arrow); C. DSA after clot injection, indicating complete occlusion of distal aorta (white arrow).

(Filename: TCT_2953_ClotmodelimagewithlegendsforASNR.jpg)

3577

2:55PM - 4:25PM

Calibrating to Hit a Moving Target: The Need for Evaluating and Modifying CT Perfusion Parameters for Acute Ischemic Stroke Following Initial Implementation

R Cody[1], J Hartman[1], J Sharpe[1], W Cohen[1], M Mossa-Basha[1]
[1]*University of Washington, Seattle, WA*

Purpose
Recent studies have demonstrated the ability to extend the treatment window for acute ischemic stroke (AIS), using physiologic imaging to identify patients with favorable ratios of potentially salvageable ischemic brain (penumbra) to non-salvageable infarcted parenchyma (core). (1-4) As a result, there is an increased installation and use of computed tomography perfusion (CTP) software packages in the AIS algorithms of many medical centers. Following automated CTP software implementation at our institution, a number of sequential protocol adjustments have been required to improve study quality and accuracy.
Materials and Methods
Beginning 9/1/17, our institution began using RAPID commercial CTP software (iSchemaView, Redwood City, CA) in the following AIS algorithm: Non-contrast head CT (NCCT) obtained immediately upon ED arrival and reviewed while patient in scanner; if no acute hemorrhage, CTP using RAPID performed to assess perfusion, followed by CTA head and neck to assess vessel patency. After initial implementation of the CTP software, there was an expected "learning curve" for the stroke team, including CT technologists, stroke neurologists, neurointerventionalists and neuroradiologists. Following this period of acclimation, accumulated suboptimal scans were reviewed, and protocol adjustments made. Initial CTP protocol: 2-second delay between contrast injection and image acquisition; perfusion images acquired over 30 seconds. First adjusted protocol: 5-second delay following contrast injection; images acquired over 60 seconds; immobilization of all patients' heads with tape in CT head holder. Beginning 12/5/17, the order of acquisition was changed to perform a CTA immediately following initial NCCT, which was reviewed while patient was in the scanner; if large vessel occlusion (LVO) was detected, CTP was then performed. In May 2018, additional alterations to the protocol were made in patients with low cardiac output. These patients were identified from the contrast kinetic curve from the CTA smartprep. Patients with a delay in contrast rise >15 seconds would undergo CTP cardiac protocol, which included a scan delay of 7 seconds and extended imaging window of 75 seconds to accommodate the prolonged and delayed perfusion window.
Results
Following the adjustments of contrast-to-scan time and CTP acquisition interval, significant improvement in RAPID attenuation curves was appreciated. Routine immobilization of patients' heads in the scanner gantry (even in those with no initial movement) eliminated the need for reinjection and rescanning for adequate CTP data, when sudden motion occurred during image acquisition. Changing the algorithm to perform CTA immediately after NCCT allowed patients with no LVO to forego CTP, thus reducing radiation dose. More recently, further adjustments to the CTP timing in patients with low cardiac output appear to improve the quality of CTP maps, helping to better identify salvageable penumbra in these patients.
Conclusions
Automated CTP software is a useful tool in the evaluation of AIS that can better triage patients for stroke intervention. However, after the software package is implemented into an institution's AIS algorithm, inherent variabilities in each institution's CT equipment and patient populations preclude a simple "set it and forget it" approach. Proper utilization necessitates ongoing evaluation of results and adjustment of CTP parameters in order to maximize performance and accuracy.

3112

3:02PM - 3:09PM

Comparative-Effectiveness of Endovascular Thrombectomy in Elderly Stroke Patients

X Wu[1], A Malhotra[2], K Seifert[3], V Kalra[4], D Gandhi[5], P Sanelli[6]
[1]Yale University School of Medicine, New Haven, CT, [2]YALE UNIVERSITY SCHOOL OF MEDICINE, NEW CANAAN, CT, [3]YALE NEW HAVEN HOSPITAL, NEW HAVEN, CT, [4]MCRG ORLANDO HEALTH, TAMPA, FL, [5]University of Maryland School of Medicine, Baltimore, MD, [6]NORTHWELL HEALTH NSUH, MANHASSET, NY

Purpose
Strokes in patients aged ≥ 80 years are common and advanced age is associated with relatively poor post-stroke functional outcome. The current guidelines do not recommend an upper age limit for endovascular thrombectomy (EVT). The purpose of this study is to evaluate the effectiveness of EVT in acute stroke due to large-vessel-occlusion (LVO) for elderly patients above age 80 years.
Materials and Methods
A Markov decision-analytic model was constructed from a societal perspective to evaluate health outcomes in terms of quality-adjusted life years (QALYs) after EVT for acute ischemic stroke due to LVO in patients above age 80 years. Age-specific input parameters were obtained from the most recent/comprehensive literature. Good outcome was defined as mRS score ≤ 2. Probabilistic, one-way, and two-way sensitivity analyses were performed for both healthy patients and patients with disability at baseline.
Results
Base case calculation showed in functionally-independent patients at baseline, intravenous thrombolysis (IVT) with tissue plasminogen activator only to be the better strategy with 3.76 QALYs compared to 2.93 QALYs for patients undergoing endovascular thrombectomy (EVT). The difference in outcome is 0.83 QALY, which is equivalent to 303 days of life in good health. For patients with baseline disability, IVT only yields a utility of 1.92 QALYs and EVT yields a utility of 1.65 QALYs. The difference is 0.27 QALYs which is equivalent to 99 days of life in good health. Multiple sensitivity analyses showed that effectiveness of EVT is significantly determined by the morbidity and mortality after both IVT and EVT strategies, respectively.
Conclusions
The study results do not support using EVT widely in all patients above 80 years of age. Selective use of EVT may be more appropriate in acute stroke patients with LVO in the older population.

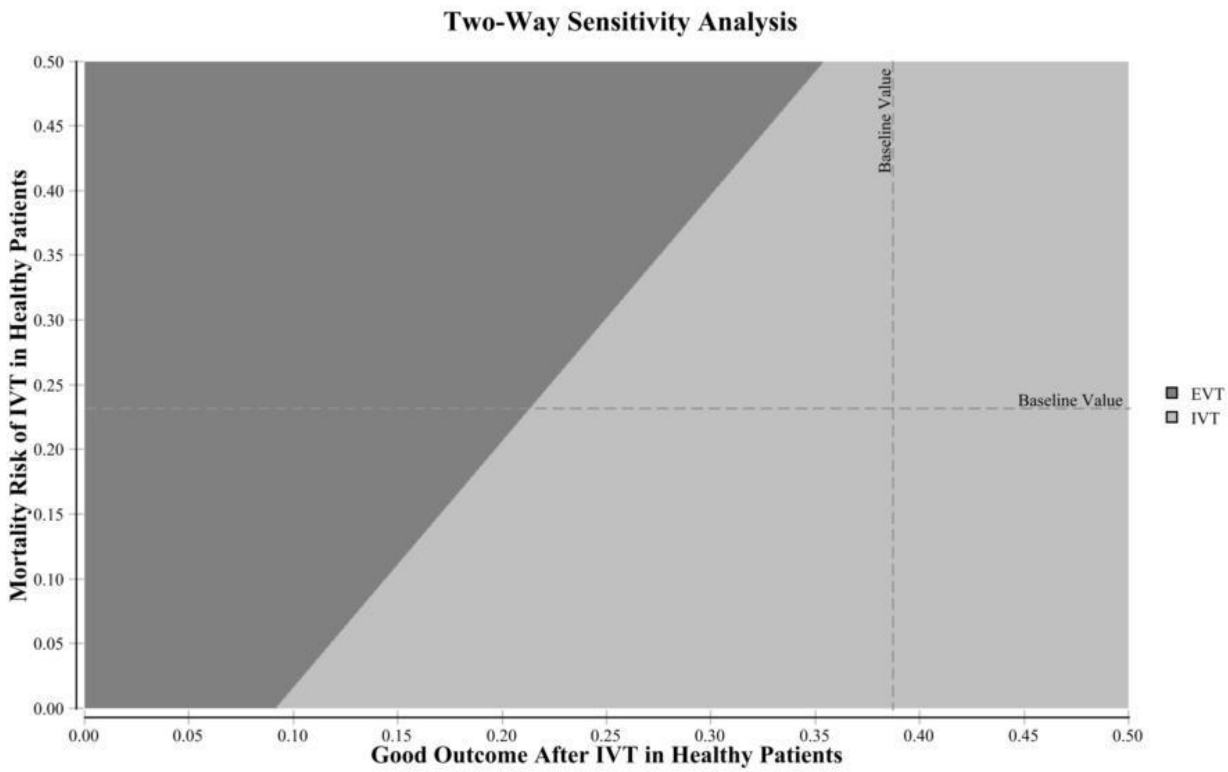

(Filename: TCT_3112_Figure2.jpg)

2151

3:09PM - 3:16PM

Defining Ischemic Core in Acute Ischemic Stroke: A Multiparametric Bayesian-Based Model

K Nael[1], E Tadayon[2], A Metry[3], J Fifi[4], S Tuhrim[5], D Wheelwright[5], H Chang[5], J Mocco[5]
[1]ICAHN SCHOOL OF MEDICINE AT MOUNT SINAI HOSPITAL, NEW YORK, NY, [2]Department of Neurology, Beth Israel Deaconess Medical Center, Boston, MA, [3]Icahn School of Medicine at Mount Sinai, new york, NY, [4]Mount Sinai Hospital, New York, NY, [5]Icahn School of Medicine at Mount Sinai, New York, NY

Purpose
Bayesian model has shown promising results to offset noise-related variability in perfusion analysis (1,2). Using baseline CTP we aim to find optimal Bayesian-estimated thresholds to construct a multiparametric model that can provide the most accurate estimate of ischemic core in patients with acute ischemic syndrome (AIS).
Materials and Methods
AIS patients with anterior circulation stroke who had baseline CTP, and achieved successful recanalization (≥ IIb IIB) were included. CTP data were processed using a Bayesian probabilistic method. Five CTP parameters including delay, TTP, MTT, CBV and CBF and 5 additional "difference maps" were generated by subtracting the mean of a cube (27 voxels) on the contralateral side of each voxel (delay diff, TTP diff, CBV diff, CBF diff, MTT diff). We did our analysis in 2 steps: 1) To build our imaging model, in a subset of patients, the brain was extracted from CTP and coregistered with the follow up MRI. An infarction mask and non-infarcted masks were drawn on MRI. We used a robust logistic regression to assess the binary outcome of our voxel-based analysis (infracted vs non-infarcted) by adjusting for intra-subject correlations. 2) The CTP-estimated ischemic core volume obtained from our model (logit-score) and circular singular value decomposition (cSVD)- rCBF <30% (that is used in

routine practice) were compared against MRI-derived infarction volume by using Bland-Altman and correlation analysis.
Results
In our imaging model constructed from 20 patients, 4 variables (threshold/AUC) remained independent predictor of infarction: TTP (28.8/0.76); rCBF (22.1/0.73); ATD diff (0.87/0.80); and MTT diff (1.38/0.69). The score given by the logistic model was Logit score = -3.9170 + 0.0601*TTP - 0.0095*CBF + 0.4629*ATD diff + 0.0989*MTT diff. At score of 0.109 this model identified infracted voxels with overall AUC of 0.88. The mean, median and 95%CI difference between CTP-estimated ischemic core and MRI volume (mL) were -6, 3, -13 -- +2 for cSVD and +1, 2, and -3 -- +4 for Bayesian logit model. Bland-Altman analysis showed the limits of agreement ranging from -61 to +50 mL for cSVD-CBF and -25 to +26 mL for Bayesian-logit model. The correlation coefficient (r) between CTP-estimated ischemic core volume and MRI were 0.73 and 0.94 for cSVD and Bayesian-logit model respectively.
Conclusions
We established thresholds for Bayesian model to estimate ischemic core. Our multiparametric Bayesian-based model improves variability in CTP-estimation of ischemic core in comparison to methodology used in current clinical routine.

3252

3:16PM - 3:23PM

Different Pathophysiology Underlies Different Cerebellar Intracerebral Hemorrhage Locations

S Marini[1], M Pasi[2], F Testai[3], D Woo[4], J Rosand[1], C Anderson[1], J Romero[1]
[1]Massachusetts General Hospital, Boston, MA, [2]Centre Hospitalier Universitaire de Lille, Lille, France, [3]University of Illinois College of Medicine, Chicago, IL, [4]University of Cincinnati, Cincinnati, OH

Purpose
Cerebellar intracerebral hemorrhage (C-ICH) has been reported to be mainly associated with hypertension-related vasculopathy. We aimed to identify risk factors associated with superficial C-ICH and deep C-ICH, under the hypothesis that these locations may represent different pathophysiologies
Materials and Methods
We collected data of C-ICH cases from the Ethnic/Racial Variations of Intracerebral Hemorrhage (ERICH) study, a multicenter cohort study of patients with primary ICH. Patients were divided into (1) superficial C-ICH (cortex and vermian involvement) and (2) deep C-ICH (white matter and nuclei). Three multivariate models were tested to identify risk factors associated with each location: vascular risk factor (VRF) model (hypertension, kidney function, left ventricular hypertrophy, diabetes), neuroimaging model based on CT and MRI (number of microbleeds and Leukoaraiosis and cortical atrophy), and genetic model (any copy of APOE ε2 and ε4). All models were adjusted for age and sex
Results
Out of 3000 subjects enrolled in ERICH, 211 presented with isolated C-ICH (43% female, median age 63y, 15.6% superficial C-ICH). In univariate analysis, the two locations did not differ for any listed variables. No variables in the VRF model reached the statistical significance. Severe Leukoaraiosis in the neuroimaging model (Odd Ratio (OR): 1.38, 95% Confidence Intervals (CI):1.03-1.86, p:0.03) and absence of APOE ε2 in the genetic model (OR: 0.26, 95%CI:0.11-0.63, p:0.003) associated with risk of deep C-ICH
Conclusions
Superficial C-ICH are associated with APOE ε2, whereas deep C-ICH are associated with severe WMH. Given the strong relationship between APOE and cerebral amyloid angiopathy and between Leukoaraiosis and hypertension related vasculopathy, our results support the hypothesis that these two

pathologic mechanisms may result in two different cerebellar hemorrhage locations, with implications on outcome and management of patients suffering from C-ICH

2647

3:23PM - 3:30PM

Early Experiences with Mobile Stroke CT Angiography

M Bates[1], J Wu[1], A Russman[1], K Uchino[1], J Lee[2]
[1]Cleveland Clinic Foundation, Cleveland, OH, [2]Cleveland Clinic Foundation, Cleveland , OH

Purpose
Use of nonenhanced head CTs in a mobile stroke treatment unit (MSTU) for acute stroke patients has drastically decreased the time to treatment and improved patient outcome. To date, few studies have investigated the use of additional computed tomography angiography (CTA) imaging of the head in a MSTU to enable faster and more appropriate triage. We hypothesize that MSTU CTA will result in faster CTA acquisition times, reduced alarm to report times, reduced alarm to puncture times, and result in improved patient triage and outcome.
Materials and Methods
Between 7/28/17 and 8/27/18, our MSTU was dispatched on 118 cases for which 38 cases also underwent CTA imaging. Alarm to CT reported, alarm to CTA completed and reported, alarm to TPA and alarm to puncture times were recorded.
Results
38 patients underwent CTA imaging in our MSTU. Out of those patients, 12 were transferred to a comprehensive stroke center (CSC) with a large vessel occlusion (LVO). 5 patients qualified for subsequent mechanical thrombectomy. Based on historic controls, all of our time metrics downstream from the nonenhanced head CT were reduced. Mean alarm to nonenhanced CT reported time was 38 minutes versus 32 minutes. Mean alarm to CTA completed time was 50 minutes versus 1 hour 12, with alarm to CTA report time of 1 hour 11 minutes. Mean alarm to TPA was 39 minutes versus 1 hour 57. Mean alarm to puncture time was 2 hours and 7 minutes versus 3 hours 15 minutes.
Conclusions
The implementation of CTA imaging in our MSTU reduced the alarm to CTA completion and reported time, appropriated triaged patients to a comprehensive stroke center that had thrombectomy capabilities which reduced alarm to puncture times and thus achieved faster recanalization in patients presenting with large vessel occlusions.

2877

3:30PM - 3:37PM

Early Lesion Water Uptake Predicts Clinical Outcome in Ischemic Stroke Patients after Successful Recanalization: An Observational Study

G Broocks[1], F Flottmann[2], A Kemmling[3], H Leischner[4], J Nawabi[5], P Sporns[6], G Schön[7], U Hanning[8], G Thomalla[7], J Fiehler[9]
[1]University Medical Center Hamburg-Eppendorf, Hamburg, Germany, [2]UKE Hamburg, Hamburg, HH, [3]University Hospital Münster, Münster, NRW, [4]University Hospital Hamburg, Hamburg, HH, [5]UNIVERSITY MEDICAL CENTER HAMBURG-EPPENDORF, HAMBURG, Germany, [6]University Münster, Münster, NRW, [7]University Hamburg, Hamburg, HH, [8]University of Hamburg-Eppendorf, Hamburg, Germany, [9]University Medical Center Hamburg-Eppendorf, Hamburg, AK

Purpose
PURPOSE: Endovascular thrombectomy (ET) is of benefit to patients with acute ischemic stroke and proximal vessel occlusion. However, clinical outcome after ET varies. Net water uptake (NWU) is a

novel quantitative imaging biomarker of ischemic edema, which can be measured in computed tomography (CT). We hypothesized that early-elevated NWU is associated with poor clinical outcome despite successful recanalization.
Materials and Methods
Acute middle cerebral artery stroke patients with multimodal admission CT who received successful endovascular recanalization (TICI 2b/3) and follow-up CT were analyzed. NWU was quantified in admission CT and was tested as predictor of functional outcome compared to NIHSS and ASPECTS using modified Rankin Scale (mRS) after 90 days.
Results
72 patients were included. The mean NWU (SD) in patients with poor outcome (mRS 5-6) was 12.1% (±5.4%), which was higher compared to patients with mRS 0-4: mean (SD) NWU: 5% (±3.4%), (p<0.0001). The time from symptom onset to imaging was not different in both patient groups (2.6h versus 2.4h, p=0.7). Based on univariate receiver operating curve analysis, early NWU above 10% identified patients with poor outcome with high discriminative power (AUC 0.85) and was superior to NIHSS (AUC: 0.72) and ASPECTS (AUC: 0.75).
Conclusions
Quantification of NWU in early infarct lesions improved the prediction of poor clinical outcome after successful ET. Early-elevated NWU could be tested prospectively as selection criteria for treatment especially in patients with a low initial ASPECTS.

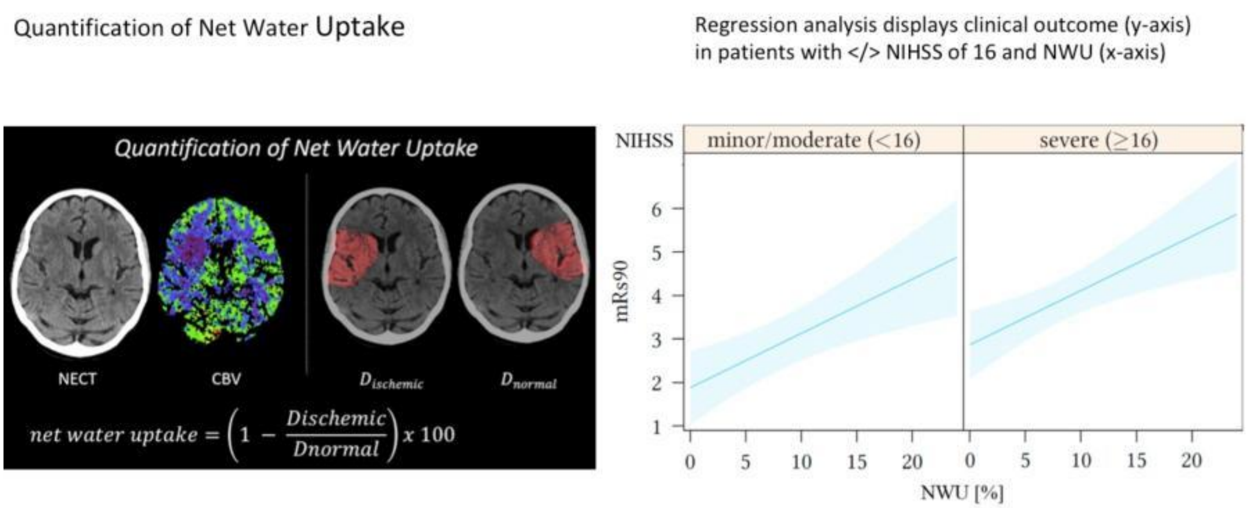

(Filename: TCT_2877_fig_mrsnwu.jpg)

2749

3:37PM - 3:44PM

Impact of Admission Blood Glucose Levels on Early Brain Edema and Clinical Outcome in Patients with Ischemic Anterior Circulation Stroke

G Broocks[1], A Kemmling[2], M Bechstein[3], T Faizy[4], G Schön[5], G Thomalla[5], J Fiehler[6], U Hanning[7], F Flottmann[8], H Leischner[9], P Sporns[10]
[1]University Medical Center Hamburg-Eppendorf, Hamburg, Germany, [2]University Hospital Münster, Münster, NRW, [3]UNIVERSITY MEDICAL CENTER - HAMBURG, HAMBURG, Germany, [4]UNIVERSITY

MEDICAL CENTER - HAMBURG, HAMBURG, GERMANY, [5]University Hamburg, Hamburg, HH, [6]University Medical Center Hamburg-Eppendorf, Hamburg, AK, [7]University of Hamburg-Eppendorf, Hamburg, Germany, [8]UKE Hamburg, Hamburg, HH, [9]University Hospital Hamburg, Hamburg, HH, [10]University Münster, Münster, NRW

Purpose
The impact of blood glucose levels on functional outcome in ischemic stroke has been discussed controversially. Elevated levels of early ischemic edema are a known predictor of poor outcome, but the association of BGL and ischemic edema are yet uncertain. We hypothesized that higher levels of BGL are associated with elevated ischemic edema and declined clinical outcome.
Materials and Methods
166 patients with acute middle cerebral artery stroke were included. BGL were analyzed as part of the standard laboratory at admission and early ischemic brain edema was determined by quantifying net lesion water uptake (NWU), a biomarker that is based on CT-densitometry. Collateral status was assessed using an established 5-point scoring system. Clinical outcome was determined using modified Rankin Scale (mRS) score after 90 days.
Results
The median blood glucose level at admission was 126 mg/dl (IQR: 108-150, range: 81-255 mg/dl) and the mean (SD) NWU at admission was 9.1% (0.05; range: 0.03- 26.9%). In linear regression analysis, there was a significant relationship between increasing BGL and early NWU as well as clinical outcome. Every increase in BGL of 25 mg/dl was associated with a 1% increase in NWU (95%CI [per 1 mg/dl BGL]: 0.3-1.5; p=0.004). However, this association was not significant in patients with good collaterals. A BGL increase of 25 mg/dl was associated with an increased mRS of 0.43 (95%CI: 0.18-0.75; p<0.001). The effect of BGL on outcome was higher in patients with good collaterals (mRS increase of 0.55 versus 0.35 for every BGL increase of 25 mg/dl).
Conclusions
Elevated admission BGL were associated with increased early brain edema and declined clinical outcome modified by collateral status. Formation of early brain edema was elevated in patients with poor collaterals; however, the effect of increasing BGL on clinical outcome was higher in patients with good collaterals.

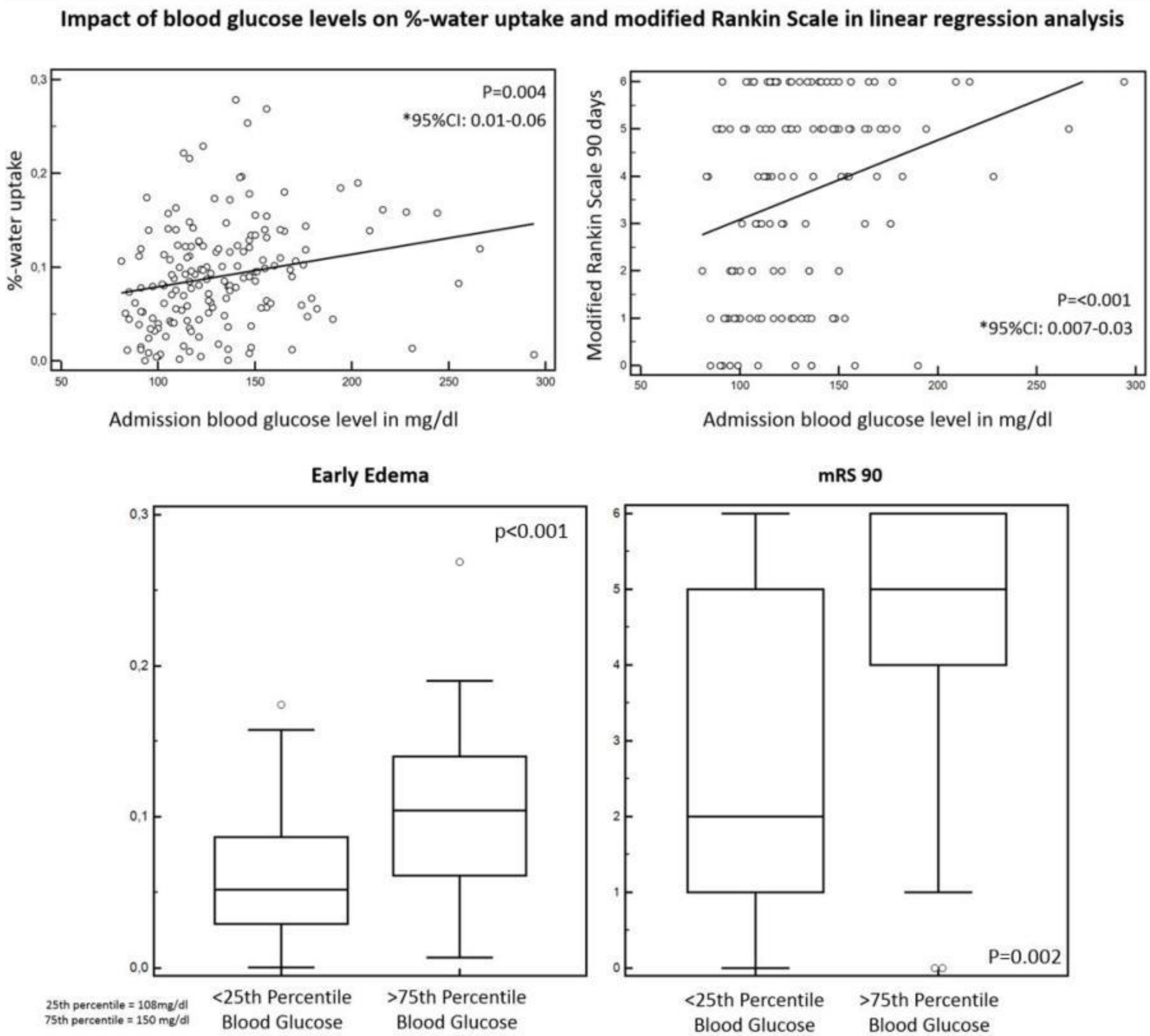

(Filename: TCT_2749_asnr_diabetes.jpg)

3320

3:44PM - 3:51PM

Measuring Degree of Conjugate Gaze Deviation May Help Distinguish Acute PICA Occlusion as Potential Mimicker from Anterior Large Vessel Occlusion on Computed Tomography

N Jiang[1], w wu[2], C Fong[3], D Sahlas[4], R Larrazabal[5]
[1]MCMASTER UNIVERSITY, HAMILTON, ON, [2]McGill University, Montréal, Quebec, [3]N/A, Hamilton, ON, [4]McMaster University, Hamilton, Ontario, [5]McMaster University, Hamilton, AK

Purpose
Conjugate gaze deviation (CGD) is a predictor of acute large anterior vessel occlusion and may help expedite patients to CTA and endovascular capable sites to maximize patient outcome. However, patients with acute cerebellar infarcts have also been observed to exhibit CGD, particularly in the PICA territory. Thus, acute PICA occlusion may be a potential mimicker of large vessel occlusion on non-enhanced CT

(NECT). So far, the association of CGD with acute PICA infarction has not been examined. We investigated whether measuring degree of CGD on NECT may help differentiate these two groups.
Materials and Methods
We retrospectively reviewed imaging and clinical records of 27 patients with CTA proven acute PICA occlusions within 12 hours after symptom onset. This was compared against 114 patients with CTA proven proximal vessel occlusion (ICA, M1, and M1/2). Degree of CGD was measured for each group. A positive CGD was defined as ipsilateral eye deviation with > 5° on imaging. Demographics and comorbid conditions were also collected.
Results
Twenty-seven patients with acute PICA occlusions, 9 (33%) have positive gaze deviation (6 with ipsilateral and 3 with contralateral gaze deviation). Of the 72 out of 114 (63%) patients with proximal vessel occlusion have +CGD. The median degree of CGD between the two groups is statistically significant (32° vs 25°, $p < 0.05$). Infarct location is predominantly in the vermis or inferior medial aspect of cerebellar hemisphere.
Conclusions
Radiographic CGD seems relatively common in patients with acute PICA occlusion and may be a potential mimicker of proximal ischemic stroke in stroke code evaluation. However, our study demonstrates a higher median degree of gaze deviation in acute PICA than proximal anterior vessel occlusions. Thus, measuring degree of CGD may help detect mimickers and streamline patients for the endovascular pathway.

3474

3:51PM - 3:58PM

Posterior Frontal Lobe Involvement is a Highly Specific Imaging Marker for Prediction of Large Final Infarct Despite Successful Intra-Arterial Thrombectomy in Patients with Large Vessel Occlusion.

F Noro[1], M Lev[2], R Gonzalez[3], R Almeida[3], B Canedo Bizzo[3], W Mehan[3], S Kamalian[3], T Leslie-Mazwi[3]
[1]MGH, BROOKLINE, MA, [2]MASSACHUSETTS GEN'L HOSP./HARVARD MED. SCHL., NEWTON CENTER, MA, [3]Massachusetts General Hospital, Boston, MA

Purpose
Multiple recently published trials established the benefit of intra-arterial thrombectomy (IAT) in acute ischemic stroke (AIS) patients up to 24 hours. However, several patients have large final infarcts despite successful IAT. Our purpose was to determine if involvement of specific region(s) on initial MR-DWI predicts likelihood of large final infarcts despite successful IAT.
Materials and Methods
In this retrospective study, 117/221 consecutive acute ischemic stroke patients who underwent IAT between 6/1/2012 and 12/31/2017 met out inclusion criteria: (1) Available admission DWI; (2) IAT; and (2) Follow-up imaging performed between 12 hours and 5 days after IAT. Large final infarct was defined as core infarct volume >100 ml on follow-up imaging. We calculated sensitivities and specificities for involvement of different brain regions separately for prediction of a large final infarct size.
Results
The final infarct size following IAT was <70 mL in 69/115 (60%), 70-100 mL in 6/115 (5%), and >100 mL in 42/115 (35%) patients. The sensitivities and specificities for prediction of a large final infarct size based on involvement of each region at presentation were: insula (<50% involvement) – 52% and 36%; insula (>50% involvement) – 47% and 64%; deep gray matter – 73% and 28%; periventricular white matter – 52 and 44%; anterior frontal – 57% and 87%; posterior frontal 25% and 91%; temporal lobe – 71 and 58%; and parietal lobe – 35% and 73%.
Conclusions
Involvement of the posterior frontal lobe on admission imaging may serve as a highly specific marker for

prediction of large final infarct in stroke patients with proximal artery occlusions despite successful IAT. Our findings may provide a helpful tool in making treatment decisions; further study in late-window patients is currently being performed.

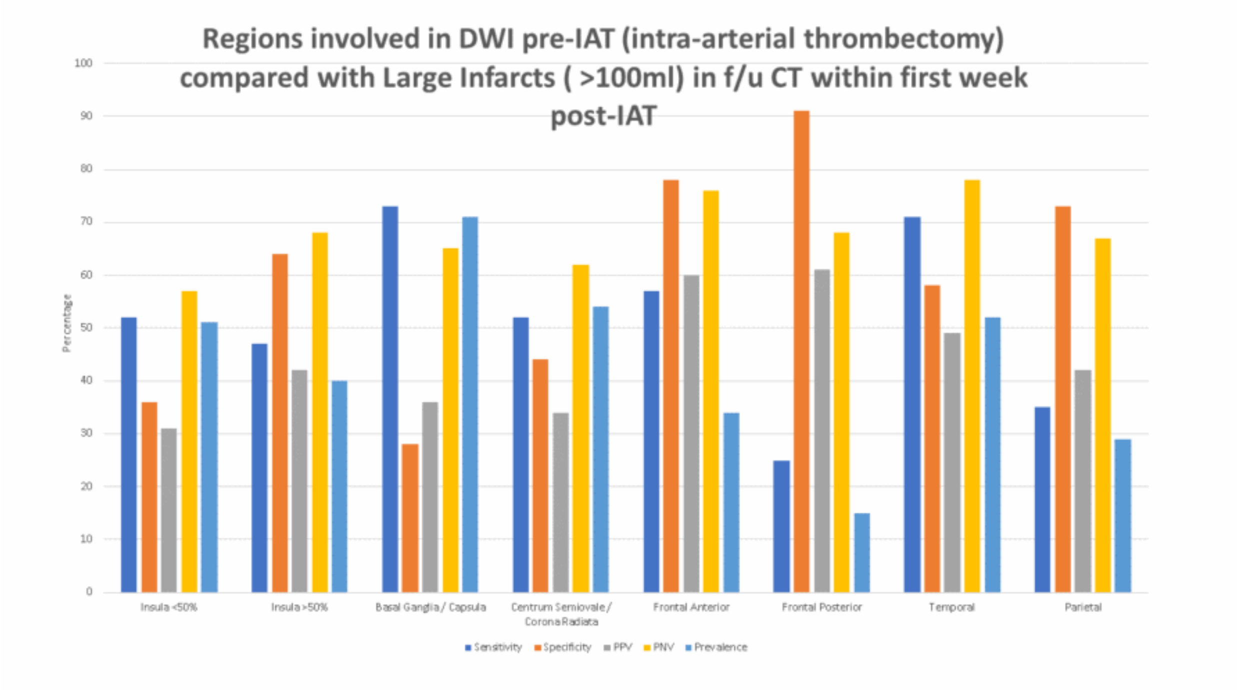

(Filename: TCT_3474_Slide1.GIF)

3429

3:58PM - 4:05PM

The Intrinsic Iodine Content of the Thyroid is Correlated to the HU Value of the Thyroid on True Non-Contrast Scans

A Kroonenburgh[1], S van Kuijk[2], A Jacobi-Postma[3]
[1]MUMC+, Maastricht, europe, [2]MUMC+, Maastricht, Europe, [3]MUMC+, MAASTRICHT, Limburg

Purpose
Virtual non-contrast (VNC) scans from Dual energy CT are thought to reflect True non-contrast (TNC) images and could therefore be used as a substitute to lower radiation dose. The difference in thyroid imaging however exceeds the normally accepted 15 HU, this is thought to be due to the intrinsic iodine content of the thyroid. We investigated the correlation between Thyroid Stimulating Hormone (TSH) and the density measurements on TNC and VNC.
Materials and Methods
In the period from November 2016 until June 2018 we included forty-seven patients who underwent a DECT scan of the head neck region. The correlation of TSH values and density measurements on TNC and VNC, as well as the ΔHU between VNC and TNC were calculated.
Results
There is a positive correlation between TSH and the HU value on the true non contrast scan of 0.32 (p = 0.050). Such correlation does not exist for VNC reconstructions (correlation of -0.08, p = 0.64)
Conclusions
No correlation between TSH and VNC is found as expected, because the intrinsic iodine is subtracted from the images. The increased organification of iodine due to higher TSH levels is reflected in the

density measurements of the TNC. Therefore the Δ HU measurements reflect the intrinsic iodine content of the thyroid.

2460

4:05PM - 4:12PM

Thrombus Permeability and Histopathology: Is a Clot's Perviousness on CT Imaging Correlated with its Histologic Composition?

J Benson[1], S Fitzgerald[1], R Kadirvel[1], D Kallmes[1], W Brinjikji[1]
[1]*Mayo Clinic, Rochester, MN*

Purpose
In acute ischemic stroke (AIS), RBC-rich thrombi are associated with shorter procedure times and successful thrombectomy rates. This study sought to evaluate the association between clot perviousness, measured using thrombus attenuation increase (TAI) between NCCT, and histologic composition of thrombi.
Materials and Methods
Included patients had AIS secondary to large-vessel occlusion, NCCT and CTA images, and histologic analysis of the retrieved thrombi. Patients were excluded if the thrombus was outside the field of imaging on either NCCT or CTA, or if the clot was too small to be visualized on CT. TAI was measured by subtracting clot attenuation on NCCT from the attenuation on CTA. Up to 3 regions of interest (ROIs) were evaluated on each thrombus; the average attenuation was used for analysis if multiple ROIs were assessed. Both absolute and relative TAIs were measured. Histologically, thrombi were evaluated for degree of both RBC and fibrin density.
Results
30 patients were included, 14 of which were female (47.7%). 31 thrombi were assessed (one patient had bilateral clots). Average patient age at time of imaging was 68.0 ± 12.2. The most common location of thrombi were the MCA (n=24), followed by the ICA (n=6), basilar artery (n=1), PCA (n=1) and ACA (n=1); 3 patients had clots that involved more than one artery. Thrombi with an absolute increase in attenuation of ≥10 had greater RBC density than those with absolute increase <10 HU (mean difference of RBC density = 24.6, 95% CI [4.8-44.5]. Clots with ≥25% increase in attenuation on CTA relative to NCCT also had higher RBC density (mean difference in density = 22.5, 95% CI [4.4-40.6].
Conclusions
Thrombus perviousness assessed on CT and CTA imaging is correlated with higher RBC density, offering a possible explanation for the higher rates of successful thrombectomy and favorable clinical outcome seen in such patients.

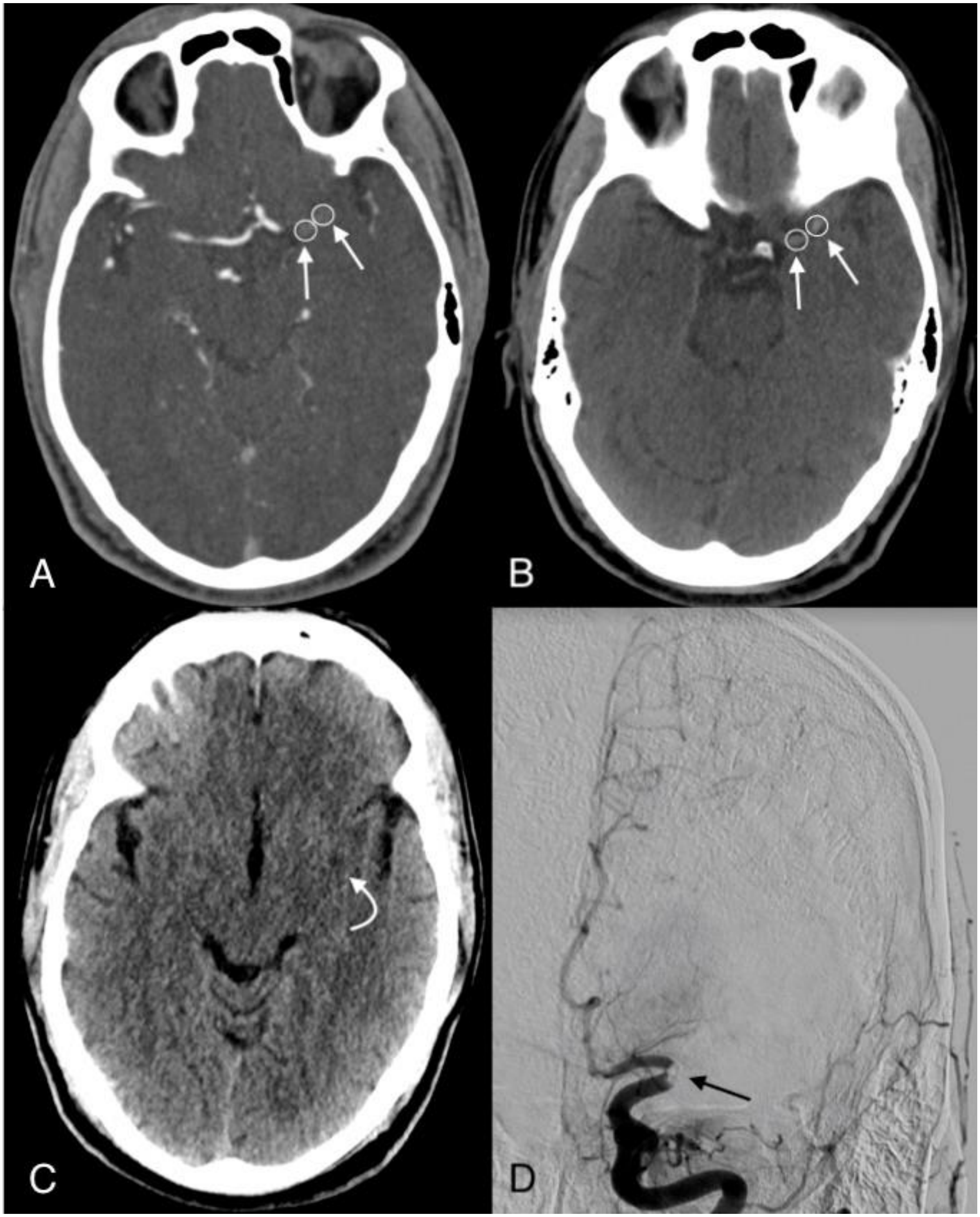

(Filename: TCT_2460_ASNR4image.jpg)

2553

4:12PM - 4:19PM

Where Did the Time Go? Packaging, Transfer and Imaging Time Course of Patients Who Undergo Neuro-endovascular Intervention for Acute Stroke

J Coburn[1], G Avey[2], A Kuner[1], R Zea[3]
[1]University of Wisconsin Hospitals and Clinics, Madison, WI, [2]UNIVERSITY OF WISCONSIN, MADISON, WI, [3]University of Wisconsin, MADISON, WI

Purpose
Endovascular thrombectomy improves outcomes in selected patients with acute stroke. However, barriers remain in providing this therapy outside the immediate vicinity of a stroke center. The purpose of this study was to evaluate if imaging factors impacted groin puncture time and transfer patient outcomes at a single academic stroke center.
Materials and Methods
Transfer patients who underwent endovascular treatment for acute stroke from 2016-2017 were included. Clinical, imaging and timestamp variables were collected from our institutional neuroendovascular database and the medical record. ASPECTS scores from baseline head CT and any repeat head CT prior to intervention were analyzed. Outcome measures, including modified Rankin score at 90 days, were documented.
Results
91 patients were included in the study. 68 (75%) were referred from a facility within 90 miles. Median time to groin puncture was 225 minutes. There was no difference in time to groin puncture or outcomes between those who had advanced imaging at the referral or receiving center. There was a relationship between change in ASPECTS score and time, such that the odds of the ASPECTS score decreasing almost doubled every hour spent between initial head CT and repeat head CT prior to intervention ($p<.001$). The ASPECTS score on the presenting head CT did not predict functional independence or disability/death at 90 day follow up. The ASPECTS score on CTs performed immediately prior to intervention was predictive of outcome.
Conclusions
Significant delays exist between presentation and endovascular therapy for patients transferred to stroke centers. The location that advanced imaging is performed does not impact time to skin puncture or patient outcome. The odds of an ASPECTS score decay increases with time and only the imaging performed immediately prior to intervention was predictive of patient outcome. Therefore, expedited imaging should be considered in transferred patients, particularly those nearing exclusion criteria.

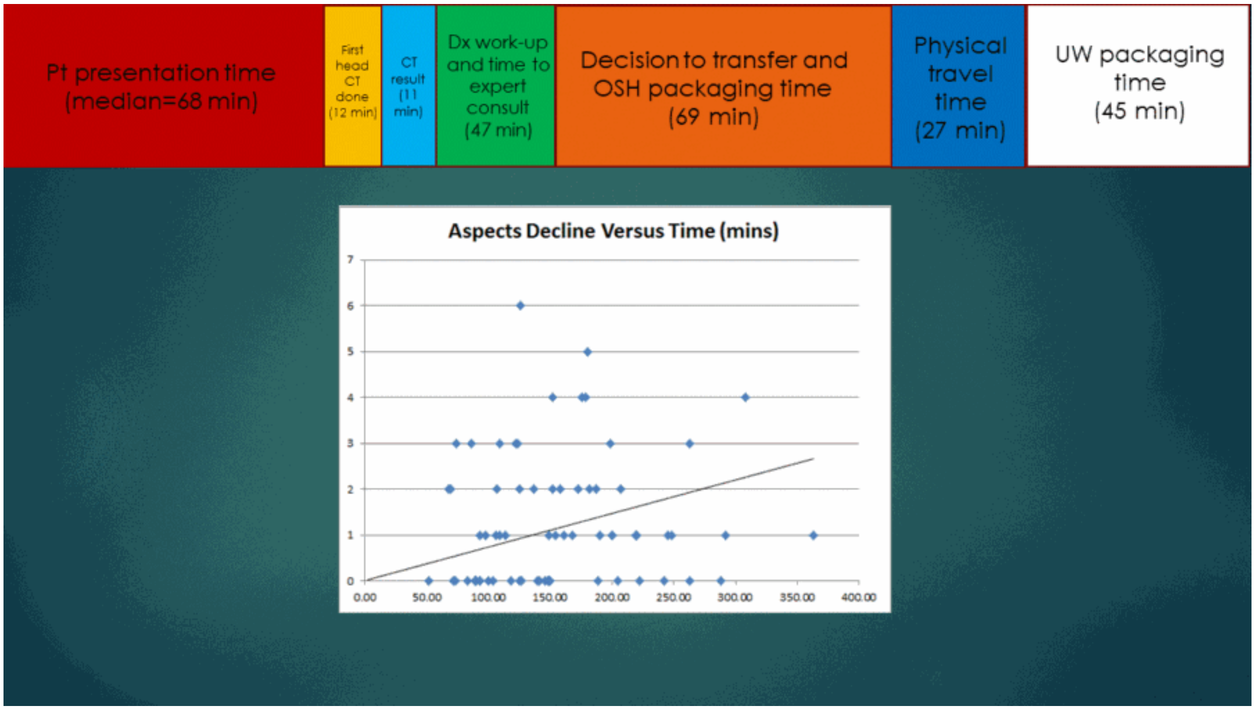

(Filename: TCT_2553_Wheredidthetimego_Coburn.gif)

Wednesday, May 22, 2019
4:30PM - 6:00PM
Epilepsy and Neuropsychiatric Imaging Adult Brain

2952

4:37PM - 4:44PM

Assessment of Explicitly Stated Interval Change on Non-Contrast Head CT Radiology Reports

M Braileanu[1], K Crawford[2], R Key[3], M Mullins[4]
[1]Emory University Hospital, Atlanta, GA, [2]Emory University, Atlanta, GA, [3]EMORY UNIVERSITY SCHOOL OF MEDICINE, DECATUR, GA, [4]EMORY UNIVERSITY, ATLANTA, GA

Purpose
Assessment of interval change is important to the radiology consultation when comparison to prior is appropriate. The purpose of this study is to assess when interval change (IC) is explicitly stated in non-contrast head CT radiology reports.
Materials and Methods
A retrospective review was preformed of radiology reports from January 2014. Reports with at least one prior non-contrast head CT and one diagnosis were include. Normal studies and comparisons to other modalities (MRI) were excluded. Whether IC was mentioned in the body or impression of the report was collected. All abnormalities were grouped into: 1=microvascular/lacunar, 2=infarct, 3=volume loss, 4=ventricular caliber, 5=hemorrhage, 6=postsurgical, 7=mass effect, and 8=other. Descriptive and subgroup (Fisher's exact test) statistical analyses were performed. This study was IRB approved.
Results
In total 45 patients with 165 radiographic abnormalities were identified; mean age was 66±19 years with 44%(n=20) females. Average interval between studies was 386±765 days. Interval change was mentioned

57.6%(n=95) in the body, and 54.5%(n=90) in the impression of all reports. Subgroup analysis is displayed in Table 1.

Conclusions

Interval change reporting is variable, mentioned in just over half of radiology report bodies and impressions. In the body, IC of "microvascular/lacunar" were significantly less likely to be reported, while "mass effect" was more likely. In the impression, IC of "volume loss" and "other" were less likely to be report, while "hemorrhage" was more likely. However, even reporting for important diagnoses, such as mass effect and hemorrhage, was only 80-90%. Consistent and standardized reporting of interval change for certain diagnoses may improve the clinical utility of radiology reports.

Table 1: Subgroup Analysis of Interval Change (IC) (n=165)

Group	n(%)	IC Body (n=yes[%])	Fisher's exact test p-value	IC Impression (n=yes[%])	Fisher's exact test p-value
Microvascular/lacunar	34(20.6%)	11(32.4%)	0.002*	17(50.0%)	0.6
Infarct	9(5.5%)	4(44.4%)	0.5	3(33.3%)	0.3
Volume loss	17(10.3%)	9(52.9%)	0.8	5(29.4%)	0.04*
Ventricular caliber	18(10.9%)	13(72.2%)	0.2	11(61.1%)	0.6
Hemorrhage	18(10.9%)	14(77.8%)	0.08	15(83.3%)	0.01*
Postsurgical	25(15.2%)	19(76.0%)	0.05	18(72.0%)	0.08
Mass effect	12(7.3%)	11(91.7%)	0.01*	10(83.3%)	0.07
Other	32(19.4%)	14(41.2%)	0.11	11(32.4%)	0.02*

*statistically significant with a p<0.05

(Filename: TCT_2952_Table1.jpg)

2707

4:44PM - 4:51PM

Default Mode Network Functional Connectivity Post Stroke and Association with Depression

V Nair[1], R Mohanty[2], B Moreno[2], N Tellapragada[2], T Kang[2], V Prabhakaran[3]
[1]University of Wisconsin Madison, School of Medicine and Public Health, Madison, WI, [2]University of Wisconsin Madison, School of Medicine and Public Health, MADISON, WI, [3]University of Wisconsin Madison, MADISON, WI

Purpose

To identify differences in resting functional connectivity (rsFC) in the default mode network (DMN) after stroke and to explore the predictive accuracy of DMN connectivity on post-stroke depression scores.

Materials and Methods

Resting-state data from 36 stroke patients (SP) and 19 healthy controls (HC) were analyzed. The Center for Epidemiological Scale-Depression (CES-D) scores were recorded for all. After standard rsFC preprocessing (SPM12; Matlab; DPABI toolbox) (ref1) the time-series for 6 regions in the DMN were extracted (ref2) and a 15x15 correlation matrix computed. Correlation coefficients were input in the Network Based Statistic (NBS) toolbox (ref3) to examine group differences. In Model 1, age, gender, and intracranial volume were entered as covariates, and in Model 2, CES-D score was entered as an additional covariate. Associations between CES-D score and DMN FC were investigated using a linear-kernel support vector regression (SVR) analysis with non-parametric permutation tests based on root mean squared error. Group differences for rsFC were considered significant at $p < .05$ (FWE corrected) and for the SVR at $p < .05$.

Results

Patients had significantly higher depression scores (mean=7.8, stdev=7.18) compared to HC, (mean = 4,

stdev=3.6), p <.05. Model 1 identified decreased connectivity in SP in the medial PFC (mPFC) and posterior cingulate cortex (PCC), and between the mPFC and the right lateral parietal cortex connections (R.LPC; p = .04). Model 2, with CES-D as covariate revealed reduced connectivity in SP in mPFC and L LPC as well (p=.01). SVR analysis showed a significant correlation between rsFC and CES-D in HC ($R2=0.37$; p = 0.02) based on connectivity in mPFC (with PCC and L.LPC) but not the SP ($R2=0.04$; p = 0.61) due to lack thereof.
Conclusions
These results suggest that rsFC within the DMN is associated with the processing of affect and that impairment in these connections may be associated with depression after stroke.

3403

4:51PM - 4:58PM

Diffusion Kurtosis Imaging of Temporal Lobe Epilepsy Patients with Bilateral Temporal Encephalocele and Unilateral Seizure Focus Reveals Microstructural Pathology

D Roberts-Wolfe[1], M Yazdani[2], L Bonilha[1]
[1]*Medical University of South Carolina, Charleston, SC,* [2]*Medical University of South Carolin, Charleston, SC*

Purpose
Learning objectives: describe the role of diffusion kurtosis imaging in identification of microstructural pathology in patients with temporal lobe epilepsy and temporal encephalocele Patients suffering from temporal lobe epilepsy may possess temporal encephaloceles (TEs) - herniations of brain through skull. TEs are thought to be epileptogenic based on curative resection. Seizure focus does not always correlate with TE location, suggesting that additional microstructural pathology may moderate the relationship between TE and epilepsy. The purpose of this study was to identify this pathology using diffusion kurtosis imaging (DKI) which models non-gaussian diffusion of water in brain tissue.
Materials and Methods
26 patients (23 F, age 42 +/- 11.3 years) with bitemporal encephalocele and unilateral seizure focus (18 left) underwent diffusion kurtosis imaging (DKI). DKI parameters included (NEX 10) b0 images and (NEX 1) 30 diffusion directions for 2 gradient strengths (b=1000 and 2000). Diffusivity and kurtosis tensors were estimated using DKE software, and were orthogonalized to calculate mean, axial, and radial kurtosis and diffusivity, as well as conventional and kurtosis-based fractional anisotropy (FA and KFA) for each voxel. These images were non-linearly normalized to MNI152 standard coordinates, and non-parametric permutation inference testing (500 permutations) was conducted using threshold free cluster estimation (family-wise error corrected alpha of 0.05) was used to compare patients with left vs. right temporal seizure focus.
Results
Fractional anisotropy revealed differences between patients with left and right seizure focus despite the presence of bitemporal encephaloceles. Differences were most pronounced in anterior corpus callosum.
Conclusions
Use of diffusion metrics can provide important additional information in the approach to temporal lobe epilepsy patients with temporal encephalocele. Future directions include comparison of TE patients to those with hippocampal sclerosis and healthy controls, prediction of TE resection based on DKI metrics, and histological examination of tissue with high kurtosis signal for downregulated glutamate transporter GLT1.

3462

4:58PM - 5:05PM

Global and Local Efficiency of Brain Networks in Treated HIV Infection

E O'Connor[1], T Zeffiro[1]
[1]*University of Maryland Medical Center, Baltimore, MD*

Purpose
There is abundant evidence that HIV infection, even when treated, has enduring and progressive effects on brain structure and function (1,2). These changes are accompanied by behavioral impairments. Nevertheless, the mechanisms linking these neural and behavioral phenomena are incompletely understood. The central purpose of this study was to determine whether network resting state (rs-fMRI) measures of inter-regional intrinsic functional connectivity and sensorimotor behavior could provide an integrated account of network dysfunction in HIV infection.
Materials and Methods
We studied 31 seropositive and 20 seronegative participants, ages 41-64, all receiving anti-retroviral therapy. First, serostatus effects, controlling for age and drug use, on neuropsychological test performance were modeled. Next, we used functional connectivity analysis of 3T rs-fMRI (TR 2 sec, 150 time points) to investigate changes in network global and local efficiency related to HIV infection.
Results
HIV infection was associated with decreases in attention (digit span), sensorimotor speed (pegboard), and spatial skills (block design) ($p<0.05$). Functional connectivity analysis using network metrics revealed higher overall global, but not local, efficiency in HIV infected participants. Regional analysis revealed higher global efficiency in the cerebellum, posterior parietal and lateral temporal cortices in HIV infected participants (Figure 1). ($p<0.05$ FDR corrected).
Conclusions
HIV infection has effects on neural information transfer that do not reverse with anti-retroviral therapy. These effects are evidenced by higher global efficiency, the information exchange efficiency in parallel processing systems in which nodes exhibit exchange information using the shortest paths. In contrast, local efficiency, the extent of integration among immediate neighbors, was unaffected by HIV infection. The regional pattern of global efficiency changes revealed effects in corticocerebellar systems responsible for multimodal sensory integration and movement control, consistent with the observed pattern of neuropsychological effects. Global network efficiency measured using rs-fMRI may be a useful marker of HIV effects on regional brain function.

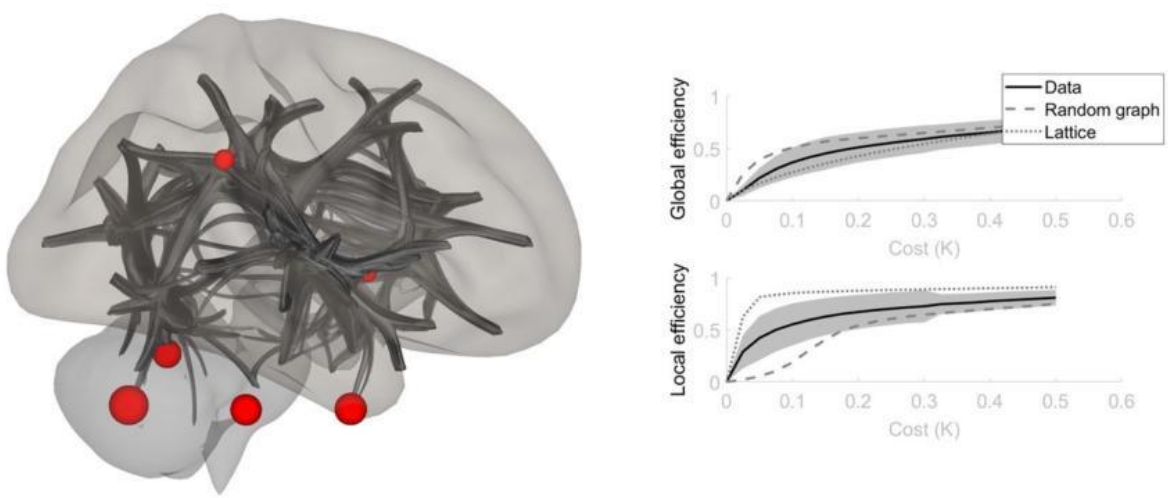

Figure 1. (LEFT) Nodes exhibiting higher global efficiency in the seropositive participants. Right lateral view. (RIGHT) Effects of various cost thresholds on overall global and local efficiency estimates, compared to lattice and random graphs. A cost threshold of 0.2 was used in the present study.

(Filename: TCT_3462_ASNR_2018_fig.jpg)

3377

5:05PM - 5:12PM

Initial Experience with PET-MR for the Evaluation of Temporal Lobe Epilepsy

J Rispoli[1], P Dugan[1], M Holmes[1], E Zan[2], T Shepherd[1]
[1]NYU Langone Health, New York, NY, [2]NYU Langone Health, New York , NY

Purpose
Imaging plays an important role in the management of medically refractory epilepsy, as these patients often become surgical candidates. We aim to determine the benefit of integrated PET-MRI in the evaluation of patients with epilepsy, specifically those with temporal lobe epilepsy. We hypothesize that there is a synergistic effect of PET and MRI for the detection of epileptogenic lesions that are otherwise not detected on conventional MR imaging.
Materials and Methods
We retrospectively reviewed the first 395 integrated PET-MRI cases performed at our institution for the evaluation of "epilepsy". Patients were scanned on a 3-T integrated PET-MRI scanner with an epilepsy protocol and dedicated temporal lobe imaging. All cases were adjudicated by an expert epileptologist utilizing, pre-operative EEG, seizure semiology and imaging. For patients that underwent subsequent surgery, surgical outcomes and pathology were recorded.
Results
Of the 395 patients with PET-MR examinations, overall 140/395 PET-MRI patients were determined to have temporal lobe epilepsy by an expert epileptologist. Of those with TLE and prior MR negative cases, there was an increase in detection rate of findings of up to 45% in bilateral TLE (5/11 patients), 33% in right TLE(9/27 patients) and 27% in left TLE.(9/33 patients). In patients with frontal lobe epilepsy, the second most common group, 7/34 patients with prior negative MRI had frontal lobe findings on PET-MR . Pathology and Engel outcomes will also be reviewed.
Conclusions
Integrated PET-MRI has the potential to play a crucial role in pre-operative planning for epilepsy beyond conventional MRI. Previous studies utilized separately acquired PET and MR studies and focus on focal cortical dysplasia as a cause of epilepsy. Integration of PET and MRI can have a synergistic effect in detecting causes of focal epilepsy.

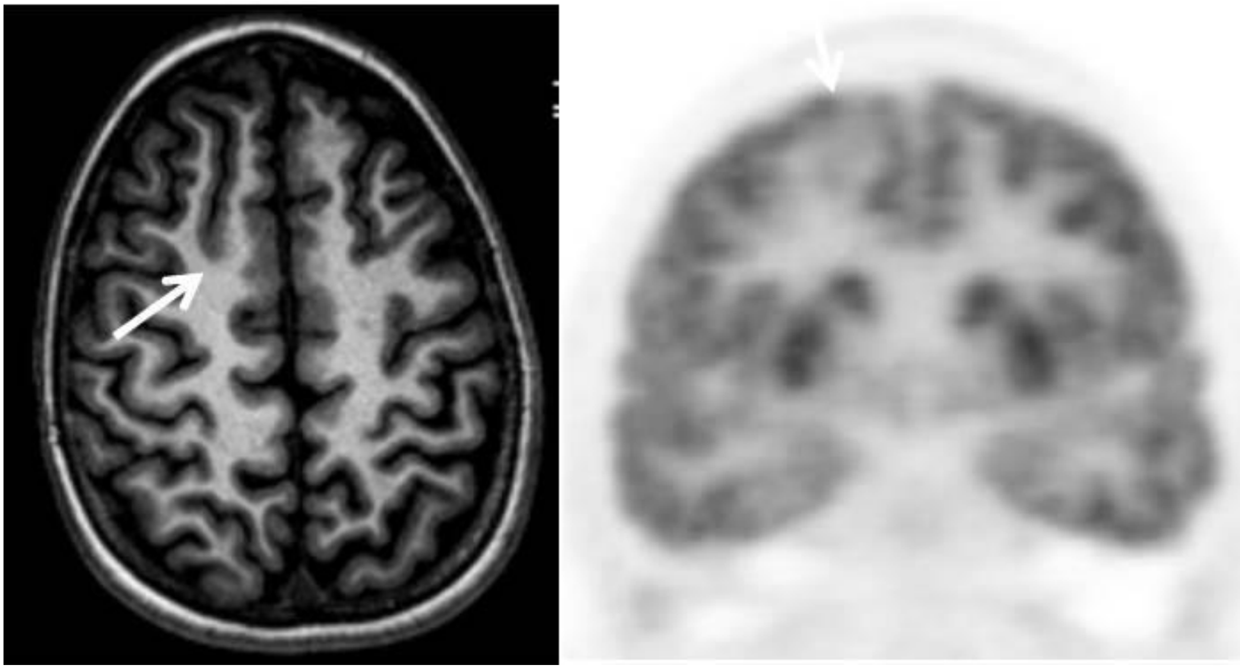

(Filename: TCT_3377_PETMRIASNR.jpg)

2488

5:12PM - 5:19PM

Noninvasive Neuromodulation in Rat Models of Pain and Depression

D Martin[1], J Bishop[2], Z Huang[2], J Wang[2], R Airan[2]
[1]STANFORD UNIVERSITY, STANFORD, CA, [2]Stanford University, Stanford, CA

Purpose
Focused ultrasound mediated drug release is a promising technique for noninvasive neuromodulation whereby ultrasound is used to selectively release neuroactive agents in targeted regions of the nervous system, combining the spatial precision of ultrasound with the robust, clinically validated principles of neuropharmacology. In this work we have applied focused ultrasound to animal models of various neuropsychiatric disorders, including depression and chronic/neuropathic pain.
Materials and Methods
Perfluorocarbon poly(ethylene glycol)-poly(lactic-co-glycolic acid) (PEG-PLGA) nanoparticles were prepared and loaded with different neuroactive agents, including ketamine and ropivacaine. The physical properties of the particles, including size, drug loading, and in vitro drug release, and the toxicity and pharmacokinetics in rats were evaluated. After initial characterization of the particles was completed, both central (ketamine release in the infralimbic cortex for depression) and peripheral (ropivacaine release in the sciatic nerve for neuropathic pain) nervous system applications of focused ultrasound were evaluated using standard animal behavior models.
Results
Ketamine- and ropivacaine-loaded polymeric nanoparticles demonstrated appropriate size, drug loading, and in vitro drug release. Toxicity and biodistribution of the drug-loaded nanoparticles were similar to previous compounds and appropriate for in vivo use. Using a combination of imaging and stereotactic guidance, we were able to successfully use focused ultrasound to release drug in a spatially and temporally controlled manner in order to modulate the behavior of the animals.

Conclusions
Noninvasive neuromodulation via focused ultrasound mediated drug release shows great potential for diagnosis and therapy of neuropsychiatric illnesses, including depression.

2552

5:19PM - 5:26PM

Temporal Encephaloceles in Patients with Refractory Epilepsy: Underdiagnosed but Uncommon

K Bhatia[1], R Mohanraj[1], P Cooper[1], M Bailey[1], V Josan[1], A Ponnusamy[1], O Thomas[1]
[1]*Salford Royal Hospital, Manchester, United Kingdom*

Purpose
Temporal lobe encephaloceles, herniation of brain parenchyma through the floor of the middle cranial fossa, can act as potential foci for seizures. However, they remain an under recognised structural cause of refractory temporal lobe epilepsy as they are easily overlooked on imaging. Recent literature suggests that the prevalence of these lesions is up to 13-14%. We examined imaging for patients referred to our regional epilepsy surgery service to review the prevalence in this cohort.
Materials and Methods
Patients were identified using electronic records of referrals to our regional service over a 6 year period (June 2012-June 2018). Those with refractory seizures of temporal lobe semiology, based on clinical and EEG findings referred for surgical evaluation, were retrospectively reviewed. Those without available pre-operative imaging were excluded. All imaging was performed using our local epilepsy protocol, which includes high-resolution T2 and T1 weighted sequences and was performed on 1.5T or 3T scanners.
Results
A total of 151 patients were referred within this period with refractory temporal lobe seizures. In 3 patients, the available imaging was of inadequate quality to assess for encephaloceles. 111 had an alternative underlying temporal lesion that could be attributed as the cause for seizures, the commonest being medial temporal sclerosis, others including tumours and cavernomas. 8 were demonstrated to have temporal encephaloceles, equivalent to 5% (8/149) of those referred with refractory temporal lobe seizures. Of these cases, 3 were identified before review at the regional service.
Conclusions
Whilst it remains true that temporal encephaloceles are an under reported cause for refractory temporal lobe seizures, and should be an important review area for all involved in reporting epilepsy imaging, with detection potentially reducing further investigations such as invasive EEG in these patients, the prevalence in our regional population is significantly lower than reported in recent literature.

Wednesday, May 22, 2019
4:30PM - 6:00PM
MRI of Neurovascular Diseases

2818

4:37PM - 4:44PM

Spot Sign in Secondary Intraventricular Hemorrhage (IVH) Predicts Early Neurological Decline

J Soun[1], D Montes[1], F Yu[2], J Goldstein[3], J Romero[1]
[1]*Massachusetts General Hospital, Boston, MA,* [2]*University of Texas Southwestern Medical Center, Dallas, TX,* [3]*Massachusetts General Hospital and Harvard Medical School, Boston, MA*

Purpose
The spot sign has been shown to play an important role in intracerebral hemorrhage expansion and neurological decline. However, the relationship of the spot sign to secondary IVH has not been well established. We aimed to investigate the role of the spot sign in clinical outcomes of patients with secondary IVH.
Materials and Methods
We examined secondary IVH patients (n=57) who had CTAs in the Antihypertensive Treatment of Acute Cerebral Hemorrhage II (ATACH-II) randomized clinical trial. We evaluated for the presence of a spot sign on CTA and measured IVH volumes on admission and 24-hour non-contrast CT scans. Early neurological decline (END) was assessed by the Glasgow Coma Scale (GCS) and NIH Stroke Scale (NIHSS) in the first 24 hours. The relationship of the spot sign to END, hydrocephalus, need for a ventricular drain, IVH expansion, and modified Rankin score at 90 days was evaluated.
Results
The spot sign was a significant predictor of END in univariate ($p < 0.004$ for GCS and $p < 0.01$ for NIHSS) and multivariate analyses. Multivariate analyses showed clinically significant decline (decrease of ≥ 2 points) of GCS scores (OR= 4.9, CI 1.3 to 18.74, $p < 0.019$; see Figure 1) and significant change in GCS and NIHSS scores in the first 24 hours (β coefficient = -2.52, $p < 0.008$, CI -4.36 to -6.68 for GCS and β coefficient = 4.72, $p < 0.02$, CI 0.77 to 8.68 for NIHSS). No significant association was seen between the spot sign and other outcome measures.
Conclusions
The presence of the spot sign is linked to early neurological deterioration in patients with secondary IVH. Identifying this radiologic feature could have important implications for triaging patients to the appropriate level of care.

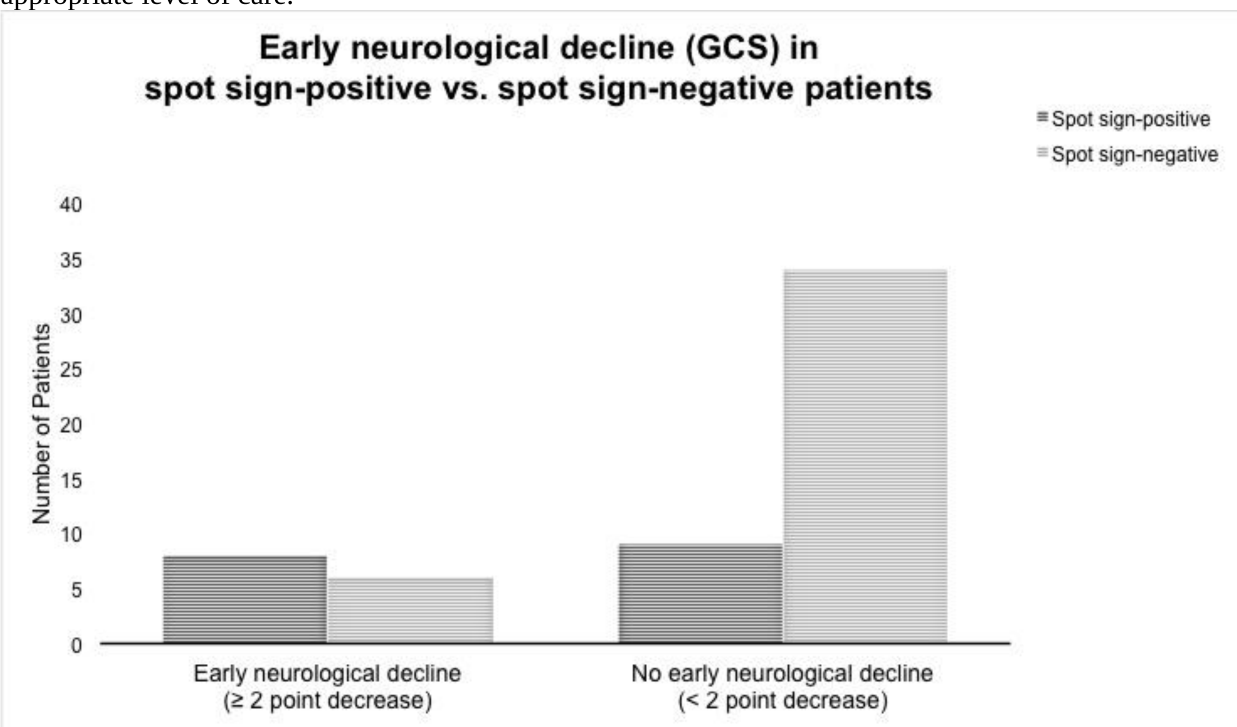

(Filename: TCT_2818_Figure1.jpg)

2711

4:44PM - 4:51PM

Identification of Patients Within Thrombolysis Time Window: Direct Comparison of DWI-FLAIR Mismatch and CT-Based Lesion Water Uptake Quantification in Acute Stroke Patients Receiving Both Imaging Modalities

G Broocks[1], A Kemmling[2], U Hanning[3], T Faizy[4], G Schön[5], G Thomalla[5], J Fiehler[6], F Flottmann[7], P Sporns[8], H Leischner[9]
[1]University Medical Center Hamburg-Eppendorf, Hamburg, Germany, [2]University Hospital Münster, Münster, NRW, [3]University of Hamburg-Eppendorf, Hamburg, Germany, [4]UNIVERSITY MEDICAL CENTER - HAMBURG, HAMBURG, GERMANY, [5]University Hamburg, Hamburg, HH, [6]University Medical Center Hamburg-Eppendorf, Hamburg, AK, [7]UKE Hamburg, Hamburg, HH, [8]University Münster, Münster, NRW, [9]University Hospital Hamburg, Hamburg, HH

Purpose
Mismatch in visibility of an acute ischemic lesion between diffusion-weighted MRI (DWI) and fluid-attenuated inversion recovery (FLAIR), as well as computed tomography (CT) based quantification of lesion water uptake can be used to identify wake-up stroke patients with lesion age <4.5 hours from symptom onset. However, it is uncertain whether CT may replace MRI in wake-up stroke patients to enable thrombolytic treatment. The purpose of this study was to test the performance of both methods to identify patients within 4.5 hours in patients who received both imaging modalities at admission.
Materials and Methods
In this pilot study, 34 patients with acute anterior circulation stroke and known time of symptom onset were analyzed who received both imaging modalities at admission. DWI-FLAIR mismatch was diagnosed by consensus reading and quantitative lesion water uptake (NWU) was calculated in admission CT. An established cut-off for NWU was applied to distinguish patients within and beyond 4.5 hours in a blinded fashion.
Results
In 17 patients, the time from symptom onset to admission imaging was <4.5h (range: 2-3.9h) and 17 patients presented after 4.5h (range: 4.6-7.8h). The mean (SD) time from CT to MRI was 30.8 (12.7) minutes. DWI/FLAIR mismatch correctly assigned 20/34 patients (59%) with a sensitivity of 47% and specificity of 71%. CT-based NWU correctly assigned 27/34 (80%) with a sensitivity of 82% and specificity of 76% using 11.5% as established threshold.
Conclusions
In this pilot study, CT-based quantitative NWU was superior to DWI-FLAIR mismatch in identifying patients within thrombolysis time window. After validation of these results with a higher number of patients, future trials could use quantitative NWU as imaging biomarker to stratify wake-up stroke patients enabling thrombolytic treatment.

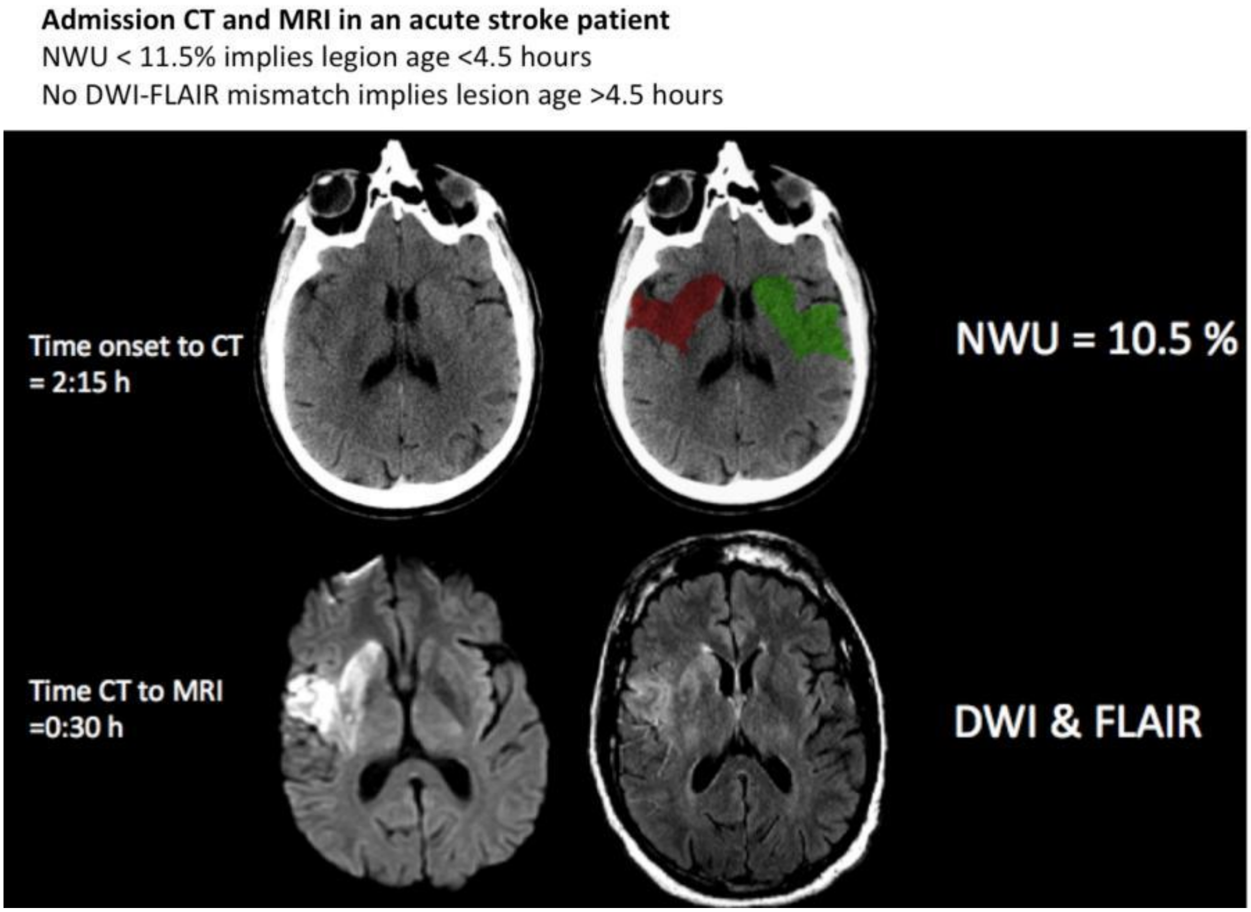

(Filename: TCT_2711_Prsentation1.jpg)

2900

4:51PM - 4:58PM

in Non-Recanalizing Stroke Patients as a Sign of Collateral Involvement Using DSC-MRI: A Substudy of the Observational 1000Plus Study

K Villringer[1], S Zimny[2], I Galinovic[3], C Nolte[3], J Fiebach[1], A Khalil[4]
[1]Charité Universitätsmedizin Berlin, Berlin, N/A, [2]Ev.-Luth. Diakonissenanstalt zu Flensburg, Flensburg, NA, [3]Charité-Universitätsmedizin, Berlin, NA, [4]Charité Universitaetsmedizin Berlin, Berlin, N/A

Purpose
The aim of this study was to evaluate the use of dynamic susceptibility contrast MRI (DSC-MRI) in acute stroke patients as a sign of collateral involvement.
Materials and Methods
Retrospective analysis of 186 patients enrolled into the prospective observational 1000Plus study (clinicaltrials.org NCT00715533). Inclusion criteria were vessel occlusion on day1 MR-angiography, imaging within 24 hours after stroke onset and follow-up perfusion imaging. MRI examination was performed on a 3 T MRI scanner with a standard stroke imaging protocol1. Reperfusion in non-recanalizers (the interaction between reperfusion and recanalization), hypoperfusion intensity ratio (HIR=Tmax>8s/Tmax>2s) on day1 and the Higashida score using substracted dynamic MR perfusion source images2 on day1 were used as markers of collateral flow. The influence of these variables on clinical and imaging outcome was assessed using robust linear regression.

Results
Sixty-seven patients (36%) showed persistent vessel occlusion on follow-up examination (29.6% of whom reperfused), 64 (34.4%) partial and 55 complete recanalization. There was a significant relationship between Higashida score and HIR (b=-1.67, t=-5.26, p<0.0001), however not between Higashida score and the interaction between recanalization and reperfusion (reperfused partial recanalizers: b=0.23, t=0.52, p=0.607; reperfused non-recanalizers: b=0.18, t=0.38p=0.704). The interaction between recanalization and reperfusion was however associated with HIR (b=-0.18, t=-2.45, p=0.016). NIHSS on admission (b=0.15, t=5.01, p<0.0001) was associated with higher mRS day90, and thrombolysis (b=-0.91, t=-3.17, p=0.002) as well as Higashida scores 2, 3, 4 (b=-2.09, T=-2.63, p=0.001; b=-2.13, t=-2.54, p=0.01; b=-2.45, t=-2.90, p=0.005 respectively) were associated with lower mRS day90. There was no interaction between recanalization status and reperfusion on long-term outcome.
Conclusions
Patients with favorable Higashida scores have better clinical outcomes. The presence of reperfusion in non-recanalizers was not associated with clinical outcome, but was associated with HIR.

2612

4:58PM - 5:05PM

Longitudinal Analysis of Quantitative Brain MRI in Astronauts Following Microgravity Exposure

R Riascos[1], A Kamali[1], R Hakimelahi[2], B Mwangi[1], P Rabiei[1], B Bagheri Behzad[3], L Kramer[1], K Hasan[1]
[1]The University of Texas Health Science Center at Houston, Houston, TX, [2]Memorial Sloan Kettering Cancer Center, New York, NY, [3]Texas Tech University Health Sciences Center at El Paso, El Paso, TX

Purpose
To retrospectively evaluate the effects of microgravity on the brains of astronauts by obtaining and analyzing micro- and macro-structural measures using quantitative magnetic resonance imaging (qMRI), before and after microgravity exposure. We hypothesize that subtle structural change, manifested by alterations in diffusion tensor imaging (DTI) metrics including fractional anisotropy and mean diffusivity, will affect regions involved in visual function.
Materials and Methods
Quantitative MRI data sets in 19 astronauts were acquired before the flight and repeated after completion of each mission. Both anatomical (volumetric) and microstructural (diffusion tensor imaging-based) measures were analyzed. Paired t-tests were used to compare pre- and post-flight measures. Pearson correlation coefficient and linear regression were used to test the association of qMRI measures with age of the astronauts.
Results
The fractional anisotropy was reduced in the right posterior thalamic radiations (Fig-1, p=0.0009). An increase in the mean diffusivities of different sub-regions of the occipital cortex on the right side (Fig-2), including calcarine (p=0.01), middle occipital (p=0.02), inferior occipital (p=0.03) and fusiform gyri (p=0.04) was noted. There was cortical thinning involving the right occipital lobe (p=0.03, t=2.4) and bilateral fusiform gyri (Fig-3). The volume of thalamus showed a reduction on the left side (Fig-4, p=0.02, t=2.6). An increase in lateral ventricular volume in the post-flight scans was found.
Conclusions
Our findings could be secondary to microgravity-induced intracranial hypertension, intracranial fluid redistribution, brain volume loss, micro-anatomic changes, rearrangement of the white matter or psychological stress during space flight. This study may provide neuroanatomical evidence of brain dysfunction or neuroplasticity in microgravity conditions and may offer an improved understanding of the mechanisms involved in intracranial pressure elevation and vision changes in a subset of crewmembers. Further research is still needed to corroborate some of the mechanisms proposed in this study.

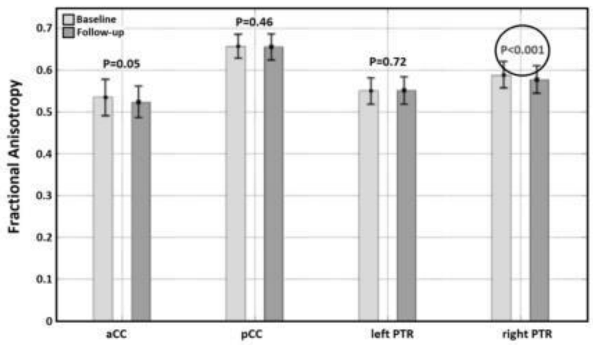

Figure-1. Pre-flight vs. post-flight fractional anisotropy (FA) of selected white matter regions.

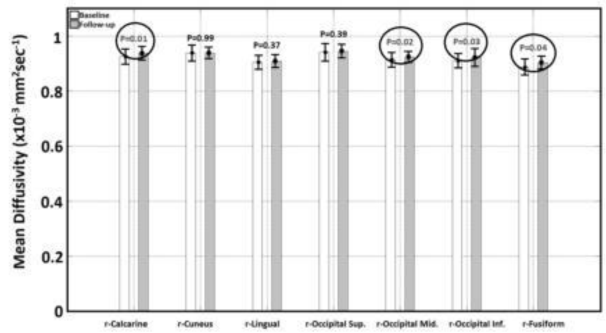

Figure-2. Mean diffusivity in the right occipital cortical domains.

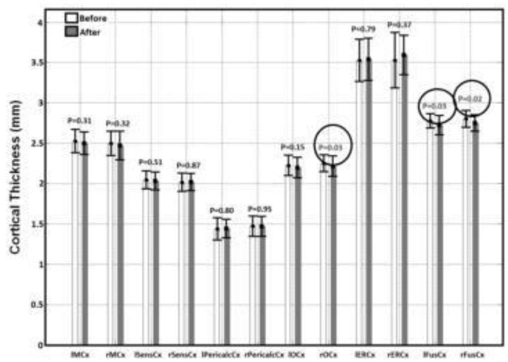

Figure-3. Pre-flight vs. post-flight regional cortical thickness.

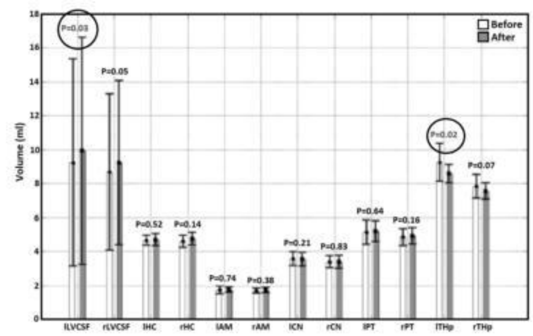

Figure-4. Post-flight volumetric data compared with the pre-flight baselines.

- "r" before the name of the domain is referring to the right side.
- MCx=motor cortex, SensCx=sensory cortex, PericalcCx=peri-calcarine cortex, OCx=occipital cortex, ERCx=entorhinal cortex, FusCx=fusiform cortex
- Lateral ventricular CSF (LVCSF), Hippocampi (HC), Amygdalae (AM), Caudate nuclei (CN), putamina (PT), and Thalamus proper (THp)

(Filename: TCT_2612_dti_BW_700dpi_FINAL.jpg)

2610

5:05PM - 5:12PM

Pre- and Post-Flight Size Comparison of the Major Dural Venous Sinuses in Astronauts

P Rabiei[1], B Behzad[2], K Hasan[1], A Kamali[1], L Kramer[1], R Riascos[1]
[1]The University of Texas Health Science Center at Houston, Houston, TX, [2]Texas Tech University Health Sciences Center at El Paso, El Paso, TX

Purpose
Intracranial hypertension can alter the configuration of anatomic structures of the central nervous system. Astronauts have shown signs of increased intracranial pressure after returning from space flights. We aimed to determine if there is a statistically significant difference in the size of transverse and superior sagittal sinuses pre and post flight in astronauts.
Materials and Methods
Seventeen astronauts were scanned pre- and post-flight, using a 3Tesla Verio MRI (Siemens). 3D isovolumetric T1 Weighted images of their brains with isotropic voxel size of 1 mm were obtained in sagittal planes. The area of the sagittal sinus in the axial plane and the area of the left and right transverse sinuses in the coronal plane were measured using MRIcron (Fig, A, B, C). The averages of pre- and post-flight areas of the transverse and superior sagittal sinuses were compared using paired t-test.

Results

MR images of seventeen astronauts were evaluated with average age of 47.3 years and average time in flight of 82.7 days. Post flight average sizes of the right and left transverse venous sinuses were significantly decreased compared to pre-flight status (Fig. D), from 130.47 mm2 and 128.59 mm2 to 126 mm2 and 124.12 mm2 respectively (both p-values < 0.05). Although post-flight superior sagittal sinus sizes also showed an average decrease (compared to pre-flight) from 108.29 mm2 to 106.29 mm2 in the astronauts, this decrease was not statistically significant (p-value = 0.139).

Conclusions

Our study showed post flight decrease in the size of the venous sinuses. These changes are similar to the ones described in patients with idiopathic intracranial hypertension. They can also be attributed to other structural brain changes in astronauts such as an increase in the size of the ventricles due to intracranial fluid redistribution or overproduction of CSF due to microgravity-related dynamic changes.

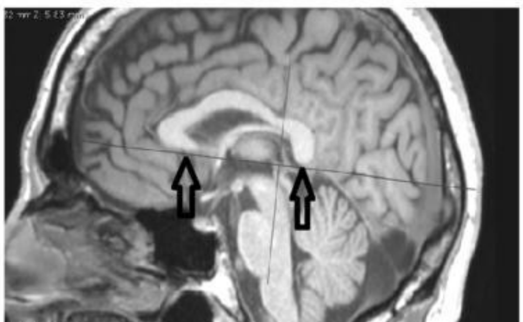

Fig. A

An axial plane was reconstructed that crossed the inferior aspect of the corpus callosum anteriorly and posteriorly.

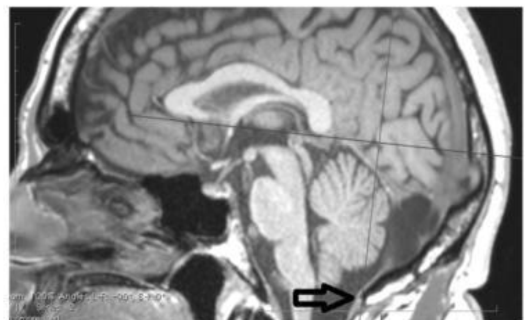

Fig. B

A coronal plain, perpendicular to the axial plane that crosses through the opisthion was also obtained.

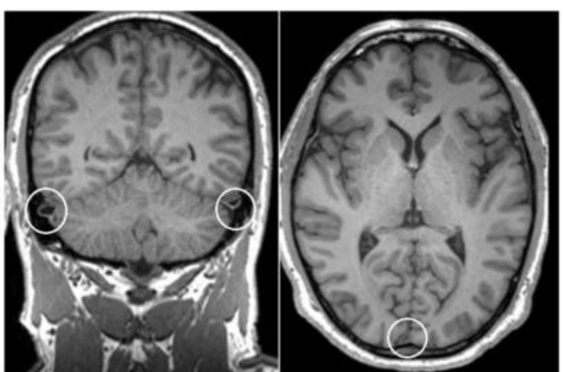

Fig. C

In the axial plane the area of the sagittal sinus and in the coronal plane, the area of the left and right transverse sinuses were also measured using MRIcron.

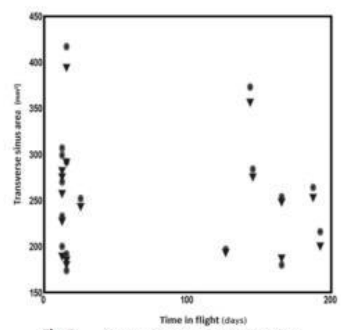

Fig. D (circle=pre flight , triangle=post flight)

This diagram shows that most astronauts showed decreases in size of transverse sinus after being exposed to microgravity.

(Filename: TCT_2610_venous_BW_700dpi_FINAL.jpg)

3529

5:12PM - 5:19PM

Prediction of Upper Extremity Motor Recovery after Stroke Using Diffusional Kurtosis Imaging

M Spampinato[1], W Feng[2], M Beasley[3], I Kabakus[4], N Somayaji[5]
[1]Medical University of South Carolina, Charleston, SC, [2]N/A, N/A, IN, [3]MUSC, Charleston, SC, [4]Department of Radiology and Radiological Science Medical University of South Carolina 96 Jonathan Lu, Charleston, SC, [5]Medica university of South Carolina, Charleston , SC

Purpose
The recovery of upper extremity (UE) motor function remains challenging to predict in acute stroke patients with severe motor impairment. Our purpose was to evaluate the association between diffusional kurtosis imaging (DKI)-derived measures of CST integrity and 3-month UE motor outcome in acute stroke patients with severe motor impairment.
Materials and Methods
Eight acute stroke patients with severe motor impairment underwent a brain MRI including DKI within four days after the onset of symptoms. Neurological evaluation included the Fugl-Meyer Motor Scale Upper Extremity (FM-UE) in the acute phase and 3 months post-stroke. For the CST in the lesioned and contralateral hemispheres, we estimated with DKI both pure diffusion metrics, such as the mean diffusivity and mean kurtosis, as well as model-dependent quantities, such as the axonal water fraction. Lesional hemisphere/contralateral hemisphere CST ratios were calculated for each diffusion metric. We also calculated diffusion metrics for the region of the CST caudal to the infarction (5-nearest slices region of interest). We evaluated the correlation between CST diffusion metrics, 5-nearest slices CST diffusion metrics, and motor outcome at 3 months using Spearman's rho correlation coefficient. Results were considered significant when $p < 0.05$.
Results
Mean kurtosis of the entire CST and axial kurtosis of the 5-nearest slices CST had the strongest associations with 3-month motor outcome measured using the FM-UE (respectively rho = -0.95 and rho = -0.95). Axial kurtosis and axial diffusivity of the entire CST had the strongest associations with 3-month motor recovery, defined as observed recovery/maximal possible recovery (respectively rho = -0.83 and rho = 0.81).
Conclusions
CST diffusion metrics related to the kurtosis have strong associations with 3-month motor outcome in stroke patients with initial severe motor impairment, and may have potential value in the prediction of motor recovery.

2756

5:19PM - 5:26PM

Spectrum of Perfusion and Diffusion Changes in the Setting of Hypoxic Ischemic Brain Injury: A Translational Pilot Study Using Swine Models

M Peckham[1], J Mcnally[2], S Kim[3], A DeHavenon[3], S Mckellar[4], J Tonna[3], S Youngquist[3]
[1]UNIVERSITY OF UTAH HEALTH SCIENCE CENTER, SALT LAKE CITY, UT, [2]UNIVERSITY OF UTAH, SALT LAKE CITY, UT, [3]University of Utah, Salt Lake City, UT, [4]University of Utah Health Sciences Center, Salt Lake City, UT

Purpose
Hypoxic ischemic brain injury (HIBI) results from hypoxia or low blood flow in cardiac and cardiopulmonary arrest. Because of the potential for profound disability, neuroprotective measures are critically important. Diagnostic tests are crucial to identify irreversible injury thresholds and for neuroprognostication. MRI can detect cellular injury and perfusion changes in response to HIBI, but time and severity of hypoxia are widely variable and response to treatment is often uncertain. To better understand and test recovery methods in a controlled fashion, an animal model is required. Our goal was to develop and test an MRI-compatible animal model of HIBI with rescue treatment.

Materials and Methods

Two healthy swine were placed under general anesthesia and underwent MRI with the following sequences: DTI at b2000/20 directions to measure cellular injury, and dynamic susceptibility contrast (DSC) to measure tissue perfusion. Following this, extracorporeal membrane oxygenation (ECMO) catheters were placed in the distal aorta and right atrium, and ventricular fibrillation (VF) was induced by a bipolar pacing catheter in contact with the right ventricle. The first animal underwent 10 minutes of VF and the second underwent 20 minutes VF to induce HIBI prior to ECMO rescue. Both animals were re-imaged two hours post-resuscitation using the same pre-arrest protocol with regions of interest drawn bilaterally above the level of the lateral ventricles.

Results

After 10 minutes of VF there was a +191% increase in CBF, +194% increase in CBV, and -6% change in ADC. After 20 minutes of VF there was a -25% decrease in CBF, +568% increase in CBV, and -35% change in ADC indicating profound cellular injury.

Conclusions

A spectrum of perfusion and diffusion changes was observed in two swine models undergoing 10 and 20 minutes of ischemia, with variable changes in CBF, increased CBV, and decreased ADC values with duration of cardiac arrest. These preliminary findings demonstrate feasibility of an MRI-compatible animal model to further understand the spectrum of injury in HIBI and devise better therapies and clinical measures of prognosis.

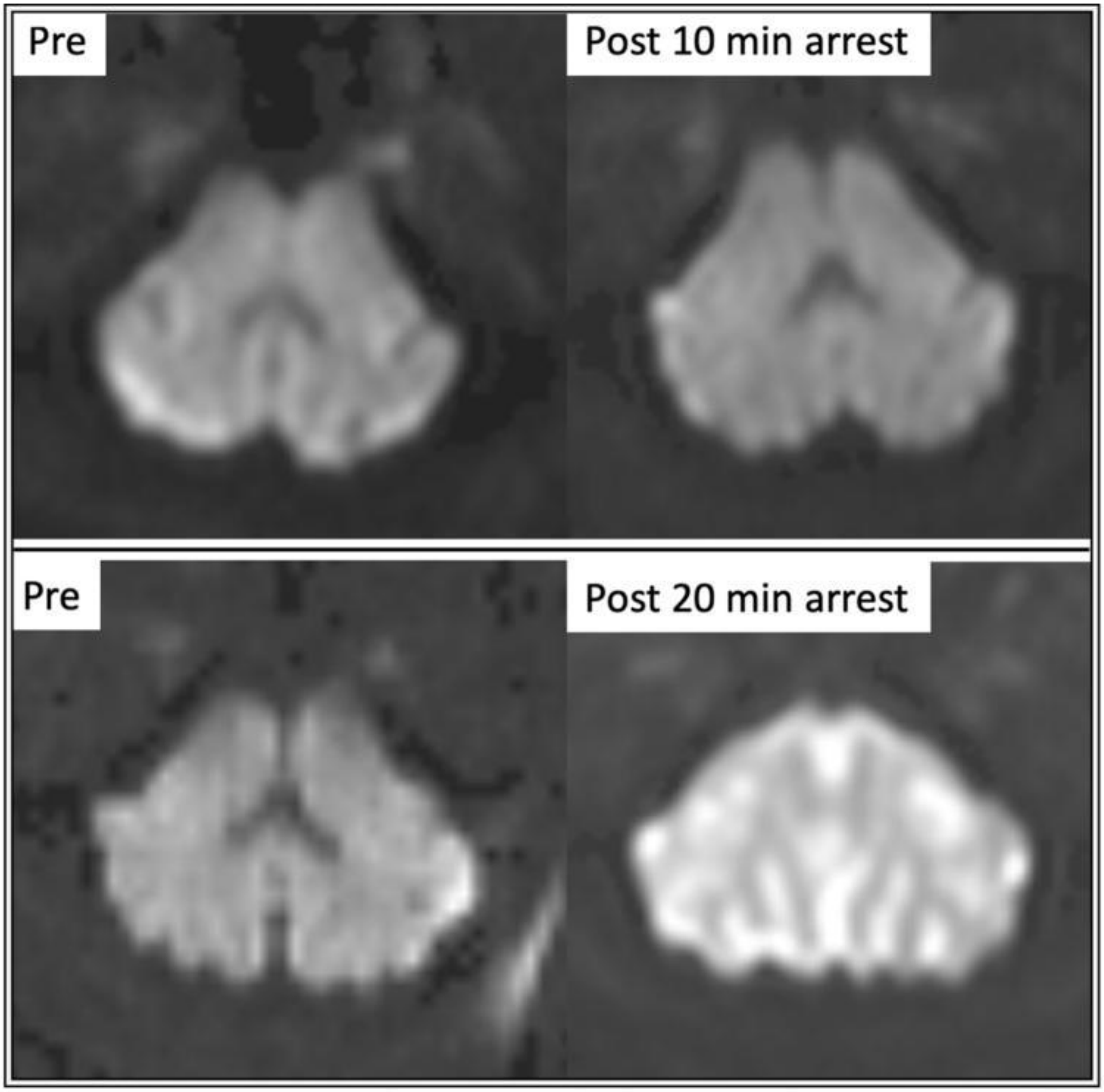

Figure: Brain MRI DTI of two swine before and after ischemia with ECMO rescue. The first animal demonstrated imperceptible changes on DTI after 10 minutes of ischemia (top row). After 20 minutes of ischemia, the second animal demonstrated global diffusion restriction and diffuse edema (bottom row).

(Filename: TCT_2756_HIBIfigure.jpg)

2511

5:26PM - 5:33PM

Stroke of Underterminded Source and Carotid Intraplaque Hemorrhage on MRI: A Systemic Review and Meta-Analysis

I Mark[1], P De Sanctis[2], L De Maria[3], D Nasr[4], L Saba[5], G Lanzino[4], V Lehman[1], W Brinjikji[4]
[1]MAYO CLINIC - ROCHESTER, MN, ROCHESTER, MN, [2]Humanitas University, Milan, Italy, [3]P.O. Gaspare Rodolico, Catania, CATANIA, [4]Mayo Clinic, Rochester, MN, [5]AOU Cagliari, Cagliari, Italy

Purpose
We performed a systemic review of the literature to determine the prevalence of carotid artery intraplaque hemorrhage on MRI vessel wall imaging in patients with embolic stroke of undetermined source (ESUS).
Materials and Methods
A literature search was performed of all studies with patients who had ESUS, carotid artery stenosis of less than 50%, and MRI vessel wall imaging published through October 2018.
Results
A total of 6 studies with 231 patients were included. The mean age was 67.8 years old. 69 patients were female (33.0%). The overall prevalence estimate for prevalence of plaque hemorrhage ipsilateral to the ischemic lesion was 26.3% (95%CI=10.9-41.8). The odds of having a plaque hemorrhage on the ipsilateral side versus the contralateral side was 7.52 (95%CI=2.15-26.37).
Conclusions
Patients with ESUS are shown to have ipsilateral unstable carotid atherosclerosis in approximately 25% of cases. Carotid artery vessel wall MRI should be considered in patients with cryptogenic stroke.

2939

5:33PM - 5:40PM

Stroke Stratification of Carotid Plaque by MRI Diffusion Weighted Imaging

M Peckham[1], S Kim[2], D Parker[2], G Treiman[2], J Mcnally[3]
[1]UNIVERSITY OF UTAH HEALTH SCIENCE CENTER, SALT LAKE CITY, UT, [2]University of Utah, Salt Lake City, UT, [3]UNIVERSITY OF UTAH, SALT LAKE CITY, UT

Purpose
Plaque rupture and embolization lead to stroke, the fifth leading cause of death and a large public health issue due to high morbidity and cost. Noninvasive imaging has been important for determining plaque stability for stroke prevention, with vulnerable plaque components including intraplaque hemorrhage (IPH) and lipid-rich necrotic core (LRNC). DWI has shown promise in further delineating these components, but can been limited due to motion at the carotid bifurcation. We sought to develop a motion-insensitive DWI sequence to evaluate ADC values of LRNC and hemorrhage in relation to stroke status.
Materials and Methods
DWI was obtained using motion insensitive 3D Diffusion Weighted Driven Equilibrium Stack of Stars (3D DW-DE SoS) (0.6 x 0.6 x 2 mm3 resolution). This sequence was optimized on phantom studies, then 22 patients with carotid disease were recruited to an IRB-approved study. DWI was performed at b20 and b450. ADC values were calculated and correlated with IPH and stroke status. Clinical cerebrovascular risk factors were recorded.
Results
22 patients (1 female) were recruited, (age = 66.7±10.1 years, BMI = 26.3±3.6kg/m2), 11 with smoking history, 17 with hypertension, 15 with dyslipidemia, and 10 with diabetes. Of 22 patients, 43 carotid plaques were analyzed after excluding 1 occluded carotid. 20/43 plaques were IPH-positive, and had lower ADC values than IPH-negative plaques (0.72±0.15 versus 1.01±0.18 x10-3mm2/sec, two-tailed t-test $p<0.001$). IPH volume negatively correlated with ADC over all patients ($r=-0.57$, $p<0.001$). Plaques associated with ipsilateral stroke (14/43) had lower ADC values compared to asymptomatic plaques (0.65±0.13 versus 0.98±0.17 x10-3mm2/sec, $p<0.001$). ADC values were lower in symptomatic plaques

that were either IPH-positive (0.63±0.10 vs. 0.83±0.13 x10-3mm2/sec, p=0.001) or IPH-negative (0.71±0.23 vs. 1.05±0.13 x10-3mm2/sec, p<0.001).
Conclusions
3D DW-DE SoS technique allows motion insensitive evaluation of carotid plaque diffusion parameters. Significantly lower ADC values are present in IPH-positive plaque, and ADC values negatively correlate with IPH volume. Additionally, there are lower ADC values in symptomatic plaques regardless of IPH-status. These results suggest that carotid plaque DWI may further stratify stroke sources and future risk and should be evaluated in larger studies.

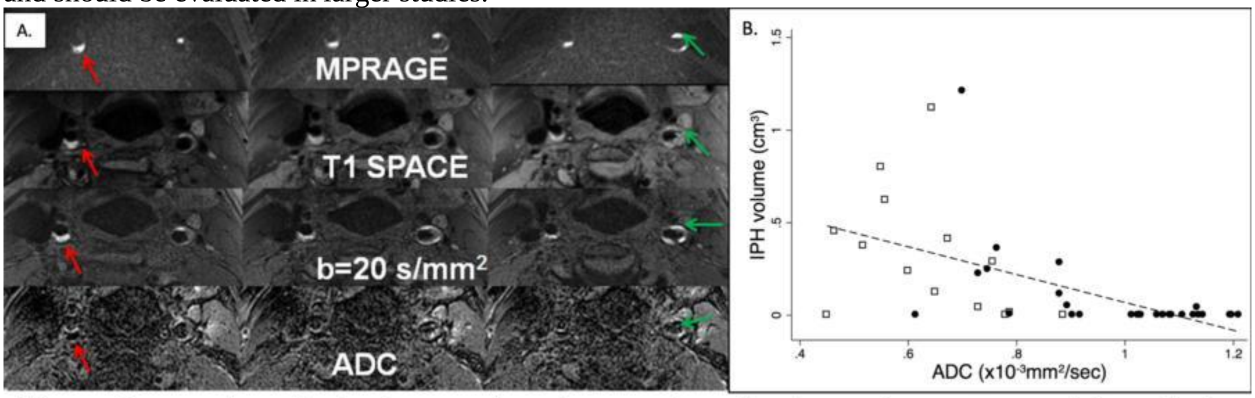

Figure A: symptomatic (red arrows) and asymptomatic plaque (green arrows) in a single patient demonstrate ADC differences (Symptomatic Hemorrhage=$0.32x10^{-3}$ mm²/s, Asymptomatic Hemorrhage =$0.92x10^{-3}$ mm²/s).

Figure B: Pooled data show the negative correlation between IPH volume and ADC value, with symptomatic carotid plaques in white squares and asymptomatic plaques in black circles.

(Filename: TCT_2939_carotidplaqueabstractfigure.jpg)

3175

5:47PM - 5:54PM

Vessel Wall MRI Contrast Enhancement in Cerebral Amyloid Angiopathy and Association with Stroke

J Mcnally[1], A Sakata[2], M Alexander[2], D Dewitt[2], S Kim[2], A DeHavenon[2]
[1]UNIVERSITY OF UTAH, SALT LAKE CITY, UT, [2]University of Utah, Salt Lake City, UT

Purpose
Arterial wall enhancement detected on vessel wall MRI (vwMRI) is associated with stroke risk in intracranial atherosclerosis. Other pathologies affect the intracranial arteries, including β-amyloid deposition in cerebral amyloid angiopathy (CAA). Our goal was to determine the association of vwMRI enhancement in CAA with acute ischemic stroke.
Materials and Methods
IRB approval was obtained for this retrospective study on patients undergoing 3T intracranial vessel wall MRI (vwMRI) from 2015-18. Chart review was used to collect patients diagnosed with CAA using modified Boston criteria. Vessel wall, leptomeningeal and focal parenchymal enhancement were detected on 3D pre and postcontrast flow-suppressed T1-weighted images. Interrater agreement was determined by prevalence/bias-adjusted Kappa analysis. Diffusion weighted imaging was used to detect recent infarction. Logistic regression was used to determine the association of each enhancement pattern with acute ischemic stroke.

Results

Out of 642 patients undergoing vwMRI, 42 patients were found to have CAA by modified Boston criteria (35 'probable' and 7 'possible'). These patients had an average age of 71.5±7.5 (mean±SD), 24/42 (57.1%) were female, and 28/42 (66.7%) had acute ischemic stroke on diffusion weighted images (DWI). CAA patients demonstrated vessel wall (26/42, 61.9%), leptomeningeal (26/42, 61.9%), and focal parenchymal (24/42, 57.1%) enhancement with prevalence/bias-adjusted Kappas of 0.80 (95%CI: 0.66-0.94), 0.72 (95%CI: 0.56-0.88) and 0.49 (95%CI: 0.29-0.70), respectively. Vessel wall enhancement was associated with acute ischemic stroke (OR=6.6, p=0.009) as was leptomeningeal enhancement (OR=5.4, p=0.017), but focal parenchymal enhancement was not (OR=1.5, p=0.509). Female gender (OR=2.4, p=0.190) and age (OR=1.03, p=0.510) were not associated with ischemic stroke status. Figure 1. Representative case of a 76-year-old male with mild cognitive decline and episodes of altered sensation was found to have probable CAA. DWI showed a small acute right anterior frontal infarct (A, arrow). SWI demonstrated with multiple peripheral and subcortical microhemorrhages meeting modified Boston criteria for probable CAA (B, arrowheads). Vessel wall imaging with postcontrast T1 weighted black blood (C and D) revealed arterial wall enhancement (C, arrows, inset). Posterior predominant leptomeningeal enhancement (D, arrows, inset) and parenchymal foci of enhancement (D, arrowhead) were also present.

Conclusions

In CAA, vessel wall and leptomeningeal enhancement was highly associated with acute ischemic stroke. In this population at high risk of ischemic stroke, vwMRI may have important diagnostic and prognostic impact.

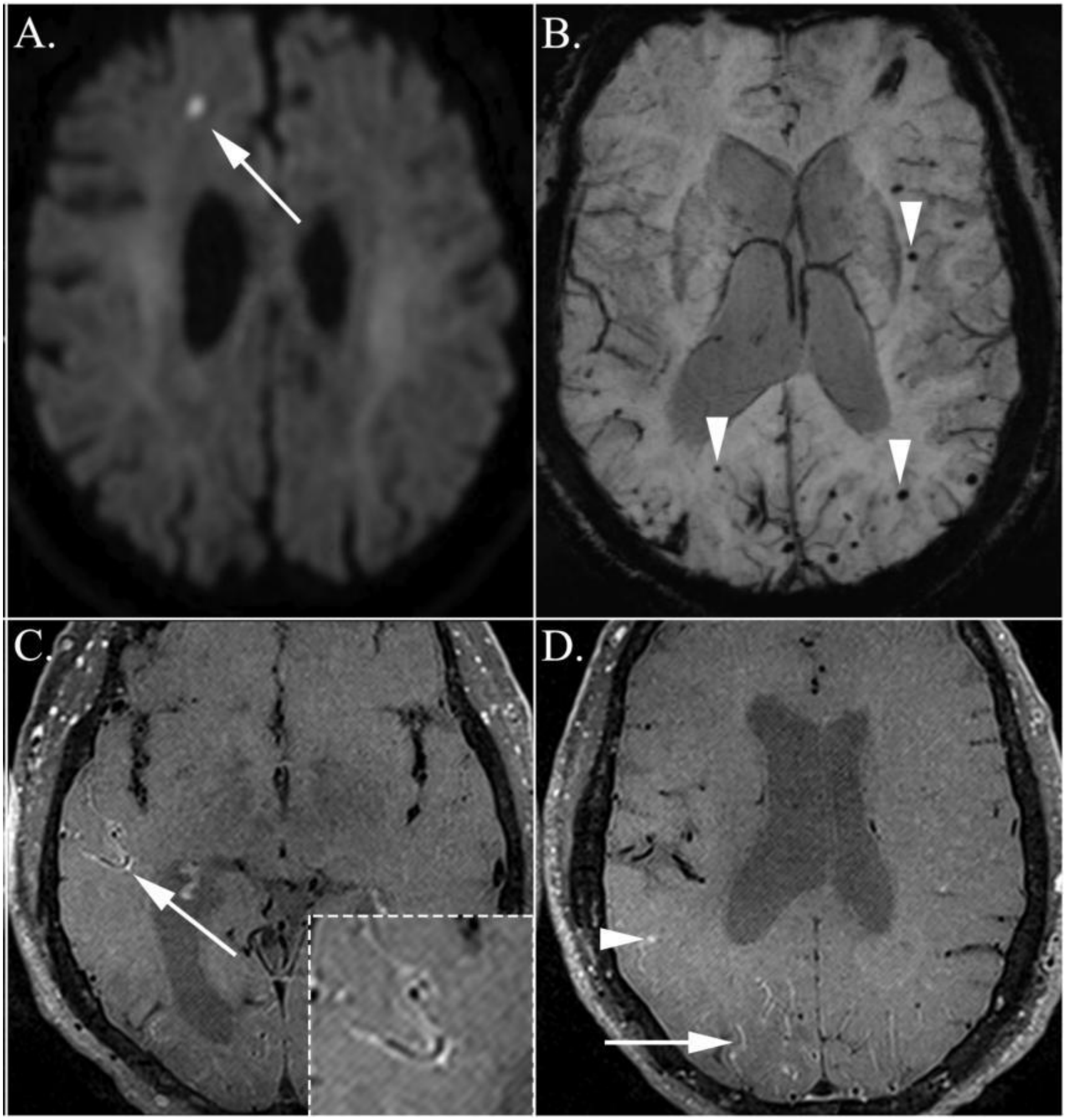

(Filename: TCT_3175_CAAASNRabstractfig1110618.jpg)

Wednesday, May 22, 2019
4:30PM - 6:00PM
New MR Imaging Techniques

2577

4:30PM - 4:37PM

3D Fast Low Angle Shot (FLASH) Imaging for Detection of Intracranial Enhancing Lesions: Comparison with MPRAGE

K Schallert[1], T Huerta[2], S Abbas[2], S Mukherjee[2], J Mugler[3], S Patel[2]
[1]UNIVERSITY OF VIRGINIA HEALTH SYSTEM, CHARLOTTESVILLE, VA, [2]University of Virginia Health System, Charlottesville, VA, [3]University of Virginia, Charlottesville, VA

Purpose
3D fast low angle shot (FLASH) imaging is a spoiled gradient echo technique that allows for a very short repetition time (TR) resulting in rapid image acquisition. Our purpose was to compare 3D FLASH brain MRI imaging (0.9-mm isotropic resolution, acquisition time = 0:49 minutes) with magnetization-prepared rapid gradient echo (MPRAGE) (0.9-mm isotropic resolution, acquisition time = 4:35 minutes) for the detection of abnormal intracranial contrast enhancement as well as prevalence and degree of motion and susceptibility artifacts.
Materials and Methods
A retrospective review was performed on contrast-enhanced 3D FLASH and MPRAGE sequences sequentially obtained in consecutive patients who underwent a 3T brain MRI scan for various clinical indications (n=115). Two neuroradiologists independently recorded the number of abnormal enhancing intracranial lesions, the degree of motion artifact, and the prevalence and degree of susceptibility artifact obscuring intracranial anatomy for each case.
Results
The measurement of enhancing lesions for 3D FLASH and MPRAGE were strongly correlated: Pearson correlation coefficient for Reader 1 = 0.9804 ($p<0.0001$) and Reader 2 = 0.9488, ($p<0.0001$). A Bland-Altman plot examining the agreement between the 3D FLASH and MPRAGE measurements of enhancing intracranial lesions showed no evidence of systematic bias (95% limits of agreement were -1.0704 to 1.0704 and -1.6213 to 1.6213 enhancing lesions for Reader 1 and Reader 2, respectively). There was significantly greater motion artifact for MPRAGE versus 3D FLASH ($p=0.0028$ for Reader 1) ($p=0.02$ for Reader 2) and significantly greater incidence of susceptibility artifact obscuring intracranial anatomy for MPRAGE versus 3D FLASH ($p<0.0001$ for Reader 1) ($p<0.001$ for Reader 2).
Conclusions
Contrast-enhanced 3D FLASH is a very rapid, motion robust, isotropic whole-brain imaging sequence demonstrating comparable performance to MPRAGE for detecting enhancing intracranial lesions.

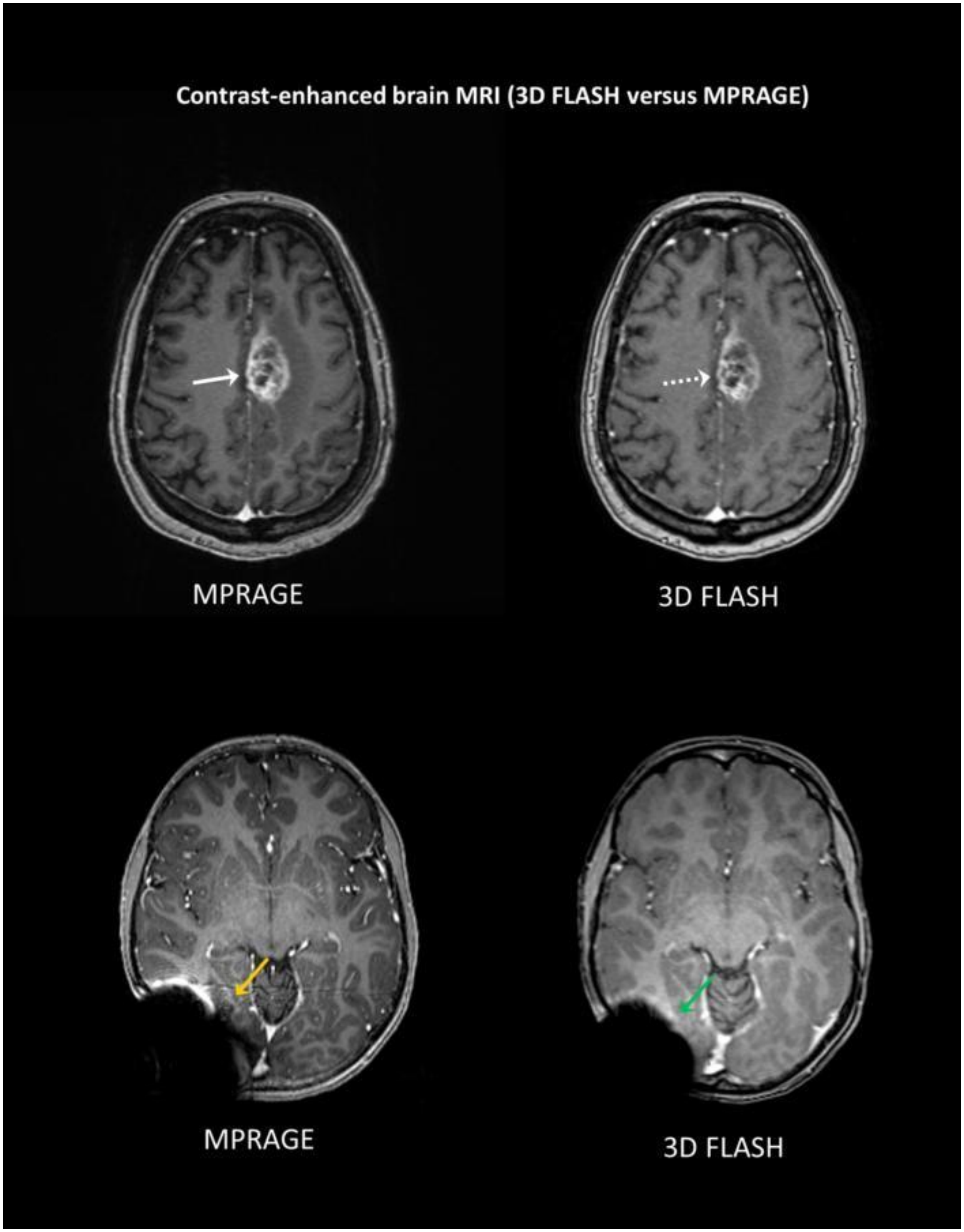

(Filename: TCT_2577_ASNR193DFLASHSubmissionGraphicFINAL.jpg)

3642

4:37PM - 4:44PM

A Diffusion Tractography-Based Atlas of Human Thalamic Ventral Intermediate Nucleus for Neurosurgical Guidance

Q Tian[1], C Ngamsombat[1], B Bilgic[1], Q Fan[1], Y Hu[2], J McNab[2], T Witzel[1], K Setsompop[1], J Polimeni[1], S Huang[1]
[1]Athinoula A. Martinos Center for Biomedical Imaging, Massachusetts General Hospital, Boston, MA, [2]Stanford University, Stanford, CA

Purpose
Tremor suppression in the hands of patients with essential tremor can be achieved by lesioning the ventral intermediate nucleus (Vim) of the thalamus using transcranial MRI-guided focused ultrasound [1]. The Vim cannot be delineated on standard structural MR images due to its small size and low intrinsic contrast. Recent work has shown that diffusion MR tractography identifies the Vim more precisely and predicts the degree of tremor suppression [2]. We aim to create a tractography-based atlas of Vim location using data of a large population.
Materials and Methods
236 healthy subjects from the Human Connectome Project [3] (https://www.humanconnectome.org/) were included. A convolutional neural network (CNN) [4] was trained on 30 subjects and tested on 6 to segment the thalamus from diffusion tensor imaging fractional anisotropy and mean diffusivity map, red nucleus (RN) and dentate nucleus (DN) from non-diffusion-weighted image, hand-knob region (HR) of pre-central gyrus from gray/white matter segmentation of the pre-central and post-central gyrus. The training targets were manually segmented by a neuroradiologist. The brain regions of interest (ROIs) of the rest 200 subjects were automatically segmented using CNN for probabilistic tractography from the thalamus to the pre-central gyrus, HR, and DN (with RN as the waypoint).
Results
Dice coefficients between manual and CNN segmentations were ~90% for thalamus, RN, DN and ~80% for HR. Figure 1a shows the averaged tractography results in MNI152 space followed the expected anatomy of the thalamocortical radiation and the dentatothalamic tract. Figure 1b-c display the averaged structural connectivity maps in MNI152 space representing the probability of each thalamic voxel belonging to the Vim.
Conclusions
We utilized a CNN to segment subject-specific ROIs for diffusion tractography of tremor circuits and created a tractography-based atlas of Vim location using 200 healthy subjects, which could aid in neurosurgical guidance.

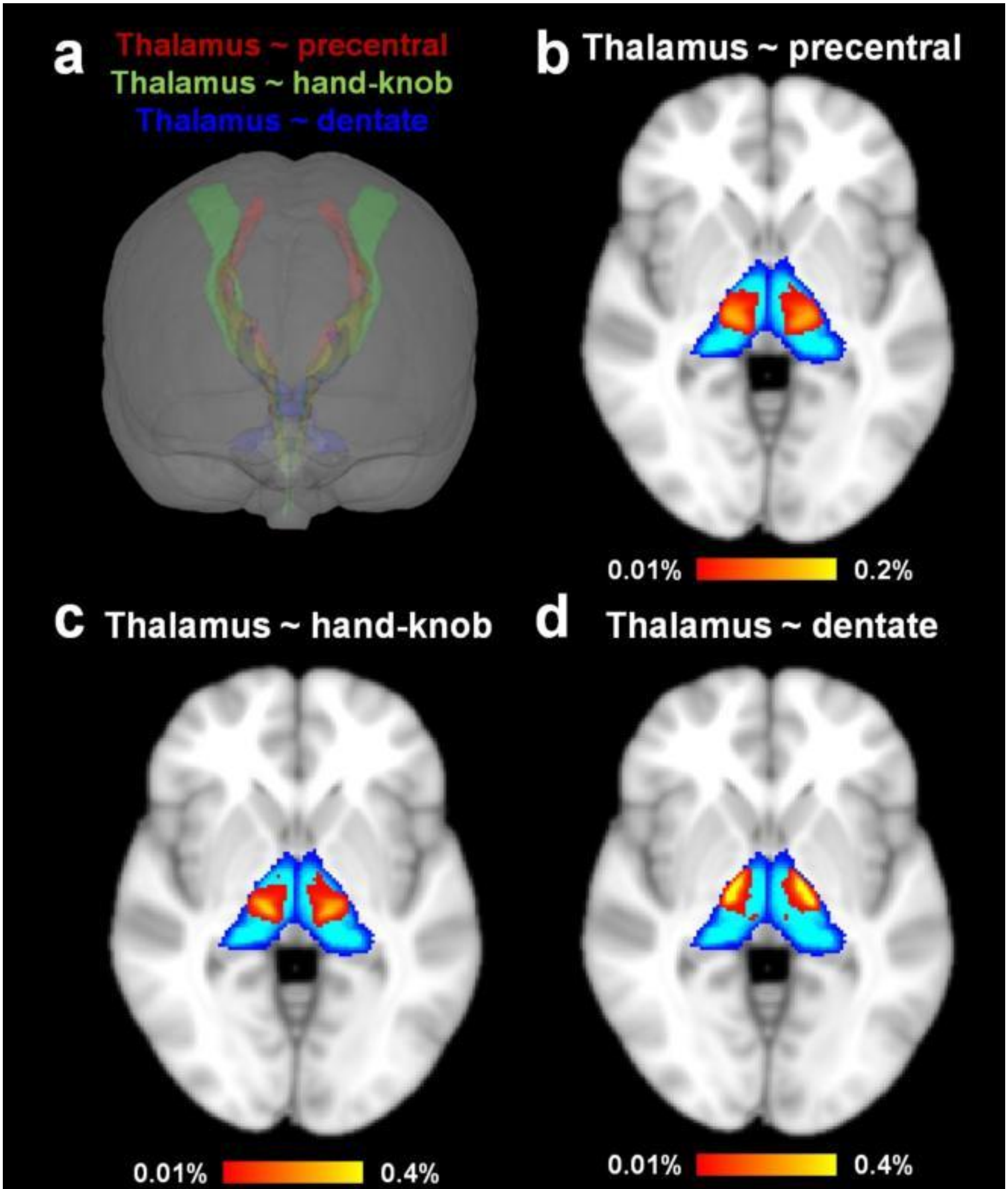

Figure 1. (a) Binarized and volume rendered probabilistic tractography results in MNI152 space. (b-c) Maps of normalized counts (red-yellow) of streamlines reconstructed between the thalamus and pre-central gyrus, hand-knob region of the pre-central gyrus, and dentate nucleus in MNI152 space.

(Filename: TCT_3642_figure-caption.jpg)

2345

4:44PM - 4:51PM

Application of Compressed Sensing Technique to Quantitative Susceptibility Mapping

M Azuma[1], T Hirai[2], M Enzaki[1]
[1]Miyazaki University, Miyazaki, Miyazaki, [2]UNIVERSITY OF MIYAZAKI, MIYAZAKI, MIYAZAKI

Purpose
Quantitative susceptibility mapping (QSM) is an MR technique that depicts and quantifies magnetic susceptibility sources. Although QSM has many important clinical applications in diagnosing, monitoring, and treating diseases of the central nervous system, the scan time is relatively long. Compressed sensing (CS) is a new strategy to accelerate data acquisition by nonlinear iterative reconstruction of sparsely undersampled k-space data. We aimed to determine whether a CS technique can apply to QSM to reduce scan time.
Materials and Methods
In 10 healthy volunteers (7 men, 3 women; age range 23 - 35 years, mean 28 years), the image quality and quantitative values were compared among QSM images using CS with acceleration factors of 0, 4, and 5.5. All subjects were scanned on 3T MR scanners using standard 32 channel head coil. Two radiologists independently rated image quality and artifacts of QSM images using a 4-point scale. They also measured the mean susceptibility values (MSVs) in the bilateral substantia nigra (SN), red nucleus (RN), caudate nucleus (CN), globus pallidus (GP), and putamen (PT). In each structure the region of interest was placed in the maximal area. The differences of image quality and degree of artifact among the 3 groups were evaluated with Kruskal-Wallis test. Interobserver agreement of them was analyzed with Cohen's kappa coefficient. The differences of MSVs among the 3 groups were evaluated by using Friedman test. Interobserver agreement of MSVs were analyzed with interobserver agreement (ICC).
Results
The MR scan time for CS with acceleration factors of 0, 4, and 5.5 was 422, 295, and 210 seconds, respectively. Interobserver agreement of image quality and degree of artifact and ICC of the MSVs among three groups showed good to excellent. QSM images using CS with acceleration factors of 5.5 showed significantly worse image quality and degree of artifact than those using CS with acceleration factors of 0 and 4 ($p<0.05$). There were no significant differences of MSVs among three groups.
Conclusions
Compared to conventional QSM images, QSM images using CS with acceleration factors of 4 yield similar image quality and quantitative values of the brain while reducing scan time.

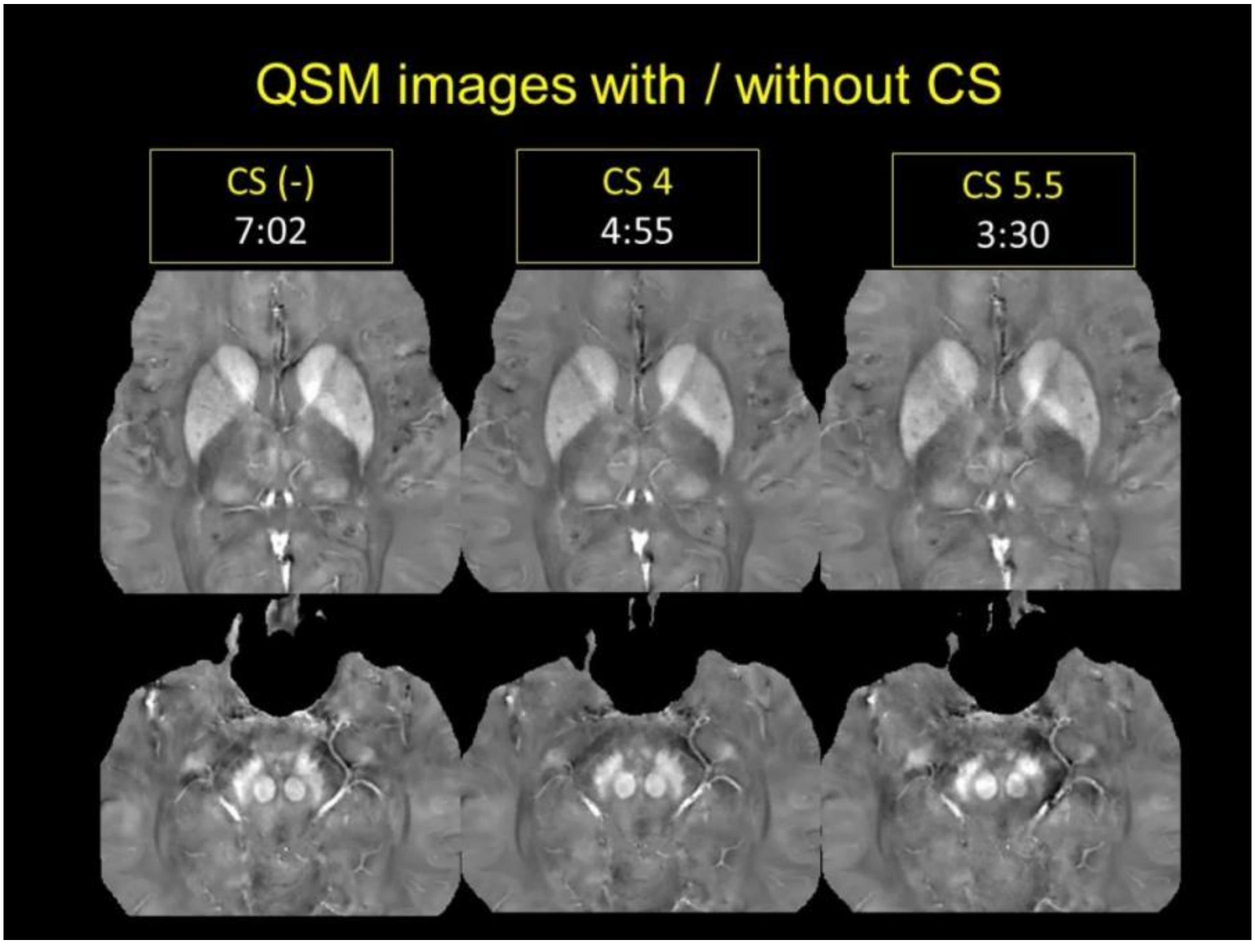

(Filename: TCT_2345_QSMASNR.jpg)

2167

4:51PM - 4:58PM

Association Between Tumor Acidity and Hypervascularity Within Human Gliomas Using pH-Weighted Amine Chemical Exchange Saturation Transfer Echoplanar Imaging (CEST-EPI) and Dynamic Susceptibility Contrast (DSC) Perfusion MRI at 3T

Y Wang[1]
[1]*PLA General Hospital, Beijing, China*

Purpose
To investigate the association between image contrast obtained from pH-sensitive amine chemical exchange saturation transfer echoplanar imaging (CEST-EPI) and relative cerebral blood volume (rCBV) measurements obtained from dynamic susceptibility contrast (DSC) perfusion MRI in patients with diffuse gliomas.
Materials and Methods
pH-weighting was obtained using CEST-EPI estimation of the magnetization transfer ratio asymmetry (MTRasym) at 3ppm and rCBV was estimated using DSC-MRI. The correlation between median MTRasym at 3ppm and rCBV within T2 hyperintense lesions were evaluated in a total of 66 patients with histologically proven gliomas (WHO II, N=20; WHO III, N=20; WHO IV, N=26 gliomas).
Results
Both MTRasym at 3ppm and rCBV within T2 hyperintensity increased with increasing tumor grade . A

strong correlation was observed between median MTRasym at 3ppm and rCBV within areas of T2 hyperintensity ($R2=0.335$, $P=0.0043$). No association was observed between MTRasym at 3ppm and rCBV within areas of necrosis or enhancing tumor.

Conclusions

The general degree of tumor acidity, measured with amine CEST-EPI, was correlated with hypervascularity, measured with DSC-MRI. These data confirm a potential association between tumor glycolysis and angiogenesis in human gliomas.

2967

4:58PM - 5:05PM

Comparison of Highly Accelerated Wave-CAIPI Susceptibility-Weighted Imaging (SWI) and Standard T2*-Weighted 2D Gradient-Echo (GRE) Imaging for Routine Clinical Brain MRI

J Conklin[1], M Longo[1], S Cauley[2], K Setsompop[2], J Kirsch[3], W Liu[4], T Beck[4], S Ahn[5], R Gonzalez[1], P Schaefer[6], S Huang[7], O Rapalino[1]

[1]Massachusetts General Hospital, Boston, MA, [2]Harvard Medical School, Boston, MA, [3]Massachusetts General Hospita (MGH), Boston, MA, [4]Siemens Healthineers, Erlangen, Erlangen, [5]Siemens Medical Solutions, Pleasanton, CA, [6]MASS GENERAL HOSPITAL, WAYLAND, MA, [7]Massachusetts General Hospital / Athinoula A. Martinos Center for Biomedical Imaging, Boston, MA

Purpose

Improvements in parallel imaging and reconstruction have enabled high-resolution 3D brain imaging with dramatically reduced acquisition times. We evaluated highly accelerated 3D-Wave-CAIPI SWI (Wave-SWI) compared to a commonly used alternative (T2*-weighted 2D Gradient-Echo, T2*w-GRE).

Materials and Methods

Consecutive patients (n=139) underwent 3T brain MRI (MAGNETOM Prisma and MAGNETOM Skyra; Siemens Healthcare GmbH, Erlangen) using 20 or 32-channel head coils, for a variety of clinical indications. Each scan included a standard 2D T2*w-GRE (slice thickness=5mm, acquisition time=73-141s) and a highly accelerated prototype 3D Wave-SWI sequence (slice thickness=1.8mm, acquisition time=60-110s). Two neuroradiologists reviewed all images for clinical pathology, including the number of cerebral microbleeds (<5 mm) when present. For abnormal studies, Wave-SWI and T2*w-GRE were compared side-by-side using a predefined 5-points scale: (0) indicates equivalence, (-1/+1) indicates that one sequence is preferred but the final diagnosis is not affected, and (-2/+2) indicates that one sequence is preferred and the difference would impact the final diagnosis. Discrepancies were adjudicated by a third reader.

Results

The observers detected more microbleeds with Wave-SWI compared to T2*w-GRE ($p<0.001$, kappa=0.73), including 11 cases where microbleeds were only seen on Wave-SWI and T2*w-GRE appeared normal (Figure Panel A). In the accompanying balloon plot (Figure Panel B), the size and color of each circle indicates the number of cases receiving a given score. Wave-SWI was preferred over T2*w-GRE for visualization of pathology, visualization of normal structures, artifacts, and overall diagnostic quality (all $p<0.01$). Wave-SWI images had slightly increased noise within the central brain likely due to the smaller voxel size, but there were no cases where this difference impacted the final diagnosis.

Conclusions

Compared to standard T2*w-GRE, highly accelerated Wave-CAIPI SWI provides improved overall diagnostic quality, increased sensitivity for small foci of hemorrhage, and reduced artifacts, in a comparable acquisition time. These findings support use of Wave-SWI over T2*w-GRE for routine clinical brain imaging

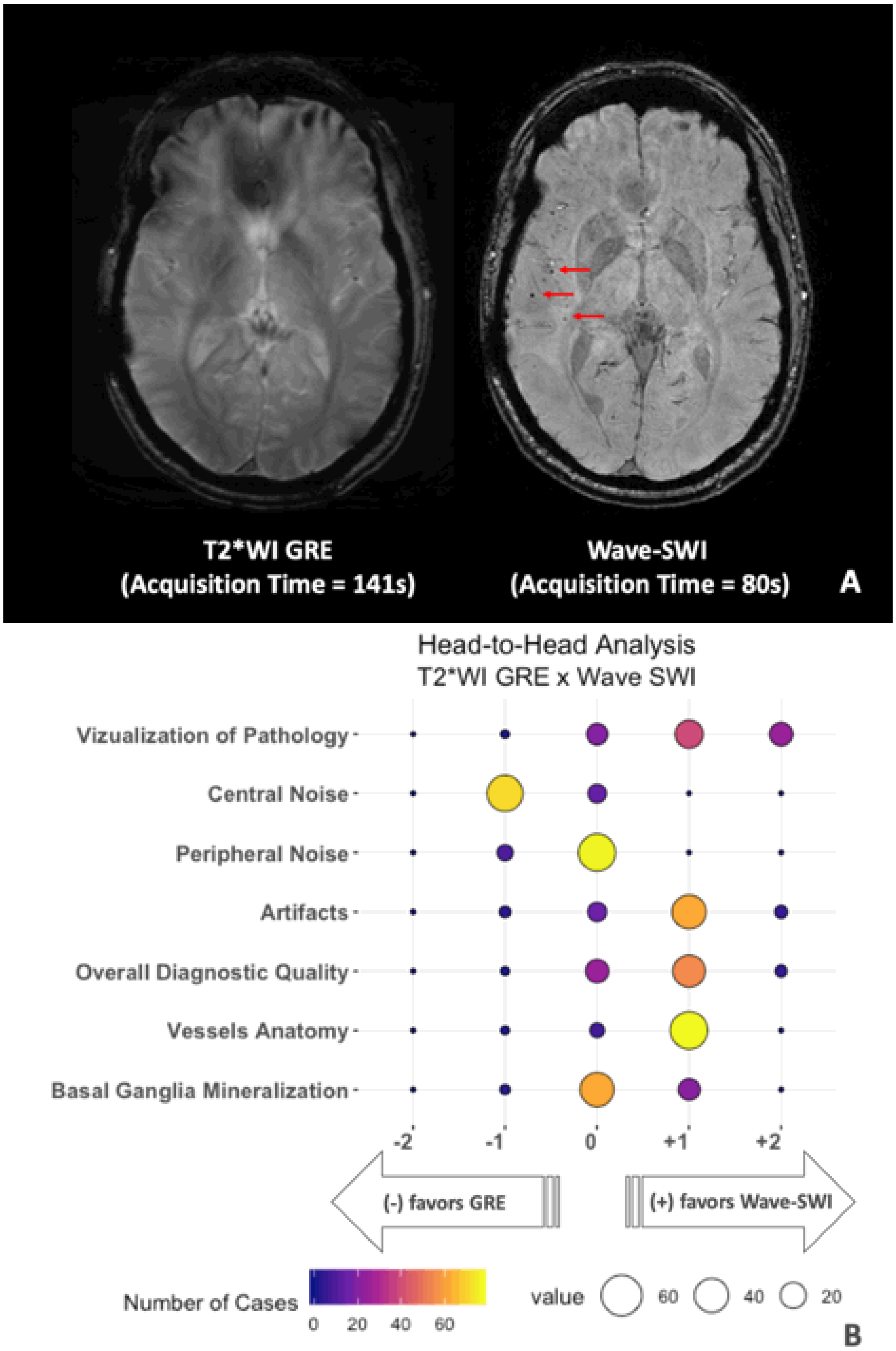

(Filename: TCT_2967_gre_asnr.gif)

2946

5:05PM - 5:12PM

Comparison of Highly Accelerated Wave-CAIPI Susceptibility-Weighted Imaging (Wave-SWI) with Conventional 3D SWI for Routine Clinical Brain Imaging

M Longo[1], J Conklin[1], S Cauley[2], K Setsompop[2], J Kirsch[3], W Liu[4], T Beck[5], S Ahn[6], R Gonzalez[1], P Schaefer[7], O Rapalino[1], S Huang[8]
[1]Massachusetts General Hospital, Boston, MA, [2]Harvard Medical School, Boston, MA, [3]Massachusetts General Hospital (MGH), Boston, MA, [4]Siemens Shenzhen Magnetic Resonance Ltd., Shenzhen, Guangdong, [5]Siemens Healthineers, Erlangen, Erlangen, [6]Siemens Medical Solutions, Pleasanton, CA, [7]MASS GENERAL HOSPITAL, WAYLAND, MA, [8]Massachusetts General Hospital / Athinoula A. Martinos Center for Biomedical Imaging, Boston, MA

Purpose
Wave-CAIPI (controlled aliasing in parallel imaging) enables highly accelerated 3D imaging with negligible g-factor penalties, and may facilitate broad clinical application of SWI. We evaluated the image quality and diagnostic performance of Wave-SWI and conventional SWI in a prospective study of patients undergoing brain MRI for a variety of clinical indications.
Materials and Methods
Consecutive patients (n=107) undergoing 3T clinical brain MRI were prospectively enrolled, including both inpatient and outpatient settings. The most common indications for MRI were brain tumor (n=34), altered mental status (n=13), intracranial hemorrhage (n=13), and stroke (n=10). In addition to the clinical protocol, all scans included a conventional SWI (R=2, acquisition time AT=300s) and a matched prototype Wave-SWI sequence (R=6, AT=100s on 20-channel coil, and R=9, AT=60s on the 32-channel coil). Studies were performed on two clinical 3T MRI scanners (MAGNETOM Prisma and MAGNETOM Skyra; Siemens Healthcare GmbH, Erlangen). Two neuroradiologists reviewed the images for clinical pathology, including the number of cerebral microhemorrhages (<5 mm) when present. For abnormal studies, Wave-SWI and Conventional SWI were compared using a predefined 5-point scale, where 0 indicates equivalence, -1 or +1 indicates that one sequence is preferred but the final diagnosis is not affected, and -2 or +2 indicates that one sequence is preferred and the difference would impact the final diagnosis. Any discrepancies were adjudicated by a third reader.
Results
There was no difference in the number of microhemorrhages detected using Wave-SWI versus conventional SWI ($p>0.05$, kappa=0.73) (Figure A). In the balloon plot (Figure B), the size and color of each circle indicates the number of cases receiving a given score. There was no difference between the two sequences for visualization of pathology, visualization of normal anatomy, peripheral image noise, or overall diagnostic quality ($p>0.05$, kappa=0.42-0.59). Wave-SWI images had slightly fewer artifacts ($p=0.04$) and slightly increased image noise within the central brain compared to standard SWI ($p<0.001$). However, there were no cases where these differences impacted the final diagnosis.
Conclusions
Wave-CAIPI SWI provides comparable performance to standard SWI across a range of clinical pathologies, with an approximate 5-fold reduction in acquisition time and fewer motion artifacts. The findings support clinical application of Wave-SWI over conventional SWI for routine clinical brain imaging.

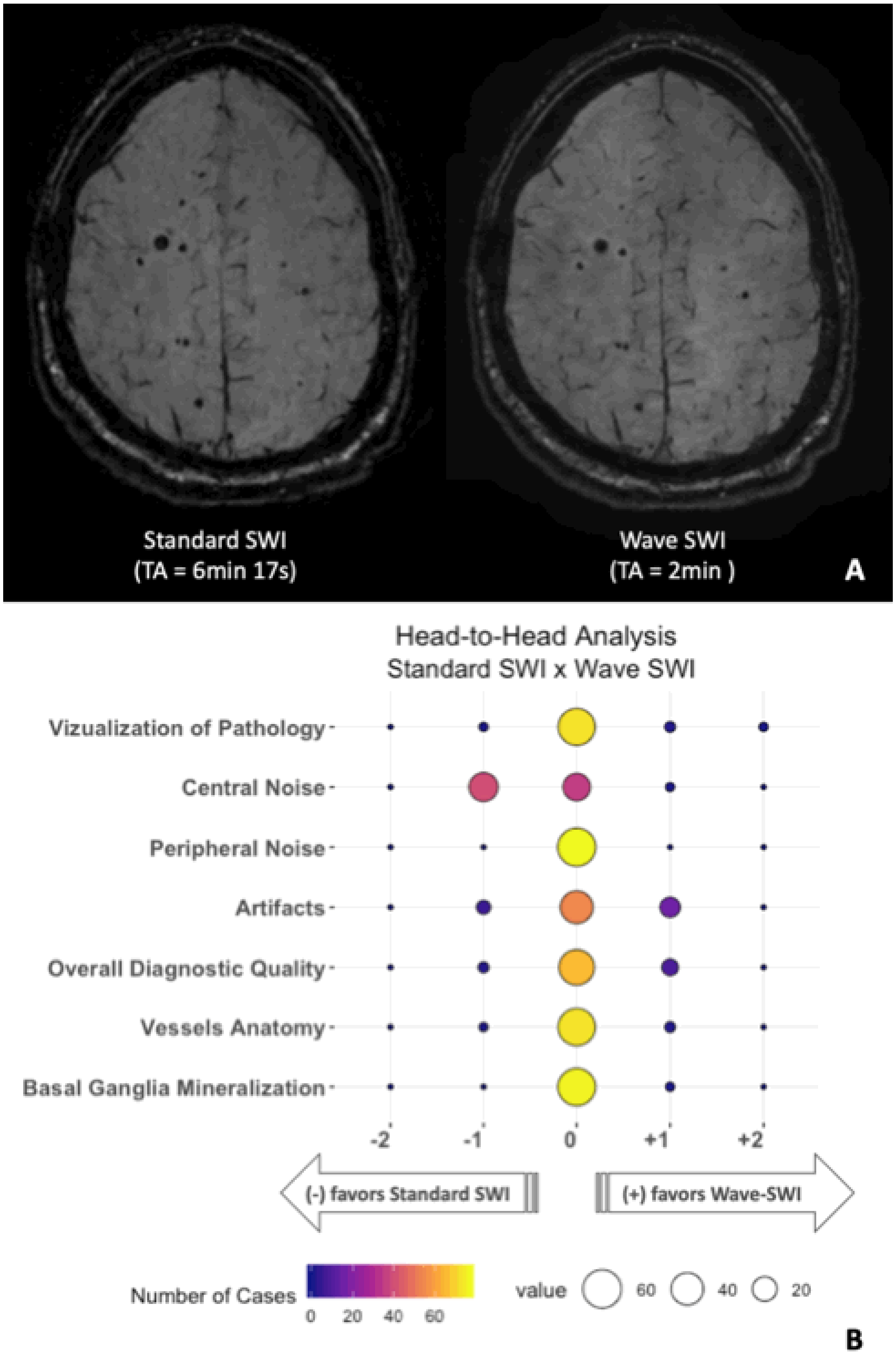

(Filename: TCT_2946_swi_asnr.gif)

2484

5:12PM - 5:19PM

Delineation of Thalamic Substructures Based on Ultra-High B-Value DWI-Measurement with Reasonable Acquisition Time

N Nuessle[1], B Bender[1], U Klose[1]
[1]*University Hospital Tuebingen, Tuebingen, Germany, Tuebingen, Baden-Württemberg*

Purpose
As shown in recent publications, deep brain stimulation (DBS) is becoming more and more important in therapies of various neurological and psychological diseases(1-3). A lack of reliable pre-interventional and individual target identification presents a problem for implantation. Pre-interventional MR-imaging could serve as a new and promising technique to localize new target regions(4). It has been shown, that ultra-high b-value diffusion weighted imaging reveals new intrathalamic substructures which correlate very well with the histological anatomy found in stereotactic atlases(5). Nevertheless, the proposed protocols are time consuming and therefore vulnerable to movement artefacts especially when applied in patients with neurological movement disorders. The purpose of this study was to evaluate the capability of optimized and faster ultra-high b-value DWI in separating and identifying intrathalamic substructures and to compare the new technique with the previously described protocol and histological data.
Materials and Methods
For this prospective MRI-study, approved by the local institutional review board of our university hospital, 7 healthy subjects (4 male, 3 female) were recruited. All subjects provided written informed consent, had to be healthy without any cerebral illnesses or injuries, never underwent surgical intervention in the brain region and didn't receive steroid therapy at that time. No contrast medium was used. Measurements were performed on a 3T-MRI-scanner, able to obtain ultra-high b-values with good noise and vibration levels (PRISMA Fit, Siemens, Erlangen). MPRAGE 3D sequence was applied to reconstruct anatomical images of the subjects' brains and to plan acquisition of diffusion-weighted images (DWI) in AC/PC orientation. Optimized spin-echo echo-planar imaging DWI sequence with b-values of 0 (b0) and 5000 s/mm2 (b5000) was used and diffusion was encoded in 5 directions. For b0, two and for b5000, 25 averages were measured (8:23 minutes acquisition time). A second previously described sequence with the same b-values, encoded in 64 directions with 5 averages at b5000 was added to the protocol (17:56 minutes acquisition time) (5). DWI acquisition was not performed as full brain imaging but focused on thalamic and subthalamic regions. Following to the MRI-Scan, images were denoised using total generalized variation. Intrathalamic substructures, defined prior to the evaluation, were semi-automatically identified in the slice 4 mm above the AC/PC line. Later, the defined substructures were compared between the two sequences and with a histological stereotactic atlas of the brain.
Results
In all subjects and in both protocols, all seven intrathalamic substructures could be identified due to different signal variations. The accordance between the original sequence and the new speeded-up measurement was high. The acquisition time was reduced by more than 50% (8:23 minutes compared to 17:56 minutes). Nuclei, which were delineated based on DWI in both sequences, corresponded very well with the histological data from the atlases. In addition, high concordance between the drawn in nuclei in the different subjects and the two acquired sequences could be shown. No movement artefacts were identified on the images and no noise and vibration problems were declared by the patients as it is sometimes the case in ultra-high b-value MR-scanners.
Conclusions
Ultra-high b-value DWI showed great potential in identifying different thalamic substructures. In this study, a significantly shorter and therefore more easily applicable protocol showed comparable results to the previously described method. Especially in patients with motoric disorders, the acquisition times need to be as short as possible. Reducing them by 9:30 minutes, more than 50% of the original acquisition time, with comparable results therefore is a great step towards fast and reliable identification of thalamic target structures in ultra-high b-value DWI. In conclusion, ultra-high b-value DWI, encoded in only five directions with 25 averages showed comparable potential in determining thalamic nuclei with high signal-to-noise ratio and high concordance with histological data. Further investigations need to be done to

evaluate the described protocols in DBS-patients and to correlate anatomical identification with clinical outcome.

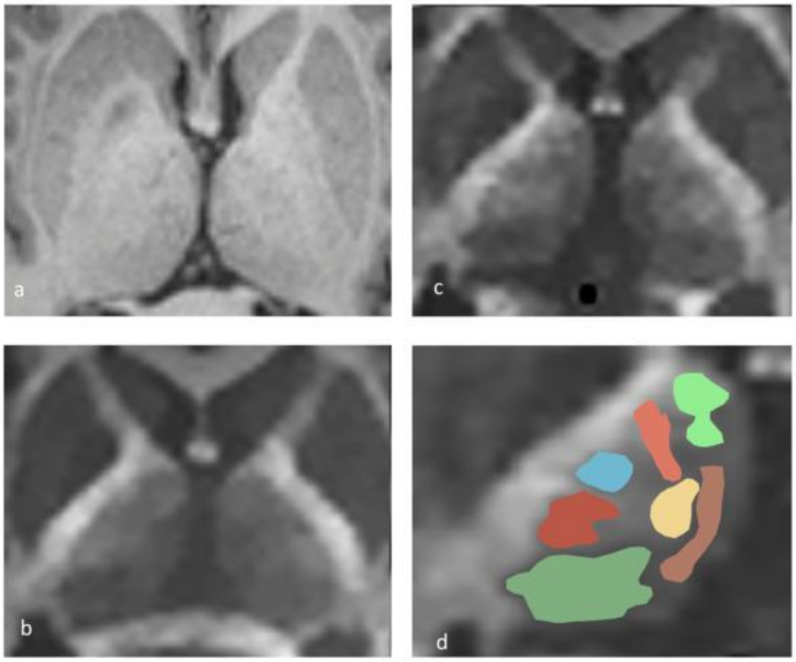

Fig. 1: MRI-scan of the thalamic region
a) T1 MPRAGE
b) DWI at 5000 s/mm², previously described sequence
c) speeded-up sequence, saving more than 50% of acquisition time
d) DWI with delineated substructures at 5000 s/mm²

(Filename: TCT_2484_Thalamus_Comparison_003.jpg)

3265

5:19PM - 5:26PM

Diagnostic Performance of a Multi-Contrast EPI Sequence Compared to Routine MRI Sequences in the Emergency Department: Initial Results

O Rapalino[1], J He[1], P Schaefer[1], M CHRISTENSEN[1], A Guidon[2], J Kirsch[1], T Sprenger[3], S Skare[4], R Gonzalez[1]
[1]Massachusetts General Hospital, Boston, MA, [2]GE HEALTHCARE, Boston, MA, [3]GE Healthcare, Stockholm, Stockholm, [4]Karolinska Institute, Stockholm, SE-171 76 Stockholm

Purpose
To compare the diagnostic performance and diagnostic quality of a novel multicontrast EPI sequence with routine brain MRI sequences in the assessment of acute intracranial pathologies in the Emergency Department
Materials and Methods
190 cases were consecutively acquired using a 1.5T GE SIGNA Artist MR scanner (GE Healthcare, Chicago, Illinois) including conventional brain MRI sequences and a novel multi-contrast EPI sequence (Multi-EPIMix). GRE, T2 FLAIR, T2W, T1 FLAIR, ISO DWI, and ADC images were generated from the multi-contrast EPI sequence. Data collection was approved by the institutional review board. The conventional brain MRI protocol included axial FLAIR, axial DWI, axial GRE, and axial T2W sequences. The average acquisition time of the multi-contrast EPI sequence was 89 seconds (compared to at least 8 minutes and 13 seconds for the conventional sequences). From these 190 cases, a sample of 20 cases was analyzed for the detection of DWI hyperintense lesions, intra-parenchymal or extra-axial foci of susceptibility signal, white matter and extra-axial FLAIR hyperintensities and intracranial masses. Images were also evaluated for the presence of motion artifacts and for their value in achieving the final imaging-based diagnosis.

Results
7 cases (33%) showed DWI hyperintense lesions that were equally identified on both the multicontrast EPI and conventional DWI sequence. 6 of these cases represented acute to subacute infarcts and 1 case had intracranial metastases. 7 cases showed intraparenchymal foci of susceptibility signal likely representing microhemorrhages. 1 of these cases showed a microhemorrhage in the multicontrast EPI that was not seen in the conventional GRE sequence. 5 cases showed better visualization of these lesions on the multicontrast EPI. The number of white matter FLAIR hyperintensities identifiable on both FLAIR sequences was the same. Motion artifacts were equal in 95.2% of cases and slightly worse in the conventional sequence in 1 case. Imaging-based diagnosis could be equally achieved in all cases.
Conclusions
A multi-contrast EPI sequence could potentially provide an acceptable diagnostic alternative to the core conventional brain MRI sequences in selected populations that cannot tolerate long MRI examinations in the Emergency Department.

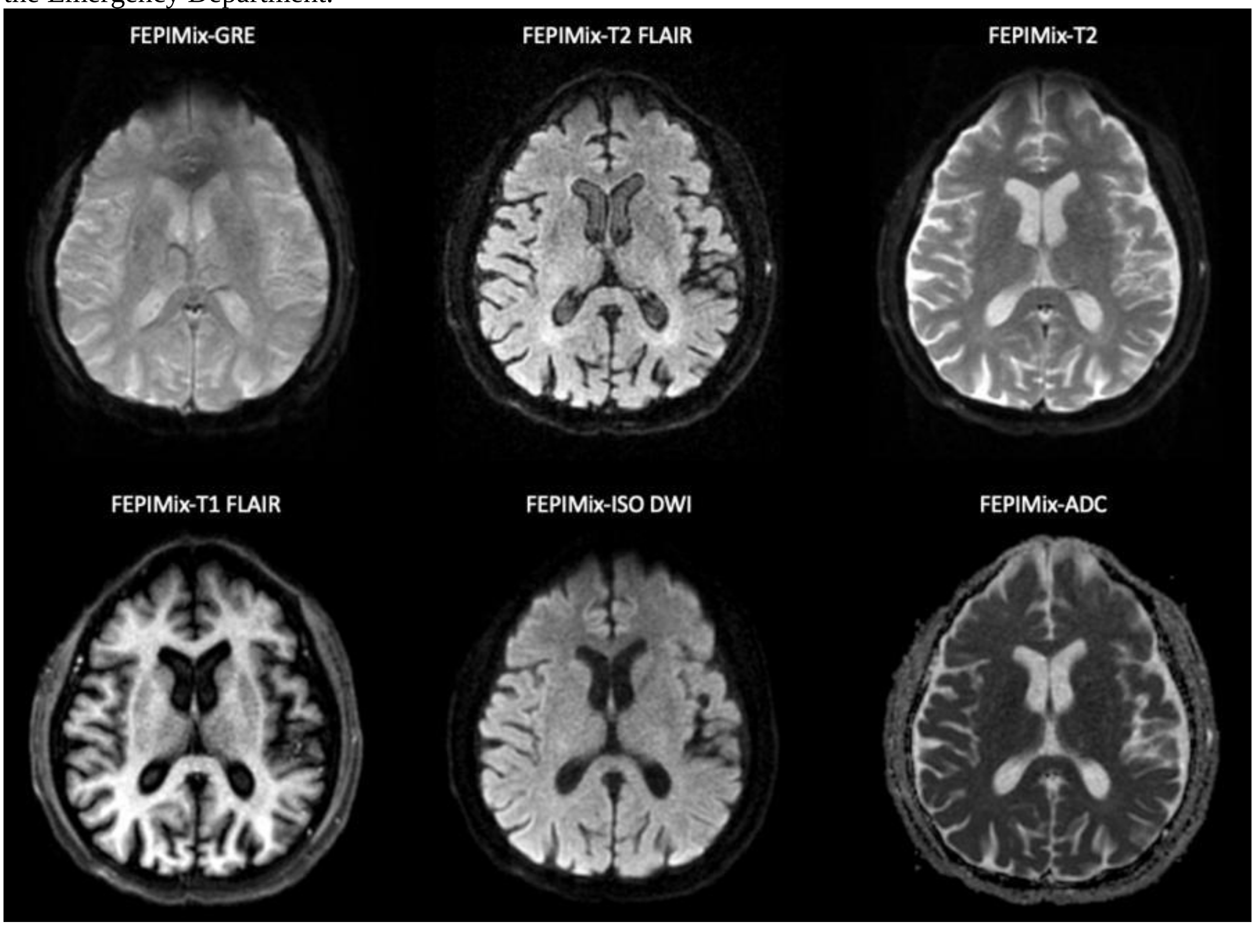

(Filename: TCT_3265_EPIMIX.jpg)

3605

5:33PM - 5:40PM

In-Vivo Diffusion Imaging of Hippocampal Network with 600 Micrometer Isotropic Resolution at 7T

F Sepehrband[1], R Cabeen[1], A Toga[1]
[1]*University of Southern California, Los Angeles, CA*

Purpose

Neuroimaging findings indicate that neurological disorders differentially target distinct subregions of the hippocampal circuit [1]. Therefore, the ability to image hippocampal network is essential to study the mechanism of the disease pathophysiology. Recently, 1mm isotropic diffusion MRI of the hippocampus was achieved [2] in a clinically feasible time frame by acquiring an axial slab around hippocampus and by utilizing a low b-value EPI strategy. Intra-hippocamapl connectivity analysis demand even higher resolutions given the large complexity of the hippocampal formation. Pushing the imaging resolution decreases the SNR and CNR, which could negatively affect the power to resolve intricate subfields of the hippocampus. Here we take advantage of 7T MRI technology, readout segmented diffusion MRI and a robust SNR enhancement technique, to enable diffusion MRI of the hippocampal network at 600 µm isotropic resolution.

Materials and Methods

Readout segmented diffusion MRI sequence [3] was used to acquire 40 axial slices around hippocampus with isotropic resolution of 600 µm, 12 diffusion-encoding gradient directions with one non-weighted diffusion image with b-value of 1000 and total scan time of 18 minutes. on a 7 Tesla whole-body scanner (Magnetom Terra, Siemens Healthcare, Erlangen, Germany) using a single-channel quadrature transmit radiofrequency (RF) coil, and a 32-channel receive array coil (Nova Medical Inc., MA), we used 11 readout segments, TR=7800ms, TE(b0)=77, TE=129, flip angle=170-degree, and acceleration factor=3. The institutional review board of the University of Southern California approved the study. In order to enhance SNR without a substantial sacrifice in spatial resolution and to denoise the magnitude images, we used a similar technique as what described in Ref [4]. Tractography was performed using Quantitative Imaging Toolkit (QIT) [5]. Deterministic tensor-based tractography was performed within a region of interest that was drawn around the hippocampus. We used registered high-resolution T2w images to accurately pinpoint a spherical seed in a multilayer region of the hippocampus. The T2w was acquired with in-plane resolution of 300 µm and slice thickness of 2 mm.

Results

Subfields of the hippocampal formation were resolved using the proposed framework (Figure 1.b-c). The SNR enhancement technique improved the diffusion MRI quality (Figure 1c), without over-smoothing the data (Figure 1.d shows that the diffusion-weighted signal in gradient encoding domain was preserved). Diffusion-weighted signal was higher than the noise level (Figure 2.a) and contained orientational information (Figure 2.b) across subregions of the hippocampus. The expected fiber architecture of the CA1, startum radiatum and collateral white matter regions were captured (Figure 3). In addition, the expected along-hippocampal and intra-hippocampal connectivity were extracted and corroborate neuroanatomical topology (Figure 4).

Conclusions

We were able to perform diffusion imaging of hippocampal network with 600 µm isotropic resolution, by taking advantage of higher signal in ultra-high field and by combining a high-resolution diffusion imaging sequence [3] and a post-processing diffusion signal enhancement technique [4]. This resolution is 4.6 times higher than the state-of-the-art diffusion imaging at 1 mm and 37 times higher than what is being used in the advanced diffusion MRI of many modern studies such as ANDI-3 (i.e. 2 mm resolution).

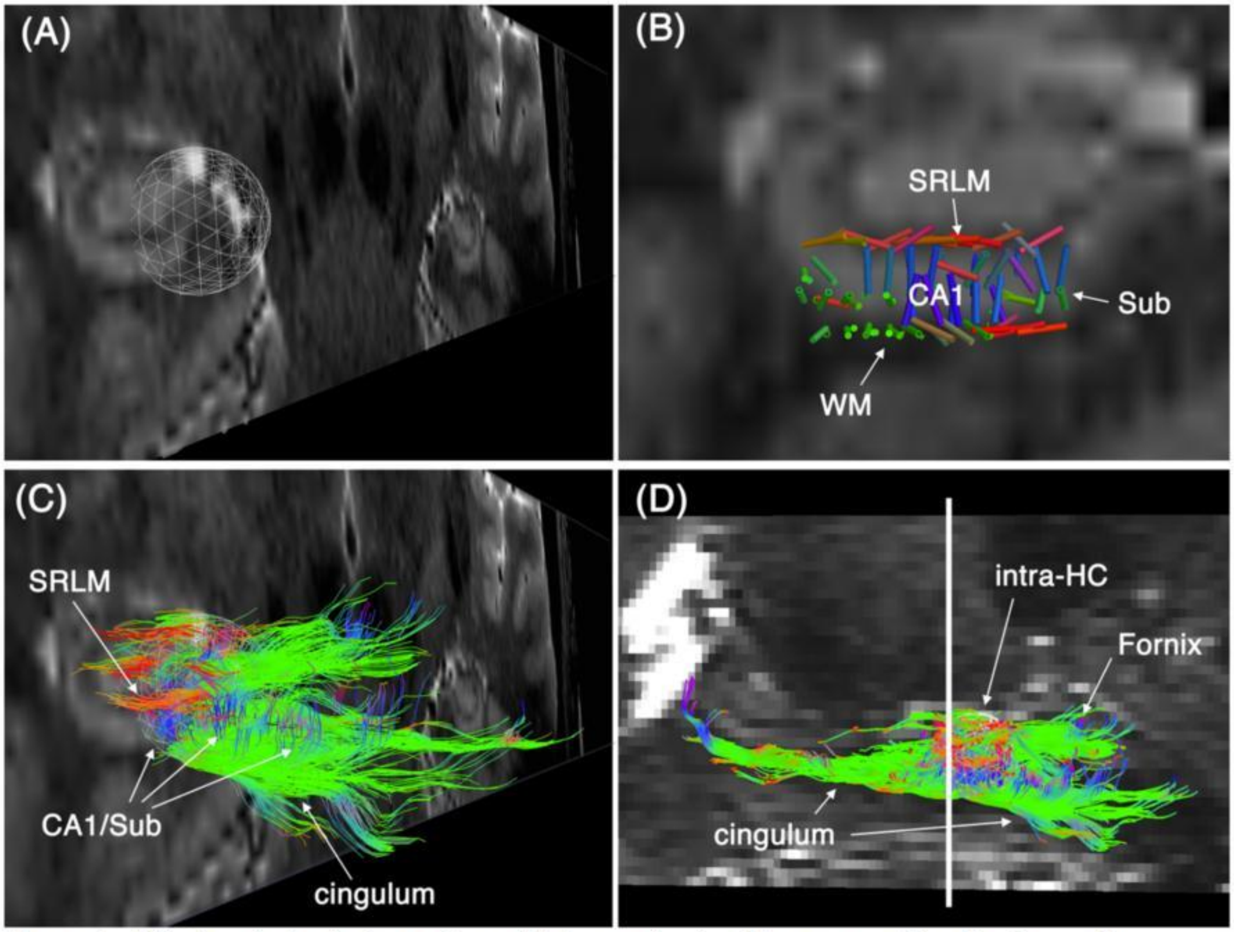

Figure 4. diffusion-derived streamlines of intra- and extra-hippocampal tracts. Streamlines were generated by seeding a sphere in the boundary of CA1, subiculum, collateral white matter, SRLM and dentate gyrus. Expected anterior-posterior projection of the cingulum and fornix were obtained.

(Filename: TCT_3605_figure.jpg)

2812

5:40PM - 5:47PM

Markerless Prospective Motion Correction Improves Diagnostic Image Quality of T2 and FLAIR

C Jaimes[1], P Grant[2], J Conklin[3], F Karahanoglu[4], M Tisdall[5], P Wighton[4], A van der Kouwe[6], R Frost[4]
[1]Boston Children's Hospital, Boston, MA, [2]Children's Hospital Boston, Boston, MA, [3]University of Toronto, Toronto, Ontario, [4]Massachusetts General Hospital, Charlestown, MA, [5]Perelman School of Medicine. University of Pennsylvania, Philadelphia, PA, [6]Athinoula A. Martinos Center for Biomedical Imaging, Charlestown, MA

Purpose
To evaluate the effectiveness of markerless prospective motion correction (PMC) in decreasing motion artifacts for TSE-T2 and FLAIR
Materials and Methods
The study was IRB approved. Five adult volunteers were recruited. We performed experiments using 3 sequences: fast-T2 (TR/TE 8310/106 ms, 1 average, acquisition time [AT]: 1:16 min), high-resolution

(HR)-T2 (TR/TE11750/93, 2 averages, AT: 4:55 min), and fat-suppressed FLAIR (TR/TE/IR: 9000/85/2500ms, 1 average, AT: 1:50 min). Experiments included a combination of motion states (still/discrete motion) and PMC (ON/OFF). PMC was performed with a commercial markerless system (Tracoline-TCL3.01 [TracInnovations, Denmark])1, 2. For motion experiments, subjects received a verbal directive to perform a single 3-10 mm discrete change in head position once every minute. Prior to scanning, subjects were coached on the magnitude of motion (monitored with Tracoline). Two blinded neuroradiologists assessed image quality with a previously validated 5 point Likert scale, ranging from 1 (no diagnostic information) to 5 (diagnostic, no artifact)3. ANOVA and a series of t-tests were used to compare image quality across groups. Inter-rater reliability was assessed with weighted kappa.

Results

A total of 48 series were analyzed by each radiologist (weighted kappa=0.84). Table 1 (fig1a) summarizes data on the overall image quality and that of various sequences. ANOVA showed significant differences in scores between groups ($p<0.001$)(fig1b). When subjects were still, image quality was no different with PMC on and off ($p>0.05$), indicating that PMC does not introduce artifacts when subjects are still. In moving subjects, image quality for all sequences was significantly improved with PMC on ($p<0.02$), although image quality remained lower than with non-moving subjects ($p<0.01$).

Conclusions

Markerless PMC during T2 and FLAIR acquisition does not introduce new artifacts in still subjects and significantly reduces artifacts related to motion. PMC-acquired data are reconstructed in the standard way on the scanner (unchanged image reconstruction time). This can improve patient care, workflow, and reduce the need for sedation in vulnerable populations (e.g. children).

Figure 1a.

	Motion, PMC-off		Motion, PMC-on		Still, PMC-off		Still, PMC-on	
	n	Mean (SD)	n	Mean (SD)	n	Mean (SD)	n	Mean (SD)
All	28	1.8 (0.7)	30	3.5 (0.6)	20	4.2 (0.7)	18	4.4 (0.7)
Fast T2	18	1.9 (0.7)	18	3.5 (0.6)	10	4.4 (0.5)	10	4.4 (0.7)
HR T2	6	1 (0)	8	3.4 (0.6)	6	4.2 (0.9)	4	4.5 (0.6)
FLAIR	4	2.5 (0.6)	4	3.7 (0.5)	4	4 (0.8)	4	4.3 (0.9)

Table# 1. Number of subjects, mean, and standard deviation (SD) of quality scores for various acquisitions, grouped by motion and PMC. N= number of subjects. PMC= Prospective Motion Correction.

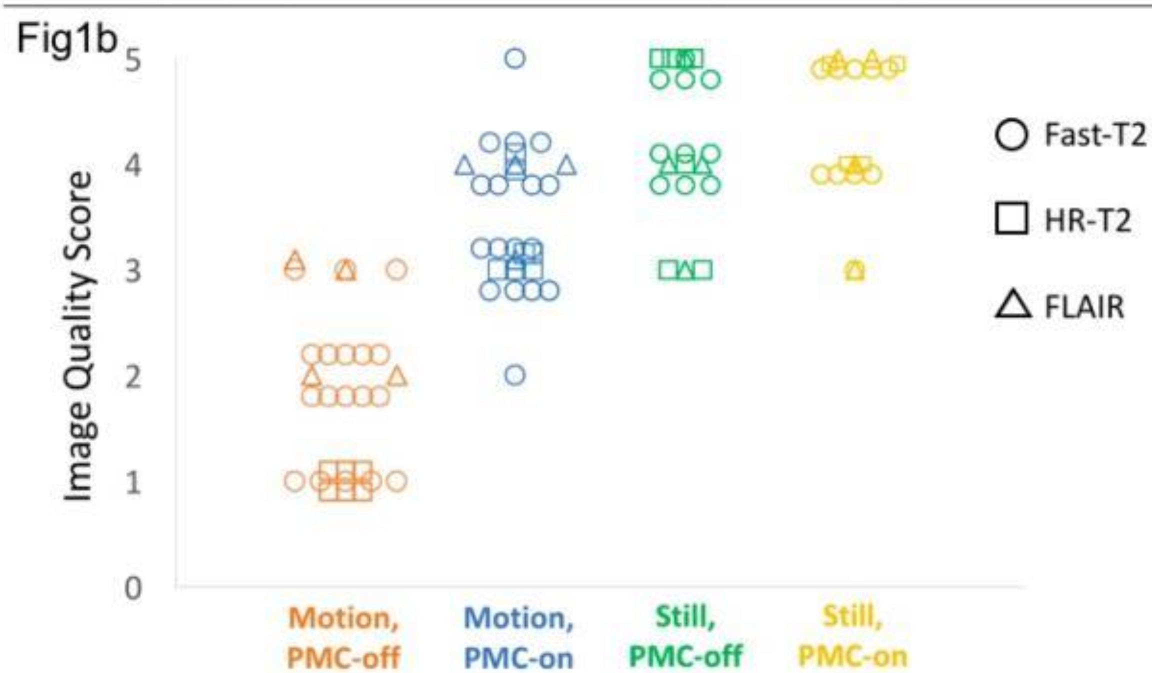

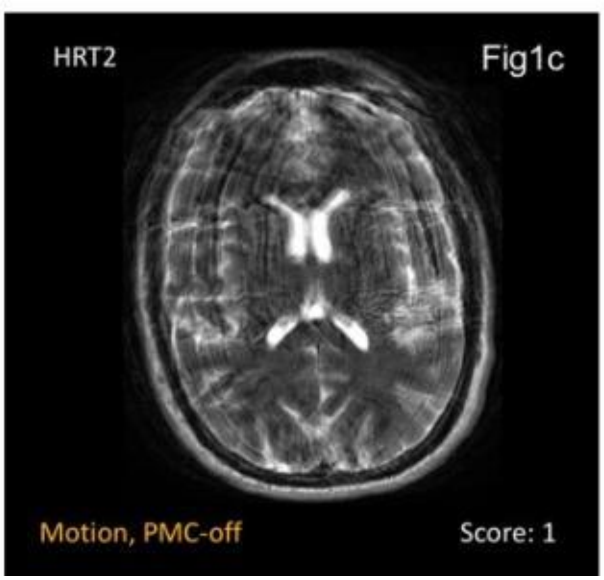

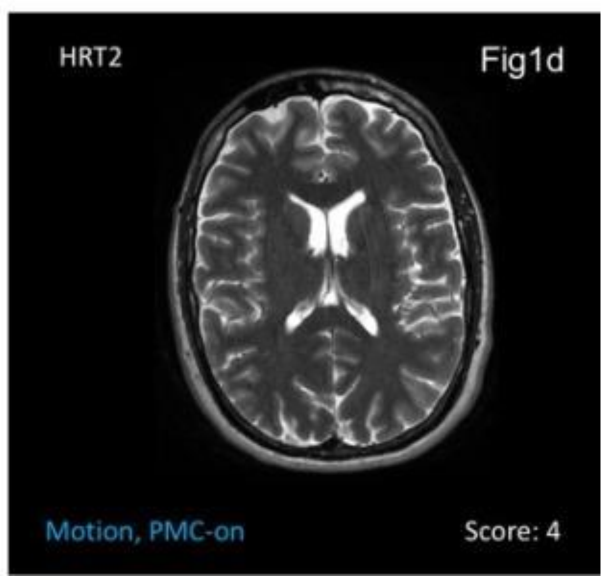

(Filename: TCT_2812_11upload.jpg)

3522

5:47PM - 5:54PM

Myeloarchitectonic Mapping of Cortical Gray Matter with 3D Inhomogeneous Magnetization Transfer (IHMT)

F Munsch[1], G Varma[1], M Taso[1], O Girard[2], A Guidon[3], G Duhamel[2], D Alsop[1]
[1]Beth Israel Deaconess Medical Center, Harvard Medical School, Boston, MA, [2]Aix Marseille Univ, CNRS, Marseille, Provence Alpes Cote d'Azur, [3]GE HEALTHCARE, Boston, MA

Purpose
Cortical gray matter demyelination appears in the early stages of Multiple Sclerosis (MS) and is associated with cognitive and physical disability (1). Nevertheless, the pathological process behind it is still unclear. Inhomogeneous magnetization transfer (ihMT) is a novel MRI technique that can be made selectively sensitive to relatively long-lasting dipolar couplings within lipid chains, making it more specific to the high membrane density in myelin (2,3). This work aims to make use of an ihMT 3D sequence to investigate the distribution of myelin in the cortex using the inverse ihMT ratio (ihMTRinv).
Materials and Methods
Five healthy volunteers aged 18 to 35 years were scanned on a 3T scanner (GE Discovery MR750) and a 32-ch head coil (Nova Medical) with a 1mm isotropic 3D T1w FSPGR sequence and a 1.6mm isotropic 3D ihMTRAGE sequence composed of an ihMT preparation combined with a rapid gradient echo (RAGE) sequence. A high-flip angle (hfa) reference was also acquired for calculation of ihMTRinv, by substitution of the ihMT preparation with 1s of RF spoiled FA=45° pulses applied on-resonance every 25ms. We computed a cortical surface-based analysis of ihMTRinv in order to assess the sensitivity of ihMT to cortical myelination using FreeSurfer (http:// surfer.nmr.mgh.harvard.edu). We sampled the z-transformed ihMTRinv map at the mid-distance between white and pial surfaces (50% depth) and projected it to an average surface (fsaverage), averaging across subjects and smoothing along the surface with a 5mm FWHM Gaussian kernel.
Results
Cortical surface-based analysis of ihMTRinv displays regional differences in cortical myelination. The primary motor, primary somato-sensory, visual cortices and posterior cingulate display high myelination while the insula and the temporal lobe display low myelination (Figure). This spatial distribution of myelin is in agreement with postmortem studies (4) and previous in vivo MR-based analyses (5).
Conclusions
IhMT MRI, and especially calculated ihMTRinv, is specifically sensitive to myelin content in cortical gray matter. These results also broadly support the myelin sensitivity and specificity of the ihMT technique for applications in the CNS, like early prognosis in MS.

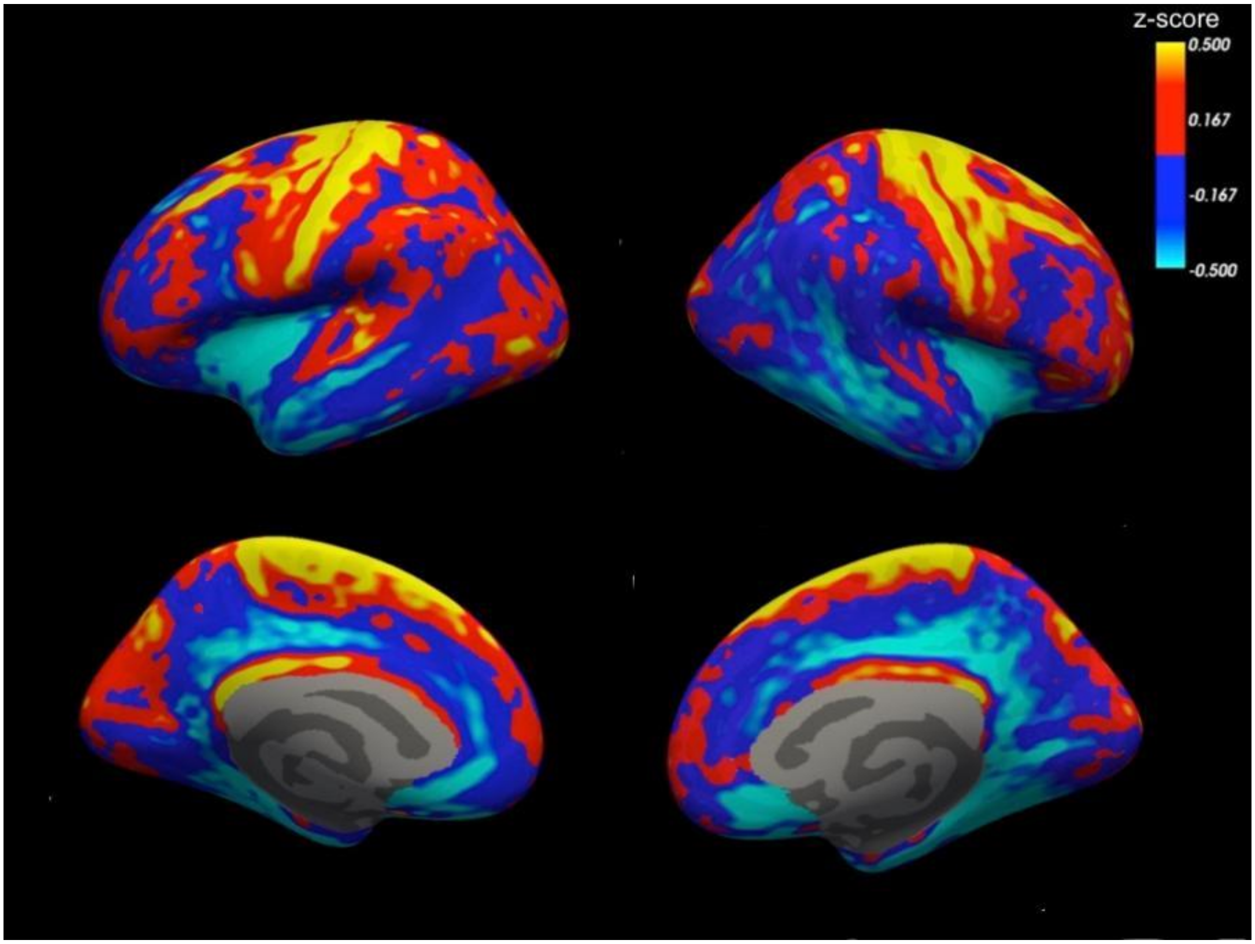

(Filename: TCT_3522_Figure.jpg)

3156

5:54PM - 6:00PM

Reproducibility of Amide Proton Transfer-weighted Signal in Brain According to Clinical Conditions and Anatomical Location: A Prospective Evaluation

J Lee[1], J Park[2], S Jung[3], H Kim[4], S Kim[5]
[1]Soonchunghyang univ hospital, Puchun, Select One, [2]Asan Medical Center, Seoul, 05555, Korea, Republic of, [3]Asan medical center, Seoul, -, [4]Asan Medical Center, Seoul, NA, [5]ASAN MEDICAL CENTER, SONGPA-GU, SEOUL, KOREA-REPUBLIC OF (KOR)

Purpose
To prospectively investigate the reproducibility of amide proton transfer-weighted (APTw) magnetic resonance imaging (MRI) in the brain.
Materials and Methods
Three sets of APTw MRI data were acquired (two intrasession and one separate intersession acquisition) from each of 19 healthy subjects, 15 glioma patients, and 12 acute stroke patients. The mean APTw signals from five anatomical locations in healthy brain (supratentorial and infratentorial locations) and from entire tumor and stroke lesions (supratentorial location) were calculated. The within-subject coefficient of variation (wCV) and intraclass correlation coefficient (ICC) were calculated for each clinical condition, intra- and intersession acquisitions, and supra- and infratentorial locations. Differences in APTw signals between sessions were analyzed using repeated-measures analysis of variance.

Results
The ICC and wCV were 0.96 (95% confidence interval [CI]: 0.91–0.99) and 16.1 (12.6–21.3), respectively, in glioma, 0.93 (0.82–0.98) and 15.0 (11.4–20.6) in stroke, and 0.84 (0.72–0.91) and 34.0 (28.7–41.0) in healthy brain. There were no significant differences in APTw signal between the three sessions, irrespective of disease condition and location. The ICC and wCV were 0.85 (0.68–0.94) and 27.4 (21.8–35.6), respectively, in supratentorial locations, and 0.44 (−0.18–0.76) and 32.7 (25.9–42.9) in infratentorial locations. There were significant differences in APTw signal between supra- (mean, 0.49%) and infratentorial locations (mean, 1.09%; $P<.001$).
Conclusions
The reproducibility of the APTw signal was excellent in supratentorial locations, irrespective of disease condition, while it was poor in infratentorial locations. Therefore, APTw signals measured in infratentorial locations may not be considered reproducible values.

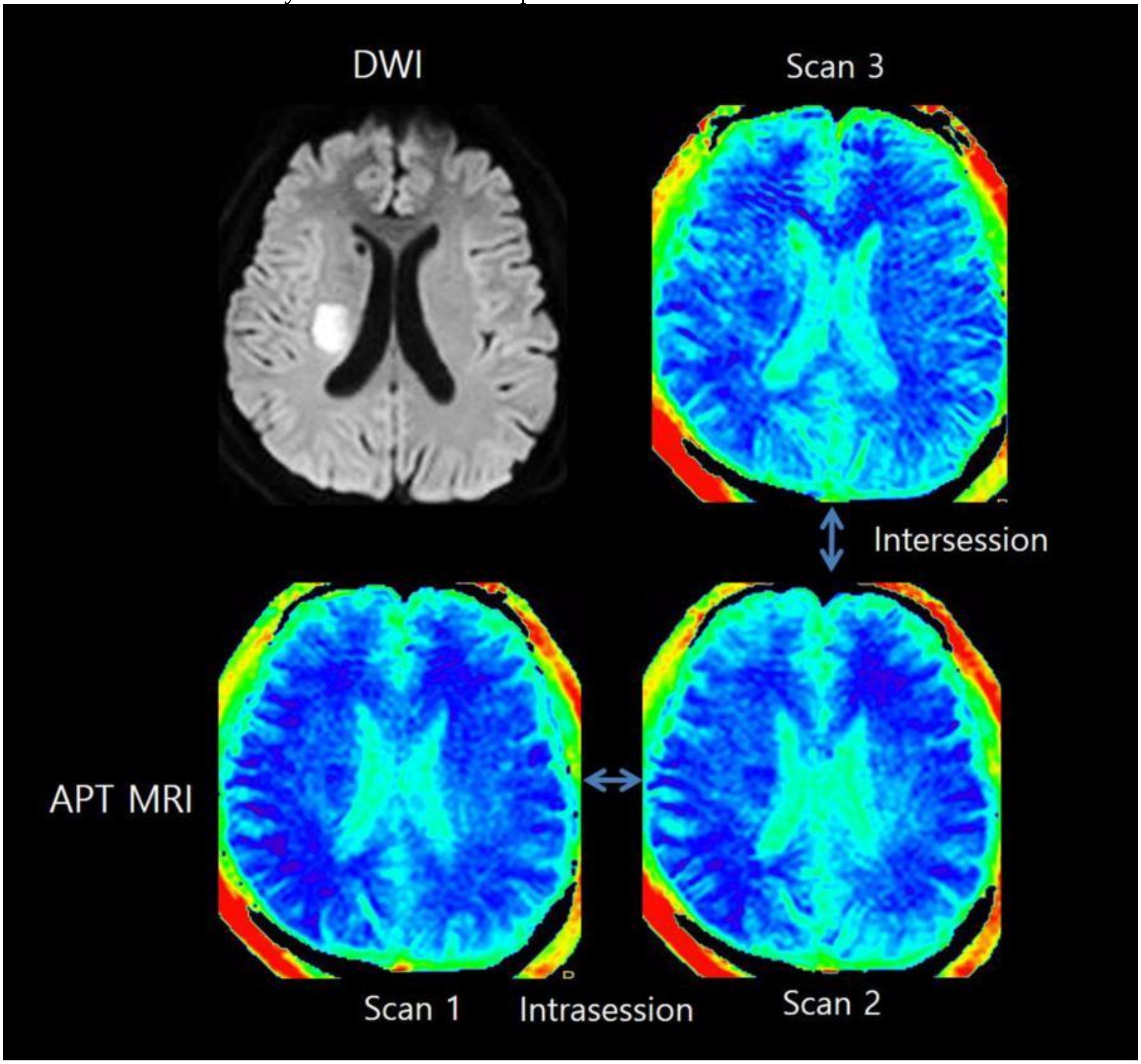

(Filename: TCT_3156_Fig1.JPG)

Thursday, May 23, 2019
9:30AM - 10:30AM
Head and Neck Potpourri Topics 2

3250

9:30AM - 9:37AM

A Rare Case of Metastatic Glomangiocpericytoma

C Harvey[1], O Raslan[1], A Ozturk[2], J Chang[3], M Bobinski[4], B Dahlin[5], J Ziegler[6], N Pham[6]
[1]University of California Davis, Sacramento, CA, [2]University of California, Davis Medical Center, Sacramento, CA, [3]UC Davis medical center, Sacramento, CA, [4]UC DAVIS SCHOOL OF MEDICINE, SACRAMENTO, CA, [5]UNIVERSITY OF CALIFORNIA AT DAVIS, SACRAMENTO, CA, [6]UC Davis Health, Sacramento, CA

Purpose
The purpose of this paper is to report a rare case of locally invasive glomangiopericytoma with distant metastatic disease.
Materials and Methods
A 40 year old male presented with six months of worsening right face, jaw, and eye pain. His pain originally was thought to be dental in nature and tooth extraction was performed. However, his pain progressively worsened, and he went on to develop ocular pain and diplopia at which time he was referred to our institution. His workup revealed a large locally invasive mass centered in the masticator space with locoregional invasion, perineural spread, and intracranial extension. Additional workup demonstrated disseminated pulmonary metastases.
Results
Contrast enhanced CT of the sinuses demonstrated a large mass centered within the right masticator space which was locally invasive involving the parapharyngeal space, suprazygomatic masticator space, and abutted the distal cervical ICA. MRI of the brain with contrast demonstrated extensive perineural spread along the pathways of the pterygopalatine fossa as well as V2 and V3 divisions of the trigeminal nerve. Perineural spread along the V3 division extended through the cavernous sinus with dural enhancement along the middle cranial fossa. Perineural spread along the V2 division of the trigeminal nerve involved Meckel's cave, foramen rotudum and infraorbital foramen. CT chest demonstrated cervical lymphadenopathy and disseminated pulmonary metastasis.
Conclusions
Glomangiopericytoma is a rare sinonasal tumor accounting for less than 0.5% of all sinonasal tumors usually seen in the 7th decade. Histologically the tumor is characterized as a subtype of hemangiopericytoma. Given its vascular nature, it often presents as nasal obstruction and epistaxis. It is generally of low malignant potential though does have a high local reoccurrence rate. This case is unique because malignant glomangiopericytoma is exceedingly rare. Even more unique is the extent of perineural spread, intracranial involvement, and extent of metastatic disease. Although the prognosis of glomangiopericytomas is generally good, much of the prognosis is dependent on curative resection. Postoperative radiation is sometimes recommended as a means to alter angiogenesis in these vascular tumors, though they are largely radiation resistant. Our patient was not a surgical candidate and at the time of this paper was undergoing palliative chemotherapy and radiation therapy.

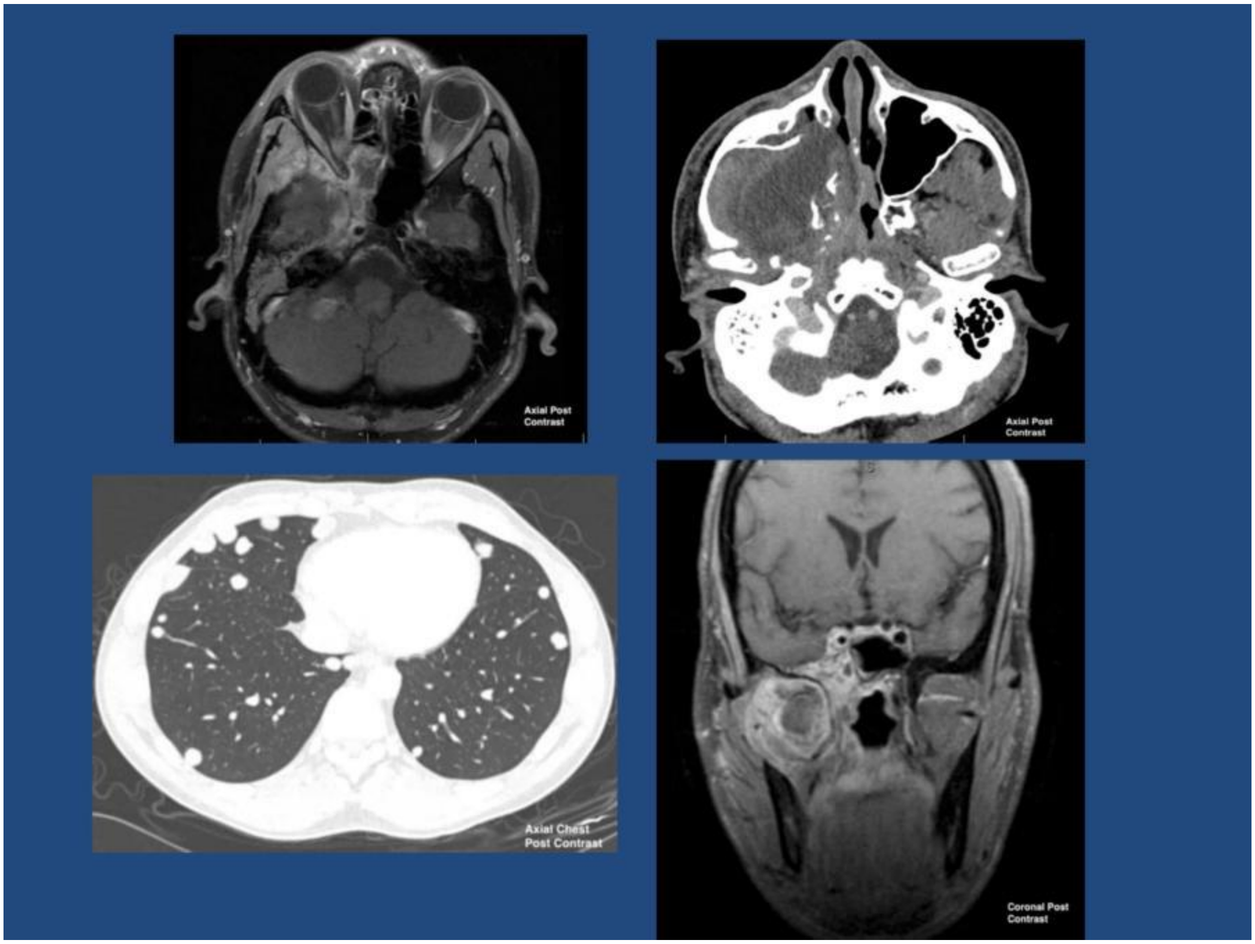

(Filename: TCT_3250_CHGlomangiopericytoma2.jpg)

2841

9:37AM - 9:44AM

Looking for Brain Tissue in all of the Wrong Places: A Rare Case of Middle Ear Neuroglial Heterotopia

A Zlochower[1], G Parnes[1], W Mallon[2], K Hsu[3], S Roknsharifi[1], J Bello[1], K Shifteh[1]
[1]Montefiore Medical Center, Bronx, NY, [2]Montefiore Medical Center, New York, NY, [3]Stanford University, Stanford, CA

Purpose
Present a case report of a neuroglial heterotopia within the middle ear in a patient presenting with tinnitus and hearing loss.
Materials and Methods
A 60 year old female presented to the otolaryngologist with a history of right sided tinnitus, hearing loss and dizziness. Temporal Bone CT and MRI Brain demonstrated a non-enhancing mass in the right tympanic cavity. The patient underwent surgery for resection of the lesion. The intraoperative findings demonstrated a mass within the epitympanum segment of the tympanic cavity lateral to the lateral semicircular canal. The dura was intact and there was no connection to the central nervous system These findings, along with the histologic appearance of non-neoplastic neuroglial tissue was consistent with neuroglial heterotopia. The differential diagnosis of tympanic cavity soft tissue lesion includes:

cholesteotoma, adenoma, paraganglioma, encephalocele/meningocele, inflammatory lesion or facial nerve schwannoma.

Results

MRI Brain 4/11/16 – Right non-enhancing tympanic cavity lesion within the epitympanum. The lesion is isointense to gray matter on T1 and T2 weighted imaging. CT Temporal Bones - 6/17/16 – Right tympanic cavity lesion with dehiscence of the tegmen tympani.

Conclusions

Neuroglial heterotopia, also known as neuroglial choristoma, is defined as normal brain tissue in an abnormal location. Although neuroglial heterotopias are classically found in the nasal cavity, nasopharynx or other midline structures, they can rarely present in non-midline structures such as the middle ear. Midline neuroglial heterotopias are generally found in infants and represent congenital lesions of abnormal embryonic development. On the other hand, non-midline neuroglial heterotopias typically occur in adults with a history of surgery, trauma, infection or inflammation to the affected area. There may be dehiscence of the osseous structures separating the brain from the extracranial location of the neuroglial heterotopia, as is true in our case where there was dehiscence of the tegmen tympani. These lesions are believed to be a variant of encephalocele whereby the brain tissue herniates into the affected structure with resorption of the intracranial pedicle. In this manner, neuroglial heterotopia can be distinguished from encephalocele by the presence of intact dura and no direct connection to the central nervous system.

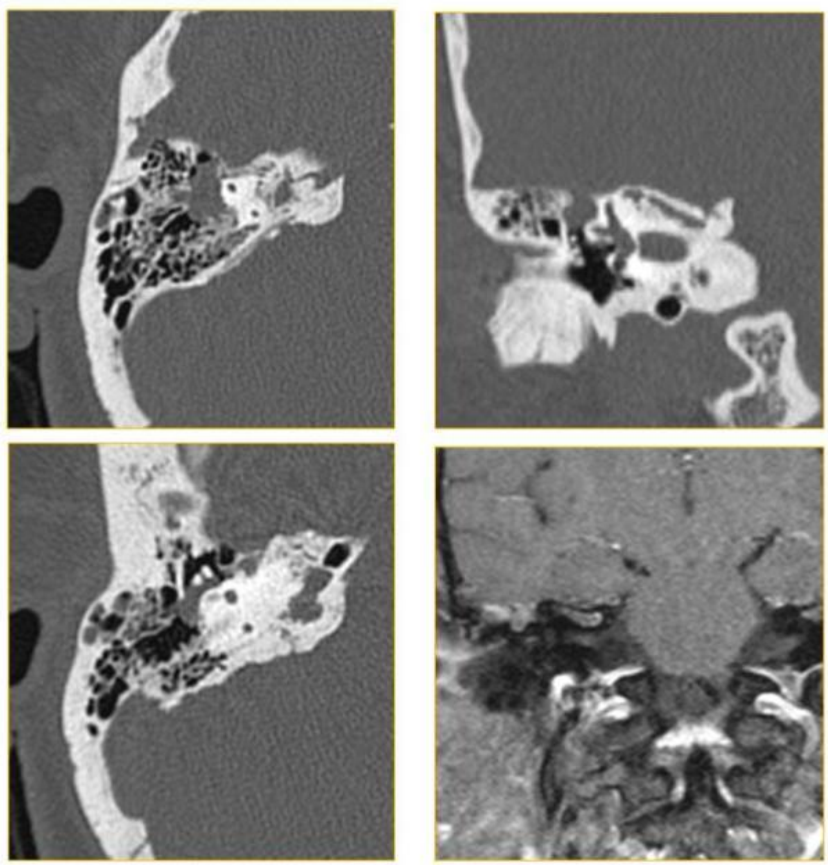

(Filename: TCT_2841_Presentation4.jpg)

2684

9:44AM - 9:51AM

Lupus-associated Vasculitis Mimicking an Invasive Sinonasal and Orbital Infection

S Galvis Vega[1], O Arevalo[2], C Soto[3], R Riascos[2], A Kamali[2]
[1]Universidad el Bosque, Bogota, Colombia, [2]Department of Diagnostic and Interventional Imaging, McGovern Medical School. UTHealth., Houston, TX, [3]National University of Colombia, Bogota, Colombia

Purpose
To present a case of lupus-associated vasculitis mimicking an invasive sinonasal and orbital infection.
Materials and Methods
37 years old woman with a history of Systemic lupus erythematosus (SLE) on treatment with prednisone and Hydroxychloroquine, complaining of nasal congestion and non-purulent discharge. The patient also presented malaise, fever, right eye swelling, and erythema, associated burry vision. CT and MR of the facial bones demonstrated an extensive sinonasal, orbital and meningeal inflammatory process. Further biopsy confirmed changes of lupus angiitis without undelaying infection. The patient was placed on DMARD therapy and showed clinical improvement.
Results
Mucosal thickening and enhancement within the right ethmoidal air cells and frontal sinuses with inflammatory changes in the extraconal space of the right orbit with associated thrombosis of the superior ophthalmic vein. There is myositis of the superior rectus, levator palpebrae, medial rectus, and superior oblique muscles. The lacrimal gland also inflammatory changes. The adjacent meninges demonstrate inflammatory changes.
Conclusions
Non-infectious inflammatory diseases of the paranasal cavities and orbits comprise a wide range of such as sarcoidosis, granulomatous vasculitides (Wegener, Churg–Strauss), eosinophilic angiocentric fibrosis, chronic rhinosinusitis and nasal perforations secondary to cocaine inhalation. SLE is a well-known cause of secondary vasculitis that may involve the central nervous system and the head and neck. Vasculitis in SLE patients show a prevalence ranging between 11% and 20%, and ulcers on the nasal mucosa and cartilaginous septum perforation are reported in less than 5% of patients. However, a destructive and invasive transpatial sinonasal and orbit presentation is uncommon and deserves to be revisited.

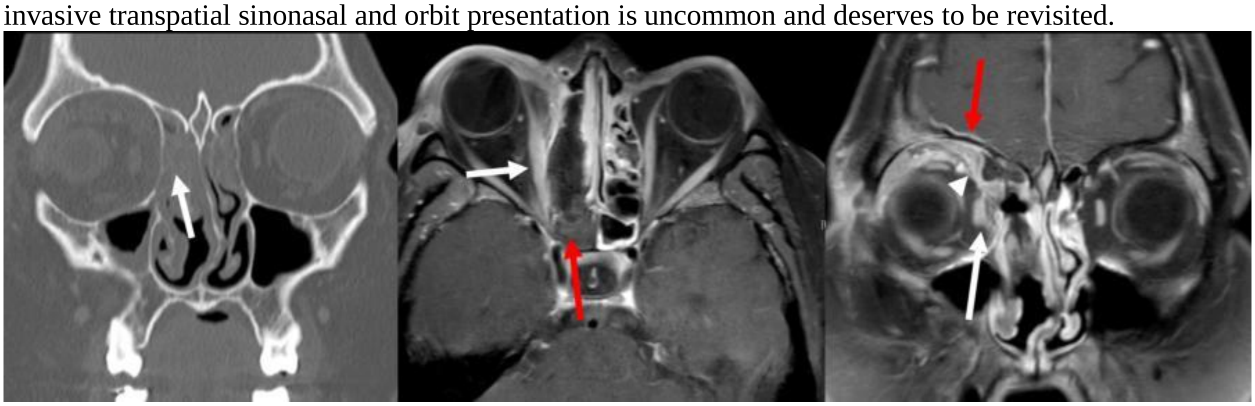

(Filename: TCT_2684_ExcerptaSLEVasculitis.jpg)

2673

9:51AM - 9:58AM

Regressed Pneumatization - Fatty Osseous Replacement of Previously Aerated Air Cells Mimicking Arrested Pneumatization

S Montoya[1], H Wang[1], D Gilroy[2]
[1]University of Rochester Medical Center, Rochester, NY, [2]University of Rochester Medical Center, N/A

Purpose

Pneumatization of the paranasal sinuses and skull base structures begins in utero and continues into adolescence. It is known that this is preceded by fatty marrow conversion. Arrested pneumatization is characterized by the failure of pneumatization, resulting in persistent fatty marrow within the air cells. We present a case of acquired fatty osseous replacement of a previously pneumatized petrous bone.

Materials and Methods

A woman initially presented in 2010 with eye pain; a CT was obtained and did not reveal an etiology for the eye pain, nor any other abnormalities. Subsequent presentation for pain 2018 resulted in another CT, which showed interval air cell opacification or matrix-forming lesion of the left petrous apex. An MRI was obtained for further characterization; this demonstrated no mass lesion, and fat signal within the air cells of the left petrous apex.

Results

CT obtained in 2010 (a) shows normal pneumatization of the petrous apices bilaterally. CT obtained in 2018 (b) shows interval opacification of the left petrous apex by a nonexpansile "lesion" with internal curvilinear sclerotic structures and no mass effect. T2-weighted MRI without (c) and with (d) fat suppression demonstrate fatty content of the "lesion" and preservation of architecture. Findings are compatible with "arrested" pneumatization, however the left petrous apex is known to have been previously pneumatized.

Conclusions

Arrested pneumatization is a normal variant which should not be mistaken for pathology; however, perhaps not all cases are development. We present a case of acquired fatty osseous replacement of the petrous bone, which is neither developmental nor pathologic.

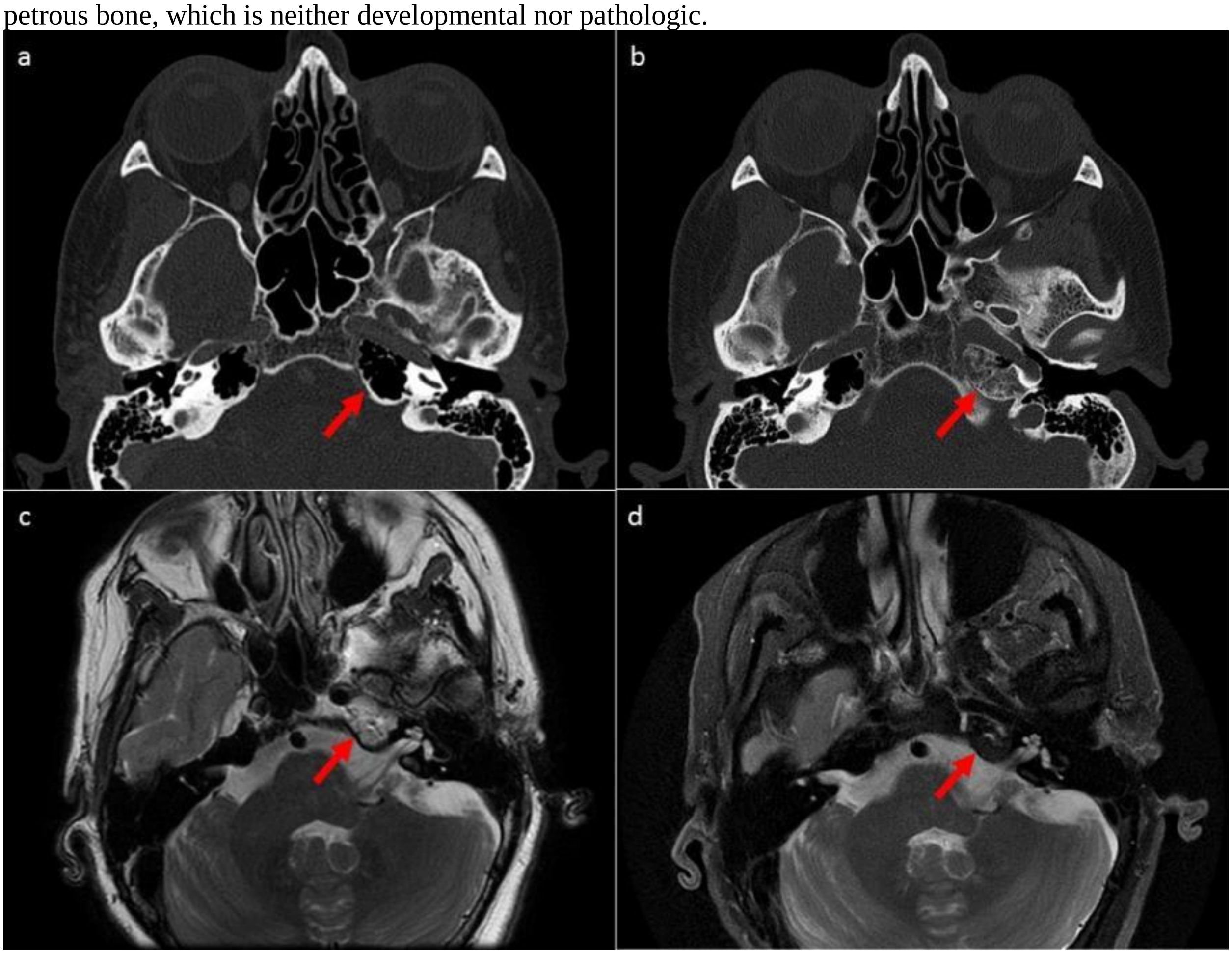

(Filename: TCT_2673_AP_abstract_images300.jpg)

3608

9:58AM - 10:05AM

Silicone Lymphadenopathy in Papillary Thyroid Carcinoma: Potential Mimickers of Metastatic Lymphadenopathy

J CHOI[1], W Moon[2], J Lee[2], H Roh[2]
[1]Konkuk University Medical center, Seoul, Seoul, [2]Konkuk University Medical Center, Seoul, Seoul

Purpose
To aware silicone lymphadenopathy related to liquid silicone injection in the face which can be misinterpreted as metastatic lymphadenopathy from the papillary thyroid carcinoma
Materials and Methods
We have 4 cases of silicone lymphadenopathy which were initially misinterpreted as metastatic lymphadenopathy from the PTC. All patients were female (47, 60, 68, and 70 years old), had subcentimeter PTC, and were confirmed as stage I (T1aN0M0) PTC via total thyroidectomy (three patients) and lobectomy (one patient) accompanied by central lymph node dissection. During routine follow-up using HRUS, we found several subcentimeter-sized ovoid non-necrotic lymph nodes with echogenic spots (arrows, A) or hyperechoic band-like area (arrows, B) in cervical lymph node level III or IV in 2 to 4 years after surgery. The thyroglobulin level was very low. According to the US criteria for metastatic lymphadenopathy from the PTC, we considered these lymph nodes were metastasis. However, subsequent repeated US-FNA upto 3 times revealed no evidence of malignancy on aspirates. During the conference for lateral neck dissection for these suspicious metastasis with surgeon, we reviewed preoperative CT and found innumerable silicone granulomas in the lower face (C). Although they were not willing to confess history of the liquid silicone injection to the face several decades ago, we concluded the lymph nodes with suspicious US-feature for metastasis were silicone lymphadenopathy related to liquid silicone injection in the face. These patients are still in good condition without any evidence of recurrence except US findings for 1 to 7 years.
Results
US showed several subcentimeter-sized ovoid non-necrotic lymph nodes with echogenic spots (arrows, A) or hyperechoic band-like area (arrows, B) in cervical lymph node level III or IV. CT showed innumerable non-enhancing nodular lesions in the subcutaneous fat of the face (C) suggesting silicone granulomas.
Conclusions
Silicone lymphadenopathy related to liquid silicone injection in the face can be misinterpreted as metastatic lymphadenopathy in patients with PTC. US-feature of silicone lymphadenopathy were ovoid non-necrotic lymph nodes with echogenic spots or hyperechoic band-like area. When the repeated FNA revealed no malignant cell in old female patients with suspicious metastatic lymph nodes, silicone lymphadenopathy should be included one of differential diagnosis for metastatic lymphadenopathy from PTC.

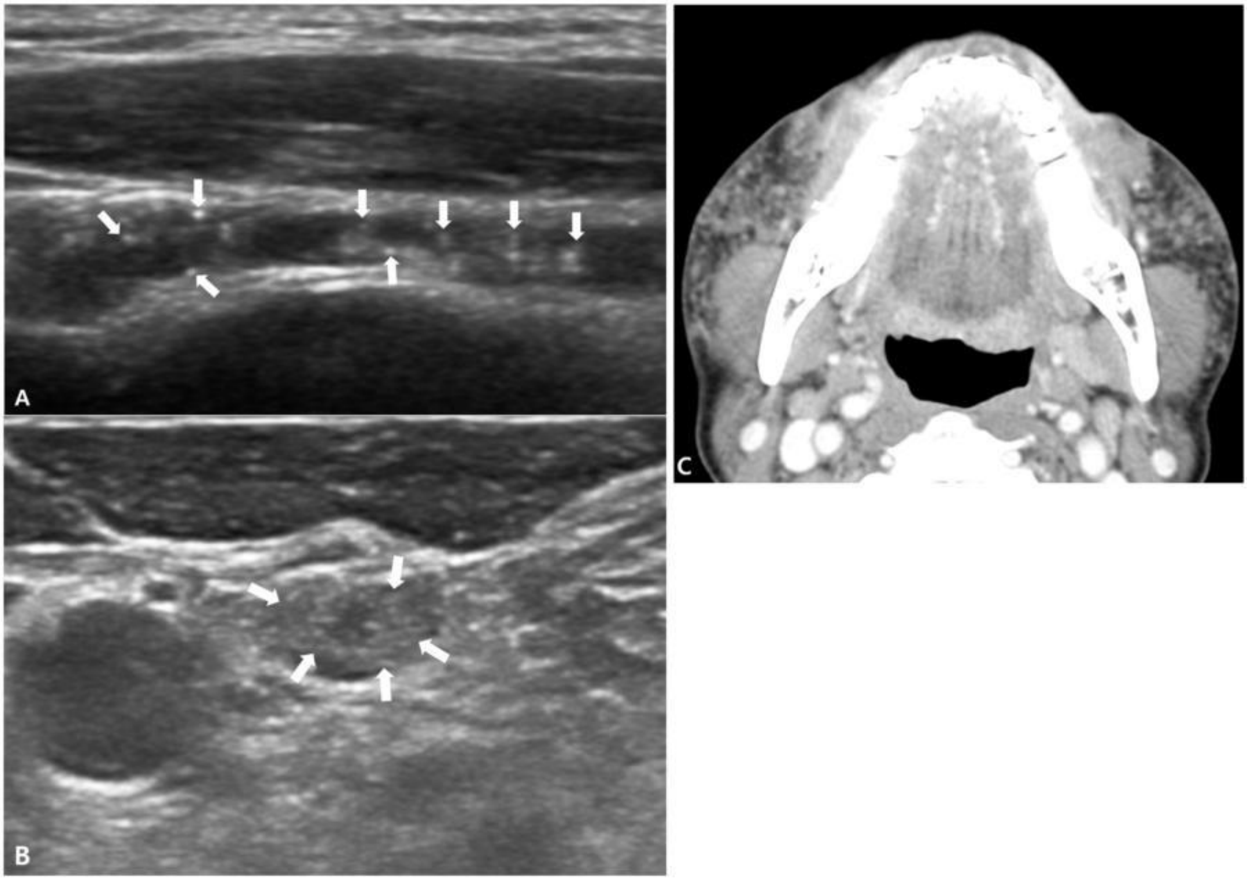

(Filename: TCT_3608_Figure.JPG)

2875

10:05AM - 10:12AM

Risk Stratification for Oropharyngeal Carcinoma Using Texture Analysis - a Step Beyond HPV Status

Y Chang[1], J NAIR[2], C McDougall[3], M Joshi[4], J Lysack[5]
[1]University of Calgary, Calgary, Alberta, [2]McMaster University, Hamilton, Ontario, [3]University of Calgary, Calgary, AB, [4]UNIVERSITY OF CALGARY, CANADA, CALGARY, AB, [5]University of Calgary, Foothills Medical Centre, Calgary, Alberta

Purpose
1) To develop, multivariable risk assessment models for oropharyngeal squamous cell carcinoma, based on 3D high order texture analysis of both the primary tumor and metastatic lymph node on enhanced CT scan, to accurately and consistently establish response / failure to treatment. 2) To compare the two models and determine their efficacy in predicting response/failure to treatment. 3) Use Texture Analysis to determine P16 status of oropharyngeal squamous cell carcinomas on CT.
Materials and Methods
80 patients with oropharyngeal squamous cell carcinoma and minimum follow-up of 24 months were retrospectively evaluated. 376 texture features were extracted from both the contoured tumor and metastatic lymph node on enhanced CT images. For each segmented tumor and lymph node, 376 texture features were produced using code written in MATLAB. These were grouped into three different sub-groups: First Order Statistics, Volume-Based measurements, and higher order matrix statistics. Texture features were then truncated to avoid multicollinearity and over fitting. The construction of prediction

models was performed by combining non-redundant texture features (top 10 features) using logistic regression. The performance of the resulting models for the prediction of response/ treatment failure, were evaluated using receiver operating characteristic (ROC) metrics on 100 bootstrap samples to maximize their generalization to out-of-sample data.

Results

The best multi variable model, based on contoured tumors, which showed association to treatment failure had an area under the curve (AUC) of 0.981. Similarly, the best model for association based on contoured lymph nodes to treatment failure had AUC of 0.965 . Model based on contoured tumors, for association with P16 status had an AUC of 0.990.

Conclusions

Multi variable models based on 3D Volumetric CT texture features of both primary tumor and metastatic lymph node appears to be a promising tool in the work-up of patients with oropharyngeal squamous cell carcinomas to estimate treatment response and determining P16 status. Combining feature analysis with known p16 status further increases the prognostic ability to treatment response compared to radiomics signature alone.

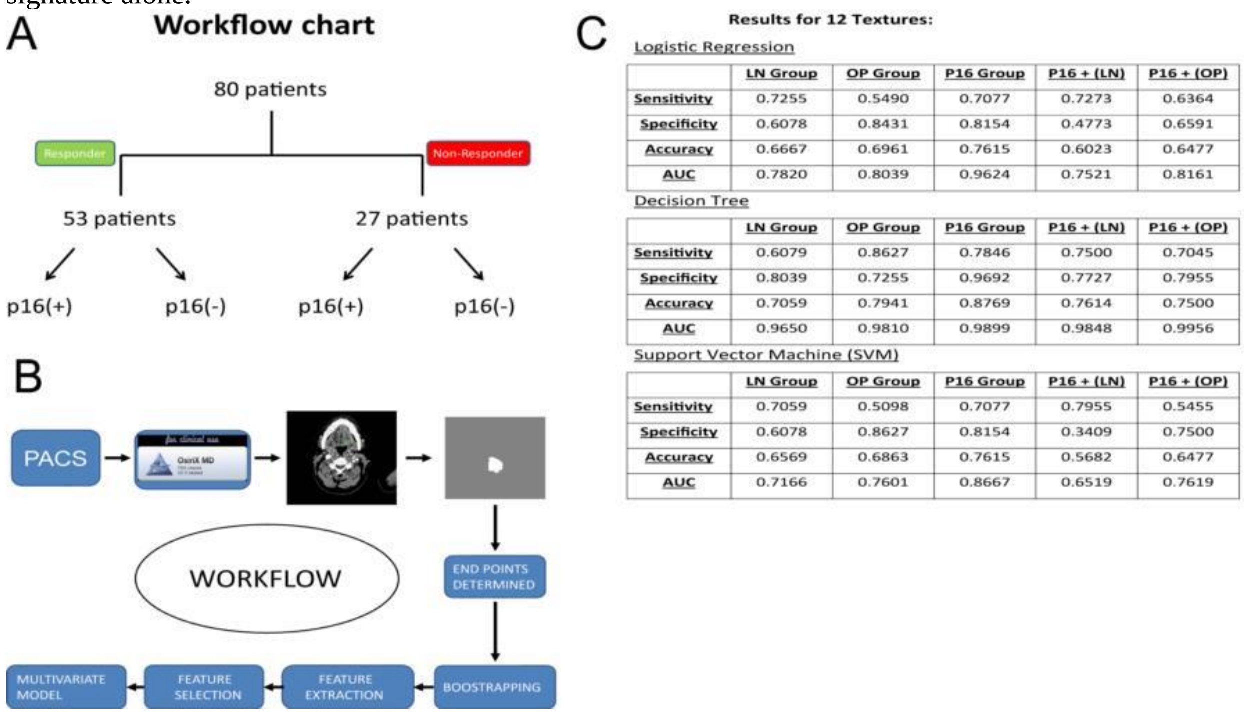

Logistic Regression

	LN Group	OP Group	P16 Group	P16 + (LN)	P16 + (OP)
Sensitivity	0.7255	0.5490	0.7077	0.7273	0.6364
Specificity	0.6078	0.8431	0.8154	0.4773	0.6591
Accuracy	0.6667	0.6961	0.7615	0.6023	0.6477
AUC	0.7820	0.8039	0.9624	0.7521	0.8161

Decision Tree

	LN Group	OP Group	P16 Group	P16 + (LN)	P16 + (OP)
Sensitivity	0.6079	0.8627	0.7846	0.7500	0.7045
Specificity	0.8039	0.7255	0.9692	0.7727	0.7955
Accuracy	0.7059	0.7941	0.8769	0.7614	0.7500
AUC	0.9650	0.9810	0.9899	0.9848	0.9956

Support Vector Machine (SVM)

	LN Group	OP Group	P16 Group	P16 + (LN)	P16 + (OP)
Sensitivity	0.7059	0.5098	0.7077	0.7955	0.5455
Specificity	0.6078	0.8627	0.8154	0.3409	0.7500
Accuracy	0.6569	0.6863	0.7615	0.5682	0.6477
AUC	0.7166	0.7601	0.8667	0.6519	0.7619

(Filename: TCT_2875_ASNRabstractgraph.jpg)

Thursday, May 23, 2019
9:30AM - 10:30AM
Health Policy Analytics

2490

9:30AM - 9:37AM

Changing Characteristics of Inpatient Hospital Stays and Associated Neuroimaging in Brain Cancer Patients

G Tewkesbury[1], M Hoch[2], R Duszak[1], D Coleman[3], G Sadigh[1]
[1]Emory University School of Medicine, Atlanta, GA, [2]Emory University Hospital, Atlanta, GA, [3]Emory University, Atlanta, GA

Purpose

To study changing characteristics of US inpatient hospital stays in brain cancer patients and associated neuroimaging utilization.

Materials and Methods

Using 2006-2014 data from the Nationwide Inpatient Sample (NIS), the largest publicly available all-payer inpatient health care database in the US, we identified inpatient stays for patients with a primary diagnosis of primary brain cancer. We assessed utilization and using logistic regression, identified independent predictors of neuroimaging examinations.

Results

A total 47,281 weighted cohort patients (mean age 52; 57% male; 76% white) with primary brain cancer were hospitalized for a mean 6.5 days. Admissions increased from 4,067 in 2006 to 6,140 in 2014 (+51%). Patients' primary insurance was Medicare in 34%, Medicaid in 14%, commercial in 44%, other in 5%, and self-pay in 3%. Of all patients, 8.9% underwent brain imaging (with 6.7% and 3.8% undergoing MRI and CT, respectively). Between 2006 and 2014, the rate of inpatient brain imaging increased 39% (from 7.2% to 10%). Total hospitalization charges increased from a mean $37,141 in 2006 to $75,456 in 2014 (+103%). Independent factors associated with a higher likelihood of neuroimaging utilization (p all <0.05) were hospital stay >6 days (OR 1.9), age <50 (OR 1.8), non-elective admissions (OR 1.5), female sex (OR 1.3), hospitalization in urban counties (OR 1.6), and not dying during admission (OR 2.1). Neuroimaging utilization did not differ significantly with patient race, payer, or income quartile.

Conclusions

In patients with brain cancer, the frequency of inpatient hospitalizations, utilization of inpatient neuroimaging, and total charges associated with hospitalizations have all increased over time. A variety of sociodemographic characteristics are associated with a higher likelihood of imaging utilization.

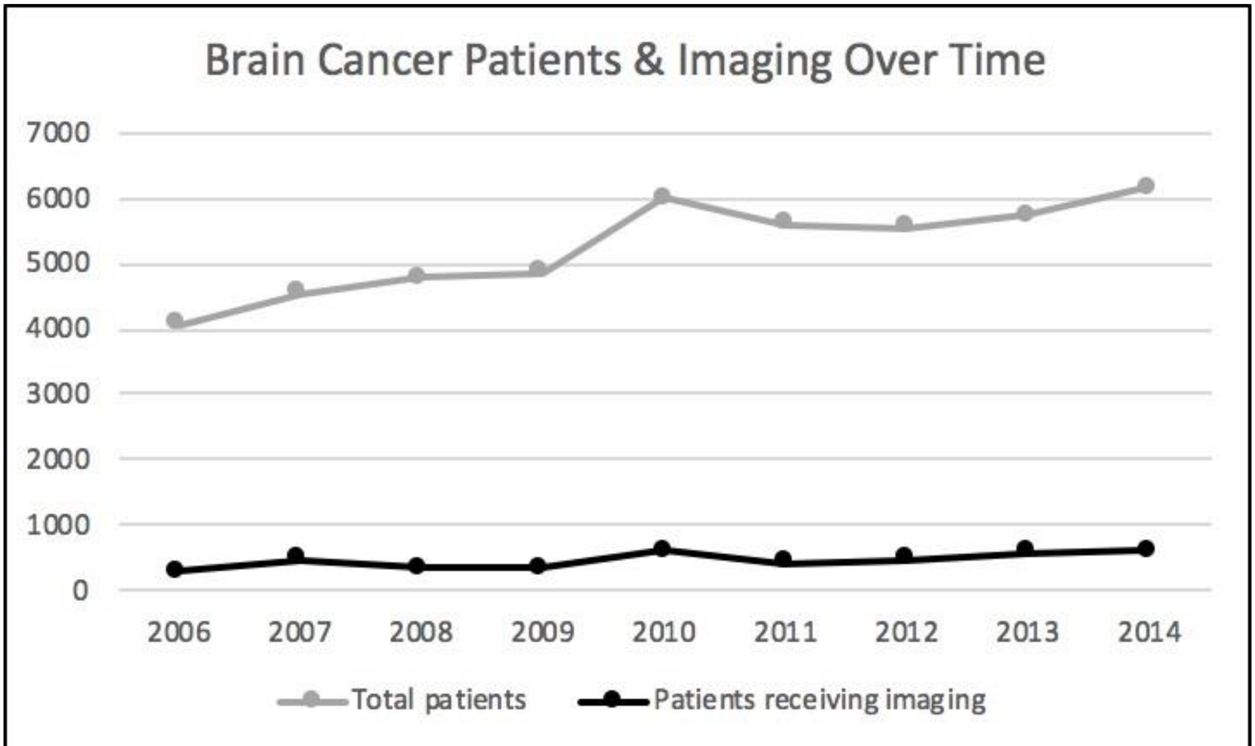

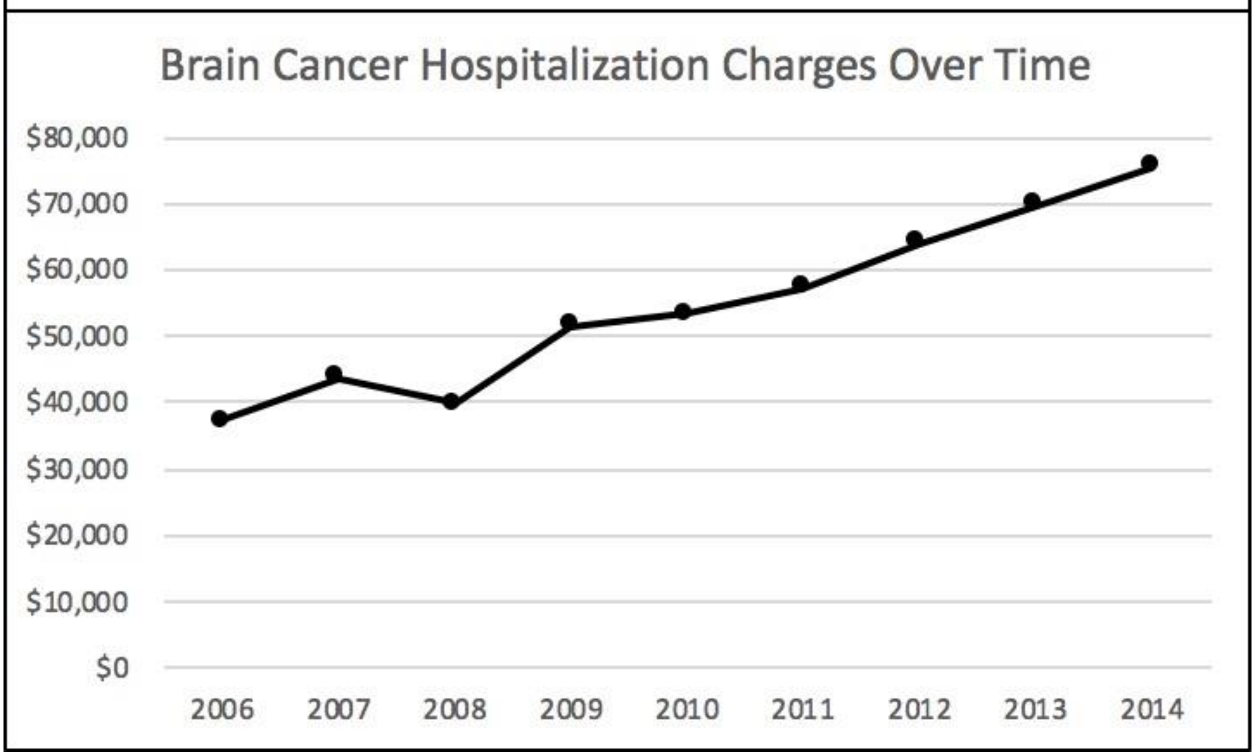

(Filename: TCT_2490_ScreenShot2018-10-23at21137PM.jpg)

2363

9:37AM - 9:44AM

Clinical Impact of Emergent Total Spine MRI Scans Performed at a Major Academic Medical Center

A Ali[1], C Huang[1], E Wiklund[1], Y Chang[1], A Bezuidenhout[1], D Hackney[1], R Bhadelia[1]
[1]*Beth Israel Deaconess Medical Center, Boston, MA*

Purpose

Total spine MRI scans are resource-intensive and are frequently requested by Emergency Room (ER). However, their utility in guiding immediate clinical decision making has not been assessed (1). We evaluated the radiological and clinical outcomes of emergent total spine MRI studies to determine their clinical impact.

Materials and Methods

Consecutive total spine MRI studies requested by the ER at our institution over one-year period were evaluated. A positive radiological outcome was: Cord Compression-CC (compression of the spinal cord and lack of surrounding CSF-Figure 1), Cauda Equina Compression-CEC (>75% narrowing of the lumbar spinal canal), Intramedullary Spinal Cord Lesion-IMSCL or Other Significant Findings-OSF (trauma-related findings not identified on CT, and infection/tumor without CC/CEC). The clinical outcome was considered positive if a patient was treated with surgery, radiation or intravenous antibiotics based on imaging findings during the same visit and further refined to include treatment within 24 hours of arrival to the ER.

Results

78/230 (33.9%) total spine MRI scans had positive radiological outcome of which 39/230 (17.0%) had positive clinical outcomes: CC/CEC= 28 (neoplasm= 10, degenerative= 9, infection= 5, hematoma= 3, trauma= 1), IMSCL= 1 (neoplasm) and OSF= 10 (neoplasm= 4, infection= 5, trauma= 1). 18/230 (7.8%) received treatment within 24-hours: Surgery= 15 (neoplasm= 4, degenerative= 1, infection= 6, hematoma= 3, IMSCL= 1), and IV antibiotics for infection= 3. None of the patients with negative radiological outcome had positive clinical outcome.

Conclusions

Although our results indicate a high radiological yield of emergent total spine MRI scans, their actual impact on immediate clinical management was low. Further stratification of clinical data may be required to develop a pre-test probability scale that could help targeted utilization of total spine MRI scans.

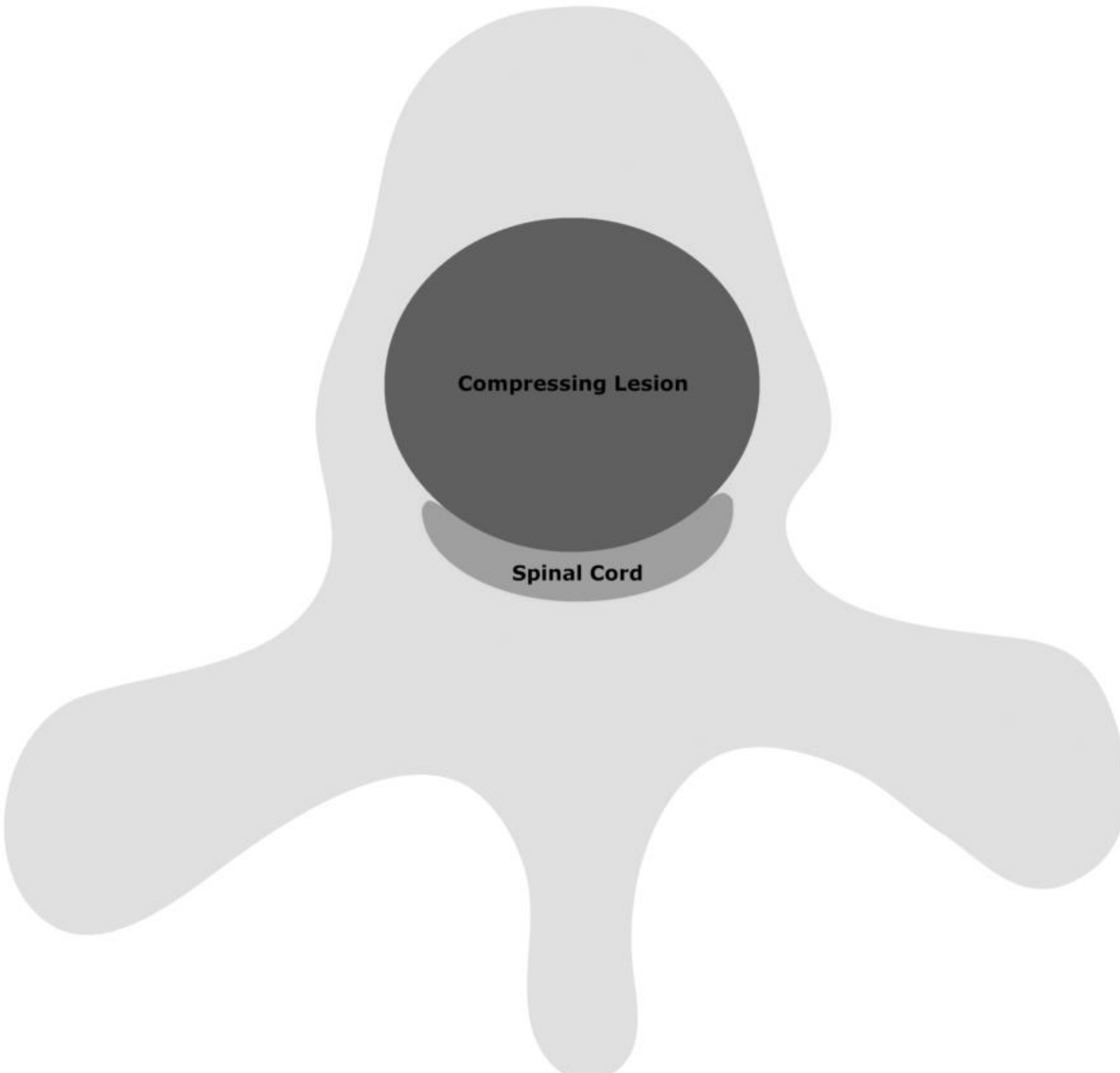

(Filename: TCT_2363_cordcompression2.gif)

3624

9:44AM - 9:51AM

Current Procedural Terminology in the United States and Canada: Differences and Similarities in 2 North American Health Systems

H Valand[1], O Chohan[2], S Chu[3], R Tu[4]
[1]American University of Integrative Sciences, Toronto, ON, [2]Christiana Care Health System, Newark, DE, [3]Vancouver Coastal Health Authority, Vancouver, BC, [4]Progressive Radiology, Washington, DC

Purpose
Current procedural terminology in radiology is a alphanumeric catalog of accepted procedures in medicine. The coding systems in Canada and the United States are both used to track radiology procedures. The similarities and differences between the Canadian and US coding systems are reviewed.

Materials and Methods
The Canadian Classification of Health Interventions, Canadian Coding Standards and the American Medical Association Current Procedural Terminology standards and policy are reviewed.
Results
The coding of radiology procedures in Canada is specific to the individual province. There are 10 Canadian provinces and 10 different radiology code sets in each province's imaging family. The specificity of radiology codes is provided by modifiers applied to the code. The American Medical Association (AMA) publishes a standard code set, Current Procedural Terminology (CPT) used by all 50 States and territories of the United States (US). CPT is a rigorous coding standard with Category 1, widely used procedures approved by the Food and Drug Administration and Category 3 investigational procedures. The AMA meets regularly to review new, retire old or review existing codes. Both the Canadian and US coding systems use modifiers to provide additional specificity. The US CPT category 2 codes are non procedure quality codes used for tracking.
Conclusions
The Canadian coding system is decentralized and different among the providences as each establishes individual coding methodology, coverage and reimbursement policy. In the US a single CPT code set is applied. The existence of the procedure code in both countries has no guarantee of payment or coverage but does provide a mechanism to evaluate exam type, volumes and statistical analysis. The Canadian Coding Standard of the Canadian Institute of Health Information is similar to the International Classification of Disease Procedural Coding System (ICD-10 PCS) which the US recently adopted for facility reporting of inpatient procedures whereas CPT is used for all outpatient procedures.

2668

9:51AM - 9:58AM

Disproportionate National Contributions to Subspecialties of Neuroradiology

S Emamzadehfard[1], V Eslami[1], S Sahraian[2], D Yousem[3], Z Fulton[4]
[1]University of Texas Health Science Center, San Antonio, TX, [2]John Hopkins, Baltimore, MD, [3]Johns Hopkins Medical Institution, Baltimore, MD, [4]University of Texas Health Science Center San Antonio, San Antonio, TX

Purpose
The contribution to the American Journal of Neuroradiology by foreign institutions has dramatically increased in recent decades. We examined whether all areas of neuroradiology have been equally affected in the AJNR. We hypothesized that, while foreign authors would dominate all branches of neuroradiology, the greatest impact would be on neurointerventional publications.
Materials and Methods
We assessed the country of the first author's institution of published manuscripts in the last 30 AJNR issues (January 2016-June 2018) to determine the contributions to the brain, head, and neck (H&N), spine, neurointerventional radiology (NIR), and pediatric (Ped) sections. In addition to calculating the percentage of US authorship, we determined which countries were contributing most to each branch of neuroradiology.
Results
We reviewed 793 articles. The overall percentages of manuscripts from US institutions were 44.4% in 2016, 47.2% in 2017, and 37.4% thus far in 2018. The percentage of US authorship was least in NIR (31.8%; p-value < 0.001) and brain (41.5%; p-value = 0.21), while It was significantly higher than non-US authorship in spine (60.7%; p-value = 0.002), followed by H&N 53.7%, and Ped 51.3%. The foreign countries that had the highest contributions in the brain, H&N, spine, Ped, and NIR were Japan, Korea, Canada, Italy, and Germany, respectively. Figures legend: Part 1: Ratio of US Contribution to different subsections of AJNR from 2016 to July 2018. IR = Interventional Radiology Part 2: Contribution of US and Non-US countries to different categories of articles in AJNR *The Chi-Square independence test

assessed the association between the contribution and the country of origin and showed statically significant values for these groups compared to the other categories. Brain was the only category that was not significant. Part 3: Top Two Non-US Countries Contributing to Each Category of AJNR (2016-2018). Data were presented as numbers and percentages.
Conclusions
The contributions to the AJNR from non-US authors dominate in the NIR category, whereas the US prominence is foremost in the spine. Overall, the contributions from nonUS authors exceed those originating from the US.

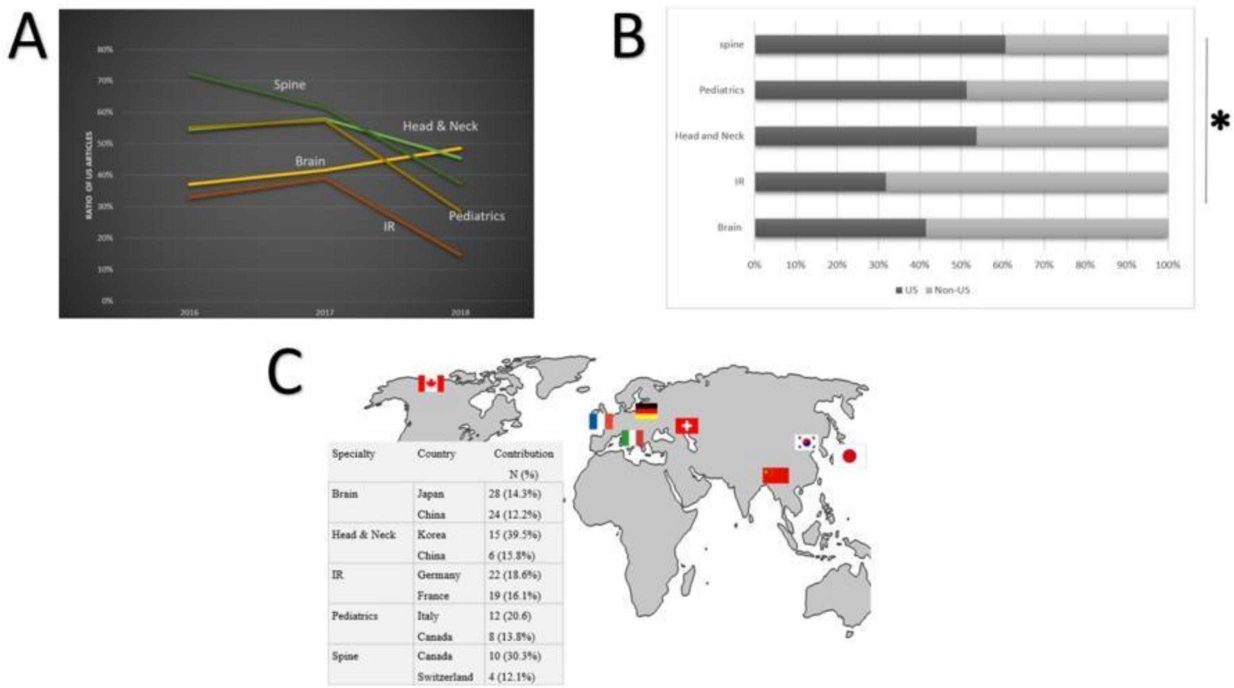

Specialty	Country	Contribution N (%)
Brain	Japan	28 (14.3%)
	China	24 (12.2%)
Head & Neck	Korea	15 (39.5%)
	China	6 (15.8%)
IR	Germany	22 (18.6%)
	France	19 (16.1%)
Pediatrics	Italy	12 (20.6)
	Canada	8 (13.8%)
Spine	Canada	10 (30.3%)
	Switzerland	4 (12.1%)

(Filename: TCT_2668_Neuroraddistribution.JPG)

3295

9:58AM - 10:05AM

Standardization of Imaging Strategies in Acute Stroke Care: A Cost-Effectiveness Approach

M Martinez[1], A Pandya[2], J Katz[3], A Malhotra[4], J Wang[3], P Sanelli[3]
[1]Siemens Healthineers, Manhasset, NY, [2]Harvard T.H. Chan School Of Public Health, Boston, MA, [3]Northwell Health, Manhasset, NY, [4]Yale University School Of Medicine, New Canaan, CT

Purpose
Stroke is a leading cause of death and serious long-term disability, with a high impact on the healthcare system and costs. Imaging plays a critical role in the diagnosis and subsequent treatment decisions in acute stroke care, but optimal imaging strategies remain uncertain according to national guidelines. This results in wide variations in clinical care, which may ultimately lead to suboptimal downstream variations in patient outcomes and healthcare costs. The purpose of this study was to determine cost-effective imaging guidelines in acute stroke care, assess the potential role of MR imaging prior to stroke treatment decisions, and elucidate the main drivers of patient outcomes and healthcare costs in acute stroke care
Materials and Methods
We developed a decision model to compare several CT- and MRI-based imaging strategies that utilized conventional imaging techniques, which reflects current practice, with advanced imaging (angiography and perfusion), including CTAP, MRAP, or combination of CT and MR (HYBRID). The clinical

pathways were based on published guidelines from the American Heart Association. The modified Rankin scale was used to model patient health states based on functional outcomes. Brain cancer risk for radiation exposure from CT was calculated using National Cancer Institute methodology. The input parameters and probabilities of the model were based on published literature and clinical trials data. Willingness-to-pay (WTP) thresholds were set at $100,000 and $50,000 in the analyses.

Results

The model results demonstrate advanced imaging is the most cost-effective strategy in acute stroke care even with a low WTP ($50,000). However, sensitivity analyses revealed the type of advanced imaging preferred (CT or MRI) is dependent on the time-delays from MR imaging and symptom onset time (SOT). Importantly, radiation-induced brain cancer has minimal impact on the effectiveness of CT-based strategies.

Conclusions

Our results demonstrate that utilization of advanced imaging is cost-effective in acute stroke care and provide insight into developing new guidelines based on SOT and imaging time delays.

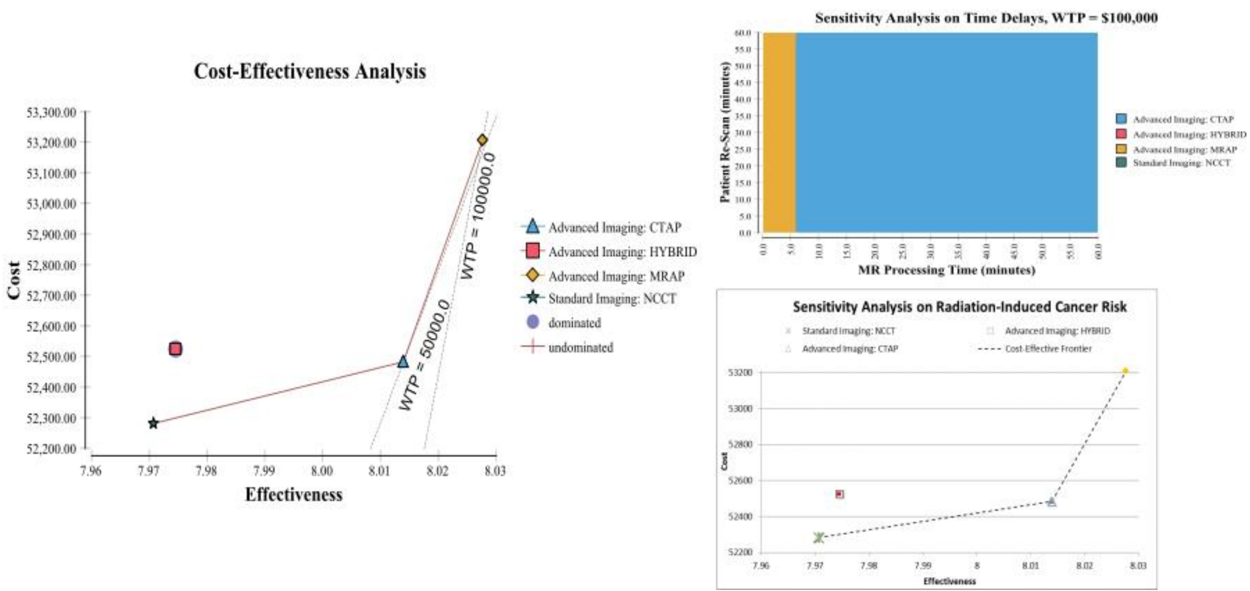

(Filename: TCT_3295_asnr_martinez_sanelli.jpg)

Thursday, May 23, 2019
9:30AM - 10:30AM
Temporal Bone Hour

2453

9:30AM - 9:37AM

Expected Evolution of Inner-Ear MR Findings after Vestibular Schwannoma Resection: Comparison of Translabyrinthine, Retro-Sigmoid, and Middle-Cranial Fossa Approaches

J Benson[1], M Carlson[1], J Lane[2]

[1]Mayo Clinic, Rochester, MN, [2]MAYO CLINIC, ROCHESTER, MN

Purpose

Changes following vestibular schwannomas resection have prognostic and surgical planning implications, including for future cochlear implants. This study aimed to delineate the expected evolution of MR findings after resection via translabyrinthine (TL), retro-sigmoid (RS), and middle cranial fossa (MCF) approaches.

Materials and Methods

A retrospective review was completed of patients with MR imaging following vestibular schwannoma resection. Examinations were numerically ordered based on their relation to the surgery: e.g. first post-operative MR (PO1), second post-operative MR (PO2), etc. Inner ear structures were evaluated on T2WI and/or FIESTA, FLAIR, T1WI, and post-gadolinium images. Signal intensity was compared to pre-operative exams.

Results

After TL approach resections, PO1 tended to show blood products within, and early obliteration of, the semicircular canals (SCCs) and vestibule; the basal turn of the cochlea (BTC) had inflammation but no internal heme. BTC obliteration appeared on PO2 in >50% of patients; diffusely decreased enhancement and resolution of blood products was seen on PO3. Post-RS approach resection, approximately half of patients had early inflammatory changes in the BTC, a SCC, and/or the vestibule on PO1. BTC obliteration occurred in about 30% of cases on PO2; fewer patients had obliteration of one or more SCC. Heme was present in at least 1 area in approximately 25% of patients on PO1, which progressively decreased on PO2 and PO3; enhancement likewise decreased over the course of sequential examinations. After an MCF approach resection, early inflammatory changes were seen in the superior SCC in about half of patients on PO1. Superior SCC enhancement resolved on PO2; findings otherwise remained stable on PO3-4. No patients had BTC obliteration on PO1 or PO2; 10% had BTC obliteration on PO3.

Conclusions

Each surgical approach for vestibular schwannoma resection has characteristic evolution of post-surgical findings in the inner ear. BTC obliteration occurred most frequently after TL approach, and least after MCF approach.

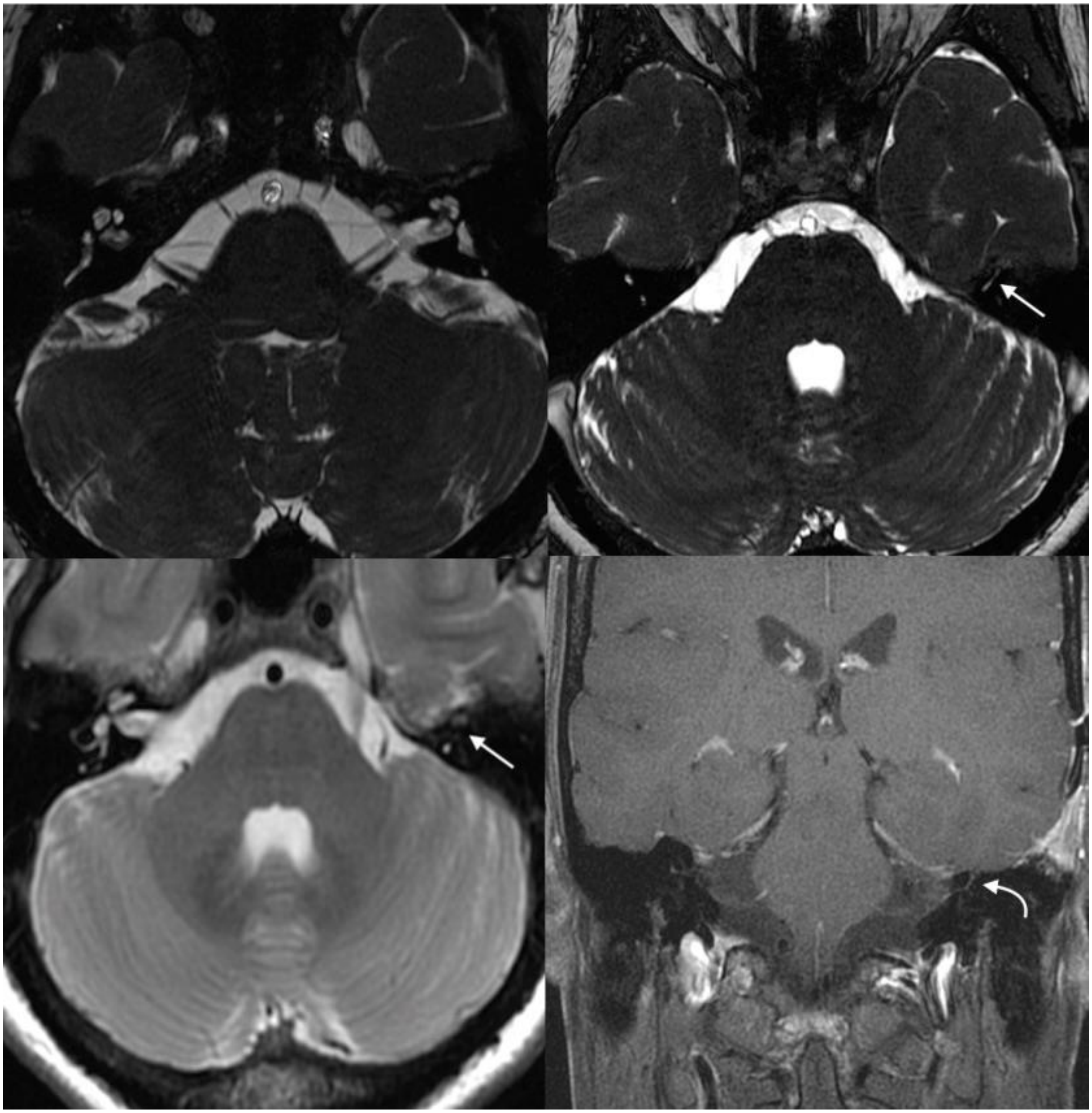

(Filename: TCT_2453_ASNRImage.jpg)

2666

9:37AM - 9:44AM

Inner and External Ear Malformations as Assessed on Fetal Ultrasound and MRI

J Choi[1], J Estroff[1], C Robson[2]
[1]Boston Children's Hospital, Boston, MA, [2]BOSTON CHILDREN'S HOSPITAL, BOSTON, MA

Purpose
Previous literature has documented associations between external ear abnormalities with syndromes as assessed on ultrasound. The purpose of this study is to review abnormalities of the inner and external ears

as assessed on ultrasound and 3T fetal MRI and to document their association with syndromes, thus better informing patients, clinicians, genetic counseling and workup.
Materials and Methods
An IRB approved retrospective review was performed of fetal ultrasound and MRI examinations performed between 8/1/2013-8/1/2018. Examinations were reviewed for the presence of malformations of the inner and /or external ears. When available, genetic testing and postnatal clinical documents and imaging were also reviewed.
Results
From the dates of 8/1/2013-8/1/2018, 41 pregnant females were imaged in whom ear malformations were observed in their fetuses. The most commonly observed external ear malformations included malformed pinnae (n = 20) including microtia (n = 9); low set ears (n = 17); external auditory canal malformation or atresia (n = 9); mass involving or abutting the external ear (n = 4, most commonly lymphatic malformations); preauricular skin tags (n = 3); and anotia (n = 2). The most commonly observed inner ear malformations included cochlear malformation (n = 6); absence and / or malformation of the semicircular canals (n= 4); vestibular malformation (n = 3); malformed internal auditory canals (n = 3); and absence of the inner ear structures (n = 1). Ear abnormalities were associated with syndromes on the basis of additional imaging findings, genetic testing and / or postnatal examination in a large number of cases (18/41) with the most commonly observed syndromes including CHARGE (n = 4), Trisomy 18 (n = 3), Trisomy 13 (n = 3), 22q11.2 duplication (n = 2), Brachio-Oto-Renal syndrome (n = 1), Trisomy 21 (n = 1), Trisomy 22 (n = 1), Goldenhar syndrome (n = 1), Klinefelter Syndrome (n = 1), and Cat-Eye Syndrome (n = 1). Syndromic associations were suggested in 5/41 cases, but were not confirmed due to redirected care. Vascular anomalies counted for 4/41 cases involving the external ear. In the remainder of the ear malformations, no syndromic correlation, genetic abnormality or unifying diagnosis was made.
Conclusions
Our findings suggest that detailed evaluation of the inner and external ears should be performed in every evaluation of the fetus and malformation may suggest the presence of underlying syndromic condition.

3444

9:44AM - 9:51AM

Inner-Ear Fluid Compartment Accumulation of Gadolinium after Intrathecal Gadolinium Injection for the Work-Up of Suspected CSF Hypotension/Hypovolemia Syndrome

A Hedjoudje[1], W Dillon[2], D San Millán[3]
[1]Johns Hopkins University, Baltimore, MD, [2]UNIV OF CALIFORNIA, SAN FRANCISCO MED CTR, SAN FRANCISCO, CA, [3]Sion Hospital, Sion, Valais

Purpose
Patients in our Institution routinely undergo MR myelography and MR cisternography for suspected SIH. During these studies, Gadolinium (Gd) accumulation was observed in the inner ear fluid compartment. The purpose of this study is to report this observation and to discuss the possible pathways allowing for Gd to cross from the CSF spaces to the inner ear fluid compartments.
Materials and Methods
Ten patients with suspected SIH underwent MR-myelo-cisternography after intrathecal Gd injection using 3DT1 fat saturated space sequence in 1.5 and 3 Tesla MRI. MR-cisternography was performed on average 3.8 hours after intrathecal Gd injection (2.5-5 hours). 5 patients had repeat MRI 5.5-29 hours after intrathecal Gd injection.
Results
Contrast accumulation in the inner ear fluid compartments was visible in all patients, including 2 patients that turned out not to have SIH and where no extra-thecal CSF accumulation and no CSF leak were demonstrated. It was particularly conspicuous in the cochlea, around the modiolus and basal turn and in studies performed 5-7 after intrathecal Gd enhancement. Signal intensity decrease in delayed studies. No

Gd was observed in the cochlear and vestibular aqueduct and very faint high T1 signal was observed in the vestibule and semi-circular canals.

Conclusions

Accumulation of Gd in the inner ear fluid compartments is observed after intrathecal Gd injection and likely represents a normal phenomenon as it was observed both in patients with documented SIH and in a patient without SIH. It should not be considered a pathological finding or thought to represent a type of CSF leak in patients with SIH. The most likely communication route between the CSF spaces to the inner ear fluid compartments is across the fundus of the inner ear, through the modiolus into the cochlea. These findings provide further insight as to the close physiological relationship between the CSF spaces and inner ear fluid spaces. Figure legend : Coronal T1-weighted images in 8 patients who underwent MR-cysternography illustrating bilateral gadolinium accumulation in the inner ear fluid compartments.

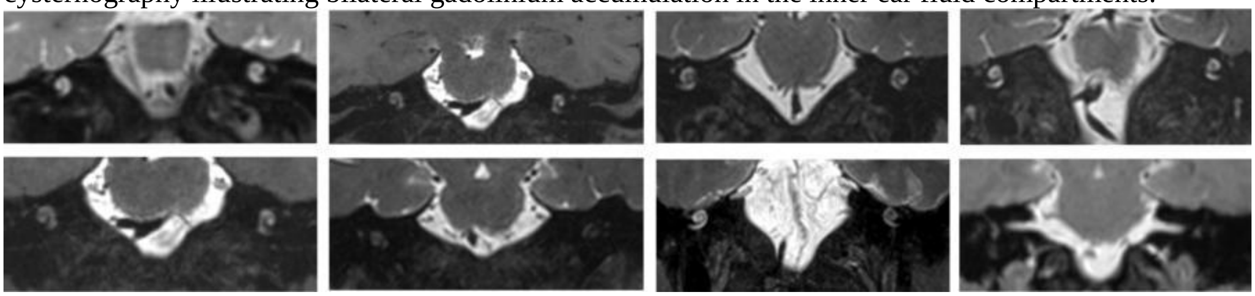

(Filename: TCT_3444_Figure1.jpg)

3489

9:51AM - 9:58AM

Jugular Foramen Tumors: The Role of Imaging from the Surgeon's Perspective

A Winn[1], M Nachiappan[2], F Contreras[3], D To[4], S Sur[3], R Kuker[5], N Nagornaya[6], R Bhatia[6]
[1]University of Miami, Jackson Memorial Hospital, Miami, FL, [2]Jackson memorial hospital, Miami, FL, [3]Jackson Memorial Hospital, Miami, FL, [4]Jackson Memorial Hospital / University of Miami, Miami, FL, [5]University of Miami Miller School of Medicine, Miami, FL, [6]University of Miami/Jackson Memorial Hospital, Miami, FL

Purpose

Define the current knowledge base necessary for neuroradiologists to cogently report the advanced imaging findings that surgeons require in the planning of established and novel surgical approaches to paraganglioma and non-paraganglioma tumors of the jugular foramen.

Materials and Methods

Review of multidisciplinary Pubmed and Embase-indexed articles, and collaboration with the Neurosurgery, Otolaryngology, and Radiation Oncology departments of the University of Miami and Jackson Memorial Hospital, pictorially define the current role of advanced imaging of jugular foramen tumors from the surgeon's perspective.

Results

The complex anatomopathology of jugular foramen tumors demands an unmitigated multidisciplinary understanding and interplay for optimal treatment planning. As a clinically inaccessible crossroad of cranial nerves, critical hindbrain structures, and vital, frequently variable vascular structures, advanced multimodality imaging plays a fundamental and increasingly consequential role in the diagnosis and treatment planning of previously inoperable tumors of the jugular foramen. As imaging and surgical techniques continue to advance, so must the neuroradiologist's acumen for identifying and describing previously indiscernible microanatomic and pathologic details that will dictate management of jugular foramen tumors.

Conclusions
Gleaned through the study of current peer reviewed literature, this article will illustrate the essentials that neuroradiologist should know in order to effectively communicate with surgeons for the management of jugular foramen tumors, including surgically relevant detailed anatomy, anatomic variants, multimodality imaging interpretation, pearls, and pitfalls.

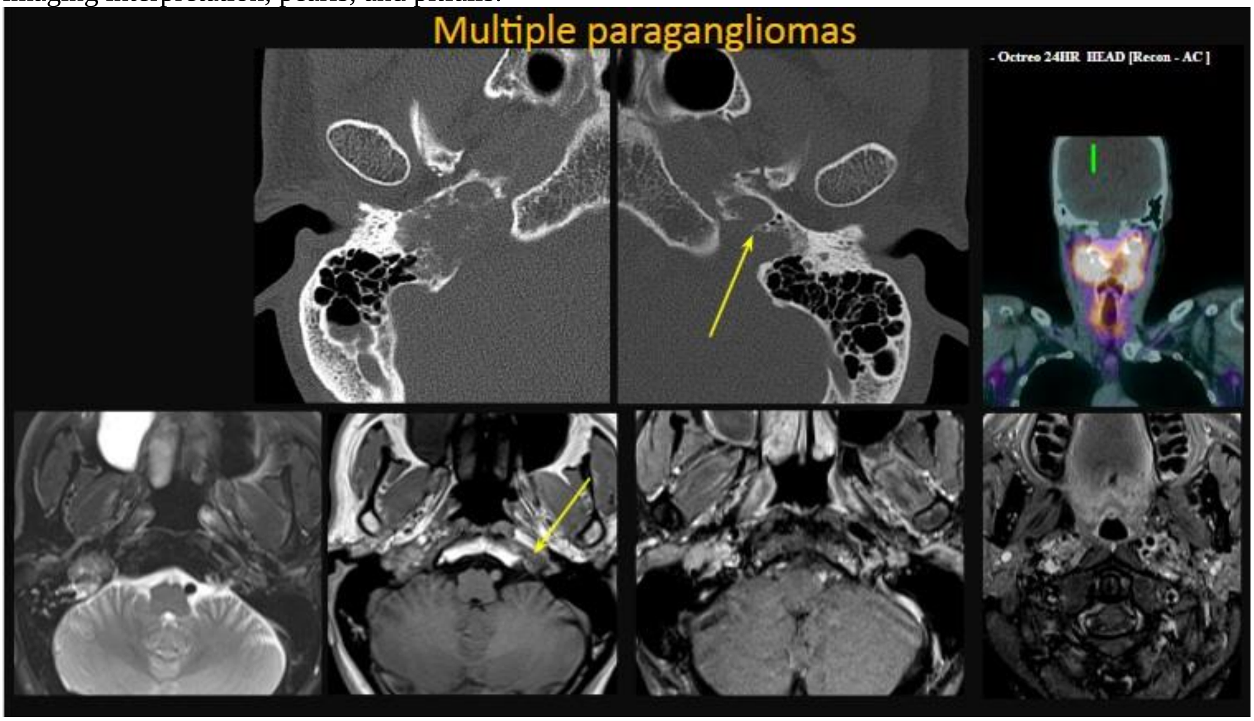

(Filename: TCT_3489_multiplepara.jpg)

2566

9:58AM - 10:05AM

Novel MRI Characterization of Auditory Pathways for Preoperative Assessment in Cochlear Implant Patients

M Yuhasz[1], G Lemberskiy[1], B Ades-aron[1], M Hagiwara[1], J Roland[1], T Shepherd[1]
[1]*NYU Langone Medical Center, New York, NY*

Purpose
Patients with sensorineural hearing loss (SNHL) benefit from cochlear implantation (CI), however preoperative risk-benefit assessment is challenging. Diffusion MRI can demonstrate components of the auditory pathway, but results are inconsistent, hard to reproduce and lack independent validation. We assessed the potential for a combination of novel MRI strategies to provide in vivo MRI assessment of the entire auditory pathway.
Materials and Methods
All MRIs were obtained with a 20-channel coil on a 3-T Prisma MRI scanner. First, a high spatial resolution turbo spin echo (TSE) sequence of the whole brain (350-micron in-plane resolution, 2 hrs) was obtained in 14 postmortem whole brains to identify the different anatomic components of the hearing pathways as a ground truth. Next, 10 normal hearing adult subjects were scanned using a Fast Gray Matter Acquisition T1 Inversion Recovery (FGATIR) sequence to identify the same structures in vivo. Finally, adult subjects returned for a 1-mm isotropic high angular resolution diffusion scan using random matrix theory denoising. Size, morphology and orientation of auditory pathway structures were obtained and regions-of-interest drawn to extract diffusion parameters.

Results

Brainstem auditory pathway structures, including the cochlear nucleus, superior olivary complex, lateral lemniscus, inferior colliculus and medial geniculate nucleus were identified in all ex-vivo brains and healthy controls using FGATIR. Size, position and orientation were obtained of all structures. In vivo diffusion properties were extracted using manual segmentation with coregistered FGATIR MRI data. Tractography using MRTRIX software was obtained from the cochlear nucleus to the MGN.

Conclusions

Modified TSE and FGATIR MRI sequences provide an independent ground truth for discrimination and morphological assessment of the brainstem auditory structures. These data can validate quantitative diffusion MRI characterization and tractography. Future work will employ this combined FGATIR and high resolution diffusion approach to potentially identify MRI predictors of CI success or failure in patients with SNHL.

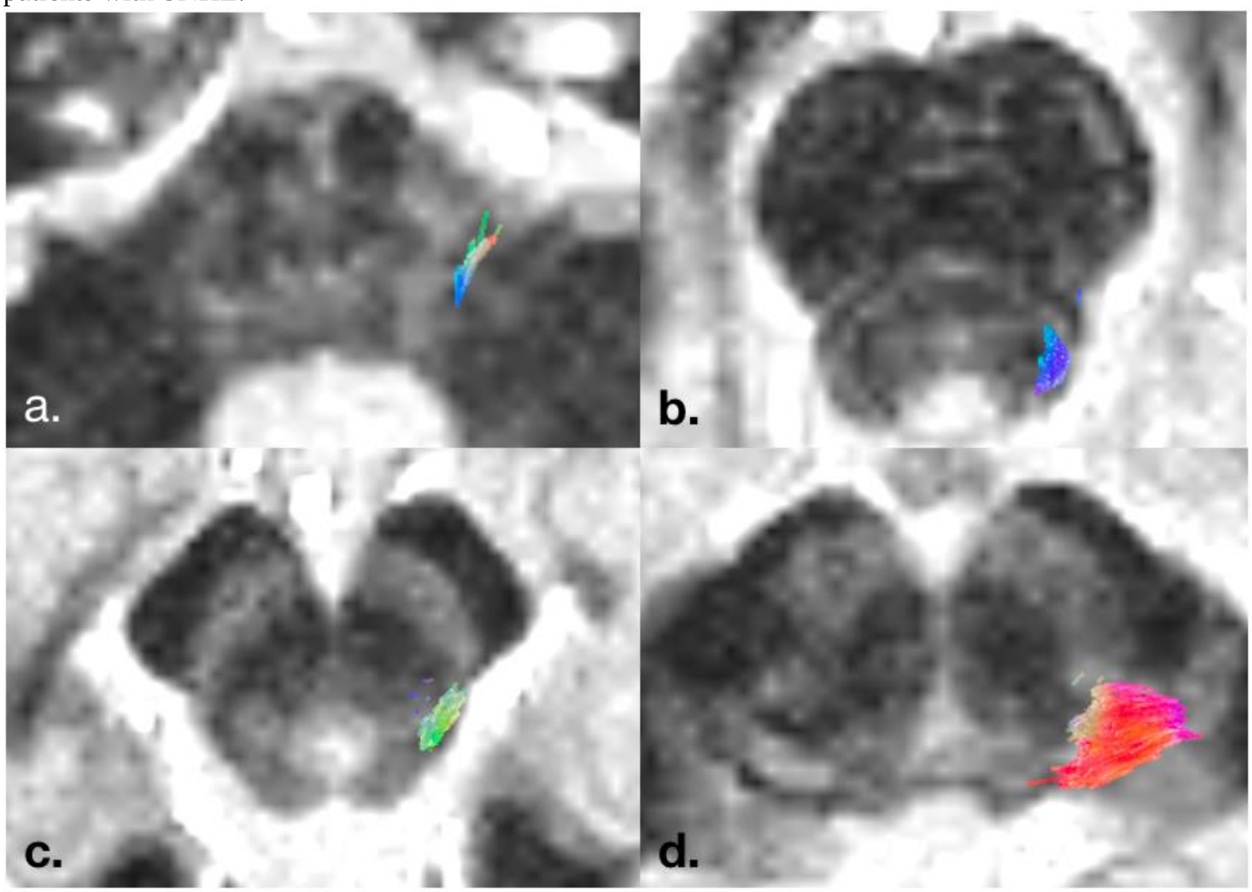

Figure 1. High angular resolution 1.0mm-isotropic diffusion weighted sequence showing seeded auditory pathway through regions of interest in the cochlear nucleus (a), the lateral lemniscus (b), the inferior colliculus (c), and the medial geniculate nucleus (d).

(Filename: TCT_2566_ASNRCompositeFigure.jpg)

2197

10:05AM - 10:12AM

Prevalence of Internal Auditory Canal Diverticulum in Subjects without and with Otosclerosis and its Association with Internal Auditory Canal Morphology

M Peterson[1], D Palipana[1], C Hsu[1], T Watkins[2], G Kwan[1], S Bhuta[1], K Singh[1]
[1]Gold Coast University Hospital, Australia, [2]Princess Alexandra Hospital, Australia

Purpose
Diverticulum at the anteroinferior wall of the internal auditory canal (IAC) has been recently described as cavitary otosclerotic plaques in recent publications. The purpose of this study is to establish the prevalence of IAC diverticulum in both subjects without and with otosclerosis and its association with IAC morphology.
Materials and Methods
A retrospective review of high resolution computed tomography temporal bones was conducted at a tertiary hospital from February 2015 to September 2018. Clinical records and HRCT temporal bones of 262 consecutive patients (131 male, 131 female, mean age 50.21 years) were evaluated for the presence of IAC diverticulum at the anteroinferior wall and severity of otosclerosis. IAC morphology was classified into four groups: patulous, normal, stenotic or atretic. Relevant clinical histories were also recorded.
Results
Diverticulum at the anteroinferior wall of the IAC were present in 19 subjects without otosclerosis (7.3%;19/262) and 6 subjects with otosclerosis (2.3%;6/262). Majority were bilateral (76%;19/262) and less commonly unilateral (24%;6/262). A statistically significant association was found between patulous IAC and either unilateral or bilateral IAC diverticulum ($p=0.009$). Other IAC morphologic types were not statistically associated with IAC diverticulum. A statistically significant association was found between IAC diverticulum and otosclerosis ($p= 0.004$). Otosclerosis severity in our series only ranged from grade I-II. Hearing impairment was not a clinical feature of IAC diverticulum as an isolated finding or in subjects without otosclerosis.
Conclusions
IAC diverticulum are more prevalent in subjects with otosclerosis and patulous IAC morphology. Aetiology remains uncertain but we hypothesized that this could be an acquired structural anomaly formed at a potential weak transitional point between the dense bone of the otic capsule and the IAC canal. Both patulous morphology (presumed greater degree of bony remodeling from cerebrospinal fluid pulsation) and "bone softening" disease such as otosclerosis serve as potential predisposing factors for the formation of IAC diverticulum.

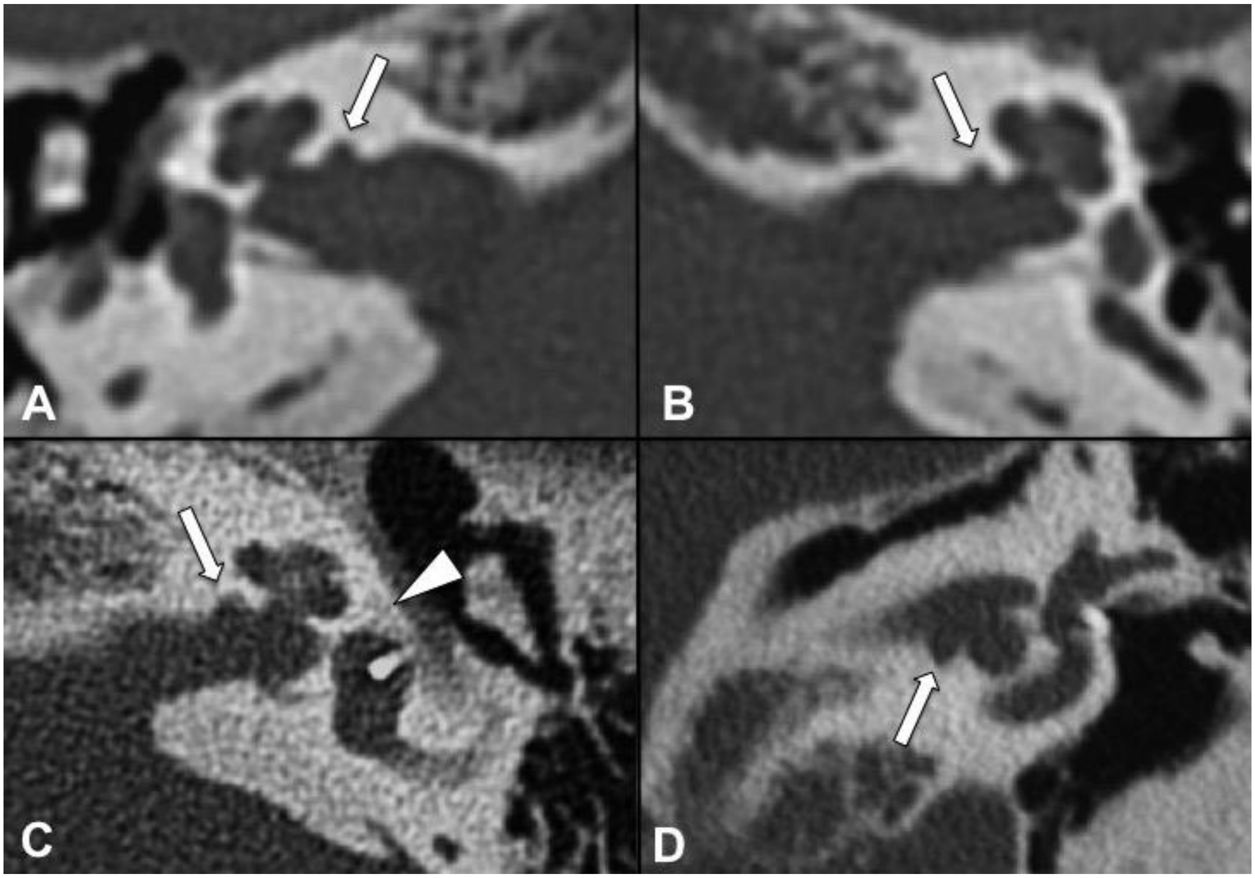

(Filename: TCT_2197_Figure300.jpg)

3013

10:12AM - 10:19AM

Reversed Fast Imaging with Steady-State Precession Diffusion-Weighted Imaging for the Detection of Middle Ear Cholesteatoma

M Azuma[1], Z Khant[1], T Hirai[2]
[1]Miyazaki University, Miyazaki, Miyazaki, [2]UNIVERSITY OF MIYAZAKI, MIYAZAKI, MIYAZAKI

Purpose
Three-dimensional reversed fast imaging with steady-state precession (3D-PSIF) diffusion-weighted imaging (DWI) has not been applied for the evaluation of cholesteatoma. We aimed to investigate the diagnostic performance of 3D-PSIF-DWI sequence for the detection of middle ear cholesteatoma compared with echo-planar (EP) DWI sequence.
Materials and Methods
Our study population consisted of 81 patients who underwent 3D-PSIF-DWI and EP-DWI studies at 3T. Both qualitative and quantitative evaluations were performed. Kappa (κ) statistics, interclass correlation coefficient (ICC), independent t-test, and receiver operating characteristic (ROC) analysis were used for statistical analysis. Pair-wise comparison of ROC curves was performed to compare diagnostic performance [area under the ROC curve (AUC)] of the two DWI sequences.
Results
Five of 81 patients were excluded due to severe susceptibility artifacts interfering with interpretation and apparent diffusion coefficient (ADC) measurement on EP-DWI studies. For the finally included 76 patients (68 cholesteatoma, 5 otitis media, and 3 cholesterol granuloma patients), interobserver

agreements for the qualitative evaluations were moderate to very good (κ = 0.60-0.90). ICCs for the quantitative evaluations were good to excellent (ICC = 0.626-0.972). ADC value and ADC ratio were significantly lower in cholesteatoma than noncholesteatoma lesions (P < .0001). 3D-PSIF-ADC ratio provided highest diagnostic performance (AUC = 1). The diagnostic performance of the qualitative evaluations for < 5mm cholesteatomas was significantly better for 3D-PSIF-DWI than EP-DWI sequence (P < .01) although there were no significant differences in the quantitative evaluations between the two sequences.
Conclusions
The diagnostic performance of 3D-PSIF-DWI sequence is superior to EP-DWI sequence especially for the qualitative detection of < 5mm middle ear cholesteatomas.

2615

10:19AM - 10:26AM

The Prognostic Significance of Bony Cochlear Nerve Canal Width in Sudden Sensorineural Hearing Loss

M Cetin[1], S Karakurt[1], H Hatipoglu[1]
[1]*Health Sciences University Ankara Numune Research and Training Hospital, Ankara, Turkey*

Purpose
To study the bony cochlear nerve canal (BCNC) width in the affected and unaffected ears of adults with sudden sensorineural hearing loss (SNHL).
Materials and Methods
Medical records were reviewed from January 2010 through May 2017 to identify patients presenting with sudden SNHL. SNHL was defined as a rapid onset of hearing loss of at least 30dB in three consecutive frequencies in the pure-tone audiogram within 72 hours or less. High resolution temporal bone CT examinations were reviewed by a neuroradiologist with 16 years of experience. The BCNC widths were measured on PACS. Mann-Whitney U test was employed to study the differences in BCNC between the affected and unaffected ears. Correlation between BCNC widths and initial pure tone audiograms and hearing thresholds were examined (Spearmn rho correlation test). The affected ears of patients were classified as healed (Recovered group: F/M:5/17, mean age:52) according to the recovery observed in one month of follow-up (pure tone average within 10 dB hearing levels of initial hearing loss or within 10 dB of the hearing loss of the unaffected ear). Correlation between the BCNC widths and healing was sought (Mann-Whitney U test).
Results
There were 38 patients (F/M:11/27, aged 27 to 79 years, mean age:56). There was a statistically significant difference between the mean BCNC widths of the affected and unaffected ears ($p = 0.001$, 1.78 ± 0.2 mm (need the range for all measurements) and 1.93 ± 0.2 mm). A statistically significant negative correlation was found between the BCNC widths of the affected ears and the initial pure tone audiogram and the hearing thresholds at frequencies of 4000 Hz and 8000 Hz ($p= 0.036$, $r= -0.342$; $p=0.012$, $r= -0.406$; $p=0.008$, $r=-0.427$). 22 patients were healed. The mean BCNC widths were different between the healed and unhealed groups were ($p = 0.021$; 1.85 ± 0.22 and 1.69 ± 0.13, respectively).
Conclusions
The mean BCNC width is smaller on the affected side compared with the unaffected side in patients with sudden SNHL. The mean BCNC width is larger in patients who recovered their hearing compared with the patients who did not.

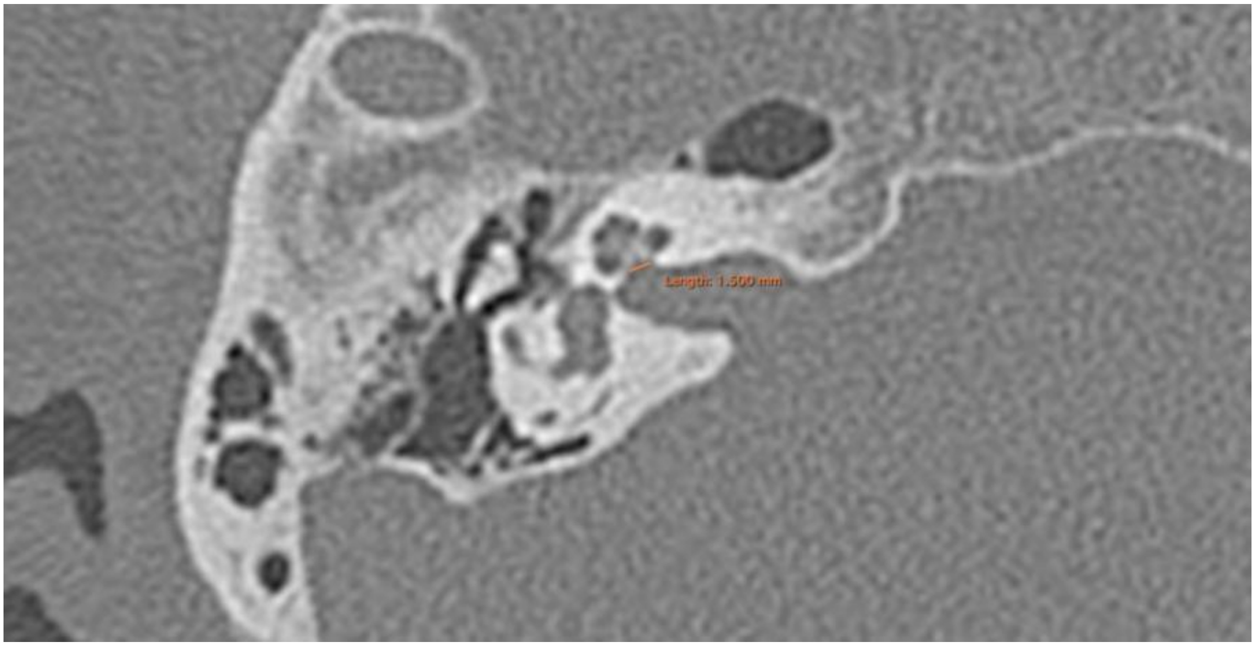

(Filename: TCT_2615_Cochlea.jpg)

Thursday, May 23, 2019
9:30AM - 10:30AM
Vascular Malformations and Embolization

2298

9:37AM - 9:44AM

Ear Arteriovenous Malformation Management

W Yakes[1]
[1]*The Yakes Vascular Malformation Center, Englewood, CO*

Purpose
To determine the efficacy of Ethanol Endovascular Repair of Ear Arteriovenous Malformation (AVMs).
Materials and Methods
14 patients (9 female, 5 males; age range 6-39 years; mean age: 22 years) with ear AVMs presented for therapy. Two patients had failed prior embolizations (PVA/coils/nBCA/steroids) and 2 patients had other therapies (laser/excisions/grafting). All presented with a grossly enlarged painful ear, and 5 patients had intermittent bleeding. All patients underwent transcatheter and direct puncture ethanol treatments. (86 procedures).
Results
All 14 patients were cured of their AVM at long-term follow-up (mean follow-up: 52 months). One patient had transient partial VII nerve palsy. Two patients had minor blisters and ear injuries that healed on the outer tragus. The longest follow-up demonstrating cure was 12 years.
Conclusions
Ethanol endovascular repair of Ear AVMs can achieve cures in this vexing lesion that previously was treated with resection of the ear and with high recurrence rates. This series documents long-term cures of AVMs of the ear and scalp that were not treatable by endovascular approaches as previously documented in the world's literature. Permanent treatment of the auricular AVMs is documented and no recurrence

occurred in any patient. Only one article is published (group from Shanghai, China) emulating this technique.

2303

9:44AM - 9:51AM

Ethanol and Coil Embolization of Complex Dural AVF

W Yakes[1]
[1]*The Yakes Vascular Malformation Center, Englewood, CO*

Purpose
To evaluate the efficacy of ethanol, ethanol and coils, nBCA, and Onyx management of complex dural AVF.
Materials and Methods
13 patients (mean age 39 years; 8 females, 5 males). All patients presented with dural AVF involving the transverse sinus, sigmoid sinus and cavernous sinus. One patient suffered from high output cardiac state due to the massive size of her combined dural fistula and scalp AVM. All patients underwent MR and cerebral arteriogram evaluations. Patients underwent ethanol embolization, coil embolization, ethanol and coil em-bolization, nBCA embolization and Onyx embolization to treat these acquired dural AVF.
Results
12/13 patients were endovascularly cured of their disease at a mean follow-up of five months. One patient's therapy is on going. In those patients who had thrombosed sig-moid sinuses and partially thrombosed transverse sinuses with venous drainage being cortical because of the occluded sinuses, novel approaches were utilized to reach the point of fistualization and treat with coils and ethanol. Sacrifice of the diseased trans-verse and sigmoid sinus was also utilized to treat the large dural AVF involving these segments. In the cavernous sinus coil embolization and nBCA embolization was utilized via surgical cut-down to access the Superior Ophthalmic Vein to navigate to the Cavern-ous Sinus when the Inferior Petrosal Sinus was incomplete. In those patients presenting with pulsatile tinnitus it was absent at follow-up. Headaches also resolved. Except for one patient with a transient homonymous hemianopsia, no other complication occurred.
Conclusions
Complex acquired dural AVF can be treated and cured by endovascular means. With meticulous technique complications can be avoided. Many embolic agents are success-ful in ablating dural AVF in all dural sinuses.

3216

9:51AM - 9:58AM

Evaluation of Hemorrhagic Risk in Quantitative Digital Subtraction Angiography

C Lin[1], W Guo[2]
[1]*Taipei Veterans General Hospital, Taipei, Taipei,* [2]*TAIPEI VETERANS GENERAL HOSPITAL, BEITOU DISTRICT, TAIPEI, 11217, TAIWAN*

Purpose
Hemorrhage risk assessment for arteriovenous malformations (AVMs) has recaptured the attention of cerebrovascular specialists since the ARUBA trial demonstrated that medical treatment was superior to intervention. In previous studies, assessments of hemorrhage risk based on angioarchitecture have yielded inconsistent results, and quantitative hemodynamic assessments have been limited to small numbers of patients. In the present study, we examined whether cerebral hemodynamic analysis using quantitative digital subtraction angiography (QDSA) can outperform angioarchitecture observations in evaluating the risk of hemorrhage associated with cerebral AVM

Materials and Methods
We retrospectively reviewed adult supratentorial cerebral AVM patients who had undergone both digital subtraction angiography and magnetic resonance (MR) imaging studies between 2011 and 2017. Angioarchitecture parameters, QDSA parameters, age, sex, and nidus volume measured from MR imaging were analyzed using univariate and multivariate logistic regression. Stasis index was defined as the absolute value of inflow gradient divided by outflow gradient of the region of interests. The receiver operating characteristic curve was used to compare the diagnostic performance of the angioarchitecture and hemodynamic models.
Results
A total of 119 cerebral AVM patients were included in this study after the exclusion of ineligible. After adjustment for age at diagnosis, sex, and nidus volume, multivariate logistic regression revealed that exclusive deep venous drainage ($p = 0.005$), observed through conventional angioarchitecture examination, and the stasis index of the most dominant drainage vein ($p = 0.018$), measured in hemodynamic analysis, were independent risk factors for hemorrhage. The areas under the receiver operating characteristic curve were similar between the conventional angioarchitecture (0.76) and hemodynamic analyses (0.78).
Conclusions
In QDSA, a higher stasis index of the most dominant drainage vein is an objective warning sign for AVM rupture. Both qualitative angioarchitecture and quantitative hemodynamic analysis should be considered in assessments of cerebral AVMs in patients.

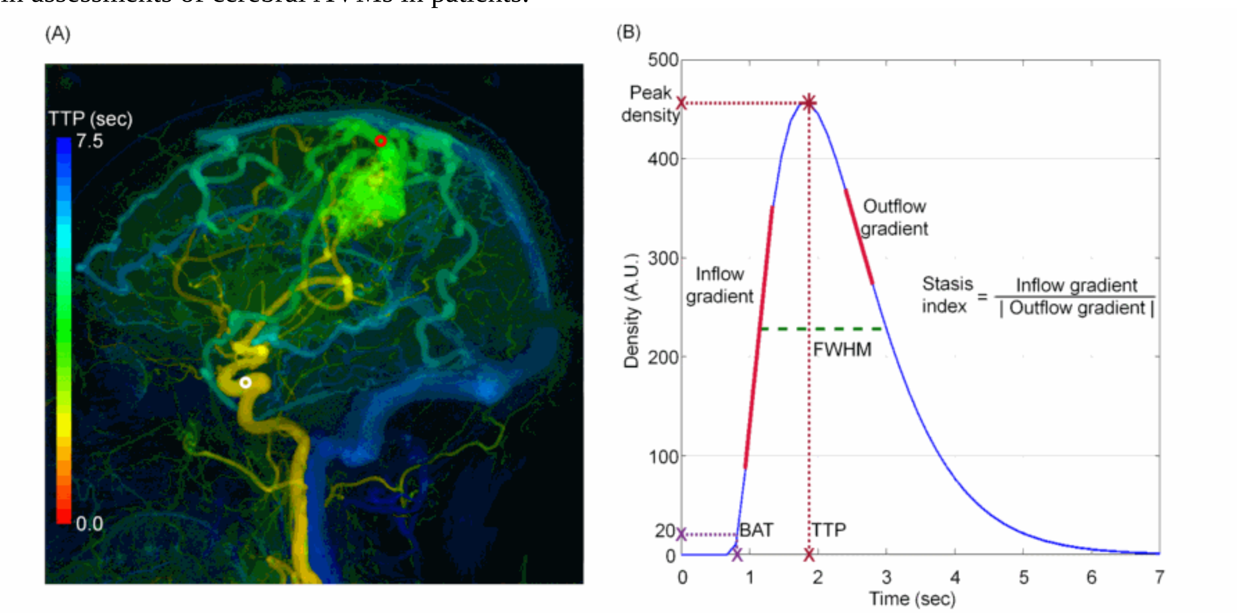

(Filename: TCT_3216_Fig1.gif)

2301

9:58AM - 10:05AM

Management of Tongue Venous & Lymphatic Malformations

W Yakes[1]
[1]The Yakes Vascular Malformation Center, Englewood, CO

Purpose
To determine the efficacy of ethanol embolization in management of tongue venous and lymphatic malformations.

Materials and Methods
40 patients (23 females, 17 males; mean age: 38 years) presented with tongue low-flow malformations. Forty-seven patients had undergone 61 failed previous procedures (embo, laser, surgery, steroid injection, alpha-interpheron, radiation). All patients had baseline arteriograms and MRs. All patients underwent direct puncture ethanol endovascular therapy.
Results
Of 40 patients with venous and lymphatic malformations, 32 patients had dramatic reduction and 7 patients' therapy is on-going with concurrent reductions (mean f/up: 60 months). One patient with AVM required additional surgery and 1 patient with mixed veno-lymphatic malformation required surgical debulking of excess tissues. Minor complications such as tongue blisters (9 instances) healed spontaneously; 3 tongue focal areas of necrosis healed spontaneously; 3 infections responded to antibiotic treatment; 1 focal tongue hemi numbness resolved. 1 patient with dense VMs had a portion of the tongue slough and the tongue healed and remolded with no treatment required.
Conclusions
Ethanol embolotherapy is a primary and consistent form of therapy to eradicate low-flow vascular malformations of the tongue permanently at long-term follow-up. Rarely is concurrent surgery required. Ethanol sclerotherapy is a curative treatment in which recurrences do not occur and permanent ablations are the rule. Complications are minor and rare.

2302

10:05AM - 10:12AM

Mandibular AVM Diagnosis and Curative Treatment

W Yakes[1]
[1]*The Yakes Vascular Malformation Center, Englewood, CO*

Purpose
To determine optimal management strategies for the treatment of intraosseous mandibular AVM.
Materials and Methods
Twelve patients (9 females, 3 males), age 9 -14; mean age 10, underwent endovascular therapy to treat their mandibular AVMs. Nine patients had distinct intraosseous AVMs. Three had additional multiple facial and intra-maxillary AVMs requiring treatment. Outside institutions recommended massive hemi-facial resections in these patients. Four patients had prior PVA and gel foam embolization, one patient had a lip graft, one had prior mandible surgery, all that had failed.
Results
All twelve patients have demonstrated MR and angiographic cure of their AVMs. One patient's therapy is not completed and is on-going. The patients mandibular AVMs cured, a third AVM in this patient in the infratemporal fossa is still undergoing treatment. The follow-up range is 11 months – 41 months, with a mean follow-up of 29 months. No complications were noted in treatment of mandibular AVMS. One patient required a minor gingival surgery after treatment of an additional intramaxillary AVM with inferior extension.
Conclusions
Endovascular approaches to manage mandibular AVM can be curative. The mandibular intraosseous variety is largely a fistula between artery and vein within the bone and the bulk are Yakes Type IIIa/IIIb AVMs. All respond and can be cured by endovascular ethanol therapy alone. Surgery was not required in any patient. Surprisingly no complications were encountered in this patient series. Long-term cures are noted in this patient series with endovascular approaches alone. No massive surgical resections in any patient, even in patients with multiple AVMs of the soft tissues, mandible and maxilla, was required to effect cure. In patients who suffered hemorrhages from floating teeth, bone formed and stabilized the teeth and no further hemorrhages occurred. Ethanol sclerotherapy proved curative in mandibular

intraosseous AVMs in patients who had additional facial soft-tissue and intramaxillary AVMs that were cured as well at long-term follow-up.

2682

10:12AM - 10:19AM

Recurrence of Brain Arteriovenous Malformations Following Complete Angiographic Obliteration: A Large Single Center Experience

A Copelan[1], R Khangura[2], R Higashida[3], M Amans[4]
[1]University of California, San Francisco, San Francisco, CA, [2]UC San Francisco Medical Center, San Francisco, CA, [3]UCSF Medical Center, San Francisco, CA, [4]UCSF, San Francisco, CA

Purpose
Arteriovenous malformation (AVM) recurrence following complete angiographic obliteration is thought to be a rare entity but has been described, predominantly in children. As a high volume center in the management of AVMs, we present our own experience and offer insights into both risk factors for recurrence and recommendations for follow up.
Materials and Methods
We retrospectively reviewed 433 consecutive patients from 1996-2017 who underwent cerebral angiography following the treatment of brain AVMs with surgery, gamma knife, endovascular, or combination therapy. One hundred ten patients were excluded as complete angiographic obliteration was not achieved, giving us a total of 323 patients with angiographic cure. Recurrence was defined as a new AVM within or immediately adjacent to the treatment bed on follow up catheter cerebral angiography.
Results
AVM recurrence was demonstrated in 5.9% of patients (19/323) with previously documented angiographic cure. In those with recurrence, the mean patient age at initial angiographic cure was 9.4 years (range, 3-19 years) and at the time of angiographic recurrence was 13.5 years (range, 4-25 years). Hemorrhage was seen at initial presentation in 94.7% of patients (18/19) and deep location with deep venous drainage in 84.2% of patients(16/19). While 73.7% (14/19) of recurrences were incidental at follow up, 26.3% (5/19) presented with repeat intracranial hemorrhage.
Conclusions
AVM recurrence following complete angiographic cure is not extraordinary, particularly in the pediatric population. While the majority of recurrences are discovered incidentally at routine follow up, patients may present with a more ominous clinical picture, including recurrence of intracranial hemorrhage. At a minimum, we espouse a 5 year follow up angiogram in those patients treated prior to 18 years of age.

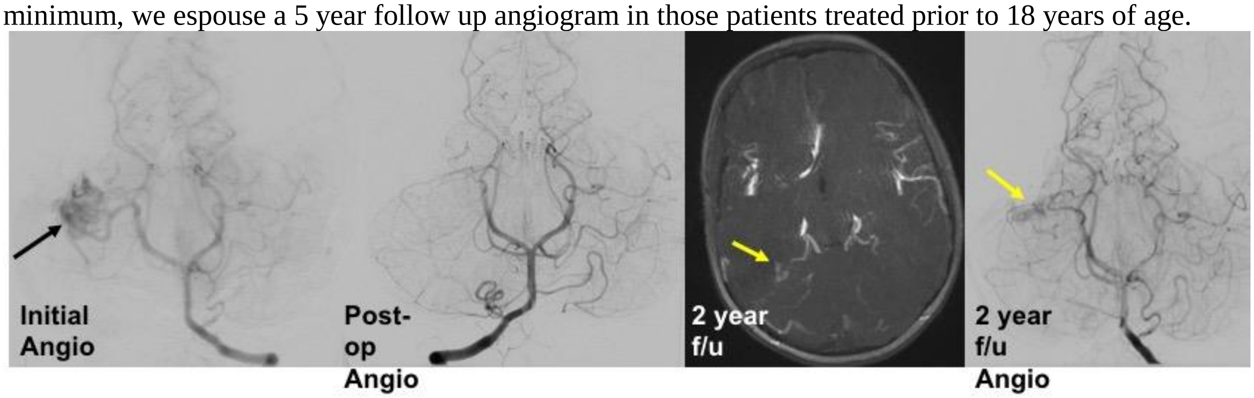

(Filename: TCT_2682_ASNR.jpg)

3500

10:19AM - 10:26AM

Transarterial Hemispheric Embolization For Intractable Seizures In Neonates With Hemimegalenchephaly

M Pearl[1], C Oluigbo[2], P Kratimenos[2], G Vezina[2], W Gaillard[2], T Tsuchida[2], T Chang[2]
[1]Johns Hopkins University School of Medicine, Baltimore, MD, [2]Children's National Medical Center, Washington, DC

Purpose
Management of the newborn with intractable seizures due to hemimegalenchephaly is challenging. Unrelenting seizures and the multiple anti-seizure medications used impairs the neurodevelopment of the brain. Anatomic or functional hemispherectomy is the establish treatment for intractable seizures in patients with hemimegalencephaly; however, in infants < 3 months of age, this can be life threatening due to intra-operative blood loss. We present our experience with 5 neonates with intractable seizures due to hemimegalenchephaly who underwent transarterial glue embolization.
Materials and Methods
A multidisciplinary team including a Level 4 Pediatric Epilepsy Program, a Level 4 neonatal ICU, a neonatal neurocritical care service, and an interventional neuroradiology program agreed a staged transarterial glue embolization was the best approach in 5 newborns presenting with hemimegalencephaly and intractable seizures who presented between 2013-2018. The region of highest seizure burden was selected for initial and subsequent embolization. During and between embolization, seizure control was maximized with prolonged continuous EEG monitoring. Preventive measures to minimize cerebral edema, intracranial bleeding and vasospasm was established.
Results
There was 1 boy and 4 girls, ages 11 days to 51 days old, with intractable seizures due to hemimegalenchephaly who underwent staged transarterial glue embolization. Seizure burden improved with each stage of embolization allowing for reduction of anti-seizure medication and complete resolution was achieved by the final stage allowing for patient discharge. Three were later treated with anatomic or functional hemispherectomy when seizures re-emerged from brain remnants and they were no longer at risk of demise from surgery.
Conclusions
Staged transarterial hemispheric embolization of the affected hemimegalencephalic brain is an effective option for the management of intractable seizures in the newborn. Technical considerations, challenges, and results will be discussed.

Thursday, May 23, 2019
10:45AM - 12:15PM
Data Crunching, Pretty (and Pretty Useful) Pics in H&N

2809

10:45AM - 10:52AM

ACR TI-RADS Reduces Biopsy Recommendations for Thyroid Nodules while Increasing the True Positive Rate

M Kuruva[1], J Watts[2], F Tessler[3], J Hoang[4]
[1]Duke University Medical Center, Durham,NC, [2]Cone Health imaging, Greensboro, NC, [3]University of Alabama at Birmingham School of Medicine, Birmingham, AL, [4]Duke University Medical Center, Durham, NC

Purpose

The American College of Radiology Thyroid Imaging, Reporting, and Data System (ACR TI-RADS) guides management of thyroid nodules based on ultrasound. Studies have shown a reduction in thyroid nodule biopsies by 20-35%, but these studies were limited because they assessed the effect of ACR TI-RADS on cohorts of previously-biopsied nodules (1). The aim of this study was to compare biopsy referrals and results before and after implementing ACR TI-RADS.

Materials and Methods

We retrospectively determined biopsy rates and findings during the 12-months immediately prior to and following implementation of ACR TI-RADS at Canopy Partners, a private practice radiology group, on July 1, 2017. The two periods were compared for the number of thyroid biopsy recommendations and cytology results. We also determined the malignancy rates for each of the five ACR TI-RADS risk categories.

Results

Prior to ACR TI-RADS, there were 878 biopsy referrals out of 3487 thyroid ultrasound studies (25.2%). After ACR TI-RADS, there was a statistically significant reduction in biopsy referrals to 691 out of 3441 thyroid ultrasounds (20.1%) ($p = 0.0001$) (Table 1). The malignancy rate increased to 8%, compared to 6.4% before ACR TI-RADS ($p = 0.27$), and the percentage of benign results decreased to 66%, compared to 81.3% before ACR TI-RADS ($p = 0.0001$). Malignancy rates post TI-RADS were 2.9%, 8.2%, and 13.6% for TR3, TR4 and TR5, respectively.

Conclusions

ACR TI-RADS implementation led to significant decreases in the number of biopsy referrals and benign (false positive) biopsies.

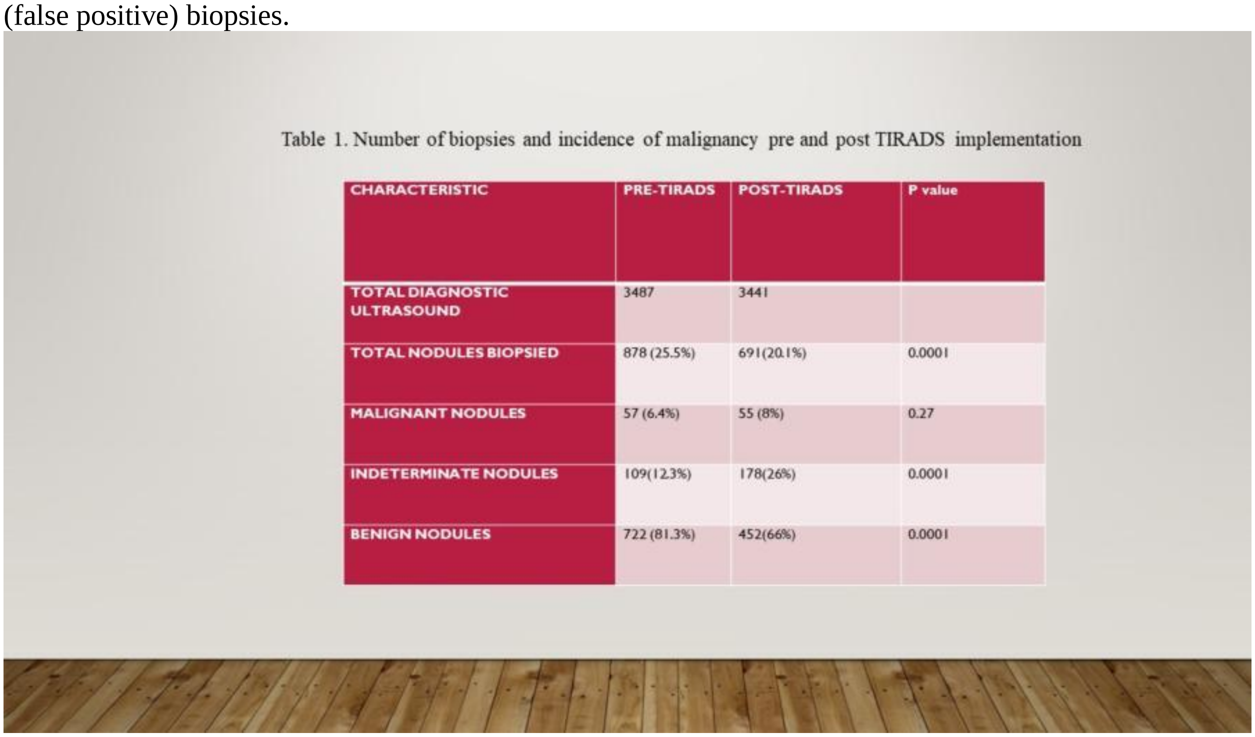

Table 1. Number of biopsies and incidence of malignancy pre and post TIRADS implementation

CHARACTERISTIC	PRE-TIRADS	POST-TIRADS	P value
TOTAL DIAGNOSTIC ULTRASOUND	3487	3441	
TOTAL NODULES BIOPSIED	878 (25.5%)	691(20.1%)	0.0001
MALIGNANT NODULES	57 (6.4%)	55 (8%)	0.27
INDETERMINATE NODULES	109(12.3%)	178(26%)	0.0001
BENIGN NODULES	722 (81.3%)	452(66%)	0.0001

(Filename: TCT_2809_Table1.jpg)

3431

10:52AM - 10:59AM

CT features of head and neck amyloidosis: Correlation with clinicopathological characteristics

K Takumi[1], P Staziaki[1], R Hito[2], R Nadgir[3], O Sakai[1]

[1]Boston Medical Center, Boston University School of Medicine, Boston, MA, USA, [2]Veteran Affairs Hospital, Boston University School of Medicine, West Roxbury , MA, USA, [3]Johns Hopkins Medical Institution, Baltimore, MD, USA

Purpose
To characterize the CT imaging features of amyloidosis in the head and neck and correlate with clinical outcomes and amyloidosis subtype.
Materials and Methods
The population of this retrospective study consisted of 75 consecutive patients with head and neck amyloidosis who underwent unenhanced head and neck CT examinations between November 2003 and April 2018. The CT imaging features including distribution and number of lesions, lesion morphology (focal or diffuse), presence of calcification, calcification pattern (punctate or diffuse), and mucosal thickness of lesion were evaluated. The CT features were correlated with the amyloidosis clinical subtype (localized or systemic), and clinical course (stable, progressive, requiring surgical treatment). Clinical subtype and clinical course were compared with imaging characteristics including the location of lesion, lesion morphology, presence of calcification and calcification pattern using Fisher's exact test. The Mann-Whitney U test was used for comparing thickness of the lesion and number of affected locations.
Results
Localized (89.3%,67/75) was the most common form of amyloidosis and AL (98.0%,50/51) was the most common amyloid type in the head and neck. The most commonly affected region was the larynx (61.3%,46/75), specifically the glottis (45.3%,34/75). Calcification was seen in 64.0% of patients (48/75). Non-airway and tongue lesions were significantly associated with systemic type (100%,8/8) rather than localized type (4%,3/70;$p<0.001$). Necessity of repeated surgical treatment was significantly associated with presence of laryngeal amyloidosis (35.3%,12/34) compared to absence of laryngeal amyloidosis (0%,0/22;$p=0.002$). A statistically greater number of repeat surgical interventions was observed among patients with increased lesion burden and thickness ($p=0.022$,0.004 respectively).
Conclusions
This is the first report systematically evaluating the CT features of head and neck amyloidosis in a large cohort. The knowledge of the imaging features of head and neck amyloidosis can aid the diagnosis and monitoring of amyloidosis as well as potentially predicting patients that will require repeated surgical intervention.

Table. Distribution of head and neck amyloidosis with clinicopathological and CT imaging features

	Clinicopathological features			CT imaging features				
	Form of amyloidosis		Type of amyloid	Morphology		Calcification(%)	Calcification feature	
	Localized (%)	Systemic (%)	AL:AA:unknown	Focal (%)	Diffuse (%)		Punctate (%)	Diffuse (%)
Whole region (n=75)	67/75 (89.3)	8/75 (10.7)	50:1:24	13/75 (17.3)	62/75 (82.7)	48/75 (64.0)	36/48 (75)	12/48 (25)
Nasal/paranasal sinus (n=6)	6/6 (100)	0/6 (0)	4:0:2	1/6 (16.7)	5/6 (83.3)	6/6 (100)	5/6 (83.3)	1/6 (16.7)
Nasopharynx (n=19)	18/19 (94.7)	1/19 (5.3)	13:1:5	4/19 (21.1)	15/19 (78.9)	16/19 (84.2)	15/16 (93.8)	1/16 (6.2)
Oropharynx (n=16)	15/16 (93.8)	1/16 (6.2)	10:1:5	1/16 (6.2)	15/16 (93.8)	14/16 (87.5)	13/14 (92.9)	1/14 (7.1)
Tongue (n=2)	0/2 (0)	2/2 (100)	2:0:0	0/2 (0)	2/2 (100)	0/2 (0)	-	-
Hypopharynx (n=4)	4/4 (100)	0/4 (0)	2:0:2	1/4 (25)	3/4 (75)	2/4 (50)	2/2 (100)	0/2 (0)
Larynx (n=46)	45/46 (97.8)	1/46 (2.2)	29:0:17	8/46 (17.4)	38/46 (82.6)	16/46 (34.8)	13/16 (81.3)	3/16 (18.7)
Supraglottis (n=26)	25/26 (96.2)	1/26 (3.8)	13:0:13	16/26 (61.5)	10/26 (38.5)	8/26 (30.8)	6/8 (75)	2/8 (25)
Glottis (n=34)	34/34 (100)	0/34 (0)	22:0:12	9/34 (26.5)	25/34 (73.5)	6/34 (17.6)	4/6 (66.7)	2/6 (33.3)
Subglottis (n=27)	27/27 (100)	0/27 (0)	18:0:9	3/27 (11.1)	24/27 (88.9)	8/27 (29.6)	7/8 (87.5)	1/8 (12.5)
Trachea (n=38)	37/38 (97.4)	1/38 (2.6)	25:0:13	14/38 (36.8)	24/38 (63.2)	23/38 (60.5)	18/23 (78.3)	5/23 (21.7)
Orbit (n=1)	1/1 (100)	0/1 (0)	1:0:0	0/1 (0)	1/1 (100)	1/1 (100)	1/1 (100)	0/1 (0)
Lymph node (n=5)	1/5 (20)	4/5 (80)	5:0:0	0/5 (0)	5/5 (100)	3/5 (60)	2/3 (66.7)	1/3 (33.3)
Salivary gland (n=2)	0/2 (0)	2/2 (100)	2:0:0	0/2 (0)	2/2 (100)	1/2 (50)	1/1 (100)	0/1 (0)
Soft tissue (n=4)	1/4 (25)	3/4 (75)	4:0:0	0/4 (0)	4/4 (100)	2/4 (50)	1/2 (50)	1/2 (50)

(Filename: TCT_3431_figure.jpg)

3039

10:59AM - 11:06AM

Diffusion-Weighted Imaging for the Evaluation of Post-Treatment Squamous Cell Carcinoma in the Neck: Image Optimization and a New Quantitative Assessment Metric

G Guzman Perez-Carrillo[1], S Han[2], K Johnson[2], R Khan[3], N Chen[2]
[1]UNIVERSITY OF ARIZONA, TUCSON, AZ, [2]UNIVERSITY OF ARIZONA, Tucson, AZ, [3]Dartmouth Hitchcock Medical Center, Lebanon, NH

Purpose
Current DWI sequences utilized for the evaluation of head and neck tumors have significant issues with fat saturation, distortion, aliasing/ghosting and resolution that limit their utility, even though the Quantitative Imaging Biomarkers Alliance [QIBA, 2015] has attempted to address these shortcomings through optimized image parameters. Multiple new improvements in sequence acquisition - such as readout-segmented, multi-shot EPI RESOLVE (iShim, Siemens Medical Solutions, Erlangen, Germany) and multiband echo planar imaging (MultiBand, Siemens Medical Solutions, Erlangen, Germany) - can significantly improve DWI quality and thus increase diagnostic accuracy. We propose a study to quantitatively evaluate the difference in fat saturation, distortion and aliasing/ ghosting artifacts as well as signal to noise ratio and contrast to noise ratio between conventional DWI sequences and optimized DWI sequences with RESOLVE and MultiBand in post-treatment head and neck squamous cell carcinoma patients.
Materials and Methods
A cohort of 14 adult patients with biopsy-proven diagnosis of head and neck tumor that presented with suspicion of tumor recurrence after completion of either surgical and/or chemoradiation treatment was evaluated. Qualitative calculation of geometric distortion [Chen, 1999], ghosting [Chen, 2013] and residual fat signal [Chen, 2013] was carried out as detailed below. The geometric distortion was quantified by the bandwidth and matrix size, based on which we can calculate the pixel's width Δw.

Assuming that the frequency difference caused by geometric distortion at one pixel at B0 is Δf, then we could calculate the distortion (corresponding to the number of pixels) is $\Delta f/\Delta w$. To evaluate ghosting artifact, tumor and residual of fat signal, we manually contoured ROIs for muscle (SMuscle), tumor(STumor), background signal (SBackground) and fat (SFat). To evaluate ghosting artifacts, two approaches were used to calculate the SNR of ghosting artifact: (1) SNRArtifact1 = SArtifact/SBackgound; (2) SNRArtifact2 = SArtifact/SMuscle. Images with no ghosting will have a SNRArtifact1 close to 1 and a low SNRArtifact2 close to 0. In RESOLVE images, since there is visible ghosting, we could assume that the SNRArtifact1 $\approx$ 1 and SNRArtifact2 $\approx$ 0. For residual fat signal evaluation, we contoured the area with residual fat and compared the average signal intensity and standard deviation. With lower signal intensity and standard deviation for fat, it indicates that the fat suppression is better. The evaluation was shown in Figure 1 and 2.

Results

3 out of 14 patients could not be evaluated as there was so much signal loss due to artifact and distortion in the conventional DWI sequence that quantitative values could not be acquired for comparison. Of the remaining 11 patients, the pixel's width Δw for the optimized images are 34.722 Hz and for conventional DWI are 15.727 Hz. With the frequency difference Δf at B0, we know that the distortion for RESOLVE image is $\Delta f/34.722$ and for conventional DWI is $\Delta f/15.727$, meaning that the distortion is smaller in RESOLVE/MultiBand images. Signal to noise ratio was significantly improved in our optimized sequence, in cases increased up to 1,604% as compared to conventional DWI for mean SNR muscle, 703% for mean SNR tumor and 200% for CNR tumor (See Table 1). Fat saturation was at least 52% better in our optimized sequence as compared to conventional DWI (See Table 1). For ghosting artifact, the SNRArtifact1 in RESOLVE/MultiBand images decreased 76.1% and SNRArtifact2 decreased 97.6% (See Table 1).

Conclusions

Our optimized DWI sequence demonstrates quantitatively significant increases in SNR and CNR, as well as significantly decreased fat saturation artifact, distortion artifact and ghosting/aliasing artifact. We believe this optimized sequence has the potential to significantly improve diagnostic accuracy in evaluating recurrent tumor versus treatment changes as compared to conventional DWI imaging.

	Median		Difference	Mean		Difference
	RESOLVE	DWI		RESOLVE	DWI	
SNR muscle	38.91	4.19	34.72	85.51	5.33	80.18
SNR tumor	77.3	14.02	63.28	104.63	14.89	89.74
CNR tumor	19.76	9.24	10.52	19.12	9.56	9.56
	Median		Difference	Mean		Difference
	RESOLVE	DWI		RESOLVE	DWI	
SNR1 artifact	1.00	4.07	-3.07	1.00	4.19	-3.19
SNR2 artifact	0.02	0.51	-0.49	0.04	0.52	-0.48
Fat Mean Intensity	Median		Difference	Mean		Difference
	RESOLVE	DWI		RESOLVE	DWI	
	75.08	159.75	84.67	80.55	166.1	85.55

Table 1- Quantitative signal-to-noise (SNR) of muscle, tumor and contrast-to-noise ratio (CNR) of conventional DWI versus optimized sequence; quantitative mean fat intensity of conventional DWI versus optimized sequence; quantitative mean SNR of artifact.

- ROI Definition
  - Muscle: green, total area of 151.516 mm^2
  - Background: orange, total area of 996.5 mm^2
  - Tumor: red, total area of 1.002 mm^2
  - Fat: yellow, total area of 513.6 mm^2
  - Artifact: blue, total area of 538.2 mm^2
- Calculation
  - $SNR_{Muscle} = \frac{S_{Muscle}}{S_{Background}}$
  - $SNR_{Tumor} = \frac{S_{Tumor}}{S_{Background}}$
  - $CNR_{Tumor} = \frac{S_{Tumor} - S_{Muscle}}{S_{Background}}$
  - $SNR_{Artifact} = \frac{S_{Artifact}}{S_{Background}}$ or $SNR_{Artifact} = \frac{S_{Artifact}}{S_{Muscle}}$

Figure 1. Calculations for SNR muscle, SNR tumor, CNR tumor and SNR artifact.

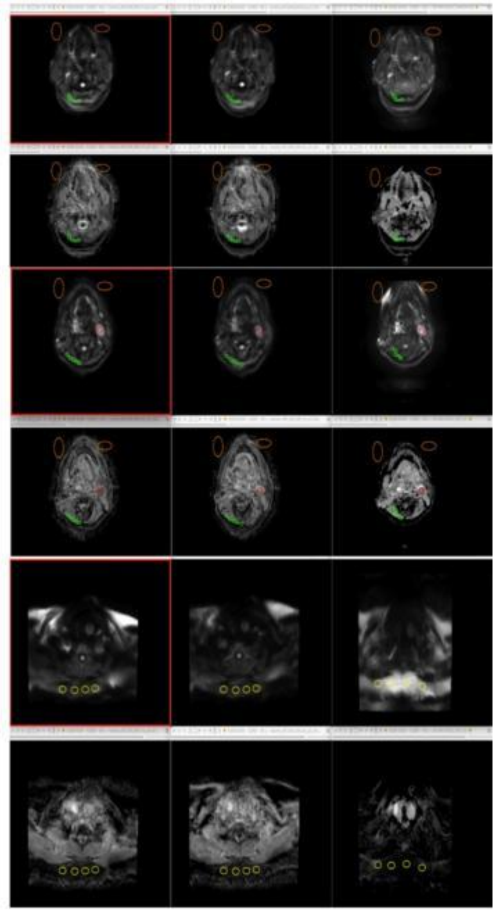

Figure 2 – Single patient example of ROI placement for quantitative measurement calculations.

(Filename: TCT_3039_asnr2019finalfigure.jpg)

2399

11:06AM - 11:13AM

Fly-through Virtual Reality-Assisted Training Module of the Pterygopalatine Fossa.

R Javan[1], M Lipman[2], S Singhal[2], A Herur-Raman[3], A Goyal[1], A Javan[4], J Sherman[1]
[1]George Washington University Hospital, Washington, DC, [2]George Washington University School of Medicine and Health Sciences, Washington D.C. , DC, [3]Surgical Theater, Mayfield Village, OH, [4]Bon Secoures Hospital, Baltimore, MD

Purpose
We describe the methodology for developing a virtual reality (VR)-based educational module for teaching the complex anatomy of the Pterygopalatine Fossa (PPF) designed by using computed tomography (CT) data combined with custom graphic design.
Materials and Methods
The osseous structures that make up the walls of the PPF were segmented on a normal high-resolution maxillofacial CT in Materialise Mimics to allow for an initial 3D reconstruction. This 3D model was exported in STeroeLithography (STL) format and then imported in Autodesk 3D Studio Max, where the intricate neurovascular anatomy of was graphically added and color-coded. A Surgical Theater surgical planning workstation was utilized to import the 3D models into a VR scene, which can be viewed on a

flat touch screen and simultaneously through a VR headset (Oculus Rift). Additionally, Oculus Touch controllers and a Logitech F310 gamepad were used to view and control the scene in VR. Flythrough videos of the VR rendering were exported as standard MP4, 360 Video, and Stereoscopic VR Video file format to allow for viewing outside of the rendering platform. A 3D printed version of the model was also created as an additional aid.

Results

An anatomically accurate color 3D model of the PPF was created with intricate detail in a VR environment for the specific use of teaching anatomy, especially by visualizing a complex anatomic space from within. This VR model allowed for visualization at various magnification levels, from any angle, and allowed the trainee to place him/herself inside the structures and examine their relationship in minute detail. The necessary software, graphic design skills and the available options for VR are discussed.

Conclusions

Neuroanatomists, neuroradiologists, and surgeons can take advantage of VR technologies in creating numerous custom tools for teaching complex anatomical spaces and their contents to medical students and trainees in radiology, otolaryngology and neurosurgery.

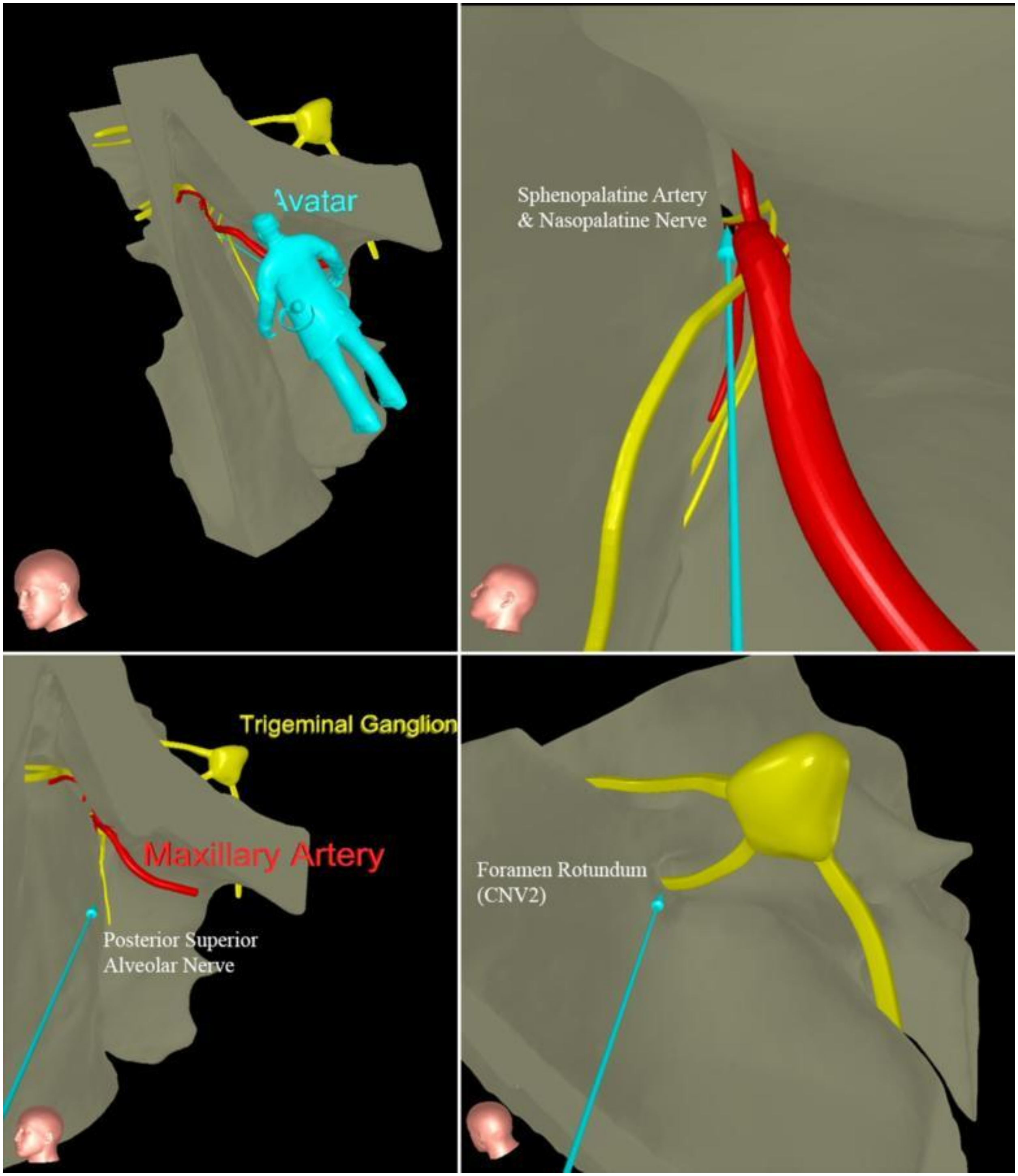

(Filename: TCT_2399_PPF.jpg)

2613

11:13AM - 11:20AM

Imaging Surveillance of Head and Neck Cancer using NI-RADS: 36 % of recurrences were clinically NED and Detected by Imaging Alone

A Gore[1], K Baugnon[1], J Beitler[2], N Saba[2], P Mihir[3], A Aiken[4]

[1]*EMORY UNIVERSITY, ATLANTA, GA,* [2]*Winship Cancer Institute of Emory University, Atlanta, GA,* [3]*Emory University, Atlanta, GA,* [4]*Emory University Hospital, Atlanta, GA*

Purpose
Accurately detecting recurrent disease is important for salvage treatment planning in patients with head and neck cancer. The Neck Imaging Reporting and Data System (NI-RADS) involves numeric assessment of suspicion of tumor recurrence in patients with head and neck cancer. The National Comprehensive Cancer Network (NCCN) guidelines recommend post-treatment imaging within six months after treatment; however, does not recommend standard surveillance imaging beyond this point. Our purpose was to evaluate the frequency of recurrence in "asymptomatic" patients (defined as no clinical suspicion of recurrence) using the NI-RADS recommended surveillance imaging protocol.
Materials and Methods
This IRB approved retrospective database search from June 2014 to March 2018 yielded 331 consecutive CECT or PET/CECT cases with NI-RADS scores of 2 or 3. The electronic medical records, specifically clinical, radiology and pathology reports, were reviewed to determine clinical evidence of disease around the time of imaging and pathology proven recurrence. Inclusion criteria included clinical exam by either otolaryngology, radiation or medical oncology within 3 months of the imaging exam and either biopsy or imaging follow up of NI-RADS 2s and 3s. Cases with non-squamous cell carcinoma primary tumors, squamous cell carcinoma primary outside the head and neck, or those that were lost to follow-up were excluded.
Results
A total of 255 cases with NI-RADS scores of 2 or 3 met the inclusion criteria. A total of 59 patients (23%) demonstrated recurrence. Approximately 21 patients (36%) of all recurrences (14% had a NI-RADS score of 2 and 22%, a score of 3) had no clinical evidence of disease at the time of imaging. Mean time to recurrence after treatment completion was 18.6 months (range 1-170 months).
Conclusions
Imaging surveillance beyond the first post- treatment baseline study was critical for detecting recurrent disease, as of over one third of all recurrences were seen in patients with no clinical evidence of disease.

2491

11:27AM - 11:34AM

Patient-Specific Bench-Top Models of Venous Pulsatile Tinnitus

M Amans[1], K Valluru[2], H Haraldsson[1], E Kao[1], J Leach[3], A Wright[4], M Ballweber[2], K Meisel[2], D Saloner[1]
[1]*UCSF, San Francisco, CA,* [2]*University of California, San Francisco, San Francisco, CA,* [3]*UCSF, San Francisco , CA,* [4]*ucsf, San Francisco, CA*

Purpose
Pulsatile tinnitus (PT) can be caused by aberrant blood flow in large cerebral veins near the cochlea. To investigate the sound production mechanism, we created 3D printed flow models based on patient-specific cerebral venous anatomies.
Materials and Methods
Patients with venous etiology PT were recruited from the UCSF PT Clinic. Patients underwent MR imaging, including phase contrast and time-resolved venous phase contrast-enhanced MRA (CE-MRA) of the head. The venous sinus outflow was segmented from the CE-MRA using in-house software. The anatomy and extensions were 3D printed in wax and set in silicone. The wax was then melted out of the model yielding a hollow patient-specific venous lumen. Water was pumped through each model at the MR-derived patient-specific time-dependent flow rate. Sound was measured using a Bluetooth enabled recording stethoscope (Littmann St. Paul, MN) sensitive to frequencies between 80 and 2kHz, coupled to the models with ultrasound gel. Maximum amplitude and reproducibility studies were performed.

Results
Four separate patient-specific 3D models of venous anatomy were printed, including: two with high-riding jugular bulbs, and two models of a single patient with idiopathic intracranial hypertension (IIH) based on pre- and post-lumbar puncture (LP) imaging. This patient's PT symptoms improved following LP, and imaging similarly demonstrated reduced transverse sinus stenosis (Figure 1 A and B). Sounds recorded over the anticipated venous anatomic source of PT were very similar to those reported by all patients. Sound amplitude rapidly decayed with increasing stethoscope distance from the anticipated PT source. The post-LP flow model for the IIH patient produced nearly no sound, correlating with the patient's resolution of symptoms (Figure 1C, 1D). Ten recordings at the location of maximum signal pre and post LP yielded significantly louder sound pre-LP with peak-to-rms amplitude values 3.31 ± 0.45, and 1.98 ± 0.41 for post-LP ($p<0.001$).
Conclusions
We have created patient-specific cerebral venous flow models that reliably produce sounds similar to those reported by PT patients.

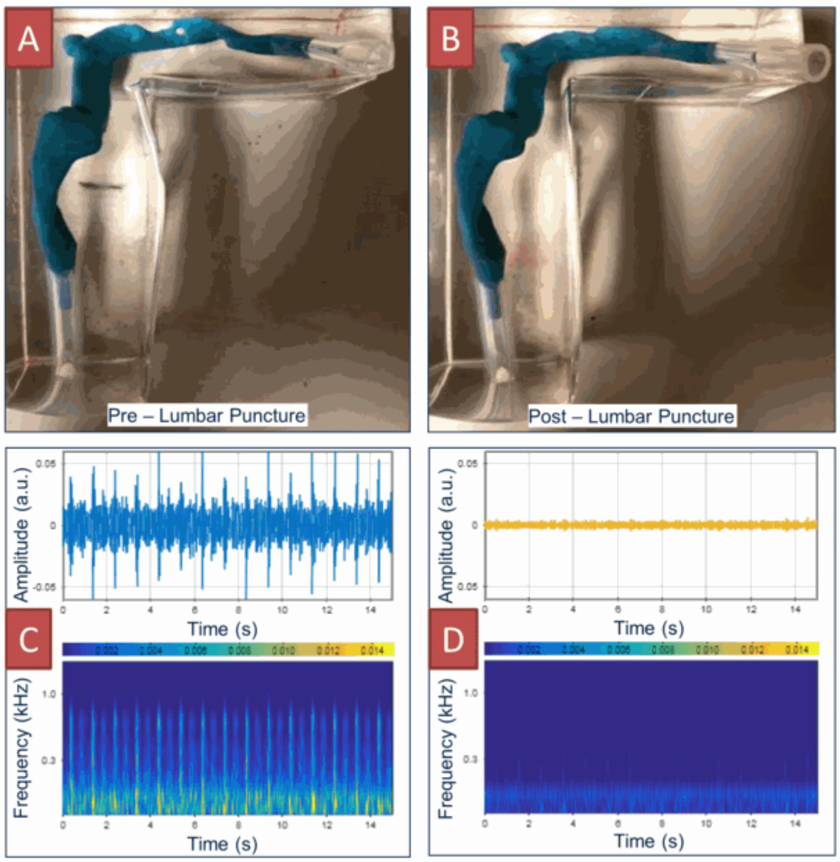

(Filename: TCT_2491_fig1_abstract_ASNR.gif)

3129

11:34AM - 11:41AM

Positive Predictive Value of NI-RADS Categories 3 and 4 Post-treatment FDG PET/CT in Head and Neck Squamous Cell Carcinoma

P Wangaryattawanich[1], B Branstetter[1], J Ly[2], U Duvvuri[1], D Heron[3], T Rath[1]
[1]University of Pittsburgh Medical Center, Pittsburgh, PA, [2]UPMC, Pittsburgh, PA, [3]UPMC Hillman Cancer Center, PITTSBURGH, PA

Purpose
The Neck Imaging Reporting and Data System (NI-RADS) is a standardized reporting system intended to risk stratify patients treated for head and neck squamous cell carcinoma (HNSCC). The purpose of this study is to investigate the positive predictive value (PPV) of NI-RADS Categories 3 and 4 on post-treatment FDG PET/CTs in patients treated definitively for HNSCC.
Materials and Methods
We retrospectively identified patients treated definitively for HNSCC with surgery, radiation therapy, chemoradiotherapy or a combination thereof between 2006 and 2018. Patients whose post-treatment FDG PET/CT were interpreted as NI-RADS category 3 (suspicious) or 4 (definitive recurrence) at the primary site (P), regional nodes (N) or at distant sites (D) on any post-treatment PET/CT were included. The reference standard was histopathology or unequivocal imaging or clinical evidence of treatment failure. The PPV of NI-RADS categories 3 and 4 post-treatment FDG PET/CT were calculated.
Results
72 of 128 patients interpreted as NI-RADS category 3 at P, N, or D were proven to have treatment failure at the suspicious sites yielding an overall PPV of 56%. The PPV of NI-RADS category 3 by subsite was as follows - P: 56% (44/79), N: 65% (34/52) and D: 79% (42/53). In contrast, all 69 patients with post-treatment FDG PET/CT interpreted as NI-RADS category 4 had true treatment failure, yielding a PPV of 100% - P: 100% (28/28), N: 100% (35/35) and D: 100% (27/27). .
Conclusions
The PPV of NI-RADS category 3 on post-treatment PET/CT is relatively low, particularly at the primary tumor site. Confirmation of NI-RADS category 3 findings should be performed with tissue sampling prior to instituting new treatment regimens to avoid unnecessary overtreatment and treatment-related toxicities.

Thursday, May 23, 2019
10:45AM - 12:15PM
Adult Brain Excerpta 3

3575

10:45AM - 10:49AM

A Case of Pial Arteriovenous Malformation(AVM) with Jugular Vein Aplasia and Stenosis: Is Pial AVM an Acquired Venous Outflow Restriction Disease?

Y Kikuchi[1]
[1]KAMEDA MEDICAL CENTER, KAMOGAWA CITY, Chiba prefecture

Purpose
To present a case of pial AVM associated with the right jugular vein aplasia and high grade stenosis of the left jugular vein.
Materials and Methods
A previously healthy forty-year old man suddenly lost consciousness and caused a motor vehicle accident. He was brought to the emergency room.
Results
The head CT showed parenchymal calcifications of the brain at gray-white junction more prominent on the right side. On the bone-window images, there was diffuse thickening of the calvarium. The groove of right sigmoid sinus was absent. From these findings, high-flow dural arteriovenous fistula(AVF) was suspected. MRI revealed dilated and tortuous vessels around the right temporal lobe and brain stem. DSA showed a temporal lobe pial AVM without contribution from the dural branches. DSA and contrast-enhanced CT confirmed the absence of the right jugular vein and high-grade stenosis of the left jugular vein.
Conclusions
Pial AVM is considered a congenital lesion and its primary pathophysiology being arteriovenous shunt.

Dural AVF, another intracranial lesion with arteriovenous shunt, is established as an acquired lesion and the arteriovenous shunt being the secondary pathology due to venous outflow restriction and resultant venous hypertension. This unique case of pial AVM with jugular occlusion and stenosis suggests that pial AVM might also be an acquired lesion caused by the venous stenosis and venous hypertension sharing the same pathophysiology with the dural AVF. If that is the case, pial AVM could be treated with the dilatation of stenotic venous segment with intravascular stent placement in the future.

3157

10:49AM - 10:53AM

A High-Resolution Vessel Wall MRI-Histopathology Study of Cerebral Amyloid Angiopathy

Q Hao[1], N Tsankova[1], A Banihashemi[1], H Shoirah[1], C Kellner[2], K Nael[3]
[1]Icahn School of Medicine at Mount Sinai, New York, NY, [2]Icahn School of Medicine at Mount Sinai, New York , NY, [3]ICAHN SCHOOL OF MEDICINE AT MOUNT SINAI HOSPITAL, NEW YORK, NY

Purpose
High-resolution vessel wall MRI (vwMRI) is an emerging image technique that can better visualize vessel wall abnormalities in various vasculopathies. Little is known about the features of cerebral amyloid angiopathy (CAA) on vwMRI. We reported a case with vwMRI findings of CAA that was confirmed on histology.
Materials and Methods
A 75 year old woman with history of hypertension and diabetes presented with progressive memory loss, inappropriate behavior over 6 months and acute worsening over 5 days. Upon admission, her vital signs showed blood pressure of 172/82 mmHg and heart rate of 100 /min. The neurological exam showed that patient was awake with impaired attention and language; cranial nerves, motor strength and gait were unremarkable. Blood and CSF analysis did not show signs of CNS infection or metabolic abnormalities except for blood glucose of 340 mg/dl. Patient had fluctuating mental status during the first three days and developed seizure on the fourth day with subsequent non-convulsive status epilepticus that was revealed on video EEG and required multiple antiepileptic agents.
Results
MRI brain at admission did not show hemorrhagic or ischemic stroke. There was regional increased cerebral blood flow on arterial spin labeling (ASL) perfusion in the left parietal and temporal lobes presumably related to postictal status. The conventional angiogram was normal without intracranial or extracranial arterial stenosis or other vasculopathy. On the eighth day of admission, vwMRI showed significant arterial wall enhancement along distal cortical branches of left MCA in left parietal and temporal lobes (Figure A-B). Biopsy of left temporal lobe on the ninth day showed thickening and hyalinization of several small and medium-sized arteries within the leptomeninges and superficial cortical gray matter (Figure C). Immunostain confirmed amyloid accumulations (Figure D); there were no inflammatory cells surrounding the vessels.
Conclusions
This case demonstrates that beta-amyloid accumulation by itself in the absence of inflammation can result in post-contrast enhancement on high-resolution vwMRI.

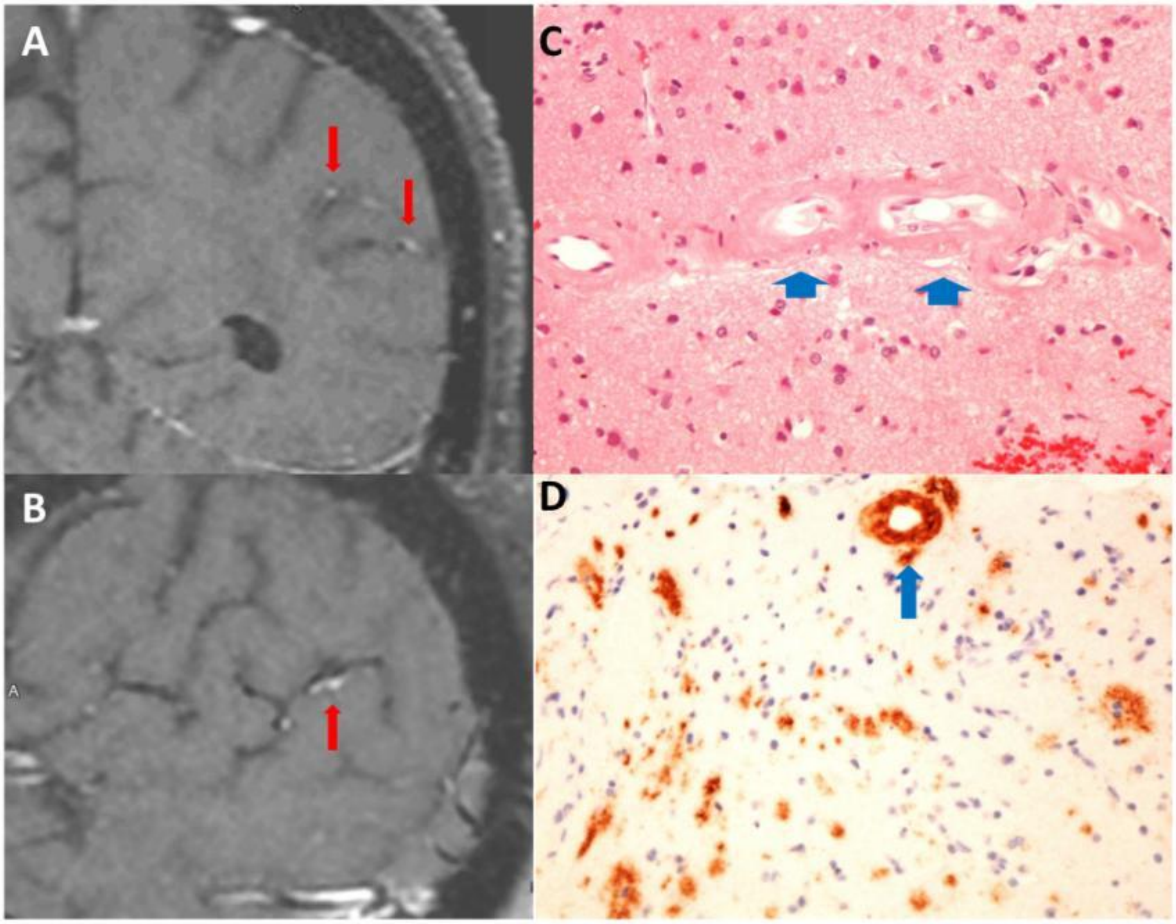

A-B: vwMRI post-contrast T1 image showed enhancement in the superficial cortical branches (red arrow);
C: H&E stain showed thickened and hyalinized blood vessels, containing pale eosinophilic material (arrow head);
D: Immunostain for beta-amyloid showed abnormal amyloid accumulation within these blood vessel walls (blue arrow)

(Filename: TCT_3157_ASNRabstractpiccopy.jpg)

3174

10:53AM - 11:57AM

Cerebral Microbleeds and Superficial Siderosis: Iron Deposition in the Brain Leading to Neurodegeneration?

M Shams[1], J Martola[2], T Granberg[3], M Wintermark[4], M Kristoffersen Wiberg[2], E Westman[2], S Shams[5]
[1]Karolinska Institute, Menlo Park, CA, [2]Karolinska Institutet, Stockholm, Stockholm, [3]Karolinska Institutet, Stockholm, MA, [4]Stanford, San Carlos, CA, [5]Stanford, Menlo Park, CA

Purpose
Metal homeostasis in the brain is essential for brain health, and deregulation can result in oxidative stress in the brain parenchyma. Cerebral small vessel disease is very common with ageing, and the hallmark of the disease is fragile and leaking microvasculature of the brain. Leaking hemosiderin from vessels can deposit in the brain, and the imaging findings are cerebral microbleeds and cortical superficial siderosis. We decided to explore how this focal hemosiderin deposition in the brain may impact cognition and brain health by studying patients with cognitive impairment and dementia.
Materials and Methods
This is a cross sectional study with 196 enrolled patients (Alzheimer's disease, n=85; mild cognitive

impairment, n=72; subjective cognitive impairment, n=32, vascular dementia, n=7). All patients underwent memory clinic investigation including an MRI brain. Blood samples were analyzed for ApoE genotype. Cerebrospinal fluid (CSF) analysis was done on metals, Amyloid β (Aβ) 42, total Tau (T-tau), phosphorylated tau (P-tau) and CSF/serum albumin ratios. Results were analyzed with generalized linear models.

Results

There was no significant difference between metal CSF levels among the different groups. Higher iron and copper levels were associated with higher levels of Aβ 42, T-tau, P-tau and CSF/serum albumin ratios ($P<0.05$). CSF iron levels were high with cerebral microbleeds in ApoE ε4 carriers. There was no other association between cerebral microbleeds and cortical superficial siderosis and iron levels.

Conclusions

There was no significant difference between metal CSF levels among the different groups. Higher iron and copper levels were associated with higher levels of Aβ 42, T-tau, P-tau and CSF/serum albumin ratios ($P<0.05$). CSF iron levels were high with cerebral microbleeds in ApoE ε4 carriers. There was no other association between cerebral microbleeds and cortical superficial siderosis and iron levels.

3171

11:01AM - 11:05AM

Dural Venous Sinus Cephalocele in the Setting of Intracranial Hypertension

J Villanueva-Meyer[1], L Eisenmenger[2], M Amans[3]
[1]University of California - San Francisco, San Francisco, CA, [2]UNIVERSITY OF CALIFORNIA - SAN FRANCISCO, SAN FRANCISCO, CA, [3]UCSF, San Francisco, CA

Purpose

We report a unique case of intracranial hypertension in the setting of a dural venous sinus cephalocele and discuss our institutional experience and implications of this recently recognized entry.

Materials and Methods

A 44-year-old man presented with vision loss, pulsatile tinnitus, and headaches. On clinical examination he was found to have papilledema. Neurologic examination was otherwise unremarkable. Neuroimaging revealed findings consistent with papilledema, a partially empty sella, and bilateral transverse sinus stenoses. Additionally, he was found to have a small focal left occipital lobe herniation into the transverse sinus. He was started on oral acetazolamide and despite maximal doses, had progressive vision loss. Further evaluation with catheter angiography was performed where venous manometry showed bilateral transverse sinus stenoses with pressure gradients and no other source for intracranial hypertension. A venous stent was placed in the right transverse sinus (contralateral to cephalocele) with resolution of previously noted stenosis. At follow-up the patient's papilledema had resolved and his headaches were improving.

Results

Intracranial hypertension in the setting of a left transverse sinus cephalocele. (A,B) Coronal FLAIR and T1 post-contrast MR images show a small herniation of the left occipital lobe into the transverse sinus (dotted circle). (C) Axial T2 MR image shows flattening of the posterior globes and protrusion of the optic nerve heads as well as prominent subarachnoid space in the optic nerve sheaths suggesting papilledema. (D) MR venogram shows bilateral, left greater than right, transverse sinus stenosis, most pronounced at site of cephalocele (white arrow).

Conclusions

Familiarity with the rare finding of cerebral herniation into a dural venous sinus is important for the neuroradiologist to appropriately identify a potential source of intracranial hypertension or pulsatile tinnitus, particularly in an otherwise normal examination.

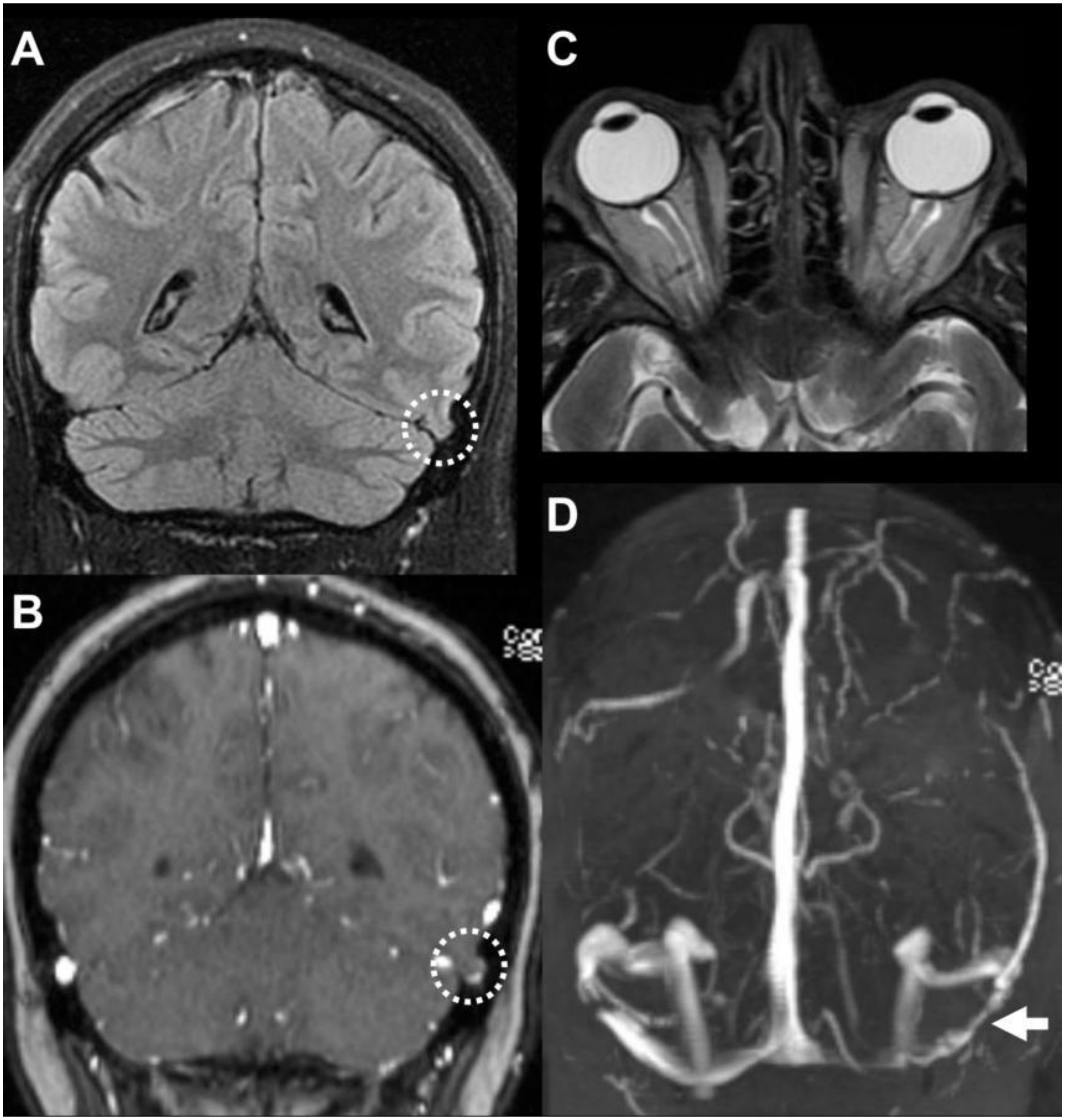

(Filename: TCT_3171_ASNR2019ExcerptaFig.jpg)

3113

11:05AM - 11:09AM

Giant De Novo Cavernoma and Associated Developmental Venous Anomaly

Y Sun[1], J Hoang[1]
[1]*Duke University Medical Center, Durham, NC*

Purpose

Cavernoma is a subtype of slow-flow vascular malformation that is common in clinical practice. The majority of these lesions are small with mean size of 1.4 cm. Because of their small sizes, cavernomas are often incidental findings and cause no neurologic symptoms. Giant cavernomas (greater than 6 cm) are rare and present with symptoms such as headache, focal neurologic deficits and seizures. We present a case of a patient with de novo giant cavernoma associated with de novo developmental venous anomaly (DVA).

Materials and Methods

20 year-old female with history of PFO and prior stroke presents with one month of intermittent headache that had progressively worsened and became daily accompanied by nauseas and vomiting. Brain CT and MRI showed a large left frontal hemorrhagic mass. The patient underwent craniotomy and resection of large hemorrhagic mass, which was a pathologically proven cavernoma.

Results

Prior MRI two years ago showed a small DVA in the left frontal lobe but otherwise normal. At presentation, non-contrast CT head found a 6 cm left frontal lobe mixed density hemorrhagic mass with surrounding vasogenic edema and mass effect including subfalcine herniation. CTA and CTV of head showed no evidence of arteriovenous malformation or dural venous thrombosis. On MRI brain, hemorrhagic left frontal mass was multicystic, nonenhancing and had varying age of blood products. The previously seen DVA was at the superior aspect of the mass and new developmental venous anomalies were found at the inferomedial margin of the mass.

Conclusions

Although rare, giant cavernoma should be included as a diagnostic consideration of a new large intra-parenchymal hemorrhagic mass. Adjacent DVAs support the diagnosis. Absence of smaller cavernoma on prior imaging should not deter from making the diagnosis. Correct diagnosis and detection of possible associated developmental venous anomaly of these lesions have both surgical and prognostic implications.

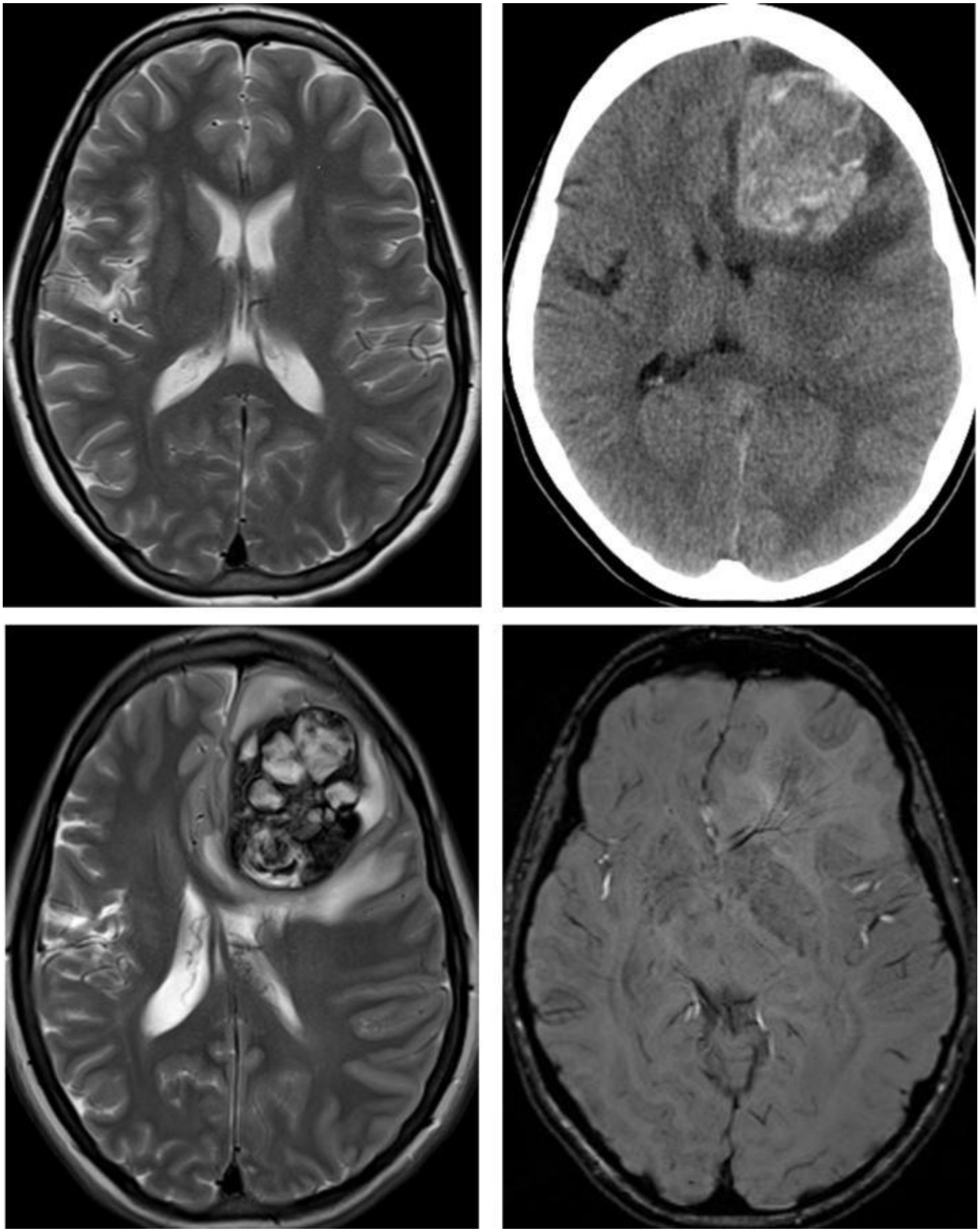

(Filename: TCT_3113_ASNR.jpg)

2782

11:09AM - 11:13AM

Identification of a Ruptured Basilar Artery Sidewall Perforator Aneurysm by Vessel Wall MR Imaging

J Song[1], S Nabavizadeh[1], P Ramchand[1], L Loevner[2], D Kung[1], O Choudhri[3]
[1]University of Pennsylvania, Philadelphia, PA, [2]University of Pennsylvania, Philadelphia , PA, [3]University of Pennsylvania, Phildadelphia, PA

Purpose
Perforator aneurysms are rare and challenging to detect given their size and tendency to intermittently thrombose. We describe a case of a ruptured basilar artery sidewall perforator aneurysm not detected by conventional vessel imaging but identifiable by vessel wall MRI imaging (VWI).
Materials and Methods
A 53-year-old man presented with acute onset headache and nausea. CT head revealed diffuse basilar and prepontine subarachnoid hemorrhage (Fig 1A, asterisk; Hunt-Hess 2, Fisher scale 3). Upon presentation, a CTA head (Fig 1A) and cerebral angiogram (Fig 1B) did not reveal a dissection, ruptured aneurysm, or other etiology for the hemorrhage. A MRI brain with VWI was subsequently performed, which showed a focal punctate focus of enhancement along the posterolateral wall of the basilar artery (Fig 1C, arrowhead). A repeat cerebral angiogram 9 days later revealed a 2 mm basilar artery perforator aneurysm (Fig 1D, arrowhead). Two overlapping LVIS Blue braided stents were placed without complication. Post-intervention angiogram showed decreased aneurysm filling (not shown).
Results
(A) Diffuse subarachnoid hemorrhage (asterisk) in the posterior fossa suggested a posterior circulation vasculopathy. A CTA head and assessment of the basilar artery (A, rectangle) revealed no appreciable aneurysm. Representative orthogonal planes of the basilar artery lumen are depicted in A'. (B) A cerebral angiogram was unrevealing, presumably due to thrombosis of the aneurysm at the time of imaging. (C) MRI Brain with VWI performed the next day revealed a focal outpouching (inset, C', proton density inset) with punctate enhancement along the basilar artery posterolateral wall (insets, C''-C'''). (D) Follow-up cerebral angiogram confirmed a 2mm perforator aneurysm at this site, which was subsequently stented (not shown).
Conclusions
Ruptured aneurysms have high morbidity and mortality, and expedient detection and treatment is imperative. VWI can play a role in detecting small ruptured aneurysms that intermittently thrombose and are challenging to detect by conventional vessel imaging.

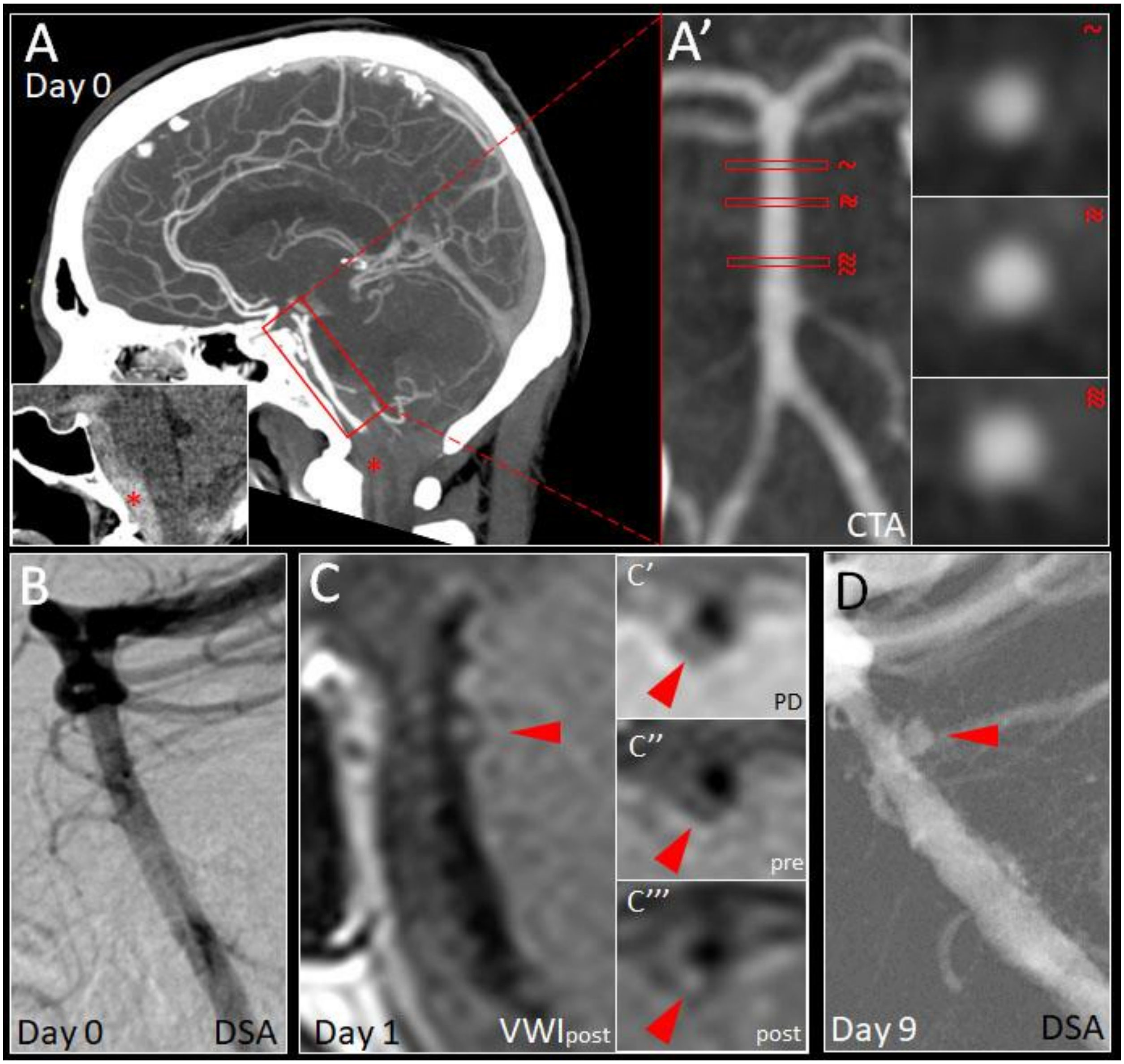

(Filename: TCT_2782_blisteraneurysm.jpg)

2735

11:13AM - 11:17AM

Imaging Features of Non-Ketotic Hyperglycemic Hemichorea

S Kamalian[1], K Wang[1], Y Parikh[1], S Teoh[1], P Sasson[1]
[1]*Mount Auburn Hospital, Cambridge, MA*

Purpose
Hemichorea is commonly due to a pathologic process in the contralateral basal ganglia. Differential diagnosis is broad, such as stroke, metabolic, autoimmune or medication induced. Familiarity with imaging features of non-ketotic hyperglycemic hemichorea can help with the timely diagnosis and treatment of this reversible condition.
Materials and Methods
A 62 year-old right handed male with a history of hemochromatosis complicated by hepatic

encephalopathy, status post liver transplantation and poorly controlled type II diabetes, presented to ER with confusion, involuntary mouth movements and slight left facial droop. The initial physical exam revealed action tremor of the right hand and mild right arm drift. No history of neurologic disorders or dopamine antagonist medication use. Laboratory studies revealed blood glucose level of 412, HBA1c of 14%, and mildly elevated liver enzymes. The patient was treated for non-ketotic hyperglycemia and symptoms improved. After hospitalization, the patient was noncompliant with his diabetes medications. Approximately 8 months later, the patient presented to the Neurology clinic with right-sided involuntary movements involving face, right upper and lower extremities (Video). Laboratory studies revealed blood glucose level of 358, HBA1c of 13% and normal liver function tests. The patient was diagnosed with non-ketotic hyperglycemic hemichorea.

Results

Noncontrast head CT shows hyper-attenuation in the left caudate and putamen (Figure). MR images show increased T1 signal intensity, decreased T2 signal intensity and subtle susceptibility effect in the left caudate and putamen (Figure). Along with high clinical suspicion, these imaging findings are characteristic of non-ketotic hyperglycemic hemichorea.

Conclusions

Familiarity with the imaging features of non-ketotic hyperglycemia, along with the supporting clinical symptoms and laboratory findings is crucial for the timely diagnosis and treatment of this reversible condition.

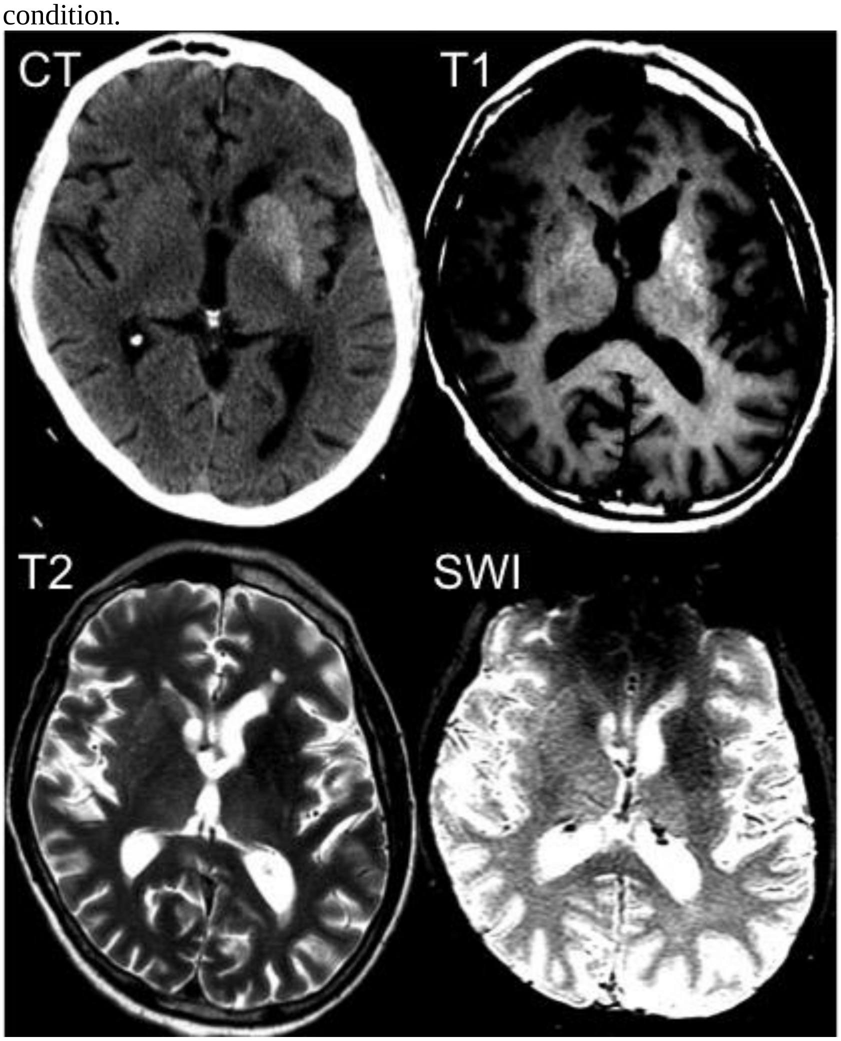

(Filename: TCT_2735_NKHHC.jpg)

2723

11:17AM - 11:21AM

Imaging Illustration of a Rare Case of Trigeminal artery Variant Resulting in Trigeminal Neuralgia

M Gupta[1], E Velez[2], M Ling[3], A Rajput[1], B Ng[4], J Go[5], A Rajamohan[5], J Acharya[6]
[1]USC Keck School of Medicine, Los Angeles, CA, [2]LAC+USC, Los Angeles, CA, [3]USC Keck School of Medicine, Los angeles, CA, [4]University of Southern California, Los Angeles, CA, [5]UNIVERSITY OF SOUTHERN CALIFORNIA, KECK SCHOOL OF MEDICINE, LOS ANGELES, CA, [6]UNIVERSITY OF SOUTHERN CALIFORNIA, KECK SCHOOL OF MEDICINE, Monrovia, CA

Purpose
Illustrate and be able to recognize imaging findings of persistent trigeminal artery anatomy resulting in trigeminal neuralgia.
Materials and Methods
Patient is a 74-year-old female with no significant past medical history who presents with twelve years of progressively worsening left facial pain. Patient has seen multiple dentists without diagnosis of the problem and has self-medicated with pain medication.
Results
A : 3-D time-of-flight MR angiogram axial image demonstrates left persistent trigeminal artery variant originating from the left precavernous internal carotid artery which terminates in the left anterior inferior cerebellar artery. B: MRI IAC 3D Fiesta image demonstrates a vascular loop of the persistent trigeminal artery variant which results in mass effect at the entry/exit of trigeminal nerve. C: MRI IAC Sagittal image demonstrating persistent trigeminal artery variant compressing on the trigeminal nerve.
Conclusions
Trigeminal arteries connect the cavernous portions of the internal carotid arteries (ICA) with the paired vessels that form the basilar arteries. The trigeminal arteries are usually obliterated in utero, but rarely can persist throughout adulthood. They are the most common persistent primitive carotid-basilar anastomosis and have been classified into two types. In Saltzman Type I, the persistent trigeminal artery (PTA) supplies the upper basilar artery and the PCOM is absent, while in Type II, the PTA supplies the superior cerebellar arteries, and the PCOM supplies PCAs. The vessel in this is classified as a persistent trigeminal artery variant (PTAV), in which the trigeminal artery arises from the cavernous ICA without communicating with the basilar artery. In this case, the artery terminates in an anterior inferior cerebellar artery, which results in mass effect on the cisternal component of the left trigeminal nerve. The frequency of PTA and PTAV is 0.1-0.2% and 0.18-0.76%, respectively. Trigeminal neuralgia may be caused by a PTAV due to the proximity of its course to the trigeminal nerve. PTA is a less likely cause because it courses medially relative to the trigeminal nerve to join the basilar artery. PTA or PTAV compression of the trigeminal nerve is the cause of 0.2-0.6% of trigeminal neuralgia cases. In several such cases, trigeminal neuralgia resolved after the patient underwent microvascular decompression surgery. Although rare, it is important to recognize PTA and PTAV as potential causes of trigeminal neuralgia, especially in medically refractory cases.

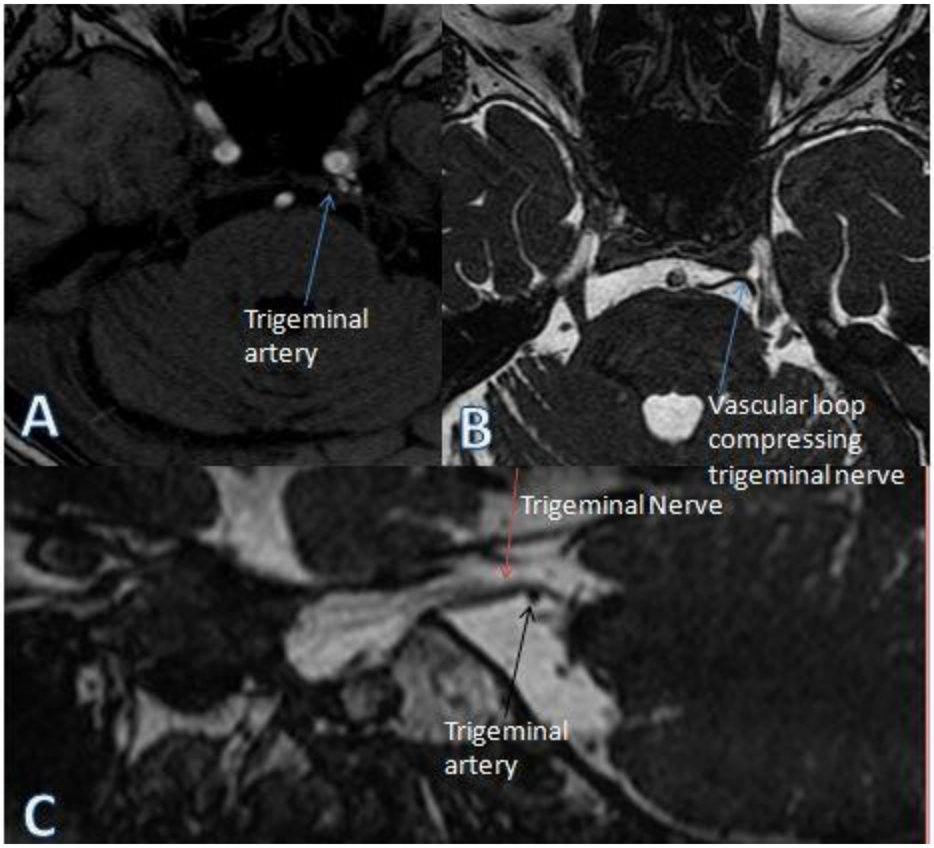

(Filename: TCT_2723_ASNR.JPG)

2128

11:21AM - 11:25AM

Improved Visualization of Cerebral Blood Flow in Mice and Neonates Using Angular Coherence Based Doppler Ultrasound

B Yoon[1], M Jakovljevic[2], L Abou-Elkacem[3], D Hyun[2], E Rubesova[4], J Dahl[2]
[1]*Massachusetts General Hospital, Boston, MA,* [2]*Stanford University School of Medicine, Palo Alto, CA,* [3]*Stanford University Medical Center, Palo Alto, CA,* [4]*Stanford University Medical Center, Stanford, CA*

Purpose
High resolution Doppler ultrasound has been proposed as a new modality for assessing cerebral perfusion (1). These techniques are based on power Doppler (PD) and employ synthetic aperture focusing and large ensemble lengths to separate slow-flow signals from stationary clutter in the cerebral cortex. However, they require long processing time and are susceptible to high acoustic and thermal noise. We demonstrate a novel Doppler strategy based on coherent flow power Doppler (CFPD) imaging and short-lag angular coherence (SLAC) beamforming that has short processing time and improved noise suppression.
Materials and Methods
Images were obtained using a Verasonics Vantage 256 research scanner with 9 MHz, 12L-3v linear array transducer. Stationary tissue signals were removed using spatiotemporal filtering. Angular coherence function was computed from the filtered beam-summed data. Matched PD and CFPD/SLAC images were created. Doppler data were acquired on mice through intact skull and on neonates through the anterior fontanelle. Neonate scans were approved by Institutional Review Board (IRB).

Results
Signal-to-noise ratio of the cerebral blood flow in vivo through the intact mouse skull was greater with CFPD/SLAC by up to 4 dB. This allowed better delineation of the venous sinuses. CFPD/SLAC was also less affected by motion, and the neonate scans through the fontanel showed improved visualization of the cortical veins (Fig 1A, yellow arrow; scale bar = 5 mm). Changes in the cortical blood flow were captured over time (Fig 1B, white arrows; scale bar = 5 mm).
Conclusions
CFPD with SLAC beamforming is a promising technique for assessing cerebral blood flow in neonates with good noise suppression and fast processing of Doppler data with potential application in functional brain imaging by ultrasound.

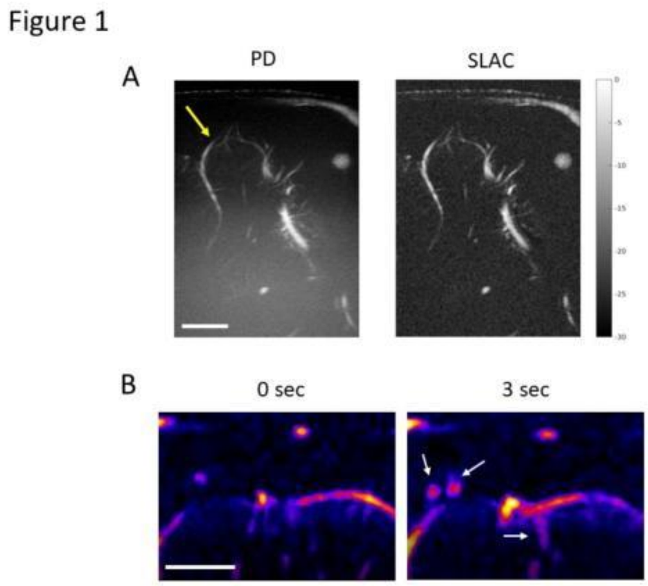

(Filename: TCT_2128_ASNRFigures_YoonB.jpg)

3033

11:25AM - 11:29AM

Intracranial Involvement in a Giant Cell Arteritis: The Role of Imaging in Reaching the Underlying Diagnosis

K Bhatia[1], S Mathur[1]
[1]*Royal Preston Hospital, Preston , United Kingdom*

Purpose
Giant cell arteritis is a common vasculitis of medium to large vessels, usually presenting with headache. Early recognition and treatment initiation is crucial to prevent complications such as permanent visual loss. A small proportion of patients present atypically with infarcts rather than headache, which can lead to delayed recognition. We demonstrate a radiological pattern of involvement of intracranial vessels which is suggestive of this diagnosis to improve recognition in this subset of patients not presenting classically.
Materials and Methods
A 66 year old male presented to the emergency department with one year history of transient visual disturbances, gait disturbances and dysarthria. Initial blood tests demonstrated mildly raised inflammatory

markers but were otherwise unremarkable. After neurological assessment, CT and MRI were performed to further investigate.

Results

Initial MRI demonstrated multiple acute infarcts in the deep watershed territories bilaterally, with attenuation of both cavernous internal carotid flow voids. Enhancement of the vessel walls could be appreciated on conventional post contrast sequences, specifically involving the cavernous internal carotid arteries bilaterally and the right vertebral artery at the V3/V4 junction, at the point of entry into the dura. MR angiography confirmed multifocal stenosis.

Conclusions

Multiple infarcts with vessel wall enhancement led to the diagnosis of vasculitis. In particular, the pattern of vessel wall enhancement located at the point of dural entry of the intracranial vessels led to the suspicion of giant cell arteritis as the underlying cause of the patient's presentation based on a previously encountered case. This is postulated to be a susceptible area due to a change in calibre of the vessels at the dural margin, with reduction in elastic tissue within the wall. The suspicion based on radiological appearances led to biopsy of the superficial temporal artery, which confirmed the diagnosis.

3154

11:33AM - 11:37AM

Neuroimaging of Leukostasis, a Rare Complication of Leukemia

B Wang[1], L Ketonen[2]

[1]MD ANDERSON CANCER CENTER, HOUSTON, TX, [2]M.D. Anderson Cancer Center, Houston, TX

Purpose

Leukostasis occurs in patients with high blast counts due to aggregates of leukemic cells in vessels. This may involve multiple organs but the lung and brain are more susceptible for damage. We illustrate the imaging findings of 2 cases of leukostasis in the brain, which to our knowledge has not received much attention in the radiological literature. Our purpose is to raise awareness of the neuroradiology community concerning this entity.

Materials and Methods

One of our two patient is a 21-year-old man initially diagnosed with Philadelphia chromosome negative pre B- acute lymphoblastic leukemia (ALL)/lymphoblastic lymphoma at age of 19. He presented with bilateral lower extremity weakness and paresthesia due to epidural mass causing cord compression. He underwent urgent upper thoracic laminectomy of T1-T5 and opted not to proceed with radiation. The patient underwent treatment induction according to pediatric protocol on a very high risk arm. Because of severe neuropathy the patient did not receive intrathecal methotrexate. He continued on maintenance therapy until he was found to have relapse after presentation with right cervical and supraclavicular lymphadenopahty. Subsequent biopsy showed B-cell malignancy, CD10, CD19, CD4 positive lymphoblasts. Recently, the patient experienced difficulty swallowing of solid food as well as severe neck pain. When his symptoms became worse, he decided to present to EC in our institution to have second opinion.

Results

On MRI, there are innumerable scattered lesions throughout the brain that show blooming on T2 gradient echo images. Some of the lesions have a T2 FLAIR hyperintense rim, compatible with edema. There is no definite superimposed enhancement. None of the lesions demonstrate diffusion restriction. There is no abnormal leptomeningeal enhancement. On follow up MR 6 months later, the previously seen innumerable susceptibility foci are again seen consistent with microhemorrhages. The surrounding edema has resolved. The microhemorrhages are not conspicuous on CT.

Conclusions

The hyperleukocytosis that can be observed in acute myeloid leukemia (AML) may lead to leukostasis, a life-threatening complication caused by leukemic cell sludging in blood capillaries. In the absence of treatment, cellular hyperviscosity caused by extreme leukocyte count elevation may rapidly lead to multiple organ failure and death. Leukostasis is more frequently observed in patients with AML or chronic myelocytic leukemia than in patients with acute lymphoblastic or chronic lymphocytic leukemia. It is now becoming increasingly evident that leucostasis results from the adhesive interactions between leukemic blasts and the endothelium. Although leucostasis can affect any organ system, symptoms usually arise from the involvement of the pulmonary and cerebral microvasculature and early deaths are due to respiratory failure and intracranial hemorrhage. Patients can present with exertional dyspnea due to severe respiratory distress. Neurological manifestations range from mild confusion to stupor and coma. Focal central nervous system deficits may herald intracranial hemorrhage. Fatal intracerebral hemorrhage may occur. This condition is a medical emergency which needs prompt recognition and therapy. Prompt reduction in the number of circulating blast cells (leucoreduction) is essential to prevent leucostasis in patients with acute hyperleucocytosis and to treat or halt the progression of established leucostasis. This report intends to increase awareness of this life threatening condition and the need to implement urgent patient management.

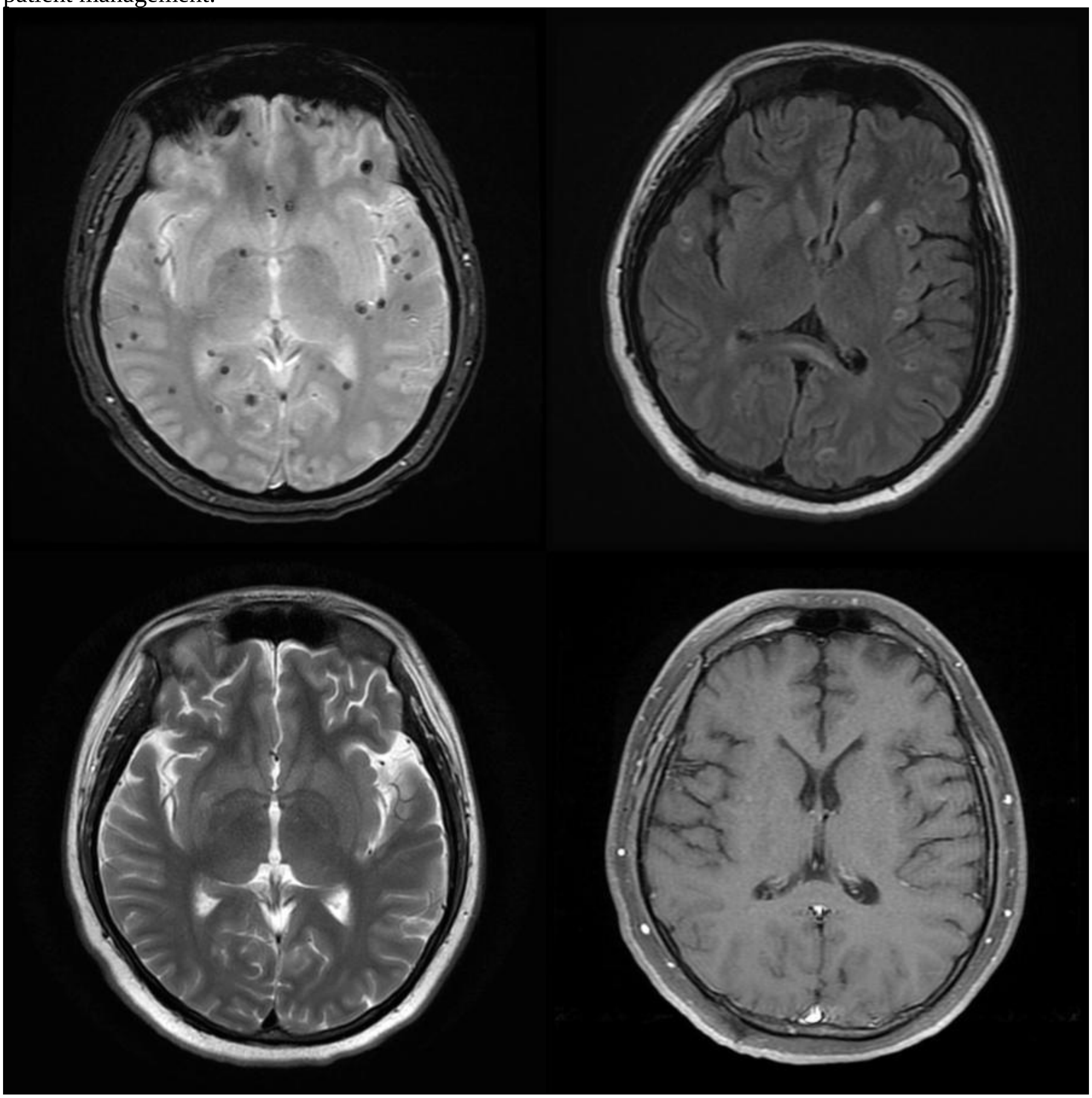

(Filename: TCT_3154_LeukostasisASNR2019Images.jpg)

2655

11:37AM - 11:41AM

Nonketotic Hyperglycemia: Brain MRI Findings and Serial Follow-Up

F SEPULVEDA[1], P Yañez[2], M CARNEVALE[3], L Carballo[4]
[1]DIAGNOIMAGE, SANTIAGO, NC, [2]FLENI, Buenos Aires, Buenos Aires, [3]FLENI, Buenos aires, Buenos Aires, [4]FLENI, Buenos Aires, Argentina

Purpose
The purpose of this case report is to show the brain MRI findings of Nonketotic hyperglycemia and its time evolution.
Materials and Methods
A 52-year-old woman presented with phosphenes and lost of the right eye acuity. The patient has a history of diabetes type II and diabetic retinopathy. Imaging workup with MRI revealed classic finds of nonketotic hyperglycemia with a hyperosmolar state in the left parietal and occipital subcortical white matter. The patient received hypoglycemic therapy with normalization of blood glucose and improvement of the symptomatology. 1 month and 20 days later a follow up was performed. MRI showed signal changes in the affected region with the presence of edema. 3 month later she showed a complete resolution of the symptoms and normalization of the signal changes on the brain MRI.
Results
Figure. T2WI (A) show hypointense signal in the parietal subcortical white matter. ADC map (B) shows diffusion restriction in the cortex and subcortical white matter of the affected lobes. First follow up (C): T2WI shows hypertense signal in the parietal and occipital subcortical white matter corresponding to edema. Second follow up (D): T2WI shows normal signal intensity in the previously affected area.
Conclusions
Given the characteristic brain MRI features (T2 subcortical hypointensity) and the history of diabetes type II the diagnostic of nonketotic hyperglycemia was made. The brain MRI in the patient with nonketotic hyperglycemia in the hyperosmolar state is usually normal. In the presence of seizure or ophthalmologic symptom, brain MRI can show a reversible T2 signal changes and diffusion restriction in the parietal-occipital region.

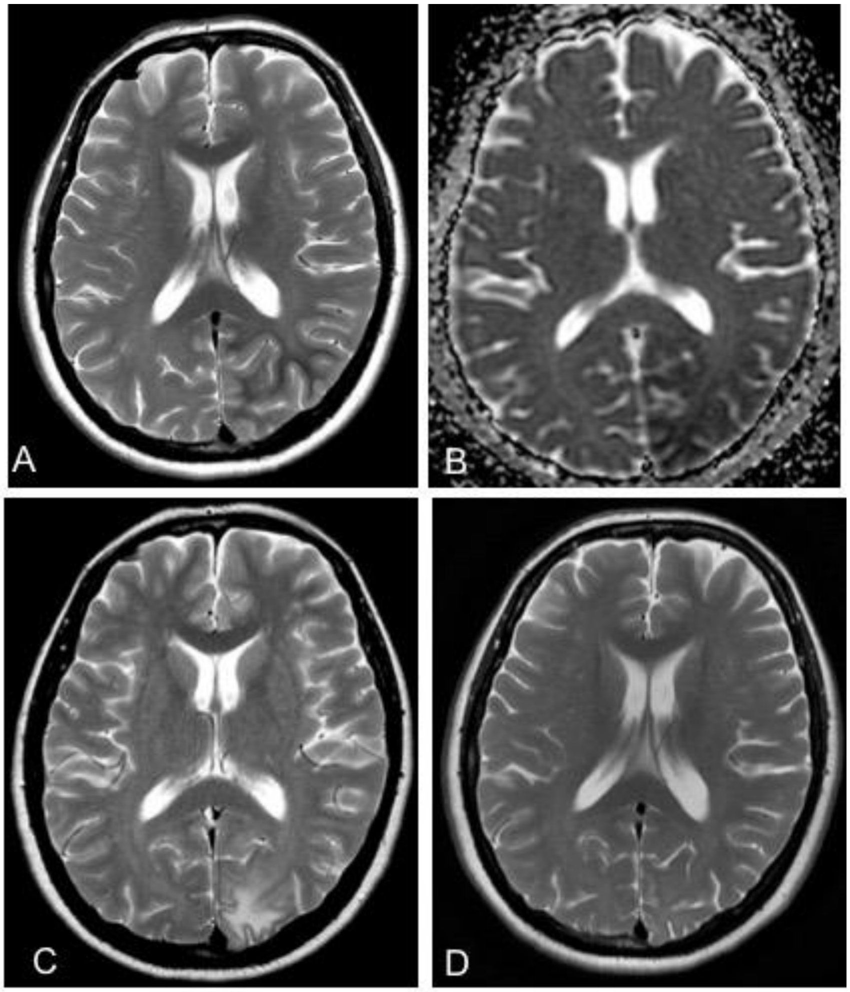

(Filename: TCT_2655_Figure.jpg)

Scientific Posters

2474

ASL Outperforms DSC Perfusion in Differentiating Recurrent High Grade Glioma Versus Radiation Change

V Ivanovic[1], Y Chang[1], I Chiali[1]
[1]*Beth Israel Deaconess Medical Center, Boston, MA*

Purpose
Distinguishing recurrent glioma from post-treatment change is important. Both Arterial Spin Labeling (ASL) and Dynamic Susceptibility Contrast (DSC) perfusion have been used for this purpose. The aim of our study was to evaluate the performance of ASL versus DSC perfusion imaging in distinguishing recurrent glioma from post-treatment change.
Materials and Methods
Sixteen patients with worsening MRI and distant history of treatment for high grade glioma (Grade IV=9, grade III=7) were included. 15 of 16 patients had prior surgery and chemo-radiation, and 1 patient had prior surgery and chemotherapy. Pre biopsy MRI brain included routine sequences, ASL and DSC perfusion imaging. ASL and DSC perfusion findings were assessed qualitatively by 2 neuroradiologists. ASL/DSC was considered to be positive and suggestive for recurrent glioma when signal higher than white matter was observed within worsening MRI abnormality. ASL/DSC perfusion was considered to be negative and suggestive for post-treatment change when signal equal to or less than white matter was observed within worsening MRI abnormality. Findings were correlated with biopsy results.
Results
Biopsy showed recurrent glioma in 14 patients (Grade IV=10, Grade III=4) and post-treatment change in 2 patients. Cohen's kappa coefficient for inter-reader agreement was 1.00 for ASL perfusion (perfect agreement) and 0.74 for DSC perfusion (substantial agreement). ASL was positive in 14/14 cases of recurrent tumor, and negative in 2/2 cases of post radiation change, yielding sensitivity of 100% (95% CI 76.84-100.00%) and specificity of 100% (95% CI 15.81-100.00%). DSC was positive in 7/14 of cases of recurrent tumor and negative in 2/2 cases of post radiation change, yielding sensitivity of 50% (95% CI 23.04-76.96%) and specificity of 100% (15.81-100.00%).
Conclusions
ASL outperforms DSC perfusion in distinguishing recurrent high grade glioma from post treatment change and should be part of a routine imaging protocol.

2710

Assessment of Obstructive Sleep Apnea on Cerebrovascular Health in Children with Obesity Using MRI

A Bhatia[1], T Naik[2], I Narang[2], A Kassner[2]
[1]*University of Toronto, Toronto, Ontario,* [2]*The Hospital for Sick Children, Toronto, Ontario*

Purpose
Obstructive sleep apnea (OSA) is a significant contributor to co-morbid disease in obese children. Cerebral endothelial dysfunction and neurocognitive deficits have been linked to obesity-related OSA. However, the effect of the chronic hypoxic environment caused by untreated OSA on cerebrovascular health remains unclear. Non-invasive imaging strategies can assess vessel distensibility by quantifying the

relative changes in cerebral blood flow (CBF) in response to a vasoactive stimulus. The resulting measure, cerebrovascular reactivity (CVR), is a useful tool in the clinical assessment of cerebrovascular disease. The purpose of this study is to assess the effect of OSA on cerebrovascular health in a pediatric obese population.

Materials and Methods

33 obese patients, 10 with no, 9 with mild and 14 with moderate-to-severe OSA, between 9 and 18 years old were included and imaged on a clinical 3T MRI. Blood-oxygen level-dependent (BOLD) imaging was used to assess changes in CBF during the administration of a computerized CO_2 stimulus as previously described (Leung et al.). CVR maps were computed offline using FSL by correlating the voxel-wise BOLD signal to the measured CO_2 waveform. CBF was measured using a PICORE arterial spin labeling sequence and quantified with the vendor pipeline. CVR and CBF values were averaged over grey matter (GM) and white matter (WM) regions and Pearson correlation analysis was performed on the resulting data.

Results

Higher CBF was inversely associated with CVR in obese patients with moderate-to-severe OSA for both GM and WM ($r=-0.331$ and $r=-0.590$, respectively). Furthermore, in patients with moderate-to-severe OSA, a decline in CVR was observed for both GM and WM when plotted against the Obstructive Sleep Apnea Index (OAHI) ($r=-0.297$ and $r=-0.508$, respectively).

Conclusions

In this study, we have demonstrated higher CBF values in obese patients with moderate-to-severe OSA compared to those with no or mild OSA. Reduced CVR in children with obesity and moderate-to-severe OSA may be exposed to a higher risk of cerebrovascular damage. If left untreated, this may present behaviourally as neurocognitive deficits and serious vasculopathies such as stroke. Further studies are needed to confirm our results in a larger cohort and to assess the effectiveness of CPAP therapy.

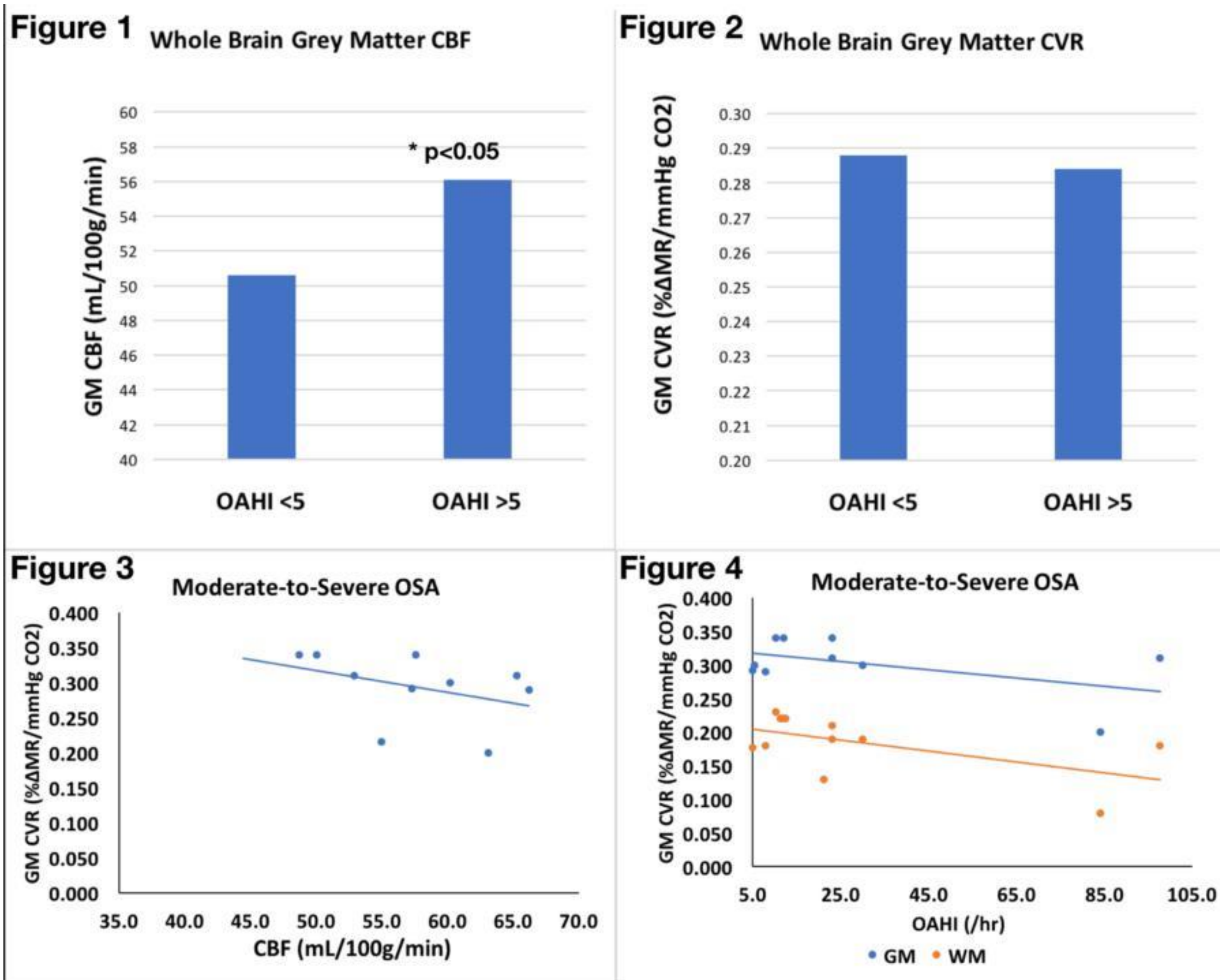

Figure 1: Average CBF measures for combined no and Mild OSA group (OAHI<5.0) and moderate-to-severe OSA group (OAHI>5.0).
Figure 2: Average measures for combined no and Mild OSA group (OAHI<5.0) and moderate-to-severe OSA group (OAHI>5.0).
Figure 3: Negative correlation between CBF and CVR in whole brain Grey Matter.
Figure 4: Negative correlation between OAHI and CVR in Grey Matter and White Matter

(Filename: TCT_2710_OSACVR_ASNRFigure.jpg)

3408

Automated Segmentation of Areas of Abnormal Susceptibility on MRI Using a 3D Convolution Neural Network.

J Choi[1], L Xie[1], J Wang[1], J Gee[1], A Rauschecker[2], J Rudie[1]
[1]University of Pennsylvania, Philadelphia, PA, [2]University of California San Francisco, San Francisco, CA

Purpose
Abnormalities on susceptibility-weighted imaging are an important imaging finding used to support the diagnosis of many neurological diseases, including hemorrhage, amyloid angiopathy, primary and metastatic tumors, and traumatic brain injury, among others (Haller et al 2018 Radiology). The ability to automatically detect and quantify areas of abnormal susceptibility has the potential to improve the radiologist's workflow and allow for more advanced quantitative assessment. Our study utilized a

convolutional neural network to automatically segment areas of abnormal signal on gradient echo (GRE) imaging from brain MRI scans.

Materials and Methods

GRE sequences from 249 brain MRI scans (including 77 normal and 172 abnormal) were split into training (n = 175) and validation samples (n = 74) with gold standard segmentations performed by a radiologist. Images were resampled into 1x1x1 mm3 using linear interpolation. Segmentation was achieved using a tailored 3D U-Net algorithm based on Ronneberger et al 2015. 3D 96x96x96 patches were augmented with elastic transformations prior to training. The U-Net consisted of four consecutive down-sampled blocks followed by four consecutive up-sampled blocks with skip connections (Figure 1).

Results

The median Dice score of the validation set segmentation was 0.54. The false positive fraction was 0.22 and the false negative fraction was 0.52 There was a high correlation between true volume of abnormalities, as judged by a radiologist, and the estimated volume of abnormalities, as judged by the U-Net (Spearman rank coefficient r = 0.87, p < .0001). The overall accuracy relative to radiologists' assessment for the presence or absence of abnormal susceptibility was 91% (sensitivity = 100%, specificity = 63%).

Conclusions

We trained a 3D convolutional neural networks to detect abnormal susceptibility on brain MR GRE sequences with high accuracy, providing quantitative assessments of abnormalities automatically. The performance is expected to improve with more training data and advanced network architectures.

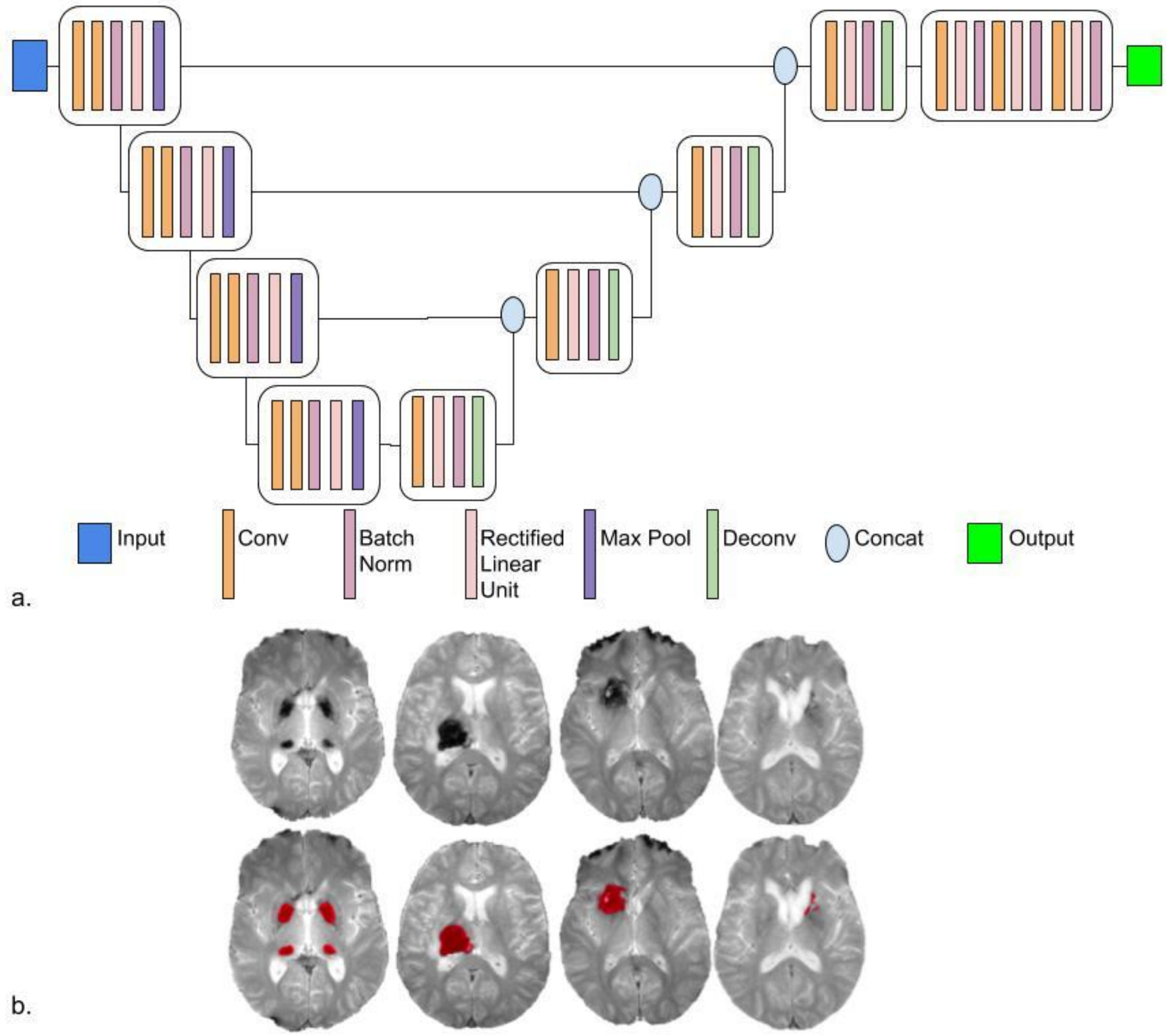

Figure 1. (a) Schematic of U-Net algorithm showing four consecutive blocks of down-sampling followed by four consecutive blocks of up-sampling, noting skip connections between each layer of sampling. After the final up-sampling block, and additional block of convolution, rectification and normalization was performed. (b) Examples of axial GRE images with areas of abnormal susceptibility (top row) and the corresponding automatically generated segmentations from the U-Net algorithm (bottom row).

(Filename: TCT_3408_Figure.jpg)

2317

Axonal Damage in the Optic Radiation Detected by Advanced Diffusion MR Metrics is Associated with Retinal Thinning in Multiple Sclerosis

C Ngamsombat[1], Q Tian[1], Q Fan[1], A Russo[2], T Witzel[1], L Wald[1], E Klawiter[2], S Huang[1]
[1]Massachusetts General Hospital / Athinoula A. Martinos Center for Biomedical Imaging, Boston, MA, [2]Department of Neurology, Massachusetts General Hospital, Harvard Medical School, Boston, MA

Purpose
Damage to white matter of the visual pathway is common in MS. DTI has been used to demonstrate

microstructural damage to the optic radiation (OR) in MS.[1,2] Advanced multi-compartment diffusion MR models [3,4,5] may provide better specificity to axonal integrity. Here, we determine the presence of changes in white matter tract integrity (WMTI) and neurite orientation dispersion and density imaging (NODDI) metrics in the OR in MS and investigate the association of these metrics with retinal thinning.

Materials and Methods

Thirty MS patients and 30 age-matched healthy controls (HC) were recruited. Subjects were scanned using a multi-shell diffusion imaging protocol on the 3T-Connectome MRI scanner equipped with 300 mT/m maximum gradient strength. DTI (b=800s/mm2), WMTI (b=50-2400s/mm2) and NODDI metrics (b=950,2400s/mm2) were assessed within lesions and normal-appearing-white-matter (NAWM) of OR. The OR region-of-interest was generated by probabilistic tractography with seed and target regions in the LGN and V1 region (Figure 1). Evaluation of diffusion metrics between groups and their relationship with same-day OCT data was performed with linear regression analysis and Pearson partial correlation adjusted for age and sex.

Results

Optic radiation NAWM of MS patients showed decreased FA ($p=0.003$), increased RD ($p=0.001$), decreased axonal water fraction (AWF,$p<0.0001$) and decreased intracellular volume fraction (FICVF,$p<0.0001$) compared to HC, with similar trends seen in MS lesions compared to NAWM. Thinning of the retinal nerve fiber layer (RNFL) on average and in the nasal retinal quadrant correlated with reduction in FA, AWF, and FICVF in NAWM OR.

Conclusions

Our results suggest that axonal damage may be the underlying substrate of previously observed DTI alterations in the OR. RNFL thickness in the nasal retinal quadrant was specifically correlated with FA, AWF and FICVF in the synaptically connected contralateral OR. Our results support the notion that axonal damage is widespread throughout the visual pathway in MS and may be mediated through trans-synaptic degeneration.

Figure 1: (A) Tractography of the optic radiation superimposed on a NODDI FICVF map. (B) Clinical data of MS patients and HC. (C and D) OCT images show how the retinal nerve fiber layer (RNFL) was analyzed.

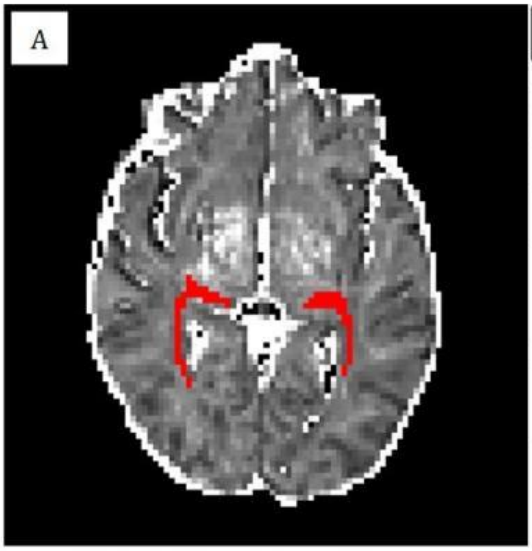

B

	Healthy controls	Multiple sclerosis
Subjects	30	30
Gender (M/F)	13/17	6/24
Age (Y)*	39.87 (13.98)	43.87 (11.17)
Disease duration (Y)*	-	10.63 (6.61)
MS subtype (RRMS/SPMS/PPMS)	-	23/5/2
Clinical history of optic neuritis in both/right/left eye(s)	-	17 (56.67%), 6/5/6
Median EDSS**	-	2.5 (1-7.5)
Mean retinal nerve fiber layer (RNFL) thickness in um*	-	73.3 (12.3)

*Data are mean +/- standard deviation
** Data in parentheses represent the range

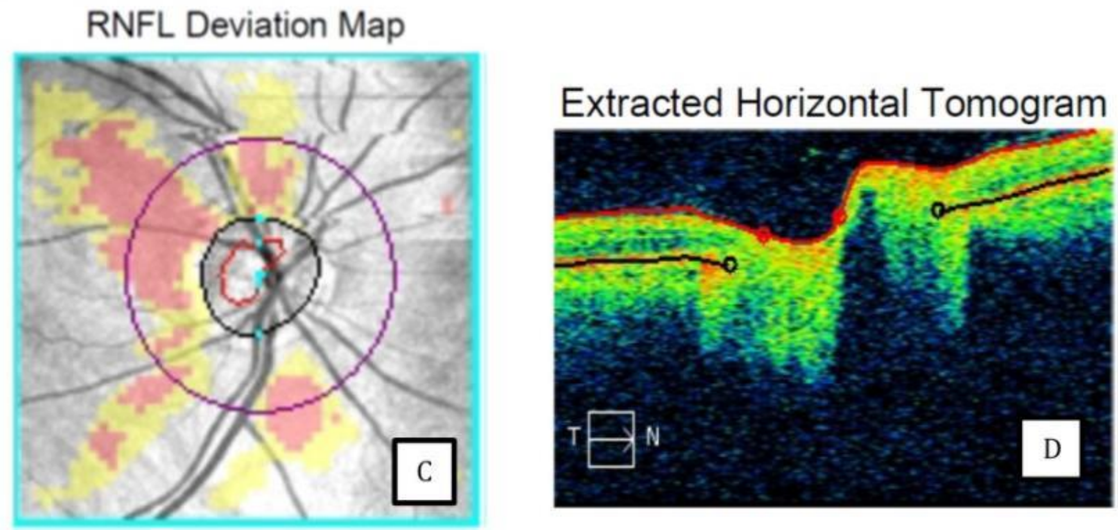

(Filename: TCT_2317_figure1.jpg)

3506

Cerebrovascular Reactivity and Neuropsychological Outcomes in Children with Moyamoya Disease

N Dlamini[1], E Choi[1], R Westmacott[1], M Shroff[1], P Krishnan[1], A Robertson[1], T Williams[1], W Logan[1]
[1]*The Hospital for Sick Children, Toronto, Ontario*

Purpose
Moyamoya is a major arteriopathy of childhood, which is caused by progressive steno-occlusion of the arteries at the base of the brain. A network of lenticulostriate collaterals develops to bypass the primary steno-occlusion, and vasodilation at the level of the capillary bed occurs to maintain cerebral blood flow (CBF), resulting in a reduction of cerebrovascular reserve. In vivo assessment of cerebrovascular reserve

can be performed by measurement of cerebrovascular reactivity (CVR), defined as a change in CBF in response to vasoactive stimuli such as carbon dioxide. A negative response to the vasoactive stimulus is termed "steal", representing reduced CBF. This is an independent predictor of ischemic injury and stroke. Blood oxygen level-dependent (BOLD) MR imaging is a noninvasive technique of measuring dynamic changes in local and global CBF at the level of the microvascular tissue bed. Using carbon dioxide as a vasoactive stimulus, hypercapnic challenge BOLD MR imaging CVR maps can be generated and provide a visual representation of normal "positive reactivity" and abnormal "negative reactivity/steal", with steal representing ischemic risk and impending tissue demise. The breath-hold (BH) method of hypercapnic challenge uses the accumulation of endogenous alveolar carbon dioxide during short periods of voluntary apnea. This method has been shown to be reliable and reproducible for the assessment of CVR in childhood (Dlamini et al., AJNR, Sep 2018). Cognitive difficulties or decline in moyamoya has been rarely investigated and is complicated by a number of factors, such as underlying disease condition (e.g. Sickle Cell disease or neurofibromatosis Type 1) or duration of symptoms (Hogan et al., 2005; Williams et al., 2012) or individual variabilities (age at diagnosis). However, it is important to understand how patients' neurological presentation predict various kind of neuropsychological outcomes, especially in pediatric stroke.

Materials and Methods

Participants 31 BH-CVR cases of 7 years of age or older with a diagnosis of moyamoya (Recruited from the Hospital for Sick Children Toronto Stroke Registry between 2010 to 2018) Breath-Hold CVR paradigm Five 60-second periods of breath holding and normal breading and 30-seond rest period (Figure) Children underwent two BH-CVR studies on the same day during the same MR imaging session (1A and 1B) and some of them also have done follow-up studies over the years (2A-2B, 3A-3B, 4A-4B). MR Imaging Acquisition 3T scanner (Achieva; Philips Healthcare, Best, the Netherlands) using an 8-channel head coil BH-CVR acquisition using EPI-gradient recalled echo lasting 6 minutes, 6 seconds (25 slices; TR/TE = 2000/30 ms; voxel size = 3.4 × 3.4 × 5 mm3; FOV = 22 cm; 180 dynamics). High-resolution 3D T1-weighted structural image (160 slices; voxel size = 0.86 × 0.86 × 1 mm3; FOV = 22 cm) Image processing and CVR estimation MR imaging data processing was performed using locally developed tools Neuropsychological assessment Intelligent Quotient was assessed using WISC-IV or V (The Wechsler Intelligence Scale for Children Version 4 or 5) and WAIS-IV (Wechsler Adult Intelligence Scale Version 4) Statistical analysis CVR measures: Mean of positive, negative and combined CVR estimates, representing the magnitude of CVR value and their respective voxel counts Neuropsychological outcomes: Correlation analysis between ICC or CVR estimates and IQ (Full scale IQ and subscales of IQ) and regression analysis to examine the relationship between CVR estimates and IQ scores.

Results

Study population Thirty one (12 males; mean age, 12.29 ± 3.01 years range, 7 to 17 years) BH-CVR cases from 25 patients were included. Participants demographics and neurological characteristics are shown in [Table 1] and [Table 2]. The CVR estimates for group mean and SD are shown in [Table 3]. The Correlation matrix ([Table 4]) between the CVR estimates and IQ scores demonstrated significant correlations between the full scale IQ and the positive mean magnitude CVR in grey and white matter. We performed linear stepwise regression analysis to examine the effects of CVR estimates on IQ sub-scales and the results are shown in [Table 5]. -Mean Magnitude of Positive CVR in GM significantly predicted FSIQ (beta = 0.209, p = 0.004) -Mean count of negative CVR in GM predicted PRI performance (beta = -0.488, p=0.04) -Mean magnitude of positive CVR in WM predicted WMI performance (beta = 0.45, p = 0.013)

Conclusions

These are preliminary results, but we suggest that the breath-hold paradigm may be useful to examine the relationship between CVR estimates and neuropsychological outcomes in children with moyamoya disease. Positive CVR mean magnitude in grey and white matter may predict children's intellectual outcomes. Further analysis will be performed using other cognitive measures (executive function), and hemispheric / regional CVR estimates.

[Table 1] Demographics

Demographics and neurological characteristics		
Number of participants	31 BH-CVR cases from 25 patients	
Number of males/females	12 males	
Mean age at diagnosis (Mean±SD, range)	7.14 ± 2.35 years (1.40-11.30 years)	
Mean age at scan (Mean±SD, range)	12.29 ± 3.01 years (7.00-17.00 years)	
Moyamoya classification	Familial	1 patient
	Neurofibromatosis Type 1	4 patients
	Sickle cell disease	2 patients
	Idiopathic	11 patients
	ACTA 2 mutation	1 patient
	Radiation vasculopathy	1 patient
Presentation	Stroke	2 patients
	Asymptomatic	4 patients
	TIA	7 patients
	HA	5 patients
	Headache	2 patients
	Pallor and lethargy	1 patient

[Table 2] IQ outcomes

IQ scores	
Scales	Mean±SD, Range
FSIQ (Full-scale IQ)	94.65 ± 18.15, 59-131
VCI (Verbal Comprehension Index)	94.58 ± 12.96, 65-127
PRI (Perceptual Reasoning Index)	86.00 ± 18.29, 54-111
WMI (Working Memory Index)	96.52 ± 13.15, 67-122
PSI (Processing Speed Index)	92.07 ± 15.30, 64-127

[Table 3] CVR estimates

	Mean Magnitude				Mean Count				Mean Magnitude CVR (Positive and Negative Combined)	
	Positive CVR		Negative CVR		Positive CVR		Negative CVR			
	GM	WM	GM	WM	GM	WM	GM	WM	GM	WM
Mean	0.94	0.59	-0.43	-0.56	0.62	0.66	0.19	0.20	0.46	0.28
SD	0.30	0.30	0.17	0.25	0.13	0.15	0.13	0.49	0.22	0.17

[Table 4] Correlations matrix

	FSIQ	VCI	PRI	WMI	PSI
Mean Magnitude Positive CVR in GM	.490**	.358*	.314	.440*	.219
Mean Magnitude Positive CVR in WM	.502**	.308	.337	.445*	.235
Mean Magnitude Negative CVR in GM	-.125	.098	-.046	-.048	.111
Mean Magnitude Negative CVR in WM	-.212	-.017	-.049	-.259	-.060
Mean Count Positive CVR in GM	.097	.211	.374	.102	.078
Mean Count Positive CVR in WM	.013	.194	.091	-.037	-.014
Mean Count Negative CVR in GM	-.203	-.243	-.491*	-.292	-.253
Mean Count Negative CVR in WM	-.130	-.028	-.394	-.154	-.220
Mean Magnitude CVR in GM (Positive and Negative Combined)	.367*	.450*	.314	.345	.238
Mean Magnitude CVR in WM (Positive and Negative Combined)	.385*	.404*	.289	.337	.251

[Table 5] Regression analysis results

Variables	B	Std.Error	Beta	t	p
Constant	-1.564	0.532		-2.941	0.006
Mean Magnitude Positive GM	1.701	0.543	0.209	3.132	0.004

$R = 0.51$, $R^2 = 0.26$, Adj. $R^2 = 0.23$

(Filename: TCT_3506_Tables.jpg)

2832

Click Larynx: Cross Sectional Imaging Findings and Relevance

F Hebroni[1], S Karnezis[1], A Vijayasarathi[2], A Azizyan[1]
[1]UCLA, Los Angeles, CA, [2]University of California Los Angeles, los angeles, CA

Purpose
A clicking larynx is a rare entity described as a clicking sensation in the neck with swallowing or head movement. Abnormalities of the hyoid bone, styloid process, and thyroid cartilage have been identified as possible etiologies. Enlargement or displacement of the greater cornu of the hyoid bone and displacement of the cornu of the thyroid cartilage are the most commonly reported. Prior studies have demonstrated these abnormalities with x-ray or fluoroscopy. We present the first cross-sectional study.
Materials and Methods
Retrospective clinical and imaging review of four patients with confirmed click larynx and literature search of the 17 previously reported cases. Imaging of an additional 50 patients, randomly selected from patients referred for reasons not related to larynx mobility issues, was reviewed to assess the prevalence

of these anatomic abnormalities. We assessed the length of the styloid processes, and looked for any displacement or significant deviation of the hyoid bone and thyroid cartilages.

Results

Of the 50 cases reviewed, only 1 case (1/50) had any significant anatomic abnormality of the hyoid bone, or laryngeal cartilages; a medially deviated greater cornu of the hyoid bone. In addition, there were 10 cases (10/50) with one or more elongated styloid processes and 4 of which had both elongated (above 30 mm). The four confirmed cases at our institution had displacement of the hyoid bone, proximity between thyroid cartilage and hyoid bone, and elongated styloid process.

Conclusions

This is the first cross sectional review of the abnormalities associated with click larynx. Review of 50 CT examinations of the neck, revealed that some of the associated abnormalities are common in the general population, while others are rare. The objective of this study is to aid radiologists in identifying potential abnormalities on CT or MRI, and to help determine whether these abnormalities are related to the patient's symptoms or incidental.


(Filename: TCT_2832_DeviatedHyoid.jpg)

3179

Comparison of 3D Double Inversion Recovery Sequence with Conventional MRI Sequence in the Detection of Multiple Sclerosis Lesion

A Lai[1], C Chu[1], W Shiu[2], W Kan[1], K Leung[3]
[1]Pamela Youde Nethersole Eastern Hospital, HONG KONG, HONG KONG, [2]Pamela Youde Nethersole Eastern Hospital, Hong Kong, HONG KONG, [3]Pamela Youde Nethersole Eastern Hospital, Hong Kong, Hong Kong

Purpose
To compare the detection rate of multiple sclerosis lesion located in different regions of the brain and the interrater agreement between three-dimensional (3D) double inversion recovery (DIR) sequence and combination of T2 TSE and FLAIR (T2/FLAIR) sequences
Materials and Methods
Consecutive patients known to have multiple sclerosis who underwent MRI (including 3D DIR, T2 TSE and FLAIR sequences) in a single institution between January 1 to December 31, 2017 were retrospectively reviewed. DIR MRI images were reviewed independently by two neuroradiologists. This was repeated for T2/FLAIR after 3 months with the study list in a different random order. Lesions were counted and localized to 7 anatomic regions: intracortical, mixed white matter (WM)-gray matter (GM), juxtacortical, deep WM, deep GM, periventricular WM and infratentorial. The mean lesion counts and interrater agreement between the two imaging techniques were compared using Mann-Whitney U test and intraclass correlation respectively
Results
18 MRI were performed among 17 patients (mean age: 39.8; M:F = 5:12). More lesions were detected on DIR than T2/FLAIR in total (26.6 vs 15.7) and in almost all individual anatomical regions, except deep gray matter. The differences are more pronounced for intracortical (mean 1.7 vs 0.4, p=0.01). There was excellent interrater agreement in lesion detection in the entire brain on DIR (ICC 0.89), while that on T2/FLAIR was fair only (ICC 0.40). The interrater agreement for lesion detection in juxtacortical and periventricular regions on DIR was also excellent (ICC 0.81 and 0.91 respectively), while that on T2/FLAIR was fair to moderate (ICC 0.22 and 0.62 respectively).
Conclusions
Our study suggested that DIR sequence can depict more lesions in patients with multiple sclerosis and offers better interrater agreement when compared with T2 and FLAIR sequences in combination.

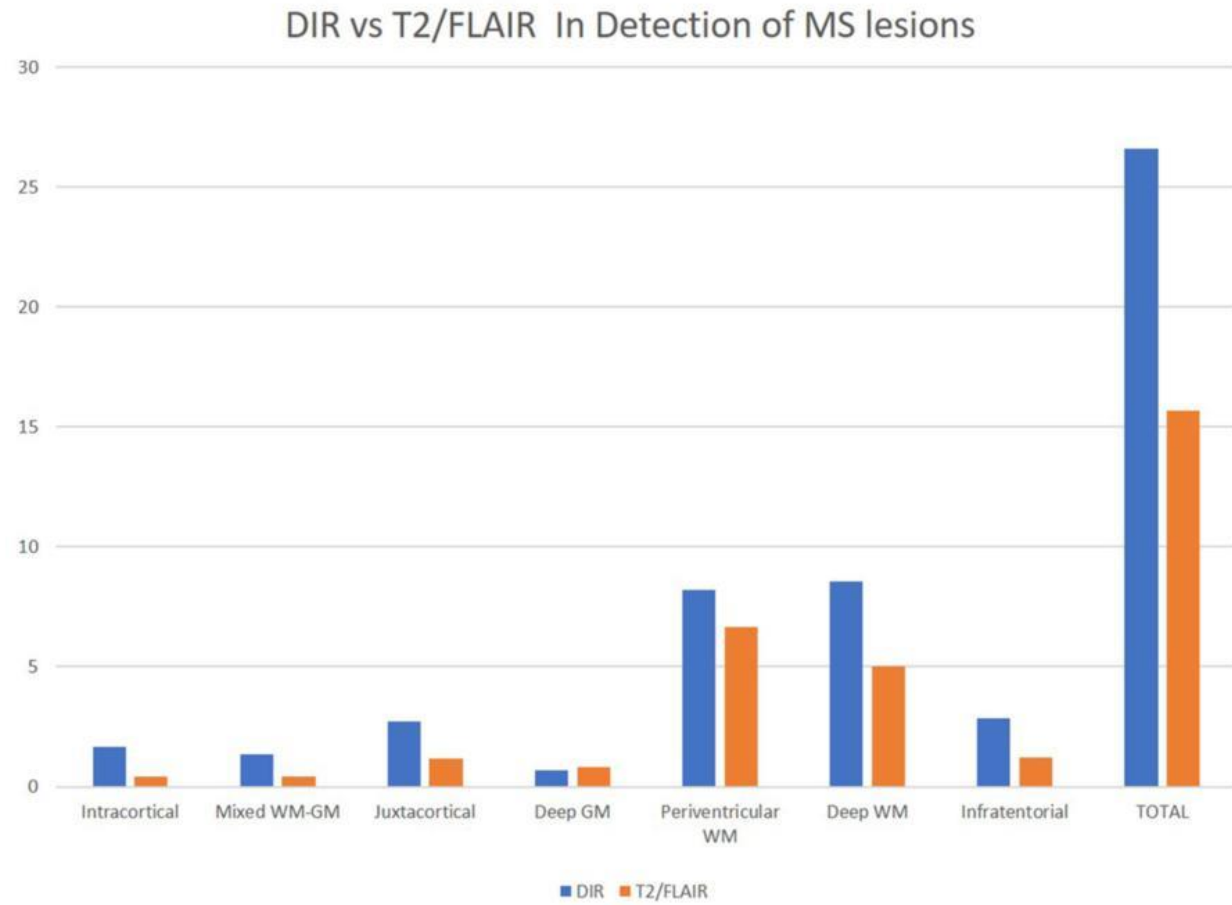

(Filename: TCT_3179_Figure1.jpg)

2787

Comparison of Cerebrovascular Disease Load Between Amnestic and Non-amnestic Mild Cognitive Impairment

M Agarwal[1], K Reiter[1], A Correro[1], S Franczak[2], E Ulmer[3], C Kleefisch[1], L Umfleet[4]
[1]Medical College of Wisconsin, Milwaukee, WI, [2]University of Notre Dame, Notre dame, IN, [3]Rhodes College, Memphis, TN, [4]Medical College of Wiscosnin, Milwaukee, WI

Purpose
Amnestic (aMCI) and non-amnestic MCI (naMCI) are presumed to be distinct neurobehavioral syndromes with the former at greater risk for conversion to Alzheimer's disease (AD) and the latter reflecting a more heterogenous group. Of the naMCI, individuals with histories of vascular risk factors and frontosubcortical profiles on formal cognitive testing are presumed to be at greater risk for vascular cognitive impairment and vascular dementia. The purpose of this study was to compare the severity of cerebrovascular disease between aMCI with consolidation deficits and naMCI with frontosubcortical dysfunction.
Materials and Methods
79 individuals participated in a comprehensive neuropsychological evaluation and brain MRI. Participants were divided into amnestic (N=43; no benefit from recognition) and non-amnestic profile (N=36; intact memory, encoding-based weaknesses, or retrieval-based weaknesses). Of the non-amnestic profiles,

frontosubcortical profiles were identified (N=19; weaknesses in retrieval-based memory, processing speed, and executive functioning). Cerebrovascular disease load was assessed by a neuroradiologist using the standard Fazekas grading scale to determine low (grade 0 and 1) (N=55) vs. high (grade 2 and 3) disease burden (N=24).

Results

Chi-square analysis revealed no difference in the disease load between aMCI vs. naMCI (x2 (N=79)=0.273, p=0.601) and aMCI vs. frontal-subcortical neuropsychological profiles (x2 (N=64)=0.03, p=0.863).

Conclusions

By interruption of the connections of prefrontal cortex, cerebrovascular disease may cause naMCI. However, in the current study, cerebrovascular disease did not differ between aMCI and naMCI groups. It is possible that there is unknown disease overlap between groups and future research is needed to better appreciate naMCI with and without significant vascular burden.

3130

Correlating MR Imaging Features of Small Cell Lung Cancer Brain Metastases with Patient Outcomes With and Without Prophylactic Cranial Irradiation.

T Richards[1], R Devita[1], E Kikano[1], N Ramaiya[1]
[1]University Hospitals Cleveland Medical Center, Cleveland, OH

Purpose

The purpose of this study is to correlate MR imaging characteristics of brain metastases in patients with small cell lung cancer (SCLC) with patient survival outcomes after either prophylactic cranial irradiation (PCI) or therapeutic whole brain radiation (WBRT).

Materials and Methods

In this observational study, the MRI brain examinations of twelve patients with SCLC that developed imaging findings consistent with brain metastases were evaluated. MR imaging characteristics including diffusion weighted imaging were characterized for patients at the time of initial development of brain metastases including T1 and T2 weighted signal, surrounding edema, hemorrhage, diffusivity, location, size, and number of lesions. Progression free survival (PFS), overall survival (OS), and time to local progression (TLP) in the brain were calculated for these patients. At time of presentation there will be a significantly expanded cohort of patients that will be analyzed and included in the results of the study.

Results

Of the 12 patient evaluated in this preliminary data, the patients that received PCI had the longest mean overall survival of 25.5, however these patient also had a shorter mean time to local progression of 3.8 months. In patients treated with therapeutic whole brain radiation therapy (WBRT), there was a trend towards a shorter mean time to local progression in patients with T2 hypointense lesions and basal ganglia metastases.

Conclusions

In patients with SCLC that developed brain metastases, different conventional and diffusion weighted MRI characteristics of their metastases may provide imaging biomarkers to predict which patients will respond well to radiation therapy and help guide clinical management.

	% of patients	Time in month		
		Overall survival	Progression free survival	Time to local progression
Brain mets after PCI (n=4)	33	25.5	12.2	3.8
T2 hypointense signal	25	31.9	21.9	8.6
Diffusion restriction	75	28.9	14.5	4.6
Marked surrounding edema	25	31.9	21.9	8.6
Cerebral hemisphere mets	100	25.5	12.2	3.8
Cerebellar mets	50	80.3	44.2	15.5
Basal ganglia mets	25	22.5	8.1	1.4
Brainstem	50	27.4	10.8	2.6
Brain mets treated with WBRT (n=5)	42	13.5	7.6	7.0
T2 hypointense signal	60	13.4	8.9	6.4
Diffusion restriction	80	14.8	8.4	8.4
Marked surrounding edema	60	14.2	8.1	7.0
Cerebral hemisphere mets	100	13.5	7.6	7.0
Cerebellar mets	80	15.8	8.9	8.9
Basal ganglia mets	40	6.6	5.4	5.4
Brain mets not treated with radiation (n=3)	25	21.3	15.8	5.7
T2 hypointense signal	33	39.5	30.3	9.3
Diffusion restriction	100	21.3	15.8	5.7
Marked surrounding edema	66	20.5	15.9	5.0
Cerebral hemisphere mets	100	21.3	15.8	5.7
Cerebellar mets	33	22.8	15.6	7.2
Basal ganglia mets	33	22.8	15.6	7.2

Table 1. The survival data for small cell lung cancer patients who developed brain metastases according to some of the imaging characteristics of their lesions and the type of cranial radiation they received.

(Filename: TCT_3130_Table1.jpg)

3198

Crossover Intraindividual Comparison of Ionic and Non-ionic Macrocyclic GBCA in Orthotopic Glioblastoma Model: Pathologic Correlation of DCE Characteristics at 9.4T MRI

C Choi[1], K Yi[1], J Cho[2], S Cha[3]
[1]Chungbuk National University Hospital, Cheongju-si, Chungchungbuk-do, [2]Chungbuk National University, Cheongju-si, Chungchungbuk-do, [3]Chungbuk National University, College of Medicine and Medical Research Institute, Cheongju-si, Chungchungbuk-do

Purpose
Dynamic contrast enhancement (DCE) patterns of DCE-MRI depending on chelate ionicity of macrocyclic gadolinium-based contrast agents (GBCA) are expected to be different in brain glioblastoma. This experiment aimed to intra-individually compare the ionic and non-ionic macrocyclic GBCAs in orthotopic human glioblastoma model with DCE-MRI.
Materials and Methods
The orthotopic human glioblastoma model was established stereotactically (U373-MG, 1 x 106 cells) in 92 nude mice (BALBc nude, female, 18~20g). DCE-MRI (9.4-T, Varian Inc., Palo Alto, CA) scans were performed in 8~13 days tumor incubation period. The crossover DCE-MRI scans (T1W-GRE sequence, TR/TE = 160.0/2.5msec, flip angle = 30o, 30 dynamic, every 1 minute up to 30) were performed with two different macrocyclic GBCAs 6 hours apart in 65 mice (ionic: n=41, nonionic: n=44) including crossover set (n=20). DCE-parametrical maps by model free and pharmacokinetic model (TOFT by Nordic) were compared. Ktrans and Ve maps were compared with Ki67 proliferation index (Ki67index, on Ki67 stain) and microvessel counts (MVC, on CD31 stain) voxel-wisely.
Results
Time intensity curves were different depending upon the ionicity of GBCA. The mean relative SI of tumor were washed-in slowly reached high in a short period of time, and washed-out rapidly in ionic GBCA both of total set ($p < 0.001$) and crossover set ($p < 0.001$) (figure 1). The Ve of ionic was small significantly by voxel wise comparison in 20 crossover set ($p < 0.01$) (table 1). Ki67index was more correlated with Ve of ionic GBCA ($p<0.01$). MVC was also more correlated with Ktrans and Ve of ionic GBCA ($p<0.01$) (figure 2).
Conclusions
DCE patterns of ionic macrocyclic GBCA were different in glioblastoma DCE MRI and reflected tumor pathology more than nonionic one. This suggests possible advantage of ionic GBCA in characterizing globlastoma in patients in DCE-MRI study.

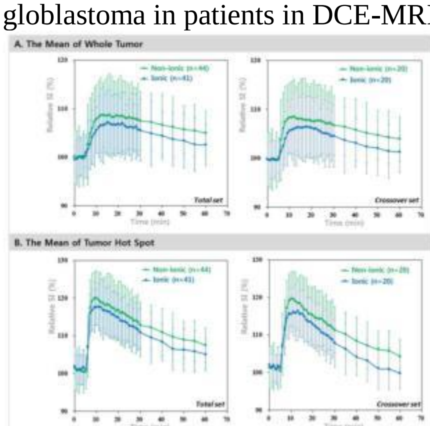

Figure 1. Time intensity curves after contrast media injection: DCE patterns were different depending upon the ionicity of GBCA. The mean relative SI of tumor (both entire tumor (A) and hot spots (B)) and total set (left column) and crossover (right column) showed same patterns.

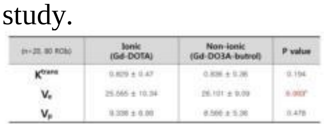

(n=20, 80 ROIs)	Ionic (Gd-DOTA)	Non-ionic (Gd-DO3A-butrol)	P value
K^{trans}	0.829 ± 0.47	0.836 ± 0.36	0.194
V_e	25.665 ± 10.34	26.101 ± 9.09	0.003*
V_p	9.338 ± 6.00	8.566 ± 5.36	0.479

Table 1. Voxel-wise comparison of parametrical maps by pharmacodynamic modeling (TOFTs by Nordic): The V_e of ionic GBCA was small significantly in crossover set ($p < 0.001$)

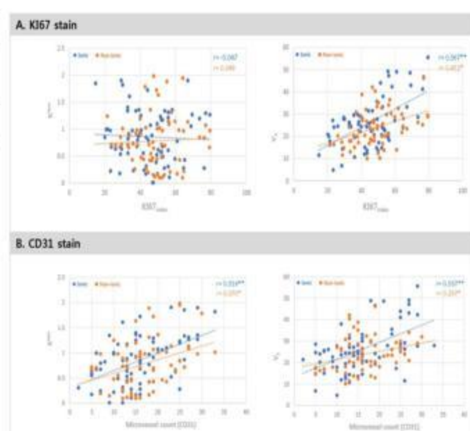

Figure 2. Pathologic correlations between parametrical maps and $KI67_{index}$ and microvessel counts: $Ki67_{index}$ was more correlated with V_e of ionic GBCA ($p<0.01$). MVC was also more correlated with K^{trans} and V_e of ionic GBCA ($p<0.01$)

(Filename: TCT_3198_ASONR_2019_fig.jpg)

3630

CT Scan Following Orbital Exenteration: Lesion Mimic Tumor Recurrence

S Elkhamary[1]
[1]*Manosura university Faculty Of Medicine, Egypt, Riyadh, Riyadh*

Purpose
To describe CT scan findings following orbital exenteration in 27 patients and to identify the factors involved in the development of post exenteration hyperostosis
Materials and Methods
review of preoperative and postoperative CT imaging of the orbits in 27 patients ranging in age from 33 to 99 years, who underwent unilateral orbital exenteration. Data regarding patient demographics, surgical procedure, clinical diagnosis were obtained. The relationship between hyperostosis and postoperative time, gender, age, adjuvant radiotherapy, and cavity coverage was evaluated by multivariate stepwise logistic regression
Results
Seventeen (73.9 %) orbits had postoperative orbital hyperostosis. No soft tissue masses were detected in the affected orbits except in 2 cases with tumor recurrence. The only factor associated with hyperostosis was immediate intraoperative socket rehabilitation (odds ratio = 0.13, 95% confidence interval: 0.01-0.89). There was an 87.0% lower chance of hyperostosis in patients whose socket was covered with musculocutaneous flaps. Sequential CT scans showed that orbital hyperostosis followed a specific pattern. Initially, bone thickening appeared as either uniform or undulating endo-osteal minimal thickening along the roof and then on the lateral and medial walls. More advanced hyperostosis had a laminated/lamellated appearance progressing to homogeneous and diffuse circumferential bone thickening. New bone formation and bone overgrowth were late findings. Hyperostosis extended to involve the adjacent facial bone, more obviously on the maxilla. Some patients had minimal thickening of the adjacent frontal and squamous temporal bone. Over-pneumatization of the paranasal sinuses was evident in all cases of hyperostosis.
Conclusions
Development of hyperostosis following exenteration is not rare. Radiologists and surgeons should be aware of the need to monitor the orbital healing process closely to avoid misdiagnoses of tumor recurrence/radionecrosis or infection. Obliteration of the orbital cavity with musculocutaneous flaps significantly reduces the chances of bone hyperostosis

3093

CT-Angiography and CT-Perfusion in Patients with Aneurysmal Subarachnoid Hemorrhage - Correlation with Cerebrospinal Fluid Markers of Blood-Brain Barrier Degradation and Clinical Outcomes

Y Oh[1], S Glynn[1], N Smith[2], A Segal[3], A Gupta[4], P Sanelli[5], J Ivanidze[6]
[1]*Weill Cornell Medicine, New York, NY,* [2]*N/A, N/A,* [3]*NewYork-Presbyterian Hospital - Weill Cornell, New York, NY,* [4]*WEILL CORNELL MEDICAL COLLEGE, NEW YORK, NY,* [5]*NORTHWELL HEALTH NSUH, MANHASSET, NY,* [6]*N/A, New York, NY*

Purpose
The lack of quantitative clinical and imaging-based biomarkers poses a major limitation in early detection and monitoring of aneurysmal subarachnoid hemorrhage (aSAH) complications, including cerebral vasospasm (VS) and delayed cerebral ischemia (DCI)-manifestations of blood-brain barrier (BBB) dysfunction. Matrix metallopeptidase-9 (MMP-9) degrades tight junctions, thereby compromising BBB

integrity. Our purpose was to prospectively correlate cerebrospinal fluid (CSF) MMP-9 levels with clinical and radiological measures of disease severity and BBB dysfunction. Furthermore, we evaluated the relationship between MMP-9 and AQP-4, a glial water channel protein implicated in BBB disruption.

Materials and Methods

28 prospectively enrolled aSAH patients underwent serial axial shuttle CT-Angiography (CTA) and CT-Perfusion (CTP) per clinical standard-of-care. MMP-9/AQP-4 proteins were analyzed in CSF collected via ventriculostomy catheter placed for intracranial pressure measurement. CTA reports were assessed for presence of VS in segments 1-2 of the bilateral anterior, middle and posterior cerebral arteries and basilar artery, and scored as none, mild, moderate, severe VS (1-4). Patients were stratified into "none-mild" (sum scores<20 for all CTA examinations; Hunt Hess (HH)1-3) and "moderate-severe" (scores≥20; HH1-2) cohorts. CTP data were post-processed into quantitative BBB-permeability maps using Olea-Sphere software (Olea-Medical, France). Mann-Whitney-tests and Spearman-Rank correlations were performed.

Results

MMP-9 CSF levels correlated significantly with clinical scores (HH3-5= 12.77, HH1-2= 5.76 ng/mL, p=0.039), degree of VS (moderate-severe= 13.45, none-mild= 6.38 ng/mL, p=0.047), and BBB dysfunction (CTP WASHIN rs= 0.42, p=0.027) (Figures 1A-C). Furthermore, there was a moderate positive correlation (rs=0.44, p=0.019) between MMP-9 and AQP-4 (Figure 1D).

Conclusions

Elevated CSF MMP-9 levels correlated with presence of moderate-severe VS, clinical disease severity, and BBB dysfunction in this prospective aSAH cohort, while it also exhibited moderate correlation with AQP-4 levels. This pilot study lays the groundwork for future trials exploring a potential role for MMP-9, AQP-4 and advanced imaging, ultimately developing a multimodal biomarker in aSAH.

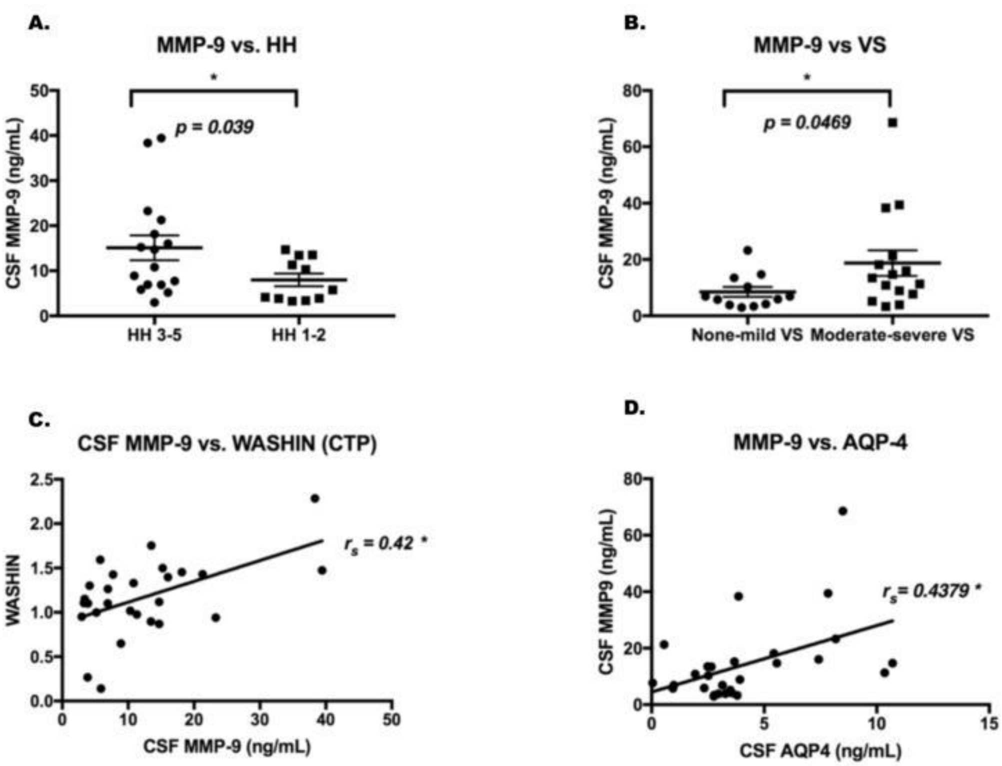

Figure 1: CSF MMP-9 Correlation with Hunt Hess Scores, Cerebral Vasospasm, BBB Dysfunction (CTP WASHIN), and AQP-4. Top Left (A): Patients with HH 3-5 had significantly higher CSF MMP-9 levels compared to patients with HH 1-2 (12.77 versus 5.76 ng/mL, p=0.039). Top Right (B): Patients with moderate-severe VS had significantly higher CSF MMP-9 levels compared to patients with mild-moderate VS (13.45 versus 6.38 ng/mL, p=0.047). Bottom Left (C): CSF MMP-9 Levels exhibited a moderate positive correlation with WASHIN, a CTP BBBP parameter (rs= 0.42, p=0.027). Bottom Right (D): CSF MMP-9 levels exhibited a moderate positive correlation with CSF AQP-4 Levels (rs= 0.44, p=0.019).

(Filename: TCT_3093_ASNR_Figure_YunaOh.jpg)

2808

Deep Learning Algorithm for Detection of Intracranial Aneurysms on Computed Tomography Angiography

D Plasto[1], K Shpanskaya[2], L Kim[2], R Jabarkheel[2], M Kuwabara[3], K Yeom[2]
[1]St. Joseph's Hospital and Medical Center, Phoenix, AZ, [2]Stanford University, Palo Alto, CA, [3]Barrow Neurological Institute, Phoenix, AZ

Purpose
Despite recent advances in the use of deep learning for automated diagnosis in medical imaging, the potential for clinician augmentation has been relatively unexplored. We propose applying deep learning to generate model segmentations, or precise voxel-by-voxel predictions, of intracranial aneurysms and to augment clinician decision-making.
Materials and Methods
A 3-D convolutional neural network architecture was developed using a training set of 611 head CT Angiography exams to generate aneurysm segmentations. Exams used had at least one clinically significant, non-ruptured intracranial aneurysm. Exams with hemorrhage, ruptured aneurysm, pseudoaneurysm, arteriovenous malformation, or surgical hardware were excluded. A test set of 115 exams was used to generate segmentation outputs from this support model, which were provided to clinicians. Eight board-certified clinicians diagnosed the presence of aneurysm on the test set twice, once with and once without model augmentation, in randomized order with a 14-day washout period.
Results
Sensitivity, specificity, accuracy, and inter-rater agreement for aneurysm diagnosis were measured and compared prior to and following model augmentation. Augmentation with segmentation predictions resulted in statistically significant improvements in sensitivity, specificity, and inter-rater agreement when compared with no augmentation. Mean sensitivity for aneurysm detection improved from 0.831 to 0.890 (adjusted p-value: 0.035), mean accuracy improved from 0.893 to 0.932 (adjusted p-value: 0.046), and inter-rater agreement (Fleiss' kappa) improved from 0.799 to 0.859 (adjusted p-value: 0.046).
Conclusions
Artificial intelligence is an undeniable part of the future of neuroradiology, and the development, integration, and ownership of the technology is of utmost importance to those who practice it. Our study results suggest that segmentation models for aneurysm detection offer a promising approach for integrating deep learning into clinical workflows. The benefits in diagnostic accuracy as a result of this integration have the opportunity to not only improve upon the ultimate goal of patient care, but also positively affect the neuroradiologist's speed, satisfaction and confidence.

3482

Deeper Levels of Systemic Hypotension Increase AVM Retropermeation during Simulated Endovascular TRENSH—Transvenous Retrograde Nidus Sclerotherapy under Controlled Hypotension: Hemodynamic Analysis Using a Computational Network Model

M Jain[1], T Massoud[1]
[1]Stanford University School of Medicine, Stanford, CA

Purpose
TRENSH is a proposed new concept for endovascular treatment of brain arteriovenous malformations (AVMs). Using a novel biomathematical AVM model, we tested the hypothesis that greater degrees of

systemic hypotension (Syst-hypo) could enhance retrograde nidus permeation extent while averting rupture risk during a simulated TRENSH procedure.
Materials and Methods
The AVM model was a theoretical electrical circuit with four arterial feeders, three draining veins (DV1-3), and a 3D nidus of 97 interconnected plexiform and fistulous vessels. We assigned known values of pressure to vessels outside the AVM nidus and used network analysis to determine consequent pressure and flow within each nidus vessel. We simulated TRENSH by first inducing Syst-hypo and then introducing a retrograde 'injection' pressure (Inj-P) through a DV. We performed 36 TRENSH simulations using different combinations of Syst-hypo, DVs, and injection pressures. We varied systemic pressures between 74mmHg (normotension), 70 mmHg (minor Syst-hypo), 50mmHg (moderate hypotension), and 25mmHg (profound hypotension). Inj-Ps were at 10, 20, and 30mmHg.
Results
Deeper Syst-hypo allowed increasing retrograde permeation using stronger transvenous Inj-Ps. Nidus rupture was avoided if the transvenous Inj-P did not cause intranidal pressures to exceed those at baseline normotension. Initial induction of moderate or profound Syst-hypo caused drops in intranidal vessel pressures between 0.1-26mmHg and 0.1-20mmHg, respectively. In subsequent TRENSH simulations using Inj-P of 20 mmHg through DV1, there was 56% and 100% retrograde filling of the nidus, at moderate and profound Syst-hypo, respectively. Nidus decompression during injection occurred via the other DVs.
Conclusions
Biomathematical models offer approaches to investigate complex intranidal AVM hemodynamics that are challenging to study clinically. Our theoretical results support the feasibility of TRENSH established previously in a pig AVM model. This technique may allow future sclerotherapy of large AVMs while reducing the risks of nontarget arterial embolization. Continued investigations of this novel neuroendovascular technique are ongoing prior to clinical translation.

2579

Dural Venous Sinus Stenting for the Treatment of Papilledema in Idiopathic Intracranial Hypertension

J Oros[1], M Mian[2], J Hise[1]
[1]Baylor University Medical Center, Dallas, TX, [2]Texas A&M College of Medicine, Dallas, TX

Purpose
This study examines the effectiveness of using dural venous sinus stenting for the treatment of papilledema in patients with idiopathic intracranial hypertension and dural venous sinus stenosis.
Materials and Methods
21 patients (20 female, 1 male) with papilledema secondary to idiopathic intracranial hypertension presented to a single center between 3/2016-8/2018 for dural venous sinus stenting. These patients had a mean age of 36.4 (range 19-53) with evidence of papilledema on initial fundoscopic examination. MR or CT venogram was then performed demonstrating dural venous sinus stenosis; these patients were then referred to the radiology department for catheter venogram and dural sinus stenting. Venous pressure measurements were taken proximal to and distal to the stenosed section before and after stent deployment and were reported as a pressure gradient in mmHg. All procedures were performed at a single center in a biplane neurointerventional suite. Follow-up fundoscopic examinations were subsequently performed by the referring clinician.
Results
Mean pre-treatment pressure gradient across the stenosed section was 13.3 mmHg (range 7-24 mmHg). Mean post-treatment pressure gradient section was 1.3 mmHg (range 0-4), with a reduction in the mean pressure gradient by 12 mmHg. No major or minor complications were reported after the procedures.

Follow up fundoscopic examination demonstrated interval resolution of papilledema in all patients. 2 patients had late recurrence (greater than 1 year after initial procedure) of their papilledema; repeat venography on these patients demonstrated stenosis distal to the existing stent and were subsequently re-treated with stenting.
Conclusions
Dural venous sinus stenting is a safe and effective treatment for papilledema in appropriately selected patients with idiopathic intracranial hypertension and dural venous sinus stenosis. This single-center study demonstrates a decrease in both mean transstenosis pressure gradient and papilledema after dural venous sinus stenting. Two patients had late recurrence of their papilledema secondary to re-stenosis distal to the previously placed stent.

(Filename: TCT_2579_CollageFINAL.jpg)

2300

Efficacy of a Modern AVM Classification System that Directs Curative Endovascular Therapies Accurately

W Yakes[1]
[1]The Yakes Vascular Malformation Center, Englewood, CO

Purpose
To determine if AVM angioarchitecture characteristics can be predictive and direct specific curative endovascular procedures accurately and consistently to cure high-flow malformations.
Materials and Methods
Angiographic analysis of high-flow AVMs determined 4 major angioarchitectures. Type I: Direct arterial/arteriolar to vein/venule connection; e.g., as commonly seen in pulmonary AVF, congenital renal AVF, etc. Type II: Arterial/arteriolar connections to a "nidus" that then have several out-flow veins with no intervening capillary beds in any of the vascular interconnections. Type IIIa: Arterial/arteriolar connections to an aneurysmal vein ("nidus" is the vein wall) that drains into a dominant out-flow vein with no intervening capillary bed in these connections. Type IIIb: Same angioarchitecture as Type IIIa, except that there are more than one (several) out-flow veins. Type IV: "Infiltrative" form of AVM whereby innumerable micro-arteriolar branches fistulize through a tissue (e.g., ear AVMs) totally infiltrating it, shunting into multiple out-flow veins. Capillary beds also exist in the tissue and are admixed with the innumerable AVFs. Without the capillaries the tissue could not be viable, therefore must be present.
Results
Type I: Can be effectively treated with mechanical devices; e.g., coils, Amplatzer Plugs, etc. Type II: Can be effectively treated with ethanol embolization; trans-cath and direct puncture. Type IIIa: Can be

effectively treated by transcatheter ethanol, retrograde vein catheter access or direct puncture access of the aneurysmal vein and treatment with ethanol and coils, or even by coils alone. Type IIIb: Can be effectively treated as above, but can be more challenging by the vein route as more veins (not a single out-flow vein) require closure. Type IV: Can be effectively treated by transcatheter or direct puncture of the innumerable microfistulous AVFs by embolization with 50% -50% ethanol non-ionic contrast mixture.

Conclusions

This newly reported classification system has a direct impact on determining the curative endovascular and direct puncture embolization procedures and also determines the embolic agents that will successfully treat complex AVMS in the body.

3335

Follow-up of MR Vessel Wall Imaging Findings in Patients with Primary Central Nervous System Vasculitis

E Obusez[1], J Song[2], D Montes[1], J Romero[1]

[1]*Massachusetts General Hospital, Boston, MA,* [2]*Hospital of the University of Pennsylvania, Philadelphia, PA*

Purpose

Vessel wall magnetic resonance imaging (VWI) is a technique that can differentiate between intracranial vasculopathy (1). Several VWI studies have described enhancement of arterial wall segments in patients with primary central nervous system (PCNS) vasculitis (2, 3). The follow-up VWI changes of these enhancing arterial wall segments and relationship with disease activity while undergoing immunosuppressive management have not been established. The aim of the study was to investigate the relationship of VWI enhancement and clinical symptoms in patients with PCNS vasculitis undergoing immunosuppressive management over a follow-up period.

Materials and Methods

A retrospective study was conducted on 7 patients with biopsy-proven, or clinical-confirmed diagnosis of PCNS vasculitis from a database of 81 patients that underwent vessel wall imaging from January 2017 to June 2018. The VWI protocol included pre and post-contrast 3D SPACE T1-weighted sequences, TOF-MRA and routine sequences. VWI characteristics of enhancement and wall thickening were collected at initial imaging and at follow-up (if imaging was performed). The VWI findings were graded by consensus between two neuroradiologists.

Results

Four patients had follow-up VWI, with a mean follow-up period of 134 (R,13-255) days. The initial VWI findings were short segment, multifocal concentric wall thickening and enhancement in the anterior and/or posterior circulation. These 4 patients were managed on immunosuppression with high dose prednisone and/or mycophenolate throughout the follow up period. The initial enhancing arterial segments showed persistent enhancement in the 4 patients over the follow-up period (Figure 1). Clinical symptoms were either decreased or worsened over the follow up period. Figure 1: Patient 1 - 55-year-old male with a history of PCNS presented with multiple small acute infarcts and right thalamocapsular hemorrhage (not shown). On initial VWI (A, B), axial post-contrast 3D-SPACE T1WI (A) showed multifocal areas of concentric enhancement in the anterior (not shown) and posterior circulation, and acute infarcts (white arrows) on axial DWI (B). Follow-up at 255 days (C, D), showed persistent enhancement of the initial enhancing segments (C) without acute infarcts.

Conclusions

Our VWI results appear to show that enhancement of arterial segments persists, despite variation in clinical symptoms over the follow-up period, and while on immunosuppression therapy. The clinical implications of these findings are unclear, and a larger prospective study maybe warranted.

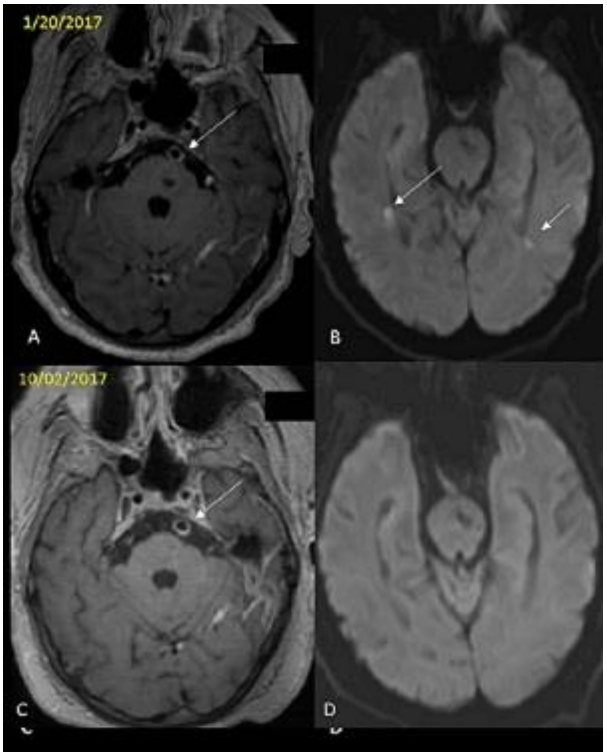

(Filename: TCT_3335_Figure1ASNR2019TemporalVesselwallimaging300dpi.jpg)

2828

Free Text Radiology Reports for Cancer Surveillance: How Often are Correct Recommendations Made based on ACR NI-RADS?

J Reese[1], J Mitsky[2], U Rawal[3], A Huang[4], X Wu[1], A Aiken[5]
[1]Emory University School of Medicine, Atlanta, GA, [2]Radiology Partners, Portland, OR, [3]Radiology Partners, El Segundo, CA, [4]Radpartners, El Segundo, CA, [5]Emory University Hospital, Atlanta, GA

Purpose
The Neck Imaging Reporting and Data System (NI-RADS) surveillance template for head and neck cancer was designed to steam-line communication for suspicion of recurrence and management recommendations. The purpose of this study was to evaluate free-text radiology reports from private practices for management recommendations of abnormal findings for treated head and neck cancer and compare to standards based on NI-RADS.
Materials and Methods
Contrast Enhanced CT (CECT) and PET/CT free-text reports from 16 private practices by 32 radiologists were analyzed for abnormalities and whether correct recommendations were offered. Inclusion criteria required the imaging to be done post-treatment. Findings concerning for recurrence were categorized as primary site, lymph node, or distant. Note was made whether management recommendation was offered, including direct inspection, short term follow up, or biopsy. Recommendation rates and accuracy of the recommendations based on ACR NI-RADS were recorded.
Results
Of the 84 reports, 43 met inclusion criteria requiring imaging be post-treatment. 18 abnormalities were identified including 4 primary site, 5 lymph node, and 9 distant. Recommendation rates were 0% for primary site, 80% for lymph node, and 33% for distant. In 50% of the primary site and lymph node cases, recommendations corresponded to the appropriate NI-RADS category. In 2 of the 4 primary site cases

where no recommendation was offered, a NI-RADs category of 3 would have been appropriate. In the lymph node case where no recommendation was offered, a NI-RADS category of 2a would have been appropriate.
Conclusions
In this preliminary multi-center retrospective review, we show rates at which radiologists offer correct management recommendations in their free-text reports for imaging abnormalities discovered during surveillance for treated head and neck cancer. The next phase will be to analyze if correct recommendation rates improve after a structured reporting template based on the NI-RADS lexicon is implemented.

2326

Functional MRI Shows Altered Task-Induced Deactivation of the Default Mode Network in Glioma Patients

Y Maniar[1], K Peck[1], M Jenabi[1], M Gene[1], A Holodny[1]
[1]Memorial Sloan Kettering Cancer Center, New York, NY

Purpose
The default mode network (DMN), consisting of the medial prefrontal cortex (mPFC), posterior cingulate cortex (PCC), and bilateral inferior parietal lobules (RIPL and LIPL), is a functional brain network that normally deactivates during tasks requiring external attention(1). Although many neurological conditions disrupt this pattern(2-4), no studies have examined task-based deactivation of the DMN in glioma patients. We investigated DMN deactivation with task-based functional MRI (tb-fMRI) and DMN connectivity with resting-state fMRI (rs-fMRI) in glioma patients, including the effects of tumor location, hemisphere, and grade on DMN deactivation and connectivity.
Materials and Methods
We retrospectively analyzed 10 healthy controls and 30 glioma patients, separated by tumor location (posterior DMN=14, anterior DMN=8, outside the DMN=8), hemisphere (right-sided=7, left-sided=23), and grade (II=11, III=7, IV=12). Seed-based correlation analysis was performed on each subject's language tb-fMRI data. The region of the PCC negatively correlated with the task paradigm was used to generate tb-fMRI and rs-fMRI correlation maps in order to measure functional connectivity between the PCC and the other DMN regions. We statistically compared average correlation values in each DMN region between patients and controls using the Mann-Whitney U test.
Results
PCC deactivation was significantly decreased with posterior DMN tumors ($p<0.0001$) and tumors outside the DMN ($p=0.04$), but not with anterior DMN tumors ($p=0.15$). mPFC connectivity was significantly decreased with anterior (tb-fMRI $p<0.001$, rs-fMRI $p<0.01$) and posterior (tb-fMRI $p=0.03$, rs-fMRI $p=0.03$) DMN tumors, but not with tumors outside the DMN (tb-fMRI $p=0.08$, rs-fMRI $p=0.25$). RIPL connectivity was significantly decreased only with right hemisphere tumors (tb-fMRI $p=0.04$, rs-fMRI $p=0.03$); LIPL connectivity was significantly decreased with left hemisphere tumors in tb-fMRI only ($p=0.04$). No significant effect was observed between grades II and III/IV.
Conclusions
The location-dependent decrease in task-based DMN deactivation and functional connectivity in glioma patients suggests that tumors near posterior DMN regions have a greater impact on the DMN.

2705

Gadolinium Deposition within the Brain 10 years After Undergoing Up to 26 Monthly Triple-Dose Gadopenetate Dimeglumine in Multiple Sclerosis Patients.

J DeBevits[1], D Bageac[1], L Wang[1], R Munbodh[1], L Wolansky[1], D Karimeddini[1], R Naismith[2], S Dhib-Jalbut[3]
[1]UConn Health, Farmington, CT, [2]Washington University in St. Louis, St. Louis, MO, [3]Rutgers University, Newark, NJ

Purpose
It has been well-documented by both radiologic and postmortem studies that gadolinium (Gd) deposition likely occurs in the brain even in patients with normal renal function, but data regarding the long-term presence of Gd within the brain are not readily available. Our aim was to study gadolinium deposition in patients receiving up to 26 monthly triple-doses of gadopentetate dimeglumine (over 70 dose-equivalents in some cases) as part of a randomized controlled study for the evaluation of drug efficacy in multiple sclerosis. Monthly MRI examinations using this high dose gadolinium protocol provided an opportunity to study Gd deposition within the brain. This study provided the additional opportunity to study patients longitudinally 8 years after the cessation of gadolinium (10 years after initiation). Thus, we were able to assess not only for Gd deposition, but also washout versus retention over a prolonged period.
Materials and Methods
The data from 18 MS subjects who received monthly triple-doses (0.3 mmol/kg) of gadopentetate dimeglumine over 12-24 months (mean number of doses 58, median 52.5, range 30-75) were analyzed. MRIs were evaluated at baseline (Y0), year one (Y1), year two (Y2) and at year 10 (Y10) following the start of monthly triple-dose Gd and used to evaluate Gd retention. For each subject, a manual segmentation of ROIs of the globus pallidus (GP) was carried out by a radiologist using T2-weighted images at a single timepoint using the open-source software ITK-SNAP. T1-weighted precontrast images for each subject were then registered and mean voxel signal intensity (SI) within each overlay of the ROI was measured at each time point using an automated algorithm without normalization.
Results
The mean(SD) signal intensity of the globus pallidus at each time point were: Baseline=505.96(35.3), Year 1=523.36(60.49), Year 2=523.42(26.28), LTFU=536.38(44.83) (Fig. 1A). With analysis using mixed model for repeated measures, we found a significant increase of signal intensity over time in the globus pallidus ($F=3.35$, $p=0.04$). The median signal intensity of the globus pallidus was higher at Y10 than at Y1, but not higher than that of Y2 (Fig. 1B)
Conclusions
The results suggest that deposition and subsequent retention of gadolinium is long-term and possibly can be permanent under certain conditions. It is noteworthy that GP mean SI continued to rise after the cessation of the high-dose Gd protocol of our study. We suspect the skeletal system, another documented site of Gd deposition in the literature, may serve as a reservoir and thus "exposure" of the brain to Gd may extend far beyond its administration for medical imaging purposes.

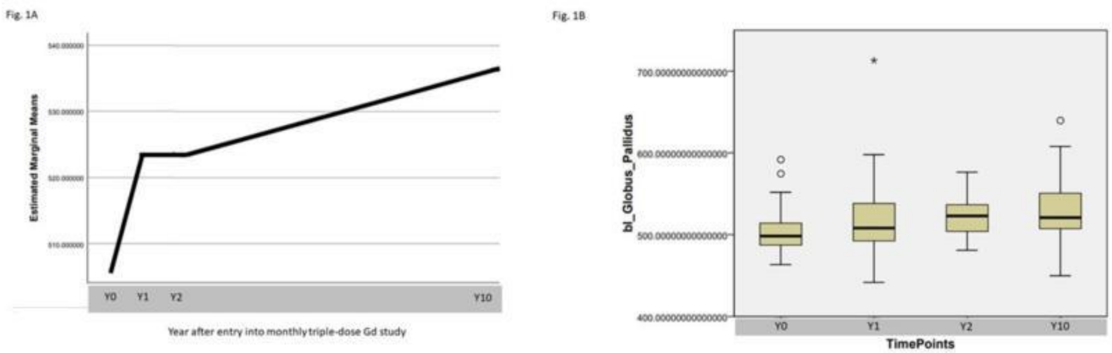

(Filename: TCT_2705_GdASNR.JPG)

2241

Gadolinium-Enhanced 3D-FLAIR MRI of Uveitis

D Titelbaum[1], L Rifkin[2], G Velez[3], R Engisch[4]
[1]Shields Health Care, Brockton, MA, [2]New England Eye Center, Boston, MA, [3]Central Mass Retina and Uveitis Center, Worcester, MA, [4]Luzerner Kantonsspital, Lucerne, Switzerland

Purpose
FLAIR MRI can identify low-concentration Gd (1). Gd-enhanced 3D-FLAIR has been shown to identify leptomeningeal enhancement in such entities as multiple sclerosis (2) and Susac's Syndrome (3), not visible on T1W, thought to be due to inflammation-mediated blood-brain barrier disruption resulting in leakage of low-concentration of Gd. We sought to determine if Gd-3D-FLAIR MRI can identify disruption of blood-retinal barrier in the setting of uveitis.
Materials and Methods
3 patients with 5 globes affected by clinically documented uveitis underwent Gd-3D-FLAIR MRI using CUBE or VISTA FLAIR at 1.5T or 3T. The unaffected globe in one patient with unilateral uveitis and 3 age-matched patients without uveitis who underwent Gd-3D-FLAIR MRI for other indications were selected as controls. In each patient with uveitis, all 4 posterior ocular quadrants were assessed for ocular enhancement on MRI, and compared to areas of inflammation seen at slit-lamp, fundoscopy, OCT, or retinal or choroidal angiography.
Results
Two globes that were assessable by ophthalmological exam showed inflammation in 6/8 quadrants by ophthalmology and 8/8 revealed enhancement on Gd-3D-FLAIR MRI. In 3 globes, ophthalmological assessment was not possible due to vitreal opacification, but MRI showed enhancement in 6/12 quadrants. Additionally, 4/5 globes MRI revealed enhancement in the anterior inferior globe, outside of the limits of visualization by ophthalmological methods. No enhancement was seen in any quadrant on Gd-2D-T1W fat-suppressed imaging. The 7 control globes showed no abnormal enhancement on MRI.

Conclusions
We provide preliminary evidence that Gd-3D-FLAIR MRI can identify uveitis, presumably due to disruption of blood-retinal barrier resulting in leakage of low concentration Gd. This method may be useful to confirm inflammation seen on clinical exam, to identify inflammation when ophthalmological exam is not possible in cases of severe anterior chamber inflammation or vitreal opacification, and to visualize inflammation anterior to the limits of ophthalmological techniques.

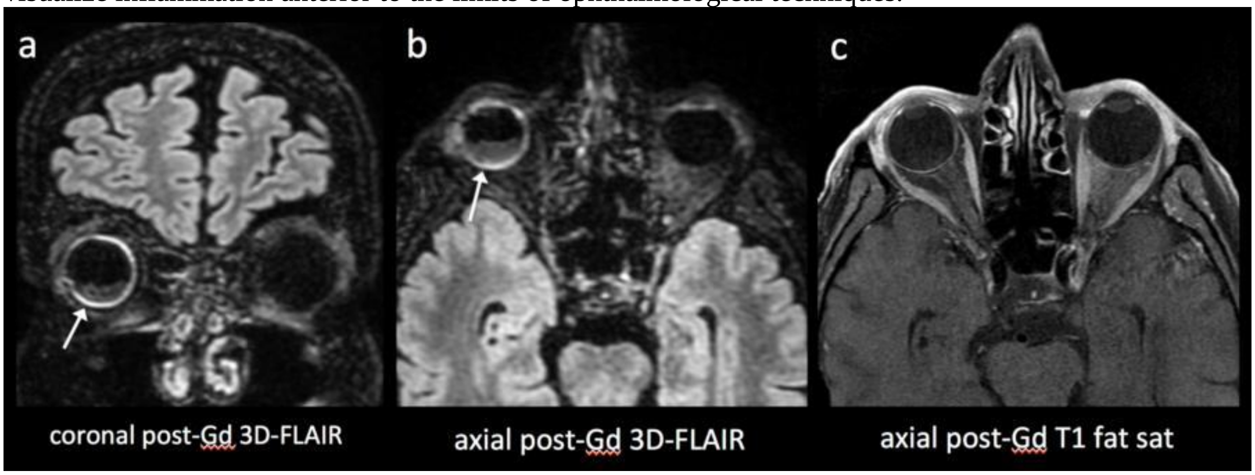

(Filename: TCT_2241_uveitis.jpg)

3464

Going Against the Norm: A Novel Approach for the Creation of a Normative Dataset for Clinical Brain SPECT

L Quandt[1], S Quint[1]
[1]*CereMetrix Corp., Littleton, CO*

Purpose
Quantitative analysis of single photon emission computed tomography (SPECT) brain perfusion imaging is dependent on comparison to normal control datasets [1-3], which are heavily protected and difficult to produce. As a result, the number of people per commercially owned SPECT brain dataset are rather small, ranging from 35 to 90 subjects. This study investigated an alternative approach to traditional normative databases by creating a "composite average" that combines SPECT brain scans from a large number of clinical patients instead of a few healthy individuals. We hypothesized that a large heterogeneous clinical dataset would prove equivalent to a smaller control dataset for comparison purposes, and therefore provide a viable substitute for use in identifying and quantifying brain perfusion abnormalities in SPECT scans.
Materials and Methods
1,463 patient SPECT brain scans were acquired and processed according to protocols set forth by the American College of Radiology and the supervising imaging clinic, CereScan. Each scan was reconstructed and attenuation corrected in Segami Oasis software before being registered with MIMneuro's BrainAlign to their single brain atlas [3]. The registered scans were then averaged to form a single image. This "composite average" image was imported into MIMneuro and quantitatively compared against their normal control dataset through their region and voxel analysis tools.
Results
MIMneuro classifies any voxels or regions with an average z-score value outside +/- 1.65 as abnormal. No regions of the composite average fell outside +/- 1 z-score, and over 80% were within +/- 0.5 z-score. Voxel analysis determined that the composite average contained 5 clusters of voxels that met the

minimum volume and z-score parameters, but the statistical significance of each cluster (>0.97) rendered these findings immaterial.
Conclusions
These results demonstrate that, despite inherent abnormalities, combining heterogeneous clinical scans is a valid alternative to traditional normal datasets when used to quantify perfusion patterns in brain SPECT.

2299

Head and Neck Endovascular Repair of Vascular Malformations

W Yakes[1]
[1]The Yakes Vascular Malformation Center, Englewood, CO

Purpose
To determine the efficacy of ethanol embolotherapy of extracranial head and neck vascular malformations of all types, particularly after failure of other endovascular and surgical treatments.
Materials and Methods
One hundred and sixty-six patients (64 males, 102 females; mean age: 38 yrs) presented with extracranial arteriovenous malformations (AVMs) of the head and neck area. Over half of the patients had undergone previous failed therapies(Glue, Onyx, PVA, Coils). All patients underwent ethanol embolotherapy under general anesthesia. Forty-five patients had AVMs and 121 patients had venous malformations (VM).
Results
Of 45 AVM patients, 26 patients are cured (mean follow-up 2 ½ years); of 121 venous malformation patients, 65 are at end-therapy (mean follow-up 4 ½ years). The remaining patients are not at end-therapy and are being treated for their residual malformations. In AVM follow-up, arteriography is the main imaging modality to determine cure or residual AVM as MR is less sensitive in the evaluation of residual AVM. In VM follow-up, MR is the main imaging tool, particularly with T- 2 fat suppression and/or STIR imaging. All patients demonstrated improvement post-therapy. Complications were 4.5%, to include bleeding (self-limited), partial 7th nerve palsy (with recovery), skin injury (not requiring skin grafts), infection, and pain.
Conclusions
Ethanol has proven its consistent curative potential at long-term follow-up for high-flow AVMs and low-flow VM lesions at long-term follow-up as lesions in the periphery. Complication rates remain low. The procedures are tolerated well by the patients and done on an out-patient basis. Prior surgery and embolization procedures can cause difficulty in lesion access but does not obviate further ethanol endovascular treatment.

2239

Hereditary Spasticity and Ataxia Syndromes: MRI findings.

D Titelbaum[1], P Greenstein[2], R Engisch[3], O Kendall[4], F Wagner[5]
[1]Shields Health Care, Brockton, MA, [2]Beth Israel Deaconess Medical Center, Boston, MA, [3]Luzerner Kantonsspital, Lucerne, Switzerland, [4]Harvard Vanguard Medical Associates, Boston, MA, [5]Inselspital, Bern, Switzerland

Purpose
Hereditary spastic paraplegias and ataxias are a heterogeneous group of genetic disorders characterized by ataxia and progressive lower limb spasticity resulting from pyramidal tract dysfunction (1). Diagnosis is often difficult due to variable clinical features and certain imaging findings that may go unrecognized (2). By being able to identify critical imaging findings within the clinical context of spasticity and ataxia,

radiologists are uniquely positioned to recommend specific genetic testing, and thus facilitate diagnosis. We present a series of patients with hereditary causes of spasticity or ataxia, several of whom had gone clinically unrecognized, and in whom radiology played a critical role in the diagnosis. It is hoped that greater awareness of hereditary causes of ataxia and spastic paraplegia by radiologists will result in more accurate diagnosis in the future.

Materials and Methods

Imaging and genetic findings of 7 patients found to have hereditary causes of spasticity or ataxia were reviewed, and unique or characteristic MRI findings were identified that corresponded to the genetic diagnosis.

Results

2 females and 5 males between the ages of 17-60 with progressive spasticity or ataxia underwent MRI and were ultimately diagnosed by genetic testing. MRI features and genetic results included: pontine striations in ARSACS (fig a); thin corpus callosum (fig b) and "ears of lynx" in SPG11; degeneration of the decussation of the superior cerebellar peduncles in POLR3A-related leukodystrophy (fig c); isolated cerebellar atrophy in ataxia telangiectasia; dentate nuclei degeneration and cataracts in cerebrotendinous xanthomatosis; and spinocerebellar atrophy in SCA 3 and SCA7.

Conclusions

Certain hereditary ataxia and paraplegia syndromes may present with identifiable neuroradiological findings. Awareness of hereditary ataxia among radiologists will expedite neurogenetic evaluation and accurate diagnosis, explanation of patient symptoms, recommendation for syndrome-specific treatment, and family planning considerations.

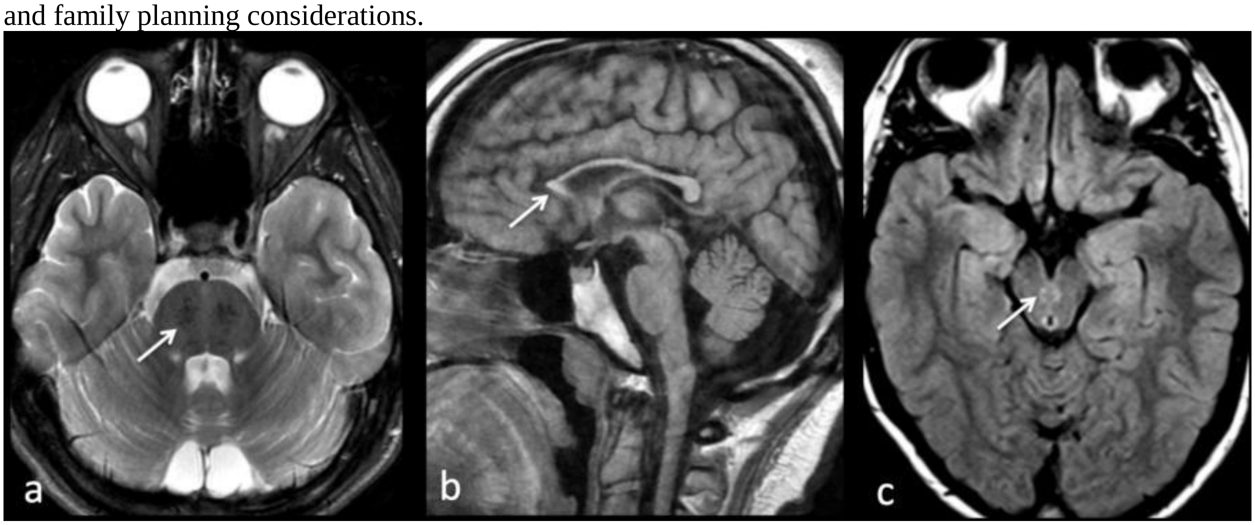

(Filename: TCT_2239_HSAabstractfig1.jpg)

2112

Impact of Commodities on the Clinical Outcome of Endovascular Coil Embolization of Intracranial Aneurysms in Asian Population: A 3-Year Retrospective Study

S Ahmad[1]
[1]*Lahore General Hospital, Lahore, Outside U.S. and Canada*

Purpose

Intracranial aneurysms are treated with either microsurgical clipping or endovascular coiling, the last being a much more recent treatment strategy. Hence, long term result after endovascular coiling are as yet scarce. Endovascular embolization of ruptured and unruptured intracranial aneurysms gives an adequate treatment and long-term results with less morbidity and mortality . Endovascular treatment has turned into

a built up technique for treating intracranial aneurysms since the International Subarachnoid Aneurysm Trial (ISAT) of neurosurgical clipping versus endovascular coiling in 2143 patients with ruptured intracranial aneurysms. In patients with a ruptured intracranial aneurysm, for which endovascular coiling and neurosurgical clipping are helpful alternatives, the result as far as survival free of disability at 1 year is altogether better with endovascular coiling. Independent risk factors that influence recuperation incorporate age, sex, smoking and hypertension. Smoking is viewed as a standout amongst the most imperative hazard factors causing intracranial aneurysm formation and subarachnoid hemorrhage, however no exact data is available. There is scarce data accessible on impacts of hypertension on clinical result in post coiling patients. Postoperative blood pressure variability has an effect on clinical outcomes and this study will guage the exact impact of that risk factor.
Materials and Methods
This is a 3-year retrospective analysis, performed to assess the clinical outcomes of patients with cerebral aneurysms treated with detachable coils in Asian population and impact of comorbidities including smoking and hypertension in relation to age and gender. From July 2015 to August 2018, a total of 297 consecutive patients (mean age: 45.5 years) with cerebral aneurysms (ruptured and un-ruptured) were treated with endovascular coiling procedures included in the study. We have obtained clinical information included age, sex and aneurysm location. Concomitant clinical data such as hypertension and smoking were also evaluated to determine risk factors that might affect the functional outcome. Clinical information and radiological outcomes were retrospectively evaluated on regular follow-ups and telephonic interviews. A modified Rankin Scale was used to measure the clinical outcome of patients.
Results
The mean age of patients was 45 years, 171 Women and 126 Men participated in the study. It was seen that smoking was found to be lower in women and hypertension was equally distributed across men and women. A multivariable linear regression model was run comparing age, gender, smoking and hypertension with treatment outcome. Treatment outcome was measured on the modified Rankin scale and lower the scale better the outcome. The results showed that women in the sub-continent have not only far higher frequency of aneurysms but also poorer outcomes. Poor recovery is compounded by the presence of comorbidity of hypertension. Smoking does not play a major role in women's recovery or at least this fact was not discernable by this study most likely due to a lack of data as most women in this part of the world due to religious and cultural reasons are mostly non-smokers. Men with comorbidity of smoking and hypertension were seen to be at higher risk and age played a major role in recovery. Men in their 20s and 30s saw the best recovery rates which is highly encouraging with hypertension and comorbidity only having a minor impact on their recovery. It was seen however that men who were 40+ in age had far more negative impacts of smoking and hypertension in their recovery and showed very poor results.
Conclusions
As a conclusion we find that smoking and hypertension both adversely affect the outcome of endovascular treatment of intracranial aneurysms. It is found that while aneurysms are more prevalent in women than men, women have a poor chances of recovery. Similarly, patients who were above the age of 40 had a less chance of recovery compared to younger patients.

2156

In the Pit. Imaging Characteristics of Rathke's Cleft Cysts

K Seifert[1], A MAHAJAN[2], S Omay[3], R Bronen[4]
[1]YALE NEW HAVEN HOSPITAL, NEW HAVEN, CT, [2]Yale University, NEW HAVEN, CT, [3]Yale School of Medicine, New Haven, CT, [4]Yale University, New Haven, CT

Purpose
The purpose of this study was to assess the imaging characteristics, pathology, and changes over time of

cystic lesions in the sella/suprasellar region. This study was performed to specifically evaluate imaging characteristics of Rathke's cleft cysts and allow for a confident diagnosis of these benign lesions.
Materials and Methods
We performed a retrospective search to create list of patients with a differential diagnosis that included Rathke's cleft cyst. Each patient's imaging was reviewed to include the location and extension of the cystic lesion, T1 and T2 signal characteristics, presence of calcifications or intracystic nodule, enhancement pattern, size and change over time, mass effect of optic chiasm, and pathology if resected.
Results
A total of 342 patients with cystic sellar/suprasellar lesions had a differential diagnosis that included Rathke's cleft cyst. 45 of these patients underwent resection; 13 patients had pathology proven Rathke's cleft cysts, while 32 patients had pathology of another lesion type, such as cystic adenoma, arachnoid cyst, and cystic craniopharyngioma. The remaining 297 patients were managed conservatively and followed with biochemical and imaging data. Our data show that the majority of lesions with a differential of Rathke's cleft cyst are nearly entirely cystic in appearance, with little to no solid component or calcifications, homogenous in signal with T1 and T2 characteristics of simple cysts or cysts with proteinacous/hemorrhagic components, and subcentimeter in size. These cystic lesions tend to have minimal to no growth over time, despite being followed for multiple years, with average follow up of 1.75 years and a range of up to 16 years.
Conclusions
This study reviewed the imaging characteristics of lesions that included Rathke's cleft cyst in the differential to provide a standard to diagnose these benign lesions. Given the minimal to no growth of Rathke's cleft cysts, a subcentimeter purely cystic lesion in the sellar/suprasellar space with no laboratory abnormalities or mass effect can be treated conservatively and does not require prolonged imaging follow up, beyond 2 years if stable.

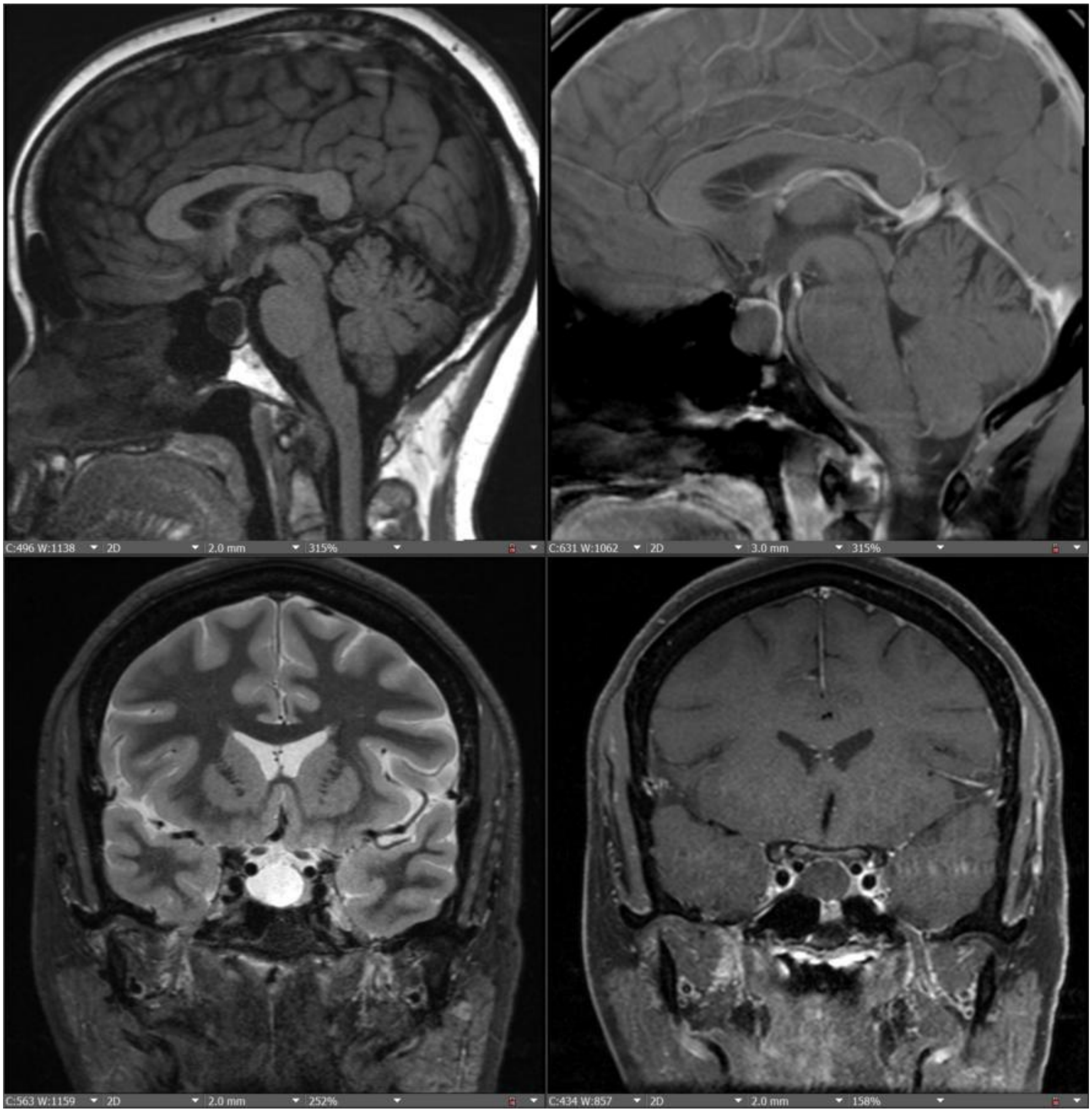

(Filename: TCT_2156_Pit.jpg)

2278

Incidence of Dilated Perivascular Spaces in Young Athletes Evaluated for Concussion.

P Rathousky[1], E Biondo-Savin[2]
[1]Ascension Providence Hospital / MSUCHM, Southfield, MI, [2]Michigan State University, East Lansing, MI

Purpose
Recent studies have demonstrated an increased prevalence of dilated, high convexity perivascular spaces, or Virchow-Robin spaces (VRS) in individuals with a history of traumatic brain injury and other

neurologic disorders. This suggests that they may be a marker of inflammatory change. The goal of this study was to assess the incidence of dilated VRS in college athletes with a clinical diagnosis of concussion, a mild form of traumatic brain injury.

Materials and Methods

This is a retrospective study where 23 patients (14 women, 9 men; mean age: 20; range: 18.3 – 22.4 years) who received MR imaging following the clinical diagnosis of concussion were reviewed for the presence of dilated VRS. Axial T2-weighted images were used to identify the presence or absence of dilated VRS. Dilated VRS were defined as punctate areas of high T2 cerebrospinal fluid-like signal conforming to the path of penetrating arteries, measuring greater than 2mm. Normal variants such as the anterior commissure and basal ganglia were not reported for the purposes of this study. The remaining sequences were also evaluated for areas of white matter signal abnormality as well as incidental findings.

Results

In our study group, 12/23 (52%) patients were found to have dilated VRS. Five of the twenty-three patients demonstrated nonspecific FLAIR signal abnormalities involving the white matter tracts and deep gray nuclei.

Conclusions

The results of the study reveal that the majority of our cohort, consisting of college aged athletes with a clinical diagnosis of concussion, demonstrated dilated high convexity VRS. When compared to an earlier study demonstrating the low prevalence of dilated VRS in the pediatric population, this suggests a possible link between dilated VRS and inflammatory changes associated with concussions. This is something that can easily be assessed on routine T2-weighted imaging.

Table 1 - Demographic Data and Imaging Findings in 23 Athletes Evaluated for Concussion

Patient	Age (y)	Sex	Presence of Dilated Perivascular Spaces	Location	Other Findings
1	20.2	Male	No	-	Right Frontal Lobe 2mm Juxtacortical FLAIR Lesion
2	18.5	Female	Yes	Frontal and Parietal Lobes	Cavum Septum et Vergae
3	20	Female	Yes	Frontal and Parietal Lobes	-
4	21.7	Male	No	-	7mm Pineal Cyst
5	21.2	Male	Yes	Frontal and Parietal Lobes	Minimal Tonsillar Ectopia
6	18.9	Female	Yes	Parietal Lobes	-
7	21.4	Male	Yes	Parietal Lobes. Centrum Semiovale	-
8	20.5	Female	Yes	Left Mesotemporal Lobe	Left Frontal Lobe 4mm FLAIR Lesion
9	18.5	Male	No	-	-
10	19.5	Male	Yes	Parietal Lobes	-
11	22.4	Female	Yes	Parietal Lobes	Scattered Subcortical FLAIR Lesions
12	20.8	Female	No	-	-
13	19.5	Female	No	-	-
14	19.5	Female	Yes	Parietal Lobes	Left Cerebellar Developmental Venous Anomaly
15	20.9	Male	No	-	-
16	20.9	Male	No	-	Posterior Fossa Arachnoid Cyst
17	21.6	Male	No	-	-
18	18.3	Female	Yes	Parietal Lobes and Deep Gray Matter	Scattered FLAIR Lesions
19	18.6	Female	No	-	-
20	18.5	Female	Yes	Left Parietal and Temporal Lobes	-
21	20.8	Female	No	-	-
22	19.2	Female	Yes	Right Posterior Parietal Lobe	-
23	19.2	Female	No	-	Right Globus Pallidus 4mm FLAIR Lesion Rathke's Cleft Cyst or Hemorrhagic Microadenoma

(Filename: TCT_2278_Table01.JPG)

2990

Incidence of T2 and SWI Hypointensity in the Pulvinar Nucleus of Healthy Subjects at 3T MRI

S Tufik[1], R Moreno[1], L Lucato[1], C Leite[1], G vieira[1]

[1]*HOSPITAL DAS CLINICAS DA FACULDADE DE MEDICINA DA USP, SAO PAULO, SAO PAULO*

Purpose
To investigate thalamic pulvinar hyposignal incidence in T2 and susceptibility sequences among healthy subjects in different ages in order to avoid erroneous radiological interpretation.
Materials and Methods
Sixty asymptomatic subjects (25 men and 35 women; age range from 25 to 82) with unremarkable brain 3T magnetic resonance (MR) findings were enrolled. The images were analysed with regard to signal intensity of the pulvinar nucleus (PN) relative to the thalamus on T2 spin echo (T2SE), T2 fast spin echo (T2FSE) and susceptibility weighted image (SWI) and classified as either negative or positive for PN hypointensity.
Results
A progressive higher incidence of pulvinar nucleus hypointensity was observed with age progression in all the sequences analysed. This finding was observed 56%, 55% and 31% respectively in the T2SE, T2FSE and susceptibility sequences.
Conclusions
Our study evaluated and confirmed a progressively higher incidence of T2 and susceptibility sequences hypointensity of the pulvinar nucleus with age in healthy subjects. This finding is in accordance with other few studies in literature [1] and it is important to relativize the analysis of neuroradiologists so as not to always consider it as a pathological finding.

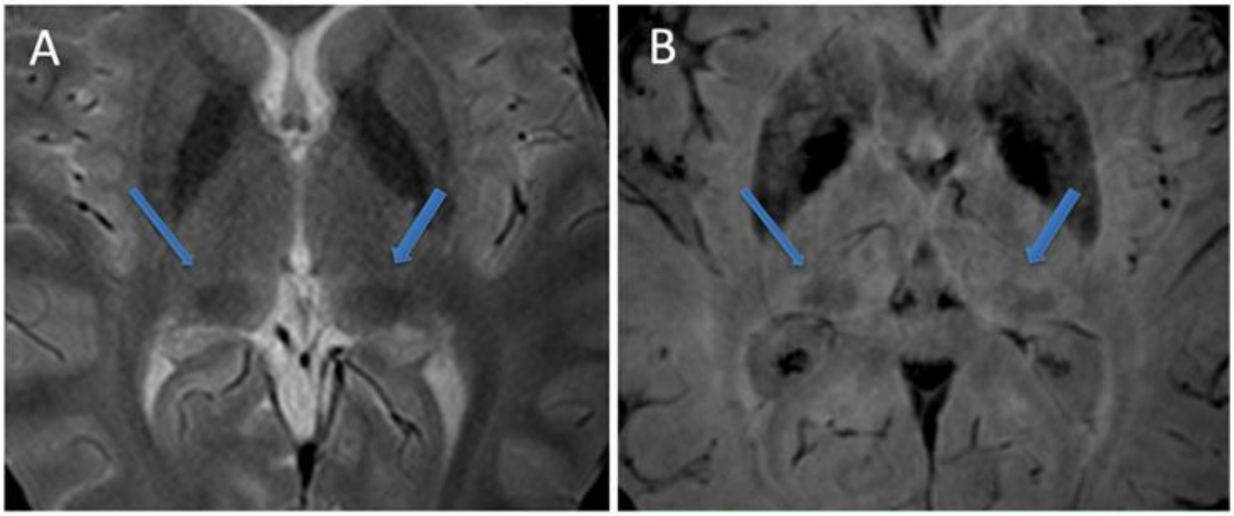

T2SE Hypointensity	Absent	Present
25-29 years	6	4
30-39 years	5	5
40-49 years	5	5
50-59 years	2	8
60-69 years	4	6
≥ 70 years	4	6
Total	26	34

SWI Hypointensity	Absent	Present
25-29 years	8	2
30-39 years	8	2
40-49 years	9	1
50-59 years	5	5
60-69 years	5	5
≥ 70 years	6	4
Total	41	19

A) Axial T2SE showing bilateral pulvinar nucleus hypointensity. Below a table showing the distribuition of this finding among different ages.
B) Axial SWI showing bilateral pulvinar nucleus hypointensity. Below a table showing the distribuition of this finding among different ages.

(Filename: TCT_2990_PulvinarNucleus.jpg)

2115

Inter-scanner Variability May Lead to Differences in Detection Rate of Leptomeningeal Enhancement on 3D-FLAIR MRI in Multiple Sclerosis.

D Titelbaum[1], R Engisch[2], E Schwartz[1], S Napoli[3], J Sloane[4], j katz[5], E Lathi[5]
[1]Shields Health Care, Brockton, MA, [2]Luzerner Kantonsspital, Lucerne, Switzerland, [3]Neurology Center of New England, Foxboro, MA, [4]Beth Israel Deaconess Medical Center, Boston, MA, [5]The Elliot Lewis Center for MS Care, Wellesley, MA

Purpose
Meningeal inflammation has been implicated in cortical grey matter demyelination and disability progression in multiple sclerosis (MS) (1). Gadolinium-enhanced 3D-FLAIR (Gd-3D-FLAIR) MRI has been shown to identify foci of leptomeningeal enhancement (LME) in MS (2), thought to be an imaging biomarker for leptomeningeal inflammation. However, there has been considerable variability in the rate of LME detection by different investigators. We sought to determine if MRI scanner variability can explain different rates of LME detection by different investigators.
Materials and Methods
A phantom was made containing vials of increasing concentrations of Gd from 0.01 to 3.0 mmol, as previously described by Mathews et al, 1999 (3). The phantom was placed over the forehead of one volunteer, and scanned using 3D-FLAIR on all imaging platforms available. Signal intensity (SI) was normalized by dividing by thalamic signal, and concentration-SI curves were generated and compared by scanner type, including type of FLAIR and field strength. The effects of various surface coil intensity correction algorithms and fat suppression were also assessed. Phantom stability was verified by repeated scanning.
Results
SI vs Gd concentration curves for various scanner are shown in the Figure. Scanners using CUBE FLAIR showed notably higher SI compared to scanners using SPACE FLAIR. When using CUBE, 3T produced a moderate increase in SI over 1.5T, whereas there was no difference between 1.5T and 3T when using SPACE. VISTA showed intermediate SI at both 1.5 and 3T. Use of fat suppression had no effect on SI. Surface coil corrections produced variable signal attenuation.
Conclusions
Signal intensity of low concentrations of Gd vary by scanner type and FLAIR method. Controlling for scanner variability will be essential in future studies of LME.

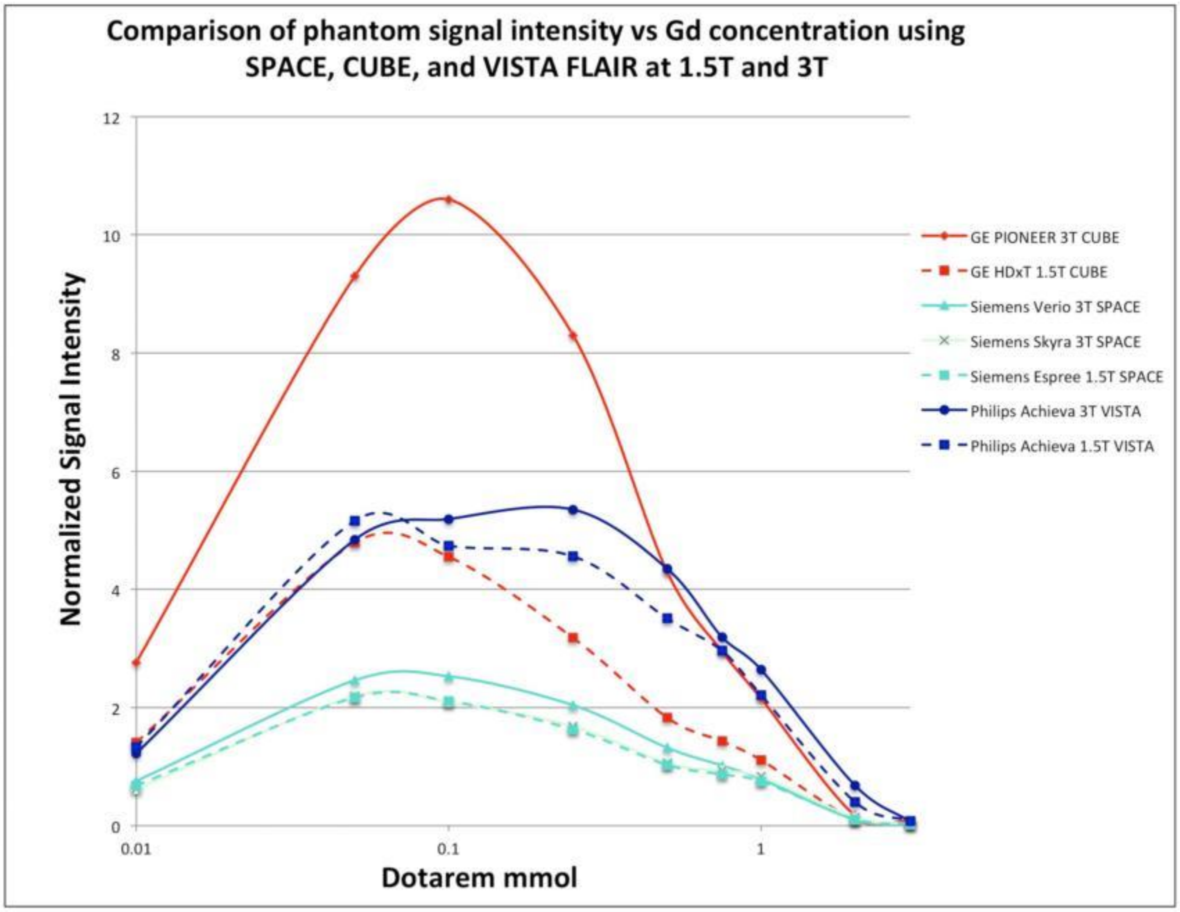

(Filename: TCT_2115_phantomgraphjp.jpg)

3280

Morphological Changes in the Third Ventricle and Cerebral Aqueduct in Idiopathic Normal Pressure Hydrocephalus Related to Stroke Volume

R Chen[1], L Chan[2], W Go[3], H Li[3], S Lim[3], S Kumar[4], N Keong[5]
[1]Singapore General Hospital, Singapore, Not Applicable, [2]Department of Diagnostic Radiology, Singapore General Hospital,, Singapore, Singapore, [3]Singapore General Hospital, Singapore, Singapore, [4]National Neuroscience Institute, Singapore, Singapore, [5]National neuroscience institute, Singapore, Singapore

Purpose
The morphological changes in the third ventricular and cerebral aqueduct of patients diagnosed clinically with idiopathic normal pressure hydrocephalus (iNPH) have been sparsely described in the literature. We described (1) the third ventricular and aqueduct morphological changes in a cohort iNPH patients, (2) semi-quantitative measures of the third ventricle in iNPH compared to age-matched healthy controls, (3) correlates of these measures with stroke volume on CSF flow study, and (4) temporal changes in these measures in iNPH patients with and without ventricular shunting.
Materials and Methods
This prospective study was approved by the institutional ethics committee. Patients diagnosed with iNPH based on key clinical and neuroimaging features after exclusion of secondary causes and confirmation

with neuropsycholoical testing and CSF lumbar tap tests over 3 consecutive days were recruited. All patients, with or without ventricular shunting, underwent brain MRI on a 3T scanner at baseline, 6-month and 1-year follow-up. The MR sequences included axial FLAIR, DTI, 3D MPRAGE & SPACE, and CSF flow study at the cerebral aqueduct. Age-matched healthy controls (HC) were also recruited for brain MRI.

Results

Twenty iNPH patients and 26 HC were included in this study; 1 patient was excluded due to a suprasellar cyst grossly compressing the third ventricle. Three iNPH patients demonstrated gross third ventricular ballooning, flaring of the supra-optic and infundibular recesses, and cerebral aqueduct; and grossly pathological stroke volumes (SV) of >200microlitres. Statistical differences in 4 semi-quantitative measures of the third ventricle were found between between iNPH and HC, and before and after ventricular shunting in iNPH patients at 6- and 12-month MRI.

Conclusions

Unusual ballooning of the third ventricles and aqueductal flaring occurred in a minority of iNPH patients with grossly pathological SV of >200microlitres. Semi-quantitative measures of third ventricular morphological changes were different between iNPH and HC, and in iNPH patients pre- and post-shunting.

3319

Most Relevant Brain Regions to Discriminate Idiopathic Generalized Epilepsy from Healthy Controls Using Multiple Kernel Learning: Comparison Between VBM, DTI and MTI.

L Avila Lessa Garcia[1], C TOYAMA[2], C da Silva[2]
[1]Grupo Fleury, Sao Paulo, Sao Paulo, [2]FLEURY, SÃO PAULO, SÃO PAULO

Purpose

The purpose of this study is to evaluate the differences between the group of patients with idiopathic generalized epilepsy and the control group, by means of artificial intelligence, and indicate which differences contributed most to patient selection. Patients with generalized epilepsy usually have neuroimaging tests within the limits of normality, so with the help of artificial intelligence, we think of using the computer to evaluate these subtle differences between the groups and from there to see which or which differences are the most important in the classification of the individual as patient or control. In addition, we employ several MRI sequences to try to find out more about the brain and possible secondary or disease-related changes, especially changes in white matter and brain gray matter.

Materials and Methods

The patients were recruited from the epilepsy clinic of the medical school of the University of São Paulo and the exams were performed in a 3 Tesla (Philips) device. After exclusion of the patients according to the selection criteria, 21 exams were selected from individuals from the control group and 37 from the sick group. The sequences used were to evaluate brain morphometry (sagittal T1 of high resolution and volumetric), diffusion tensor (DTI) and magnetization transfer imaging (MTR). The images were converted to the NIFTI format and processed on the workstation through the SPM program package and the PRONTO toolbox. We used the supported vector vector machine for the classification of groups and multiple kernel learning to generate weights for the areas of interest and thus to indicate which or which brain structures most contribute to the classfication of the groups.

Results

The evaluation through artificial intelligence was able to distinguish the groups appropriately and classify the individual with high precision, besides indicating differences that contributed the most to this selection. Differences were found in the corpus callosum and in the cerebral hemispheres that contributed most to the classification.

Conclusions
Unlike other isolated studies of VMB, we did not identify significant changes in the thalamus or frontal lobes of patients with generalized idiopathic epilepsy, perhaps because of the heterogeneity of the sample. There was only significant reduction of the corpus callosum in patients. The evaluation of the white matter by means of DTI and MTI has shown, as well as other studies, that there is a great difference between the groups, mainly in brain withe matter substance, and that perhaps compromised function of the tracts and fascicles is related to disease. When we use only one of the techniques employed, we can not classify subjects as well as when we use all techniques, suggesting that diseases in which the structure or function are discreetly compromised, the more information we add the computer, the better . The evaluation of all the techniques together was more effective than an isolated technique. The findings suggest that not only neurons (gray matter) are involved in these diseases, but also white matter, being that this dysfunction may be secondary to disease or be part of the pathophysiology.

2677

MR-based Radiomic Analysis on Peritumoral Brain Edema of Glioblastoma Patients: Comparison of Survival Prediction to Conventional Clinical Parameters

Y Choi[1], K Ahn[1], Y Nam[1], J Jang[1], H Choi[1]
[1]Seoul St. Mary's Hospital, The Catholic University of Korea, Seoul, Korea (the Republic of)

Purpose
To assess whether radiomic features extracted from peritumoral brain edema (PBE) of pre-treatment MRI reliably predict patients' long-term survival and to compare their predictive performance to the conventional prognostic parameters.
Materials and Methods
A total of 114 patients with pathologically confirmed glioblastoma were retrospectively selected from March 2008 and May 2018 (61 from our institution and 53 from the Cancer Imaging Archive, TCIA). All patients were randomly divided into either test or validation set (n=80; n=34). Long-term (LTS) and short-term survivors (STS) were defined based on overall survival (OS) period of 400 days. Clinical variables included age, sex, MGMT (O-6-methylguanine-DNA-methyltransferase promoter methylation) promoter methylation status, and type of surgical resection. On conventional MR sequences (T1, T2, FLAIR, T1CE), PBE were manually segmented and analyzed via radiomics from which 105 features per patient were computed. A Cox proportional hazards model via penalized maximum likelihood (Lasso) was fitted on the test set for feature reduction. Cox regression analyses were fitted to the clinical variables as well as the selected subset of radiomic features. Clinical and radiomic Cox models were tested on a separate validation set using prediction error curves (PEC) for risk prediction.
Results
The median OS of all patients were 435 days. No significant differences were found between LTS and STS in MGMT methylation status, type of surgical resection, preoperative tumor volume and PBE volume. Among the 105 radiomic features, a subset of six relevant features were obtained (2 shape, 2 grey level and 2 first order). The concordance indices of clinical and radiomic models were 0.608 and 0.679, respectively. On validation set, the radiomic model showed lower error rate in survival prediction than the clinical model.
Conclusions
The prognostic model derived from radiomic features of PBE in glioblastoma patients showed higher predictive performance than that of conventional clinical parameters, suggesting radiomics' potential as non-invasive prognostic imaging biomarker.

3279

MRI Tracking the Kinetic Distribution and Therapeutic Effect Iron Dioxide Particles Labeled Chimeric Antigen Receptor T-cells on Glioblastoma

W Zhang[1]
[1]*Daping Hospital, Army Medical University, Chongqing, China*

Purpose
To noninvasively track the kinetic distribution and persistence and therapeutic effect of Ultrasmall superparamagnetic iron oxide particles labeled chimeric antigen receptors (CAR) T cells on glioblastoma (GBM) by MRI.
Materials and Methods
Ultrasmall superparamagnetic iron oxide (USPIO) was used to label CAR-T cells, and we checked its effect on biological property and functionality of CAR-T cells. EGFRvIII-U87MG and U87MG cells were injected into the right basal ganglia of 60 mice. Animals were stratified into Saline, USPIO-T, USPIO-EGFRvIII/IL13Rα2-CAR-T group (n=15, respectively). MRI, including anatomical and advanced sequences, were performed longitudinally post infusion of USPIO labeled CAR-T cells to track their kinetic phases of distribution and therapeutic effect on GBM model. Standard immunohistochemical analysis was performed to verify in vivo results.
Results
USPIO inserted no effect on apoptosis, proliferation and functionality of CAR-T cells in vitro. Dynamic infiltration and persistence of CAR-T cells in tumor parenchyma could be tracked in vivo via MRI ranging from 3 days to 14 days following USPIO-CAR-T cells infusion, mainly locating at periphery regions of tumors. Prussian blue staining at each given time points also indicated effective infiltration of labeled CAR-T cells. Further, advanced MRI revealed significant elevated ADC value, decreased Ktrans value and contrast enhancement at 3 days after treatment， which concurrently happened with the destruction of tumor cells and increased of intercellular tight junction on immunostaining.
Conclusions
Our study established a new imaging platform and evaluation system for in vivo tracking of CAR-T cells in orthotropic model of GBM， and its corresponding therapeutic efficiency. Our research potentially guides the design and improvement of new CAR with highly infiltrating ability into the tumor core.

3210

Non-invasive Brain Temperature Monitoring with 3T MRI in a Hyperacute Monkey Stroke Model: a Feasibility Study

K Yi[1], C Choi[1], S Cha[2]
[1]*Chungbuk National University Hospital, Cheongju, Chungbuk,* [2]*Chungbuk National University Hospital, College of Medicine and Medical Research Institute, Cheongju, Chungbuk*

Purpose
Systemic and local hypothermia is considered a promising therapeutic strategy in acute ischemic stroke patients. Non-invasive monitoring is essential for the assessment of temperature changes and the optimization of therapeutic target temperature in acute ischemic brain. We tried to compare fiber optic thermometry and MR thermometry (MRT) for the temperature change assessment in phantoms. And this is to apply sequential MRT in a monkey stroke model.
Materials and Methods
A phantom of agar-gel in a glass container was warmed up to 40℃ and prepared in the 3T MR magnet prior to temperature monitoring. While temperature of the agar-gel phantom was monitored by an MRI-compatible fiber optic thermometry system every 2 minutes, MRI with Proton Resonance Frequence

(PRF) shift technique was repeated for 40 minutes. In a monkey stroke model with focal infarction, brain temperature changes in regions of interest (ROIs) were monitored using same PRF shift technique for phantoms on 3T MR scanner for 110 minutes (6 scans) immediately after the endovascular middle cerebral artery occlusion. MRT presented temperature difference between the times of 1st MR scan and scan of interest.

Results

Temperature measurement of the phantoms with fiber optic thermometry showed linear decrease (-5.5℃) from mean 38.6℃ to 33.1℃ during 40 minutes (Fig 1). Results of MRT also showed linear decrease from the start to the end (mean temperature difference, -4.9℃) and coincided those of fiber optic thermometry (Fig 2). In the monkey stroke model, temperatures in the infarction ROI and normal ROIs (ipsilateral and contralateral) were elevated continuously for 110 minutes. The temperature differences in the infarction ROI was 7.6℃ and in the normal ROIs (ipsilateral and contralateral) 6.0℃ and 5.9℃ respectively (Fig 3).

Conclusions

In this preliminary study, we showed MRT with PRF shift technique can follow the temperature changes in the hyperacute ischemic stroke.

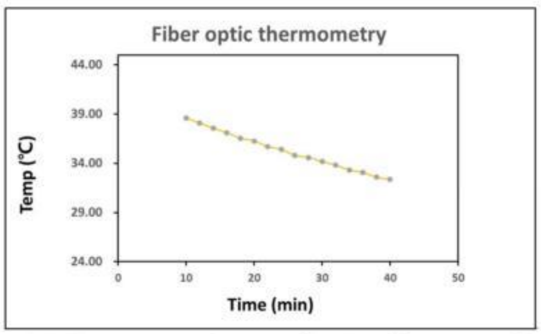

Fig 1. Temperature changes of in vitro phantom on fiber optic thermometry.

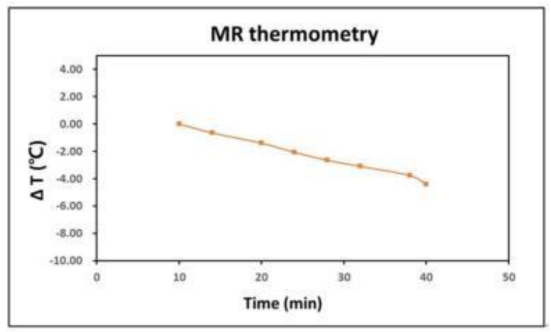

Fig 2. Temperature changes of in vitro phantom on MR thermometry.

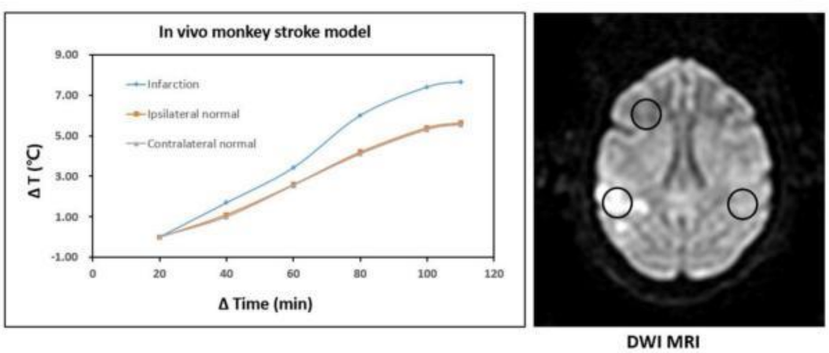

Fig 3. Temperature changes of a monkey hyperacute infarction model in the infarction and ipsilateral / contralateral normal areas.

(Filename: TCT_3210_Figures.JPG)

3220

Novel Practical Optical Tracking-system for Prospective Motion-Correction of Neuroimaging at 7T

E Tong[1], P DiGiacomo[1], J Maclaren[1], M Aksoy[1], M Zeineh[1]

[1]*STANFORD MEDICAL CENTER, STANFORD, CA*

Purpose

Ultra-High-field 7T MRI can produce images with higher signal-to-noise-ratio(SNR) and spatial-resolution than clinical MRI(1.5, 3T). However, these ultra-high-resolution images are sensitive to minute motion-artifact. Additionally, long acquisition-times may provoke subjects' motion. Susceptibility to motion-artifact is one of the major hurdles hindering broad deployment of this powerful imaging equipment. Retrospective motion-correction methods are available but require long post-processing time and may degrade images from overlaps and gaps in K-space. Prospective motion-correction methods monitor motion in real-time and update acquisition parameters regularly to compensate. Existing motion-correction systems typically utilize MR-compatible cameras mounted inside the bore of the magnet for optical tracking and mouthpieces as tracking targets. Our study aims to design a novel, practical, comfortable optical tracking-system for 7T MRI.

Materials and Methods

Our prospective motion-tracking system consisted of an MR-compatible camera (mounted between Transmit and Receive coils), a checkerboard optical-marker securely taped on subject's forehead, and a tracking computer. In-vivo testing was performed on volunteer-subject while (1) lying still with only subtle physiologic motion and (2) rotating deliberately ~45 degree to either side periodically. T1-weighted isotropic-3D-BRAVO sequence(256x256, 1.5mm slice-thickness) and 2DFAST sequences(512x512, 1.5mm slice-thickness) (Figure) were obtained with and without motion-correction. To demonstrate the utility of this system in producing high-quality images, a high-resolution 2DFAST sequence(1024x1024, 0.14x0.14x1.0mm3 voxel-size, 20min scan) was acquired.

Results

Motion-correction for both deliberate and involuntary motion was successfully demonstrated on human subjects, producing superbly high-quality high-contrast images, without introducing spurious artifacts during correction. Figure shows 2D-FAST-sequences acquired (A) without deliberate motion and without motion-correction, (B) with deliberate motion and without motion-correction, and (C) with deliberate motion and with motion-correction. Figure D was acquired using ultra-high-resolution 2D-FAST-sequence with motion-correction, which demonstrates exquisite details of the hippocampus, delineating the dentate gyrus and cornu ammonis.

Conclusions

Addressing motion-artifact is a pivotal prerequisite to unleashing the full potential of 7T MRI. Our prospective motion-correction system demonstrates potential to overcome motion-artifact at 7T. This practical and user-friendly design allows longer scan-times, producing superbly high-quality high-contrast images with ultra-fine image-resolution, which may facilitate discovery of novel imaging-biomarkers of aging, neuropathology, and neurodegenerative diseases.

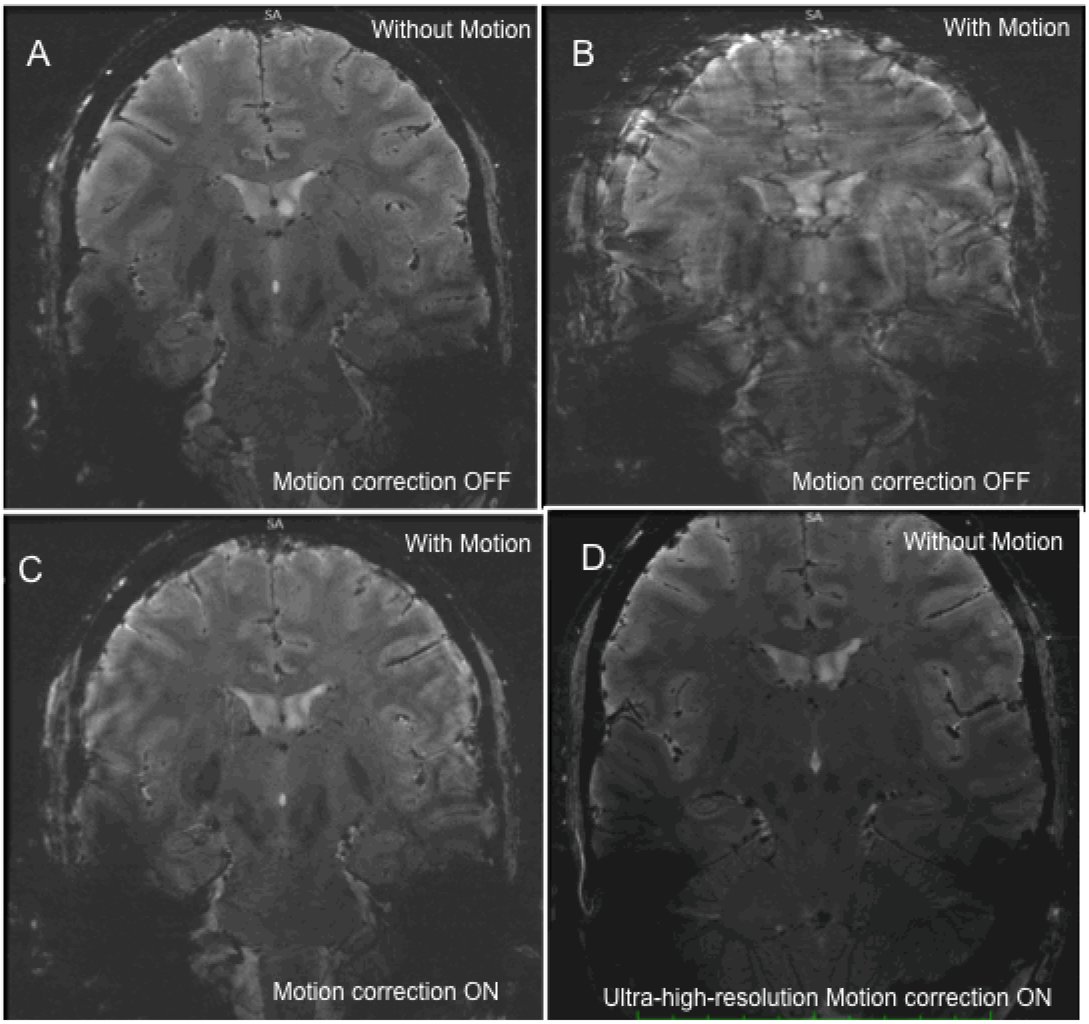

(Filename: TCT_3220_Figure.gif)

2886

Orthostatic Headaches in Spontaneous Intracranial Hypotension: Prevalence and Clinical Predictors

X Lu[1], A Griffin[1], J Campbell[1], S Peacock[1], P Kranz[2], L Leithe[1], T Amrhein[3]
[1]DUKE UNIVERSITY MEDICAL CENTER, Durham, NC, [2]DUKE UNIVERSITY MEDICAL CENTER, CARY, NC, [3]DUKE UNIVERSITY MEDICAL CENTER, DURHAM, NC

Purpose
Spontaneous intracranial hypotension (SIH) patients suffer from pervasive misdiagnosis (up to 94% in one case series), leading to delayed treatment and significant morbidity (Schievink, Arch Neurol, 2003). This occurs, in part, because the hallmark clinical feature of SIH, orthostatic headache (one that is improved when recumbent), is not present in all patients. Orthostatic headache prevalence in SIH has not been previously reported. The purpose of this study is to establish orthostatic headache prevalence in confirmed SIH patients and to determine factors predictive for orthostatic headaches in SIH.
Materials and Methods
We retrospectively reviewed headache questionnaires, myelograms, and brain MRIs in consecutive

patients referred for possible SIH between 1/1/2013 and 1/1/2017. Patients meeting ICHD-3 criteria for SIH were included. Age, sex, CSF leak subtype, time since symptom onset, CSF opening pressure, and orthostatic headache presence or absence were recorded.

Results

We identified 90 SIH patients. Only 69%(62/90) reported orthostatic headaches. Orthostatic headaches were more common in women (76%,46/60) than men (57%, 16/30)(p=0.05). Patients with dural tears were more likely to report orthostatic headaches (80%,33/41) compared to other CSF leak subtypes (meningeal diverticulum: 62%,13/22; CSF-venous fistulas:57%,8/14; and non-specified leaks:67%,8/12)(p=0.03). Patients with opening pressures less than 6 cm2H2O were more likely to have orthostatic headaches than those with pressures greater than 6 cm2H2O (82% vs 69%, P=0.2). Neither duration of symptoms nor patient age predicted orthostatic headache presence

Conclusions

SIH is a commonly misdiagnosed disease partly because nearly one third of these patients present without orthostatic headache, the expected hallmark symptom. SIH therefore cannot be excluded by the absence of an orthostatic headache, particularly in male patients. Furthermore, in the context of SIH, dural tears and low opening pressures (<6 cm2H2O) are predictive for orthostatic headache, findings that may have therapeutic significance.

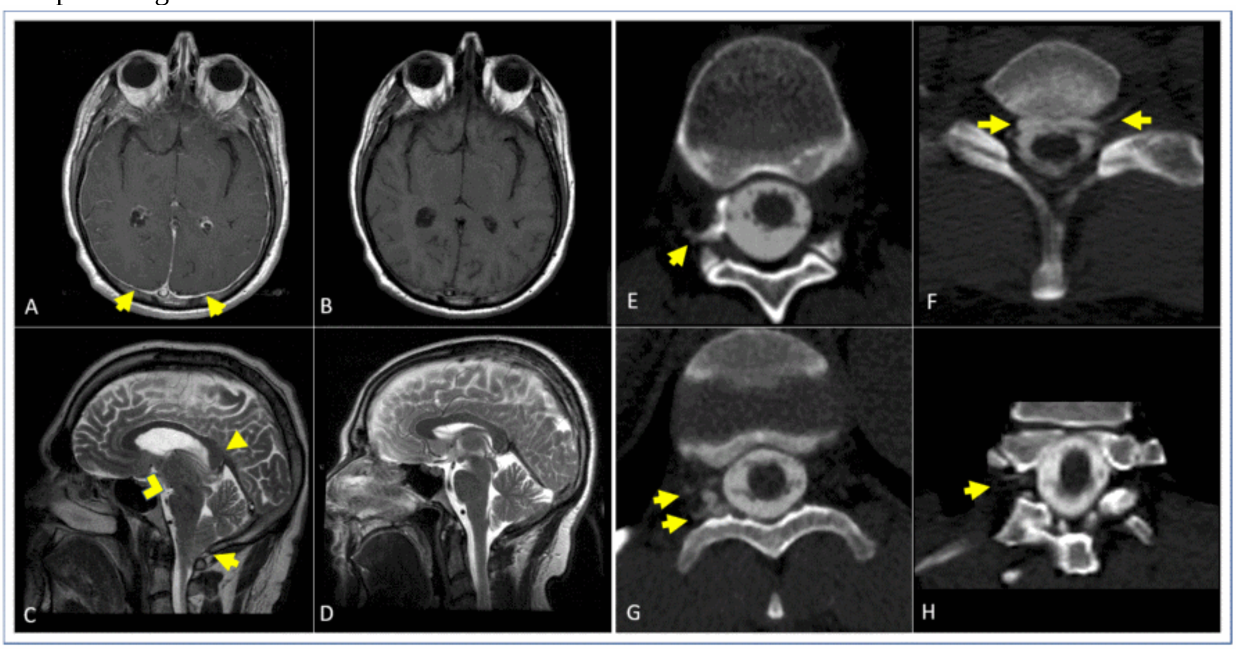

Figure 1: Imaging findings of intracranial hypotension and of CSF Leaks by subtype. MRI images in patients with (A&C) and without (B&D) intracranial hypotension. (A) Axial gadolinium enhanced T1-weighted magnetic resonance imaging showing diffuse pachymeningeal enhancement, as compared to (B) T1-weighted MRI without gadolinium enhancement. (C) Sagittal T2 weighted MRI - findings of ICH as compared to sagittal T2 weighted MRI of a normal brain (D), including decreased mamillopontine distance and decreased pontomesencephalic angle ( ), downwards drooping of the splenium( ), and tonsillar ectopia ( ). (E) Axial CT myelogram imaging, showing tear of a meningeal diverticulum. (F) Axial CT myelogram showing large dural tear and ventral fluid collection. (G) Axial & (H) coronal reformation CT myelogram images showing extravasation of CSF contrast into adjacent venous channels

(Filename: TCT_2886_figure1.gif)

2924

Outcome Differences Between Intra-Arterial Iso- and Low-Osmolar Iodinated Radiographic Contrast Media Use in Stroke Management

Z Smith[1], T Tomsick[2], P Shirani[3], A Grossman[4], S Voleti[1], J Vidovich[1]
[1]University of Cincinnati College of Medicine, Cincinnati, OH, [2]University of Cincinnati Hospital, Cincinnati, OH, [3]University of Cincinnati, Cincinnati, OH, [4]University of Cincinnati, CINCINNATI, OH

Purpose
Despite its utility, Iodinated radiographic contrast media (IRCM) use may be associated with deleterious outcomes. In rat stroke models, intracarotid low-osmolar IRCM infusion demonstrated greater hemorrhagic transformation (HT) and infarct size compared to iso-osmolar IRCM. Initial human studies suggested similar, though inconclusive, clinical advantages of iso-osmolar IRCM. Our aim is to evaluate clinical and imaging outcome differences following administration of low-osmolar iohexol versus iso-osmolar iodixanol during revascularization of MCA-M1 occlusion.
Materials and Methods
A retrospective chart and image review for M1 segment MCA occlusions treated with IA thrombectomy/thrombolysis procedures at University of Cincinnati Medical Center from July 2016-2018 was performed. Patients grouped by iodixanol (n=38) or iohexol (n=17) were compared for pre-specified endpoints (90-day % mRS 0-2, mTICI reperfusion score ≥ 2B, contrast extravasation/enhancement, presence and type of hemorrhagic transformation, 24-hr ASPECTS). Baseline and other procedural variables of interest were compared for balance between groups and associations with outcomes via stepwise linear regression. Fisher's exact test analysis was performed to compare outcomes between contrast groups.
Results
Multiple relevant baseline covariates numerically favored positive outcome for iodixanol, including age and capillary index score. CTA prior to thrombectomy, without additional CTP, was associated with better mRS, mTICI, and fewer hemorrhagic transformations, for both contrast groups. IV or IA tPA use predicted poorer outcomes, with higher % use amongst iodixanol patients (50% vs 29%; p=0.23). Of the procedural, imaging, and clinical endpoints, iodixanol demonstrated fewer contrast extravasations (5% vs 18%; p=0.16). Each instance of contrast extravasation was followed by hemorrhagic transformation, irrespective of IRCM type. No significant difference in mRS, mTICI, or hemorrhagic transformation was observed between contrast groups.
Conclusions
Contrast extravasation, less common with iodixanol, predicts hemorrhagic transformation. Additional contrast administration from combined CTA and CTP may predispose patients to less favorable outcomes. Identified numerical differences in the propensity for extravasation support further investigation in a prospective analysis of all proposed modulating baseline and endovascular treatment variables that may also affect clinical outcome in MCA occlusion diagnosis and treatment.

Figure 1. Association between Basline Clinical/Procedural Variables and Outcomes

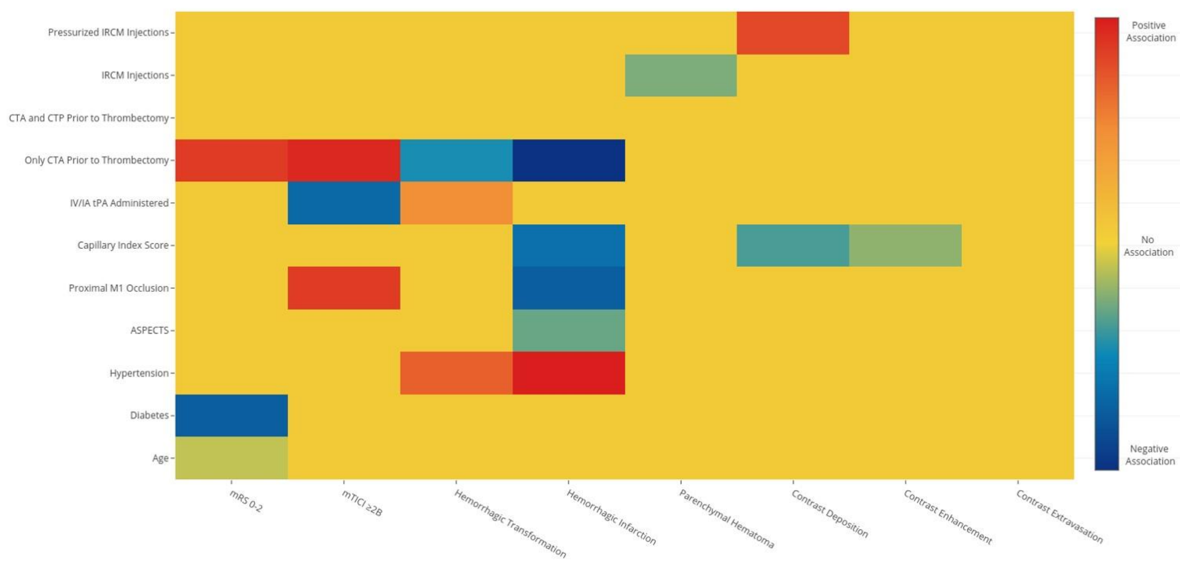

(Filename: TCT_2924_ASNRIRCMFigure1.jpg)

3322

Patterns of Thalamic Lesions in Leigh Syndrome

S Teixeira[1], C Alves[1], F Gonçalves[1], K Shekdar[2], J Martin-Saavedra[1], A Goldstein[1], G Zuccoli[3]
[1]Children's Hospital of Philadelphia, Philadelphia, PA, [2]CHILDREN'S HOSPITAL OF PHILADELPHIA, PHILADELPHIA, PA, [3]CHOP, Philadelphia, PA

Purpose
LS is characterized by symmetrical signal intensity alterations in the basal ganglia (i.e. pallidus, putamen and caudatus), and brainstem. Seldom, the thalami are affected in LS patients. The purpose of this study is to describe the imaging patterns of thalamic involvement in LS.
Materials and Methods
This is a retrospective IRB approved study including patients seen from 2000 to 2018 at an academic children's hospital. Inclusion criteria were: confirmed genetic mutation related to MC, availability of brain magnetic resonance imaging (MRI), and final diagnosis of LS. Diagnosis of LS was made according to the previous clinical described criteria retrieved from the medical notes. MRIs were reviewed by experienced pediatric neuroradiologists.
Results
Out of 105 patients with confirmed genetic mutation of MC and available brain MRI, 34 met our inclusion criteria. Eleven (32%) patients disclosed bilateral thalamic lesions. All of them, showed association with classical LS brainstem and/or basal ganglia abnormalities. Four patients (36%) showed stroke-like appearance in the artery of Percheron vascular territory, 3 patients (27%) showed striking medial thalamic lesions, 2 patients (18%) subtle medial thalamic lesions, one patient (9%) showed diffuse thalamic involvement, and one patient (9%) demonstrated lateral thalamic lesions.
Conclusions
Thalamic lesions are present in LS with presentation patterns mimicking acute infarction.

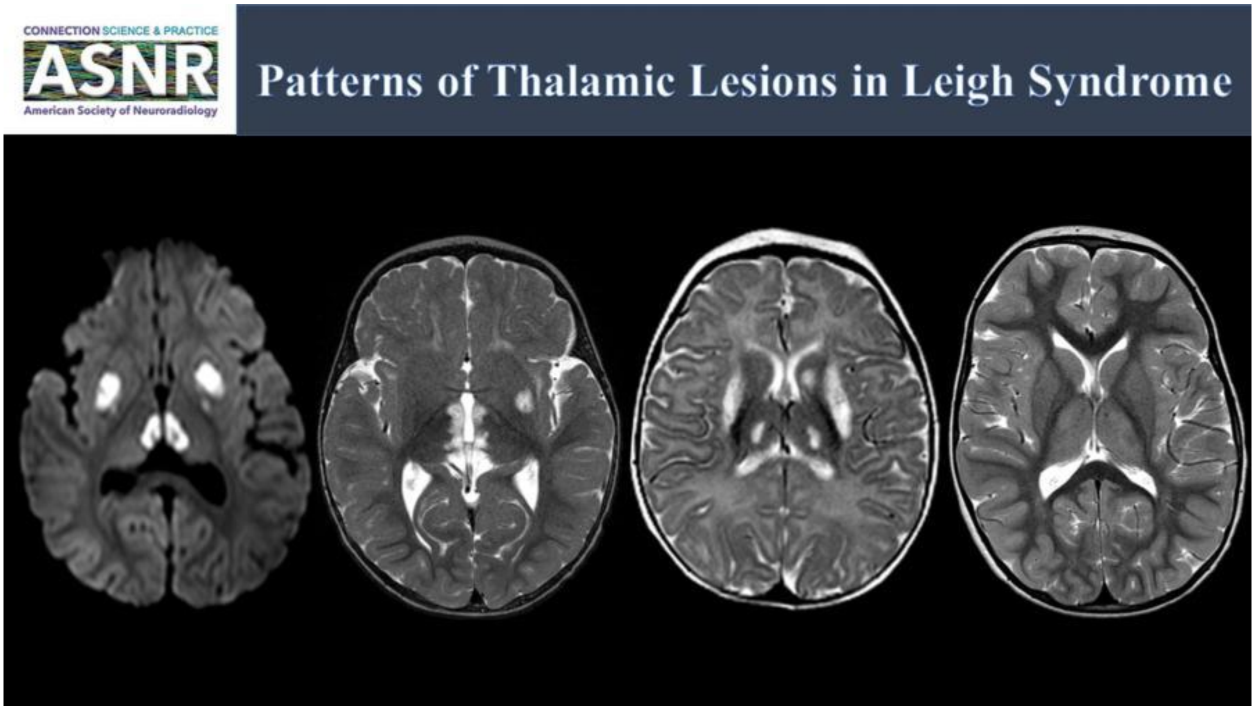

(Filename: TCT_3322_ABSTRACTThalamus300.jpg)

3587

Primary Central Nervous System Lymphoma and Glioblastoma: Differentiation Based on Venous Architectural Ddistortion in High-resolution Susceptibility Weighted Imaging

O Arevalo[1], S Calle[1], S Khanpara[1], A Kamali[1], X Zhang[2], C Soto[3], Y Esquenazi[4], L Ballester[5], R Riascos[1]
[1]Department of Diagnostic and Interventional Imaging. McGovern Medical School, UTHealth., Houston, TX, [2]Center for Clinical and Translational Sciences. University of Texas Health Science Center at Houston, Houston, TX, [3]National University of Colombia, Bogota, Colombia, [4]Vivian L. Smith Department of Neurosurgery. McGovern Medical School, UTHealth., Houston, TX, [5]Department of Pathology and Laboratory Medicine. McGovern Medical School, UTHealth., Houston, TX

Purpose
To determine the usefulness of venous architectural distortion in high-resolution susceptibility-weighted imaging to differentiate Glioblastoma versus primary central nervous system lymphoma.
Materials and Methods
Fifteen and nine patients with pathology-proven GBM and PCNSL respectively were retrospectively reviewed. Patients underwent standard technique susceptibility-weighted imaging (SWI) MRI on a 3T magnet preoperatively. Patients included in the study had not initiated any therapy before imaging. Four blinded readers with different levels of experience visually classified the distortion of the medullary veins of the brain on SWI MinIP images into two main groups: vein damage Vs. Non-damage using an OsiriX™ workstation. The inter-rater variability was measured by the Fleiss' Kappa.
Results
The prevalence of vein damage in the GBM vs the PCNSL group were 66% Vs. 33% for rater 1 (p=0.13), 66% Vs. 22% for rater 2 (p=0.035), 46% Vs. 11% for rater 3 (p=0.07), and 53% Vs. 44% for rater 4 (p=0.63). The readings among four raters were non agreeable. The Fleiss' Kappa value was 0,23 for the whole cohort, 0,200 for the GBM subgroup, and 0,77 for the PCNSL subgroup.

Conclusions
Overall, GBM caused medullary vein architectural distortion more frequently than PCNSL; however, no statistically significant difference was reached. It is hypothesized that with a bigger sample size, and by using a standardized visual scale a statistically significant difference and a better inter-rater correlation can be achieved.

Table 1. Vein damage comparison between GBM and lymphoma (# and % of vein damage are shown in the table)

	GBM (N=15)		Lymphoma (N=9)			
	Vein damage	%	Vein damage	%	Difference in %	P value
Rater 1	10	66.7	3	33.3	33.3	0.113
Rater 2	10	66.7	2	22.2	44.4	0.035
Rater 3	7	46.7	1	11.1	35.6	0.074
Rater 4	8	53.3	4	44.4	8.9	0.673

The score test was used to compare vein damage rate between GBM and lymphoma groups

Table 2. Inter-rater variability - Fleiss' Kappa for four raters is shown in the table

Cohort	Fleiss' Kappa	P value
Whole cohort	0.233	0.005
GBM subgroup	0.200	0.058
Lymphoma subgroup	0.077	0.572

(Filename: TCT_3587_SWI.jpg)

3209

Pseudo-occlusion of The Proximal Internal Carotid Artery Predicts Poor Outcome After Mechanical Thrombectomy in Acute Ischemic Stroke

W Jung[1], J Choi[2], M Han[3]
[1]Ajou University Hospital, Suwon, Korea, Republic of, [2]Ajou University School of Medicine, Suwon-si, Gyeonggi-do, [3]Ajou University Medical Center, Suwon-si, Gyeonggi-do

Purpose
The pseudo-occlusion (PO) on computed tomographic angiography (CTA) in the cervical ICA (cICA) in acute ischemic stroke can be caused by distal ICA occlusion. We aimed to investigate its relationship with clinical outcome after mechanical thrombectomy (MT).
Materials and Methods
All patients who received MT with acute distal ICA occlusions evaluated by CTA between July 2012 and March 2018 were retrospectively reviewed. cICA-PO was defined when CTA showed a gradual contrast decline located above the level of the carotid bulb on arterial phase whereas DSA proved that this artery was patent. Poor outcome was defined as 3-month modified Rankin Scale (mRS) of 4 to 6. Binary logistic regression analysis was used to investigate the relationship of cICA-PO with poor outcome. In cICA-PO group, the relationship between successful recanalization and outcome was also evaluated.
Results
A total of 71 patients with distal ICA occlusion were included and 40 (56.3%) had cICA-PO. Patients

with cICA-PO were more likely to have poor outcome (80.0% vs. 25.8%, P<0.001), hemorrhagic transformation (32.5% vs. 9.6%, P=0.01) and a lower rate of successful recanalization (65.0% vs. 90.3%, P=0.014) than non-PO group. cICA-PO was independently associated with poor outcome (odds ratio, 4.278; 95% CI, 1.080-33.006; P=0.045) after adjustment using binary logistic regression analysis. In cICA-PO group, all patients who did not achieved successful recanalization (n=15) after MT underwent poor outcome, whereas 69.2% patients with successful recanalization underwent poor outcome (P=0.018).
Conclusions
The prevalence of cICA-PO in the distal ICA occlusion is relatively high in acute ischemic stroke and most of them show poor outcome if they are not achieved successful recanalization. Therefore, we suggest that more aggressive recanalization approaches to get successful recanalization may be needed in patients with cICA-PO.

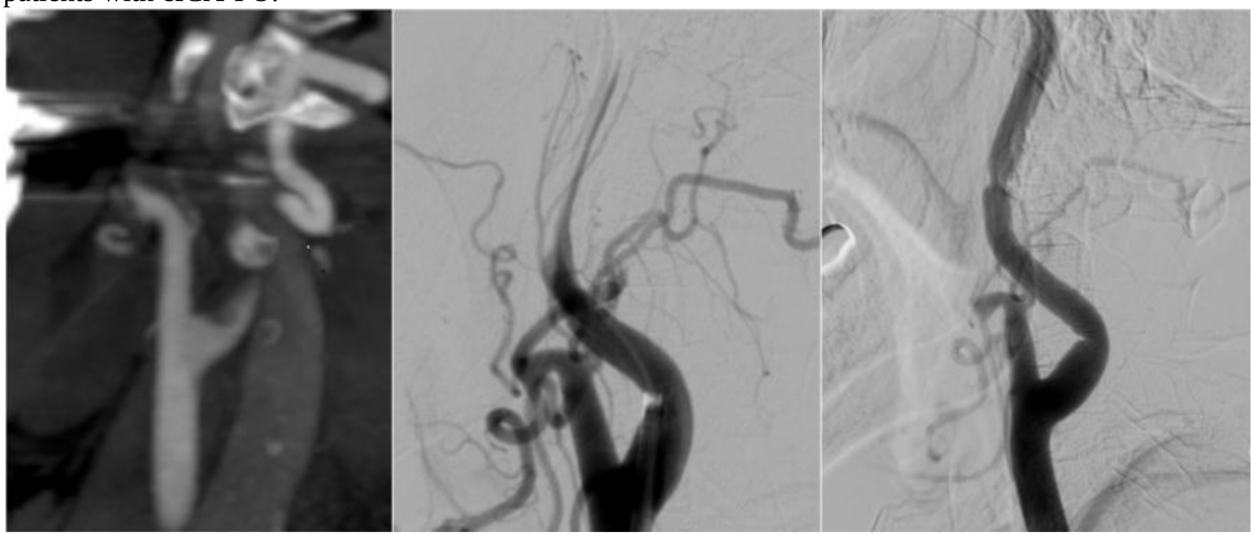

(Filename: TCT_3209_.jpg)

3541

Quantitative Evaluation of Imaging Markers for Intracerebral Hematoma Expansion Prediction Using Single and Dual Energy CT

C Tan[1], D Kuppens[2], R Bergmans[2], R Gupta[3]
[1]Harvard Medical School / Massachusetts General Hospital, Cambridge, MA, [2]University of Twente, Enschede, The Netherlands / Massachusetts General Hospital, Boston, MA, [3]Massachusetts General Hospital, Boston, MA

Purpose
Hematoma expansion after intracerebral hemorrhage (ICH) is strongly associated with increased mortality, worse functional outcome, and neurologic deterioration. Early recognition of patients at risk for hematoma expansion, therefore, is critical for selection of patients for targeted intervention. Many qualitative radiographic markers to predict hematoma expansion have been described, such as spot sign, texture-based signs, and other quantitative indices derived from non-contrast computed tomography (CT), CT angiography (CTA), and dual-energy computed tomography (DECT) scans. Each of these markers of hematoma expansion reflects a specific property of ICH such as active hemorrhage, its time course, or its multifocal nature. Individually, these markers have been found to be highly specific for expansion but lack sensitivity. In this research, we assess whether a combination of quantitative markers would substantially improve predictive performance.

Materials and Methods
Using 115 hematomas in 107 patients, we derived 15 previously identified markers and estimated their relative and combined predictive contributions to the risk of hematoma expansion.
Results
Individually, the best performing predictors were the DECT-based iodine content in the hematoma and in spot signs (area under ROC >0.75 for all); these markers performed remarkably better than those based on textural characteristics of the hematoma (area under ROC <0.60 for all). A forward/backward model selection approach showed that two markers out of these 15 – namely, iodine within the hematoma and the iodine in the brightest spot sign (if any) – optimally predicted the risk of hematoma expansion. The lack of significant contribution from other markers is attributed to high correlation among them and the fact that the information they contribute is subsumed in these two iodine based markers.
Conclusions
DECT-based iodine markers of hematoma expansion offer a reliable method for selecting ICH patients at highest risk of hematoma expansion.

2703

Radiogenomics of Blood Brain Barrier Disruption in Patients with Aneurysmal Subarachnoid Hemorrhage Stratified by Age and Sex.

S Glynn[1], Y Oh[1], N Smith[2], A Segal[3], A Gupta[4], P Sanelli[5], J Ivanidze[6]
[1]Weill Cornell Medicine, New York, NY, [2]N/A, N/A, [3]NewYork-Presbyterian Hospital - Weill Cornell, New York, NY, [4]WEILL CORNELL MEDICAL COLLEGE, NEW YORK, NY, [5]NORTHWELL HEALTH NSUH, MANHASSET, NY, [6]N/A, New York, NY

Purpose
Aneurysmal subarachnoid hemorrhage (aSAH) is a devastating disease with high morbidity and mortality. The incidence of aSAH is higher in females and older patients, with worse prognosis. The pathophysiological implications of these differences remain poorly understood. There is a lack of quantitative outcome biomarkers in aSAH. Blood-brain-barrier (BBB) disruption after aSAH is associated with poor outcomes. Matrix metalloproteinase 9 (MMP-9) is inflammation-inducible and cleaves the BBB, and has been implicated in poor outcomes in aSAH. The purpose of this study was to assess BBB disruption and MMP-9 levels in the context of age and sex.
Materials and Methods
In this prospective IRB-approved study, 39 patients underwent axial shuttle CTP on day 0-3 after aSAH. Cerebrospinal fluid (CSF) was collected via ventriculostomy catheter placed for clinical monitoring. MMP-9 levels were measured using ELISA assay. CTP data were post-processed into quantitative BBB permeability (BBBP) maps using Olea Sphere software (Olea Medical, France). Mann-Whitney-U tests and 2-way-ANOVA were performed.
Results
Mean age was 58.6 years (range: 35-86); 63% (22/30) were female; mean Hunt-Hess-score was 3. Patients were stratified as either 60 years and younger (n=16) or older than 60 years (n=15). Younger females tended to have higher BBBP values compared to younger males, while this relationship reversed in the older cohort, although these findings did not reach statistical significance (p=0.17, 0.18, 0.11 and 0.52, respectively). Females had significantly higher MMP-9 levels (p=0.04), and young females had the highest MMP-9 levels.
Conclusions
We found a statistically significant increase in MMP-9 in young female patients with aSAH. Further, there appear to be disctinct patterns of BBBP versus sex depending on age. Given the higher incidence of aSAH in females and the possible role of BBB disruption in aSAH, these findings suggest potential sex

and age-related physiological differences related to BBB and neuroinflammation in aSAH, with diagnostic and therapeutic implications.

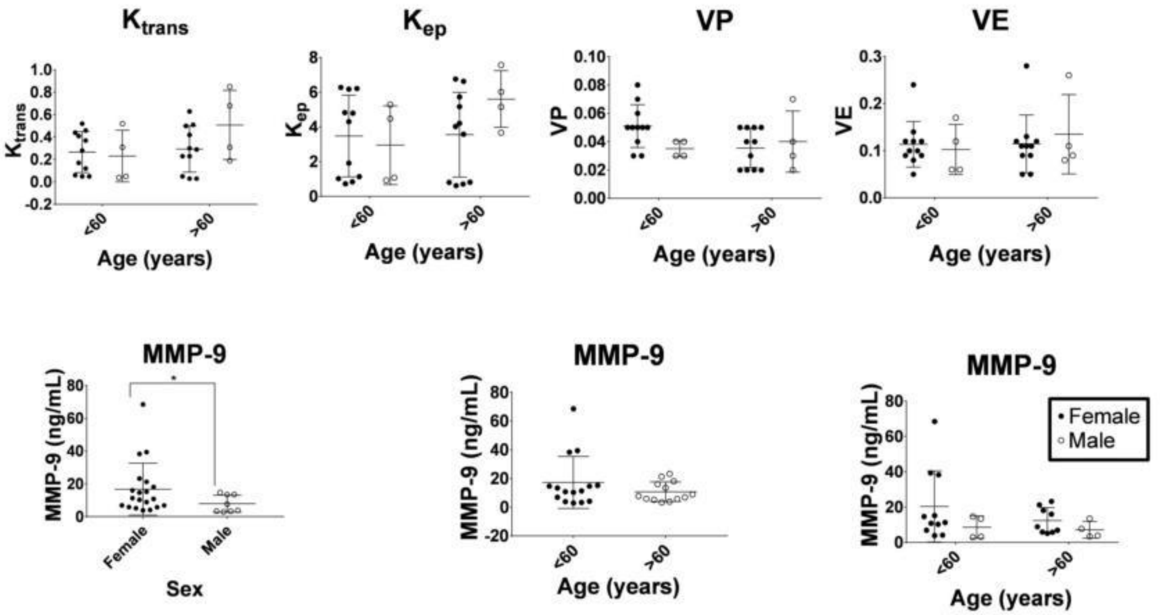

Blood brain barrier permeability parameters and MMP-9 levels stratified by age and sex. BBBP parameters, K_{trans} (volume transfer constant from the blood plasma to EES), K_{ep} (EES-to-IVS washout rate), VP (plasmatic volume per unit tissue volume) and VE (volume in the EES per unit of tissue volume), as well as MMP-9 levels in patient cerebrospinal fluid, were analyzed in patients 60 years old and younger (n=16) or older than 60 years (n=15) and stratified by sex. Mann-Whitney U tests and 2-way ANOVA tests were performed to determine statistical significance.

(Filename: TCT_2703_ASNRFigure.jpg)

2270

Radiomics MRI Pheynotyping of Oropharyngeal Squamous Cell Carcinoma According to the Status of Human Papillomavirus

B Sohn[1], J Kim[2], S Bae[3], C Park[4], J Kim[4], S Ahn[5], S Lee[6]
[1]Yonsei University College of Medicine, Seoul, Korea, [2]Yonsei University College of Medicine, Seoul, CA, [3]Yonsei University College of Medicine, Seoul , Korea, Republic of, [4]Yonsei university, Seoul, Korea, [5]Yonsei University College of Medicine, Seoul, Korea, Republic of, [6]Yonsei University College of Medicine, Seoul, Seoul

Purpose
To investigate potential of MRI based radiomics features as a biomarker that predicting human papillomavirus phenotype in oropharyngeal cancer.
Materials and Methods
73 patients who diagnosed as oropharyngeal squamous cell carcinoma from our institution with

pretreatment MRI were consecutively enrolled, from January 2012 to December 2017. Patients without 3D T1 contrast enhanced T1 image or axial T2WI were excluded. (4 patients) Patient with inadequate image quality due to severe motion artifact were excluded. (1 patient). Finally, total 68 patients were included for the study.The test set for validation was prepared, by temporally divide the patients group into two subgroups. The patients who underwent MRI before Jan 01 2016 were classified as training set and who underwent MRI after Jan 01 2016 were classified as test set. The p16 immunohistochemistry analysis was used as a surrogate marker for HPV phenotyping. Enhancing tumors were semiatutomatically segmented on each slice of the postcontrast T1-weighted images and T2-weighted images were registered. Then, an in-house radiomics feature extracting python code, based on Pyradiomics was used. The DICOM images were resampled with 1x1x1mm resolution and subjected to N4 bias correction. The T2WI were registered to 3D CE T1WI by elastic ITK. We apply histogram matching to normalize the MRI images of all patients. Total 170 features (78 features from 3D CE T1WI and T2WI, and 14 shape features) were extracted from the ROI area of the MRI images. SMOTE was adopted for resolve imbalance in training set. After that, the LASSO method was adopted in selecting statistically valuable predictive features from 3D CE T1WI, T2WI and combination of T2WI/3D CE T1WI. The selected features were added linearly to make a radiomics score. Internal cross validation and temporal external test set validation were done.

Results

The proportion of the HPV status between training and test sets are not statistically different by chi-square test ($p = 0.055$). After adopting SMOTE, the modified training set shows relatively balanced proportion of HPV status. By applying LASSO, there was no statistically valuable features from CET1WI and T2WI separately. With features from combination of these two sequences, LASSO selected 7 features to induce the Radiomics score. The radiomic score model yielded excellent performance with Bootstrapped internal validation (AUC was 0.982 (0.942-1.000)) and moderate performance with test set (AUC was 0.744 (0.496-0.991)) to differentiate oropharyngeal squamous cell carcinoma according to HPV status.

Conclusions

The results suggests that radiomics based phenotyping might differentiate oropharyngeal carcinoma according to HPV status, and thus has potential as a practical imaging biomarker.

Selected features with its selection probability by LASSO

Features	Selection probability
T1_3d_original_firstorder_Skewness	0.95
T1_3d_original_firstorder_Median	0.86
T2_original_firstorder_Skewness	0.83
T1_3d_original_glszm_GrayLevelVariance	0.65
T1_3d_original_gldm_GrayLevelVariance	0.6
T2_original_glcm_JointEnergy	0.56
T2_original_glcm_ClusterProminence	0.5

Logistic regression with top 3 features

Features	Odds ratio (95% CI)	p
T1_3d_original_firstorder_Skewness	8.130 (1.859, 42.179)	0.0077
T1_3d_original_firstorder_Median	0.984 (0.977, 0.989)	<.0001
T2_original_firstorder_Skewness	0.790 (0.383, 1.582)	0.5101

Discrimination ability

	c-statistic	95% CI	Bootstrap validated c-statistic	95% CI
Training set	0.9542	(0.926, 0.982)	0.9539	(0.9245, 0.978)
Test set	0.7456	(0.449, 1.000)		

(Filename: TCT_2270_tables.jpg)

3636

Reconstruction of Osseous Structures in MRI Scans of the Cervical Spine with BoneMRI: a Quantitative Analysis

B van der Kolk[1], M van Stralen[2], M Podlogar[3], F Zijlstra[4], M Florkow[4], D Slotman[5], J van Osch[3], E Oost[6], J Hendrikse[7], P de Jong[4], R Castelein[4], M Viergever[4], M Maas[8], P Seevinck[2], M Boomsma[3]
[1]Isala / Amsterdam UMC, Zwolle, The Netherlands, [2]UMC Utrecht / MRIguidance BV, Utrecht, The Netherlands, [3]Isala, Zwolle, The Netherlands, [4]UMC Utrecht, Utrecht, The Netherlands, [5]University of Twente, Enschede, The Netherlands, [6]MRIguidance BV, Utrecht, The Netherlands, [7]Utrecht University Medical Center, Utrecht, The Netherlands, [8]Amsterdam UMC, location AMC, Amsterdam, The Netherlands

Purpose
To investigate the accuracy of the visualization of 3D osseous structures using BoneMRI, based on a cervical spine MRI.
Materials and Methods
In this feasibility study, 25 consecutive patients referred to the Department of Radiology of the Isala Hospital (Zwolle, The Netherlands) for a cervical spine MRI were enrolled. After obtaining written informed consent, patients underwent an MRI scan (1.5 Tesla) and a CT scan of the cervical spine. The MRI exam included a sagittal 3D multiple gradient echo (T1w-MGE) sequence for BoneMRI reconstruction. With a deep learning-based approach, a mapping from MRI to CT was optimized to visualize the radiodensity contrast based on the T1w-MGE MRI [1], denoted BoneMRI. The T1w-MGE was registered to the CT images for training and voxelwise comparison. In a fivefold cross-validation, data of 20 patients were used for training, 5 datasets served as test cases. Quantitative comparison

between BoneMRI and CT consisted of ROI-based analysis (air, fat, muscle and vertebral bone), voxelwise comparisons (mean absolute error (MAE)) and assessment of geometrical accuracy (distance measurements by 3 observers). Reproducibility of BoneMRI was assessed in 5 healthy volunteers at the University Medical Center Utrecht (Utrecht, The Netherlands).
Results
BoneMRI accurately reproduced radiodensity contrast of the gold standard CT (Figure 1), demonstrated by ROI-based quantitative analysis, rendering MAE of 83.9 ± 6.6 HU (n=25) and scan-rescan difference of 34.5 ± 2.7 HU (n=5). No significant differences were found between BoneMRI and CT in geometric accuracy of vertebral morphology, with excellent interobserver agreement (intraclass correlation coefficient (ICC) 0.91-0.98, n=10).
Conclusions
BoneMRI is promising for 3D osseous visualization of the cervical spine. BoneMRI reproduces CT radiodensity contrast accurately, without the need for ionizing radiation. Our future research will focus on qualitative assessment, evaluation of the impact on clinical workflow and quantification of both clinician and patient's benefits; thus, validating its contribution to value-based healthcare.

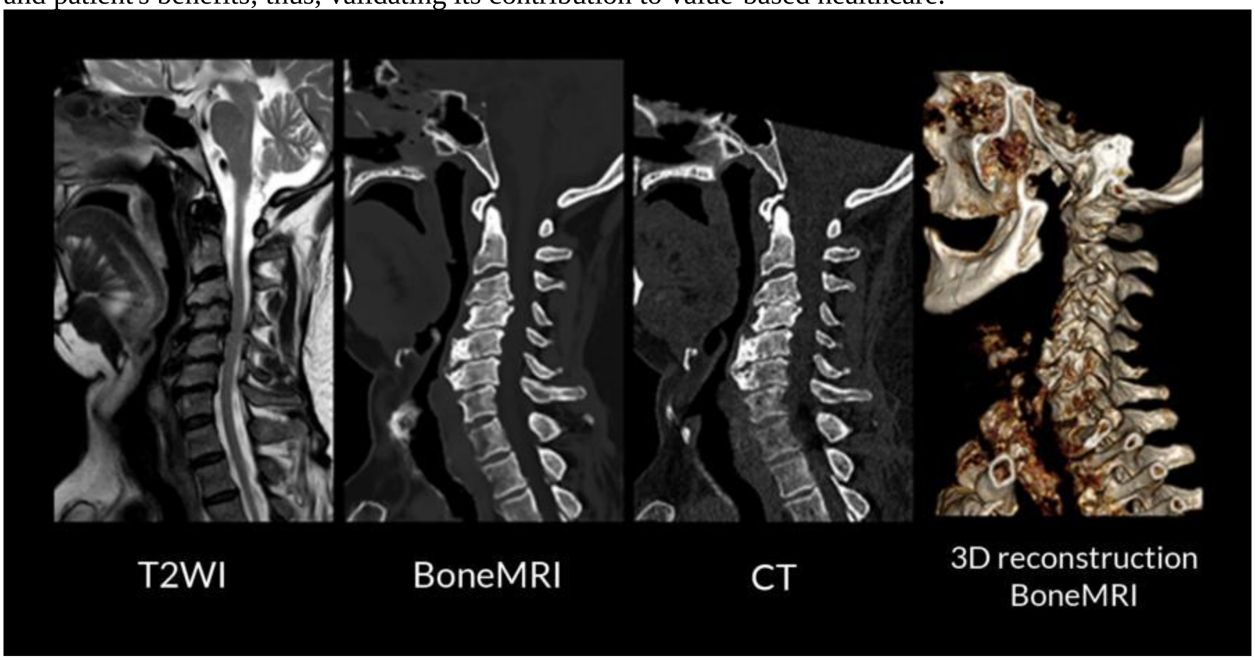

(Filename: TCT_3636_ASNR2019_Figure_T2w_BoneMRI_CT_3D_def.jpg)

2328

Recurrent Pattern Prediction Based on Conventional MRI in GBM Patients: a Retrospective Study

X Du[1]
[1]*Department of Radiology, Daping Hospital, Chongqing, Chongqing*

Purpose
To investigate the significance of preoperative conventional MRI abnormalities on patterns of recurrence and outcomes in patients with GBM.
Materials and Methods
Sixty-five patients with recurrent GBM were retrospectively evaluated. Conventional MRI including T1W, T2W, FLAIR, DWI and T1W contrast images were acquired for all patients preoperatively. Quantitative MRI features were extracted using VASARI features criteria. Recurrence patterns were defined in T1W contrast images. Progression free and overall survival was determined for patients with

different patterns. Potential risk factors for outcomes were assessed using univariate models followed by multivariate analysis.
Results
Thirty VASARI features were identified in all cases. The recurrence pattern in these cases was local in 49/65 (75.4%) and distant in 16/65 (24.6%). VASARI features including Definition of the non-enhancing margin (F13), Cortical involvement (F20) and Deep WM invasion (F21) overlapped with recurrence patterns. Kaplan–Meier analysis revealed inferior progression free survival (PFS) in patients with an Age over 48 or with an irregular non-enhancing margin compared to those without, despite similarities between the groups in terms of IDH status, performance status, and F20, F21 status. Followed cox multivariate analysis revealed F13 was an independent prognostic factor on PFS in recurrent GBM patients.
Conclusions
The presence of conventional MRI based features were associated with the location of tumor recurrence as demonstrated by frequent overlap in this series, and was associated with a trend toward inferior outcomes. This may indicate warrants consideration with respect to treatment planning.

3271

Risk Factors of Symptomatic Intracerebral Hemorrhage after Endovascular Thrombectomy: The Predictive Value of Collateral Status on Multiphase CT Angiography.

B Kim[1], B Kim[1], S You[1]
[1]*Korea University Anam Hospital, SEOUL, KOREA-REPUBLIC OF (KOR)*

Purpose
Symptomatic intracranial hemorrhage (sICH) is major concern in the patient with acute ischemic stroke (AIS) after endovascular thrombectomy (EVT). We sought to determine sICH definition with the highest clinical relevance and identify predictors of sICH after EVT.
Materials and Methods
Retrospective single center analysis performed in the consecutive patients treated with EVT for AIS in the anterior circulation from March 2014 to July 2018. The variables of interests were pial collateral status on CT angiography, baseline infarct volume on CT perfusion, and sICH defined by several common definitions. Multivariate logistic regression analysis was used to find the sICH definition associated with clinical outcome and risk factors associated with the sICH.
Results
Of the total 86 study patients (mean age 70 ± 11 and median NIHSS score of 15 (11 – 19)), 40 patients (47%) showed good neurologic outcome with mRS from 0 to 2. There were 13 (15%), 15(17%) and 7(8%) patients who met the sICH criteria of ECASS1, ECASS2 and ECASS3, respectively. Univariate and multivariate analysis showed higher initial NIHSS score, poor pial collaterality status, lower rates of successful recanalization and presence of sICH in the patients with poor clinical outcomes ($p < 0.05$). Of 70 patients with available CT perfusion data, ASPECT score of CBV and pial collaterality status were independent predictors for development of sICH.
Conclusions
Pre-procedural evaluation with CT angiography and CT perfusion is important for predicting sICH development after EVT. Pial collaterality status may associate with sICH development and influence clinical outcome.

2605

Sagittal DTI of the Spinal Cord in Lesion Positive and Negative MS patients

N Khanna[1], S Agarwal[2], C Bhamani[1], S Faro[2], J Pillai[3], E Mowry[4], I Izbudak[5]
[1]Johns Hopkins Hospital, Baltimore, MD, [2]Johns Hopkins School of Medicine, Baltimore, MD, [3]JOHNS HOPKINS HOSPITAL, BALTIMORE, MD, [4]The Johns Hopkins Hospital, Multiple Sclerosis Center, Baltimore, MD, [5]Johns Hopkins University, Baltimore, MD

Purpose
The purpose of our study is to determine group differences in advanced diffusion metrics of the spinal cord in patients with multiple sclerosis who have demyelinating spinal cord lesions on conventional MRI (lesion positive) those who have multiple sclerosis but do not have demyelinating lesions (lesion negative) as measured by sagittal DTI.
Materials and Methods
We first queried our institutional PACS for all MRIs of the cervical and thoracic spine performed between 01/01/2013 and 01/01/2018 that included a sagittal DTI sequence (Siemens resolve) performed in an identical number of directions (20) in order to maintain consistent diffusion measurements between examinations. The results were screened to identify patients with a history of multiple sclerosis. These exams were reviewed to identify those with and those without demyelinating lesions involving the spinal cord as evidenced by T2-weighted hyperintensity, which were designated as lesion positive and lesion negative, respectively ($n = 10$ for each group) The images were pre-processed in FSL to correct for eddy current-induced distortions and subject movements. Region of Interests (ROIs) were then drawn in the upper, mid and lower segments for both the cervical and thoracic spinal cord. In the cervical spine, the upper cervical cord was defined as C2-C3, the mid spinal cord was designated C4-C5 and the lower cervical spinal cord as C6-C7. In the thoracic spine, the upper segment was defined as T1-T4, mid was defined as T5-T8 and the lower segment as T9-T12. The presence or absence of a demyelinating plaque within the segmented ROI of the lesion positive group was designated. Subsequently diffusion matrix was obtained and diffusion parameters-- fractional anisotropy (FA), mean diffusivity (MD), axial diffusivity (AD) and radial diffusivity (RD) from the ROIs were calculated using FSL toolbox. When then compared the segments within the spinal cord with demyelinating plaques in the lesion positive group to the corresponding segments in lesion negative group.
Results
Our data showed that the mean FA for the upper, mid and lower cervical spinal cord in the lesion positive cord containing demyelinating plaques was 0.769 ($n=9$), 0.707 ($n=9$) and 0.538 ($n=7$), respectively. In the lesion negative group, the values in the upper, mid and lower cervical spinal cord were 0.722 ($n=10$), 0.704 ($n=10$) and 0.627 ($n=10$), respectively. In the thoracic cord, the FA for the upper, mid and lower segments in the lesion positive cord containing demyelinating plaques was 0.463 ($n = 8$), 0.546 ($n = 9$) and 0.579 ($n = 6$), respectively The intergroup differences in FA were statistically significant differences in the lower cervical spinal cord segments ($p = 0.029$). The differences were not statistically significant in the upper cervical cord group ($p = 0.1341$) and in the middle cervical cord group ($p = 0.91$). No statistically significant difference was found for the mean, radial and axial diffusivity of the upper, mid and lower segments of cervical spinal cord with demyelinating plaques as compared to lesion negative for any segment at this point in data collection. No statistical significance was found in the FA values at this time.
Conclusions
As has been previously reported reported, advanced diffusion metrics in lesional and non-lesional spinal cord has been established with both sagittal and axial DTI techniques. Our goal, specifically to identify intergroup variability in diffusion metrics has thus far shown statistically significant differences in FA values of the lower third of the cervical spinal cord in MS positive patients with demyelinating plaques and those without, and near statistical significance ($p = 0.13$) between these groups in the upper segment of the cervical spinal cord. We hope to expand upon these preliminary results with more cases to detect other potentially statistically significant intergroup differences in diffusion metrics.

3068

Salivary Gland Mass Fine Needle Aspiration Diagnostic Yield by Preprocedural Imaging Morphological Characteristics

S Poliashenko[1], A Chen[1], A Aiken[1]
[1]Emory University, Atlanta, GA

Purpose
Salivary gland lesions include a wide variety of both benign and malignant pathology and are frequently difficult to definitively evaluate on the basis of clinical exam and imaging alone. Ultrasound guided fine need aspiration (FNA) for tissue sampling is often the next step in evaluation, however its utilization is not standardized in management guidelines. While salivary gland FNA sensitivity/specificity and accuracy has been reported in the literature fairly extensively, there is little research on the correlation of salivary gland lesion imaging characteristics and FNA diagnostic yield. Our goal is to examine this correlation to determine if there is a subset of patients that may not benefit from a preoperative FNA or have higher non-diagnostic rates.
Materials and Methods
Inclusion criteria were: 1. Ultrasound-guided salivary gland performed biopsies at our institute with available pre-procedural US, CT, or MR images. 2. Final cytopathology reports at our institution. A search of the imaging data warehouse was performed for all CPT codes for ultrasound guided salivary gland biopsies performed between 2013 and 2018. This search yielded 156 patients who met the inclusion criteria. The imaging was reviewed for the morphology (cystic, cystic/solid, or solid). Cytopathology reports were reviewed to document diagnostic yield.
Results
Of the 156 total patients included in the study, 16 had purely cystic lesions, 34 had cystic/solid lesions, and 106 had solid lesions determined on pre-procedure imaging. When stratified by these morphologic characteristics, patients with purely cystic lesions had a cytopathologic non-diagnosis rate (either non-diagnostic specimen or findings of neoplasm of uncertain benign or malignant etiology) was 69%, as opposed to patients with solid lesions 21% (P=0.002) or mixed cystic/solid lesions 32% (P=0.02).
Conclusions
The subset of patients with cystic salivary gland lesions (as determined on pre-procedural imaging) have much higher rates of effectively non-diagnostic FNA results thus providing no significant further management guidance.

2616

The (Mis)use of Imaging Criteria in the Assessment of Glioblastoma Treatment Response

J Buwanabala[1], A Mirchandani[2], T Booth[3]
[1]Cambridge University Hospitals NHS Foundation Trust, Cambridge , UK, [2]King's College London, London, UK, [3]King's College Hospital NHS Foundation Trust, London, UK

Purpose
Imaging is used as a monitoring biomarker in treatment response assessment. The purpose of our study is to analyse whether imaging criteria used in the assessment of treatment response in glioblastoma clinical trials are adhered to. We also see whether published imaging criteria can fully capture the relevant information required to accurately determine treatment response.
Materials and Methods
Key MeSH terms were applied to PubMed and Scopus databases to extract clinical trials conducted from 2012. The resulting articles and their references were reviewed and publications that were not relevant to the study were excluded. Forty publications were selected for the study. A pre-formed data collection tool

was used to extract the data set from the selected papers pertaining to areas such as the use of medication that are known to influence imaging patterns, the use of pre-defined imaging criteria and mitigating for pseudoprogression. The extracted data set was then collated into a traffic light system table to better visually display the collated data.
Results
We demonstrate that there are many unmeasured variables and confounding factors pertaining to the use of imaging as a monitoring biomarker. Examples of problematic areas include the following: greater than 60% of reviewed trials used medications/immunotherapy therapies that are known to impact imaging appearances, many trials don't use a pre-defined 'gold-standard' imaging criteria and ones that did often use modifications/combinations of several criterion and not utilising imaging timelines that would allow for cases of pseudoprogression or pseudoresponse to be demonstrated.
Conclusions
There are confounding factors in the current use of imaging as a monitoring biomarker in glioblastoma treatment response trials. This is due to a high degree of heterogeneity in how imaging criteria are applied in the assessment of treatment response in glioblastoma clinical trials. Furthermore, relevant information required to accurately determine treatment response may not be included in published imaging criteria.

(Filename: TCT_2616_trafficlight.jpg)

3307

The Value of Spectroscopy and Perfusion MRI in Differentiating Tumor Recurrence From Treatment Necrosis in High-grade Gliomas

N Freedman[1], E Saraf Lavi[2], M Goryawala[1], A Lavi[3], A Maudsley[1]
[1]University of Miami, Miami, FL, [2]University of Miami, Coral Gables, FL, [3]University of Miami, CORAL GABLES, FL

Purpose
To compare choline/creatine (Cho/Cr), choline/N-acetylaspartate (Cho/NAA) ratios, and perfusion weighted imaging (PWI) in patients with high-grade primary brain neoplasm and to evaluate their usefulness in the differentiation between tumor progression/residual tumor and radiation related injury.
Materials and Methods
26 studies of adult patients (age range 31-78) with high-grade primary brain neoplasm (17 Grade IV glioblastomas, 5 anaplastic astrocytomas, and 4 anaplastic oligodendrogliomas) who underwent 3T MRI

were retrospectively analyzed. Out of the 20 studies, 15 were tumor and 5 were radiation related injury on pathology or clinical follow up. The MR examination included conventional MR imaging (T1-MPRAGE without and with CE, T2-TSE, T2 FLAIR), PWI and short TE volumetric MR spectroscopic imaging (MRSI) and single-voxel spectroscopy. Lesion rCBV values were calculated. Cho/Cr and Cho/NAA ratios from voxels that were placed on the solid/enhancing part of the tumor were calculated.

Results

Cut off values of 1.7 for Cho/Cr,1.8 for Cho/NAA, and 1.75 for rCBV were used as residual tumor/tumor progression criteria. All tumor cases (Image 1) showed elevated Cho/Cr and Cho/NAA ratios, with the exception of one case of anaplastic astrocytoma, which showed no contrast enhancement but showed elevated rCBV. In two tumor cases there were elevated Cho/Cr and Cho/NAA ratios with no elevation of rCBV and variable contrast enhancement (Image 2). All cases of radiation related injury showed no elevation of Cho/Cr, NAA/Cr ratios or rCBV (Image 3).

Conclusions

Although PWI is considered to be the most reliable MR imaging sequence in the differentiation between high-grade tumor/ tumor recurrence and radiation necrosis, MR spectroscopy has an important complimentary role in those cases where conventional MR images and PWI are inconclusive.

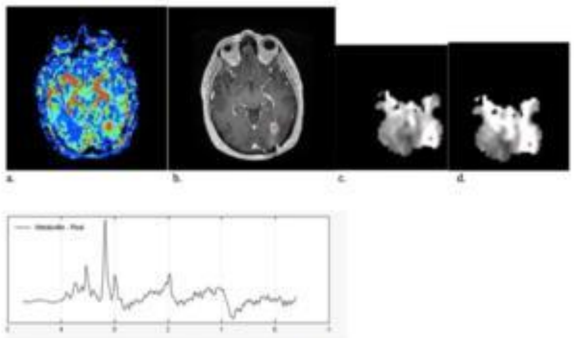

Image 1. 57-year-old male with a grade 4 glioblastoma multiforme. a) PWI map showing high rCBV in the area of tumor in the left parietal lobe. b) T1PC imaging showing enhancement in the region of tumor. C and d) Cho/Cr and Cho/NAA metabolite maps, respectively, showing increased signal within the examined region. e) MR Spectroscopy showing increased Choline peak and significantly decreased NAA peak consistent with increased cellular turnover and significant neuronal loss, respectively, with Cho/Cr of 3.009 and Cho/NAA of 3.921 consistent with tumor progression.

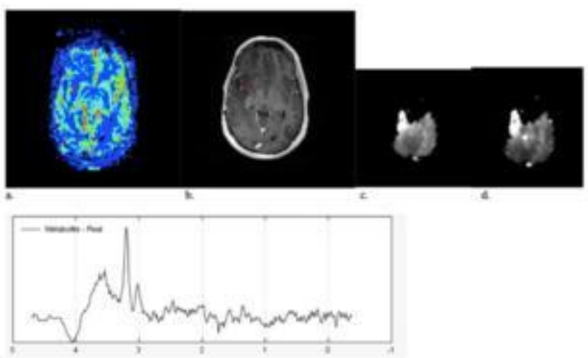

Image 2. 40-year-old male with anaplastic astrocytoma degenerated to high-grade glioblastoma multiforme. a) PWI map showing low rCBV in the area of tumor in the right temporal and parietal lobe. b) CET1 image shows lack of enhancement in the region of tumor. C and d and e) Spectroscopy shows markedly elevated choline peak with no appreciable NAA peak with elevated Cho/Cr and Cho/NAA ratios.

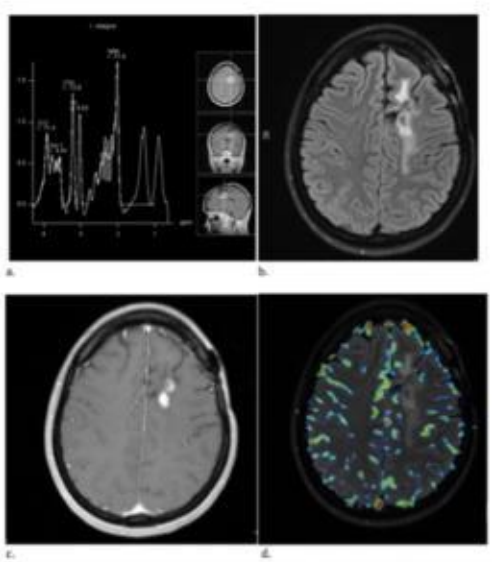

Image 3. Radiation necrosis. 31-year-old female with history of grade 4-glioblastoma multiforme a) MR Spectroscopy shows elevated NAA peak with Cho/Cr of ratio of 1.42 and Cho/NAA ratio of 0.734 b) FLAIR image showing surrounding signal hyperintensity favoring post treatment gliosis in the left frontal lobe. c) CET1 image showing nodular enhancement at the inferior margin of the surgical cavity. d) PWI showing no evidence of increase rCBV in the area of enhancement.

(Filename: TCT_3307_Images1-3.jpg)

3329

Usefulness of Neurite Orientation Dispersion and Density Imaging for Evaluation of the Epileptogenic Zone in Patients with Temporal Lobe Epilepsy

H Uetani[1], M Kitajima[1], T Hamasaki[1], T Yoneda[2], K Morita[3], H Kawaguchi[4], M Tateishi[5], A Mukasa[5], Y Yamashita[1]
[1]Kumamoto University, Kumamoto, Kumamoto, [2]Department of Medical Physics in Advanced Biomedical Sciences, Kumamoto University, Kumamoto, Kumamoto, [3]Department of Radiology, Kumamoto University Hospital, Kumamoto, Kumamoto, [4]Siemens Healthcare K.K, Osaka, Osaka, [5]Kumamoto university, Kumamoto, Kumamoto

Purpose
Identification of the epileptogenic zone is critical in planning surgical treatment for temporal lobe epilepsy (TLE). In some patients with TLE, identification of the epileptogenic zone is difficult on structural MRI. Neurite orientation dispersion and density imaging (NODDI) is a recently developed diffusion technique and provides brain microstructural information.1 The purpose of this study was to evaluate the usefulness of NODDI for identification of the epilptogenic zone in patients with TLE.
Materials and Methods
This study included 16 patients with TLE and 5 healthy controls. At a 3T MRI, axial and coronal T2WI and diffusion images were acquired using 3 diffusion weightings (b = 0, 700, 2000 sec/mm2) along 96 non-collinear directions. For image processing of NODDI, we developed intra-neurite volume fraction (ICVF) map by a publicly available toolbox. Two neuroradiologists independently assessed the signal intensity of the affected hippocampi suggested by clinical data on ICVF and T2WI using a three-points grading system: definitely abnormal, probably abnormal, and equivocal. We compared the confidence of the hippocampal abnormal intensity and the extent of the abnormal intensity between ICVF and T2WI. We also compared ICVF value of the hippocampi between 16 TLE patients and 5 healthy controls.
Results
The confidence of the hippocampal abnormal signal was significantly higher on ICVF map than on T2WI ($p = 0.0147$ and 0.0246, respectively) in both readers. In 88% of the patients, the area with decreased ICVF was larger than that with high signal on T2WI. The mean value of ICVF in the affected hippocampi in TLE patients (0.30 ± 0.06) was significantly lower than that in healthy controls (0.38 ± 0.02) ($p = 0.005$).
Conclusions
In TLE patients, ICVF decreased in the epilptogenic medial temporal lobe even in the area with no abnormality on T2WI. NODDI may be useful for estimating the epileptogenic zone in patients with TLE.

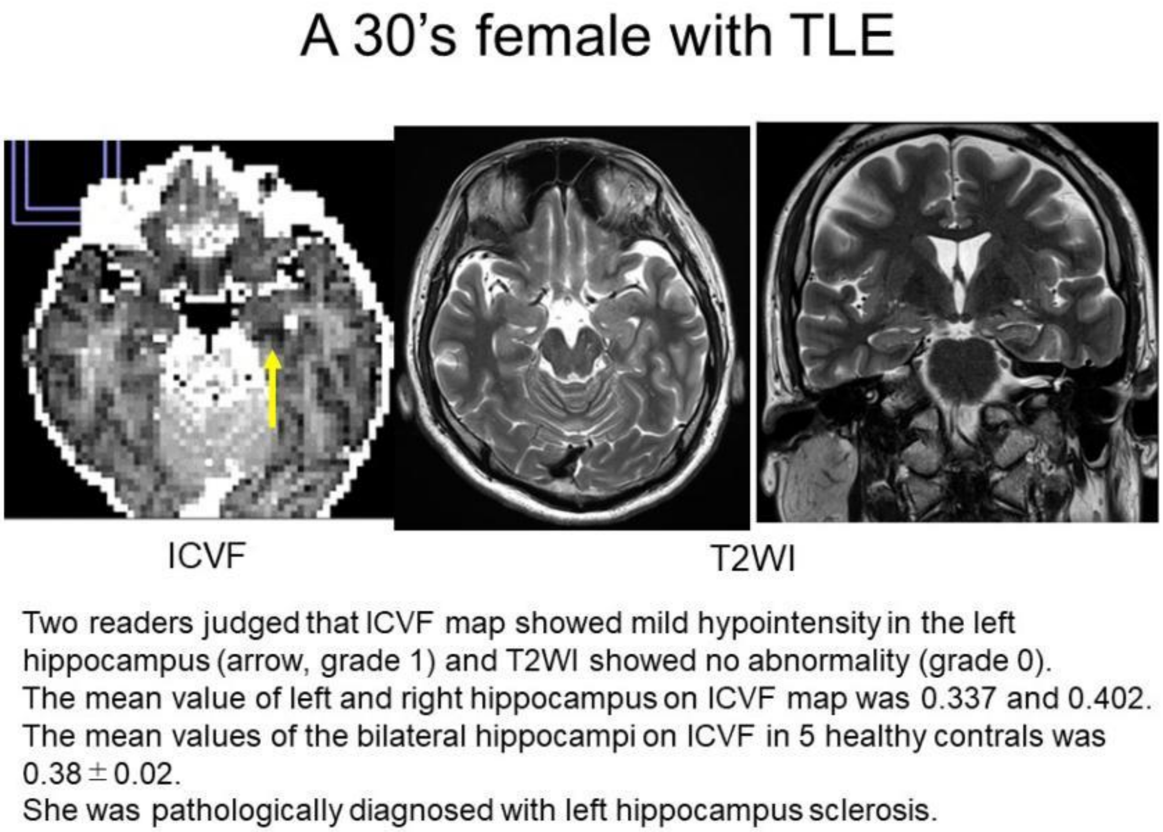

(Filename: TCT_3329_ASNR2019NODDIepilepsyabstruct.jpg)

2650

White Matter Disease Burden Predicts Clinical Outcome in Small Thalamocapsular Hemorrhages

J Vidovich[1], V Vagal[1], V Khandwala[1], T Behymer[2], C Prestigiacomo[3], A Vagal[4], D Woo[2]
[1]University of Cincinnati College of Medicine, Cincinnati, OH, [2]University of Cincinnati, Cincinnati, OH, [3]University of Cincinnati Medical Center, Cincinnati, OH, [4]UNIV. HOSP./UNIV. CINCINNATI COLLEGE OF MEDICINE, CINCINNATI, OH

Purpose
Although intracerebral hemorrhage (ICH) is the deadliest stroke subtype with significant morbidity and mortality rates, prognostic accuracy regarding functional outcome remains a major challenge. We radiologically characterized ICH injury according to hematoma morphology and underlying small vessel disease to determine association with functional outcome in small ICH. We hypothesized that functional outcomes are better predicted by the additional imaging parameters versus traditional risk factors.
Materials and Methods
The Ethnic/Racial Variations of Intracerebral Hemorrhage (ERICH) is a large, multicenter prospective study of hemorrhagic stroke. We analyzed baseline CTs in a homogenous group of patients from the ERICH database with small (<30cc) left thalamocapsular hemorrhages. We graded morphological characteristics of the primary ICH (shape, density, fluid-fluid levels, hounsfield values, and perihematomal edema) and measures of small vessel disease (Van Swieten score, prior infarcts).

Outcomes were measured with the 3-month modified Rankin Scale (mRS) and dichotomized as good (mRS 0-3) or poor (mRS 4-6). We performed univariate and backward-elimination multivariate regression.

Results

Our criteria included 125 patients (age mean/SD 51.2+ 5.8, 36 % females). ICH characteristics including irregular shape (p = 0.001), mean hounsfield value (p = 0.0237), and moderate to severe perihematomal edema (p = 0.0456) were significant in univariate analysis. In multivariate analysis, severe white matter disease (OR [CI] = 1.53 [1.05, 2.23]; p = 0.0265), Glasgow Coma Score (GCS) (OR [CI] = 0.80 [0.68, 0.93; p = 0.0041) and ICH volume (OR [CI} = 4.79 [2.00, 11.51]; p = 0.0005) were predictive of a poor outcome, while hispanic ethnicity (OR [CI] = 0.16 [0.04, 0.66]); p = 0.0113) and black ethnicity (OR [CI] = 0.15 [0.04, 0.65]; p = 0.0114) were protective.

Conclusions

Severe white matter disease is an independent baseline predictor of poor outcome for small thalamocapsular hemorrhages. Further study for inclusion into outcome measures like the ICH and FUNC scores should be considered.

3019

Application of Compressed Sensing Technique to Synthetic MRI

M Azuma[1], M Enzaki[1], T Hirai[2]
[1]Miyazaki University, Miyazaki, Miyazaki, [2]UNIVERSITY OF MIYAZAKI, MIYAZAKI, MIYAZAKI

Purpose
Synthetic MRI (Sy MRI) can create various contrast-weighted images and quantitative maps from a single scan. Although there are many reports of the usefulness of Sy MRI, this technique requires relatively long acquisition time. Compressed sensing (CS) is a new strategy to accelerate data acquisition by nonlinear iterative reconstruction of sparsely undersampled k-space data. We aimed to determine whether a CS technique can apply to Sy MRI images to reduce scan time.
Materials and Methods
In 10 healthy volunteers (5 men, 5 women; age range 23 - 45 years, mean 30 years), the image quality and quantitative values were compared among Sy MRI images using CS with acceleration factors of 0, 2.8, 3.8, and 5.7. All subjects were scanned on 3T MR scanners using standard 32 channel head coil. We produced synthetic T1-, T2- and proton density (PD)-weighted images and T1-, T2-, PD maps after quantification of the T1 and T2 values and the proton density. All images were performed with a 4-mm slice thickness. Two radiologists independently rated image quality and artifacts of QSM images using a 5-point scale. They also independently measured T1 and T2 values and the proton density on bilateral six brain structures (the frontal cortex, caudate nucleus, putamen anterior limb of the internal capsule, posterior limb of the internal capsule and occipital white matter). Qualitative and quantitative results were assessed with the Kruskal-Wallis test and Tukey-Kramer test.
Results
The Sy MRI scan time for CS with acceleration factors of 0, 2.8, 3.8, and 5.7 was 371, 299, 226 and 154 seconds, respectively. In image quality, there was no significant difference between the Sy MR images with CS with acceleration factor of 2.8 and without CS. The Sy MRI of CS with acceleration factor of 3.8 and 5.7 showed significantly lower grading scale than that without CS. In quantitative analysis, T1 and PD values on CS with acceleration factor of 5.7 showed significant changes in the putamen and internal capsule compared to those without CS ($p<0.05$). On the other hand, T2 values showed no significant differences between the CSs with acceleration factors of 0, 2.8, 3.8, and 5.7.
Conclusions
Compressed sensing technique can reduce acquisition time maintaining the image quality and quantitative values of Sy MRI. However, CS with excessive acceleration factors affects image quality and quantitative values.

3258

Assessment of Relationship Between the Pattern of Disk Displacement and Joint Effusion in Temporomandibular Joint Disorders Using MR Imaging

Y Kawashima[1], O Sakai[2], Y Hara[1], S Tokunaga[1], T Kaneda[1]
[1]Nihon University School of Dentistry at Matsudo, Matsudo, Chiba, [2]BOSTON UNIVERSITY SCHOOL OF MEDICINE, BOSTON, MA

Purpose
Temporomandibular joint disorders (TMDs) are disorders associated with the temporomandibular joint (TMJ) and the masticatory muscles. Only the disk displacement and degenerative changes can be detected on images. Fibrous tissue fraying may be an inciting factor for disk displacement. Disk displacement is important because it is a critical sign of TMDs. Most often the disk displaces in an anterior direction. It is important to detect early MR imaging signs of TMDs, thereby avoiding the evolution of this condition to condylar flattening or osteophytes. However, disk displacement is frequently seen in asymptomatic volunteers, and presence of joint effusion may be more indicative of TMDs. The purpose of this study was to reveal the relationship between the pattern of the disk displacement and joint effusion in TMDs using MR imaging.
Materials and Methods
We evaluated 350 TMJs (54 men and 159 women, mean age, 46.3 years). MR imaging of the TMJs was performed at a 1.5-Tesla unit with a 5-channel phased array coil. We recorded the pattern of disk displacement as follows; anterior, anteolateral, anteomedial, posterior and medial, and presence/absence of joint effusion in each disk displacement.
Results
Anterior disk placement was the most common pattern of displacement seen in 271 TMJs (77%), followed by anteolateral disk displacement seen in 55 (16%) TMJs, and anteomedial disk displacement seen in 22 (6%) TMJs. Joint effusion was seen in 75 out of 271 (28%) TMJs with anterior disk displacement, 37 out of 55 (67%) TMJs with anterolateral disk displacement, and 3 out of 19 (13%) TMJs with anteomedial displacement.
Conclusions
Our results revealed anterior disk displacement was the most common pattern of disk displacement, often with joint effusion. The highest incidence of joint effusion was seen with anterolateral disk displacement, although this disk displacement pattern is less common compared to anterior disk displacement.

3010

Automatic Measurement of Cerebral Vessels Diameters

D Ben-Bashat[1], O Geri[1], S Shiran[1]
[1]Tel Aviv Sourasky Medical Center and Tel Aviv University, Tel-Aviv, Israel

Purpose
Accurate characterization of the cerebral vascular system including vessels dimension are crucial for understanding its function, development and pathology. Using magnetic resonance imaging a number of angiography methods were developed in order to investigate the cerebral vessels properties. Measurement of vessels dimensions is usually done manually, by choosing one slice of the vessel, presumably, perpendicular to the direction of the vessel, and manually estimating the vessel cross section and diameter. A few studies, suggested semi-automatic methods for estimation of the vessels cross-section area in order to improve the measurement accuracy and decrease measurement time. However, all these methods require manual identification of the vessel of interest and choosing a slice of interest. The aim of this study was to develop a fully automatic algorithm for measuring the vessels diameter with high repeatability, based on the entire vessel volume, using tine-of flight (TOF) MRI data.
Materials and Methods
The automatic method: A fully automatic method was developed. The algorithm detect the different vessels sequentially from TOF data, with the previously detected vessels used to define reference points for a region-growing process, using the maximum segmentation threshold which satisfies defined conditions on the boundaries or shape of the detected vessels. The current method detect 15 cerebral vessels including: The right and left (R/L) internal carotid artery (ICA), each divided into 3 segments (extra-cranial, petrous and cavernous-supraclinoid), R/L M1 segment of the middle cerebral artery

(MCA), R/L A1 segment of anterior cerebral artery (ACA), R/L vertebral arteries, the basilar artery, and the R/L posterior cerebral artery (PCA). After the detection of the vessels, the length of the detected vessel is measured based on the sum of distances between each two adjacent voxels of the skeleton vessel. The vessel is then dilated and the vessel cross section area is calculated by dividing the segmented volume with the vessel length. Vessel diameter is calculated assuming a circular shape. D=(4A/pi)0.5.
Subjects and MRI protocol Fourteen healthy subjects (aged 23-53) were scanned twice with an interval of 1-3 weeks. All imaging was performed on a 3 Tesla Siemens system (MAGNETOM Prisma, Germany), using a twenty channel head coil. TOF imaging parameters were: time to repeat / time to echo (TR/TE) = 20/3.43, field of view: 240X195 mm, slice thickness: 0.7 mm, 5 slabs, 48 slices per slab, in-plane spatial resolution of 0.6X0.6 mm (interpolated to 0.3X0.3), parallel acquisition (IPAT) factor 2, partial Fourier 7/8 in slice direction, total scan time of 7:09 minutes.

Results

Automatic identification and diameter analysis was successfully performed in all subjects and all scans. Table 1 shows the mean, the inter-subject standard deviation and the within-subject standard deviation for each vessel segment. For all the vessels the within-subject standard deviation was lower than the inter-subject standard deviation. There were no significant difference between right and left vessel dimensions except for the vertebral arteries (L>R $p<0.05$). Table 1 shows the vessels diameter mean, inter-subject standard deviation (Std) and within-subject standard deviation (Sw), N=14. (R/L) – Right/Left, ICA1- Internal carotid (extra-cranial segment), ICA2- Internal carotid (petrous segment), ICA3- Internal carotid (cavernous-supraclinoid segment), M1 – MCA-M1 segment, A1-ACA A1 segment, Vert- Vertebral artery, Bas- Basilar artery, PCA – Posterior cerebral artery.

Conclusions

In this study we demonstrated the ability to fully automatically detect and measure the dimensions of the cerebral vessels with high test-retest repeatability in healthy subjects. This method could be used to assess vessel dimensions without the need for manual identification and measurement, therefore making this a practical method for investigating the cerebrovascular structure in normal and pathological conditions. Our current efforts are to improve vessel segmentation; increase the resolution of the diameter measurements and the visual presentation of the results.

Table 1.

Vessel	Mean (mm)	Std (mm)	Sw (mm)
R ICA1	5.08	0.36	0.15
L ICA 1	5.00	0.29	0.10
R ICA2	5.12	0.34	0.14
L ICA2	5.09	0.22	0.18
R ICA3	4.51	0.23	0.15
L ICA3	4.56	0.20	0.08
R Vert	3.56	0.41	0.10
L Vert	3.90	0.43	0.12
R A1	3.28	0.25	0.10
L A1	3.27	0.33	0.09
R M1	3.82	0.30	0.18
L M1	3.90	0.27	0.17
Basilar	3.74	0.41	0.10
R PCA	3.05	0.32	0.19
L PCA	3.07	0.28	0.06

(Filename: TCT_3010_Picture-Vessesld.jpg)

2435

Cerebral Computed Tomography Angiography in a 160mm Coverage Axial Scan Mode Using a Low Tube Voltage (70-kVp) Protocol: Comparison with the 120-kVp

P Lai[1]

[1]*KAOHSIUNG VETERANS GENERAL HOSPITAL, KAOHSIUNG, Taiwan*

Purpose
To assess the image quality by using a 70-kVp protocol in a 160mm axial scan mode in comparison with a 120-kVp protocol for the CCTA, and to investigate a probable reduction in the volume of contrast medium (CM) in the 70-kVp protocol.
Materials and Methods
A total of 121 individuals (47 men and 74 women; mean age, 50 years; range, 19-79 years) were enrolled and divided to one of three groups: group A: 120 kVp, 170 mAs, and 60 mL of CM; group B: 70 kVp, 350 mAs, and 60 mL of CM; group C: 70 kVp, 350 mAs, and 45 mL of CM. All of these three groups were scanned in a 160mm axial scan mode in a 256-slice CT machine (Revolution, GE Healthcare) with the slice thickness of 0.625 mm, and the radiation dose was controlled as close as to each other (12.71 to 13.38 mGy of volume CT dose index [CTDIvol]. Objective image quality (Hounsfield units, signal-to-noise ratio [SNR], and contrast-to-noise ratio [CNR] of cerebral arteries) and subjective image quality were compared in these three groups. The one-way ANOVA with Bonferroni post hoc test was used to evaluate the objective image quality. The subjective image quality was analyzed by Kruskal-Wallis test in three groups and Mann-Whitney U test between any two groups. Two experienced radiologists independently evaluated the subjective image quality, and inter-observer reliability was calculated by kappa (k) analysis. For all statistical analyses, P value < 0.05 was considered significant.
Results
In objective image quality, both of group B and C had significantly higher arterial attenuation, SNR, and CNR than group A (all $P<0.001$). In subjective evaluation, the image quality of group B was significantly better than group A (all $P<0.05$), and there was no significant difference between group A and group C. The inter-observer reliability was substantial (k= 0.84).
Conclusions
The arterial enhancement, SNR, and CNR can be improved by using 70-kVp protocol, and better subjective image quality can be provided. Moreover, the lesser amount of CM might be used in the 70-kVp protocol without interference of imaging quality, and needed to be verified by using a larger sample size in the future.

2366

Changing Utilization of Neuro-Imaging in Primary Brain Cancer Patients During Emergency Department Visits

Y Cho[1], R Duszak[2], M Hoch[3], D Coleman[1], G Sadigh[2]
[1]*Emory University, Atlanta, GA,* [2]*Emory University School of Medicine, Atlanta, GA,* [3]*Emory University Hospital, Atlanta, GA*

Purpose
To study changing neuroimaging utilization in primary brain cancer patients in US emergency departments (EDs).
Materials and Methods
Using 2006-2014 data from the Healthcare Cost and Utilization Project (HCUP) Nationwide Emergency Department Sample (NEDS), the largest all-payer ED database in the US, we identified patients with primary brain cancers vising EDs, and studied both their utilization and independent predictors of neuroimaging examinations using logistic regression.
Results
An estimated total 40,862 weighted cohort of patients with primary brain cancer visited a US ED between 2006 to 2014 (mean age 54; 56% male), increasing from 3,932 in 2006 to 5,625 in 2014 (+43%). Patients' primary insurance was Medicare in 36%, Medicaid in 16%, private in 39%, others in 4.8% and self-pay in

4.2%. Of those patients, 14.4% underwent brain imaging, with 2.3% undergoing MRI and 13.2% undergoing CT. In this cohort from 2006 to 2014, there was 104% increase in rate of ED brain imaging (from 9.7% in 2006 to 19.8% in 2014). Independent factors associated with higher utilization of ED neuroimaging were an ED visit year after 2009 (OR, 1.9), private insurance as compared to Medicare (OR, 1.2), and not dying during the subsequent admission (OR 9.1) (All p values < 0.05).
Conclusions
In patients with primary brain cancer, the frequency of ED visits and the utilization of neuroimaging tests during those ED visits have both increased in recent years. A variety of sociodemographic characteristics are associated with a higher likelihood of imaging.

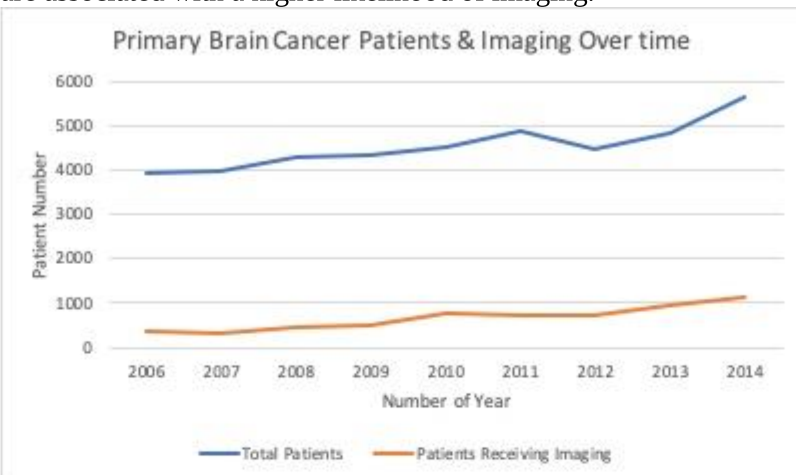

(Filename: TCT_2366_Figure1NEDS.jpg)

2451

Chondro-osseous Respiratory Epithelial Adenomatoid Hamartoma (COREAH)

J Benson[1], J Lewis[2], P Luetmer[3]
[1]Mayo Clinic, Rochester, MN, [2]Mayo Clinic, Rochester , MN, [3]MAYO CLINIC, ROCHESTER, MN

Purpose
To present an example of a chondro-osseous respiratory epithelial adenomatoid hamartoma (COREAH) of the nasal cavity, an extremely rare entity first described by Wenig and Heffner in 1995. COREAHs are benign lesions that contain both epithelial and mesenchymal components, and represent a type of respiratory epithelial adenomatoid hamartoma (REAH).
Materials and Methods
A 68-year-old woman with a history of a known thyroglossal duct cyst presented to outpatient clinic with longstanding post-nasal drip, snoring, and difficulty sleeping with her head turned to the right. On exam, a soft tissue mass was visualized in her oropharynx behind the uvula. Laryngoscopy performed during her subsequent otorhinolaryngology referral noted a polypoid mass arising from the posteroinferior border of the right superior turbinate. The patient underwent an excisional biopsy of the mass approximately 1 week later with significant symptomatic improvement. Histopathological analysis demonstrated a hamartomatous lesion with both seromucinous and respiratory epithelial glands and central osseous trabeculae. To date, the patient has not had any evidence of lesion recurrence.
Results
Non-contrast CT of the paranasal sinuses and contrast-enhanced CT of the neck demonstrated a 4.1 x 2.3 x 2.9 cm (AP x RL x SI) non-enhancing polypoid mass lesion with internal mineralization extending from the posterior right nasal canal into the oropharynx. The mass partially obstructed the right choanae. Thin soft tissue stranding along the superior margin of the mass was thought to represent a polyp-like

extension of the mass to the site of origin, near the right sphenoethmoidal recess. There was no evidence of osseous erosion or hyperostosis. No enlarged lymph nodes were identified.
Conclusions
This case demonstrates characteristic imaging and histopathological features of an extremely rare COREAH, a benign lesion that classically arises from the posterior nasal cavity.

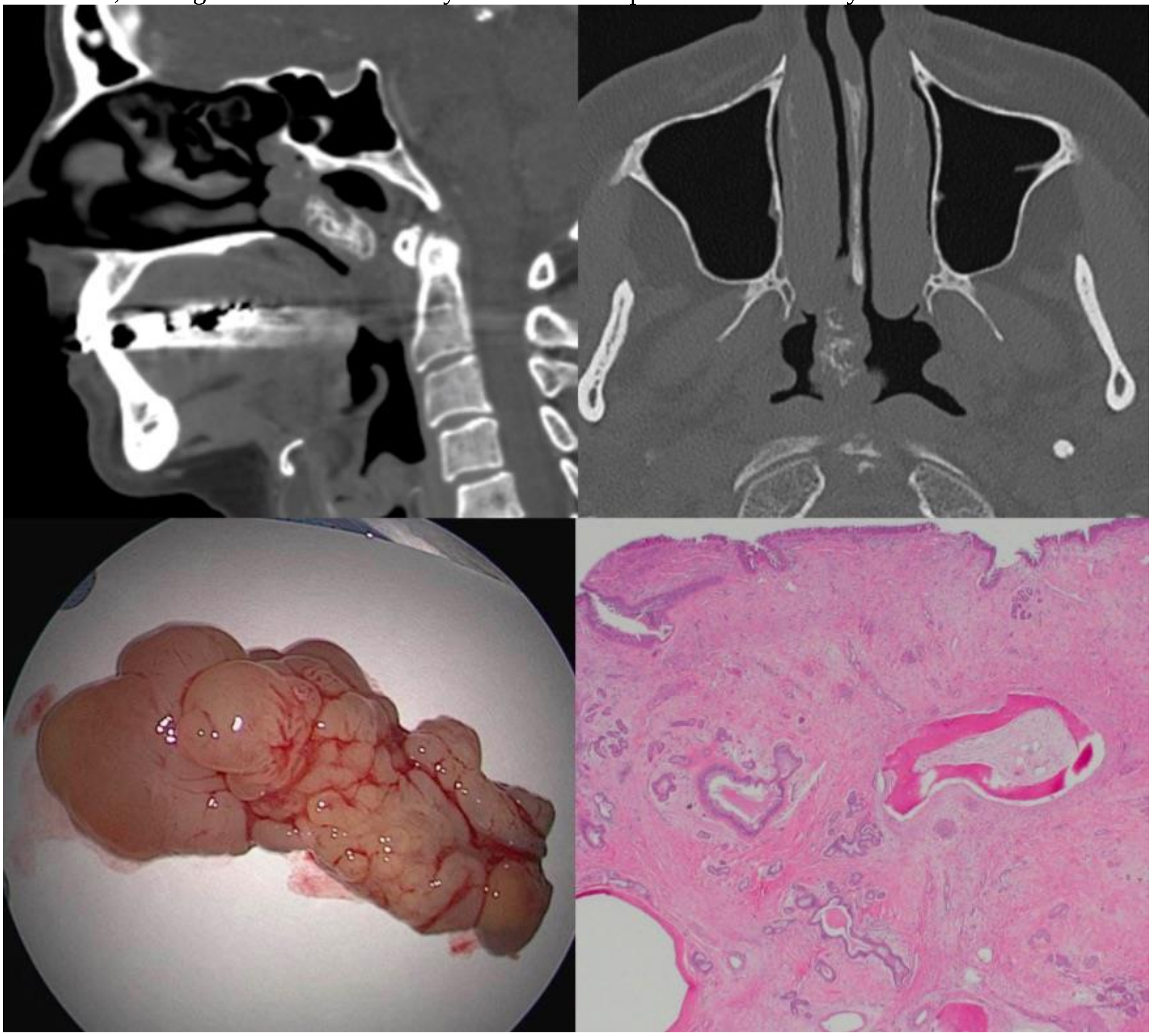

(Filename: TCT_2451_Abstractimage.jpg)

2178

Classification of Multigland Parathyroid Disease versus Single Parathyroid Adenomas Using Support Vector Machines

O Kohannim[1], G Hathout[1], J Huang[1]
[1]University of California, Los Angeles, Los Angeles, CA

Purpose
The most common cause of primary hyperparathyroidism is a single parathyroid adenoma, followed by multigland parathyroid disease, double adenomas and parathyroid carcinoma in order of frequency.

Differentiating single parathyroid adenomas from multigland parathyroid disease has important implications for parathyroid surgical planning. Our aim is to combine imaging and chemical markers using machine learning to accurately distinguish the two entities.

Materials and Methods

We performed a retrospective study, considered exempt by our institutional review board from review. All dynamic CT parathyroid studies performed within 2015-2016 were collected and corresponding calcium and parathyroid hormone levels were obtained via chart review. The subset of patients who underwent surgery at UCLA with available pathology results showing single adenomas or multigland hyperplasia were selected. Patients with double adenomas, unavailable laboratory measures or equivocal findings in radiology reports were excluded from analysis. The number of identified candidate lesions and the maximal dimension of the largest candidate were identified from radiology reports. Support vector machines analysis with leave-one-out cross-validation was then performed to obtain diagnostic classification accuracy measures.

Results

A total of 87 patients were included in the study, 62 of which were diagnosed with a single adenoma and 25 of which had multigland disease. We integrated age, sex, calcium levels, parathyroid hormone levels, number of candidate lesions detected on CT and the maximal dimension of largest identified lesion as features of our machine learning model. Support vector machines in the classification of multigland disease versus adenoma resulted in 83% accuracy, 95% specificity and 52% sensitivity. Corresponding receiver-operating characteristic (ROC) curve analysis yielded an area under the curve of 0.85.

Conclusions

We applied a machine learning algorithm to predict the diagnosis of single adenomas versus multigland disease based on imaging markers, calcium and parathyroid levels. When compared to previously published scoring systems in the field, our machine learning approach demonstrates improved specificity, while maintaining sensitivity. Our results thereby have potential implications for accurate surgical planning in cases of primary hyperparathyroidism.

2774

Clinico-Radiological Correlation of Magnetic Resonance Imaging findings in Patients with Idiopathic Intracranial Hypertension

J Shankar[1], H Wong[2], K Sanghera[3], A Neufeld[3], C Maxner[3]

[1]university of Manitoba, Winnipeg, MB, Manitoba, [2]Dalhousie Unversity, Halifax, Canada, [3]Dalhousie University, Halifax, Nova Scotia

Purpose

Although several studies have reported imaging findings associated with idiopathic intracranial hypertension (IIH), less is known about the correlation between imaging findings and IIH-related symptoms or signs. This study aimed to determine if clinical presentation of IIH correlated with radiological findings. We focused on magnetic resonance imaging (MRI) and presenting complaints with severity of vision loss, and laterality of ocular symptoms and signs.

Materials and Methods

A retrospective chart review was conducted on consecutive patients presenting at the neuro-ophthalmology department within our institution over last 15 years. All patients diagnosed with IIH were identified and those with available MRI were included in final analysis. All MRI images were reviewed by neuroradiologists who were blinded to the presenting symptoms and signs. Statistical analysis was performed to determine the correlation between the MRI findings with each clinical symptom or sign.

Results

Thirty-one out of eighty-eight patients with the initial diagnosis of IIH had MRI available and were included in study. Significant correlations were observed between clinical presentation and MRI imaging:

(1) Colour vision and amount of perineural fluid around the optic nerve on MRI (r = -0.382; p=0.004); (2) disc assessment and intraocular optic nerve protrusion (r = 0.364; p = 0.004); (3) disc assessment and perineural fluid around the optic nerve (r = 0.276; p = 0.033); and (4) disc assessment and venous sinus stenosis (r = 0.351; p = 0.009).
Conclusions
Our findings suggests that MRI imaging in IIH may be useful in ruling out ominous causes of intracranial pressure and risk stratifying ophthalmologic intervention and management of patients with headaches possibly due to IIH.

3256

Comparison of Bedside US to MRI for the Detection of Longstanding Increased Intracranial Pressure– Feasibility Study

A Goyal[1], H Shokoohi[1], M Pyle[1], E Kuhl[1], M LeSaux[1], k boniface[1], M Taheri[2]
[1]George Washington University Hospital, Washington, DC, [2]George Washington University, Washington, DC, DC

Purpose
Patients with longstanding increased intracranial pressure (IICP) present to the Emergency Department (ED) with various symptoms, some of which if unrecognized can become irreversible. A constellation of MRI findings, including optic nerve sheath diameter (ONSD), is predictive of IICP. MRI is not readily available to many ED physicians. Nearly all EDs are equipped with bedside US. Increased ONSD measured by US has been proposed for the diagnosis of patients with IICP. Direct comparison between MRI and US in the evaluation of ONSD has not been performed. Before ONSD measured by US and MRI can be compared, the correlation between the measurements of a structure unaffected by IICP needs to be established. The purpose of this study is to compare the measurements of optic nerve diameter (OND) by MRI and US. This analysis will provide a context for the comparison of ONSD measurements by these techniques.
Materials and Methods
In this IRB approved retrospective study, ED patients with both orbital US and MRI were included. The OND was measured in the coronal plane by US and MRI (T2-FS sequence). OND on MRI was measured independently by two Radiologists. The mean of this measurement was compared to a single measurement of OND with US obtained in the ED. Correlation and agreement between different readings was assessed using Pearson's correlation and Bland-Altman analysis.
Results
A total of 25 patients with 50 OND measurements by MRI and US were included. The MRI measurements by the two Radiologists showed good inter-class correlation(r=0.67, p<0.001). On Bland-Altman analysis, there was generally good agreement between US and MRI measurements (95% limits of agreement=-0.15 to 0.28). Measurements of OND by US were significantly smaller than the measurements by MRI (mean difference =-0.0625, CI=-0.03. -0.09, p<0.001).
Conclusions
US underestimates the size of the OND when compared to MRI.

2734

Comparison of PET Imaging with Neuropathological Staging for Amyloid β Deposition in the Brain

L Wang[1], S Flores[2], R Perrin[1], J Morris[3], T Benzinger[4]

[1]Washington University in St Louis, St Louis, MO, [2]Washington University in St Louis, St. Louis,, MO, [3]Washington University in St. Louis, St. Louis, MO, [4]Washington University in St. Louis, Saint Louis, MO

Purpose
To determine the spatial pattern of PET imaging changes with advancing amyloid β phase in neuropathological assessment
Materials and Methods
Forty-three older participants were studied for amyloid β deposition using PET imaging with the tracer Pittsburgh Compound B (PiB) and neuropathological assessment at autopsy. Dynamic PET scans were acquired after intravenous administration of approximately ~12 mCi of PiB. The PET images were reconstructed on a 128 x 128 x 109 matrix using filtered back-projection. Structural MRI scans were acquired using T1-weighted magnetization-prepared rapid gradient echo sequence and processed with FreeSurfer software to generate 34 cortical regions of interest (ROI). PET data acquired between 30 and 60 minutes post injection was summed and transformed into patient MRI space. For each ROI, PET data were estimated using standardized uptake value ratios (SUVRs) with cerebellar cortex as the reference region. Partial volume correction was performed using a regional spread function technique. In the neuropathological assessment, postmortem brain sections from the middle frontal gyrus, hippocampus, basal ganglia, midbrain and cerebellum were stained immunohistochemically with amyloid β antibody (10D5, Lilly, IN) and examined. The phase of amyloid β distribution was determined using Thal criteria. The participants were classified as either low Thal phase (0-3) or high Thal phase (4-5). For each ROI, the partial volume corrected SUVRs were compared between low vs. high Thal phase groups.
Results
Nineteen and twenty-four participants were classified into low and high Thal-phase groups, respectively. No difference was seen for the time interval between PET imaging and death between the 2 groups. An increase in SUVR was observed in the high Thal-phase compared to low Thal-phase groups in several frontal and temporal regions (corrected for multiple comparisons at $p < 0.05$) (yellow areas in the Figure).
Conclusions
Advanced phase of amyloid β deposition in autopsy is associated with elevated PiB binding in the frontal and temporal areas.

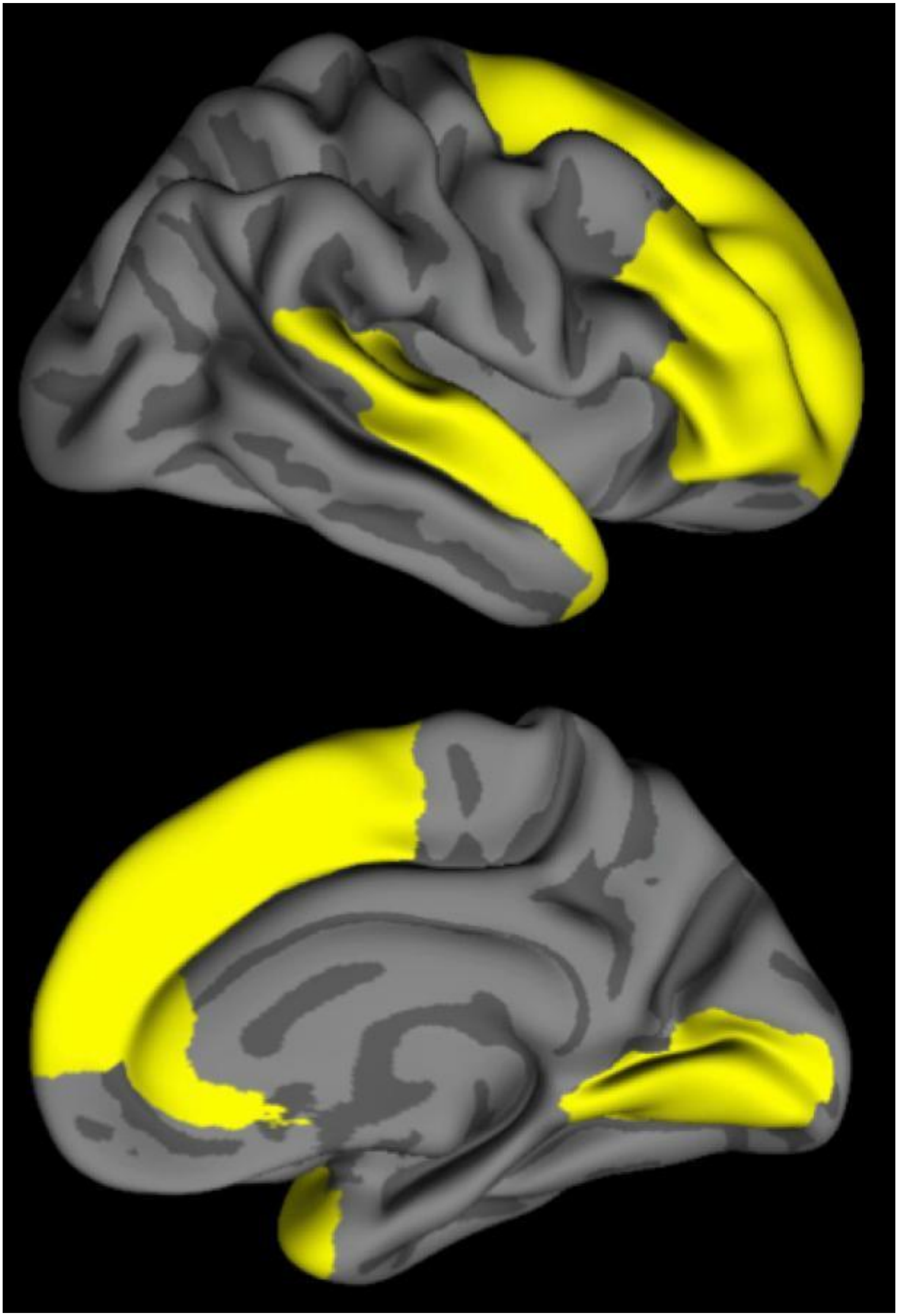

(Filename: TCT_2734_Figure_ASNR.jpg)

2342

Cranial Nerve Abnormalities in Spontaneous Intracranial Hypotension and Their Clinical Relevance

S Kim[1], A Castilho[2], M Hoch[3], J Allen[4], A Saindane[4], B Weinberg[3]
[1]Emory University, Atlatna, GA, [2]Emory, Atlanta, GA, [3]Emory University Hospital, Atlanta, GA, [4]Emory University, Atlanta, GA

Purpose
Spontaneous intracranial hypotension (SIH) is a known cause of headaches and neurologic symptoms, but the frequency of cranial nerve symptoms and corresponding abnormalities on MRI has not been well described in the literature. The purpose of this study was to document cranial nerve findings in patients with SIH and correlate them with patient's clinical symptoms.
Materials and Methods
A retrospective cohort study of patients diagnosed with SIH and treated with CT guided blood patch at a single institute from September 2014 to July 2017 was performed. Chart review was completed to determine the frequency of clinically significant neurologic symptoms, with findings divided into those affecting cranial nerves 3 and 6 (vision changes and diplopia) and cranial nerve 8 (hearing changes and vertigo). Blinded review of the patient's brain MRI was conducted to assess for cranial nerve abnormalities, specifically abnormal post contrast enhancement of cranial nerves 3, 6, and 8. Statistical analysis was then performed to correlate clinical symptoms with MRI findings.
Results
30 patients treated for SIH with corresponding brain MRIs were identified. Overall, 66% of these had clinically significant neurologic symptoms (vision changes, diplopia, hearing changes, and/or vertigo). Cranial nerve 8 enhancement was present in 20 patients on MRI. 13 of these patients experienced hearing changes and/or vertigo, odds ratio 16.7 (p=0.015, 95% CI 1.7-160.6). Cranial nerve 3 or 6 enhancement was present in 9 patients on MRI. 7 of these also experienced visual changes and/or diplopia, odds ratio 14.9 (P=0.006, 95% CI 2.2-100.8).
Conclusions
Patients with cranial nerve findings on MRI in the setting of SIH were significantly more likely to have associated neurologic symptoms. When present on brain MRI in the setting of other findings of SIH, cranial nerve findings should be reported, as they can contribute a potential source of symptoms and may affect prognosis when treating SIH.

Cranial Nerve Abnormalities in Spontaneous Intracranial Hypotension and Their Clinical Relevance

	Oculomotor symptoms		
Cranial nerve 3 or 6 enhancement	Yes	No	Odds ratio (p-value)
Yes	7	2	14.9
No	4	17	p=0.006

	Hearing/vestibular symptoms		
Internal Auditory Canal Enhancement	Yes	No	Odds ratio (p-value)
Yes	13	7	16.7
No	1	9	P=0.015

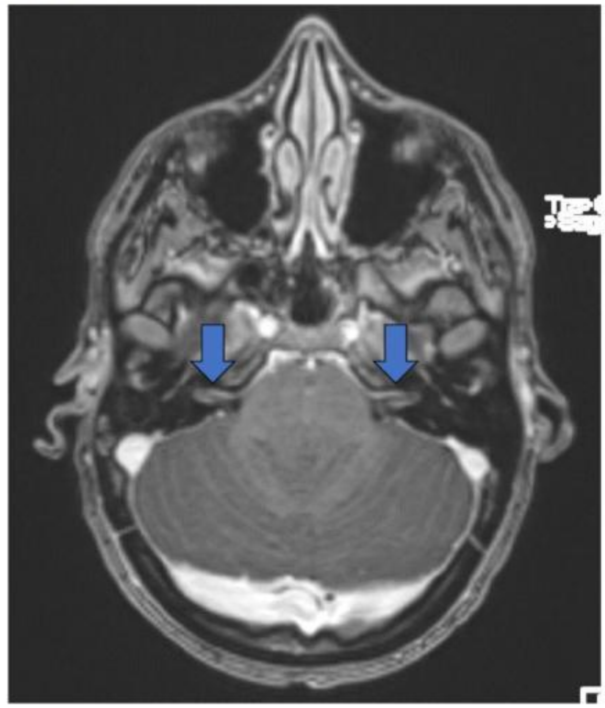

(Filename: TCT_2342_GraphsandImage.JPG)

2941

CT Assessment of the Nasofrontal Angle and Frontal Prominence to Mid-Sellar Distance in Facial Feminization Surgery: A Retrospective Study

A Callen[1], E Wang[1], S Lee[1], J Talbott[1], C Glastonbury[1], J Pomerantz[1], J Narvid[1]
[1]*University of California, San Francisco, San Francisco, CA*

Purpose
Facial feminization surgery (FFS) is a collection of facial bone and soft tissue procedures designed to adjust masculine features to feminine proportions. Along with gender reassignment surgery, it is a component of the gender transition process for transgendered individuals. The osseous components of feminization involve reshaping the frontal calvarium and nose, as well as adjusting the angles and proportions of the entire mandible. Routine preoperative assessment of the patient undergoing FFS includes computed tomography (CT) of the face in order to assess various osseous anatomic features and relationships which could alter the surgical approach for reshaping both the upper and lower face. Two of the facial features considered most contributory to identification of gender are the nasofrontal angle and prominence of the brow. In the female face, the nasofrontal angle is considerably more obtuse, and the there is a reduced prominence of the frontal bone. These areas are evaluated on preoperative imaging in order to inform the surgical approach, and their surgical modification can be quantified pre- and post-operatively. The purpose of this study was to conduct a retrospective review of patients who have undergone facial feminization surgery at a single institution under a single surgeon and quantitatively characterize the modifications performed on both the nasofrontal angle and brow prominence.
Materials and Methods
A retrospective review of imaging reports was performed of all CT studies performed between 1/1/16 and

9/30/18 using the term "feminization" to identify routinely obtained pre- and post-operative CT assessment of the face for individuals undergoing male to female gender reassignment surgery. The nasofrontal angle, formed from a line tangent to the glabella and a line tangent to the nasal bridge with its apex at the nasal radix, was measured pre and post operatively. The frontal prominence to sellar distance, formed from a line originating at the anterior most point of the outer table of the frontal sinus and terminating at the mid-sella, was also measured pre and post operatively. Measurements were performed according to osseous, rather than soft tissue anatomy, given the distortion of soft tissues post operatively. The type of frontal sinus was characterized according to the Ousterhout classification system where a type 1 sinus is characterized by a thick outer table with a minimally pneumatized sinus, a type II sinus is characterized by a thin outer table with a moderately pneumatized sinus and moderate anterior projection of the supraorbital rims, and a type III sinus is characterized by a thin outer table with a hyperpneumatized sinus and a large anterior projection of the supraorbital rims. Paired t-tests were performed to evaluate for significant differences between mean measurements pre- and post-operatively.

Results

A total of 9 patients were identified with adequate pre- and post operative imaging. All patients underwent a procedure to reshape the frontal bone and nasofrontal angle, consisting of frontal contouring in 9 (100%) patients, frontal osteotomy in 8 (89%) patients, and rhinoplasty in 8 (89%) patients. Preoperatively, 1 patient was classified as Ousterhout type I frontal sinus, 5 patients were classified as Ousterhout type 2 frontal sinus, and 3 patients were classified with Ousterhout type 3 frontal sinus. The mean (SD) frontal prominence to mid sellar distance pre-operatively was 7.7 cm (0.4), and post operatively was 7.3 cm (0.4), ($p < 0.01$). The mean (SD) nasofrontal angle preoperatively was 108.2 (18.2), and post operatively was 130.1 (12.6), ($p < 0.01$).

Conclusions

As gender identity disorders become increasingly recognized, medical procedures aimed to aid in the process of gender transition are happening with greater frequency. As facial feminization surgery includes routine preoperative CT assessment of the face, radiologists will encounter these studies in clinical practice. In order to communicate effectively with our surgical colleagues as well as provide the best care possible to our patients, understanding the components of facial feminization surgery as well as the key anatomic features of the face which inform the surgical approach are critical. While gender-conforming alteration of facial proportions comprises much more than two measurements, this study aims at quantifying the measurable aspects of facial feminization surgery which can readily be assessed pre- and post- operatively by CT imaging. It is our hope that this study will facilitate improved communication between radiologists and plastic surgeons regarding the care of transgendered patients.

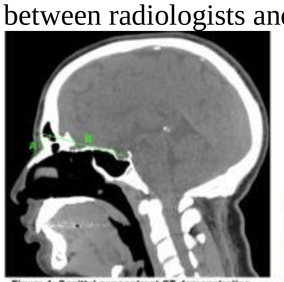

Figure 1: Sagittal noncontrast CT demonstrating measurements of the nasofrontal angle (A) and frontal prominence to sellar distance (B)

N		9
Ousterhout Type	1	1 (11%)
	2	5 (56%)
	3	3 (33%)
FP to S pre, mean (SD)		7.7 (0.4)
FP to S post, mean (SD)		7.3 (0.4)
NFA pre, mean (SD)		108.2 (18.2)
NFA post, mean (SD)		130.1 (12.6)

Table 1: Summary characteristics pre- and post-operatively

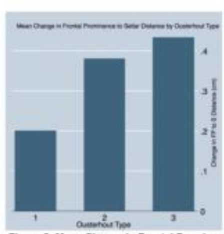

Figure 2: Mean Change in Frontal Prominence to Sellar Distance by Ousterhout Type


Figure 3: 3D rendering of craniofacial CT demonstrating frontal osteotomy and genioplasty surgical changes

(Filename: TCT_2941_FFSASNRgraphicfile.jpg)

2242

Deep Learning-Assisted Diagnosis of Hyperdense MCA Sign In Acute Ischemic Stroke

Y Shinohara[1], N Takahashi[1], Y Lee[2], T Ohmura[1], F Kinoshita[1], A Umetsu[3], K Kuya[4], A Kato[5], T Kinoshita[1]

[1]*Research Institute for Brain and Blood Vessels-Akita, Akita, Akita,* [2]*Niigata University, Niigata, Niigata,* [3]*Tohoku University Graduate School of Medicine, Sendai, Miyagi,* [4]*SECOMEDIC Hospital, Funabashi, Chiba,* [5]*Tottori University, Yonago, Tottori*

Purpose
Non-contrast computed tomography (CT) of the brain enables estimation of middle cerebral artery (MCA) occlusion by identifying high attenuating vasculature that reflects the acute embolus (hyperdense MCA sign; HMCAS). However, HMCAS is not necessarily highly accurate for diagnosing MCA occlusion. This study aimed to evaluate whether the deep learning method could help in diagnosing HMCAS by comparing the diagnostic performance test of neuroradiologists.

Materials and Methods
Deep convolutional neural network (DCNN) model (Xception, arxiv.org/abs/1610.02357) learned with 35 HMCAS-positive and 39 HMCAS-negative training samples extracted by 50-pixel-diameter circle regions of interest was employed. Test data of 46 HMCAS-positive and 52 HMCAS-negative samples were prepared. First, five neuroradiologists conducted an initial diagnostic performance test for the test samples by describing the HMCAS-positive prediction rate (%) in each. The readers then conducted a second diagnostic performance test with reference to the prediction rate of the DCNN model in each sample. Statistical analysis was performed with SPSS software (version 19.0; SPSS Inc., Chicago, IL, USA) and EZR software (version 1.37; Saitama Medical Center, Jichi Medical University, Saitama, Japan) (Bone Marrow Transplantation 2013; 48: 452-8).

Results
The initial diagnostic performance and the second with reference to the results of the DCNN model of five neuroradiologists for HMCAS respectively showed 89.1±11.1% and 92.2±5.3% sensitivity, 69.6±8.0% and 80.2±10.3% specificity, 78.8±3.4% and 84.7±3.6% accuracy, and area under the curves of receiver operating characteristics (AUCs) of 0.884±0.059 and 0.930±0.029 (mean ± standard deviation). All five readers showed higher AUCs in the second diagnostic performance test compared to the initial, including one reader with significant improvement ($p=0.000646$). A representative case is shown in a graphic file.

Conclusions
Deep learning-assisted diagnosis can potentially improve HMCAS detection on non-contrast CT in acute ischemic stroke.

A case of 80-year-old female with sudden left hemiparesis and loss of consciousness (NIHSS=10).

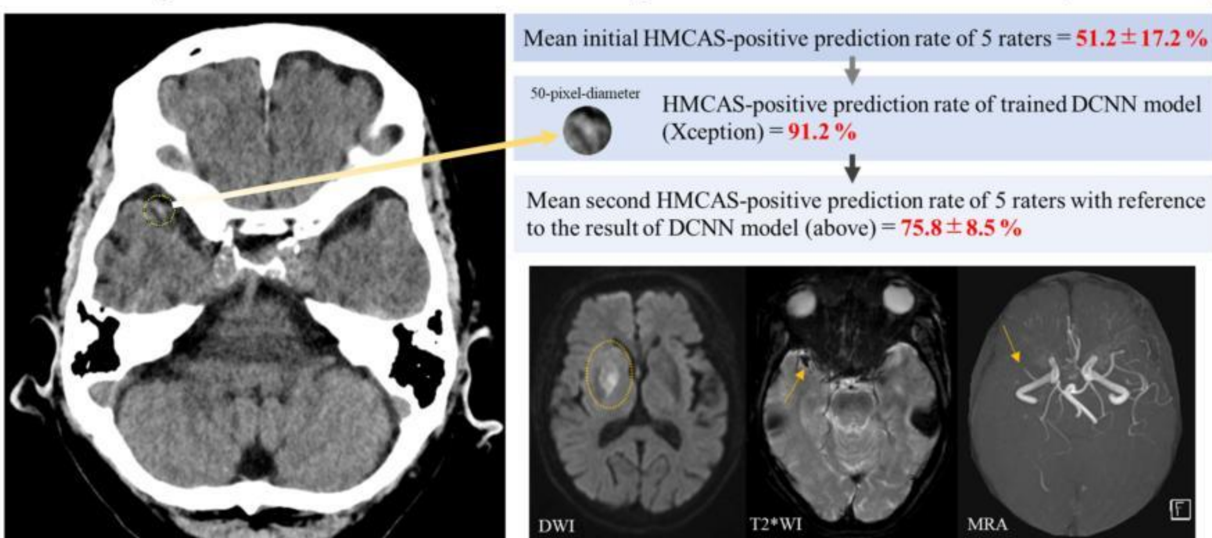

MRI immediately after CT shows acute infarction in the right basal ganglia with right MCA embolism.

(Filename: TCT_2242_ASNR2019Fig.jpg)

2219

Distinguishing Normal From Abnormal Brain CT Scans Using 3D Convolutional Neural Networks: a Tool to Improve Emergency Neuroradiology Workflow

S Dupont[1], D McCoy[1], A Callen[2], J Narvid[1]
[1]University of California, San Francisco, San Francisco, CA, [2]University of California San Francisco, San Francisco, CA

Purpose
Radiology departments are under increasing pressure to reduce delays in reporting despite an increasing volume of studies 1,2. In neuroradiology, computed tomography is critical for triaging stroke and trauma patients due to its wide availability and rapid acquisition 3. This time-sensitive workflow could be accelerated by assigning a priority order to scans for reading. This study aimed at developing a deep-learning method for the automatic detection of abnormality in brain CT scans to improve daily neuroradiology workflow.
Materials and Methods
A 3D convolutional neural network was implemented and trained for the classification task, the model architecture is described in Figure 1. 1428 brain non-contrast CT scans were retrospectively collected from two clinical centers for the training, validation and testing of the proposed model. Hyper-parameters were optimized with the Taguchi method for experiment design 5. Briefly, this technique quantitatively evaluates the effect of several controlled factors on the result of a given experiment and is commonly used in various fields of industry for quality engineering. The result of the experiment has to be quantitative, each controlled factor needs to be discrete with multiple levels, and only a few carefully chosen combination are tested based on specific orthogonal arrays 5. The result of each experiment is stored and used to compute the effect of each level of each factor on the final result compared to the average result across all experiments. This allows to quantify the effect of the different levels of each factor on the final result and select the appropriate level of each factor that optimizes the final result, with an estimation of the expected best result. Four models trained with the best parameters chosen by experiment design were evaluated on the test set by computing the final accuracy, specificity (true-negative rate), sensitivity (true-positive rate), precision (positive predictive value) and F1-score.
Results
The proposed hyper-parameter optimization approach allowed a quantification of the effect of each level of each parameter on the model performance. The best combination of parameters found for the proposed model reached excellent classification accuracies (0.88 ± 0.04, see Table 2).
Conclusions
We implemented, optimized and validated a 3D convolutional neural network for the detection of abnormality in brain CT scan. This model was trained using real-life data from active hospitals. The proposed hyper-parameter approach allowed to test several values of parameters and have a quantitative evaluation of the effect of each tested value on the model's accuracy with only few experiments, representing a few days of training vs. months if the same parameters had been evaluated with a gridsearch. Future work will integrate this tool in the daily neuroradiology practice as a real-time triage tool and evaluate efficiency gains in patient care.

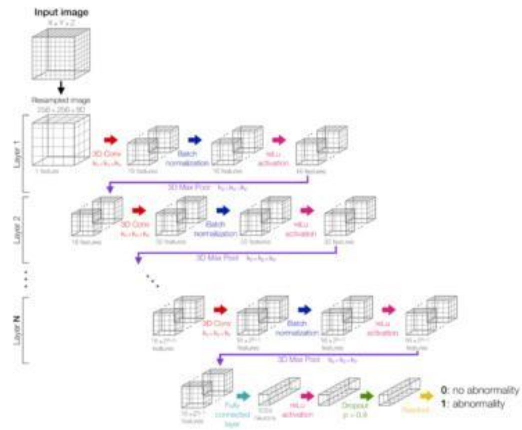

Figure 1: Architecture of the 3D convolutional neural network used for classification. The common image size after resampling was 256x256x80 voxels, 16 features were generated after the first and the number of features was doubled during the 3D convolution in each layer, 1024 neurons were used in the last fully connected layer, and the probability of dropout was set to 0.9 (i.e. 90% chances of keeping a weight). Other hyper-parameters were left to be optimized: the kernel size of the 3D convolution (k_c), the kernel size of the 3D max pooling (k_p), the initial training rate of the optimizer (tr), the batch size (B) and the depth of the network, i.e. the number of convolutional layers (N). The model was trained for 5000 epochs.

	3D convolution kernel size	3D max pooling kernel size	Initial training rate of the Adam optimizer	Batch Size	Number of layers (depth of the network)
Exp.	k_c	k_p	tr	B	N
#1	3	2	$1e^{-4}$	1	7
#2	3	2	$1e^{-3}$	3	4
#3	3	4	$1e^{-4}$	3	5
#4	3	4	$1e^{-3}$	1	6
#5	5	4	$1e^{-3}$	3	7
#6	5	4	$1e^{-4}$	1	4
#7	5	2	$1e^{-3}$	1	5
#8	5	2	$1e^{-4}$	3	6

Table 1: Detail of the L_8 matrix defining the combination of factors used in the experimental design. Each row corresponds to one experiment, i.e. training, validation and testing of the model with the specified parameters. Splitting between training, validation and testing sets remained the same between the eight experiments.

Bootstrap iteration	#1	#2	#3	#4
Accuracy	0.93	0.82	0.90	0.85
Specificity	1.0	1.0	0.94	1.0
Sensitivity	0.92	0.80	0.90	0.83
Precision	1.0	1.0	0.99	1.0
F1-score	0.96	0.89	0.94	0.91

Table 2: Performance metrics for the four bootstrap iterations: accuracy, specificity (or true-negative rate), sensitivity (or true-positive rate), precision (or positive predictive value) and F1-score.

(Filename: TCT_2219_FigureandTables.jpg)

3235

Double Inversion Recovery (DIR) Imaging in Glioblastoma

T Matys[1], F Zaccagna[1], S Price[2], J Gillard[3]
[1]University of Cambridge, Cambridge, UK, [2]University of Cambridge, Cambridhe, UK, [3]University of Cambridge, Cambridge , UK

Purpose

Glioblastoma is a highly malignant brain neoplasm characterized by infiltrative growth pattern, with malignant cells penetrating beyond the central contrast enhancing region into surrounding area of T2/FLAIR signal hyperintensity. As the latter is usually a combination of non-enhancing tumor and vasogenic edema, it is not possible to reliably establish the true tumor extent. It has been previously suggested by others that double inversion recovery (DIR) sequence, which in addition to nulling fluid signal similar to FLAIR also nulls signal from normal white matter by using an additional inversion recovery pulse, may provide additional information. In particular, the authors observed discrepancies between FLAIR- and DIR-defined regions in postoperative setting (ref 1). The aim of this study was to attempt to further assess potential utility of DIR with a view to characterize any regions of signal discrepancy by biopsy.

Materials and Methods

We scanned 10 patients with newly diagnosed glioblastoma using Siemens Prisma 3T system including matching 3D DIR (1.3 mm isotropic resolution, TI for DIR of 450 ms and 3000 ms). In addition, we scanned 8 patients using 3T GE Signa system (1 x 1 mm in plane and 2 mm axial resolution). DIR images were compared with 3D FLAIR images of matched plane and resolution by an experienced neuroradiologist.

Results

DIR images provided better contrast between the region of infiltrative tumor/edema and surrounding normal appearing white matter, and in the case of tumors containing hemorrhage DIR provided different contrast to FLAIR. However, we were not able to identify any differences in the spatial extent of DIR and FLAIR signal abnormality on either scanner.

Conclusions

In our experience, DIR does not provide any practical advantage compared to FLAIR with regards to characterization of tumor extent, at least in the preoperative setting.

3233

DTI Metrics for Different Penumbral Tissue Fate in Stroke Animals by Reperfusion

C Chen[1], Y Kao[2], J Tazoe[2], C Lu[3]

[1]Taipei Medical University Hospital, Taipei, Taiwan, [2]Taipei Medical University, Taipei, Taiwan, [3]National Yang-Ming University, Taipei, Taiwan

Purpose

As Intra-arterial (IA) mechanical thrombectomy (MT) is incorporated into the early management of acute ischemic stroke [1], it is emerging to evaluate the salvageable tissue after MT by the performance of surgery [2]. We aim to explore the microstructure change in the penumbra as early as the reperfusion after transient middle cerebral artery occlusion (tMCAo) by diffusion MRI and investigate DRI-derived metrics for the evaluation of final tissue fate.

Materials and Methods

Sprague-Dawley rats (n=7) were anesthetized with 1-2 % isoflurane following by tMCAo with 60 min occlusion [3]. Multi-parametric MRI was performed in under occlusion and immediately after the suture removal. T2w images at 24 h were acquired to determine the final infarct region. DTI metrics including fractional anisotropy (FA), apparent diffusion coefficient (ADC), q- and L-value, and relative cerebral blood flow (rCBF) were analyzed as the previous work [4]. The reperfusion status and tissue survival of each penumbral pixel was determined by the threshold of 80 % rCBF after suture removal and T2w images at 24 h, respectively. The DTI metrics in the destined survival vs. destined-infarct pixels, as well as the well- vs. poor-reperfused pixels at the measurement before and after reperfusion were delineated correspondingly.

Results

Inhomogeneous penumbral tissue regarding the reperfusion and survival status was observed and described by DTI metrics after stroke. Higher FA and q-value were observed in destined survived tissue before and after reperfusion. No significant difference in ADC and L-value was found between survival status in the penumbra. Lower q-value was observed in the pixels with well-reperfusion before and after reperfusion. In addition, pixels with poor reperfusion showed lower q-value after reperfusion. More importantly, lower FA and q-value were observed in the infarcted penumbra regardless of reperfusion status compared with the destined-survived penumbra tissue (Figure).

Conclusions

The FA and q-value decoding the property of anisotropy in the microstructure may reflect the penumbral tissue fate by mechanical thrombolysis.

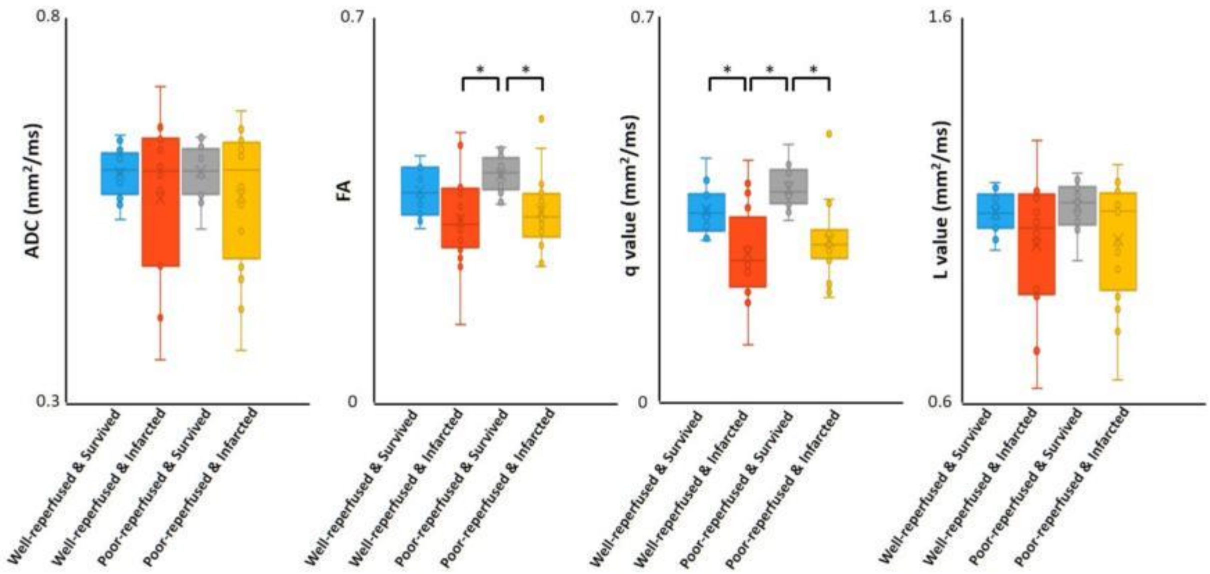

Figure. Tensor metrics including ADC, FA, q- and L-value derived from DTI acquired post-reperfusion shows the difference between destined-survived and destined-infarcted penumbral tissue with well- and poor-reperfusion status in tMCAo animals. *, $P<0.05$ from one-way ANOVA.

(Filename: TCT_3233_Figure.jpg)

3394

Effect of Tumor Sidedness on Resting State Functional Connectivity in Patients with Glioma

S Zhang[1], S Gohel[2], A Holodny[3], B Vachha[4]

[1]Lewis Katz School of Medicine at Temple University, Philadelphia, PA, [2]Rutgers University School of Health Professions, Newark, NJ, [3]MSKCC, NEW YORK, NY, [4]MEMORIAL SLOAN KETTERING CANCER CTR, NEW YORK, NY

Purpose

Patients with glioma often show disruptions in three resting state networks (RSNs) important to consciousness and cognition: the default mode network (DMN), central-executive network (CEN), and salience network (SN). However, the extent to which such disruptions are lateralized across these networks remains largely unexplored. This study used resting state fMRI (rsfMRI) to investigate the effect of tumor sidedness (left vs. right hemisphere) and location (frontal vs. non-frontal) on resting state functional connectivity across these three networks.

Materials and Methods

rsfMRI data were acquired on 74 patients with glioma (mean age 48.69; 60.8% male) sub-divided into left-sided tumors (n=45), right-sided tumors (n=29), frontal tumors (n=48), and non-frontal tumors (n=26). 10 spatially distinct brain regions (4 for CEN, 2 for DMN, 4 for SAL) were defined for rsfMRI analysis. A linear regression-based approach and GLM based model were implemented to understand effects of tumor sidedness and location, respectively, on functional connectivity.

Results
Functional connectivity was reduced between the left anterior cingulate cortex of the SN and the left dorsolateral prefrontal cortex and bilateral intraparietal sulci of the CEN in patients with right-sided tumors compared to those with left-sided tumors ($p<0.05$). Functional connectivity was also reduced across DMN, CEN, and SN with frontal tumors compared to non-frontal tumors ($p<0.05$).
Conclusions
Right-sided and frontal tumors produced greater disruptions in overall functional connectivity across three major RSNs as compared to left-sided and non-frontal tumors in our sample. These findings are potentially useful in understanding how tumor sidedness and location contribute to altered brain function in patients with glioma.

2164

Efficacy and Safety of Bleomycin Sclerotherapy for Lymphovenous Malformations

J Kang[1], S Shankar[2]
[1]Dalhousie University, Halifax, NS, [2]university of Manitoba, Winnipeg, MB, Manitoba

Purpose
Lymphovenous malformations are low flow, vascular lesions that commonly occur in the head and neck. Sclerotherapy has become the mainstay of treatment for these lesions as sclerotherapy is less invasive than surgical excision. Bleomycin is one of the sclerosing agents used for these malformations. The aim of our study was to assess the efficacy and safety of percutaneous Bleomycin embolization in head and neck lymphovenous malformations.
Materials and Methods
Prospectively maintained procedural records were retrospectively reviewed to identify all patients with lymphovenous malformations who underwent percutaneous Bleomycin therapy between 2012 and 2018. Demographic information, lesion and treatment details were collected through chart review. Treatment responses were evaluated objectively by manual volume measurements of the lymphovenous malformations on pre and post treatment MR/CT imaging. Subjective treatment evaluations were obtained with patient satisfaction responses during their clinic visit. Paired t test was used for pre and post treatment volume comparison and $p<0.05$ was considered significant.
Results
16 patients (9 Female; age range 6-67 yrs) were treated in this time period for a total of 30 sessions . All patients were followed clinically and were satisfied with their treatment and improved symptomatically. All lesions reduced in size on follow up subjective evaluation. Pre and post treatment imaging, available on 13 patients, showed a mean reduction of lesion by 57% ($p= 0.02$) after treatment. No peri-procedural complication was seen except for one patient (5 %) who developed hyperpigmentation at the site of ECG leads.
Conclusions
Percutaneous sclerotherapy with Bleomycin for lymphovenous malformations of head and neck appeared safe and efficacious in our study.

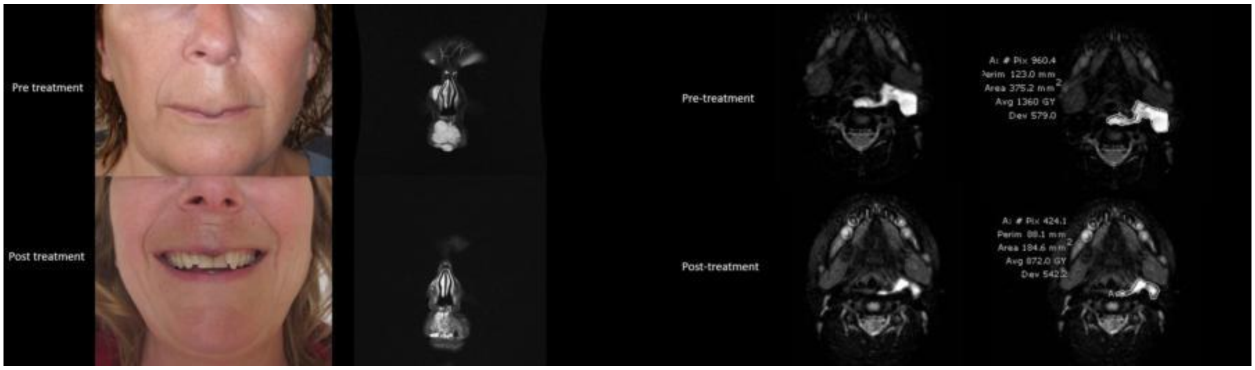

(Filename: TCT_2164_merge.jpg)

2621

Endovascular Management of Spontaneous Delayed Migration of the Flow-Diverter Stent

Y TSAI[1]
[1]Chang-Gung Memorial Hospital, Chiayi, Taiwan

Purpose
Spontaneous delayed migration of the flow-diverter stent (FD) is an unusual complication that can be fatal. The purpose of this study is to report our experience and review of the literature for the management of delayed FD migration.
Materials and Methods
Between Nov. 2013 and June 2017, 122 patients were treated by FD at our institution. Six patients (4.9%) were found to have spontaneous delayed migration of their FD. We also performed a comprehensive review of the literature.
Results
The device migrated proximally in 4 patients and distally in 2 patients. One patient had temporal lobe infarction due to stent migration, and another had subarachnoid haemorrhage. Three patients were treated with a 2nd or 3rd FD, while 2 were treated with stent-assisted coiling, and one was treated with sacrifice of the parent internal carotid artery. According to our results and the literature, the prevalence rate of delayed FD migration ranges from 2.2% to 4.9%, and the mortality and morbidity rate of delayed FD migration is 40%.
Conclusions
Neurointerventionalists should be aware of this complication and be familiar with risk factors, preventive methods and treatment options. If there is any concern regarding the size or position of the FD, early imaging follow-up and endovascular treatment should be indicated.

2676

Endovascular Treatment of Acute Ischemic Stroke in Octogenarians and Nonagenarians Compared with Younger Patients

Y Kawabata[1], S Fukuda[2], N Nakajima[3], T Tsukahara[2], H Miyake[3]
[1]Kyoto Katsura Hospital, Kyoto, Japan, [2]National Hospital Organization Kyoto Medical Center, Kyoto, Kyoto, [3]Kyoto Katsura Hospital, Kyoto, Kyoto

Purpose
Endovascular therapy (EVT) for emergent large vessel occlusion has been established as the standard

therapy in acute ischemic stroke. However, the effectiveness and safety in the very elderly population have not been proved. Objective: To determine the safety and effectiveness of EVT in octogenarians and nonagenarians.
Materials and Methods
We retrospectively reviewed all patients who underwent EVT at two stroke centers between April 2012 and July 2018. Functional outcome was assessed using mRS at 90-day or at discharge. Favorable outcome was defined mRS of 0 to 2 or not worsening of the mRS before stroke, and compared between younger patients (age 46-79; n=42) and octogenarians and nonagenarians (age 80-97; n=19).
Results
Patients in octogenarians or nonagenarians more frequently had poor pre-stroke functional deficit (mRS >1) than younger patients (57.9% vs. 19.0%, p value=0.0059). No difference was observed between very elderly and younger patients in the rate of successful recanalization of TICI 2b/2c or 3 (89.5% vs. 69.1%, p value =0.11), favorable functional outcome (47.3% vs. 47.6%, p value=1.00), and mortality (21.1% vs. 26.2%, p value=0.76). (Nearly) complete recanalization of TICI2c or 3 recanalization was observed more frequently in very elderly patients (57.9% vs. 28.6%, p value=0.045). Procedure time did not change between the groups (63.2 min vs. 80.0 min, p=0.95).
Conclusions
Patients in octogenarians or nonagenarians often had prestroke morbidity. However, age depedency of clinical outcome after EVT was not observed in our analysis. EVT should not be withheld for large vessel occlusion in octogenarians and nonagenarians in acute ischemic stroke.

safety and efficacy outcome

variable	age<80 (n=42)	age>=80 (n=19)	p value
TICI2b/2c/3	29(69.1)	17 (89.5)	0.11
TICI2c/3	12 (28.6)	11(57.9)	0.045
symptomatic ICH	1 (2.38)	0	1.00
mRS 0-2	18 (42.9)	6 (31.6)	0.57
mRS0-2 or no worsening of mRS	20 (47.6)	9 (47.3)	1.00
mortality	11(26.2)	5(21.1)	0.76
Procedure time	79.97(37.47)	63.22(30.78)	0.95

(Filename: TCT_2676_JSNET2018001.jpg)

2752

Evaluation of Volume of the Amygdala in Psychogenic Nonepileptic Seizure

H Tatekawa[1], N Salamon[1]
[1]*UCLA, Los Angeles, CA*

Purpose
Psychogenic nonepileptic seizures (PNES) resemble partial or generalized epileptic seizures, such as temporal lobe epilepsy (TLE), but do not show abnormal brain electrical activity in video-electroencephalogram. The symptoms of PNES are perpetuated by ongoing or recurrent stress, which would also cause conversion disorder. The functional connectivity due to contiguous stress was supposed to influence the amygdala, and chronic psychosocial stress was also known to lead to excessive release of glutamate in the projection areas to the amygdala. Elevation of glutamate levels in the amygdala was reported to occur in TLE as well as PNES, and long-lasting inflammation may be associated with amygdala enlargement (AE). Although AE was reported in patients with TLE at rates that range from 12% to 63%, the relationship and occurrence frequency of AE in PNES have not been revealed. The purpose of this study is to evaluate the volume of the amygdala in PNES.
Materials and Methods
We retrospectively selected 46 patients (mean age, 39.6 years old; male : female, 13 : 33) who presented to the UCLA between 2004 and 2018 and were diagnosed as PNES by group consensus during weekly case conferences. We used T1-weighted MPRAGE sequence, measured the volume of amygdala, and calculated z-score by using NeuroreaderTM.
Results
Mean amygdala volume was 2.78 ml (standard deviation {SD}, 0.39 ml). Mean z score was -0.03 (SD, 0.18). Z-score of amygdala volume in all PNES patients was included in the range of 1 SD of the healthy control database.
Conclusions
Although the volume of amygdala in PNES was similar to that in healthy control database, this result has not been reported before and may help to differentiate PNES from other true epileptic seizures.

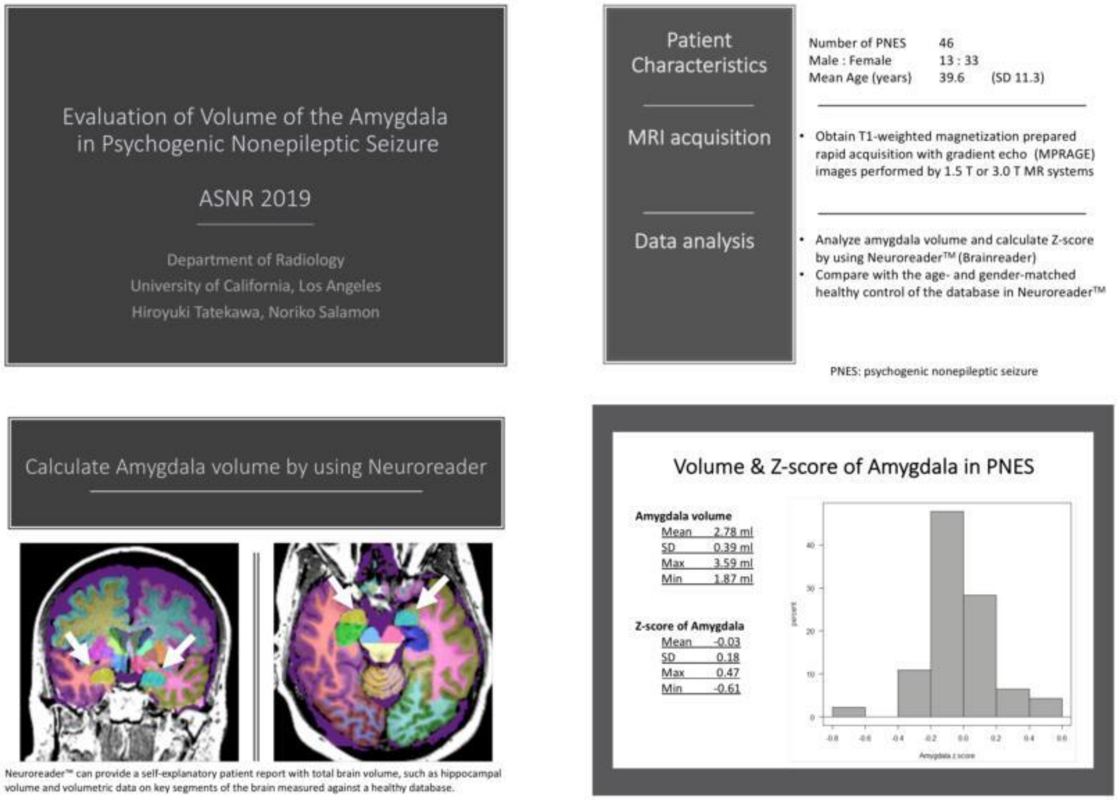

(Filename: TCT_2752_ASNRabstract4.jpg)

2667

External Auditory Canal Ceruminous Adenocarcinoma

G Parnes[1], A Zlochower[1], W Mallon[2], S Roknsharifi[1], R Zampolin[1], K Hsu[3], S Slasky[1], J Burns[1], J Bello[1], K Shifteh[1]
[1]Montefiore Medical Center, Bronx, NY, [2]Montefiore Medical Center, New York, NY, [3]Stanford University, Stanford, CA

Purpose
To describe the imaging features of a rare case of ceruminous adenocarcinoma of the external auditory canal. To understand how ceruminous adenocarcinomas are treated and managed. To learn the differential diagnosis of lesions originating from the external auditory canal.
Materials and Methods
The patient is a 75-year-old female with a history of diabetes presenting with a week of severe left ear pain and facial nerve palsy. A non-contrast CT of the temporal bone and a contrast enhanced MRI of the temporal bone were performed.
Results
Non-contrast CT of the temporal bone demonstrates a soft tissue mass within the bony and cartilagenous segment of the external auditory canal with bony destruction along the anterior wall. The soft tissue mass extends anterior and superior through the mastoid segment of the temporal bone. There is also abnormal soft tissue within the entire tympanic cavity without ossicular erosion. 4 months later post contrast MRI of the temporal bone demonstrates moderate progression of disease process. There is abnormal enhancing

soft tissue within the external auditory canal, mastoid segment of the temporal bone, and intracranial extension along the floor of the middle cranial fossa. There is abnormal enhancement along the facial nerve consistent with perineural spread of tumor.

Conclusions

Ceruminous glands are modified apocrine sweat glands found in cartilagenous portion of the external auditory canal. Secretions from sebaceous glands and ceruminous glands drain into the hair sacs of the the fine hairs in the external auditory canal to form cerumin. Tumors originating from the ceruminous glands have varied clinical and histological manifestations making diagnosis difficult. The typical patient with ceruminous tumors is over 50 years old, however there are cases affecting adolescents. The common clinical symptoms reported in the literature includes otalgia, mass and hearing changes. Facial nerve involvement may result in facial nerve paralysis. These lesions more commonly metastasize to the bones, lungs, and brain than to the cervical lymph nodes. CT of the temporal bones is helpful to detect bony erosion, destruction, and tumor extension. MRI can show local spread of tumor to adjacent soft tissues including intracranial invasion and perineural spread of disease. The differential diagnosis includes squamous cell carcinoma, melanoma, cholesteatoma, malignant otitis externa, neuroendocrine adenoma, metastasis and lymphoma. Prognosis can be hard to predict with these neoplasms. Complete surgical excision with radiation has been found to give the best long term prognosis. Important prognostic factors for cases described in the literature include positive surgical margin at initial surgery, perineural invasion, local recurrence, and bone extension.

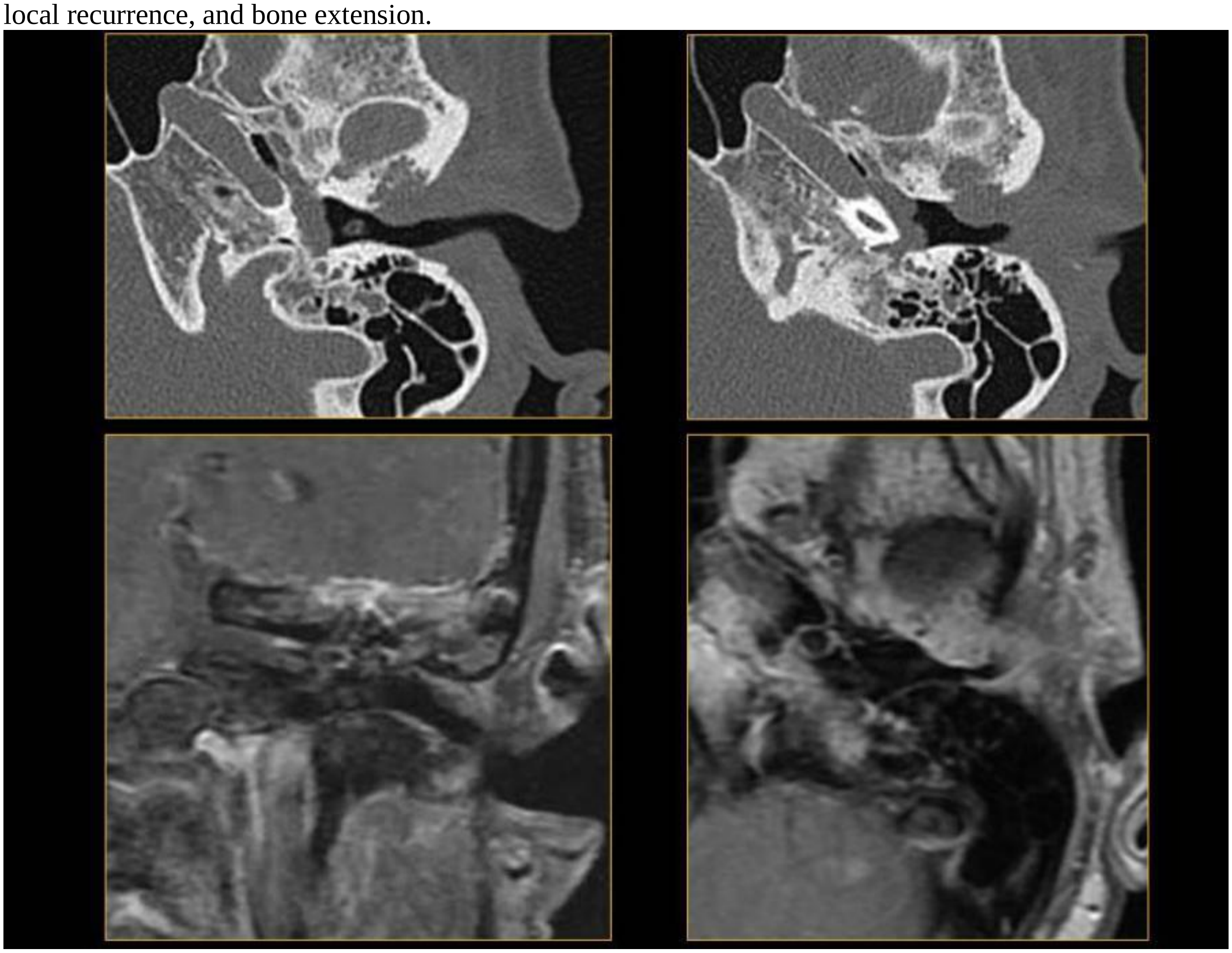

(Filename: TCT_2667_Presentation21.jpg)

2982

Hedging in Neuroradiology

A Callen[1], S Dupont[1], V Bartle[1], J Talbott[1], M Kohli[1], J Narvid[1]
[1]*University of California, San Francisco, San Francisco, CA*

Purpose
The purpose of this study was to assess the degree of hedging present within radiology reports generated by the neuroradiology section at a single academic institution, and compare it to that of other radiology subspecialties. We hypothesized there would be substantial variability among neuroradiologists with regard to their use of hedging in radiology reports. Likewise, we hypothesized that substantial variability exists within use of hedging among radiology subspecialities.. To test these hypotheses, we a validated Natural Language Processing (NLP) algorithm that automatically labels radiology reports as hedging or not and used it to evaluate a large database of neuroradiology and general radiology reports.
Materials and Methods
An algorithm was created to detect usage of expressions of uncertainty (hedging). For validation, 452 unstructured reports were reviewed by two radiologists who determined whether the reporting radiologist expressed uncertainty. Cohen's kappa was calculated, with $k = 0.67$. The software was 93% sensitive and 94% specific for detecting hedging, with an average precision value of 0.78, and average F1 score of 0.84. Once validated, the software was then used to prospectively analyze all radiology reports from our institution from 2011-2015. To evaluate the effect of radiology subspecialty on hedging, chi-squared tests were used to assess the relationship of hedging with subspecialty of origin. The level of significance was adjusted according to the Bonferonni correction for multiple comparisons.
Results
642569 radiology reports were collected from a 5-year long period from 2011 through 2015. Of the 642569 reports, 435392 (67.8%) were from general radiography, 76407 (11.9%) neuroradiology, 54881 (8.5%) ultrasound, 42883 (6.7%) abdominal, 24258 (3.8%) chest, and 7752 (1.2 %) musculoskeletal radiology. Within neuroradiology, 47.1% of reports were from patients in the emergency room, 29.6% of reports were from patients admitted to the hospital, and 23.3% of reports were from outpatients. 72.7% of reports were from CT studies, and 27.3% of reports were from MRI studies. The differences in rates of hedging between neuroradiology and other specialities was statistically significant (<0.003), Figure 1. Computed tomography had the highest rate of hedging, with 44% of reports containing uncertainty terms. Significant differences in hedging were present between CT and ultrasound and between radiography and each other modality within all radiology reports ($p<0.008$), Figure 2. There was no statistically significant correlation between rates of hedging and years of experience (Spearman's $R = 0.19$, $p=0.44$), Figure 3.
Conclusions
We developed and validated an algorithm to detect the presence of uncertainty in radiology reports. Using this validated tool, we analyzed large numbers of reports to elucidate the use of ambiguous language within a neuroradiology subsection, and compare it to that of other subsections within the same hospital. Future work may identify the factors that influence individual variability in hedging and develop curricula to improve standardization.

Figure 1:

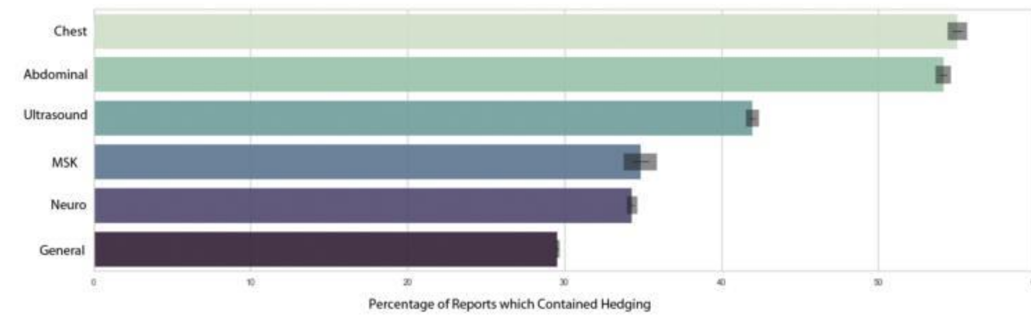

Figure 2:

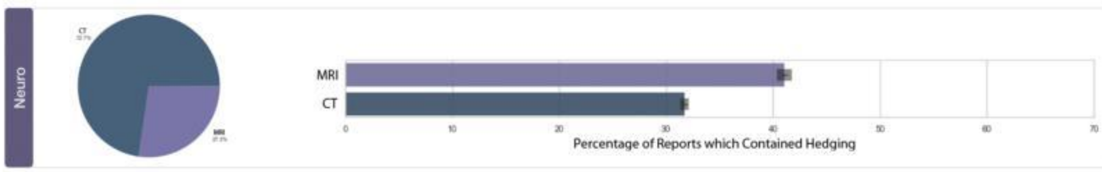

Figure 3:

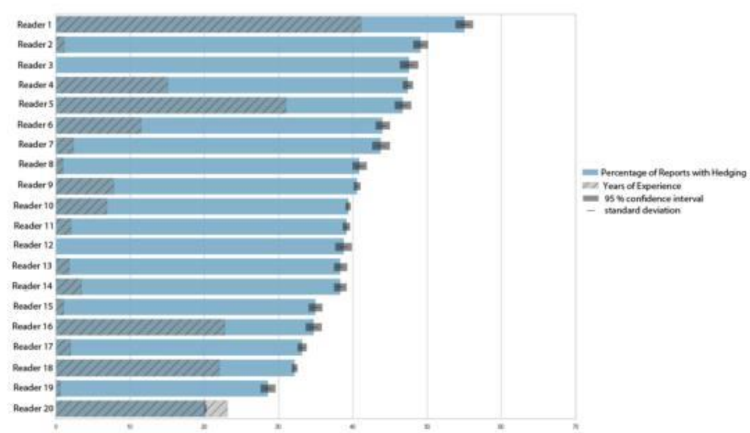

(Filename: TCT_2982_ASNRHedgingFigure.jpg)

2419

Improved Diagnostic Value of Combined CT Angiography and CT Perfusion Studies for Detection of Acute Ischemic Stroke.

O Kutsenko[1], K Durwas[1], D Sun[1], C Tsetse[1], R Mangla[1]
[1]*SUNY Upstate University Hospital, Syracuse, NY*

Purpose
To determine if combined CT angiography with CT perfusion studies are superior to CT angiography alone in imaging interpretation for acute ischemic stroke.

Materials and Methods
This is a retrospective IRB-exempt HIPPA compliant study. We selected a random sample of 50 patients with acute cerebral hypoperfusion symptoms who had simultaneous CT angiography (CTA) and CT perfusion (CTP) imaging at the time of suspected ischemic event. A randomized experimental block design was used where two radiology residents blinded to patient data each assessed all exams using CTA only and combined CTA/CTP configurations evaluating for presence of acute infarction, territorial location, source artery, and time required for interpretation. Evaluations were spaced four weeks apart. This experimental design allowed for estimation of benefit of additional CTP while controlling for carryover effects. Experimental results were compared with final diagnosis based on arteriograms and/or magnetic resonance imaging. Diagnostic significance (sensitivity, specificity, positive and negative predictive values) and interrater agreement were evaluated using SPSS statistical software.
Results
Sixteen patients (32%) had an acute ischemic infarction with 18 total arteries occluded. Thirty-four patients did not have acute ischemia. Specificity increased with added CT perfusion (CTA only 0.81; CTA/CTP 0.96) without sacrifice in sensitivity (CTA only 0.69; CTA/CTP 0.72). Positive predictive value significantly increased (CTA only 0.64, CTA/CTP 0.9). Mean interpretation time improved from 3.2 mins to 1.63 mins. Overall interrater agreement (Kappa) similarly increased from moderate to substantial (CTA only 0.6; CTA/CTP 0.76, p<0.001).
Conclusions
When assessing for acute cerebral arterial occlusion on CT angiogram, additional CT perfusion imaging increases specificity, positive predictive value, and interpretation speed per study. Overall agreement between readers for diagnosis of acute stroke, territory, and arterial source also improves. This analysis shows that addition of CT perfusion imaging to CTA has high diagnostic value in detecting cerebral ischemia and intracranial occlusion.

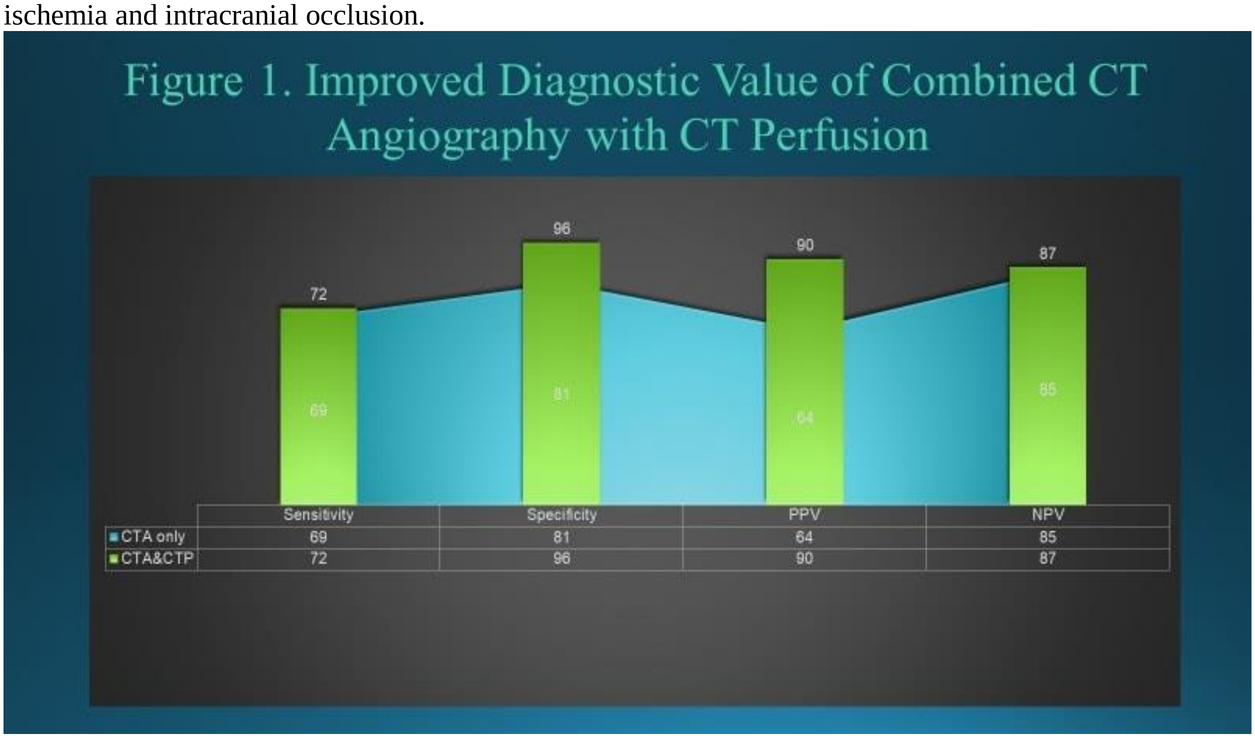

	Sensitivity	Specificity	PPV	NPV
CTA only	69	81	64	85
CTA&CTP	72	96	90	87

(Filename: TCT_2419_CTACTP-min.jpg)

3598

Improving Accuracy and Confidence of Radiology Residents in the Diagnosis of Otosclerosis

B Ozgen Mocan[1], A Allen[1], M Patel[1], L Brown[2], M Redleaf[1]
[1]University of Illinois at Chicago, Chicago, IL, [2]University of Ilinois at Chicago, Chicago, IL

Purpose
Otosclerosis (OS) is a cause of progressive hearing loss with specific exam and audiogram findings. However many patients present with only few typical features and symptoms can be confused for other causes of conductive or mixed hearing loss. CT of the temporal bones is the imaging of choice to evaluate OS and has reported high accuracy however this evaluation is challenging for the inexperienced eye. The purpose of this study was to assess the effect of a focused tutorial on the diagnostic accuracy of radiology residents for the diagnosis of OS.
Materials and Methods
The preoperative temporal bone CTs of 17 patients with surgical diagnosis of OS were evaluated. The control group consisted of 21 patients who had no evidence of OS clinically and who were operated for other diagnoses. First a neuroradiologists with extensive head and neck experience retrospectively evaluated both groups. Then, two radiology residents (PGY-4 and PGY-3) performed the assessment, before and after reviewing a didactic tutorial. The observers remained blinded to the diagnosis and clinical information. The observers were not given the self-administered tutorial until one week after submitting the initial review of the images to allow for adequate time between the pre and post tutorial evaluations. A degree of confidence (DOC) with the diagnosis (high, medium, or low) was given. Sensitivity, specificity and accuracy were calculated before and after the didactic tutorial.
Results
The neuroradiologist was able to diagnose OS in all 17 test ears, and ruled out OS in all of the 21 control ears, giving a sensitivity and specificity of 100%. The combined results for the two residents before the tutorial were: 40% sensitivity, 66% specificity, and 54% accuracy. After the tutorial the combined results were: 56%, 93%, and 76% respectively with p- values of 0.295 for sensitivity, 0.073 for specificity and 0.036 for accuracy.
Conclusions
Otosclerosis can be diagnosed with a very high accuracy using temporal bone CT when evaluated by an experienced neuroradiologist. The accuracy of the trainees can also be increased by reviewing a short didactic tutorial and radiology training programs can help trainees gain not only accuracy but confidence in the difficult but clinically relevant diagnosis of otosclerosis.

2669

Is a Didactic Lecture Effective in Teaching Ultrasound Technologists the TIRADS Scoring System for Stratifying Thyroid Nodules?

V Patel[1], J Roberts[1], M Koenigsberg[1], B Cohen[1], S Frank[1], R Orentlicher Fine[2], J ROSENBLUM[3], M Stein[1]
[1]Montefiore Medical Center, Bronx, NY, [2]Montefiore Medical Center, White Plains, NY, [3]Jacobi Medical Center, WHITE PLAINS, NY

Purpose
Thyroid nodules have a reported prevalence of up to 68% in adults. The majority of these nodules are benign. Moreover, malignant nodules less than 1 cm often exhibit indolent or nonaggressive behavior. Hence, the vast majority of nodules do not require fine-needle aspiration or biopsy. Recent publications sought to standardize terminology for ultrasound reporting of incidental thyroid nodules using a system termed TI-RADS (Thyroid Imaging, Reporting and Data System). As ultrasonographers are generally the first members of the imaging team to select and capture images of the thyroid nodules, it is essential that they be well versed in the imaging features involved in the TI-RADS lexicon. The aim of this study is to

present and familiarize ultrasonographers with the TI-RADS lexicon for the purpose of improving their recognition of malignant nodules according to the TI-RADS criteria.
Materials and Methods
After obtaining institutional review board approval, we presented 20 ultrasonographers with the TI-RADS lexicon using an image rich 45 minute didactic lecture which encompassed the diagnostic criteria for thyroid malignancy and how to properly scan patients. Our study examined the effects of the lecture by comparing the results of a pre-test, an immediate post-test and a 2-week delayed post-test. The tests were composed of the same 15 multiple-choice questions, with varying question order. Assessment scores were compared using a matched pair t-test.
Results
The pre-lecture assessment scores ranged from 25-55% with an average of 39%. Immediately after the lecture, the assessment scores ranged from 40- 75%, average of 60%. Two weeks after the lecture, scores ranged from 30%-70%, average 55%. Compared to the pretest, there is a statistically significant difference in average scores immediately after and 2 weeks after the lecture (p-value < 0.00001 and <0.000016 , respectively).
Conclusions
A didactic lecture can successfully teach, result in knowledge retention and increase ultrasonographer's confidence in the TI-RADS lexicon.

2979

Lipogenic Graves' Orbitopathy: Clinicoradiologic Correlation

P Shoor[1], G Moonis[1], A Tooley[1], M Kazim[2]
[1]Columbia University Medical Center, New York, NY, [2]Columbia, New York, NY

Purpose
To describe the lipogenic or fat-predominant variant of Graves' orbitopathy (GO) from a radiologic point of view using both computed tomography (CT) and Magnetic Resonance Imaging (MRI) in order to make radiologists aware of the unique radiological findings of this variant form of GO, as the diagnosis has important clinical implications for patients.
Materials and Methods
All final radiology reports from our hospital system were searched for key words including "lipogenic graves," "lipogenic orbitopathy," "fat orbitopathy," and "type 1 graves." This search yielded 27 patients (23 female, 4 male) where lipogenic GO was suggested by the radiologist. The search also provided characteristics of the patients including age, sex, and gender. Ophthalmologists then provided clinical data including physical exam, diagnosis, clinical activity score (signs of inflammation), and prognosis.
Results
CT and MRI of patients with the lipogenic form of GO demonstrate increased intraconal fat but the size of the extraocular muscles (EOM) are preserved or even decreased compared to the more common myogenic or muscle-predominant form of GO, which presents with increased EOM size. Lipogenic GO patients are more like to have proptosis, be young and female, have better clinical activity scores, and better clinical prognosis from ophthalmologists.
Conclusions
Unlike the more usual myogenic form of GO, lipogenic GO presents radiographically with increased intraconal fat and relative preservation of the EOMs. This entity has not been described in the radiology literature and radiologists must be aware of the unique imaging findings of the lipogenic form of GO. Suspicion should be particularly high in young female patients with proptosis. The diagnosis has prognostic and management implications.

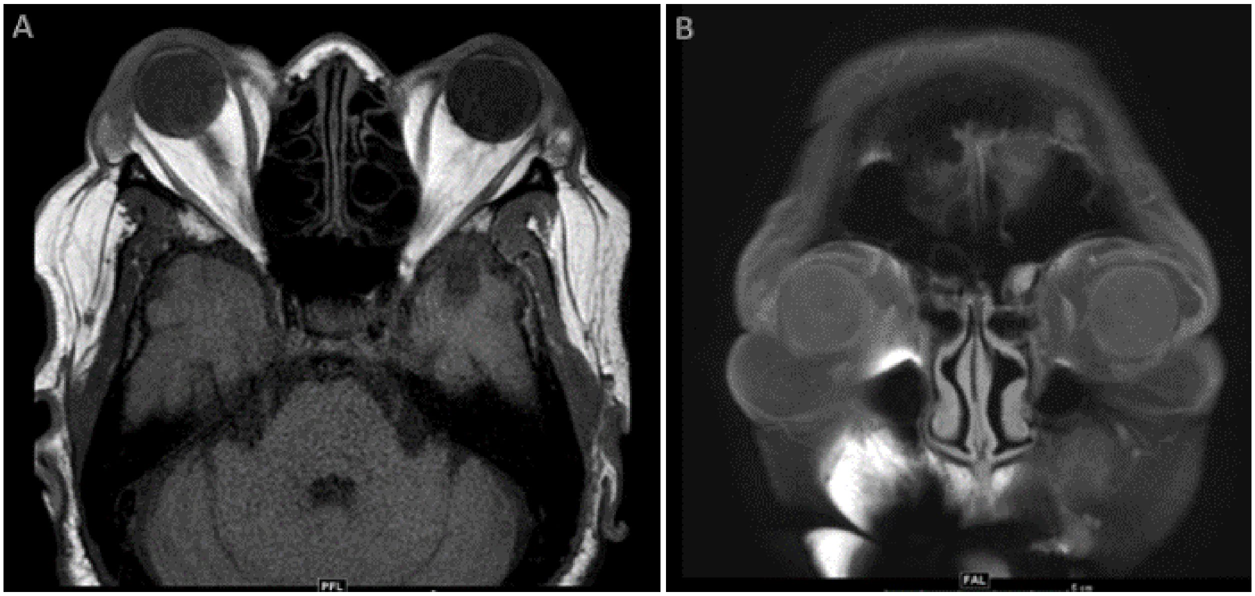

(Filename: TCT_2979_LipogenicImageSingleMRI.gif)

2775

Mismatch T2-FLAIR Sign and its Prognostic Value in Diffuse Gliomas

C Coelho Neto[1], T Rocha[2], G Simao[1], A Santos[1]
[1]University of São Paulo - Ribeirão Preto Medical School, Ribeirão Preto, Brazil, [2]University of São Paulo- Ribeirão Preto Medical School, Ribeirão Preto, SP

Purpose
The low grade gliomas (grade 2 WHO) have glial tissue origin and habitual slow growth, with possible progression to anaplastic types (grade 3 WHO). These two tumor are together referred as lower grade gliomas in this abstract. Nowadays, in addition to histologic diagnosis, the molecular analysis has been a important diagnostic step in these cases, considering the fact that different tumor subtypes have different biological behaviors, with impact in treatment and survival rates. There has been a recent description of a MRI sign, named Mismatch T2-FLAIR, which has straight relation to a certain molecular subtype of diffuse gliomas (IDH mutated, codeleted 1p/19q). The purpose of the study was to find the presence of this sign in diffuse gliomas and compare the prognostic of these patients with the ones in which the signal was not found.
Materials and Methods
We have studied 96 patients with diffuse gliomas, including histologic types oligodendrogliomas, astrocytomas and oligoastrocytomas, reviewing their first diagnostic MRI, including T2 and FLAIR sequences, searching for the presence of the mismatch T2-FLAIR sign, caracterized by hypersignal in T2 sequences and relative hyposignal in FLAIR sequences, with possible hyperintenseT2 rim. Then, each patient's records has been analysed to colect prognostic data, such as survival rates and disease progression after first surgical treatment. We have then compared these data among different groups to find out if the presence of the T2-FLAIR mismatch sign is an independent prognostic marker in these cases. The MRI's were analyzed by two independent neuroradiologists and the patients information were collected by the author of the project. The patients were then divided in two big groups, regarding the presence or absence of the mismatch T2-FLAIR sign, and then they were once again divided in alive x dead patients, and progression of disease x no progression in 5 years after diagnosis/first surgery.

Results
Among 96 patients with diffuse gliomas, we had 22 patients with T2-FLAIR mismatch sign (22%), with 4 death (18%) and 18 alive patients (82%) in this group by the time of the study. Among these 18 patients, we had 9 patients with progression of disease and 9 patients without progression (in 5 years after first surgical treatment). Considering the group with the T2-FLAIR mismatch sign, we had 74 patients (77%), with 22 death (29%) and 52 alive patients (70%) in this group by the time of the study. Among these 52 alive patients, we had 27 patient with progression of the disease and 25 without progression (in 5 years after first surgical treatment).
Conclusions
The study tries to point to the fact that the presence of the T2-FLAIR mismatch signal may be a good prognostic marker in diffuse gliomas. The recent studies have shown that its presence is highly especific for IDH mutated with 1p19q codeletion diffuse gliomas, that correspond to astrocytomas. We try to prove that the patients who present the sign in the first diagnostic MRI may have a better evolution with higher survival rates and less progression of the disease. In addition to this fact, we try to understand the meaning of the T2-FLAIR sign, for example if it has any relation with low cellularity. Imaging markers with such a high correspondence with molecular tumor types are important in the first diagnostic step and therefore must be studied and well understood in the clinical practice.

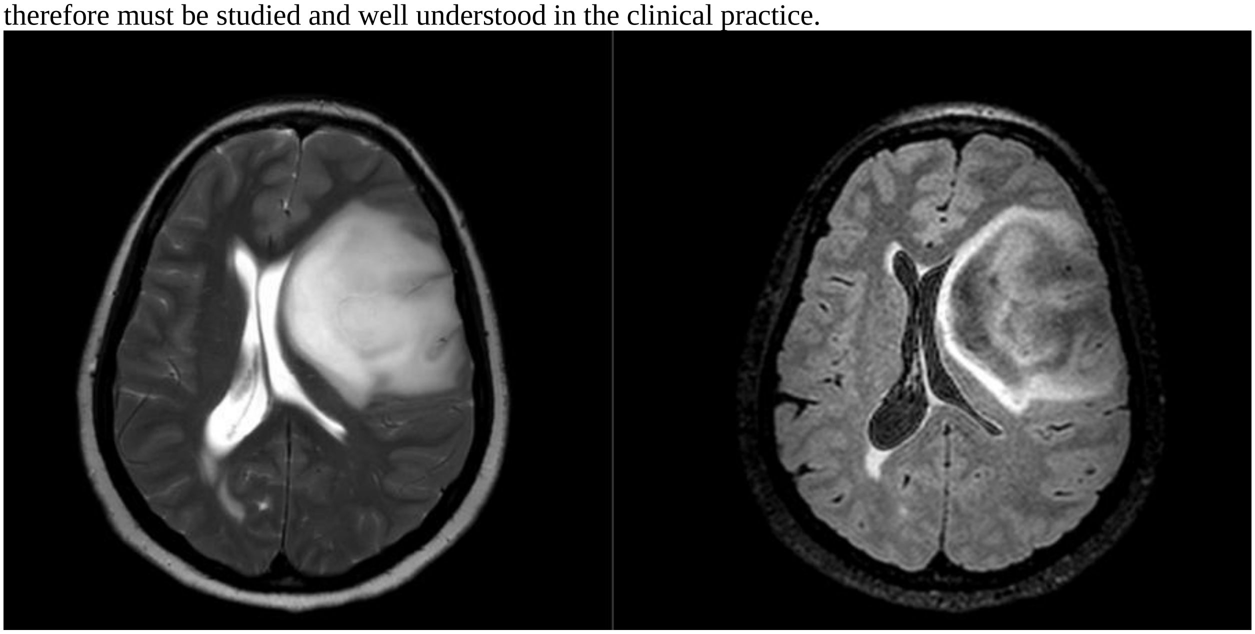

(Filename: TCT_2775_ScreenShot2018-11-06at093126.jpg)

2872

Neuroimaging Evaluation of Chimeric Antigen Receptor (CAR) T-Cell Therapy Neurotoxicity

W Klejch[1], A Artz[2], M Bishop[2], S Ali[2]
[1]University of Chicago, Chicago, IL , [2]University of Chicago, Chicago, IL

Purpose
CAR-T cell therapy is a novel form of immunotherapy approved for patients with relapsed or refractory diffuse large B-cell lymphoma (DLBCL) and B-cell precursor acute lymphoblastic leukemia (ALL). Initial clinical trials have demonstrated promising results in refractory disease but have been tempered by high rates of neurotoxicity. The pathophysiology of this complication is poorly understood, with recent studies suggesting a role of endothelial activation and increased blood brain barrier permeability. Only

scarce case reports are available on the neuroimaging manifestations, and we sought to evaluate the neuroradiological findings of neurotoxicity after CAR-T cell therapy in a retrospective study.

Materials and Methods

Retrospective chart review was performed of patients from a single academic center who underwent CAR-T cell therapy and developed neurotoxicity according to standard CARTOX criteria. All brain CT and MR studies performed in these patients immediately pre- and post- CAR-T cell therapy were independently reviewed by two radiologists.

Results

A total of 22 adult patients with DLBCL treated with axicabtagene were evaluated. 17 (77%) patients had available immediate pre-lymphodepleting therapy CT or MR imaging, all of which were normal or demonstrated no acute findings. 17 (77%) patients received post-therapy neuroimaging (15 with head CT, 10 with brain MR studies) due to neurotoxicity. Positive imaging post-therapy findings were seen in 3 patients with DLBCL including punctate acute left cerebellar infarct (n=1), acute subdural hematoma (n=1), and reversible punctate foci of T2 hyperintensity in the cerebral white matter noted on sequential post-therapy MR exams (n=1). No abnormal enhancement was observed in any case. Clinical severity of neurotoxicity did not correlate with presence of positive imaging findings although sample size was small.

Conclusions

Neuroimaging findings of CAR-T cell related neurotoxicity are heterogeneous. Future studies should investigate pre-symptomatic neuroimaging, ideally with MRI, which may help elucidate the pathophysiology of neurotoxicity and facilitate early recognition and treatment.

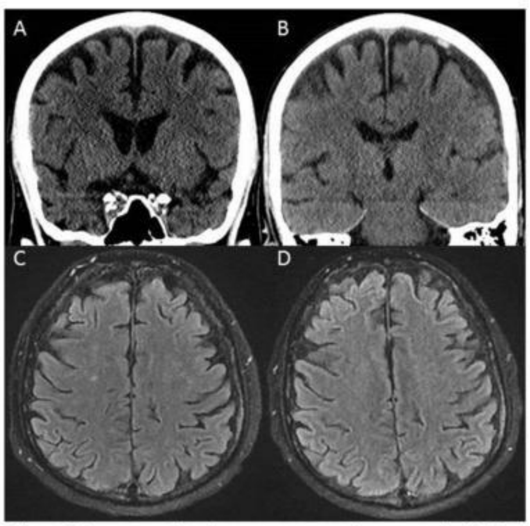

Figure 1: Pre-treatment (A) and post-treatment coronal noncontrast head CT 3 days later (B) in patient with neurotoxicity demonstrating development of bilateral subdural hemorrhage. Different patient (C, D) with axial FLAIR images demonstrating punctate foci of T2/FLAIR hyperintensity in the white matter (C) which resolved 5 days later (D). Other foci of white matter hyperintensity not shown.

(Filename: TCT_2872_CARTASNR2019FIG1.jpg)

3089

Neuroimaging Metrics Associate with Overall Survival in Patients with IDH-mutant, 1p/19q Non-codeleted Astrocytomas

A Bansal[1], E Young[2], S Abbas[3], P Batchala[3], D Schiff[3], C Fadul[3], M Lopes[3], S Patel[3]

[1]*University of Virginia, Charlottesville, VA,* [2]*UVA, Charlottesville, VA,* [3]*University of Virginia Health System, Charlottesville, VA*

Purpose
To determine neuroimaging metrics that associate with overall survival in patients with IDH-mutant 1p/19q non-codeleted astrocytomas.
Materials and Methods
IRB approval was obtained for this HIPAA compliant retrospective study. 76 IDH-mutant astrocytomas with available preoperative neuroimaging were accrued from an institutional database. Demographic information, histologic grade, surgery type, and neuroimaging metrics (tumor laterality, tumor size, lobe involvement, maximum tumor diameter, tumor morphology [predominantly infiltrative versus predominantly circumscribed], T2-FLAIR mismatch sign, necrosis, hydrocephalus, midline shift) were associated with patient overall survival using Cox proportional hazards regression modeling. Significant metrics were associated with overall survival after adjustment for tumor grade.
Results
Of the 76 IDH-mutant astrocytomas, 47 tumors were grade II, 21 were grade III, and 9 were grade IV. Higher tumor grade was associated with shorter overall survival [hazard ratio (HR) = 2.72, p=0.015]. After adjusting for tumor grade, maximum tumor diameter (HR: 2.62, p=0.027), tumor morphology (infiltrative versus circumscribed) (HR: 3.80, p=0.019), number of involved lobes (HR: 2.31, p=0.024), and surgery type (biopsy versus sub-total or gross-total resection) (HR: 5.41, p=0.008) were significantly associated with patient overall survival.
Conclusions
Among patients with IDH-mutant 1p/19q non-codeleted astrocytomas, several neuroimaging metrics and surgery type associate with patient overall survival. Such metrics can be useful for prognostic counseling in patients with IDH-mutant astrocytomas.

3294

Non-invasive Assessment of Gioma Microstructure Using VERDICT MRI: Correlation with Histology

F Zaccagna[1], F Riemer[1], A Priest[2], M Mclean[1], K Allinson[3], J Grist[4], T Matys[1], J Gillard[1], C Watts[4], S Price[1], M Graves[2], F Gallagher[1]
[1]*University of Cambridge, Cambridge, UK,* [2]*Cambridge University Hospitals NHS Foundation Trust, Cambridge, UK,* [3]*Addenbrooke's Hospital, Cambridge, UK,* [4]*University Hospitals Birmingham NHS Foundation Trust, Birmingham, UK*

Purpose
This prospective study evaluated the use of VERDICT MRI to investigate the tissue microstructure in glioma. VERDICT-derived parameters were correlated with both histological features and tumor subtype and were also used to explore the peritumoral region.
Materials and Methods
Fifteen consecutive treatment-naïve patients (age 43.5±15.1 years, 6 males) with suspected glioma underwent diffusion weighted imaging including VERDICT modelling. Tumor cell radius, intracellular (IC) and combined extracellular/vascular (EC) volumes were estimated using a framework based on linearization and convex optimization. An experienced neuroradiologist outlined the peritumoral edema, enhancing tumor and necrosis on T2W and contrast-enhanced T1W. The same regions-of-interest were applied to the co-registered VERDICT maps to calculate the microstructure parameters. Pathology sections were analyzed with semi-automated software to measure cellularity and cell size.
Results
VERDICT parameters were successfully derived in all patients. The imaging-derived results showed a

larger intracellular volume fraction in high grade glioma compared to low grade glioma (0.13±0.07 vs. 0.08±0.02 respectively; p=0.05) and a trend towards a smaller extracellular/vascular volume fraction (0.88±0.07 vs. 0.92±0.04 respectively; p=0.10). The conventional ADC was higher in LGG compared to HGG but this difference was not statistically significant (1.22±0.13x10-3mm2/s vs. 0.98±0.38x10-3mm2/s, respectively; p=0.18).

Conclusions

This feasibility study demonstrated that VERDICT MRI can be used to explore the tissue microstructure of glioma using an abbreviated protocol. The VERDICT parameters of tissue structure correlated with those derived on histology. The method shows promise as a potential test for diagnostic stratification and treatment response monitoring in the future.

3029

Obstructive Sleep Apnea and White Matter Hyperintensities: Correlation or Causation?

T Vandewater[1], N Schammel[2], C Wilson[3], S Self[3], C Schammel[4], A Cowley[5], D Gault[6], L Madeline[6]
[1]University of South Carolina School of Medicine Greenville, Greenville , SC, [2]University of South Carolina School of Medicine Greenville, Greenville, SC, [3]Clemson University, Clemson, SC, [4]Pathology Associates, Greenville, SC, [5]Greenville Health System, Greenville , SC, [6]Greenville Health System, Greenville, SC

Purpose

Obstructive sleep apnea (OSA) is a common medical condition affecting approximately 12% of the adult population and causes hypoxic events thought to cause small vessel ischemic episodes in the brain, identified on MRI as white matter hyperintensities (WMH) which have been implicated in cognitive dysfunction and decline. This study sought to investigate this relationship.

Materials and Methods

A retrospective evaluation of adults who underwent polysomnography and a brain MRI between 4/1/2002 and 4/30/2017 was completed. Patients with comorbidities that would create ambiguity with WMH on MRI were excluded.

Results

For the 72 patients, demographic/clinicopathologic/polysomnography data, treatment and outcomes were collected. MRI evaluation of WMH using Fazekas scores were collected blind of clinical data. Collated clinical/MRI data were stratified and then analyzed using chi-square, fishers t-tests, ANOVA and linear regression. Stratification by OSA category revealed no differences in demographics, clinicopathologic or comorbidities; however, none of the WMH measures were significantly different. Similarly, stratification by BMI and HTN did not expose indicators of OSA differences. Mean Fazekas (2.09; p=0.0032) and DWMH (1.22; p=0.008) were different with HTN stratification. Stratification by Fazekas, PVWM and DWMH revealed increasing incidence and number of lesions with age (p=0.0001), while hypertension and hyperlipidemia were significantly different between Fazekas (p=0.0032 and p=0.0005, respectively) and DWMH groups (p=0.0008 and p=0.0005, respectively). Hyperlipidemia was significant between PVWMH lesion groups (p=0.0076).

Conclusions

Our results indicate no association between total WMH, PVWMH, or DWMH and OSA, suggesting OSA is not an independent risk factor for the development of WMH. Additionally, hypertension and hyperlipidemia are significantly associated with both Fazekas and DWMH, with PVWMH significantly associated with hypertension only. These results suggest small vessel atherosclerosis may play a role in the development of WMH; however, OSA alone is not associated with WMH. Unanticipated, our results may provide insight into future study design for evaluating these clandestine but ubiquitous white matter findings.

2940

Parapharyngeal Mesenchymal Chondrosarcoma

H Sotoudeh[1], O Shafaat[2]
[1]University of Alabama at Birmingham, Birmingham, AL, [2]Isfahan University of Medical Sciences, Isfahan, MD

Purpose
The parapharyngeal masses(PPS) account for about 0.5-1.5% of head and neck masses. Calcification of the PPS mass a rare phenomenon and although it has been reported in polymorphic adenoma which is the most common parapharyngeal neoplasm, is not specific for polymorphic adenoma. In this report I am presenting a case of heavily calcified parapharyngeal mesenchymal chondrosarcoma with unusual presentation.
Materials and Methods
The patient is a 30-year old man with history of gout who presented with sudden onset nausea and vomiting with subsequent syncope. After waking up, He felt paresthesias and numbness around right jaw which improved in 15 minutes. MRI was order by his PCP that showed a mass arising from the parapharyngeal or carotid space in the right neck. CT angiogram was performed for surgical planning. The CTA showed a 4.4 x 2.4 x 5.3 cm heterogeneously and heavily calcified parapharengeal mass which abuts and partially encases the distal cervical right internal carotid artery without mass effect on the vessel itself. There was no appreciable enhancement. Because of unusual presentation, the patient was reviewed at tumor board and was decided to be likely a salivary gland tumor, most likely pleomorphic adenoma (based on one case report about calcified parapharengel polymorphic adenoma). The patient underwent selective neck dissection at right level II, parotidectomy with facial nerve dissection and transcervical approach and removal of parapharyngeal space mass. On pathology evaluation, the tumor consists of two elements: an Ewing sarcoma-like proliferation of small round blue cells with a striking "staghorn"/"hemangiopericytoma"-like vascular pattern that transitions either abruptly or gradually to mature chondromatous elements with varying degrees of calcification/ossification. Immunohistochemical stains for CD99, Fli-1, ERG, Desmin, Sox10, STAT6* and D2-40 were performed. The lesional cells are immunoreactive for D2-40, a marker that was described to be positive in chondroid lesions while being negative for all other markers, basically ruling out the possibility of unusual variants of either Ewing sarcoma, Solitary Fibrous Tumor, peripheral nerve sheath tumor or a myogenic tumor. The morphologic and immunohistochemical features were consistent with Mesenchymal Chondrosarcoma (MCS).
Results
CTA showed a 4.4 x 2.4 x 5.3 cm heterogeneously and densely calcified mass in the right para pharyngeal space with encasement of right internal carotid artery without mass effect on the vessel itself. There was no appreciable enhancement. There was mass effect on the right oropharynx. There was no lymphadenopathy.
Conclusions
The parapharyngeal space (PPS) is a fat containing space of the suprahyoid neck, lateral to the pharynx. The PPS is divided to prestyloid and poststyloid compartments by the styloid process. The prestyloid space contains the deep parotid lobe and minor salivary glands. The poststyloid space contains the IX, X, XI and XII cranial nerves, the cervical sympathetic chain, the internal jugular vein, the internal carotid artery and lymph nodes. Neoplasms of the PPS are not common, 0.5–1.5% of all head and neck tumours with 80% being benign. The most common neoplasm in prestyloid space originate from the salivary glands with the polymorphic adenoma being the most common one. The most common neoplasm of the poststyloid space are neurogenic tumours. Other less common PPS tumors include Adenocarcinoma NOS, Acinic cell carcinoma, Myoepithilial carcinoma, Paraganglioma ,Rhabdomyoma /rhabdomyosarcoma, Branchial cyst and metastasis. The most common presentation of PPS tumors are neck mass, intraoral mass and dysphagia. Chondrosarcomas (MCS) are rare mesenchymal tumors. They

include 10–20% of all malignant bone tumors. Mesenchymal chondrosarcoma is a rare tumor . It includes 3% to 10% of all chondrosarcoma and 0.2% to 0.7% of all bone tumors. Histologically, MCS has a typical biphasic pattern of small cells and islands of atypical cartilage. The MCS are differ from the classical chondrosarcomas by higher prevalence in females and more aggressive behavior with less survival rate. The MCS often originate from bones but 22% to 50% of them originate from soft tissues especially the brain and the meninges with high rate of metastasis to the lungs, lymph nodes, and other bones. The MCS originating from the PPS is a very rare tumor and so far very few similar cases have been reported. The clinical presentation of this case was unusual as well since the patient was presented by nausea and syncope likely because of right ICA compression.

2391

Patient Selection for Thrombectomy based on CT perfusion Derived Ischemic Core Volumes: A Retrospective Study

A Callen[1], K Lewis[1], J Talbott[1], R Cheng[2], V Singh[1], J Narvid[1]
[1]UCSF, San Francisco, CA, [2]Rutgers Robert Wood Johnson Medical School, New Brunswick, NJ

Purpose
Various patient selection criteria for thrombectomy in large vessel occlusion stroke have been utilized to predict favorable outcomes. Specifically, ideal perfusion eligibility strata on the basis of size of ischemic core volumes is not established. The purpose of this study was to evaluate the capacity of various CT perfusion based-selection models to predict favorable clinical outcomes (90-day modified Rankin Scale).
Materials and Methods
Review was conducted of a prospectively acquired database of consecutive patients from two community based hospitals under the purview of a single academic institution with large vessel anterior circulation stroke and underwent thrombectomy from January 2016 through August 2017. Patients were retrospectively assessed for thrombectomy eligibility based on CT perfusion derived ischemic core volumes. Post processing was performed using either Syngo Volume Perfusion CT (Siemens Healthcare, Erlangen, Germany), where ischemic core is defined as CBV <1.2 ml/100 mL, or RAPID (iSchemaView Inc, Menlo Park, CA), which uses a delay-insensitive algorithm, with ischemic core defined as relative CBF <30% of that in normal tissue. The ischemic core volume selection paradigms of the DEFUSE-3 trial (greater than or less than 70 cc), DAWN trial (<21, <31, and <51 cc) and an unique schema (<20, <40, <60, <80 cc) were compared. Outcome measures were inclusion rates for each selection paradigm and the 90-day modified Rankin Scale (mRS). Nonparametric test of trend (Spearman's rank correlation coefficient) and multivariate analysis was used to evaluate for differences in mean 90 day mRS between groups. All statistical analysis was performed with Stata version 14.2.427.
Results
We identified 63 patients who met criteria for the study. A total of 55 studies were post-processed using RAPID and eight studies were post-processed using Syngo Volume Perfusion CT. Patient inclusion was highest based on DEFUSE-3 core volume criteria (90%) and DAWN criteria (57%). A statistically significant difference in mean 90 day mRS was seen in the DEFUSE-3 inclusion group (2.8 vs. 5.0, p = 0.033). No differences in mean 90 day mRS were observed between DAWN subgroups or the exploratory schema. Ischemic core volume as a continuous variable did not correlate with 90 day mRS. The presentation NIHSS also did not correlate with 90-day mRS. In multivariate analysis, only DEFUSE-3 inclusion criteria demonstrated a statistically significant association with 90-day mRS (Coef: 3.53, p= 0.027).
Conclusions
DEFUSE-3 criteria performs better than DAWN criteria for the prediction of favorable 90-day mRS. In addition, selection using DAWN criteria appears to disqualify more patients without demonstrable differences in 90-day mRS.

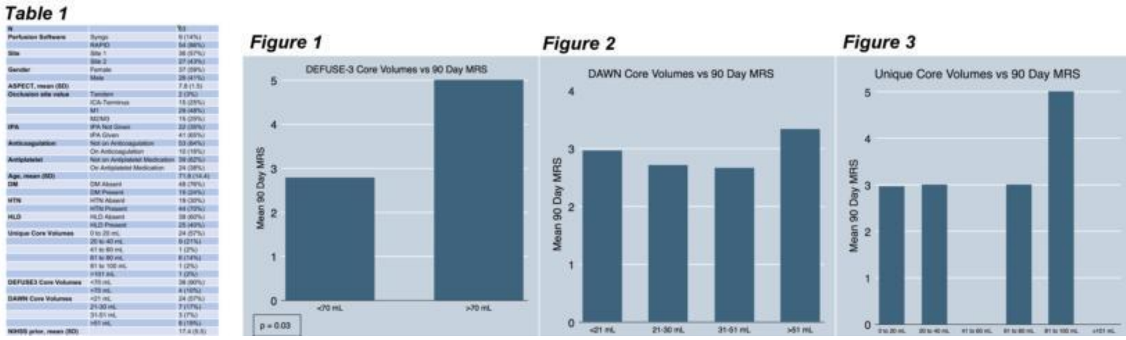

(Filename: TCT_2391_updatedgraphicfile.jpg)

2235

Quantitative Diffusion Tensor Imaging and Ventricular/Sulcal CSF Volumetry: A Marker to Diagnose the Normal Pressure Hydrocephalus.

A Kamali[1], P Rabiei[2], K Younes[3], R Riascos[2], R Patel[2], K Hasan[4]
[1]UT HEALTH, HOUSTON, TX, [2]The University of Texas Health Science Center at Houston, Houston, TX, [3]University of California San Francisco, San Francisco, CA, [4]UTHSC-Houston, Houston, TX

Purpose
The iNPH is one of the most common treatable causes of dementia in the elderly. iNPH is a form of chronic communicating hydrocephalus that results in a treatable syndrome characterized by the triad of gait impairment, progressive dementia, and urinary incontinence. The diagnosis of iNPH requires performing invasive procedures in rather elderly patients with multiple comorbidities. To date, there is no sensitive, non-invasive test that could help in screening, diagnosis and prognostication of the outcomes of iNPH. In patients with iNPH, shearing forces are exerted on the periventricular white matter as the ventricles enlarge. As the superior thalamic radiation (STR) runs most closely to the lateral ventricles, these tracts would most likely be affected by the tangential shearing forces. This study investigates the Diffusion Tensor Imaging (DTI) metrics of the STR for the first time in patients with iNPH. Decreased sulcal CSF volume especially at the top of the brain is a characteristic finding in MRI in patients with iNPH, due to crowding of gyri at the vertex. Investigation of the trends of ventricular and sulcal volumes in iNPH patients compared to healthy controls is also planned in this study. Our preliminary data support significant differences in diffusion tensor metric values of STR as well as the sulcal/ventricular CSF volume, in iNPH compared to normal controls.
Materials and Methods
15 patients with diagnosis of iNPH and 15 age/sex matched healthy controls were selected. MRI scan of the brain including DTI sequences was performed in both groups. MRI Technique: 3D-MPRAGE sequence with a slice thickness of 1.5 mm was utilized for image registration and volumetric analysis of evaluated brain structures outlined in this proposal. Additional sequences include a 1 mm slice thickness sagittal FLAIR, axial T2-weighted, axial double inversion recovery (DIR) and T1-weighted phased-sensitive inversion recovery (PSIR) sequences, each with 0.94 mm × 0.94 mm in-plane resolution (256 × 256 matrix and 24 cm FOV). Whole brain diffusion-weighted data was acquired using a single-shot spin-echo diffusion-sensitized echo-planar imaging sequence with balanced alternating polarity Icosa21 tensor encoding scheme at different b-factors = 100, 500, 1500, 3000. s mm-2, TR/TE = 12000/75 msec; isotropic voxel = 2mm. Finally, dedicated imaging was performed using a 1.5 mm slice thickness 3D axial fast spin echo (FSE) SPIR sequence with 128 x 128 matric and 10 cm FOV. Ventricular CSF Volumes (vCSFV) and the sulcal CSF volumes (sCSFV) were parcellated using the fully automated online MRI-cloud software packet for both the iNPH patients and healthy control data. DTI Studio software (http://cmrm.med.jhmi.edu/) was used for measurement of the DTI metric values including the

fractional anisotropy (FA), mean diffusivity (MD), axial diffusivity (AD), radial diffusivity (RD) of the STR tract in iNPH and healthy controls.

Results

Our results demonstrated that the ratio of the ventricular/Sulcal CSF volumetry is significantly higher in iNPH patients than in age/sex matched healthy controls (p value = 0.010). The mean diffusivity values of the superior thalamic radiations (STR) in iNPH patients were also significantly higher than in normal aging healthy brain controls (p value = 0.046).

Conclusions

Our results demonstrated that using quantitative diffusion tensor metric values of the superior thalamic radiation along with the ventricular/sulcal CSF volumetric values, its feasible to diagnose and differentiate the patients with iNPH from age/sex matched healthy controls.

	Mean vCSFVp and SD	Mean sCSFVp and SD	vCSF/sCSF	Mean Sylvian CSFVp and SD	Mean sCSFV minus Sylvian CSF and SD
iNPH	0.078 (0.023)	0.073 (.012)	1.07	0.014 (0.004)	0.059 (0.01)
Healthy Control Elderly (HC)	0.01 (0.004)	0.058 (.0105)	0.20	0.008 (0.0017)	0.05 (0.01)

Table 1. Ventricular/sulcal CSF ratio in healthy controls and iNPH patients. Higher sulcal CSF/ventricular CSF ratio is seen in iNPH patients compared to normal controls. CSF: Cerebrospinal Fluid. vCSFVp: ventricular cerebrospinal fluid volume percentage adjusted to intracranial volume, sCSFVp: sulcal cerebrospinal fluid volume percentage adjusted to intracranial volume, SD: Standard deviation.

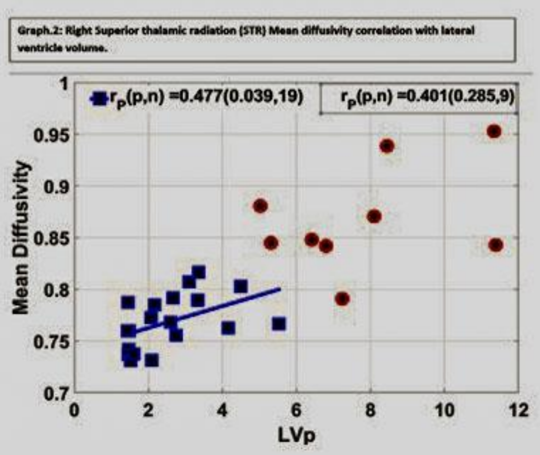

Graph 1. Superior thalamic radiation (STR) mean diffusivity correlation with lateral ventricular volume in iNPH patients compared to healthy controls.

(Filename: TCT_2235_tableandgraph_edited.jpg)

3024

Radiation Dose in CT Fluoroscopy-Guided Cervical Nerve Root Injections

N Asmar[1], N Ahmed[1], T Matys[1]
[1]*University of Cambridge, Cambridge, UK*

Purpose

Selective cervical nerve root injections (CNRIs) are used to confirm the level of foraminal nerve root compression prior to spinal surgery, and to provide relief from radicular symptoms. In our institution the procedure is performed under CT fluoroscopy (CTF) using modified indirect technique with the needle introduced from a posterolateral approach to the anterior border of the ipsilateral facet joint (Figure 1). While the advantages of CTF compared to standard fluoroscopy are well recognized, concerns have been raised in the past about associated radiation exposure. However, there is almost no data on the radiation dose incurred during CNRIs. In this study, we evaluate the effective dose associated with CNRIs using standard and reduced scanning parameters.

Materials and Methods

We compared effective dose (ED) in 35 injections performed using standard tube voltage and current (planning scan: 120 kV and automatic current up to 802 mAs, CTF: 100-120kV and 80 mAs) and 148 injections after we defaulted to reduced parameters (planning scan: 80 kV and 80 mAs, CTF: 70-80 kV and 40-50 mAs). ED was calculated from dose-length product (DLP) using conversion factor of 0.0057 mSv/mGycm (BJR 2016; 89: 20150346).

Results

With standard parameters the total ED (from planning scan and CTF) averaged 1.27 mSv (range 0.64-7.47 mSv), and 64% of the total dose resulted from CTF component. Low dose protocol allowed 91% reduction of ED which averaged 0.11 mSv (range 0.05-0.64 mSv) with 47% of radiation attributable to CTF. In only 9 cases (6%) it was necessary to revert to standard parameters for CTF due to unsatisfactory image quality.

Conclusions

Using reduced CT voltage and current it is possible to achieve successful CNRI in the majority of patients with average ED comparable to a single chest radiograph.

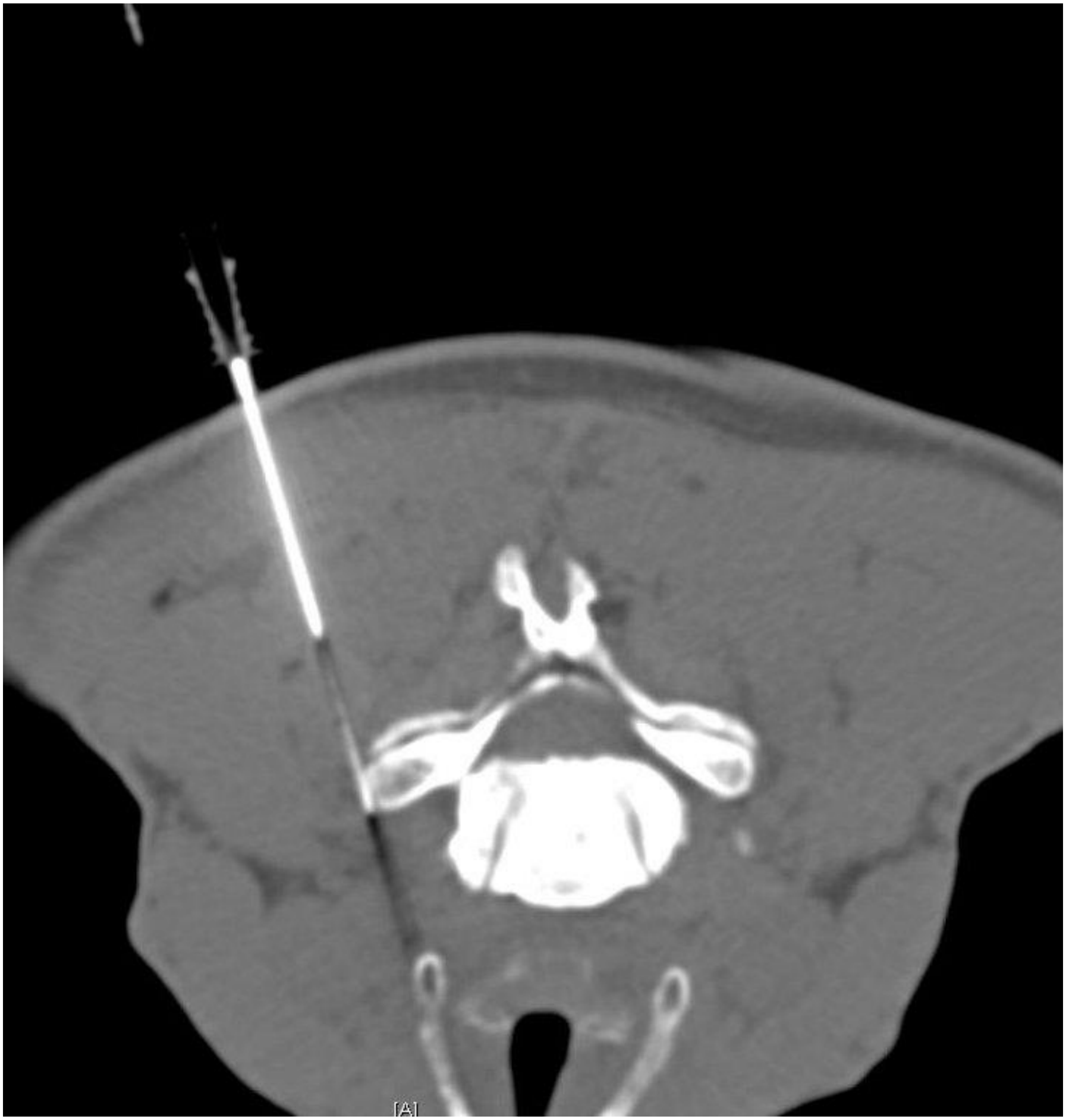

(Filename: TCT_3024_NRI.jpg)

2256

Revealing the Anatomical Connectivity of the Thalamo-limbic Connections of the Human Limbic System

A Kamali[1], S Choi[2], K Meissner[2], N Doyle[3], P Rabiei[4], R Patel[4], R Riascos[4]
[1]UT HEALTH, HOUSTON, TX, [2]University of Texas Houston Medical School, Houston, TX, [3]University of Texas Medical School at Houston, Houston, TX, [4]The University of Texas Health Science Center at Houston, Houston, TX

Purpose

Although, the thalamus is not primarily considered a limbic structure, it has central role in many limbic connections in the human limbic system. Lack of adequate neuroimaging sensitivity and spatial resolution, so far, impeded depiction of the major thalamo-limbic pathways in the human brain. The purpose of the current study is to demonstrate the feasibility of demonstration of the major thalamolimbic connectivity in the human limbic system using a high spatial resolution DTI data on 3T.

Materials and Methods

Study Subjects This work was approved by our institutional review board (IRB) and was health insurance portability and accountability act (HIPAA) compliant. Fiftheen right-handed healthy adults (age range 24-37 years) were included in this study and written informed consent was obtained from all the subjects. Conventional MRI Data Acquisition All MRI studies were performed on a 3T Philips Intera scanner with a dual quasar gradient system with a maximum gradient amplitude of 80 mT/m, maximum slew rate 200 mT/ms/m, and an eight channel SENSE-compatible head coil (Philips Medical Systems, Best, Netherlands). The conventional MRI (cMRI) protocol included axially prescribed 3D spoiled gradient (repetition time /echo time/ flip angle = TR/TE/a = 8 ms / 4ms / 6o), 3-D proton density-weighted (TR/TE/a = 10,000 ms / 10 ms / 90o and 3-D T2-weighted (TR/TE/a = 10,000 ms / 60 ms / 90o), with a square field-of-view (FOV) = 256 mm x 256 mm and a matrix of 256x256 pixels. The slice thickness for the cMRI sequences was 1.0 mm with 120 contiguous axial slices covering the entire brain (foramen magnum to vertex). The number of b-factor ~ 0 (b0) magnitude image averages was four. The total DTI acquisition time was ~ seven minutes for the diffusion-weighted acquisition. The DTI acquisition was repeated three times to enhance signal-to-noise ratio (SNR). The selection of the b-factor, parallel imaging, repetition and echo times enabled entire brain coverage using single-shot and interleaved EPI. Tractography of the major thalamo-limbic pathways was performed using DTI Studio software from John's Hopkins University.

Results

We demonstrate major connectivity of the thalamus with the hypothalamic nuclei and amygdala via the amygdalothalamic tract, mammillothalamic tract and thalamo-hypothalamic tract for the first time in the human brain.

Conclusions

We demonstrate the tractography of the amygdalothalamic tract, mammillothalamic tract and thalamo-hypothalamic tract for the first time in the human brain.

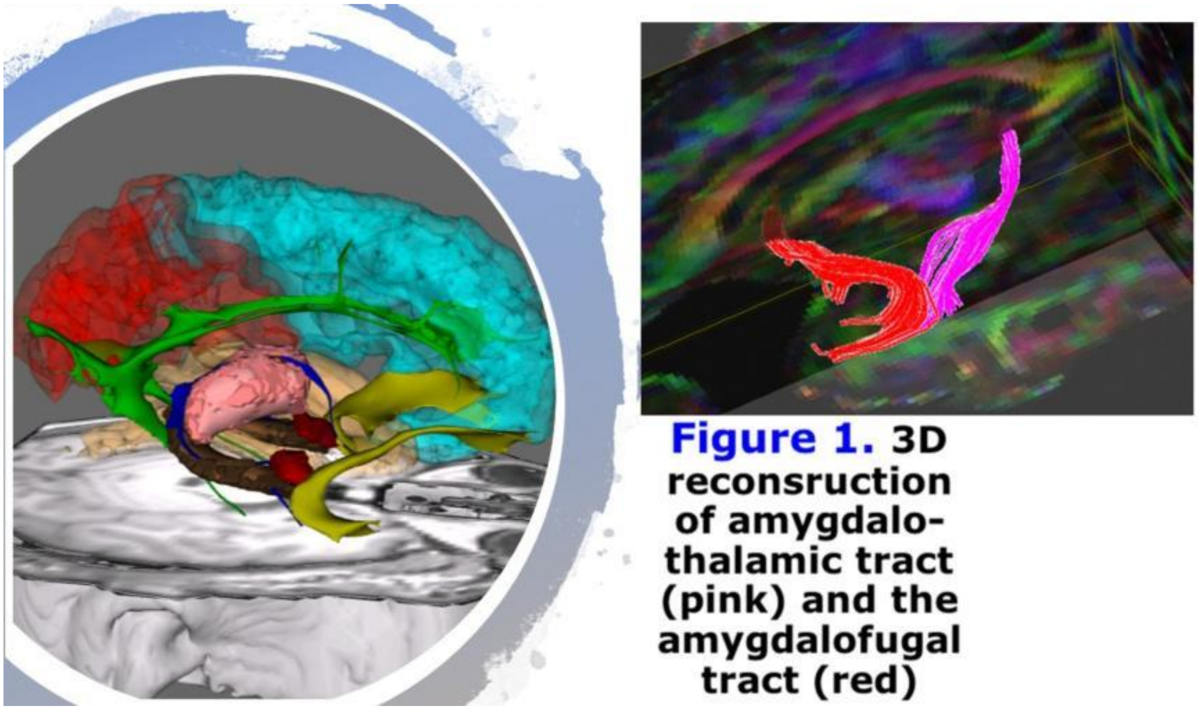

Figure 1. **3D reconsruction of amygdalo-thalamic tract (pink) and the amygdalofugal tract (red)**

(Filename: TCT_2256_Thalamo-limbic.jpg)

3136

Risk Assessment of Osteoradionecrosis by Periodontitis Using 18F-FDG PET/CT Imaging

K Ito[1], K Takumi[2], S Meibom[3], M Qureshi[4], M Truong[4], A Salama[5], O Sakai[3]
[1]Boston University School of Medicine, Boston, MA and Nihon University School of Dentistry at Matsudo, Chiba, Japan, [2]Boston Medical Center, Boston University School of Medicine, Boston, MA and Kagoshima University, Kagoshima, Japan, [3]Department of Radiology, Boston Medical Center, Boston University School of Medicine, Boston, MA, [4]Department of Radiation Oncology, Boston Medical Center, Boston University School of Medicine, Boston, MA, [5]Boston Medical Center, Boston University School of Dental Medicine, Boston, MA

Purpose
The purpose of this study was to evaluate whether assessment of periodontitis using pre-radiotherapy FDG-PET/CT can help predict osteoradionecrosis (ORN) in patients with head and neck squamous cell carcinoma (HNSCC) undergoing radiotherapy (RT).
Materials and Methods
Nineteen HNSCC patients who developed ORN between October 2007 and June 2016 were identified (17 men, 2 women; age mean, 60.0, range 44-82). Thirty-four HNSCC patients who underwent RT without ORN were identified as controls (29 men, 5 women; age, 60.1, range 46-74). Diagnosis of ORN was made clinically based on presence of exposed mandibular bone secondary to necrosis following RT not related to progression of disease with failure to heal after a period of 3 months. All patients underwent FDG-PET/CT before radiotherapy. The SUVmax of periodontal regions identified on CT was measured for all patients and periodontitis was classified by American Academy of Periodontology staging system using CT. The SUVmax and CT staging of periodontitis were compared between patients with and without ORN using the Mann-Whitney U test. Results are presented as mean ± standard deviation. Receiver-operating characteristic (ROC) curve analysis was performed to assess the ability of SUVmax

and periodontitis staging to predict ORN and area under the curve (AUC) was calculated. A P-value <0.05 was considered to indicate statistical significance.
Results
SUVmax of the periodontal region of patients with ORN was significantly higher (3.71±1.6) than that of patients without ORN (2.74±1.5), p=0.01. CT periodontitis staging of patients with ORN was significantly higher (2.56±0.63) than that of patients without ORN (1.96±0.84), p=0.02. SUVmax at the cut-off value of 2.8 and periodontitis staging at the cut-off value of 2 had AUC of 0.72 and 0.69, and accuracy of 68.0% and 65.1%, respectively. 75% (3/4) of edentulous patients who developed ORN had high SUVmax (>2.8) with high specificity (100%).
Conclusions
SUVmax of the periodontal region and CT staging of periodontitis in patients with ORN were significantly higher than those of patients without ORN. In the subset of edentulous patients FDG-PET imaging with an SUV max over 2.8 was highly specific for ORN, where CT evidence of periodontal disease was lacking. Pretreatment PET/CT may help identify high risk patents for ORN.

2714

RSI Imaging of a Head and Neck Tumor

M Baris[1], P Quarterman[2], J Shin[3], M Fung[3], S Jambawalikar[1], G Moonis[1]
[1]Columbia University Medical Center, New York, NY, [2]GE Healthcare, Brooklyn, NY, [3]GE Healthcare, New York, NY

Purpose
Restriction Spectrum Imaging (RSI) is a new diffusion weighted imaging (DWI) MRI technique in that enhances the ability to differentiate aggressive cancer from low-grade or benign tumors and guides treatment and biopsy. RSI method has shown improved delineation of tumor and reduced sensitivity to edema and necrosis compared with DWI and ADC image contrast. Its contribution to imaging of brain and prostate tumors has been previously published. However, there is no prior experience using RSI sequence in head and neck tumors due to anticipated problems with susceptibility and shimming as well as patient motion. The purpose of this report is to evaluate the feasibility of doing RSI imaging in head and neck cancer.
Materials and Methods
A 51 years old, male patient with recently diagnosed laryngeal cancer was admitted with worsening of the symptoms. Routine Neck MR imaging with contrast and additional RSI sequence (with 0, 500, 1500, 4000 s/mm2 b values and 29 directions including one b=0 image with reverse polarity gradient for distortion correction) was performed for better evaluation of the tumor before treatment plan. RSI cellularity map was produced and evaluated.
Results
MR imaging revealed a large left transglottic cancer with involvement of the cricoid cartilage and no metastatic lymph nodes. However, increased signal intensity of the tumor and its extralaryngeal component could be seen on RSI cellularity map better than the corresponding ADC map (Figure 1).
Conclusions
RSI is a promising tool which has shown greater sensitivity and specificity to tumor cellularity in the presence of edema compared with DWI and ADC image in brain tumors and prostate cancer. This is the first case of RSI imaging in head and neck cancer. It is feasible to perform this sequence in the neck. There are some limitations to the technique due to anatomical considerations. RSI images show wraparound artifact of the subcutaneous fat and low signal to noise ratio. To improve image quality we propose increasing the number of excitations (NEX) and placement of fat suppression band on the posterior subcutaneous fat area. Also, suitable shimming and smaller scanning area coverage should be considered. We will make these changes in future imaging studies.

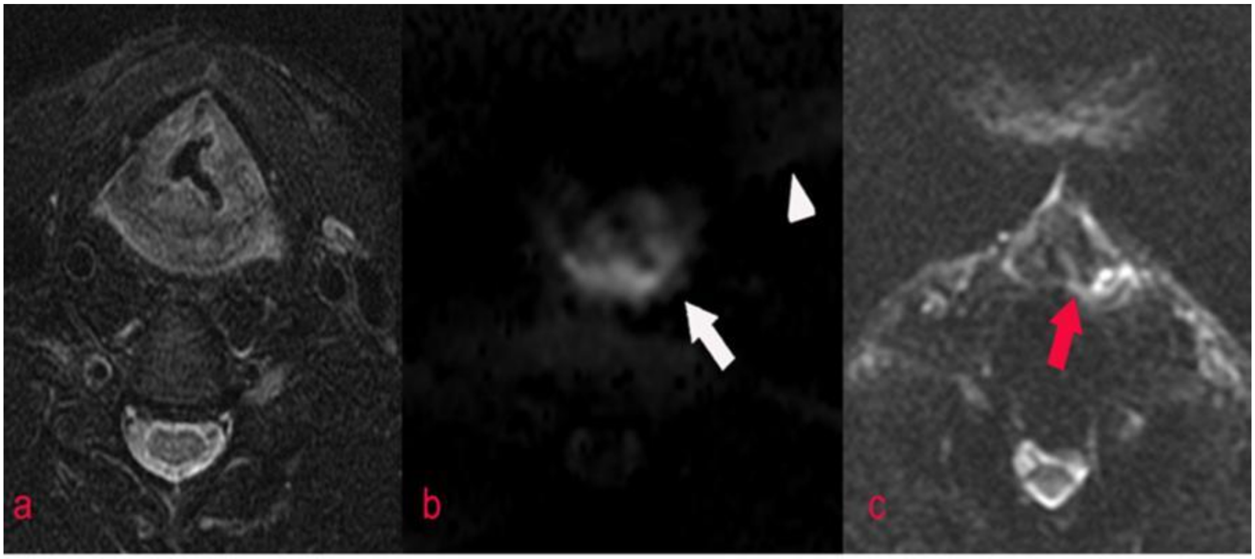

Figure 1 : a. Axial T2 weighted image (left) shows a large supraglottic mass. b. On RSI cellularity map at the same level, the tumor and its extra laryngeal component can be seen as increased signal (arrow). Also wraparound artifact can noticed (arrow head). c. On the corresponding ADC map the lesion is not as well visualized as on the RSI image.

(Filename: TCT_2714_Figure1.jpg)

3264

Significant Dose Reduction While Preserving Diagnostic Quality: Advancing the Application of Iterative Reconstruction Using a Live Animal Model

F Raslau[1], E Escott[2], H Ganesh[1], D Feigal[1], C Adams[1], J Zhang[1]
[1]University of Kentucky, Lexington, KY, [2]UNIVERSITY OF KENTUCKY, LEXINGTON, KY

Purpose
Although iterative reconstruction can reduce radiation dose, its full implementation has not yet been reached due to limited understanding of the relationship between radiation dose and image quality. Our goal is to achieve significant dose reduction without compromising image quality. But this objective cannot be met with phantoms and mathematical models alone. We present an in-vivo study using a live animal model both assessed visually by neuroradiologists for diagnostic quality as well as by quantitative analysis. We demonstrate a dose-image relationship that will advance clinical applications for significant dose reduction in patients.
Materials and Methods
A live sheep was scanned under anesthesia using Definition Force CT scanner at different exposures (120 kV, ranging 82-982 effective mAs). Images of the sheep brain were reconstructed with Filtered Back Projection (FBP) and Advanced Modeled Iterative Reconstruction (ADMIRE) at different strengths (levels 1-5). With FBP as the reference image, various combinations of exposure and reconstruction technique were visually rated by two neuroradiologists. Diagnostic quality consisted of two scores on a 4-point scale, for gray-white distinction and for image texture. Quantitative analysis for signal-to-noise (SNR) and contrast-to-noise (CNR) was also performed across all exposure-technique combinations.
Results
Gray-white distinction is compromised at lower radiation exposure as expected, but image quality recovers at higher ADMIRE strength. Image texture acquires excessive smoothness with higher ADMIRE

strength, but image quality recovers at lower radiation exposure. According to neuroradiologists' visual rating, the same diagnostic quality (gray-white distinction and texture) as the reference image is achieved with ADMIRE-5 at 58% dose reduction. Objective analysis shows that the same CNR is achieved with 67% dose reduction.

Conclusions

Both qualitative and quantitative results show that diagnostic quality (gray-white distinction and texture) can be preserved with approximately 60% dose reduction. These results can serve as a guide for translating the advanced implementation of iterative reconstruction to the clinical practice.

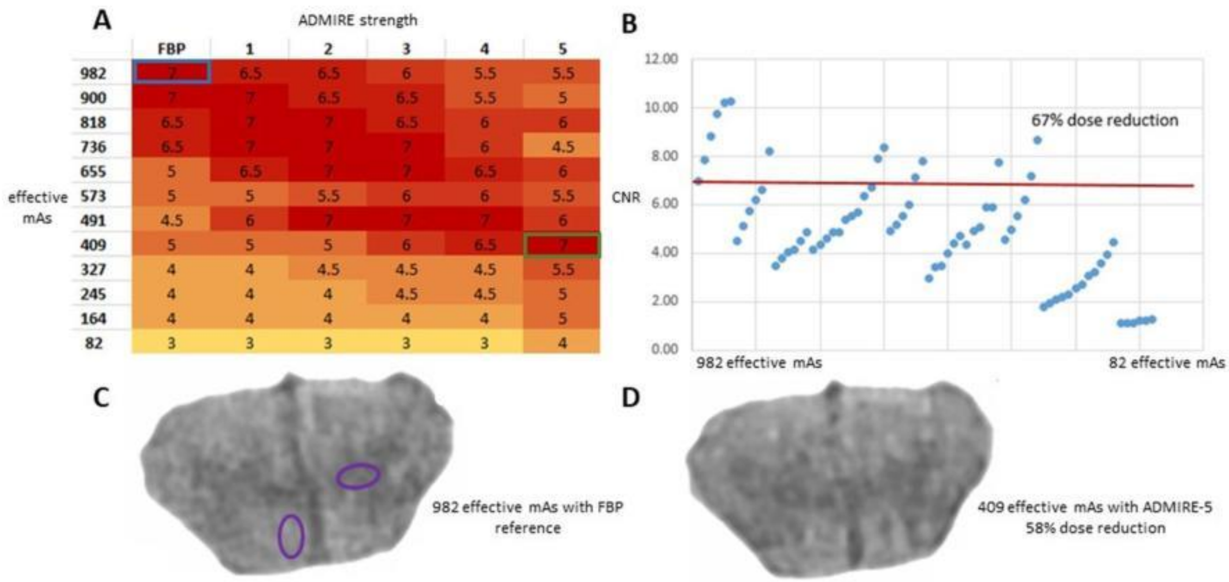

Figure. A) Heat map of diagnostic quality as rated by neuroradiologists, combining scores for gray-white differentiation and texture. Combination of 409 effective mAs with ADMIRE-5 (green outline) yields comparable quality to reference image at 982 effective mAs with FBP (blue outline). B) Plot of CNR for all FBP and ADMIRE strengths 1-5, from highest to lowest radiation exposures. Red line demarcates CNR of reference image, showing that high iterative strength can achieve same CNR with 67% dose reduction. C) Coronal CT image of live sheep brain at reference settings 982 effective mAs with FBP. Regions-of-interest are marked for CNR analysis. D) CT image at 409 effective mAs with ADMIRE-5, achieved with 58% dose reduction.

(Filename: TCT_3264_figure.jpg)

3285

Susceptibility-Weighted Imaging (SWI): Preoperative Grading of Gliomas and its Correlation with Perfusion and Molecular Biomarkers

A Hilario[1], E Salvador[1], P Martin[1], L Koren[2], J Sepulveda[1], A Hernandez-Lain[3], A Perez-Nuñez[1], A Lagares[1], A Ramos[4]
[1]Hospital 12 de Octubre, Madrid, Spain, [2]Hospital 12 de Octubre, madrid, spain, [3]Hospital 12 de Octubre, Madrid, WY, [4]Hospital 12 de Octubre, Madrid, Madrid, Spain

Purpose

Prognosis and treatment strategy of diffuse gliomas depends upon the WHO tumor grade. SWI is a technique that complements structural imaging allowing better visualization of blood and microvessels

without contrast agents. Our objectives in a group of diffuse gliomas were: 1) to assess the role of SWI in the preoperative grading and 2) to correlate SWI with DSC and DCE perfusion MRI-derived parameters.
Materials and Methods
We enrolled 43 histologically confirmed diffuse gliomas (WHO 2017 classification). SWI was performed in addition to conventional MR sequences, DSC and DCE perfusion imaging. Intratumoral susceptibility signal intensity (ITSS) was classified on the basis of morphology (dots, linear structures or mixed) and grade (grade 0 = no ITSS; grade I =1-5 dotlike or fine linear ITSS; grade II = 6-10 and grade III >11). Parametric maps of DSC and DCE perfusion parameters were calculated using Olea Sphere software. Univariate analysis was performed with Xi square test.
Results
Degree of ITSS of grade III gliomas was lower than in grade IV tumors ($p<0.05$). Regarding ITSS, anaplastic gliomas show more frequently (66.7%) a grade O and glioblastomas a grade III (67.6%). Contrast enhancement was also related to ITSS. 80% of non-enhancing tumors show a grade O and 68.6% of enhancing tumors show a grade III. We have demonstrated a relationship between ITSS and permeability parameters. Parameters significantly related to ITSS were rCBV, Ktrans, Vp and Ve. ITSS were no statistically different in high-grade gliomas classified according to ATRX status. When demonstrated differences in patterns of ITSS on the basis of IDH status. IDH non-mutated tumors show more frequently (68.8%) an ITSS grade III. On the other hand, 62.5% of IDH-mutated gliomas show a grade O. Grading gliomas preoperatively, the combination of SWI and perfusion MRI resulted in higher sensitivity and specificity.
Conclusions
ITSS morphology and grade was useful for preoperative assessing of the WHO tumor grade. IDH mutated and non-mutated tumors were different on SWI. Combination of SWI and PWI improves diagnostic accuracy of glioma grading.

3021

Synthetic MR Imaging for the Visualization of the Corticospinal Tract

M Azuma[1], Z Khant[1], T Hirai[2]
[1]*Miyazaki University, Miyazaki, Miyazaki,* [2]*UNIVERSITY OF MIYAZAKI, MIYAZAKI, MIYAZAKI*

Purpose
Hyperintense foci in the posterior internal capsule on T2-weighted MR images represent the fibers of the corticospinal tract (CST). However, its identification can be sometimes difficult. We investigated whether synthetic- yield better visualization of the CST than conventional MR images.
Materials and Methods
Our prospective study included 10 healthy volunteers (5 men, 5 women; age range 24 - 31 years, mean 26.9 years). They underwent conventional- and synthetic MRI studies on a 3T scanner. We produced synthetic T1-, T2- and proton density (PD)-weighted-, FLAIR-, and double-inversion recovery images and produced T1-, T2-, PD-, and myelin maps after quantification of the T1 and T2 values and of the proton density. Conventional T1-, T2- and PD-weighted-, and FLAIR images were also obtained. All images were performed with a 3-mm slice thickness. Two neuroradiologists independently graded the visibility of the CST in the posterior internal capsule on all MR images by using a 4-point scale. The CST-to-thalamus contrast-to-noise ratio (CNR) on conventional- and synthetic MR images was calculated and compared. Qualitative and quantitative results were assessed with the Kruskal-Wallis test, ANOVA and the Scheffe test.
Results
Among 13 images, synthetic T2 maps yielded the best visibility of the CST. It was significantly better on synthetic T2 maps than on conventional T1-, T2-, and PD-weighted-, and FLAIR images ($p<0.05$). The

CST-to-thalamus CNR was significantly higher on synthetic T2 maps than on conventional T1-, T2- and PD-weighted images ($p<0.05$). Visibility of the CST was lowest on conventional PD-weighted images.
Conclusions
Synthetic MR imaging, especially T2 maps, yielded better visualization of the CST than conventional MR images.

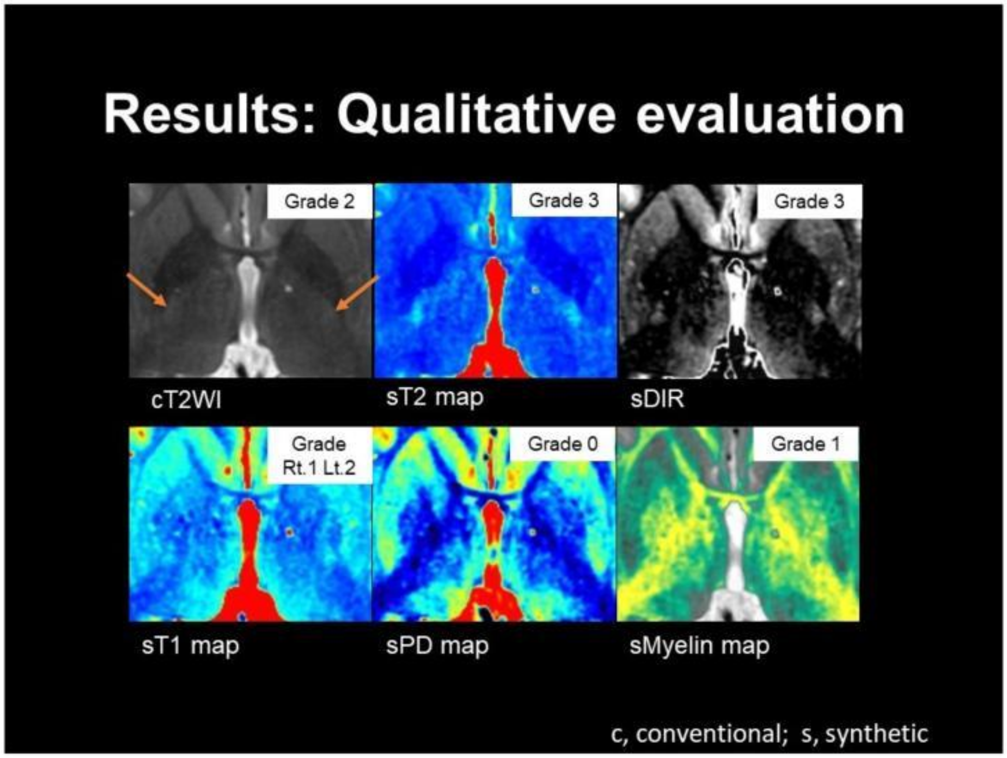

(Filename: TCT_3021_CSTASNR2.jpg)

3026

Synthetic MR Imaging for Visualization of the Mamillothalamic Tract

M Azuma[1], Z Khant[1], T Hirai[2]
[1]Miyazaki University, Miyazaki, Miyazaki, [2]UNIVERSITY OF MIYAZAKI, MIYAZAKI, MIYAZAKI

Purpose
The purpose of this study was to determine whether synthetic- yield better visualization of the mamillothalamic tract (MTT) than conventional MR images.
Materials and Methods
Our prospective study included 10 healthy volunteers (5 men, 5 women; age range 24 - 31 years, mean 26.9 years). They underwent conventional- and synthetic MRI studies on a 3T scanner. We produced synthetic T1-, T2- and proton density (PD)-weighted (T1WI, T2WI and PDWI)-, FLAIR-, and double-inversion recovery images and produced T1-, T2-, PD-, and myelin maps after quantification of the T1 and T2 values and of the proton density. Conventional T1WI, T2WI, PDWI, and FLAIR images were also

obtained. All images were performed with a 3-mm slice thickness. Two radiologists independently graded the visibility of the MMT at the level of the anterior and posterior commissure on all MR images by using a 4-point scale. Semiqualitative results were assessed with the Kruskal-Wallis test and the Scheffe test.
Results
Among 13 images, synthetic myelin maps yielded the best visibility of the MTT. It was significantly better on synthetic myelin maps than on conventional T1WI, T2WI, PDWI, and FLAIR ($p<0.05$).
Visibility of the MTT was similar between synthetic PD maps and PDWI. It was lowest on conventional T1WI.
Conclusions
Synthetic MR imaging, especially myelin maps, yielded better visualization of the MTT than conventional MR images.

3225

T1/T2 Matching In the Assessment of Treatment Response Post Stereotactic Radiosurgery

J Murphy[1], M Bowen[1], G Heyes[1], S Ramalingam[1]
[1]*University Hospitals Birmingham NHS Foundation Trust, Birmingham, West Midlands*

Purpose
Differentiation between tumor progression and radiation necrosis (RN) within brain metastases following treatment with stereotactic radiosurgery (SRS) often poses a clinical and diagnostic challenge. Many studies have evaluated the use of advanced imaging techniques in the differentiation between tumor progression and RN. We sought to identify parameters which could predict a good response to treatment and to evaluate the use of T1/T2 matching as an indicator of tumor progression.
Materials and Methods
Patients treated with SRS as a primary or adjunctive treatment for solitary or multiple brain metastases in our institution were identified. Pre and post SRS MRI studies were evaluated. Dimensions of the lesions on T2 and post contrast T1 weighted sequences were recorded and the rate of growth and T1/T2 matching were assessed. The presence of haemorrhage, surrounding vasogenic oedema and a T2 hyperintense rim on MRI were also recorded.
Results
One-hundred and thirteen patients were included in our database. Mean age was 53 years (range 41-75 years), with a mean follow-up period of 573.5 days. Mean tumor volume prior to SRS was 2.02 cm3, with a mean growth rate of 0.003 cm3/day. Preliminary results demonstrate 42% of patients demonstrated response to treatment. 8% had delayed resection of the index lesion and pathologically proven viable tumor at resection. Based on response to treatment, there was no significant difference in lesion volume pre and inital post SRS studies. In patients with poor response, there was a matched increase in tumor volume on T1 and T2 weighted sequences over sequential studies. T1/T2 mismatch was greatest in patients with radiation necrosis on the first post SRS MRI, and was persistent over sequential studies.
Conclusions
T1/T2 matching is a useful sign in the assessment of brain metastases post SRS. Where there is recurrent or residual tumor, matched increase in tumor volume on T1 and T2 weighted sequences is observed over sequential studies.

3195

The change of cerebral cortex in children with Tourette syndrome

L Kong[1], Y Liu[1]

[1]*Beijing Children's Hospital, Capital Medical University, National Center for Children's Health, Beijing, Beijing*

Purpose

To investigated microstructural changes of cortical thickness , cortical sulcus, cortical curvature, and LGI in TS children.

Materials and Methods

60 children with TS(age 8.79 ± 3.07 years, range 3–16 years; 11 female) and 52 age and gender matched health controls (age 10.82±3.36 years, range 3–16 years; 18 female)were scanned by 3.0T MR scanner with three-dimensional T1-weighted image (3DT1WI). We then extracted some surface-based features by using FreeSurfer and performed the statistical analysis between two groups.

Results

Surface analyses revealed altered cortical thickness, cortical sulcus, cortical curvature and LGI in TS compared to controls. The brain regions with significant differences in cortical thickness between TS patients and healthy subjects were postcentral， superiorparietal， rostralanteriorcingulate in left hemisphere and frontalpole, lateraloccipital, inferiortempora in right hemisphere(Figure 1).The cortical sulcus changed in superiortemporal, medialorbitofrontal, supramarginal， medialorbitofrontal, superiorparietal and lateraloccipital between TS and healthy subjects(Figure 2). The brain regions with significant differences in cortical curvature between TS patients and healthy subjects were caudalanteriorcingulate, supramarginal, inferiorparietal and lateraloccipital(Figure 3). The changes of LGI were most prominent in the inferortemporal and insula. Additionally,there was no statistical difference in brain surface area with controls(Figure 4).

Conclusions

Motor portions of CSTC circuits have long been postulated to be involved in the pathogenesis of Tourette syndrome[2]. Until now, the involvement of cortical portions of those circuits has not been widely suspected. In this study, We explain the structural correlates of the diversity of symptoms.Our study results prove that TS patients have abnormal changes in cortical structure. Combined with previous studies of basal ganglia[3,4] and thalamus[5] , we think that the nervous system develops rapidly in childhood, which may lead to the imperfect structure of CSTC circuit. Then the children show some tic. During adolescence, the physical growth and neurodevelopment of children is rapidly. The structure of CSTC circuit in some children may become perfect and the clinical symptoms will decrease. However, the structure of CSTC circuit in some children are still not perfect. The symptoms of this part of the TS children may continue into adulthood. Therefore, it is important to treat children before puberty.

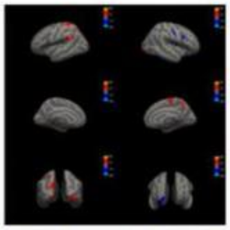

Figure 1. Dark gray areas on the inflated cortical surface represent the sulci while light gray areas represent gyri. The color scale bar is on a -log (p value). The clusters with warm colors indicate that the cortical thickness is thinner in TS patients than in the normal control group, and the clusters with cold colors show that TS patients have the thicker cortical thickness.

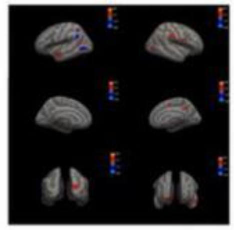

Figure 2. Dark gray areas on the inflated cortical surface represent the sulci while light gray areas represent gyri. The color scale bar is on a -log (p value). The clusters with warm colors indicate that the cortical sulcus is smaller in TS patients than in the normal control group, and the clusters with cold colors show that TS patients have the larger cortical sulcus.

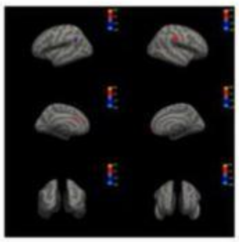

Figure 3. Dark gray areas on the inflated cortical surface represent the sulci while light gray areas represent gyri. The color scale bar is on a -log (p value). The clusters with warm colors indicate that the cortical curvature is smaller in TS patients than in the normal control group, and the clusters with cold colors show that TS patients have the larger cortical curvature.

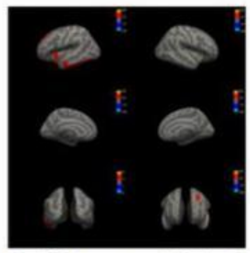

Figure 4. Dark gray areas on the inflated cortical surface represent the sulci while light gray areas represent gyri. The color scale bar is on a -log (p value). The clusters with warm colors indicate that the LGI is smaller in TS patients than in the normal control group, and the clusters with cold colors show that TS patients have the larger LGI values.

(Filename: TCT_3195_fig.jpg)

3475

The Clinical Significance of Large or Asymmetric Foramen of Vesalius

A Haboosheh[1], S Nabavizadeh[2]
[1]University of Pennsylvania, Philadelphia, PA, [2]UNIVERSITY OF PENNSYLVANIA HEALTH SYSTEM, WYNNEDWOOD, PA

Purpose
Foramen of Vesalius (FV) is a small, variable and frequently symmetrical structure located in the greater wing of the sphenoid bone, and anteromedial to the foramen ovale (FO). It transmits an emissary vein through which the cavernous sinus and pterygoid plexus communicate. Our aim was to study the morphological and morphometric variations of FV on CT angiography (CTA) of brain. There have been only few imaging studies evaluating this foramen. Some claim that an asymmetric FV is likely the result of a pathologic process than a normal variant. This is not consistent with our clinical experience and wanted to investigate the incidence of asymmetry with associated skull base pathologies.
Materials and Methods
We retrospectively studied one hundred consecutive CTA of the brain for variations in size, shape, presence or absence and any duplication of the FV, surface area, distance from FO, and any associated skull base pathology. After collecting data, statistical analysis was done
Results
FV was present in 56% of the total studies, 48% bilateral, 46% symmetric, and was assimilated in FO in 22% of the cases. There was no associated skull base pathology with asymmetry. There was no significant difference between the unilateral FV on the right or left sides of the skulls. Although based on our results left sided was slightly higher, which is consistent with other prior studies.
Conclusions
FV is an inconsistent foramen of sphenoid bone, but we found no association between the incidence of asymmetry or large FV with any skull base pathologies. The morphological and morphometric variations

of FV on CTA of the brain are important to the clinicians in diagnosis and management of various conditions where micro-neurosurgical and microvascular approach is a needed.

2160

The Co-Existence of the Matched Large Artery Stenosis (LAS) May Corroborate the Perfusion Deficit To Identify the Patients With High Risk Imminent Progress to Acute Ischemic Stroke After Transient Ischemic Attack (TIA)

Y Cai[1], Y Chen[2]
[1]Seton Family Hospital, Austin, TX, [2]Burke Neurological Institute, White Plain, NY

Purpose
Around 5%-20% of patients with TIA progress to the acute tissue-based defined stroke within 90 days, half of whom are imminent within the first 48 hours. Identifying these patients is critical but more challenging since its initial negative DWI findings and mild clinical symptom. The non-imaging factors, ABCD2 (Age, BP, Clinical Feature, Duration, Diabetes) method, attracted the research focus for this task. Its low specificity (around 30% in 90 days follow-up) restricted its wide clinical application. The imaging marker, the large artery stenosis (LAS), defined as >70% occlusion, has even lower sensitivity and specificity, especially for the imminent acute stroke. The other well known imaging marker perfusion deficit, though widely investigated in stroke mismatch, few literature reported its application to predict TIA progress to acute ischemic stroke. In light of the concept of ABCD2 method and DWI-Perfusion mismatch, combination of risk factors, we assumed that the matched LAS would corroborate the perfusion deficit to identify these patients.
Materials and Methods
Since no need of contrast, the arterial spin labeling (ASL) perfusion was adopted and implemented at Siemens Skyra 3.0T scanner. With IRB's approval, ASL perfusion was added into the standard clinical stroke MRI protocol. 227 TIA/stroke suspected patients from age 40 to 93 (72±12.4 year) received ASL scan. The study followed the clinical practice guideline. ASL imaging was not used for any clinical decision. Angiogram was acquired by CT or MRI. The Follow-up scans were performed only on the patients for whom the physician thought it necessary according to clinical guideline (for patients without follow-up scan, the clinical defined TIA would be diagnosed if the symptoms resolved within 24h according to clinical TIA criterion). The data were retrospectively analyzed. The inclusion criterion: 1) No tissue defined acute ischemic stroke at the initial MRI scan, defined by DWI completely normal. 2). Definite ASL perfusion deficit, defined by background signal at the surface cortical area and volume > 2ml. MIPAV software was used to segment and calculate the perfusion deficit volume. Using $\chi 2$ analysis, two groups, perfusion deficit with/without the matched LAS, were compared its proportion that the patients would develop the ischemic stroke in 90 days.
Results
6 patients were satisfied the inclusion criterion. Table 1 summarized the details. 3 patients developed the stroke who had both the perfusion deficit and the matched LAS. 3 patients without LAS or not available were diagnosed as TIA. There was a statistically significant difference ($\chi 2$ =6.0, P value = 0.0143). Except one patient (ID6), all other 5 patients had mild syndrome and some of them symptoms fluctuated (stuttering fashion) even to NIH Stroke Scale (NIHSS) 0 when arrived at Emergency Room (ER). 3 patients whose symptom onset time to perfusion imaging was more than 3h, the longest one was 13h. Figure 1 compared two patients (ID1 vs ID4) who had the similar perfusion deficit findings (left temporal lobe, deficit size around 25ml) and mild symptom (NIHSS 4 vs 0) but patient (ID4) who had the left middle cerebral artery (MCA) stenosis, the matched LAS to the left temporal lobe, developed the ischemic stroke detected by DWI 18h later.
Conclusions
Our preliminary study showed the patients with both perfusion deficit and the matched LAS may have

higher possibility to develop imminent ischemia stroke from TIA than those who had perfusion deficit only. The perfusion imaging reflects the brain ischemia directly caused by different etiologies (thrombotic, embolic, vasospastic, systemic hypotension et al) but not etiology itself. Thus it is suitable for prediction of the imminent ischemia event. However, the perfusion deficit snapshot by one scan cannot determine whether the ischemia is temporary (TIA) or steady (ischemic stroke). In the imaging mismatch study, the co-existence of positive DWI findings corroborates to indicate it is steady; or in clinical mismatch, the severe symptom (high NIHSS) also indicates it. For TIA patients with mild symptom, the alternate corroborations need to be found. Our study indicated that the LAS may serve this role. The perfusion deficit with the matched LAS may be steady and thus cause the ischemia stroke in the imminent time period, even though the clinical symptoms are mild. It is also noticed that the perfusion deficit of two patients detected beyond 4-5h after symptom onset time (5h, 13h respectively) did not develop stroke. Similar to the stuttering fashion of clinical symptom, this indicates the perfusion may fluctuate also and is just snapshot at that time. Finally, due to the limited sample size and retrospective study nature, further study is needed.

Table 1

ID	Age-Gender	NIHSS at ER/Symptom / onset time to ASL Image	Large Artery Severe Stenosis (>%70)	ASL perfusion deficit size and area / DSC confirmed?	Follow-up DWI / days to ASL imaging/Stroke defined by follow-up DWI ?	Recanalization Treatment
1	89/F	4/Slurred Speech, Word difficulty/5h	Normal	22.6mL, Left temporal lobe / Yes	No	No
2	57/M	0/Face tingling/ N/A	N/A	26.5mL, Left occipital lobe, partial left temporal lobe / No	No	No
3	75/F	0 / Loss of peripheral vision / 13h	Normal	7.1mL, Left occipital Lobe / No	No	No
4	73/F	0 /weakness/ 8h	Left MCA severe stenosis	24.3mL, Left temporal lobe / Yes	Yes/ 18h/ Yes	No
5	56/F	0 / Syncope/ N/A	left ICA severe stenosis	31.7mL, mixed with many collateral flow, Left temporal, partial left frontal lobe / No	Yes/ 26 days / Yes	Angioplasty 27 days after ASL
6	92/F	24/Aphasia, weakness / 2h	Right MCA severe stenosis	68.3mL/Right temporal lobe / No	Yes/ 1 days/Yes	tPA 30min after ASL imaging

Figure 1

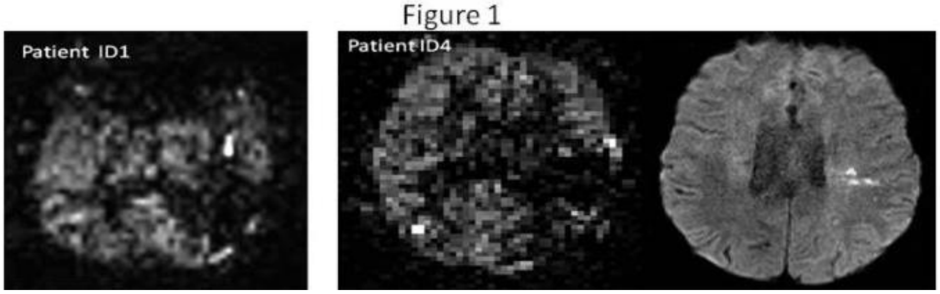

(Filename: TCT_2160_pic.jpg)

3042

The Impact of Ultra-high Resolution CT on the Evaluation of Small Intracranial Arteries: Phantom Study and Visual Evaluation

A Yogi[1], H Tomita[2], J Ito[2], M Okuma[1], S Yogi[3], K Ishigami[4], S Murayama[2]

[1]University of the Ryukyus Hospital, Nakagami-gun, Okinawa, [2]Graduate School of Medical Science, University of the Ryukyus, Nakagami-gun, Okinawa, [3]Graduate School of Medical Science, University of the Ryukyus, Nishihara-cho, Okinawa, [4]Graduate School of Medical Science, University of the Ryukyus, Namagami-gun, Okinawa

Purpose
To examine the performances in visualizing intracranial small arteries on CT angiographies (CTAs) scanned by ultra-high resolution CT (U-HRCT) (Aquilion Precision, Canon Medical Systems, Tokyo, Japan) and conventional HRCT (C-HRCT) (Aquilion ONE, Canon Medical Systems, Tokyo, Japan).
Materials and Methods
We scanned TOS phantom (Canon Medical Systems, Tokyo, Japan) on both of C-HRCT and U-HRCT and analyzed modulation transfer function (MTF) by circular edge to evaluate their spatial resolution. For qualitative evaluation, we retrospectively selected nine patients, who underwent CTAs by both of U-HRCT and C-HRCT. The acquired images were reconstructed using enhanced Adaptive Iterative Does Reduction (eAIDR) (Canon Medical Systems, Japan), and subsequently, axial, coronal and sagittal 3-mm maximum-intensity projection (MIP) were also generated. Two radiologists evaluated the visualization according to the origin and the periphery of bilateral ophthalmic arteries (OpthAs), anterior choroidal arteries (AChoAs), lenticulostriate arteries (LSAs), medial striate arteries (MSAs) and thalamoperforating arteries (TPAs) on both CTAs, using five-point visual scale in consensus. Variables were compared using paired t test and Wilcoxon signed-rank test.
Results
U-HRCT demonstrated higher MTF at each spatial frequency ($p < 0.001$). On the qualitative evaluation, U-HRCT visualized the origin of right OpthA and left AChoA better than C-HRCT(p values < 0.03) and did the periphery of right OpthA, right AChoA, right LSA, left OpthA, left AChoA and left LSA better than C-HRCT ($p = 0.01$, $p < 0.02$, 0.03, 0.05, 0.01, and 0.01, respectively).
Conclusions
U-HRCT demonstrated better spatial resolution on phantom study, which led to the better visualizing performance of small intracranial arteries.

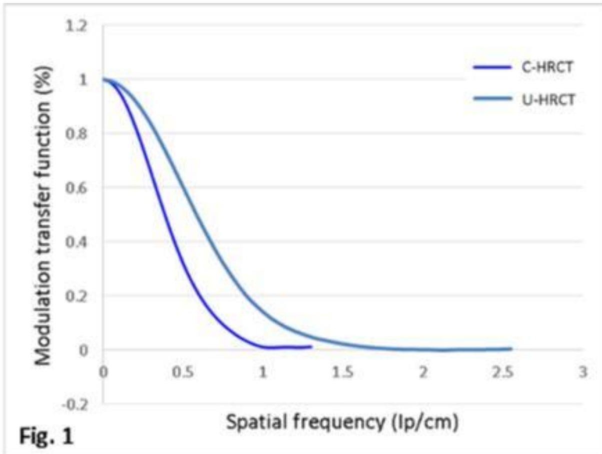

Fig. 1: Graph shows modulation transfer function (MTF) curve for the conventional high resolution CT (C-CT) and ultra-high resolution CT (U-HRCT). U-HRCT demonstrated higher MTF at every spatial frequency.
Fig. 2: Axial MIP image with 3mm thickness obtained by U-HRCT demonstrates right medial striate artery (MSA) (arrow) and left MSA (arrow heads) originating from left ACA (not shown).
Fig. 3: Axial MIP image with 3mm thickness obtained by C-HRCT does not show any of MSA.

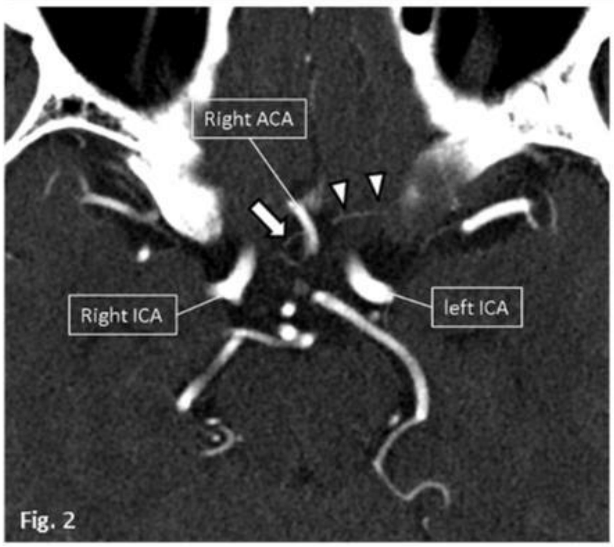

(Filename: TCT_3042_figures.jpg)

2680

The Use of Descriptive Terms for Ventricular Size on Head CTs

R Key[1], M Braileanu[2], K Crawford[3], M Mullins[4]
[1]EMORY UNIVERSITY SCHOOL OF MEDICINE, DECATUR, GA, [2]Emory University Hospital, Atlanta, GA, [3]Emory University, Atlanta, GA, [4]EMORY UNIVERSITY, ATLANTA, GA

Purpose
Numerous radiographic terms can be used to describe abnormally enlarged ventricles on non-contrast head CTs, such as "hydrocephalus," "dilated ventricles," "ventriculomegaly," and "ex vacuo dilation." We have noticed that these terms are sometimes used incorrectly in radiology reports. As the ventricles are implicated across a broad spectrum of brain diseases and may be clinically managed differently, it is important to use accurate terminology. This helps both referring clinicians and other radiologists who may interpret future studies on the same patients. The purpose of this study is to characterize how ventricular size is described in radiology reports.
Materials and Methods
We performed a single institution retrospective review of all adult patients with at least two consecutive non-contrast head CTs from 2010-2016. IRB approval was obtained. We grouped reports based on

descriptions of the ventricles into three categories: "acceptable," "unclear," and "not acceptable." "Acceptable" reports indicated (1) if the ventricle size was normal or abnormal, (2) the presence or absence of hydrocephalus, and (3) the presence or absence of interval change from the prior exam. "Unclear" reports fulfilled criterion (1), but did not fulfill either or both of criteria (2) and (3). "Not acceptable" reports did not fulfill criterion (1). An additional subgroup was created for exams which mentioned "hydrocephalus" as the study indication. Descriptive statistics and subgroup analysis were performed.

Results

We found that slightly more than half of radiology reports at our institution had an "acceptable" description of the ventricles. Most of the "unclear" reports used broad or vague terms such as "ventriculomegaly" or "prominent ventricles", without ascribing an etiology such as hydrocephalus or volume loss to the ventricular appearance. Most of the "not acceptable" reports described the ventricles relative to the prior exam, using words such as "increased" or "stable", without further characterization. When "hydrocephalus" was in the indication, the report was more likely to have an "acceptable" description of the ventricles. Documenting the presence or absence of hydrocephalus on every exam, regardless of indication, may improve the clinical utility of the reports. The importance of such practice could potentially be emphasized through faculty and resident training, as well as through modification of standardized templates.

Conclusions

We found that only slightly more than half of radiology reports at our institution had an "acceptable" description of the ventricles. Most of "unclear" reports used broad or vague terms such as "ventriculomegaly" or "prominent ventricles", without ascribing an etiology such as hydrocephalus or volume loss to the ventricular appearance. Most of the "not acceptable" reports described the ventricles relative to the prior exam, using words such as "increased" or "stable", without further characterization. When "hydrocephalus" was in the indication, the report was more likely to have an "acceptable" description of the ventricles. Documenting the presence or absence of hydrocephalus on every exam, regardless of indication, may improve the clinical utility of the reports. This could potentially be emphasized through faculty and resident training, as well as modification of standardized templates.

2665

Tympanic Cavity Melanoma

G Parnes[1], A Zlochower[1], W Mallon[2], S Roknsharifi[1], S Slasky[1], K Hsu[3], J Burns[1], R Zampolin[1], J Bello[1], K Shifteh[1]
[1]Montefiore Medical Center, Bronx, NY, [2]Montefiore Medical Center, New York, NY, [3]Stanford University, Stanford, CA

Purpose

To describe the imaging features of a rare case of melanoma of the tympanic cavity To understand how tympanic cavity melanoma is treated and managed To review the anatomy of the middle ear To learn the differential diagnosis of masses within the tympanic cavity

Materials and Methods

The patient is a 74-year old female with no significant past medical history presenting with hearing loss and fullness in her left ear. A contrast enhanced CT and MRI of the temporal bone was obtained. A PET-CT was also performed.

Results

Contrast enhanced CT of the temporal bone demonstrates complete opacification of the left tympanic cavity, mastoid antrum, and mastoid air cells/ without bony destruction. Subsequent contrast enhanced MRI of the brain demonstrated a T1 hyperintense, T2 hypointense lesion within the left tympanic cavity. There is no intracranial extension of the tumor. There is no abnormal enhancement of the cranial nerves.

Conclusions
Malignant melanoma is a neoplasm of the melanocytes or cells that develop from melanocytes. Mucosal melanomas of the head and neck typically affect patients in the fifth through seventh decades of life and have a slight male predominance. Primary mucosal melanomas of the head and neck represent approximately less than two percent of melanomas. Of that small fraction malignant melanoma of the temporal bone may rarely involve the mucosa of the middle ear and the mastoid cavity. CT is useful to look for bony erosions however this is usually a negligable finding in regards to melanoma. MRI is useful for contrast resolution of soft tissue and extent of soft tissue spread to the surrounding structures. The unique tissue signal characteristics make MRI particularly useful to confirm the diagnosis of melanoma. The differential diagnosis for middle ear soft tissue masses includes cholesteaotoma, facial nerve schwannoma, adenoma, and glomus tympanicum. The middle ear or tympanic cavity includes the space between the tympanic membrane and inner ear. The contents includes the ossicles (stapes, incus, and malleus), the oval window, the round window, and the eustacian tube. Treatment is controversial however involves surgery with radiation therapy and chemotherapy.

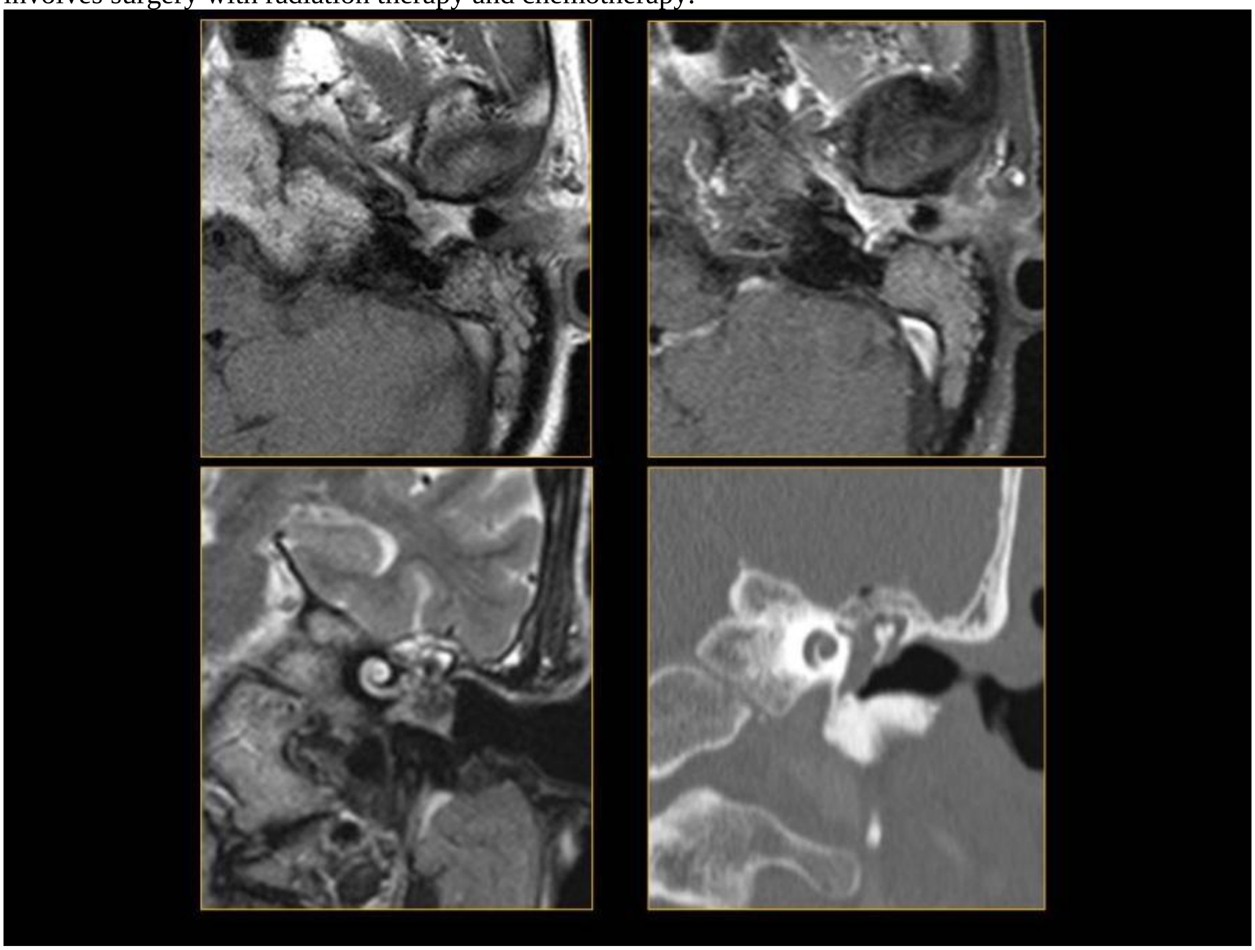

(Filename: TCT_2665_Presentation3.jpg)

2614

Typical Versus Atypical Acute Necrotizing Encephalopathy (ANEC) – a Clinico-Radiological Correlation.

H Vanjare[1]
[1]*CHRISTIAN MEDICAL COLLEGE AND HOSPITAL, VELLORE, VELLORE, TAMIL NADU*

Purpose
ANEC is a rare disorder affecting younger individuals and is associated with poor outcome. Not all the patients fulfill the case definition for ANEC (1). These may be considered as atypical form of the disease. The purpose of this single center retrospective study was to look at the imaging features and outcomes between ANEC vs. atypical ANEC cases.
Materials and Methods
Radiology database was searched for all the brain imaging (both CT and MRI) for cases with bilateral thalamic involvement from 2006 to 2017. All patients who had presented with acute encephalitic illness were included in the study. Based on the imaging and laboratory findings, patients were divided into ANEC vs. atypical-ANEC group. Outcome at discharge (alert vs. minimally conscious state / death group) and status of patients during follow up was documented.
Results
Of the twenty seven cases, 17 were in ANEC group (image 'a' showing significant thalamic involvement) while 10 were in atypical-ANEC group (image 'c' showing partial thalamic involvement). Imaging parameters which had significant difference between ANEC vs. atypical-ANEC cases were involvement of periventricular white matter, substantia nigra, presence of diffusion restriction and hemorrhage. Trilaminar pattern on ADC images (image 'b') was specific for ANEC cases. There was no significant difference between the management of ANEC vs. atypical-ANEC cases. Higher proportions of the patients in ANEC group (59%) were in minimally conscious state / death group as compared to atypical-ANEC group (30%); however, this was not statistically significant.
Conclusions
In presence of bilateral thalamic involvement the clinical outcome is poor. However, ANEC cases have higher proportion of poor outcome.

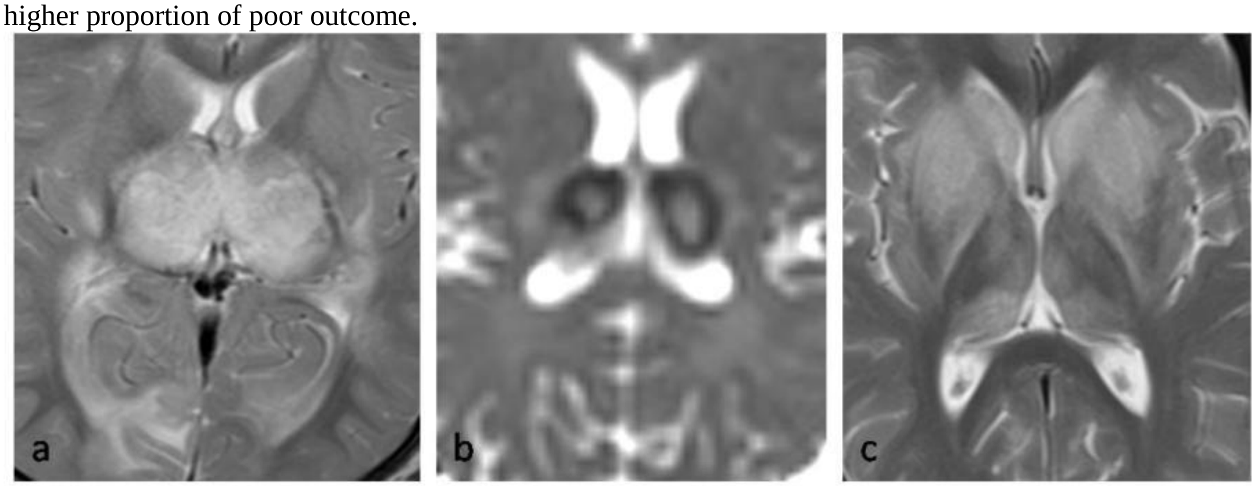

(Filename: TCT_2614_ANECvsatypicalANEC300.jpg)

2961

Update to Management of Very Small Intracranial Aneurysms: Outcomes for Patients with 3 mm Aneurysms

A Saha[1], K Seifert[2], X Wu[1], A Malhotra[3], L Tu[4]
[1]Yale University School of Medicine, New Haven, CT, [2]YALE NEW HAVEN HOSPITAL, NEW HAVEN, CT, [3]YALE UNIVERSITY SCHOOL OF MEDICINE, NEW CANAAN, CT, [4]Yale School Of Medicine, New Haven, CT

Purpose

Unruptured intracranial aneurysms (UIAs) are a common entity, present in 6-8% of the general population. Small aneurysms measuring are often followed for many years with angiographic imaging. The utility of this imaging surveillance is unclear given the infrequent rates of rupture or growth reported in the literature. In this study, we examine follow-up trends for patients with 3 mm aneurysms at a single tertiary referral center. We assess the number of follow up studies employed, the number of multiple aneurysms, the rates of de novo aneurysm formation, growth, rupture, and treatment. These data inform evidence-based recommendations for patients with aneurysms measuring 3mm.

Materials and Methods

Retrospective review of cases from a single institution was performed over a 5-year period from 5/1/2010 to 5/1/2015. Patients with aneurysms measuring 3mm were identified, and these patients were tracked until 5/1/2017. Pertinent patient and aneurysm-specific data were collected.

Results

Review of institutional cases revealed 155 patients with 3mm aneurysms. Over a total of 769 imaging studies (CTA, MRI/MRA, and DSA), a total of 334 aneurysms were identified in this population. Among these, 126 aneurysms were described as having maximum dimension of 3mm. The range of reported size was 1 - 15 mm. Of the 126 aneurysms measuring 3mm, 9 (7%) aneurysms grew over the study period, 5 (4%) were treated, and 2 (2%) appeared de novo. Zero ruptured during the study period. A subset of 63 patients had a 3mm aneurysm as their largest aneurysm. Among these patients, there were 107 total aneurysms detected via 284 imaging studies (CTA, MRI/MRA, and DSA). 67 of these measured 3mm. Within this subgroup, zero (0%) 3mm aneurysms grew, zero (0%) ruptured, and 4 (6%) were treated. A single (1.5%) 3mm aneurysm was de novo.

Conclusions

In patients with 3mm aneurysms, routine surveillance reveals low rates of de novo aneurysm formation, growth, and rupture. We found growth only of 3mm aneurysms in patients with also larger aneurysms. No 3mm aneurysms were found to rupture during our study period. In view of these finding, it frequent surveillance of 3mm aneurysms found in isolation, or as the largest of multiple aneurysms, is likely of low utility.

3374

Updated Imaging Findings in Hyperostosis Corticalis Generalista using 3D reconstructions

E Peters[1], K Tong[2]
[1]Loma Linda University Medical Center, Loma Linda, CA, [2]LOMA LINDA UNIVERSITY SCHOOL OF MEDICINE, LOMA LINDA, CA

Purpose

Demonstrate updated imaging findings using 3D reconstructions in a rare disease, Worth Syndrome, a subtype of hyperostosis corticalis generalista.

Materials and Methods

42 year old male with history of motor vehicle collision presented with multifocal trauma and facial pain from suspected nasal bone fracture, and underwent maxillofacial CT with 3D reconstructions.. Genetic test results are pending.

Results

Extensive mandibular and maxillary buccal exostoses and anterior mandibular cortical thickening consistent with hyperostosis corticalis generalista, presumably Worth Syndrome. The patient also had prominent frontal bossing, which has been described in Worth Syndrome.

Conclusions

Extensive buccal exostoses have been reported with Worth syndrome and have been evaluated with panoramic radiographs, plain film, and more recently cone beam CT in the dental literature. These are considered benign findings. Worth syndrome is a controversial entity with often inaccurate or incomplete descriptions, making it difficult to distinguish from other subtypes of hyperostosis, which vary based on inheritance patterns and whether or not they cause cranial nerve palsy. We present a case of incidental presumed Worth syndrome which was identified using maxillofacial CT. The use of 3D reconstructions facilitate the interpretation of the findings, and have not been previously described in the literature.

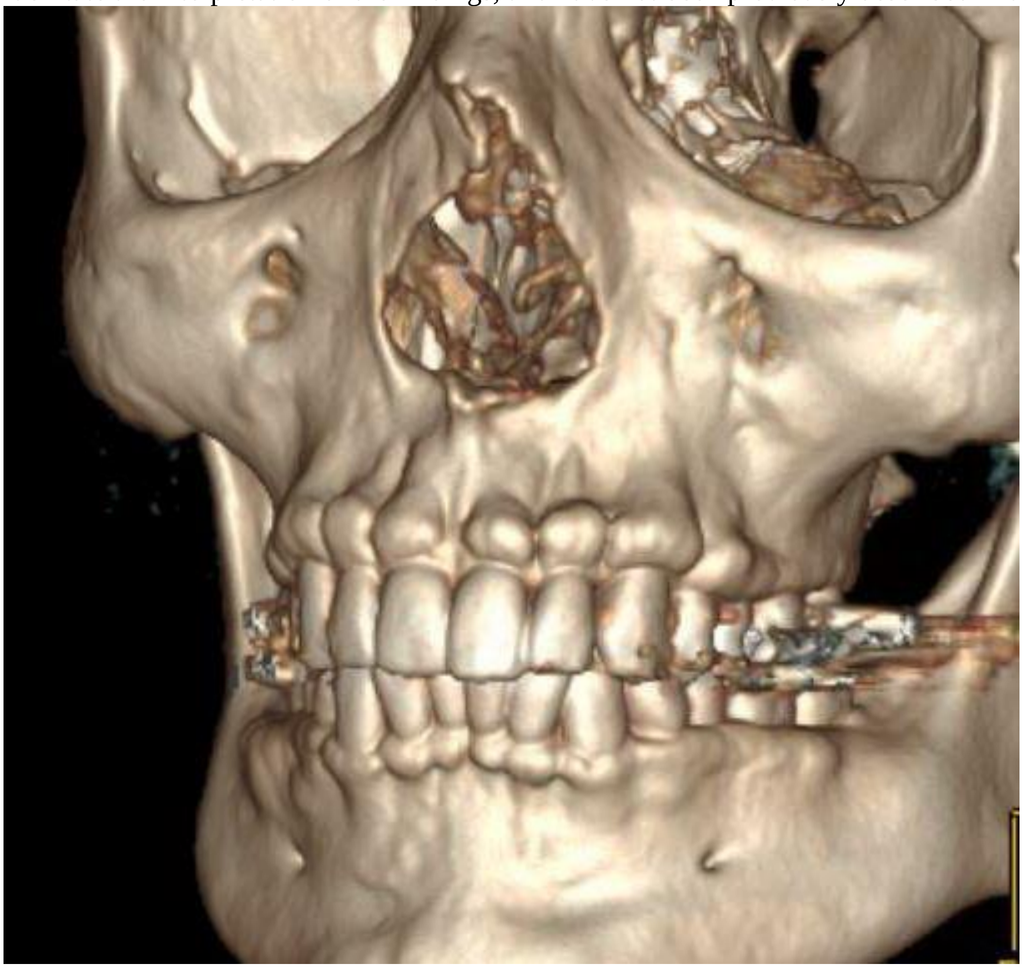

(Filename: TCT_3374_buccalexostosis3dct.JPG)

2180

Usefulness of Contrast-enhanced 3-Dimensional T1-weighted Turbo Spin Echo Sequence in Detection of Brain Metastases at 3T Magnetic Resonance Imaging: Comparison with Contrast-enhanced 3-Dimensional T1-weighted Gradient-recalled-echo Volumetric Interpolated Brain Examination

S Prakkamakul[1], S Kongpromsuk[2], N PITAKVEJ[3], N Jittapiromsak[4]
[1]King Chulalongkorn Memorial Hospital the Thai Red Cross Society, Chulalongkorn University, Bangkok, Thailand, [2]King Chulalongkorn Memorial Hospital the Thai Red Cross Society, Bangkok, Thailand, [3]King chulalongkorn Memorial Hospital, the Thai Red Cross Society, Chulalongkorn University, Bangkok, Thailand, [4]Chulalongkorn University, Bangkok, Thailand

Purpose
Accurate identification of brain metastases is crucial for cancer treatment. This study aims to compare the

detectability of brain metastases between contrast-enhanced 3D T1-weighted turbo spin echo sequence (SPACE; Sampling Perfection with Application optimized Contrasts using different flip angle Evolutions), and contrast-enhanced 3D T1-weighted nonmagnetization-prepared spoiled gradient-echo sequence with asymmetric k-space sampling and zero filling (VIBE ; Volumetric Interpolated brain sequence) at 3 Tesla. Studies have shown superiority of 3D T1-weighted SPACE over 3D T1-weighted magnetization-prepared rapid gradient-echo sequence (MPRAGE) for the detection of brain metastases, however a comparison between 3D T1-weighted SPACE and 3D T1-weighted VIBE is lacking.

Materials and Methods

This IRB-approved retrospective study included 27 consecutive adult patients with brain metastases who underwent both contrast-enhanced 3D T1-weighted SPACE and contrast-enhanced 3D T1-weighted VIBE sequences at 1-mm-thickness using 3 Tesla MRI between April 2017 and February 2018. Blinded neuroradiologist and neuroradiology fellow independently determined the number of enhancing lesions on each sequence. Wilcoxon signed rank test was used to compare the difference between the number of detectable parenchymal enhancing lesions. Interobserver reliability was calculated using intraclass correlation.

Results

Significantly more parenchymal enhancing lesions were detected on 3D T1-weighted SPACE compared with 3D T1-weighted VIBE (total 424 vs 378 lesions; median 6 vs 5; $p = 0.008$). Fifteen patients (55.6%) showed equal number of parenchymal enhancing lesions across both sequences. Ten patients (37%) showed more detectable parenchymal enhancing lesions on 3D T1-weighted SPACE (up to 9 more lesions), while only 2 patients (7.4%) showed more enhancing lesions on 3D T1-weighted VIBE (up to 2 more lesions). Interobserver reliability between readers was excellent.

Conclusions

Contrast-enhanced 3D T1-weighted SPACE sequence demonstrates higher detectability of brain metastases compared with contrast-enhanced 3D T1-weighted VIBE sequence at 3 Tesla. Contrast-enhanced 3D T1-weighted turbo spin echo is a promising alternative technique for the detection of brain metastases.

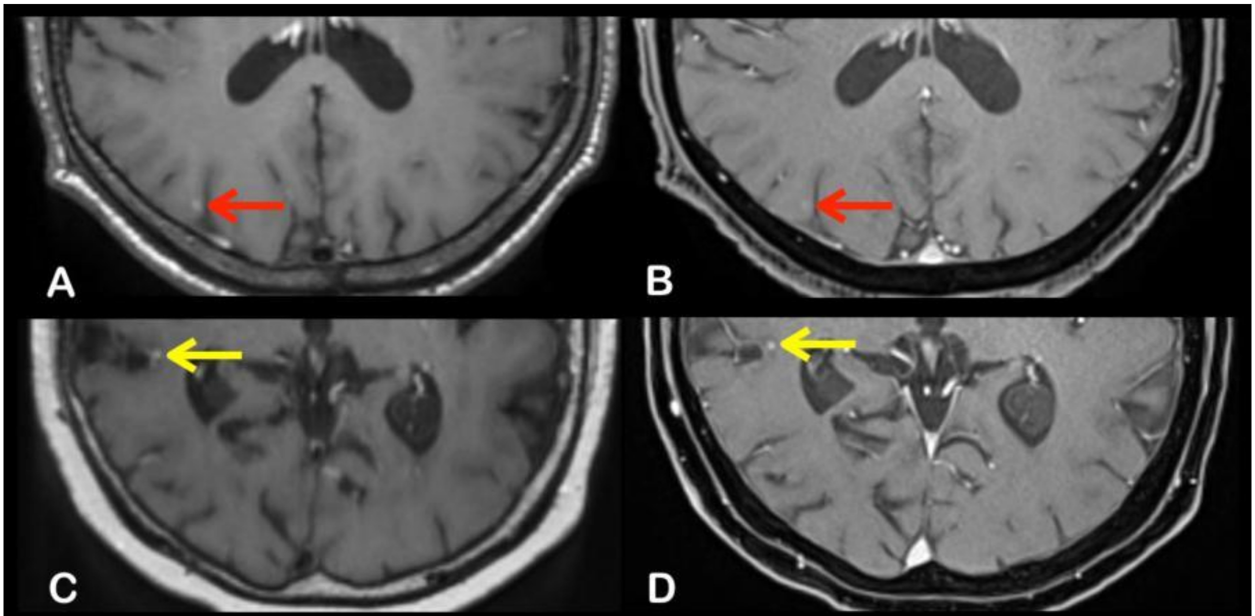

(A) and (B) images from a 58-year-old lung cancer patient exemplify an enhancing metastatic lesion in the right temporo-occipital lobe that was missed by readers on contrast-enhanced 3D T1-weighted VIBE (red arrows). The degree of enhancement and lesion conspicuity are higher on contrast-enhanced 3D T1-weighted SPACE (A) compared with contrast enhanced 3D T1-weighted VIBE (B).
(C) and (D) images from a 76-year-old lung cancer patient exemplify an enhancing metastatic lesion in the right temporal lobe that was missed by readers on contrast-enhanced 3D T1-weighted SPACE (yellow arrows). The degree of enhancement is similar on both sequences. However, this lesion was missed because it located close to a vessel and was mistaken for an incompletely suppressed vascular signal on contrast-enhanced 3D T1-weighted SPACE (C). Axial contrast-enhanced 3D T1-weighted VIBE (D) clearly distinguishes parenchymal enhancing lesion (yellow arrow) from an adjacent vascular structure.

(Filename: TCT_2180_abstract_EPos2180_ASNR2019.jpg)

3391

Using Convolutional Neural Networks to Predict Infarct Development in Acute Ischemic Stroke Patients: Does Reperfusion Status Matter?

Y Xie[1], Y Yu[1], T Thamm[1], C Huang[1], E Gong[2], S Christensen[1], M Lansberg[3], G Zaharchuk[4]
[1]Stanford University, Stanford, CA, [2]Stanford University, Sunnyvale, CA, [3]Stanford, Stanford, CA, [4]STANFORD UNIVERSITY, STANFORD, CA

Purpose
For acute ischemic stroke (AIS) patients, predicting final infarction is a key element for triage. Using input data from baseline multimodal MRI, deep learning models have been found useful in final infarct prediction. However, the patient's reperfusion treatment outcome can greatly influence the actual prognosis. In this study we investigated whether knowledge of the patient's reperfusion status improves deep-learning-based prediction performance.
Materials and Methods
AIS patients were reviewed and selected from the prospective, multi-center Imaging Collaterals in Acute Stroke (iCAS) and DEFUSE2 studies. We included patients who underwent baseline MRI including perfusion-weighted imaging with dynamic susceptibility contrast (DSC), diffusion-weighted imaging (DWI), and gradient echo (GRE) imaging; and follow up imaging with T2-FLAIR performed 3-5 days after stroke onset. The ground truth was defined as the stroke lesions on follow-up T2-FLAIR, which

were manually delineated by readers blinded to clinical information. Perfusion maps (Tmax, cerebral blood flow, cerebral blood volume, and mean transient time) were reconstructed by RAPID software (IschemaView, Redwood City, CA). All images were co-registered to Montreal Neurological Institute template space with SPM software. Three U-Net models were trained with the above-mentioned 7 different contrasts as inputs (Figure 1). The first model was trained on 50 reperfused patients, the second on 50 non-reperfused patients and the third on 50 patients randomly selected from previous two training sets, with 25 reperfused and 25 non-reperfused patients. Reperfusion was determined based on follow-up DSA images by neurointerventional radiologists based on a TICI score of >= 2b. The models were trained based on a mixed loss function of cross-entropy and SSIM. The three models were evaluated on a test set with 26 patients, 13 reperfused and 13 non-reperfused patients. The predictions and the results are reported as area under the receiver operator curve (AUC), Dice score, and predicted stroke volumes.
Results
The study included a total of 126 patients (63 males, age 65±16, baseline NIHSS 15±6). 7 patients received IV tPA only, 57 with IV tPA plus thrombectomy, 33 with thrombectomy only, and 4 without reperfusion therapy. Overall, the model trained on non-reperfusers showed a significantly higher Dice score (0.47±0.047, pval = 0.045) and AUC (0.94±0.0021, pval = 0.00069) than the model trained on reperfused patients (Table 1). Comparing between the reperfused and non-reperfused test sets, the reperfused model had a significantly higher AUC when tested on reperfused patients (0.93±0.0016, pval = 0.013), in comparison to testing on non-reperfused patients (0.89±0.0029). When predicting reperfused stroke lesion volumes, (Figure 2) non-reperfused model shows highest correlation with ground truth volume (R = 0.669). The largest volume error is 271.4 cm3 predicted by the reperfused model on non-reperfused test set.
Conclusions
Deep learning models trained using patients with the same reperfusion results does not uniformly improve the prediction outcome of stroke lesions on similar patients in the test set, a surprising finding that requires further investigation.

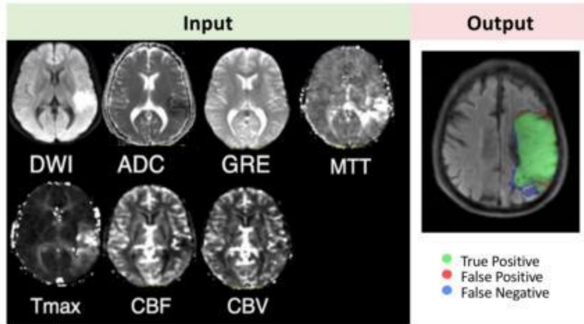

		Training set		
Test set	**Dice**	Non-reperfused	Reperfused	Mixed
	Non-reperfused	0.470	0.332	0.368
	Reperfused	0.472	0.416	0.472
	All	0.471 (p = 0.99)	0.374 (p = 0.27)	0.42 (p = 0.26)
	AUC	Non-reperfused	Reperfused	Mixed
	Non-reperfused	0.930	0.892	0.912
	Reperfused	0.948	0.933	0.944
	All	0.939 (p = 0.34)	**0.912 (p = 0.012)**	0.928 (p = 0.17)

Table1. This table shows Dice and AUC for the 3 models trained on three training sets (n = 50) tested on reperfused and non-reperfused test sets(n=13) as well as both sets combined (n = 26). Only AUC from the reperfused model showed a significant increase when testing on reperfused test set.

(Filename: TCT_3391_ASNR_YX.jpg)

2838

Utility of Advanced Imaging in the Evaluation and Resection of Epileptogenic Foci: A Single Institution Survey

M Hirano[1], J Templer[2], B Liu[1], A Korutz[1]
[1]Northwestern Memorial Hospital, Feinberg School of Medicine, Chicago, IL, [2]Neurology Department at Northwestern Memorial Hospital, Chicago, IL

Purpose
Multiple advanced modalities are utilized to identify epileptogenic foci as well as to plan intracranial electrode placement and surgical resection. We surveyed neurologists and neurosurgeons to determine their perspectives on the value of BOLD fMRI, DTI/Tractography, and PET in epilepsy surgery.
Materials and Methods
Neurologists (n=4) and neurosurgeons (n=2) at our institution completed a survey assessing their perception of the value of fMRI, DTI/tractography, and PET in epilepsy surgery. Responses were recorded on a 5 point Likert scale, ranging from "Not Helpful" to "Extremely Helpful."
Results
83% (n=5) rated fMRI as very or extremely helpful in pre-operative planning. 100% reported fMRI as somewhat or extremely helpful in guiding electrode placement. There was no consensus regarding the

helpfulness of fMRI during surgical resection (range 2-5). Responders were split between rating DTI tractography as somewhat helpful and extremely helpful in pre-operative planning. There was no consensus regarding the helpfulness of DTI in guiding electrode placement (range 2-5). 83% reported tractography as very or extremely helpful for surgical resection. 83% found PET very or extremely helpful in pre-operative planning, with 83% agreeing that the location of hypo/hyper-metabolism helped guide electrode placement. 67% found PET very or extremely helpful during surgical resection. The consensus among neurologists was that PET is the most helpful modality for pre-operative evaluation and surgical resection. Neurosurgeons agreed that fMRI is the most useful for pre-operative evaluation and DTI is the most helpful for surgical resection.

Conclusions

Neurologists and neurosurgeons hold different perspectives about the value of advanced imaging in evaluating seizure patients. Neurologists favor PET in pre-operative evaluation and surgical resection, while neurosurgeons favor fMRI for pre-operative evaluation and DTI for surgical resection. Additional clinicians within our institution as well as other institutions will be surveyed in the near future to supplement these initial results.

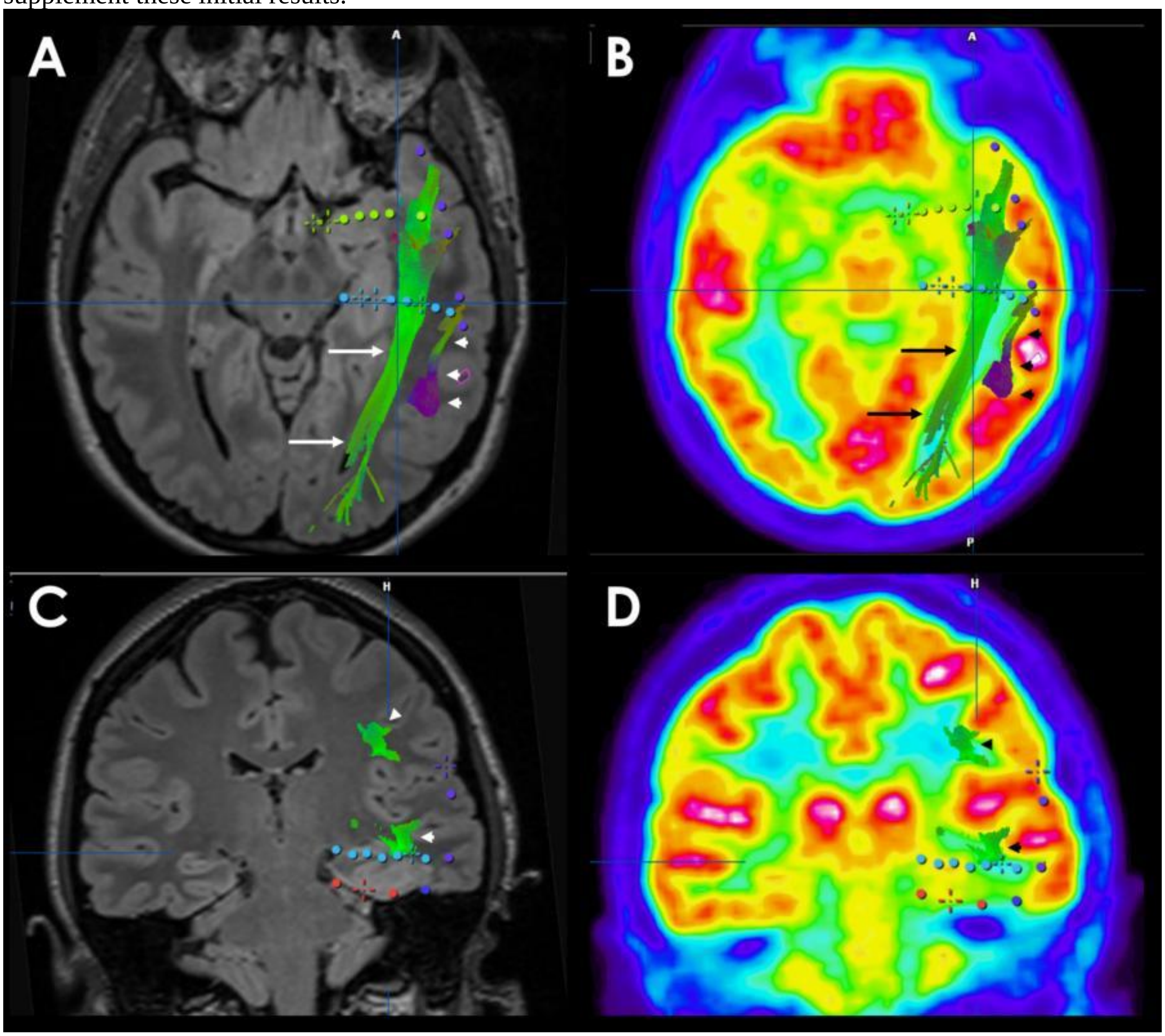

(Filename: TCT_2838_asnr1106fig.jpg)

2969

Validation of Post-operative Residual Contrast Enhancing Tumor Volume as an Independent Prognostic Factor for Overall Survival in Patients with High Grade Glioma

M Fernandez-Taranilla[1], A Hilario[1], E Salvador[1], P Martin[1], A Perez-Nuñez[1], J Sepulveda[1], A Hernandez-Lain[1], V Perez Garcia[2], J Perez Beteta[3]
[1]Hospital 12 de Octubre, Madrid, Spain, [2]MATHEMATICAL ONCOLOGY LABORATORY (MOLAB), CIUDAD REAL, CASTILLA-LA MANCHA, [3]Mathematical Oncology Laboratory, CIUDAD REAL, CASTILLA-LA MANCHA

Purpose
In the current study, we pooled imaging data in newly diagnosed Glioblastoma (GBM) patients from our institution to identify the relationship between postoperative residual enhancing tumor volume and overall survival (OS).
Materials and Methods
Retrospective review of clinical and imaging data from 96 patients newly diagnosed GBM were reviewed from 2012 to 2018. Post-surgical residual enhancing disease was quantified using T1 contrast-enhanced 3D images always comparing with T1 3D sequences without contrast administration to avoid false positive enhanced areas ((hematoma, postsurgical changes…). We used Philips Intellispace Portal software and tumor tracking tool, to quantify residual enhanced volume (measure in cubic centimeters). Multivariate Cox regression models were used to determine influence of clinical variables such as age at diagnosis, days after first post surgical MRI, amount of macroscopic surgical resection followed by neurosurgeons reports (complete, partial and biopsy) and its correlation with imaging, IDH status, everything in overall survival rates (OS).
Results
A long- linear relationship was observed between postoperative, residual enhancing tumor volume and OS in newly diagnosed GBM treated with standard chemoradiation.Post-operative tumor volume is a prognostic factor for OS (P <0.01), regardless of therapy, age and IDH status.
Conclusions
Post-surgical, residual contrast-enhancing disease significantly influences survival in patients with newly diagnosed glioblastoma treated with chemoradiation with or without concomitant experimental therapy. Knowledge of the residual tumor volume is extremely important to clinicians to predict the overall survival in these patients.

2836

Vessel Wall Imaging in Previously Unruptured, Untreated Brain Arteriovenous Malformations (bAVM)

L Eisenmenger[1], D Saloner[1], D Cooke[1], S Hetts[1], N Ko[1], A Abla[1], C Hess[1], H Kim[1]
[1]University of California, San Francisco, San Francisco, CA

Purpose
Advanced imaging techniques such as vessel wall imaging (VWI) and 4DFlow MRI promise improved anatomic characterization and quantification of flow and inflammation in bAVMs. In particular, VWI has been hypothesized to help in identifying the site-of-rupture in ruptured bAVMs, and enhancement may be a marker of unstable lesions prone to rupture. The purpose of this study was to present a series of unruptured, untreated bAVM cases with VWI.
Materials and Methods
VWI was obtained using black-blood pre- and post-gadolinium 3D CUBE T1 (images). Two neuroradiologists identified the number of feeding arteries and draining veins, evidence of remote

hemorrhage, and the distribution and degree of AVM enhancement (yellow arrow). Presence or absence of vessel wall and/or perivascular enhancement inside and outside the nidus was assessed. Percent of AVM enhancement (0-25%, 25-50%, 50-75%, or 75-100%) was also evaluated.

Results

VWI was obtained in 6 cases with no prior definitive bAVM treatment (resection, stereotactic radiosurgery, or embolization) or history of symptomatic hemorrhage. 4/6 were Spetzler-Martin grade (SMG) 4 and 2/6 were SMG 5 bAVMs, ranging in size from 3.4 to 9.5cm. All lesions exhibited enhancement on VWI both inside and outside the nidus, and 5/6 had perivascular enhancement in the nidus. No subjects had perivascular enhancement outside the nidus. Most patients had >50% enhancement (3/6 had 50-75%, 2/6 had 25-50%, and 1/6 had 0-25%).

Conclusions

While contrast enhancement has been seen in ruptured and post-treatment AVMs, our cases all had vessel wall enhancement prior to any treatment or large hemorrhage. Although the cause of enhancement is uncertain, altered vascular flow is likely a contributing factor. Future studies with clinical and radiographic follow-up using 4Dflow MRI and histopathology could help to further understand the underlying etiology.

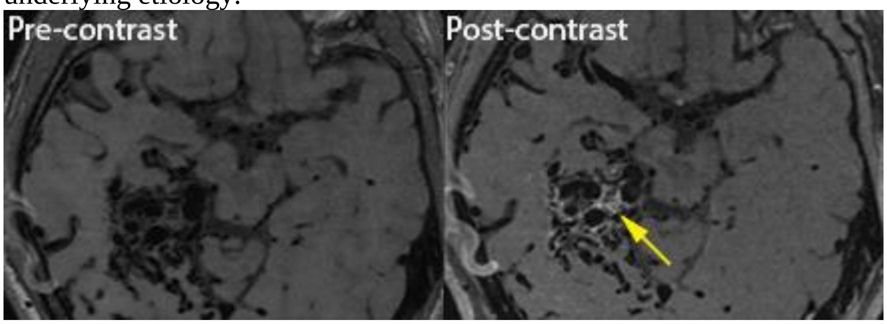

(Filename: TCT_2836_avm-hor.gif)

3065

Amyotrophic Lateral Sclerosis: Mimickers and Chameleons.

I Padilha[1], A Araújo[2], R Hoffmann Nunes[3], A Alves Fonseca[4], A Pettengill[5], F Pacheco[3], A MAIA[6], A da Rocha[7]
[1]Irmandade da Santa Casa de Misericórdia de São Paulo, São Paulo, São Paulo, [2]Irmandade da santa casa de misericórdia de são paulo, São Paulo, São Paulo, [3]DASA, Sao Paulo, Sao Paulo, [4]Irmandade da Santa Casa de São Paulo, Sao Paulo, Sao Paulo, [5]Irmandade da Santa Casa de Misericórdia de São Paulo, São Paulo, Brazil, [6]SANTA CASA DE SÃO PAULO, SAO PAULO, SAO PAULO, [7]IRMANDADE SANTA CASA DE MISERICORDIA DE SAO PAULO, Sao Paulo, Sao Paulo

Purpose
Amyotrophic lateral sclerosis (ALS) is a progressive and devastating neurodegenerative motor neuron disorder, with typical involvement of both upper motor neuron (UMN) and lower motor neuron (LMN), and age peaks between 50 and 75 years. Objective diagnostic criteria systems is established. There are many different disorders that can mimic ALS and its misdiagnosis has many implications for patient, leading to different outcomes. Our purpose is reviewing and discussing typical and atypical ALS presentations, highlighting differential diagnosis based on clinical presentation, imaging findings and additional red flags to support this differentiation.
Materials and Methods
After reviewing our institution teaching files, we selected cases demonstrating typical and atypical (chameleons) cases of ALS. Differential diagnosis (mimickers) were grouped according to specific findings, highlighting the contribution of different imaging methods/sequences. Patient selection and data collection were performed using the electronic patient's database.
Results
Population-based studies have indicated that nearly 10% of patients diagnosed with ALS ultimately turn out to have another condition. The progressive improvement of magnetic resonance imaging into clinical practice has contributed to advances in degenerative disorders comprehension, such as the use of magnetization transfer imaging and gradient-echo sequences in ASL diagnosis. The appropriate correlation of clinical and imaging findings is crucial to differentiate from alternative disorders, particularly in atypical presentations. Mimickers can be grouped into those presenting with isolated LMN/UMN involvement or those with mixed signs, including possible differentials, such as Hirayama's disease, duropathies, cervical polyradiculopathy, multiple sclerosis and metabolic myelopathies. Considering its variable forms of presentation, some important chameleon-like presentations, such as Mills Syndrome, must be recognized in order to attenuate diagnostic delay and specific treatment.
Conclusions
Besides the consolidated use of ALS diagnostic criteria systems, there are still many misdiagnosis. In order to reduce potential delays on treatment, clinical and anatomical red flags are important tools to identify chameleons and potential mimickers.

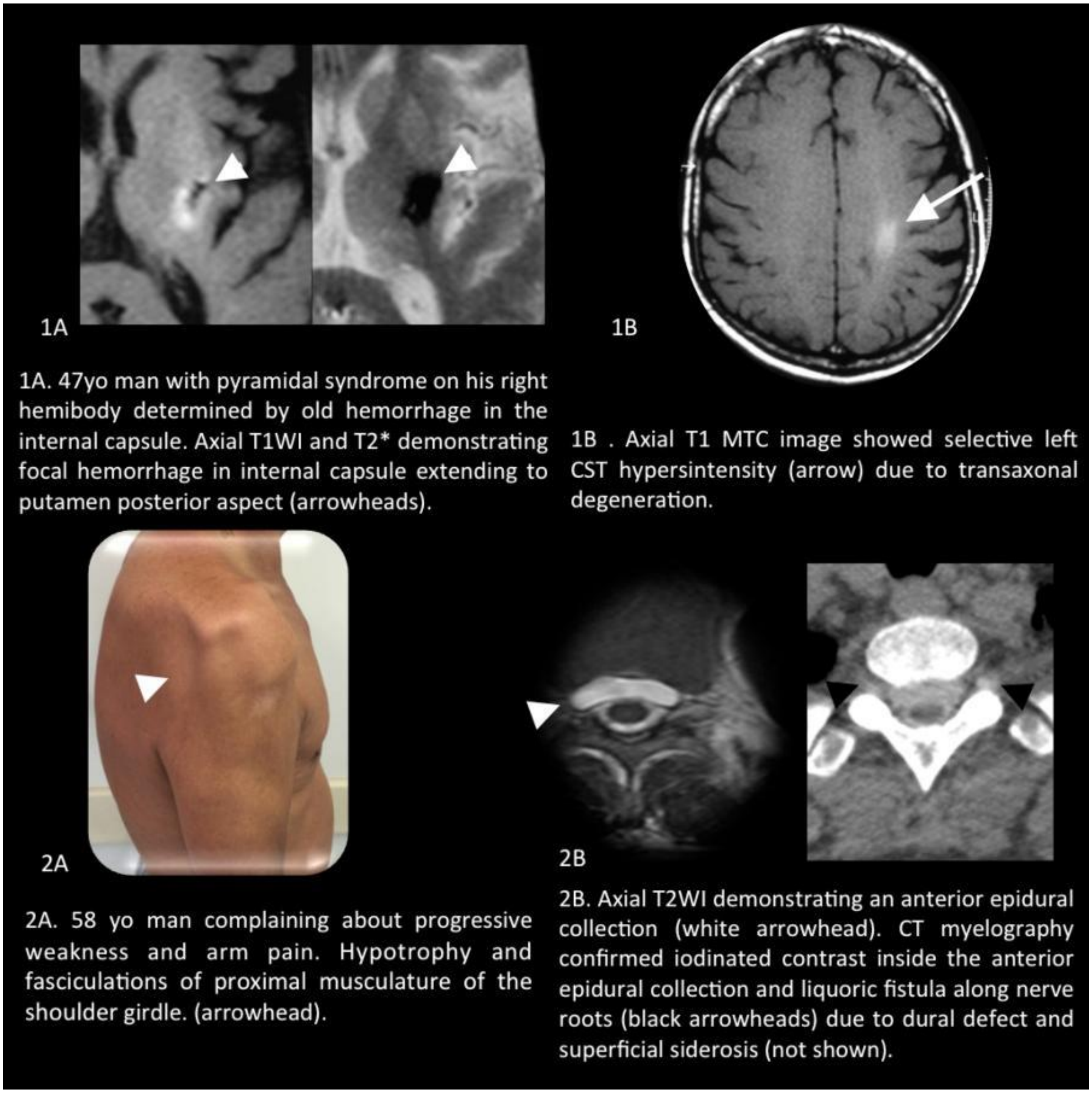

(Filename: TCT_3065_Slide1.jpg)

2173

Cerebral Vasoconstriction and its Differentials – Guideline for Residents

J Ospel[1], T Demerath[2], K Blackham[3]
[1]UNIVERSITY HOSPITAL BASEL, BASEL, Switzerland, [2]University Hospital Basel, Basel, Basel, [3]University Hospital of Basel, Basel, BS

Purpose
To illustrate imaging findings of cerebral vasoconstriction and point out the characteristic radiographic features of frequent underlying pathologies.

Materials and Methods
Case-based illustration of cerebral vasoconstriction in the setting of SAH, PRES, RCVS, meningitis, vasculitis and atherosclerosis.
Results
Cerebral vasoconstriction findings in general: Caliber irregularities and narrowing of intracerebral arteries, diffuse or focal, beads-on-a-string appearance, caliber changes in comparison to prior exams. Treatment options in general are oral, intravenous and intraarterial calcium channel blockers. In addition, etiology-specific treatment options are available, e.g. steroids and immunosuppressants in vasculitis or antibiotic treatment in meningitis. SAH: Aneurysm, blood in the basal cisterns and perisylvian area, vasospasms are pronounced in the basal cerebral arteries/ Circulus Wilisii PRES: Vasogenic edema with parietooccipital predominance, associated hemorrhage and infarction in up to 25% RCVS: Typically no other findings besides vasospasm, although SAH, hemorrhage and infarcts can occur Meningitis: Leptomeningeal enhancement, effacement of sulci and basal cisterns with exsudate, mild ventricular enlargement Vasculitis: Multifocal narrowing with predominant involvement of small and medium-sized arteries, multiple infarcts of different age and without vascular distribution pattern, meningeal enhancement can be present Atherosclerosis: Calcification, dilatation and elongation of ICA, vertebral and basilar arteries, old infarcts may be present
Conclusions
Early and confident detection of cerebral vasoconstriction is important to initiate appropriate treatment. Cerebral vasoconstriction per se is an unspecific finding and can be seen in the context of different pathologies. Common causes are aneurysmal SAH, PRES, RCVS, meningitis/meningoencephalitis, vasculitis and atherosclerosis. Additional imaging features are crucial to determine the underlying etiology in a given case.

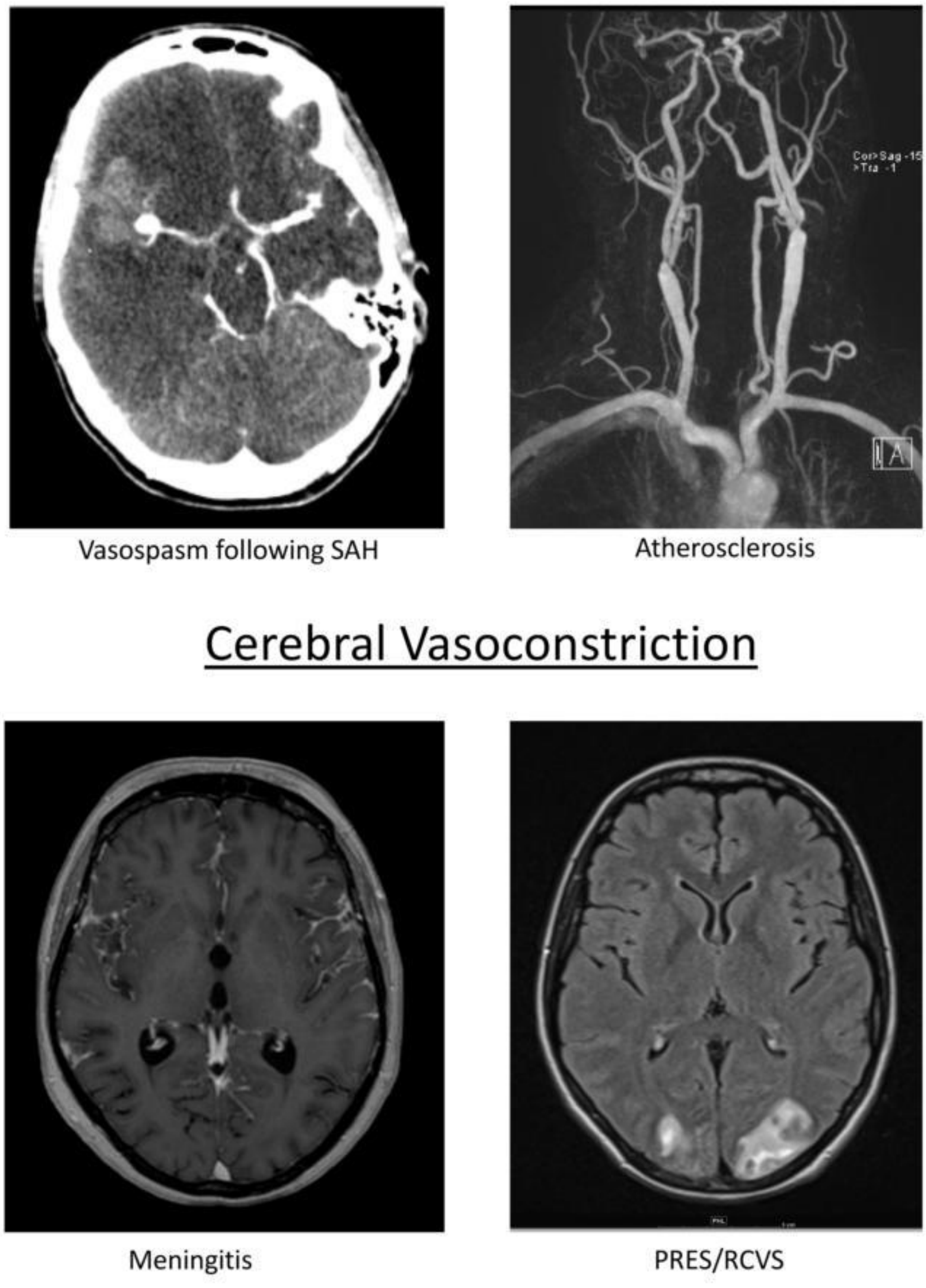

(Filename: TCT_2173_EducationalExhibitBilder09102018.jpg)

2777

Dysraphism Spinal: Imaging and Embriology Evaluation

H Silva[1], M Caliani[2], L Nelli[2], M Akuri[3], M Akuri[4]
[1]FAMEMA, Marília , São Paulo, [2]FAMEMA, Marília, São Paulo, [3]Famema, Marília, São paulo, [4]Universidade de Marília, Marilia , São Paulo

Purpose
Discuss the most common forms of closed spinal dysraphism and provide an overview of embryologic development and congenital anomaly image findings of the spine and spinal cord.
Materials and Methods
Embryology will be evaluated and correlated with developmental abnormalities that give rise to spinal dysraphisms, illustrated with interesting cases of our service, highlighting the main imaging findings that must be recognized by the radiologist.
Results
Spinal dysraphism is due to faults in the embryological development between the second and sixth weeks of gestation, where three consecutive embryonic stages occur: gastrulation (weeks 2-3), where the neural tube, notochord, spine and brain and spinal cord;primary neurulation (weeks 3-4), where neural tube closure and secondary neurulation (weeks 4-6) occurred, where it formed the tip of the medullary cone and the terminal phylum. It´s encompasses a spectrum of congenital anomalies ranging from complex lesions, incluiding lipomyelomeningocele (LMM) to subtle anatomical abnormalities like fibrolipoma of the filum terminale (FFT). We will discuss some of them. LIPOMIELOCELE, LIPOMYELOMENINGOCELE AND SACRAL LIPOMA - Characterized by a midline subcutaneous fatty mass rigth above the intergluteal crease, usually extending asymmetrically into one buttock. Embryologically, are abnormalities of primary neurulation. DERMAL SINUS - The Dermal Sinus is an epithelium-lined fistula that extends inward from the skin surfasse and can connect with de CNS and its meningeal coating. It´s found more frequently in the lumbosacral region. Embryologically, result from focal incomplete disjunction of the neuroectoderm from the cutaneous ectoderm. CAUDAL AGENESIS - Categorized into two types depending on the location and shape of the conus medullaris: either high and abrupt (type I) or low and tethered (type II). Embriologically, related disordered primary or secondary neyrulation, respectively. FILAR LIPOMA - Characterized by fibrolipomatous thickening of the filum terminale. Embriologically is an abnormality of secondary neurulation. TETHERED CORD SYNDROME - Involves traction on a low-lying conus medullaris with progressive neurologic deterioration due to metabolic derangement.
Conclusions
Congenital anomalies of the spine, spinal cord and envelopes comprise a wide spectrum of clinical presentations and malformations dependent on the embryological phase in which the failure occurs, being of the utmost importance the radiologist's knowledge of the several alterations found since early diagnosis and therapy are necessary for the patient's good prognosis.

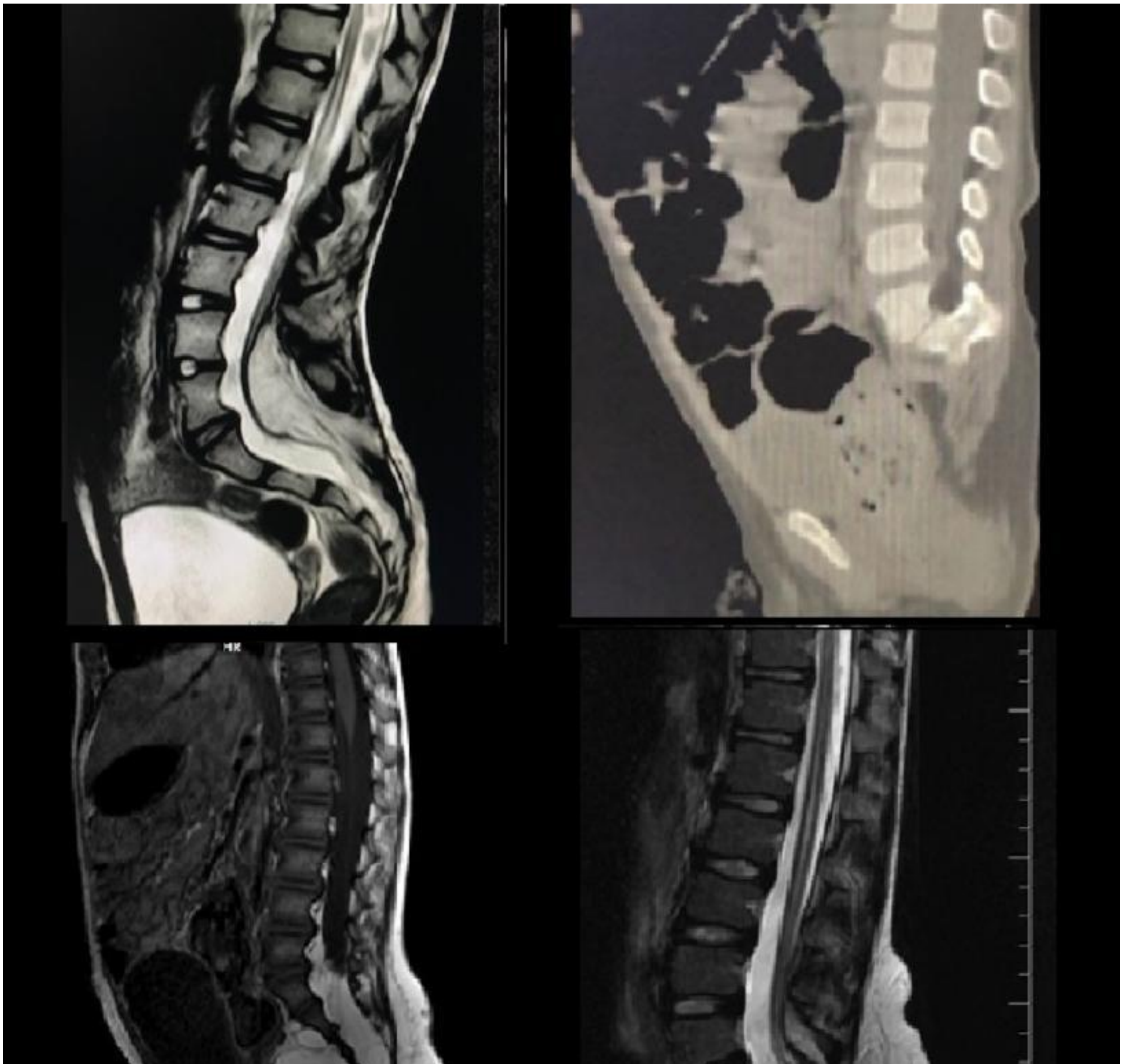

(Filename: TCT_2777_IMAGEDysraphismSpinal-ImagingandEmbriologyEvaluation.jpg)

3117

From Diagnosis to Treatment: Clinical Role of the Neuroradiologist in Caring for Patients with Spontaneous Intracranial Hypotension

J Spivey[1], V Timpone[1], A Thaker[1]
[1]*University of Colorado Anschutz Medical Campus, Aurora, CO*

Purpose
To describe the pathogenesis, clinical presentation, imaging features, and treatment of spontaneous intracranial hypotension, with specific attention to techniques employed by neuroradiologists to localize and treat CSF leaks.
Materials and Methods
The radiology database at our institution was searched for cases of intracranial hypotension. Representative cases were selected, and images from both diagnosis and treatment are reviewed.
Results
The pathogenesis and clinical presentation of intracranial hypotension are briefly summarized. Classic imaging features of intracranial hypotension are reviewed. We discuss the benefits and limitations of various diagnostic methods used to localize dural defects, including conventional MRI, CT myelography, dynamic CT myelography, and MR myelography. Finally, treatment approaches are reviewed, including empiric autologous epidural blood patch, targeted autologous epidural blood patch (using both interlaminar and transforaminal approaches under CT and fluoroscopic guidance), epidural fibrin glue patch, and intrathecal saline infusion.
Conclusions
Neuroradiologists are uniquely positioned to both diagnose and treat spontaneous intracranial hypotension. Familiarization with the various diagnostic and image-guided therapeutic tools available to care for this patient population can help maximize the potential for favorable outcomes.

3544

Gadolinium-Enhanced Magnetic Resonance Imaging Findings in Cervical Spondylotic Myelopathy

C Auger[1], L Pessini[1], F Doniselli[1], E Maciag[1], A Rovira Canellas[1]
[1]*Section of Neuroradiology, Department of Radiology, Hospital Vall d'Hebrón, Barcelona, Barcelona, Spain*

Purpose
Cervical spondylotic myelopathy (CSM) is the most common cause of spinal cord dysfunction worldwide. It consists of clinical myelopathy secondary to a spinal cord compression due to cervical spondylosis. Contrast-enhanced MRI sequences have not been routinely used in cervical degenerative disease imaging protocols; however, intramedullary contrast enhancement might indicate a local hyperpermeability or areas of disruption of the blood-spinal cord barrier. The recognition of a specific enhancing pattern in CSM could contribute to an accurate diagnosis and to the exclusion of other causes of myelopathy. Therefore, it may help define the treatment strategies avoiding unnecessary interventions.
Materials and Methods
We present 5 patients who were referred for evaluation of suspected myelopathy with an insidious clinical onset, including mild gait impairment, weakness and paresthesias in the upper and mainly lower extremities. All patients underwent MRI scans with and without gadolinium administration on 1.5 Tesla magnets, in both sagittal and axial planes.
Results
All patients presented a typical transverse pancakelike and circumferential gadolinium enhancement in the sagittal and axial plane respectively. The imaging findings we describe in this case series favors the assertion that this enhancing pattern is strongly indicative of CSM, in agreement with Flanagan et al (2014).
Conclusions
The recognition of a pancakelike gadolinium enhancement in the sagittal post-gadolinium T1 sequences with a circumferential enhancement pattern in the axial plane is strongly indicative of CSM when located immediately below the narrowest diameter of the cervical canal in a patient with a compatible clinical picture.

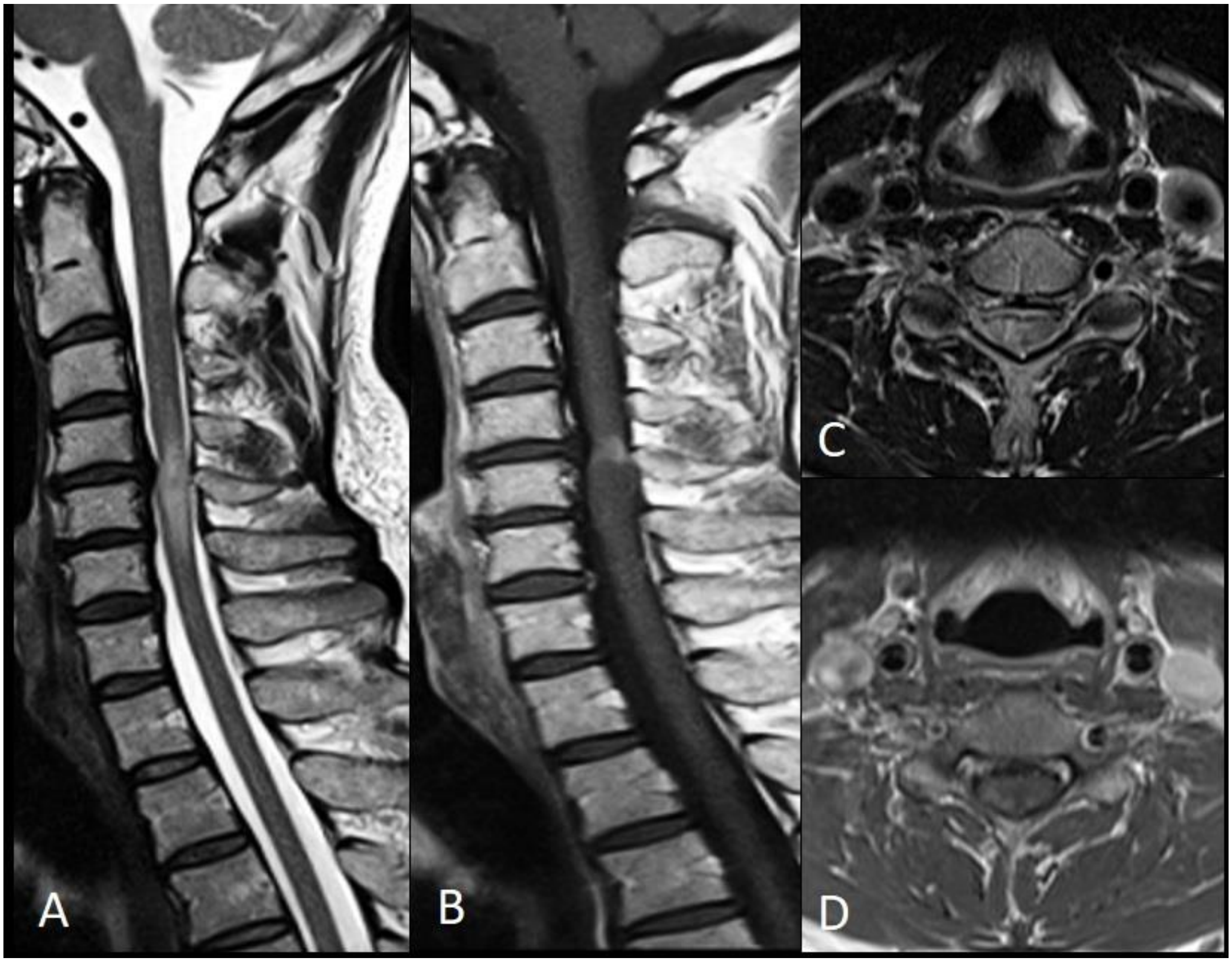

(Filename: TCT_3544_IMGM.jpg)

3560

Giant Intracranial Tumors in the Newborn and Infant

F Torres[1], R Ourfalian[2], J Kang[3], E Christian[4], H Tran[5], A Rajamohan[6], J Acharya[7], B Tamrazi[8]
[1]Kaiser Permanente, Los Angeles Medical Center, Los Angeles, CA, [2]Kaiser Permanente Los Angeles Medical Center, Los Angeles, CA, [3]Kaiser Permanente, Los Angeles, CA, [4]USC, Los Angeles, CA, [5]Kaiser Permanente LAMC, N/A, [6]UNIVERSITY OF SOUTHERN CALIFORNIA, KECK SCHOOL OF MEDICINE, LOS ANGELES, CA, [7]UNIVERSITY OF SOUTHERN CALIFORNIA, KECK SCHOOL OF MEDICINE, Monrovia, CA, [8]Children's Hospital Los Angeles, Los Angeles, CA

Purpose
The purpose of this educational exhibit is to review the few rare giant-sized intracranial tumors that present during the first year of life, including both the newborn and infancy time period. Although intracranial tumors in this time period are rare, they are commonly devastatingly large and are characteristically of a handful of histologic sub-types. We hope to provide a basic review of the neuroimaging findings of giant intracranial tumors during the first year of life, for trainees, general radiologists, and adult neuroradiologists, given these tumors are very rarely seen outside of dedicated children's hospitals.

Materials and Methods
The Southern California Permanente Medical Group cares for over 4 million patients throughout 12 medical centers. However, at our specific Los Angeles Medical Center, we have the only two Pediatric Neurosurgeons and Pediatric Neuro-oncologists, that care for our pediatric patients with brain tumors. With the help of the long detailed patient lists of our pediatric neuro-oncology and neurosurgery team, as well as my own personal patient list, we have cared for over 15 patients with rare, however, devastating giant intracranial tumors.
Results
We will review multiple examples of giant intracranial immature teratomas, both based within the brain parenchyma, as well as extending intracranially from the skull base and orbits. In addition, we will review the classic multicystic appearance of desmoplastic infantile ganglioglioma. We will also present a terribly aggressive posterior fossa atypical teratoid rhabdoid tumor during infancy, and uncommon but devasting embryonal tumor. We will review a case of a giant choroid plexus carcinoma, that in retrospect, demonstrated findings suggesting an intraventricular location, which may have aided in the pre-operative diagnosis. Will review a few infiltrative astrocytomas. Lastly, we will review a rare intracranial, and recently defined, Ewing's Sarcoma with CIC-DUX4 translocation.
Conclusions
We will review the neuroimaging findings, and histological sub-types, of the few rare giant-sized intracranial tumors that present during the first year of life.

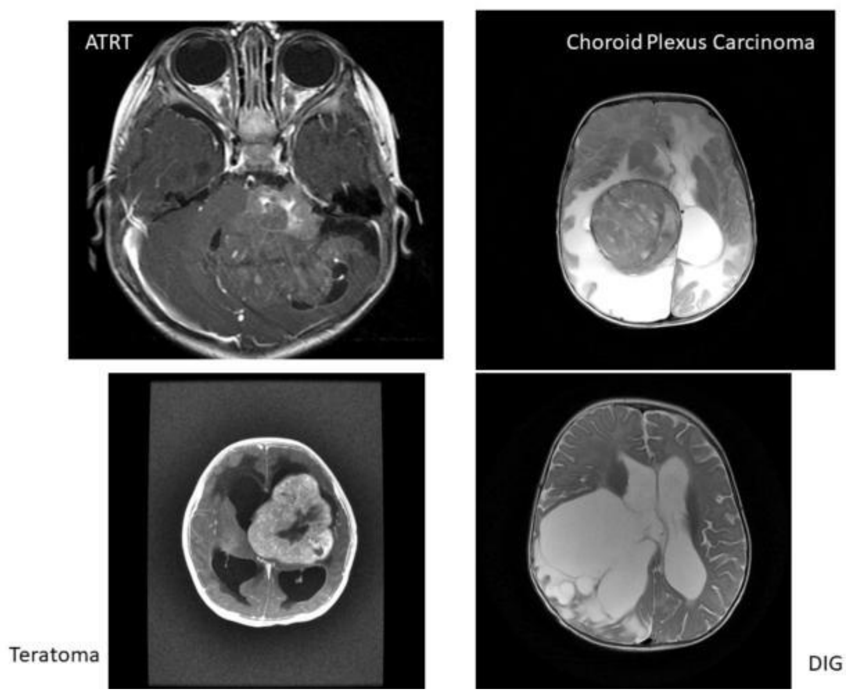

(Filename: TCT_3560_ASNR.jpg)

2627

Hop into the Saddle; Learn the Common and Uncommon Lesions of the Sella

A Patel[1], J Almast[2], A Bhatt[3], K Skalski[4]
[1]University of Rochester Medical Center, Rochester, NY, [2]Univeristy of Rochester, Rochester, NY, [3]UNIVERSITY OF ROCHESTER, STRONG MEMORIAL HOSPITAL, ROCHESTER, NY, [4]University of Rochester Medical Centre, Rochester, NY

Purpose
After participating in this educational presentation, the learner will be familiar with the anatomy and imaging of the sella turcica and pituitary gland and surrounding anatomic structures. Most importantly, the learner will learn the imaging findings for sellar lesions and how imaging can help differentiate between these lesions and help clinicians determine which lesions need intervention and which do not. The learner will become familiar with not only common lesions of the sellar but with uncommon lesions, which are important to keep in the differential.
Materials and Methods
Educational Exhibit powerpoint including images depicting the anatomy of the pituitary gland and surrounding structures. Multimodal imaging including CT, CTA and MRI of Pathology, both common and uncommon, involving the Sella. Epidemiology and and pathophysiology of pathology arising from the sella turcica and surrounding structures.
Results
TABLE OF CONTENTS/OUTLINE -Sella turcica and pituitary gland anatomy and physiology, including surrounding structures -Clinical presentation of sellar/suprasellar lesions Incidence and prevalence of pathology -Common sellar/suprasellar lesions: pituitary adenoma, Rathke's cleft cyst, craniopharyngioma, arachnoid cyst, ectopic posterior lobe -Uncommon sellar/suprasellar lesions: pituitary metastasis (ex. lung), ipilimumab induced hypophysitis, pituitary abscess, pituitary gland calcifications, extramedullary acute myeloid leukemia with involvement of the pituitary, Aneurysm, Meningioma, Hamartoma, Chordoma
Conclusions
After participation in this educational exhibit the learner will be able to name the anatomic structures involving the pituitary gland and sella turcica as well as be able to help clinicians identify pathology and give accurate differentials.

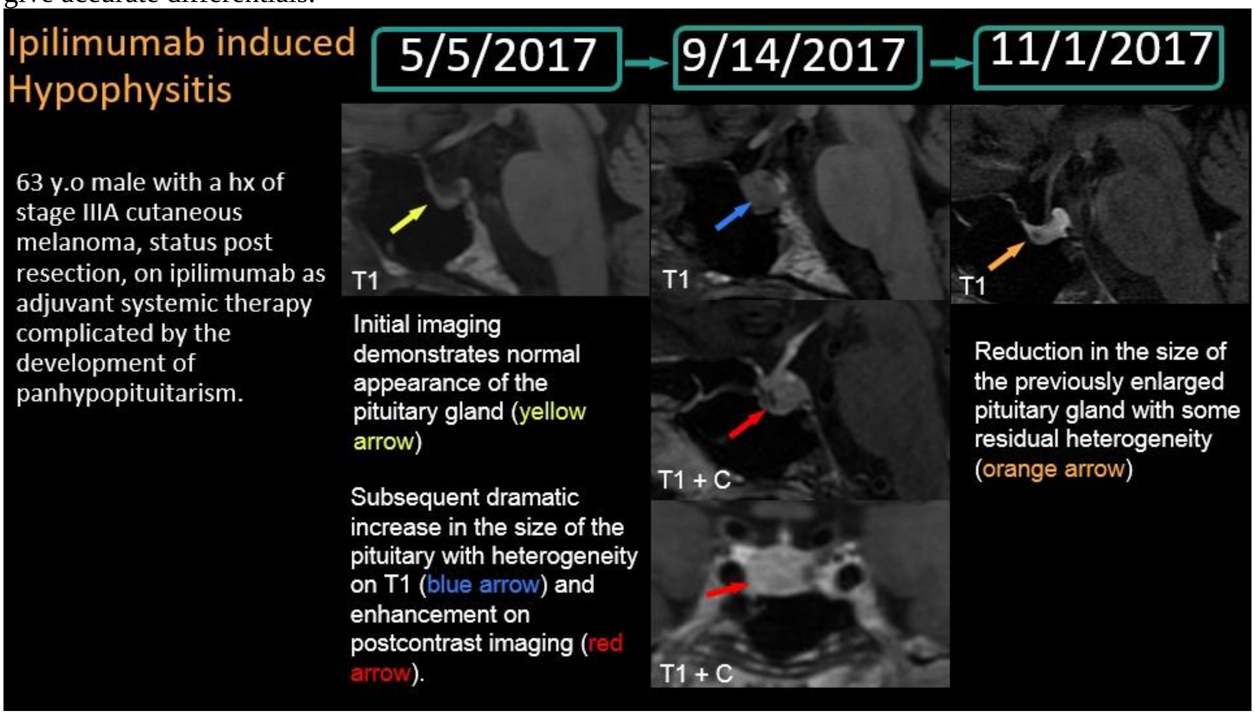

(Filename: TCT_2627_Slide3.jpg)

2837

Imaging of Intravenous Drug Use (IVDU) Related Infections and Infection-related Complications in the Head and Neck

C Farris[1], B Baylosis[1], M Abdalkader[2], A Mian[3]
[1]Boston University Medical Center, Boston, MA, [2]Boston Medical Center, Boston, MA, [3]BOSTON MEDICAL CENTER, BOSTON UNIVERSITY, CAMBRIDGE, MA

Purpose
Purpose: To review imaging findings for IVDU related infections and infection-related complications of the head and neck, their pathophysiology, their treatment, and appropriate imaging follow-up. Learning Objectives: 1. Review imaging findings for IVDU related infections and infection-related complications of the head and neck. 2. Examine the pathophysiology underlying VDU related infections and infection-related complications of the head and neck. 3. Discuss treatment options for IVDU related infections and infection-related complications of the head and neck. 4. Evaluate the role of follow up imaging in IVDU related infections and infection-related complications of the head and neck.
Materials and Methods
We selected twenty case examples to illustrate a wide range of IVDU related infections and infection-related complications of the head and neck performed during the last 10 years at our urban academic medical center. Many case examples include multi-modal imaging with CT and MRI, and occasionally also with digital subtraction angiography. Case examples include cerebral septic embolic with their associated complications such as embolic infarcts, intraparenchymal hemorrhage, mycotic aneurysm formation, brain abscesses, ventriculitis, and extra-axial infections. Case examples of local consequences of direct injection into neck veins such as venous thrombosis and local soft tissues infections are also reviewed. The pathophysiology, treatment, and appropriate imaging follow-up is discussed for each of the case examples.
Results
Figure 1 illustrates the initial finding of intraparencymal hemorrhage in the setting of septic emboli in the absence of any detectable mycotic aneurysms, but short interval follow-up imaging demonstrates rapid interval development of a pseudoaneursym of the right superior cerebellar artery.
Conclusions
Understanding the imaging findings for IVDU related infections and infection-related complications of the head and neck, their pathophysiology, their treatment, and appropriate imaging follow-up is extremely important in the setting of the current IVDU epidemic to help optimize care for this large underserved population.

Figure 1.
33 year-old women with history of IVDU that presented with altered mental status.

A. Initial Non-contrast Head CT demonstrated multifocal intraparenchymal hemorrhage with the largest hemorrhage shown in the right temporal lobe. These ultimately proved to be secondary to septic emboli.

B. Initial CTA Head was negative for evidence of pseudoaneursym with an example image shown.

C. Follow-up CTA Head performed 6 days after the initial CTA demonstrates rapid interval development of a superior cerebellar artery pseudoaneurysm.

D. Digital subtraction angiogram demonstrates the superior cerebellar artery pseudoaneurysm.

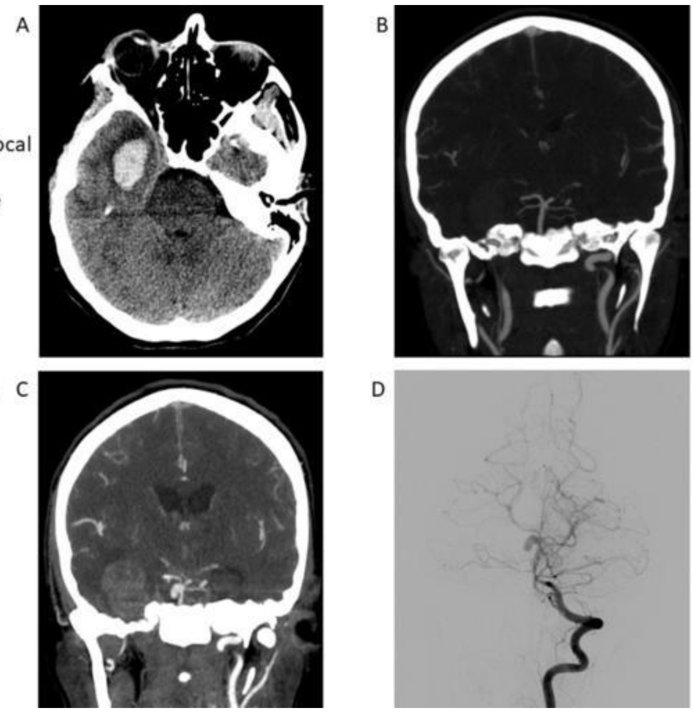

(Filename: TCT_2837_Figure1rescale.jpg)

3282

Imaging of Neuro-oncology Emergencies

A Eran[1], O Kaidar - Person[2]
[1]RAMBAM HEALTH CARE CAMPUS, HAIFA, Israel, [2]Rambam health care campus, Haifa, non

Purpose
Several emergent conditions that require immediate recognition, diagnosis and therapeutic management might be encountered in patients with systemic or CNS malignancy. Prompt and accurate diagnosis is essential in order to preserve and improve patient outcomes. Radiologist should be familiar with the spectrum of clinical presentations and know how to differentiate them based on imaging. In this presentation the various clinical patterns of neuro-oncology emergencies are discussed and demonstrated.
Materials and Methods
We searched our radiology and oncology database to find cases matching the various clinical and imaging patterns of neuro-oncology emergencies.
Results
Patients suffering from CNS or systemic tumors may present as a neuro-oncology emergency in various ways. 1. The first pattern is an emergency situation caused by a direct effect of the tumor on the central nervous system such as edema, increased intracranial pressure, hydrocephalus, major bleed, spinal cord compression and paraneoplastic syndromes. 2. The second pattern is treatment related CNS complications causing an emergency, like PRES and radiation necrosis. 3. Additional 3rd pattern is a malignancy with superimposed emergency condition, such as stroke and venous thromboembolism. 4. The 4th pattern is a malignancy mimicking an emergency status, such as a tumor presenting with seizure complicated by Todd's palsy and therefore suspected for stroke in the ED. 5. Lastly, the 5th pattern is incidental diagnosis of a malignancy in a trauma victim. The various scenarios will be demonstrated in this pictorial presentation.

Conclusions
There are various imaging and clinical presentations of neuro oncology emergencies. Radiologists should be familiar with the spectrum of clinical and imaging finding to assure appropriate and prompt treatment.

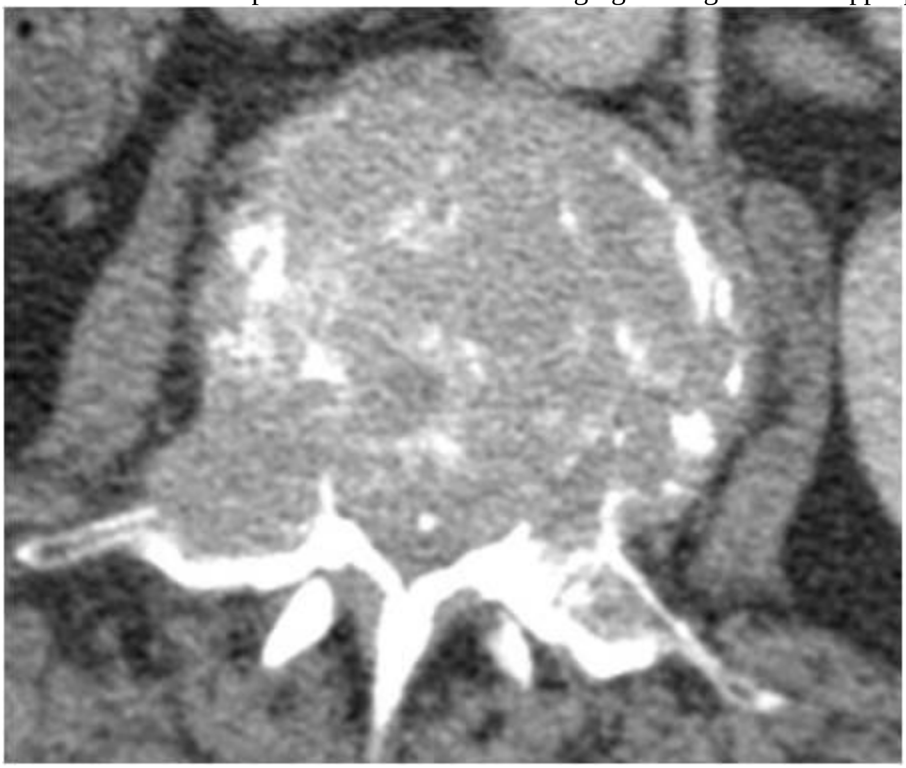

(Filename: TCT_3282_no-ED-2.jpg)

2623

Imaging of Parkinson-Plus Syndrome

A Meng[1], E Lin[1]
[1]*Weill-Cornell, New York, NY*

Purpose
Parkinson disease continues to be diagnosed by clinical recognition of characteristic signs and symptoms. However, accuracy of diagnosis is suboptimal with up to 20% of patient's incorrectly diagnosed [1]. False positives are often associated with atypical parkinsonian syndromes such as multiple system atrophy, progressive supranuclear palsy, dementia with Lewy bodies, and corticobasal degeneration [2]. Several of these neurodegenerative disorders have unique imaging characteristics that may help differentiate these entities from Parkinson disease, allowing for appropriate treatment of patients [3]. The goal of this presentation is to give an overview of parkinsonism and its' differential considerations as well as expected imaging characteristics of these entities.
Materials and Methods
Imaging characteristics of Parkinson disease, progressive supranuclear palsy, multiple system atrophy, dementia with Lewy bodies, and corticobasal degeneration will be discussed.
Results
NA
Conclusions
Imaging can aid in distinguishing Parkinson plus syndromes from Parkinson disease.

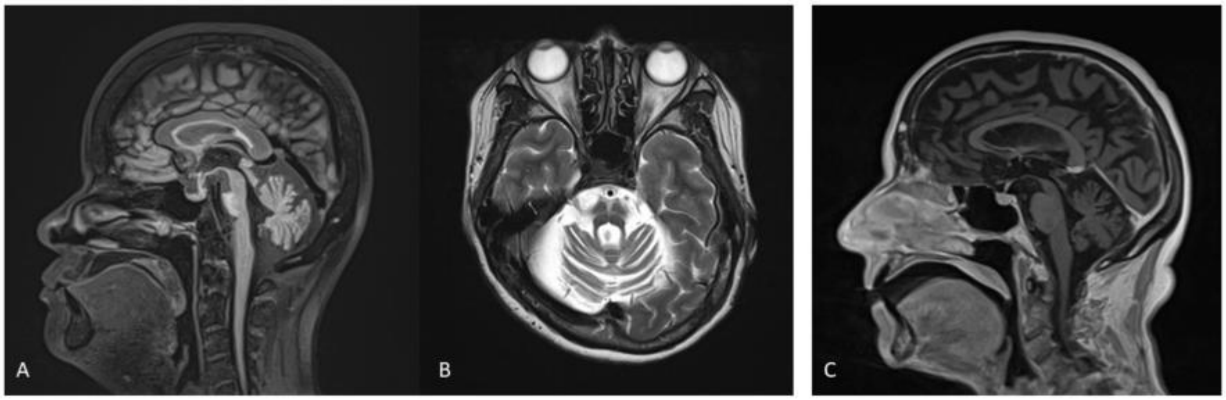

A: Sagittal FLAIR demonstrates marked atrophy of the pons and cerebellum, which is seen in multiple system atrophy.
B: Axial T2 weighted image through the pons show a "hot cross bun" sign, characteristic of multiple system atrophy.
C: Sagittal T1 weighted image demonstrates marked atrophy of the midbrain relative to the pons and medulla, a finding typical of progressive supranuclear palsy.

(Filename: TCT_2623_images.jpg)

3302

Imaging Pattern in Demyelinating Optic Neuritis: Could the Optic Nerves Predict CNS Involvement?

A Alves Fonseca[1], I Padilha[2], A Pettengill[3], F Pacheco[4], R Hoffmann Nunes[4], A MAIA[5], A da Rocha[6]
[1]Irmandade da Santa Casa de São Paulo, Sao Paulo, Sao Paulo, [2]Irmandade da Santa Casa de Misericórdia de São Paulo, São Paulo, São Paulo, [3]Irmandade da Santa Casa de Misericórdia de São Paulo, São Paulo, Brazil, [4]DASA, Sao Paulo, Sao Paulo, [5]SANTA CASA DE SÃO PAULO, SAO PAULO, SAO PAULO, [6]IRMANDADE SANTA CASA DE MISERICORDIA DE SAO PAULO, Sao Paulo, Sao Paulo

Purpose
The optic nerve is frequently involved in demyelinating disease and optic neuritis (ON) may be present in Clinically Isolated Syndrome or as part of Multiple Sclerosis (MS), Acute Disseminated Encephalomyelitis (ADEM), Neuromyelitis Optica spectrum disorders (NMOSD) and MOG antibody-related disorders. Our purpose is to review and discuss the different patterns of optic nerves involvement in demyelinating diseases, predicting central nervous system (CNS) imaging changes in this setting. Furthermore, exemplify mimicking disorders in order to scrutinize a practical approach for the differential diagnosis.
Materials and Methods
After reviewing our institution teaching files, we selected cases demonstrating ON in demyelinating diseases. Disorders were presented according to specific findings highlighting the pattern of involvement: laterality, symmetry, extent of optic nerve involvement (short or longitudinal), the most affected optic nerve segment (retrobulbar, canalicular or intracranial), optic chiasmal involvement, contrast enhancement and perineuritis. Patient selection and data collection were performed using the electronic patient's database.

Results
The pattern of ON involvement in demyelinating disorders can predict the CNS imaging findings. The main diagnoses reported are MS, NMOSD, ADEM, and MOG antibody-related disorders. There are relative specific imaging patterns that could aid to predict the potential diagnosis between these disorders. Different patterns are also depicted in other inflammatory, infectious, neoplastic and vascular diseases disorders, such as cat scratch disease, neurosyphilis, ocular toxocariasis, Susac syndrome, IgG4-related disease, perineural spread of lymphoproliferative disorders, granulomatosis with polyangiitis, neurosarcoidosis, among others.
Conclusions
The approach of ON in demyelinating disorders requires an understanding of specific patterns of nerve optic involvement and its main pitfalls in order to prevent misinterpretation and predict CNS impairment. This radiological characterization may assist with an expedited diagnosis, appropriate institution of specific treatment and have prognostic implications on visual outcomes.

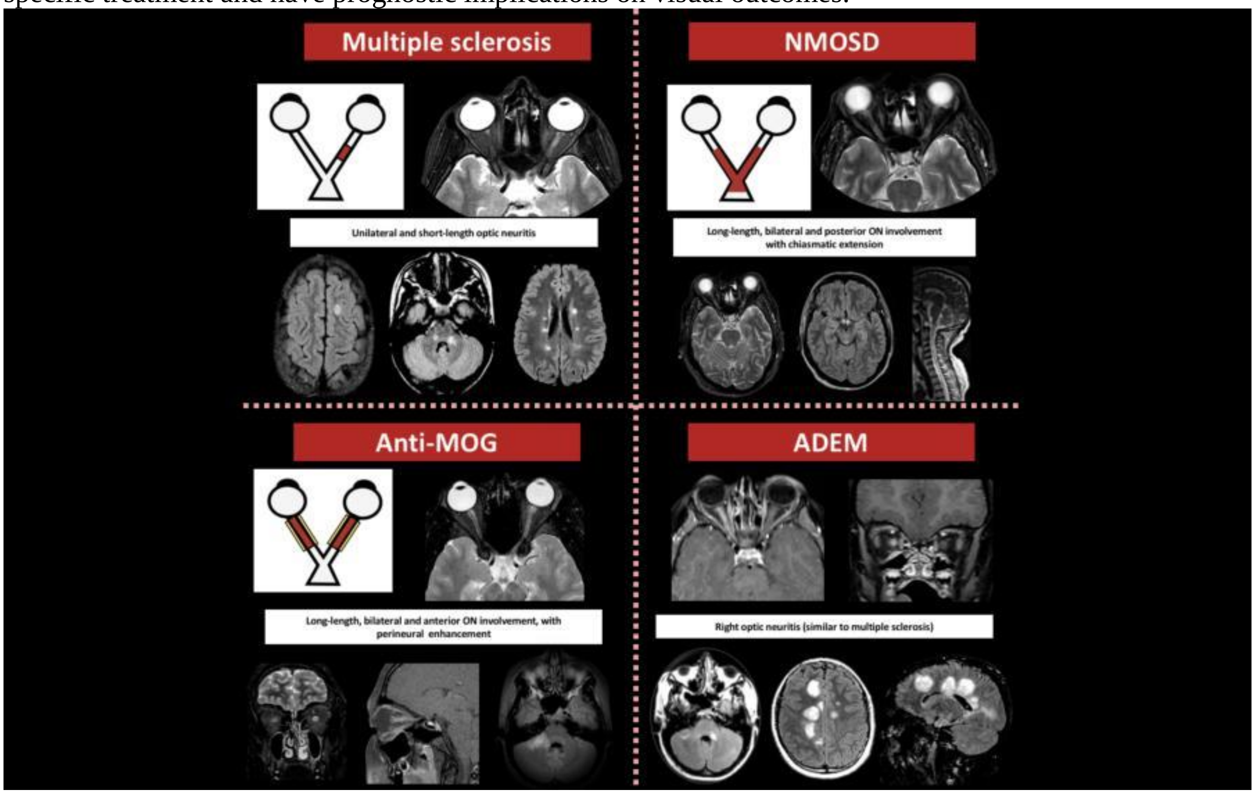

(Filename: TCT_3302_ASNR-Image.jpg)

3545

Li-Fraumeni Syndrome: Epidemiology, Genetics, Imaging Findings and Management

T Donohue[1], T Moritani[2], J Kim[1], A Capizzano[3]
[1]University of Michigan, Ann Arbor, MI, [2]UNIVERSITY OF MICHIGAN, ANN ARBOR, MI, [3]UNIVERSITY OF MICHIGAN, Ann Arbor , MI

Purpose
• Discuss clinical definition of Li-Fraumeni syndrome and role/function of tumor protein 53 • Review select neuroradiological and non-neuroradiological imaging findings in patients with Li-Fraumeni • Review screening criteria for patients with known Li-Fraumeni syndrome

Materials and Methods
• Overview of Li-Fraumeni syndrome definition • Discussion of tumor protein 53 including chromosome location, normal protein function, and consequences of protein function disruption • Review some neurological and non-neurological tumorogenic imaging manifestations of Li-Fraumeni syndrome o Oligodendroglioma/Astrocytoma o Brainstem glioma o Choroid plexus tumor o Rhabdomyosarcoma/Osteosarcoma o Adrenal carcinoma with metastasis o Lymphoma • Current imaging screening guidelines for patients with known Li-Fraumeni syndrome
Results
• Li-Fraumeni syndrome (LFS) is an autosomal dominant tumorogenic disorder characterized by early neoplastic development within an adult population younger than 45 years of age. LFS is caused by a germline mutation within the tumor suppressor gene 53 (TP53), located on chromosome 17p13.1. TP53 is implicated in multiple intracellular functions, including DNA repair, apoptosis, angiogenesis, metabolism, and cell-cycle arrest. Disruption of normal TP53 gene function results in malignancies of the brain, brainstem, choroid plexus, head and neck mucosa, breast, adrenal gland, bone, muscle, lung, pancreas, skin, gastrointestinal tract or leukemic/ lymphomatous dyscrasias. There is an estimated lifetime risk of primary cancer of 73% in men and 90-100% in women, as well as an increased risk of developing secondary or tertiary malignancy, in patients with LPS. • We demonstrate neuro and non-neuro imaging findings in individuals that have met radiologic and/or genetic confirmation of LFS. Whole body MRI for surveillance is recommended due to the reduction of radiation related tumor induction risk, although malignancy/organ appropriate imaging may alter clinical decision making, as patient/neoplasm/organ appropriate.
Conclusions
• After viewing this exhibit, the reader will be familiar with epidemiology, genetics, various neurological and non-neurological imaging findings of Li-Fraumeni syndrome and management, including current screening recommendations.

3148

Mass Lesions in Multiple Sclerosis and its Variants—Frequent Sources of Misdiagnosis: An Educational and Neuroimaging Review

V Yedavalli[1], Z Chaudhry[2], D Martin[2], F Zaccagna[3], T Matys[4], S Hashmi[2], T Massoud[2]
[1]Stanford University, San Francisco, CA, [2]Stanford University School of Medicine, Stanford, CA, [3]University of Cambridge, Cambridge, UK, [4]University of Cambridge, Cambridge, Cambridgeshire

Purpose
Brain multiple sclerosis (MS) lesions are typically small, discrete, ovoid lesions. However, some atypical cases uncommonly present us with diagnostic challenges on MRI. There are few accounts in the literature emphasizing how the consideration of giant MS plaques is generally underestimated in the differential diagnosis of large mass-like white matter lesions. This exhibit will be valuable for accurate recognition of normal and atypical patterns of mass lesions in MS and its demyelinating variants.
Materials and Methods
Using a case-based approach, we review the MRI appearances of mass-like lesions in MS and its variants.
Results
Demyelinating diseases range widely in severity and appearance. Uncommonly, mass-like MS lesions may have atypical imaging features, such as >2 cm in size, perilesional edema, central necrosis, concentric demyelinating bands, or presence of ring enhancement, which may all be frequent sources of diagnostic misinterpretation on MRI. In this exhibit we review the varied imaging appearances and possible differentiating features of tumefactive MS, Balo's concentric sclerosis (BCS), solitary sclerosis, and ring enhancing MS lesions. In particular, the MRI features of BCS are distinctive and include concentric hyperintense T2 rings interleaving with isointense bands corresponding to zones of myelin loss

and myelin preservation, with a peripheral ring of active demyelination. This is a rare and severe demyelinating disease, and although the exact immunopathogenesis of BCS remains unknown, its oligoclonal bands and IgG index manifestations suggest that it is immunologically distinct from MS. We also review the contrasting imaging features of other enhancing mass-like brain lesions, i.e. tumor, abscess, radiation necrosis, metastases, infarct, and hematoma.

Conclusions

Mass-like MS lesions are frequently misdiagnosed as primary malignancy, metastatic disease, or abscess. This may lead to unnecessary surgical interventions and treatments. A thorough understanding of these uncommon and challenging lesions, and their differentiating imaging features, are essential for neuroradiologists and MS specialists alike.

3447

Misrepresentation of Intracranial Cerebrovascular Disease by RAPID Software: A Case Series

Z Stewart[1], M Kassar[2], J Little[3], P Britt[4]

[1]Memorial Health University Medical Center, Savannah, GA, [2]Memorial Health University, Savannah, GA, [3]Mercer University School of Medicine, Savannah, GA, [4]Memorial Health Universty, Savannah, GA

Purpose

This educational case series illustrates how RAPID computed tomography angiogram (CTA) analysis color mapping may misrepresent cerebrovascular disease. Specifically, this software uses volumetric CTA data to generate a cerebral blood vessel density map. The cerebral blood vessel density of the affected side is related to the unaffected side and a relative percentage is generated. A technologist is responsible for sending the "peak arterial" volume data set to iSchemaView RAPID © (Menlo, CA). We have found that in a variety of cerebral vascular diseases, this software will misrepresent cerebral blood volume density. These cases reinforce the need for radiologists to use CTA analysis software judiciously, to review all volumes in a digital subtraction CTA and obtain neck imaging with every RAPID CTA study.

Materials and Methods

A CAQ certified Neuroradiologist reviewed a number of head CTA examinations that were sent to RAPID. A selection of these studies were identified in which the cover overlay CTA map-provided by RAPID to reflect relative blood vessel density on the affected side relative to the contralateral side-misrepresented the actual cerebral blood vessel density.

Results

Three unique cases are submitted which demonstrate misrepresentation of blood vessel density by the CTA color overlay map provided by RAPID. These cases include a common carotid stenosis, internal carotid stenosis and an M2 segment of the middle cerebral artery stenosis. In these cases, the 3D CTA dataset at peak arterial density was shown to overestimate the degree of contrast density over time within the affected vasculature. Had a non-peak arterial density series been sent, a markedly different relative density would have been detected.

Conclusions

In summary, we illustrate the potential for misrepresentation of cerebrovascular disease by RAPID software utilizing peak arterial 3D CTA datasets to generate relative cerebral blood vessel density map.

3219

Myelopathies: How Magnetic Resonance Imaging Can Help?

V Brito[1], K Schumacher[1], F Reis[2], P Okuda[1]

[1]UNICAMP, Campinas, São Paulo, [2]University of Campinas, Campinas, NA

Purpose

Review cases with typical and atypical findings of acute and subacute myelopathies, on magnetic resonance imaging (MRI), in a didactic and illustrative way, in order to facilitate the learning process and memorization of these patterns by radiologists in their clinical practice. The cases were selected in our archive of images and included: schistosomiasis, neuromyelitis optica (NMO), multiple sclerosis, disseminated paracoccidioidomycosis, spinal cord ischemia, spondylodiscitis with abscess and cord compression and neoplastic diseases. The MRI findings were then matched with clinical history of the patient.

Materials and Methods

All the images and medical data were compiled from patients with acute and subacute myelopathy in the Clinical Hospital of the State University of Campinas – Brazil.

Results

The underlying etiologies for myelopathy symptoms were found in 25 patients including demyelinating, infectious, expansive and ischemic injuries. In patients with MRI findings, nine presented with demyelinating disease and four with infectious etiology, which was composed by two cases secondary to discitis, one case of schistosomiasis myelitis and one case of paracoccidioidomycosis myelitis. Expansive lesion was found in nine cases of myelopathy, three of them were intramedullary lesions and the others extramedullary lesions. We saw other etiologies such as spinal cord ischemia, actinic myelitis and vasculitis, accounting for one case for each.

Conclusions

Patients with acute or subacute myelopathy may present a variable symptomatology, depending on the etiology and the neurologic localization of the finding in the spinal cord. MRI may play a key role in the accurate localization of the neurological finding, identifying the correct etiology and guiding the clinical management.

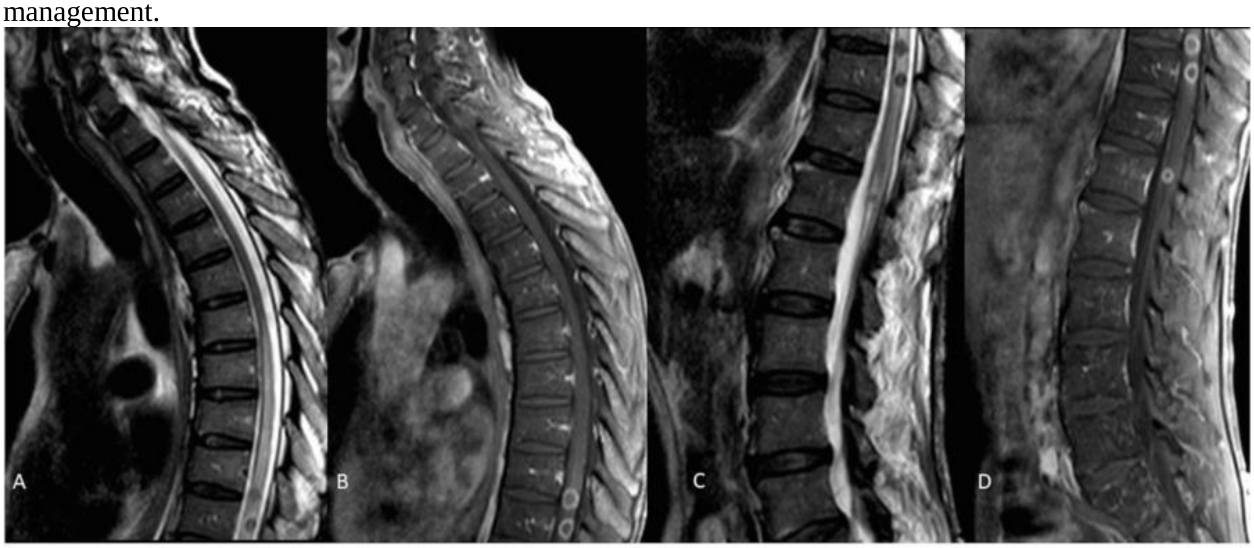

Figure 1: Male, 62 years old, gardener, with lower limb paresthesia, muscle weakness, urinary and bowel incontinence and skin lesions. The skin biopsy shows *Paracoccidioides brasiliensis*. The spine MRI shows intramedullary nodular lesions at T10-11 level with hyposignal on T2 weighted sequences (A) and peripheral enhancement after paramagnetic contrast administration (B). More intramedular lesions can be seen in lumbar spine with hyposignal on T2 (C) and peripheral enhancement after paramagnetic contrast administration (D). There is hyperintense signal on T2 weighted images at adjacent medular spine (A).

(Filename: TCT_3219_imagensasnr.jpg)

3472

Navigating the MRI "Spin Zone:" MRI Arterial Spin Labeling Perfusion with Angiographic Correlates – No Contrast Needed!

J Yetto[1], A Condos[2], M Cathey[2], A Cho[1]
[1]Naval Medical Center San Diego, San Diego, CA, [2]NAVAL MEDICAL CENTER, SAN DIEGO, SAN DIEGO, CA

Purpose
Arterial spin labeled (ASL) perfusion is a magnetic resonance (MR) imaging technique the relies on endogenous magnetically labeled blood protons as the tracer and is a proven and increasingly recognized invaluable tool for assessing a wide variety of neuropathologies, most often applied for stroke and brain neoplasm evaluation. However, ASL has many other applications and can be used as a surrogate for brain metabolism and has shown promise in multiple arenas, including the imaging evaluation of dementia as an adjunct in the localization of an epileptogenic focus. ASL is particularly promising in that it can provide non-invasive functional diagnostic imaging in the setting of neurovascular diseases without relying on gadolinium-based contrast agents (GBCA). The aim of this poster exhibit is to familiarize neuroradiologists already accustomed to interpreting dynamic vascular neuroimaging parameters using conventional angiography and/or magnetic resonance angiography (MRA) with magnetic resonance imaging (MRI) perfusion; specifically, the pseudocontinuous ASL (pcASL) method. Additionally, this exhibit is heavily focused on the physics specific to the pcASL technique.
Materials and Methods
Case-based approach featuring high resolution 3.0 Tesla (3T) MRI with pcASL and corresponding conventional angiogram. When appropriate, computed tomography (CT) and/or magnetic resonance (MR) angiography may also accompany cases.
Results
Practical review of pcASL physics followed by several-illustrative neurovascular cases. Extrapolate functional diagnostic imaging from the MRI prior to entering the angiography suite. Highlight the utility and limitations of pcASL through high-resolution side-by-side comparison of 3T MRI with MR angiograms versus conventional angiograms.
Conclusions
For neurovascular diseases, pcASL provides a non-invasive means for obtaining dynamic functional diagnostic information that highly correlates with conventional and MR angiogram findings. Understanding how to interpret pcASL is a skill best taught through illustrative cases.

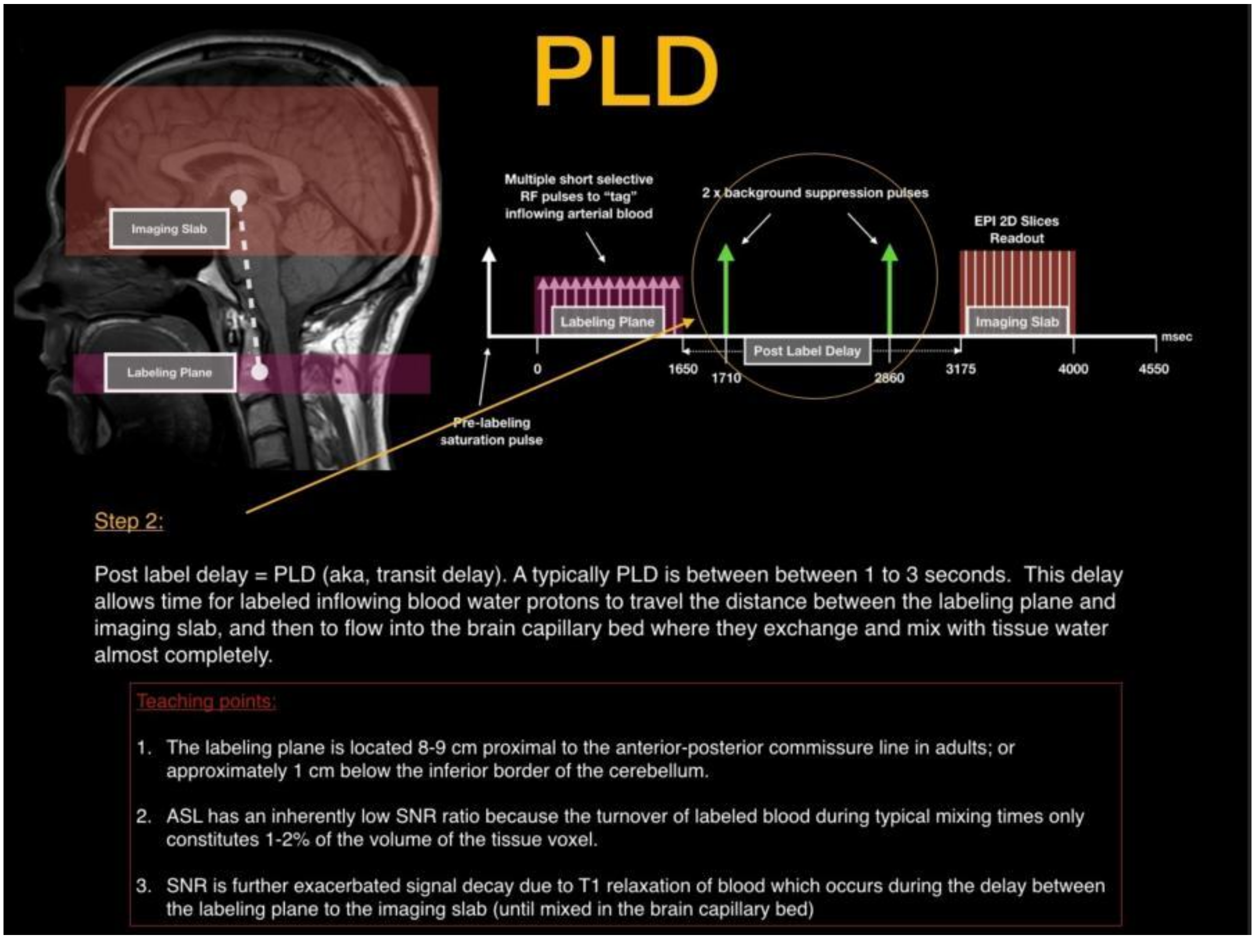

(Filename: TCT_3472_pcasl.JPG)

2404

Neuroradiological Manifestations of Pediatric IgG4-Related Disease

A Hsu[1], C Prause[2], S Kralik[1], H Tran[1]
[1]*Texas Children's Hospital, Houston, TX,* [2]*Baylor College of Medicine, Houston, TX*

Purpose
IgG4-related disease is a multisystem fibro-inflammatory disorder. Neurological manifestations have been described in the lacrimal gland, salivary glands, pituitary gland, and skull base in adults. The purpose of this exhibit is to present neuroradiological findings of IgG4-related disease in the pediatric population.
Materials and Methods
CT and MRI exams of biopsy-proven IgG4-related disease in the brain, head, neck, and spine from 1999 to 2018 were collected by a retrospective search of PACS in our children's hospital, the largest in the nation.
Results
Three pediatric cases of biopsy-proven IgG4-related disease were found. Case 1 is a 14-year-old female presenting with right ear pain. Brain MRI shows an enhancing mass in the floor of right middle cranial fossa with bony destruction and extension into ipsilateral cavernous sinus and infratemporal fossa (Fig 1); abnormal pachymeningeal and leptomeningeal enhancement of right middle cranial fossa;

intraparenchymal T2 hyperintesnity of right temporal lobe; bilateral, right greater left, mastoid enhancing soft tissues. Disease improves following surgical debulking and immunosuppressive therapy but relapses in the left mastoid bone several years later. Case 2 is a 14-year-old male presenting with right submandibular swelling. Neck CT shows enlargement and heterogeneous enhancement of submandibular glands, much worse on the right (Fig 2); multiple enhancing masses in parotid glands (Fig 3). Face MRI several months later following immunosuppressive therapy shows disease resolution in salivary glands but reveals an enhancing mass in central skull base with extension to bilateral petrous and mastoid temporal bones. Case 3 is a 7-year-old male with a history of pulmonary IgG4-related disease status post left pneumonectomy at an outside facility presenting to our institution with a left paraspinal mass on surveillance chest radiograph. Thoracic spine MRI shows a left enhancing paraspinal mass with minimal epidural extension through multiple neural foramina (Fig 4).

Conclusions

Neuroradiological manifestations of pediatric IgG4-related disease are rare based on our anecdotal experience and seen in the skull base and temporal bones in two cases (with additional meningeal and brain parenchymal involvement in one and involvement of salivary glands as early presentation in the other) and paraspinal region with epidural extension in one case.

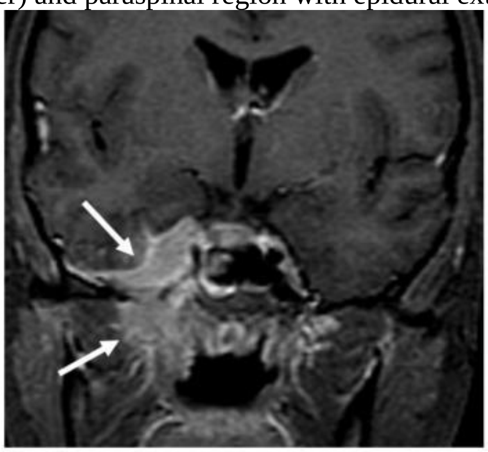

Fig 1. Lytic enhancing mass in floor of right middle cranial fossa extending into right cavernous sinus and infratemporal fossa with abnormal pachymeningeal and leptomeningeal enhancement. Involvement of bilateral temporal bones not shown on this image.

Fig 2. Abnormal enhancing right submandibular mass with perilesional edema in conjunction with heterogeneous enhancement of left submandibular gland

Fig 3. Multiple bilateral intraparenchymal parotid enhancing masses

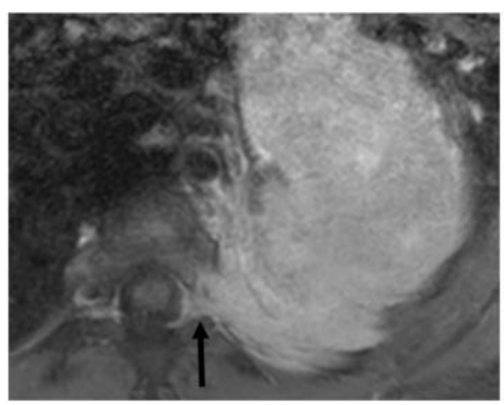

Fig 4. Left enhancing paraspinal mass with minimal epidural extension through the foramina

(Filename: TCT_2404_IgG4picture.jpg)

2540

New Imaging Patterns of Treatment Response of Brain Tumors in Cancer Patients Treated with Immune Checkpoint Inhibitors

S Prakkamakul[1], p aouad[2], C Cankurtaran[3], A Korutz[4], B Liu[3]
[1]King Chulalongkorn Memorial Hospital the Thai Red Cross Society, Chulalongkorn University, Bangkok, Thailand, [2]northwestern university, chicago, IL, [3]Northwestern University Feinberg School of Medicine, Chicago, IL, [4]Northwestern University, Feinberg School of Medicine, Chicago, IL

Purpose
Educational objectives: 1) To learn that the rising use of immunotherapy has led to appearance of new imaging patterns of treatment response 2) To understand the imaging patterns of treatment response in cancer patients treated with immunotherapy focusing on immune checkpoint inhibitors
Materials and Methods
Planned presentation: 1) Definition, mechanism of action and commonly used FDA-approved immune checkpoint inhibitors 2) Response to immune checkpoint inhibitors may be delayed or unconventional due to variations of patients' immune response, as well as their interactions with tumors. 3) Four recognized patterns of response after immune checkpoint inhibitor treatment a. Decreased size of tumor without new tumor b. Stable size of tumor followed by eventual decrease in tumor size c. Initial increased tumor size followed by eventual decrease in tumor size d. New lesion followed by eventual decrease in tumor size 4) Pseudoprogression - Initial increase of tumor burden followed by eventual reduction of tumor burden may be a flare up of inflammatory reaction or delayed effect of the treatment. The appearance of new lesions does not necessarily mean progression in patients receiving immune checkpoint inhibitors. 5) New assessment criteria (i.e. irRC, irRECIST, iRANO), and suggested follow up interval. 6) Emerging terms, for example "hyperprogression" , "unconfirmed progressive disease".
Results
N/A
Conclusions
Summary: Rising use of immune checkpoint inhibitors in cancer treatment has led to appearance of new imaging patterns of treatment responses. Radiologists' understanding of this novel treatment is helpful for imaging evaluation.

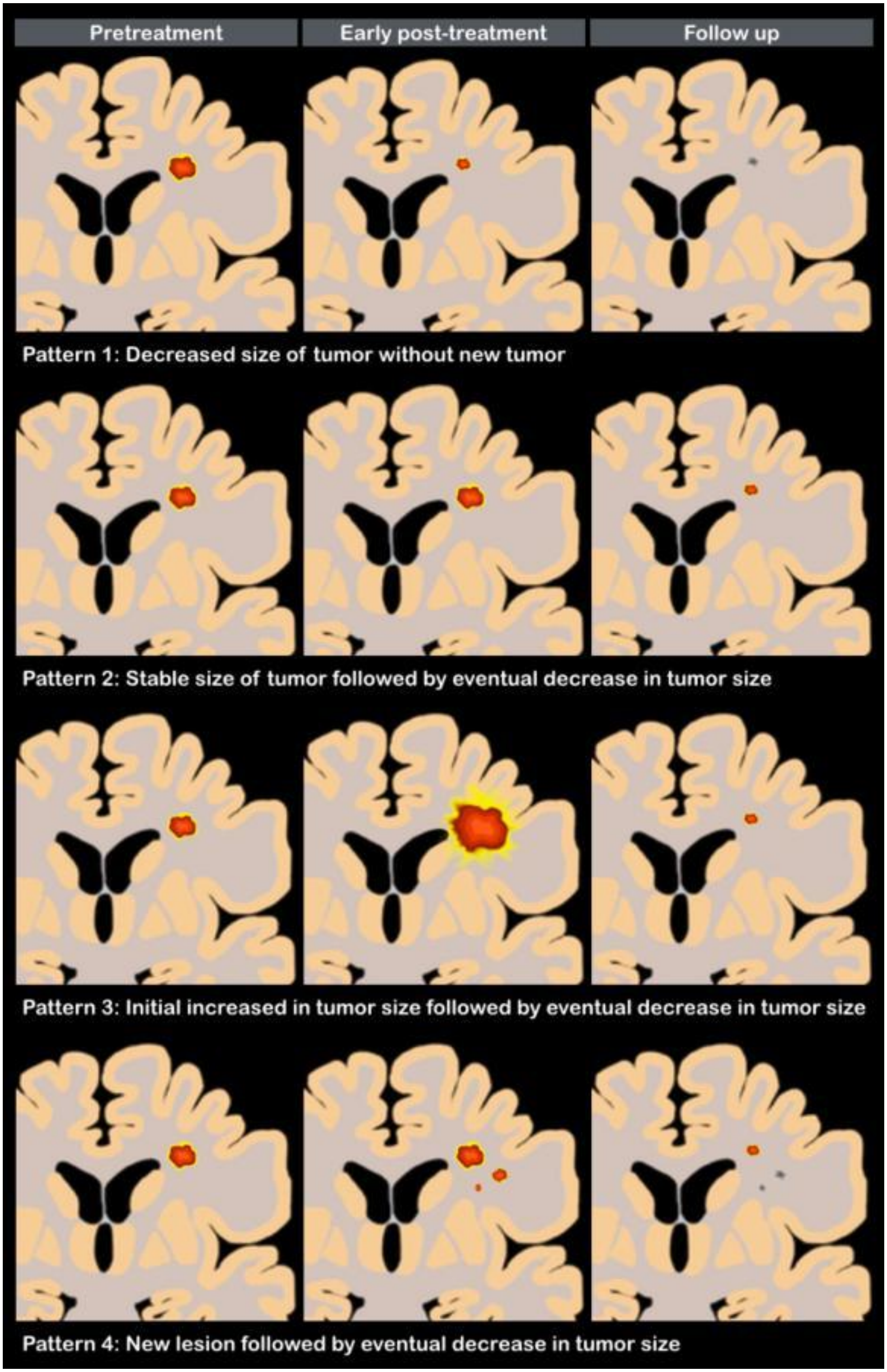
Pretreatment
Early post-treatment
Follow up
Pattern 1: Decreased size of tumor without new tumor
Pattern 2: Stable size of tumor followed by eventual decrease in tumor size
Pattern 3: Initial increased in tumor size followed by eventual decrease in tumor size
Pattern 4: New lesion followed by eventual decrease in tumor size

(Filename: TCT_2540_ASNR2019_Abstract_EdEx_figure.jpg)

2200

Overcalls: A Pictorial Review of Atypical Mimickers in Neuroimaging

G Calles[1], L Dixon[2], A Tenreiro[3]
[1]University of Texas Medical Branch, Galveston, TX, [2]UTMB, Houston, TX, [3]The University of Texas Health Science Center at Houston UTHealth, Houston, TX

Purpose
To review a series of atypical or uncommon benign processes or normal variants incidentally observed in imaging of the brain, head and neck, and spine which can be misinterpreted as pathological processes.
Materials and Methods
Over a period of a year, we collected cases that were overcalled by radiology residents or faculty at our institute as pathology. This poster focuses on atypical findings which can be overcalled by even experienced radiologists. We provide radiological imaging of a group of unusual, incidental and benign findings in CT and MRI emphasizing their radiologic appearance and an explanation for the finding.
Results
One early difficulty in radiological training is distinguishing benign entities from pathological ones. This difficulty persists as one advances in training, though the number of benign entities radiologists are aware of increases with experience. This review focuses on rarer or more unusual variants or imaging appearances, for example the external sagittal stratum mimicking band heterotopia, which mimic pathology and can fool even an experienced radiologist. Our goal is to bring awareness to these entities to avoid unnecessary follow-up imaging, procedures or undue patient anxiety.
Conclusions
Even experienced radiologists can be fooled by unusual findings they have not come across before. While the entities we discuss have been described elsewhere, they are not widely known and have not been collected in one convenient location for reference.

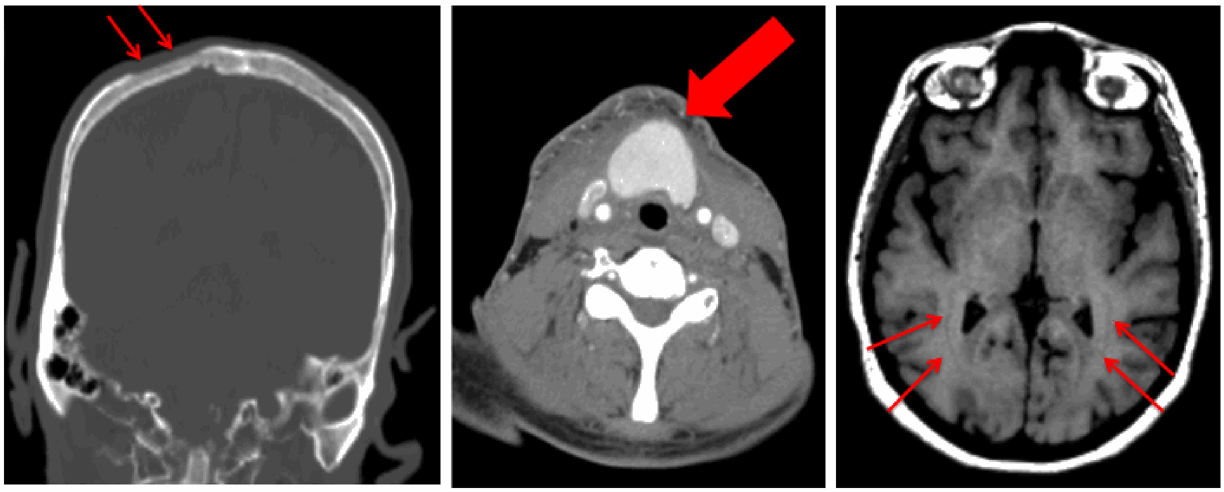

Figure 1. CT Coronal view bone window. Parietal osteodystrophy case. Focal right parietal bone thinning and erosion of outer table (Red arrows)

Figure 2. Axial view soft tissue neck CT scan with contrast. Thyroidopexy sample case. Enhancing lesion at anterior aspect of the neck which represents reposition of the thyroid gland in patient with total laryngectomy. (Red Arrow)

Figure 3. 3 Tesla MRI, Axial T1weighted sequence without contrast. External sagittal stratum sample case. Thin, linear isointense to grey matter signal paralleling the posterior horns of the lateral ventricles mimickening band heterotopia. (Red arrows)

(Filename: TCT_2200_Slide1.gif)

2649

Primary Lateral Sclerosis, an Under-Diagnosed Entity in the Setting of Progressive Weakness

A Rajput[1], J Branchcomb[2], E Velez[2], M Gupta[1], M Lin[1], J Scheibal[1], J Acharya[3], A Rajamohan[4], M Law[5], P Kim[6]
[1]USC Keck School of Medicine, Los Angeles, CA, [2]LAC+USC, Los Angeles, CA, [3]UNIVERSITY OF SOUTHERN CALIFORNIA, KECK SCHOOL OF MEDICINE, Monrovia, CA, [4]UNIVERSITY OF SOUTHERN CALIFORNIA, KECK SCHOOL OF MEDICINE, LOS ANGELES, CA, [5]Keck Medical Center of USC, Los Angeles, CA, [6]Keck School of Medicine of USC, La Crescenta, CA

Purpose
The goal of this educational exhibit is to review the incidence, prevalence, and clinical presentation of an uncommon idiopathic upper motor neurodegenerative disorder, Primary Lateral Sclerosis (PLS). Knowing the typical imaging appearances and clinical presentation of PLS will narrow the differential diagnosis substantially and clarify common misdiagnoses of demyelinating or other neurodegenerative disorders. This will allow the radiologist to correctly distinguish this entity and recommend appropriate workup and treatment.
Materials and Methods
Primary Lateral Sclerosis (PLS), is an upper motor neurodegenerative disorder caused by the absence of Betz cells in layer 5 of precentral cortex. Typically, symptoms present after the age of 50, are slowly

progressive (greater than 3 years), begin in the lower extremities, preserve overall muscle bulk, demonstrate considerable spasticity, and are pseudobulbar in nature. Most presenting symptoms may overlap with other neurodegenerative disorders such as amyotrophic lateral sclerosis (ALS), HTLV-1 myelopathy (HAM), or hereditary spastic paraplegia, making it difficult for clinicians to diagnose and provide appropriate supportive treatment early on. In addition to clinical examination, frequent imaging modalities are ordered of the brain to evaluate for underlying etiologies of patient's symptoms. The goal of our exhibit is to discuss neurodegenerative disorders, with focus on primary lateral sclerosis. Clinical clues such as specific physical exam findings and natural history of symptoms play an enormous impact in distinguishing PLS from other disorders, most considerably, ALS. We discuss a case of PLS which was not immediately diagnosed until careful clinical and radiographic correlation was made. Awareness of this rare entity is vital as prognosis and treatment approaches vary. Currently, supportive treatments that are approved for ALS are not applicable to PLS, and mainly used in individuals who are progressing rapidly.

Results

The discussion will include a review of primary lateral sclerosis including epidemiology, clinical presentations, diagnostic criteria using the Pringle criteria, imaging findings, and available treatments. Further discussion will highlight differences between primary lateral sclerosis and other neurodegenerative disorders with focus on comparison with amyotrophic lateral sclerosis. The exhibit will provide a case based review of PLS with characteristic image findings that will help a radiologist to distinguish between other possible considerations.

Conclusions

Review of this educational exhibit will enable a radiologist to be familiar with primary lateral sclerosis (PLS) and use this information to distinguish it from other more progressive neurodegenerative disorders such as ALS.

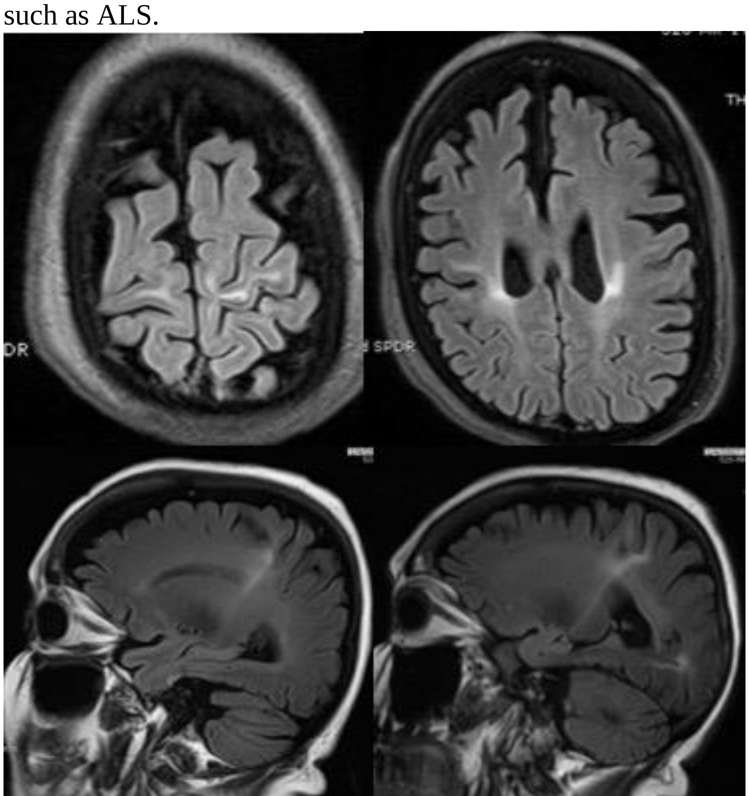

(Filename: TCT_2649_PLS.jpg)

3600

Quiz Yourself: Traumatic Injuries of the Cervical Spine

K Launier[1], A MLIKOTIC[2]
[1]Harbor UCLA Medical Center, Torrance, CA, [2]HARBOR UCLA MEDICAL CENTER, TORRANCE, CA

Purpose
There are a variety of possible presentations of traumatic cervical spine injuries that are essential for the radiologist to recognize. Lack of timely and accurate diagnosis can lead to potentially devastating injuries. This educational exhibit will focus on critical findings in the cervical spine with an emphasis on pathology appropriate for the resident level of training. Pathologies will include flexion and extension injuries, axial loading injuries, and spinal cord injuries seen on a mixture of CT and MR presented in an interactive, quiz-type format. In addition to the imaging findings, the discussion for each case will include important associated injuries and relevant appropriate recommendations for addition imaging.
Materials and Methods
A mixture of CT and MR cases will be presented that were compiled in a retrospective review of cervical spine studies performed with an indication of "trauma."
Results
The reader will enhance their knowledge of imaging findings in cervical spine trauma.
Conclusions
The reader will enhance their knowledge of imaging findings in cervical spine trauma.

2765

Review of Spinal Epidural Disease and Spinal Cord Compression: Time is Cord

M White[1], Y Zhang[2], J Cramer[2], C Johnson[2], M Keiper[3], M Punsoni[2]
[1]University of Nebraska Medical Center, omaha, NE, [2]University of Nebraska Medical Center, Omaha, NE, [3]UNIVERSITY OF NEBRASKA MEDICAL CENTER, OMAHA, NE

Purpose
Spinal epidural diseases can result in serious consequences with spinal cord damage and neurologically devastating deficits. Also, a wide variety of processes affect the spinal epidural space. Up to 5-10% of patients with systemic cancer present with spinal cord compression. Traumatic spinal epidural hemorrhage is an infrequent but serious cause of neurological injury. Spinal degeneration is ubiquitous after the age of 40 and not infrequently results in a disc herniation in the epidural space. Secondary to the confined space of the spinal canal epidural disease can quickly result in neurological complications. Clinically many of these processes have similar presentations. A neuroradiologists needs to be an expert on the anatomy and disease processes that can involve the epidural space due to the risk of spinal cord damage and the gravity of these potential outcomes.
Materials and Methods
Cases of spinal epidural diseases were collected from the authors' teaching collection and imaging database. Imaging modalities demonstrated include CT, MRI, and FDG-PET scans. Pathological correlation will be included. A review of the literature was performed and is incorporated in the presentation.
Results
The imaging characteristics of spinal epidural diseases have a number of similarities but there are also differences that can help to discriminate between them. One can evaluate if the disease process is focal or diffuse. Processes that are usually focal are synovial cysts, disc herniations and schwannomas. Processes that are usually more diffuse, traversing multiple levels, are epidural hematomas, lymphoma and epidural abscesses. Metastatic disease often presents with compression at one level but with multiple lesions

throughout the spine. It is important to evaluate for ancillary findings: disc spaces for evidence of discitis, adenopathy, lesions in liver, adrenals or other organs. CT densities, enhancement characteristics and MRI signal intensities can also help to differentiate the etiologies.

Conclusions

A neuroradiologist has the opportunity to make a critical diagnosis in cases of epidural disease and facilitate patients receiving appropriate treatments.

◀ **Fig.1 Epidural abscess**

22 y.o. male with back pain and progressive lower extremity weakness and numbness. A) Sag T1 image shows a thickened posterior epidural space with fat signal that is heterogenous and thickened (arrows). B) Sag T1-Gd fat-sat image that shows diffuse increased signal (small arrows) in the epidural space with a non-enhancing focus consistent with an abscess (big arrow). C) Sag T2 fat-sat demonstrates the epidural space to have increased T2 signal.

▲**Fig.2 Ossification of the posterior longitudinal ligament (OPLL)** (A,C) **and disc herniations** (B,D)

A) Sag T2 shows hypo-T2 anterior epidural thickening with spinal canal stenosis and CSF effacement. B) Sag T2 fat-sat shows a similar anterior epidural thickening with hypo-T2 and cord compression. There are also areas of mild increased T2 signal. The differential for the areas of T2 thickening include disc herniations, epidural blood and OPLL. Epidural abscess is unlikely given the hypo-T2. Epidural tumor is a possibility but is unlikely given no evidence of tumor in the adjacent vertebral bodies and the profound hypo-T2. OPLL on MRI can have signal intensities similar to bone marrow or be diffusely hypointense on T2 & T1. This second type is most similar in appearance to extruded disc herniations. The CTs clearly show the difference between ossification and the soft tissue of disc herniations.

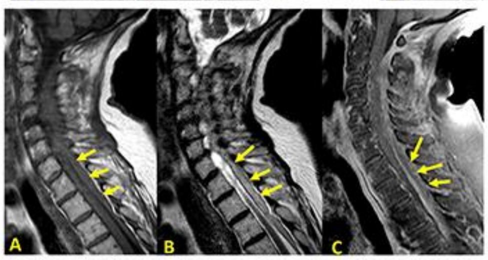

◀ **Fig.3 Epidural hemorrhage**

77 y.o. female presented with acute myelopathy. A) Sag T1 image demonstrates diffuse epidural collection that is isointense on T1. B) Sag T2 image demonstrates the epidural collection to have minimal hyperintensity compared to the spinal cord. There is diffuse spinal cord compression. Operation confirmed a spontaneous epidural hematoma. C) T1 sag-Gd fat-sat demonstrates diffuse rim enhancement and small internal foci of enhancement that can be seen with an epidural hemorrhage.

Table, Epidural Disease : Imaging Appearances and Differential ▼

Disease	T1	T2	Diffusion	T1 Gadolinium	CT	Other
Herniated disc	Similar to disc	Similar to disc	Not reported	Usually no enhancement, can have rim enhancement, rarely diffusely enhances	Soft tissue density	Can have MRI signal intensity different than the adjacent disc if a free fragment
OPLL	Similar to bone marrow or hypointense	Similar to bone marrow or hypointense	No signal	No enhancement	Bone density	Can be segmental
Epidural tumor	Isointense to spinal cord	Variable but usually hyperintense, lower signal with increased cellularity	Variable, can be restricted where there is hypercellularity	Diffuse enhancement	Soft tissue density	Look for vertebral lesions, adenopathy, lesions in other bones and organs
Epidural hemorrhage	Variable related to the age of the hemorrhage, typically iso- to hyperintense	Variable related to the age of the hemorrhage, typically hyperintense with hypointense foci	Can be hyperintense and diffusion can help to visualize, varies depending on serum versus clotted component, depends on age and state of hemoglobin	Can have multiple enhancing foci, can see rim enhancement	Blood density, variable depending on age	use susceptibility/gradient-echo imaging to evaluate
Epidural abscess	Hypointense	Hyperintense	Hyperintense	Areas of abscess will not enhance, areas of phlegmon enhance	Fluid density, can be slightly increased	look for associated discitis/osteomyelitis, rare to be due to facet infection
Hirayama Disease	Isointense	Flow voids with hyperintensity	Not described	Diffuse enhancement	Soft tissue density	Cord volume loss and increased T2 signal in spinal cord, homogenous enhancement
Synovial Cyst	Hypointense to isointense	Hyperintense predominantly, but variable	Limited data, not restricted	Rim enhancement	Soft tissue density	Facet degeneration

(Filename: TCT_2765_epiduraldiseaseimage.jpg)

3155

Spectrum of Abnormalities/Complications in the Brain on Imaging

A Jain[1], B Setty[1]
[1]Boston Medical Center, Boston University School of Medicine, Boston, MA

Purpose
To illustrate the spectrum of abnormalities/complications seen in the brain in patients with a documented/confirmed use of intravenous (IV) heroin and cocaine, also known as "speedball".
Materials and Methods
A retrospective review of our database from 2007-2017 revealed 113 patients with documented use of cocaine and heroin and having either CT brain/ CT angiogram of the head and neck/Magnetic Resonance (MR) imaging of the brain.
Results
A wide variety of secondary complications from "speed balling" were seen in the brain. Septic emboli and infarcts (territorial and basal ganglia) were the most common manifestations in this group. Other abnormalities included cerebral abscess, ventriculitis, venous sinus thrombosis, hypoxic ischemic injury, and posterior reversible encephalopathy syndrome.
Conclusions
Recreational drug use has risen at an alarming rate over the past decade in the United States, particularly the use of illicit intravenous drugs (IV) such as heroin and cocaine. The combination of the two is commonly known as "speedball" and is a popular form used by IV drug abusers. It is important for the radiologist to be able to recognize secondary complications from its use and key imaging features.

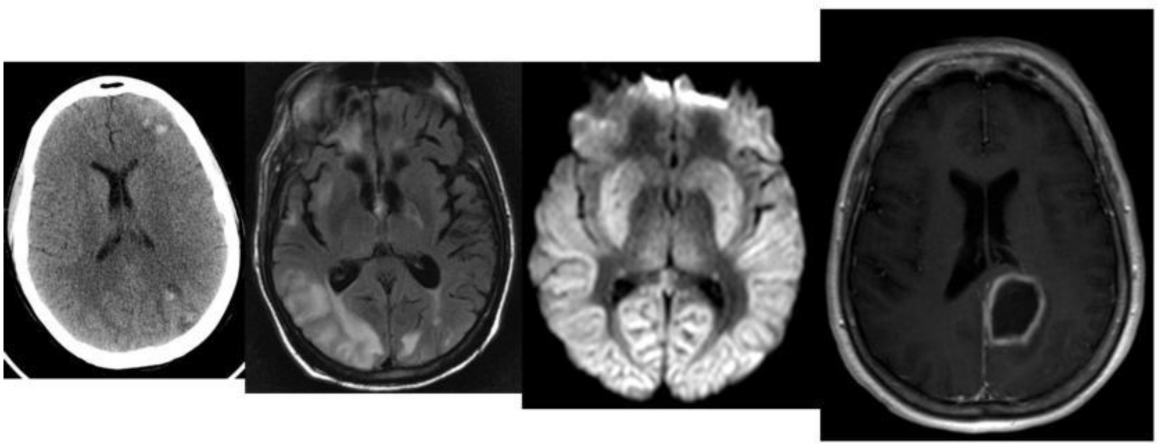

4 different patients with history of speedballing: a) septic emboli in left cerebral and right cerebellar hemisphere (not shown). b) White matter changes seen secondary to PRES which subsequently resolved c) Global hypoxic ischemic injury involving the bilateral cerebral hemispheres and the basal ganglia and d) Cerebral abscess in the left occipital lobe which was drained.

(Filename: TCT_3155_Presentation1.jpg)

3009

Structural Yin-Yang of the Brain: An Educational Review of Right-Left Torque and Regional Asymmetries Observed on Neuroimaging

D Martin[1], A Trinh[2], S Ghaderi Niri[2], V Yedavalli[3], B Lanzman[2], S Hashmi[2], T Massoud[2]
[1]STANFORD UNIVERSITY, STANFORD, CA, [2]Stanford University School of Medicine, Stanford, CA, [3]Stanford University, San Francisco, CA

Purpose
A fundamental feature in interpreting brain images is reliance on the high degree of morphologic symmetry of bilateral hemispheres. However, the brain is not perfectly symmetrical, and the small extent of natural right-left asymmetry must be taken into account when symmetry/asymmetry is used as a diagnostic cue for the presence of pathology. Neuroradiologists should be aware of the existence of normal asymmetry that could potentially confound the process of extracting abnormal asymmetry, and if a given brain structure or region can be asymmetrical so as to relate this to its function.
Materials and Methods
We review and illustrate asymmetrical brain structures that may be seen in neuroimaging.
Results
Brain structural asymmetries may be considered either rotational or pure right-left asymmetries. Many of these asymmetries are related to a uniquely human ability-language. 'Yakovlevian torque' is the tendency of the right side of the brain to be warped slightly forward relative to the left, i.e. the midsagittal plane is rotated clockwise. This may make the right frontal lobe bigger and wider, often protruding forward beyond the left frontal lobe; while the left occipital lobe becomes wider and protrudes further backwards. In keeping with this torque, the left Sylvian fissure is longer and less steep, causing a larger planum temporale. Language is lateralized to the left hemisphere and the planum temporale is heavily implicated in auditory processing. We will also review and discuss implications of right-left asymmetries in the ventricles, basal ganglia, cortex, hippocampus, and amygdala.
Conclusions
Neuroanatomical asymmetries are not random, but are distinct patterns in structural design that confer functional evolutionary advantages. Asymmetrical brain structures may at times be unexpected or puzzling on neuroimaging. This presentation will aid in identifying and understanding them for improved diagnostic interpretation, and for when constructing symmetry-based paradigms for automatic localization and segmentation of brain lesions.

2322

The Different "Faces" of Image in the Facial Aesthetic Procedures

A Wolosker[1], L De Abreu Jr.[2], A Torres[3], M Borri[4]
[1]Fleury Group Hospital and Federal University of Sao Paulo, sao paulo, -- SELECT --sao paulp, [2]Fleury Group Hospital, Sao Paulo, Brazil, [3]Fleury Group Hospital, SAO PAULO, BRAZIL, [4]Fleury Group Hospital and Federal University of Sao Paulo, sao paulo, -- SELECT --sao paulo

Purpose
The goal of this study is to report many cases of aesthetic facial procedures including injectable facial fillers (like hyaluronic acid and collagen); silicone implants; facial lifting; buccal fat pad remove; rhinoplasty and orthognathic surgery, found incidentally on radiological imaging studies, showing the usual aspects that must be known by radiologists, to avoid misinterpretation. The authors also show the main related complications.
Materials and Methods
The authors report the imaging features observed in Computed Tomography (CT) and Magnetic Resonance Imaging(MRI) of patients submitted to aesthetic facial procedures, found incidentally and as complications of the procedures. The study was performed in the past 2 years showing usual aspects and the main complications. A comprehensive search of medical literature was performed via Pubmed.
Results
Many studies has shown that aesthetic procedures can significantly improve overall quality of life. It includes the demand for facial rejuvenation procedures driven by societal ideals of youth and beauty and facial reconstruction related to congenital or traumatic causes. Our study shows the imaging features of

different aesthetical facial procedures and some of the main complications like as abscess formation, granulomas, migration of fillers , overfilling and silicone implant protrusion.

Conclusions

Aesthetic facial procedures are widely used for rejuvenation or reconstruction. This study summarizes the imaging features of common procedures and the main complications. This knowledge helps to avoid misinterpretation and the recognition and prompt management of complications.

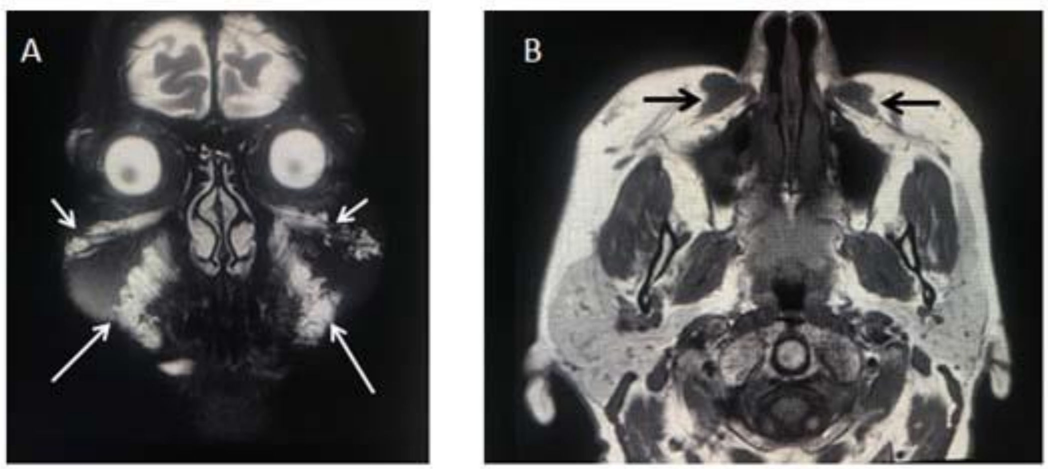

Fig. 1 - **A** - Coronal STIR MRI image shows the typical hyperintensity of the bilateral hyaluronic acid injections in the inferior orbital compartments (short arrows) and nasolabial fat compartments (long arrows) and **B** - axial T1 MRI shows the hypointense signal in the nasolabial fat compartments (arrows)

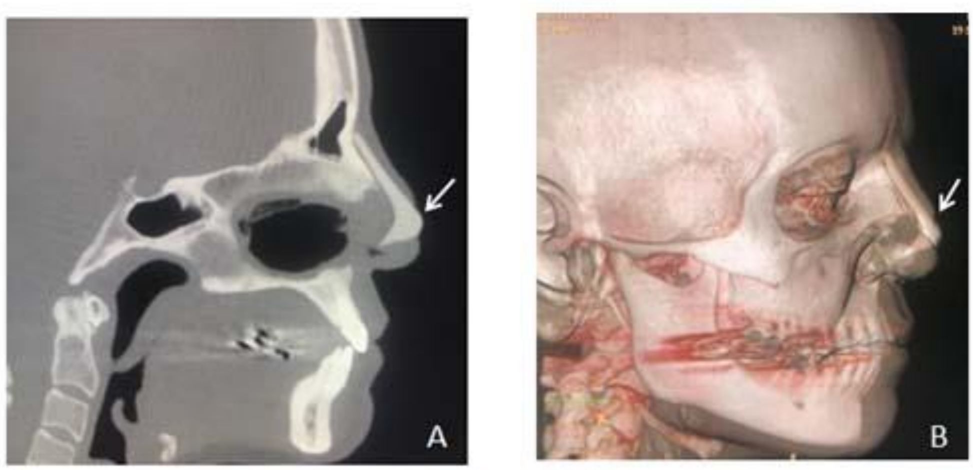

Fig. 2 - **A** - CT sagital reformatation and **B** - 3D volumetric redering showing silicone nasal implant complication with extrusion (white arrows)

(Filename: TCT_2322_ASNR2019FIG01.jpg)

2860

The Feasibility of Deep Learning Algorithm in Final Stroke Lesion Prediction Using Baseline Diffusion-Weighted Imaging Only in Non-reperfused Acute Ischemic Stroke Patients

Y Yu[1], Y Xie[1], T Thamm[1], E Gong[2], S Christensen[1], M Lansberg[3], G Zaharchuk[4]

[1]Stanford University, Stanford, CA, [2]Stanford University, Sunnyvale, CA, [3]Stanford, Stanford, CA, [4]STANFORD UNIVERSITY, STANFORD, CA

Purpose

Previous work shows that using baseline MRI, deep learning models are useful in final infarct prediction. We aim to investigate if baseline diffusion-weighted imaging (DWI) can predict final stroke lesion in acute ischemic stroke patients.

Materials and Methods

Acute ischemic stroke patients were reviewed and selected from Imaging Collaterals in Acute Stroke (iCAS) study and from DEFUSE2 study. Patients who underwent baseline MRI including perfusion-weighted imaging, diffusion-weighted imaging, angiography; and follow up imaging with angiography 24 hours after arrival and T2-FLAIR 3-5 days after stroke onset; and who had a TICI score ≤2a or no arterial recanalization within 24 hours were included. The ground truth was defined as the final stroke lesions on follow-up T2-FLAIR, which were manually delineated by readers blinded to clinical information. A 2.5 dimension U-Net model was trained using baseline DWI b1000 and apparent diffusion coefficient (ADC) as input. The model was trained based on a mixed loss function of cross-entropy and SSIM. Five-fold cross-validation was performed to evaluate the predictions and the results are reported as area under the receiver operating curve (AUC), DICE score, precision, recall, and absolute volume difference. The model prediction was also compared with clinically used threshold of Tmax > 6s.

Results

In total, 63 patients were eligible for inclusion. (30 males, age 65±16, onset-to-imaging time 288±154 min, median NIHSS 14 [IQR 11-19], 3-month mRS 4 [IQR 2-4], final stroke lesion volume 168.7±128.9 ml).Compared to Tmax >6s, the U-net model had an area under curve of 0.90±0.09 vs 0.78±0.11, dice score of 0.48±0.21 vs 0.37±0.19 ($p<0.0001$), sensitivity of 0.57±0.22 vs 0.65±0.22 ($p=0.016$), specificity of 0.97±0.02 vs 0.83±0.10, volume difference of 1.4±95.6 ml vs 82±109 ml.

Conclusions

The U-net model with DWI and ADC only as input may help estimate final stroke lesion without major reperfusion, which may be useful when perfusion scans are not available. Further validation and improvements are required.

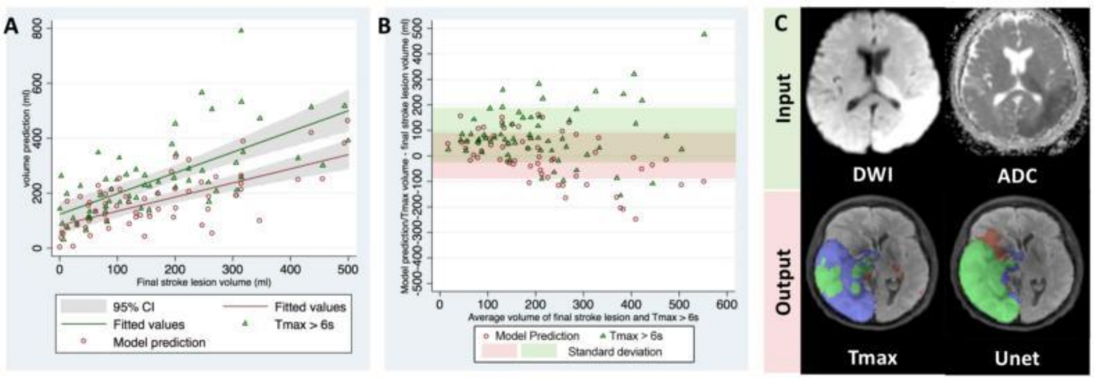

(Filename: TCT_2860_ASNR_YX.jpg)

3153

The Sphenoidal Crescent of Foramina: A Review of Normal and Variant Anatomy, and a Spectrum of Neuroimaging Abnormalities

A Trinh[1], S Ghaderi Niri[1], D Martin[2], V Yedavalli[3], S Hashmi[1], T Matys[4], N Fischbein[2], T Massoud[1]
[1]Stanford University School of Medicine, Stanford, CA, [2]STANFORD UNIVERSITY, STANFORD, CA, [3]Stanford University, San Francisco, CA, [4]University of Cambridge, Cambridge, Cambridgeshire

Purpose
The 'sphenoidal crescent of foramina' (Grant, 1948) are several endocranial skull base foramina arranged in the form of an arc sweeping from the orbital apex toward the midline, where the greater wing and sphenoid body merge, and then extending posterolaterally. We review in detail the neuroimaging appearances of the four common and the three less common foramina, as well as a spectrum of associated abnormalities depicted on cross sectional imaging. This review will be valuable for accurate diagnostic interpretation of skull base CT and MRI, avoidance of misdiagnosis in cases of lytic lesions of the skull base, accurate diagnosis of cranial nerve abnormalities, and appreciation of these foramina during image-guided skull base interventional procedures.

Materials and Methods
We comprehensively review the imaging of normal and variant anatomy and morphometry of these sphenoidal foramina, and categorize their associated abnormalities according to etiology.
Results
We first describe the imaging features of the seven sphenoidal foramina, from posterior to anterior: (1) Foramen spinosum; (2) The innominate foramen or canal of Arnold which may lie between foramen ovale and spinosum; (3) Foramen ovale, which along with spinosum form the 'high heel footprint' sign on CT, but they may be conjoined or incomplete. (4) Foramen of Vesalius anteromedial to foramen ovale; (5) Foramen rotundum; (6) Superior orbital fissure; and (7) The meningo-orbital or lacrimal foramen of Hyrtl, which is occasionally lateral to the apex of the superior orbital fissure. Much variability results from different routes taken by emissary veins connecting the middle meningeal plexus to the pterygoid plexus. We also illustrate a wide spectrum of pathologies (traumatic, neoplastic, vascular, inflammatory, and iatrogenic) specifically affecting these foramina.
Conclusions
A thorough appreciation of imaging findings for a wide spectrum of normal or variant anatomy, and pathologies affecting the sphenoidal crescent of foramina is essential for neuroradiologists and skull base neurosurgeons.

2932

Thrombotic Microangiopathy: Spectrum of Neuroimaging Findings

A Mas-Bonet[1], M Picado Valles[2], A Calleja Bonilla[3], A Moll Servera[4], C Gassent Balaguer[5], M Uriol Rivera[3], M Orozco Botero[6]
[1]Hospital Son Espases, Palma de Mallorca, Spain, [2]Hospital son Espases, Palma de Mallorca, I.picado@ssib.esslas Baleares, [3]H. Son Espases, Palma Mallorca, Balearic Islands, [4]Hospital Son Espases, Palma de Mallorca, Islas Baleares, [5]Hospital Son Espases, Palma de Mallorca, IIslas Baleares, [6]Hospital Son Espases, Palma de Mallorca, Illes Balears

Purpose
To provide a evidence based review of neuroimaging findings in Thrombotic Microangiopathy (TM). TM is a spectrum of microvascular occlusive disorders, which endothelial injury incites platelet aggregation with thrombus formation and vascular occlusion. The mechanical injury to erythrocytes results in intravascular hemolysis and schistocytosis in the peripheral blood smear. The intraluminal platelet thrombosis results in partial or complete obstruction of the vessel, thrombocytopenia and organ malfunction of variable intensity, mainly including renal impairment and central nervous system involvement. The most important forms of primary TM are Thrombotic Thrombocytopenic Purpura (TTP) and Haemolytic Uremic Syndrome (HUS). TM can also be secondary to autoimmune diseases, drugs, among others. TM is a seldom disorder, and the incidence of TM varies with the underlying diagnosis. The most frequent forms in adults are idiopathic TTP and secondary TM. Clinical manifestations are end-organ ischemia/infarction and/or haemorrhage. According to literature review, up to 60% of patients with TTP may develop neurological symptoms, as well as 25 to 40% of patients with HUS. Neurological symptoms are multiple and include focal neurologic deficits, seizure and mental status alteration. In PTT these manifestations are classically described as fluctuating-recurrent. MRI pattern typically consist in hyperintensities on T2 and FLAIR sequences, with or without diffusion abnormalities (edematous lesions or infarctions), and micro- and macrohaemorrhage. We described the lesion´s distribution in multiple locations frequently in both thalami and basal ganglia, but also cerebral cortex, white matter, corpus callosum, brainstem, and cerebellum involvement has been detected. Other findings include changes in white matter consistent with PRES syndrome, multiple punctate white-matter hyperintensities, a "beaded" appearance of large- and medium-sized arteries and venous thrombosis.

Materials and Methods
We retrospectively reported a series of 28 patients that fulfilled the criteria of TM in our institution, during the four year period (January 2015 to October 2018). Eighteen patients presented neurological symptoms, who underwent MRI exploration to evaluate the brain damage. Among them, we noted 12 cases with pathologic findings in neuroimaging. The studies were performed using a GE Signa HDxt 3T and a GE Optima MR450w 1.5T, and they included SWAN and 3D TOF sequences.
Results
We detected brain MRI abnormalities in 12 patients, who have demonstrated five different neuroimaging patterns: Haemorraghic pattern (4 cases). Brain cortical aedema (2 patients). Diffuse white matter lesions (2 cases). Vasogenic aedema suggestive of PRES (2 patients). Bilateral mesiotemporal lobe T2 hyperintensities (2 cases); just one with bilateral hippocampal atrophy. The presence of pathologic findings in imaging was a inclusion criteria for the treatment with Eculizumab in our institution. All patients with severe brain damage had both a diagnostic and a follow-up MRI, performed after being treated with Eculizumab,
Conclusions
MRI is a very useful resource to evaluate cerebral involvement in TM. Early MRI performed in patients with TM and neurological symptoms has allowed us to detect in two-third of cases brain MRI abnormalities as different image patterns, most of them revealed severe brain damage.

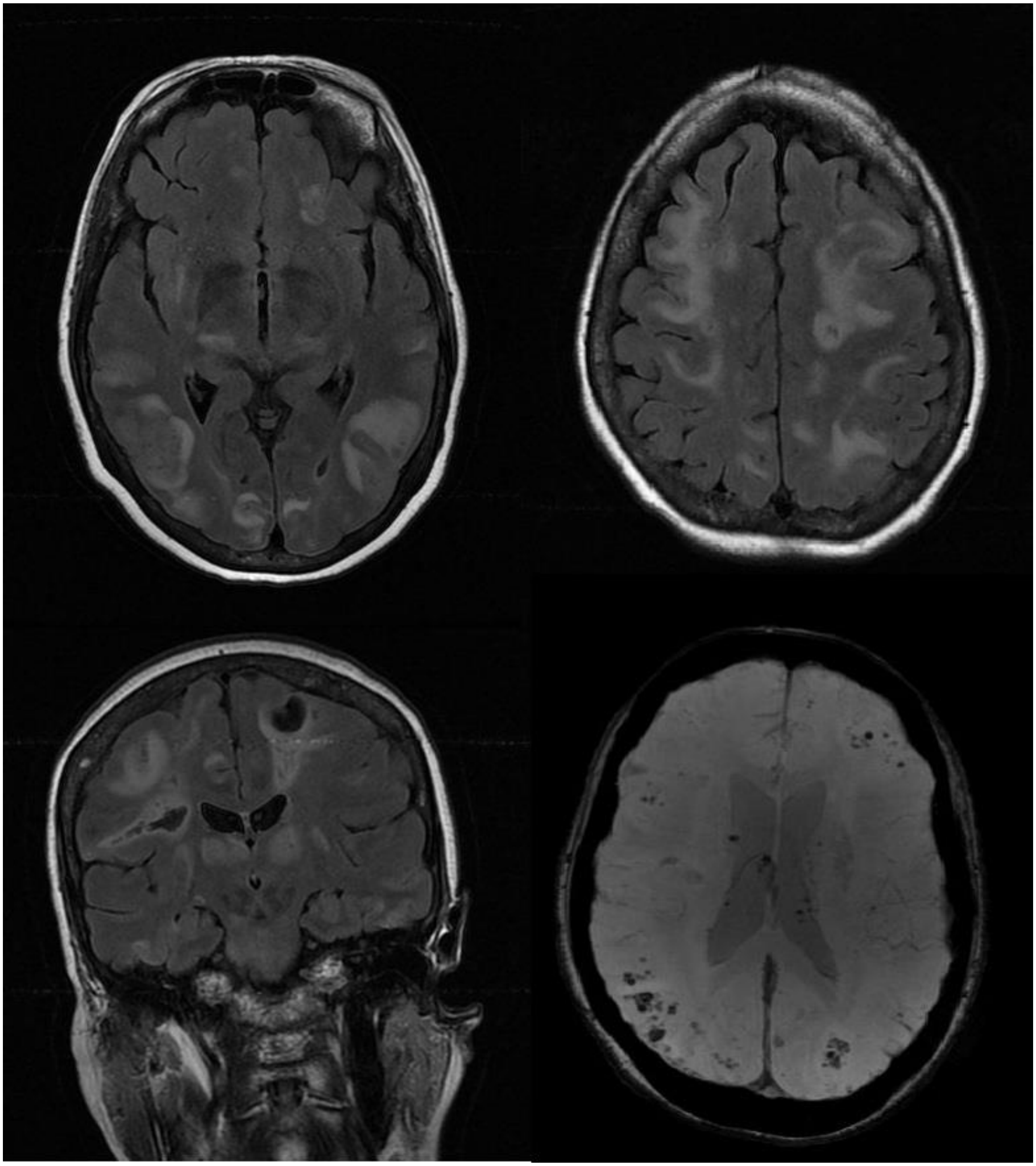

(Filename: TCT_2932_MATJPG.jpg)

2594

Tumefactive Demyelinating Lesions: the Spectrum of Imaging Appearances and the Differential Diagnosis

M White[1], Y Zhang[2], J Cramer[2], R Zabad[2], M Punsoni[2], M Keiper[3]

[1]*University of Nebraska Medical Center, omaha, NE,* [2]*University of Nebraska Medical Center, Omaha, NE,* [3]*UNIVERSITY OF NEBRASKA MEDICAL CENTER, OMAHA, NE*

Purpose
Tumefactive demyelinating lesions (TDLs) have been defined large (usually > 2 cm) demyelinating brain lesions and can be solitary or multifocal in number. TDLs present with clinical and radiologic features similar to brain tumors and cerebral infections. The purpose of this exhibit is 1. To present the clinical, pathological, and radiological (CT and MRI) features of TDLs. 2. To illustrate examples of the differential diagnostic considerations including glioblastoma (GBM), primary CNS lymphoma (PCNSL) and cerebral infections.
Materials and Methods
Patients with pathologically proven TDLs, GBM, PCNSL, cerebral abscess were included in this study. All patients with TDLs were not previously established multiple sclerosis (MS) diagnosis. Neurologic symptoms (especially those not common in MS), pathological findings, and radiological features in TDLs were compared with those in GBM, PCNSL, and cerebral infections. This exhibit will illustrate the lesion topography, lesion multiplicity, perilesional edema, mass effect, enhancement pattern, diffusion and perfusion features, and MR spectroscopy (MRS) findings for the pathologies.
Results
TDLs were mostly solitary and mainly involved the supratentorial white matter. On conventional imaging, TDLs showed perilesional edema, mass effect, and peripheral (or occasionally diffuse) enhancement, which were similar to GBM, PCNSL, and cerebral infection. However, TDLs tended to have relatively little mass effect or perilesional edema for lesion size. The enhancement pattern of TDLs were mainly in the form of an open ring. On DWI, TDLs had predominantly high diffusion center and was therefore in contrast to abscesses that was associated with restricted diffusion centrally. Although TDLs could have a rim of reduced diffusion, the minimum ADC values were higher in TDLs than in PCNSLs and also GBMs. On PWI, TDLs were predominantly hypoperfused with lower rCBV than GBMs and even PCNSLs. MRS features of TDLs included elevation of choline and lactate. Cho/NAA ratio was lower in TDLs than in GBMs and PCNSLs.
Conclusions
This exhibit enhances knowledge of the imaging characteristics of TDL and its differential diagnostic considerations. It is important to know the unique imaging characteristics of TDL to optimize early diagnosis and therapy.

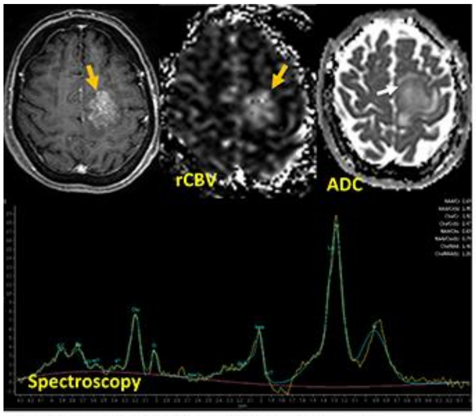

Fig.1 Tumefactive demyelinating lesion ▲
The mass (yellow arrow) in this case shows prominent irregular enhancement, high perfusion (elevated rCBV) and slightly peripheral restricted diffusion (white arrow), which are more similar to imaging features of high-grade glioma. However, there is only minimal effacement of the adjacent sulci and relatively mild surrounding edema given the size of lesion. The diagnosis of active demyelination was confirmed through biopsy.

MR spectroscopy demonstrates elevated choline and prominent lipid lactate peaks. The creatine and NAA are decreased.

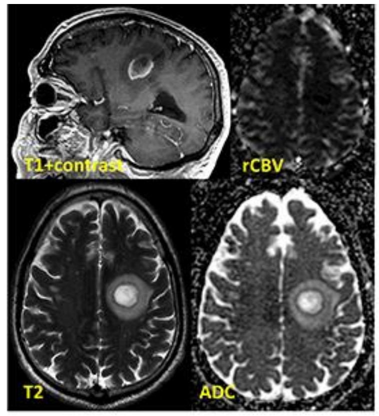

◀ Fig.2
Tumefactive demyelinating lesion

Tumefactive demyelinating lesions tend to have contrast enhancement in an open-ring pattern, high ADC values, and low perfusion. The appearances of the lesion may be diffusely infiltrative, megacystic, or Balo-like.

The demyelinating lesion in this case shows a Balo-like pattern with low perfusion, high ADC in the center, and mild mass effect. The lesion has prominent asymmetric enhancement with greater enhancement inferiorly than superiorly in the rim reflecting the advancing front of demyelination that favors the white matter side of the lesion. The ADC map shows restricted diffusion of the ring that is thought to represent demyelination as well. This is associated with a thin rim of T2 hypointensity. The restricted diffusion occurs in a minority of these lesions. There is mild surrounding edema with little mass effect.

Table, Tumefactive demyelinating lesions: Imaging Appearances and Differential ▼

Imaging characteristic	Tumefactive demyelinating lesions	Tumor	Abscess
CT without contrast	Low density	Low to increased density	Low Density
Enhancement pattern - typical	Incomplete ring	Complete ring, solid, irregular walls	Thin rim
Enhancement pattern - unusual	Balo type, solid	Along CSF surfaces (lymphoma)	Irregular – more likely in fungal
Mass effect	Absent or mild	Present	Present
Vasogenic edema	Mild	Prominent	Prominent
Perfusion	Low CBV	Elevated CBV metastasis and high grade glioma, Low CBV lymphoma	Usually mild increased, Sometimes prominently increased
Diffusion	Mixed: Predominantly elevated in the rim, minority have restricted rims of diffusion, few have normal diffusion, increased in center	Have restricted diffusion in areas of hypercellularity, more nodular or mass like restricted diffusion, but can be irregular rims of restricted diffusion	Rim has increased diffusion, Center has restricted diffusion
Spectroscopy	elevated choline and decreased NAA peaks in addition to lactate and lipid peaks	Elevated choline and decreased NAA peaks in addition to lactate and lipid peaks	Valine, leucine and isoleucine; (0.9 ppm), acetate (1.9 ppm), alanine (1.5 ppm) and succinate (2.4 ppm)
T2 hypointense border	Mild hypointensity - location of macrophages	Areas of hypointesity where hypercellularity or potentially from hemorrage	Hypointense rim from free radicals, usually not hemorrhagic

(Filename: TCT_2594_TDLfigure2019NEW-Copy.jpg)

2804

Tumors and Mimics on Perinatal Head and Brain

M Beasley[1], I Kabakus[2], M Matheus[3], M Yazdani[4]
[1]MUSC, Charleston, SC, [2]Department of Radiology and Radiological Science Medical University of South Carolina 96 Jonathan Lu, Charleston, SC, [3]MEDICAL UNIVERSITY OF SOUTH CAROLINA, MT. PLEASANT, SC, [4]Medical University of South Carolin, Charleston, SC

Purpose
The etiology of tumors and tumor-like lesions in the head and brain during the perinatal stage differs significantly from older pediatric groups. Fetal and newborn MRI studies are the ideal method to describe

and differentiate these lesions. We propose to review MRI findings of perinatal tumors and mimics covering a diagnostic spectrum ranging from intra and extra-axial neoplastic processes, migrational disorders, vascular events and abnormalities, as well as calvarial and scalp aberrations that are common in this age group and unusual for older children.
Materials and Methods
Explanatory cases from our institution's fetal and newborn MRI teaching files and review of the current literature will illustrate the most common neoplastic processes and mimics, as well as their most common clinical presentation. The cases will include desmoplastic infantile astrocytomas and gangliogliomas, atypical teratoid/rhabdoid tumors, teratomas, lipomas, fetal intracranial hematomas, fetal and neonatal infarctions, subpial hemorrhages, nodular gray matter heterotopia, encephaloceles, dermal inclusion cysts, dermal sinuses, and sinus pericranii.
Results
The distinct types of pathological processes have peculiar characteristics on clinical presentation (including maternal pathologies and newborn metabolic abnormalities), location, aggressiveness, and signal characteristics. A systematic review of the current literature and schematic/illustrative explanation of the lesions characteristics will help to organize the imaging search pattern and description.
Conclusions
Although complex and rare, the tumors and mimics of the perinatal head and brain can be accordingly classified and debriefed by their clinical and imaging features, revealing the adequate diagnosis and disease extension, which conveys a significant impact on patient care and treatment plans.

3141

Unintended Consequences: Review of New Artifacts Introduced by Iterative Reconstruction CT Metal Artifact Reduction in Spine Imaging

N Kim[1], A Kuner[1], A Grayev[2], B Otto[3], D Wayer[3]
[1]University of Wisconsin Hospitals and Clinics, Madison, WI, [2]University of Wisconsin Hospital and Clinics, Madison, WI, [3]University of Wisconsin, Madison, WI

Purpose
Review imaging artifacts that are introduced by iterative reconstruction CT metal artifact reduction (MAR) software in patients with spinal hardware.
Materials and Methods
Learning Objectives: • Understand the role of iterative reconstruction CT MAR software in evaluating patients with spinal hardware • Understand the imaging techniques underlying CT MAR software • Discuss the limitations of CT MAR software • Identify the spectrum of imaging artifacts introduced by MARS in evaluating spine CT and CT myelogram.
Results
Table of Contents: • Description of the indications and imaging techniques for CT MAR software • Review of limitations of MAR software • Overview of unexpected imaging artifacts introduced by MAR software
Conclusions
Although CT MARS is useful for reducing metal artifact when imaging patients with spinal hardware, several unintentional imaging artifacts can be introduced that radiologists should be aware of when interpreting these images.

2501

Usage of the Term "Hemorrhagic Stroke" in Neuroradiology and Neurology Literature. A Systematic Review.

M Aftab[1], M Salman[2], J Iordanou[3]
[1]Michigan State University College of Human Medicine, Flushing, MI, [2]University of Michigan - Flint, Fenton, MI, [3]Michigan State College of Osteopathic Medicine, Rochester Hills, MI

Purpose
To assess how often and in what sense the term "hemorrhagic stroke" is used in the neuroradiology and neurology literature. To determine if the term conveys any clinically precise and useful information. To understand ifalternative and better terminology which can be employed to replace the vague term of "hemorrhagic stroke" such as intraparenchymal hemorrhage, subarachnoid hemorrhage and hemorrhagic transformation of ischemic stroke. To study if this transition has already taken place in the neuroradiology literature.
Materials and Methods
An electronic literature search of major academic journals in neuroradiology such as AJNR and major publications in neurology such as the journal Neurology will be conducted. The use of the term "hemorrhagic stroke" will be assessed in each of these publications in the last 10 years. The 5 year period before and after the 2013 ASA/AHA guide on stroke terminology will be separated. The prominence of the term in the study title, body, or foot-note will also be recorded. The mode of usage of the term will be assessed, is it used to describe the etiology of the stroke? A rate comparison using Chi square analysis (also calculating the Odds Ratio) will be performed. A Repeated Measures ANOVA (either for medians or for rates) to compare the term usage over time (year by year) will be performed to assess for trends over time.
Results
The results of the Chi-squared and ANOVA analysis will be presented. This will include a descriptive analysis of the form in which the term "hemorrhagic stroke" is being used in these publications. An analysis of the pattern of usage of the term will be presented. Is the term being used as a substitute for hemorrhagic transformation and intracranial hemorrhage, or is it used to convey any other meaning? Has there been a change in stroke terminology in the neuroradiology or neurology literature after the publication of the ASA/AHA 2013 guidelines? Results will be presented in chart and graphical format.
Conclusions
Using correct nomenclature for stroke is becoming increasingly more important because of the emphasis upon prompt stroke diagnosis and therapy, including IV-tPA and the advent of endovascular options. Therefore, we propose that clear and unambiguous terminology should be used by all those involved in stroke care. The term "hemorrhagic stroke" may cause confusion in the setting of acute stroke particularly in medical training programs. When juxtaposed with ischemic stroke the term hemorrhagic stroke implies a different mechanism of stroke symptoms but this is not always the case. The current widely accepted use of the term hemorraghic stroke encompasses "ischemic" strokes with hemorrhagic transformation, and primary intracranial bleeds such as intraparenchymal or subarachnoid hemorrhages. The new 2013 ASA/AHA definition of stroke downplays the use of "hemorrhagic stroke" instead using the classification "stroke due to intracerebral hemorrhage" and "silent cerebral hemorrhage." This is a step in the right direction, which is yet to fully adopted in everyday clinical use and in the general medical literature.

2722

"Double Trouble" in Neuroimaging - Similar Imaging Features of Different Pathologies.

R Thakkar[1], C Lee[2], E Makariou[2]
[1]MEDSTAR GEORGETOWN UNIVERSITY HOSPITAL, Washington, DC, [2]Medstar Georgetown University Hospital, Washington, DC

Purpose
There are many instances where one can encounter two "identical cases" with very similar imaging findings but from different etiologies. The purpose of this educational exhibit is to highlight "key features" of the individual cases to enable differentiation between the two cases and to reach the correct diagnosis.
Materials and Methods
We are presenting multiple pairs of cases with almost identical imaging appearance, with relevant clinical history. We will discuss key diagnostic imaging characteristics and the approach to differential diagnosis with further advance imaging including MRI, MRA/CTA or cerebral angiogram wherever applicable.
Results
Clinical presentation for each pair of cases will be discussed. Similar imaging findings will be discussed with special emphasis on "key imaging" feature distinguishing two cases. Role of advance imaging with further approach to final diagnosis will be discussed.
Conclusions
This exhibit will present multiple pairs of cases with almost identical imaging findings. The characteristic diagnostic imaging features for each pair of the cases will be highlighted and approach to diagnosis discussed.

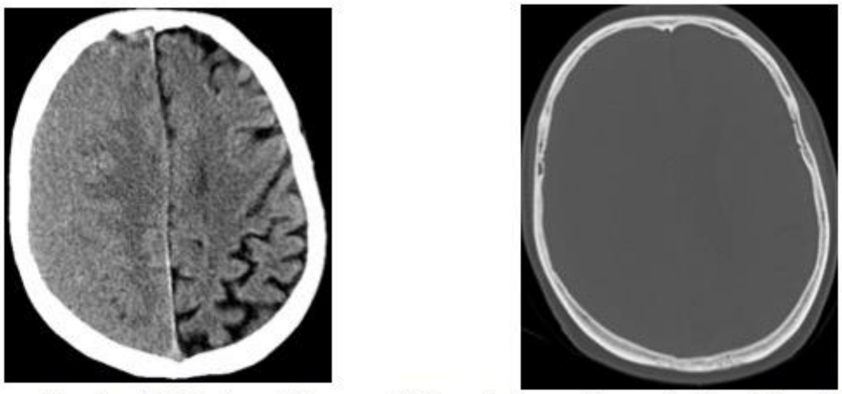

35 year old male with history of trauma. CT head – hyperdense right subdural hematoma with effacement of cortical sulci and mass effect. No calvarium abnormality. Following craniotomy there was complete evacuation of the hematoma.

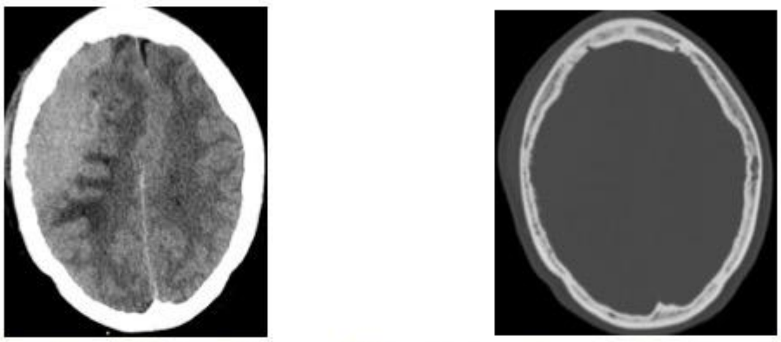

38 year old female with history of trauma. CT head – hyperdense right extra-axial mass with vasogenic edema and mild soft tissue swelling of the scalp. Calvarium - Subtle irregularity and spiculations of the inner table. Further on MRI and subsequent biopsy revealed lymphoma as the final diagnosis.

(Filename: TCT_2722_Doubletroublegraphicfile.jpg)

2920

3-D Stereoscopic Display of High Resolution Flat Panel Computed Tomography Temporal Bone Imaging

M Kiczek[1], M Solaiyappan[2], M Pearl[3], J Zinreich[1]
[1]Johns Hopkins, Baltimore, MD, [2]Johns Hopkins, Baltimore , MD, [3]Johns Hopkins University School of Medicine, Baltimore, MD

Purpose
The objective of this preliminary presentation is to show the advantages of the application of 3D stereoscopic imaging technology to high resolution flat panel computed tomography (FPCT), in the evaluation of normal and pathologic temporal bone.
Materials and Methods
Our study represents a retrospective evaluation of the temporal bones of five patients with high resolution FPCT imaging data performed on Dyna CT (Siemens) between July 2017 and July 2018. Four of these patients were considered to be normal and one had an erosion of the incus as well as superior semicircular canal dehiscence. The data from these imaging examinations was de-identified and uploaded into a 3-D stereotactic imaging (3DSI) display unit, (an advanced evolution of the Dextroscope imaging device) and virtually evaluated by board certified neuroradiologists. An essential key feature of our software is that it provides a 3D stereoscopic representation of the anatomy that can be viewed using a pair of electronic

glasses, which helps us perceive the depth of an object, just as one would naturally perceive it, naturally, in the "real-world". To date, our challenge is, to create the same effect, as we display the 3D formatted structure, created by our software, onto a "flat" paper media, without having the viewer use of electronic glasses, in a reasonably practical or economic way. Therefore the results are presented as volume-rendered images displayed on a flat surface, without the depth perception effect, and therefore a "simulated" 3D display, or if we might be allowed to say "a 2.5D display".

Results

The FPCT imaging data viewed and evaluated on the 3DSI unit provided an intuitive, clear three dimensional highly detailed evaluation of the temporal bone anatomy. Details not well evaluated on conventional temporal bone CT, on the case with pathology, were brought into clearer light. Furthermore, the ability to manipulate the imaging data in a 3D workspace provided an additional dimension and clarity to the regional anatomy and specifically the ossicular chain. The intricate anatomic architecture of the temporal bone has been investigated extensively. Most recently, ultra-high resolution computed tomography (UHRCT) techniques using 0.25 mm collimation have been used to image the temporal bone structures in greater detail. Evaluation of the temporal bone infrastructure has also been performed with high resolution flat panel computed tomography (FPCT) Dyna CT with voxel sizes ranging from 0.08 to 0.1 mm. Evaluation at this resolution produces a clear and detailed evaluation of both normal and pathologic temporal bones. Evaluation of high resolution FPCT source data augmented with 3DSI display has not been reported to date. Our objective is to show the advantage of combining these imaging technologies and show the benefit in the evaluation of the temporal bone anatomy and pathology.

Conclusions

Evaluation of this high resolution data on a 3-D stereotactic imaging display would serve to benefit several regional morphologic evaluations. The ability to manipulate the images in a 3-D workspace would great benefit to surgeons in their operative planning. Regarding the temporal bone, precise evaluation of ossicular pathology, cochlear implant position and function would be facilitated. This presentation provides a preliminary display of the above mentioned capabilities.

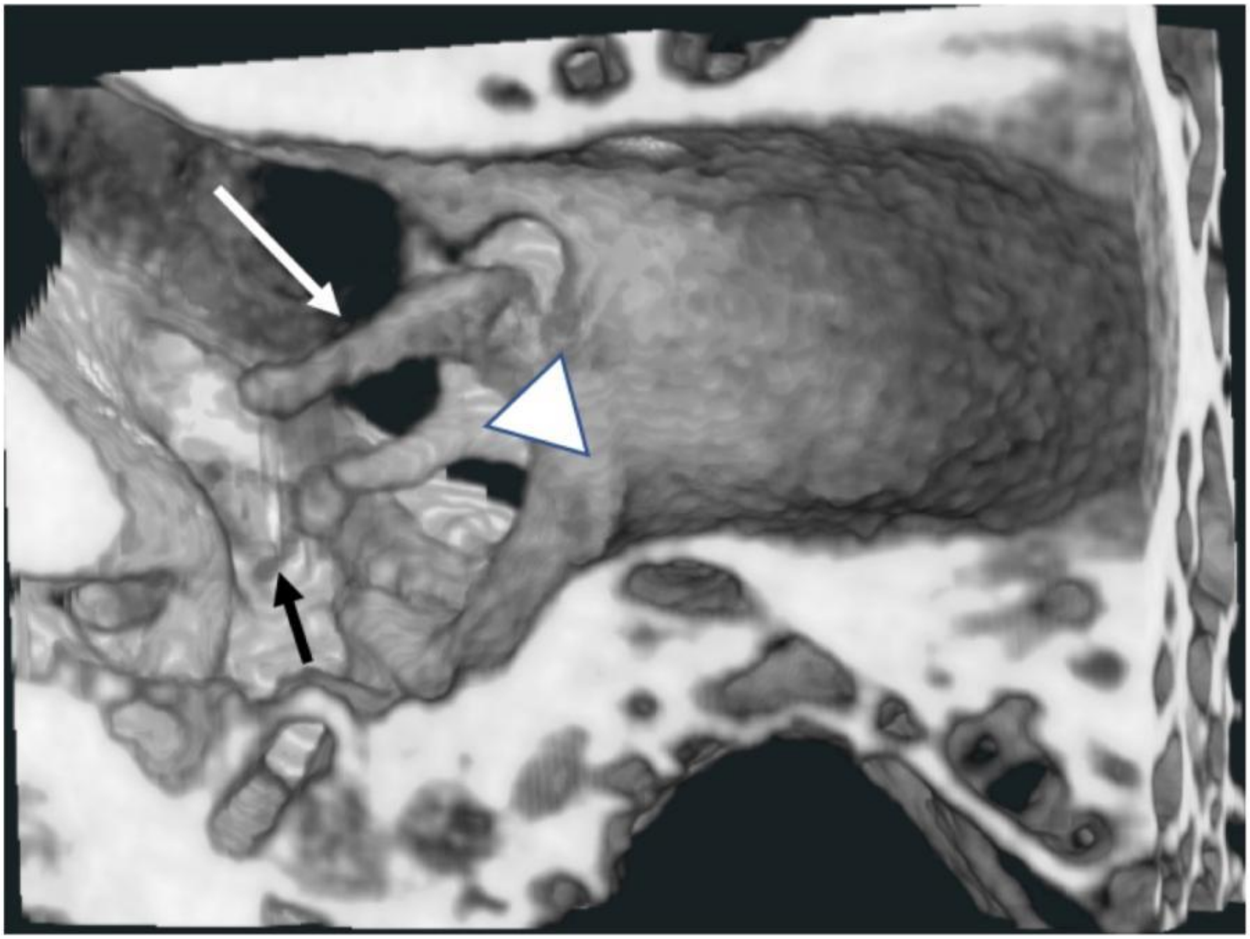

Fig 1: Cut away orthogonal 2-D projection of the 3-D volume rendered display demonstrating the relationship of the malleus (white arrow), incus (white arrow head), and stapes (black arrow).
(Filename: TCT_2920_tempbonefig1.jpg)

3375

3D Cinematic Rendering: An Emerging Tool to Visualize Cerebrovascular Anatomy and Disease

M Caton[1], W Wiggins[1], D Nuñez[1]
[1]*Brigham & Women's Hospital/Harvard Medical School, Boston, MA*

Purpose
3D cinematic rendering (3DCR) is an emerging post-processing technique that allows the user to generate and manipulate photorealistic reconstructed images (ref. 1). As educators and clinical consultants, neuroradiologists face challenges in teaching the relational anatomy of the cerebral vessels and skull base. Here, we describe the use of 3DCR in visualizing cerebrovascular pathology with a focus on building intuitive educational tools for trainees and referring clinicians.
Materials and Methods
3DCR creates life-like shadowing and surface reflection by simulating a non-uniform distribution of irradiation which can improve perception of depth and complex anatomic spatial relationships (ref. 2). We processed a range of cerebrovascular cases with a 3DCR post-processing package (Syngo.via, Forchheim,

Germany) using CTA head/neck source images. The spectrum of disease included arterial, arteriovenous, and venous lesions, as well as surgical and endovascular treatments.
Results
Using 3DCR, we developed patient-specific models highlighting both normal anatomy and cerebrovascular diseases which are presented as a series of cases. The underlying physics and technology of 3DCR are also addressed. 3DCR models were both visually intuitive and practical; images could simulate neurosurgical perspective ("virtual craniotomy") or emphasize salient imaging features (e.g. EC-IC bypass, Fig 1A). 3DCR was particularly useful for visualizing structures at the vessel-skull interface such dural AV fistulas (Fig 1B) which are difficult to assess with traditional modalities.
Conclusions
3DCR is a powerful tool for the academic neuroradiologist that complements traditional 2D and 3D imaging. Visually striking, patient-specific 3DCR images may be easier for non-radiologists to intuit. Thus, familiarity with 3DCR can energize teaching materials and aid in communication with referring clinicians, elevating the role of the neuroradiologist as educator. This exhibit will provide a technical and practical "how to" guide which will prepare the viewer to implement 3DCR in daily practice.

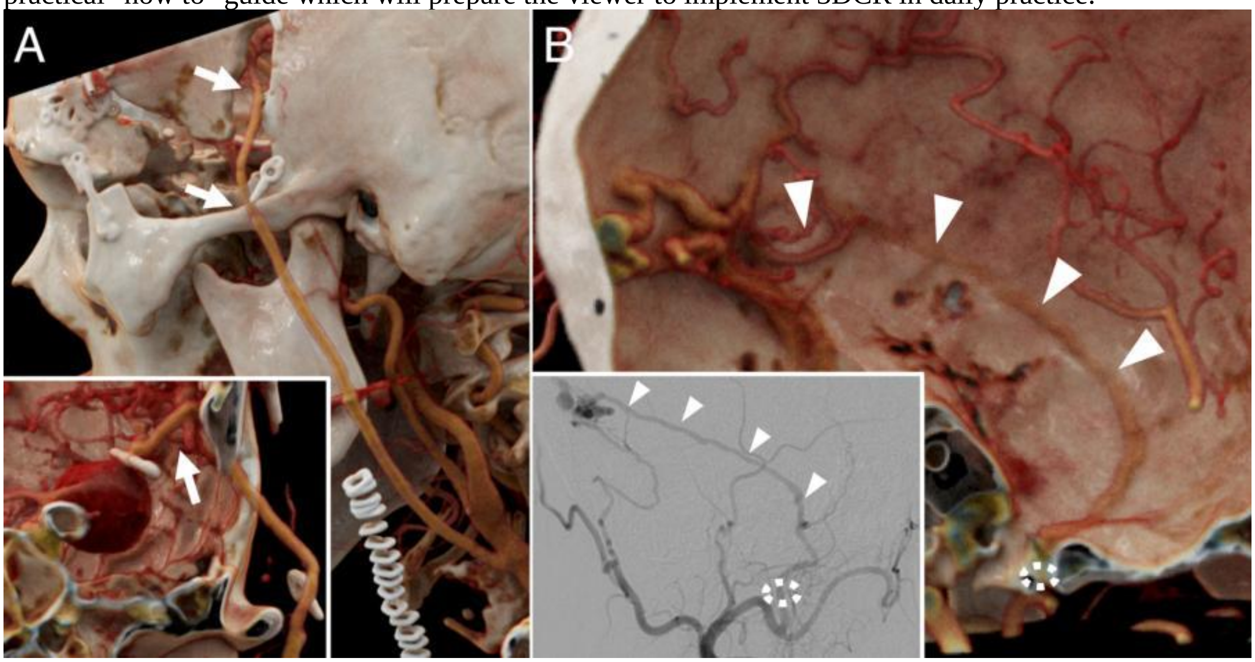

(Filename: TCT_3375_Figure1.jpg)

2232

A Far Out Approach to the Jugular Fossa and Central Skull Base Lesions

M Kulzer[1], J Ly[2], T Rath[3]
[1]UNIVERSITY OF PITTSBURGH MEDICAL CENTER - PITTSBURGH, PA, PITTSBURGH, PA, [2]UPMC, Pittsburgh, PA, [3]University of Pittsburgh Medical Center, Pittsburgh, PA

Purpose
This exhibit will present a case-based review of jugular fossa and skull base lesions treated via a far lateral approach and its variants with a focus on anatomy, landmarks, and critical areas to address on preoperative and postoperative imaging.
Materials and Methods
1) Review the anatomy of the jugular fossa and posterolateral skull base, relevant to far lateral surgical

approaches. 2) Discuss the far lateral approach skull base surgery and its variants. 3) Present cases of pathology treated via a far lateral approach and its variants.
Results
The anatomy and imaging of the jugular foramen and skull base is complex and challenging. Tumors in the jugular foramen are deep, surrounded by numerous critical vascular and neural structures and may be vascular, complicating access. Modern imaging techniques provide a detailed assessment of the jugular foramen useful for guiding treatment. There are multiple advanced surgical approaches to lesions of the jugular foramen, often requiring a combination of techniques for adequate exposure. The far lateral approach and its variants, is an effective means for addressing intradural lesions of the jugular foramen, lower third of the clivus, foramen magnum, or upper cervical spine. A thorough understanding of the anatomy of the posterolateral skull base is crucial for the radiologist and surgeon to avoid postoperative morbidity.
Conclusions
As both imaging and surgical techniques evolve, it is imperative for the radiologist to be cognizant of the potential treatments available to lesions detected in the skull base and particularly the jugular foramen. The far lateral approach and its variants, while uncommon, are a means for addressing pathology at the posterolateral skull base.

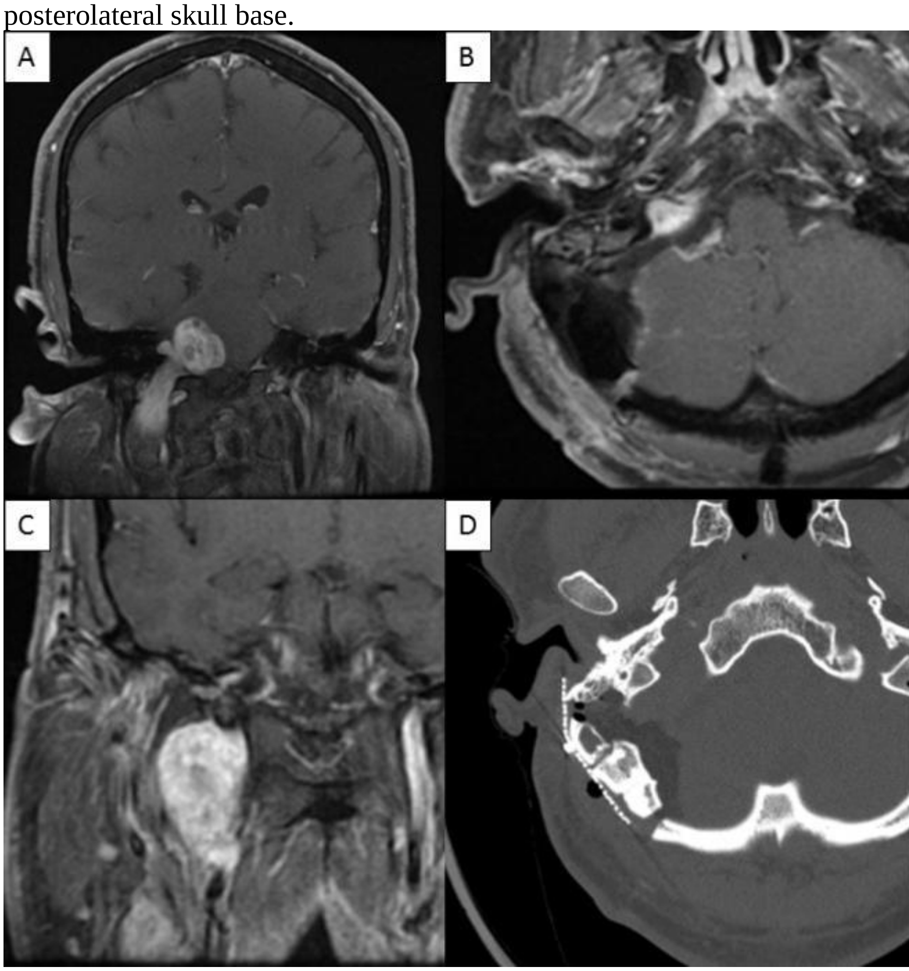

Figure 1 (A) Coronal T1 post-contrast image. Multilobulated, enhancing vagal schwannoma centered within and extending both above and below the jugular foramen causes mass effect on the brainstem. (B) Axial and (C) coronal T1 fat-supressed post contrast images and (D) skull base CT in bone algorithm demonstrate the intracranial portion of the schwannoma was resected via a right far lateral retro and transmastoid approach with resolution of mass effect on the brainstem. Residual schwannoma in the carotid space was subsequently debulked via a transcervical approach.

(Filename: TCT_2232_jugfossafigure.jpg)

3513

A Focus on the Spinal Cord: A Focused Case Based Review on Lupus Related Transverse Myelitis, Multiple Sclerosis, Neuromyelitis Optica, and Acute Disseminated Encephalomyelitis

C Smith[1], A Chouhdry[2], B Martin[1]
[1]University of South Alabama, Mobile, AL, [2]USAmc, Mobile, AL

Purpose
To describe the clinical presentations and imaging findings typical for Multiple Sclerosis (MS), Acute Disseminated Encephalomyelitis (ADEM), Neuromyelitis Optica (NMO) and Transverse Myelitis (TM). To review pertinent associations for the above spinal cord disorders to guide the differential diagnosis. To describe, compare non-contrast and contrast MR imaging findings for MS, ADEM, NMO and TM. To describe laboratory immunologic findings that may be reviewed and/or suggested to help narrow the differential.
Materials and Methods
Institutional review of 4 cases of demyelinating myelopathies including transverse myelitis, multiple sclerosis, neuromyelitis optica, and acute disseminated encephalomyelitis. Review of current literature to identify the epidemiology and pathophysiology associated with these entities.
Results
Case 1: Lupus Related Transverse Myelitis Epidemiology Pathophysiology Clinical History Imaging Findings: Sagittal and axial T2 Weighted MR images of the thoracic spine on a patient with TM and a history of lupus shows a long segment T2 hyperintense lesion expanding the spinal cord at the level of T2-T3 (left), with follow up sagittal and axial T2 weighted images demonstrating spinal cord atrophy (right). Case 2: Multiple Sclerosis Epidemiology Pathophysiology Clinical History Imaging Findings: Sagittal T2 Weighted MR images of the cervical spine in a patient with MS shows short segment T2 hyperintense lesions at the level of C1-C2 anteriorly and C2-C3 posteriorly. Post-contrast fat saturated sagittal T1 weighted image demonstrate enhancement of these lesions. Sagittal FLAIR weighted image demonstrates demyelinating plaques through the corpus callosum. Case 3: Neuromyelitis Optica Epidemiology Pathophysiology Clinical History Imaging Findings: Coronal STIR weighted image (upper left) and postcontrast coronal fat saturated T1 weighted image (lower left) demonstrate an enlarged, enhancing right optic nerve, consistent with optic neuritis, and sagittal STIR weighted image from the same patient demonstrates a long segment central spinal cord lesion extending from the medulla oblongata to the level of C4 in this patient with neuromyelitis optica. Case 4: Acute Disseminated Encephalomyelitis Epidemiology Pathophysiology Clinical History Imaging Findings: Initial Axial FLAIR weighted image (upper left) demonstrates a hyperintense lesion predominantly involving the left cerebral peduncle and causing mass effect. Postcontrast axial T1 weighted image (upper right) demonstrates corresponding enhancement in the central pons. Follow up axial FLAIR weighted image (bottom left) shows complete resolution and postcontrast axial T1 weighted image demonstrates no enhancement.
Conclusions
Comon spinal cord demyelinating myelopathies including transverse myelitis, multiple sclerosis, neuromyelitis optica, and acute disseminated encephalomyelitis have typical imaging characteristics and clinical associations. It is important to be aware of these associations to aid in narrowing and guiding the differential diagnosis.

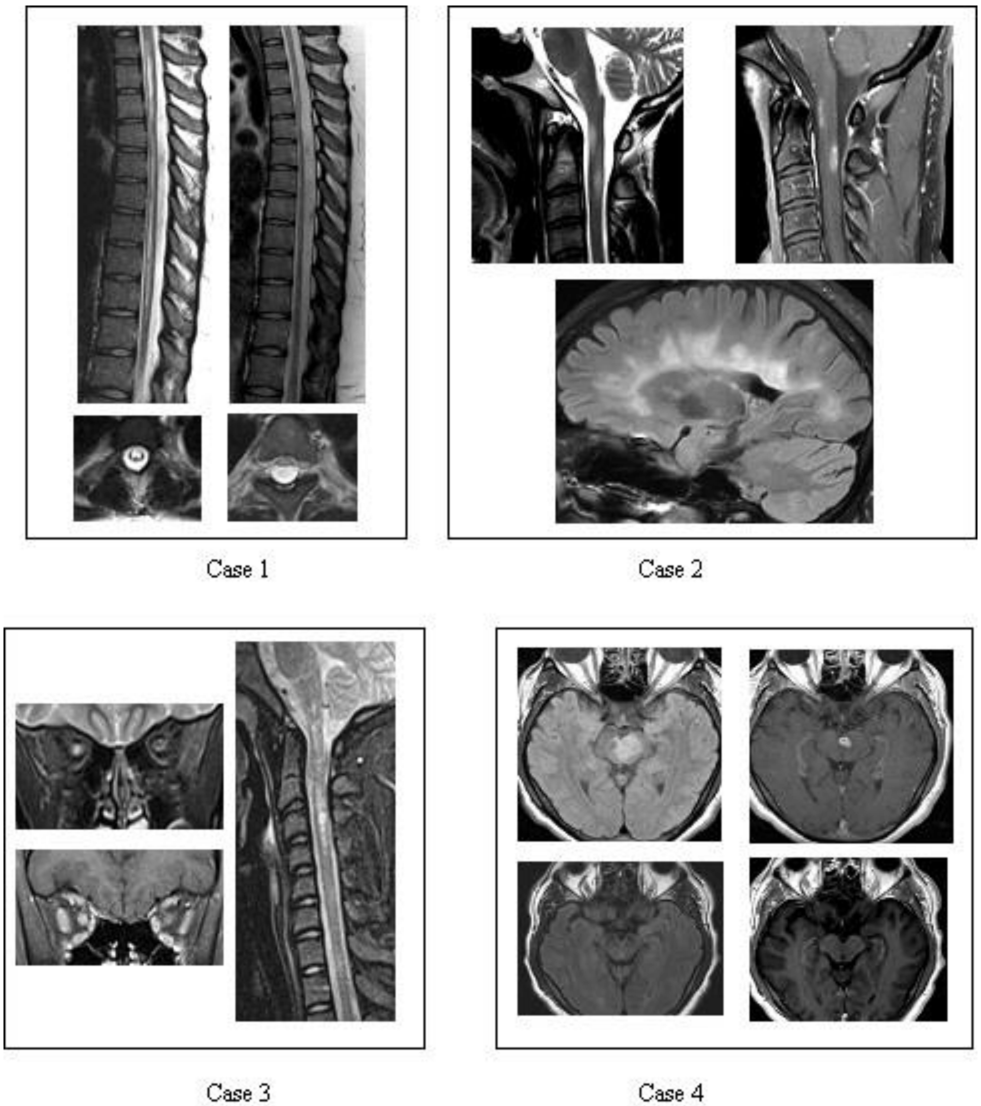

(Filename: TCT_3513_pictures.jpg)

3115

A Look Beyond the Neck Spaces: Pictorial Review of Pathology Involving the Strap Muscles.

J Hassan[1], A Soroka[1], G Weinstein[1]
[1]Tufts Medical Center, Boston, MA

Purpose
This educational exhibit will review basic anatomy of the infrahyoid muscles and provide an illustrative essay of multiple pathologies involving the strap muscles of the neck. The purpose is to establish a list of differential diagnoses a radiologist should consider when such a lesion is encountered in daily practice.
Materials and Methods
The exhibit will review appearance of multiple pathologies involving the infrahyoid muscles through a series of cases collected from our institution. Each case will provide a clinical history, a series of representative images and a brief discussion. The cases will be organized by etiology including neoplasm, vascular, congenital, trauma, iatrogenic, infectious and inflammatory.

Results
There is a variety of pathology that involves the infrahyoid neck muscles and includes infection, inflammation, congenital abnormalities, metastatic disease and iatrogenic causes amongst other etiologies. Abnormality in this region may be isolated or may represent extension of a disease process from suprahyoid or infrahyoid neck and vice versa. Metastatic disease is also an important differential consideration when history of primary malignancy is present.
Conclusions
Variety of pathology involves the strap muscles of the infrahyoid neck. Familiarity with the anatomy of this region is beneficial; clinical information accompanied with secondary imaging findings in addition to an understanding of common etiologies would help a radiologist establish an accurate list of differential diagnoses.

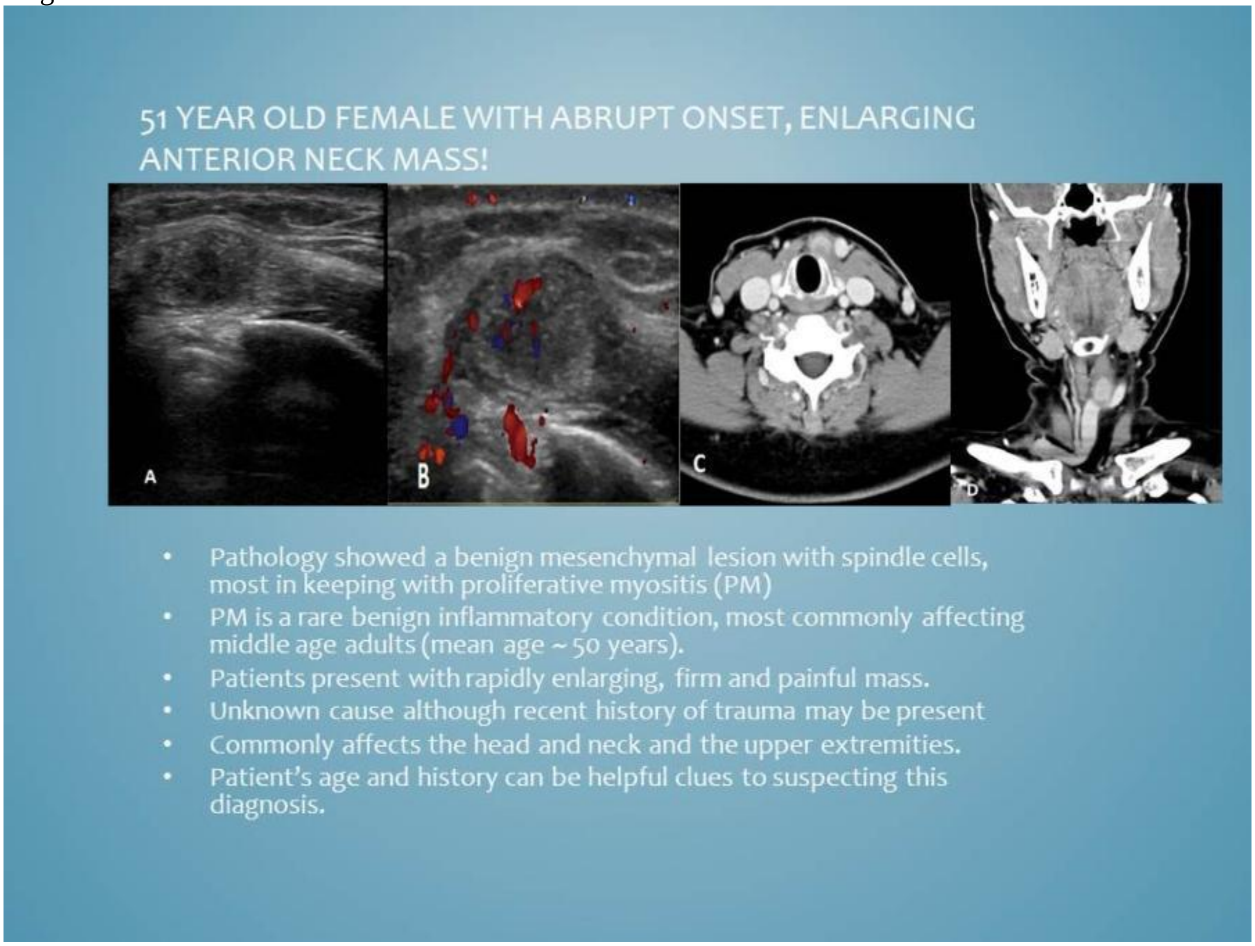

(Filename: TCT_3115_51yearoldfemalewithabruptonset.jpg)

3538

A New Era: Performing MRI Scans in Patients with Non-Conditional Cardiac Devices

M Antonucci[1]
[1]*MEDICAL UNIVERSITY OF SOUTH CAROLINA, CHARLESTON, SC*

Purpose
Implanted cardiac devices were traditionally considered a contraindication to magnetic resonance imaging (MRI). Over the past few years, the safety considerations in scanning this population have dramatically

shifted, first with the advent of specifically designed MR-conditional implants (1), and more recently, following studies underscoring the relative safety of "legacy" (non-MRI-conditional) devices. The latter include two large, recent publications which stand to revolutionize everyday neuroradiology practice (2,3). Concurrently, there has been a dramatic (but largely under-recognized) change to federal guidelines governing reimbursement for this new demographic (4). The goal herein is to review the expanding relevant data regarding MR safety, examine emerging best care practices and guidelines, and discuss new national coverage parameters.

Materials and Methods

Review of the recent literature regarding MR scans in patients with legacy devices and an examination of ways in which multidisciplinary protocol design can be facilitated at the institutional level. This framework is needed to comply with emerging mandates and to allow reimbursement under new Centers for Medicare and Medicaid Services (CMS) coverage determinations.

Results

Two large, prospective trials were recently published. These include the results of the MagnaSafe Registry with 1500 (1000 pacemaker, 500 ICD) 1.5T MRI exams & Nazarian et al's description of 880 pacemaker/ 629 ICD 1.5T MRI exams. Both studies had extraordinarily low complication rates and the latter included thoracic region exams and studies performed in pacer-dependent patients. These results, compiled data from smaller studies, and the overwhelming support obtained during a public comment solicitation period, compelled the CMS to re-examine their long-standing policy of non-coverage for MR examinations in patients with legacy cardiac devices. A final coverage determination was made this year allowing financial remuneration when scans are performed in a method designed to maximize patient safety. Our institution has incorporated a protocol addressing pre-scan device assessment, patient and technical safety parameters before and during imaging, post-MR evaluation, and report/billing compliance. This protocol will be reviewed as a model to facilitate scan performance and reimbursement at facilities wishing to expand imaging services to this growing patient population.

Conclusions

The past year has seen a revolution in MRI acquisition in patients with non-conditional cardiac devices. By understanding the science, implementing guiding policies at the institutional level, and realizing a new financial benefit to providing these services, neuroradiologists can offer valuable diagnostic imaging to an expanding group of vulnerable patients.

3289

A Tangled Tell: Post Treatment Changes of Arterial Venous Malformations (AVMs) After Different Neurosurgery Therapies

A Soroka[1], J Hassan[2], G Weinstein[3]
[1]Tufts Medical Center, Boston , MA, [2]Tufts medical center, Malden, MA, [3]Tufts Medical Center, Boston, MA

Purpose

Brain arterial venous malformations (bAVMs) are rare, generally congenital, lesions of arterial blood flow communicating directly with venous systems without intervening capillaries. Abnormal high arterial flow into the venous system can disrupt associated blood vessel walls, leading to aneurysms or subarachnoid hemorrhage (SAH). Additionally, bAVMs can cause seizures, headache, or neurologic deficit. Because of the SAH risk, bAVMs require full work up and neurosurgery consultation for management. Multiple treatment modalities exist including microsurgery, endovascular embolization, and stereotactic radio-ablation, which can be used independently or in combination. Patient traits and bAVM anatomy influence the optimal surgical approach, and patients are best served by neurosurgery teams with expertise in multiple therapies and strong interdisciplinary ties.

Materials and Methods
Brain AVMs have specific imaging characteristics multiple imaging modalities including NCCT, CT angiography, MRI, MRA, and digital subtraction angiography (DSA). The diagnostic radiologist needs to be effective in identifying bAVMs and communicating the meaningful findings that initiate neurosurgical planning. Moreover, the radiologist should proficiently understand the post treatment changes of the various neurosurgical methods. In this way, the radiologist can provide information that the bAVM is resolving appropriately or alert the neurosurgeon to adverse complications. This educational review highlights the diverse specific findings which occur after treatment of bAVMs by different modalities. Cases are organized in sequence from acute presentation to full evaluation to post treatment followup. This provides broad perspective. Possible treatment complications are discussed.
Results
Images are obtained from multiple cases at Tuft Medical Center. Emphasis is placed on endovascular embolization, treating associated aneurysms, and Gamma knife radiosurgery. This review facilitates understanding of AVM disease resolution and possible adverse complications after neurosurgery treatment, including AVM persistence, radiation induced gliosis, and adverse tissue necrosis. Associated image: Example bAVM and treatment changes. Healthy young adult presents with headache and SAH on NCCT. CTA (A) and DSA (B) demonstrate parietal occipital lobe AVM and P1 aneurysm (arrowheads). (C) T2 MRI, AVM demonstrates flow voids. (D) Post Gamma knife, AVM is decreased and there is radiation induced gliosis.
Conclusions
Understanding changes in bAVMs after various neurosurgical interventions is an essential skill for diagnostic radiologists.

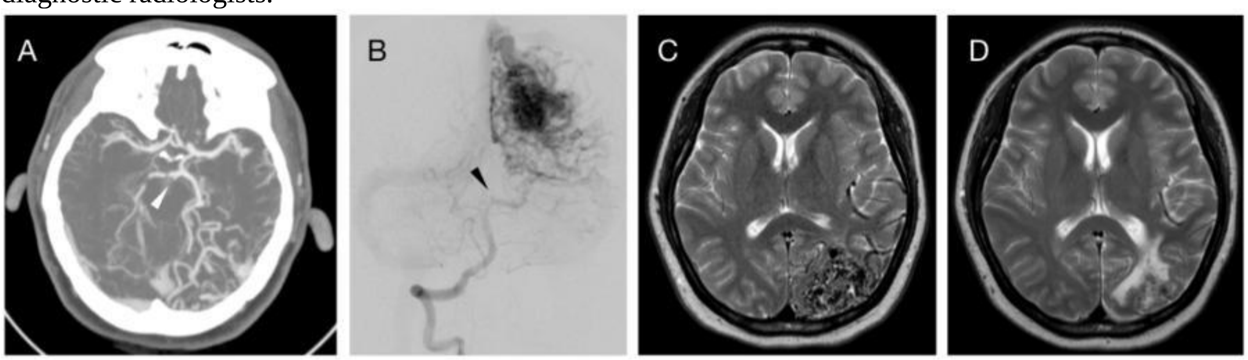

(Filename: TCT_3289_SorokaAVMCase.jpg)

3267

Acute Arterial Ischemic Stroke in Children

P GOYAL[1], J Sapire[2], G Thomas[3], A Malhotra[4], p Nepal[5], J Almast[6], R Mangla[7]
[1]St. Vincents Medical Center, Bridgeport, CT, [2]St. Vincent's Medical Center, Bridgeport, CT, Bridgeport, CT, [3]St Vincent's Medical Center, Bridgeport , CT, [4]YALE UNIVERSITY SCHOOL OF MEDICINE, NEW CANAAN, CT, [5]St. Vincent's Medical Center, Bridgeport, CT, [6]Univeristy of Rochester, Rochester, NY, [7]SUNY upstate, syracuse NY, NY

Purpose
Unlike adult stroke population, there are differences in clinical manifestations, stroke mechanism and risk factors in childhood acute ischemic stroke (AIS). There are numerous causes of childhood ischemic stroke. Prompt diagnosis of AIS is essential to limit injury and prevent recurrent stroke. This presentation will illustrate key imaging characteristics of various causes childhood AIS, and the specific role and use of imaging modalities for providing an accurate diagnosis and lesion localization when appropriate.

Materials and Methods
Multiple examples of childhood acute ischemic stroke resulting from various etiologies were reviewed with various imaging modalities. We will highlight distinguishing imaging characteristics and elucidate key imaging findings that are of particular use to the clinician.
Results
For healthcare providers, the ability to distinguish between varying causes of childhood AIS carries a major prognostic implication for acute management and secondary stroke prevention as well as screening for systemic complications and counseling.
Conclusions
We have described the imaging and clinical features of childhood AIS that may allow trained neuroradiologists and neurologists who are non-experts in childhood AIS to generate a reasonable differential diagnosis.

2572

Acute Viral Encephalitis Neuroimaging Spectrum: Clinical Correlation

A Kirsch[1], F Memon[2], A Wang[3], A Krishnan[4], R Silbergleit[1], K Barry[5], M Al-Hakim[1]
[1]Beaumont Health, Royal Oak , MI, [2]William Beaumont Hospital, detroit, MI, [3]BEAUMONT HOSPITAL, ROYAL OAK, MI, BLOOMFIELD HILLS, MI, [4]OAKLAND UNIVERSITY WILLIAM BEAUMONT SCHOOL OF MEDICINE, TROY, MI, [5]William Beaumont Hospital, royal oak, MI

Purpose
Viral encephalitis can be a challenging diagnosis. Neuroimaging guides diagnosis, early intervention, and improves clinical outcomes. We present classical imaging features of common and uncommon cases of viral encephalitis.
Materials and Methods
CT and MRI brain imaging findings were reviewed from confirmed cases of viral encephalitis. Findings will be discussed for each etiology of viral encephalitis including herpes simplex virus (HSV), West Nile, and influenza encephalitis, and progressive multifocal leukoencephalopathy (PML).
Results
HSV encephalitis presents with abnormal signal in the temporal lobes, insular cortex, and limbic region on MRI. PML presents in immunocompromised patients with involvement of U-fibers and T2 prolongation in subcortical white matter. MRI in West Nile encephalitis demonstrates T2 hyperintensity in the basal ganglia, brainstem, and mesial temporal lobes. MRI findings in influenza encephalitis is not well studied and may demonstrate multifocal areas of diffusion restriction with corresponding low T1 and increased T2 signal abnormality involving bilateral hippocampi, periaqueductal gray matter, and superior colliculus.
Conclusions
The cause of encephalitis may be unknown in some patients, although it is often viral in etiology. Neuroimaging can identify potential complications and differentiate from other causes of altered mental status. Neuroradiologists should be aware of these findings to determine a diagnosis in an efficient manner.

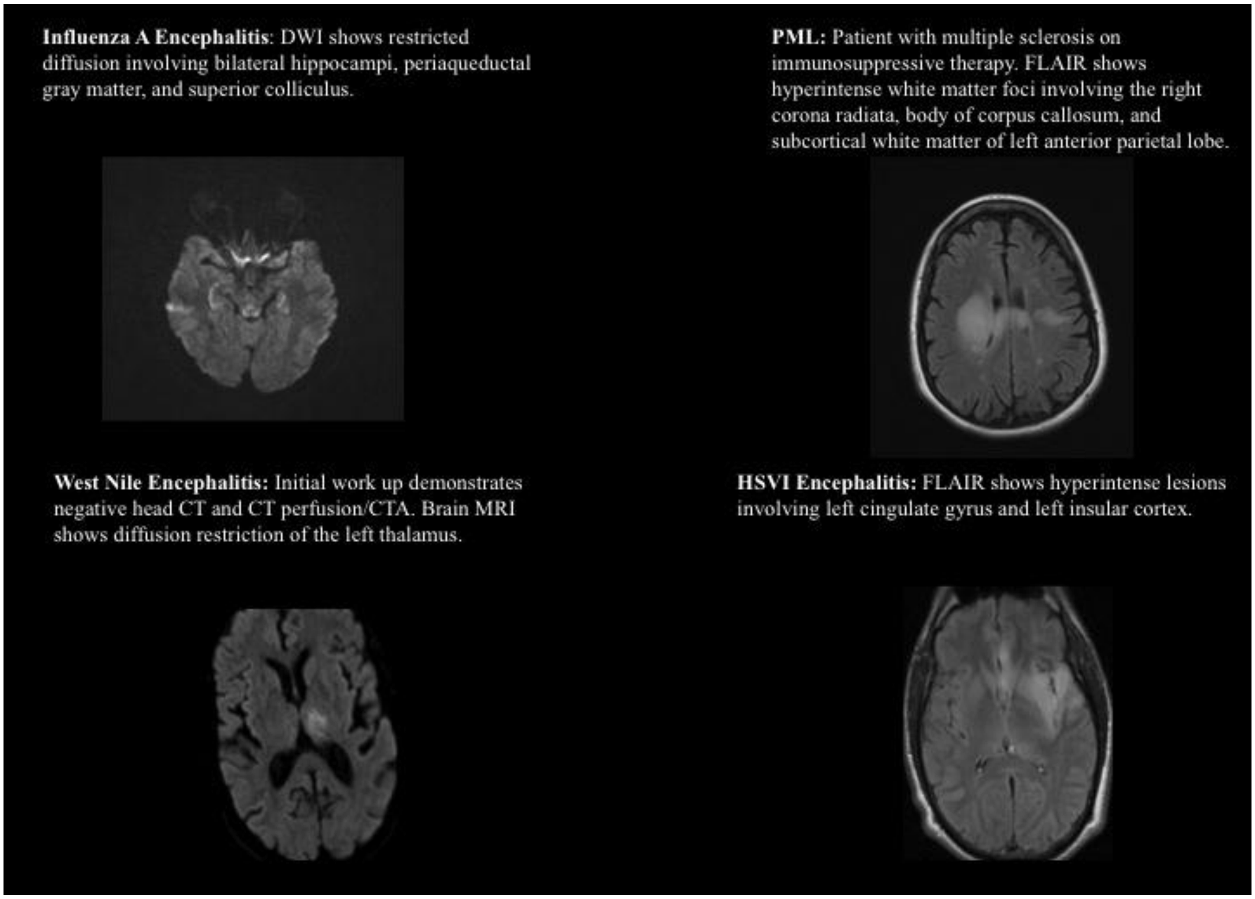

(Filename: TCT_2572_CasesFINAL.jpg)

3379

Advanced Imaging for Neurosurgical Planning: A Single Academic Medical Center Experience

L Marple[1], C Raji[2], S Keefe[1], J Shimony[3], M Miller-Thomas[4], T Benzinger[5]
[1]Washington University in St. Louis, St. Louis, MO, [2]Washington University in St. Louis, ST LOUIS, MO, [3]Washington University School of Medicine, Saint Louis, MO, [4]Mallinckrodt Institute of Radiology, St. Louis, MO, [5]Washington University in St. Louis, Saint Louis, MO

Purpose
The purpose of this presentation is to provide an overview of the functional neuroradiology clinical pipeline for neurosurgical planning as part of the Mallinckrodt Institute of Radiology advanced imaging service at Washington University School of Medicine and Barnes-Jewish Hospital.
Materials and Methods
In 2017, a total of 318 presurgical planning exams were post-processed using the following pipeline at Washington University. Each patient with a malignant eloquent cortical lesion managed by neurosurgical intervention is scanned under one of two pre-surgical, advanced functional neuroimaging protocols on a 3-Tesla Siemens scanner (PRISMA, Trio, Skyra): a resting-state protocol (rs-fMRI) and a resting-state and task-based protocol (tb-fMRI). Both protocols contain a 3D T1-weighted magnetization prepared rapid gradient echo (MPRAGE) sequence, two resting-state blood oxygen level dependent (BOLD) functional magnetic resonance imaging sequences, a susceptibility-weighted (SWI) sequence, a fluid-attenuated inversion recovery (FLAIR) sequence, a perfusion sequence, a T2-weighted sequence, a

diffusion tensor imaging (DTI) sequence, and a post-contrast T1-weighted sequence. The tb-fMRI protocol utilizes a dedicated task presentation system and processing software to administer finger tapping, word generation, verb generation, and visual stimulation task paradigms. The rs-fMRI analysis is performed using a previously trained machine-learning algorithm, a multi-layer perceptron, for identifying resting-state networks on an individual basis as described by Hacker et al. (2013). Task-based fMRI (tb-fMRI) analysis is performed using commercial fMRI processing software. Seed-based tractography analysis is performed using a commercial neurosurgical planning software package. Three-dimensional maps of corticospinal tracts, arcuate fasciculi, optic radiations, and both resting-state and task-based (if acquired) motor, language, and visual networks are created and utilized for both preoperative planning and intraoperative navigation.

Results

Figure 1 shows an example of tractography and fMRI networks in a single patient. By utilizing advanced imaging techniques such as DTI and BOLD fMRI, the radiology and neurosurgery departments at Washington University collaborate to achieve maximal tumor resection while minimizing the risk for post-surgical motor, language, and visual deficits. Because rs-fMRI is not dependent on patients' ability to perform a task, eloquent cortex mapping is possible in patients with paralysis, aphasia, and altered mental status. The utility of rs-fMRI is not compromised when patients are scanned while under general anesthesia, thus enabling populations who cannot typically tolerate MRI (claustrophobia, young age, etc.) to be scanned.

Conclusions

The development and continuous improvement of an imaging pipeline for neurosurgical planning at our institution enables maximal tumor resection while minimizing risk of post-surgical deficits in patients with malignant eloquent cortex lesions.

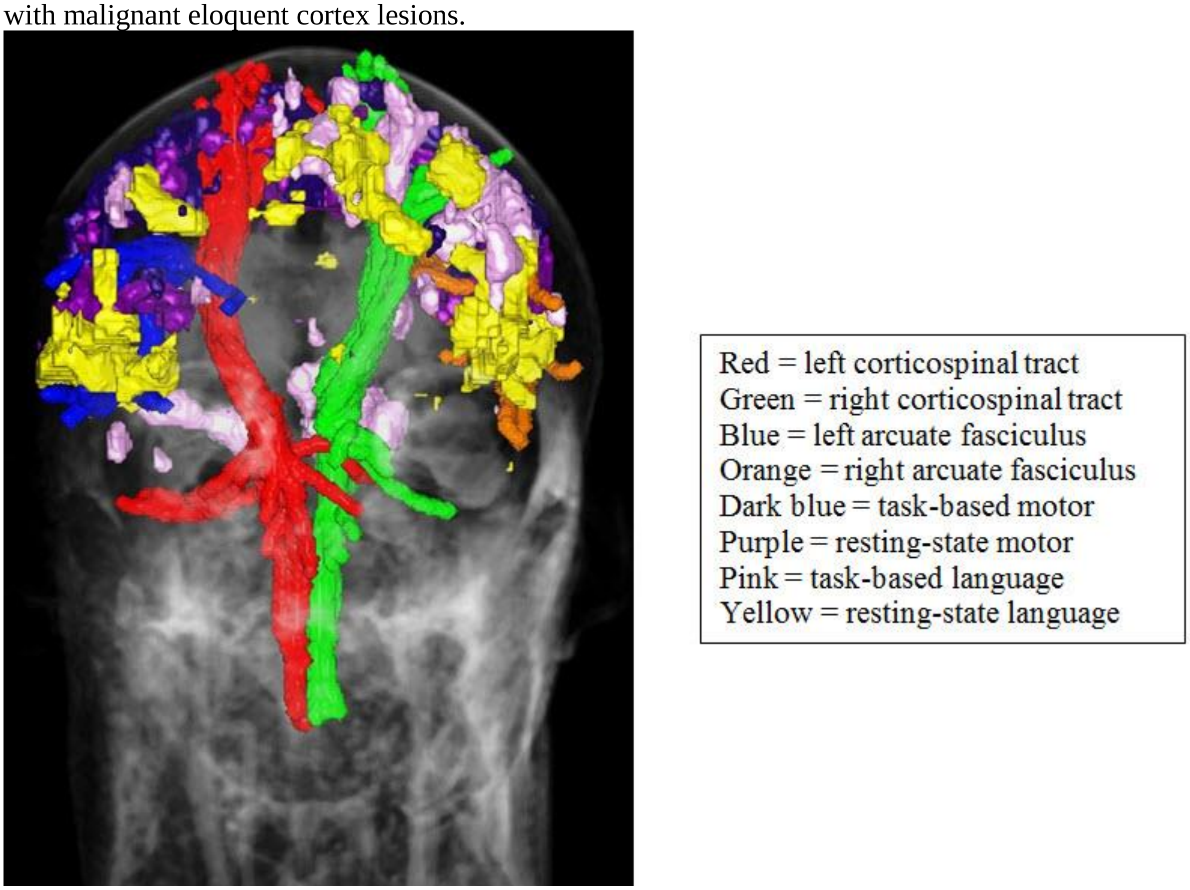

(Filename: TCT_3379_AI_Workflow_Abstract_Figure1.jpg)

3528

Advanced Imaging of the Larynx

J Ortiz Jimenez[1], E Yu[2], R Forghani[3]
[1]JEWISH GENERAL HOSPITAL & MCGILL UNIVERSITY, MONTREAL, QC, [2]University of Toronto, Toronto, Ontario, [3]JEWISH GENERAL HOSPITAL & MCGILL UNIVERSITY, COTE ST LUC, QC

Purpose
The larynx is a complex structure with a critical function that is composed of different cartilages, muscles, and membranes. Optimal evaluation of laryngeal pathology requires familiarity with its anatomy, variants that may pose a diagnostic challenge, and advanced imaging techniques that can be used for characterizing pathology and staging disease.
Materials and Methods
An interactive electronic presentation will be used to review the imaging anatomy of the larynx, familiarize the reader with important variants, review TNM staging using the 8th edition of the AJCC manual, and briefly overview the common surgical and non-surgical approaches used for treating squamous cell carcinoma of the larynx. Thereafter, different imaging techniques (single energy CT, dual-energy CT, MRI) will be reviewed for optimal evaluation and staging of laryngeal pathology.
Results
Knowledge of anatomy, anatomical variants such as variable ossification of the thyroid cartilage, TNM staging, and different approaches and selection criteria for management of laryngeal squamous cell carcinoma is pivotal for an optimal and clinically relevant diagnostic evaluation.
Conclusions
This interactive presentation will provide the reader with the necessary knowledge to perform a comprehensive, clinically oriented advanced imaging evaluation of the larynx.

3007

All About the Facial Nerve: A Detailed Review of the Facial Nerve and its Relationship to Parotid Gland Pathology and Surgery

J Ball[1], E Flores[1], E Lindsey[1], J Krumholt[1], J Gupta[2], D Casey[3]
[1]LSUHSC New Orleans, New Orleans, LA, [2]Southeastern Veterans Healthcare Administration, New Orleans, LA, [3]LSUSHC New Orleans, New Orleans, LA

Purpose
This electronic educational exhibit provides an extensive review of parotid gland pathology, including cases from our institutions. The exhibit places specific emphasis on the relation of the primary parotid lesions to the underlying facial nerve in order to help the viewers learn to produce reports that are valuable to the surgical team's preoperative planning. The imaging examples of parotid pathology include infectious, neoplastic, and developmental processes. It has been shown that three dimensional high-resolution magnetic resonance imaging can show the spatial relationship between the intra-parotid facial nerve and adjacent structures. Our ultimate goal is to decrease morbidity secondary to intra-operative facial nerve injury by offering detailed information within our reports during the preoperative imaging phase (1).
Materials and Methods
To review normal anatomy of the parotid gland and the course of the facial nerve with illustrations and real scan images. To review the approach to dictating a useful report on parotid gland lesions for preoperative planning. To review how to describe and image both common and uncommon parotid gland pathology.

Results
This exhibit provides the tools to create a more detailed imaging report of parotid gland pathology, especially in regards to the course of the facial nerve. The exhibit reviews the interaction of the lesions with surrounding soft tissues including the deep and superficial parotid gland lobes and lymph nodes as well as osseous and vascular structures with special attention to the facial nerve course. All components of this review enable the meeting attendees to write detailed and useful reports for preoperative imaging to decrease patient postoperative morbidity in regards to iatrogenic facial nerve injury.
Conclusions
After reviewing of the extensive collection of parotid gland pathology from our institutions with the detailed facial nerve anatomy, the attendees will be able to add more value to their radiology reports as well as potentially decrease patient morbidity with their detailed reports of preoperative parotid gland pathology.

2803

All That Tremors is Not Parkinson's: How Volumetric MRI Helped Us Characterize Extrapyramidal Syndromes.

M Agarwal[1], K Reiter[1], A Correro[1], E Ulmer[2], S Franczak[3], A Klein[4], L Umfleet[5]
[1]Medical College of Wisconsin, Milwaukee, WI, [2]Rhodes College, Memphis, TN, [3]University of Notre Dame, Notre dame, IN, [4]Medical College of Wisconsin - Froedtert Hospital, Milwaukee, WI, [5]Medical College of Wiscosnin, Milwaukee, WI

Purpose
Neurodegenerative disorders are a very diverse group of neurologic pathology where impairment of cognitive function may occur in various combinations. Prevalence of extrapyramidal symptoms among patients with various forms of cognitive impairment is not uncommon and is not always due to Parkinson's disease. Symptoms could be due to an underlying tauopathy - progressive supranuclear palsy (PSP) and corticobasal syndrome (CBS) or due to an underlying synucleopathy - dementia with Lewy bodies (DLB) and Parkinson's disease dementia (PDD). Different, and sometimes distinct areas of the brain are affected in different forms of these extrapyramidal syndromes. The affected brain regions lose volume, which is subtle earlier in the disease process. Automated segmentation and volumetric MRI however can detect these subtle changes and can help in differentiating these syndromes. The objectives of this exhibit are: 1. To describe the different forms of neurodegenerative disorders with extrapyramidal symptoms. 2. To demonstrate the use of volumetric MRI in the differentiation of these disorders.
Materials and Methods
Individuals with mild cognitive impairment were evaluated with an FDA approved software program that provides z-scores for 45 brain regions relative to same-age healthy controls. The software used thin section MRI images acquired on a 1.5 or 3T scanner.
Results
Using Volumetric MRI non-specific generalized brain volume loss was seen in patients with Parkinson's disease while the volume loss was more specific in other types of extrapyramidal syndromes. Involvement of occipito-parietal regions with relative sparing of the hippocampi was seen on volumetric analysis in DLB, involvement of the midbrain and superior cerebellar peduncles was seen in PSP and asymmetric atrophy of the posterior frontal and parietal lobes contralateral to the side of the motor symptoms was seen in CBS.
Conclusions
Extrapyramidal symptoms in a patient with cognitive impairment are not always due to PDD. Volumetric MRI can help in differentiating between different extrapyramidal syndromes.

3385

Alzheimer Disease: A Review of Recent Developments and the Role of Imaging

H Ismail[1], L Wang[2]
[1]University of Cincinnati, Cincinnati, OH, [2]University of Cincinnati Medical Center, Cincinnati, OH

Purpose
Alzheimer's disease (AD), the most common form of dementia, is a devastating illness that will affect an estimated 5.7 million Americans and almost 50 million people worldwide in 2018, with numbers expected to nearly triple by 2050. While mortality related to heart disease and stroke has continued to decline, the rate of AD-related death in the United States more than doubled in the period from 2000-2015. Now the 6th leading cause of death, it is the least preventable and treatable of the major causes, and places a tremendous financial, physical, and emotional burden on the estimated 16 million unpaid caregivers who provide the majority of care to Alzheimer's patients. Following the recent lack of success of numerous therapeutic trials aimed at slowing the progression of cognitive impairment in AD patients, there has been an increased emphasis on the early, preclinical detection of Alzheimer's disease, in which diagnostic imaging plays a key role. This educational exhibit aims to provide a brief but comprehensive review of recent developments related to AD with an emphasis on imaging.
Materials and Methods
Summarize current understanding regarding the pathophysiology of AD. Describe relevant diagnostic imaging findings for current and evolving techniques such as MRI and PET/CT. Provide a general discussion of the role of imaging in AD going forward.
Results
The use of MRI is recommended and approved for the initial evaluation of patients with cognitive dysfunction, with well-described imaging findings that can aid in the diagnosis of Alzheimer's disease. Additional findings have been described on 18F-FDG PET that can provide further diagnostic clarification. Although current belief is that AD symptoms are a result of neuronal loss, synaptic dysfunction, and resultant atrophy related to the deposition of β-amyloid (Aβ) plaque and tau/neurofibrillary tangles (NFT), recent drug trials using anti-plaque agents in symptomatic patients have failed to slow the progression of cognitive impairment. Given that the development of Aβ plaque is believed to precede the onset of AD symptoms by 10-20 years, these trials may have been unsuccessful due to the advanced stage of disease. Additionally, patients may have been improperly selected on the basis of a clinical rather than biologic (i.e. imaging) diagnosis of AD. Thus, more recent imaging techniques such as Amyloid PET, tau PET, functional MRI, and diffusion weighted imaging are crucial in the early and accurate detection of patients with or at risk for developing AD.
Conclusions
Diagnostic imaging, including MRI and PET/CT, is critical in the early and accurate detection of Alzheimer's disease. This has implications for the appropriate selection of patients for therapeutic trials, as well as long-term disease management and potential preventative therapies. Imaging also serves as a useful tool for further understanding the mechanism behind AD.

2641

Ambiguous Amyloidosis

J Dennison[1], A Leyva[1], A Cibulas[1], R Beegle[1]
[1]Advent Health, Orlando, FL

Purpose
Cerebral amyloidosis is a pathologic process in which amyloid-β plaques are abnormally deposited within the brain and its supporting structures. This process has been implicated in multiple highly-prevalent

disease pathologies, including intracranial hemorrhage, Alzheimer's dementia, and vascular dementia. In 2010, the prevalence of Alzheimer's dementia alone amounted to approximately 5.2 million people in the United States. Given the multiple associated disease processes and relatively high prevalence of these conditions, it is advantageous for the practicing radiologist to become familiar with the imaging features of CA. There are multiple possible radiologic manifestations, some of which are quite rare, or that may overlap with other disease processes, making the diagnosis quite challenging. This educational exhibit will present the underlying pathology, typical imaging characteristics, unusual possible presentations, as well as common mimics of cerebral amyloidosis.

Materials and Methods

This educational exhibit will utilize a PowerPoint presentation to depict the multiple ways, both common and unusual, that cerebral amyloidosis (CA) can present itself using high quality, annotated images. Educational objectives include: 1. Understand the basic pathophysiology behind CA. 2. Discuss the common pathologic conditions associated with CA. 3. Review the cross-sectional imaging findings of the various types of CA with an emphasis on MRI. Imaging review will include classical cerebral amyloid angiopathy, amyloidoma, inflammatory amyloidosis, and CA with diffuse white matter involvement. 4. Understand the appropriate imaging and specific MRI sequences to obtain when evaluating for CA. 5. Compare and contrast the imaging characteristics of CA with other entities that may have similar imaging findings such as PRES, diffuse axonal injury, multiple cavernous hemangiomas, hemorrhagic metastases, hypertensive microhemorrhages, and hemorrhagic stroke.

Results

Findings and discussion of this educational exhibit will be included throughout the PowerPoint presentation in order as each item is presentated. This will include cross-sectional imaging with an emphasis on MRI. High quality images of the multiple, previously mentioned presentations of cerebral amyloidosis will be reviewed, annotated, and discussed in detail.

Conclusions

Cerebral amyloidosis exhibits a wide range of possible radiologic manifestations, which may vary from one individual to another, often making it a challenging diagnosis. Given its association with several disease processes, many of which are highly prevalent, prompt recognition of these findings and various presentations is important for expedient and appropriate subsequent management.

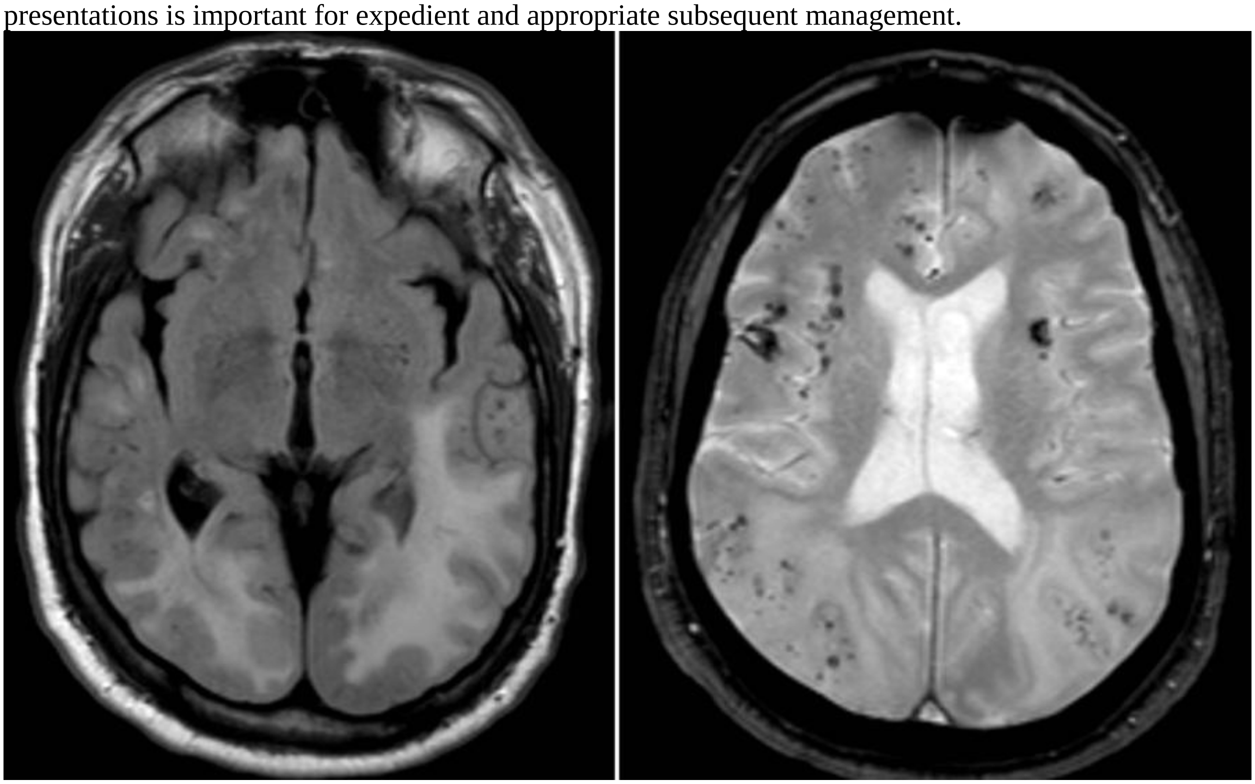

(Filename: TCT_2641_InflammatoryCAAandClassicFindings.jpg)

3298

An Essence of Making Differential Diagnosis of Acquired Corpus Callosum Lesions

A Tsukabe[1]
[1]*Osaka International Cancer Institute, Osaka, Osaka*

Purpose
The purpose of this presentation is to review and discuss the anatomy of corpus callosum and differential diagnosis of acquired corpus callosum lesions.
Materials and Methods
We provide comprehensive commentaries on the anatomy of pericallosal structures and essential of differential diagnosis, through presenting case series. (Infarction, Hemorrhage ,Fat embolism, Multiple sclerosis, acute disseminated encephalomyelitis (ADEM), Demyelination due to Nivolumab, Adrenoleukodystrophy, Progressive Multifocal Leukoencephalopathy (PML), glioblastoma multiform, Lymphoma, Metastasis, Clinically mild encephalitis/encephalopathy with a reversible splenial lesion (MERS), Reversible splenial lesion due to hypoglycemia, Charcot-Marie-Tooth disease type X (CMTX), Marchiafava-Bignami Disease, Werniche encephalopathy, Diffuse axonal injury)
Results
Acquired corpus callosum lesions are classified roughly into Vascular lesions, Demyelinating lesions, Inflammatory lesions, Trauma, Neoplastic lesion, Infection, Metabolic/Toxic disease, Transient lesion, and Leukoencephalopathy. We should pay attention to the localized distribution inside the corpus callosum for proper diagnosis. Not only the abnormal findings in the corpus callosum, the existence of other findings outside the corpus callosum is important.
Conclusions
You can understand the underlying pathologies and the mechanism of localized distribution in the corpus callosum through this presentation.

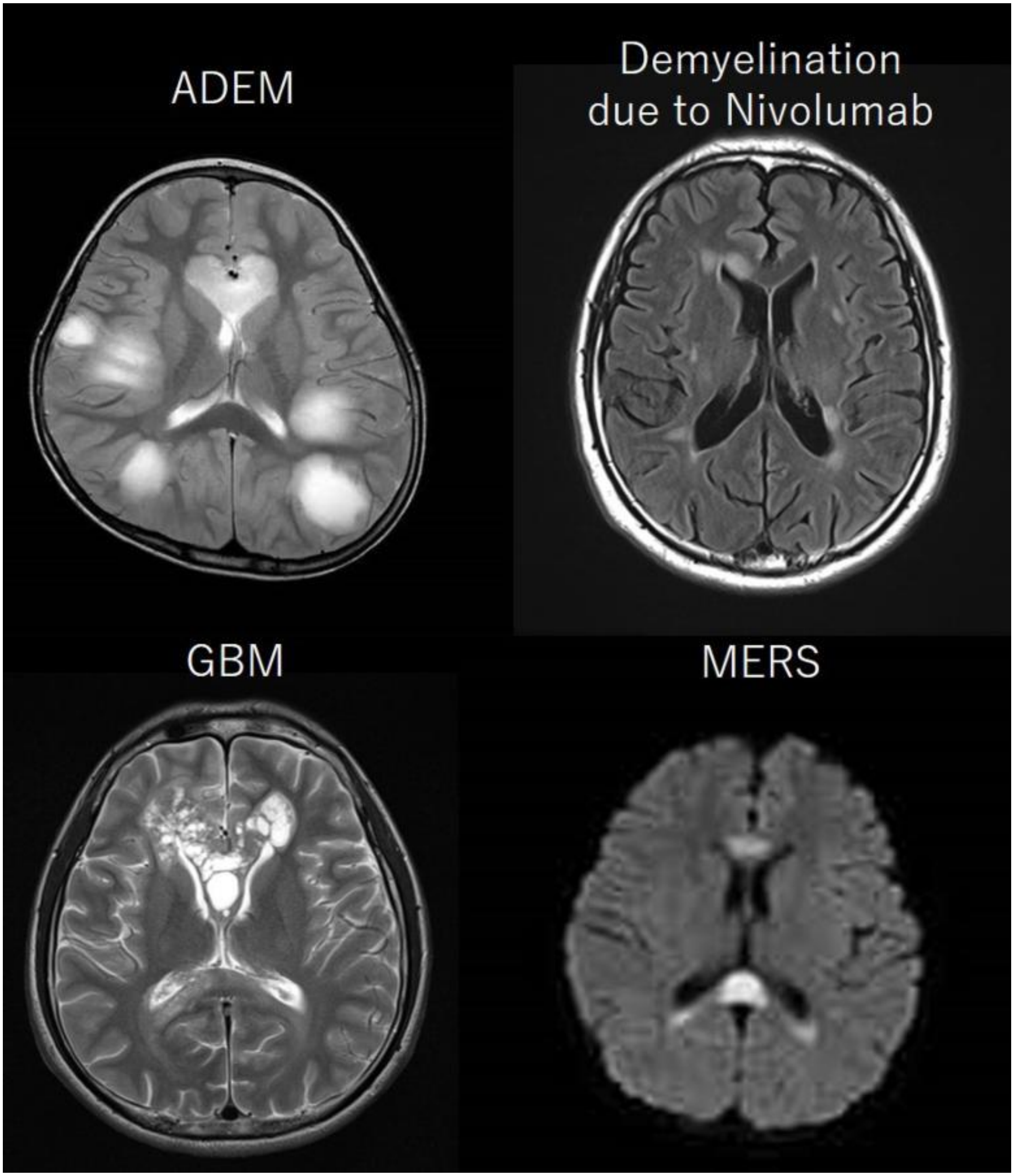

(Filename: TCT_3298_a.jpg)

2915

Anatomic Approach to Non-Traumatic Lesions of the Visual Pathway

V Pai[1], B Purohit[1], W Yu[1], Y Sitoh[1], K Joshi[2], K Gupta[2], B Pai[2]
[1]*National Neuroscience Institute, Singapore, Singapore,* [2]*SevenHills Hospital, Mumbai, Maharashtra*

Purpose
The purpose of this exhibit is to provide: 1. A review of the anatomy of the visual pathway. 2. A comprehensive pictorial essay of the various lesions that affect the visual pathway, thus providing a systematic approach for Resident Education.
Materials and Methods
Cross-sectional imaging of the brain and the visual pathway is routinely performed for the evaluation of diminution or loss of vision. CT scans and multisequence MRIs, performed for such indications were reviewed and a collection of lesions affecting the visual pathway were included in the final data set.
Results
Our observations were divided according to the anatomic location involved by the lesion. The lesions to be discussed will be classified as follows: (I) Lesions of the retina: Retinal Detachment, Retinitis, Retinoblastoma. (II) Lesions of the optic disc: Papilledema, Metastasis, Optic Drusen. (III) Lesions of the Optic nerve: (A) Congenital: Colobomas. (B) Vascular: Optic nerve infarction. (C) Inflammatory: Demyelination, Neurosarcoidosis. (D) Infective: Optic nerve perineuritis and exudates. (E) Neoplasms: Gliomas. (F) Optic sheath lesions: Meningioma. (G) Miscellaneous: Optic atrophy, Radiation Neuritis, Idiopathic Intracranial Hypertension. (IV) Lesions of the Optic Chiasm: (A) Congenital: Septo-optic dysplasia. (B) Infections: Opto-Chiasmatic tuberculosis. (C) Neoplasms: Hypothalamic Optochiasmatic Glioma. (V) Lesions affecting the Occipital lobes: Adrenoleukodystrophy, Posterior Cerebral Artery Territory Infarction, Posterior Reversible Encephalopathy Syndrome.
Conclusions
Lesions along the visual pathway are common place at the office. As most of the visual pathway is inaccessible for histopathology, radiology may be the only diagnostic modality available. Hence knowledge of the radiological appearance is of utmost importance, as it will aid early diagnosis and management with the aim to preserve vision or prevent further visual loss. This poster will help radiologists-in-training approach lesions of the visual pathway with ease and serve as a ready one-stop reference.

3452

Anatomical Variations and Don't Touch Lesions in Patients with Epilepsy

A Haboosheh[1], S Nabavizadeh[2], A Vossough[3]
[1]University of Pennsylvania, Philadelphia, PA, [2]UNIVERSITY OF PENNSYLVANIA HEALTH SYSTEM, WYNNEDWOOD, PA, [3]UNIVERSITY OF PENNSYLVANIA - CHOP, PHILADELPHIA, PA

Purpose
There are brain anatomical variants and structural alterations, particularly within the anterior temporal lobe region, hippocampus and motor cortex that can be misinterpreted as potentially epileptogenic foci and may cause unnecessary diagnostic follow-up imaging or worse unnecessary treatment. The purpose of this exhibition is to describe normal variants and discuss their imaging findings. Radiologist must be familiar with both the normal brain anatomy as well as numerus variants that mimic pathology in the context of epilepsy imaging. After reviewing this exhibit, the viewer will have a comprehensive understanding of numerus anatomical variants that can be mistakenly interpreted as tumors, heterotopia and cystic lesions.
Materials and Methods
1. Review normal anterior temporal lobe and hippocampal anatomy in relationship with anatomical variants mimicking potentially epileptogenic lesions in patients with epilepsy. 2. Highlight imaging appearances of these CNS structural alterations findings. 3.Demonstrate how familiarity with normal anatomical variants and structural findings. can play a critical role in accurate imaging diagnosis, MEG/PET interpretation, clinical decision making, and management.

Results

This educational exhibit will review these anatomic variations: choroidal fissure cyst, hippocampal sulcal remnants, malrotation of hippocampus, asymmetric gyri (e.g., split motor cortex), caudate tail mimicking heterotopia, nodularity of hippocampus, perivascular space in anterior temporal lobe mimicking a cystic tumor, DVA causing hypoperfusion on PET imaging mimicking seizure focus, among others.

Conclusions

Radiologists may be less familiar with normal anatomical variants and structural changes. After reviewing this exhibit, the viewer will have a comprehensive understanding of various don't touch lesions and anatomical variations that may mimic a seizure focus in patients with epilepsy and thereby minimizing interpretive errors.

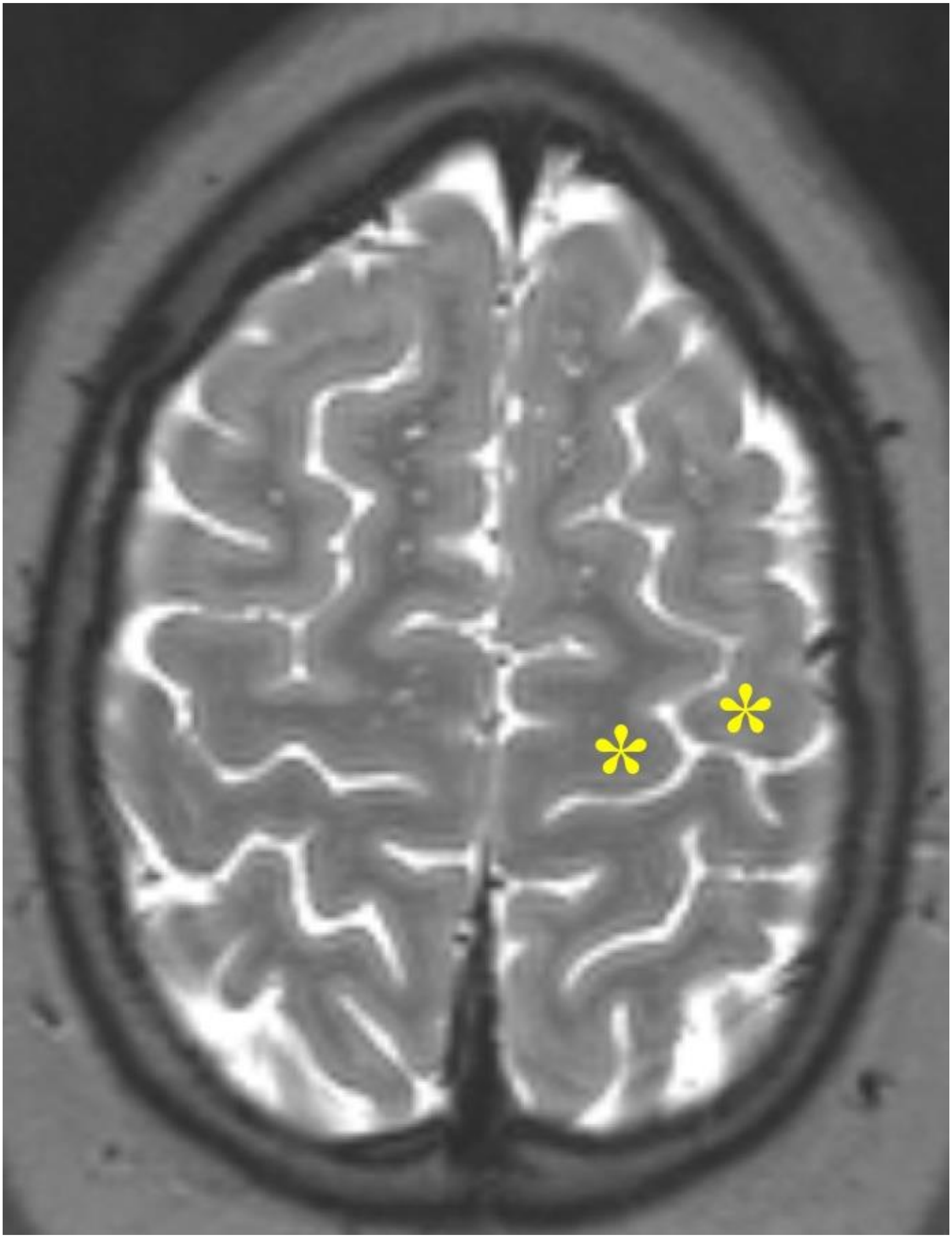
(Filename: TCT_3452_Variant20gyral20anatomy20-20split20motor20cortex202.jpg)

3412

Anatomy, Function, and Pathology of the Amygdala

H Tatekawa[1], A Azizyan[1], N Salamon[1]
[1]*UCLA, Los Angeles, CA*

Purpose
The amygdala is a complex structure, located dorsomedially in the temporal lobe, forming the ventral superior, and medial walls of the inferior horn of the lateral ventricle. The amygdalae are considered part of the limbic system, performing a primary role in the processing of memory and emotional responses (including fear, anxiety, and aggression). There are multiple subdivisions in the amygdala with specific connections to the certain areas of the cortex. This presentation will review functional anatomy to better understand the clinical presentation in the different types of pathology of the amygdala lesions.
Materials and Methods
Table of contents 1. Anatomy of the amygdala a)MRI structural anatomy b)White matter pathway around amygdala c)Vascularization of amygdala 2. Function of the amygdala a)Afferent and Efferent 3. Clinical examples of the diseases in the amygdala a)Tumors b)Dysplasia c)Infection d)Vascular diseases e)Metabolic process
Results
The amygdala has three major compartments: dorsomedial, central and lateral. In particular, central nucleus leads to ventral amygdalofugal pathway, which connects to the hypothalamus. This pathway is related to motivation and drives, through the limbic system and the injury can cause emotional blindness. Many disease processes may involve amygdala including tumors; the most common amygdala tumor is hamartoma, followed by dysembryplastic neuroepithelial tumor and low-grade glioma. Amygdala enlargement can be sometimes identified due to seizures or other processes such as focal cortical dysplasia, tumors, or clustering hypertrophic neurons. Aura of the seizures may be related to the amygdala; including gastrointestional symptoms, cardiovascular, respiratory changes, or anxiety.
Conclusions
Radiologists may not be familiar with detailed amygdala functions. Knowing the anatomy and functional connections will help better understanding mechanism and pathology of the amygdala. This presentation will facilitate the clinical correlation and pay more attention to the process involving amygdala which leads to accurate diagnosis in some cases.

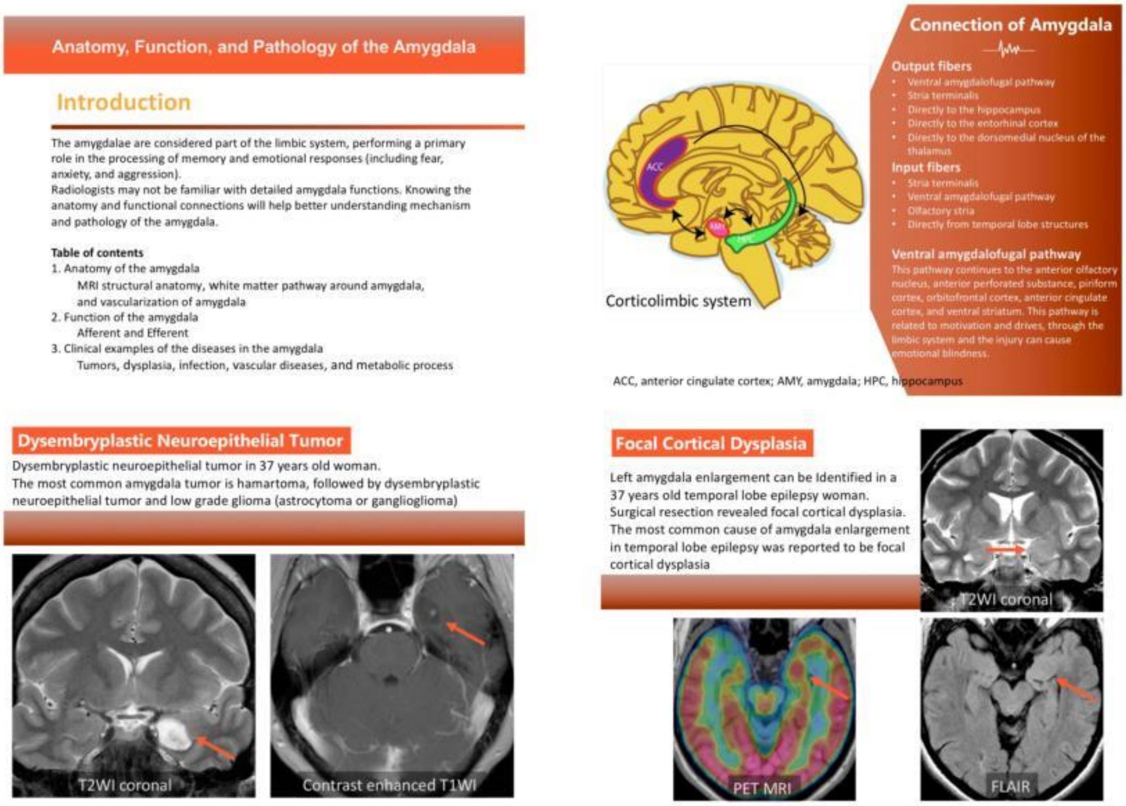

(Filename: TCT_3412_ASNReducational_submit.jpg)

2132

Antiangiogenic Therapy: Understanding What is Happening to the Brain in Patients with High-Grade Gliomas Treated with Bevacizumab: A Case-Based Approach

L Brandao[1]
[1]Felippe Mattoso Clinic-Grupo Fleury, RIO DE JANEIRO, RJ

Purpose
The purpose of this study is to demonstrate the imaging findings associated with bevacizumab (BV) therapy in patients with recurrent high grade gliomas (HGGs) and to clarify the meaning of restricted diffusion and T2/FLAIR abnormalities in these patients.
Materials and Methods
MRI of 45 patients with recurrent HGGs treated with bevacizumab were visually analyzed. The study was conducted over a 8 year period from January 2010 to September 2018. MRI studies were performed on 1.5T GE Signa Horizon and 1.5 T GE Excite units. Available sequences included sagittal T1, axial T1, T2, FLAIR, GRE and DWI, coronal T2, as well as contrast enhanced axial, sagittal and coronal T1 and T13D SPGR. Dynamic susceptibility contrast enhanced (perfusion) MRI, dynamic contrast enhanced (DCE) permeability studies and MR spectroscopy were performed in all cases.
Results
The main imaging findings related to bevacizumab therapy were: 1-Marked decrease in contrast enhancement and perilesional edema; 2-Deposits of paramagnetic material with high signal intensity on T1; 3-Reduced permeability and blood volume in patients that responded to BV therapy; 4-New areas of

restricted diffusion, some that remained stable and some that progressed; 5-Non enhancing tumor progression; 6-Hemorrhage and brain infarcts.
Conclusions
While there is no established standard of care for recurrent GBM, bevacizumab (BV) has emerged as a potential treatment option. Familiarity with the imaging abnormalities associated with BV therapy will help interpret MR imaging studies in these patients, including the detection of non-enhancing tumor progression.

2469

Application of an Emerging Machine Learning Modality to Bring Deep Learning to the Workbench

B Ellison[1], S Soman[1]
[1]*Harvard Medical School, BIDMC, Boston, MA*

Purpose
Deep learning is a subset of machine learning inspired by neural networks with potential to become an integral component of radiologic problem solving and image interpretation. Similar to other clinical support systems, it is of critical importance that radiologists be involved in the early development of this powerful technology; however, many of the pioneering tools used in deep learning are available only to the computer scientist and are difficult to access for most clinical radiologists. We propose using an emerging machine learning modality called TensorFlow to address this deficiency. Using all publically available resources, we hope to demystify the mechanics of setting up a deep learning experiment and to provide a practical approach to bring this promising new technology to the workbench.
Materials and Methods
TensorFlow (www.tensorflow.org) is a freely available, open source machine learning framework recently developed by the Google Brain Team. TensorFlow is based in Python (www.python.org), a relatively intuitive and approachable programming language, which is pre-installed on MacOS and Linux based systems and freely available for Windows machines. In order to perform deep learning, the radiologist must have appropriate radiologic data, which include multiple cases with an accompanying diagnoses or regions of interest, which will serve as the "ground truth." TensorFlow acts as the base machine learning engine; however, to customize its use for neuroradiology, the user must add additional application program interfaces (APIs), which are pre-built Python base packages easily downloaded and installed often from a single line of code. For example, the Deep Learning Toolkit is an API that converts images in NIFTI format to "tensors," the format read by TensorFlow. This process can be surprisingly challenging as radiologic data is often heterogeneous, such as in DICOM files containing header a variable amount of necessary or unnecessary information or spread across multiple folders. Thus, customization may be required to the Python scripts in order to suit the user's dataset. Once the data is read in, the user must select a type of neural network to train the data, which can be programmed by hand or more conveniently acquired from APIs such as NiftyNet. The next step is to train the model on a random subset of data, carefully adjusting variables such as the learning rate and the number of training cycles to optimize the performance of the model. Finally, once the algorithm is created, it must be tested on novel data to evaluate its accuracy and reliability.
Results
TensorFlow provides a fully functioning machine learning engine freely available for use on Windows, MacOS, and Ubuntu devices with step-by-step instructions as well as comprehensive tutorials and a wealth of online trouble shooting resources. For the radiologist less versed in computer programming, excellent educational resources are available including fully interactive online programming courses, such as HarvardX (www.edx.org). Even without extensive expertise in programming, the number of publically available software packages for TensorFlow and Python is growing rapidly, which will allow the user to find methods of loading in their radiologic data and testing different machine learning models, effectively

bringing the power of machine learning into the hands of radiologists. We demonstrate here the basic mechanics and challenges of a deep learning experiment including the selection of appropriate radiologic data, technologic setup of TensorFlow, the use and customization of Python software packages and APIs, as well as the complexities of data input, neural network model selection, and analysis of model quality.
Conclusions
By bringing machine learning technology into the hands of more clinical radiologists, we will improve the quality and accuracy of deep learning techniques to aid the radiologist in image interpretation and clinical decision-making.

2251

Application of Susceptibility Imaging (SWI) in Neurodegenerative Disorders.

H Sotoudeh[1]
[1]*University of Alabama at Birmingham, Birmingham, AL*

Purpose
The number of Americans surviving into their 80s and beyond is expected to grow dramatically and it is expected that 72 million older (>65 years of age) Americans will make up to 20% of the total population by 2030. As the number of older Americans grows rapidly, neurodegenerative diseases (NDDs) and brain diseases associated with aging are also expected to rise significantly. Micro-hemorrhages, calcium and iron deposition are common in neurodegenerative disorders in distribution which can be used for diagnosis which emphasize the role SWI as the best MR sequence to detect these hemorrhages, calcium and iron deposition. Unfortunately mineral deposition in brain can be a part of "aging process" so being familiar with age-related SWI findings versus abnormal abnormal SWI is critical for the radiologists.
Materials and Methods
In this presentation the basic concept of SWI will be reviewed. Then the age-related SWI signal changes will be reviewer. The abnormal patterns of SW signal changes in the most common neurodegenerative diseases will be reviewed which includes: Parkinson's disease, Huntington's disease, Alzheimer's disease, Multiple sclerosis (MS), Amyotrophic lateral sclerosis, Wilson's Disease, Hallervorden-Spatz syndrome/Pantothenate kinase-associated neurodegeneration (PKAN), Cerebral amyloidosis and Multiple system atrophy (MSA). Finally a structural report for SWI sequence will be provided to be added in " Neurodegenerative Brain MRI protocol ".
Results
N/A
Conclusions
At the end of this presentation radiologist will be able to differentiate the age related pattern of SW versus abnormal pattern and recognize the classical pattern of SWI in major Neurodegenerative disorders.

2866

Applying Automated Segmentation and Radiomics Feature Extraction to Brain Tumors: A Review of Open Source and Commercially Available Software Options and Lessons Learned

J Vera[1], S Gonzales[2], J Ormsby[3], C Wilson[2], K SantaCruz[4], R Selwyn[2], M Mabray[2]
[1]*UNIVERSITY OF NEW MEXICO, ALBUQUERQUE, NM,* [2]*University of New Mexico, Albuquerque, NM,* [3]*University of New Mexico, Albuquerque , NM,* [4]*University of New Mexico Hospital, Albuquerque, NM*

Purpose
We aim to provide education for neuroradiologists and trainees on various open source and commercially

available software packages used for manual and automated segmentation of images and extraction of radiomics features. We hope to introduce attendees to available software packages that our group has used for setting up a pipeline of both segmentation and radiomics feature extraction of brain tumors on MRI. These software packages are potentially powerful tools for enabling future computer analysis of brain tumors that may assist with research and clinical analysis of these tumors.

Materials and Methods

We will introduce and discuss multiple available software packages that our group has used for both manual and automated segmentation of brain tumors (including the 3D convolutional neural network architecture, "DeepMedic") and for radiomics feature extraction (including commercial and open-source options). We will highlight challenges and lessons learned with each software package and the various formats required for each task/package. We will demonstrate the workflow for setting up an image processing pipeline and will give examples of results/outputs at each step.

Results

Tools are available for setting up image processing pipelines that allow segmentation and feature extraction from MRI images of brain tumors. There are various options available for each task, each with advantages and disadvantages to their use and potential challenges that may be encountered. Ultimately, we demonstrate an example image processing pipeline that can be replicated to successfully provide quantifiable features about brain tumors and develop "tumor signatures".

Conclusions

Attendees will gain familiarity with the process for setting up an image processing pipeline and various open-source and commercial software packages available for accomplishing the necessary tasks. The brain tumor segmentation and quantitative feature extraction that results will be important processes for developing "tumor signatures" that can ultimately be used to predict histology and genetic features of brain tumors. This will serve as an educational primer that will improve attendees familiarity with these topics and the challenges in this arena.

3669

Assessment of the Sagittal Mid-Line Section of the Brain: A Systematic Approach.

A True[1], P Sideras[1], G Singh[1], J Matthews[1], V Spektor[1]
[1]Newark Beth Israel Medical Center, Newark, NJ

Purpose

Learning Objectives: 1. Recognize normal and variant anatomy of mid-line brain structures. 2. Acquire a basic understanding of normal mid-line structure development. 3. Review pathologies that affect mid-line structures. 4. Construct a systematic approach in evaluating mid-line structures and discussing differential diagnoses.

Materials and Methods

Many non-neuro trained radiologists have a difficult time evaluating the structures of the brain. Of the wide array of topics, mid-line structures of the brain is an appropriate starting point for evaluation of neuroradiological exams. The purpose of this educational exhibit is to provide a systematic approach reviewing and recognizing the mid-line structures of the brain, detect developmental anomalies, pathologies, and minimize misses. This would provide a sense of relief and confidence in those who are not yet comfortable with neuroradiological examinations.

Results

In order to examine the mid-line structures of the brain, a systematic approach much best taken. We present one such approach where the reader recognizes the structures and keeps a constant pattern of search. One of the main issues, unique to the brain and in evaluations of mid-line structures is the fact that there is no contra-lateral structure to examine. First, normal anatomy must be assessed. Viewing the sagittal midline allows us to view, in a single slice to determine pathologies of the corpus callosum, midbrain, hindbrain, and the continuity of the CSF pathway. Starting anteriorly, the corpus callosum can be evaluated to differentiate normal anatomy, agenesis, or dysplasia/hypoplasia. We believe that this should be the approach in assessing the corpus callosum as its formation starts anteriorly with the genu and proceeds posteriorly along the body to the splenium and lastly, the rostrum. Any contour deformities of the corpus callosum may also reveal signs of hydrocephalus or intracranial hypotension. The fornix can also be evaluated for any disruption of the pre- and post-commissural fibers. Secondly, the superior aspect of the midbrain can be evaluated. It should develop with a convex contour forming the posterior floor of the third ventricle. The cerebral aqueduct should be observed for patency as stenosis can lead to an obstructing hydrocephalus. Continuing inferiorly, one can assess the development of other structures such as the pons and at the same time the cerebellar vermis. Lastly, more anteriorly starting at the nose and nasal septum moving more posteriorly to include the clivus and pituitary gland depending on how far inferiorly the examination allows, incidental abnormalities within the upper cervical spine may be evaluated.

Conclusions

Neuroradiology exams can be intimidating to new trainees and those without neuro fellowship training. We hope that after reviewing this presentation, the trainee will have acquired and will be able to utilize a systematic approach in interpreting normal mid-line structures,associated pathologies, and be able to provide discussion of an array of differential diagnoses.

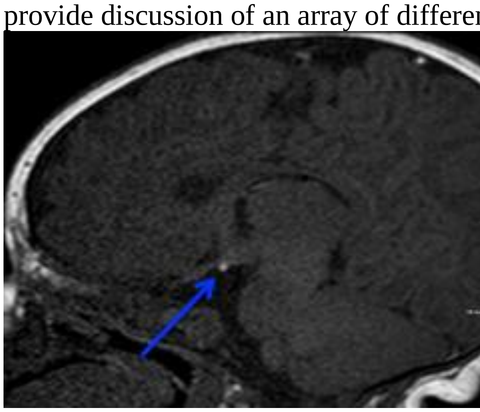

(Filename: TCT_3669_Ectopicpituitarygland.jpg)

2292

Automated Processing of CT Perfusion Imaging in Ischemic Stroke Triage Workflow: Clinical Utility and Potential Pitfalls

C Chung[1], R Hu[1], R Peterson[1], J Allen[1]
[1]*Emory University School of Medicine, Atlanta, GA*

Purpose

Favorable outcomes in recent stroke trials led to expansion of the endovascular thrombectomy window in management guidelines (1), launching a shift from the 'time-is-brain' paradigm to imaging-based patient selection criteria for intervention (2). Computed tomography perfusion (CTP) data processed with the Rapid Processing of Perfusion and Diffusion (RAPID) platform (iSchemaView, Menlo Park, CA), a fully automated software that computes and exports perfusion maps directly to mobile devices, was the basis for eligibility determination in both trials (3,4), and is increasingly accepted as a component of stroke triage workflow (5). However, over-reliance on readily available, computationally complex processed data may predispose interpreting physicians to diagnostic errors unless there is an understanding of the limitations and pitfalls associated with user-independent, automated CTP processing programs.

Materials and Methods
This exhibit presents an overview of CTP data processing with the RAPID platform and discusses the technical and diagnostic pitfalls of interpreting CTP data.
Results
Educational objectives include: 1. Review general CTP source data acquisition and processing as well as commonly-used perfusion parameters. 2. Illustrate the role of RAPID in stroke triage workflow and the validity of perfusion parameter thresholds. 3. Highlight technical pitfalls of automated CTP perfusion maps due to suboptimal image acquisition (insufficient scan length or coverage, motion), variation in post-processing (arterial and venous output selection), and failure to reach pre-defined parameter thresholds. 4. Demonstrate CTP perfusion abnormalities in alternative diagnoses such as stroke mimics, proximal arterial stenosis, vasospasm, chronic infarcts, and cerebral hyperperfusion. Accompanying multimodal neuroimaging and clinical findings aiding correct diagnosis will be stressed.
Conclusions
Increasing availability of standardized automated CTP perfusion maps has drastically improved data accessibility to front-line physicians, streamlining stroke patient triage and selection for late window thrombectomy. Knowledge of the inherent limitations in CTP data acquisition, processing and interpretation pitfalls, as well as review of all available imaging data are imperative for accurate interpretation and treatment decision-making.

2158

Bilateral Parotid Swelling: Trying to "MR" Differentiate Kussmaul vs Sjögren Diseases

B Brea Alvarez[1], J SANZ SANZ[2], M Tuñón Gómez[3], R Ruiz Peralbo[4], Y Garcia Hidalgo[1]
[1]Hospital Puerta de Hierro, Majadahonda, Madrid, [2]HOSPITAL UNIVERSITARIO PUERTA DE HIERRO-MAJADAHONDA, Majadahonda, Madrid, [3]Hospital Universitario Puerta de Hierro-Majadahonda, Majadahonda, Madrid, [4]Hospital Universitario Puerta de Hierro-Majadahonda, Majadahonda, Madrid

Purpose
Sialodochitis fibrinosa (Kussmaul disease, KD) is a rare disease characterized by recurring episodes of pain and swelling of the salivary glands due to the formation of mucofibrinous plugs. Analytic studies show elevated levels of eosinophils and immunoglobulin E. Sjögren's syndrome (SS) is a chronic autoimmune inflammatory disease characterized by diminished lacrimal and salivary gland function characterized by dryness of the eyes and mouth and swelling of salivary glands. It can occur as a primary form, or not associated with other diseases, and as a secondary form associated with other rheumatic conditions. Analytic studies reveal anti- Ro/SSA antibodies with or without anti- La/SSB antibodies. MRI is useful for diagnosis of salivary gland diseases. MRI especially with heavily T2-weighted sequences (Sialography MR) can shows diffuse intraglandular sialectasis in SS. However typical pattern of the KD has not clearly described. We have tried to identify the differential MRI pattern of these two entities
Materials and Methods
We have reviewed the SS MRI pattern and compare with our cases of KD that can occur in our centre in the last two years. We have reviewed the last five years english publications of MRI findings (biomarkers) in both diseases
Results
SS is characterized by the presence of variable size sialectasis, presence of solid nodules and intraglandular fibrosis that vary according to the evolutive of the disease. Kussmaul disease presents structurally normal glands with intra and extraglandular sialectasis.
Conclusions
In conclusion, we believe that patients who present with salivary swelling and findings of intra and /or

extraglandular sialectasis in MRI should be considered the infrequent Kussmaul disease in the differential diagnosis.

2519

Case Series: Imaging Findings in Acute Flaccid Myelitis Caused By Enterovirus D68

G Ciavarella[1], M Baumann[2], W Millar[1]
[1]Geisinger Medical Center, Danville, PA, [2]Geisinger Health System, Danville, PA

Purpose
Enterovirus D68 (EV-D68) is an emerging pathogen in the United States that has important pediatric public health implications because of its ability to cause acute polio-like neurological symptoms including acute flaccid paralysis with permanent sequelae. The purpose of this abstract is to highlight common imaging findings found on MRI of the brain and spine of pediatric patients who develop acute flaccid myelitis (AFM) secondary to enterovirus D68, discuss potential differential diagnoses, and how to distinguish them.
Materials and Methods
Several cases of AFM among young pediatric patients were subsequently found to have infection with EV-D68 at our institution over the past several years. These cases were evaluated as a series to assess for common imaging characteristics that can help distinguish this entity from other diagnostic considerations such as demyelinating disease, acute disseminated encephalomyelitis (ADEM), acute transverse myelitis, Guillain-Barre syndrome, and other autoimmune or infectious causes of acute myelitis.
Results
The typical age range for AFM is 2-8 years of age. Several imaging findings in the brain and spine were characteristic of AFM caused by EV-D68. Typical findings in the brain included brainstem, and less commonly cerebellar, lesions with T2 hyperintensity and variable enhancement with a midline predominance. Findings in the spine included central gray matter T2 hyperintensity in numerous segments in all cases, with variable enhancement and sparing of the white matter. These findings help distinguish AFP from other causes of similar clinical scenarios. For example, ADEM and demyelinating disease are not as confluent and affect the white matter of the brain and spinal cord rather than gray matter. Multiple sclerosis commonly affects the dorsolateral spinal cord. Acute transverse myelitis generally has holocord involvement, affects greater than two-thirds of the cord, does not spare the white matter, and may cause cord expansion. Guillain-Barre syndrome would rarely have brain findings or involve the upper spinal cord, which are both common features of AFM.
Conclusions
AFM caused by EV-D68 is an emerging virus that causes polio-like symptoms with long term sequelae, and produces characteristic imaging findings. These imaging findings can be utilized to raise suspicion for this entity as a cause of acute onset paralysis after a viral respiratory infection in young children.

3283

Caught in the Middle—Imaging Anatomy and Lesions of the Corpus Callosum: A Case-Based Review

K Hewitt[1], A Sajan[1], D Reede[2], V Velayudhan[3], W Smoker[4]
[1]SUNY Downstate, Brooklyn, NY, [2]SUNY downstate University Hospital, Brooklyn, NY, [3]SUNY Downstate Medical Center, Brooklyn, NY, [4]University Of Iowa Hospitals & Clinics, Iowa City, IA

Purpose
1. Review the anatomy and embryology of the corpus callosum (CC). 2. Demonstrate imaging findings

of common congenital and acquired abnormalities encountered in this region. 3. Learn to use an algorithm based on anatomy, embryology, clinical history, and imaging findings on specific MR pulse sequences to improve diagnostic accuracy.

Materials and Methods

After a review of the embryology and normal anatomy (gross and imaging) of the CC, cases are presented to emphasize the best MR sequence, imaging planes and locations of different congenital and acquired diseases.

Results

The CC forms in a specific fashion. Sagittal images, especially T1-weighted images, can be used to evaluate the CC for areas characteristically involved with various congenital anomalies, i.e., agenesis and dysgenesis of the CC (splenium and posterior body absent), holoprosencephaly (genu and anterior body absent) and abnormal fat in pericallosal lipomas. Axial and coronal images are useful to identify the parallel orientation of the lateral ventricles and colpocephaly with dysgenesis and agenesis and for fusion anomalies. FLAIR images, particularly sagittal images, are useful in demyelinating diseases. In multiple sclerosis (MS) there are smaller lesions along the undersurface of the CC and Dawson's fingers are characteristically seen. In acute disseminated encephalomyelitis (ADEM) larger lesions may be present with involvement of the midbrain and basal ganglia. In neuromyelitis optica spectrum disorders there may also be longitudinally extensive myelitis, medullary lesions and optic neuritis. Clinical and laboratory findings used in diagnosing demyelinating diseases, including oligoclonal bands, aquaporin 4 receptor and anti-MOG antibodies are reviewed. Diffusion-weighted images best demonstrate infarcts, acute demyelination and occasionally transient lesions of the CC. Marchiafava-Bignami disease can involve the central layers of the CC diffusely or focally and best demonstrated on FLAIR and sometimes on DWI in the acute settings. Gradient echo and susceptibility weighted imaging is useful in evaluating post-traumatic diffuse axonal injury (typically located in the posterior body and splenium). Lesions that cross the CC include lymphoma, gliomas, tumefactive MS lesions and isolated tumefactive demyelinating lesions. Clinical history, patterns of enhancement and MR perfusion and spectroscopy can aid in making the diagnosis. Lastly, iatrogenic callosal abnormalities are discussed, including callosotomy for epilepsy and transcallosal resection of masses.

Conclusions

A variety of congenital and acquired lesions can affect the corpus callosum. The involvement of the CC in many neurologic diseases can be characteristic, but easily overlooked. Knowledge of pertinent anatomy, embryology, clinical and laboratory findings, and key imaging features on different MR pulse sequences improves diagnostic accuracy. This information is summarized in an image-based algorithm.

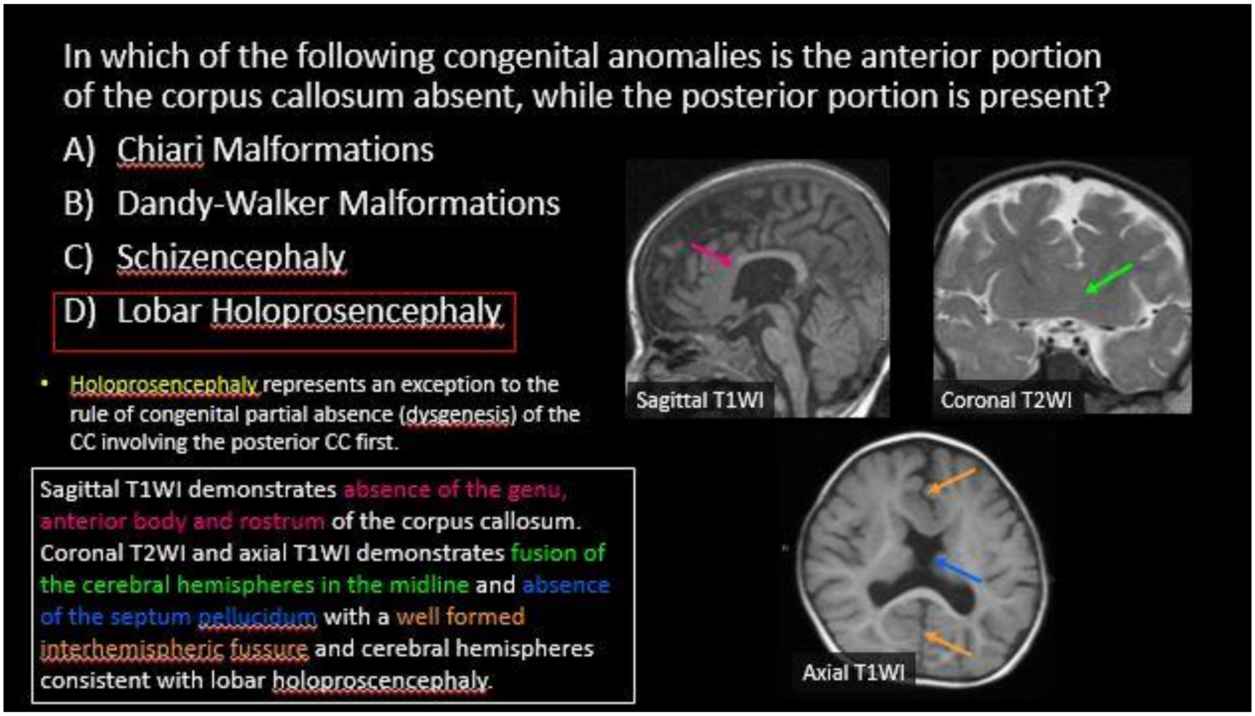

(Filename: TCT_3283_ASNRslidesample.JPG)

3292

Cavernous Sinus Lesions: What the Surgeon Needs to Know?

F Contreras[1], A Winn[2], D To[1], R Bhatia[3], S Sur[1], N Nagornaya[3]
[1]Jackson Memorial Hospital, Miami, FL, [2]Jackson Memorial Hospital, University of Miami, Miami, FL, [3]University of Miami/Jackson Memorial Hospital, Miami, FL

Purpose
Understanding pertinent surgical landmarks for approaching lesions of the cavernous sinus, serving to define the role of advanced imaging techniques and neuroradiologists for optimal treatment planning.
Materials and Methods
Review the imaging characteristics of cavernous sinus lesions, understand the pertinent anatomic landmarks relevant to the various surgical approaches, and discuss the role of radiologists in guiding treatment at a tertiary academic medical center.
Results
Examples of particular relevance to neurosurgeons approaching lesions of the cavernous include specific characterization of the anterior clinoid process, internal carotid artery, and bony boundaries. Since surgical removal of the anterior clinoid process is often required when entering the cavernous sinus from a superolateral trajectory, precise determination of a calcified petroclinoid ligament, subclinoid aneurysm, or atypical pneumatization of the clinoid process itself is essential. The presence of an atypical course of the internal carotid arteries or its branches is also of great surgical significance. Even small cavernous segment aneurysm can pose challenges to surgical entry into the cavernous sinus. Certainly, the presence of variant vascular anatomy such as a persistent trigeminal artery or evidence of collateral orbital supply through a recurrent meningeal branch is vital for surgical planning as these dural branches are often sacrificed during the approach. Finally, the endoscopic endonasal approach to cavernous sinus lesions requires a clear understanding of the carotid course and specific mention of bony irregularities such a dehiscence at Sternberg's canal can aid the surgeon in planning the safest possible to the cavernous sinus.

Remarking specifically on the relationship between bones and vascular anatomy is often useful as well. Examples include mentioning the relationship between the sphenoid septi and internal carotid arteries coursing alongside the sella.
Conclusions
Successful cavernous sinus surgery requires a complex, multidisciplinary collaboration between neurosurgery, otolaryngology, radiation oncology and neuroradiology. To achieve an optimal post-surgical outcome it is not only necessary to have an accurate radiologic diagnosis, but equally important to identify pertinent surgical landmarks such as variant osseous and vascular anatomy. This review discusses the imaging techniques, pearls and pitfalls in the diagnosis of cavernous sinus lesions, and the role of imaging in the surgical decision making process.

2646

Cephalocele of the Craniopharyngeal Canal: A Rare Remnant with a Rare Entity

A Rajput[1], J Branchcomb[2], E Velez[2], M Gupta[1], J Scheibal[1], J Acharya[3], P Kim[4], J Go[5], A Rajamohan[5]
[1]USC Keck School of Medicine, Los Angeles, CA, [2]LAC+USC, Los Angeles, CA, [3]UNIVERSITY OF SOUTHERN CALIFORNIA, KECK SCHOOL OF MEDICINE, Monrovia, CA, [4]Keck School of Medicine of USC, La Crescenta, CA, [5]UNIVERSITY OF SOUTHERN CALIFORNIA, KECK SCHOOL OF MEDICINE, LOS ANGELES, CA

Purpose
The goal of this educational exhibit is to review the incidence, prevalence, and clinical presentation of common and uncommon sellar and suprasellar lesions with focus on a cephalocele of the craniopharyngeal canal. Knowing the typical imaging appearances of embryological remnants of the central skull base and pituitary gland will help rule out various other pathologies and give referring physicians a precise explanation for the clinical findings. This will allow the radiologist to correctly distinguish this entity as congenital and recommend appropriate workup and treatment.
Materials and Methods
The craniopharyngeal canal is a remnant of the embryological tract between the floor of the sella and the nasopharynx. It exists because of incomplete closure of the Rathke's pouch, a diverticulum of the primitive buccal cavity, which is the precursor of the adenohypophysis of the pituitary gland. With this defect, many congenital lesions of development may form or persist, such as ectopic pituitary tissue primitive mesenchymal neoplasms. Additionally, the canal may serve as a site for herniation of normal intracranial tissue or as a site for tumors to grow. Our aim is to discuss the imaging findings and consider a differential diagnosis of lesions within the craniopharyngeal canal with focus on a case demonstrating a cephalocele herniating into the canal. Awareness of this rare entity is vital as diagnosing and treatment approaches.
Results
The discussion will include a brief review of sella and central skull base anatomy with embryological development of the pituitary and its vascular supply. Further discussion will highlight abnormalities in development of the normal pituitary gland resulting in a range of pathological conditions. The exhibit will provide a case based review of more common sellar and suprasellar lesions with focus on a cephalocele of the craniopharyngeal canal. The review will further include imaging characteristic that will help a radiologist to distinguish between possible considerations and offer appropriate recommendation regarding follow up and further management.
Conclusions
Review of this educational exhibit will enable a radiologist to be familiar with the development of the normal pituitary gland and associated structures. With this information, one can confidently and systematically diagnose and narrow relevant differential considerations while offering appropriate recommendations.

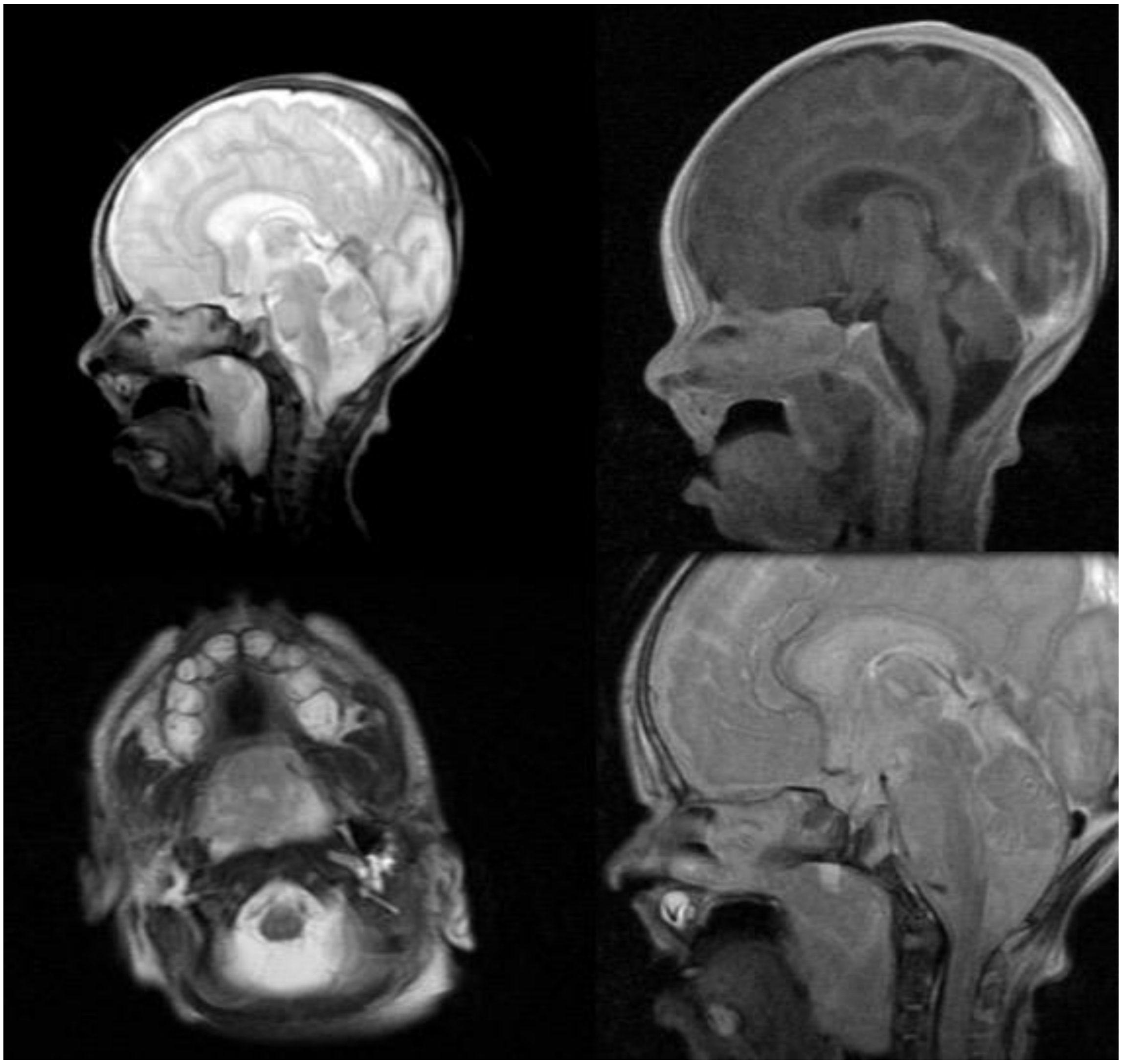

(Filename: TCT_2646_CPC.jpg)

3440

Clinical Potential of Dual-layer Detector CT for Diagnosing Head and Neck Lesions

R Aayushi[1], K Takumi[2], S Onderi[1], O Sakai[1]
[1]Boston Medical Center, Boston University School of Medicine, Boston, MA, USA, [2]Boston Medical Center/Boston University School of Medicine, Kagoshima University, Boston, MA, USA

Purpose
The utility of dual energy CT has been reported in several organs including the head and neck. Recently, dual-layer detector CT (DLCT) has been introduced into clinical practice with the advantage of routinely acquiring spectral data sets and enabling retrospective dual energy data analysis. The purposes of this exhibit are: 1. To illustrate basics of the technique of dual energy CT and demonstrate the characteristics of DLCT 2. To review clinical applications, current evidence and potential utility of dual energy CT for evaluation of head and neck region 3. To review clinical cases with DLCT and indicate future directions of DLCT in the head and neck

Materials and Methods

We summarized the basics of the technique of dual energy CT in all vendors. We retrospectively reviewed our radiological database to identify clinical cases with dual energy CT imaging in the head and neck.

Results

The representative cases with DLCT will be shown, especially the cases with incidental lesions, emergency cases, and follow-up study cases because the advantage of DLCT is to get dual energy data not only in prospective pretreatment studies but in all clinical studies. By using dual energy CT analysis, we can add to the diagnostic value of the conventional CT images, for example, leading to the improvement in image quality with or without metal artifact reduction for the conspicuity and delineation of lesions on virtual monochromatic images, accurate quantitative analysis on iodine and effective-Z maps, and detection of bone marrow edema on calcium suppression images.

Conclusions

DLCT which can perform dual energy analysis for all routine clinical images makes it possible to use dual energy analysis not only in research but also in routine clinical practice. It is important for radiologists to be familiar with the technique and clinical applications of dual energy CT for diagnosing head and neck lesions.

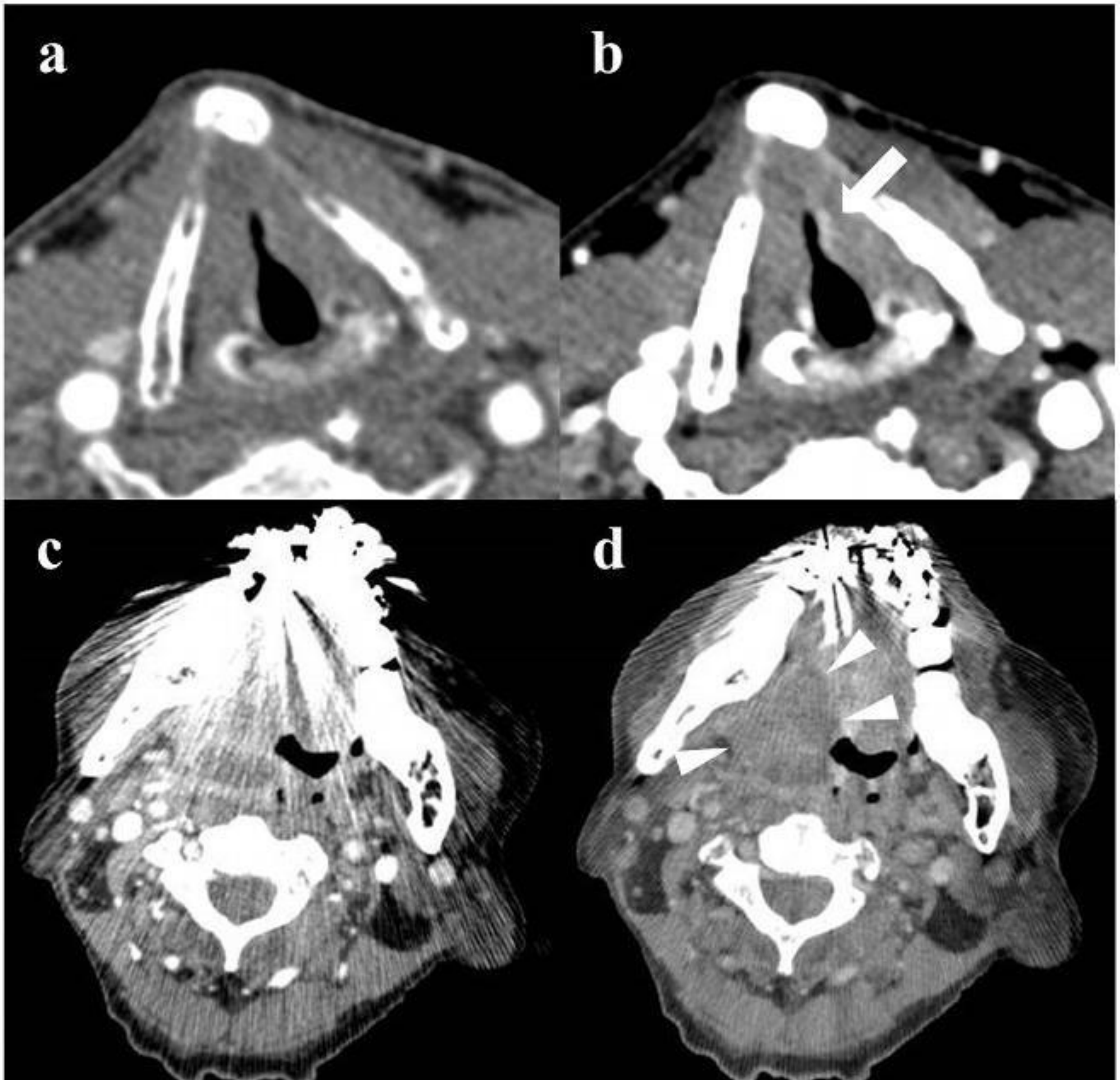

Figure. CT images of a 73-year-old male with glottic cancer (**a,b**) and a 67-year-old male with right tonsil cancer (**c,d**). The conspicuity of the tiny lesion (arrows) is greater on the 40 keV virtual monochromatic image (**b**) than on conventional 120 kVp image image (**a**). A tonsil tumor (arrow heads) is clearly detectable on the 120 keV virtual monochromatic image with metal artifact reduction technique (O-MAR) (**d**), whereas it is difficult to identify on conventional 120 kVp image image (**c**)

(Filename: TCT_3440_ASNReducationfigure600dpi.jpg)

3301

Clinical-Radiological Correlation of Isolated Brainstem Pathologies

A Habboub[1], S Mohammed[2], H Al-Jadiry[3], J Heymann[4], U Chaudhry[2], K Raghuram[2]
[1]utmb, galveston, TX, [2]UTMB, Galveston, TX, [3]UTMB Galveston, Galveston, TX, [4]University of Texas Medical Branch at Galveston, Galveston, TX

Purpose
The brainstem controls several vital functions including respiratory, cardiac, eating and sleep/activity cycles. Additionally the major white matter tracts connecting the motor and sensory systems of the brain to the rest of the body pass through the brainstem. In this exhibit, we are presenting a broad spectrum of pathologies including but not limited to infarcts, glioma, Bechet's disease, Tuberculosis and Neurosarcoidosis. Given the deceptive clinical presentation and insidious symptomatology, imaging plays a crucial role in the identification and characterization of brainstem pathologies. We present several brainstem lesions and correlate the imaging findings with the clinical presentation based on the tracts/nuclei or systems involved.
Materials and Methods
Our section database was reviewed for brainstem lesions and patient studies collected over the past two years were reviewed by the Neuroradiology fellow and fellowship trained neuroradiology faculty. Additionally clinical data was reviewed and the clinical presentation and physical exam findings were correlated with the imaging findings using standard anatomical maps of the brainstem.
Results
We will start by reviewing brainstem anatomy, then we will show the cases in a quiz-based mode; we will provide a brief history followed by the MR images showing the pathology, then there will be a slide showing the diagnosis followed by the discussion of the disease process including the symptomatology, pathophysiology and imaging findings with buzzwords to help in the differential diagnosis.
Conclusions
The purpose of this exhibit is to provide guidance to the interpretation of brainstem pathology in a clinically relevant fashion with correlation of the imaging findings and anatomical lesions.

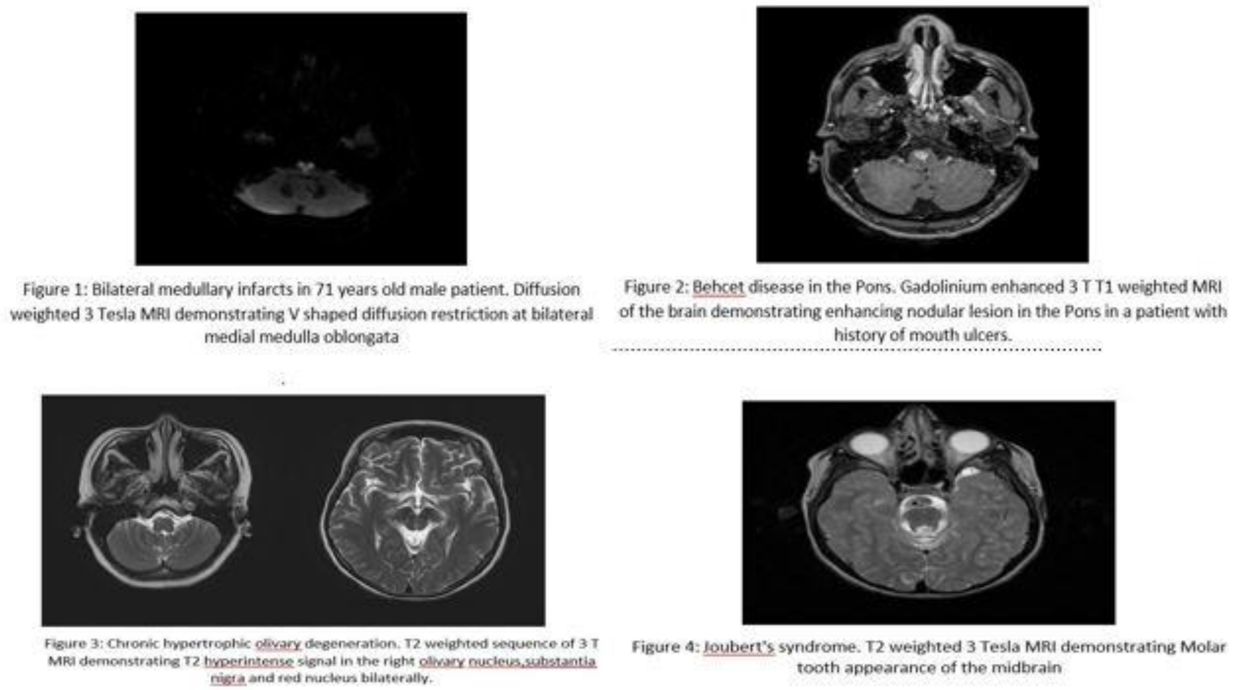

Figure 1: Bilateral medullary infarcts in 71 years old male patient. Diffusion weighted 3 Tesla MRI demonstrating V shaped diffusion restriction at bilateral medial medulla oblongata

Figure 2: Behcet disease in the Pons. Gadolinium enhanced 3 T T1 weighted MRI of the brain demonstrating enhancing nodular lesion in the Pons in a patient with history of mouth ulcers.

Figure 3: Chronic hypertrophic olivary degeneration. T2 weighted sequence of 3 T MRI demonstrating T2 hyperintense signal in the right olivary nucleus,substantia nigra and red nucleus bilaterally.

Figure 4: Joubert's syndrome. T2 weighted 3 Tesla MRI demonstrating Molar tooth appearance of the midbrain

(Filename: TCT_3301_Capture4.JPG)

2789

Cognitive Errors in Neuroradiology

A Hussien[1], A hussain[2]
[1]SUNY upstate, JAMESVILLE, NY, [2]University of Rochester Medical Center, Rochester, NY

Purpose
Neuroradiology has a unique nature as a radiology subspecialty. The scope of diseases is wide and full of subtle signs that if missed could be life threatening or could pose potential harmful consequences. Radiologists interpret neuroradiology may need to be aware of the potential sources of cognitive errors, especially emergency /general radiologists who may also interpret other types of studies in a very busy night. The purpose of this presentation is to emphasize the various types of cognitive errors that radiologist may need to know.
Materials and Methods
In this presentation we will enumerate the various types of cognitive errors and the our vision of suggested ways to overcome.
Results
Anchoring bias Confirmation bias Satisfaction of search Attribution bias Premature closure Thinking fast and slow Suggested strategies to overcome such biases
Conclusions
Radiologist awareness of the possible sources of cognitive errors and the ways that may be used to overcome them may have good effect in minimizing the mistakes and errors and improve the quality of radiology report.

2737

Common and Uncommon Masses of the Lacrimal Gland: Clinical, Radiologic, and Pathologic Correlation

M Siddiqi[1], M Dakhel[1], H Lee[2]
[1]Rutgers New Jersey School of Medicine, Newark, NJ, [2]Rutgers New Jersey Medical School, Newark, NJ

Purpose
We present 6 pathology proven lacrimal gland masses from our institution to review the CT and MR findings with clinical and pathology correlation. Approximately 50% of lacrimal masses are infectious or inflammatory in origin and 25% are salivary gland tumors. Although exceptions and overlaps exist, familiarity with certain features may help an accurate deduction of the pre-surgical diagnosis.
Materials and Methods
A chart review was performed of 6 pathology proven lacrimal gland masses from our institution in order to determine the clinical and pathologic correlation with radiological findings.
Results
Dacryoadenitis: Idiopathic orbital inflammation, subclassified based on anatomical target, dacryoadenitis (32%), myositis (29%), optic nerve (22%). CT and MRI demonstrate diffuse oblong enlargement of gland with preservation of gland shape. Post contrast reveals avid enhancement. Sarcoid: multisystem granulomatous disorder. Ocular involvement in 22%. 75% are bilateral. On MRI, the glands may appear hypointense to isointense on T1 and T2 weighted images1. Homogeneous enhancement on CT and MRI without bony involvement. Pleomorphic Adenoma: the most common benign epithelial tumor1. 20% of these may become malignant. Painless, slow growth causes smooth bony scalloping on CT1. MRI may demonstrate low to intermediate signal on T1 and intermediate signal on T2 weighted sequence. Adenoid Cystic Carcinoma: most common malignant epithelial tumor, accounting for 50% of epithelial tumors. Unilateral, painful mass, characterized by perineural spread. CT demonstrates homogeneous orbital mass with bony destruction and diffuse enhancement1. MRI demonstrates hypointensity on T1 and intermediate to high signal on T2 weighted images with diffuse enhancement. Lymphoma: Relatively rare, with the most common type being mucosa associated lymphoid tissue. CT demonstrates diffuse involvement of bilateral glands with mild enhancement. MRI demonstrates homogeneous, isointense lesion on T1 and isointense to slightly hyperintense on T2 weighted images with moderate enhancement and diffusion restriction. Canalicular Adenoma: Less than 1% of gland tumors, most commonly in the 7th decade. Arises purely from ductal luminal cells without stromal component. Painless, slow growth with bony erosion on CT. MRI demonstrates heterogeneous high signal on STIR sequence with diffuse heterogeneous enhancement.
Conclusions
Familiarity with imaging features of benign and malignant etiologies of the lacrimal gland will enable the neuroradiologist to arrive at an accurate pre-surgical diagnosis.

2304

Cricoarytenoid – the Forgotten Joint: Imaging Findings and Literature Review

K Lam[1]
[1]Rochester General Hospital, Rochester, NY

Purpose
a. Arytenoid dislocation/subluxation is a rare but underdiagnosed condition and can mimic vocal cord paralysis. b. Knowledge of the clinical history, anatomy, and pathophysiology of arytenoid dislocation are important in making prompt and accurate diagnosis, which is critical since it can be surgically corrected if not delayed, unlike vocal cord paralysis.

Materials and Methods
a. Discuss embryology of the cricoarytenoid joint. b. Review the important pertinent anatomy. c. Demonstrate important imaging findings of cricoarytenoid dislocation/subluxation. d. Review of the literature regarding incidence, risk factors, etiologies, symptomatology, injury mechanisms, and treatment.
Results
The fetal arytenoid cartilages can be identified at approximately 30-32 days of gestation. The cricoarytenoid joint is diarthrodial, strengthened posteriorly by the cricoarytenoid ligament. Located atop the posterior cricoid cartilage, the pair of arytenoid cartilages is pyramidal in shape, which is thought to contribute to the joint stability. The vocal and muscular processes are at the level of the true vocal cord. The vocal processes are anterior projections where the posterior margins of the true vocal cords attach. Arytenoid dislocation/subluxation is rare and was first described in 1973. Its incidence is less than 0.1%, with less than 200 cases reported. Etiologies include difficult intubation, external laryngeal trauma, and procedures involving direct laryngoscopies. There are numerous risk factors, such as cardiovascular operation, BMI, laryngomalacia, diabetes mellitus, chronic renal failure, acromegaly, chronic steroid use, rheumatoid arthritis, laryngeal cancer, chondroradionecrosis, cricoarytenoid arthritis. Most common symptoms include dysphonia, dysphagia, sudden onset of odynophagia, and voice fatigue. Official diagnosis is usually made by a combination of computed tomography, laryngeal electromyography, and laryngoscopy. Differential diagnoses include vocal cord paralysis (recurrent laryngeal nerve mediated), laryngeal hematoma (which can be life-threatening), and tumor invasion. Several theories on postintubation arytenoid dislocation injury are postulated. Insertion of the endotracheal tube with the right hand allows for the distal one-third tip to exert the most pressure on the left arytenoid, causing subluxation. Extubation with the balloon incompletely deflated may result in posterior arytenoid dislocation. It is critical for the endoscopist or anesthesiologist to ensure good visualization of the arytenoids before instrumentation of the airway. Treatment options include voice therapy, surgery (closed reduction only or with additional procedure).
Conclusions
a. Cricoarytenoid dislocation/subluxation is a rare but important diagnosis and can be easily misdiagnosed by the more common diagnosis of vocal cord paralysis. b. Improved awareness and knowledge of the relevant anatomy and imaging findings are critical in making prompt and accurate diagnosis, which has important surgical implications.

3467

Current Treatment Protocols for CNS Metastases

J Jenkins Fernandez[1], A MAHAJAN[2]
[1]Yale University, New Haven, CT, [2]Yale University, NEW HAVEN, CT

Purpose
Metastatic lesions are the most common intracranial malignant tumors. Radiotherapy, both Whole Brain Radiotherapy (WBRT) and Stereotactic Radiosurgery (SRS) are currently the most widely employed treatment modalities. But with rapid progress being made in development of targeted therapies and immunotherapy regimens for brain metastases, an up-to-date algorithm is required to aid in the selection of the most appropriate treatment plan for each patient. We aim to review all available information to create an up-to-date algorithm for this purpose.
Materials and Methods
Systematic review of the latest available literature about the current protocols and trends in management of CNS metastases. Selection of an appropriate approach for the management of CNS metastases depends of various factors, such as the site of the primary tumor, the number of metastatic lesions, size, location, expected survival benefit, age, histological features etc.

Results
We put forth the current treatment algorithm for the management of CNS metastases. We also include relevant examples, with radiological images before and after treatment, to highlight the effect of the selected treatment in these patients.
Conclusions
This is the current algorithm for the management of CNS metastases, based on available information for each patient. This would enable treatment providers with the most appropriate treatment plan for each patient based on the patient variables and tumor characteristics, and in the selection of the most appropriate immunotherapy trial for each patient.

2592

Decipering Collateral Flow: Anatomical and Imaging Correlate

C Liang[1], M Taheri[2]
[1]George Washington University Hospital, Washington, DC, [2]George Washington University, Washington, DC, DC

Purpose
The CDC estimates that approximately 1 out of every 20 American deaths each year are caused by stroke. Most of these strokes are caused by lack of adequate arterial blood supply. The selection of the group of patients who would benefit from therapy has transitioned from the time of symptom onset towards the extent of tissue at risk. CT Perfusion scans have been shown to play a key role in the selection of potential candidates for intra-arterial therapy. More recently, new evidence has emerged that Multiphase CTAs may have similar utility as CT perfusion scans in the selection of these patients. The degree of collateral flow is typically determined based on the comparison of the degree of contrast opacification of the branches of MCA as compared to the contralateral side. The purpose of this exhibit is to explore the mechanisms by which this collateral flow is recruited.
Materials and Methods
We review existing anatomical and angiographic literature and personal experience for details regarding these pathways.
Results
The concept of collateral circulation makes most sense when viewed as a pathophysiological response to loss of perfusion pressure in an adjacent vascular bed. The physical existence of a collateral pathway and its (patho) physiological response are equally important clinically. However, the latter factor is often overlooked and under-emphasized. Leptomeningeal collaterals consist of pial plexus vessels bridging neighboring branches of major cerebral vessels as well as meningeal vessels with connection between the cerebral and meningeal arteries. Many leptomeningeal collaterals are often underdistended and angiographically occult in the absence of pathology and may re-disappear after reestablishment of flow, as sometimes seen in post-thrombectomy patients. Factors that affect the number and presence of leptomeningeal collaterals includes innate variation of Willisian circulation, long standing intra- and extracranial stenosis, and chronic hypoxia. Equally important are physiological factors dictating cerebral blood flow. The most important is the ability to autoregulate (vasodilate) which is adversely affected by many factors. This includes an age related decline in the number and diameter of collaterals with their increased tortuosity, resulting in an increased collateral resistance. History of chronic hypertension is associated with poor collaterals whereas pretreatment with statins have been shown to increase the probability of good collaterals.
Conclusions
Understanding cerebral collateral circulation as a dynamic response to a pathophysiologic state in both anatomical and physiological terms aids a neuroradiologist in the interpretation of Multiphase CTA as well as its implication on CT and MR perfusion studies.

2887

Decompressive Craniectomy and Cranioplasty: A Review of the Current Literature

R Sinha[1], A Herwadkar[2], R Siripurapu[3], R Hyde[4], I Russell[5]
[1]Salford Royal Hospital, UK, Manchester, United Kingdom, [2]Salford Royal Hospital, Manchester, Greater Manchester, [3]Greater Manchester Neurosciences Centre & Salford Royal NHS Foundation Trust, Salford, Manchester, [4]Salford Royal Hospital, Manchester, United Kingdom, [5]Salford Royal NHS Foundation Trust, Manchester, Greater Manchester

Purpose
Several studies have evaluated the role of decompressive craniectomy (DC) as part of a second level measure in the management of refractory raised intracranial pressure. Raised intracranial pressure can be secondary to various causes including severe head injury, subarachnoid haemorrhage, infection and acute ischaemia.
Materials and Methods
Whilst DC is thought to be effective, several factors should be taken into consideration including patient selection, optimal time for intervention, risk of associated complications and patient outcomes. Many of these patients subsequently undergo cranioplasty (CP), which involves repair of the skull vault defect created by the craniectomy. A summary review of the current literature on the use of DC and CP will be discussed in detail during the presentation.
Results
The main indications for CP include protection of the brain surface and for cosmetic purposes. There are however several small scale studies that have postulated a therapeutic role associated with cranioplasty in the form of improvement in patient's functional outcome. Several different materials can be used including biological and non-biological substitutions however there is yet to be a consensus regarding the optimal material. These procedures are not without its risks and these can be divided into two subgroups: 1. Complications relating to the initial DC – herniation of the cortex, subdural/subgaleal effusion, infection, syndrome of the trephine, paradoxical cerebral herniation, external brain tamponade, seizures, hydrocephalus. 2. Complications relating to the subsequent CP – subdural and epidural haematomas, cerebral edema, infection, bone flap resorption
Conclusions
In conclusion, the aims of this presentation include discussion of the rationale for DC and CP, an overview of the different techniques used for cranioplasty and a summary of the imaging appearances including the associated complications.

3388

Deep Learning for Radiology: How to Get Started

J England[1], A Vijayasarathi[1]
[1]University of California Los Angeles, Los Angeles, CA

Purpose
The purpose of this educational exhibit is to demonstrate how to go from knowing next to nothing about computer coding, artificial intelligence, or deep learning to starting a well-chosen, potentially publishable research project on deep learning in radiology.
Materials and Methods
Deep learning is a sub-field of machine learning that has allowed breakthrough performance in computer vision. Some deep learning algorithms have achieved expert or near-expert performance in radiology

tasks, such as diagnosis of hip fracture or pulmonary tuberculosis on plain radiograph. Many radiologists are excited by these advances and would like to learn more but lack the computer science background necessary to implement deep learning in their research endeavors.

Results

Our presentation will include a review of deep learning, how it works, and how it fits into the larger fields of artificial intelligence and machine learning. We will recommend a curriculum of online courses and books totaling approximately 24 weeks that can be completed in parallel with other clinical, research, and administrative responsibilities. Finally, we will provide useful advice for choosing an early project that will solidify this new knowledge and skill, answer an important research question, and lead to publication in a peer-reviewed journal. To concretize this advice, we will use the example of classifying T1- and T2-weighted MRI images of the brain.

Conclusions

Deep learning is an exciting field in the early phases of application to radiology. Many radiologists are interested in learning more but lack the background in computer science to make quick headway. We present a review of deep learning and published applications of deep learning in radiology, recommend a curriculum to quickly acquire the necessary skills to understand and apply deep learning to new problems, and provide advice on designing an early project that will solidify these skills.

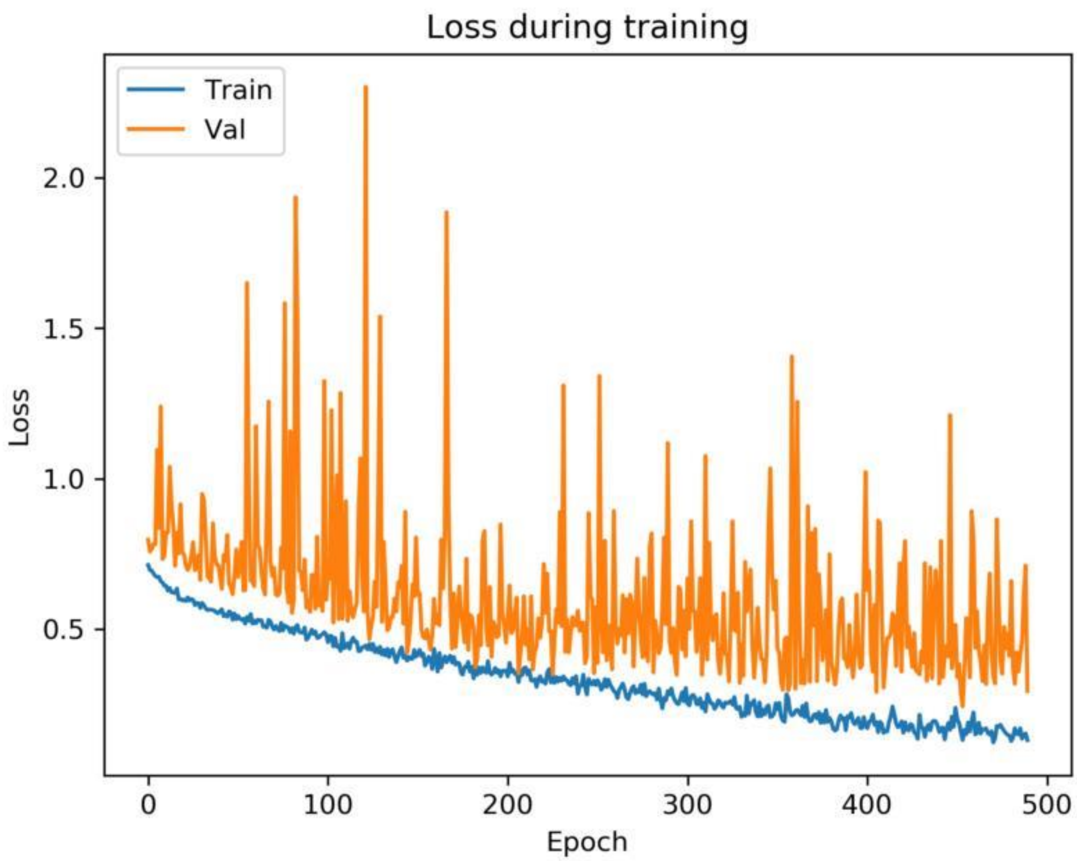

(Filename: TCT_3388_DeepLearningAbstractImage.jpg)

2730

Diagnosis and Beyond: Utility of Imaging across a Variety of Clinical Scenarios Encountered in Multiple Sclerosis

M Bhatt[1], A Krishnan[2]
[1]Beaumont-Royal Oak (William Beaumont Hospital), Royal Oak, MI, [2]OAKLAND UNIVERSITY WILLIAM BEAUMONT SCHOOL OF MEDICINE, TROY, MI

Purpose
Magnetic resonance (MR) imaging plays a critical role in the diagnosis and management in Multiple Sclerosis (MS). The utility of MR imaging continues to evolve with advances in MS management and therapeutics. Our purpose is to review common clinical applications of MR imaging in MS and how the radiologist can provide more relevant interpretations based on the particular clinical question.
Materials and Methods
We will present multiple clinical scenarios in MS for which MR imaging is obtained. Each case will discuss a myriad of relevant points: specific protocol used for the particular clinical question, utility of gadolinium, key imaging findings, potential pitfalls and pertinent details to include in the report. These scenarios include: 1. Making the Diagnosis 2. Establishing an imaging baseline at time of initial clinical evaluation 3. Imaging of acute symptoms/relapses (Including Brain, Optic Nerves, Spinal Cord) 4. Routine follow-up imaging 5. Beginning new disease modifying therapies (DMTs) [Including baseline and response to therapy] 6. Evaluating for opportunistic infections/side effects of DMTs (example, progressive multifocal leukoencephalopathy) 7. Additional miscellaneous topics (Limitations of Conventional MR imaging in MS and Future applications of advanced MR imaging techniques)
Results
Following our case based review; the radiologist should be aware of current clinical applications of MR in MS. The reader should also have an understanding of the technical differences in each scenario and knowledge of the pertinent details that aid the Neurologist in the management of patients.
Conclusions
MR imaging has multiple roles in MS beyond making the diagnosis or assessing for increased disease burden. Comprehension of the different clinical situations in which MR is used for MS can aid the radiologist in reporting the relevant information that can assist in patient care.

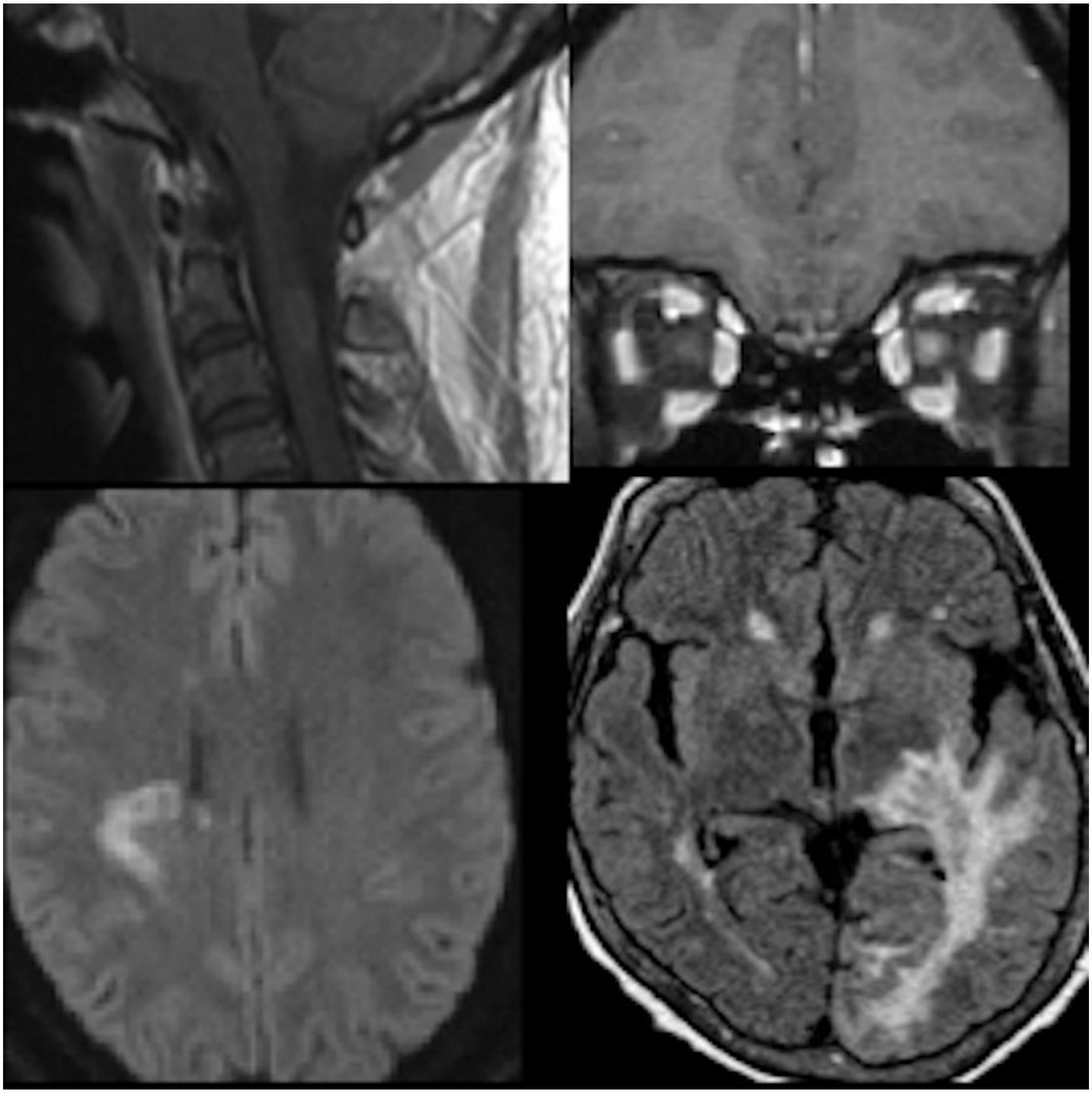

(Filename: TCT_2730_ASNRMSabstractimages.jpg)

2518

Differentiating Treatment Related Response from Progression in Intracranial Neoplasms: A Diagnostic Challenge

W Chang[1], A Sohn[1], M Spearman[1], C Li[1], M Goldberg[1]
[1]*Allegheny Health Network, Pittsburgh, PA*

Purpose
Given the myriad techniques available for treatment of intracranial neoplasms including surgery, radiotherapy, systemic chemotherapy, local chemotherapy, anti-angiogenic therapy, immunotherapy, vaccines, and laser/thermal ablation, differentiating tumor progression from treatment related response

can be very challenging. In this presentation, we will discuss the common imaging findings from the treatments described above, illustrate findings that can help differentiate progression from treatment related effects, and introduce techniques that can help differentiate treatment related effects from tumor progression, including MR perfusion, MR spectroscopy, gallium, FDG-PET, ADC histogram analysis and F-DOPA.

Materials and Methods

We will discuss the different treatment paradigms, showing examples of their typical presentations on CT/MRI, as some of these techniques are relatively new or uncommonly used, and may present in the community without adequate history or clinical information. We will then discuss differences between tumor and treatment related response on conventional MRI. Subsequently, we will discuss techniques that can help differentiate treatment from tumor progression, and how they can be best employed to differentiate the two clinical scenarios. Finally, an interactive quiz will be provided to reinforce key teaching points.

Results

Many treatment related responses may have characteristic imaging findings/features suggestive of treatment related response as opposed to true progression. This may include time course of lesion emergence, intensity of T2/FLAIR signal, distribution of lesions, and other features. For more difficult diagnostic cases, the different techniques described above can be employed. MR perfusion can demonstrate decreased cerebral blood volume in areas of treatment related change as opposed to increased CBV in regions of tumor, while spectroscopy can demonstrate findings characteristic of normal brain versus tumor. Nuclear medicine studies, such as FDG-PET and F-Dopa, may also have clinical utility. ADC histogram analysis can also show decreased ADC in regions of tumor.

Conclusions

In this presentation, we will demonstrate typical imaging findings for treatment related effects, describe techniques for differentiating them from tumor progression, describe techniques that can help in identifying treatment related response, and show how they can be used to differentiate tumor progression from treatment related changes.

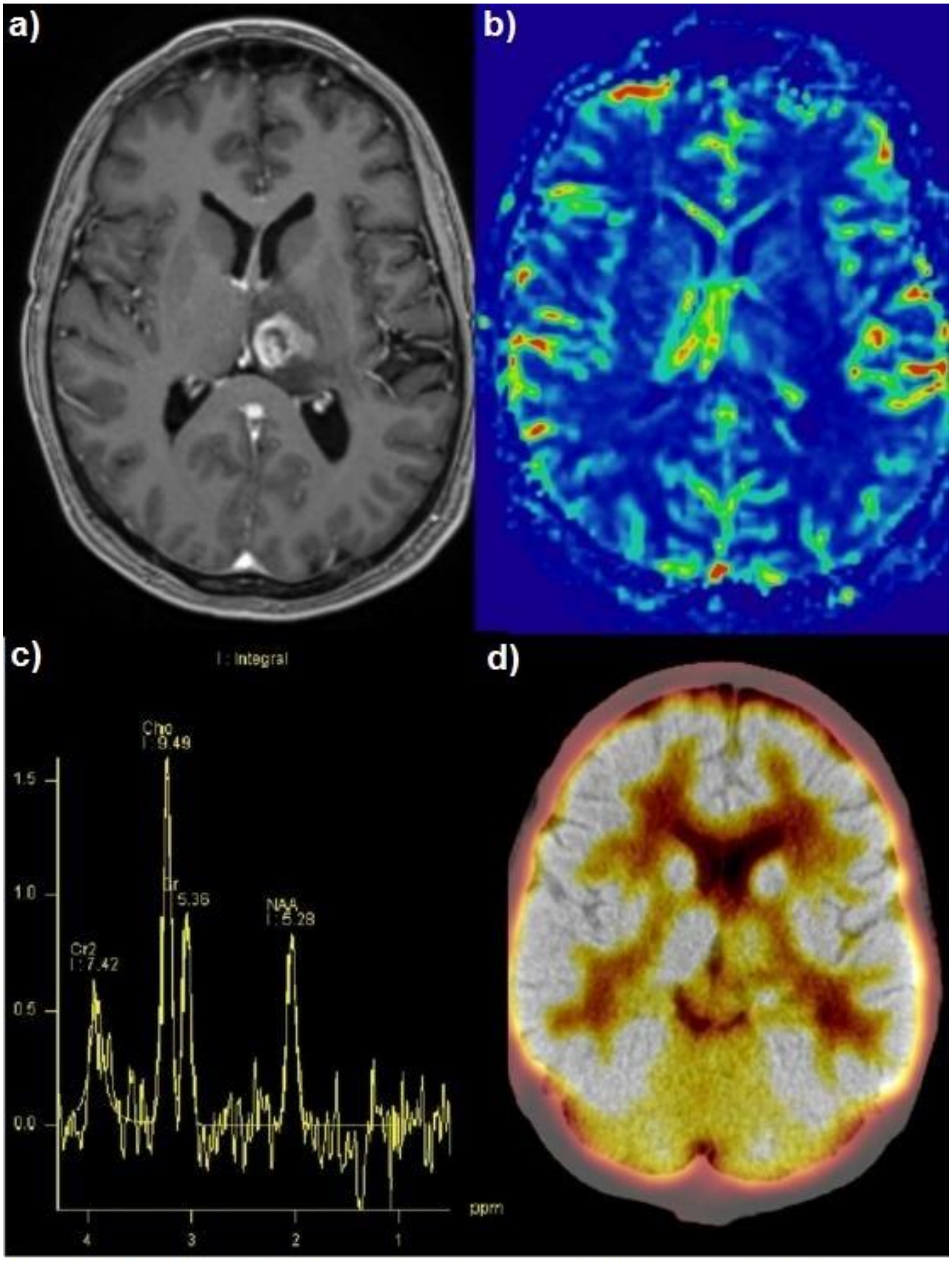

Figure 1: a) Enhancing lesion is seen within the left thalamus, concerning for recurrent glioblastoma. **b)** The lesion demonstrates decreased cerebral blood volume compared to the contralateral unaffected thalamus. **c)** The lesion demonstrates elevated Choline-NAA ratio, which can be seen in early radiation necrosis. **d)** The lesion demonstrates decreased FDG update on PET/CT. Overall, findings are consistent with treatment related effects.

(Filename: TCT_2518_treatment2.jpg)

3127

Diffuse Tensor Imaging Quantification Analyzing: A Success Way to Differentiation Gliomas Versus Brain Metastases Accurately

S Emamzadehfard[1], V Eslami[1], H Sair[2], K Clark[1]
[1]University of Texas Health Science Center, San Antonio, TX, [2]JOHNS HOPKINS MEDICINE, BALTIMORE, MD

Purpose
High-grade gliomas and metastases are the most common intracranial lesions, with different management paradigm. However, their differentiation is still in a deep gap of knowledge. Although sets of cross-sectional imaging (MR and CT) are often used as primary neuroimaging steps, differentiation still mostly relies on correlating clinical history with biopsy or searching for primary lesions throughout the body in cases of malignancy involvement. Nonetheless, relying on clinical history and cross-sectional imaging may be challenging when the patient presents with a solitary enhancing mass as both gliomas and metastases may exhibit ring-enhancement and extensive edema on MR.
Materials and Methods
Measurements computed from diffusion tensor imaging (DTI) such as fractional anisotropy (FA) and mean diffusivity (MD) have demonstrated pathological changes within brain tumors. FA and MD have been measured based on chemical and physical properties of individual voxels. Anisotropy describes the tendency of water to travel along a single axis. High FA values are expected in white matter tracts that move along a single axis, while low FA values are expected in free water areas such as ventricles. High MD is expected in voxels with low anisotropy. Clinically, FA values are lower and MD values are higher in the damaged white matter when compared to healthy tissue. Also, apparent diffusion coefficient (ADC) has been measured recently and has proven to be lower in gliomas than metastases. In contrast to metastatic lesions, the vasogenic edema surrounding gliomas is characterized by infiltrating tumor cells. Both intratumoral and peritumoral FA, MD measurements could be applied for differentiation between high-grade gliomas and metastases.
Results
Recent literature consensus showed significantly more pronounced vasogenic edema effects on the FA and MD in metastases than in gliomas with high-grade gliomas demonstrating a significantly higher peritumoral FA and significantly lower MD than metastases.
Conclusions
Outline: • Mean diffusivity or ADC map; which is defined as the summed of all three eigenvalues of a voxel's tensor to quantify the amount of diffusion, increased in metastasis compared to gliomas. • Due to the difference in the selection of the region of interests for the peritumoral region, all of these parameters including ADC map are non-conclusive. • Systematic measurements of DTI metrics from different regions of the tumor, robust way of characterizing. • DTI metrics (categorized into four main segments including pixel-wise ADC, FA, linear measure (cl) and planar measure (cp) maps), from segmented regions, were combined to generate an optimal regression model to differentiate these two tumors. • The ROC analysis showed that FA and CL from the enhancing region of the tumor (ER) have the highest prediction accuracy when used alone. • Tumor wise, the overall sensitivity, specificity, and accuracy for all the measurements in the peritumoral areas were lower than in the enhancing part of the tumor. • Combination of ADC, FA, and CP from the enhancing part is the most powerful classifier of tumor types DTI metrics, used individually or combined, have a potential as a non-invasive measure to differentiate glioblastomas from metastases. Figures legend: Figure1. A 68-year-old female with a glioblastoma in the left frontal lobe. There was no hemorrhage based on T1- and T2-weighted images (not shown). Transverse contrast-enhanced T1-weighted (A) and FLAIR (B) images show ring-enhancement and

extensive edema. ADC map (C) shows restricted diffusion of the enhancing part. FA (D), CL (E) and CP (F) from the enhancing part are lower than normal appearing white matter but higher than that for brain metastases.

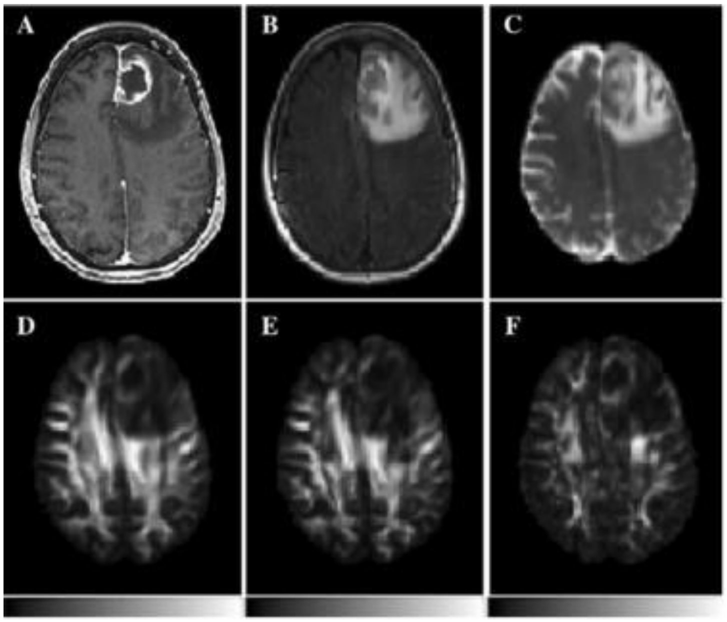
A
B
C
D
E
F

(Filename: TCT_3127_DTI.jpg)

2882

Diffusion-Weighted Imaging in Head and Neck Cancer: What do We Know and Where do We Intend to Go?

D Fragoso[1], L Garcia[2], T Scoppetta[3], A MAIA[4], A Goncalves Filho[4], C TOYAMA[5], C da Silva[5]
[1]Santa Casa de São Paulo, SÃO PAULO, Brazil, [2]Hospital das Clínicas, Sao Paulo, Sao Paulo, [3]Santa Casa de São Paulo, São Paulo, Brazil, [4]Santa Casa de São Paulo, SAO PAULO, SAO PAULO, [5]FLEURY, SÃO PAULO, SÃO PAULO

Purpose
Discuss how DWI can potentially be used to characterize head and neck lesions as either benign or malignant, predict the response of head and neck cancer to various types of treatment, monitor tumor to determine the effectiveness of treatment, and determine whether a residual mass detected after treatment represents scar or recurrence.
Materials and Methods
We conducted a review in the literature with the following search terms: Diffusion-weighted imaging, intravoxel incoherent motion, apparent diffusion coefficient, head and neck cancer, and head and neck squamous cell carcinoma). The work was organized in a brief introduction, which included some relevant techniques details. Then, most clinical applications were discussed: - Characterizing the malignant potential of a lesion; - Prediction of treatment response; - Monitoring of treatment response; - Recurrence versus posttreatment changes; Finally, we discussed the limitations and perspectives. All examples of each situation (diagnosis, pre- and post-treatment / recurrence evaluation) were cases of our institution.
Results
Multiple studies have been testing the ability and reliability of diffusion-weighted (DW) in characterizing the malignant potential of a lesion based on ADC measurement. These were based on the hypothesis that malignant tumors would demonstrate lower ADC values compared with benign tumors owing to their relatively higher cellularity. Besides that, the potential of DWI is not just limited to differentiating benign versus malignant head and neck lesions, as in some instances can help to distinguish different malignant tumors, according to some authors. Despite some controversies in the literature, several past and current studies have explored the ability of DWI to predict a tumor's response to treatment before the intervention, helping to predict treatment response, guide treatment strategies, and assess the overall prognosis. Once treatment has commenced, be it radiation, chemotherapy, or a combination of both, it is desirable for radiation and medical oncologists to not only assess whether the treatment is effective but also to quantify its efficacy and tailor further treatment to the individual patient. Many studies have looked at ADC and also intravoxel incoherent motion (IVIM) changes and their correlation to treatment response. DWI has also been investigated for its potential to distinguish posttreatment changes from recurrent neoplasm.
Conclusions
DWI of head and neck represents a distinct method of MR imaging with far ranging current and potential applications. Current research continues to improve the capabilities of DWI in characterizing masses as benign or malignant, predicting their response to treatment, monitoring and assessing the response to treatment as therapy progresses and surveilling areas of prior intervention to detect posttreatment and recurrent neoplastic changes.

2263

Disease Processes that Cause Cranial Nerve Symptomatology

R Embertson[1], M Altenburg[2], V Summers[3]
[1]University of North Carolina, Chapel Hill, NC, [2]University of North Carolina at Chapel Hill, Chapel Hill, NC, [3]University of North Carolina, DURHAM, NC

Purpose
The range of pathology affecting the cranial nerves is broad, and many of the relevant disease processes are not classically discussed within the framework of cranial nerves. The goal of this educational exhibit is to present various disease processes that affect the cranial nerves, with pathophysiologic and anatomic correlation, in an image-rich format using real case examples. Common entities will be covered, in addition to some more rare disease processes, and uncommon manifestations of familiar pathology.
Materials and Methods
A retrospective review of cases collected over several decades are used to present the imaging findings, pathology, and clinical presentation of disease processes affecting the cranial nerves, including but not limited to many of the entities listed below: CN I: Kallmann's syndrome, dermoid/epidermoid, nasal glioma, encephalocele, trauma, septo-optic dysplasia, esthesioneuroblastoma, Granulomatosis with Polyangiitis, and SNUC CN II: Papilledema, optic neuritis, Juvenile pilocytic astrocytoma, lymphoma, IgG4-related disease, pseudotumor, chloroma, cavernous and capillary hemangioma, and meningioma CN III: P-Comm aneurysm, meningioma, stroke, neuritis, lymphoma, leukemia, schwannoma and ophthalmoplegic migraine, and Horner's syndrome from multiple etiologies including Pancoast tumor and birth injury CN IV: Cavernous sinus thrombosis, cavernous/carotid fistula, carcinomatosis, hemosiderosis, and Rosai Dorfman. CN V: Schwannoma (including Meckel's cave and infraorbital nerve), chordoma, sarcoidosis, metastases, pseudotumor, mucormycosis, and perineural tumor spread CN VI: MS plaque, schwannoma, and dolichoectasia CN VII: Bell's palsy, prolapsing nerve, aberrant nerve course, Ramsay Hunt Syndrome, schwannoma, hemangioma, and nerve agenesis CN VIII: Schwannoma, cochlear nerve agenesis, and Herpes Zoster Oticus CN IX: Glomus Jugulare tumor, platybasia, and meningioma. CN X: Vocal cord paralysis from multiple etiologies including H&N/thyroid malignancy, and skull base masses. CN XI: Paraganglioma with secondary SCM and trapezius atrophy CN XII: Synovial cyst, schwannoma, paraganglioma
Results
Etiologic categories of cranial nerve dysfunction include congenital, infectious, neoplastic, trauma-associated, and pathology related to hemorrhage/vascular lesions. Cranial nerves can easily be overlooked, and it is important to thoroughly evaluate the cranial nerves when interpreting diagnostic imaging studies of the head and neck, and to keep in mind the range of pathology that can affect them.
Conclusions
Numerous disease processes, including their pathophysiology, anatomic relationships, and imaging features must be well understood to improve diagnostic accuracy when evaluating patients with cranial nerve dysfunction. Keeping these disease processes and their cranial nerve relationships in mind will help radiologists be more helpful to ordering providers when interpreting neuroimaging studies.

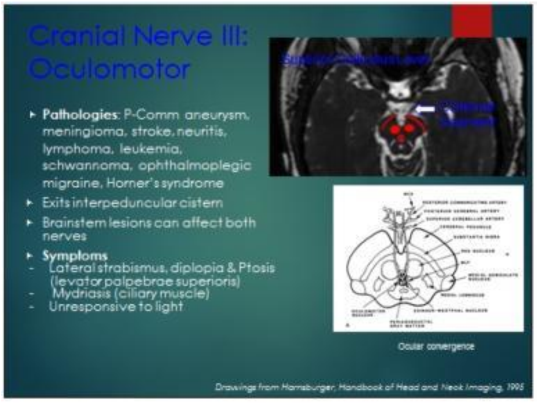

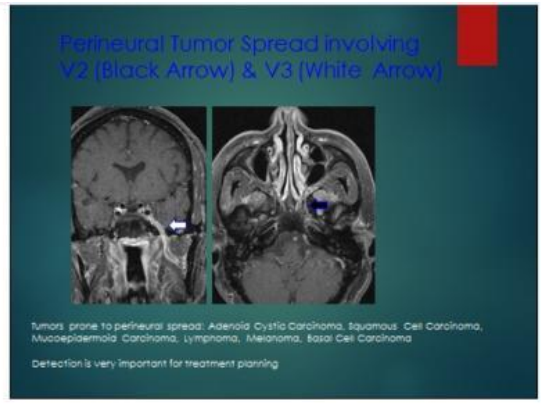

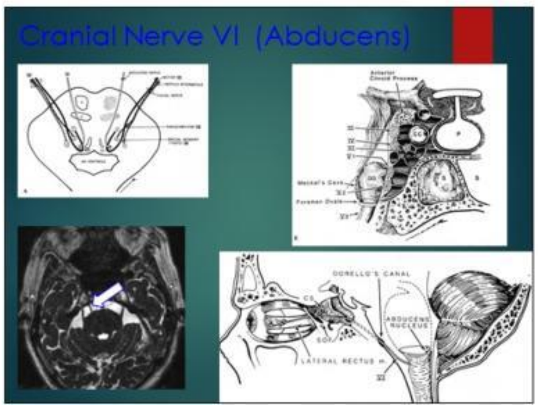

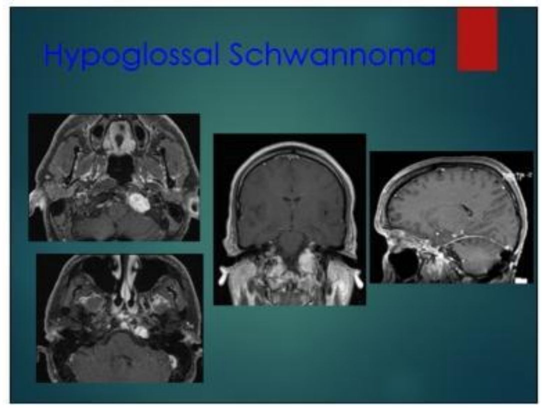

(Filename: TCT_2263_CN.jpg)

3063

Don't Be Fooled: It's Not a Meningioma

T Scoppetta[1], D Fragoso[2], F Pacheco[3], R Hoffmann Nunes[3], A da Rocha[4]
[1]Santa Casa de Misericórida de São Paulo, São Paulo, Brazil, [2]Santa Casa de Misericórida de São Paulo, SÃO PAULO, Brazil, [3]DASA, Sao Paulo, Sao Paulo, [4]IRMANDADE SANTA CASA DE MISERICORDIA DE SAO PAULO, Sao Paulo, Sao Paulo

Purpose
Illustrate a series of cases that mirrors meningioma in neuroimaging scans, including ordinary and rare pathologies.
Materials and Methods
Was conducted a retrospective, descriptive and analytic study of brain CT and MRI scans performed in our institutions. Present a series of cases that mimics meningioma, debate its peculiar imaging findings and point out when and which others imaging techniques will guide the final diagnosis.
Results
Meningiomas are extra-axial tumours and represent the most common tumour of the meninges. They are generally easy diagnosed. However, a constellation of pathologies can mirrors meningioma neuroimaging findings. Pathologies belonging to distinct groups were presented, including vascular (aneurysm), inflammatory (post-operative changes, sarcoidosis), neoplastic (hemangiopericytoma, lymphoma, metastasis, tumor-to-tumor metastasis), traumatic (extra-axial haematoma) and iatrogenic (mucocele and

foreign body). All pathologies were histologically proven. Peculiar imaging characteristics were dissected to simplify the differential diagnosis.
Conclusions
Meningioma are often treated as a child's play diagnosis. A collection of pathologies can mimic meningioma on brain scans. Radiologists should be familiarized with all these conditions, in view of its wide treatment options, considering it can shift from conservative approach to surgery and chemotherapy. Therefore, it cannot be underestimated and certainly not misdiagnosed.

2750

Don't Get Stumped by Lumps and Bumps - Imaging of Calvarial Lesions

R Thakkar[1], T Deklotz[2], A Jay[3]
[1]MEDSTAR GEORGETOWN UNIVERSITY HOSPITAL, Washington, DC, [2]MedStar Georgetown University Hospital, Washington, DC, DC, [3]MEDSTAR Georgetown University Hospital, Washington, DC

Purpose
Calvarial and scalp masses are common presenting symptoms in both children and adults. Given the wide spectrum of benign and malignant lesions that can affect the skull and the overlapping of associated presenting symptoms, these lesions can often be diagnostic dilemmas. However, the accuracy in diagnosis is critical because imaging strategy and management can vary significantly.
Materials and Methods
The radiology database using departmental search engine was queried for calvarial and scalp lesions from 2008-2018.
Results
This exhibit will describe the normal anatomy and the differential diagnosis for multiple skull/scalp. Furthermore, we will discuss the importance of complete and appropriate imaging for preoperative assessment of these skull lesion. The characteristic imaging finding for diagnosing these lesions will be highlighted, which will enable radiologist to narrow the differential diagnosis. The final diagnosis will be correlated with histopathology whenever possible.
Conclusions
Calvarial and scalp masses are common symptoms presenting in children and adults. It is important that the radiologist understands how to recommend appropriate imaging strategies and provide narrow differential diagnoses to guide management. Don't get stumped by these lumps and bumps!

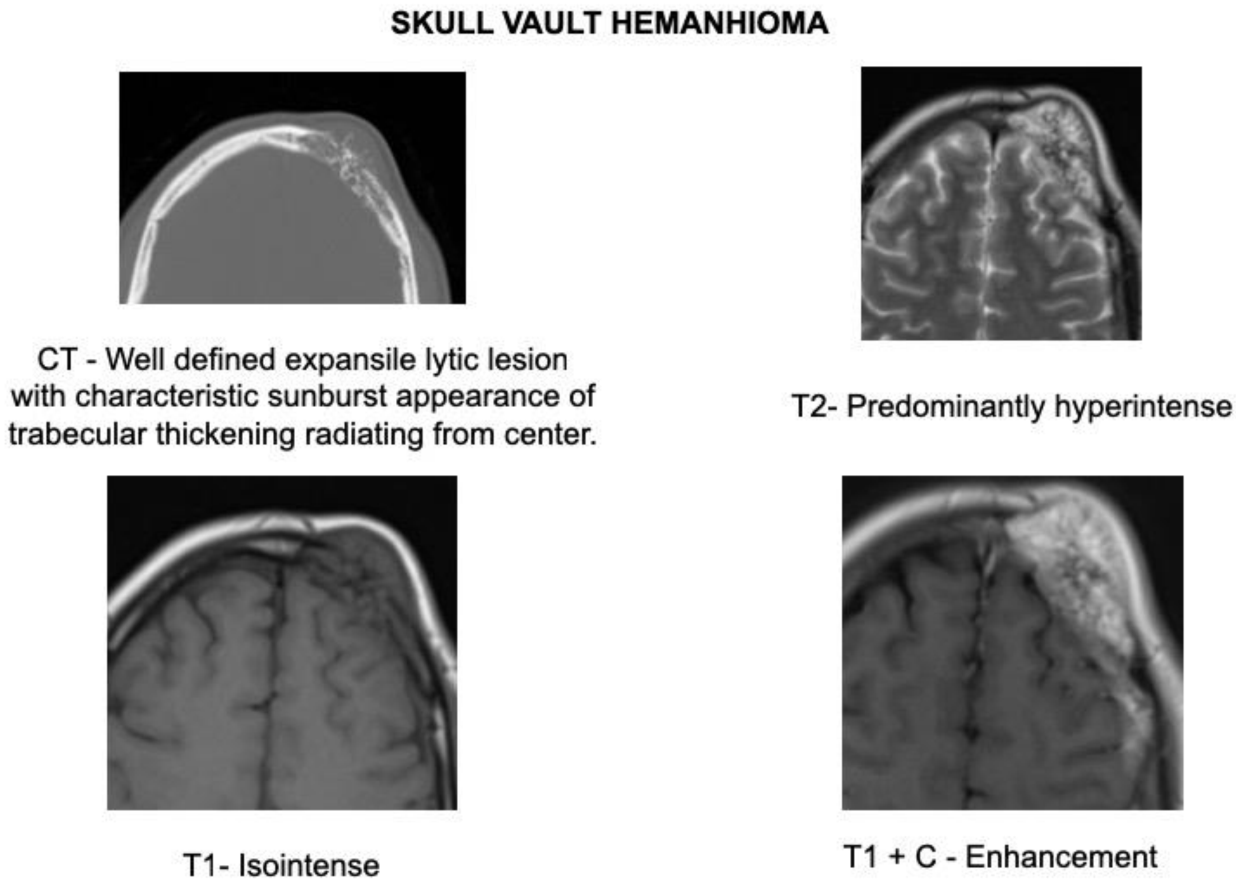

(Filename: TCT_2750_Skulllesion.jpg)

2674

Don't Miss the Gorilla in the Reading Room: Prevent Residency Burnout

T Arusoo[1], A Goyal[1], R Bhojwani[1], M Taheri[2]
[1]*George Washington University Hospital, Washington, DC,* [2]*George Washington University, Washington, DC, DC*

Purpose
Medical school admission and diagnostic radiology residency placement have increased in competitiveness over the last five years. Those who have succeeded have a strong personal history of achievement. Meanwhile, burnout is disproportionately increasing in the radiology profession, affecting half of practicing radiologists and nearly 85% of radiology residents. Studies have identified causative factors, preventative measures and mitigating solutions regarding radiology resident burnout. A majority of solutions focus on multifactorial and organizational approaches over personal factors. In an effort to decrease resident burnout, we propose annual resiliency training tailored to the intricacies of diagnostic radiology residency with a departmental focus on bidirectional constructive feedback.
Materials and Methods
A PubMed literature review focused on radiology resident burnout and proven feedback models in aviation, military, business and surgical fields was conducted.

Results
Current radiology residents with personal histories of unprecedented success are matriculating into a field intertwined with inevitable error and ever increasing productivity demands. The conventional approach to teaching radiology has been based upon weakness-oriented feedback. However, this routinely implemented approach has evidence detailing the associated harms of utilizing such a model. Data supporting the importance for effective, strength-based performance feedback are sound and ripe for implementation within radiology. We have instituted a combination of strength-based feedback with emotional readiness training tailored to the uniqueness of the radiology field with promising results.
Conclusions
Current radiology residents with strong personal histories of success are encountering perceived relative failure early in their training. This juxtaposition places residents at an increased risk of longstanding burnout early in their careers. Educators play a pivotal role in shaping this new generation's emotional IQ and resiliency. In an effort to take personal responsibility for trainee and specialty burnout, we suggest educators enact similar resiliency training of residents while focusing on delivering feedback via one of the many strength-based frameworks.

3626

Dual Energy CT : A Step Ahead in Head and Neck Imaging

J NAIR[1], L Ribeiro[2], R Forghani[3], R Gupta[4], E Yu[5]
[1]McMaster University, Hamilton, Ontario, [2]HAMILTON GENERAL HOSPITAL - MCMASTER, DUNDAS, ON, [3]JEWISH GENERAL HOSPITAL & MCGILL UNIVERSITY, COTE ST LUC, QC, [4]Massachusetts General Hospital, Boston, MA, [5]University of Toronto, Toronto, Ontario

Purpose
1) Discuss the relevant applied physics of Dual Enegy CT (DECT). 2) Review the various clinical applications of DECT in head and neck imaging. 3) Introduce future applications of DECT, combining texture imagings /radiomics in head and neck oncology.
Materials and Methods
PACS search was undertaken to identify selected cases. Highlight various common pathological conditions of the head and neck, where DECT has an edge over conventional CT using a case based approach.
Results
We shall use a case-based approach to show case appearance of normal anatomy and different pathologic entities of head and neck, on specialized DECT reconstructions for optimal use and diagnosis. Different clinical applications of DECT discussed would include A)Head and Neck Squamous Cell Carcinoma, Salivary Gland Tumors, Recurrent Head and Neck Squamous Cell Carcinoma and Post-treatment Changes, Perineural Spread of Tumor.(Enhancing tumor visualisation, increase detection of nodal disease and accurate staging of tumor. For eg: laryngeal cartilage invasion) B) Inflammatory and Infectious Diseases C) Benign Neck Lesions and Variants D) Artifact Reduction
Conclusions
DECT has the potential to enhance detection and characterization of head and neck lesions, enabling us to make confident and accurate diagnosis, thus impacting patient management.

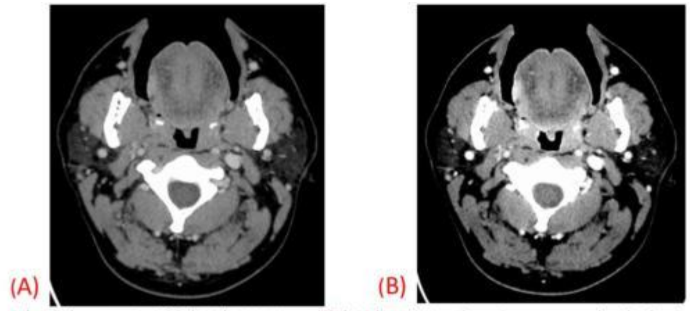

Squamous cell carcinoma of the right oral tongue Axial (A) 65 keV VMIs and (B) 40 keV VMIs. The primary tumor has higher attenuation and its margin is better delineated on the 40 keV VMI compared with the 65 keV VMI. (VMI-Virtual Monochromatic Images)

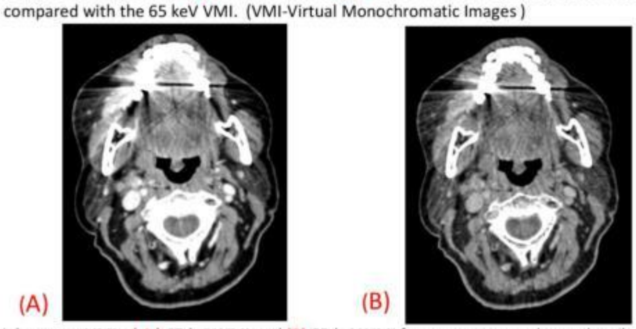

Dental artifact reduction using high-energy VMIs. (A) 65 keV VMI and (B) 95 keV VMI from a contrast-enhanced neck CT with dental artifact. Note artifact reduction on the 95 keV VMIs, enabling confident enabling visualization of the posterior part of the tumor on the right, that is much less well-seen on the 65 keV VMI.

(Filename: TCT_3626_Headandneck-page-001.jpg)

3627

Dual Energy CT: A Step Ahead in Brain and Spine Imaging

J NAIR[1], L Ribeiro[2], R Forghani[3], R Gupta[4], E Yu[5]
[1]McMaster University, Hamilton, Ontario, [2]HAMILTON GENERAL HOSPITAL - MCMASTER, DUNDAS, ON, [3]JEWISH GENERAL HOSPITAL & MCGILL UNIVERSITY, COTE ST LUC, QC, [4]Massachusetts General Hospital, Boston, MA, [5]University of Toronto, Toronto, Ontario

Purpose
1) Discuss the relevant applied physics of Dual Enegy CT (DECT). 2) Review the various clinical applications of DECT in brain and spine imaging.
Materials and Methods
1) PACS search was undertaken to identify selected cases. 2) Highlight various common pathological conditions of the brain and spine where DECT can be a problem solving tool, using a case based approach.
Results
We shall use a case-based approach to show case different applications of brain and spine on specialized DECT reconstructions for optimal use and diagnosis. Different clinical applications of DECT discussed would include A)Brain : i)Evaluation of the intracranial vessels and presence of vascular malformations like aneurysms. ii)Estimation of vessel integrity in the presence of calcifications iii) Early differentiation between hemorrhage and contrast. B)Spine: i)Bone Marrow Imaging ii)Postoperative spine iii)Urate deposition disease like Gout
Conclusions
DECT can be used as an important adjuvant to conventional CT in brain and spine imaging enabling us to make confident and accurate diagnosis, thus impacting patient management.

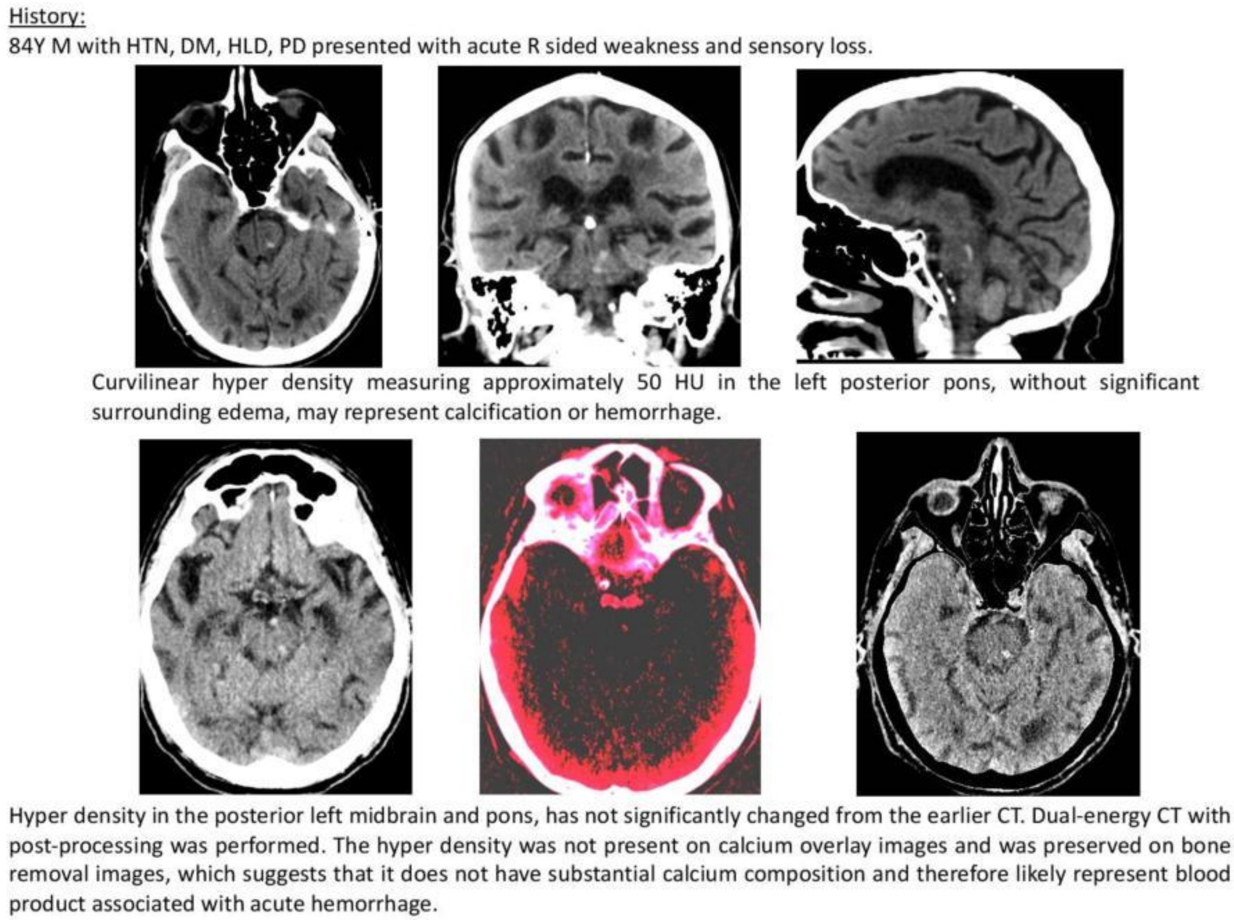

(Filename: TCT_3627_Hemorrhagevscalcificationjpg.jpg)

2130

Essentials of Subaxial Cervical Spine Trauma Imaging: Radiographs, CT and MRI

Z Wilseck[1], A Jo[2], M Manganaro[2], S Chong[2], M Ibrahim[2]
[1]University of Michigan Health System, Canton, MI, [2]University of Michigan Health System, Ann Arbor, MI

Purpose
The purpose of this electronic exhibit is to discuss the AOSpine subaxial classification system and to review spinal imaging in the trauma setting including the description of imaging modalities, basic anatomy, and common fracture patterns.
Materials and Methods
Subaxial cervical spine injury classification will be discussed. 1. Indications for imaging the cervical spine in the setting of trauma 2. Review of the complex anatomy of the craniovertebral junction and subaxial cervical spine 3. Commonly encountered injuries of the craniovertebral junction and subaxial cervical spine
Results
Imaging of the cervical spine in the setting of trauma should be determined based on the NEXUS low-risk criteria or the Canadian Cervical-Spine Rule (CCR). Although no set guidelines exist for imaging of the thoracolumbar spine in the setting of trauma, the concept of clearance is similar to that of the cervical

spine. MRI should be reserved for those who are persistently symptomatic, those who cannot undergo clinical examination for at least 48 hours, those with injury morphologies on CT that are often associated with ligamentous injuries, and for the purpose of treatment planning. The AOSpine subaxial classification system is a simple, yet reliable and reproducible system for classifying subaxial spinal column injuries which takes into account injury morphology, injury mechanism, facet joint integrity, neurologic status, and other additional comorbidities which are important in the treatment of cervical spine injuries.

Conclusions

Early diagnosis and intervention of unstable injuries of the CVJ and the subaxial spine in the setting of trauma is of utmost importance in preventing further neurologic deterioration. Radiologists should be familiar with the utility of each imaging modality and its indication in the setting of trauma. Injury morphology should be determined on CT, with further characterization with MR reserved for a select few. Furthermore, understanding of the AOSpine classification for the evaluation of the subaxial spine can help determine stability of the traumatic spine and assist in clinical decision making.

Cervical-spine imaging is indicated for patients with trauma unless they meet all of the following criteria:
No posterior midline cervical spine tenderness on palpation
No evidence of intoxication
Normal level of alertness (GCS=15)
No focal motor or sensory neurologic deficit
No painful distracting injuries *

Table 1: NEXUS Low-Risk Criteria

Cervical-spine imaging is indicated for patients with trauma unless they meet ALL of the following criteria:
Normal level of alertness (GCS=15)
Less than 65 years of age
No dangerous mechanism of injury -Fall from height of more than 3 feet -Axial loading injury -High-speed MVA of more than 100km/hr (approximately 62miles/hr) -MVA with rollover or ejection -Recreational motor vehicle, motorcycle or bicycle injury -Pedestrian struck by motor vehicle
No paresthesia in the extremities
Able to rotate neck left and right by 45 degrees (after meeting criteria for assessing range of motion*)

Table 2: The Canadian Cervical-Spine Rule

(Filename: TCT_2130_SLICTablesASNRAbstract-1.jpg)

3192

Evaluation and Pre-treatment Planning of Pediatric Epilepsy: A Team Based Approach

M Bhatt[1], A Krishnan[2], P Laoprasert[1], D Arndt[1]
[1]Beaumont-Royal Oak (William Beaumont Hospital), Royal Oak, MI, [2]OAKLAND UNIVERSITY WILLIAM BEAUMONT SCHOOL OF MEDICINE, TROY, MI

Purpose
Pediatric epilepsy is often managed conservatively, however some patients with drug-resistant epilepsy (DRE) may necessitate the need for surgical treatment. Thorough presurgical evaluation is essential, as a multitude of physiologic, anatomic, and psychosocial factors are involved in planning for epilepsy surgery. Detection of a surgically treatable lesion and its volume, can define the feasibility and type of treatment. This necessitates a combination of optimized imaging in concert with multiple other disciplines. Our purpose is to present a multidisciplinary approach used at our institution for presurgical evaluation in pediatric epilepsy surgery.
Materials and Methods
We will first review the components of our multidisciplinary epilepsy team (Pediatric Epileptologists/Neurosurgeon, Neuroradiologist, Neuropsychologist, among others). Subsequently we will review cases of DRE and highlight, step-by-step, our preoperative planning process and review each of the key components. •Medical history/physical exam (semiology of seizure) •Clinical testing: Scalp electroencephalography [EEG], Neuropsychological testing, Magnetoenecephalography [MEG], relevant laboratory studies •Imaging: MRI with epilepsy and presurgical protocol including specifics that we use to optimize detection of subtle lesions, functional MRI (fMRI), interictal FDG-PET, Ictal/ Interictal SPECT After completing the presurgical evaluation, the preimplantation "anatomo-electro-clinical" hypotheses formulation, a critical element in the process of planning the placement of Stereoelectroencephalography (SEEG) electrodes, will be generated to identify the epileptogenic region.
Results
Our multidisciplinary approach helps navigate the intricacies associated with preoperative evaluation of pediatric epilepsy. Identification of lesions by imaging is critical in seizure control. Gathered data affects the type of treatment, ranging from robotic guided laser ablation, to focal resection to functional hemispherectomy. Preoperative imaging of DRE is unique, given the subtle nature of cortical dysplasias, the necessity to correlate with other imaging (SPECT/PET, MEG), as well as correlation with the semiology of seizures.
Conclusions
Our institution has developed a multidisciplinary approach, utilizing advanced MR imaging and invasive preoperative planning (stereo EEG) to improve our ability to evaluate and treat complex cases of DRE. Following review of our workflow, the neuroradiologist, especially in centers that wish to pursue pediatric epilepsy management, should have an understanding of the steps involved and imaging protocols, in evaluating these patients.

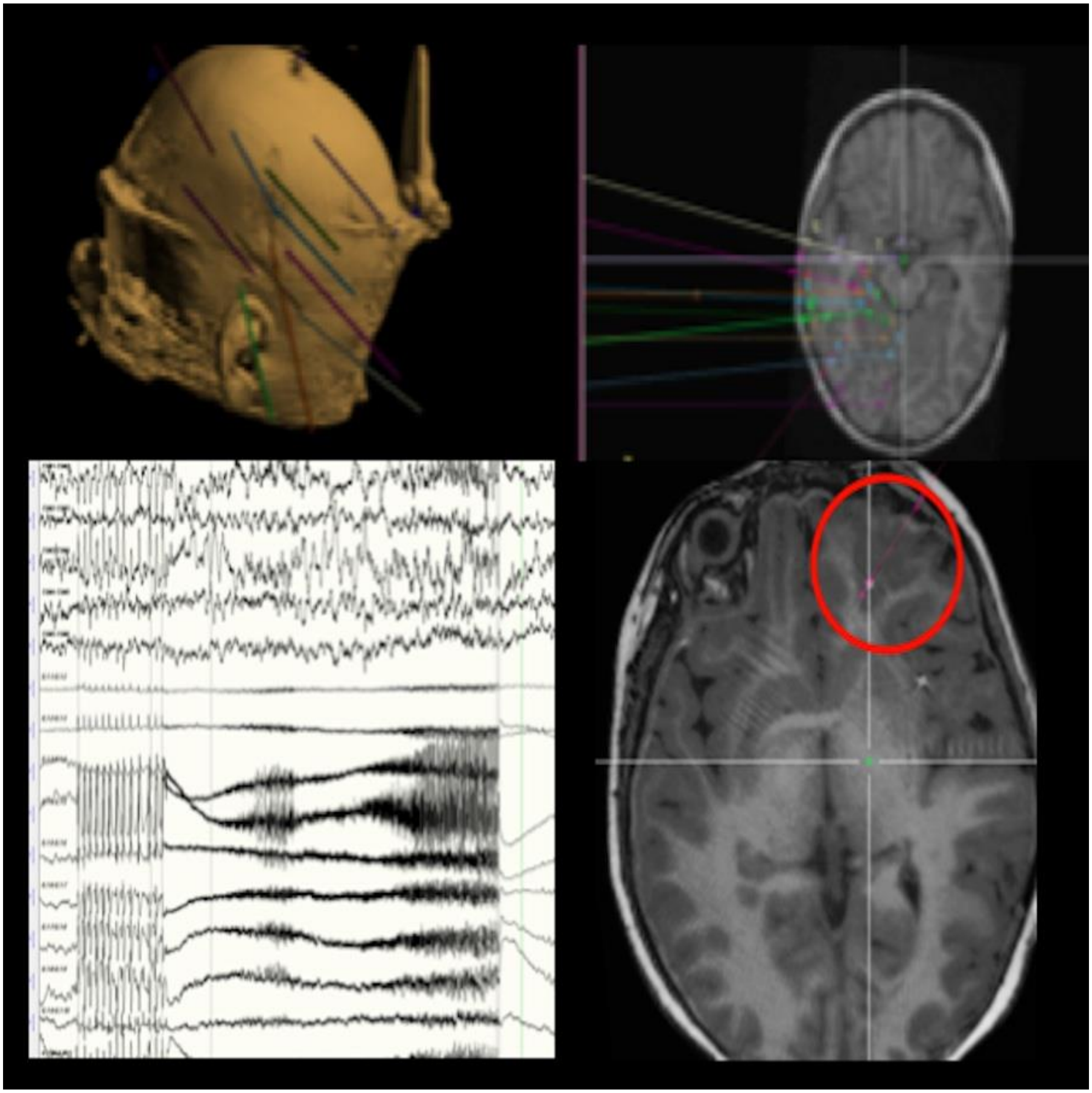

(Filename: TCT_3192_Pedsepiimagesabstract.jpg)

2427

Even the Smallest Leak Can Sink the Brain: A Review of the Clinical and Imaging Manifestations, Unusual Causes, and Atypical Presentations of Spontaneous Intracranial Hypotension.

K Soderlund[1], A Callen[2], W Dillon[3], V Shah[2]
[1]University of California, San Francisco, San Francisco, CA, [2]University of California San Francisco, San Francisco, CA, [3]UNIV OF CALIFORNIA, SAN FRANCISCO MED CTR, SAN FRANCISCO, CA

Purpose
Highlight and review major clinical and imaging presentations of spontaneous intracranial hypotension (SIH), with particular attention to more atypical or unusual clinical presentations and etiologies.

Approaches to diagnosis of SIH using various imaging modalities, as well as various therapeutic options will also be discussed.

Materials and Methods

-The material will be presented as an image-rich electronic educational exhibit. -Cases from our institution will be utilized to illustrate key imaging findings. Pertinent clinical history will be provided.

Results

-Describe typical and atypical clinical and imaging presentations of spontaneous intracranial hypotension (SIH) in the brain and spine. Some atypical presentations of SIH include coma, postural coma, ataxia and sensorineural hearing loss (related to superficial siderosis), postural tinnitus, upper and lower motor neuron symptoms (mimicking ALS), other cranial nerve deficits, and frontotemporal dementia. -Demonstrate several unusual causes and imaging findings of SIH, to include CSF-venous fistula, CSF-facet fistula, "weepy CSF sign" (related to leakage at multiple adjacent neural foramina) as well as more typical causes including meningeal diverticula and osteophyte related dural tears. -Describe role of various modalities used for diagnosis of spontaneous intracranial hypotension, including fluoroscopy, CT, and MR myelography. -Discuss various therapeutic options for treatment of SIH. -Discuss some pitfalls in the diagnosis of SIH such as intracranial hypotension misdiagnosed as Chiari I malformation, the false localizing sign of CSF leak at C1-C2, and CSF venous fistula.

Conclusions

Spontaneous intracranial hypotension (SIH) is a clinical syndrome of postural headaches as a result of leakage of CSF in the absence of prior dural injury or lumbar puncture. Atypical clinical presentations of SIH include ataxia, sensorineural hearing loss, dementia, coma, parkinsonism, and upper and lower motor neuron symptoms. These atypical clinical presentations may be associated with unusual imaging features such as superficial siderosis or anterior horn cell signal abnormality. While SIH is often the result of a leaking meningeal diverticulum or dural tear related to a disc-osteophyte at a single spinal level, more unusual etiologies and imaging findings of SIH can also be seen, including CSF-venous fistula, CSF-facet fistula, and leak at multilevel neural foramina due to a spontaneous or acquired dural defect (dubbed the "weepy CSF sign"). Given the diverse clinical and imaging findings in SIH, it is important for the neuroradiologist to be aware of its more atypical clinical presentations and unusual etiologies in order to improve patient diagnosis and treatment.

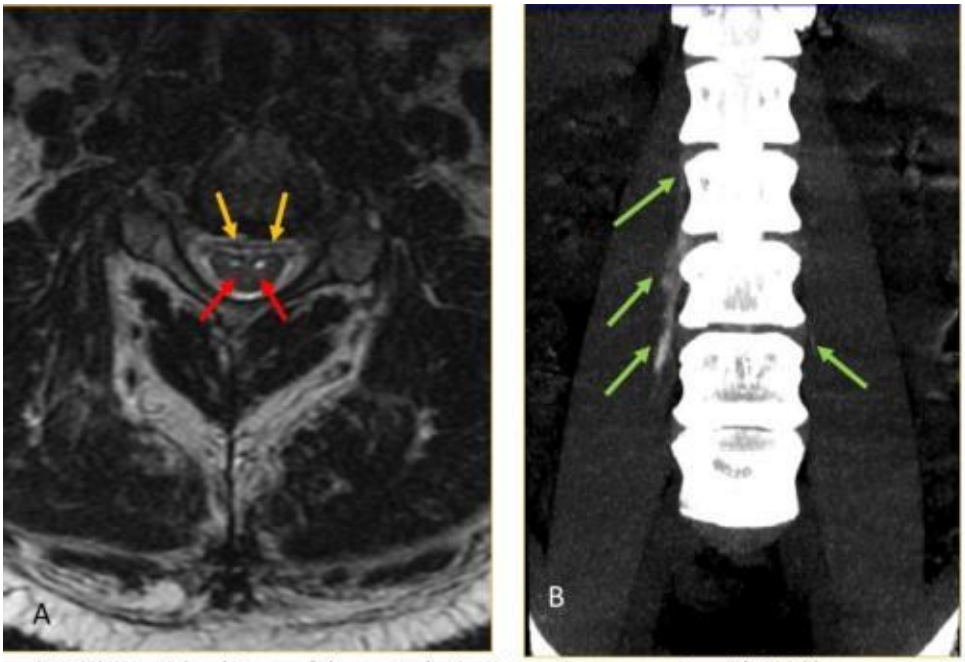

A: Axial T2-weighted image of the cervical spine in a patient presenting with ALS-like symptoms and superficial siderosis in the cerebellum demonstrates T2 hyperintense signal within the anterior horn cells of the cervical cord gray matter (red arrows). A thin ventral extradural CSF collection is also present (orange arrow).
B: Coronal MIP image from a CT myelogram performed 30 minutes after intrathecal administration of iodinated contrast in a patient who developed postural headaches following an intense weightlifting session demonstrates leakage of contrast material into the psoas muscles from multiple neural foramina (green arrows). We have named this the "weepy CSF sign".

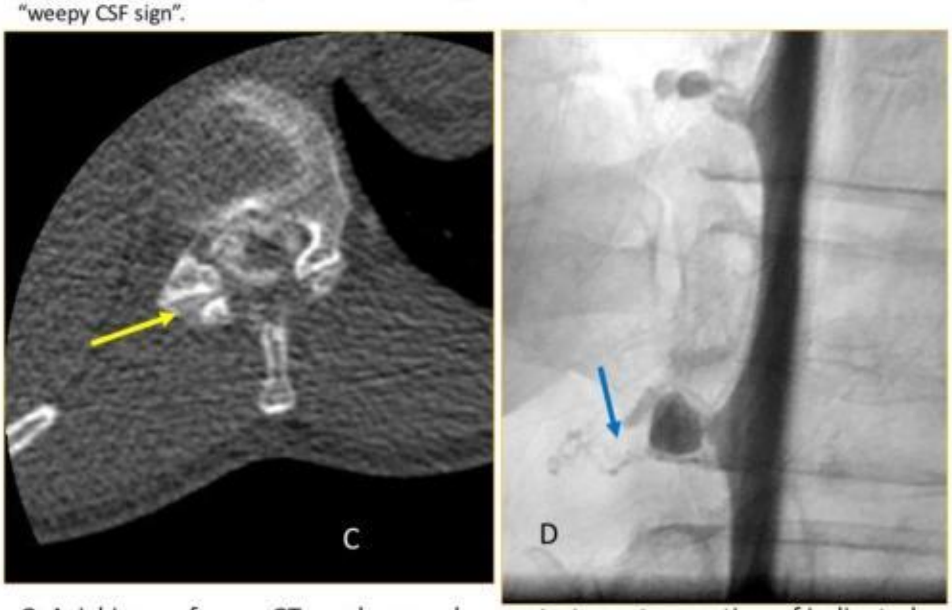

C: Axial image from a CT myelogram demonstrates extravasation of iodinated contrast material into the right T11-T12 facet joint, compatib le with CSF-facet fistula (yellow arrow).
D: Coronal oblique image from a fluoroscopic myelogram performed in the right lateral decubitus position demonstrates extravasation of iodinated contrast material from a right-sided meningeal diverticulum into a radicular vein, consistent with CSF-venous fistula (blue arrow).

(Filename: TCT_2427_SIHAbstractImages.jpg)

2747

Exploring Neurological Complications of Immunotherapy

E Jones[1], A Agarwal[2], D Schiess[1], B Shah[3], K Raj[4], J Maldjian[5]
[1]UT-Southwestern Medical Center, Dallas, TX, [2]UT SOUTHWESTERN MEDICAL CENTER, DALLAS, TX, [3]UT Southwestern Medical Center, Irving, TX, [4]UT Southwestern Medical Center, Dallas, TX, [5]University of Texas Southwestern, Dallas, TX

Purpose
With an ever increasing arsenal of immunotherapeutic agents being employed for a variety of conditions, a better understanding of their role and potential downstream neurological effects will aide in diagnostic interpretation. As such the following objectives will be addressed: To discuss the role of new and evolving immunotherapeutic agents in cancer management; To understand the difference between conventional chemotherapy and immunotherapy; To review the neurological complications of immunotherapy and the role of imaging in diagnosing these conditions; To provide representative examples of cases displaying immunotherapeutic neurological complications
Materials and Methods
The following outline of contents will be discussed via electronic educational exhibit: (A) Basics of Immunotherapy (B) Immunotherapy versus Chemotherapy (C) Common conditions being treated by immunotherapy (D) Neurological complications and select representative examples: Central neurological complications • Peripheral neurological complications • Acute encephalopathy • Chronic encephalopathy • Epilepsy • Hypophysitis • Aseptic meningoencephalitis • Progressive multifocal leukoencephalopathy • Posterior reversible leukoencephalopathy • Stroke • Myelopathy (E) Combinations with radiotherapy (F) Future of immunotherapy
Results
Unlike chemotherapy, which functions to disrupt cell synthesis at a number of specific points in the cell cycle, immunotherapy works by either blocking immunosuppression or boosting anti-tumor immune responses by modifying the body's self immune response. A number of immunotherapeutic agents are now routinely used for various malignancies (eg: Ipilmumab, Nivolumab). Despite the benefits, immune modifying drugs may result in increased levels of autoantibodies which target normal tissue, resulting in various side effects; a number of which will be discussed with representative examples provided.
Conclusions
The practicing radiologist should have an understanding of the commonly used immunotherapeutic agents and their indications. A knowledge of these potential side effects and their imaging characteristics can help delineate disease progression from immunotherapeutic complication, as the treatment of these entities is distinct.

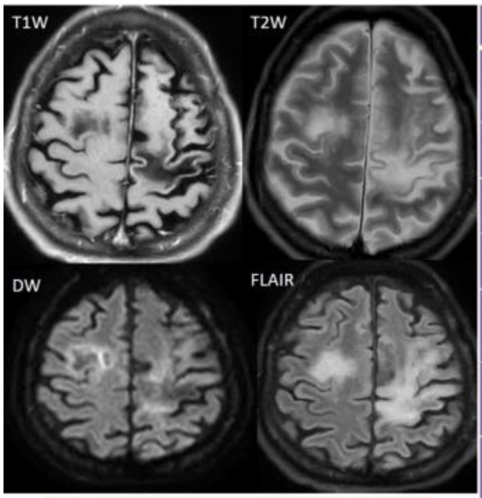

70 year old with CLL on Ibrutinib develops PML. *Multifocal, asymmetric subcortical signal changes with involvement of the subcortical fibers, no mass effect or enhancement. Note the low T1 signal characteristic of PML.CSF analysis with PCR was positive for JC virus.*

Complication	Symptoms	Agents	Pathophysiology	MRI Findings
Acute encephalopathy	Altered mental status, confusion	Blinatumomab, CAR T-cells, interferon γ, (combination, with RT)	Cytokines causing direct neurotoxicity	Cortical and deep grey matter signal changes and restricted diffusion
Chronic encephalopathy	Dementia, confusion, cognitive delay	Rituximab, alemtuzumab, brentuximab	Cytokines causing direct neurotoxicity	Confluent leukoencephalopathy
Epilepsy	Seizures	Cetuximab, panitumumab, gefitinib, erlotinib, imatinib, dasatinib, blinatumomab,	Electrolyte disturbance	Normal study or post-ictal changes
Hypophysitis	Fatigue, headaches	Ipilimumab	Immune reaction by cytokines	Thickening and enhancement of infundibulum
Aspetic meningoencephalitis	Altered mental status	Cetuximab, ipilimumab, imatinib, dasatinib, dabrafenib, antiangiogenic drugs	Immune reaction by cytokines	Meningeal enhancement and cortical signal changes
PML/IRIS	Personality change, confusion, and social deficits	Rituximab, alemtuzumab, brentuximab, infl iximab, efalizumab, ibrutinib	CD4+ or CD8+ T-cell immunosuppression and toxic effects on oligodendrocytes	Perivascular T2 signal changes with punctate contrast enhancement
PRES	Headaches, seizures, vision changes	Bevacizumab, ipilimumab, rituximab, sirolimus, sorafenib, sunitinib, tacrolimus	Failure to autoregulate cerebral blood pressure	Subcortical edema with no restricted diffusion
Stroke/Stroke like symptoms	Transient focal neurological deficit	Ipilimumab, bevacizumab	Larges vessel inflammation, coagulation disorder	Transient focal areas of restricted diffusion
Myelopathy	Sensorimotor deficits, incontinence	Ipilimumab	Immune reaction by cytokines	Cord edema
GBS	Sensory and motor deficits	Ipilimumab, pertuzumab	Cross-reactivity of activated T cells against Schwann cells	Enhancement of ventral roots

[*Table reference : Neurological sequelae of cancer immunotherapies and targeted therapies.*
Wick W, Hertenstein A, Platten M. Lancet Oncol. 2016 Dec;17(12):e529-e541]

(Filename: TCT_2747_ExampleandTablefoRASNRSubmission.jpg)

3176

Eye for an Eye: A Review of the Post-operative Orbit

J Scheibal[1], A Rajamohan[2], J Acharya[3], J Go[2], F Torres[4], P Joyce[5]
[1]USC Keck School of Medicine, Los Angeles, CA, [2]UNIVERSITY OF SOUTHERN CALIFORNIA, KECK SCHOOL OF MEDICINE, LOS ANGELES, CA, [3]UNIVERSITY OF SOUTHERN CALIFORNIA, KECK SCHOOL OF MEDICINE, Monrovia, CA, [4]Kaiser Permanente, Los Angeles Medical Center, Los Angeles, CA, [5]LAC USC, Los Angeles, CA

Purpose
To provide a review of common operations to the orbit and their post-operative appearance on multiple imaging modalities.
Materials and Methods
A multi-specialty approach will be utilized to present various orbital surgeries reviewing critical anatomy, surgical approach, normal post-operative appearance, and possible complications.
Results
Ophthalmologist perform a wide range of surgical procedures and use a variety of surgical hardware in their approach. These procedures can often be detected on CT and MRI. During this exhibit, the user will be introduced to key anatomy of the orbit, both from a radiologists and surgeons perspective, and be exposed to the expected postoperative appearance on on both CT and MRI. Possible post-procedural complications will also be discussed and illustrated with a variety of cases.
Conclusions
Post-operative changes to the orbit are commonly seen on imaging studies. By the end of this exhibit, the user will gain knowledge of key anatomy of the orbit, recognize the expected post-operative appearance of various orbital surgeries, and be able to identify common surgical hardware utilized by ophthalmologists.

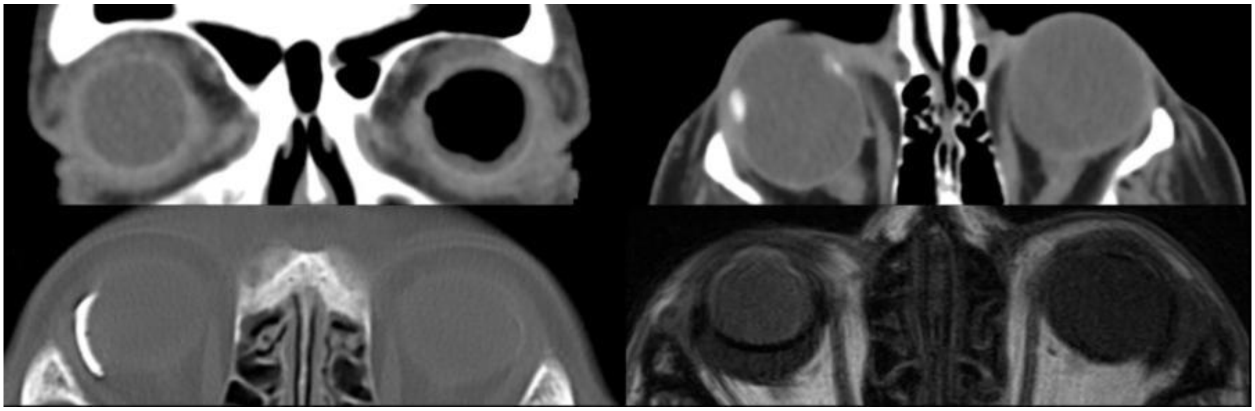

(Filename: TCT_3176_OrbitASNR.jpg)

2634

Fetal Brain MRI – Diving Below the “Tip of the Iceberg” on Prenatal US

V Onofrj[1], U Nagaraj[2], W O'Brien[3]
[1]*Cincinnati Children's Hospital, Cincinnati, OH,* [2]*CINCINNATI CHILDREN'S HOSPITAL MEDICAL CENTER, CINCINNATI, OH,* [3]*Cincinnati Children's Hospital Medical Center, Cincinnati, OH*

Purpose
Fetal MRI is an important adjunct to prenatal ultrasound (US). MRI not only allows for better characterization of intracranial abnormalities, but also frequently identifies additional CNS abnormalities not initially noted; hence, US findings are often the "tip of the iceberg." Common CNS indications for fetal MRI include ventriculomegaly, malformations of cortical development, or posterior fossa malformations identified on prenatal US. EDUCATIONAL OBJECTIVES 1. Understand the role, indications, and limitation of prenatal US and MRI. 2. Recognize and describe common brain anomalies on fetal MRI. 3. Illustrate isolated, complex, and syndromic intracranial anomalies on fetal MRI.
Materials and Methods
This exhibit is based upon a query of our institutional report database encompassing the past 10 years. We identified cases in which prenatal US abnormalities were identified and a subsequent fetal MRI was performed: ventriculomegaly, absent cavum septi pellucidi (CSP), or posterior fossa malformation.
Results
The spectrum of intracranial abnormalities found on fetal MRI largely exceeded what was initially identified on prenatal US. The gamut of anomalies noted on fetal MRI encompassed the following entities, which will be described and illustrated as part of the educational exhibit: Ventriculomegaly -Aqueductal stenosis -Destructive lesions (porencephaly, schizencephaly, hydranencephaly) -Vascular lesions (germinal matrix hemorrhage, infarct, vein of Galen malformation) Absent CSP -Dysgenesis of the Corpus callosum -Holoprosencephaly Spectrum -Hypoplastic Optic Nerve Syndrome Posterior Fossa Malformations -Dandy-Walker continuum -Cerebellar dysplasia Several entities occurred in isolation, while others were part of more complex malformations or in association with genetic syndromes.
Conclusions
Prenatal US is a valuable screening tool in identifying intracranial abnormalities; however, the obvious findings on US are often the "tip of the iceberg," as fetal MRI commonly demonstrates additional and more complex CNS abnormalities. Being able to recognize and describe these abnormalities is essential in interpreting fetal MRI examinations.

2870

Fetal MRI Diagnosis of Intracranial Tumors with Pathologic Confirmation

Y Li[1], D Xu[1], S Chetty[1], O Glenn[1]
[1]*University of California San Francisco, San Francisco, CA*

Purpose
Our educational exhibit will highlight five cases of congenital intracranial neoplasm, with a focus on the following educational objectives: 1. Added value of fetal MRI in the diagnosis of fetal brain tumors. 2. Important imaging features in each case to assist in the diagnosis. 3. Important pathologic features in each case, with radiologic-pathologic correlation.
Materials and Methods
A search of our institutional fetal MRI database, consisting of fetal MRIs performed between 1997 to 2018, resulted in 5 cases of intracranial tumors with pathologic diagnoses of immature teratoma, craniopharyngioma, medulloblastoma, atypical teratoid/rhabdoid tumor (ATRT), and choroid plexus papilloma. We describe the clinical features, fetal MR imaging findings, and pathology of these tumors in an effort to educate the audience on pertinent imaging features associated with congenital intracranial tumors on fetal MRI.
Results
In our educational exhibit, we focus on the following educational objectives: 1. Added value of fetal MRI in the diagnosis of fetal brain tumor. Indications for fetal MRI included sonographically detected brain tumor in two cases and ventriculomegaly and/or hydrocephalus in three cases. Mean gestational age at fetal MRI was 28.8 weeks (range 20.9 – 32.7). In both cases where ultrasound identified a mass, the tumors were large, measuring over 5 cm in each dimension, involved supratentorial structures, and were associated with hydrocephalus (midline supra and infratentorial immature teratoma, sellar/suprasellar craniopharyngioma). Fetal MRI confirmed the diagnosis and was able to better identify the extent and evidence of parenchymal thinning. In three cases where tumor was not suspected by ultrasound, ultrasound diagnoses were hydrocephalus in two cases and ventriculomegaly with suspected bilateral choroid plexus hemorrhage in one case. MRI identified infratentorial tumor in two of these cases (fourth ventricle medulloblastoma, pineal region ATRT), and bilateral supratentorial tumor (choroid plexus papillomas) in one case, as well as additional findings of parenchymal thinning. 2. Important imaging features in each case to assist in the diagnosis of tumor type. The location and extent of tumor, combined with signal characteristics on MRI helped to suggest specific tumor types. Diffusion weighted imaging was performed in three cases and demonstrated reduced diffusion in medulloblastoma (0.658 x10-3mm2/s) and ATRT (1280x10-3mm2/s in overall tumor, and 777x10-3mm2/s in solid component), and higher ADC (>1400x10-3mm2/s) values in choroid plexus papilloma, which is similar to published values.(1) One case had postnatal MRI which confirmed fetal MRI findings and ADC values. 3. Important pathologic features in each case, with radiologic-pathologic correlation. All five cases have pathologic proof of diagnosis with molecular subtyping in select cases.
Conclusions
Congenital brain tumors are rare, accounting for 0.5-4% of all pediatric brain tumors.(2) Brain tumors should be considered when evaluating fetuses referred for ventriculomegaly and/or hydrocephalus. In this educational exhibit, we illustrate findings on fetal MRI that aid in the diagnosis of intracranial tumor, fetal MRI imaging features associated with each of the tumor types, and radiologic-pathologic correlation. The ability to diagnosis and characterize congenital intracranial tumors prenatally by fetal MRI can help provide more accurate prenatal counseling and perinatal management.

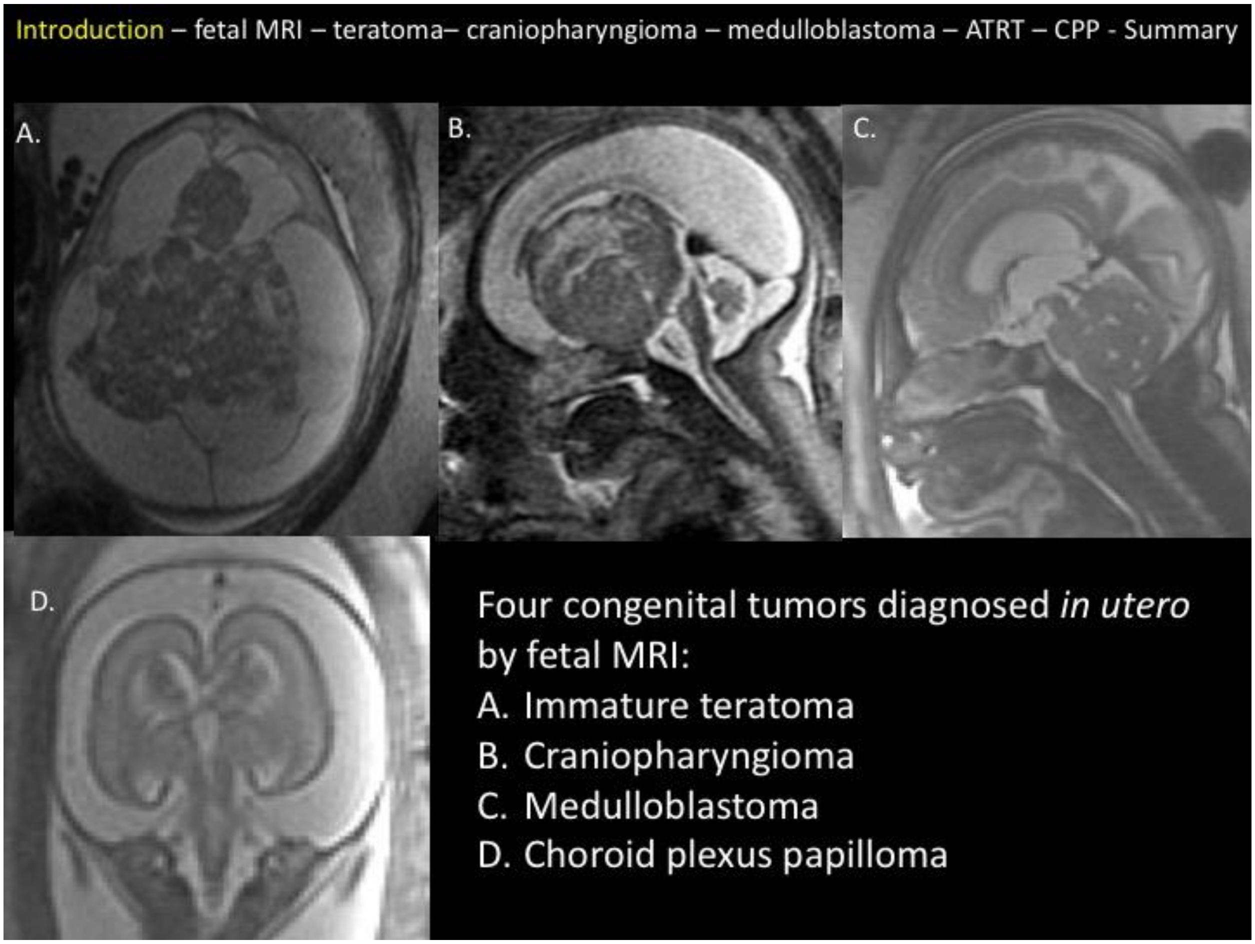

(Filename: TCT_2870_Slide1.jpg)

2815

Fluoroscopic Guided Lumbar Drain Placement: How We Do It

P Batchala[1], J Donahue[1], T Eluvathingal Muttikkal[1], S Patel[1], C Robbins[1], p Nepal[2], S Mukherjee[1]
[1]University of Virginia Health System, Charlottesville, VA, [2]St. Vincent's Medical Center, Bridgeport, CT

Purpose
Image guidance for lumbar drain (LD) placement is required when bedside attempt fails or when it is technically challenging due to spinal hardware or anatomical complexity. Here, we present an overview of the relevant radiological anatomy, indications, contraindications, step wise technique, post procedural care and complications related to image guided LD placement.
Materials and Methods
Fluoroscopy guided LD placement is performed under local anesthesia. The goal of the procedure is to gain access to the lumbar subarachnoid cistern at L3-4 or L4-5 level using a 14G Tuohy needle (Fig.1-large arrow) and placement of a 16G catheter (Fig.1 -small arrow) through the needle with tip at T9-10 level. Important procedural steps include a midline approach during dural puncture and cranial angulation of the needle bevel during catheter insertion. Procedural failure can occur from improper needle position or dry thecal sac (1).
Results
Thoraco-abdominal aortic aneurysm repair, extensive skull base surgeries, normal pressure

hydrocephalus, idiopathic intracranial hypertension and post-operative or post-traumatic CSF leaks are some of the common indications for LD placement. Lumbar drain with continuous or intermittent drainage is aimed at decreasing the CSF pressure or creating a low pressure CSF diversion in these clinical conditions. Technical success rates as high as 99% have been reported (2). Overall complications is up to 17.7% (2,3). Complications can be related to needle placement, CSF over drainage, infection (local or meningeal) or rarely retained catheter.

Conclusions

Fluoroscopy guided LD placement is an important procedure for various clinical situations. Although uncommonly performed in neuroradiology suite, it is a procedure that is well-suited to the skill-set and tools of the diagnostic neuroradiologist.

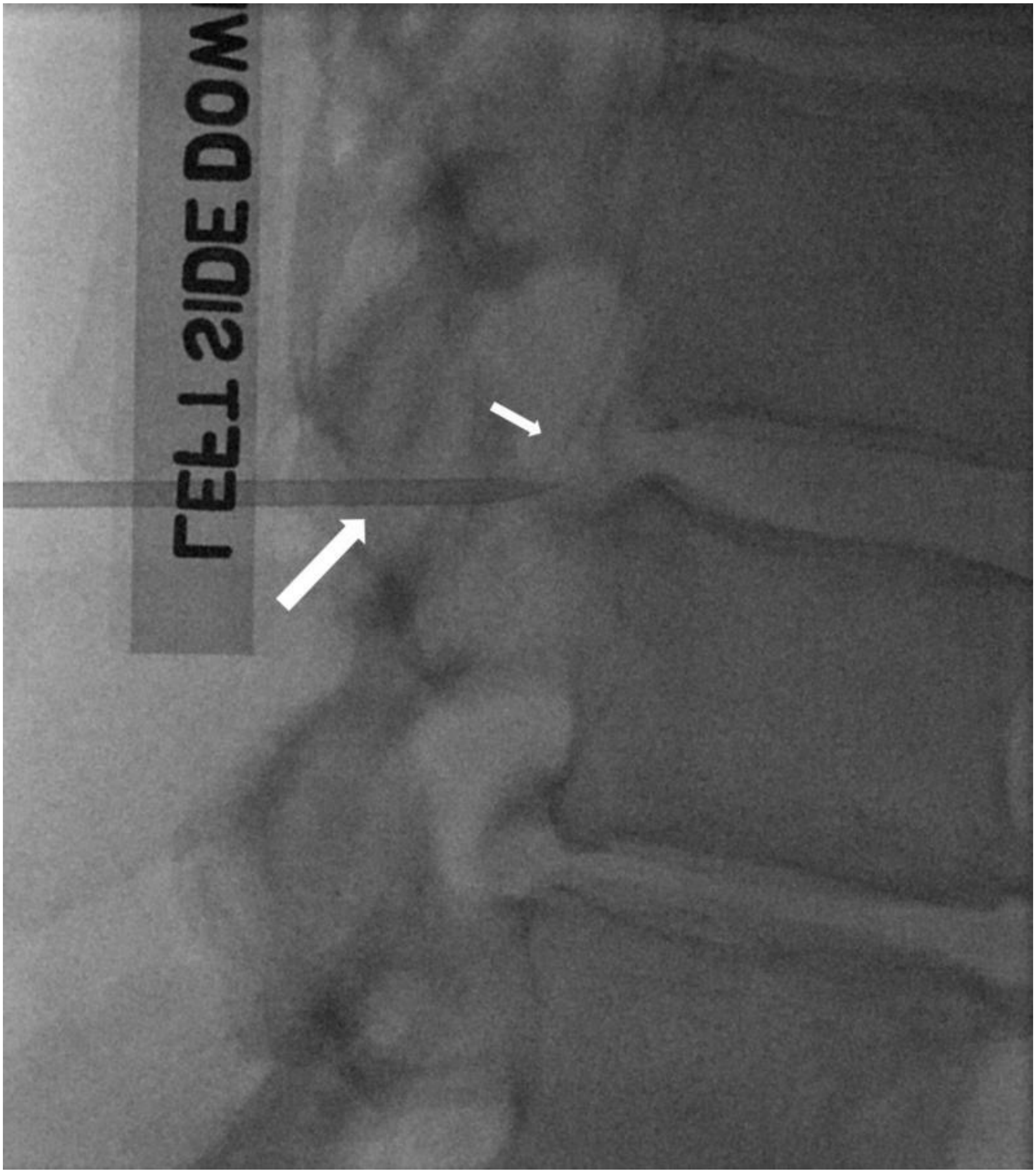

(Filename: TCT_2815_Fig1.jpg)

3580

Genotyping in Pediatric Brain Tumors, Should Neuroradiologists Care About It in The Daily Practice?. A Case-Based Review of The WHO-2016 Classification of Medulloblastomas.

O Arevalo[1], S Khanpara[1], C Soto[2], A Kamali[1], L Ballester[3], R Riascos[1], R Patel[1]

[1]Department of Diagnostic and Interventional Imaging. McGovern Medical School, UTHealth., Houston, TX, [2]National University of Colombia, Bogota, Colombia, [3]Department of Pathology and Laboratory Medicine. McGovern Medical School, UTHealth., Houston, TX

Purpose
To present a case based review of the WHO-2016 classification for medulloblastomas
Materials and Methods
Medulloblastomas are the most common malignant brain tumor in the pediatric age, commonly manifested as a midline mass in the roof of the fourth ventricle. Treatment typically consists of resection followed by chemoradiation. The 2016 update of the WHO classification of CNS tumors classifies medulloblastomas into four molecular subgroups as follows: WNT, SHH, Group 3, and Group 4. Each group shows somewhat distinctive image features such as location, size, presence of restricted diffusion, enhancement pattern, age of presentation and prognosis.
Results
The imaging features vary depending upon the histological type and molecular subtype of the mass. However, all subtypes share some of the hallmark characteristics of the small round blue cell tumors. The location at or off the midline, the involvement of the cerebral peduncle and location at the cerebellar hemisphere may aid in the prediction of the molecular subtype of the tumor.
Conclusions
Imaging features can help the neuroradiologist to predict the molecular subtype of medulloblastoma.

3478

Got Rhythm? Case-based Review of Sensorineural Hearing Loss

E Kuoy[1], C Nguyen[2], M Thompson[3], D Chow[4], A Hasso[5]
[1]UC Irvine, Orange, CA, [2]University of California, Irvine, IRVINE, CA, [3]UNIVERSITY OF CALIFORNIA IRVINE, ORANGE, CA, [4]UNIVERSITY OF CALIFORNIA, IRVINE, IRVINE, CA, [5]UNIV OF CALIFORNIA IRVINE MEDICAL CENTER, ORANGE, CA

Purpose
The purpose of this presentation is to review the American College of Radiology (ACR) appropriateness criteria for the imaging of hearing loss to assist in properly protocoling examinations, highlight relevant anatomic structures in the assessment of hearing loss, and to review the various causes of sensorineural hearing loss one may encounter on imaging studies.
Materials and Methods
A brief synopsis of the ACR appropriateness criteria for hearing loss will first be presented. Relevant CT and MRI anatomy will be reviewed that should be interrogated on exam. Finally, through a case-based presentation, various different causes of sensorineural hearing loss will be examined with key imaging findings as well as helpful clinical clues that help narrow the differential diagnosis.
Results
There are a variety of causes of sensorineural hearing loss that can manifest on imaging studies that one should be aware of including trauma-related, inflammatory/reactive, congenital, neoplastic, and vascular etiologies. Some of these include entities such as Mondini dysplasia, inner ear anomalies, cerebellopontine angle meningiomas, acoustic neuromas and schwannomas, otospongiosis, superficial siderosis and Susac syndrome. This presentation will review key imaging findings for these entities and more, with tips to help hone in these potential diagnoses.
Conclusions
A variety of causes for sensorineural hearing loss can present on imaging. Knowing the key imaging features of various entities and the relevant clinical background can help one hone in on the appropriate diagnosis and better assist in the patient's management.

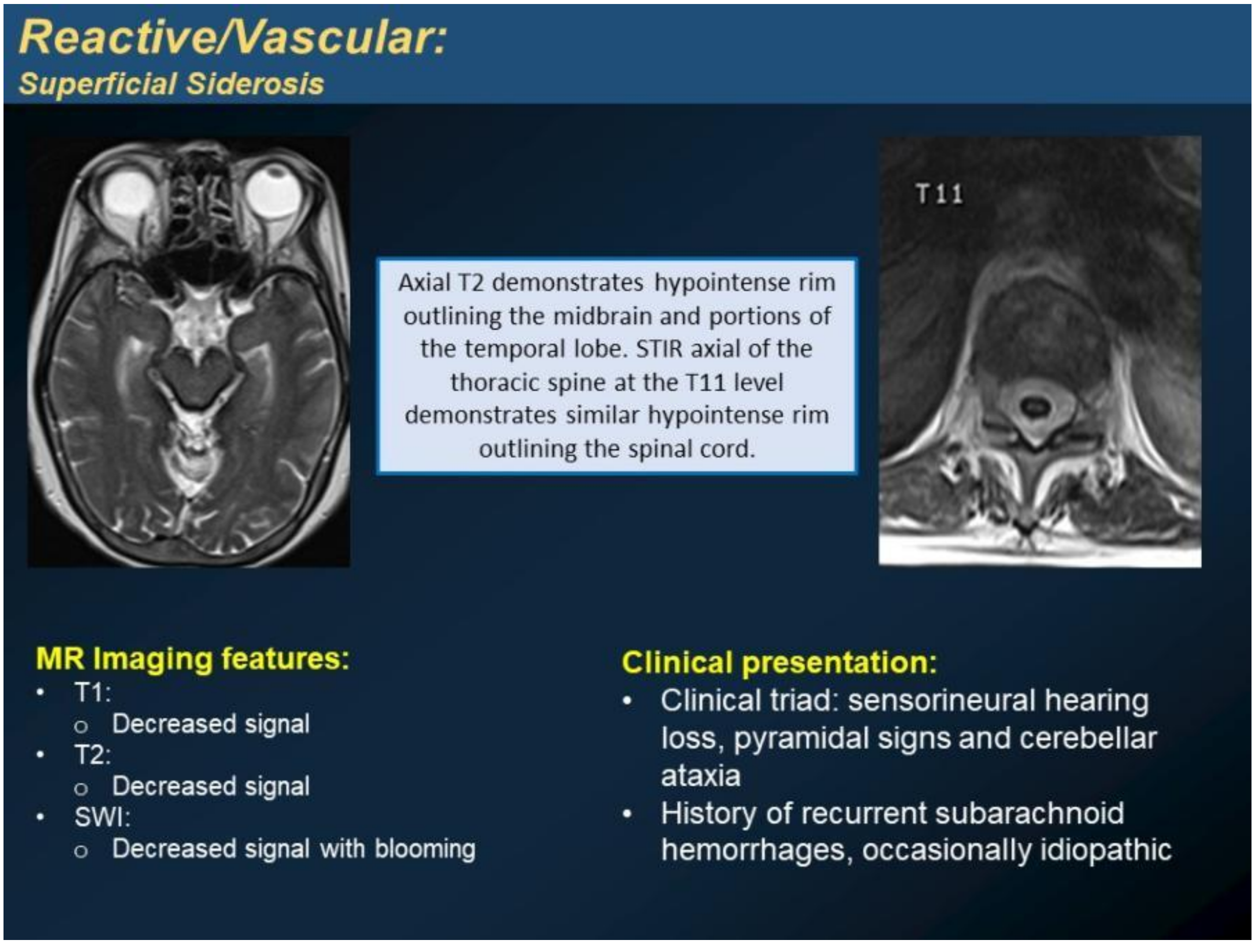

(Filename: TCT_3478_Slide2.JPG)

2801

Head and Neck Imaging with SPECTRAL CT; New Horizons & Emerging Trends

S Bhuta[1], M Peterson[2], C Hsu[3], D Palipana[4]
[1]Gold Coast University Hospital, Gold Coast, Australia, [2]Gold Coast University Hospital, Gold Coast, QUEENSLAND, [3]Gold Coast University Hospital, 1 Hospital Blvd, N/A, [4]Gold Coast University Hospital, Southport, Queensland

Purpose
Spectral CT is a promising innovation that is increasingly used in clinical practice for characterization of head and neck cancers. The purpose of this study is to investigate applications of spectral CT imaging with multiparametric maps in adding diagnostic confidence and accuracy in various head and neck pathologies.
Materials and Methods
A review of patients with a confirmed diagnosis of head and neck cancer, infections were performed at Gold Coast University Hospital from June 2018 with a prospective data collection till April 2019. All imaging was performed on the Philips IQon spectral CT scanner using a dual-layer, detector-based approach. Using the Philips IntelliSpace Portal at 40keV the parameters evaluated were: iodine concentration maps, Z-effective value. All patients had dual stage IV contrast (100 ml, Ioversol 300mg).

Parameters for normal structures, tumours and nodes were measured. Generated maps were sent to PACS for simplified workflow.

Results

Spectral CT of the head and neck assist in preoperative evaluation of oropharyngeal cancers especially in identifying primary site and nodal metastases. It helps in TNM staging of larynx to evaluate thyroid cartilage invasion (T4 disease) & thyroid neoplasms. Cystic lymphangiomas with recent bleed and tumour mimics can be well distinguished with iodine maps. Tumours demonstrate a higher iodine uptake and Z effective value compared with normal tissue. Lymph node parameters predicted metastatic potential in baseline and post-treatment neck study. Our initial experience reflects spectral CT immensely improved tumour visibility, TNM tumour staging at 40Kev influencing patient outcomes(Fig.1).

Conclusions

Spectral CT imaging is an exciting emerging CT technique. In our experience tumors and malignancy demonstrated a higher iodine uptake and Z effective value and were best seen at 40KeV. These layers of maps added diagnostic certainty and confidence and is a huge leap forward in head and neck imaging

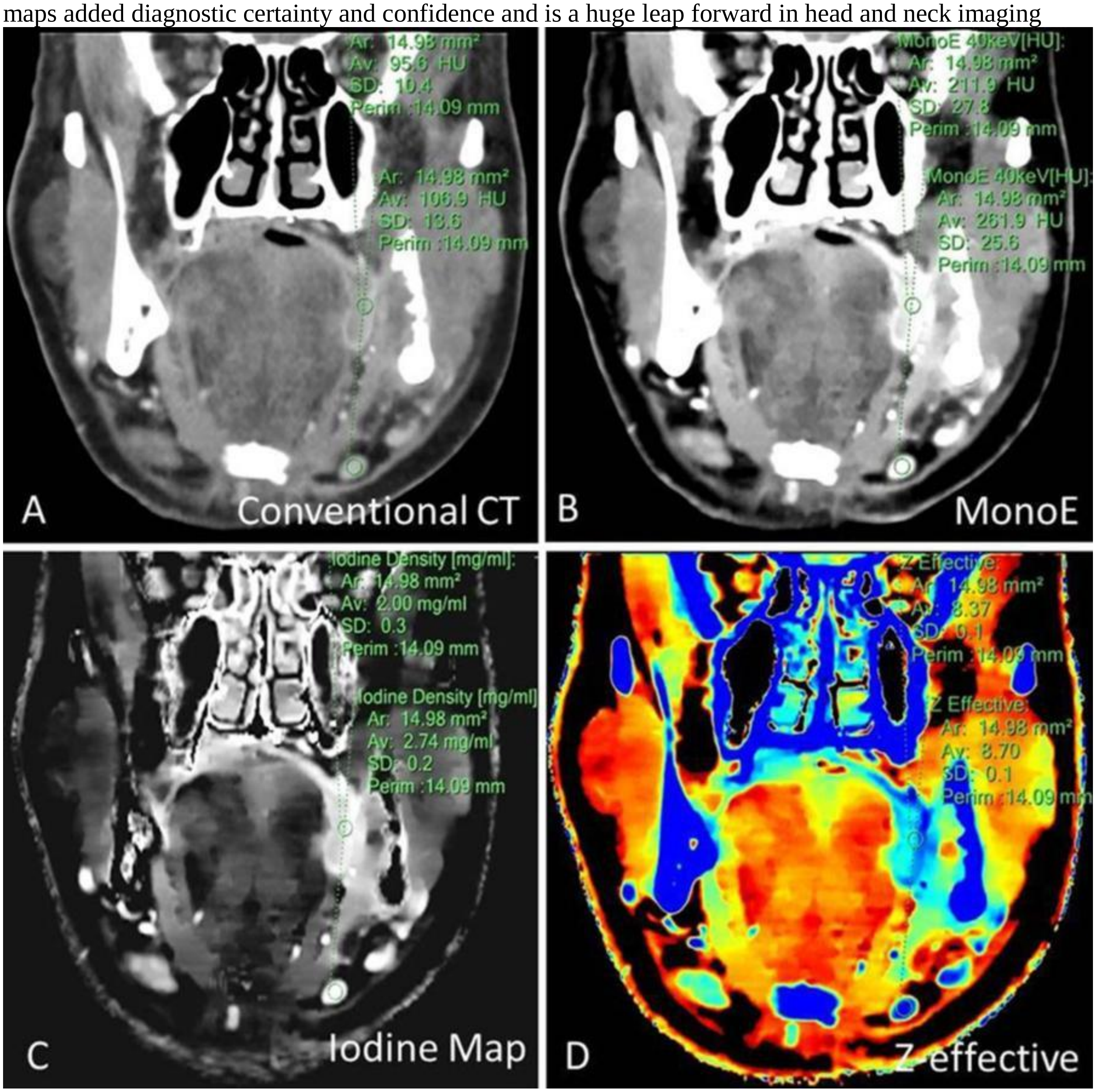

(Filename: TCT_2801_Fig1.jpg)

2397

Hemi-disease: An Imaging Review of Hemispheric Neurological disorders

A Goldman-Yassen[1], A Derman[2], D Choe[3], T Shepherd[2], Y Lui[4]
[1]NYU Langone Medical Center, New York , NY, [2]NYU Langone Medical Center, New York, NY, [3]NYU Langone Medical Center, Livingston, NJ, [4]NYU School of Medicine, New York, NY

Purpose
Asymmetric findings in the brain are typically focal, such as infarct, hemorrhage or a mass. On the other hand, diffuse abnormalities tend to involve the hemispheres bilaterally. This is an exhibit to review the unusual set of entities that defy these two categories. These are entities that involve close to an entire brain hemisphere but classically are restricted to being unilateral or grossly asymmetric. Here we will illustrate these disorders with imaging examples and discuss the unique group of differential diagnoses they form with a focus on differentiating imaging characteristics.
Materials and Methods
Exhibit will show examples and review the relevant imaging findings of asymmetric diffuse cerebral abnormalities by utilizing case examples from our academic practice including both congenital syndromes of hemiatrophy, hemimegalencephaly and acquired asymmetric hemispheric disorders.
Results
This set of unusual brain abnormalities will be presented as a set of imaging differential diagnoses and we will expand specifically on the imaging characteristics which differentiate between entities. The exhibit will cover congenital (including such entities as Dyke-Davidoff Masson, Sturge-Weber), infectious/inflammatory (such as Rasmussen's encephalitis), metabolic (such as hyperglemia induced hemiballismus hemichorea), vascular (such as neonatal ischemic insults, vascular shunting associated with congenital heart disease, post carotid endarterectomy reperfusion syndrome and hemiplegic migraine), neoplastic (including gliomatosis cerebri) and neurodegenerative etiologies (such as corticobasal degeneration and primary progressive aphasia.) There will also be a discussion on why these entities may be prone to unilateral involvement and how this impacts the resulting clinical manifestations.
Conclusions
Cases of diffuse yet asymmetric hemispheric brain abnormality present a true diagnostic challenge. Understanding the imaging characteristics of these entities and how they differ from each other will aid in appropriate image interpretation.

3428

High Resolution Orbital Anatomy and Pathology

A Matthews[1], M Beasley[2], I Kabakus[3], A Chatterjee[4]
[1]Medical University of South Carolina, Charleston, SC, [2]MUSC, Charleston, SC, [3]Department of Radiology and Radiological Science Medical University of South Carolina 96 Jonathan Lu, Charleston, SC, [4]MEDICAL UNIVERSITY OF SOUTH CAROLINA, CHARLESTON, SC

Purpose
High resolution orbital imaging using dedicated surface coils is far superior in detailing anatomy and pathology than traditional head coil orbital imaging. Numerous cases at our institution demonstrate this superior ability.
Materials and Methods
After a brief overview of orbital anatomy, several cases will illustrate the usefulness of high resolution orbital protocol to detect pathology. Case by case pathology will begin centrally to include optic neuritis

and glioma; move peripherally to elucidate intraorbital schwannoma, pseudotumor and vascular malformations among others.
Results
Each case will not only highlight the ability of high resolution imaging to depict pathology, but a brief discussion of the disease process will accompany each case geared towards the neuroradiologist and what they need to know.
Conclusions
Case by case imaging demonstrates the superior ability of high resolution MR to diagnose a variety of orbital pathology at our institution.

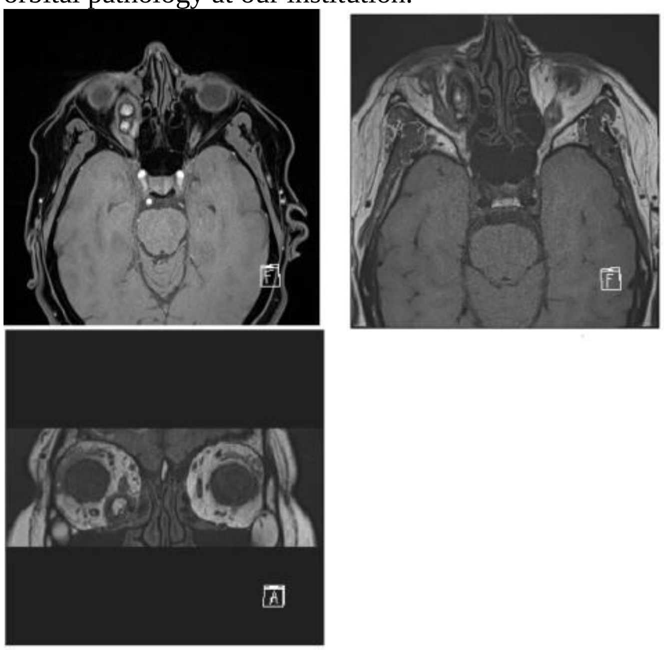

(Filename: TCT_3428_OrbitalImages.jpg)

3000

How to Differentiate Infectious Diseases of Spine from Imitating Etiologies?

H Hatipoglu[1]
[1]*Health Sciences University Ankara Numune Research and Training Hospital, Ankara, Turkey*

Purpose
The purpose of this educational exhibit is to discuss contemporary imaging of the infectious diseases of spine and its implications related to patient management.
Materials and Methods
In order to compile the cases in this exhibit, we screened our imaging database from 2010 through 2017.
Results
Some of the entities we will highlight in this exhibit are pyogenic spondylitis, tuberculous spondylitis and brucellar spondylitis and their atypical imaging patterns. Disorders that mimic spinal infection including Modic type 1 degenaration, ankylosing spondylitis and other end-plate pathologies are thoroughly discussed. Objectives are to familiarize the viewer with the 1. Epidemiology 2. Imaging anatomy 3. Imaging techniques 4. Pyogenic spondylitis 5. Tuberculous spondylitis 6. Brucellar spondylitis 7. Infection mimics of the spine.
Conclusions
At the end of this image-rich presentation, the viewer will have an improved understanding of the

imaging of infectious diseases of spine and mimics. Awareness of atypical MR imaging findings and mimics is important to avoid diagnostic delay and unnecessary diagnostic tests.

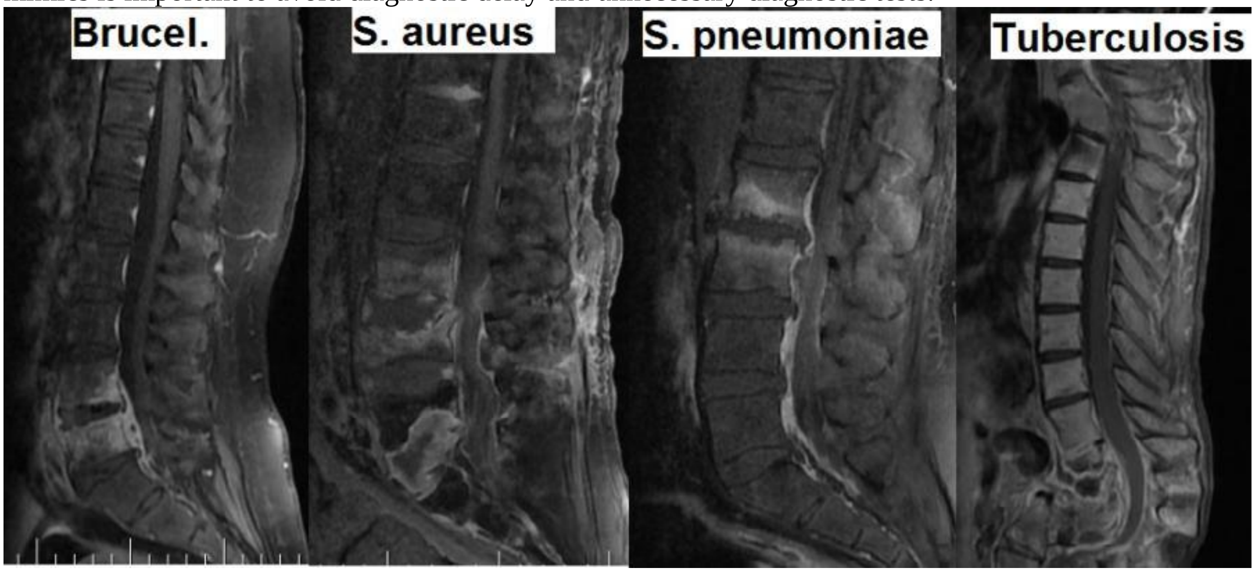

(Filename: TCT_3000_spinefigure.jpg)

3436

Hypoglossal Nerve Palsy due to Degenerative Arthropathy of the Cranio-cervical Junction

A Haboosheh[1], L Loevner[2], S Mohan[3]
[1]University of Pennsylvania, Philadelphia, PA, [2]University of Pennsylvania, Philadelphia , PA, [3]University of Pennsylvania School of Medicine, Philadelphia, PA

Purpose
Cervical spine and skull base degenerative disease may result in hypoglossal nerve palsy mimicking tongue pathology. Computed tomography and magnetic resonance imaging are necessary in the work-up of a new tongue paralysis, to evaluate for lesions along the course of the hypoglossal nerve and tongue. Radiologist must be familiar with the anatomical segments of the hypoglossal nerve from its nuclei in the medulla to its distal branches in the tongue. After reviewing this exhibit, the viewer will have a comprehensive understanding of hypoglossal nerve anatomy, differential diagnosis, and recognize imaging characteristics of tongue denervation.
Materials and Methods
1. Review relevant anatomical segments of the hypoglossal nerve and its complex relationship with surrounding structures. 2. Illustrate the distinct radiologic findings of hemi-tongue paralysis 3. Discuss the critical role that imaging plays in establishing the cause of hypoglossal nerve palsy. 4. Illustrate degenerative changes of the cervical spine and skull base that may result in tongue paralysis, and show how they may be misinterpreted as a mass.
Results
Hypoglossal nerve anatomy is complex with a spectrum of pathology that may cause denervation mimicking a tongue mass. Acute and subacute/early chronic denervation include protrusion of base of tongue into the oropharyngeal lumen, hemitongue T2 hyperintensity, and mild enhancement of the affected side. Fatty infiltration and atrophy are finding in chronic paralysis. This exhibit will use a segmental approach to scrutinize the gamut of pathology, with emphasis on degenerative disease including juxtacortical cysts at the cranio-cervical junction.

Conclusions
After reviewing this exhibit, the viewer will have a comprehensive understanding of the hypoglossal nerve anatomy and pathologies that may cause nerve palsy with emphasis on degenerative arthropathy.

(Filename: TCT_3436_hypoglossialcanalcyst1.jpg)

2585

I am All Ears! A Hemangioblastoma within the Internal Auditory Canal in the Setting of Acute Hearing Loss

A Rajput[1], S Ceglar[2], E Velez[2], J Scheibal[1], M Gupta[1], P Kim[3], J Acharya[4], A Rajamohan[5], J Go[5]

[1]*USC Keck School of Medicine, Los Angeles, CA,* [2]*LAC+USC, Los Angeles, CA,* [3]*Keck School of Medicine of USC, La Crescenta, CA,* [4]*UNIVERSITY OF SOUTHERN CALIFORNIA, KECK SCHOOL OF MEDICINE, Monrovia, CA,* [5]*UNIVERSITY OF SOUTHERN CALIFORNIA, KECK SCHOOL OF MEDICINE, LOS ANGELES, CA*

Purpose

The purpose of this educational exhibit is to review the incidence, prevalence, and clinical presentation of common and uncommon presentations of hemangioblastomas, with our main focus on a case within the internal auditory canal (IAC). Typically, the differential consideration for cerebellopontine angle masses and internal auditory canal masses are the common vestibular schwannomas, meningiomas, and epidermoid cysts. Awareness of differentiating imaging characteristics and serial examinations will help the radiologist to correctly exclude the more typical lesions found in this location. This will prompt appropriate treatment to prevent harmful consequences such as permanent hearing loss.

Materials and Methods

Hemangioblastomas are overall very rare highly vascular tumors of the central nervous system. When discovered, they are typically intracranial in location, with the vast majority in the posterior fossa. Although they have syndromic associations with von Hippel Lindau disease, they are mostly sporadic in nature. The goal of our exhibit is to discuss hemangioblastomas, with focus on a rare presentation in the internal auditory canal in a patient presenting with acute hearing loss. There are clues to the imaging findings that are atypical for common IAC lesions which should suggest to the radiologist to consider an atypical diagnosis. It is important for the radiologist to be aware of the variety of atypical lesions in this location.

Results

The discussion will include a brief review of the epidemiology, clinical presentations, diagnostic criteria, and histological findings of hemangioblastomas. The discussion will include a review of the internal auditory canal anatomy, typical lesions in the IAC, and a comprehensive review of hemangioblastomas found in common and uncommon locations, followed by presentation of a hemangioblastoma of the IAC. Images from the time of surgical resection will be included in the exhibit. Further discussion will include characteristic MRI findings of hemangioblastomas that will guide radiologists to recognize it, look for potential complications, and recommend appropriate management. The exhibit will also demonstrate a case based review of relevant differential diagnoses for IAC lesions, additional atypically located hemangioblastomas, and typical hemangioblastomas. The review will further include imaging characteristic that will help a radiologist to distinguish between these possible considerations and offer appropriate recommendations regarding follow up and further management.

Conclusions

Close evaluation of internal auditory canal lesions with serial imaging is vital to differentiate between common and uncommon pathology. After reviewing this exhibit, the radiologist should feel confident in their approach to typical and atypical IAC lesions with a comprehensive understanding of hemangioblastomas.

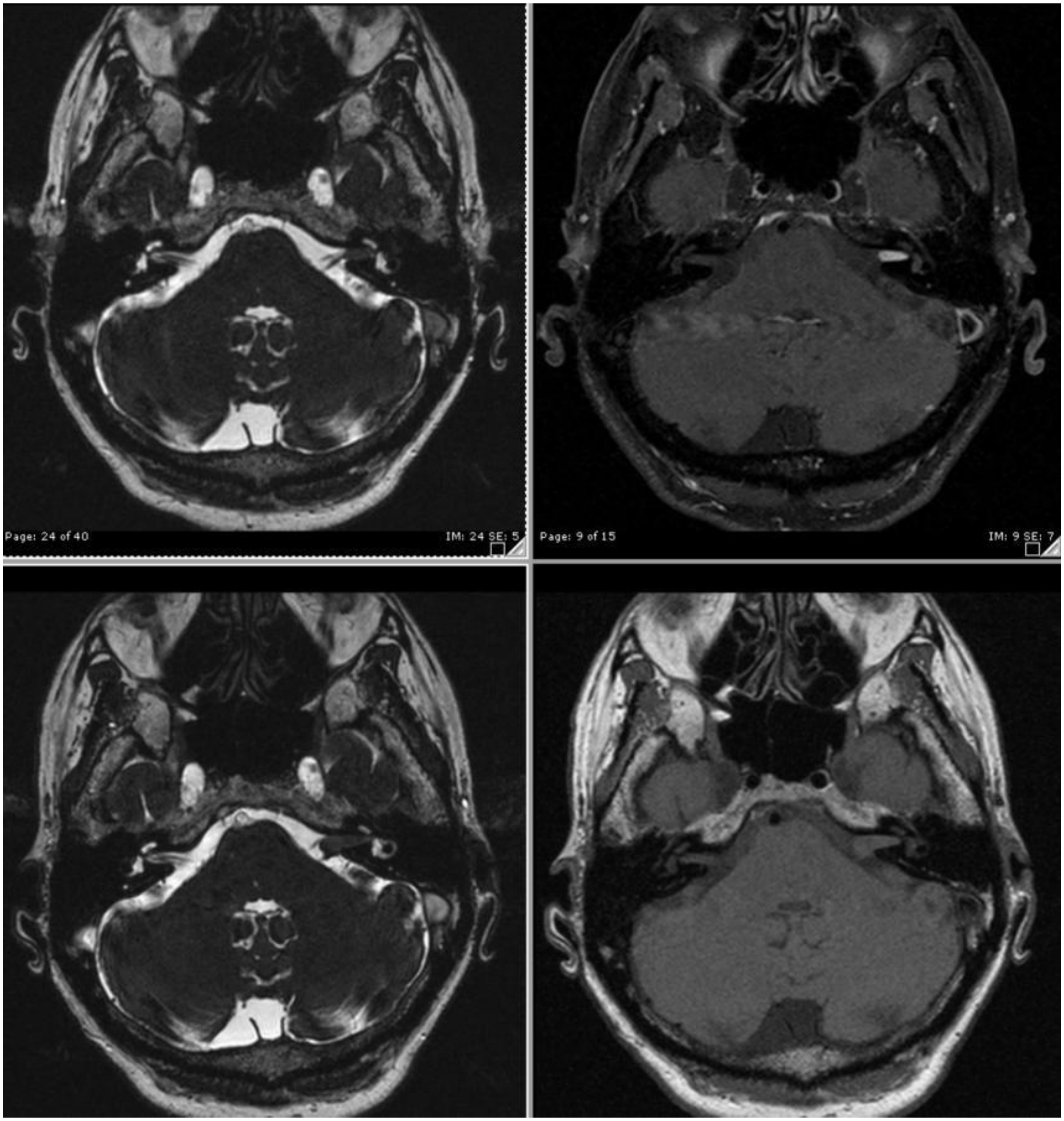

(Filename: TCT_2585_IAChemangioblastoma.jpg)

2250

I Can See Clearly Now…the Differential of Optic Nerve Enlargement

D Hill[1], L Eckel[2], F Diehn[3], K Schwartz[4], J Garrity[4]
[1]Mayo Clinic Rochester, Rochester, MN, [2]Mayo Clinic, Rochester, Rochester, MN, [3]MAYO CLINIC, ROCHESTER, MN, [4]Mayo Clinic, Rochester, MN

Purpose
This educational exhibit is designed to help general diagnostic radiologists, fellowship trained

neuroradiologists, and other providers directly involved in patient care (neurology, neurosurgery, ophthalmology, and primary care) recognize the imaging features that distinguish multiple etiologies resulting in optic nerve enlargement.
Materials and Methods
The educational exhibit will attempt to cover a broad spectrum of differential diagnoses for optic nerve enlargement including: • Optic nerve glioma • Optic nerve meningioma • Orbital pseudotumor • Optic neuritis • Sarcoidosis • Orbital lymphoma • Metastases • Orbital cavernous venous malformation • Erdheim-Chester disease • Schwannoma • IgG4 • Orbital varix • Optic nerve germinoma
Results
A short discussion of each diagnosis will cover disease epidemiology, clinical presentation, histology, and treatment options. Following the discussion will be a review of the radiology features that distinguish each diagnosis with an emphasis on high quality images.
Conclusions
Optic nerve enlargement is a common finding with a surprisingly broad differential of both benign and aggressive disease processes. Narrowing the differential based on imaging findings is of upmost importance given the difficulty and high risk nature of obtaining tissue for pathology review. Understanding the disease epidemiology, clinical presentation, histology, and treatment options for each potential diagnosis will further aid the provider in accurately diagnosing and treating the patient.

3133

Image Guided Lumbar Drainage Catheter Insertion- Technical Pearls

A Swarnkar[1], S DESHMANE[2]
[1]Upstate Medical University Hospital, Jamesville, NY, [2]SUNY upstate medical university, Syracuse, NY

Purpose
We discuss the stepwise approach for placement of the lumbar drain in technically challenging situations. A brief overview of indications, the steps of the procedure and our unique modification in cases of CSF depletion are also described.
Materials and Methods
Retrospective evaluation of Image guided lumbar drain placement during last 5 years.
Results
We discuss the technique of lumbar drain placement and technical pearls to avoid difficulties encountered during the procedure. Advantages of interlaminar vs midline approach are discussed as well. The lumbar drain placement becomes especially challenging in patients with prolonged CSF leak and CSF depletion. In such cases we describe a novel technique of infusing intra-thecal saline to recreate the temporary volume distension which helps in placement of the catheter. Complications of Lumbar drainage are also discussed.
Conclusions
Lumbar drain placement is a common procedure performed by neurosurgeons and spine surgeons for various indications. A neuroradiologist is called upon usually in difficult situations such as morbid obesity, obscured anatomy in prior lumbar spine surgery with instrumentation and failed bedside attempts. We discuss the technique of lumbar drain placement and technical pearls to avoid difficulties encountered during the procedure.

2505

Imaging Findings in Adult Medulloblastoma

W Chang[1], A Sohn[2], M Spearman[3], C Li[1], M Goldberg[1]

[1]*Allegheny Health Network, Pittsburgh, PA,* [2]*Allegheny health network, Pittsburgh, PA,* [3]*ALLEGHENY HEALTH NETWORK, BADEN, PA*

Purpose

Medulloblastoma is the most common malignant brain tumor in children but is relatively rare in adults. The presentation of medulloblastoma is also quite different in adults, when compared to children. The recent Boston classification has identified four main subtypes of medulloblastoma, some of which are more common in adults, and these genetic differences help explain the differences in tumor behavior between children and adults. These factors can greatly affect the imaging findings in medulloblastoma, carry significant differences in prognosis, and affect both treatment and patterns of recurrence for the disease. Therefore, studying this heterogeneous disease is useful for neuroradiologists to offer the best clinical care for their patients.

Materials and Methods

In this presentation, we will present the different subtypes of medulloblastoma, illustrate which subtypes are most common in adults, show their common imaging findings, recommend appropriate follow-up imaging, and discuss common patterns of recurrence. We will also discuss some of the new emerging genetic research on medulloblastoma. We will then reinforce key teaching points with an interactive quiz.

Results

The Boston classification in 2010 divided medulloblastoma into four subgroups, SHH, WNT, Group 3 and Group 4. Of these, SHH, WNT, and group 4 are the three subtypes commonly seen in adults, while group 3 is almost exclusively seen in infants and children. The WNT subtype tends to have the best prognosis, with metastases being relatively rare. This subtype tends to contact the fourth ventricle and be more well-circumscribed. The SHH subtype tends to be have poorer outcome, be more lobar, and demonstrate less enhancement. Group 4 desmoplastic tumors tend to have more direct contact with the leptomeninges while still contacting the fourth ventricle, while group 4 classic tumors tend to be more midline and more ill-defined than the WNT subtype, with poorer outcomes and more recurrence. Recurrence in medulloblastoma is commonly leptomeningeal, and imaging of the entire neuraxis for staging is recommended, as well as follow-up imaging of the brain and spine, as patients often receive craniospinal radiation, depending on the subtype and tumor biology.

Conclusions

Medulloblastoma is a tumor with a wide range of genetic heterogeneity. The different genetic subtypes tend to have significant differences in their imaging findings, allowing imaging to be used as a surrogate biomarker to a certain degree. Knowledge of the common imaging findings of the various subtypes commonly seen in adults, their molecular differences, and their prognoses and patterns of spread or recurrence may help the neuroradiologist offer value to clinicians in the evaluation of this relatively rare disease. There is a vast amount of new genetic research currently underway on medulloblastoma, which may offer additional insights and help further characterize tumor biology and behavior.

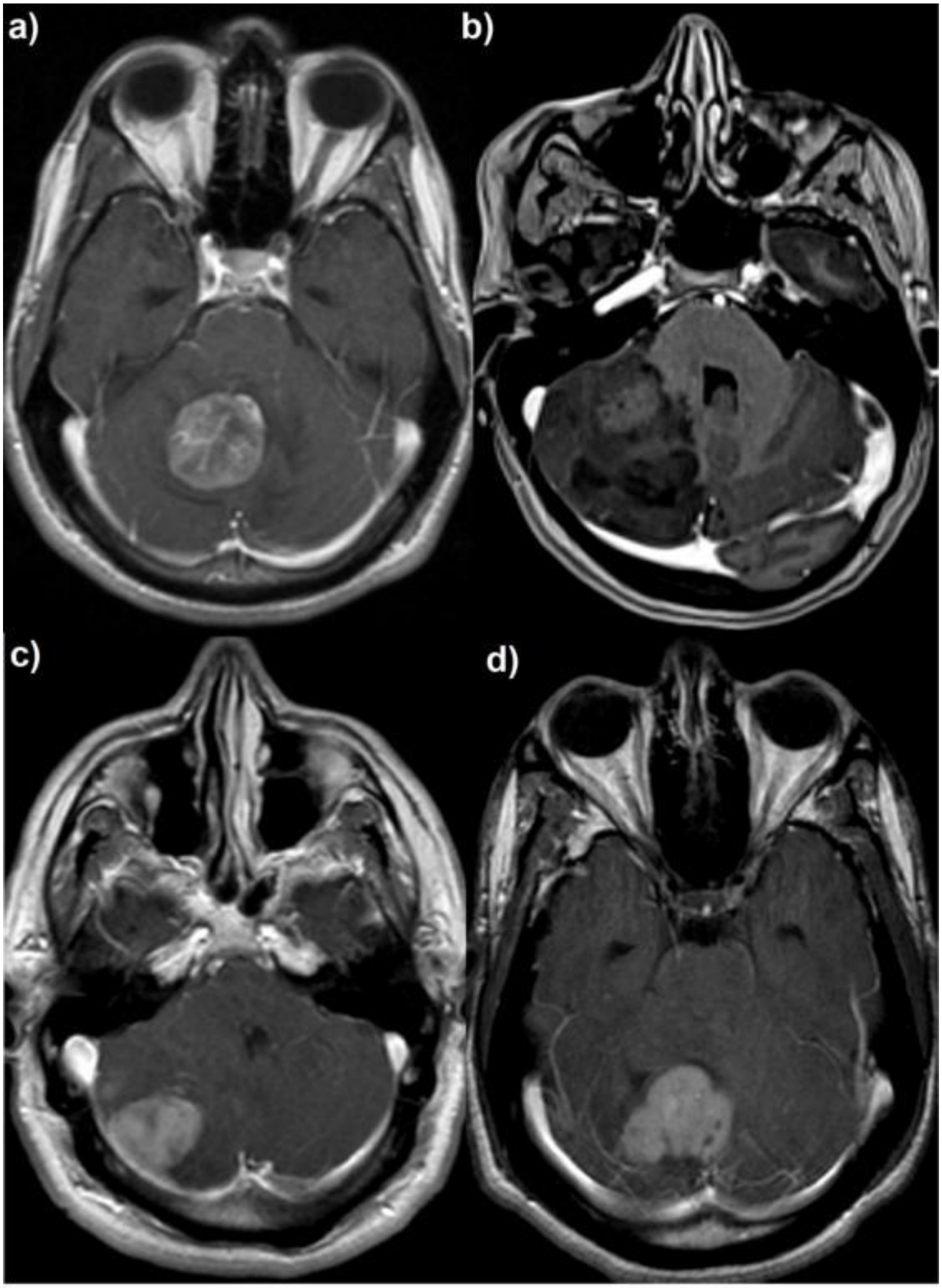

Figure 1: a) WNT phenotype medulloblastoma which is well-circumscribed and contacts the fourth ventricle. **b)** SHH phenotype medulloblastoma, which is lobar in morphology and demonstrates poor contrast enhancement. **c)** Desmoplastic group 4 medulloblastoma which contacts the leptomeninges. **d)** Classic group 4 medulloblastoma which is more midline but less well defined than the WNT variant.

(Filename: TCT_2505_medullo.jpg)

3240

Imaging Findings in Dorsal Thoracic Arachnoid Web and the Differential Diagnosis of "Scalpel Sign"

P COIMBRA[1], P BRASIL[2], L LUNA[3], T Da Silva[4], D Távora[5]
[1]CLINICA TRAJANO ALMEIDA, FORTALEZA, Brazil, [2]HOSPITAL GERAL DE FORTALEZA, FORTALEZA, CEARÁ, [3]FEDERAL UNIVERSITY OF CEARA, FORTALEZA, CEARA, [4]Hospital Geral de Fortaleza, Fortaleza , Ceará , [5]Hospital Geral de Fortaleza, FORTALEZA, CE

Purpose
To illustrate the imaging findings of dorsal thoracic arachnoid web (DTAW) and how to differentiate this particular entity from other causes of ventral cord displacement.
Materials and Methods
We report three cases of DTAW that manifested at imaging with "scalpel sign", associated or not with syrinx and other features. A review of this subject was made focused in differentiate the imaging findings presented in this rare entity of the aspect of other ventral cord displacement causes (i.e. dorsal arachnoid cyst, thoracic spinal cord herniation, tumors).
Results
Dorsal thoracic arachnoid web (DTAW) represent an intradural extramedullary transverse band of arachnoid tissue that causes mass effect and dorsal indentation, and can be associated or not with cord altered signal. On sagittal MR imaging this focal dorsal indentation of the thoracic spinal cord resemble a scalpel with its blade pointing posteriorly (called "scalpel sign"). Although very suggestive of DTAW, this sign is not specific and should be differentiate of other ventral cord displacement causes (i.e. dorsal arachnoid cyst, thoracic spinal cord herniation, tumors). In cord herniation, cord tissue protrudes through a ventral dural defect, and we can see the focal deformity along the ventral aspect of the cord on spinal axial MR imaging; while in arachnoid cysts we can identify the marginated walls and the presence of smooth wide scalloping of the cord surface.
Conclusions
Spinal MR imaging plays a fundamental role in the diagnosis of ventral cord displacement pathologies. Although clinical manifestations are usually similar, the recognition of some imaging findings (specially "scalpel sign") can help radiologists and clinicians make a correct diagnosis and a prompt treatment for the patient.

3030

Imaging Findings in Primary and Secondary Central Nervous System Lymphomas

P COIMBRA[1], P BRASIL[2], D Távora[3], T Da Silva[4], L LUNA[5]
[1]CLINICA TRAJANO ALMEIDA, FORTALEZA, Brazil, [2]HOSPITAL GERAL DE FORTALEZA, FORTALEZA, CEARÁ, [3]Hospital Geral de Fortaleza, FORTALEZA, CE, [4]Hospital Geral de Fortaleza, Fortaleza , Ceará, [5]FEDERAL UNIVERSITY OF CEARA, FORTALEZA, CEARA

Purpose
This exhibit aims to illustrate the range of imaging findings in primary and secondary CNS lymphomas; discuss the role of advanced techniques for the analysis of CNS lymphoma (DWI, MR spectroscopy, MR perfusion); and highlight the main points that may help to differentiate CNS lymphoma from other brain lesions.

Materials and Methods

We report several cases of CNS lymphoma with typical MR imaging features in both primary and secondary disease. Then we correlate these findings with the latest reports in the literature review.

Results

Primary CNS lymphoma (PCNSL) almost always present as parenchymal lesions with predilection for periventricular and central hemispheric white matter. They usually present as solitary homogeneously mass hypo- or isointense on T1-WI and iso- to hyperintense on T2-WI, with moderate-to-marked contrast enhancement, although multiple lesions can be shown in some non-AIDS PCNSLs. In contrast, secondary CNS lymphomas usually present as leptomeningeal metastases (leptomeningeal, subependymal, dural or cranial nerve enhancement; superficial cerebral lesions; and communicating hydrocephalus), with only one third of patients showing parenchymal lesions. In advanced MR imaging, CNS lymphoma shows restricted diffusion, and a recent study demonstrated that pretherapeutic ADC tumor measurements within contrast-enhancing regions might be predictive of clinical outcome in patients with PCNSL. Perfusion MR imaging of PCNSLs demonstrate low CBV (typically lower in lymphomas than in other brain tumors) and a characteristic intensity time curve. While MR spectroscopy demonstrates elevated lipid peaks combined with high Cho/Cr ratios, which besides similiar to some CNS tumors, it helps to differentiate PCNSL from other lesions.

Conclusions

MR is the imaging technique of choice to evaluate CNS lymphoma, showing some characteristic conventional imaging findings. Although none of these findings will unequivocally differentiate CNS lymphoma from other brain lesions (other CNS tumors, multiple sclerosis, infection), they can improve preoperative diagnosis, help to monitor treatment response and predict treatment outcomes, especially when associated with advanced techniques.

2504

Imaging Findings in West Nile Virus Infection

W Chang[1], M Spearman[2], M Goldberg[1], J Villablanca[3]
[1]Allegheny Health Network, Pittsburgh, PA, [2]ALLEGHENY HEALTH NETWORK, BADEN, PA, [3]UCLA, Los Angeles, CA

Purpose

West Nile Virus is an emerging pathogen in North America since first being detected in 1999, and has increased dramatically in incidence, with over 40 thousand cases and 20 thousand cases of CNS involvement being reported from 1999 to 2015. Due to its relatively recent arrival to the New World, there has been relatively little study of this entity, compared to other common viral infections. Although imaging findings in West Nile Virus infection are relatively non-specific, some classic imaging findings have been reported. In this presentation, we will discuss the classic imaging findings of West Nile Virus and review the literature on this emerging disease.

Materials and Methods

We will review the common imaging findings in West Nile Virus, and discuss how they might be differentiated from other conditions in the differential diagnosis such as demyelinating disease, other viral infections, toxic/metabolic insults and vascular etiologies. Subsequently, we will discuss common findings on follow-up imaging and discuss recent advances and study in the literature on West Nile Virus. We will conclude the presentation with an interactive quiz to reinforce key teaching points.

Results

West Nile Virus has a relatively non-specific appearance on imaging and presents in a heterogeneous manner. In a review of the literature, we found that approximately one third of patients have a classic appearance on imaging, with symmetric enhancement, FLAIR hyperintensity, and restricted diffusion, which symmetrically and preferentially affects the deep nuclei and corticospinal tracts in the brain and spine, one third of patients present with some subset of the above findings, possibly asymmetric, along with leptomeningeal enhancement, and the last third of patients presented with normal imaging. Some of the patients who presented with classic spinal cord imaging findings had normal brain imaging, as well. Therefore, making the diagnosis of West Nile Virus on imaging alone is challenging. However, in cases that present with the classic imaging findings, suggesting the diagnosis may hasten diagnosis by the clinical team.

Conclusions

West Nile Virus is a relatively new pathogen in the New World, which has increased in incidence relatively rapidly in the last 20 years. Due to changing environmental factors and the ubiquity of travel, this disease will become only more common in the future. While imaging features are often non-specific, in some cases, imaging may be useful and help in ascertaining the diagnosis in a timely manner.

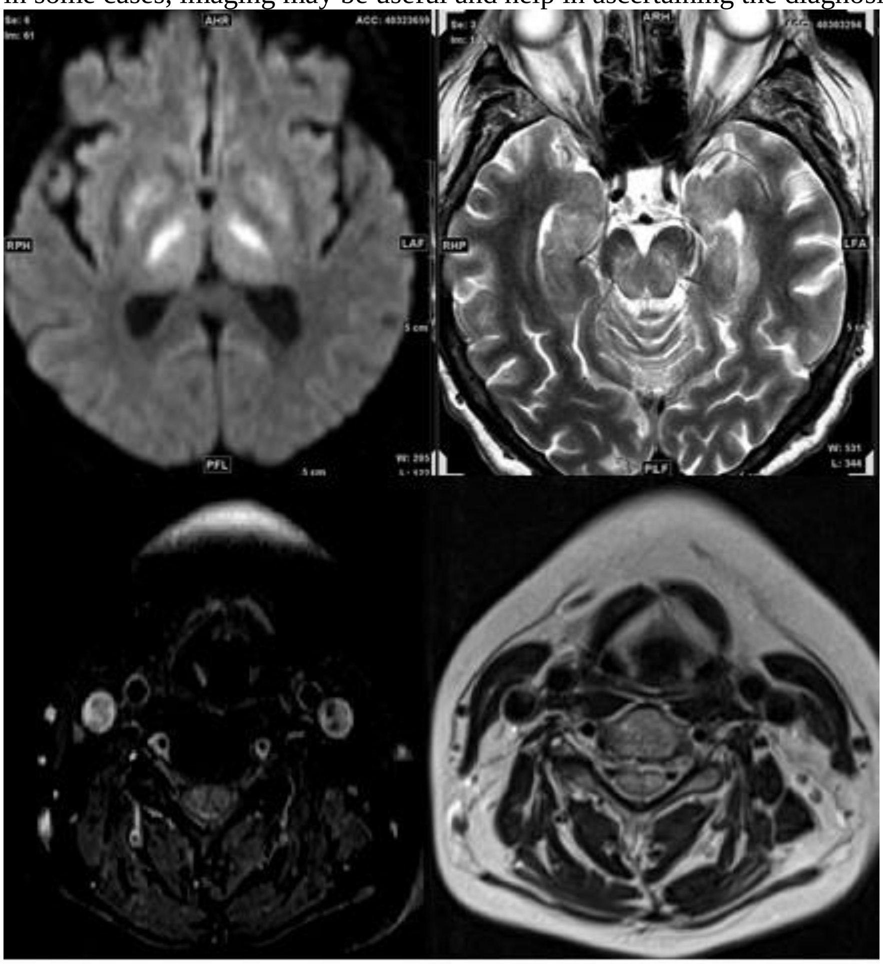

Figure 1) top left: Symmetric restricted diffusion in the bilateral thalami. **top right:** Symmetric T2 hyperintensity in the bilateral corticospinal tracts. **bottom left:** Symmetric enhancement in the bilateral corticospinal tracts. **bottom right:** Symmetric T2 hyperintensity in the bilateral corticospinal tracts. CSF was positive for West Nile Virus.

(Filename: TCT_2504_wnvasnr2.jpg)

2802

Imaging Non-melanomatous Skin Cancers of the Head and Neck: Not Just Skin Deep!

S Bhuta[1], M Peterson[2], D Palipana[3], C Hsu[4]
[1]Gold Coast University Hospital, Gold Coast, Australia, [2]Gold Coast University Hospital, Gold Coast, QUEENSLAND, [3]Gold Coast University Hospital, Gold Coast, Queensland, [4]Gold Coast University Hospital, 1 Hospital Blvd, N/A

Purpose

Australia has the highest incidence of skin cancer worldwide, and non-melanomatous skin cancer (NMSC) Basal Cell Carcinoma being most common. The purpose of this study is to analyze critical anatomical sites of head and neck NMSC, to demonstrate critical role of multimodal imaging and how it influences TNM staging and surgical management.

Materials and Methods

A retrospective review of patients with confirmed diagnosis of head and neck NMSC, from specialist head and neck clinic at the Gold Coast University Hospital from June 2016 to June 2018 was performed. Imaging was performed on 128 multi-slice Computed Tomography (CT),3.0 Tesla Magnetic Resonance Imaging (MRI). Every imaging study was analyzed under three criteria: assessment of primary for local disease and depth of invasion, regional nodal metastasis, and large nerve perineural spread. Findings were correlated with TNM staging.

Results

Critical sites of head and neck NMSC include zygoma, peri-orbital, pre and post-auricular regions. Resection criteria used for operative management are influenced by primary site, depth of invasion seen on MR. The National Health and Medical Research Council recommends 4mm excision margin for primary achieves optimal resection of SCCs. Radiotherapy is reserved for nodal metastases with extracapsular spread and as a palliative approach. Basal Cell Carcinoma (BCC) and SCC are best assessed by multimodal imaging with dual stage contrast-enhanced CT and MRI to assess soft tissue infiltration, perineural spread and lymph nodal disease(Fig.1) Merkel Cell Carcinoma (MCC) warrant a whole-body PET (Positron Emission Tomography) PET/CT.

Conclusions

Multi-modal imaging approach for assessing of head and neck NMSC is vital to characterize lesions located at critical sites. These lesions can be clinically occult or subdermal. Hi-res imaging influences surgical clearance and reconstruction and adjuvant radiotherapy regimes. Imaging almost always influences TNM staging

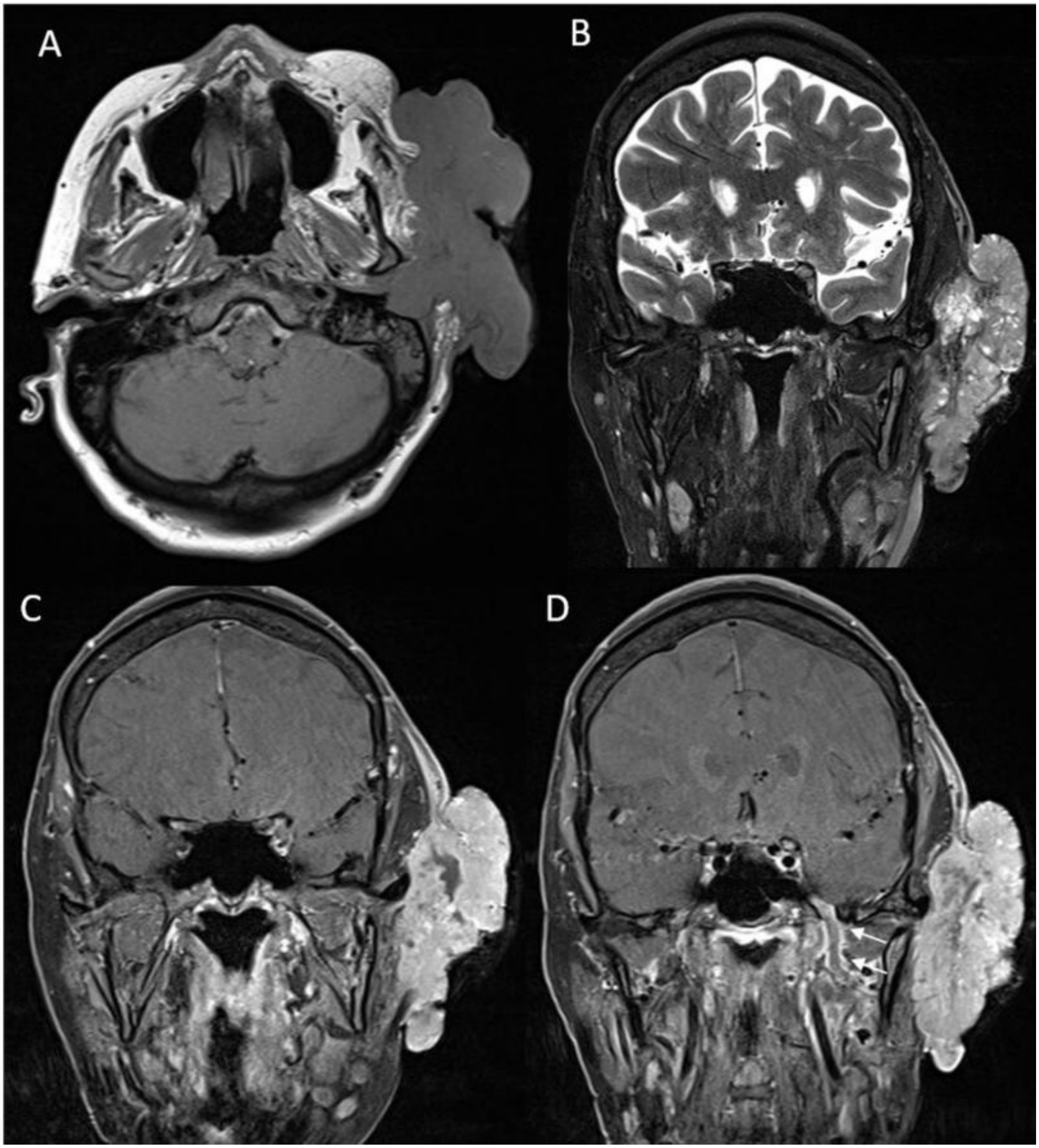

(Filename: TCT_2802_Picture1.jpg)

3532

Imaging of Auditory Brainstem Implants

K Summers[1], L Ledbetter[2], J Leever[1], N Harn[1], J Bertsch[1]
[1]University of Kansas Medical Center, Kansas City, KS, [2]UNIVERSITY OF KANSAS MEDICAL CENTER, KANSAS CITY, KS

Purpose
The auditory brainstem implant (ABI) is an infrequently encountered neuroprosthetic developed for and utilized in an attempt to restore hearing in deaf patients with pathology between the cochlea and cochlear nuclei. Though rare, it is important for the neuroradiologist to recognize and understand the device, know the relevant anatomy including optimal electrode positioning on the brainstem, conditions where ABI is indicated, the potential postoperative complications, and imaging safety recommendations.
Materials and Methods
Reviewing the ABI device, anatomy, pathologic indications, surgical approaches, potential operative complications, and imaging safety recommendations through case and literature review.
Results
The ABI is similar in principle to cochlear implants, consisting of an internal electrode and receiver stimulator component with an external worn component. Sound is converted by the device to an electrical stimulus which directly stimulates the cochlear nuclei. The cochlear nucleus complex is the target for the electrode array and is located along the dorsolateral surface of the brainstem rostral to the pontomedullary junction at the lateral recess of the fourth ventricle. The device was developed for neurofibromatosis Type 2 patients with vestibular schwannomas and hearing loss due to tumoral disruption of the cochlear nerves. Indications for ABI have since expanded to include sequelae of trauma, infection, and certain congenital anomalies. Translabyrinthine and retrosigmoid are the two surgical approaches utilized for ABI device implantation, each having inherent advantages and disadvantages. The most frequent surgical complications are CSF leak, electrode migration, and non-target stimulation of other cranial nerves. Most ABI devices are MRI conditional and require lower field strengths with or without removal of the external fixating magnet.
Conclusions
The ABI is a brain-machine interface utilized in causes of hearing loss due to disruption or deficits of the cochlear nerves. This exhibit will explore the imaging, anatomy, and clinical features associated with ABIs.

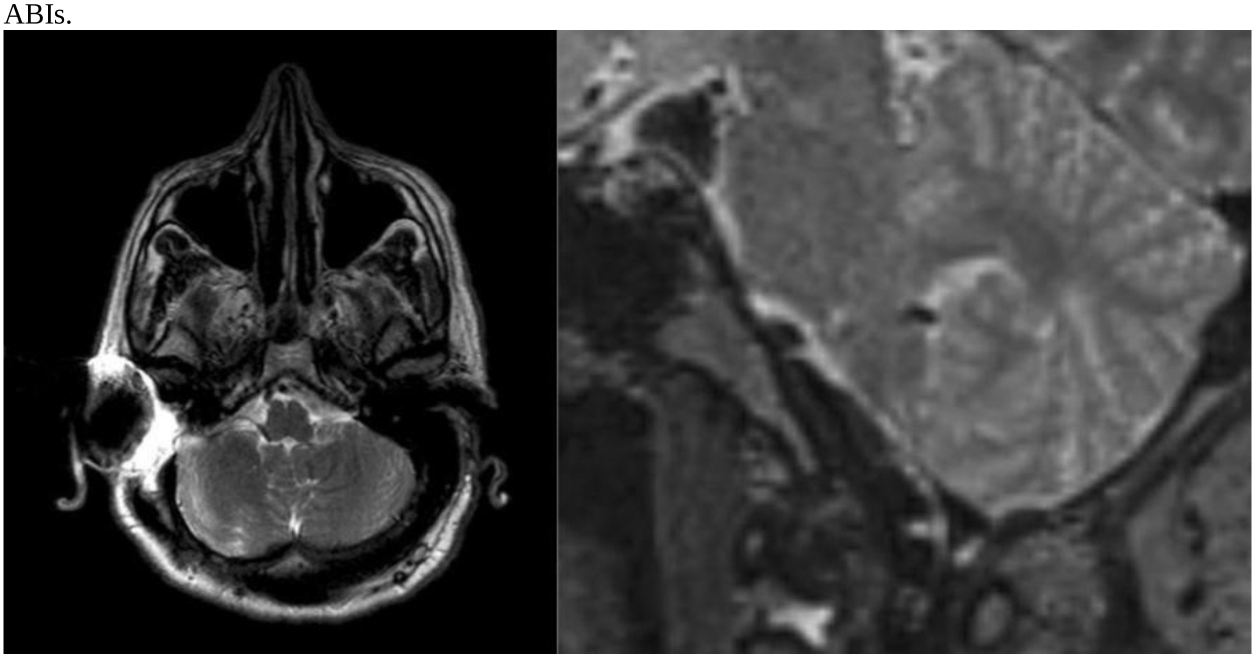

(Filename: TCT_3532_ABI.jpg)

3118

Imaging of Complicated Head and Neck Infections in Children: Beneath the Runny Nose, Red Eye and Aching Ear

A Jaju[1], J Maddalozzo[2]
[1]Ann and Robert H Lurie Children's Hospital of Chicago, Chicago, IL, [2]Ann & Robert H. Lurie Children's Hospital of Chicago, 1, IL

Purpose
Introduction: Head and neck infections in children are extremely common, and typically self-limited or resolve by medical treatment, with imaging indicated in only a minority. However, even in immunocompetent children, these can sometimes lead to complications that threaten life or function and require emergent medical and/or surgical treatment. Imaging is central to timely identification and delineation of these complications.
Materials and Methods
Learning objectives: 1. To understand the pathways for spread of infection in head and neck 2. To understand the appropriate use of imaging modalities including CT, MRI and vascular imaging. 3. To illustrate the serious complications of pediatric head and neck infections by CT and MRI.
Results
Summary: The infections will be categorized by their primary sites and the following complications will be illustrated. Paranasal sinuses: Frontal osteomyelitis with subperiosteal abscess (Pott's puffy tumor), sphenoid/skull base osteomyelitis; orbital complications including pre- and post-septal cellulitis, subperiosteal and soft tissue abscess; intracranial complications including epidural and subdural abscesses, meningitis, cerebritis, brain abscess and dural sinus thrombosis. Orbits: In addition to above, orbital compartment syndrome, endophthamitis, cavernous sinus thrombophlebitis. Temporal bone: Otomastoiditis with abscesses of the periauricular or neck soft tissues; intracranial involvement (similar to those listed above for sinus infections); petrous apicitis with cranial nerve involvement, meningitis and ICA arteritis. Superficial and deep soft tissues: Peritonsillar and retropharayngeal abscesses, airway compromise, jugular vein thrombophlebitis (Lemierre's syndrome), septic emboli, and infectious carotid arteritis with narrowing. Dental: Subperiosteal and soft tissue abscesses, mandibular osteomyelitis, Ludwig's angina. Lymph nodes and salivary glands: Necrosis/abscess formation. Congenital: Superinfection of underlying congenital anomalies including first, second, third/fourth branchial anomalies and lymphatic malformations.
Conclusions
.

2851

Imaging of IgG4 Related Disease of the Orbit

B Ozgen Mocan[1], E BULUT[2], N Saran[1], P Setabutr[1], K Oguz[2]
[1]University of Illinois at Chicago, Chicago, IL, [2]Hacettepe University, Ankara, Turkey

Purpose
IgG4-related ophthalmic disease (IgG4-ROD) consists of orbital manifestations of the systemic IgG4-related disease, characterized by dense lymphoplasmacytic infiltrations with a predominance of IgG4-positive plasma cells in the affected tissue, usually accompanied by some degree of fibrosis. The manifestations of IgG4-ROD are variable and can appear similar to other orbital inflammatory conditions such as idiopathic orbital inflammation sarcoidosis. IgG4-ROD can have aggressive and infiltrative appearance and can also be misdiagnosed as a malignant infiltrative process. This exhibit will review the important imaging features and specific differentiation sings of IgG4-ROD to assist with accurate differential diagnosis.

Materials and Methods
The imaging findings of IgG4-ROD will be reviewed with illustrative cases to demonstrate pertinent radiological findings.
Results
IgG4-ROD can involve many different soft tissue structures of the orbits but most commonly involves the lacrimal gland. Other commonly affected parts of the orbit include the extraocular muscles, orbital fat and the nasolacrimal duct system. The thickening of the infraorbital nerve has been reported to be a highly suggestive sign. Soft tissue thickening extending from the posterior orbit into the cavernous sinus and/or Meckel cave can also be seen.
Conclusions
It is important for the neuroradiologists to become familiar with the imaging findings of IgG4-ROD as the disease can mimic other inflammatory and neoplastic conditions of the orbit. The recognition of features may facilitate the accurate diagnosis and guide the clinicians for the adequate management of the patients.

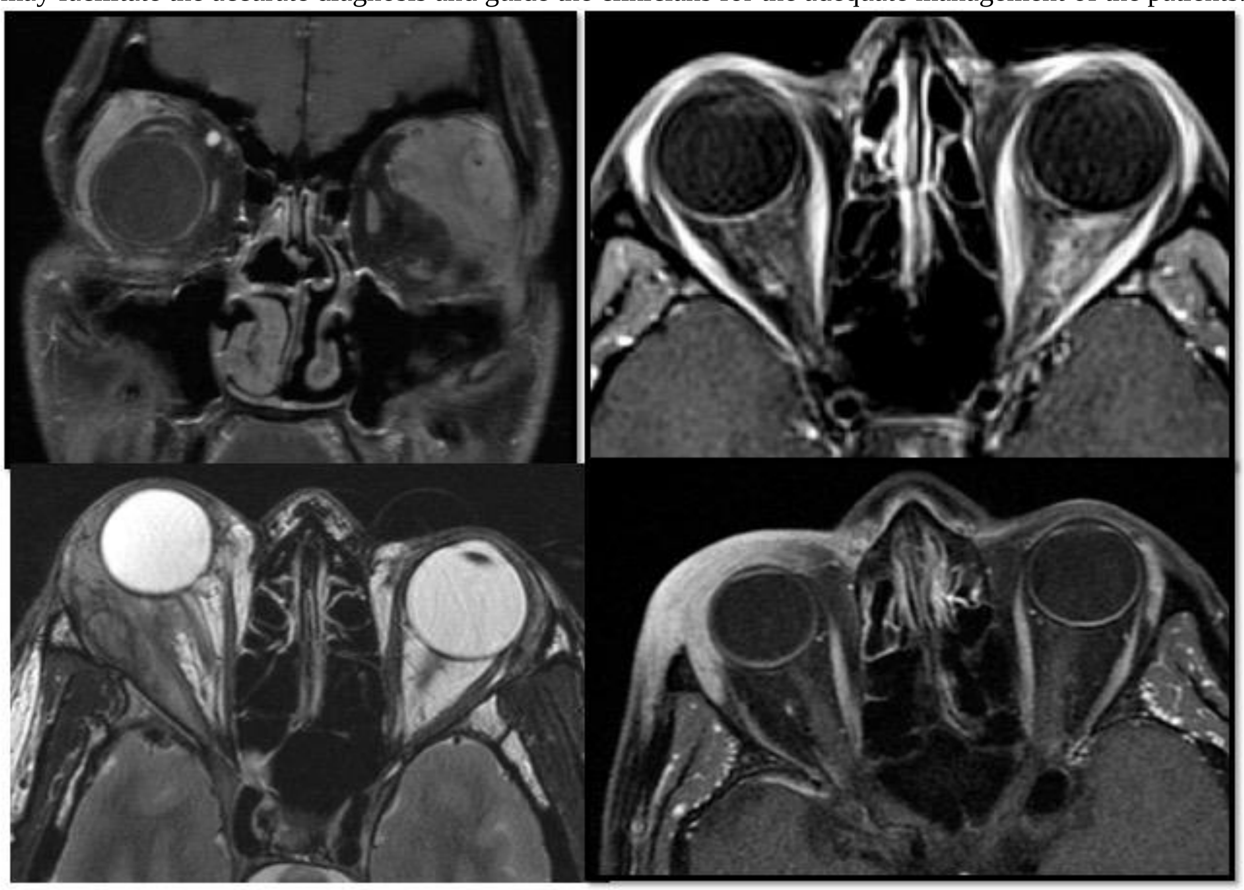

(Filename: TCT_2851_Picture1.jpg)

3477

Imaging of Ligamentous Injuries at the Craniocervical Junction (CCJ)

E Supsupin[1], N Chinapuvvula[2]
[1]The University of Texas Health Science Center at Houston, HOUSTON, TX, [2]The University of Texas Health Science Center at Houston, Houston, TX

Purpose

The craniocervical (CCJ) junction is a complex transitional zone between the cranium and the spine. Given its specific functional demands, the CCJ should be treated as a distinct anatomic and radiologic entity from the cranium, and specifically the cervical spine. This presentation aims to provide a comprehensive review of ligamentous injuries at the CCJ.

Materials and Methods

The anatomy and biomechanical demands of important ligamentous structures at the CCJ is reviewed. Illustrative cases depicting the impact of blunt trauma to the CCJ ligaments are provided. The role of MRI in the evaluation of integrity and injury to these ligaments is reviewed.

Results

The CCJ is comprised of osseous structures articulated with synovial joint, ligaments and membranes, and muscles. Given its complexity, imaging of blunt traumatic injuries (particularly ligamentous injuries) to the CCJ can be challenging, but crucial to improving morbidity and mortality to such injuries. Imaging plays an indispensable role in the management and prognostication of these injuries. Dedicated MRI sequence can provide accurate details. Knowledge of normal anatomy and biomechanics is important in the evaluation of ligamentous injuries. The CCJ has an onerous role of not only housing and protecting vital structures (such as cord, cranial nerves, and critical vessels supplying the cord and brain), but must also simultaneously provide mobility. Blunt injuries carry a significant risk for devastating morbidity and mortality. Ligaments are an important component of this vital transition between the cranium and spine. The transverse and alar ligaments are the primary stabilizers of the CCJ.

Conclusions

The radiologist plays an important role in the clinical setting of blunt CCJ ligamentous injuries. Knowledge of normal anatomy and biomechanics is crucial in making the correct diagnosis and appropriate management of such injuries.

Craniocervical dissociation with multiple ligamentous injuries at the CCJ following a high-speed motor vehicle collision

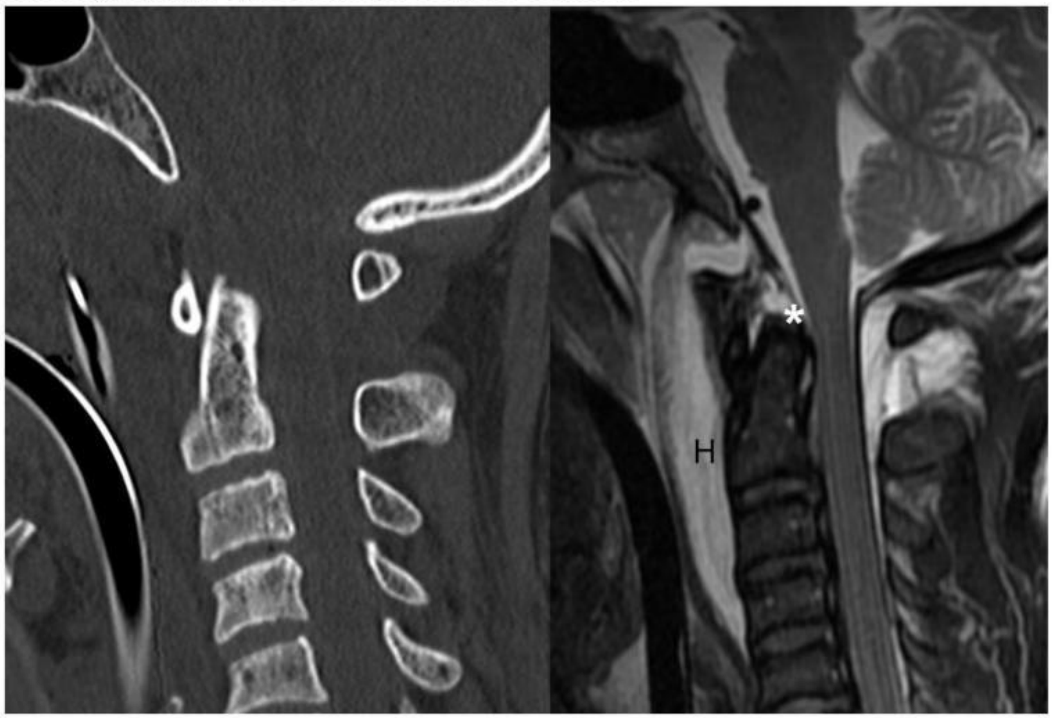

Cervical spine CT showing widening of the basion-dens interval

Sagittal T2-weighted MRI depicting multiple ligamentous injuries including tectorial membrane disruption (*). There is loss of definition of normal apical ligament and atlantooccipital membrane. A large prevertebral fluid/hematoma is present (H).

(Filename: TCT_3477_CCJLigInjury.JPG)

3126

Imaging of Oral and Dental Diseases Affecting the Systemic Health

K Ito[1], K Takumi[2], A Mecham[3], R Aayushi[4], Y Kawashima[5], N Hirahara[5], T Kaneda[5], O Sakai[4]
[1]Boston University School of Medicine, Boston, MA and Nihon University School of Dentistry at Matsudo, Chiba, Japan, [2]Boston Medical Center, Boston University School of Medicine, Boston, MA and Kagoshima University, Kagoshima, Japan, [3]Division of Oral & Maxillofacial Radiology, Boston University School of Dental Medicine, Boston, MA, [4]Department of Radiology, Boston Medical Center, Boston University School of Medicine, Boston, MA, [5]Department of Radiology, Nihon University School of Dentistry at Matsudo, Chiba, Japan

Purpose
Many oral and dental diseases or conditions can affect the systemic health. Although these may be present on CT and MR imaging studies, many might be overlooked because the exam is performed for an "unrelated" indication. The purpose of this educational exhibit is 1) to review the oral and dental disease or conditions which may cause systemic diseases in the recent literature, 2) to review imaging findings of these disease or conditions, and 3) to discuss how radiologists can contribute to predict systemic diseases from oral and maxillofacial imaging findings.
Materials and Methods
The literature search was performed to identify oral and dental diseases or conditions that may affect the

systemic health and to understand the mechanism. Our database was searched to identify patients with such disease or conditions. We will illustrate CT and MR imaging findings of various oral and dental diseases, and discuss oral and maxillofacial imaging findings to predict systemic diseases.

Results

Periodontitis has been reported to be associated with many systemic diseases such as angina pectoris, myocardial infarction, cerebral stroke, low birth weight, aspiration pneumonitis, and metabolic syndrome. Severe dental caries may result in serious regional inflammation/infection such as odontogenic sinusitis and cellulitis, and may extend to orbital or mediastinal infection. In addition, dental caries that frequently occur in the oral cavity is reminiscent of a decreased function of the salivary glands. Maxillofacial imaging is useful to detect altered craniofacial anatomy and malocclusion, which is a risk factor for obstructive sleep apnea syndrome.

Conclusions

Many oral and dental diseases and conditions are risk factors for various systemic diseases, and may be present on CT and MR images. It is important for radiologists to be familiar with the relationship between dental diseases and systemic diseases to predict the systemic disease from maxillofacial imaging findings.

2400

Imaging of Otalgia

B Ozgen Mocan[1], N Saran[2]
[1]University of Illinois, Chicago, IL, [2]University of Illinois at Chicago, Chicago, IL

Purpose

Otalgia, pain in the ear, can be the result of an otologic disease or can arise from pathologies other than the ear (referred otalgia). In children, ear pathologies and especially infectious disorders are the most common cause of otalgia, but in adults, referred otalgia constitutes more than half of cases. Otalgia can be the only presenting symptom of a severe underlying condition and is considered a "red flag" sign in the adult patient. This exhibit will review the important aspects of imaging in the evaluation of otalgia with imaging findings of the most common causes of primary otalgia, followed by the description of anatomic basis for referred otalgia with a review of different causes of secondary otalgia.

Materials and Methods

The CT and MR imaging of the temporal bone and other relevant head and neck regions will be used to illustrate the pertinent radiological findings.

Results

In primary otalgia the pain arises from the ear itself and common underlying pathologies include otomastoiditis, external auditory canal (EAC) cholesteatoma, keratosis obturans, acute external otitis, skull base osteomyelitis and EAC malignancies. Many different nerves (including cranial nerves V, VII, IX and X and spinal nerves C2 and C3) provide sensation to the various parts of the ear, and when there is irritation of those nerves at an area outside the ear, the brain is incapable of distinguishing between the sites of origin. Referred otalgia is thus related to pathologies of head and neck regions innervated by those nerves. The potential sites of pain include dental pathologies such as periodontal and periapical disease, TMJ disorders but also inflammation of the sphenoid and posterior ethmoid sinuses. Otalgia may be referred also from primary carcinoma of the head and neck; especially in oropharyngeal cancer otalgia may be the only presenting complaint. Primary neuralgia of the trigeminal, facial, glossopharyngeal and vagus nerves can all cause different degrees of otalgia.

Conclusions

This exhibit summarizes the common causes of otogenic and referred otalgia. In the setting of otalgia with negative ear findings the discussed potential sites of referred pain within the head and neck should be evaluated.


(Filename: TCT_2400_ear_pain_illustrated2.jpg)

2274

Imaging of the Diagnosis, Workup and Treatment of Moyamoya Syndrome

J Hughes[1], N Matthees[2], M Harwood[3]
[1]BNI, Phoenix, AZ, [2]St. Joseph's Hospital, N/A, [3]Medical Center in Phoenix, Phoenix, AZ

Purpose
Moyamoya syndrome is an uncommon vascular process secondary to numerous etiologies which share in common the end result of progressive narrowing of the terminal internal carotid arteries (ICA) and central intracranial arterial vasculature. Examples of implicated disease processes include sickle cell disease, neurofibromatosis type I, Down's syndrome and radiation induced vasculopathy.1 Asymptomatic moyamoya syndrome may be treated conservatively with antiplatelet therapy however when symptoms manifest patients are often treated with surgical revascularization. Revascularization methods include direct bypassing, classically from the superficial temporal artery to a recipient MCA vessel, as well as numerous indirect techniques collectively termed pial synangiosis. Indirect revascularization methods differ by surgical technique as well as the tissues used to promote neovascularization including encephalo-myo synangiosis (EMS), encephalo-duro-arterio synangiosis (EDAS), encephalo-duro-arterio-myo synangiosis (EDAMS) as well as the creation of multiple burr holes with arachnoid opening.23 Imaging plays a key role in the diagnosis and workup of the disease as well as in the evaluation of the effectiveness of direct and indirect surgical treatments.4 The purpose of this presentation is to review the imaging related to moyamoya syndrome.
Materials and Methods
A case-based format will be utilized to illustrate the typical imaging appearance of patients with Moyamoya syndrome at diagnosis, during workup and in the evaluation of the various surgical treatment options. Imaging examples will be obtained from our institutions PACS system. These case-based examples will be supplemented with discussion of expected and unexpected findings. Imaging modalities

will include computed tomography (CT), magnetic resonance imaging (MRI), computed tomography angiography (CTA), magnetic resonance angiography (MRA), digital subtraction angiography (DSA), magnetic resonance perfusion imaging (MRP) and computed tomography perfusion imaging (CTP) with and without Diamox.

Results

This presentation will highlight the imaging findings seen on various modalities in patients with moyamoya syndrome at different timepoints including initial diagnosis, workup and during the evaluation of surgical treatments. The initial diagnosis of moyamoya may be suggested on non-contrast head CT or MRI when evidence of remote infarcts is visualized, often in a watershed distribution. These findings may be unilateral or bilateral depending on the corresponding vessel involvement. Patients may also present acutely with ischemic and hemorrhagic insults. On MRI, an abnormal flow void of the affected vessel, often with associated increased collateral vasculature can provide further evidence of the disease. Following initial CT and MRI examinations suggestive of moyamoya patients typically undergo non-invasive angiographic imaging (CTA, MRA) followed by DSA. These examinations assess the angioarchitecture of the disease including the degree and location of stenosis/occlusion. Evaluation of collateral vascularity is an important factor which is best assessed by DSA. Additional workup prior to intervention may include MR/CT perfusion imaging commonly prior to and following the administration of Diamox, a vasodilator, which allows for assessment of cerebrovascular reserve. There are a myriad of imaging and clinical factors which are analyzed to determine the optimal surgical treatment for patients with moyamoya syndrome. Following direct or indirect surgical therapy imaging again plays a role in the evaluation of success of reperfusion. This often includes repeat invasive and noninvasive angiographic imaging to assess the patency of bypass grafts and assessment of collateral vascularity as well as repeat perfusion imaging to evaluate the corresponding effect on cerebrovascular reserve. This presentation will discuss the expected and unexpected findings seen on multiple imaging modalities at these various stages of the disease process.

Conclusions

Imaging plays a critical role in the diagnosis and treatment of patients with moyamoya syndrome. There are numerous direct and indirect bypass surgical techniques used to treat the disease. This presentation will discuss the expected and unexpected imaging findings seen on multiple modalities during the initial diagnosis, workup and following treatment of this complex disease.

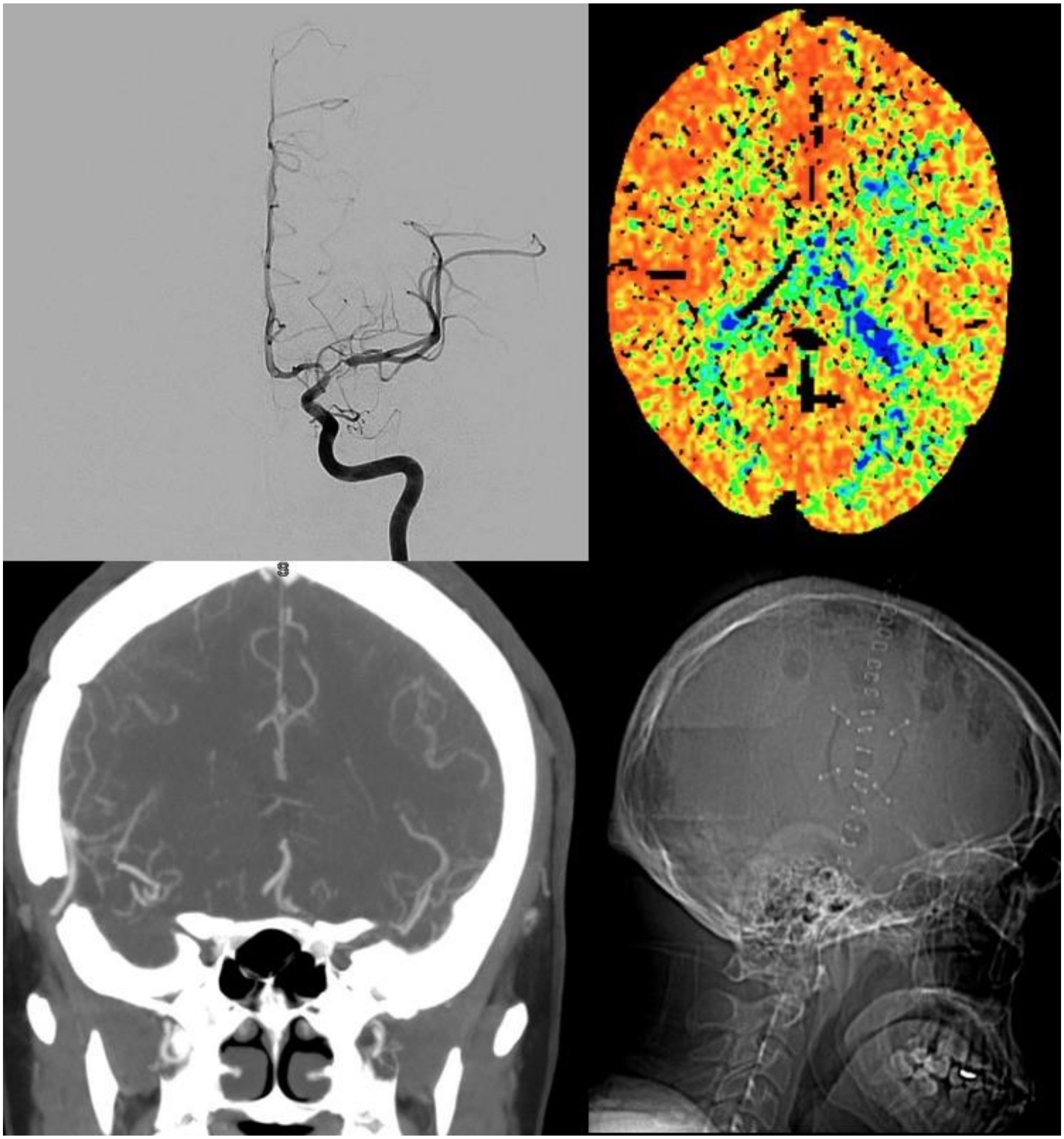

(Filename: TCT_2274_moyamoya.jpg)

2582

Imaging of the Hypopharynx Beyond Cancers.

E Rodriguez[1], J So[2], B Tantiwongkosi[3]
[1]UT Health San Antonio, San Antonio, TX, [2]Joe R. & Teresa Lozano Long School of Medicine UT Health San Antonio, San Antonio, TX, [3]University of Texas Health San Antonio, San Antonio, TX

Purpose
This pictorial review aims to illustrate pertinent imaging anatomy, common and uncommon pathology of the hypopharynx as well as post treatment that neuroradiologists should know.
Materials and Methods
Many distinct disease processes involve the hypopharynx and often present with nonspecific symptoms such as fullness, pain, dysphagia, odynophagia, etc. Endoscopic examinations may reveal nonspecific mass lesions. Pathology may be a primary hypopharyngeal process or may originate in an adjacent structure. Imaging plays critical roles in localization and characterization. This retrospective review of pathologies involving the hypopharynx at a tertiary referral center was performed with radiological and operative/pathological correlation. The anatomy of hypopharynx and relevant adjacent structures will be illustrated using multiplanar CT and MRI as well as fluoroscopic images. Images of each entity will be presented along with any distinguishing imaging features, with diagnostic pearls and pitfalls discussed.
Results
Diseases to be reviewed include cancer (with staging per 8th edition AJCC), brachial pouch anomaly type IV, foreign bodies, infections including hypopharyngitis and thyroiditis as well as infections related to brachial pouch anomaly type IV, Zenker's diverticulum and postoperative complications.
Conclusions
Familiarity with anatomy of the hypopharynx and characteristic imaging findings of pathologies involving the hypopharynx is invaluable for neuroradiologists in providing accurate diagnoses and management guidance.

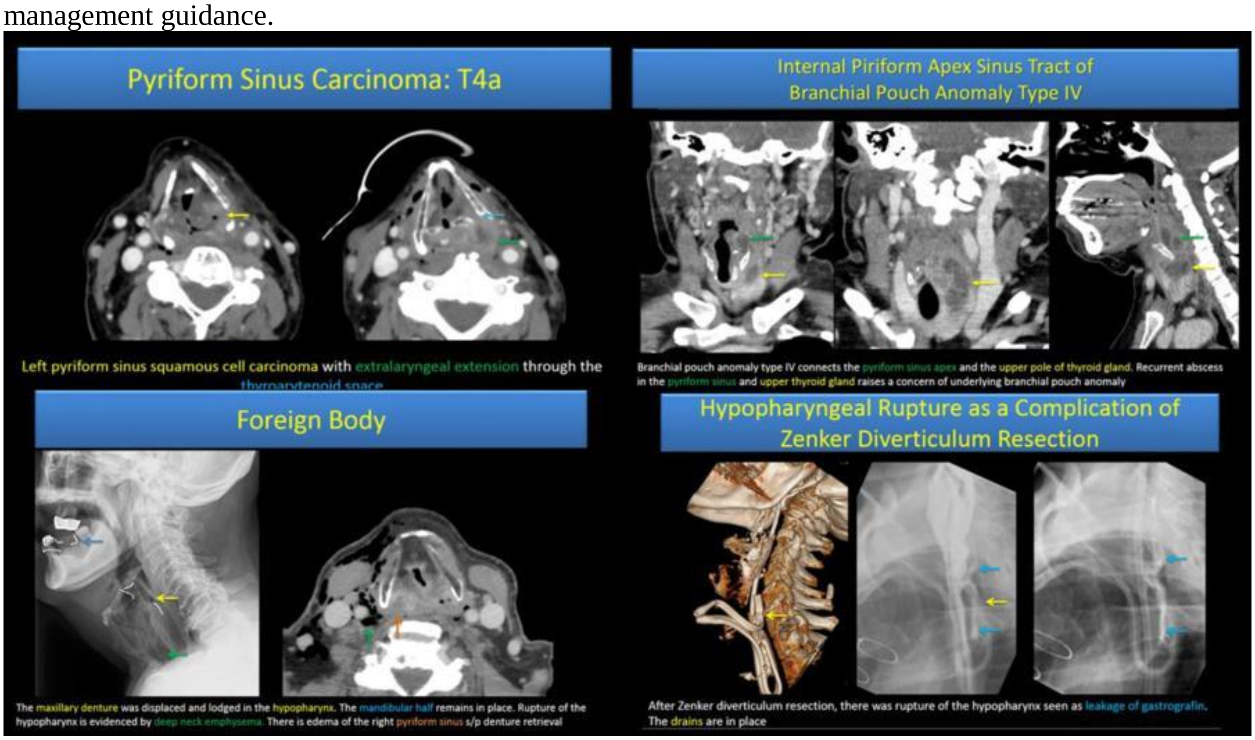

(Filename: TCT_2582_HP1.JPG)

2873

Imaging of the Post-surgical Cranium - How to Think and Speak Like a Neurosurgeon?

P Patel[1], K See[2], S Ceglar[3], A Rajamohan[4]
[1]LAC+USC Medical Center, Los Angeles, CA, [2]University of Southern California, Pasadena, CA, [3]LAC+USC, Los Angeles, CA, [4]UNIVERSITY OF SOUTHERN CALIFORNIA, KECK SCHOOL OF MEDICINE, LOS ANGELES, CA

Purpose

Post-operative imaging plays a key role in the evaluation of patients after cranial surgery. In addition, our reports add much more value to the specialized referring clinicians such as neurosurgeons. It is therefore imperative that we as radiologists are well-versed with the normal anatomy of the cranium and different imaging appearance of the post-surgical cranium to be able to appropriately communicate the findings to referring clinicians. Being familiar with different approaches and the reason behind each surgical approach allows us as radiologists to better understand post-surgical changes, recurrent disease or post-surgical complications whether they may be immediately life-threatening or indolent in nature.

Materials and Methods

The discussion of each craniotomy, craniectomy including cranioplasty will elaborate on the indications as well as accessible contents through each of the surgeries. Below is an example of the discussion which will be included in the exhibit. Pterional craniotomy: This is a standard approach to the middle cranial fossa, anterior cranial fossa, suprasellar and parasellar structures, and Circle of Willis. The pterional craniotomy is the approach of choice for resection of laterally-based skull base tumors such as meningiomas, schwannomas, epidermoids, dermoids, fibrous dysplasia, orbital tumors, arachnoid cysts among other brain masses as well as clipping of cerebral aneurysms. Retro-sigmoid craniotomy: This is a commonly employed approach to the posterior cranial fossa and cerebellopontine angle for removal of skull base tumors such as acoustic neuroma, meningioma, epidernoid, dermoid, arachnoid cyst, brain malignancies and metastatic disease as well as microvascular decompression of cranial nerves such as trigeminal neuralgia, hemifacial spasm, geniculate neuralgia, glossopharyngeal neuralgia, torticollis. Suboccipital craniectomy: This craniotomy is performed to relieve postoperative compression of posterior fossa contents or as a primary procedure to decompress intracranial contents. The indications for decompressive craniectomy include medically refractory intracranial hypertension associated with traumatic brain injury, malignant middle cerebral artery infarction, and subarachnoid hemorrhage. Supra-orbital ("Eyebrow") craniotomy: This approach is performed permit access to a number of lesions in the subfrontal corridor with minimal brain retraction and a much smaller area of potential injury of superficial structures. This craniotomy has less pain than open craniotomy, faster recovery, and minimal scarring. Image Findings: Sample images demonstrate four different types of craniotomies.

Results

Sample images demonstrate four different types of craniotomies. (Top left) Pterional craniotomy CT: Craniotomy defect is noted at the junction of frontal, temporal, and sphenoid bones for aneurysm clipping. (Top right) Translabyrinthine craniotomy CT: Craniotomy defect is noted along the temporal bone including through the inner ear structures for large cerebellopontine angle mass resection. (Bottom left) Supra-orbital ("Eyebrow") craniotomy MRI: Craniotomy defect is noted superior to the orbital region for removal of large sellar mass. (Bottom right) Cranioplasty CT: A cranioplasty flap is noted along the dura of the left frontal and parietal lobes. The patient previously had extensive transtentorial herniation secondary to ipsilateral large parenchymal hemorrhage and subsequent decompressive craniectomy.

Conclusions

It is important to be familiar with the normal CT and MR imaging appearances of the post-surgical cranium. An awareness of the specific indications and complications that may occur after each of the procedures is necessary to prevent a delay in diagnosis and treatment with an associated poorer outcome. CT is fast, accessible, and cost effective and can quickly diagnose multitude types of craniotomies and craniectomies, especially since the osseous structures are better appreciated in this modality. MR imaging is more sensitive than CT in depicting postoperative infection and ischemia. After the presentation, the audience will be better able to understand each type of surgical approach and effectively communicate findings with their referring clinicians and quickly recognize indolent and immediate life-threatening complications.

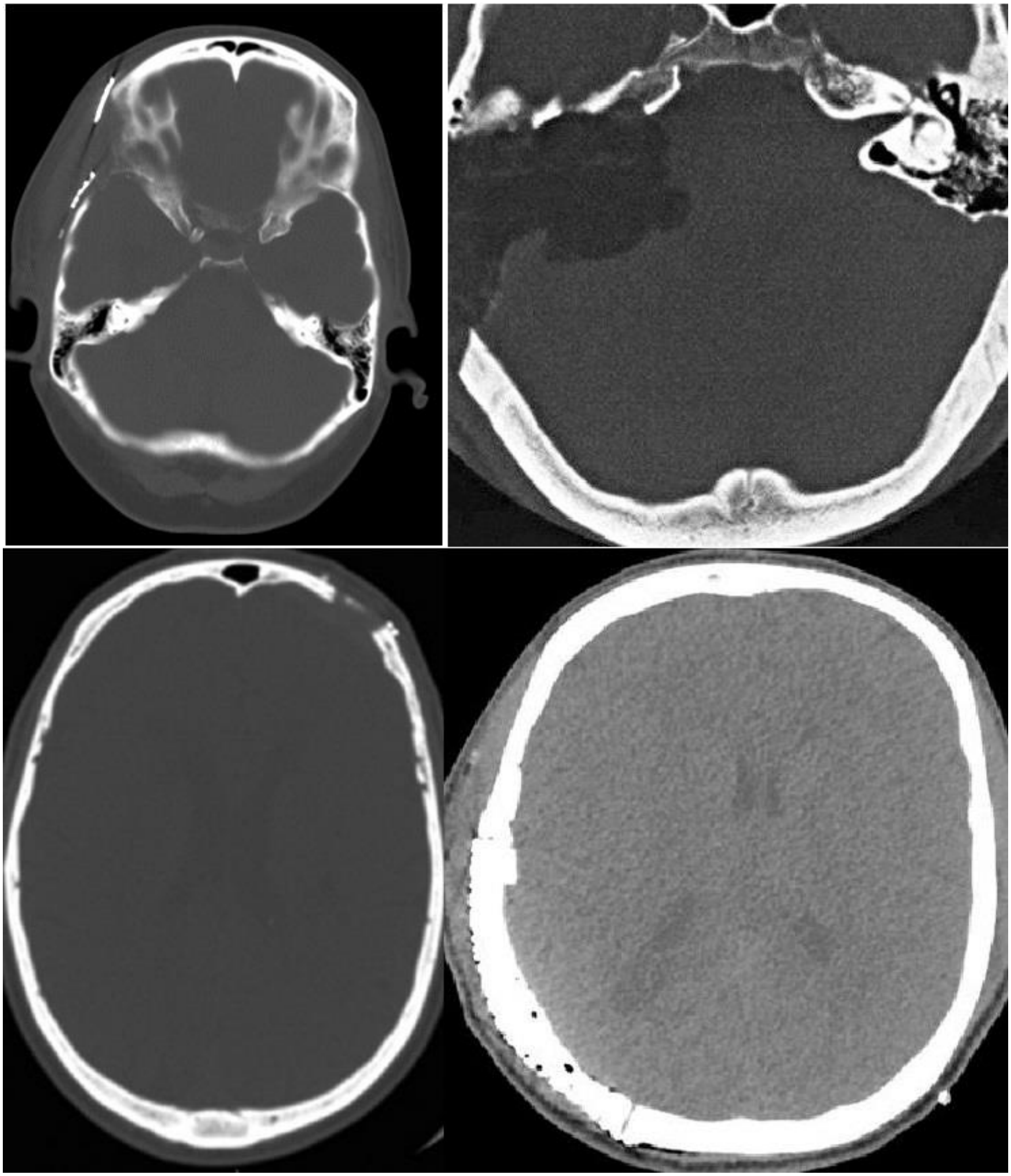

(Filename: TCT_2873_a.jpg)

2398

Imaging of Toxic and Metabolic Encephalopathy

F Memon[1], A Kirsch[2], A Wang[3], R silbergleit[2], A Khan[2], K Barry[2], A Krishnan[4], S Noujaim[1], J Wilseck[5], S Patel[6], K Tech[7]

[1]William Beaumont Hospital, Royal Oak, MI, [2]William Beaumont Hospital, royal oak, MI, [3]BEAUMONT HOSPITAL, ROYAL OAK, MI, BLOOMFIELD HILLS, MI, [4]OAKLAND UNIVERSITY WILLIAM BEAUMONT SCHOOL OF MEDICINE, TROY, MI, [5]Beaumont-Royal Oak, Royal Oak, MI, [6]Beaumont Hospital, royal oak, MI, [7]Beaumont Health - Royal Oak, Royal Oak, MI

Purpose
Clinical diagnosis may be difficult in the early stage of toxic/metabolic encephalopathy. Familiarity with the neuroimaging findings for these diseases may lead to early diagnosis and help improve clinical outcomes. We present a pictorial essay reviewing toxic/metabolic encephalopathies and their imaging features.
Materials and Methods
A review of cases of toxic/metabolic encephalopathy. The clinical course of the patients was also studied. A literature search on the topic was also performed. A review and comparison of imaging features of different types of toxic/metabolic encephalopathies was compiled. Common, uncommon and rare types of metabolic encephalopathies are included in the pictorial exhibit.
Results
There are many different types of toxic/metabolic encephalopathies. Our pictorial exhibit includes CT and/or MRI of common, uncommon and rare etiologies of encephalopathy secondary to intrathecal injection of methotrexate, methanol intoxication, Wernicke's encephalopathy, hyperammonemia, hyperglycemia, hepatic encephalopathy, hyperbilirubinemia, carbon monoxide, Wilson disease and acute alcohol intoxication.
Conclusions
Diagnosis of toxic/metabolic encephalopathy can be challenging especially if history of offending agents cannot be obtained. Familiarity with classical and non classical imaging features can help tailor the diagnosis to improve clinical outcome. In some entities, a specific diagnosis can be strongly suggested and in others, a focused differential diagnosis can be provided.

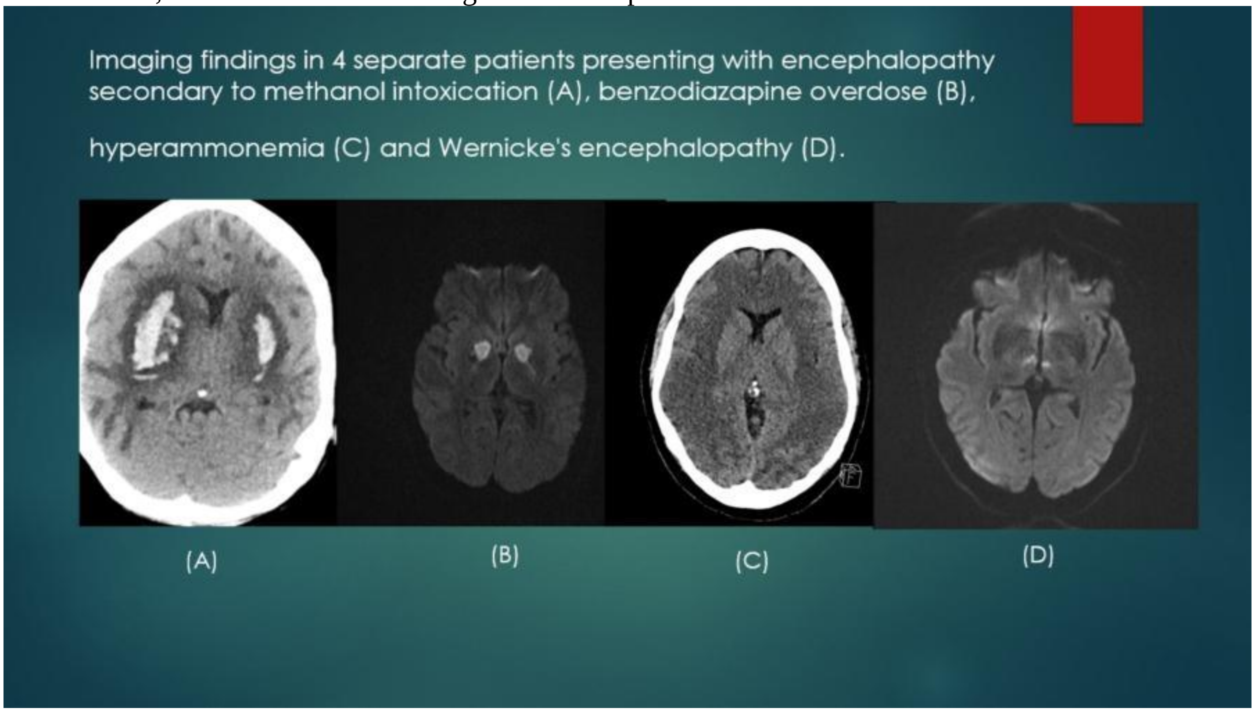

(Filename: TCT_2398_Slide1.jpg)

2769

Imaging Spectrum of Skull Base Abnormalities as Causes of Refractory Seizures: Potential Pitfalls in Epilepsy MRI

K Singhal[1], K Baugnon[1], A Saindane[1], J Willie[1], R Hu[1]
[1] *Emory University, Atlanta, GA*

Purpose
This educational exhibit will discuss skull base abnormalities that are traditionally underdiagnosed but are becoming increasingly recognized as causes of refractory seizures.
Materials and Methods
We will present cases of skull base abnormalities, such as encephaloceles and bone spurs, that have intracranial stereoelectroencephalography (SEEG) confirmation as epileptogenic foci. We will highlight important imaging features on MRI, and the benefit of CT with 3D volumetric reformatting in the evaluation of these cases. We will also summarize the role of intracranial monitoring, and surgical/ablative treatment options for these lesions.
Results
Skull base abnormalities such as encephaloceles and bone spurs can be subtle on imaging and are often underdiagnosed on imaging evaluation of seizures. Encephaloceles often occur in the temporal lobe, through enlarged skull base foramina, arachnoid pits, and osseous defects that can be associated with chronic intracranial hypertension. Rarely, encephaloceles also occur as protrusions into venous sinuses. Bone spurs can irritate the adjacent brain and be a source of seizures. These entities can occur alone or in association with other abnormalities such as mesial temporal sclerosis. Through this educational exhibit, we will highlight the importance of recognizing these potentially treatable causes of epilepsy.
Conclusions
Skull base abnormalities are an important but underdiagnosed cause of seizures. Awareness of the imaging features and clinical histories associated with these entities is crucial in the diagnostic workup and appropriate treatment of epilepsy patients.

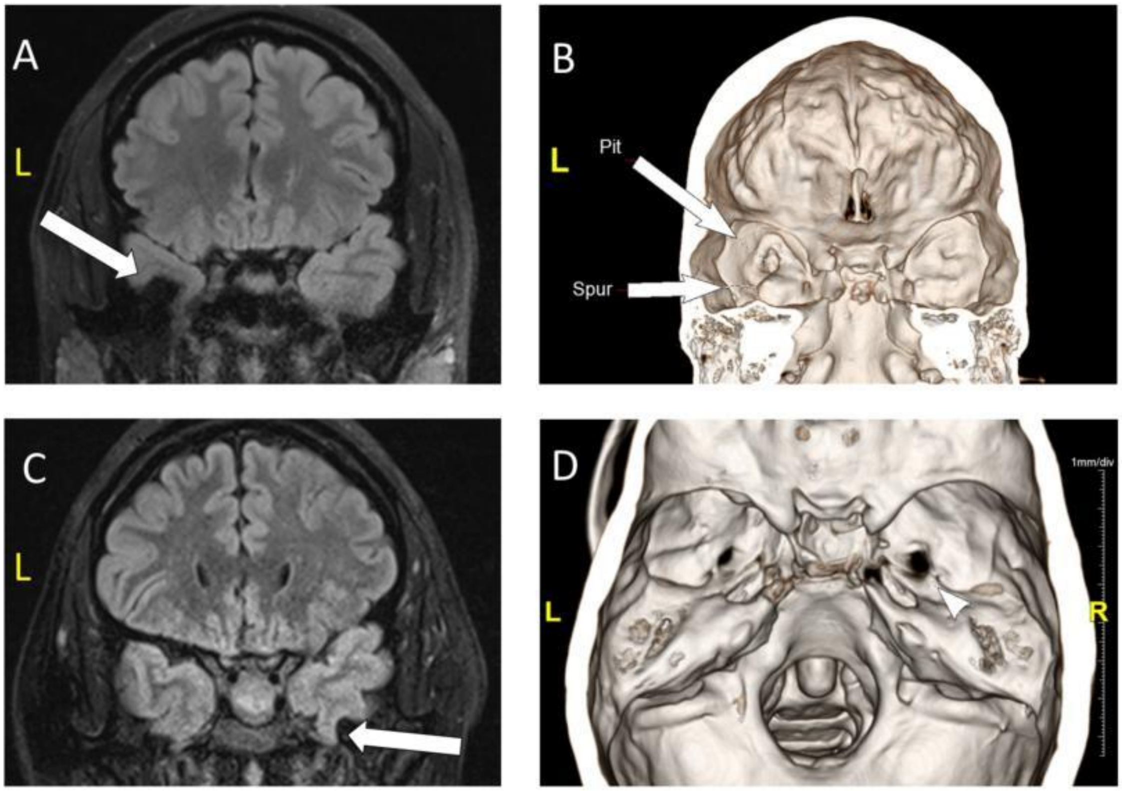

Images A, B: Left sided bone pit and spur demonstrated on T2 FLAIR (flipped) and CT 3-D reformatted images contributing to focal seizures. Images C, D: Right foramen ovale cephalocele demonstrated on T2 FLAIR (flipped) and CT 3-D reformatted images contributing to focal seizures.

(Filename: TCT_2769_EducationalExhibitSkullBaseLesions.jpg)

2587

Immune-mediated Rhombencephalitis: Neuroimaging Approach Based on Current Clinical Understanding

B Kelley[1], W Mehan[1]
[1]*Massachusetts General Hospital, Boston, MA*

Purpose
This exhibit will review: 1. Top diagnostic categories of rhombencephalitis and their most specific clinical features. 2. When to consider immune-mediated causes of rhombencephalitis by imaging. 3. Neuroimaging approach to reporting MRI findings in rhombencephalitis.
Materials and Methods
1. Review the major categories of disease and the clinical approach to narrowing the differential. 2. Neuroimaging features that prompt consideration for immune-mediated neuroinflammation. 3. For each types of pathology, case-based discussion will include: a. Diagnostic criteria and current understanding of pathophysiology. b. Unique features of different types of pathology on MR imaging. c. Useful clinical information for chart review of complex cases. d. Selective role of advanced neuroimaging techniques such as MR spectroscopy.
Results
The rhombencephalon is the portion of the brain located below the tentorium within the posterior fossa of

the cranial cavity surrounding the fourth ventricle consisting of the medulla, pons, and cerebellum which contains cranial nerve nuclei 5-12 and mediates many of the physiologic processes vital for survival. Rhombencephalitis refers to inflammation of this portion of the brain and has a wide differential within the general categories of infection, trauma, ischemia, neoplasm, osmotic myelinolysis, autoimmune, toxins/medications, vasculitis, and vascular malformations. Immune-mediated etiologies are an important part of the differential but, apart from multiple sclerosis, includes many entities that remain poorly understood. Specific autoimmune etiologies include multiple sclerosis, antibody-mediated encephalitis, lymphocytic vasculitis, lymphoproliferative conditions, and immunoregulatory disorders. Post-infectious causes of rhombencephalitis exist within this spectrum of immune-mediated disease and can be difficult to diagnose without the appropriate history. There is also a growing recognition of "autoimmune rhombencephalitis not otherwise specified" that goes by many names but remains a diagnosis of exclusion in patients without known autoantibodies that respond to therapies for autoimmune encephalitis.
Conclusions
Immune-mediated inflammation of the pons, medulla, and cerebellum is one of many possible causes for rhombencephalitis but represents a complex group of individual diseases that remain poorly understood. Radiologists familiar with the basic pathophysiology, clinical features, and imaging findings of immune-mediated CNS disorders affecting the brainstem and cerebellum can provide tremendous value and may be the first physician to suggest the diagnosis in clinical practice.

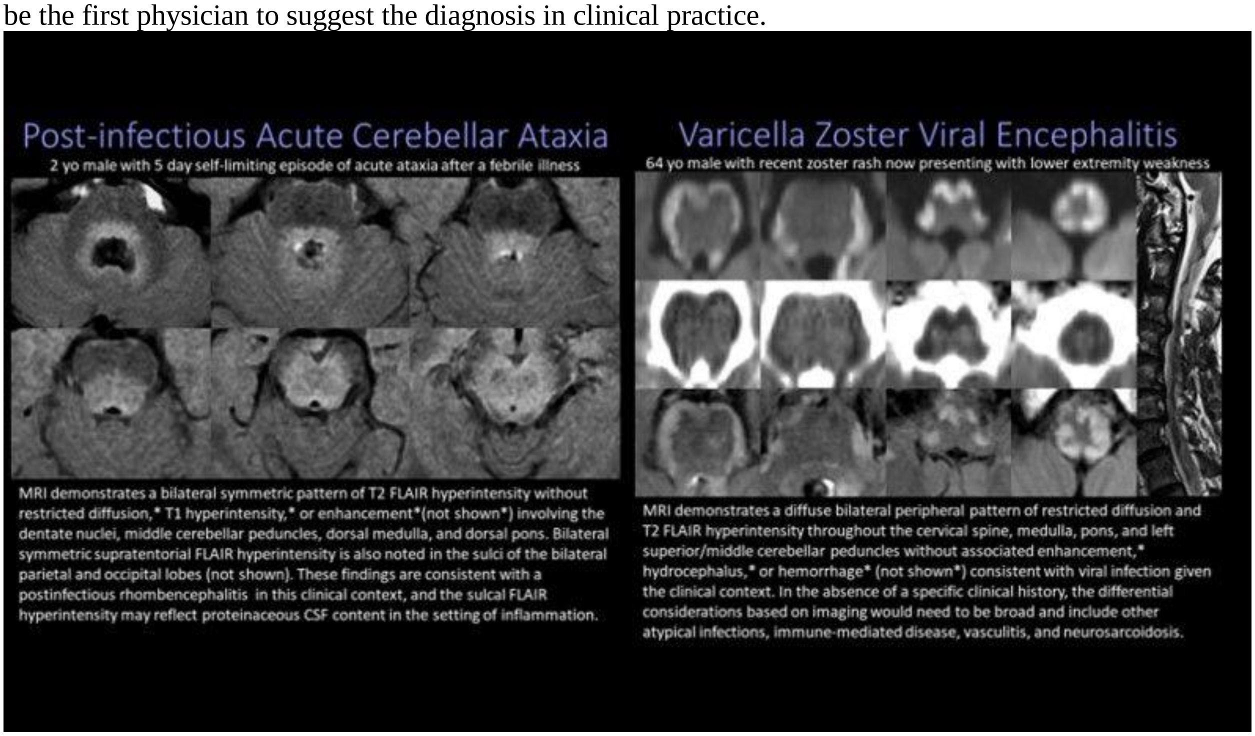

(Filename: TCT_2587_2019ASNRARslides.jpg)

3450

Infections, Inflammation, Masses and Mimics: A Pattern Based Approach to White Matter Disease of the Spine

P Manning[1], M Shroads[2], M McDonald[3]
[1]UCSD - UNIVERSITY OF CALIFORNIA SAN DIEGO, SAN DIEGO, CA, [2]UC SAN DIEGO, SAN DIEGO, CA, [3]University of California at San Diego, San Diego, CA

Purpose

Diseases of the white matter of the central nervous system range a gamut of infectious, post-infectious/inflammatory, toxic/metabolic, vascular and degenerative etiologies, many of which have similar or overlapping appearances within the brain. While many of these processes can primarily or secondary involve the white matter of the spinal cord, the unique and relatively less complex spatial organization of the major ascending and descending fibers can often help clue the radiologist in to the right diagnosis in the setting of nonspecific or equivocal intracranial findings. In this exhibit, we will review the major anatomic hallmarks of the white matter tracks of the spine and the specific imaging features of spinal manifestations of white matter diseases.

Materials and Methods

A review of our institutional imaging database and electronic medical record was performed retrospectively to identify cases of both primary and second white matter disease within the spine. When available, serial imaging inclusive of both initial diagnostic imaging and post treatment surveillance is included.

Results

By the end of this educational exhibit the participant will be able to: 1. Describe in detail the anatomic and functional organization of the spinal cord with special attention to the major ascending and descending white matter tracts. 2. Identify the imaging hallmarks of disease of the white matter of the spine, including: - Toxic/metabolic insults (subacute combined degeneration, nitrous oxide toxicity, copper deficiency/zinc toxicity) - Inflammatory/demyelinating injuries (multiple sclerosis, neuromyelitis optica, acute disseminated encephalomyelitis, sarcoidosis) - Infectious etiologies (enterovirus-associated acute flaccid myelitis, transverse myelitis, HIV myelitis, HTLV-1 myelitis) - Degenerative disorders (amyotrophic lateral sclerosis, Friederich's ataxia) - Vascular etiologies (CNS vasculitis, spinal cord infarct, spinal dural arteriovenous fistulae/malformations) 3. Consolidate learning via a brief self-assessment quiz

Conclusions

Although much attention is given to characterization of white matter disease within the brain, the spinal cord also plays host to a variety of white matter pathologies, both primarily and secondarily. The unique, often spatially specific patterns of spinal cord involvement can help clue the radiologist into the correct diagnosis, thereby aiding the timely recognition of infectious, inflammatory and degenerative etiologies critical to appropriate clinical management.

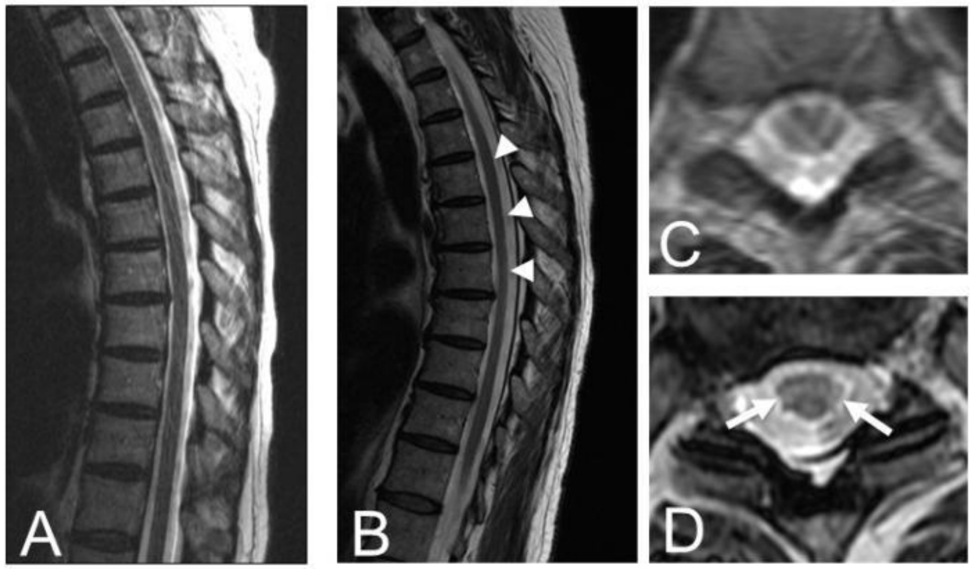

Figure 1. 61 year old female with history of chronic myelopathy and HTLV-1 infection. Substantial volume loss throughout the thoracic spinal cord (sagittal T2 series in B, arrowheads) is noted compared to thoracic spine MRI performed 3 years prior (sagittal and axial T2 sequences in A and C, respectively). Axial T2 sequences at the level of T6 demonstrate elevated T2 signal in the lateral colums (D, arrows) raising concern for HTLV-associated myelitis.
(Filename: TCT_3450_Figure1ASNRspinewhitemattertif.jpg)

3037

Intervertebral Disc Cysts: Typical and Atypical Findings

T Scoppetta[1], K Camargo[2]
[1]*Santa Casa de Misericórida de São Paulo, São Paulo, Brazil,* [2]*Hospital Sao Camilo, SAO PAULO, Solteiro*

Purpose
Illustrate and discuss the constellation of magnetic resonance imaging findings of intervertebral discal cysts.
Materials and Methods
Was conducted a retrospective, descriptive and analytic study of spine MRI scans performed in our institution. We will discuss the typical and atypical imagines findings, perform a systematic review of the literature on this topic and debate its differential diagnosis.
Results
A series of cases were presented. All patients had cervical/lombar back pain. None had history of previous spine surgery nor malignancy. Most of them presented as oval shaped, well defined and seated in the anterior epidural space cystic lesion. One case complicated with epidural space collection. An intervertebral discal cyst is defined as an extrathecal cyst, in contact with the adjacent disc in the ventrolateral epidural space. They are a rare cause of low back pain and radiculopathy, not being

considered in most differential diagnosis of cystic intraspinal lesions. Lumbar radiculopathy is a very common condition usually related to degenerative disease of the spine and herniated discs. Several other conditions have been associated with radiculopathy. Major differential diagnosis are facet joint and ligament flavum related cysts, arachnoid cysts, dermoid cyst and epidural collections (haematoma and abscess).

Conclusions

Lumbar radiculopathy is a very common condition usually related to degenerative disease of the spine and herniated discs. Epidural cyst are frequently related to joints or ligaments, naturally in the posterior space. Intervertebral disc cyst should always be considered in the differential diagnosis whenever an anterior epidural cyst is depicted. Radiologist should be familiarized with its typical and atypical findings. MRI can assuredly make the diagnosis.

2997

Intracranial Phase Contrast Quantitative MRA: What the Neuroradiologist Should Know

J Ormsby[1], J Vera[1], D Sorte[1], A Carlson[1], M Mabray[1], G Lorenzo[1]
[1]*University of New Mexico, Albuquerque, NM*

Purpose

Quantitative MRA (qMRA) is a technique that takes advantage of the high spatial resolution of a Time-of-Flight MRA and the noninvasive, in-vivo quantitative flow measurement capability of phase contrast MRA to determine blood flow for each interrogated intracranial vessel. The purpose of this exhibit is to describe the physics concepts, technical challenges, and interpretation insights of how qMRA is being used at our institution.

Materials and Methods

The exhibit will summarize the clinical utility of qMRA though a rigorous literature review. We will describe our challenges implementing and using the hardware and software. Finally, we will present examples of how qMRA is being used at our institution to direct patient care.

Results

qMRA has been used in cardiac imaging for some time providing radiologists and referring clinicians valuable quantitative physiological data including flow and velocity to characterize a disease process. More recently, the technique has been refined to be used in the neuroimaging world and is now capable of assessing in vivo fluid dynamics in the intracranial vessels, including arteries and veins. This valuable information can then be used within a given clinical context to guide neurovascular treatment. The successful performance of of intracranial qMRA is predicated on the meticulous development of imaging protocols, technologist training, quality assurance and careful interpretation. Furthermore, a close working relationship with the referring clinician is paramount to be able to fully understand the utility and limitations of this technique.

Conclusions

Intracranial phase contrast qMRA is a powerful tool that can provide valuable in vivo physiological data for complex set of patients with critical neurovascular diseases.

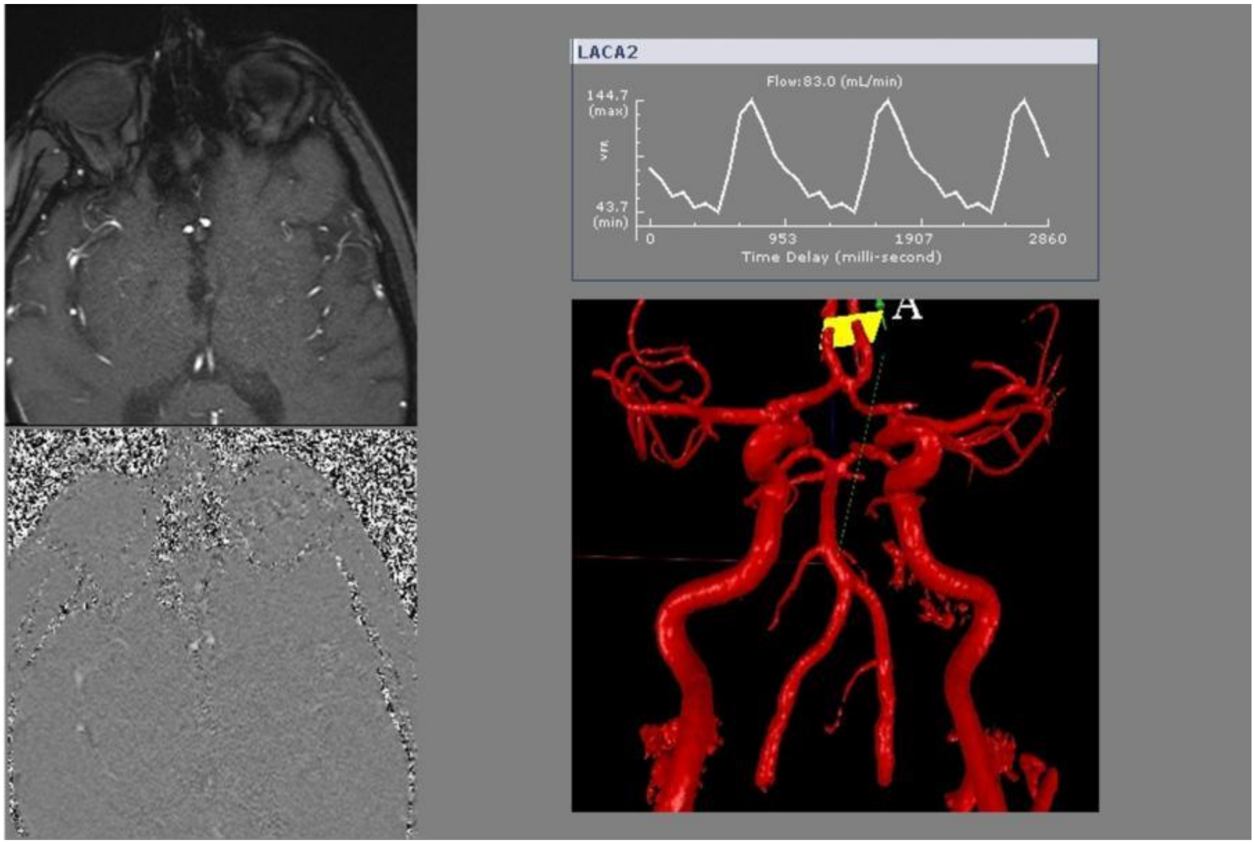

(Filename: TCT_2997_Nova.JPG)

3662

Journey Through The Cavernous Sinus

J NAIR[1], S Riaz[2], M Sharma[3], L Ribeiro[4], R Larrazabal[5], R Del Carpio[6]
[1]McMaster University, Hamilton, Ontario, [2]Montreal General Hospital, Stoney Creek, Ontario, [3]Western University, London Health Science Centre, London, Ontario, [4]HAMILTON GENERAL HOSPITAL - MCMASTER, DUNDAS, ON, [5]McMaster University, Hamilton, ON, [6]McGill University Health Centre, Montreal, Quebec

Purpose
1) To identify the normal anatomic structures that constitute the cavernous sinus and their important relationship to each other and adjacent spaces. 2) To propose adequate imaging techniques for evaluation of the cavernous sinus. 3) Discuss the imaging appearance of common and uncommon pathologies of this region and their differential diagnosis.
Materials and Methods
1) PACS search was undertaken to identify selected cases. 2) Highlight imaging findings and management of the common and uncommon pathological conditions of the cavernous sinus, using a case based approach.
Results
Imaging features of the different lesions of the cavernous sinus discussed would include: 1) Neoplastic: a) Benign (Meningioma, Schwannoma) B) Malignant (Leukaemia, Metastases) 2) Inflammatory/infectious: Tolosa Hunt Syndrome, Wegener Granulomatosis, Sarcoidosis, Lemierre syndrome, Thrombophlebitis 3)

Vascular: Hemangioma, Carotido-Cavernous fistula, Aneurysms, Arteriovenous Malformations, Cavernous sinus thrombosis 4) Congenital: Epidermoid, Dermoid cyst . 5) Trauma
Conclusions
Knowledge of the anatomy and characteristic imaging of the different disease entities of the cavernous sinus are essential for deciding therapeutic modalities such as microsurgery, radiation therapy, or medical treatment.

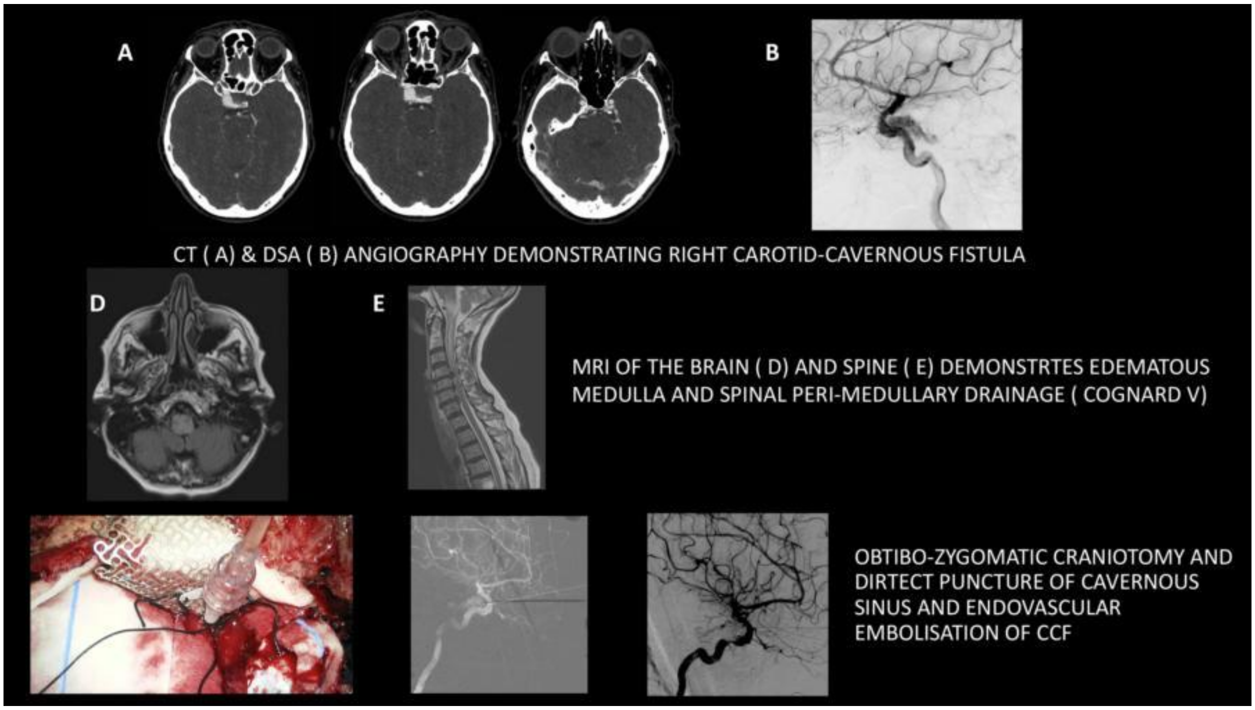

(Filename: TCT_3662_CCF-12.jpg)

3407

Large and Giant Intracranial Aneurysm Treated with Flow Diverters. What can Magnetic Resonance Imaging Offer for Follow Up?

C PARADA[1], H Lambre[2]
[1]INSTITUTO MEDICO ENERI, BUENOS AIRES, Argentina, [2]Clínica La Sagrada Familia, Capital Federal, Buenos Aires

Purpose
- Discuss the value of MRI for long-term follow up of large and giant intracranial aneurysms treated with flow diverter devices. - Discuss the strengths and limitations of MR and MRA for follow up of intracranial aneurysms after endovascular management with flow diverters and compare it with other imaging modalities. - Discuss the diagnostic imaging modality of choice for follow up of large and giant intracranial aneurysm treated with flow diverters considering specific factors and particular challenging situations.
Materials and Methods
- Role of MRI for the long-term follow up of large and giant intracranial aneurysms after endovascular treatment with flow diverters. - Benefits and limitations of MRI when assessing post-embolization intracranial aneurysm. - Limitations of TOF-MRA and CE-MRA. - Review of literature, including prior meta-analysis. - Comparison of MRI and other imaging modalities. - Diagnostic approach to consider the best imaging modality of choice for particular complex cases.

Results
The use of flow diverters for endovascular treatment of large and giant intracranial aneurysms has revolutionized the management of brain aneurysms. The risk of aneurysm's remnants and the presence of newly detected aneurysm make follow up imaging after endovascular treatment necessary. mpMRI has a high diagnostic performance and has become the preferred non-invasive imaging technique of choice for follow up of large and giant intracranial aneurysms after endovascular treatment.
Conclusions
MRI has a high diagnostic performance and has become the preferred non-invasive imaging technique of choice for follow up of large and giant intracranial aneurysms after endovascular treatment.

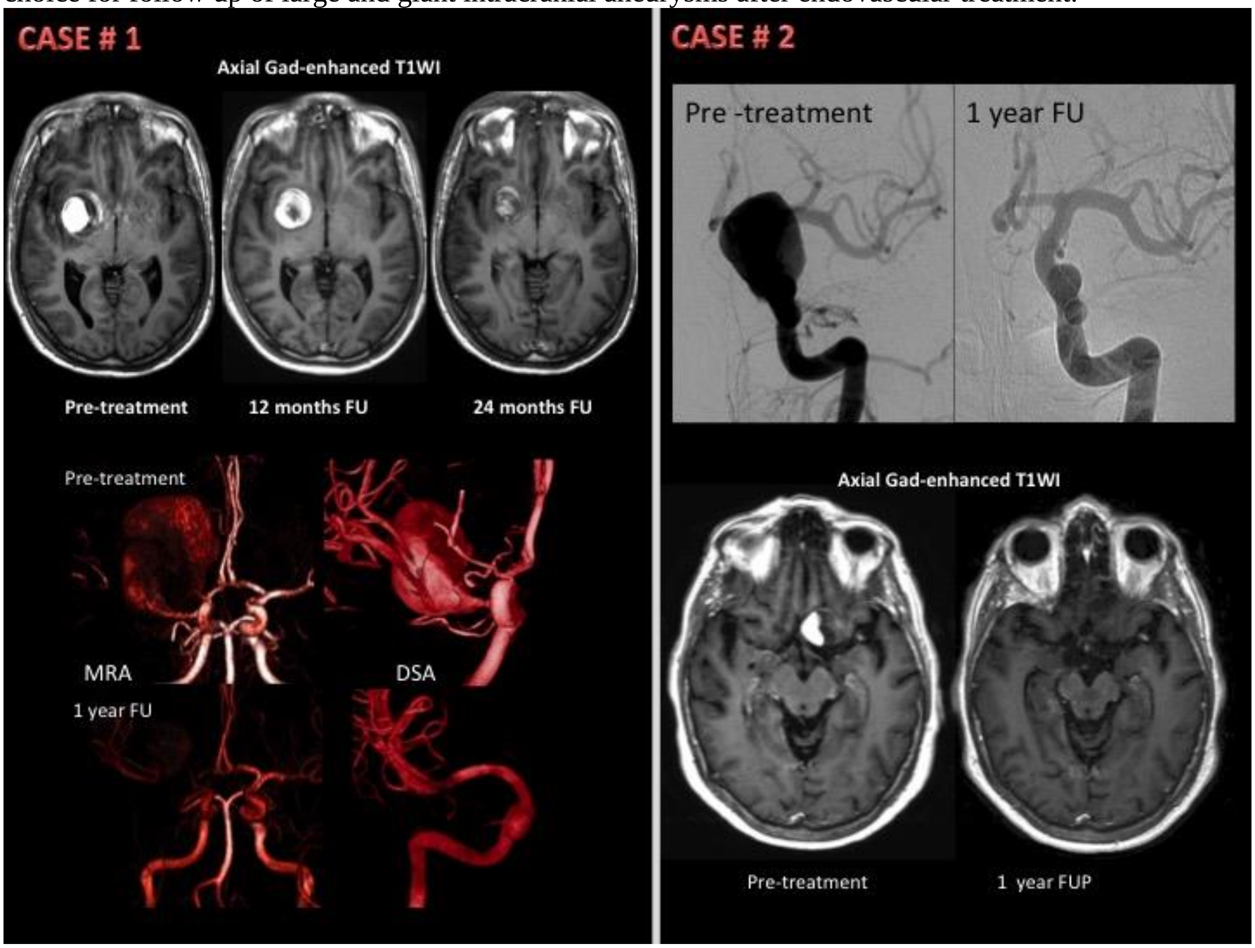

(Filename: TCT_3407_Abstract2.jpg)

2971

Lesions of the Pineal Region: an Educational Pictorial Review of Neuroimaging with Histopathological Correlation

F Zaccagna[1], K Allinson[2], T Massoud[3], T Matys[1]
[1]University of Cambridge, Cambridge, UK, [2]Addenbrooke's Hospital, Cambridge, Cambridgeshire, [3]Stanford University School of Medicine, Stanford, CA

Purpose
The pineal gland is a small pinecone-shaped organ attached to the posterior border of the third ventricle, interposed between the quadrigeminal plate and the splenium of the corpus callosum. Lesions arising in or

around the pineal gland often pose a diagnostic challenge in neuroradiology. The purpose of this exhibit is to describe the anatomy of the pineal region, imaging appearances and differential diagnosis of lesions arising in this area, and discuss further imaging and management of these conditions.
Materials and Methods
We comprehensively review and present imaging findings in a wide range of cystic and solid lesions arising in and around the pineal gland.
Results
We first describe the imaging anatomy of the pineal gland and the surrounding structures, as well as the symptomatology of pineal region tumors in reference to these anatomical relationships. We present a pictorial review of neuroradiological and histopathological findings in a wide range of lesions including non-neoplastic conditions (such as pineal cysts, epidermoid and dermoid cysts, lipoma and arachnoid cyst), pineal parenchymal neoplastic lesions (pineocytoma, pineoblastoma, and the papillary tumor of the pineal region), germ cell tumors and other neoplastic entities (such as astrocytoma, ependymoma, lymphoma and metastasis). We discuss management of these conditions, including the evidence for further imaging of the commonly encountered incidental pineal cysts.
Conclusions
Management of pineal region abnormalities differs significantly depending on the type of lesion. Due to overlap in imaging features the final diagnosis usually requires histopathology confirmation, but thorough knowledge of neuroimaging characteristics helps to identify these patients who should proceed to biopsy from those that can followed up by imaging. This educational review aids in narrowing the differential diagnosis of lesions in this region.

2581

Leukodystrophies with Centripetal Progression: A Pictorial Review

M Nicolas-Jilwan[1], M AlSayed[1]
[1]King Faisal Specialist Hospital and Research Centre, Riyadh, Saudi Arabia

Purpose
The imaging diagnosis of leukodystrophies is very challenging as there is significant overlap in the manifestations of numerous disorders. The recognition of variable patterns of selective vulnerability is highly valuable for MRI interpretation in this context. The majority of diseases, including the most common lysosomal storage disorders, result in early injury of the periventricular white matter with subsequent centrifugal progression. Early injury of the subcortical white matter with centripetal progression is a much less common MRI pattern. We highlight the characteristic imaging and clinical features of several of these disorders.
Materials and Methods
We selected the MRI and MR spectroscopy examinations of 7 patients aged 49 days to 39 years. All patients had confirmed diagnoses by molecular and biochemical testing as appropriate. Included are an 11 year-old female with L-2 hydroxyglutaric aciduria, a 12 year-old female with Alexander disease, a girl with megalencephalic leukoencephalopathy with subcortical cysts imaged at 14 months and 3 years of age, a 2 year-old girl with Canavan disease, a 39 year-old male patient with Kearns Sayre syndrome, as well as a 19 month-old girl with Sandhoff disease. Also included is a female infant with combined oxidative phosphorylation deficiency-14 imaged at 49 days and 2 months of age.
Results
We highlighted the key features which suggest a specific diagnosis in the presence of a leukodystrophy with early involvement of the subcortical white matter, including in particular the distribution and characteristics of white matter injury, presence and distribution of deep gray matter injury, presence and pattern of brainstem injury, MR spectroscopy findings, presence of macrocephaly, age at presentation and nonneurological manifestations. Our patient with combined oxidative phosphorylation deficiency-14

underscores the importance of considering mitochondrial disorders in the presence of a neurometabolic disorder involving the subcortical white matter.
Conclusions
Knowledge of the key neuroimaging and clinical manifestations of various leukodystrophies which selectively affect the subcortical white matter and exhibit a centripetal progression is crucial to potentially reach a specific diagnosis.

3578

Looking Back - A Radiological Retrospective of Non-traumatic Spinal Emergencies

A Danilenko[1], S Patel[1], C Gunn[1], S Lev[1], G Chen[1]
[1]Nassau University Medical Center, East Meadow, NY

Purpose
To review the imaging spectrum of non-traumatic spinal emergencies and provide a focused approach for the on-call spine radiologist, emphasize the importance of incorporating key clinical data. Classic and atypical presentations are illustrated. Potential pitfalls and mimics are also discussed.
Materials and Methods
We retrospectively reviewed a wide array of spine cases presenting to the ED during the past ten years at our Level 1 trauma center. Cases were categorized according to etiology, with consideration to a space-based approach. We highlight a list of relevant clinical data that a radiologist should consider when presented with a spinal emergency. We focus on identifying distinguishing radiologic features of different pathologies.
Results
When presented with non-traumatic spinal emergencies, radiologists should effectively utilize key clinical information such as oncologic data, IR procedures, steroid use, and current medications. Infectious/inflammatory conditions include a host of entities, primarily osteomyelitis/discitis together with phlegmon/abscess formation. We demonstrate examples of Guillain-barre, CMV, coccidiomycosis, tuberculosis, arachnoiditits, tranverse myelitis, and AIDS-related myelopathy. Vascular processes include AVM, cavernous malformations, infarctions, epidural hematomas, and extramedullary hematopoiesis. Neoplastic and tumor-like conditions must be distinguished and include primary and metastatic tumors. Epidural lipomatosis and intraspinal arachnoid cysts are unusual causes of compressive symptoms. Degenerative entities, such as DISH/OPLL and ankylosing spondylosis may present with acute myelopathy. Acute compression may result from osteoporotic compression fractures. The post-surgical patient deserves special consideration. Rarely, spontaneous or idiopathic cord herniation through a dural defect may occur.
Conclusions
Nontraumatic spinal emergencies may present with acute, rapidly progressive symptoms and require immediate diagnosis. Clinical data is essential in order to narrow the differential possibilities. The radiologist should employ a systematic search pattern to expedite lesion detection.

2559

Looking Pediatric Orbital Lesions Right in The Eye: A Review with focus on Orbital Rhabdomyosarcomas

A Rajput[1], E Velez[2], P Joyce[3], J Branchcomb[2], J Scheibal[1], J Acharya[4], J Go[5], A Rajamohan[5]
[1]USC Keck School of Medicine, Los Angeles, CA, [2]LAC+USC, Los Angeles, CA, [3]LAC USC, Los Angeles, CA, [4]UNIVERSITY OF SOUTHERN CALIFORNIA, KECK SCHOOL OF MEDICINE, Monrovia,

CA, [5]UNIVERSITY OF SOUTHERN CALIFORNIA, KECK SCHOOL OF MEDICINE, LOS ANGELES, CA

Purpose

The purpose of this exhibit is to review the incidence, prevalence, clinical presentation, and significance of several non-traumatic orbital pathologies in the pediatric population with our focus on orbital rhabdomyosarcoma. Knowing the appearance of the various pediatric orbital lesions will help the radiologist to correctly diagnose rhabdomyosarcoma of the orbit, exclude other differential diagnoses, and prompt treatment to prevent harmful consequences.

Materials and Methods

Diplopia, proptosis, decreased visual acuity, and eye pain are all very common presenting symptoms in pediatric patients with non-traumatic orbital pathology. In addition to clinical examination, frequent imaging modalities are ordered which include computed tomography (CT) and magnetic resonance (MR) of the orbits. It is important for the radiologist to be aware of the vast abnormalities involving the orbits and associated structures, as time is of the essence. Our aim is to discuss the clinical presentation, imaging findings, and a differential diagnosis of rhabdomyosarcoma of the orbit with its potential complications. Awareness of the key diagnostic features will guide further follow-up and aim to prevent unnecessary complications.

Results

The discussion will include a review of the orbital anatomy, the normal development of the orbital structures, followed by presentation of rhabdomyosarcoma of the orbit. Further discussion will include characteristic CT and MRI findings of an orbital rhabdomyosarcoma that will guide radiologists to recognize it, look for potential complications, and recommend appropriate management. The exhibit will also demonstrate a case based review of relevant differential diagnoses for this entity which include orbital hemangiomas, a thrombosed orbital varix, venolympathic malformations, optic gliomas, orbital metastases, and several others. The review will further include imaging characteristic that will help a radiologist to distinguish between these possible considerations and offer appropriate recommendations regarding follow up and further management.

Conclusions

Orbital rhabdomyosarcomas are typically found in children with an overall good prognosis. Review of this educational exhibit will enable a radiologist to be familiar with this entity, consider associated complications, narrow relevant differential diagnoses, and offer appropriate recommendations.

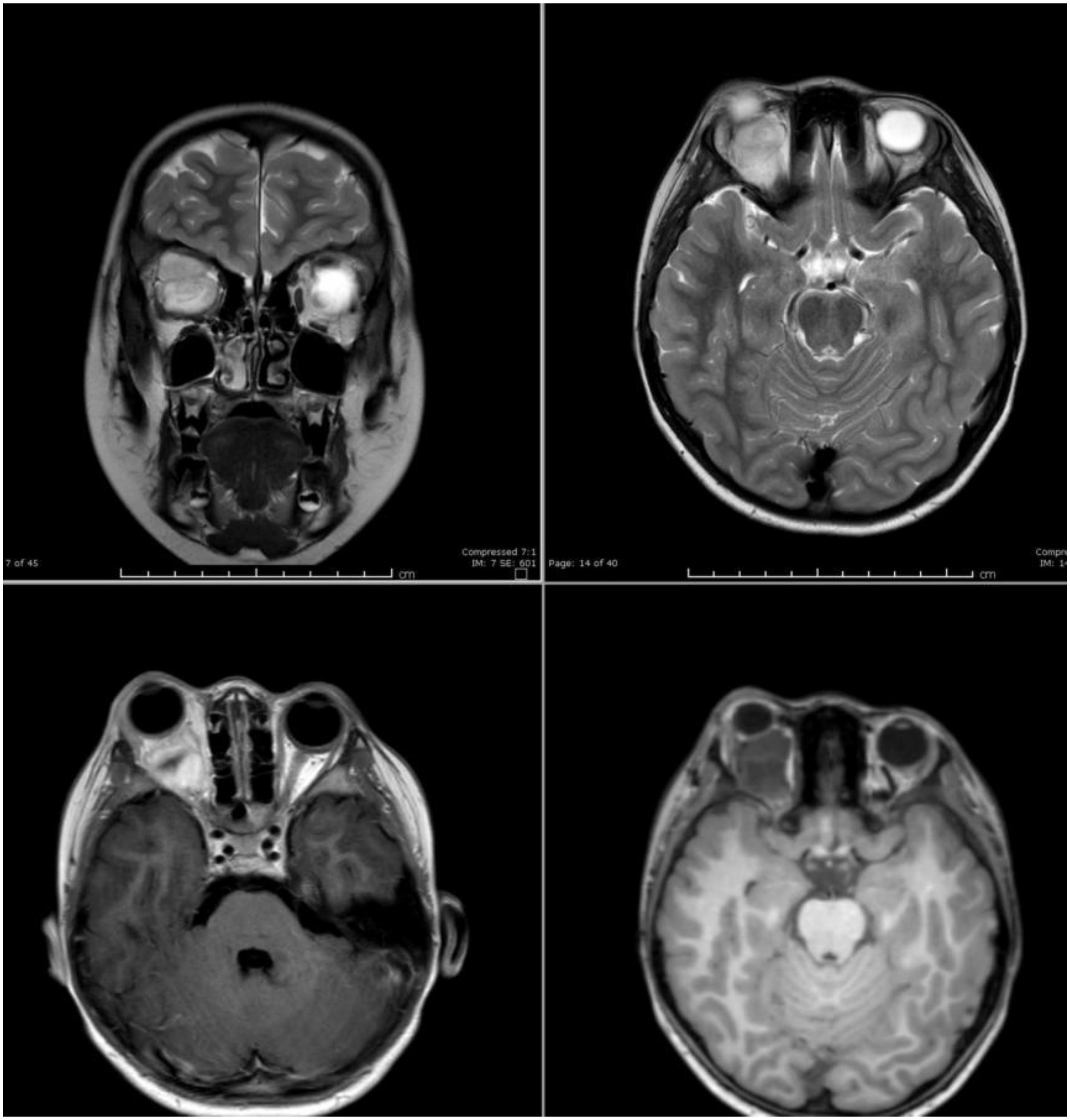

(Filename: TCT_2559_OrbitRhabdo.jpg)

2463

Malformations of Cortical Development: An Illustrative Pictorial Review of Pre- and Postnatal MRI Appearance

P Naidu[1], U Nagaraj[2], W O'Brien[3]
[1]*While at Cincinnati Children's Hospital Medical Center, Cincinnati, OH,* [2]*CINCINNATI CHILDREN'S HOSPITAL MEDICAL CENTER, CINCINNATI, OH,* [3]*Cincinnati Children's Hospital Medical Center, Cincinnati, OH*

Purpose
Background/Purpose: Malformations of cortical development (MCDs) are structural abnormalities of the cerebral cortex that result from aberrant cortical development. As a group, MCDs constitute an important cause of medically-refractory epilepsy, especially in children. While the MRI appearance of some MCDs is conspicuous, others can be subtle, making their recognition challenging. This educational exhibit presents examples of major MCDs in an effort to familiarize the audience with their imaging features on pre- and/or postnatal MRI while discussing how those features reflect their underlying pathogenesis. Educational Objectives: -Contrast normal corticogenesis with that of MCDs to define their distinguishing characteristics and classify the phase of cortical development during which each occurred -Understand the role of imaging and other data in MCD detection and the importance of an interdisciplinary approach in the care of patients with epilepsy due to MCDs
Materials and Methods
The CCHMC imaging database was searched from 2008-2018 for representative cases. Those selected for presentation include lissencephaly, microcephaly with simplified gyral pattern, pachygyria, band heterotopia, nodular gray matter (GM) heterotopia, FLNA mutation-associated confluent periventricular GM heterotopia, polymicrogyria, schizencephaly, hemimegalencephaly, PTEN-associated macrocephaly with supernumery gyration, and de novo as well as DEPDC5 mutation-associated focal cortical dysplasias.
Results
The imaging features of major MCDs will be described in the context of corticogenesis, and key phenotypic and genetic associations (such as FLNA mutation in confluent nodular GM heterotopia with Ehlers-Danlos syndrome & cardiac valvular abnormalities) discussed for each entity.
Conclusions
MCDs encompass a broad range of entities that share a disordered origin; understanding their features and etiologies provides a unique opportunity for radiologists to gain insight into normal cerebral cortical formation. Such familiarity also facilitates recognition of these at-times subtle or bizarre entities on MRI, which can profoundly impact the management of patients with refractory epilepsy.

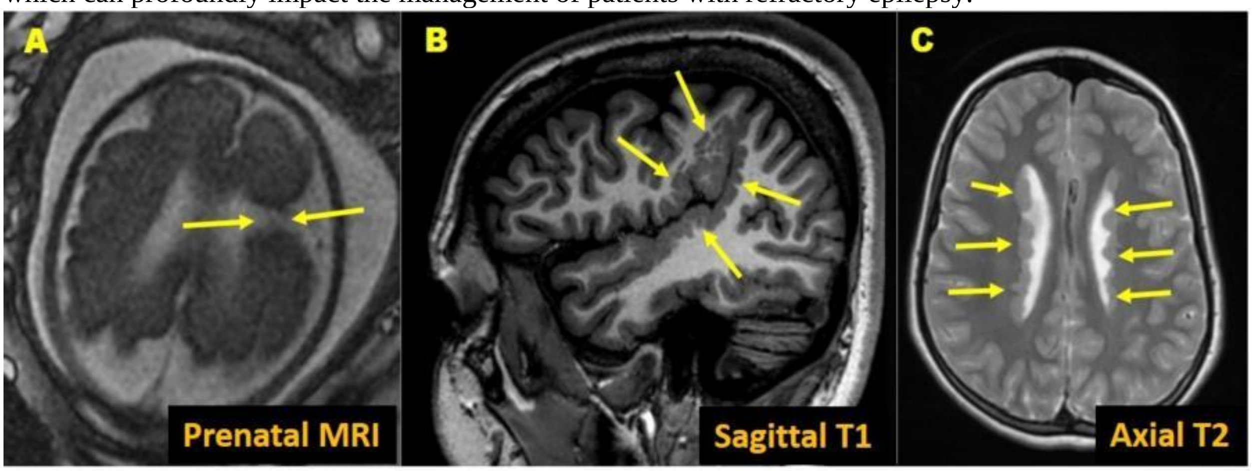

(Filename: TCT_2463_ASNR-19-Annotated-FigDPI_300.jpg)

2333

Management of Incidentalomas on MRI Spine

P Farnsworth[1], R Murtagh[2]
[1]University of South Florida College of Medicine, Tampa , FL, [2]University of South Florida College of Medicine, Tampa, FL

Purpose

To educate practicing neuroradiologists about to management and best recommendations for incidental findings encountered when reading spine MRI's.

Materials and Methods

Residents and faculty from our institution discussed a need for a streamlined resource for information on recommendations/management for commonly encountered incidentalomas on MRI of the spine. A thorough review of the literature was performed and data was compiled in order to help radiologists to make more easily make up to date, evidence based recommendations on incidental MRI findings as far as need for additional imaging, timelines for follow up exams, or management. Example cases/images were compiled from our institution to use throughout the talk and highlight the use of the presentation.

Results

Incidentalomas are something unexpected on imaging, often prompting further work up. Common incidentalomas in spine imaging include: thyroid nodules, renal lesions, abdominal aortic aneurysm, ovary lesions, and uterine lesions. Incidental thyroid nodule (ITN) is one of most common incidental findings on head and neck imaging and is defined as "nodule not previously detected or suspected clinically but seen on an imaging study. ITN have increased cost and risk to patient if biopsied. There is very high variability in management by radiologists and the Majority are benign. Renal lesions have increased frequency with age (so does spine imaging) and as a result, renal lesions are frequently seen. Management of renal lesions on dedicated imaging is well established. Many, however, are incidentally/incompletely found on other studies (i.e. spine). Increasing evidence shows indolent behavior of smaller lesions, prompting more conservative management. Abdominal aortic aneurysm is the most common true arterial aneurysm. Rupture is the 10th most common case death in western world. It is defined as greater than or equal to 3 cm in diameter. There is increased frequency of rupture over 5 cm and this is often a benchmark for treatment. The aorta is often clearly in the field of view for MRI L-spine. Ovarian lesions are common and tumors account for approx. 6% of female malignancies. They can be classified according to cellular origin: surface epithelial neoplasms, germ cell tumors, or sex cord/stromal tumors. They can also be classified according to morphology: predominantly cystic or solid. Uterine fibroids are the most common solid benign neoplasms and are seen in 25% of reproductive age females. They are more common in African American women. Fibroids are hormonally sensitive and multiple in approx. 85% of cases. Uterine fibroids rarely cause a diagnostic dilemma. However, it is still important to have uterine leiomyosarcoma on the differential.

Conclusions

Thyroid: A flow chart and examples will be shown for management. For patients with multiple nodules the flow chart should be applied to the largest nodule. Patients with diffusely heterogeneous, enlarged thyroid should have US (age and comorbidity dependent). This management scheme has shown to reduce unnecessary bx's by up to 35% in one academic institution, and another study showed decreased US follow up of ITN on CT by 46%. Another study showed a false negative rate of 13% but only missed 1.2% of malignancies; most that were missed were small papillary CA's. Renal: Management as per Bosniak classification for renal cysts. Recommendations for solid renal lesions will be discussed as well. A definite cyst can be ignored. Definite benign lesion (hemorrhagic cyst) can be ignored. Indeterminate lesions need further workup. Some authors advocate a few septa can be ignored*. For further workup, use of CT, US, or MRI, patient dependent. Question of partially imaged lesions will be addressed as well. Aorta: Recommendations based on size will be presented. If aorta is adequately imaged (usually is) and you feel confident measurements are accurate, can consider follow up based on recommendations without further imaging. If incompletely imaged, or feel that the cranial or caudal extent is not fully evaluated, may need further imaging in short term. Ovary: Follow up recommendations for cysts are based on age and size and will be presented. Benign features: predominantly cystic, thin walls, few/thin septations. Hemorrhagic cyst will have varying internal signal characteristics. Worrisome features: thick wall, mural nodularity, solid, thick septations. Uterus: Nondegenerated fibroids are low on T1 and T2 with variable heterogenous enhancement. Variable signal intensities are from cystic change, and calcification depending on degeneration. Sarcoma are difficult to differentiate based on imaging characteristics alone but are rapidly enlarging with irregular margins.

2183

Metachromatic Leukodystrophy Mimicker

T Ly[1], L Tyre[1], M Baumann[2], W Millar[1]
[1]Geisinger Medical Center, Danville, PA, [2]Geisinger Health System, Mansfield, OH

Purpose
To present the radiological characteristics of an unusual case of congenital CMV infection in a 19 month old female with global developmental delay and to review the white matter diseases in pediatric population.
Materials and Methods
We present the case of a 19-month-old female who had an uncomplicated delivery. She was first noted unable to hold her neck up at 3 months of age. Progression of symptom led to physical therapy at 6 months of age. At 8 months of age, the patient was first presented to Pediatric Neurology with global developmental delay and jerking movements of the body. Her unusual symptoms prompted imaging workup including MRI of the brain and entire spine.
Results
MRI of the brain revealed symmetric, confluent T2/FLAIR signal hyperintensity involving the bilateral periventricular and deep white matter without associated volume loss or abnormal enhancement. This appearance was highly suspicious for an underlying disorder or dysmyelination. Overall pattern of white matter involvement favored metachromatic leukodystrophy. A subsequent MRI spine was obtained. However, no abnormal signal was identified in the entire MR spine. Given patient's imaging findings, broad metabolic testing including metachromatic leukodystrophy enzyme testing was obtained. However, metabolic screening labs were normal, which ruled out many metabolic causes for leukodystrophy. She also had a formal audiologic evaluation showing bilateral sensorineural hearing loss. Patient underwent further evaluation at Children's Hospital of Philadelphia (CHOP) and found to have IgG antibodies to CMV.
Conclusions
White matter diseases can be subcategorized into subcortical white matter disease versus deep white matter disease. The deep white matter disease can be further divided based on involvement of the thalami and brainstem. Given this patient's finding of symmetric, confluent T2/FLAIR signal hyperintensity involving the bilateral periventricular and deep white matter without involvement of the thalami and brainstem, differential diagnoses include metachromatic leukodystrophy, phenylketonuria, mucopolysaccharidoses, oculocerebrorenal syndrome (AKA Lowe Disease), merosin deficit muscular dystrophy and post-radiation/chemotherapy changes. Radiological imaging features as well as patient's clinical presentations help to differentiate among these. Congenital cytomegalovirus (CMV) was a differential diagnosis of concern as a constellation of symptoms and findings can mimic that of leukodystrophy. Profound bilateral sensorineural hearing loss and MRI changes with involving the white matter could be compatible with congenital CMV disease. Positive IgG levels indicate the patient my have been exposed to CMV. In conclusion, congenital CMV presenting as nonspecific white matter disease is a relatively rare event in the literature, but awareness of CT findings on the part of the radiologist can be helpful for early diagnosis and management.

3139

Microcephaly: Small Head, Big Differential

S Verma[1], G Heller[2]
[1]Mount Sinai West, New York, NY, [2]Icahn School of Medicine at Mount Sinai, New York, NY

Purpose
The purpose of this exhibit is to review the etiologies of microcephaly, differentiate primary vs secondary microcephaly, illustrate imaging findings of common and uncommon disorders, and to discuss the severity and predictors of cognitive function.
Materials and Methods
Cases discussed include Cri du chat syndrome, perinatal hypoxia, mitochondrial chromosomal abnormalities, watershed infarcts, periventricular leukomalacia, Sturge Weber choroidal angioma, Trisomy 13 with holoprosencephaly, craniosynostosis
Results
Microcephaly is defined as a head circumference greater than 2 standard deviations below the mean, with the term "severe microcephaly" reserved for head circumference greater than 3 standard deviations. Primary microcephaly is discovered before 36 weeks gestation due to failure of neurogenesis, chromosomal disorders, or prenatal ischemic events. Careful history taking is crucial to identify prenatal causes of primary microcephaly to exclude causes such as TORCH infection or fetal alcohol syndrome. Secondary or acquired microcephaly is evident postnatally due to neuronal degeneration or genetic syndromes, such as Rett or Angelman syndrome. Etiologies for microcephaly include syndrome and non-syndromic causes. Non-syndromic are typically limited to cerebral development and include environmental factors such as fetal alcohol syndrome, hypoxic ischemic encephalopathy, intrauterine infection, and teratogens. Syndromic causes are associated with visceral malformations, skeletal malformations, and/or facial dysmorphism, and include chromosomal abnormalities and gene deletion syndromes. Syndromic and nonsyndromic causes may also co-exist in some etiologies such as fanconi anemia.
Conclusions
Imaging plays an integral role in the evaluation of microcephaly and can hint at contributory gene or external causes. More importantly, imaging can help to exclude child abuse by visualizing chronic subdurals accompanied by encephalomalacia. MR imaging is often used to identify gyral, migrational, or myelination abnormalities. CT can be helpful to visualize calcifications, suggesting TORCH or previous trauma. The severity of microcephaly is related to the severity of mental retardation. Other predictors of poor cognitive performance include atrophy, cortical dysplasia, or myelination abnormalities.

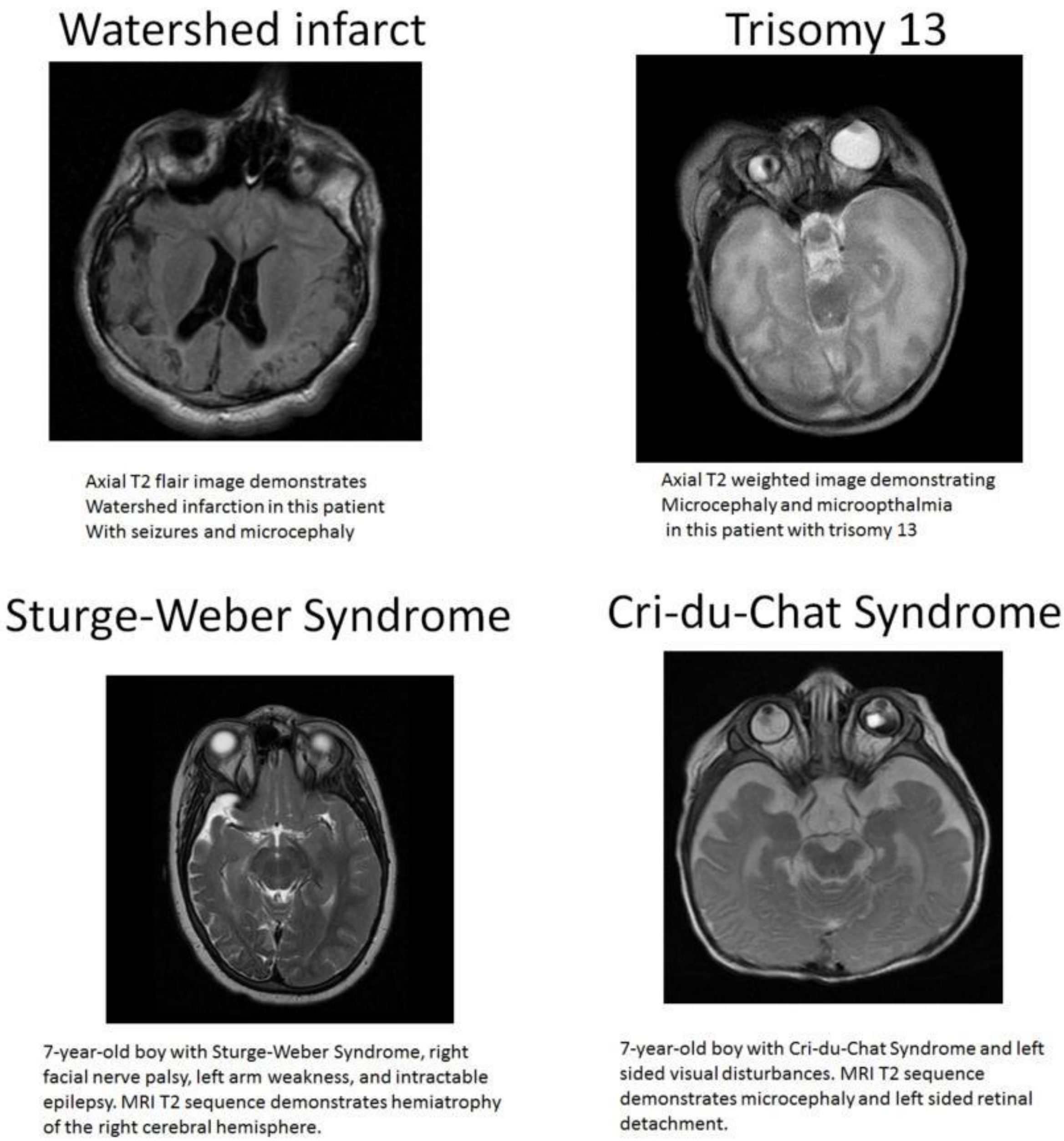

(Filename: TCT_3139_ASNRSubmissionPics.jpg)

2977

Middle Ear Implants: a Pictorial Review of Imaging and Surgical Anatomy

T Matys[1], D Scoffings[2], N Donnelly[2], M Bance[1]
[1]University of Cambridge, Cambridge, UK, [2]Addenbrooke's Hospital, Cambridge, UK

Purpose
Middle ear implants (MEI) are semi- or fully implantable hearing aids used in conductive, sensorineural or mixed hearing loss. They involve mechanical transmission of vibration via a transducer usually

attached to the ossicular chain. Available systems vary with regards to placement of their elements and point of coupling to the ossicles or round window. MEIs are increasingly encountered in radiology practice and can be mistaken for bone-anchored hearing aids or cochlear implants. Neuroradiologists should be aware of preoperative findings that influence implant choice and should be able to identify potential surgical risks. Despite the growing use of MEIs, their description in radiological literature is scarce. The purpose of this exhibit is to describe imaging appearances of MEIs and their pre- and postoperative evaluation.
Materials and Methods
We comprehensively review the available types of MEI and describe anatomical considerations that dictate the implant choice. We describe features that may pose a risk during implantation, expected postoperative appearances, and possible complications.
Results
CT is the key modality in pre- and postoperative assessment. Findings that influence the choice of MEI type include the patency and diameter of the external auditory canal, integrity of the tympanic membrane and the ossicular chain, size of the round window, size and aeration of the middle ear cleft, position of the facial nerve relative to the ossicles or round window, and presence of otosclerosis or other ossicular fixations. Features that influence the risk of surgery include the degree of mastoid pneumatization, emissary veins, dehiscence or abnormal position of the facial nerve or carotid canal, high-riding jugular bulb and persistent stapedial artery. Some patients may require MRI evaluation of inner ear structures.
Conclusions
This exhibit improves understanding of imaging appearances of MEIs required to correctly identify different device types and awareness of surgical anatomical considerations that enable neuroradiologists to issue a clinically relevant report.

3218

Mimics of Malignancy in the Calvarium and Skull Base

S Ferraciolli[1], V Gonçalves[2], J Magalhães[3], L Ramin[4], E Gebrim[5], L Lucato[6], C Leite[7], C Zamora[8], M Castillo[9]
[1]InRad - HC- FMUSP, Sao Paulo, Brazil, [2]Universidade de São Paulo, São Paulo, São Paulo, [3]InRad, Sao Paulo, NY, [4]InRad - HCFMUSP, São Paulo , São Paulo, [5]InRad, Sao Paulo, AK, [6]HOSPITAL DAS CLINICAS DA FACULDADE DE MEDICINA DA USP, SAO PAULO, SAO PAULO, [7]University Of Sao Paulo, Sao Paolo, Brazil, [8]University of North Carolina, Chapel Hill, NC, [9]UNIV. OF NORTH CAROLINA SCHOOL OF MEDICINE, CHAPEL HILL, NC

Purpose
Our purpose is to review cases of lesions that may mimic malignancy in the calvarium and skull base and to highlight imaging and clinical features that suggest their benign etiology.
Materials and Methods
For this exhibit we searched the teaching files of two academic institutions for benign calvarial and skull base lesions that may mimic malignancy on CT or MRI. We will also review and discuss the pertinent literature emphasizing distinctive features for each entity.
Results
Calvarial and skull base lesions are frequently identified on CT and MRI and include a wide spectrum of benign and malignant lesions as well as normal variants. Although they are frequently incidental their imaging features may overlap and their diagnosis can be challenging potentially leading to unnecessary biopsy. For this exhibit we have identified key cases of benign lesions such as hemangiomas, venous lakes, focal fat deposition, red marrow conversion, fibro-osseous lesions, Paget disease (sclerotic and lytic phases), arrested pneumatization, atypical/aberrant arachnoid granulations, sarcoidosis, skull base

osteomyelitis, radionecrosis, and bone infarcts, amongst others. We will discuss imaging and clinical characteristics that may aid to refine the differential diagnosis.

Conclusions

In this educational exhibit we describe lesions that may mimic malignancy in the skull base and calvarium and highlight features that suggest the correct diagnosis.

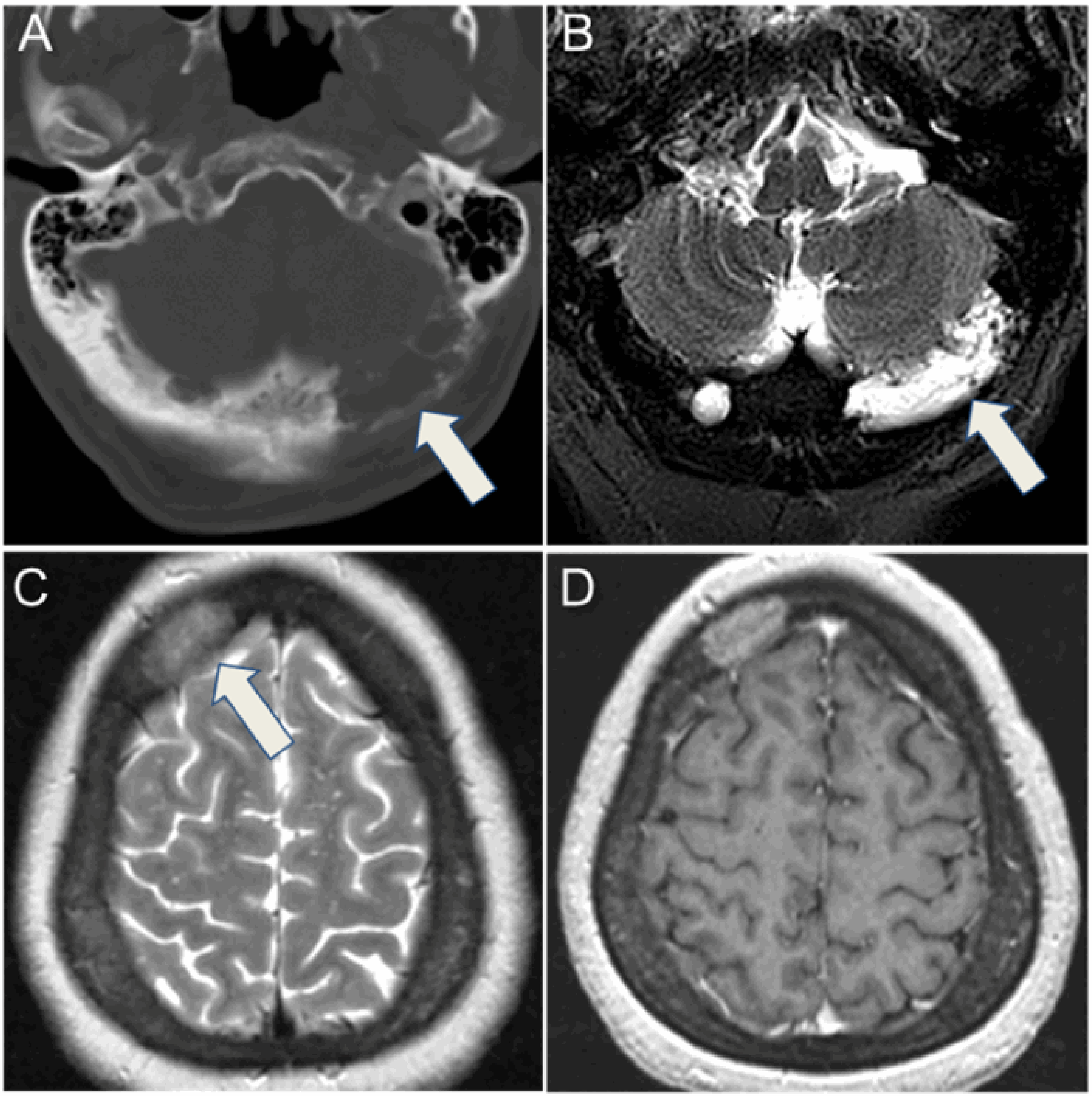

Figure.

A & B: Giant arachnoid granulations. Axial CT (A) shows a large heterogeneous lucent lesion in the left occipital calvarium (arrow) and a smaller one on the right. The lesions were markedly hyperintense on T2 (arrow, B) and suppressed on FLAIR (not shown).

C & D: Skeletal sarcoidosis. Axial T2 (C) shows a mildly hyperintense lesion in the right frontal calvarium (arrow) with diffuse enhancement on the postcontrast T1 image (D).

(Filename: TCT_3218_MIMICS.gif)

3158

More Than Just Cerumen: Lesions of the External Auditory Canal and Their Surgical Implications

M Shroads[1], J Bykowski[1]
[1]*UC San Diego Health, San Diego, CA*

Purpose
While cerumen may be the most commonly encountered entity within the external auditory canal (EAC) on imaging, there is an extensive differential diagnosis for lesions of the EAC, including benign, locally aggressive, and malignant processes. It is essential that the neuroradiologist not overlook these lesions and that imaging characteristics are appropriately identified to assist the clinician and surgeon with decisions regarding therapy.
Materials and Methods
Multiple cases of EAC lesions are reviewed from a single academic institution on cross-sectional imaging and correlated with clinical and surgical data within the institutional electronic medical record system, with particular emphasis on implications for surgical resection. A review of the literature supplements the institutional case series.
Results
Illustrative cases will include CT and MR imaging of: - Benign lesions including infectious processes (e.g. otitis externa and ruptured otitis media), post-traumatic findings (e.g. hematoma), foreign bodies, and exostosis. - Locally aggressive lesions including cholesteatoma. - Malignant involvement with squamous cell carcinoma (SCC), basal cell carcinoma (BCC), adenoid cystic carcinoma, and metastases. - Recurrence and mimics on post-surgical surveillance. Discussion will focus on key imaging findings to communicate to the clinician and surgeon regarding differential diagnoses and operative planning for sleeve resection, mastoidectomy, and parotidectomy with reconstruction.
Conclusions
The EAC is a potential site for many benign, locally aggressive, and malignant lesions. The neuroradiologist must be able to recognize and describe these lesions and formulate an appropriate differential diagnosis, as accurate characterization is crucial for potential surgical management.

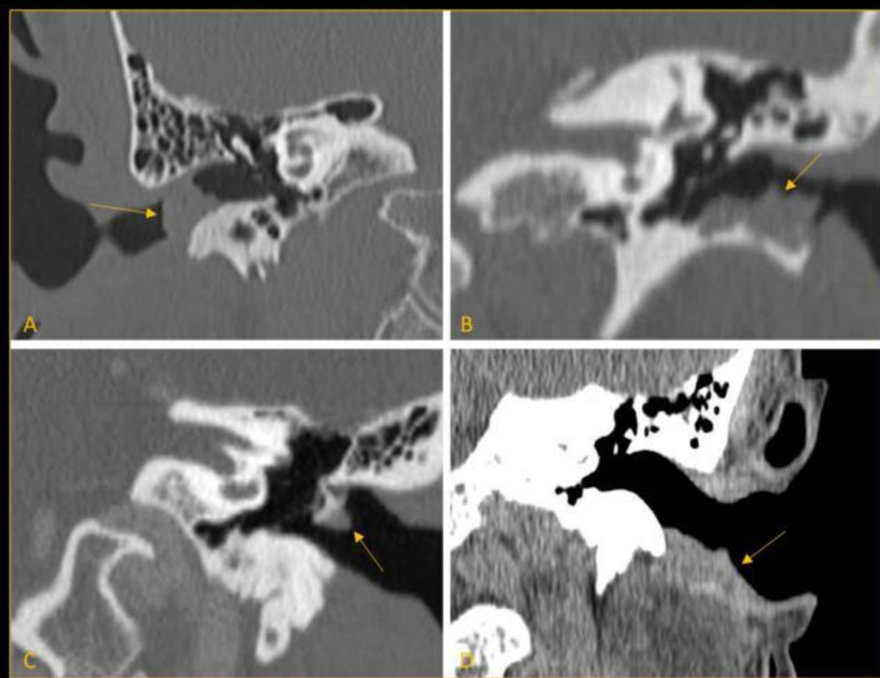

Coronal CT images through the external auditory canal (EAC) highlight features necessary to the search pattern. Soft tissue material in the right EAC (A) mimicked cerumen, however was adherent to the floor; biopsy revealed squamous cell carcinoma. Bone erosion adjacent to the mass in (B) was consistent with the diagnosed cholesteatoma, however may also be a feature of malignant processes. Central bone density in a smoothly mucosalized mass (C) was sequelae of prior incus dislocation through a perforated tympanic membrane. Adenoid cystic carcinoma along the cartilaginous canal inferiorly (D) could easily be missed if evaluating bone windows alone.

(Filename: TCT_3158_EACGRAPHIC.jpg)

3106

More Than Talk, a Visual Primer to Laryngeal Pathology

L Chan[1], K Hammoud[2], M Lang-Orsini[1], G Curaudeau[1], M Lanfranchi[3]
[1]Tufts Medical Center, Boston, MA, [2]Massachusetts General Hospital, CAMBRIDGE, MA, [3]Piedmont Atlanta Hospital, Atlanta, GA

Purpose
There are a variety of pathologies that may be found in the larynx. This exhibit will seek to help the radiologist become familiar with laryngeal anatomy and cross-sectional appearance of laryngeal pathologies, with histopathologic correlation when available. Many uncommon laryngeal pathologies manifest without mucosal abnormalities that allows for an obvious biopsy target for the endoscopist. The radiologist plays a crucial role in helping to identify the abnormality and directing the clinician to the appropriate biopsy site.
Materials and Methods
Utilizing review and reference articles we will discuss the anatomy of the larynx and the cross-sectional appearance of laryngeal pathology with histopathology correlates when available. Cases will be collected through the authors' home institution radiology department archives. The pathology department will assist with providing histopathology correlation.

Results
Overview of the anatomy of the larynx and surrounding structures Depicting laryngeal pathology through illustrative case examples and histopathology correlate: 1. squamous cell carcinoma 2. chondrosarcoma 3. paraganglioma 4. tumors of the minor salivary glands 5. pseudotumor 6. hemangioma 7. vocal cord paralysis 8. laryngocele 9. Wegener's granulomatosis 10. rheumatoid arthritis in the larynx 11. amyloidosis in the larynx 12. tracheopathia osteochondroplastica 13. nodular chondrometaplasia
Conclusions
There are a plethora of laryngeal pathologies and the radiologist plays an important role in the diagnosis of laryngeal pathology. The radiologist should be familiar with laryngeal anatomy and laryngeal pathologies. These pathologies range in spectrum from neoplasms to inflammatory disorders.

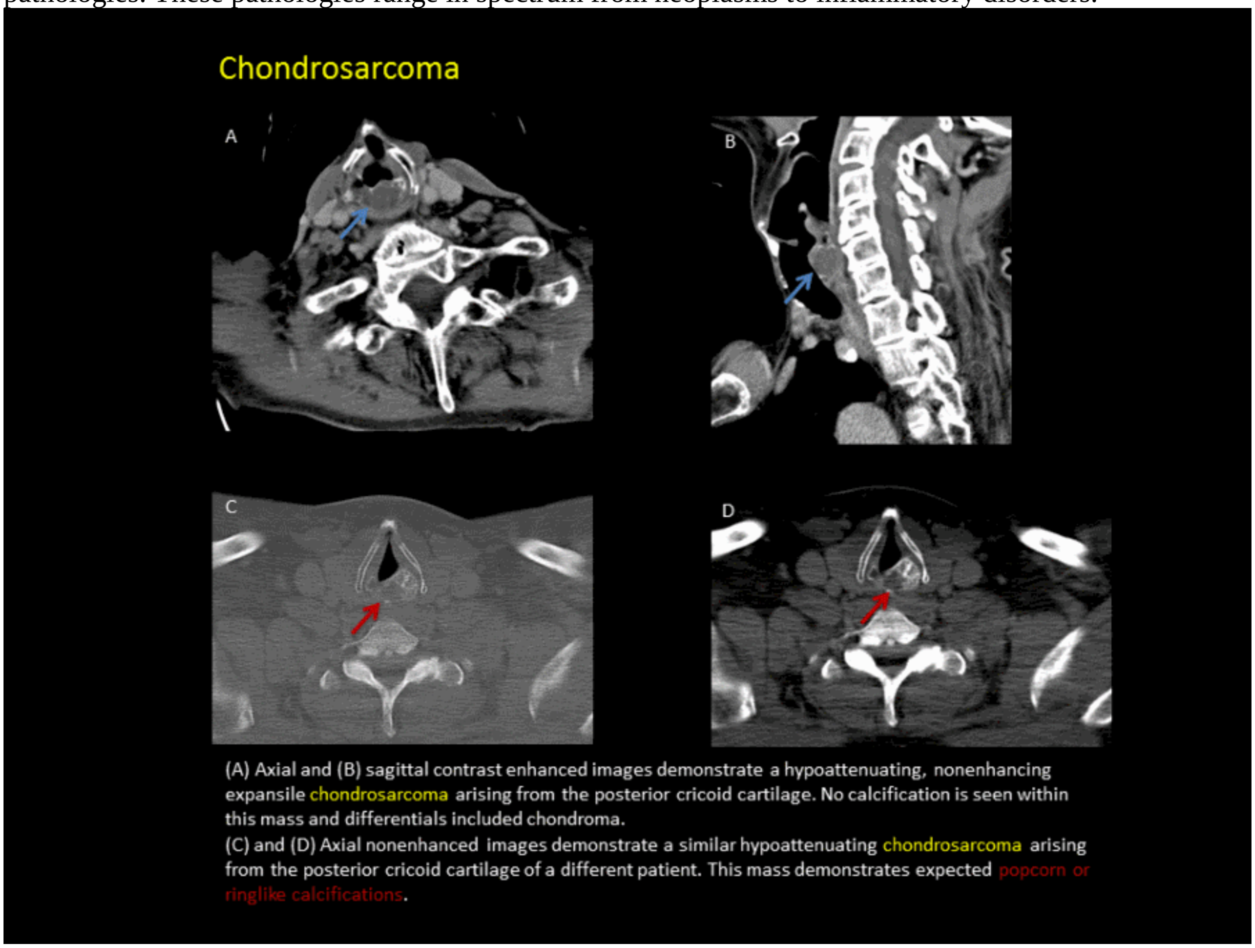

(Filename: TCT_3106_laryngealsamplepics.gif)

2985

MR Texture Analysis: Definitions, Neuro-oncological Applications, and Challenges

N Soni[1], S Priya[2], G BATHLA[3]
[1]UIHC, iowa, IA, [2]UIHC, iowa city, IA, [3]University of Iowa hospitals and Clinics, IOWA CITY, IA

Purpose
To discuss basic concepts of texture analysis (TA), potential neuro-oncological applications, limitations, challenges and future directions of MRTA

Materials and Methods
Gliomas are heterogeneous tumors, and as such brain biopsy of a representative sample may not be the true representation of the entire tumor. The conventional method for histological, molecular and genetic classification of cerebral glioma is brain biopsy that suffers from being invasive, costly and having high sampling error. This necessitates pre-operative identification of imaging biomarkers via a non-invasive means, providing entire tumor microstructure information which may help in predicting both the response to treatment and survival. TA non-invasively provide entire tumor microstructure information inclusive of cellular density, proliferation, angiogenesis, necrosis and thus predict aggressive tumor biology. TA is the quantitative analysis of radiologic images, provides information about the spatial distribution and relationship of grey-level intensities that correspond to the underlying tumor heterogeneity and thus may help in stratification of glioma based on grade, molecular subtype, and genotype. In simpler terms, TA provides a relationship between imaging signatures and histo-genomic sequencing. Recently, there have been multiple studies on application of MRTA for cerebral gliomas and have shown promising results. This educational exhibit would contribute to the value of MRTA in gliomas by evaluating data from already published studies.
Results
Despite growing knowledge, there is no agreement on the clinical utility of MRTA in routine practice, due to differences in TA techniques, analysis methods, post-processing, and classification methods. Before MRTA can be considered for clinical practice, standardization of TA techniques and methods for handling large data needs attention.
Conclusions
With continued advancement in computers power, MRTA has the potential to develop into a valuable clinical tool for oncologic imaging.

3327

MRI of the Lumbosacral Plexus: An Illustrative Review and Case Series

A Saha[1], U Sarmast[2], I Ikuta[3], L Tu[4]
[1]Yale University School of Medicine, New Haven, CT, [2]Kaiser Permanente, Atlanta, GA, [3]YALE UNIVERSITY-SCHOOL OF MEDICINE, MILFORD, CT, [4]Yale School Of Medicine, New Haven, CT

Purpose
This educational exhibit reviews the anatomy and common pathologies affecting the lumbosacral plexus.
Materials and Methods
A brief review of the literature will be followed by a case series. The cases will cover the experience of a single academic institution with MRI of the lumbosacral plexus over 5 years.
Results
The lumbosacral plexus is a complex network of nerves formed by the ventral rami of the lumbar and sacral spine. End branches supply the pelvic side wall and lower extremities. The lumbosacral plexus may be affected by neoplastic involvement, infectious/inflammatory etiologies, and traumatic injury. MRI directed at evaluating the plexus is an uncommonly performed exam. For example at our tertiary referral center, of 650,784 MRI studies performed over the past 5 years, only 64 of these (0.001%) are MRI exams of the lumbosacral plexus. Only a minority of these 12/64 (19%) demonstrated pathologic involvement of the lumbosacral plexus. Aside from degenerative neuroforaminal/spinal canal stenosis, the most common pathologic finding in our institutional cases is metastatic involvement, typically by adjacent lymph nodes or a primary pelvic mass.
Conclusions
A review of lumbosacral plexus anatomy and pathology on MRI provides an approach to this uncommonly performed exam.

3027

Multiparametric MRI Assessment of Lesions Involving the Corpus Callosum

M Bowen[1], M Patel[1], B Butler[1], J Murphy[1], N Davies[1], R Flintham[1], M Harley[1], A Moussa[1], I Ughratdar[1], V Sawlani[1]
[1]*University Hospitals Birmingham NHS Foundation Trust, Birmingham, West Midlands*

Purpose
A variety of pathologies can involve the corpus callosum and there can often be an overlap in the way in which they present clinically. Conventional MRI may not always be able to differentiate between the various pathologies. Multiparametric MRI including spectroscopy, diffusion and perfusion imaging has shown promise in being able to provide a more definitive diagnosis which may prevent unnecessary biopsies occurring. We exhibit a variety of cases to demonstrate the value of multiparametric MRI in the assessment of lesions involving the corpus callosum.
Materials and Methods
A retrospective review of 560 multiparametric MRI studies performed over the last 7 years revealed 73 cases of lesions involving the corpus callosum. PACS and online clinical records were used to review the imaging findings, clinic letters and pathology results of these cases.
Results
There were 7 cases of inflammation, 2 cases of infection, 2 cases of vascular pathology, 2 cases of metabolic disorders and 60 cases of tumour including low-grade gliomas, low-grade gliomas undergoing high-grade transformation, high-grade gliomas and lymphoma. Multiparametric MRI was frequently able to provide additional diagnostic information that affected management decisions including avoiding several proposed biopsies.
Conclusions
Distinction between the various pathologies that can involve the corpus callosum is not always possible using conventional MRI. Multparametric MRI is often able to reduce diagnostic uncertainty and differentiate between benign and malignant lesions.

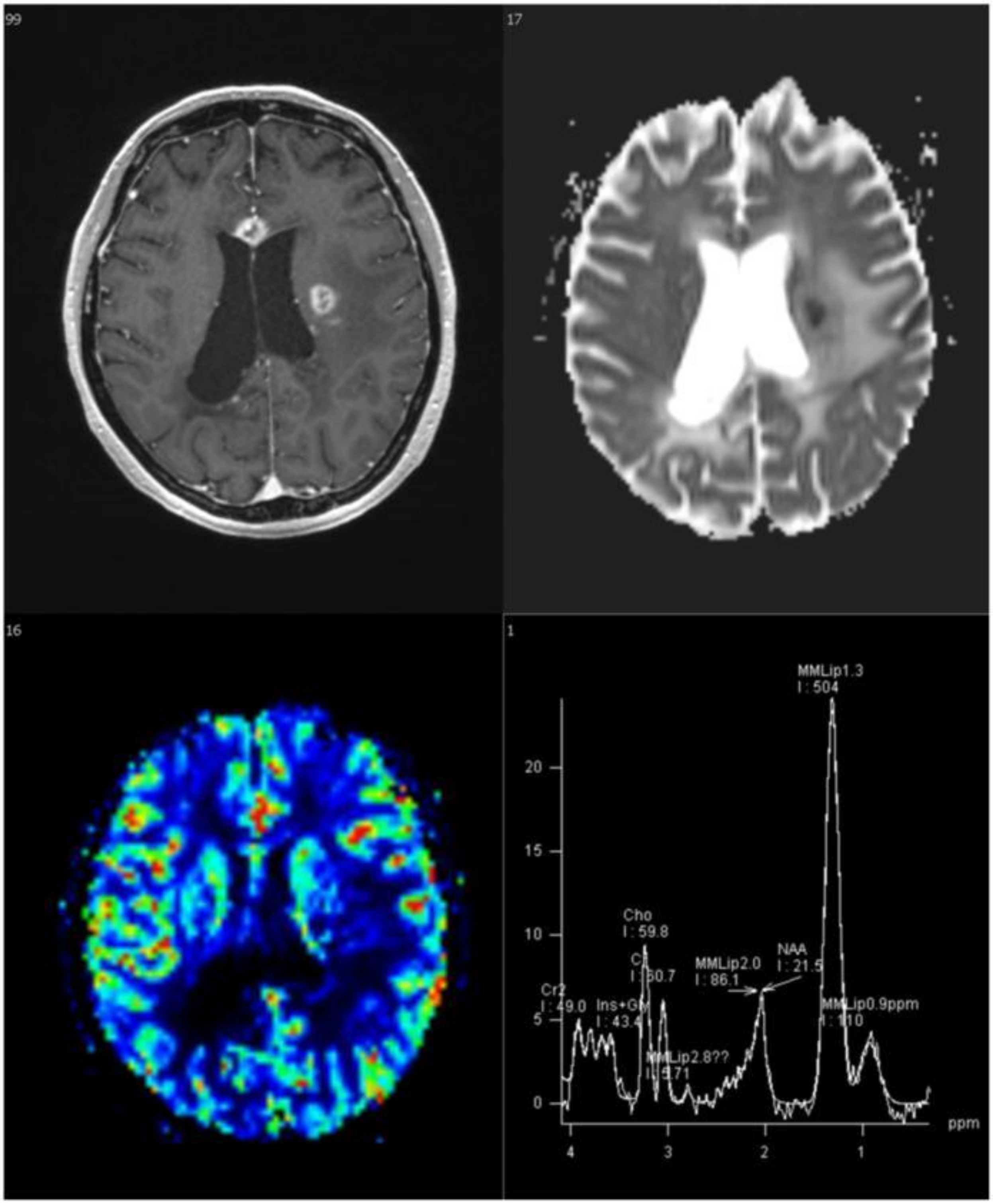

Enhancing lesions in the genu of the corpus callosum and left periventricular white matter which demonstrate restricted diffusion, bland appearances on perfusion and significantly raised lipid on spectroscopy. Appearances are in keeping with necrotic lesions not typical for tumour. Further investigation determined the underlying pathology to be retinal vasculopathy with cerebral leukoencephalopathy.

(Filename: TCT_3027_CorpusCallosumLesionsGraphic.JPG)

3091

Multiphase CTA in Acute Ischemic Stroke: Technique and Clinical Applications

R Harrington[1], M Jayaraman[2], G JINDAL[3]
[1]Warren Alpert School of Medicine, Brown University, Providence, RI, [2]RHODE ISLAND HOSPITAL, PROVIDENCE, RI, [3]Warren Alpert School of Medicine, Brown University, SHARON, MA

Purpose
Review the technique for performing multiphase CTA in the setting of Acute stroke. To learn the clinical usefulness and role of multiphase CTA in acute ischemic stroke.
Materials and Methods
Retrospective review of our PACS database to obtain illustrative cases demonstrating role of multiphase CTA in evaluation of patients presenting with acute ischemic stroke.
Results
Multiphase CTA Technique: Multiphase CTA acquisition begins with a head CT without contrast. Once intracranial hemorrhage is excluded, a head and neck CTA is obtained from the vertex to the Aortic arch in the arterial phase triggered by bolus tracking, followed by two more acquisitions through the brain, peak venous and delayed venous phases, each 8 seconds apart. Thick section axial Maximum Intensity projections(MIPs) are reconstructed to evaluate the three phases. Clinical Applications Collateral scoring Detection of distal occlusions in the anterior intracranial circulation Delayed vessel sign: Increased vascular opacification on venous and delayed venous phase distal to the site of occlusion Differentiating vascular non opacification secondary to slow flow related to distal occlusion from true occlusion. Missed initial bolus: Peak venous and delayed venous phases can capture arterial phase in case of delayed arterial filling such as related to severe carotid stenosis.
Conclusions
We describe several cases depicting the role of Multiphase CTA in evaluation of patients with acute ischemic stroke.

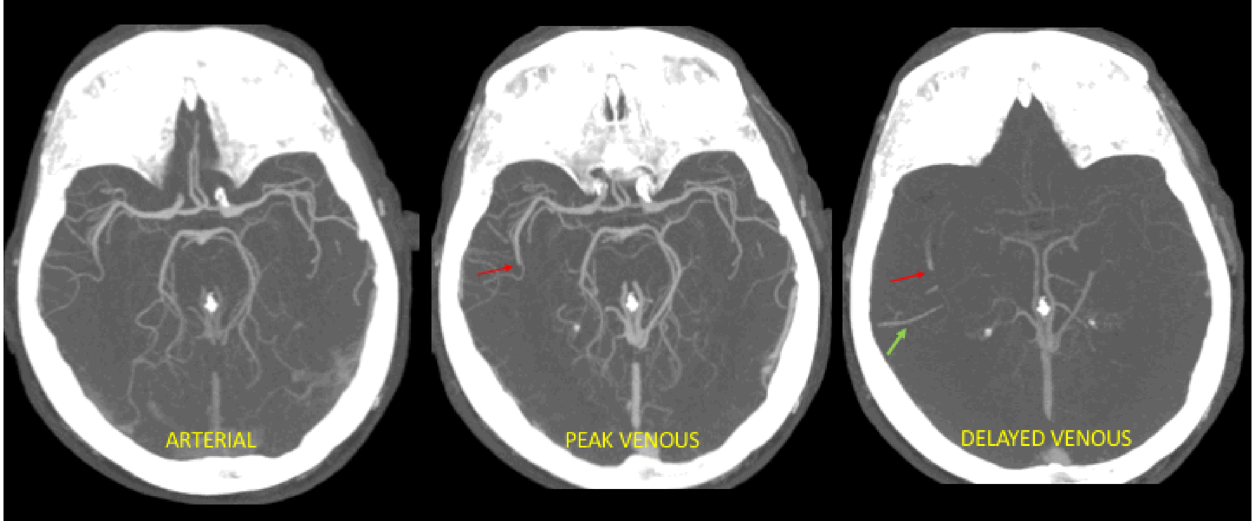

Axial Arterial phase MIP image (left) demonstrates no obvious vascular occlusion. Peak venous phase image (center)reveals right M2 occlusion (Red Arrow). Axial delayed venous phase image confirms right M2 occlusion with asymmetric increased vascular opacification distal to the site of occlusion (Green arrow, delayed vessel sign)

(Filename: TCT_3091_asnr.gif)

3186

Neuroimaging of Deep Brain Stimulators: A Review

J Scheibal[1], J Acharya[2], A Rajamohan[3], A Rajput[4], P Joyce[5], M Shiroishi[6], S Ceglar[7], F Torres[8]
[1]USC Keck School of Medicine, Los Angeles, CA, [2]UNIVERSITY OF SOUTHERN CALIFORNIA, KECK SCHOOL OF MEDICINE, Monrovia, CA, [3]UNIVERSITY OF SOUTHERN CALIFORNIA, KECK SCHOOL OF MEDICINE, LOS ANGELES, CA, [4]USC Keck School of Medicine, Los Angeles, CA, [5]LAC USC, Los Angeles, CA, [6]KECK SCHOOL OF MEDICINE, USC, SOUTH PASADENA, CA, [7]LAC+USC, Los Angeles, CA, [8]Kaiser Permanente, Los Angeles Medical Center, Los Angeles, CA

Purpose
To review current imaging guidelines, study interpretation, and potential complications associated with deep brain stimulator placement and evaluation.
Materials and Methods
Current literature as well as single institution experience with case examples will be utilized to present the current imaging guidelines for pre-operative planning, intra-operative navigation, and post-operative evaluation of deep brain stimulators.
Results
Deep Brain stimulation is an increasingly common therapy utilized for a wide variety of neurologic diseases. Neuroimaging plays a key role in in the pre-operative evaluation, intra-operative placement, and post-operative evaluation of these devices. Through this exhibit, the user will learn the neuroanatomy commonly targeted for DBS placement, review pre-operative imaging techniques, and be exposed to possible pit falls in pre-operative imaging. The user will develop an understanding of intra-operative imaging guidance techniques. Post-operative evaluation of DBS placement will also be discussed and case examples of post-procedural complications will be reviewed.
Conclusions
Neuroimaging plays a key role in evaluation of deep brain stimulators. This exhibit will review current imaging guidelines, explain key points to interpreting these studies, and review possible complications associated with deep brain stimulators.

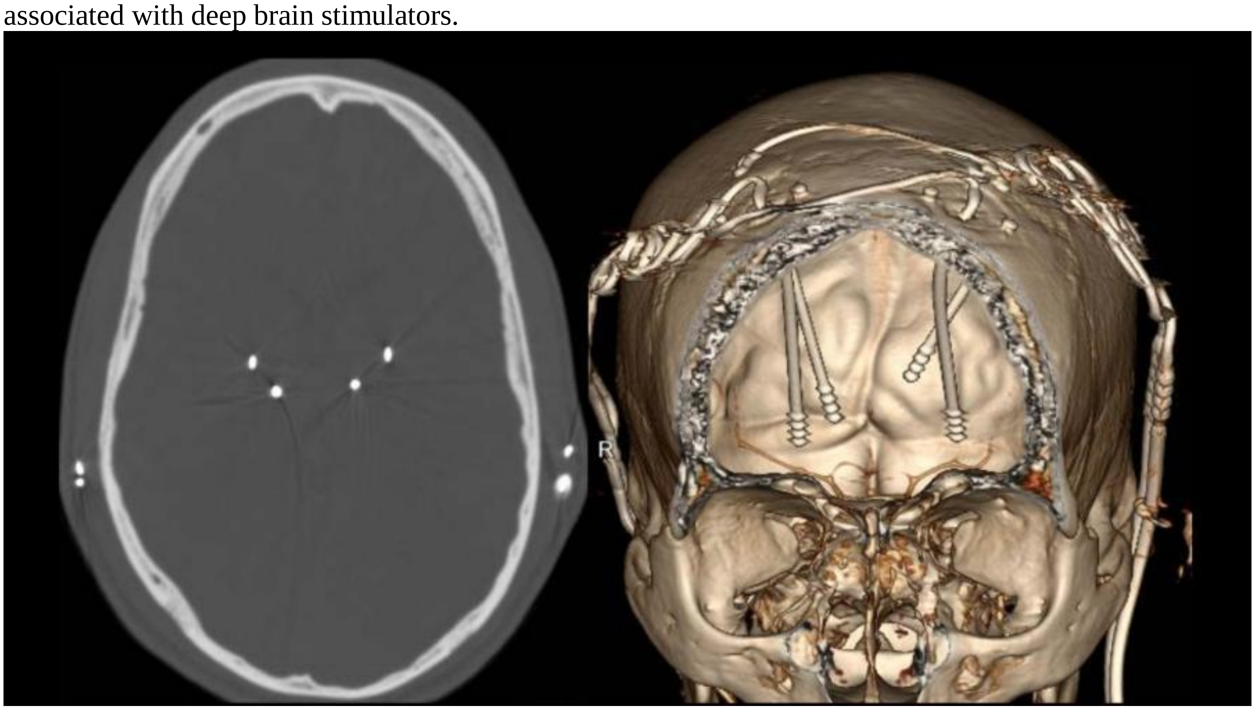

(Filename: TCT_3186_DBSASNR.jpg)

2603

Neurological Complications Related to Methotrexate Therapy

D de Oliveira[1], G BATHLA[2], B Policeni[3], L Godoy[4]
[1]Hospital do Cancer da Universidade Federal de Uberlândia, Uberlândia, Minas Gerais, [2]University of Iowa hospitals and Clinics, IOWA CITY, IA, [3]University Of Iowa, Iowa City, IA, [4]FLEURY, SÃO PAULO, SÃO PAULO

Purpose
The authors present a spectrum of cases to demonstrate the complications related to methotrexate therapy, with typical and atypical imaging findings.
Materials and Methods
We will discuss the pathophysiology related to the methotrexate toxicity in the central nervous system and demonstrate the imaging findings related to each presentation, as well as the major differential diagnosis.
Results
Methotrexate is a chemotherapy agent used systemically for a wide range of malignancies, with variable dosage regimen. It can also be administered as adjuvant therapy to brain radiation, and intrathecally to treat leptomeningeal metastases or for prophylaxis in hematologic malignancies. There are four reported presentations of methotrexate toxicity in the central nervous system: - Chronic leukoencephalopathy, the most common presentation, characterized by confluent periventricular hyperintensities, without restricted diffusion or contrast enhancement; - Subacute combined degeneration, with T2 hypersignal within the dorsal columns of the spinal cord, indistinguishable from vitamin B12 deficiency; - Toxic leukoencephalopathy, manifested as a potentially reversible lesion of the white matter, with restricted diffusion; - Necrotizing encephalopathy, the more severe presentation, in which necrotic areas develop within the white matter.
Conclusions
The onset of neurological symptoms in a patient using methotrexate should promptly alert the assistant physician about the possibility of the development of the toxic effects of the drug. Imaging techniques are essential to determine the form of involvement, the progression of the findings and to suggest possible differential diagnosis.

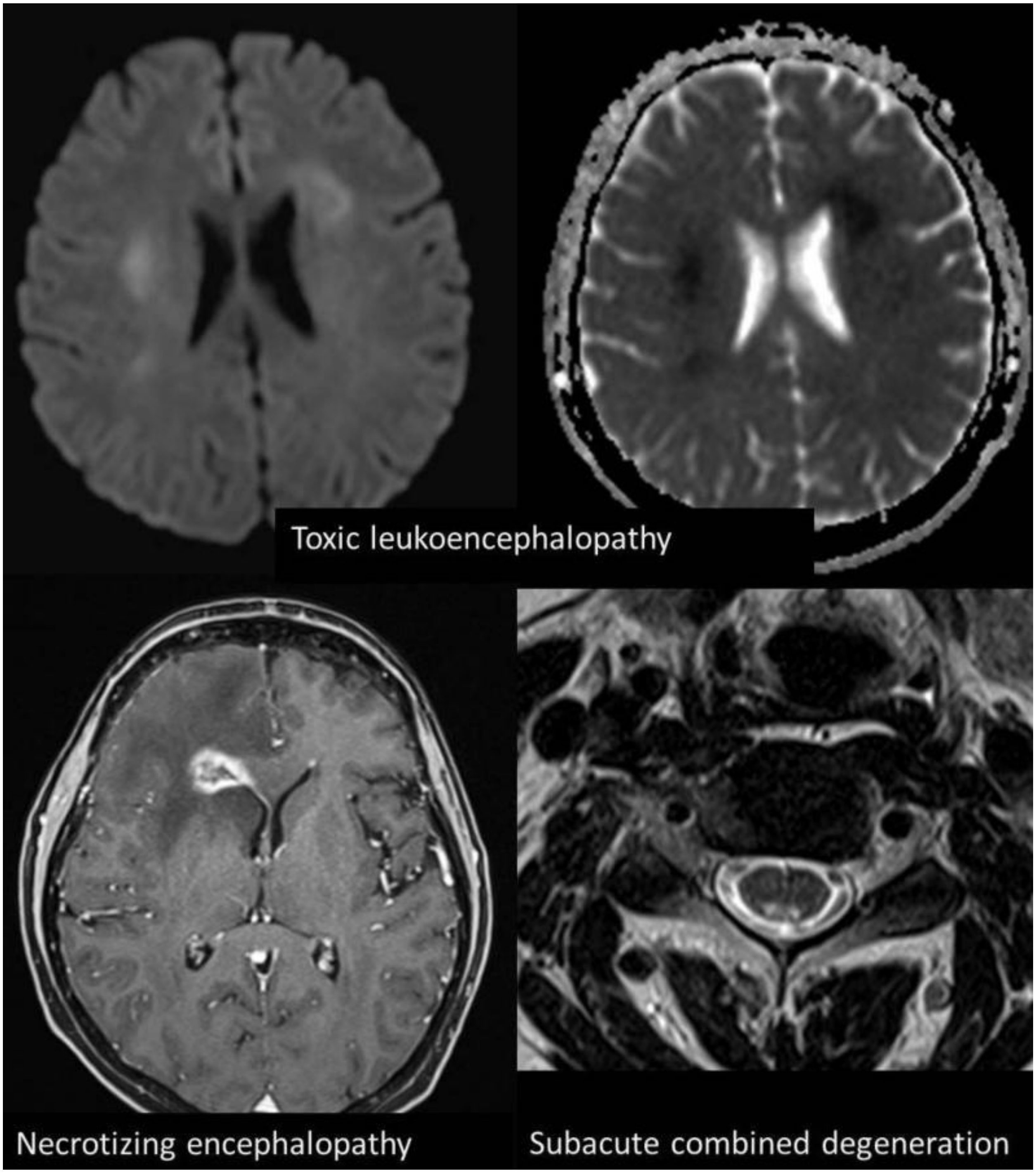

(Filename: TCT_2603_Methotrexatepic.jpg)

2792

New Look at Craniocervical Injury with 3D Surface Renderings

J Costello[1], M Peckham[2], T Hutchins[3], L Shah[1]
[1]University of Utah, Salt Lake City, UT, [2]UNIVERSITY OF UTAH HEALTH SCIENCE CENTER, SALT LAKE CITY, UT, [3]University of Utah, Neuroradiology, salt lake city, UT

Purpose
Craniocervical (CC) injury is potentially catastrophic. Early imaging recognition of ligamentous instability and associated spinal cord injury are critical and can decrease patient morbidity. Because of the multidimensional complexity of the CC articulations and supporting ligaments, injury can be easily missed initially. Through this educational exhibit, we will highlight the diagnostic value of 3 dimensional (3D) imaging in the diagnosis of CC injury and correlate ligaments on MRI to the 3D osseous articulations.
Materials and Methods
Anatomy of the CC junction will be presented in an interactive format using MRI and CT 3D surface renderings (produced with Siemens Syngo.via software), with emphasis on alignment of C0-C1 and C1-C2 articulations and the ligaments. CT 3D surface renderings are used to illustrate varying degrees of CC injury. In an interactive case presentation format, different MR patterns of ligamentous injury will be reviewed.
Results
Normal values for CC alignment have been defined on CT; however, because of the complex 3D articulations, CT surface renderings can help to identify cases of craniocervical injury. MRI delineates the extent of ligamentous injury as well as spinal cord injury. While the cruciate and alar ligaments are important for CC stability, other ligaments are being increasingly recognized for their role in CC junction stability: the occipitoatlantal membranes and C0-C1 joint capsule (i.e. occipitoatlantal ligaments). The C0-C1 joint capsule, often overlooked, is readily identified on standard sagittal T2 weighted MRI, and tearing of these ligaments has a high correlation with occipitoatlantal dislocation and CC instability.
Conclusions
Understanding of normal alignment and ligamentous anatomy is key for imaging assessment of CC injury. Because of the complex articulations at C0-C1 and C1-C2, CT 3D surface renderings as well as MRI are valuable in early diagnosis of CC injury.

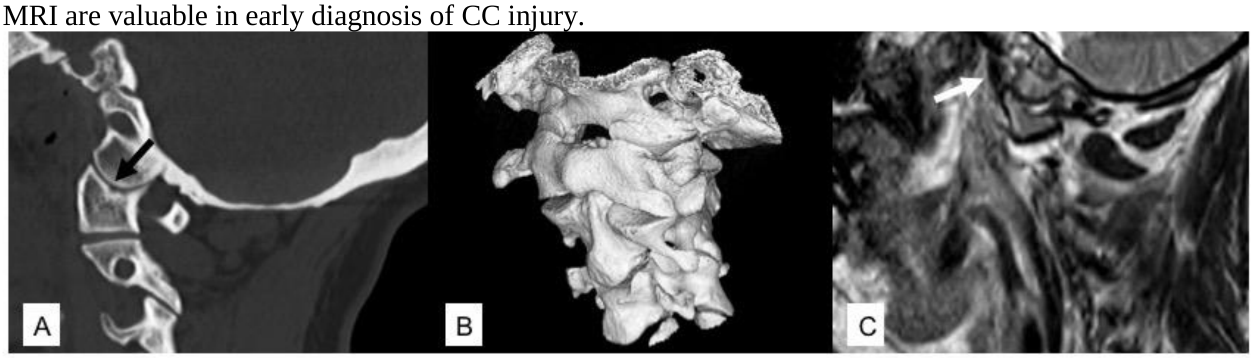

Normal craniocervical (CC) alignment has been described. (A) Demonstrates normal occipitoatlantal alignment (OA) on CT (black arrow). Because of the multidimensional complexity of CC articulations, imaging evaluation of the CC junction can be enhanced with 3D surface renderings (B). Through this exhibit, the reader will be able to rotate 3D images of the CC junction in normal cases and in patients with CC trauma. Pertinent ligamentous anatomy is also interactively reviewed with the reader. (C) What does the white arrow depict? Answer: C0-C1 joint capsule, an important stabilizer of the OA joints.

(Filename: TCT_2792_CCJFigure.jpg)

2212

Non-epithelial Tumors of the Larynx: a 12-year Single Institution Review with Radiologic-pathologic Correlation

E Huh[1], M Khan[1], N Aygun[2], S Best[1], L Rooper[1]
[1]Johns Hopkins Hospital, Baltimore, MD, [2]JOHNS HOPKINS MEDICINE, LUTHERVILLE, MD

Purpose
Non-epithelial tumors of the larynx are relatively rare entities, representing only a minority of all laryngeal neoplasms. Imaging plays an important role in the diagnosis, treatment planning and surveillance of these entities. We offer a radiologic-pathologic review of cases of non-epithelial laryngeal tumors diagnosed at a single institution over a 12 year period.
Materials and Methods
After approval was obtained from the site's Institutional Review Board, a retrospective search was conducted for cases of non-epithelial laryngeal tumors diagnosed between March 2006 and March 2018. Only cases which included pre-operative imaging and diagnoses confirmed by biopsy or unequivocal laryngoscopic appearance were included in the study. Primary imaging modalities included computed tomography and magnetic resonance imaging. Each case was reviewed for the patient's clinical presentation, radiologic findings, histologic characteristics, and clinical management.
Results
32 patients with the diagnosis of non-epithelial origin laryngeal tumors were retrospectively identified, 16 of which were male and 16 female with ages ranging from 6 to 82 years of age. Benign entities included hemangioma, chondroma, schwannoma, ossifying fibromyxoid tumor, giant cell reparative granuloma and granular cell tumor. Malignant entities included chondrosarcoma, lymphoma, alveolar soft part sarcoma, liposarcoma, histiocytic sarcoma, rhabdomyosarcoma, plasmacytoma and metastatic disease. The pre-surgical imaging primarily consisted of contrast-enhanced CT with a few cases also including MRI.
Conclusions
Although nonepithelial laryngeal tumors are relatively rare entities, it is important for radiologists to be aware of these potential diagnoses. Many of the imaging findings are nonspecific, but our review attempts to highlight certain imaging features on both CT and MRI that may be helpful in differentiating entities. We also offer histologic correlation for several cases. Differential diagnosis may be further limited by lesion location, involvement of laryngeal structures, patient age and other clinical manifestations.

2247

Notochord Remnants: A Pictorial Review

M Yao[1], V Patel[1], G Parnes[1], S Slasky[1]
[1]*Montefiore Medical Center, Bronx, NY*

Purpose
Educational Objectives 1. To review notochord development and regression during fetal life. 2. To present a pictorial review of anatomical variations of notochord remnants, from benign to malignant lesions derived from the notochord.
Materials and Methods
Background Notochord formation begins between the third and fourth week of embryonic development. As the axial skeleton develops, the notochord regresses, eventually contributing to the formation of the nucleus pulposus of the intervertebral disc. Notochord regression can be variable at the two poles of the skeleton, resulting in ectopic notochordal remnants. Although these remnants typically have an intraosseous location, they can perforate through the dorsal wall of the clivus and be found intracranially, in the epidural, subdural or subarachnoid space. Hence, these lesions often present as a diagnostic challenge.
Results
Content We plan to present a pictorial review of notochord formation to frame the basis of our discussion. There will be an image rich presentation of characteristic benign and malignant notochord remnants. Our examples will range from benign lesions such as ecchordosis physaliphora, benign notochordal cell

tumor, Tornwaldt cyst, foveola pharyngica recess and inferior median clival canal to malignant lesions such as chordoma.

Conclusions

Notochord remnants often present as a diagnostic challenge. However, familiarity with notochord development aids in understanding their characteristic location and radiographic features, which can often help narrow the differential diagnoses.

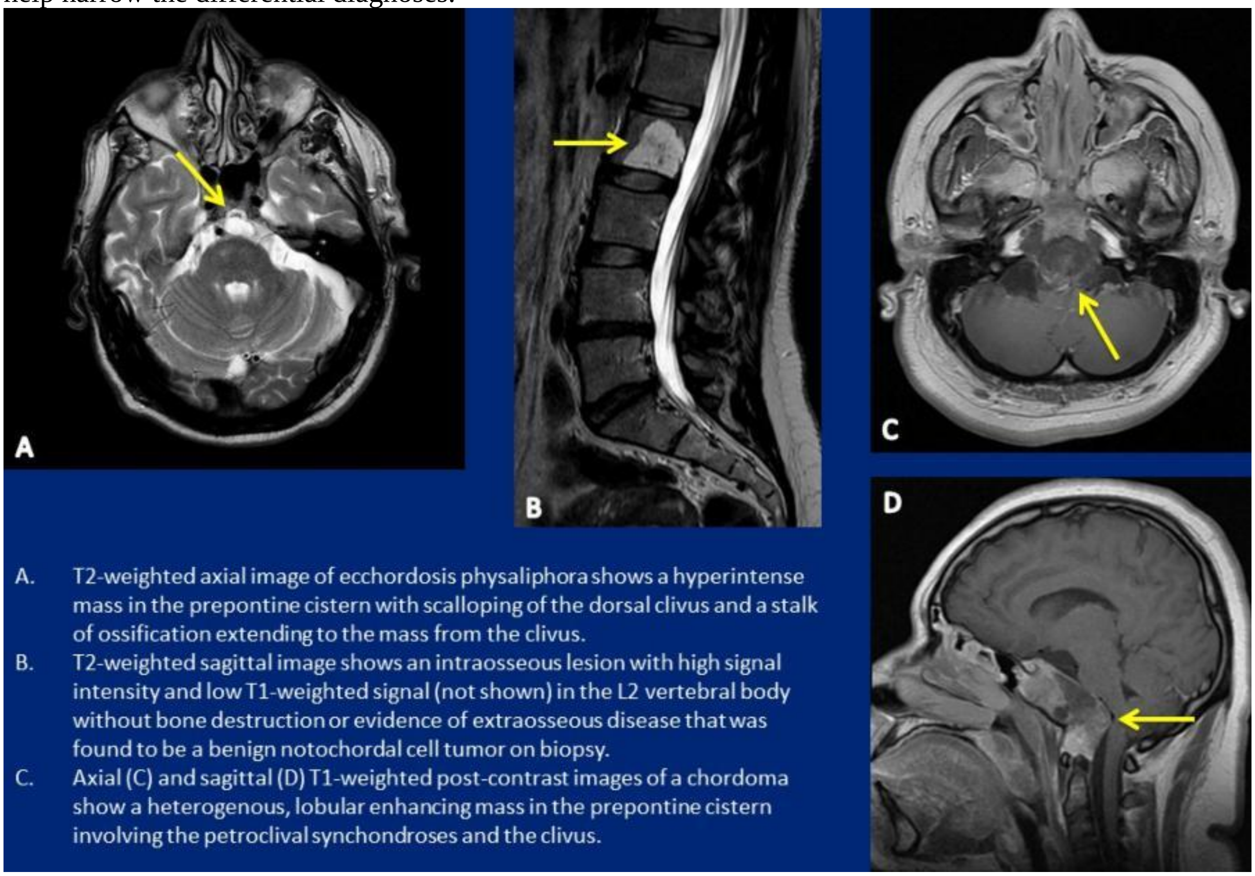

(Filename: TCT_2247_NotochordRemnantsGraphic.jpg)

3498

Novel Technique Utilizing 3D Fast Dixon Volumetric Imaging for Head and Neck Imaging

M Nachiappan[1], K Weiss[2], J Infante[3]
[1]Jackson memorial hospital, Miami, FL, [2]Miller School of Medicine, University of Miami, Miami, FL, [3]Univ of Miami, Miami, FL

Purpose

To illustrate the potential of a novel multiparametric color encoded 3D fast Dixon technique to provide rapid multi-contrast volumetric head & neck imaging and facilitate interpretation. While highlighting unique features of this technology, the exhibit will teach multiplanar anatomy with interactive labeling.

Materials and Methods

Sagittal 3D fast Dixon sequencing at 3T (TR = 4.1, TEs = 1.3 & 2.5 msec) providing 1.1 mm isotropic coverage of the head & neck in 1 min 4sec was preformed pre and post-contrast. Opposed phase (OP), in phase (IP), and derived water (W) & fat (F) image sets were further processed in MATLAB® to generate a novel color encoded composite wherein IP, OP and W signal intensities were assigned R, G & B values respectively. Coronal and axial reformations were made in Osirix®

Results

High quality T1 weighted color encoded composites were obtained. Tissues containing only W signal (e.g. brain, cord) appear gray scale (R = G = B) while tissues containing only F appear yellow (R + G). Tissues containing both W and F (e.g. red marrow) and India ink artifact (black on OP) appear red as IP (R) signal predominates. Regions of magnetic susceptibility appear green. Color-encoded Dixon provides excellent depiction of anatomy throughout the head & neck. The hyperintense neurohypophysis is readily separated from the dorsum clivus. Tissues with short T2 components (e.g. lens, ligamentum flavum) have much greater signal than on conventional T1 sequences. Vessels are extremely well visualized post contrast without appreciable flow/pulsation artifact. Various neck spaces are clearly depicted with fat being color encoded and the contents appearing in grey scale.

Conclusions

Multiparametric color encoded fast Dixon is a most promising technique for head & neck imaging and merits further exploration.

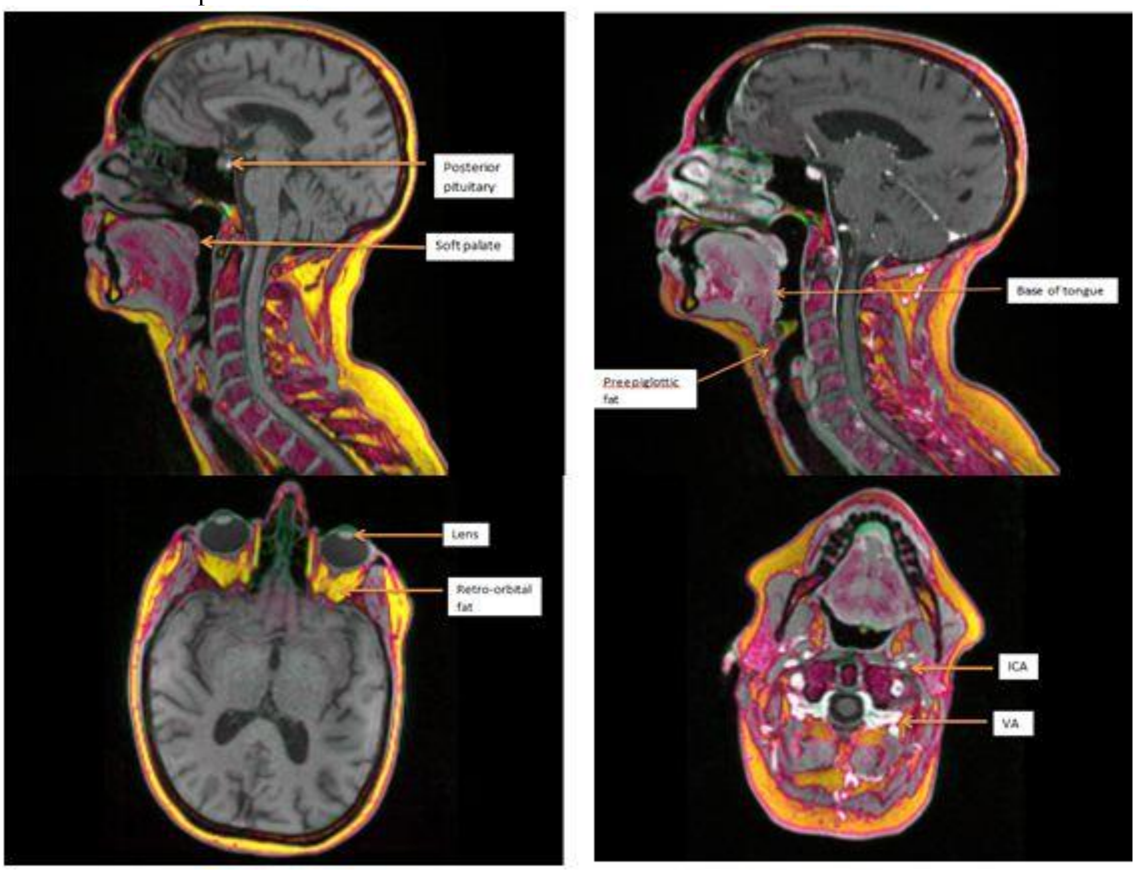

(Filename: TCT_3498_3ddixon.JPG)

2699

Our Experience in 100 Posterior Fossa Tumors in Children: A Pattern-Based Approach to Diagnosis

E Weidman[1], L Heier[2]

[1]NewYork Presbyterian - Weill Cornell Medicine, New York, NY, [2]NYP - CORNELL, NEW ROCHELLE, NY

Purpose

The purpose of our educational exhibit will be to: • Describe a pattern-based approach for diagnosis of posterior fossa tumors in the pediatric population. • Review both typical and atypical manifestations of common pediatric posterior fossa tumors. • Highlight tip-offs for uncommon posterior fossa masses. • Describe key points to address in reports to aid in treatment planning.

Materials and Methods

This educational exhibit will use annotated images from 100 cases of pediatric posterior fossa tumors at our institution to review a pattern-based approach for diagnosing these tumors. We will describe typical and atypical imaging manifestations of posterior fossa tumors, describe tumor-related syndromes, and provide a post-quiz for participants to test their knowledge.

Results

Educational objectives of this electronic presentation will include: • Demographics of posterior fossa masses in the pediatric population, including age and gender distribution, risk factors, and common clinical presentation. • Pattern-based approach to pediatric posterior fossa tumors, including tumor location, morphology, enhancement pattern, and diffusion characteristics. • Annotated examples of typical and atypical imaging characteristics of common tumors including pilocytic astrocytoma, ependymoma, and medulloblastoma. • Examples of uncommon and syndrome-related tumors in the posterior fossa. • Key information to communicate with clinicians and include in reports for treatment planning. • Post quiz of unknown tumors for readers to apply new and reinforced knowledge.

Conclusions

Readers of this exhibit will have reviewed a pattern-based approach to diagnosing posterior fossa tumors in the pediatric population, reviewed key information to include in reports, and will have been provided a post-quiz to test their knowledge.

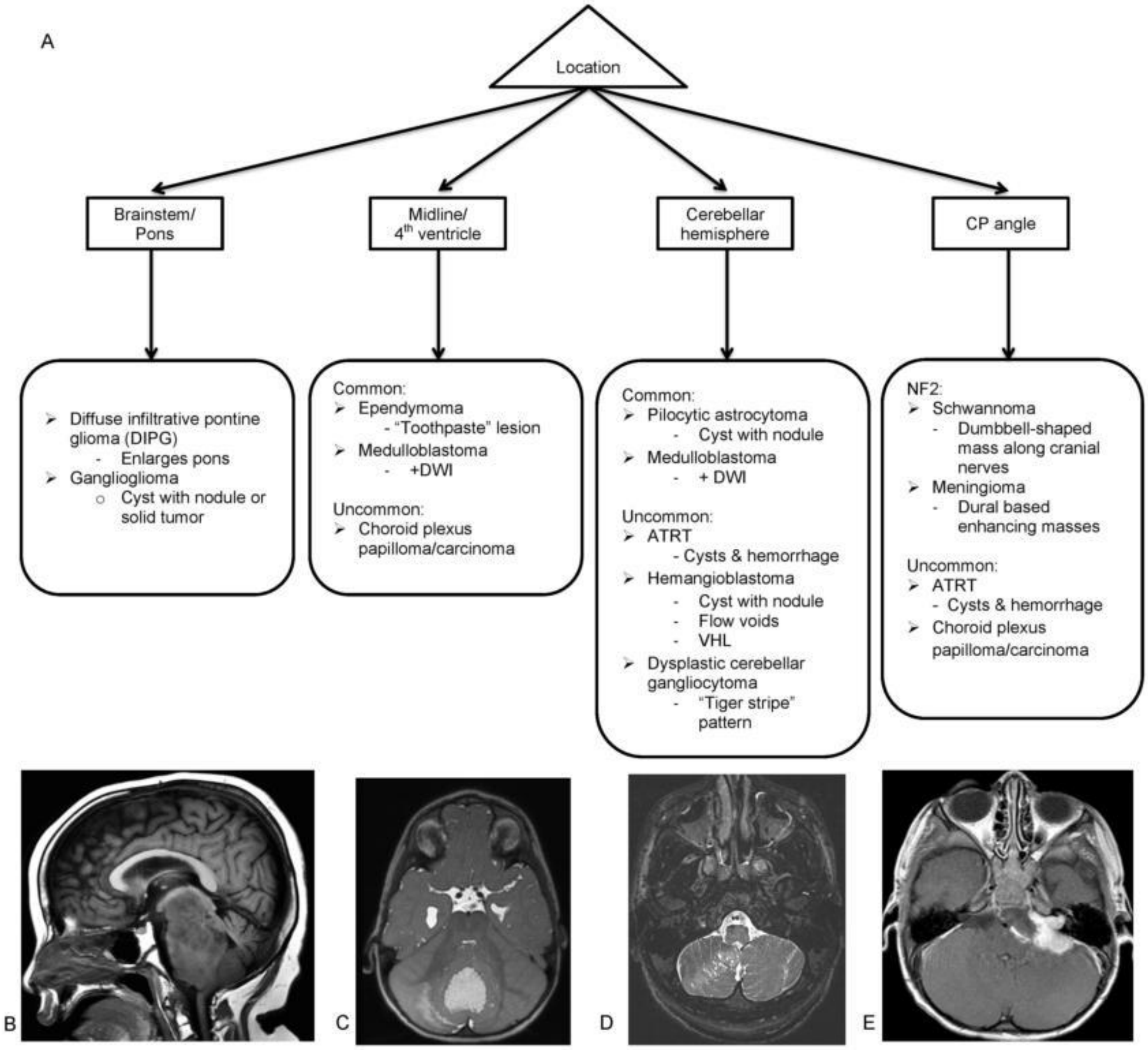

(A) Algorithm for differential diagnosis of pediatric posterior fossa mass. (B) Sagittal T2 weighted FLAIR in 6 year old with DIPG. (C) 3D T2 weighted CUBE axial reformats in 2 year old with medulloblastoma. (D) Axial 3D FIESTA in 13 year old with right dysplastic cerebellar gangliocytoma. (E) Axial T1 post-contrast in 2 year old with ATRT.

(Filename: TCT_2699_ASNRPedsPosteriorFossa.jpg)

2891

Overcoming Challenges in Adopting Magnetic Resonance Spectroscopy in to Routine Clinical Practise

V Sawlani[1], J Grist[2], M Patel[2], R Flintham[3], J Herbert[4], M Harley[3], N Davies[2]
[1]UNIVERSITY HOSPITALS BIRMINGHAM, BIRMINGHAM, United Kingdom, [2]University Hospitals Birmingham NHS Foundation Trust, Birmingham, West Midlands, [3]University Hospitals Birmingham, Birmingham, West Midlands, [4]University Hospitals Birmingham NHS Foundation Trust, Birmingham, United Kingdom

Purpose

Magnetic Resonance Spectroscopy (MRS) is a powerful technique to non-invasively inform upon metabolic processes in oncological disease. In spite of the potential utility of this technique, it is not commonly used in clinical practise due to a number of challenges in the acquisition and interpretation of spectroscopic data. At the University Hospitals Birmingham, we have optimised acquisition protocols for the routine clinical use of MRS to aid in diagnosis and monitoring of oncological disease. Here we describe simple steps to adopt MRS in to routine clinical practise.

Materials and Methods

We have performed MRS in more than 750 cases over the last seven years on a 3T scanner. We have optimised MRS acquisition in the following difficult situations: Challenging areas In order to acquire spectra from regions such as the temporal lobes and brainstem where the magnetic field is highly non-uniform, higher order shimming is utilised to improve spectral quality. (figure 1). Additional saturation pulses are also used for air and fat suppression at skull base. Small lesions Small lesion spectra were acquired using smaller voxel sizes, with additional data averaging during acquisition to increase the signal to noise ratio of spectra (figure 1). Non-enhancing lesions In order to inform upon voxel placement in non-enhancing tumours, both ADC and perfusion weighted imaging were used to guide voxel placement to ensure high yield. Hemorrhagic lesions High order shimming

Results

Through the optimisation of acquisition protocols, we have acquired a large number of high quality MRS data over last 7 years, aiding in the diagnosis and monitoring of neurological and neurosurgical diseases. Here we have shown example cases where optimisation of MRS acquisition allows for the collection of additional metabolic data in challenging regions of the brain.

Conclusions

In conclusion, with appropriate alterations to acquisition parameters, optimised voxel placement, and shimming we have shown that MRS can be reliably acquired in a number of regions that are commonly avoided, allowing for further adoption of spectroscopy in to clinical practise.

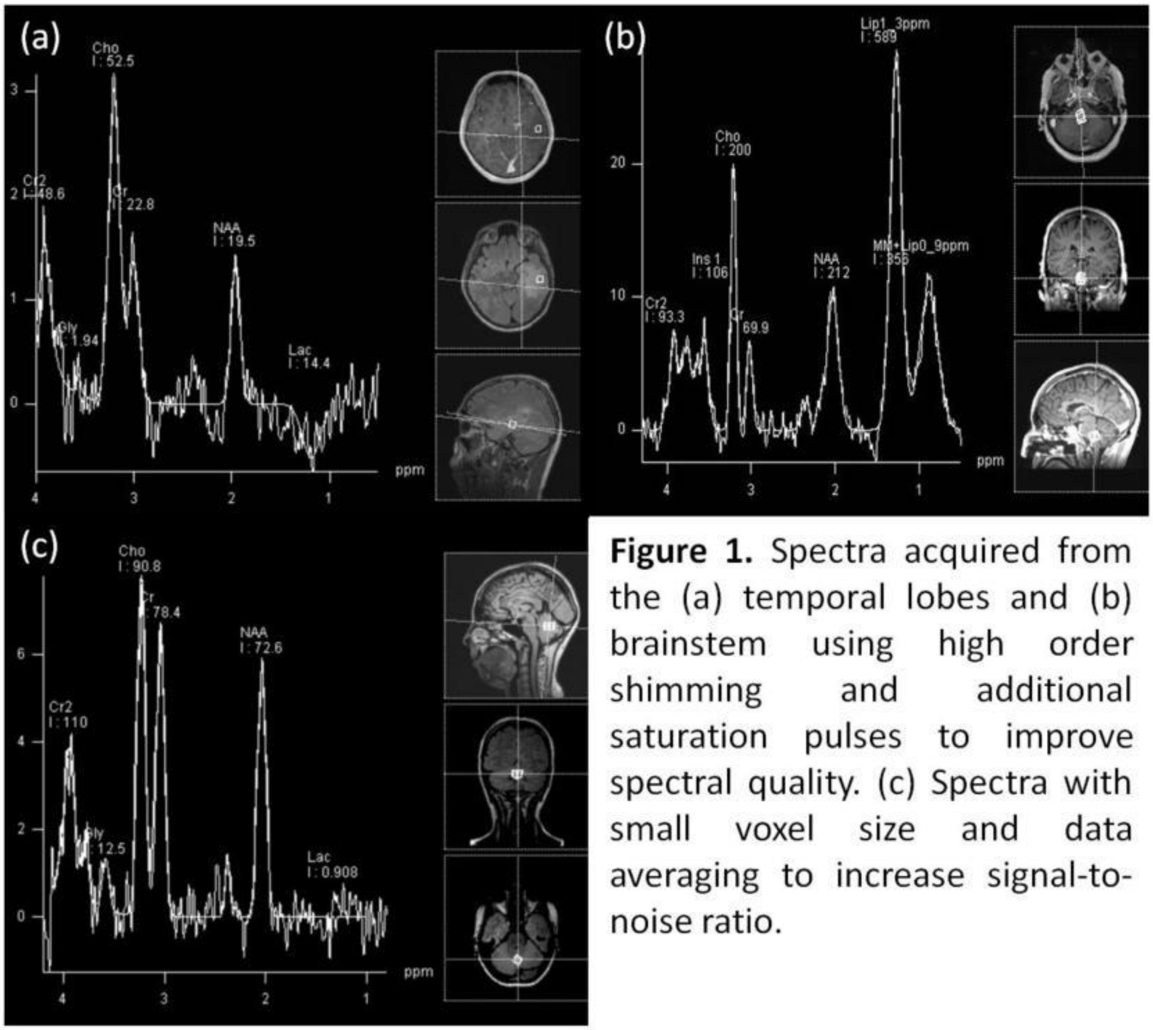

Figure 1. Spectra acquired from the (a) temporal lobes and (b) brainstem using high order shimming and additional saturation pulses to improve spectral quality. (c) Spectra with small voxel size and data averaging to increase signal-to-noise ratio.

(Filename: TCT_2891_Capture.JPG)

2190

Overview of Primary CNS Lymphoma and its Spectrum of Imaging Findings

J Mahan[1], C Glastonbury[2], S Cha[3], J Villanueva-Meyer[4]
[1]UCSF, San Francisco, CA, CA, [2]UNIVERSITY OF CALIFORNIA, SAN FRANCISCO, SAN FRANCISCO, CA, [3]University of California San Francisco, San Francisco, CA, [4]University of California - San Francisco, San Francisco, CA

Purpose
The purpose of this exhibit is to showcase the wide spectrum of imaging appearances of primary CNS lymphoma and to give an overview of clinical management and treatment.
Materials and Methods
Teaching points: - Pathologically proven cases of primary CNS lymphoma (PCNSL) involving the brain and spine will be presented to showcase the wide range of imaging appearances. - Imaging features that the radiologist can recognize will be highlighted so that the primary diagnosis may be suggested in the differential. - Review of the most recent WHO PCNSL classification. - Discuss the workup of PCNSL

and the information useful for referring providers. - The evolution of current management of PCNSL will also be briefly reviewed.

Results

Outline: - Overview and work-up of primary CNS lymphoma (PCNSL). 1) Clinical assessment and work-up to diagnose PCNSL. 2) Characteristic imaging features observed with intracranial lymphoma. 3) Factors that determine patient prognosis. - 2016 WHO classification: 1) Immunodeficient: a) AIDS-related diffuse large B-cell lymphoma (DLBCL), b) EBV-positive DLBCL, c) Lymphomatosis granulomatosis. 2) Immunocompetent: a) DLBCL, b) low-grade DLBCL, c) Intravascular DLBCL, d) T-cell lymphoma, e) NK/T-cell lymphoma, f) anaplastic large cell lymphoma ALK-positive, g) anaplastic large cell lymphoma ALK-negative, h) MALT lymphoma of the dura. - Present a wide range of cases of primary CNS lymphoma highlighting the variation of imaging appearances. - Discussion of the evolution of therapy and the current treatment regimens.

Conclusions

Primary CNS lymphoma (PCNSL) is a rare form of extranodal non-hodgkin lymphoma confined to the brain, cranial nerves, meninges, eyes, and cerebrospinal fluid (CSF) without evidence of systemic disease. PCNSL can broadly be categorized into an immunocompetent and immunocompromised patient population, with some registry studies suggesting that the former incidence is progressively increasing. The recent WHO 2016 classification describes subsets for immunodeficiency-associated, diffuse large B-cell, and non-B cell PCNSL. The objective of this exhibit is to: 1) Showcase the wide range of imaging presentations of lymphoma; 2) Discuss the most recent WHO 2016 classification; 3) Highlight information the radiologist can provide to the referring provider to help with work-up, treatment and prognostication; and 4) Discuss the evolution of treatment and the current standard of care.

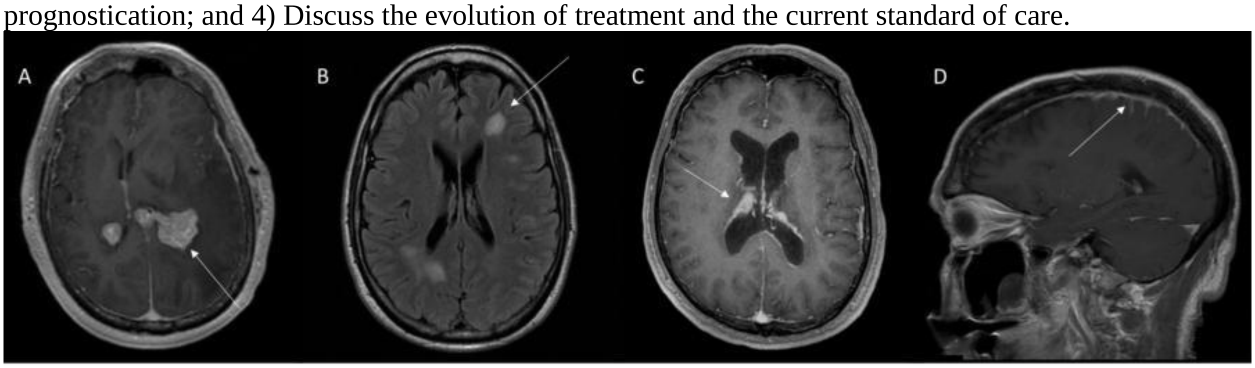

Figure 1: Cases highlighting the spectrum of Primary CNS Lymphoma (PCNSL)
A) Multifocal enhancing masses within the atria of the lateral ventricles consistent with PCNSL of the choroid plexus.
B) Multifocal periventricular FLAIR hyperintensity and faint linear enhancement in a perivascular distribution (not shown) consistent with intravascular PCNSL.
C) Periventricular subependymal nodular enhancement consistent with subependymal PCNSL.
D) Pachymeningeal and leptomeningeal enhancement overlying the cerebral convexity, consistent with MALT lymphoma of the dura.

(Filename: TCT_2190_LymphomacasesforabstractFINAL.jpg)

2822

Paragangliomas of the Head and Neck: A Practical Approach to Diagnosis and Review of Detailed Anatomy at Sites of Origin

C Hasbrook[1], S Noujaim[1]

[1]*William Beaumont Hospital, Royal Oak, MI*

Purpose

The objective of this presentation is to review related, detailed anatomy of the skull base jugular fossa, temporal bone and carotid space of the upper neck where most of the head and neck paragangliomas are found.

Materials and Methods

The authors will use original drawings to help the reader better understand the locations of the jugular fossa structures and to easily identify the location of the inferior tympanic canaliculus and mastoid canaliculus, which carry Jacobson's nerve and Arnold's nerve, branches of the CN IX and CN X, respectively. This will be followed by illustrations with MRI, CT and angiography images of the various types of paragangliomas and discussion of findings and differential diagnosis.

Results

Paragangliomas are slowly growing hypervascular neuroendocrine tumors arising from neural crest paraganglia cells distributed throughout the body. The largest concentration is in the adrenal medulla with smaller collections in the paravertebral space and head and neck region. Paragangliomas in the head and neck present with symptoms of mass effect such as cranial nerve palsy, palpable mass and tinnitus. Paragangliomas are rare, comprising <0.5% of head and neck tumors. They are classified according to their location: Carotid bifurcation (carotid body tumor), most common paraganglioma of the head and neck, > 50%. Glomus tympanicum, second most common, located within the tympanic cavity overlying the cochlear promontory. It originates from paraganglia cells of the inferior tympanic nerve (Jacobson's nerve), a branch of the glossopharyngeal nerve. Glomus jugulotympanicum arising from paraganglia cells of Arnold's nerve, a mastoid branch of the vagus nerve. Glomus jugulare, confined to the jugular fossa. Glomus vagale, originating from the inferior (nodose) ganglion of the vagus nerve.

Conclusions

The majority of paragangliomas in the head and neck occur in predictable anatomic locations. Knowledge of this anatomy along with characteristic imaging findings allows for accurate diagnosis.

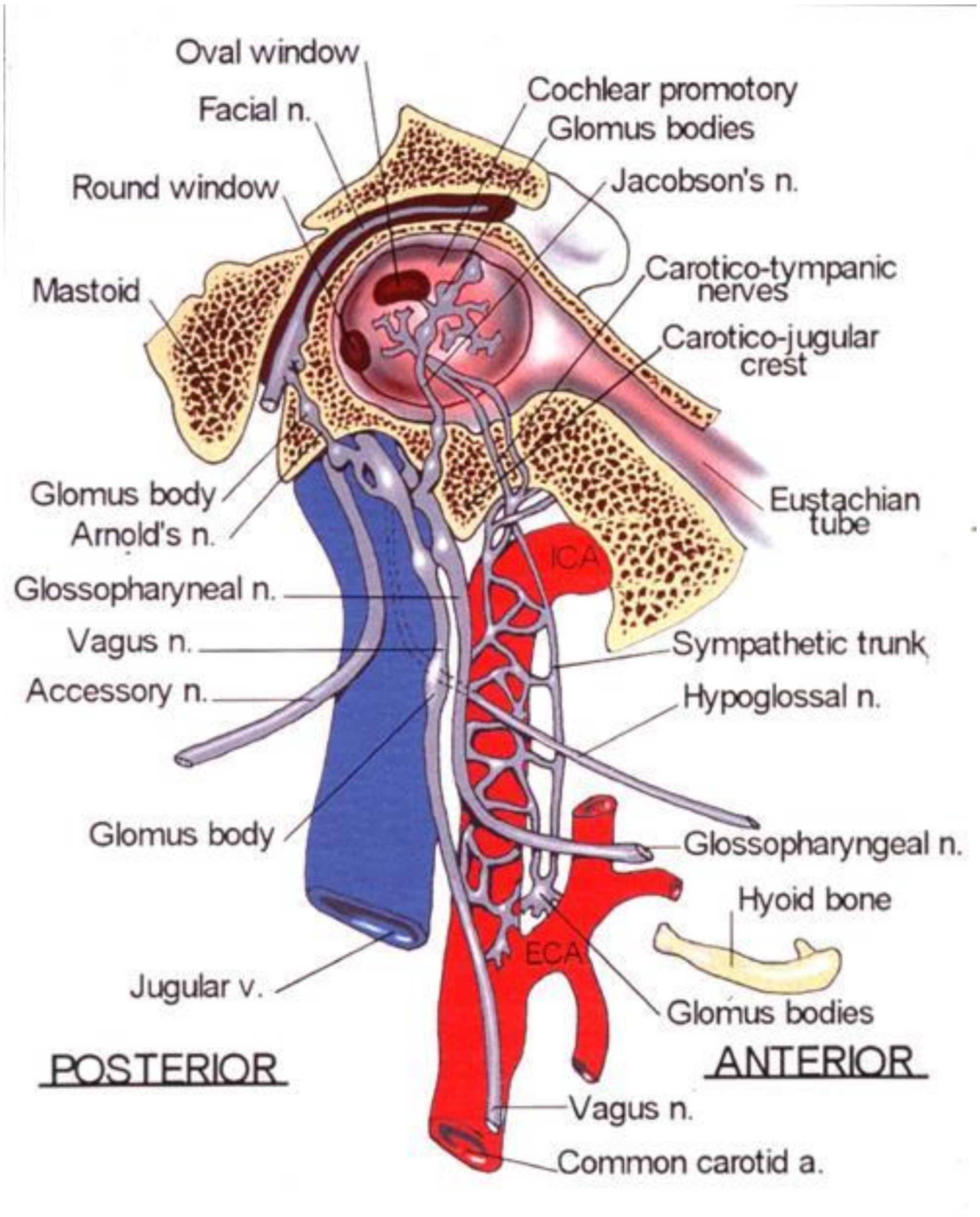

(Filename: TCT_2822_ParaganglialcellsSagittal.JPG)

2600

Parathyroid Imaging: Breaking Through the Maze

A Costacurta[1]
[1]*CLINICA FELIPPE MATTOSO, RIO DE JANEIRO, Brazil*

Purpose
Primary hyperparathyroidism is a disorder of excess secretion of parathyroid hormone leading to hypercalcemia.Most cases of primary hyperparathyroidism are caused by a solitary parathyroid adenoma (88%). Directed parathyroidectomy is a minimally invasive surgical technique and when combined with

intraoperative parathyroid hormone assay, demonstrates high cure and low complications rates. Critical to the success of a directed technique is preoperative localization of the abnormal parathyroid gland. Traditional imaging modalities such as sonography and sestamibi-SPECT demonstrate high specificity when concordant, but suboptimal sensitivity in most hands. Four-dimensional Computed Tomography (4D CT) has emerged as a useful imaging modality to detect parathyroid lesions causing primary hyperparathyroidism, particularly in some sonographically inaccessible regions such as the mediastinum. Magnetic resonance is sometimes also used. Besides the radiologist's ability to detect a candidate lesion and differentiate it from mimics, his role has evolved to a consultant position, translating different diagnostic methods into a probable diagnosis and location and helping the surgeon plan his approach. The purpose of this pictorial essay is to review the embriology and anatomy of the parathyroid glands, discuss advantages and disadvantages of different techniques and imaging findings, providing the radiologist tools for a more robust evaluation.

Materials and Methods

Review embriology and anatomy of the parathyroid glands. Briefly review the clinical aspects of hyperparathyroidism. Discuss different imaging modalities such as ultrasound, sestamibi-SPECT, 4D CT and dynamic MRI. Describe the radiological findings (with emphasis in 4D CT)

Results

Embriology and anatomy of the parathyroid glands. Clinical aspects of hyperparathyroidism. Blood tests related to clinical diagnosis. Imaging techniques such as ultrasound, sestamibi-SPECT ,4D CT and dynamic MRI : strengths and limitations of each method and current trends. Imaging characteristics of adenomas,multifocal disease, hyperplasia and carcinoma . Imaging pitfalls and mimics

Conclusions

Hyperparathyroidism can be cured with resection of the overactive gland and minimally invasive surgery emerged as the favored approach. Radiologists must be familiar with the disease and the expected location of the glands, being also aware of ectopic glands and potential mimics. It is also important to understand the different modalities currently used in the diagnostic workup to correctly evaluate and localize the lesions, guiding the clinician or the surgeon out of the maze.

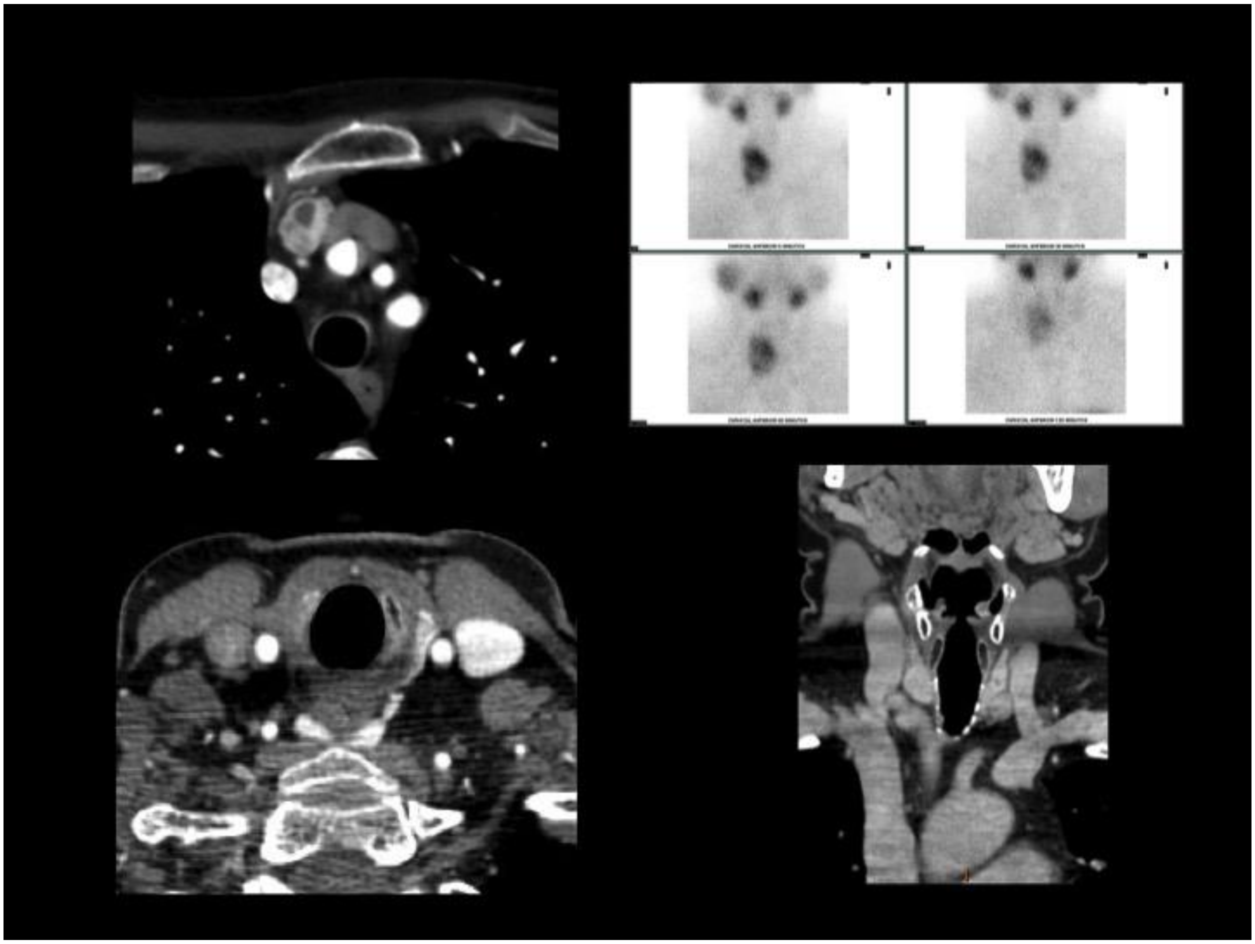

(Filename: TCT_2600_Slide1.jpg)

3622

Patterns of Anoxic Brain Injury

M Hensley[1], J Dunkin[2], C Downing[2], R McEvoy[1], M Vaitses[1]
[1]Stony Brook University at Mather Hospital, Port Jefferson, NY, [2]Stony Brook University - Mather Hospital, Port Jefferson, NY

Purpose
To review the expected pathophysiology and expected patterns of anoxic brain injury in specific anatomic locations within the brain. To familiarize the Radiologist with the acute and subacute image findings and distinct pattern distributions of anoxic brain injury, as prompt diagnosis is essential for determining the best patient management and care. To provide a case-based review of various complications and patterns throughout literature, as well as seen at our institution, to include clinical presentations, radiographic diagnoses, and management.
Materials and Methods
Acquisition and review of CT and MRI images of types of Anoxic Brain Injury to include; Focal Cerebral Ischemia, Global Cerebral Ischemia, and Diffuse Cerebral Hypoxia. Acquisition and review of CT and MRI findings of acute vs subacute patterns of anoxic injury. Cased-based review to discern different evolving patterns of Anoxic Brain Injury to include; Hypoxic-Ischemic brain injury in the Neonate, Carbon Monoxide Poisoning, Opioid Overdose, Asphyxiation, and Cardiac Arrest.

Results
Grey matter is especially susceptible to ischemia and hypoxia. The grey matter is more preferentially affected because it is more metabolically active than white matter secondary to the large number of synapses grey matter contains which are highly vulnerable to anoxic insults. Primary anatomic sites affected are the thalamus, cerebral cortex, basal ganglia, cerebellum, and hippocampus. Image findings greatly depend on the etiology of the anoxic insult, the severity of the insult, the duration of the insult, and any underlying co-morbidities.
Conclusions
The Radiologist should be familiar with the common and uncommon characteristics and patterns of Anoxic Brain Injury, as well as be able to discern the early signs of evolving injury for determining the best plan for patient management and care.

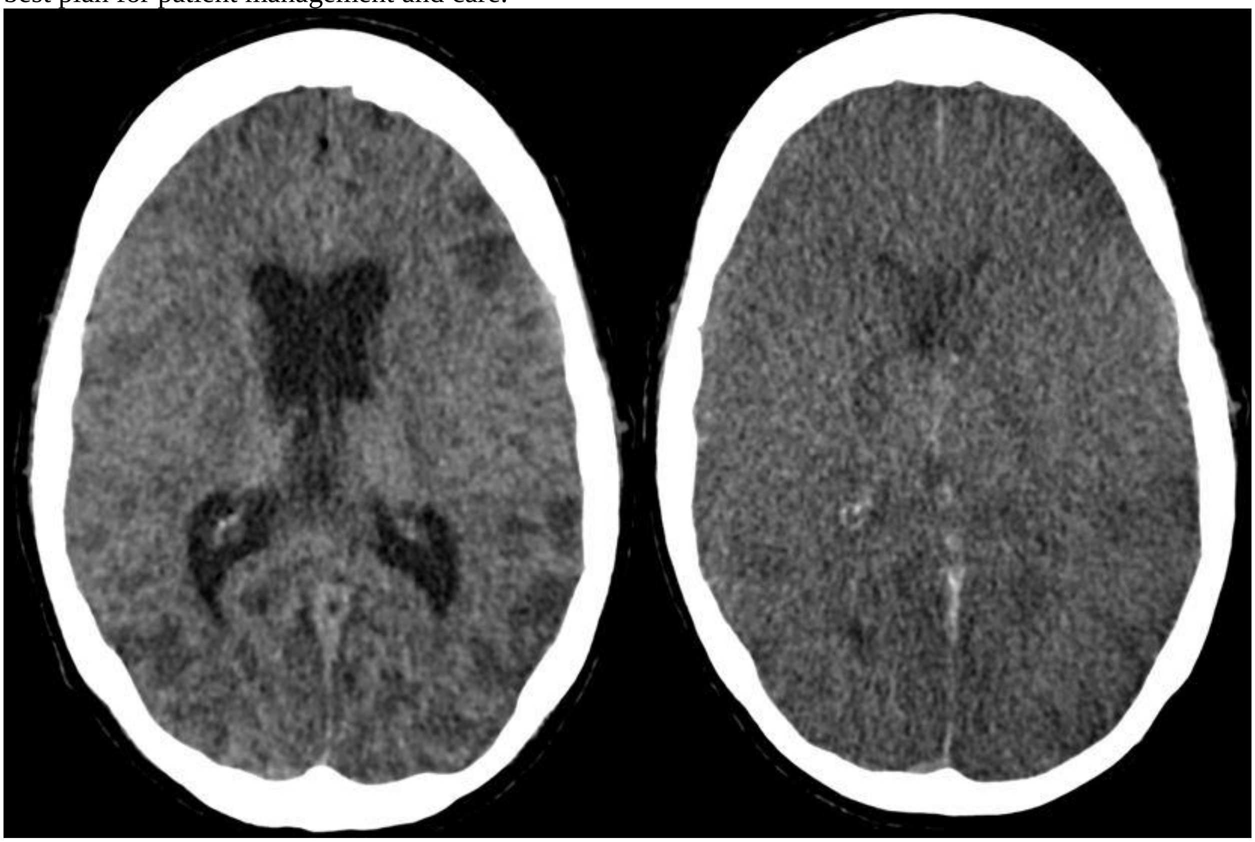

(Filename: TCT_3622_EvolvingABISecondaryOpioidAbuse.jpg)

3121

Patterns of CT Perfusion False Penumbras: What Radiologists Need To Know

R Assadsangabi[1], L Bagley[2]
[1]University of Pennsylvania, Philadelphia, PA, [2]UNIVERSITY OF PENNSYLVANIA MED CTR, BALA CYNWYD, PA

Purpose
CT perfusion (CTP) is increasingly used to assess ischemic penumbra in order to determine the potential utility of mechanical thrombectomy in cases of large vessel occlusion. However, CTP is susceptible to multiple technical and diagnostic challenges. Our aim is to discuss different causes of false penumbras, and the ways to identify them.

Materials and Methods
We reviewed literature and searched CTP studies performed at our institution. We also reviewed relevant CT, CT angiogram, MRI and cerebral angiogram when available for each patient.
Results
We identified two major categories responsible for false penumbras: technical errors, and pre-existing altered vascular anatomy/physiology. We found inappropriate contrast bolus timing or improper administered contrast amount may lead to either falsely negative or false penumbras. Other confounding technical factors are inappropriate thresholding due to infarction in contralateral hemisphere and motion. Different causes of altered vascular anatomy/physiology including upstream flow restriction, evolution of ischemic change, vascular dysregulation, and variation in anatomy of the circle of Willis were recognized as potential sources of perfusional abnormalities. We will discuss imaging patterns of each etiology with multiple examples.
Conclusions
Familiarity with technical and diagnostic challenges of CTP may help radiologists to recognize imaging patterns of false penumbras and avoid costly errors in diagnosis and treatment.

3536

Pediatric Head and Neck Vascular Anomalies Based on Most Current Revised Classification of International Society for the Study of Vascular Anomalies (ISSVA): A Radiologist's Primer

R Patel[1], H Banker[1], A Kamali[1], S Khanpara[1], R Riascos[1], E Bonfante-Mejia[1]
[1]*The University of Texas Health Science Center at Houston, Houston, TX*

Purpose
1. Overview of 2014 revised ISSVA (International Society for the Study of Vascular Anomalies) classification. 2. Describe appropriate approach and imaging modality for vascular anomalies identification. 3. Demonstrate imaging characteristics of vascular anomalies according to most recent ISSVA classification. 4. Overview of associated syndromes with vascular anomalies. 5. Brief overview of management of these vascular anomalies.
Materials and Methods
- Retrospective search in "PACS" database at a large tertiary care academic hospital was performed for the term "Pediatric Head and Neck Vascular Anomalies" in from 2002 - 2017. - The ISSVA (International Society for the Study of Vascular Anomalies) classification was utilized as a framework for discussion.
Results
Representative examples of various Pediatric Head and Neck Vascular Anomalies were presented as case based review with inclusion of clinical findings, imaging (USG, CT, MRI) findings, pathological-genetic correlation, treatment options.
Conclusions
1. Revised ISSVA Classification is an effective method for radiological diagnosis. 2. Accurate diagnosis with classification helps to determine appropriate management. 3. Diagnosis and management of vascular anomalies requires close collaboration between Neuroradiologist, Interventional Radiologists and Pediatric Plastic Surgeons.

3592

Performing and Reporting Regional Brain Volumetric Measurements (neural quantification) in a General Radiology Practice

A Yang[1]
[1]*Howard County General Hospital JHMI, Lutherville, MD*

Purpose

Quantitative volumetric analysis of regional brain atrophy or hypertrophy allows rapid quantification of regional brain pathology usually not detected on routine imaging. This is most useful in neuro degenerative disorders where the only abnormality on routine mri imaging may be regional or global atrophy .The pattern of specific regional atrophy may suggest a pattern supporting or discouraging the diagnosis of suspected specific neurodegenerative diseases. Serial measurement of brain regional brain atrophy may be used to provide an objective biomarker of the rate of disease progression in neural degenerative processes . As clinical assessment of neural degenerative functional decline is often superficial, communicating the function of the specific abnormal parts of the brain on mri morphometric measurement may help referring neurologist or internist to more precisely assess the deficit, e.g. auditory encoding vs facial recognition vs semantic memory and then suggest compensatory strategies for patients and support circle to partially compensate for the specific functional deficit. This presentation illustrate the performance , pitfalls and potential clinical uses of quantitative brain morphometric analysis in general radiology practice using commercially available software that automates the image segmentation and volumetric measurements, comparison with age matched data base and presentation in color coded chart.

Materials and Methods

Imaging protocol: Routine brain imaging was performed on each patients to detect non degenerative pathologies in the brain and reported separately. The routine brain imaging uncovers strokes, demyelination, post traumatic encephalomalacia, calcium and iron deposition and susceptibility artifacts which may prevent accurate volumetric analysis. A single 3D sagittal spoiled gradient echo (T1) weighted images is then acquired using TR 7/TE 3 ms FA 8 degrees 256 x 256 matrix 1 average 1-1.2 mm slice thickness/0 gap and sent by MR technologist for post processing. using commercially available software (in this case, NeuroQuant by Cortech Labs v. 2.3.0). Other vendors and public domain software are also available.. The result is usually available in few minutes. The quantitative regional brain volumes are segmented and are compared by the software with a data base of aged matched normal controls and listed and color coded in a brain morphometry or regional atrophy report and sent back to the radiologist for review. The areas of marked atrophy (usually at the 1-3 percentile level compared to normal) are analyzed to see if is close to a described type of dementia . The brain morphometry chart, and the description of the specific function of each of the severely affected parts of the brain are also provided to the referring physician for correlation with the patient's specific symptoms on followup clinical visit. If a longitudinal comparison is available, the deviation from age related progression is described in the report. In this presentation, the regional brain atrophy pattern in 10 patients are illustrated and some pitfalls of segmentation and interpretation illustrated. .

Results

Two illustrative case : 1. 33 year old with exposure to mold 2 years ago. marked atrophy of the inferior temporal gyrus, involved in using visual memory for identify visual pattern , NOT described for mold related chronic inflammatory response syndrome 2. 77 year old with memory loss x 1 month Neural quantification shows atrophy of superior frontal cortex (involved in self awareness), middle temporal gyrus (involved in recognition of known faces, complex characters such as in Asian languages) inferior temporal gyrus involved in using memory to identify visual objects and the fusiform gyrus, a linkage point in using memory to identify visual objects. atrophy of the pallidum and ventral diecephalon. ?frontotemporal dementia see morphometry report Currently we do not have access to a verified age, ethnic and gender specific database for most specific disease entities and cannot provide diagnosis with high specificity. If these data bases can be accumulated, it may be possible to use deep learning neural networks to improve recognition of specific dementia patterns from the volumetric atrophy patterns . A normal examination , or findings contradictory to the suspected diagnosis, however may trigger search for alternative explanations for patient's symptoms. e.g. memory loss due to chronic sleep deprivation or medication use etc. The lack of large disease specific data base and availability of large quantities of volumetric imaging data with each study may trigger utilization of brain morphometric quantification by patients and/or their medical legal advocates eager to find evidence to support injury in poorly understood entities such as mild posttraumatic brain injury syndrome, post traumatic stress disorder, exposure to toxins (such as pesticides, herbicides, building chemicals), biotoxins such as mold and chronic inflammatory response syndrome (CIRS), Little data to provide cause and effect conclusions linking regional atrophy and these entities .

Conclusions

Volumetric neural quantification is a useful tool to detect regional atrophy or hypertrophy not usually picked up on routine brain imaging. Regional atrophy implicate deficits relating to specific functions of the affected brain regions and may help clarify the patient's symptoms and potential compensatory strategies. Certain brain atrophy pattern may act like a fingerprinting suggesting specific dementia syndrome. The literature of brain morphometry quantification in specific disease states is increasing so reporting findings should include a current literature search on data on suspected diagnosis. As both radiologists and neurologists are learning the implications of regional pathologies previously not detected or reported, reviewing the known functions of those structures in the report may help referring physician reassess the symptoms. ,

MORPHOMETRY RESULTS

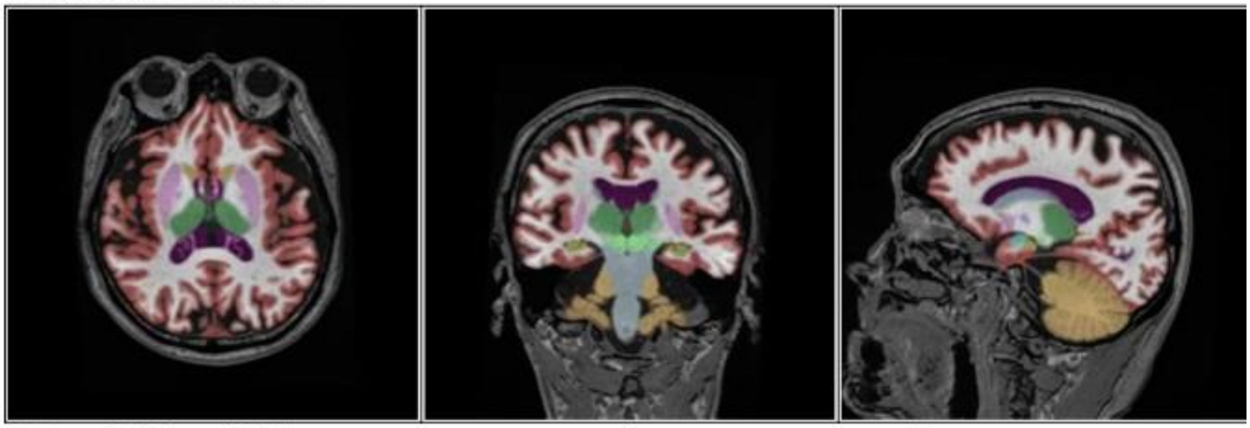

Intracranial Volume (ICV) (cm³)	ICV Percentile
1606.33	50

Total Volumes	Percentiles		
	Left	Right	Total
Cerebral White Matter	93	92	93
Cortical Gray Matter	4	6	5
Ventricles	30	29	29
Subcortical Structures			
Cerebellar White Matter	90	90	91
Cerebellar Gray Matter	81	78	80
Brainstem	-	-	44
Thalamus	86	95	92
Ventral Diencephalon	3	1	1
Basal Ganglia			
Putamen	81	93	89
Caudate	12	3	5
Nucleus Accumbens	94	93	96
Pallidum	1	1	1
Cingulate	96	93	95
Anterior Cingulate	97	90	95
Posterior Cingulate	99	96	98
Isthmus Cingulate	24	47	33

Cortical Brain Regions	Percentiles		
	Left	Right	Total
Frontal Lobes	6	15	10
Superior Frontal	1	1	1
Middle Frontal	55	47	51
Inferior Frontal	29	84	58
Lateral Orbitofrontal	41	36	38
Medial Orbitofrontal	86	89	89
Paracentral	44	17	29
Primary Motor	27	5	12
Parietal Lobes	11	9	9
Primary Sensory	13	3	4
Medial Parietal	34	27	30
Superior Parietal	34	7	16
Inferior Parietal	10	18	10
Supramarginal	21	85	50
Occipital Lobes	21	10	14
Medial Occipital	72	33	54
Lateral Occipital	7	8	4
Temporal Lobes	2	2	2
Transverse Temporal + Superior Temporal	8	10	6
Posterior Superior Temporal Sulcus	70	46	59
Middle Temporal	1	3	1
Inferior Temporal	1	13	3
Fusiform	2	1	1
Parahippocampal	15	17	13
Entorhinal Cortex	61	11	31
Temporal Pole	13	24	15
Amygdala	95	50	81
Hippocampus	79	46	65

(Filename: TCT_3592_77yearoldwithfrontotemporallobeatrophy.jpg)

3001

Perfusion and Diffusion-weighted Imaging of Pediatric Brain Tumors

M Lee[1], T Moritani[1], S Camelo-Piragua[2], J Kim[1], A Capizzano[1]
[1]UNIVERSITY OF MICHIGAN, ANN ARBOR, MI, [2]University of Michigan, Ann Arbor, MI

Purpose

• Emphasize the complementary roles that advanced MRI techniques such as diffusion and perfusion weighted imaging plays in pediatric brain tumors in addition to conventional MRI • Review specific features of diffusion and perfusion weighted imaging parameters of various types of pediatric brain tumors • Identify potential pearls and pitfalls when interpreting diffusion and perfusion weighted imaging of pediatric brain tumors

Materials and Methods

1. Overview of the basic physics and complementary roles of perfusion and diffusion-weighted imaging in pediatric brain tumors a) Perfusion: dynamic susceptibility contrast (DSC), dynamic contrast-enhanced (DCE), and arterial-spin labeling imaging (ASL) b) Diffusion: apparent diffusion coefficient (ADC), diffusion tensor imaging (DTI) - Distinguishing low-grade and high-grade tumors - Evaluating treatment effects - Differentiating recurrent tumors from pseudoprogression/radiation necrosis - Surgical planning 2. Characteristics of perfusion and diffusion-weighted imaging of various types of pediatric brain tumors a) Pilocytic/Pilomyxoid astrocytoma b) Subependymal giant cell astrocytoma (SEGA) c) Astrocytoma d) Oligodendroglioma e) Ependymoma f) Diffuse midline glioma g) Medulloblastoma h) Embryonal tumors i) Choroid plexus tumors 3. Potential pearls and pitfalls a) Perfusion: - Increased susceptibility artifacts near brain- air/bone interfaces and from blood products and calcification b) Diffusion: - ADC values can be affected by hemorrhage and calcification often found within tumors

Results

Pediatric brain tumors are a leading cause of morbidity and mortality in the pediatric patient population. Imaging evaluation for pediatric brain tumors can be challenging with nonspecific imaging features. While conventional MRI provides important information such as tumor location and size, advanced MRI techniques such as diffusion and perfusion weighted imaging provide additional meaningful information, as described in the methods section.

Conclusions

After viewing this exhibit, the reader will be familiar with the technical aspect and complementary roles of perfusion and diffusion-weighted imaging in pediatric brain tumors, their imaging features, and the pearls and pitfalls to make accurate diagnosis and treatment response assessment.

2450

Perineural Tumor Spread of Head and Neck Cancer: Anatomy and Imaging Features

I Kabakus[1], A Matthews[1], M Matheus[1], M Spampinato[1]
[1]*Medical University of South Carolina, Charleston, SC*

Purpose

Perineural tumor spread (PTS) refers to a form of contiguous neoplastic extension in which tumor cells spread to distant regions along the perineurium or endoneurium. It is considered an indicator of poor prognosis (decreased survival and greater risk of local recurrence and metastasis). The imaging findings can be subtle and easily missed, especially in the absence of known clinical findings. Our purpose is to review the normal cranial nerve (CN) radiological anatomy, and the imaging findings of PTS in head and neck cancer.

Materials and Methods

We will review the normal anatomy and cross-sectional imaging appearance of the CNs. Then, we will review cases of PTS from our institution teaching file. Each case will be accompanied by multiple-choice questions in an interactive format.

Results

The mechanism of PTS is unclear. It has been suggested that nerves represent natural conduits of least resistance for tumor cells to traverse. In the presence of PTS, primary and secondary imaging findings should be identified. Perineural tumor disrupts the blood-nerve barrier, which results in increased permeability, with leakage and accumulation of contrast agents. Tumor cell proliferation also results in thickening of the nerve, and effacement of the surrounding fat planes. Secondary imaging findings, such

as muscle edema in the acute phase or atrophy in the chronic phase, may be seen due to denervation. Imaging findings suspicious for PTS are nerve enlargement and enhancement, neuropathic muscle atrophy, obliteration of fat planes, soft tissue in the cavernous sinus and Meckel cave, foraminal enlargement, and erosion. MRI is superior to CT in the assessment of all findings, except for foraminal enlargement.
Conclusions
PTS is an important poor prognostic factor in the staging of head and neck malignancies. Knowledge of the anatomy of the CNs, and of the imaging features of perineural invasion is essential in head and neck oncology imaging.

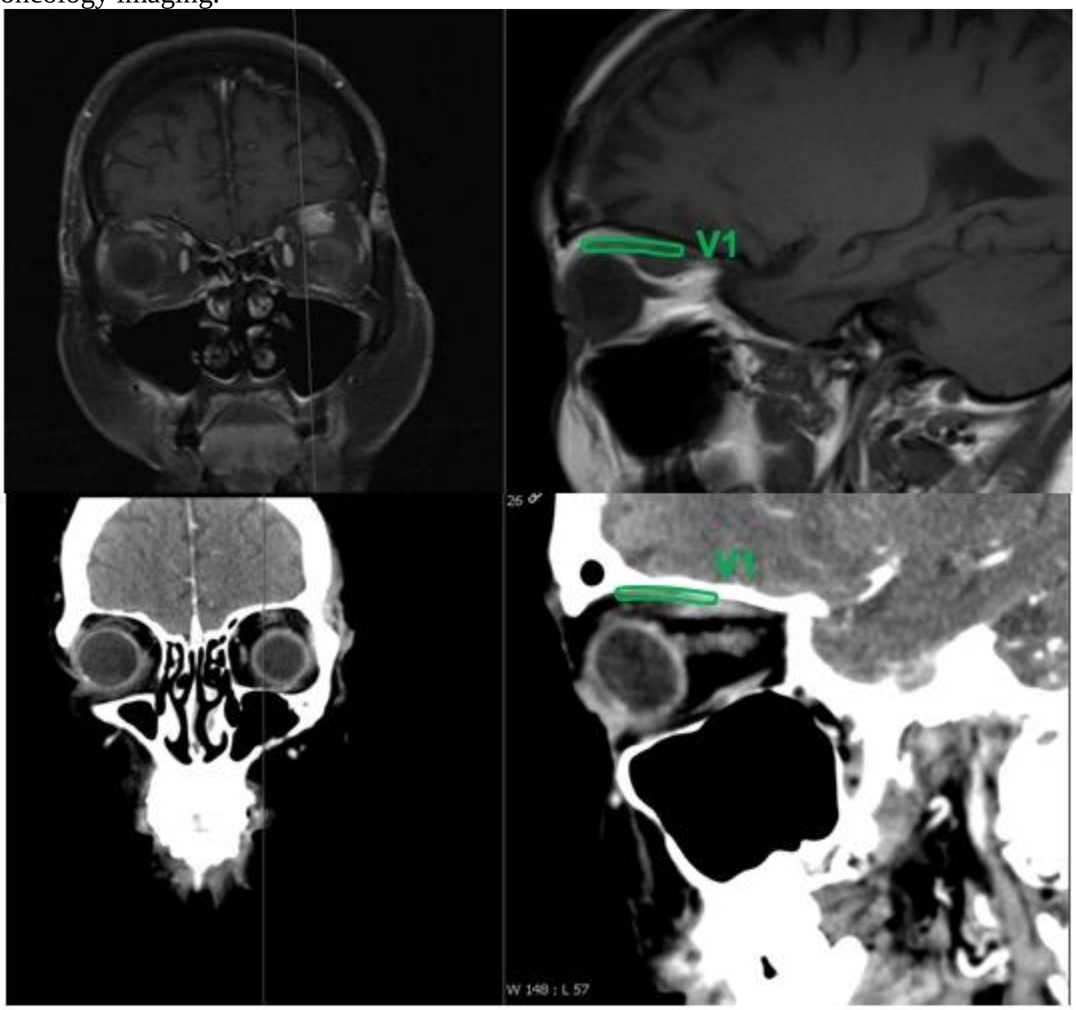

89 y.o. male patient with ulcerative skin lesion over the left eye brow.

(Filename: TCT_2450_PTS.jpg)

2835

Perivascular Spaces After Traumatic Brain Injury - Is There a Correlation?

G Barisano[1], P Patel[2], A Kathait[2], K See[3], S Ceglar[4], M Shiroishi[5], A Lerner[6]
[1]University of Southern California, Los Angeles, CA, [2]LAC+USC Medical Center, Los Angeles, CA, [3]University of Southern California, Pasadena, CA, [4]LAC+USC, Los Angeles, CA, [5]KECK SCHOOL OF MEDICINE, USC, SOUTH PASADENA, CA, [6]USC Keck School of Medicine, Los Angeles , CA

Purpose

Perivascular spaces (PVS), also known as Virchow-Robin spaces, are tubular fluid-filled structures that surround small blood vessels penetrating the brain parenchyma. Enlargement of PVS is a neuroimaging biomarker of small vessel disease and has been associated with a number of pathophysiological conditions. Inglese et al., using 1.5T MRI, reported a higher number of enlarged PVS is present in traumatic brain injury (TBI) patients, when compared with controls. Dilated PVS were identified primarily in the centrum semiovale, regardless of the interval time between the trauma and the MRI exam. Recently, the depiction and analysis of PVS significantly improved due to the increased spatial resolution achievable with the high field and ultra-high field MRI machines. Preliminary data using 3T MRI from Duncan et al. suggested that no statistically significant difference may be found in the overall number of PVS of mild TBI patients and those of normal subjects. In this study, we aim to further investigate this possible association the between number of PVS and TBI in previously reported anatomic regions at 3T MRI.

Materials and Methods

This retrospective study was performed in compliance with the Health Insurance Portability and Accountability Act. Patients were identified by using a radiology information search engine with the search term "traumatic brain injury" and their clinical charts were reviewed. Patients who suffer from mild TBI and have been previously imaged with 3T MRI of the brain were included. Age- and sex-matched subjects with normal brain MRI were used as controls. The number of PVS in centrum semiovale (PVSCS) and basal ganglia (PVSBG) was recorded on axial T2-weighted images using a validated 4-point visual rating scale. A semi-automatic and supervised segmentation method, based on PVS signal intensity and shape conforming to the path of penetrating arteries, was performed in order to evaluate the volume of PVS in the centrum semi-ovale.

Results

Nineteen subjects with unremarkable brain MRI (14 males, 5 females, mean age 42.5) and nineteen TBI patients (14 males, 5 females, mean age 41.6) were identified. In most cases, injury was related to motor vehicle accident or fall. We found that the mean number of PVSCS and PVSBG were 36.9±5.7 and 8.7±2.5 in TBI patients, respectively, and 34.1±6.2 and 9.42±2.6, respectively. The difference between groups was not statistically significant (pCS=0.152 and pBG=0.418, respectively). The estimated mean PVS volume in centrum semiovale was 1181.06±208.00 mm3 in TBI patients and 1165.79±241.88 mm3 in controls. The difference between groups was not statistically significant (p=0.836).

Conclusions

The number of enlarged PVS has been considered a potential neuroimaging marker of inflammatory changes associated with TBI particularly in the centrum semiovale. However, our results at 3T MRI demonstrate no difference in the number of PVS between TBI patients and normal subjects in the centrum semiovale as well as basal ganglia regions. Our results suggest that contrary to prior reports, PVS number, volume, and location may not be useful to establish or confirm the diagnosis of mild TBI. Further quantitative studies are required to investigate the effects of post-traumatic cerebral inflammation on PVS in order to identify morphological modifications on MRI that can be used for diagnostic, prognostic, and therapeutic purposes.

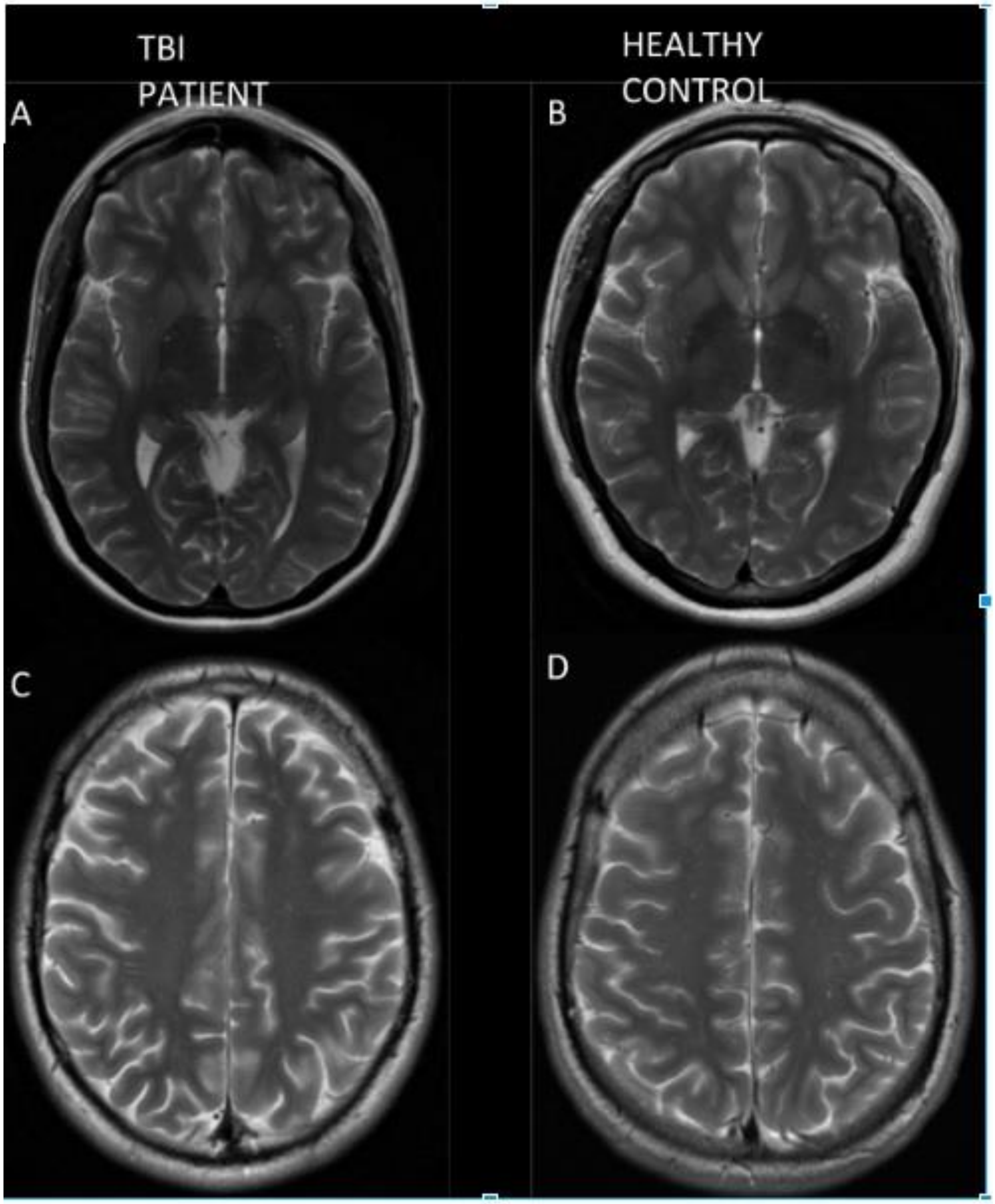

(Filename: TCT_2835_as.jpg)

2221

Pictorial Review of Current Concepts of Cerebellar Anatomic and Functional Anatomy

V Lehman[1], K Welker[2], D Black[2], D DeLone[3], T Kaufmann[3], W Brinjikji[3]
[1]MAYO CLINIC - ROCHESTER, MN, ROCHESTER, MN, [2]N/A, Rochester, MN, [3]Mayo Clinic, Rochester, MN

Purpose
The cerebellum is anatomically and functionally complex, but detail is often de-emphasized in radiology education and reporting. The seemingly complex anatomy is simplified by demonstration of a few key features of the fissures and white matter branching patterns. The cerebellum participates in multiple important functions including those of motor, language, attention, emotion, autonomics, and cognition.

The primary objectives of this educational exhibit are to: 1. Illustrate cerebellum anatomy, including lobule enumeration per Schahmann (I-X) and other common terminology with a color coded MRI overlay scheme. 2. Introduce key contemporary literature in the human brain mapping literature (connectivity with cerebral areas/networks, cerebellar lesion-symptom mapping, and automated methods for lobule parcellation with a color-coded MRI overlay scheme. 3. Illustrate functional anatomy, including zones, stripe/modules, and 3T and 7T fMRI signal. 4. Emphasize that the relatively expansive crus I and crus II have functional connectivity with the relatively large heteromodal association areas of the frontal and parietal lobes including connectivity to the default mode network about the horizontal fissure. Cerebral connectivity and cerebellar function demonstrates approximate mirror image organization about this expansion, with the majority of the motor activity localizing to the anterior lobe with somatotopic organization. 5. Demonstrate the appearance and location of the dentate, interposed, and fastigial cerebellar nuclei. Demonstrate functional organization between and within the nuclei and relevance for lesion-symptom mapping. 6. Illustrate the utility of the dentatorubral thalamocortical tractography for thalamic VIM nucleus localization for MRI-guided focused ultrasound ablation and DBS. 7. Demonstrate examples of deranged cerebellar anatomy including key congenital, toxic/metabolic, neurodegenerative, and vascular pathology.
Materials and Methods
The primary objectives will be illustrated primarily in visual form.
Results
The cerebellum demonstrates organized functional topography that corresponds to identifiable anatomic regions. Knowledge of this topography can facilitate interpretation of anatomic and functional neuroradiology studies and can facilitate clinical correlation.
Conclusions
An image-rich color-coded scheme is presented to illustrate the anatomy and function of the cerebellum.

2916

Pitfall! A Journey Through the Jungle of Head and Neck Imaging

W Stafford[1], E Escott[2], D Lukins[3], H Kapoor[3]
[1]University of Kentucky, LEXINGTON, KY, [2]UNIVERSITY OF KENTUCKY, LEXINGTON, KY, [3]University of Kentucky, Lexington, KY

Purpose
Head and neck imaging is replete with diagnostic pitfalls, which can complicate an area already fraught with anatomic and pathologic complexity. An overview of such pitfalls that include: commonly overlooked areas, normal variants that simulate disease, missing clinical history, and commonly unrecognized findings will aid the radiologist and prevent potentially costly diagnostic errors. Our exhibit will cover many of these pitfalls in an attempt to demystify a frequently daunting diagnostic challenge.
Materials and Methods
Cases encountered at our tertiary care academic medical center will be included in this educational exhibit. We will present specific cases that highlight more general categories of potential pitfalls in head and neck imaging, complete with multiple choice-type differential diagnoses to highlight common mistakes. These challenges are frequently related to the anatomic complexity of the region as stated; however, as we will demonstrate, other factors outside the radiologist's control also add to pitfalls in head and neck imaging, such as imaging artifacts, variations in imaging protocols, incomplete clinical histories, and exotic foreign bodies.
Results
Key examples will include cases that demonstrate findings including but not limited to: perineural tumor spread, retropharyngeal nodal disease, skull base meningoceles, jugular bulb pseudolesions, denervation changes, enlarged thoracic duct, alveolar ridge fractures, laryngeal cartilage fractures, soft palate

obturator, metabolic activity of nonparalyzed vocal cord misinterpreted as malignancy, and atypical retained foreign bodies.

Conclusions

At the completion of this exhibit, the radiologist will be better able to accurately interpret head and neck imaging studies by being aware of common imaging pitfalls.

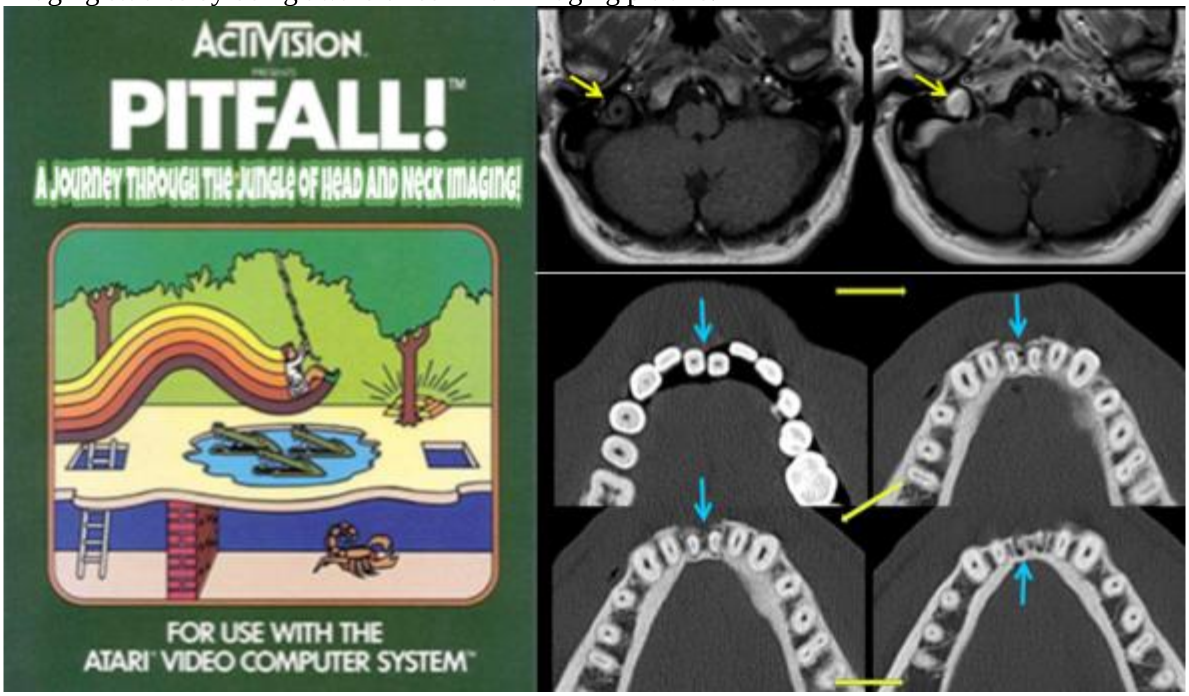

(Filename: TCT_2916_ASNR2019.jpg)

3217

Pitfalls in Post-operative Imaging of the Head and Neck

J Sommerville[1], J Van Den Heuvel[2]

[1]Royal Brisbane and Women's Hospital, Brisbane, QLD, [2]Royal Melbourne Hospital, Melbourne, Victoria

Purpose

Interpretation of imaging in the setting of previous treatment for head and neck cancer is difficult. The expected changes following surgery and radiotherapy need to be understood in order to detect potential residual disease or recurrence following treatment. This pictorial review aims to demonstrate expected findings that may be misinterpreted as disease, as well as subtle changes that should raise suspicion for recurrence.

Materials and Methods

A series of cases will be presented which will highlight the complexity of post-operative imaging following head and neck cancer.

Results

Cases will include post-surgical examples such as following hemiglossectomy, in which the residual normal tongue may be mistaken for tumour given the asymmetry within the oral cavity. Also, the residual thyroid lobe following laryngectomy which is often altered in position and can be misinterpreted as a nodal metastases. Other findings, such as denervation following nerve resection and asymmetry of soft

tissues will be presented. Cases highlighting subtle features that should raise suspicion for recurrence, including the development of new enhancement or nodularity will also be presented.
Conclusions
Knowledge of the expected findings following treatment for head and neck cancer is crucial as these changes may be misinterpreted as disease. It is important to be able to look beyond these changes in order to assess for features that may suggest tumour recurrence.

2590

Primer and Pitfalls of Deep Learning, Machine Learning and Artificial Intelligence and Its Role in Neuroradiology

A Noorbakhsh[1], D Ritchie[1], E Bergman[2], J Chen[2]
[1]Department of Radiology, University of California, San Diego, San Diego, CA, [2]Department of Radiology, San Diego Veterans Administration Medical Center, La Jolla, CA

Purpose
To review basic terminology and broad concepts in artificial intelligence as well as its limitations as it applies to the practicing radiologist. To enable viewers to evaluate better the peer reviewed published work on AI, and critically evaluate new technologies that may be implemented in the future.
Materials and Methods
Diagrams and examples of key concepts will be provided.
Results
Learning objectives in the exhibit will include: - Differences between artificial intelligence, machine learning, and deep learning. - Differences between supervised versus semi-supervised versus unsupervised learning. - Several pitfalls in machine learning including: (1) issues around causal inference and spurious associations, (2) the ability of images to be "hacked" or to have adversarial noise be added in order to intentionally cause misclassification, and (3) overfit of algorithms leading to difficulty in generalizing learning algorithms to new data. - Opportunities for machine learning to assist radiology, including improving image quality at lower radiation doses, analyzing data from images that may not be perceptible to the human eye (e.g. texture analysis in predicting tumor heterogeneity as a potential prognostic factor), and improving radiology scheduling, workflow, and prioritization of worklists.
Conclusions
Artificial intelligence is an exciting area of investigation and has several opportunities to augment radiology. Better understanding the strength and limitations of machine learning algorithms and deep learning will be critical to the practicing radiologist in order to fairly critique future peer reviewed work and to potentially apply new technologies in their future practice.

3100

Prionopathies and Prion-like Protein Aberrations in the Neurodegenerative Diseases

K Anderson[1], S Ahmad[2], M Mukhtar[3], J Brosch[1], M Veronesi[1]
[1]Indiana University, Indianapolis, IN, [2]Indiana University School of Medicine, Indianapolis, IN, [3]Indiana University School of Medicine, Plainfield, IN

Purpose
Amongst the neurodegenerative diseases (NDs), the prionopathies are best known for the ability of protein misfolding to self-propagate until neuronal dysfunction and ultimately neuronal death ensues. Rising evidence also indicates a potential role for a prion-like propogation of abnormal proteins in many other NDs. The purpose of this educational exhibit is to discuss specific neuroimaging characteristics,

diagnostic applications, and emerging therapeutics that are intended to identify and prevent the propagation of protein misfolding in prion diseases. Then we will elaborate on how a prion-like process may also be driving the progression of other neurodegenerative disease classes in a similar manner through a seeding mechanism.
Materials and Methods
The focus of this exhibit is to first highlight the role of key proteins propagating many of the known Prion diseases such as Acquired Creutzfeldt-Jakob disease (ACJD), variably protease-sensitive prionopathy (VPSPr), and genetic CJD (GCJD). We will discuss the imaging characterisitcs and emerging neuroimaging findings from our institution PACs. In the second part we will turn to detailing the prion-like attribute of multiple other neurodegenerative diseases such as Parkinson's disease (alpha synuclein), Alzheimer's disease (amyloid/tau), Huntington's disease (huntingtin), Amyotrophic Lateral sclerosis (TDP-43), and Multiple systems atrophy (tau). Neuroimaging findings and emerging therapeutics for these of NDs will be explained.
Results
In prion diseases, certain proteins in the brain lose their normal native ability to fold and instead form abnormal conformations, which then cluster into pathologic aggregates. This self-perpetuating process, known as protein misfolding, has been the focus of intense research over the past decade. The best known example is the prionopathies which spread like infections from host to host with death usually ensuing within 6 months. However, researchers are finding an underlying unifying propogation and spread of misfolded proteins in multiple other neurodegenerative diseases albeit in a more insidious and slower manner over many years.
Conclusions
Summary: Further understanding of the mechanism of prionopathies will ultimately lead to greater insight in the entire class of neurodegenerative diseases. This process will help improve earlier diagnostics of each class of diseases and help better guide emerging therapeutics. Educational Objectives: At the conclusion of this exhibit, the learner will: - Develop a better understanding of prionopathies and their neuroimaging characteristics. - Articulate the underlying mechanism that leads to prion disease. - Identify the protein abnormalities and neuroimaging characteristics in other neurodegenerative diseases. - Discuss how prion like processes underlie many of the other neurodegenerative diseases.

2852

Quantitative Diffusion Magnetic Resonance Imaging in Head and Neck Tumors

S Faerstain[1], S Payabvash[1]
[1]*Yale, New Haven, CT*

Purpose
Quantitative analysis of diffusion MRI can provide added value to structural and anatomical evaluation of head and neck tumors (HNT), by differentiation of primary malignant process, prognostic prediction, and treatment monitoring.
Materials and Methods
We will review the applications of quantitative diffusion MRI in identification of primary malignant tissue, differentiation of tumor pathology, prediction of molecular phenotype, monitoring of treatment response, and evaluation of posttreatment changes in patient with HNT.
Results
The quantitative analysis of diffusion MRI proves to offer far ranging potential applications in patients with HNT. The most common diffusion metrics evaluated in literature is the mean apparent diffusion coefficient (ADC), followed by the D value from Intravoxel Incoherent Motion (IVIM). Regarding differentiation of primary suspicious head and neck lesions, malignant tissues tend to have lower ADC values compared to benign lesions. In addition, ADC values can help with differentiation of malignant

thyroid nodules and salivary gland tumor histopathology. Similarly, ADC values can distinguish lymphomatous, metastatic, and benign lymphadenopathy from each other (in order of increasing average ADC values). In addition, lower average ADC in primary lesion of patients with oropharyngeal squamous cell carcinoma (SCC) is predictive of positive HPV status. With regards to prediction of treatment response, a low ADC or D values in pretreatment lesions, and early interval increase in ADC and D values during the treatment are harbinger of favorable response to therapy and outcome. Eventually, for distinction of post-treatment changes from residual or recurrent head and neck SCC, the malignant tissue tends to demonstrate lower average ADC.
Conclusions
Pending development of more standardized methods for image acquisition, quantitative calculation, and tissue segmentation, the diffusion MR metrics can be applied for HNT patients' selection, personalized treatment planning, and therapy surveillance in prospective trials.

3088

Radiological Requirements for Preoperative Planning in Cochlear Implant Candidates

W PHUTTHARAK[1], S Mukherji[2]
[1]Khon Kaen University, Khon Kaen , Thailand, [2]Michigan State University, East Lansing, MI

Purpose
Sensorineural hearing loss (SNHL) may result from congenital or acquired abnormalities of the membranous labyrinth or cochlear nerve. Cochlear implantation (CI) provides auditory benefits that range from simple sound detection to substantial word understanding and is considered an acceptable treatment for patients with severe to profound sensorineural hearing loss who are refractory to conventional hearing augmentation. The frequency of CI has substantially increased over the past decade and can be performed as an outpatient procedure. Imaging plays an essential part in the pre-treatment assessment of potential CI candidates and radiologists must be familiar with imaging findings that contraindicate implantation that could significantly affect surgery and outcome. The purposes are 1) Describe the components and function of a cochlear implant, 2) Discuss the imaging technique that are available to evaluate cochlear implant candidates, 3) Identify causes of hearing loss that may be amenable to CI CI, 4) Emphasize the imaging findings that contraindicate cochlear implantation, increase the likelihood of intraoperative complications, or result in poor outcome.
Materials and Methods
We review our experience in the pre-operative imaging assessment of patients for cochlear transplants. CT and MR findings are compared to assess the relative utility of the modalities and a practical, viable imaging protocol is suggested for use in the evaluation of candidates in cochlear implant surgical planning.
Results
The exhibit will describe the components of cochlear implants and the role of imaging in the pre-treatment evaluation of cochlear implant candidates. Illustration of anatomy relevant to cochlear implantation will be presented. Various causes of hearing loss that could impact surgical planning will also be illustrated. This exhibit will emphasize the imaging findings that contraindicate cochlear implantation that could significantly alter surgery.
Conclusions
Cochlear implantation has become an accepted treatment in patients with severe-to-profound sensorineural hearing loss. Radiologists have increasing role in evaluating these patients for optimizing outcome and avoiding operative complications.

2570

Rathke Cleft Cyst - What a Radiologist Needs to Know

H Nakamura[1], J Moriya[2], H Takasuna[3], M Doi[4], H Mimura[5]
[1]St.Marianna University of medicine, Kawasaki, Japan, [2]St.Marianna University of medicine, Kawasaki, Kanagawa, [3]St. Marianna University of Medicine, Kawasaki , Kanagawa, [4]St. Marianna University of Medicine, Kawasaski, Kanagawa, [5]St. Marianna University of Medicine, Kawawsaki, Kanagawa

Purpose
To demonstrate the radiological findings of Rathke's cleft cysts (RCCs) reviewing classical imaging sign and differential diagnosis. To demonstrate clinical issues regarding the natural history. To demonstrate the symptomatic cases
Materials and Methods
RCCs are congenital, non-neoplastic sellar and suprasellar cysts derived from remnants of Rathke's pouch. They are found in routine autopsies in 13% to 22%. Most of them are asymptomatic and they are more commonly discovered incidentally. From the radiological reports of recent 10 years, we investigated the radiological findings and features of clinical profile
Results
1) Radiological findings They are seen as an ovoid mass lesion in the sella, sometimes extending to suprasellar cistern, sharply demarcating itself from the surrounding tissue without remarkable mass effect. It is usually homogenous in appearance. On T1 weighted imaging, two-third of lesions are hyper intense and one third of it hypo intense. On T2 weighted imaging one fourth are iso intense, one fourth are hypo intense and rest hyper intense. But, based on signal intensity, the diagnosis is very difficult. We will demonstrate the characteristic signs. They are following: 1) intracystic nodule, 2) posterior ledge sign, 3) claw sign., 4) uncommon calcification in CT. Next, we will demonstrate the differential point between craniopharyngioma, pituitary adenoma, other cysts (including arachnoid cyst, colloid cyst). 2) Clinical profile. Most of them are stable, but some of them increase and spontaneously shrink over years, showing demonstrative cases. 3) Symptomatic cases We will demonstrate symptomatic (headache, visual loss, pituitary dysfunction) ,apoplexy (hemorrhage), and hypophysitis cases
Conclusions
RCCs themselves are silent, but the specific diagnosis is difficult unexpectedly. Because the clinical behavior is variable , sufficient knowledge bring us proper management

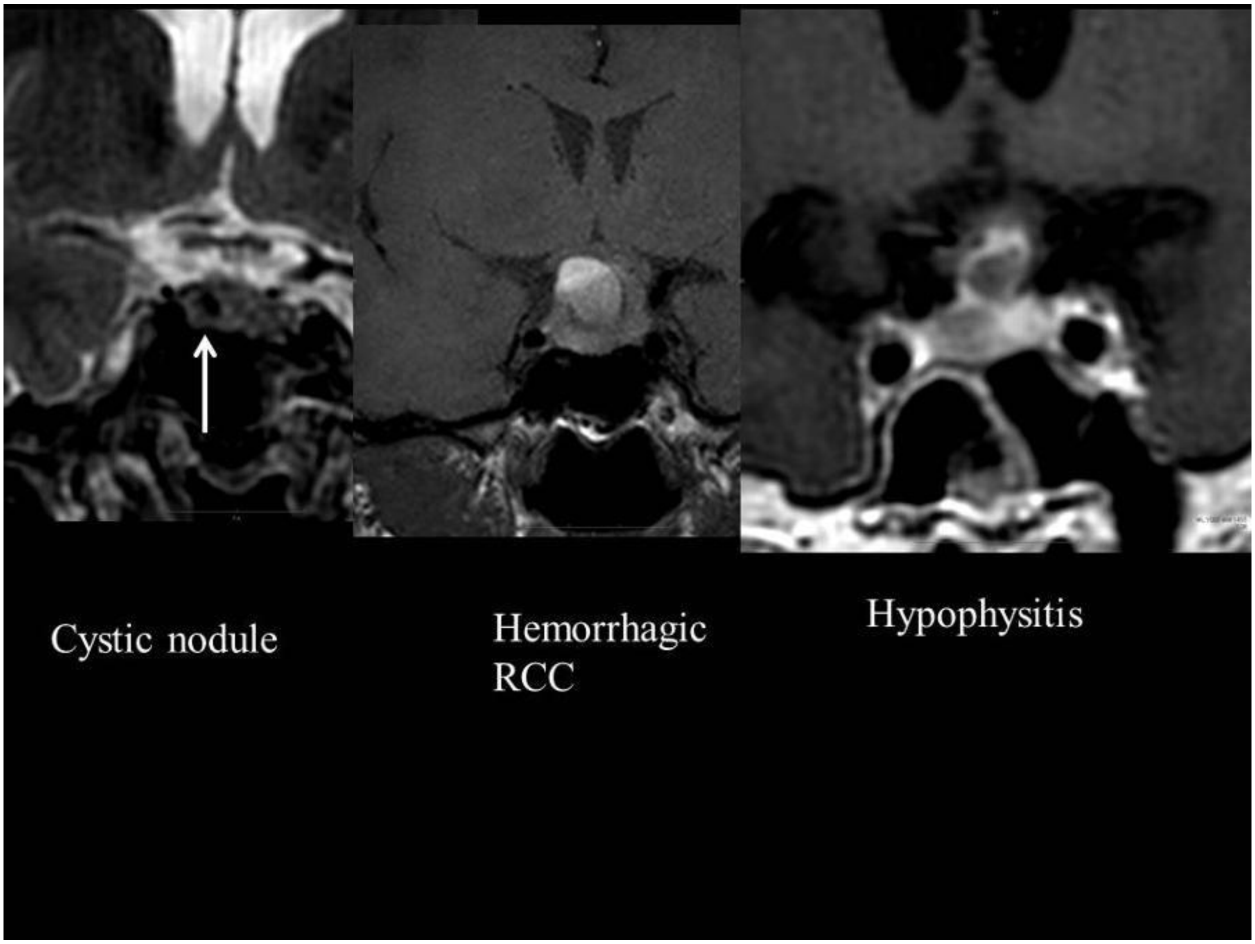

(Filename: TCT_2570_2019_ASNR_RCC_jpeg.jpg)

2479

REAHs and NUTs and SMARCBs, "WHO" knew – A Primer on the 2017 WHO Sinonasal Tumor Reclassification

E Young[1], A Bansal[1], S Patel[1], J Donahue[1], S Mukherjee[1]
[1]University of Virginia Health System, Charlottesville, VA

Purpose
The 2017 WHO Classification in Head and Neck Tumours represents both a conceptual and practical advance over its predecessor. Changes in the nasal cavity and paranasal sinus tumors classification scheme include both newer entities as well as reclassifying previously described lesions. In this exhibit, we discuss some of these new and revised entities, focusing on the more unusual tumor types with an emphasis on their imaging characteristics.
Materials and Methods
Based on the new 2017 WHO sinonasal tumor reclassification scheme, we selected a list of newly described tumors (NUT carcinomas, seromucinous hamartomas/respiratory epithelial adenomatoid hamartoma [(REAH] and biphenotypic sinonasal sarcomas) as well as some of the emerging entities (SMARCB1 [INI-1] deficient sinonasal sarcoma, renal cell-like adenocarcinoma and HPV-related carcinomas - including HPV-related carcinoma with adenoid cystic features). We present some of these cases including clinical findings, imaging characteristics, and pathology images.

Results

A complete list of changes in the 2017 WHO sinonasal tumor classification is beyond the scope of this presentation. Moreover, many of the sinonsanal tumors can have nonspecific imaging findings. However, a few of these lesions discussed here have unique imaging findings which a neuroradiologist should be familiar with. It is also important for the neuroradiologist to be acquainted with clinicopathological and molecular features of some of these lesions. Examples include the recently identified NUT and SMARCB1-deficient undifferentiated carcinomas. REAH and SH (seromucinous hamartoma) were previously thought to be the same tumor. These are now recognized as distinct entities and described under a new heading: the "Respiratory epithelial lesions". Other relevant changes include further defining HPV-related sinonasal carcinomas, including HPV-related carcinoma with adenoid cystic features, and addition of the new entity biphenotypic sinonasal sarcoma. SNUC still remains a diagnosis of exclusion. Lastly, many of the eponyms have been eliminated. For example, Schneiderian papillomas are now officially designated as sinonasal papillomas, with three unchanged subtypes (inverted, oncocytic and expophytic).

Conclusions

The new 2017 WHO sinonasal tumor reclassification scheme eliminates confusing or inaccurate nomenclature, introduces new histopathologically distinct tumors and refines relationships between tumors. Furthermore, remaining eponyms were removed, as were any neoplastic process that are not exclusive to the sinonasal region. The unique imaging and pathologic features are described in the presented cases. Although rare, the practicing neuroradiologist should be aware of these newer entities and their imaging characteristics so that accurate diagnosis and staging can be done for appropriate management.

(Filename: TCT_2479_REAHAxialT2forAbstract.jpg)

3672

Reporting Pertinent Positive and Negative Findings After CRANIOFACIAL Trauma, What the Radiologist Should Know

y levy[1], A Malhotra[2], A True[3], P A.Sideras[4], S Sakib[3]
[1]Yale, New haven, CT, [2]YALE UNIVERSITY SCHOOL OF MEDICINE, NEW CANAAN, CT, [3]Newark Beth Israel Medical Center, Newark, NJ, [4]Newark Beth Israel Medical Center, West Babylon, NY

Purpose
Imaging plays a critical role in Craniofacial trauma. It is therefore important that Radiology Residents, Fellows and Radiologists will be able to identify and communicate to the ED physician or Neurosurgeon the clinically relevant findings. In this educational presentation we will list the common imaging features of clinically and surgically relevant complications of Craniofacial trauma.
Materials and Methods
We will review pertinent Facial, Skull and Skull base anatomy. Using case based approach, we will list common injuries arising from blunt and penetrating trauma and discuss optimal imaging protocols. We

will list the common complications arising from these injuries and the importance of reporting pertinent positive and negative findings. We will conclude with case based module to review the principals mentioned above.
Results
Our educational presentation will include discussions of: Nasoseptal fractures - potential complications including impaired nasal breathing, abscess formation, and necrosis with resultant septal perforation Naso-orbitoethmoid (NOE) complex fractures - Frequent complications such as exophthalmos, telecanthus, cerebrospinal fluid (CSF) rhinorrhea Orbital fractures - Complications of orbital blowout fractures include extraocular muscle herniation and entrapment, intraorbital hemorrhage, globe injury, and injury to the infraorbital nerve in the presence of an orbital floor fracture Zygomaticomaxillary complex (ZMC) fractures - important in anticipating overall alignment and orbital volume change Isolated zygomatic arch fractures Occlusion-bearing maxillary fractures Alveolar process fractures - Because of the abundance of bacteria in the mouth, a fracture of the alveolar process is treated as an open fracture. Potential complications of alveolar process fractures include dental root avulsion, crown or root fracture, dental intrusion or extrusion, and malocclusion Frontal sinus fracture - Can result in CSF leak Paranasal sinus fractures - sinus drainage obstruction Mandibular fracture - Inferior alveolar nerve injury
Conclusions
Identification and discussion of Craniofacial related complications by the radiologist permit prompt management and an improved clinical outcome of these common traumatic injuries. This interactive educational presentation reviews the pertinent anatomy, optimal imaging protocol and imaging features of common facial fracture patterns. Interactive case based review will be provided for practice of the principals discussed.

2790

Review of Changes to Head and Neck Cancer Staging

M Beasley[1], M Matheus[2], A Matthews[3]
[1]MUSC, Charleston, SC, [2]MEDICAL UNIVERSITY OF SOUTH CAROLINA, MT. PLEASANT, SC, [3]Medical University of South Carolina, Charleston, SC

Purpose
Review changes to head and neck staging criteria in the 8th edition of the AJCC cancer staging manual.
Materials and Methods
-Brief summary of the differences in demographics, treatment, and prognosis between HPV associated and non-HPV associated head and neck cancer. -Review relevant anatomy within the head and neck, particularly as it relates to cancer staging. -Review the key changes in oropharyngeal cancer and head and neck cancer staging in the 8th edition of the AJCC Cancer Staging Manual.
Results
HPV related head and neck cancers have increased in prevalence in the last several years, even as new diagnoses of non HPV related head and neck cancers have decreased with the decline in tobacco use. HPV related cancers generally occur in younger patients (under 50 years of age), which is the demographic experiencing increased rates of new head and neck cancer diagnoses. The distinction between HPV and non HPV cancers is crucial, as HPV related cancers are associated with increased overall and disease free survival. Additionally, HPV positive cancers are more responsive to chemotherapy and radiation. Therefore, staging specific to the etiology of head and neck cancer is necessary to determine more accurate prognosis and treatment planning. By providing information in radiology interpretations relative to the new staging criteria, radiologists can better aid in the treatment of head and neck cancer.
Conclusions
The 8th edition of the AJCC Cancer Staging Manual introduces changes in the staging criteria for

oropharyngeal cancer and head and neck cancer. Accurate understanding of the updated staging criteria, relevant head and neck anatomy, and the different disease processes of HPV positive and HPV negative head and neck cancers can help radiologists become more valuable members of a multidisciplinary approach to treating head and neck cancer.

3116

Revolutionary Roles of Resting-state Functional Magnetic Resonance Imaging in Discovery and Staging of Alzheimer's Disease

S Emamzadehfard[1], V Eslami[1], Z Fulton[2], H Sair[3], K Clark[1]
[1]University of Texas Health Science Center, San Antonio, TX, [2]University of Texas Health Science Center San Antonio, San Antonio, TX, [3]JOHNS HOPKINS MEDICINE, BALTIMORE, MD

Purpose
Resting-state fMRI yields new insights into how structurally segregated and functionally specialized brain networks disconnected in AD. Hippocampus networks, the default mode network (posterior cingulate cortex and inferior parietal lobes, which also shown decreased metabolism in early AD), and the small world network (highly clustered vertex assemblies with a limited number of global shortcuts between clusters, which favors functional synchronization and resulted in high cognitive ability), were frequently discussed as the major involved networks in AD pathogenesis.
Materials and Methods
Decreased regional coherence in the posterior cingulate cortex/precuneus and increased coherence in the occipital and temporal lobe, including the bilateral cuneus, right lingual gyrus and left fusiform, meaningfully reduces with the progress of the AD.
Results
Spontaneous LFBF, (low-frequency blood oxygenation fluctuation), measured by resting-state fMRI was highly synchronous within the somatomotor system, has found to be decreased in the hippocampus of AD patients. Also, AD patients had greater persistence of resting fMRI noise in the medial and lateral temporal lobes, dorsal cingulate/medial premotor cortex, and insula.
Conclusions
1- Dysconnectivity between different brain areas are plausible explanations for many of the cognitive function deficits observed in AD. 2- Resting state fMRI, which has the advantages of no radiation exposure (versus PET/SPECT) and easy application (versus task-driven paradigms), has great potential for clinical diagnosis and treatment.

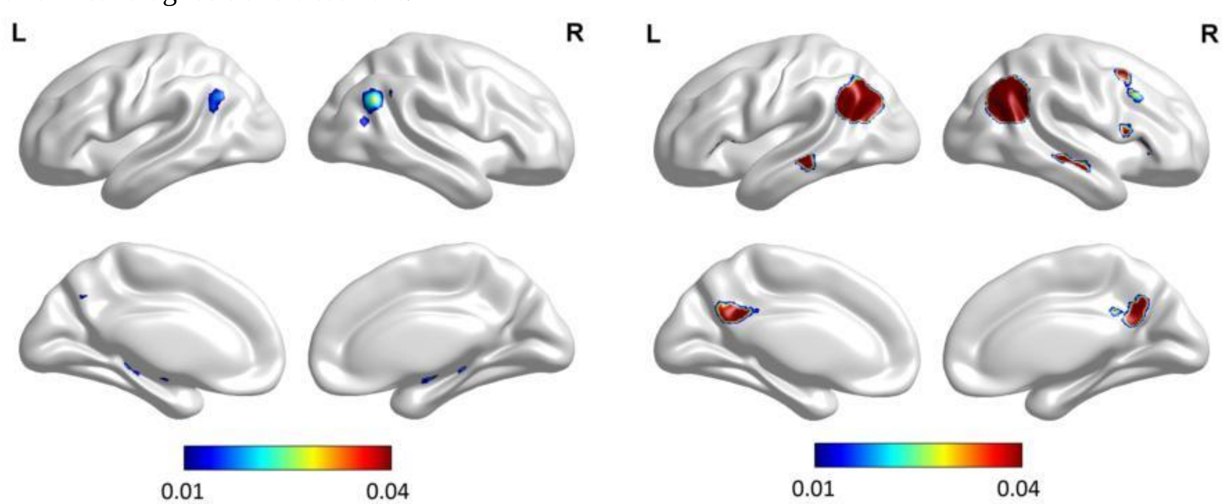

(Filename: TCT_3116_AD.jpg)

2503

Risk Stratification and Treatment Planning of Intracranial Aneurysms and Arteriovenous Malformations: The Role of Hemodynamics and 4D Flow MRA

W Chang[1], C Li[1], M Goldberg[1], J Villablanca[2]
[1]Allegheny Health Network, Pittsburgh, PA, [2]UCLA, Los Angeles, CA

Purpose
Aneurysm rupture carries high mortality/morbidity with 75% of patients with rupture suffering death or permanent neurologic deficits. However, treatment also carries significant risks. Determining which aneurysms are likely to rupture has high clinical utility. Size and growth have both been identified as risk factors. Hemodynamics and flow morphology may also have predictive value, with aneurysms with inflow jet morphology more likely to grow and rupture, while aneurysms with helical flow patterns are more stable. Wall shear stress(WSS) may also be useful, with aneurysms with high WSS demonstrating growth/rupture and those with low WSS also potentially demonstrating growth. Pressure is another hemodynamic factor that has been less commonly studied, but focal pressure differences may also predispose aneurysms toward rupture. Management of arteriovenous malformations is also challenging with both high morbidity from hemorrhage and higher morbidity from treatment. AVMs have a high risk of bleeding with 40-70% lifetime risk and annual risk of 1-33%. Risk factor analysis demonstrates the strongest predictor of hemorrhage is prior hemorrhage, which makes risk stratification on initial diagnosis challenging. Hemodynamics may offer some predictive value; some studies have noted different hemodynamic patterns in stable versus symptomatic patients. To date, acquiring these hemodynamic data have been challenging and often invasive, requiring DSA and computational flow dynamics (CFD) to calculate. The emergence of high resolution 4D Flow MRA has created an alternative technique that can acquire hemodynamic data in a non-invasive manner, without the use of intravenous contrast, in many cases.
Materials and Methods
In this presentation, we will describe the role of 4D flow in assessing both arteriovenous malformations and aneurysms, discuss how hemodynamics can be used for risk stratification, and describe new techniques and advances in both hemodynamics and 4D Flow imaging.
Results
4D Flow MRA can obtain both streamline plots to delineate flow morphology, WSS maps, and pressure maps for intracranial aneurysms in a non-invasive manner. Flow morphology can be modeled using streamline analysis to analyze the inflow jet and analyze WSS at the impact zone as well as pressure within the aneurysm dome. All of these hemodynamic factors have been shown to have value in predicting risk of rupture and growth. 3D printing is another technique that has been shown to be of value, allowing realistic vascular models to be generated that can be used with a flow pump to model flow in a realistic manner, or be used for treatment planning. 4D Flow MRA can also be used to obtain velocity/flow plots and WSS maps for arteriovenous malformations. 3D printing can also be used on these models to assess the anatomy for treatment planning.
Conclusions
4D Flow MRA has numerous applications for both risk stratification and treatment planning that can help in the assessment of aneurysms and arteriovenous malformations in a non-invasive manner.

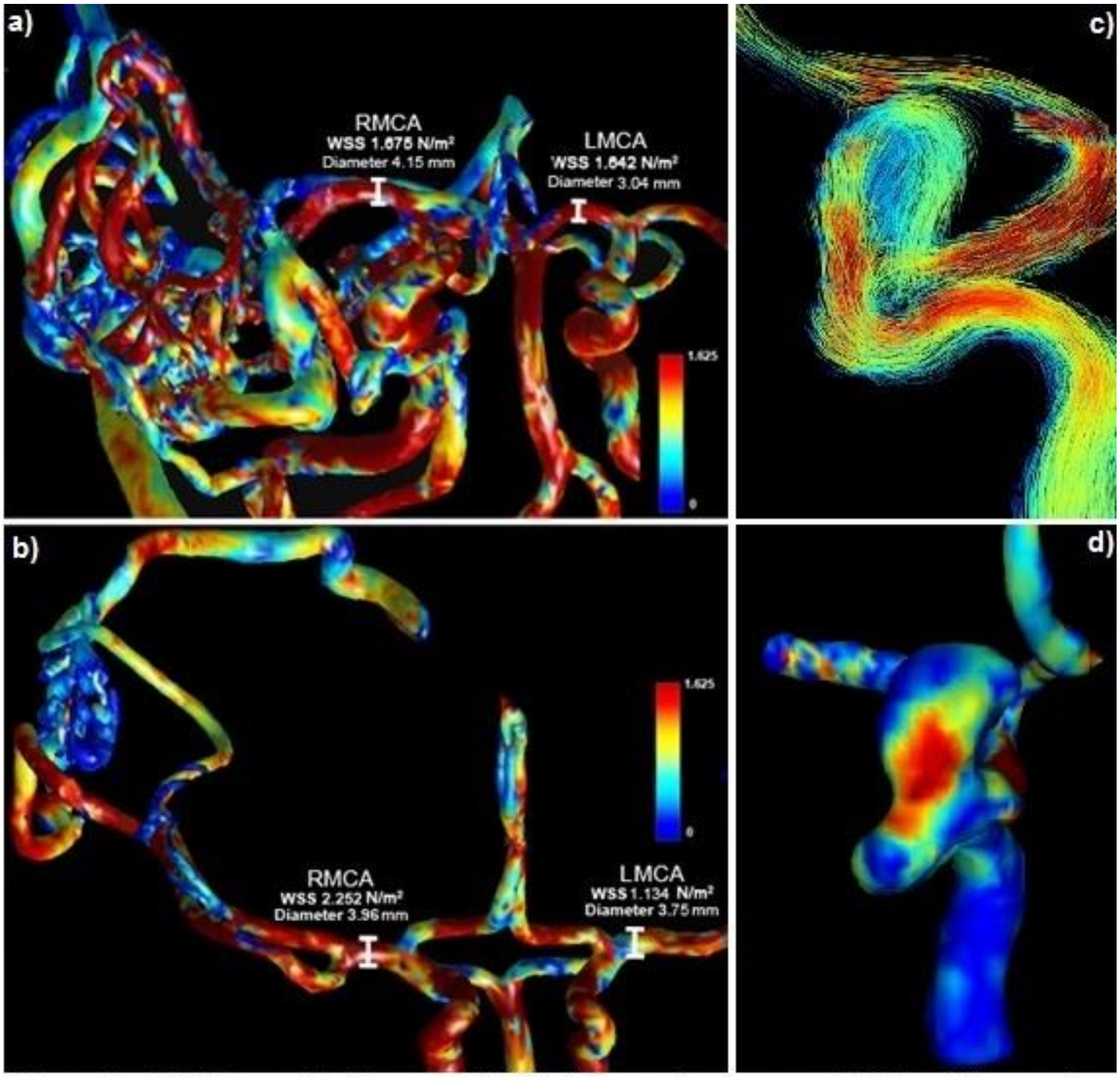

Figure 1): a) WSS map of a left temporal AVM demonstrating increased WSS and diameter in both feeding right MCA and contralateral left MCA, compatible with compensatory response in a stable patient. **b)** WSS map of a left parietal AVM demonstrating elevated WSS in feeding RMCA compared to contralateral LMCA in a symptomatic patient. **c)** Streamline map demonstrating inflow jet contacting the aneurysm dome. **d)** WSS map demonstrating focally elevated WSS at the impact zone. Findings are associated with increased risk of aneurysm growth and rupture.

(Filename: TCT_2503_hemo3.jpg)

3540

Scratching the Surface: A Resident Primer on Brain Surface Anatomy

E Kuoy[1], M Thompson[2], C Nguyen[3], D Chow[4], A Hasso[5]
[1]UC Irvine, Orange, CA, [2]UNIVERSITY OF CALIFORNIA IRVINE, ORANGE, CA, [3]University of California, Irvine, IRVINE, CA, [4]UNIVERSITY OF CALIFORNIA, IRVINE, IRVINE, CA, [5]UNIV OF CALIFORNIA IRVINE MEDICAL CENTER, ORANGE, CA

Purpose
The purpose of this presentation is to provide a primer on brain surface anatomy with practice in the context of localizing various brain tumors. This presentation is targeted to beginning residents or those looking for an anatomy refresher to be able to more specifically localize lesions to better assist referring physicians.
Materials and Methods
Brain surface anatomy can be variable across patients. This presentation will provide a systematic approach with various different methods to help discern brain surface anatomy and tips for discerning location when encountering variability. After presenting each method of localization, different brain tumor cases will be shown to allow the audience a chance to practice localizing the lesions. Radiologic tidbits will also be provided about the tumor presented along the way to help narrow the differential diagnosis when encountering similar lesions in practice.
Results
It is important for beginning radiologists to be able to localize lesions to assist referring clinicians, whether it be to confirm signs of neurological deficits on exam or for surgical planning, for example around eloquent cortex. Systematic methods of localizing lesions will be presented to boost confidence of the correct location of neoplastic lesions, especially when there is concordance of various signs.
Conclusions
Through an interactive didactic lesson followed by a case-based presentation of different neoplasms to practice, audience members should be more confident in localizing lesions. This knowledge will improve the quality of reports and better assist in the patient's management.

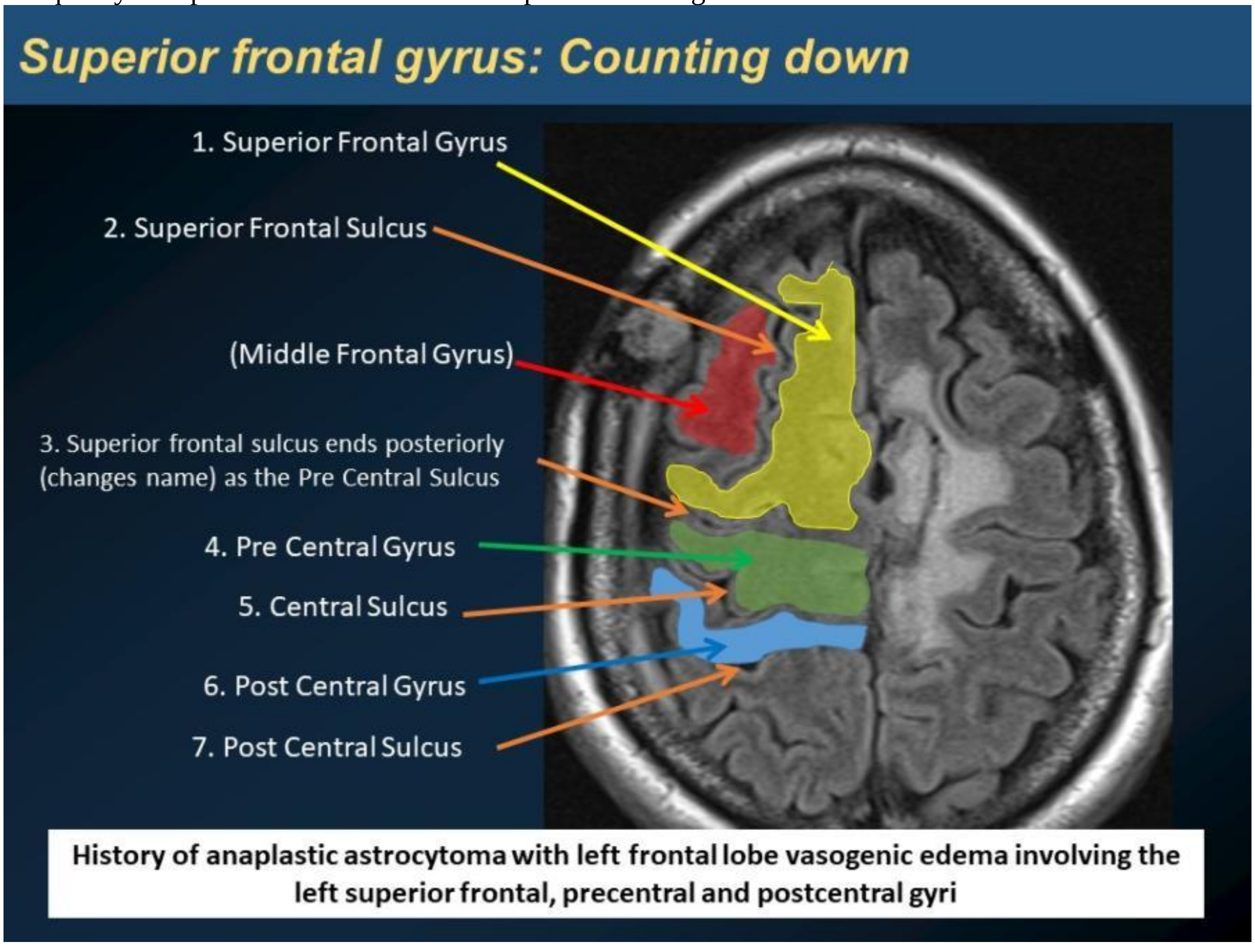

(Filename: TCT_3540_AJNRbrainsurfaceabstractslides.jpg)

2898

Shedding Light on LiTT: Institutional Experience with Laser Interstitial Thermal Therapy

L Alhyari[1], F Choudhry[1], B Cornwell[1], C Glenn[2]
[1]University of Oklahoma, Oklahoma City, OK, [2]University of Oklahoma Health Sciences Center, Oklahoma City, OK

Purpose
Laser interstitial thermal therapy (LiTT) is a surgical technique that was first introduced in the 1980s in which high temperatures are used to ablate specific areas of tissue. In the 1990s, intraoperative magnetic resonance imaging monitoring of laser ablation or "MR-guided LiTT" was introduced adding to the accuracy of this method. LiTT was initially used to stereotactically target brain tumors and subsequently was found effective in the treatment of medically-refractory epilepsy and drug-resistant cerebral edema associated with radiation necrosis. Given the growing use of this technique nationally and globally, the radiologist should be familiar with the common postprocedural imaging changes that occur following LiTT and herein we review these changes through images from our institution.
Materials and Methods
In this exhibit, we will give the reader an understanding of LiTT, both in terms of imaging and procedural technique. For example, readers may not be familiar with the mechanism by which the tissue ablation occurs, the maximal size of a solitary ablation zone, or the actual length of the procedure. We will demonstrate example images used for stereotactic localization as well as confirmatory imaging of the ablation cavity. We will expand on this by also showing temporal evolution of the ablation zone in patients with successful outcomes and examples of tumor progression following LiTT.
Results
Although going on its 3rd decade and increasing mention within peer-reviewed literature, approval for and reimbursement from LiTT procedures can be challenging as it is sometimes considered experimental. There are several compelling advantages to LiTT over standard open surgery such as affording a relatively atraumatic entry to deep seated lesions that avoids sectioning mainstem white matter tracts, less risk of development of pseudomeningoceles, a better cosmetic outcome, shorter hospital stay, and ability to treat multiple non-contiguous targets at once without need for multiple craniotomies. Despite this, the postprocedural imaging features are not widely known among radiologists, even those with subspecialty training. The postprocedural imaging features evolve over time from centrally restricting rim-enhancing lesions in the immediate postoperative phase with little or no surrounding edema. This is a combination of coagulative necrosis and devitalized charred tissue. In the subacute phase, there is decreasing enhancement and increasing edema. Hemorrhage within the lesion may be seen in acute or subacute phases. Finally, contraction of the ablated lesion occurs with residual diffusion signal abnormality and gliosis. T1 signal characteristics also evolve over time. Postprocedural MRIs are frequently ordered to look for residual tissue or for other clinical indications including persistent or worsening clinical symptoms.
Conclusions
LiTT is a novel minimally invasive stereotactic neurosurgical method offered at tertiary-care hospitals and specialized cancer centers for treating select patients with brain tumors, drug-resistant epilepsy, and cerebral edema associated with post-radiation necrosis. As LiTT is becoming more frequent and patients may be imaged at referral institutions, radiologists should be familiar with these changes in order to avoid pitfalls like misdiagnosing LiTT-associated changes with infection or tumor or failing to identify disease progression/treatment failure.

2681

Sick Sense: A Review of Cranial Nerve Schwannoma

B Litt[1], A Vijayasarathi[1], S Karnezis[1], A Azizyan[1]
[1]*UCLA, Los Angeles, CA*

Purpose
Cranial nerve (CN) schwannomas are common benign neoplasms composed entirely of Schwann cells, with a wide variety of clinical implications. Accurate diagnosis requires a detailed understanding of normal anatomy, characteristic imaging features, differential diagnoses and awareness of potential pitfalls. Knowledge of common clinical presentations, potential warning signs, and follow up with pathological confirmation can help the neuroradiologist confidently diagnose CN schwannomas, particularly in challenging and unique situations. The objective of this exhibit is to review relevant anatomy and common clinical presentations, highlight salient imaging features, provide location based differential diagnoses, and share interpretation pearls to help avoid common pitfalls.
Materials and Methods
The PACS and departmental teaching files at a large academic medical center were queried for instructive sample of cases of cranial nerve schwannomas. Clinical presentation, management strategy, and pathological characteristics were extracted from the Electronic Medical Record.
Results
The slides included in this interactive educational exhibit will demonstrate a review of normal anatomy of the brainstem, skull base, and relevant spaces of the neck, including important landmarks. For each type of CN schwannoma, common presentation, location, relevant differential diagnosis, pathology, and atypical or concerning features will be presented.
Conclusions
Understanding the features presented herein may help interpreting radiologists confidently diagnose this benign entity and differentiate it from more worrisome mimics.

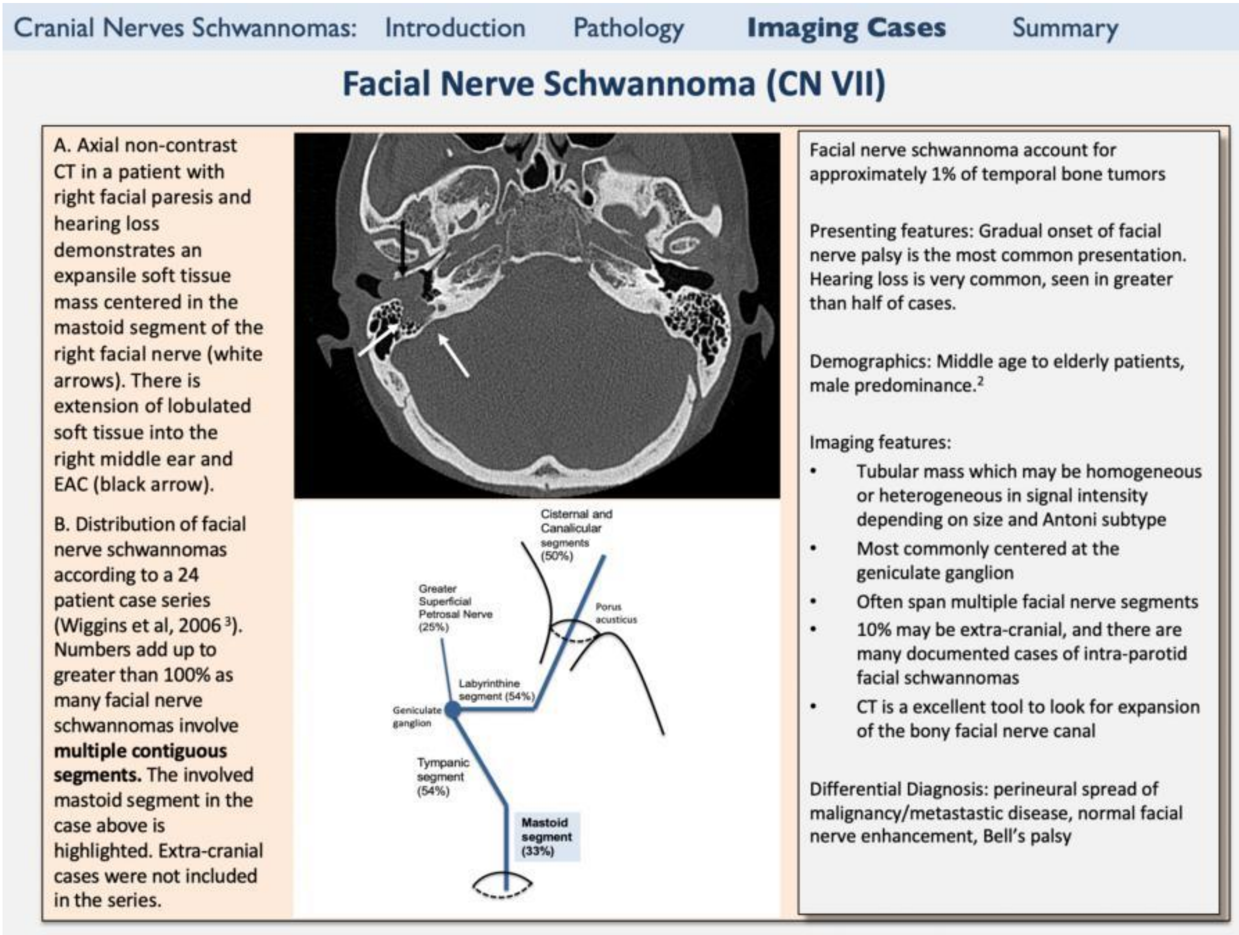

(Filename: TCT_2681_abstractupload.jpg)

3552

Simplified MRI Based Approach to Brain Myelination and Pediatric Metabolic Disorders: Case Based Review

R Patel[1], O Arevalo[1], S Khanpara[1], A Kamali[1], E Bonfante-Mejia[1], N Desai[2]
[1]The University of Texas Health Science Center at Houston, Houston, TX, [2]Texas Children's Hospital Baylor College of Medicine, Houston, TX

Purpose
1. Simplified Pattern approach of initially assessing brain myelination on MRI. 2. Distinguish normal and abnormal white matter in children. 3. Formulate an MRI based approach to Pediatric Metabolic Disorders. 4. Recognize the key clinical and imaging features of the common metabolic disorders.
Materials and Methods
Retrospective review of all confirmed diagnosis of Pediatric Metabolic Disorders from two large children hospitals was performed for patients involving the brain. Clinical presentation, Imaging (CT, MRI, MR Spectroscopy) findings, laboratory and genetic analysis were reviewed.
Results
- Simplified MRI Based pattern recognition of normal myelination was presented as case based review. - Metabolic disorders were categorized in 5 groups based on MRI findings and represented as case based review. Group 1: Disorders of Hypomyelination, Group 2: Disorders affecting Subcortical White Matter

Group 3: Disorders affecting Periventricular and Deep White Matter Group 4: Disorders affecting combined White Matter and Deep Gray Matter Nuclei Group 5: Disorders primarily affecting Deep Gray Matter Nuclei and less commonly involved white matter
Conclusions
Pediatric metabolic disorders affecting the brain are very complex, heterogeneous group of disorders. Having good understanding of Brain Myelination on MRI and pattern recognition of brain involvement categorized primarily by location can be extremely helpful to narrow the differential diagnosis and guide further evaluation and treatment.

2636

Small Posterior Fossa: What Else To Expect?

L Godoy[1], C Alves[2], L Godoy[3], C da Silva[4], C Leite[5]
[1]FLEURY GROUP,HOSPITAL SAO LUIZ, São Paulo, São Paulo, [2]Children's Hospital of Philadelphia, Philadelphia, PA, [3]FLEURY, SÃO PAULO, SÃO PAULO, [4]Fleury, São Paulo, São Paulo, [5]University Of Sao Paulo, Sao Paolo, Brazil

Purpose
Small posterior fossa (SPF) is a finding shared by several disorders. For this reason, one must consider SPF not an isolated finding, but as a part of a constellation of features that together may narrow the final diagnosis.
Materials and Methods
We retrospectively selected 24 patients with SPF in our institution from 2014 to 2018. The inclusion criteria of SPF cases was first the visual evaluation, which was later confirmed by the measurements of tentorial and infratentorial angles.
Results
SPF is classically a characteristic of Chiari malformations. However, diencephalic abnormalities involving the interthalamic and interhypothalamic adherences, among many others findings, are also found in these patients. Beyond Chiari, SPF is also observed in disorders linked to the impairment of fibroblast growth factors (FGFR) with classical temporal and hippocampal features. SPF may also be seen in some KRASopathies such as Noonan syndrome, whose manifestation may encompass multiple white matter foci in association with glial tumors and in Neurofibromatosis type-1, with multisystemic findings. Rhombencephalosynapsis and correlated syndromes, particularly Gomez-López-Hernandéz combine SPF with alopecia and absence of trigeminal nerves.
Conclusions
This presentation will separate patients with Chiari deformities from those with other different malformations associated with SPF, disclosing some distinctive features that narrow the differential diagnosis or even allow a specific one.

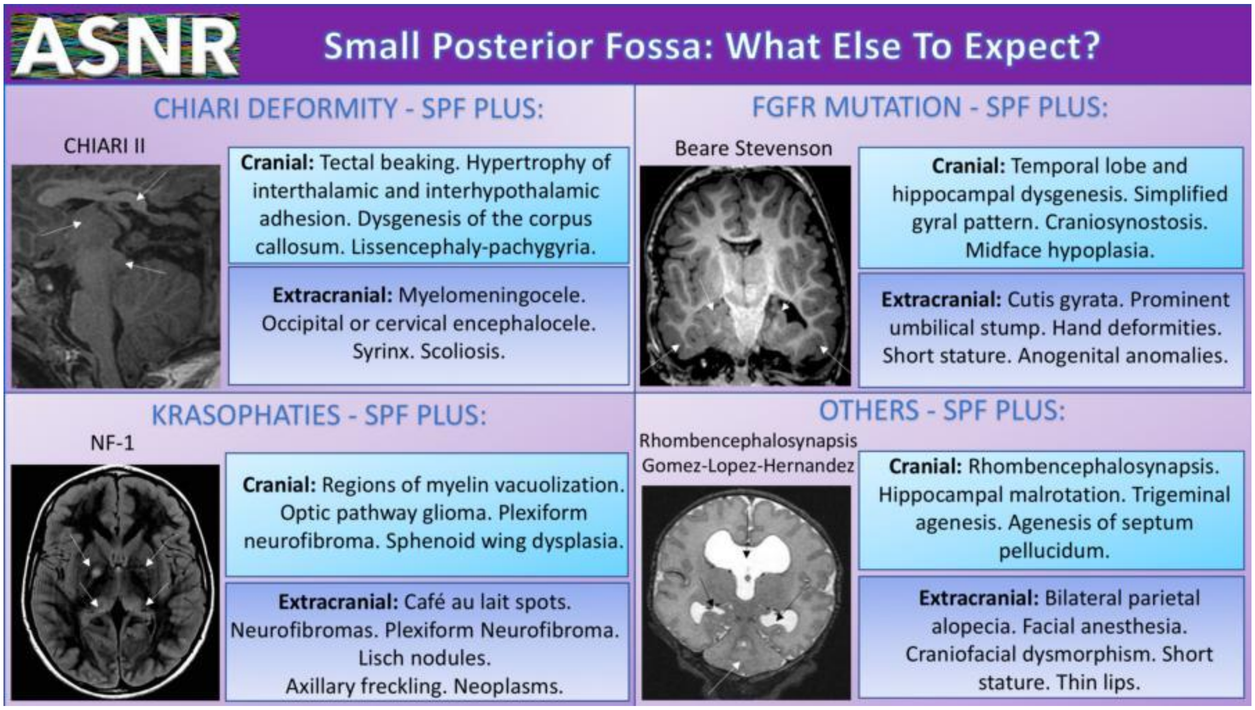

(Filename: TCT_2636_ESNRFINAL.jpg)

2950

Spectrum of FDG-PET and Amyloid-PET in Typical and Variant patterns of Alzheimer's Disease

A Kanwar[1], B Mullenbach[1], G Choudhary[1], S Gaddamanugu[2], N Adhikari[3]
[1]University of Alabama at Birmingham, Birmingham, AL, [2]University of Alabama/Veterans Affairs Medical Center, Birmingham, AL, [3]University of Alabama Medical Center, Tuscaloosa, AL

Purpose
To familiarize the reader with the pattern of FDG metabolism in early and established phases, typical and atypical variants of Alzheimer's disease (AD), using a case-based exhibit focused on FDG-PET/CT, and Amyloid-PET/CT imaging.
Materials and Methods
This exhibit will review the molecular imaging techniques and imaging findings used to diagnose Alzheimer's dementia. Normal imaging patterns and findings characteristic of Alzheimer's disease will be illustrated. In addition atypical imaging findings and dynamic changes in imaging patterns as disease progresses will also be reviewed
Results
This educational exhibit will review the pattern of FDG metabolism in typical and atypical variants of Alzheimer's disease (AD). Imaging appearance of different stages of typical amnestic AD, from pre-dementia, early, and advanced disease will be discussed with the help of clinical cases. Atypical or variant AD entities including visual variant of AD (VVAD) also called posterior cortical atrophy (PCA), frontal variant of AD (fvAD), logopenic/phonological aphasia (LPA) will be discussed. Important imaging signs and differentiating feature which can help to differentiate AD from other dementias will also be discussed.
Conclusions
FDG PET is a useful tool for diagnosis of Alzheimer's disease, with high sensitivity and specificity. Amyloid deposition precedes clinical findings of dementia by up to 15-25 years. Amyloid imaging which

serves as an imaging biomarker for pathological amyloid deposition in the brain can help in evaluating patients with cognitive decline.

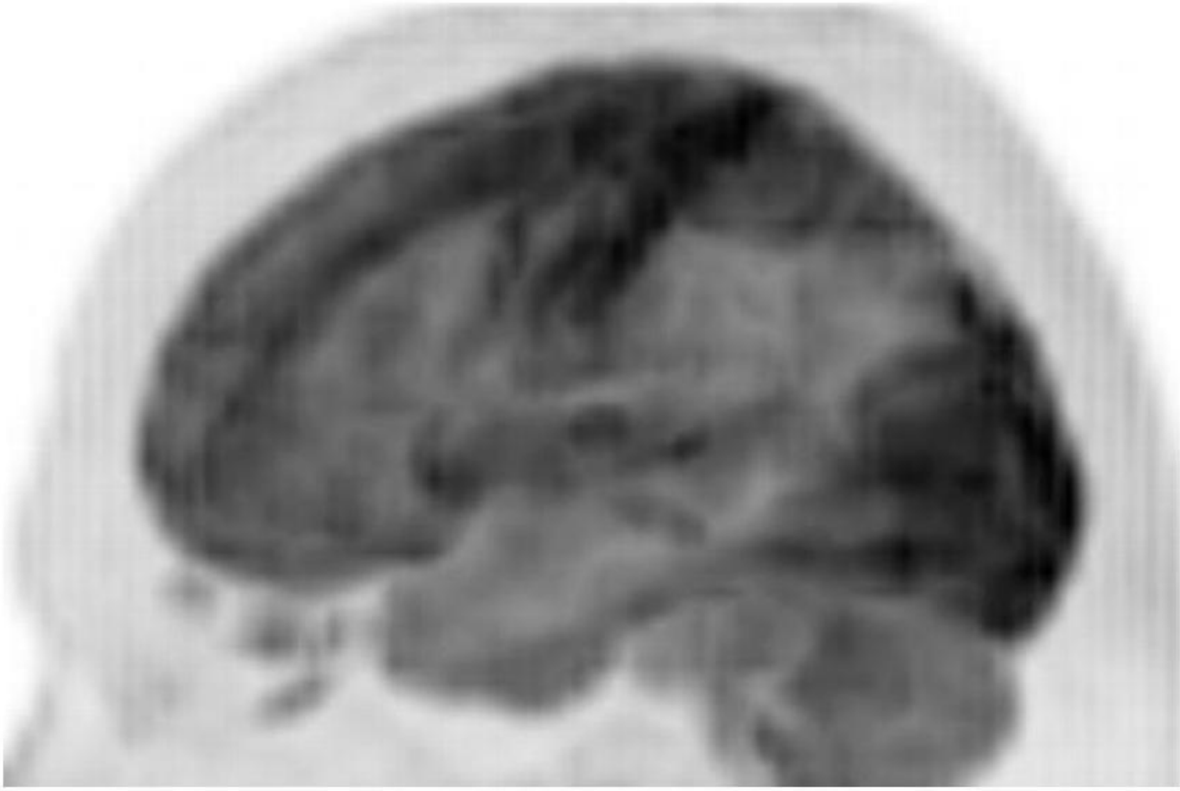

(Filename: TCT_2950_Advanced-AD-MIP-Image.jpg)

2846

Spectrum of Initial Neuroimaging Findings and Temporal Evolution of Injury in Children Admitted to PICU with Hypoxic Ischemic Injury: Impact of Mechanism and Severity of Injury from Neonates to Young Adults

J Wen[1], C Robertson[2], S Suskauer[2], S Kannan[2], T Ruddy[2], B Soares[3], A Tekes-Brady[1]
[1]Johns Hopkins Hospital, Baltimore, MD, [2]Johns Hopkins, Baltimore, MD, [3]Johns Hopkins University School of Medicine, Baltimore, MD

Purpose
Hypoxic ischemic injury (HII) results from decreased cerebral oxygenation secondary to global cerebral hypoperfusion or generalized hypoxia. Neuroimaging findings in HII are variable based on mechanism and severity of hypo-oxygenation, age of the patient, timing of imaging relative to injury, and natural evolution of the hypoxic-ischemic process. An understanding of the multifactorial pathophysiology of HII can help predict imaging findings and their evolution over time. Differentiation from potential mimickers is also important, as certain metabolic abnormalities and genetic syndromes may have overlapping features. Our goal is to review the patterns of ischemic injury from multiple different mechanisms including cardiac arrest, acute respiratory failure, asphyxia, and accidental and non-accidental traumatic brain injury. We will also highlight the temporal evolution of ischemic changes in different age groups.
Materials and Methods
Etiologies of HII will be categorized as traumatic and non-traumatic. Under each category and clinical scenario, first line imaging, initial neuroimaging findings, preferred follow-up imaging modality, and

assessment of temporal evolution of injury will be discussed. Neuroimaging findings of ischemic injury will be categorized into diffuse, central and watershed patterns. We will also highlight cases that involve the brainstem and cerebellum, along with cases that do not fit classic categorization. Additional injuries such as calvarial fractures and extra-axial hemorrhages will be mentioned when relevant. The value of advanced MRI sequences like DWI, DTI, SWI, and blackbone imaging in addition to conventional sequences will be discussed in each case. MRI also allows monitoring of the temporal evolution of HII, particularly with the use of abbreviated MRI protocols which do not require sedation or general anesthesia.

Results

Head CT is the often the first line of imaging due to fast acquisition time and wide availability. MRI has greater sensitivity and specifity for initial detection and follow-up of ischemic parenchymal injuries. Head ultrasound can also be performed, but is often limited in assessing the extent of brain injury and typically reserved as first line of imaging in neonates with open fontanelles, especially if the patient is in critical condition and cannot leave the PICU. In severe abrupt mechanisms of HII, a central pattern of involvement of the deep gray matter and perirolandic cortex is most common given the high metabolic demand in these regions. Severe prolonged cases involve even greater injury which affects the entire supratentorial brain. Peri-rolandic cortex involvement is less frequent in preterm neonates given lack of active myelination of this region, unlike term infants. Unusual cases with diffuse cerebellar ischemic injury will be also discussed. Severe cases typically demonstrate rapid progression of parenchymal volume loss in the early subacute phase of injury, even before pseudonormalization of diffusion changes. Pseudonormalization of diffusion is especially prolonged the young neonates. SWI imaging may also show additional hemorrhagic changes and highlight areas at risk for ischemic injury by identifying prominent local veins. Mild to moderate cases spare the central gray matter and involve the cortex and subcortical white matter, particularly in watershed territories. Progression of temporal changes related to ischemic injury may be less predictable in this category.

Conclusions

Pediatric HII can have different neuroimaging appearances depending on mechanism, severity and timing of injury relative to imaging. Management and prognostication is also highly guided by imaging findings. Our educational exhibit will highlight the key imaging features of pediatric HII resulting from multiple etiologies, with particular emphasis on findings which reflect severity of hypoxia and evolution of neuroimaging findings with impact on short and long term management and outcomes.

3247

Spinal Tumours: A Pictorial Review

K Mahady[1]
[1]Royal Brisbane and Women's Hospital, Brisbane, QLD

Purpose

Tumours of the spine and spinal cord are a diverse range of benign and malignant lesions that can be challenging for the reporting radiologist. Accurate diagnosis can assist treatment planning and prognostication. We present a pictorial guide to differential diagnosis of adult and paediatric spinal lesions centred around key discriminating imaging findings.

Materials and Methods

1. Anatomy: Tumor localization will be reviewed with pictorial examples of intramedullary, intradural extramedullary, mixed lesions and extradural lesions. 2. Benign and malignant: These tumors are further classified by etiology. Each will be illustrated and key diagnostic features highlighted: *Benign lesions will comprise idiopathic lesions e.g. syrinx, vascular lesions, spinal vascular malformation with focal edema e.g. cavernoma, aneurysm; inflammatory pathology mimicking tumor e.g. transverse myelitis, demyelination, granulomatous disease; infective lesions e.g. abscess, cryptococcoma and neoplastic: glial:

ganglioglioma, myxopapillary ependymoma, subependymoma; non glial: nerve sheath tumor including neurofibromatosis, haemangioblastoma, paraganglioma, meningioma, epidermoid cyst, lipoma
*Malignant lesions are separated into primary (astrocytoma, ependymoma, primitive neuroectodermal turmor, lymphoma), or secondary lesions (spinal cord and leptomeningeal metastases, direct invasion from adjacent structures including pelvic malignancy, bone tumor, multiple myeloma)
Results
We will provide an easy to use guide to differential diagnosis of spinal lesions using a clear classification structure and imaging examples of typical discerning features of each on CT, MRI, myelography and angiography. Where possible, biopsy proven examples and surgical photography will be included.
Conclusions
We hope that accurate radiological diagnosis of spinal tumors is facilitated by this pictorial guide to localization, classification and discrimination of a range of pathologies.

3461

Spinal Venous System – Anatomy and Practical Applications

E Supsupin[1], S Calle[2]
[1]The University of Texas Health Science Center at Houston, HOUSTON, TX, [2]The University of Texas Health Science Center at Houston, Houston, TX

Purpose
The spinal venous system may be involved in a wide array of pathologies. Knowledge of the anatomy of the spinal venous drainage is important in the understanding of disease conditions affecting the spine and spinal cord.
Materials and Methods
A comprehensive review of spinal venous anatomy is provided. The direction of venous drainage from spinal cord parenchyma (i.e., intrinsic) to the epidural venous plexuses is described. Cases illustrating how the spinal venous system may play a role in certain pathologic conditions (such as vascular malformations and fistulas, tumors, and infections) are shown.
Results
Like their arterial counterparts, the venous drainage of the spine and spinal cord is highly variable. Four main compartments representing different levels of intercommunicating drainage from the spinal cord and spine have been described. These include the intrinsic veins of the spinal cord parenchyma, superficial pial system, extradural-intraspinal, and extradural-extraspinal vertebral venous plexuses. Knowledge of venous anatomy is fundamental in understanding the pathology of certain conditions that afflict the spinal cord and spine. For example, dural arteriovenous fistulas draining via intrathecal veins should be clearly distinguished from spinal arteriovenous malformations. This distinction is not only important in understanding the pathogenesis of cord damage, but also crucial in the decision making for appropriate management of these two distinct entities. The vertebral venous plexus allows hematogenous dissemination of metastatic disease or infection along the spinal axis.
Conclusions
Knowledge of spinal venous anatomy is important in the understanding of a wide range of pathologies afflicting the cord and spinal axis.

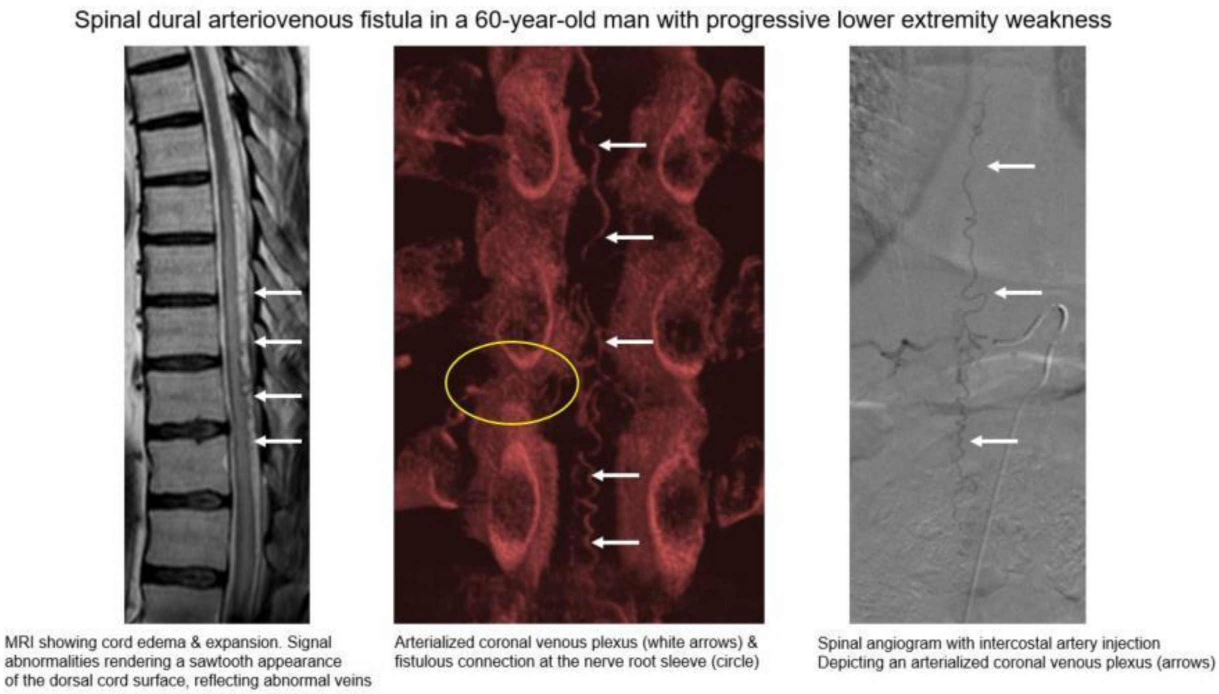

(Filename: TCT_3461_SDAVF.JPG)

3274

Sporadic and Syndromic Optic Pathway Gliomas (OPGs) in Children: Role of Imaging

F Lo Russo[1], C Alves[2], S Teixeira[2], F Gonçalves[2], D Khrichenko[1], S Avignone[3], F Triulzi[4], G Zuccoli[5]
[1]Children Hospital of Philadelphia, Philadelphia, PA, [2]Children's Hospital of Philadelphia, Philadelphia, PA, [3]Fondazione Irccs Ca Granda Ospedale Maggiore Milano, Milano, Italy, [4]Università degli Studi Milano, MILANO, Italy, [5]CHOP, Philadelphia, PA

Purpose
To review the role of imaging in the diagnosis and treatment planning of sporadic or syndromic OPGs in children with or without neurofibromatosis type 1 (NF1).
Materials and Methods
OPGs account for 1-5% of pediatric brain tumors, 50% of which affect children with NF1. Clinical presentation of OPGs is variable, being asymptomatic in 40-80% of children affected by NF1. Visual acuity loss and radiological tumor progression are the main indications to treatment which relay on chemotherapy. Difficulties assessing vision in children, especially if cognitive impairment is present, and unpredictable evolution of OPGs hinder treatment planning and follow-up. While imaging plays a pivotal role to confirm a diagnosis of OPGs in both is sporadic and syndromic cases, advanced imaging modalities could be of interest in assessing tumor progression. In particular, the volumetric measurement of the anterior visual pathway (AVP) and diffusor tensor imaging (DTI) have been correlated with visual assessment and have been able to predict clinical outcomes. Hence, imaging biomarkers able to predict vision loss could be helpful in treatment planning and follow-up.
Results
Learning points • OPGs can be sporadic or syndromic and tend to be common in pediatric patients affected by NF1 • Imaging plays a fundamental role in the diagnosis of OPGs • Evaluation of OPGs progression is challenging due to difficulties assessing visual acuity in children and unpredictability of tumor evolution. • Imaging biomarkers could be helpful in treatment planning and follow-up.

Conclusions
Assessing OPGs progression can be challenging in both clinical and radiological settings. Imaging plays a fundamental role to confirm the diagnosis, and focus on advanced techniques can further expand the role of imaging in assessing OPGs progression and treatment planning.

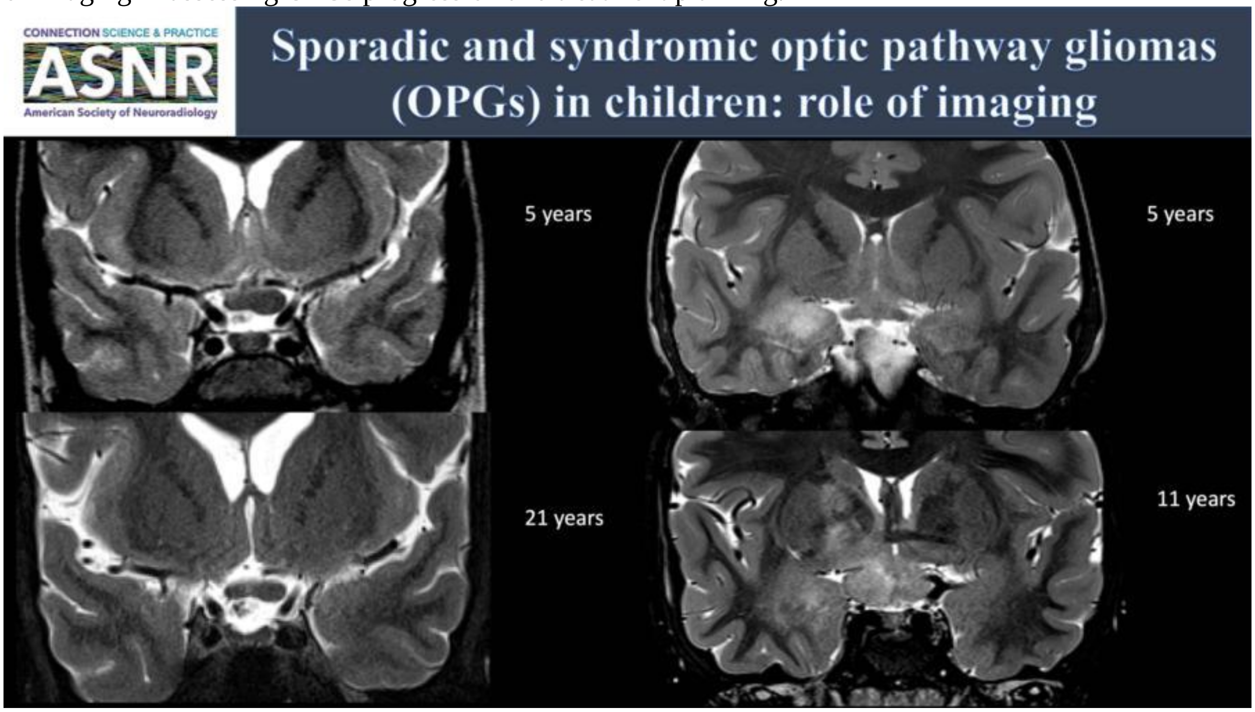

(Filename: TCT_3274_Diapositiva2.jpg)

2233

Standard Interpretation and Structural Report in Code-Stroke CT Perfusion

H Sotoudeh[1], A Bag[2]
[1]University of Alabama at Birmingham, Birmingham, AL, [2]St. Jude Children’s Research Hospital, Memphis, TN

Purpose
Regarding the most recent ischemic stroke treatment guideline, the perfusion imaging has been recommended up to 6-24 hours after initial symptoms of brain infarction and patients with a significant amount of potential salvageable peri-infarct ischemia and without contraindication benefit from delay thrombolysis and intra-arterial thrombectomy. This approach causes more and more CT perfusion to be done in subacute phase of ischemic stroke. CT perfusion findings in this "subacute phase" are slightly different from "hyper acute" ischemic stroke. The interpreting radiologist must be confident to report the CT perfusion in urgent setting since these studies are under the umbrella of "code-stroke" and should be read in minutes. In addition, result of the CT perfusion has a critical effect on the patient's outcome. Misinterpretation of stroke CT perfusion can be fatal. Underestimation of the salvageable ischemia excludes the patient from the potential effective treatment and increases the mortality and morbidity. Underestimation of infarct volume causes unnecessary thrombolysis/thrombectomy and potential fatal intracranial hemorrhage. Despite the above mentioned facts, there is no uniform approach to read the code-stroke CT perfusion.
Materials and Methods
In this presentation, the basic concept of CT perfusion, typical findings and pitfalls will be educated.

During this presentation,the radiologists will be trained about a standard structural report and template to cover the diagnostic and legal challenges of code-stroke CT perfusion. The topic which will be covered are: Basics of CT perfusion and technique Radiation dose Image processing Parameters in CT perfusion Definition of Core infarction and Ischemic penumbra Prognostic color maps Quality control-Arterial and venous selection Standard arterial and venous curves Abnormal curves Normal maps Typical presentation Complete ischemia Small core infarction, large per infarct ischemia Large core infarct, small ischemic penumbra Complete infarct False negative Field of view lacunar infarcts Watershed infarcts Luxury perfusion Ictal and post ictal phase of seizure False positive Normal variation Cervical arterial stenosis Head tilt Vasospasm Software Challenges Template and structural reporting; How to avoid misdiagnosis and legal challenges Template sample

Results

N/A

Conclusions

The "code stroke" CT perfusion is a functional imaging performed and read under urgent situation. It is prone to many pitfalls and challenges. The radiologist is responsible for image quality and should be capable to detect false positive and negative of this modality. Visual assessment of just color maps can be misleading in many ways and can be harmful for patient management. Standard processing and reporting of CT perfusion with using a uniform standard technique in interpretation is the only way that the referring physician can have real estimation of infarct and ischemia volume and select the best treatment policy.

2554

Subarachnoid Hemorrhage – Why Bleeding Patterns are Important

A Kuhn[1], K de Macedo Rodrigues[2], A Puri[2]
[1]Beth Israel Deaconess Medical Center, Boston, MA, [2]University of Massachusetts Medical Center, Worcester, MA

Purpose

Radiologic evaluation of subarachnoid hemorrhage (SAH) is important for prognosis, management and can help guide endovascular treatment of the underlying condition.

Materials and Methods

First, the exhibit will familiarize the viewer with the different etiologies of SAH, (traumatic, arterial pathology and venous bleeds) and provide a few important key points about each etiology with incidence, risk factors and symptoms at presentation. The exhibit will then focus on providing detailed description about the different imaging presentations on CT and MRI and discuss the next steps in work-up (follow-up imaging versus cerebral angiogram). The viewer will be able to learn more about aneurysms, AVM and dural AV fistula treatments by presentation of detailed case examples from our institution. The exhibit will further discuss the clinical observation of patient with SAH in the ICU with focus on vasospasm prevention, detection and treatment. The viewer will then learn about the imaging follow-up for patient with initially negative cerebral angiogram in the setting of suspected arterial pathology given a suspicious bleeding pattern or in the setting of a venous bleed with perimesencephalic SAH.

Results

Lastly, the viewer will be challenged with a few imaging examples for which he/she will need to provide the diagnosis. The correct answers to the cases will be revealed and the next follow-up or treatment steps will be discussed.

Conclusions

Clinical presentation, location and extent of SAH can often predict the underlying etiology of the bleed. Despite cerebral angiography remaining the gold standard for evaluating patients with SAH, it is an invasive procedure with a small but still significant risk of complication and should therefore only be performed if imaging studies and clinical picture suspect an underlying etiology that requires further evaluation and possible endovascular management.

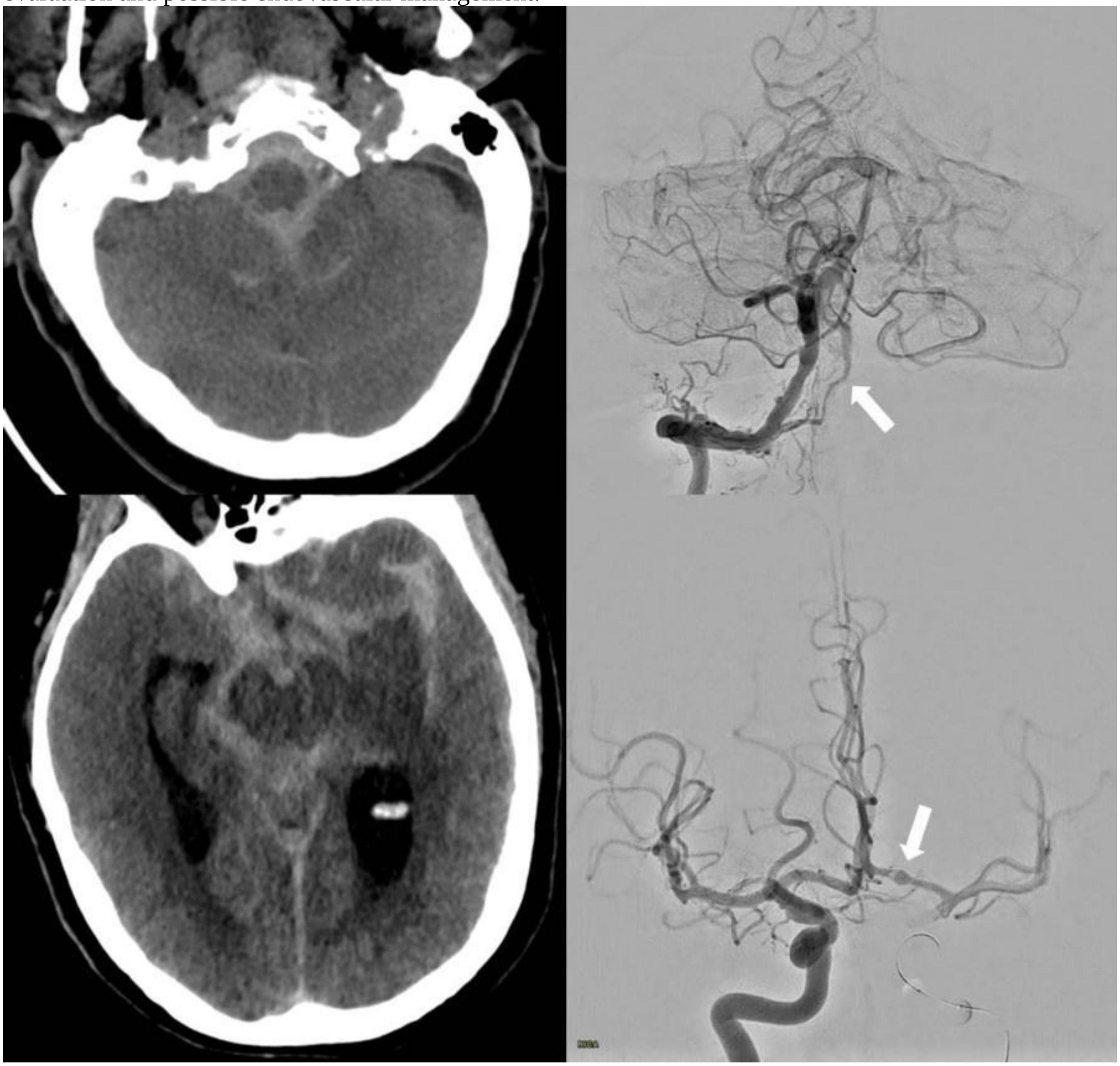

(Filename: TCT_2554_ASNRSAH.JPG)

3092

Superficial Siderosis: Where to Look

T Scoppetta[1], D Fragoso[2], L Avila Lessa Garcia[3], A MAIA[4], C TOYAMA[5], C da Silva[5]
[1]Santa Casa de Misericórida de São Paulo, São Paulo, Brazil, [2]SANTA CASA DE SP, SÃO PAULO, Brazil, [3]Grupo Fleury, Sao Paulo, Sao Paulo, [4]SANTA CASA DE SÃO PAULO, SAO PAULO, SAO PAULO, [5]FLEURY, SÃO PAULO, SÃO PAULO

Purpose
The objective of this Educational Exhibit is to illustrate and describe the cause, physiopathology, natural

history, and clinical and imaging presentations of a series of pathologies that present with superficial siderosis.
Materials and Methods
Was conducted a retrospective and descriptive study of brain and spine MRI scans performed in our institution. We will exhibit a number os pathologies that present with superficial siderosis focusing in depicting the source of the bleeding. We also propose an diagnostic algorithm.
Results
Superficial siderosis of the central nervous system results from hemosiderin deposition in the subpial layers of the brain and spinal cord. The source of bleeding is often not depicted, even with, extensive investigation, including MR imaging of the brain and spine, CT myelography, MR angiography, and cerebrospinal angiography. However, radiologists should be trained to look after for potential common and uncommon sources of bleeding, including atypical presentations of daily pathologies. The conditions covered are trauma, surgery, cerebral amyloid angiopathy, cortical and dural vein thrombosis, neoplasms and vascular pathologies. We suggest a diagnostic algorithms considering the age, location and associated findings to simplify the differential diagnosis workout.
Conclusions
Superficial siderosis is not an uncommon imaging finding in brain scans. It is imperative radiologists be enlightened of potential causes and the vast array of imaging modalities at our disposal. A diagnostic algorithm can simplify the differential diagnosis workout.

2372

Technical Aspects of Automated CT Perfusion Post-Processing Software: Basic Theory of Cerebral Perfusion, Clinical Examples, and Pitfalls

B Laughlin[1], A Chan[2], V Nwokocha[3], E Dutweiler[4], S Malik[4], A Iaia[5], B Reznikov[6], P Moftakhar[7]
[1]CHRISTIANA CARE HEALTH SYSTEM, MIDDLETOWN, DE, [2]CHRISTIANA CARE HEALTH SYSTEM, BEAR, DE, [3]Christiana Care Health System, Newark , DE, [4]Christiana Care Health System, Newark, DE, [5]Christiana Care, Newark, DE, [6]CHRISTIANA CARE HEALTH SYSYTEM, WEST CHESTER, PA, [7]Christiana Healthcare system, Newark, DE

Purpose
With the recent widespread revitalization of CT Perfusion in the acute stroke setting, there is a promise of significant improvement in the clinical decision making derived from perfusion analysis software packages. To reach this potential, Radiologists and Clinicians must understand the basic theory and different post-processing techniques inherent within the Rapid processing of Perfusion and Diffusion, RAPIDTM (Ischemaview, Menlo Park, CA). In this exhibit, we will guide the audience through the conceptual background necessary to comprehend and apply CT perfusion to their clinical practice, while being equipped with the ability to critically evaluate potential pitfalls that may lead to sub-optimal patient care.
Materials and Methods
The theoretical section will explain the principles of cerebral hemodynamics with a focus on describing and quantifying CBV, CBF, and MTT. We will conceptually illustrate the calculation of these parameters tracer kinetic theory, non-deconvolution/deconvolution techniques, and the central volume principle. The functional section will focus on some of the processing components of CT perfusion, such as AIF and VOF selection, post-enhancement cutoff, image segmentation, and vascular pixel elimination; followed by illustrating how these factors contribute to accurate parameter quantification.
Results
The clinical section will showcase real examples highlighting cases where RAPIDTM recognized acute ischemia not detected by the interpreting Radiologist in difficult imaging settings, and several examples

where technical/physiological pitfalls caused clinically significant misinterpretations. Furthermore, the majority of the cases will have additional and/or follow up imaging to corroborate the findings.
Conclusions
With the recent widespread revitalization of CT Perfusion in the acute stroke setting, there is a promise of significant improvement in the clinical decision making derived from perfusion analysis software packages. To reach this potential, Radiologists and Clinicians must understand the basic theory and different post-processing techniques inherent within the Rapid processing of Perfusion and Diffusion, RAPIDTM (Ischemaview, Menlo Park, CA). In this exhibit, we will guide the audience through theoretic and functional facets of the conceptual background necessary to comprehend and apply CT perfusion to their clinical practice. We will supplement this educational material with several case-based examples.

2704

The ABCs of Genetics Involving Malformations of Cortical Development

Y Guo[1], A Vossough[2], M Ruzhnikov[3], H Dahmoush[3]
[1]Stanford University, Stanford, CA, [2]UNIVERSITY OF PENNSYLVANIA - CHOP, PHILADELPHIA, PA, [3]Stanford University and Lucile Packard Children's Hospital, Palo Alto, CA

Purpose
Malformations of cortical development (MCD) are rare congenital anomalies due to a number of etiologies including genetic causes. MCDs may lead to varying degrees of developmental delay and epilepsy. Identifying an etiology is imperative to help guide supportive care, prognostication, family planning, and potential treatments options. Due to the increased availability of genetic testing, our understanding of the molecular pathology has substantially improved. This exhibit will introduce a framework relating imaging features of MCD to their underlying genetic mutations and associated pathways. The impact of a genetic diagnosis on image interpretation and the role of imaging in guiding genetic testing will be addressed.
Materials and Methods
CT and MR images of MCD with confirmed genetic diagnoses will be presented in this exhibit.
Results
Mutations in genes causing MCD involved in the same molecular pathways often share common imaging patterns. In particular, this exhibit will include the lissencephaly spectrum with respect to tubulin genes, tubulinopathy-associated dysgyria, cobblestone lissencephaly and dystroglycanopathies, microcephaly with simplified gyral pattern, polymicrogyria, schizencephaly, and MCDs caused by mutations in mTOR pathway genes. Imaging features attributable to specific genetic mutations or their associated pathways may be identified once a common pattern has been established.
Conclusions
Rapid advances in genetic testing and the increasing number of genetic variants implicated in MCD in recent years have led to improved understanding and classification of these malformations seen on imaging. An understanding of the genetic basis and molecular pathways involved in brain malformations can help with image interpretation and vice versa. Familiarity with the different causative genes and pathways by the neuroradiology community is often crucial in guiding further testing, genetic panel selection, and establishing a definitive diagnosis.

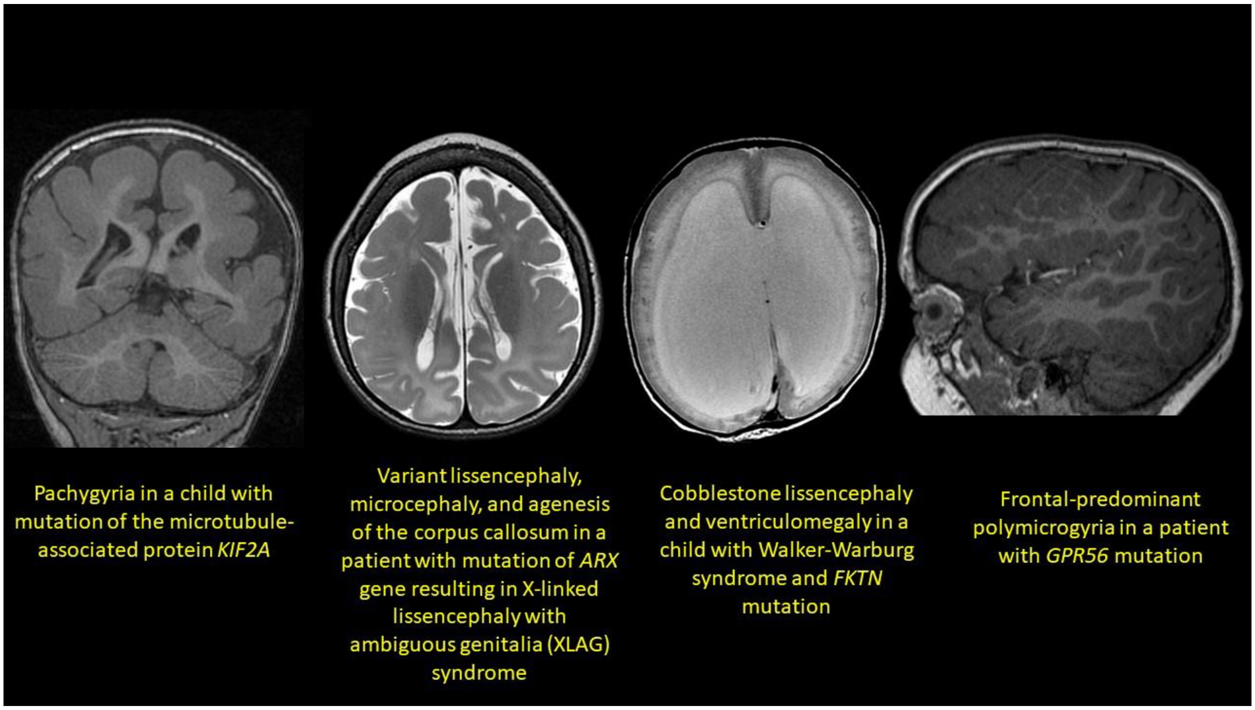

(Filename: TCT_2704_AbstractImages.jpg)

2992

The Biomarker Approach to Defeating Neurodegenerative Diseases

S Ahmad[1], K Traylor[1], J Kindler[1], B Graner[1], M Veronesi[1]
[1]*Indiana University School of Medicine, Indianapolis, IN*

Purpose
An important feature common to most neurodegenerative diseases is the accumulation of proteins with altered physicochemical properties, which lead to cellular dysfunction and ultimately neuronal loss. These abnormal proteins create tremendous opportunity for identification and exploitation as "biomarkers" of disease. The purpose of this educational exhibit is to explain the rising importance of pathologic protein biomarkers in the various neurodegenerative diseases, with an emphasis on how they are shaping emerging neuroimaging techniques and investigative therapies.
Materials and Methods
This exhibit will provide an overview of the known neurodegenerative disease imaging and laboratory biomarkers to date; specifically, alpha-synuclein, tau, beta-amyloid, TAR DNA-binding protein 43, and PrP. The contribution of these abnormal proteins to the neurodegenerative disease process will be outlined with key examples of how investigators are targeting their high-impact role for applications in diagnosis and emerging therapy.
Results
The use of biomarkers has been instrumental in the prevention, diagnosis, and treatment in other areas of medicine. For example, hypertension, hyperlipidemia and diabetes are defined by biomarkers. Interventions modulating these biomarkers have shown reduced likelihood of developing fractures and myocardial and cerebral infarctions. Biomarker mapping for NDs may allow for early disease identification and treatment initiation, perhaps well before symptom onset.
Conclusions
Biomarkers allow a critical window into the processes and cascade of aberrant events that result in a

given neurodegenerative disease, and accordingly provide high potential for diagnostic targets and disease therapy. This is especially true if the biomarker can identify the disease process prior to symptom onset. A better understanding of the disease processes and their associated biomarkers will ultimately improve patient outcomes. Educational Objectives: At the conclusion of this exhibit, the learner will: - Become familiar with specific biomarkers underlying the majority of NDs to date: alpha-synuclein, tau, beta-amyloid, TDP-43, and PrP. - Develop an understanding of the underlying mechanism leading to accumulation of abnormal proteins and how this mechanism allows for identification and exploitation of imaging and laboratory biomarkers of disease. - Understand how neurodegenerative disease imaging and laboratory biomarkers represent a logical adjunct to improve diagnosis, track disease progression, guide therapeutic molecular targets, and monitor treatment response.

2456

The Circuits of Life: Patterns and Etiologies of Brainstem Lesions

T Hinkel[1], V Patel[2], J Biren-Fetz[2], J Caskey[2], U Udayasankar[2], B Winegar[2]
[1]Tucson Hospitals Medical Education Program, Tucson, AZ, [2]University of Arizona, Tucson, AZ

Purpose
To familiarize the reader with brainstem lesions due to various etiologies, the associated clinical presentation, and the relevant anatomy through a case-based approach. The midbrain, pons, and medulla, as well as the cranial nerve nuclei and nerve tracts contained therein will be discussed.
Materials and Methods
Electronic Educational Review
Results
This educational exhibit will review multiple brainstem lesions with emphasis on the details of the anatomic circuitry and the respective clinical presentation. After a brief review of brainstem anatomy, a multitude of cases will be used to show the imaging findings, highlight the clinical presentation, and demonstrate the correlate anatomic insult. Patterns to be presented include: Dejerine Syndrome, Wallenburg Syndrome, Foville Syndrome, Gubler Syndrome, Weber Syndrome, Benedikt Syndrome, internuclear opthalmoplegia, hypertrophic olivary degeneration; various etiologies will be discussed.
Conclusions
After the reader has viewed the exhibit, they will be able to better distinguish and categorize closely related patterns of brainstem lesions and predict their clinical presentation. The reader will also be more familiar with the regional anatomic details of the brainstem.

2593

The Craniovertebral Junction: No Country for Old Men

A Costacurta[1]
[1]CLINICA FELIPPE MATTOSO, RIO DE JANEIRO, Brazil

Purpose
The craniovertebral joint is the most mobile portion of the spine and is essential to maintaining the stability of the cervical spine. The CVJ comprises the occiput and the two first vertebrae and the odontoid, along with an intricate ligamentous apparatus, is pivotal to this complex arrangement. Congenital and acquired pathologies of the odontoid may be associated with atlanto-axial dislocation and basilar invagination. Chronic mechanical dysfunction and instability may also lead to the formation of fibrous granulation tissue as a response to abnormal stress and friction, complicating the radiologic aspect. The aim of this pictorial essay is to review the relevant anatomy and anatomic variants and to

provide knowlegde for interpreting various disease processes, emphasizing the complementary roles of computed tomography and magnetic resonance imaging.

Materials and Methods

Quick review of embriology, odontoid anatomic variants, anatomy and topographic relationships of odontoid with respect to CVJ and craniometry. Explore the biomechanics of the cervical spine and the concept of the functional spinal unit, unstable injuries evolving over time and representing a risk for developing or worsening neurologic damage. Describe the roles of multidetector CT and MR imaging in the evaluation of diseases ,the respective strength of these imaging modalities in the assessment of bony and soft tissue injuries,and specifically the cord.

Results

Relevant anatomy Embriology and development anomalies of the odontoid Basic craniometry Fractures Degenerative spondylitis Infectious spondylitis Rheumatoid arthritis Ankylosing spondylitis Crowned dens syndrome

Conclusions

Craniovertebral junction ,and particularly the odontoid, is affected by a variety of congenital and acquired diseases and can be associated with chronic pain and progressive neurologic damage as in case of cord compression. Imaging this region continues to be a challenge for radiologists as often times the complex anatomy is complicated by degenerative changes superimposed on anatomic variants. Moreover the region is frequently overlooked in cervical spine studies. Multiplanar imaging with CT and MRI allows detailed evaluation of bony and soft tissue structures. Adequate knowledge of development, complex anatomy, typical disease processes , topographic relationships of odontoid with respect to CVJ and craniometry combined to the appropriate clinical background can provide meaningful diagnosis.

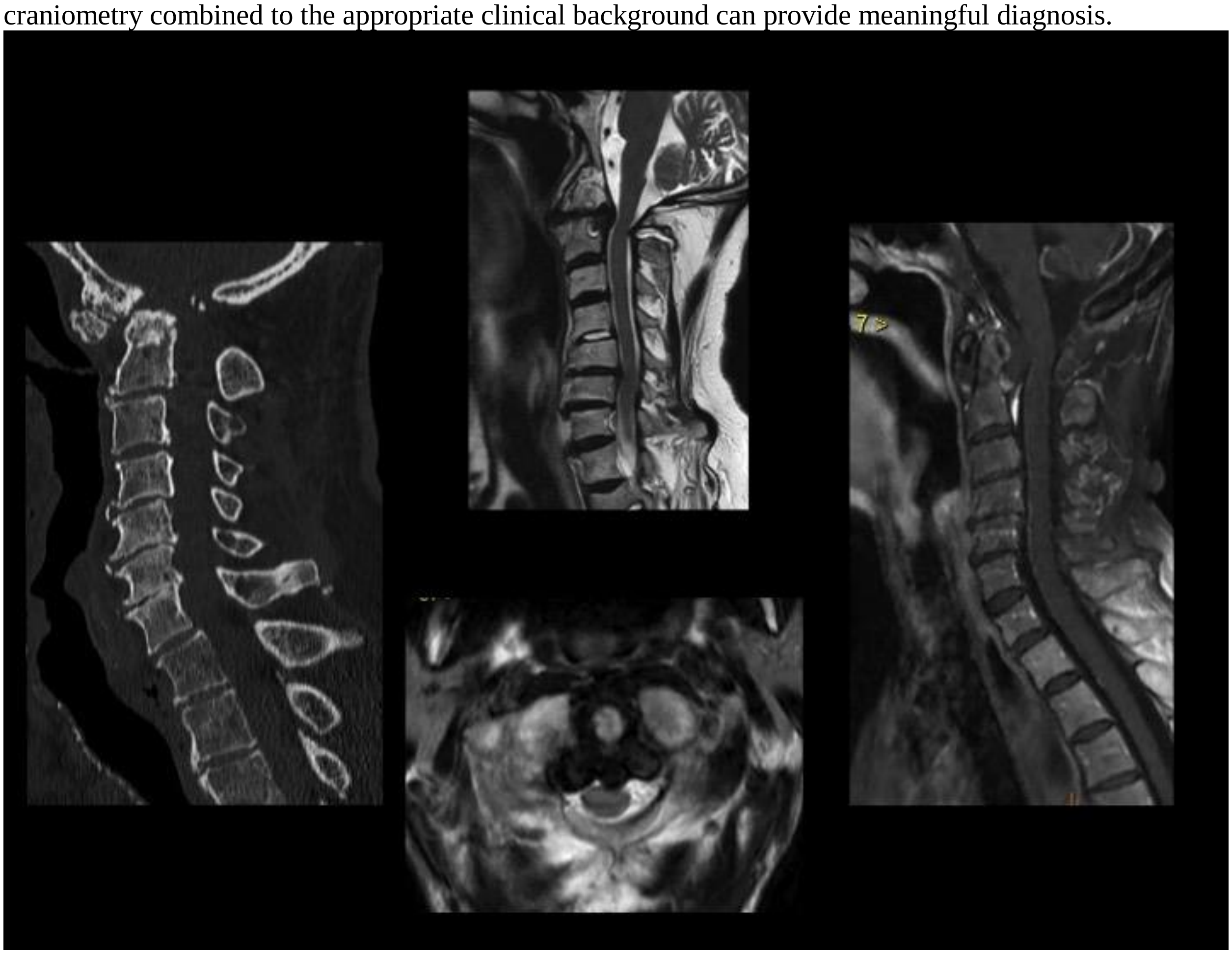

(Filename: TCT_2593_Slide1.jpg)

3057

The Exit of the Twelfth Cranial Nerve: Lesions of the Hypoglossal Canal

K Bhatia[1], S Mathur[1]
[1]*Royal Preston Hospital, Preston , United Kingdom*

Purpose
The hypoglossal canal is included in all imaging studies of the brain and often at the upper margin of studies of the cervical spine, but remains an overlooked area as pathology at this site is uncommon. However, it remains clinically important as hypoglossal nerve palsies can be disabling for patients. Certain aggressive pathologies can also be found at this site so detection of these lesions is crucial. We aim to provide a systematic approach and differential diagnosis that can be used both in patients presenting with relevant symptoms and for incidentally detected lesions affecting this region.
Materials and Methods
We will use a case based approach to highlight the key and differentiating imaging features of lesions that can be seen involving the hypoglossal canal. These include cysts, nerve sheath tumours, meningiomas, vascular anomalies and skull base metastases.
Results
We will discuss the appropriate and optimal sequences and techniques for assessment of this region, MR signal characteristics and patterns of enhancement that provide useful tools as well as focus on associated CT features with regard to assessment of the surrounding bony structures.
Conclusions
Optimal imaging techniques, as well as familiarity of appearances of classical lesions seen at this site should help ensure that this important component of the skull base is not overlooked.

2907

The Hypomyelinating Leukodystrophies: Imaging Features, Clinical Manifestations, and Genetic Underpinnings

V Patel[1], E Velez[2], S Ceglar[2], K See[3], M Shiroishi[4], B Tamrazi[5]
[1]*Keck School of Medicine of USC, Los Angeles, CA,* [2]*LAC+USC, Los Angeles, CA,* [3]*University of Southern California, Pasadena, CA,* [4]*KECK SCHOOL OF MEDICINE, USC, SOUTH PASADENA, CA,* [5]*Children's Hospital of Los Angeles, Los Angeles, CA*

Purpose
The educational exhibit will be divided into four sections, each with a distinct objective: Part 1 will review the normal CNS myelination milestones. Part 2 will briefly describe the process of oligodendrocyte differentiation, including its genetic regulation. Part 3 will provide a comprehensive review of the hypomyelinating leukodystrophies, including their imaging features, clinical manifestations, and molecular genetic underpinnings. Part 4 will teach the viewer about advanced myelin imaging and quantification techniques.
Materials and Methods
In Part 1, we will demonstrate the normal CNS myelination pattern using typical T1-weighted, T2-weighted, FLAIR, and DWI/DTI images at each time point. We will highlight the white matter regions expected to be myelinated at each age, and we will provide an aid to assist viewers in committing the expected white matter myelination patterns to memory. In Part 2, we will provide a review of oligodendrocyte differentiation from neural progenitor cells to their ultimate mature form. A limited discussion of the genes regulating this pathway will provide viewers the level of familiarity necessary to

understand the consequences of the mutations described in the subsequent section. The oligodendroglial differentiation process and its genetic regulation will be illustrated pictorially to maximize clarity and ease of recall. In Part 3, we will individually review the hypomyelinating leukodystrophies, including: 1) Pol III-related leukodystrophy, 2) oculodentodigital dysplasia, 3) Cockayne syndrome, 4) Pelizaeus-Merzbacher disease, 5) Pelizaeus-Merzbacher-like disease, 6) fucosidosis, 7) free sialic acid storage disease, 8) hypomyelination with congenital cataracts, 9) hypomyelination with brainstem and spinal cord involvement and leg spasticity, 10) hypomyelination of early myelinated structures, 11) hypomyelination with atrophy of the basal ganglia and cerebellum, 12) SOX10-associated hypomyelination, and 13) distal 18q- syndrome. For each leukodystrophy, we will provide representative neuroimaging, discuss any distinctive imaging and clinical features, and if known, provide the underlying genetic mutation and inheritance pattern. In Part 4, we will review advanced MR techniques for myelin imaging and quantification, including MWF mapping, DTI, MR spectroscopy, and magnetization transfer imaging. We will provide representative images of normally myelinated and hypomyelinated cases using each modality and briefly discuss the strengths and limitations of each technique.

Results

An example of the discussion to be contained in Part 3 of the exhibit is included below and references the attached figure: Pol III-related leukodystrophy: - This leukodystrophy is a result of pathologic mutations in the POLR3A, POLR3B, or POLR1C genes which encode subunits for the enzyme RNA polymerase III. - The inheritance pattern is autosomal recessive (AR). - Individuals with POLR3A mutations have later onset of symptoms but more rapid progression compared to individuals with POLR3B mutations. - Typical imaging findings: hypomyelinating T1 and T2 signal pattern with cerebellar atrophy (see attached figure) and thinning of the corpus callosum. - Typical clinical features: variable degrees of motor dysfunction, abnormal dentition, endocrine dysfunction (short stature, hypogonadism), and myopia. - The combination of hypomyelination, hypodontia, and hypogonadotropic hypogonadism is termed the 4H syndrome.

Conclusions

This four-part educational exhibit will provide a comprehensive review of the hypomyelinating leukodystrophies, including their basic cellular and genetic principles, the imaging and clinical features that can be used to identify and differentiate them, and the advanced imaging techniques that may soon be utilized to provide measures of disease severity. After reviewing the exhibit, we expect that viewers will better understand the unique features of this group of disorders and gain an awareness of the importance of evaluating the appropriateness of myelination in the early childhood period. We hope that this work will serve as an accessible and useful reference for radiologists in practice and in training when reviewing cases of suspected hypomyelination.

Pol III-related leukodystrophy. Left-to-right: axial T1-weighted, axial T2-weighted, and sagittal T2-weighted images of the brain of a 4-year-old male demonstrating hypomyelination and cerebellar atrophy.

(Filename: TCT_2907_poliii.jpg)

2965

The Sixth Sense: Lessons from Cranial Nerve VI Palsies

M Maher[1], P Meyers[2], J Odel[3], G Moonis[1]
[1]Columbia University Medical Center, New York, NY, [2]COLUMBIA UNIVERSITY, PHYSICIANS & SURGEONS, NEW YORK, NY, [3]Edward S. Harkness Eye Institute Columbia University Medical Center, New York, NY

Purpose
The purpose of this case is to review the course of cranial nerve (CN) VI, the presentation of a CN VI palsy and review pathologies that result in a cranial sixth nerve palsy.
Materials and Methods
In the setting of a CN VI palsy, an MRI of the orbit with contrast should be protocoled, including a gradient echo sequence, to evaluate the entire course of the nerve.
Results
Petrous chondroid tumors are classically T2 bright due to its cartilaginous origin and demonstrate enhancement; this benign chondroid tumor (A) is well circumscribed but must be distinguished from a chondrosarcoma on pathology. Angiograms of cavernous carotid fistulas (CCFs) demonstrate early filling of the cavernous sinus (B) when directly injecting the carotid artery. On non-invasive studies, CCFs typically cause dilation of the superior ophthalmic vein, enlargement of extraocular muscles and proptosis. Asymmetric flow voids may be present on MRI T2 sequences. World Health Organization (WHO) type I, II, and III meningiomas vary considerably: type I meningiomas (C) homogeneously enhance, have a dural tail, and cause hyperostosis of the underlying calvarium. Type II and III meningiomas (D) demonstrate aggressive growth pattern and invade adjacent structures. Meningioma types I, II, and II demonstrate avid dotatate uptake.
Conclusions
CN VI innervates the lateral rectus which is responsible for eye abduction. If pathology impacts CN VI at point along its course from the abducens nucleus to the lateral rectus muscle, the patient will present with double vision from gaze malalignment. Understanding the course of CN VI is critical identify the underlying pathology: the CN VI nucleus and intraparenchymal nerve reside in the caudal pons; a minority of CNVI fibers project to the medial longitudinal fasciculus to coordinate eye movements with the contralateral medial rectus. The remaining fibers exit the brain stem at pontomedullary groove. The nerve crosses the ambient cistern and enters Dorello's canal within the clivus. CN VI then passes through the cavernous sinus lateral to the carotid artery and passes through the superior orbital fissure to reach the lateral rectus. Imaging must evaluate the nerve in its entirety to identify the cause of the CN VI dysfunction.

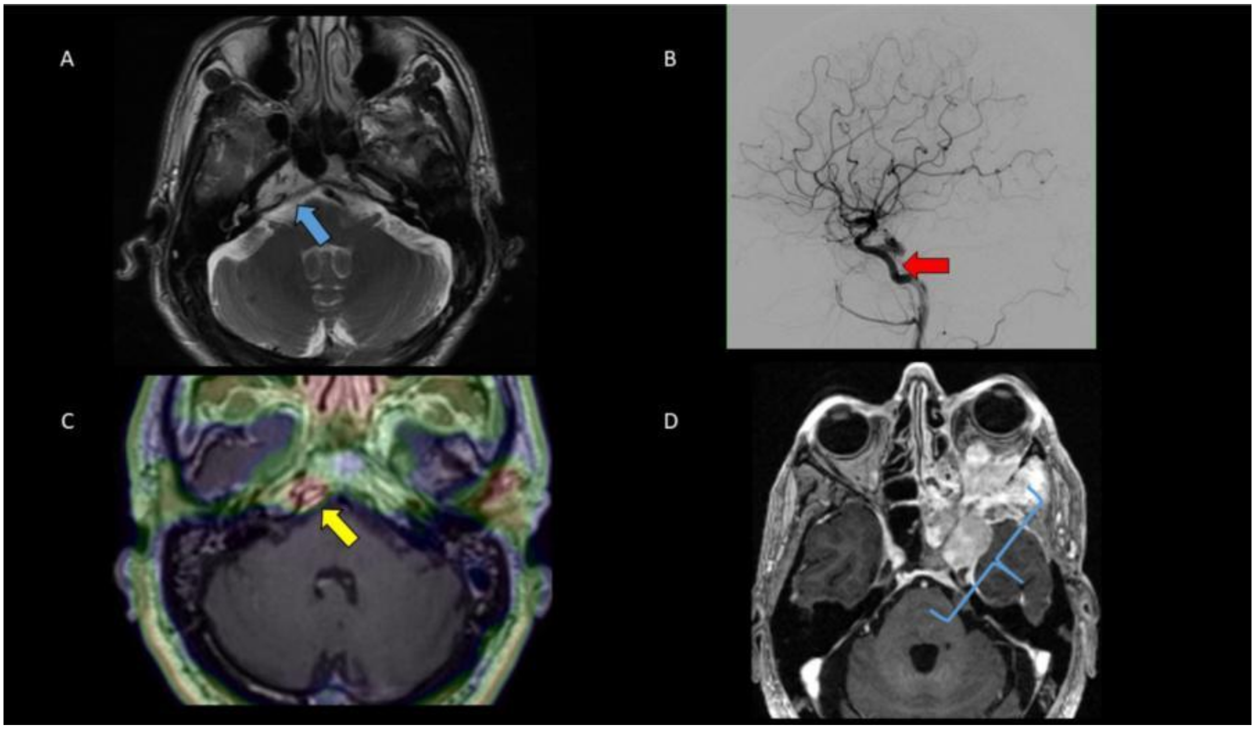

(Filename: TCT_2965_ASNRCNVI.jpg)

3325

The Spectrum of Anti-Myelin Oligodendrocyte Glycoprotein Antibody Associated CNS Demyelination in Children

B Hill[1], D Streicher[1], A Mian[1], S Narula[2], K Shekdar[2], B Banwell[2], A Vossough[2]
[1]*CHILDREN'S HOSPITAL OF PHILADELPHIA, PHILADELPHIA, PA,* [2]*CHILDREN'S HOSPITAL OF PHILADELPHIA, UNIVERSITY OF PENNSYLVANIA, PHILADELPHIA, PA*

Purpose
Summary: Myelin oligodendrocyte glycoprotein (MOG) is a protein found in the outer myelin sheath of CNS axons and the plasma membrane of oligodendrocytes. Anti-MOG antibodies have been reported to be present in up to 50% of pediatric patients presenting with incident acquired demyelination syndromes and may contribute to disease pathogenesis. Accurate, cell-based assays for the detection of serum anti-MOG antibodies have only recently become clinically available and remain time consuming, making imaging important for timely diagnosis. The clinical and imaging features of anti-MOG associated demyelination are heterogeneous and may overlap with other disorders such as vasculitis, other demyelination syndromes, and various inflammatory/infectious conditions. Importantly, disease modifying drugs used to treat multiple sclerosis may not be effective in MOG-related demyelination syndromes, whereas other medications (e.g. IVIG, rituximab) may be effective. Neuroimagers should be familiar with the spectrum of MRI findings in MOG-related demyelination in order to facilitate timely diagnosis and appropriate medical management.
Materials and Methods
Educational objectives: • Learn the basic facts about the MOG protein • Understand the basic pathophysiology and laboratory testing for MOG-related demyelination • Become familiar with the various clinical presentations of MOG-related demyelination • Become familiar with the various imaging features of MOG-related demyelination (brain, spinal cord, optic nerves) • Know when to put MOG into

your differential diagnosis • Understand that the medical management of MOG-related demyelination is different from relapsing remitting multiple sclerosis
Results
N/A
Conclusions
N/A
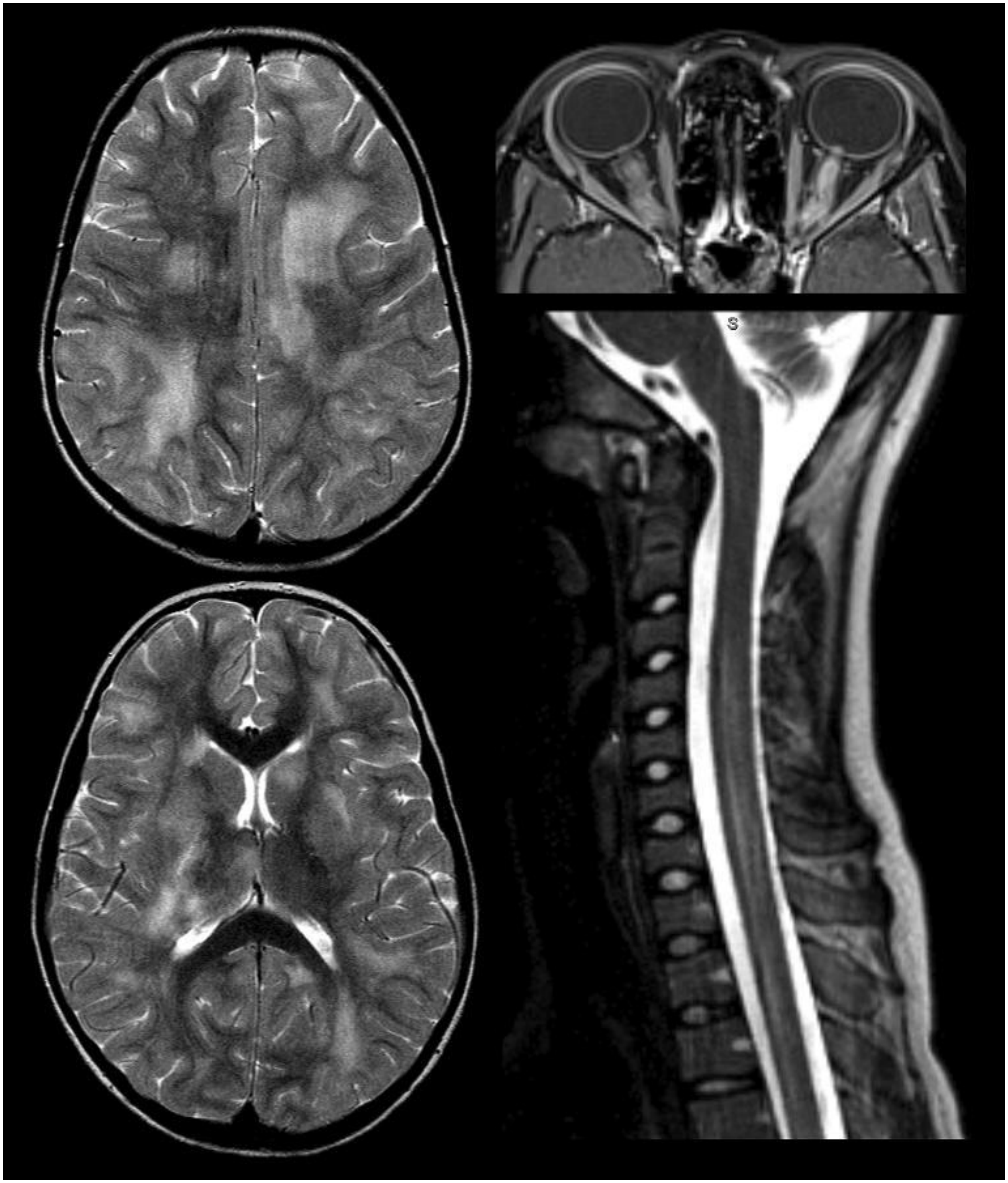

(Filename: TCT_3325_Untitled-1.jpg)

3291

The Uncinate Process and its role in Sinus Evaluation

A Madhavan[1], I Russell[2], R Sinha[3], R Hyde[4], R Siripurapu[5], A Herwadkar[6]
[1]Salford Royal NHS Foundation Trust, Manchester, Salford, [2]Salford Royal NHS Foundation Trust, Manchester, Greater Manchester, [3]Salford Royal Hospital, UK, Burnley, Lancashire, [4]Salford Royal Hospital, Manchester, United Kingdom, [5]Greater Manchester Neurosciences Centre & Salford Royal NHS Foundation Trust, Salford, Manchester, [6]Salford Royal Hospital, Manchester, Greater Manchester

Purpose
The purpose of this educational exhibit is to illustrate the normal and variant anatomy of the uncinate process and provide an overview of common sinus pathologies arising from the anatomical variations. The exhibit will also highlight management/surgical considerations and discuss pitfalls encountered based on salient CT findings.
Materials and Methods
Through logical presentation, the common CT appearances of the uncinate process will be illustrated, allowing the learner to recognise common variations of the uncinate process. Focus will be placed on CT appearances, which is the gold standard when imaging the sinuses. A description of the functional anatomy of the uncinate process will be provided such as angulations, degrees of pneumatisation, insertions and relation to adjacent structures; which will allow better understanding of why the visualised anatomy contributes towards sinus dysfunction. Commoner pathologies of the sinus will then be discussed along with surgical approaches and post-surgical imaging.
Results
The uncinate process is a major component of the ostiomeatal complex (OMC), which facilitates mucociliary drainage of the frontal, anterior ethmoidal and maxillary sinuses into the middle meatus, whilst directing inspired airflow away from the sinuses and expired sterile airflow towards them. Chronic sinusitis arises from anatomical variation or pathology of the OMC. Knowledge of the normal intricate anatomy and common anatomical variants is not just crucial for understanding functional problems, but also in planning functional endoscopic sinus surgery (FESS). Uncinectomy and maxillary antrostomy form the basis of this surgery; thus good grasp of the anatomy is key, to avoid complications and poor outcomes caused by damage to important adjacent structures.
Conclusions
The anatomy and variability of the uncinate process and its role in sinonasal pathology is often poorly understood and subtle findings can be missed when reporting. Following this exhibit, the learner will be more confident in understanding the normal anatomy of the uncinate process, its role in common sinus pathologies arising from the anatomical variations, recognizing imaging pitfalls on CT and the implications on management/surgery.

2339

The Unkempt Cauda Equina – Pathology of the Horse's Tail

V Parenti[1], F Huda[2], P Richardson[3], M Aulakh[2], M Taheri[2]
[1]The George Washington University School of Medicine and Health Sciences, Washington, DC, [2]Department of Radiology, The George Washington University Hospital, Washington, DC, [3]Department of Neurology, The George Washington University Hospital, Washington, DC

Purpose
The purpose of this presentation is to describe the diverse array of pathologies that can affect the cauda equina and to show the imaging and clinical findings associated with those conditions.
Materials and Methods
A range of abnormalities involving the cauda equina will be reviewed through case vignettes with MRI imaging.
Results
Cauda equina syndrome, which is caused by nerve root compression below the conus medullaris, is often induced by an extradural process such as disc herniation. Other indirect processes affecting the cauda equina include epidural abscess and dural arteriovenous fistula. An assortment of other pathologies involve the cauda equina directly. Although MRI findings are often not pathognomonic, a combination of MRI and clinical findings are often predictive of these disease states. For instance, clumping and contour abnormality of the nerve roots along with back/leg pain and radiculopathy are features suggestive of arachnoiditis. Diffuse nerve root thickening combined with persistent lower extremity weakness and sensory changes are indicative of chronic inflammatory demyelinating polyneuropathy. In this presentation, we will review common as well as uncommon pathologies of the cauda equina including those of inflammatory, infectious, neoplastic, and congenital etiology among others. More specifically, examples will include Guillain-Barre syndrome, tuberculous radiculomyelitis, perineural extension of lymphoma, and neurofibromatosis of the lumbar spine.
Conclusions
A variety of pathologies can involve the cauda equina. Awareness of the imaging and clinical manifestations of these entities can augment the impact of the radiologist on the management of patients with lower extremity neurologic signs and symptoms.

2931

The Utility of Multiparametric Magnetic Resonance Imaging in the Diagnosis of Brainstem Lesions

B Butler[1], M Bowen[1], M Patel[1], S Al-Ali[1], R Flintham[1], J Herbert[1], N Davies[1], V Sawlani[1]
[1]University Hospitals Birmingham NHS Foundation Trust, Birmingham, West Midlands, United Kingdom

Purpose
Brainstem lesions pose a significant diagnostic challenge. The critical nature of the brainstem renders invasive biopsy difficult, often yielding inconclusive results. Multiparametric magnetic resonance imaging (MRI) is a useful adjunct to conventional MRI sequences and can aid in the differentiation of neoplastic, inflammatory and vascular lesions. However, technical factors make obtaining multiparametric data of brainstem lesions difficult and consequently few studies have examined its utility for this purpose. Here we present our experience of characterizing brainstem lesions using multiparametric MRI at a tertiary neurosciences centre in the United Kingdom. Educational objectives: 1. Understand the sequences acquired in multiparametric MRI 2. Recognise the utility of multiparametric MRI and its appropriate application 3. Appreciate the technical limitations of multiparametric MRI in assessing brainstem lesions 4. Be able to differentiate neoplastic and inflammatory lesions in the brainstem based on multiparametric MRI features
Materials and Methods
We retrospectively reviewed all multiparametric MRI studies performed at our institution between 2013-2018. Conventional MRI failed to establish a diagnosis in all cases. Lesion characteristics on standard contrast-enhanced T1- and T2-weighted sequences, dynamic contrast-enhanced MRI, diffusion-weighted imaging (DWI), including apparent diffusion co-efficient (ADC) maps, and single and multivoxel spectroscopy were examined. Choline:creatine (Cho:Cr) peak area ratio was calculated and correlations between relative cerebral blood flow (rCBV) ratio, ADC, Cho:Cr, serological markers and follow-up imaging were recorded.

Results
Multiparametric MRI was performed on 560 patients, of which 31 (5.5%) were to assess indeterminate brainstem lesions. Of these, 18 (58%) provided useful additional diagnostic information to correctly differentiate neoplastic and inflammatory lesions. Cases of note included high-grade glioma, low-grade glioma, transformation of a low-grade to high-grade glioma, Bickerstaff encephalitis and neurosarcoid. These diagnoses were confirmed by follow-up imaging in 3 cases, biopsy in 1 case and serological markers in 1 case.
Conclusions
Conventional MRI sequences in combination with multiparametric data can provide an accurate and non-invasive means of differentiating between inflammatory and neoplastic brainstem lesions, potentially avoiding biopsy. However, significant technical factors render multiparametric assessment of brainstem lesions challenging and of limited use in a minority of cases.

2720

Tips and Tricks for Interpreting CT Perfusion Imaging: From Novice to Pro in Twenty Minutes!

A Bryant[1], G BATHLA[2], C Derdeyn[3]
[1]University of Iowa, Iowa City, IA, [2]University of Iowa hospitals and Clinics, IOWA CITY, IA, [3]University of Iowa, St. Louis, MO

Purpose
Recent trials such as DEFUSE III and DAWN have significantly expanded the role of CT perfusion (CTP) in the diagnosis and management of acute ischemic stroke (AIS). Interpreting CTP imaging however can be a daunting task, especially for the junior on-call residents, more so within the narrow time constraints of emergent situations. Nevertheless, a timely and accurate interpretation of these studies is crucial for decision making for mechanical thrombectomy. The authors provide a concise review of the CTP principles, techniques, tricks and pitfalls, allowing for more nuanced and accurate interpretation.
Materials and Methods
A review of current literature combined with our own institutional experience will be presented. Topics will include: (1) Principles and acquisition techniques for perfusion imaging, (2) perfusion output parameters, (3) interpretation of output parameters, and (4) assessment and prognostic utility of collateral vasculature. Interpretation tips and tricks will be presented in a case review format, with the reader reviewing potential pitfalls.
Results
CTP is an invaluable tool in acute stroke management, and can distinguish core infarct from potentially salvageable ischemic penumbra. Collateral vasculature is an important factor in salvageable brain, and can be assessed on CTP. Multiple automated softwares are now available to provide rapid analysis of perfusion data, and often help with image interpretation. However, there are many potential pitfalls when reviewing perfusion maps for which the interpreting radiologist should be aware. These include underlying vascular malformations, seizures, infection, improper input/output region of interest placement, and extracranial stenosis, among others. An understanding of these basic concepts will improve image interpretation and patient management.
Conclusions
The authors present a concise, yet comprehensive imaging review of CTP, its interpretation and pitfalls. These are expected to apprise the novice reader of the potential tricks and helpful hints, and hopefully make it less intimidating in emergent settings.

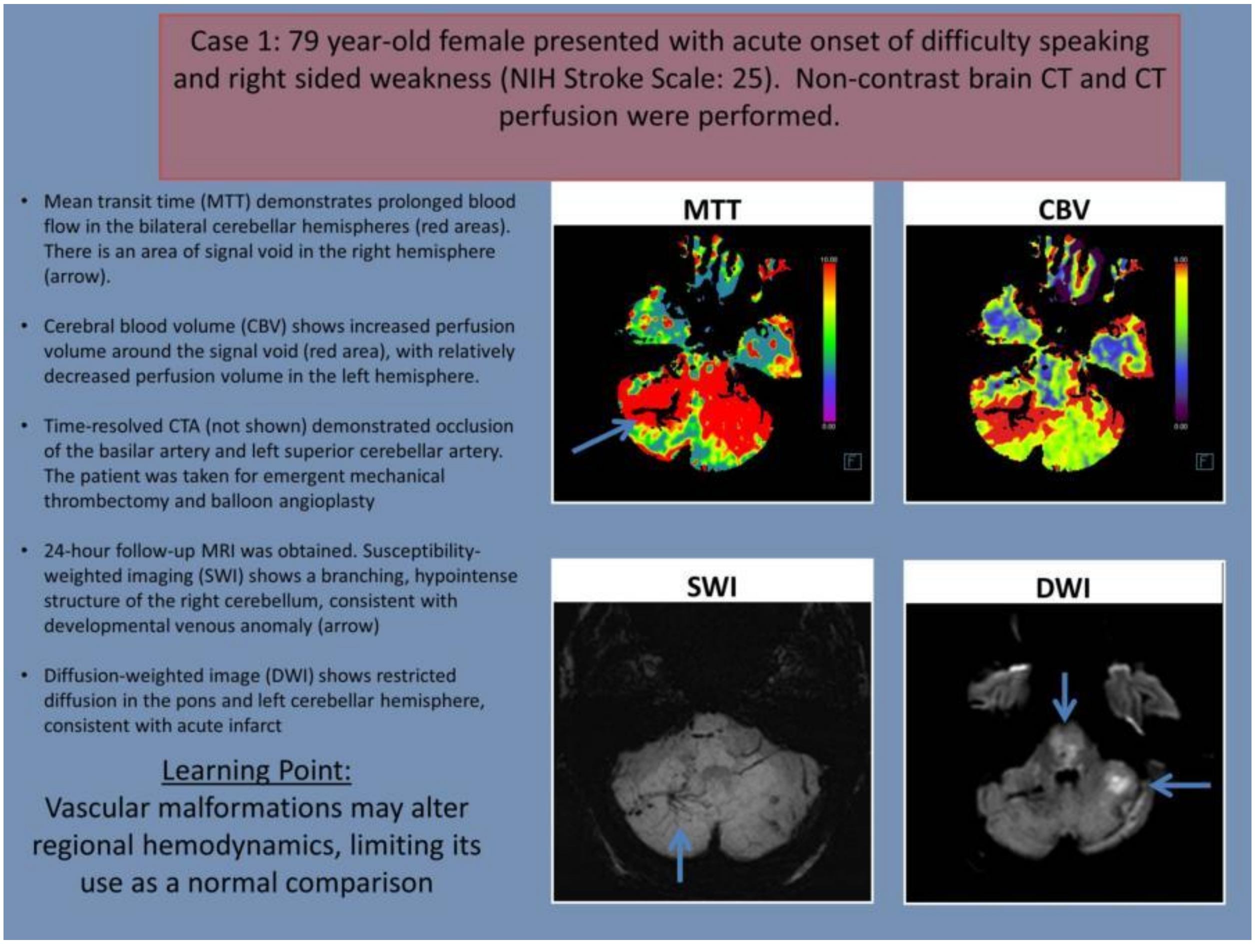

(Filename: TCT_2720_caseexample1.jpg)

3479

Tumefactive Inflammatory Leukoencephalopathy in Cocaine Users

A Rovira Canellas[1], L Pessini[1], S Kremer[2], J Castilló[1], J Pottecher[2], J de Sèze[2], E Maciag[1], C Auger[1]
[1]*Section of Neuroradiology, Department of Radiology. Hospital Vall d'Hebron, Barcelona, Barcelona, Spain,* [2]*CHU de Strasbourg. Université de Strasbourg, Strasbourg, Strasbourg, France*

Purpose
Cocaine can potentially affect the central nervous system due to a direct effect, or by means of additive drugs. Levamisole has been increasingly used as an additive drug since it extends the stimulating effects of cocaine. This has led to an increase in the detection of its adverse reactions, including levamisole-induced multifocal inflammatory leukoencephalopathy (MIL). Our purpose is to highlight the magnetic resonance imaging (MRI) findings in the tumefactive presentation of this cerebral demyelinating disease.
Materials and Methods
We present three patients with a history of chronic cocaine abuse, including a 2 month period of dose-increase in one of them before the clinical onset. Two of our patients developed acute manifestations of diffuse cortical dysfunction, while the other one had predominantly motor focal deficits. None had developed neurological symptoms before. Imaging findings on 1.5 Tesla MRI revealed the presence of tumefactive inflammatory leukoencephalopathy in all of them. The first two patients had lesions with the typical imaging pattern of Balo's Concentric Sclerosis (BCS).

Results

The pathophysiology of levamisole-induced MIL may depend on an immunological mechanism, producing multiple demyelinating lesions affecting the subcortical and periventricular white matter, basal ganglia and/or brainstem. Atypical demyelinating lesions are an unusual finding in levamisole-induced MIL. Specifically, the BCS pattern is a rare finding in these patients: to our knowledge, only two more cases mimicking BCS have been reported in the literature, which have also occurred in chronic cocaine users.

Conclusions

Based on the history and images of our patients and other two similar case reports, we suggest a probable physiopathological relationship between levamisole-adulterated cocaine use and the occurrence of MIL with atypical demyelinating lesions, even when they present following a BCS imaging pattern.

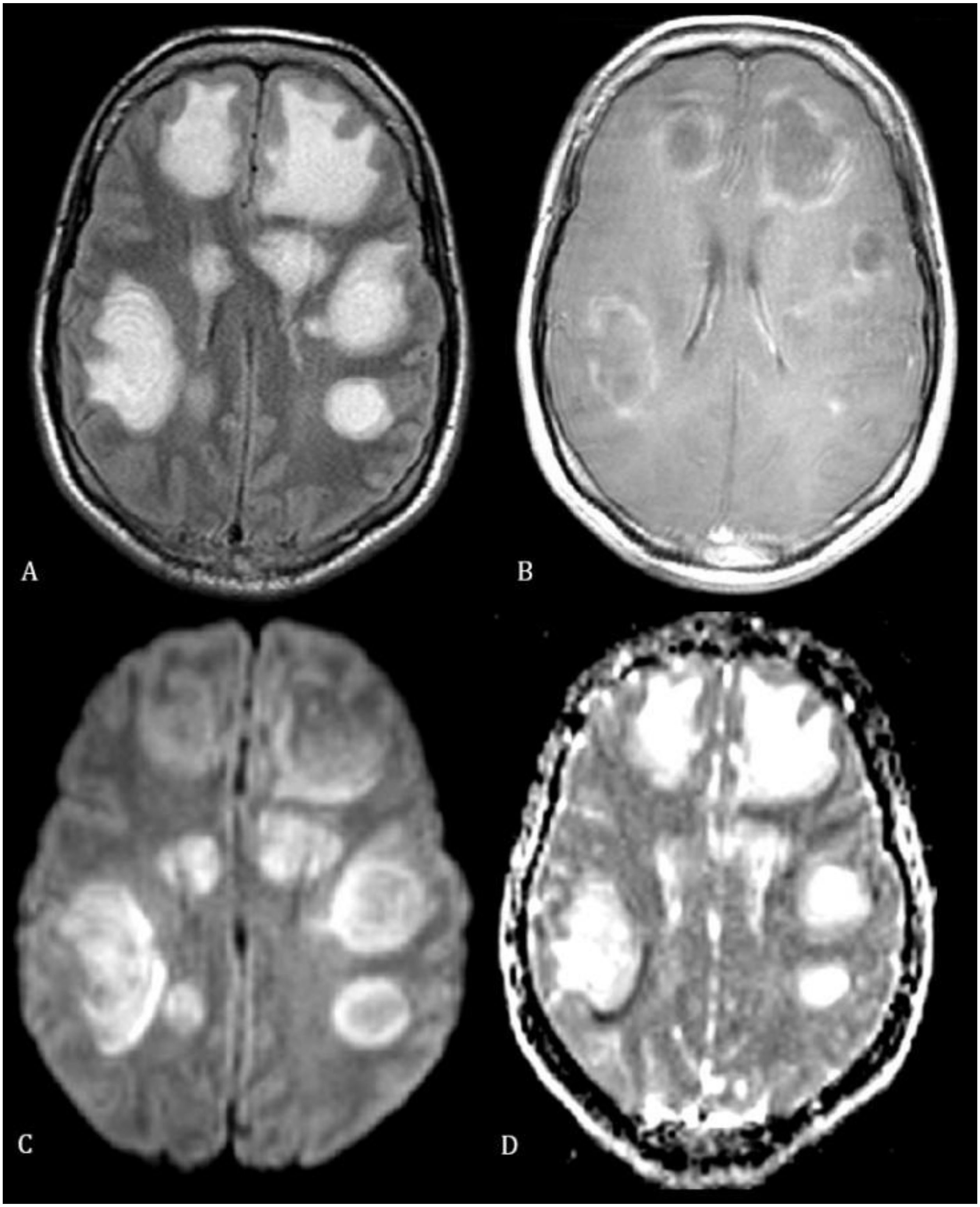

(Filename: TCT_3479_IMG.jpg)

3495

Turning up the Heat on Uncontrollable Seizures: Laser Ablation of Intractable Epilepsy.

G Curaudeau[1], L Chan[1], M Lanfranchi[2]
[1]Tufts Medical Center, Boston, MA, [2]Radiology Associates of Atlanta, Atlanta, GA

Purpose
The purpose of this abstract is to shed light on novel laser ablation techniques in the treatment of uncontrollable seizures.
Materials and Methods
With the help of a few representative cases, we will illustrate the evolution of treatment approaches from standard cortical resections to thermal-based laser ablations. Specifically we will reinforce the imaging findings pertinent for pre-operative planning, clarify the role of intraoperative imaging, and depict a few characteristic postoperative complications associated with cortical laser ablations.
Results
Epilepsy refractory to medical treatment is clinically challenging given the vast array of epileptogenic causes. A few of these etiologies driven by developmental anomalies (i.e: cortical dysplasia, heterotopia, schizencephaly), neurocutaneous syndromes (i.e: Sturge-Weber, Tuberous Sclerosis) or even gliotic scars, may not be amenable to surgical treatments. Thankfully, other causes of intractable epilepsy, including mesial temporal sclerosis, cavernous hemangiomas and epileptogenic tumors (i.e: DNET, gangliogliomas) may be mitigated or cured through cortical resection or targeted ablation. Due to the image guided nature of laser thermal ablation, radiologists are increasingly encountering laser ablation studies on their worklists. Interestingly, these studies differ significantly based on whether the study involves lesion localization, pre-operative navigation planning, intraoperative thermal monitoring or postoperative assessments. We will use a cased-based approach to highlight the salient and relevant findings associated with each type of imaging.
Conclusions
Becoming familiar with the potential applications of laser-guided thermal ablation, as well as expanding our understanding of the technique itself, can be critical in assisting our clinical colleagues in managing this difficult condition. Ultimately, radiologists can play a vital role in providing valuable information to ensure operative success and reduce postoperative complications.

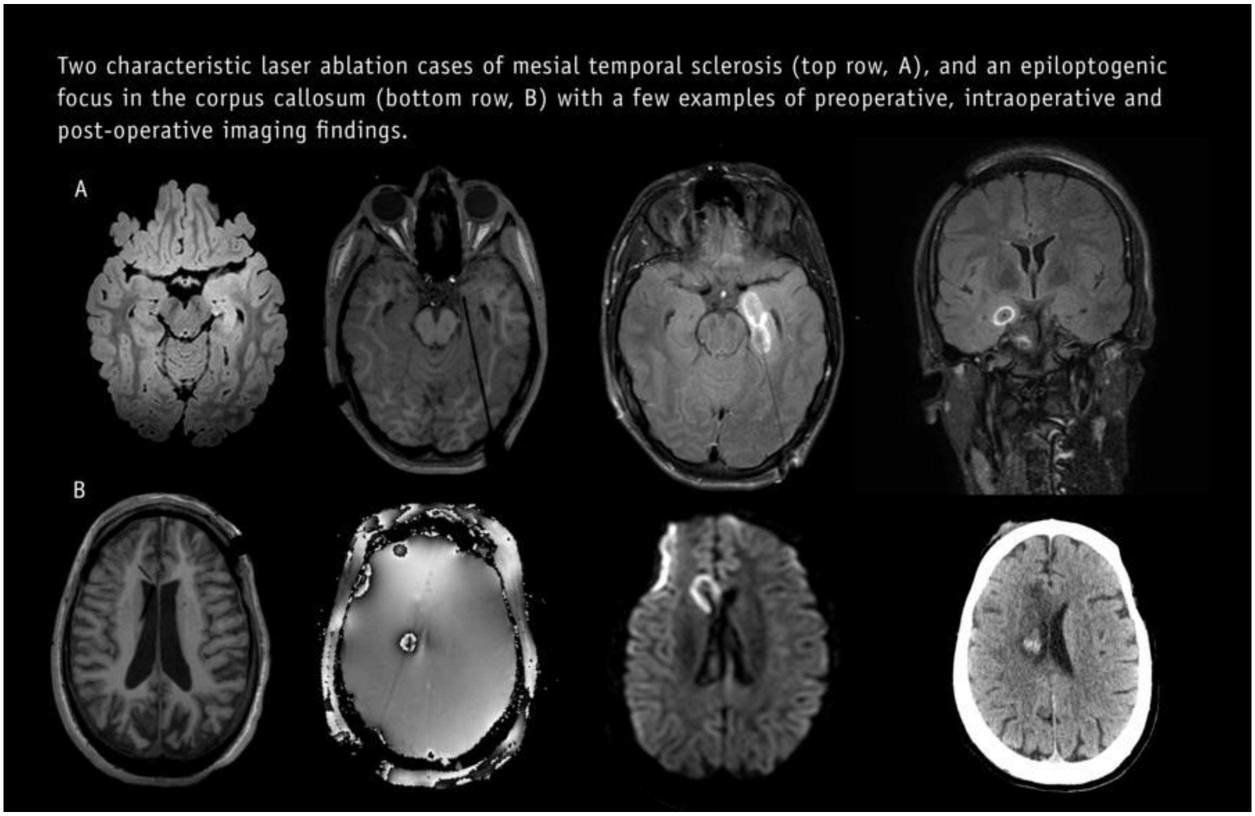

(Filename: TCT_3495_Abstract_image.jpg)

3344

Typical and Atypical Locations of Chordoma and Differential from Chondrosarcoma

C Altintas[1], E Dervisoglu[1], I Anik[1], Y ANIK[1]
[1]*Kocaeli University, Kocaeli, Turkey*

Purpose
Chordomas are rare malignant neoplasms derived from incomplete regression of notochordal tissue along the craniococcygeal axis.They are classified as sacrococcygeal, spheno-occipital, or vertebral according to their location. Also they can develop in an atypical position such as orbital, oropharyngeal and coxofemoral which are called ectopic chordomas. Because of similar anatomic location, clinical presentation, and radiologic findings chondrosarcomas can mimic chordomas. We aim to describe the typical and atypical locations of chordoma and illustrate magnetic resonance imaging (MRI) and diffusion weighted imaging (DWI) features that may distinguish chordoma from chondrosarcoma.
Materials and Methods
We retrospectively reviewed patients with pathologically confirmed chordoma (4 sacrococcygeal, 28 clival, 1 cervical spine, 1 orbital, 1 oropharyngeal and 1 coxofemoral) and skull base chondrosarcoma (n=17) who underwent MRI and DWI.
Results
In our series all atypical located chordomas revealed intermediate SI in T1-weighted images, high SI in T2 weighted images and low SI strands on the T2-weighted images, corresponding to fibrous septa like typical located chordomas. There were no significant differentiation criteria among chordomas and chondrosarcomas, with respect to morphology, SI and contrast enhancement patterns on conventional MRI. However DWI seems to differentiate chordomas from chondrosarcomas. Chondrosarcomas

revealed higher ADC values than chordomas, with the mean ADC value of the solid tumor component offering the highest accuracy for characterization.
Conclusions
Chordoma should be considered in differential diagnosis of a high T2 SI soft tissue mass with fibrous septa and lobulated margins anywhere adjacent to bone. Although conventional MRI findings are not specific, DWI seems to be promising tool for differential diagnosis of chordoma from chondrosarcoma.

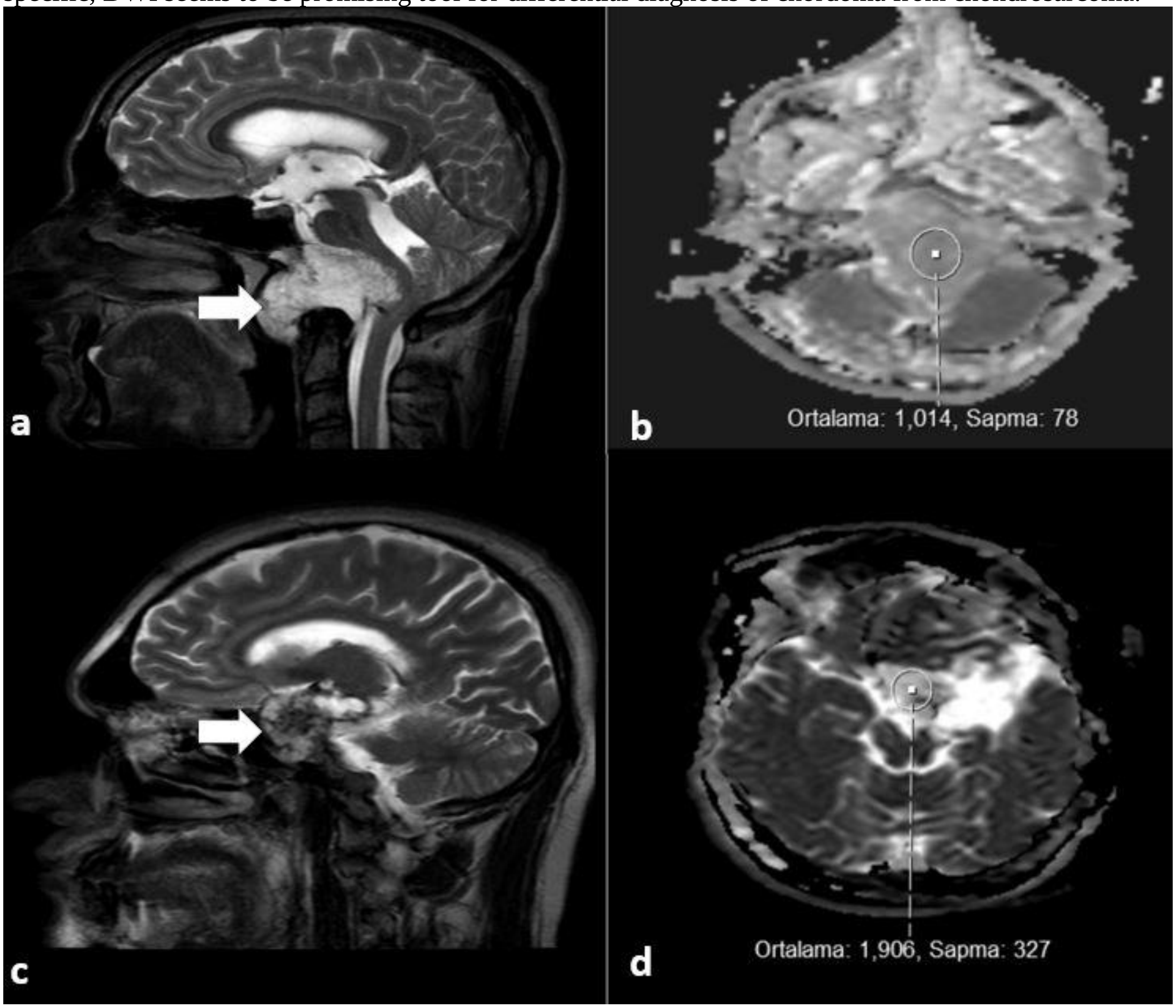

(Filename: TCT_3344_abstractpicture.JPG)

2942

Understanding the Venous Anatomy of the Cavernous Sinus

R Hyde[1], I Russell[1], R Sinha[1], R Siripurapu[1], A Herwadkar[1]
[1]*Greater Manchester Neurosciences Centre & Salford Royal NHS Foundation Trust, Manchester, United Kingdom*

Purpose
The cavernous sinus is unique among the dural venous sinuses due to its complex anatomy. It is a confluence of extracranial and intracranial venous drainage and so there are multiple afferent and efferent

tributaries, as well as crucial neurovascular contents and essential adjacent structures. Pathological processes involving the cavernous sinus and any subsequent treatments can therefore have serious potential risks and consequences.

Materials and Methods

Prior studies and reviews have established the embryological development, adult anatomy and function of the cavernous sinus [1,2]. Multiple imaging options are now available for diagnosis, including CT, MR and DSA venography, with their associated advantages and disadvantages [3]. There are also multiple management options of pathology in this region with medical, surgical, endovascular, and stereotactic treatments available.

Results

Our aim is to provide an educational overview of embryological development of the cavernous sinus in order to give a better understanding of the normal venous anatomy and, therefore a better understanding of pathological processes. We plan to use a case-based approach to the diagnosis and treatment of such lesions, with a particular focus on endovascular approaches and treatment of carotid-cavernous fistulas.

Conclusions

The cavernous sinus is a highly complex venous structure with many considerations towards diagnosis and management of lesions in this region. A good understanding of the embryological development is essential to understand the normal and therefore pathological anatomy in this region.

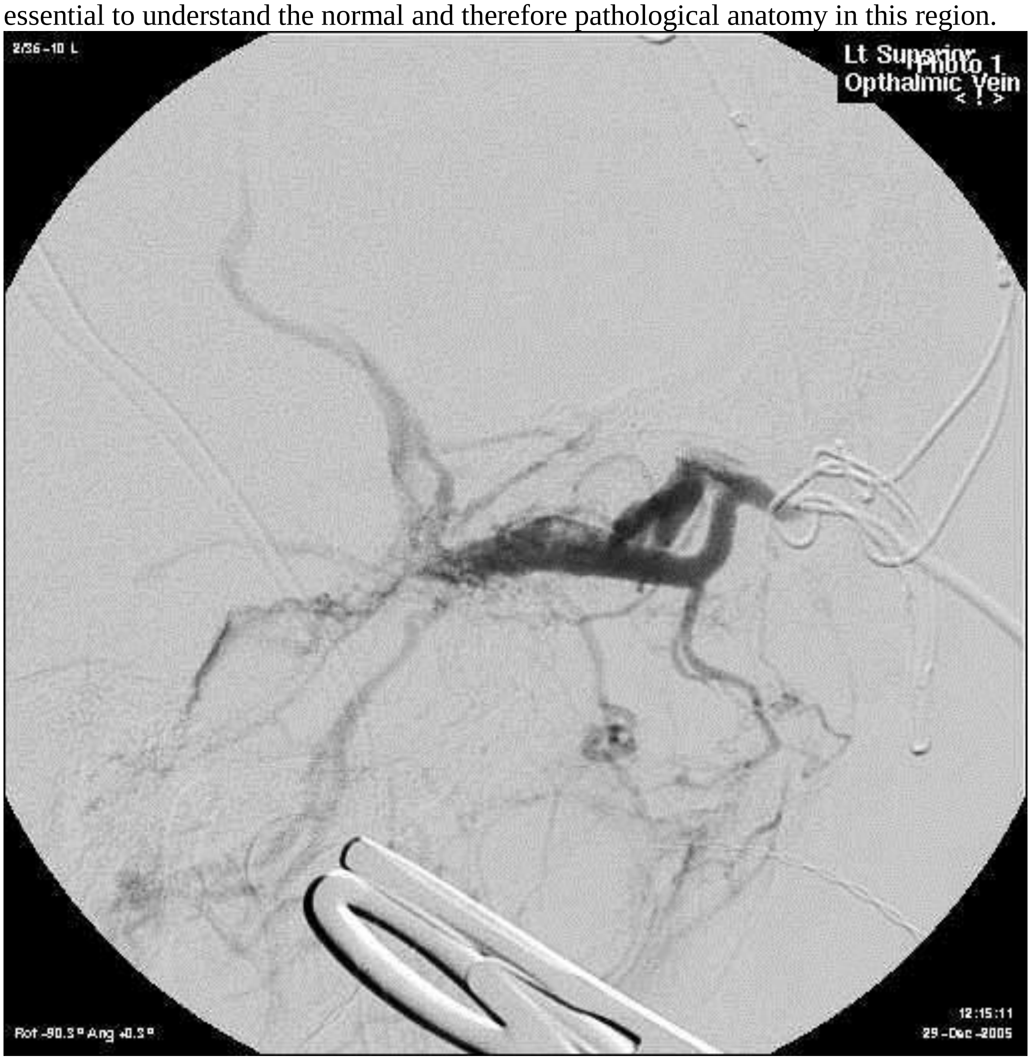

(Filename: TCT_2942_DSAcavernoussinus.jpg)

3425

Untangle Brain Vascular Malformations: Making the Diagnosis Easy!

C PARADA[1]
[1]*INSTITUTO MEDICO ENERI, BUENOS AIRES, Argentina*

Purpose
- Illustrate the major types of primary brain vascular malformations. - Discuss the imaging features that best describe each type of vascular malformations and their gold standard imaging method to evaluate them. - Discuss differential diagnosis of each vascular malformation and key points to distinguish them from other pathologies.
Materials and Methods
Invasive and non-invasive imaging methods for brain vascular malformations
Results
- Classification of brain vascular primary malformations. - Arteriovenous malformations and fistulas. Types, Imaging features and differential diagnosis. - Dural arteriovenous fistulas. Classification, Imaging features and differential diagnosis. - Cavernous malformations. Imaging features and differential diagnosis. - Telangiectasias. Imaging features and differential diagnosis. - Developmental venous anomalies. Imaging features and differential diagnosis. - Diagnostic imaging approach to distinguish vascular malformations.
Conclusions
There are a variety of brain vascular malformations. Some are aggressive high-flow lesions with risk of hemorrhage or other complications; others behave in a more benign manner. Knowledge of the imaging findings of these lesions aids in making treatment decisions.

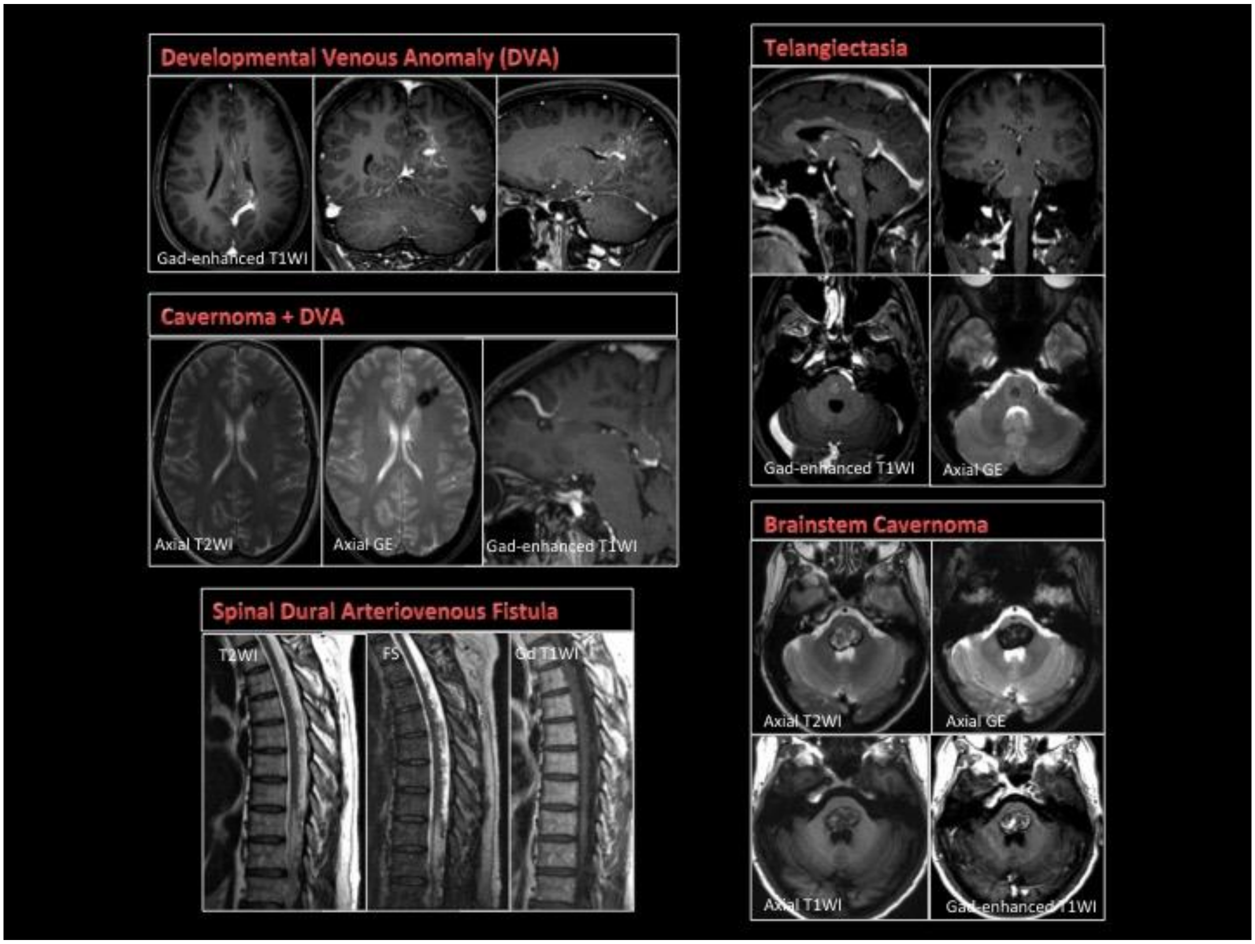

(Filename: TCT_3425_Slide1.jpg)

2374

Unusual Cases Demonstrating Leptomeningeal Enhancement

A Kamali[1], T Roberson[2], R Patel[3], R Riascos[3]
[1]UT HEALTH, HOUSTON, TX, [2]university of Texas Houston, HOUSTON, TX, [3]The University of Texas Health Science Center at Houston, Houston, TX

Purpose
The purpose of this presentation is to demonstrate multiple unusual cases of leptomeningeal disease including infectious, inflammatory, neoplastic and demyelinating disease.
Materials and Methods
We are presenting clinical and radiological representation of multiple interesting cases of infectious, inflammatory, neoplastic and demyelinating disease including the lyme disease, nocardiosis, candidiasis, cryptococcal meningitis, TB, PML, Wegener's granulomatosis, neurosarcoidosis, vasculitis, CLIPPERS, cerebral amyloid angiopathy, Glioblastoma, primary CNS lymphoma, ADEM and MS. We also provide differential diagnosis and description of the clinical course for each disease.
Results
We present multiple interesting cases of infectious, inflammatory, neoplastic and demyelinating disease including the lyme disease, nocardiosis, candidiasis, cryptococcal meningitis, TB, PML, Wegener's granulomatosis, neurosarcoidosis, vasculitis, CLIPPERS, cerebral amyloid angiopathy, Glioblastoma,

primary CNS lymphoma, ADEM and MS demonstrating leptomeningeal enhancement along with description of the clinical course and differential diagnosis for each disease.
Conclusions
We present a very informative visual illustration of leptomeningeal pathologies by variant diseases along with description of the course and differential diagnosis of each disease.

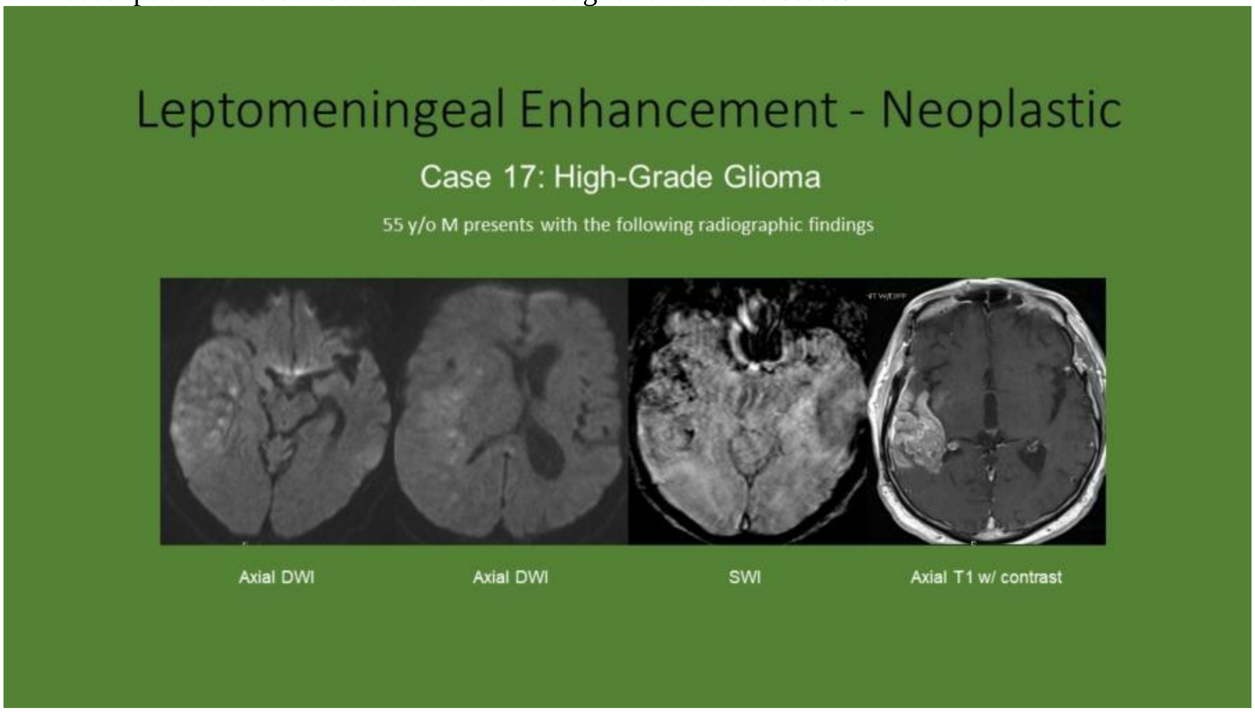

(Filename: TCT_2374_Image.jpg)

2975

Unusual Head and Neck Pathology – A Primer for Residents

C Pedersen[1], A Honarmand[1], S Roshan[2], M Brooks[1]
[1]Mercy Catholic Medical Center, Darby, PA, [2]University of Minnesota, Minneapolis, MN

Purpose
1. Head and neck pathology can be challenging with many structures in limited space and at times confusing terminology. 2. Thorough understanding of the anatomic spaces and their content help localize the pathology and narrow the list of differential diagnosis. 3. Displacement of an anatomical space by a mass can be used to localize the exact origin of the offending lesion. 4. Certain pathological conditions such as squamous cell carcinoma can spread from one anatomical compartment to another.
Materials and Methods
In this case-based educational exhibit we will show cases with unusual and also more common head and neck pathology, illustrated in a structured format with review of the most important anatomical spaces, their boundaries and content. Using CT and MRI cases from our institution, we will provide the reader with examples of pathology within these spaces and review how the list of differential diagnosis changes depending on what anatomical space the lesion is located in.
Results
1. The key anatomic spaces, their content and boundaries will be illustrated with CT and MRI images. 2. A variety of unusual and more common pathological conditions will be shown for each of the anatomic spaces, including but not limited to infectious, malignant, benign, congenital and traumatic lesions. 3. A

practical approach using displacement of the spaces will be illustrated with cases. 4. Differential diagnosis based on the content of these spaces will be highlighted.
Conclusions
The anatomy of the head and neck is complex with many important structures in small areas. The terminology is often confusing with different names for the same structures. A structured approach using the anatomical spaces helps the reader localize the disease in an anatomical compartment, create a relevant list of differential diagnosis and to arrive at a diagnosis.

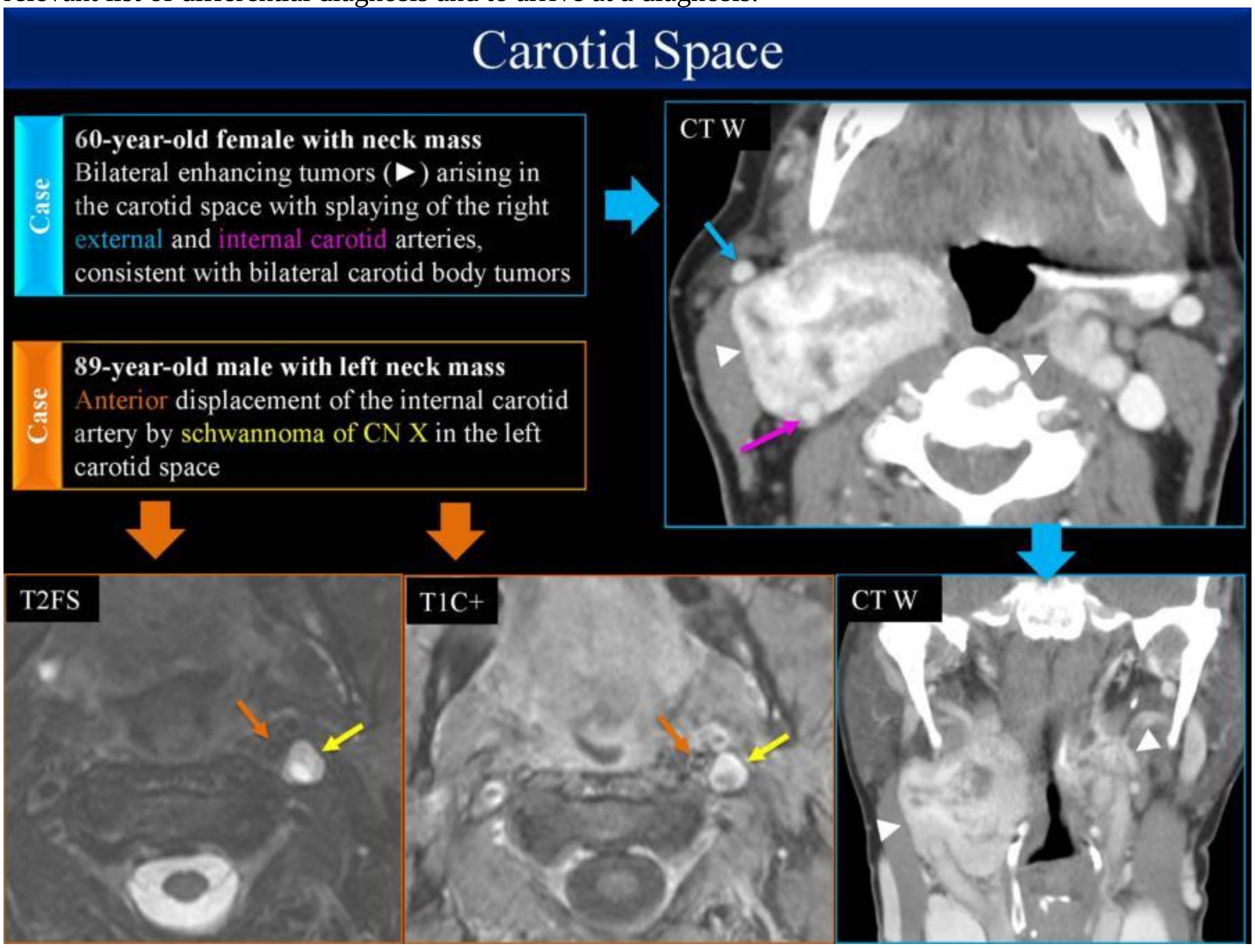

(Filename: TCT_2975_UnusualHeadNeckPathology-APrimerforResidents_Page_5.jpg)

3135

Update on Localization-Related Epilepsy: What Neuroradiologists Should Know

R Assadsangabi[1], J Stein[2]
[1]University of Pennsylvania, Philadelphia, PA, [2]Hospital of the University of Pennsylvania, Philadelphia, PA

Purpose
Neuroimaging is an important component of the pre-surgical planning for localization related epilepsy. Our aim is to review the updates in advanced structural and functional imaging techniques as well as must-know imaging features of emerging less invasive therapies for localization related epilepsy.
Materials and Methods
We reviewed the epilepsy, neuroradiology and neurosurgery literature and also identified relevant

imaging studies performed at our institution for patients with localization-related epilepsy across the spectrum of diagnosis and treatment.
Results
Following a summary of epilepsy statistics, terms and concepts, including the International League Against Epilepsy 2017 revised classification of seizures, discussion and illustrative examples cover technical aspects and pitfalls of epilepsy imaging with MRI; a checklist of structural lesions and how best to find them; adjunctive use of PET, SPECT and MEG; functional MRI for language lateralization; 7T MRI structural and glutamate imaging; intracranial EEG electrode localization; vagus nerve stimulator and responsive neurostimulator devices; and laser thermal ablation.
Conclusions
The diagnosis and treatment of medication refractory localization-related epilepsy is changing as clinicians move towards less invasive and more selective and adaptive approaches. Our review will help neuroradiologists understand new concepts, techniques and imaging aspects of emerging therapies for localization-related epilepsy.

2165

Use of fMRI in Detecting Covert Consciousnesses: The State of Imaging & its Relevance

M Aftab[1], A Sajid[2], A Concannon[3]
[1]Ascension Genesys Hospital, Flushing, MI, [2]Michigan State University, Flushing, MI, [3]Michigan State University's College of Osteopathic Medicine, Rochester Hills, MI

Purpose
Functional magnetic resonance imaging (fMRI) has enabled the detection of covert consciousness in some patients lacking a behavioral response. This educational exhibit will analyze the current state of the science in functional-BOLD imaging, current methods, clinical usages, advancements, and limitations of the use of fMRI in detecting covert consciousness.
Materials and Methods
The educational exhibit will illustrate the basic principles of fMRI-BOLD imaging, including technique, mechanisms and protocols for imaging. The exhibit will also present clinical cases of its use in detecting covert consciousness. A graphic illustration of passive, active and communicating levels of consciousnesses as detected by fMRI will be presented. This will including spatial and temporal paradigms for patient communication. The limitations of fMRI imaging will also be discussed and presented.
Results
fMRI is a noninvasive technique which can be used to detect brain activation as a response to auditory stimulation. Brain activation is mapped through the changes in blood-oxygen levels as neuronal activity is directly related to cerebral blood flow. Functional MRI, unlike PET imaging allows for more precise localization of cortical activity. Imaging protocols have been developed to assess for levels of consciousnesses for patients, this is particularly useful for patients in a clinically vegetative state. This has opened a new window and created a new set of tools for the study of disorders of consciousness. Neurological examinations have traditionally been used to diagnose patients by assessing response to commands and determining if the response is reflexive or voluntary. The assessment of passive, active and communicating levels of consciousness with fMRI in the clinical setting will be presented. The specific techniques used for each level of consciousnesses will be presented including temporal and spacial navigation paradigms. Limitation of fMRI studies include their small sample size and large false positive rate associated with these studies. Recent studies in patients who are in pharmacologically induced vegetative states and fMRI show promise in refining fMRI techniques.
Conclusions
Functional MRI imaging adds a significant new clinically relevant tool in the evaluation of disorders of

consciousness. This is new tool-kit for neurological disease is heavily imaging dependent and increasingly neuroradiologists will be required to become familiar with its protocols and clinical use. This exhibit will present an overview and brief introduction to this new imaging modality and specifically its use in the study of disorders of consciousness.

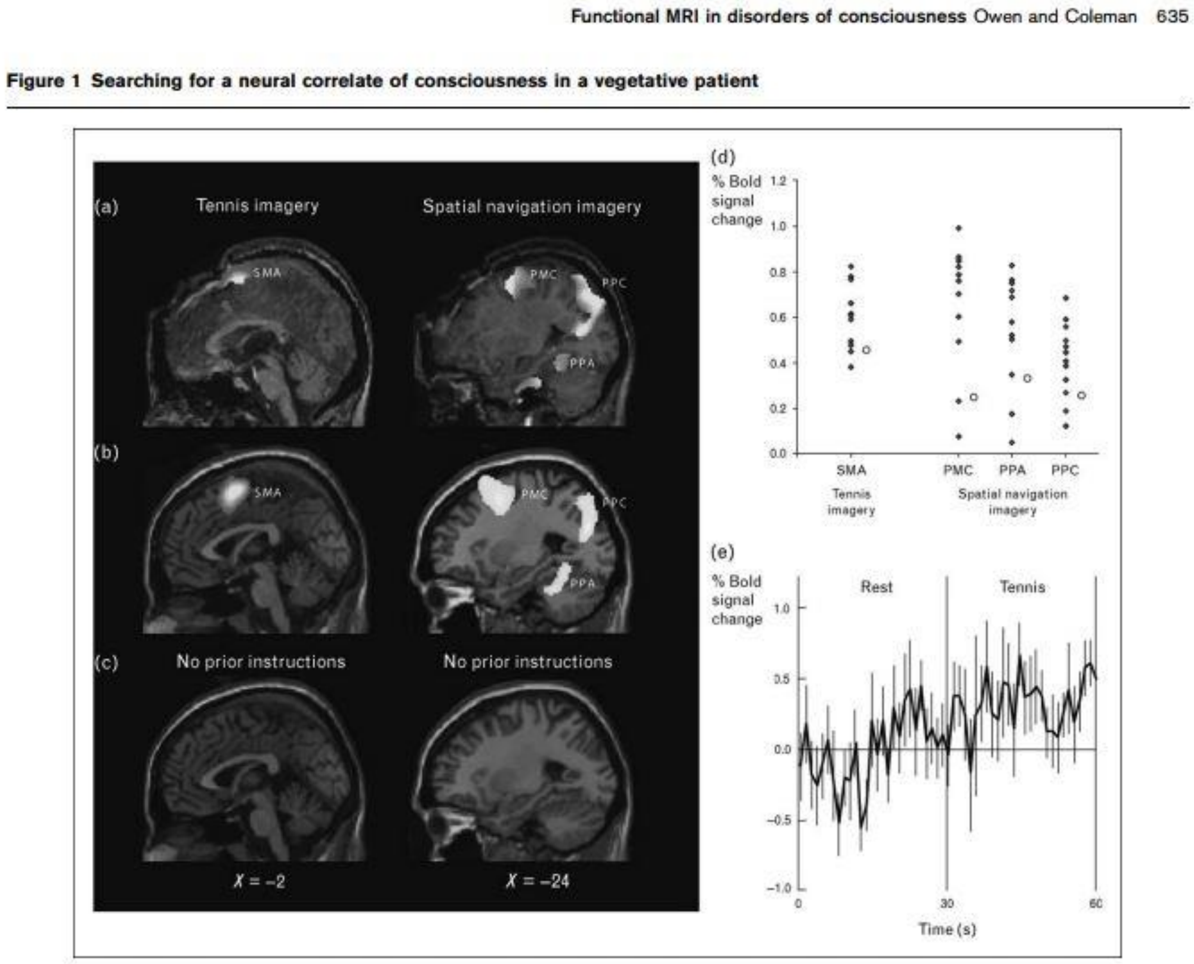

Indistinguishable functional MRI (fMRI) activity in a vegetative state patient (a) and healthy controls (b) while imagining playing tennis (left column) or moving around a house (right column) [40••]. (c) The results from healthy volunteers when noninstructive sentences involving the same key words were used [41••]. (d) Signal intensity changes in the vegetative state patient plotted against 12 healthy volunteers performing the same two tasks. Signal intensity changes for the patient are all within the normal range. (e) A sustained 30 s fMRI response in the supplementary motor cortex was observed when the vegetative state patient was asked to imagine playing tennis (right), relative to rest (left). PMC, premotor cortex; PPA, parahippocampal gyrus; PPC, posterior parietal cortex; SMA, supplementary motor area.

(Filename: TCT_2165_fMRI.JPG)

3664

Vascular Complications of Skull Base Osteomyelitis

A Malhotra[1], P GOYAL[2], y levy[3], K Seifert[4], X Wu[5], R Mangla[6], D Gandhi[7]
[1]YALE UNIVERSITY SCHOOL OF MEDICINE, NEW CANAAN, CT, [2]St. Vincents Medical Center, Bridgeport, CT, [3]Yale, New haven, CT, [4]YALE NEW HAVEN HOSPITAL, NEW HAVEN, CT, [5]Yale University School of Medicine, New Haven, CT, [6]SUNY upstate, syracuse NY, NY, [7]University of Maryland School of Medicine, Baltimore, MD

Purpose
Skull base osteomyelitis can be an aggressive, life-threatening infection that occurs predominantly in elderly immunocompromised patients or in children with normal immunological status.Potential vascular complications include carotid artery involvement with or without ischemic infarcts, septic emboli, arterial pseudoaneurysm or rupture. Sinovenous thrombosis can also be an important vascular complication. The purpose of this exhibit is to present a pictorial review of vascular complications of skull base osteomyelitis.
Materials and Methods
Cases of skull base osteomyelitis were searched through the electronic medical records, and assessed for vascular complications. Infection to the skull base may occur secondary to paranasal sinus or mastoid infection, or nasopharyngeal infections through emissary veins. A pictorial review of imaging findings will be presented on various imaging modalities including CT, MRI and nuclear medicine studies. Image optimization on MRI will be discussed to evaluate the skull base and early vascular involvement.
Results
Skull base osteomyelitis can result in both venous and arterial involvement, which can result in vascular complications. Venous involvement can result in sino-venous thrombosis of the dural venous sinuses, or cavernous sinus thrombosis with spread of infection through the venous collaterals. The internal carotid artery can also be involved as it traverses the skull base. Arterial involvement can be catastrophic and result in rapid wall thinning with pseudoaneurysm formation or rupture. In fungal infections of the skull base, arterial occlusion can occur as an indolent event. Arterial involvement can also result in distal septic emboli and intracranial abscesses, or bland infarcts.
Conclusions
Vascular complication of skull base osteomyelitis re uncommon, but early detection is critical for optimal management. Delay in diagnosis can result in significant morbidity and mortality. This pictorial review will help the clinical neuroradiologist recognize the imaging feature of vascular involvement, including vascular variants and pathways of spread of skull base infections.

2813

Vascular Emergencies of the Head and Neck

J Coburn[1], E Golden[2], J Brucker[3], T Kennedy[4]
[1]University of Wisconsin Hospitals and Clinics, Madison, WI, [2]UNIVERSITY OF WISCONSIN SCHOOL OF MEDICINE AND PUBLIC HEALTH, MADISON, WI, [3]University of Rochester Medical Center, Rochester, NY, [4]THE UNIVERSITY OF WISCONSIN-MADISON, MIDDLETON, WI

Purpose
This exhibit will review vascular emergencies of the arterial and venous system, involving the skull base as well as the soft tissues of the neck. This exhibit will examine the epidemiology of emergencies of the head and neck, identify common imaging findings, and discuss key clinical findings associated with these emergencies. This exhibit will also present a brief discussion on anatomy and management.
Materials and Methods
Vascular emergencies of the head and neck are relatively uncommon, but can be potentially catastrophic. Although rare, vascular emergencies often occur in very predictable patient populations including patients with central venous catheters, patients with head and neck infections, and patients with head and neck cancers. Many patients, especially those with head and neck cancers, have multiple significant risk factors for these emergencies. Recognizing the imaging findings of vascular complications in these patient populations is crucial to ensure expeditious detection and treatment.
Results
This presentation will be a comprehensive and case-based review of vascular emergencies highlighting

several examples of such emergencies including cavernous sinus thrombosis, massive epistaxis, thrombosis, stenosis of the major neck vessels, vascular infections, and vascular rupture.
Conclusions
Vascular emergencies of the head and neck are relatively rare, but critically important to recognize. These emergencies often occur in specific patient populations. Such patients should be evaluated with a high index of suspicion for vascular compromise as failure to detect such injury may lead to delay in diagnosis and treatment with potentially serious devastating complications.

2244

Vascular Trauma of the Head and Neck and Interventional Applications: A Pictorial Review

J Patel[1], G Brzezicki[1], P Natter[1], P Fiester[2], D Rao[1], D Haymes[1]
[1]University of Florida College of Medicine - Jacksonville, Jacksonville, FL, [2]University of Florida College of Medicine - Jacksonville, jacksonville, FL

Purpose
Traumatic vascular injuries of the head and neck can pose life-threatening emergencies. If they are not diagnosed or appropriately managed, they can result in significant morbidity. The purpose of this exhibit is to review the imaging appearance of various vascular injuries that can occur from penetrating and non-penetrating trauma to the head and neck. In addition, the exhibit will familiarize the viewer with the application of and decision-making for neurointerventional management for vascular trauma.
Materials and Methods
A case-based approach will be used to demonstrate the various forms of vascular trauma that can occur in the intracranial compartment, extracranial head and neck, and cervical spine. All patients are from a level 1 trauma center. Both penentrating and non-penetrating traumatic injuries will be demonstrated. A summary of the history will be provided as well as important details of the patient's clinical status as the imaging work-up and plans for intervention unfolded. The pertinent imaging findings on noncontrast CT and CT angiography will be highlighted. The decision-making that prompted conventional angiography and the therapeutic intervention will be addressed, and finally the imaging from successful interventions will be presented.
Results
Cases with more common pathology as well as unique and challenging cases will be presented to give the viewer an appreciation of the various scenarios that may arise. With regard to penetrating trauma, the zone 1-3 classification system for neck injuries will be reviewed to provide a background in the clinical perspective for management. The Denver grading scale for blunt vessel injury will also be reviewed, with examples of the different degrees of arterial injury. The therapeutic interventions presented will include deploying of embolization coiling, flow-diversion stents, and stent grafts.
Conclusions
Trauma radiology can be a difficult task as the radiologist might be confronted with a multitude of abnormalities simultaneously with an expectation to identify clinically significant injuries in a timely manner. Therefore, attention to vascular structures is essential. After reviewing this exhibit, the viewer will have greater knowledge of different types of vascular injuries and will have greater knowledge of the clinical management and interventional therapeutic options for these injuries

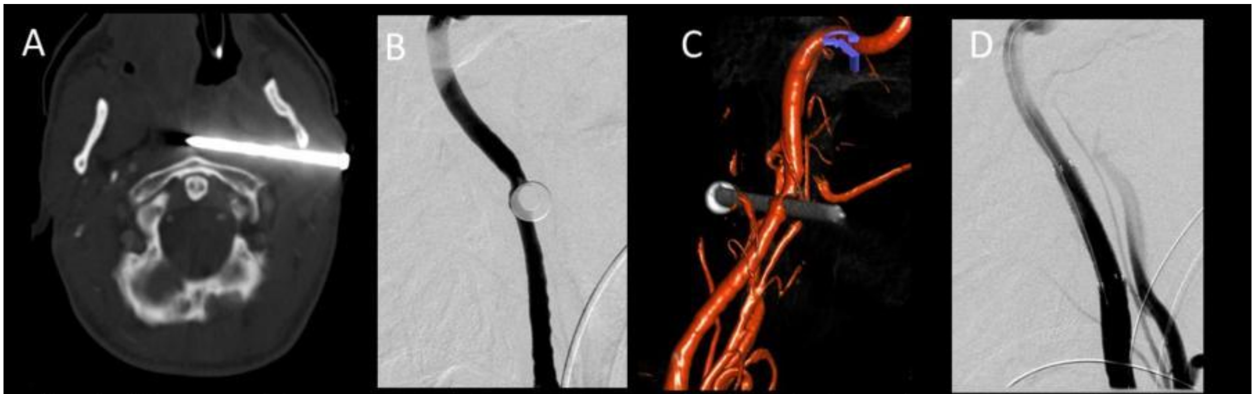

Fig 1: 49 year-old man presenting with penetrating injury above the angle of the mandible (Zone III)

1A: Axial CTA image: A metal nail penetrates through the left carotid space with tip in the posterior pharyngeal soft tissues. Streak artifact obscures evaluation of the immediately adjacent vasculature.
1B: Digital subtraction angiography left ICA injection: The nail traverses the left ICA lumen. There is preserved flow through the level of injury in the ICA.
1C: 3D rotational angiography image: The nail has partially lacerated the wall of the vessel, and there is focal dilatation at the level of injury suggesting pseudoaneurysm.
1D: DSA right CCA injection: Successful repair with placement of 5 x 25 mm Viabahn covered stent across the injury.

(Filename: TCT_2244_Graphicfile.jpg)

3409

Ventricular Catheters: Case-based Systematic Evaluation and Potential Complications

J Kim[1], M Haber[1], S Mukundan[2], C Potter[1]
[1]Brigham and Women's Hospital, Boston, MA, [2]Brigham & Women's Hospital, Boston, MA

Purpose
Ventricular catheters are commonly used for decompression in the setting of trauma, hemorrhage, mass effect, cerebral edema, hydrocephalus, and for monitoring intracranial pressure. It is important for radiologists to systemically evaluate ventricular catheters, identify expected post-operative appearances and acute and chronic complications in order to optimize patient care.
Materials and Methods
A case-based learning presentation format is planned with interactive format to teach systematic evaluation of catheters, with each case including teaching points, details of the neurosurgical procedure and potential pitfalls.
Results
1. Discuss catheter types and method of placement, evaluating for position, course, integrity, and function. The difference between externalized and internalized CSF drainage will be discussed, including indications for the different types of placement, neurosurgical placement procedures involved in each drainage type, types of drain and shunt components, and types of shunt locations, including ventriculoperitoneal, ventriculoatrial and venticulopleural locations. Shunt reservoir settings will also be discussed, including the available types of reservoirs, how to image and read them properly and how they are reset clinically. 2. Discuss the expected post-operative appearance of catheter placement, which includes small amounts of parenchymal hemorrhage or air along the catheter, and extra-axial fluid/gas collection at the surgical site. Identifying expected findings allows radiologists to reduce unnecessary communication and to recommend appropriate imaging follow up. 3. Discuss acute and chronic complications of shunt placement. Acute complications include misplacement, hemorrhage, and infection.

Infections to discuss will include meningitis, ventriculitis and abscess. Over and under-shunting will be discussed as acute and chronic complications. In the chronic setting, ventricles can become stiff, especially with prior bouts of ventriculitis, and subtle changes in ventricular size or angle should be noted to identify shunt malfunction. Over-shunting can lead to extra-axial fluid collections, such as subdural hygroma.

Conclusions

Detailed knowledge of catheter types, procedures for placement, normal post-operative appearance and complications allow the radiologist to add value and optimize neurosurgical clinical care.

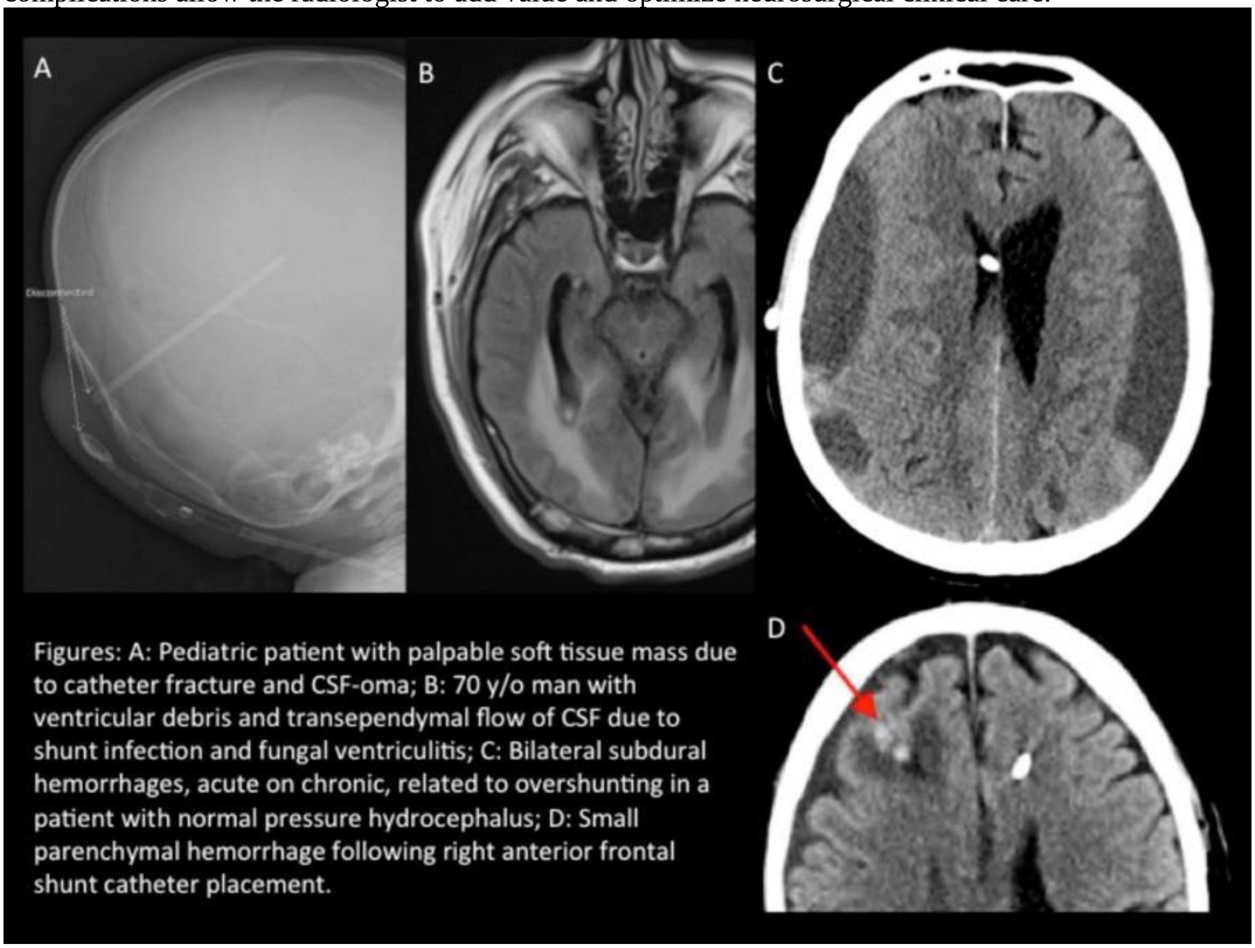

Figures: A: Pediatric patient with palpable soft tissue mass due to catheter fracture and CSF-oma; B: 70 y/o man with ventricular debris and transependymal flow of CSF due to shunt infection and fungal ventriculitis; C: Bilateral subdural hemorrhages, acute on chronic, related to overshunting in a patient with normal pressure hydrocephalus; D: Small parenchymal hemorrhage following right anterior frontal shunt catheter placement.

(Filename: TCT_3409_Shuntcomplications.jpg)

3254

What is What? When a Mitochondrial Cytopathy Mimics Common CNS Pathology in Children

F Lo Russo[1], C Alves[2], S Teixeira[2], F Gonçalves[2], G Zuccoli[3]
[1]*Children Hospital of Philadelphia, Philadelphia, PA,* [2]*Children's Hospital of Philadelphia, Philadelphia, PA,* [3]*CHOP, Philadelphia, PA*

Purpose

This pictorial essay aims to review the imaging pattern of mitochondrial cytopathies which can mimic common CNS pediatric disorders

Materials and Methods

We retrospectively searched our database for patients younger than 18 years of age who underwent brain

and/or spine MRI at our institution in which imaging findings of mitochondrial pathology have posed a diagnostic dilemma with common pathologies. Images have been reviewed for elementary imaging abnormalities: symmetric and/or signal changes in subcortical structures, leukoencephalopathy, and/or symmetric signal changes in the optic nerve and the spinal cord. Elementary imaging abnormalities have been used to classify imaging pattern further.
Results
Based on the heterogeneity of combinations of elementary imaging abnormalities the following categories of imaging patterns have been identified: tumefactive and inflammatory-like, tumor-like, and stroke-like patterns. Relevant cases of mitochondrial disease affecting CNS and their imaging findings will be displayed, with particular attention to the following learning objectives: • Elementary CNS lesions in children affected by mitochondrial disorders • Imaging patterns in which elementary can be combined • Diagnostic differentials in need to be reviewed while assessing imaging patterns of mitochondrial disorders affecting CNS • Imaging protocol and advanced imaging modalities (magnetic resonance spectroscopy) which can restrict diagnostic differential • Importance of imaging in the diagnosis of mitochondrial disease
Conclusions
Imaging patterns are an essential aspect of the diagnosis of mitochondrial disorder affecting the CNS, especially in children. This brief pictorial essay highlights the diagnostic challenge posed by mitochondrial cytopathy due to imaging pattern which can be mimicked and mimics common pathologies.

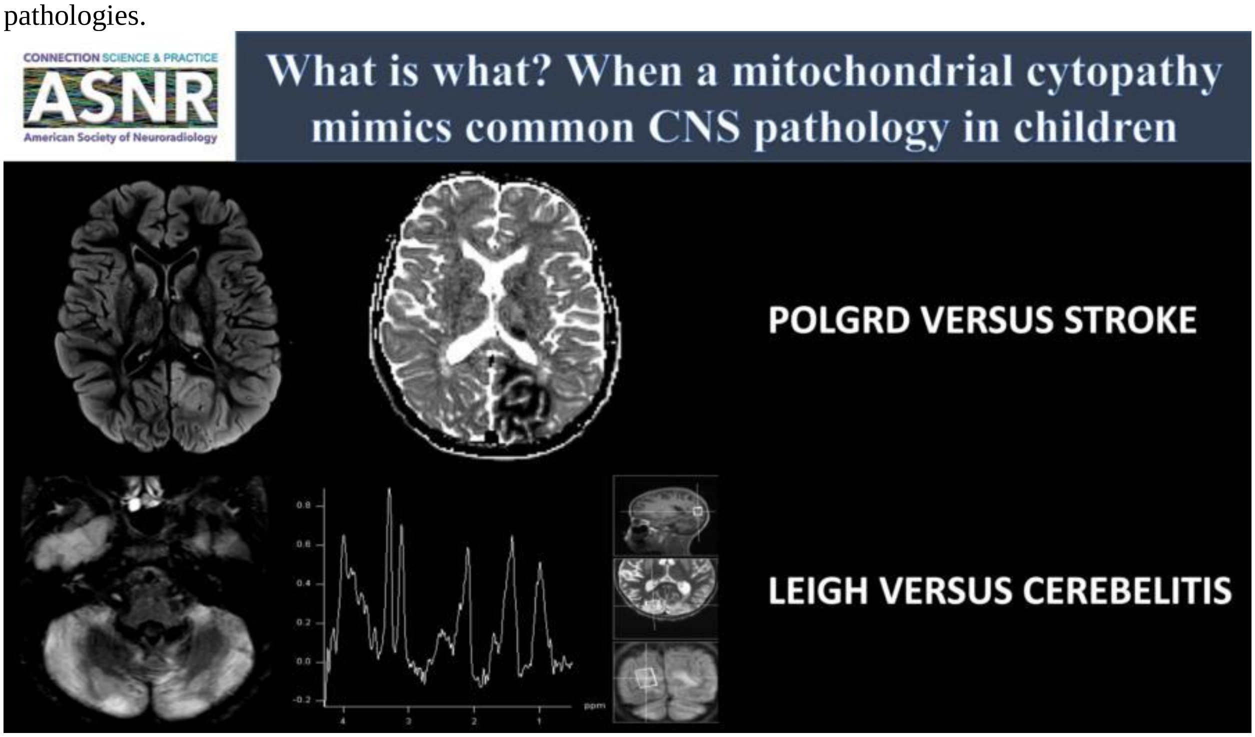

(Filename: TCT_3254_Diapositiva1.jpg)

2575

When Angry Vessels Talk: Applications, Interpretation and Pitfalls of Vessel Wall Imaging in Neuroradiology

D de Oliveira[1], J Roa[2], N Soni[3], B Policeni[4], E Samaniego[2], G BATHLA[5]

[1]*Hospital do Cancer da Universidade Federal de Uberlândia, Uberlândia, Minas Gerais,* [2]*University of Iowa, Iowa city, IA,* [3]*UIHC, iowa, IA,* [4]*University Of Iowa, Iowa City, IA,* [5]*University of Iowa hospitals and Clinics, IOWA CITY, IA*

Purpose
The authors present a spectrum of cases to demonstrate and emphasize the wide-ranging, established and emerging clinical applications of vessel wall imaging (VWI) in Neuroradiology.
Materials and Methods
VWI is emerging as an important imaging technique which has implications both in understanding the pathophysiology of different diseases as well as in diagnosis and follow up. It can be done both on a 3T or a 7T magnet. We present a spectrum of cases to highlight characteristic imaging findings related to each disease.
Results
We will present: - Atherosclerotic disease: vessel wall imaging can demonstrate plaque components, such as intraplaque hemorrhage, eccentric plaque growth and plaque enhancement, which has been associated with recent rupture or increased risk of rupture. - CNS vasculitis: Imaging may show focal or segmental wall thickening and enhancement which is often circumferential. - RCVS: Segmental wall thickening without significant enhancement. Similar changes may be seen with cocaine vasculopathy. - Aneurysm: Symptomatic and ruptured aneurysms have wall enhancement much more commonly than asymptomatic saccular aneurysms; - Post-thrombectomy: mechanical thrombectomy results in intracranial arterial wall thickening and enhancement, potentially mimicking arteritis; - Neurosarcoidosis: perivascular and vessel wall enhancement is observed in patients with sarcoidosis, presenting with cerebrovascular symptoms; - Giant cell arteritis: thickening and enhancement of superficial temporal artery wall;
Conclusions
VWI is being increasingly used as a noninvasive diagnostic tool while evaluating intra- and extracranial vascular bed. With advances in imaging, the clinical applications of VWI are expected to expand further.

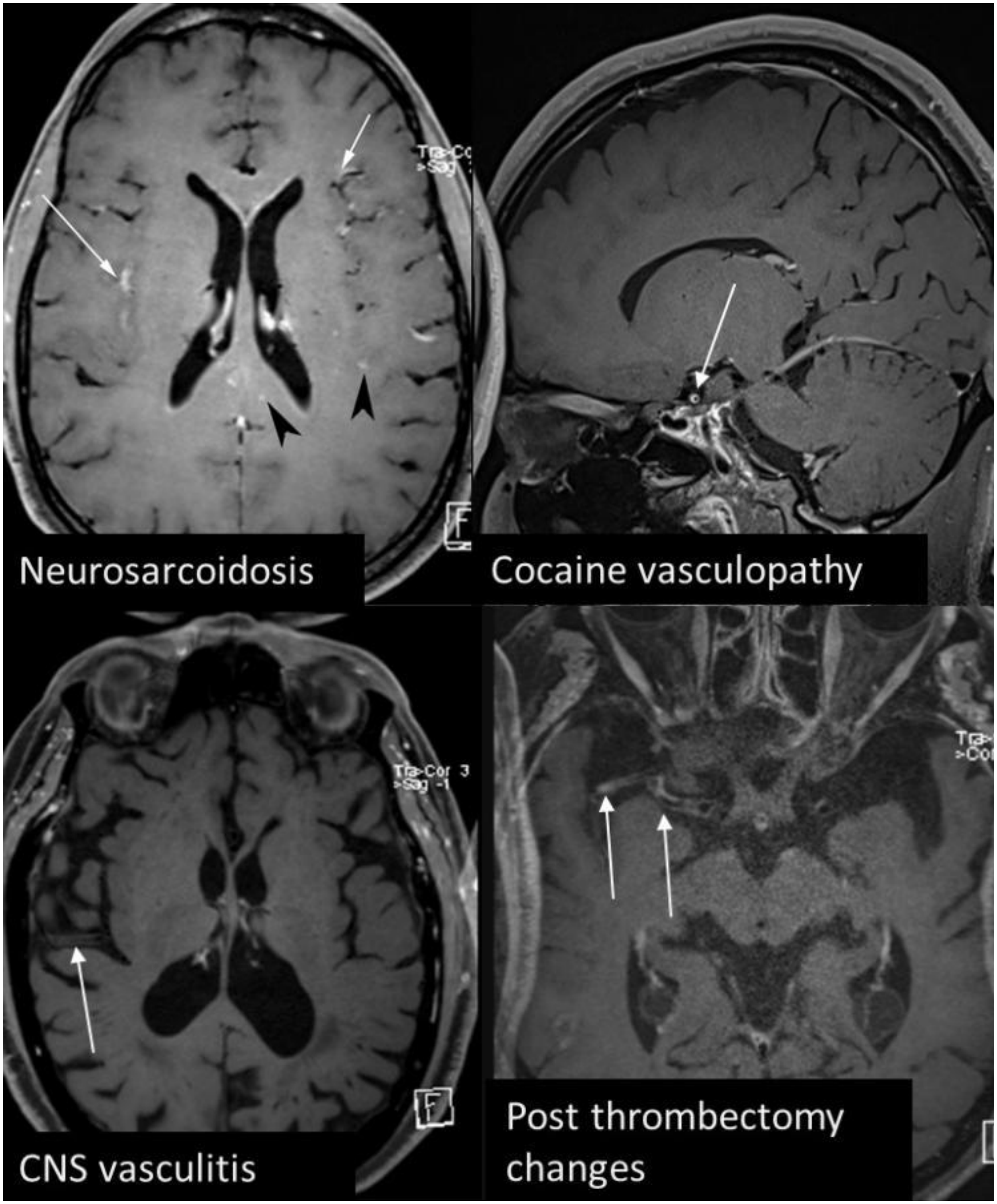

(Filename: TCT_2575_VWI.jpg)

2690

Yikes!!! There is a Stranger's Hand in My Bed: Alien Hand Syndrome: Case Series and Review of the Literature

M Thomas[1], B Harrison[2], C DeGiorgio[3], G Hathout[2]
[1]Olive View-UCLA Medical Center, Sylmar, CA, [2]University of California, Los Angeles, Los Angeles, CA, [3]University of California, Los Angeles, Sylmar , CA

Purpose

A 48 year old female with past medical history of diabetes, hypertension, hyperlipidemia and NSTEMI woke up in the morning in her bed screaming that a hairy man's hand was on her chest while she was sleeping. Her family ran in to the room and noted that the mysterious hand belonged to the patient. Over the next couple of days, the patient noticed that while she was pulling up her undergarments with her right hand, the left hand would then pull down the undergarment. Her family also noticed the patient having arguments with her left hand. Alien Hand Syndrome (AHS) is a rare, intriguing neurological disorder characterized by the inability of the patient to identify ownership of one's own limb. The patient may ignore the affected limb, consider the limb as foreign or personify the limb. The affected limb can have involuntary yet purposefully appearing movements that can at times appear contradictory or even harmful to the other limb or person. Although the clinical presentation may be fascinating, it can also be perplexing to the patient, family members and clinicians and accurate and prompt diagnosis is of paramount importance. The purpose of this exhibit is to present a series of cases of alien hand syndrome at our institutions while reviewing the spectrum of clinical manifestations, etiology, types, proposed neurological mechanism of AHS and possible treatments.

Materials and Methods

We retrospectively reviewed a series of cases of alien hand syndrome at our institutions and reviewed the clinical scenarios, underlying cause, mechanism, treatment and follow up. We also did a detailed review of the literature of reported cases of alien hand syndrome.

Results

Alien Hand Syndrome is a fascinating yet rare neurological disorder that can be due to a variety of clinical and pathological entities. The criteria for diagnosis include complaints of a foreign limb and complex involuntary motor activity that is not part of an identifiable movement disorder. The patient may personify the arm and have arguments with the limb as in one of our cases. Lesions that can cause alien hand syndrome can involve the frontal lobe, corpus callosum, parietal lobes, occipital lobes and thalamus. AHS has been reported in infarcts, vasculitis, prior surgeries, trauma, seizures, tumors, Alzheimers Disease, cortical basal ganglionic degeneration, Creutzfield Jacob Disease, progressive supranuclear palsy, focal cortical atrophy, vascular malformations, HIV, Parry Romberg Syndrome and multiple sclerosis. AHS is classified into 3 types: frontal, callosal and posterior variants. Features of the frontal variant often include groping, grasping or compulsive manipulation of tools in the affected extremity. This is thought to result from lesions in the supplementary motor area, cingulate cortex, dominant medial prefrontal cortex or the corpus callosum. The callosal variant is often characterized by intermanual conflict where there is opposing purposeful movements of the hands and is related to damage to the corpus callosum. The third type is the posterior variant characterized by unintentional withdrawal from the environment or stimuli or uncoordinated hand movements or involuntary levitation and is thought to be related to lesions from the thalamus, posterolateral parietal or occipital lobe. Although Alien Hand Syndrome has been classified into 3 types, there is considerable overlap of the symptoms and localization into a discrete type at times may not be possible. Medications such as benzodiazepines and injection of botulism toxin have been reported as useful in certain clinical situations as well as behavioral interventions

Conclusions

Alien Hand Syndrome is a complex, intriguing, rare syndrome. This little known syndrome with its often bizarre presentation can confuse the patient, family members and clinicians. It is important for the neuroradiologist to be aware of this syndrome to accurately identify it and to understand the clinical features, etiology, neurological mechanism and treatment.

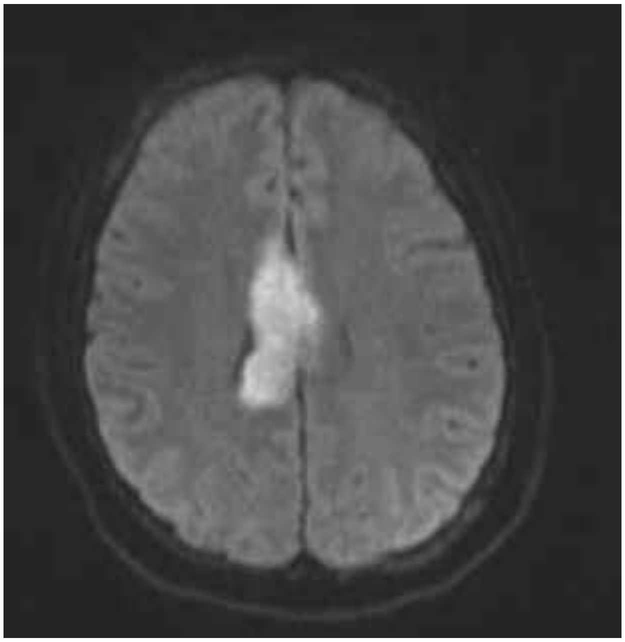
(Filename: TCT_2690_diffusion.jpg)